PHOTOCHROMIC SMALL MOLECULAR TOOLS: ALTERING BIOLOGICAL FUNCTION THROUGH LIGHT

Dissertation

Zur Erlangung des Doktorgrades der Naturwissenschaften

(Dr. rer. nat.)

Der Fakultät für Chemie und Pharmazie

Der Universität Regensburg

Vorgelegt von

Nadja A. Simeth

aus Cham

Regensburg – 2018

The experimental work was carried out at the Institute of Organic Chemistry at the University of Regensburg under the supervision of Prof. Dr. Burkhard König between November 2014 and February 2018 and in the PhotoGreenLab at the University of Pavia under the supervision of Prof. Dr. Maurizio Fagnoni between March and May 2017.

The PhD Thesis was submitted on:	May 14th 2018
Date of the colloquium:	August 3rd 2018

Board of Examiners:

Chairman:	Prof. Dr. Alkwin Slenczka
1st Referee:	Prof. Dr. Burkhard König
2nd Referee:	Prof. Dr. Reinhard Sterner
Examiner:	Prof. Dr. Julia Rehbein

DECLARATION

Eidesstattliche Erklärung

Ich erkläre hiermit an Eides statt, dass ich die vorliegende Arbeit ohne unzulässige Hilfe Dritter und ohne Benutzung anderer als der angegebenen Hilfsmittel angefertigt habe; die aus anderen Quellen direkt oder indirekt übernommenen Daten und Konzepte sind unter Angabe des Literaturzitats gekennzeichnet.

Die Arbeit wurde bisher weder im In- noch im Ausland in gleicher oder ähnlicher Form einer anderen Prüfungsbehörde vorgelegt.

Signed: _____

Date: _____

Nadja A. Simeth, M.Sc.

Regensburg

To Those who are and became Part of My Family

ACKNOWLEDGEMENTS

Firstly, I want to thank Prof. Dr. Burkhard König for the opportunity to work in his group. I'm particularly grateful for the freedom he gave me to develop own ideas and projects from the very first day but also for his friendly advice and excellent support during the last years – especially during times when projects had to be pushed hard.

Also, I would like to thank Prof. Dr. Reinhard Sterner, Prof. Dr. Julia Rehbein and Prof. Dr. Alkwin Slenczka for completing the board of examiners.

I also owe thanks to Prof. Dr. Joachim Wegener and Prof. Dr. Morten Grøtli for accepting the position as mentors within the *ChemPharm* graduate school.

I am grateful to Dr. Stefano Crespi and Prof. Dr. Maurizio Fagnoni for their excellent cooperation, advice and hospitality during my stay in Pavia, Italy. *Grazie Mille*!

Furthermore, I would like to thank Dr. Andrea Kneuttinger, Kristina Heyn, Prof. Dr. Reinhard Sterner, Karin Rustler, Dr. Steffen Pockes, Prof. Dr. Sigurd Elz, Lisa-Marie Altmann, Nathalie Wössner and Prof. Dr. Manfred Jung for outstanding joint work in various projects.

I am grateful to Burkhard König, Stefano Crespi, Andrea Kneuttinger, Anika Simeth, Martin Obst, Miriam Graf, Helena Pfeiffer and Friederike Steudel for their careful proofreading of certain parts of this thesis.

I would like to acknowledge the both financial support and the various opportunities to advance on a personal level and to meet up with great people through the Studienstiftung des Deutschen Volkes. I'm happily looking back to the Doktorandenforen in Bonn, Berlin, Düsseldorf, Bad Homburg, Heidelberg and Münster, and *Stipendiaten Machen Programm* in Potsdam that I could organize together with Friederike Steudel and Andreas Beil. I also want to thank both of them as well as my fellow Stiftis Sebastian Gohr, Elisabeth Kreidt, Manuel Hochheim, Michael C. D. Fürst and David Winnekens for their friendship and elitist company.

I further would like to express my gratitude to my lab mates Anna, Amrita, Kang, Stefano, Luca and Silvia for all the time we spent together – from regular working days to hot incidents. Thanks for making life easier!

Dem *permanent staff* des Lehrstuhls: Dr. Petra Hilgers, Britta Badziura, Regina Hoheisel, Ernst Lautenschlager, Katharina Nickl, Viola Rappenegger, Simone Strauß, Dr. Rudolf Vasold und Julia Zach möchte ich für ihre Hilfe bei Verwaltungs-, Mess- oder technischen Problemen und der Aufrechterhaltung einer hervorragenden Infrastruktur herzlich danken.

Den Mitarbeitern der Abteilungen für Massenanalyse, NMR-Spektroskopie sowie der Röntgenstrukturanalyse gilt ein großes Dankeschön für ihre hervorragende Arbeit.

I owe thanks to my students Peter Ehrnsberger, Lisa-Marie Altmann, Oliver Sarosi, Andreas Hartl, Barbara Kaiser, Carolin Koss, Tobias Karl, Franziska Funke and Thomas Kinateder and trainees Lorena Oegl, Julia Kefer, Anna Wittmann and Elisabeth Bauer for their time and commitment during their stays.

My special thanks go to:
The König group: for all the coffee breaks, after-work beers, Weißwurst Breakfasts, International Evenings, PhD Parties and the great working atmosphere during now more than four years.
The MedChem&Switches Subgroup: For being the best subgroup anyways.
Tonda Kralik: For a great friendship over the last years that all started out with a coffee and a glass of Nutella. I am very happy about all the moments we spent together – over a cup of coffee or a glass of wine, in Germany, Czech Republic, Spain, Estonia or Sweden talking about work, movies, the room of imagination, members, yesterday (when you said tomorrow) and stranger things in several languages.
Barbara Krämer: For a PhD-life-long crucial look on wannabe crystals. Aber vielmehr noch für eine nun schon mehr als neun Jahre anhaltende Freundschaft, die das Chemiestudium ermöglicht hat (auch wenn dich die AC auf die dunkle Seite gezogen hat), für all die gemeinsamen langen Tage und noch längeren Nächte beim Fertigstellen von (früher) Protokollen und (heute) anderen Projekten, für das immer offene Ohr, den konstanten Rückhalt und die unverblümte Kritik.
Karin Rustler: For your friendship that included both unicorns and cookies. Für die gemeinsamen Kaffeepausen ohne, dass du Kaffee trinkst. Für lange Gespräche bei einer Tasse heißer Schokolade und einem Nutella-Crêpes. Für zwei großartige Konferenzen zwischen Sightseeing, Hörsaal und Unmengen an Franzosen.
Martin F. Obst: Für dreieinhalb gemeinsame Jahre der Promotion – vom Verwaltungsgang am allerersten Tag bis zur Prüfungsvorbereitung war immer auf dich Verlass. Deine unübertreffliche Selbstironie und dein Humor werden mir sehr fehlen.

As I was lucky, there also was a life outside of Uni – and it was at least as important:
Steffi Landgraf: Wir kennen uns schon so lange, dass ich gar nicht mehr weiß, wo ich anfangen soll zurückzublicken - bei unseren Trips zu *Jugend forscht*, nach Berlin oder London, den vielen Teestunden im Wohnheim? Den späteren Treffen? Dem gemeinsamen – sicher nicht, aber vielleicht doch ein bisschen – Erwachsenwerden? Vielen Dank für all die wunderschönen Aktionen, die so oft im Blödsinn begannen und dann doch zu Sinnhaftigem wurden.
Helena Pfeiffer: For being the best roomie! Für lange WG-Abende, intensive Gespräche, Rat und Tat – for those nights and all nights to come. Für all die unvergesslichen Augenblicke und lustigen Momente, die oft genug dem Nerd-sein geschuldet waren oder einfach lost-in-translation zwischen Latein, Fachchinesisch und dreierlei Variationen Englisch gingen. And for having more than just ONE duck in the bathroom :)
Miriam Graf: For truly being a friend, deine Ratschläge zu allen Lebenslagen, für viele Weinabende mit tiefen Gesprächen, dein unerschöpfliches Wissen über Sprach- und

Zeitgrenzen hinweg, die vielen Mädels-Abende und (hört sich zwar unrealistisch an, stimmt mit dir als Begleitung aber wirklich) schönen Shoppingtouren.
Lisa Kaser: Für all die gemeinsamen Aktionen, die meist die besten und dümmsten Ideen zu gleich waren. Aber Hauptsache 120 Krapfen und zwölf Kürbisse in einem Abendessen vereinen! Für 17 min Noah! Für die Rettung der israelischen Robbe!
Florian Reitemann: Für deine konstante Motivation andere zu Motivieren – zum Arbeiten, Zusammenkommen, für Unternehmungen und zum Schnaps trinken. Für deine Spontanität, sich auf einen Kaffee zu treffen oder eben mal Instrumente, Umzugskartons oder Skier durch die Gegend zu fahren.
Felix Schamburger: Für die lange Kochpartnerschaft, die das Niveau der KHG-Küche hochhielt, die jahrelange Leihgabe von Umzugskartons, die vielen Fahrtdienste, das Teilen deiner Spielesammlung mit Freunden und viele, viele lustige Abende.
Lucas Lobmeier: Für dein Allzeit-Bereit-Sein, sei es mit Priestermobil, zum Brunchen, auf einen Cocktail, am Bismarckplatz, zum Film schauen oder als Ultra-Fan unseres Handballteams – der den Spielplan besser kennt als sämtliche Spieler.
Lara Bruck & Judith Kalb: Le Trio Infernal…Da ist Einiges zusammengekommen über die Jahre, das ich nicht missen möchte.
Friederike Steudel: Das war wohl Liebe auf den ersten Blick! Für deine lockere Art, das gemeinsame Vortragsbierchen und die perfekte Anmoderation. Für deine Freundschaft über Längen- und Höhenmeter.
KHG: Für einen Ort zum Ankommen und Ausruhen, zum Kreativsein, zum Schmieden verrückter Pläne, für Fahrten ins Unbekannte, für einen Ort zum Freunde treffen und Verweilen.
ESV '27 Regensburg: Für eine Heimat zwischen Harz und Teamgeist, die das Ankommen in Regensburg ein ganzes Stück leichter gemacht, ein großes Dankeschön an all die kleinen und großen Handballer mit denen ich seit 2009 Siege und Niederlagen teilen durfte.

And last but not least: to my family, besonders meinen Eltern Gisela und Helmut, weil sie mich über all die Jahre begleitet und bestärkt haben. Ihr habt mir den Freiraum gegeben meinen ganz eigenen Weg zu gehen und mich in Momenten des Zweifels ermutigt weiter zu machen. Es gibt keine Worte, um auszudrücken, wie wichtig ihr für mich seid. Gigantic thanks to my *little* sister Anika – for finding the perfect words in crucial moments.
Stefano, for your care, love and patience enduring my never-ending poutiness. Ti amo.

PREAMBLE

DESIGN AND SYNTHESIS OF PHOTOCHROMIC SCAFFOLDS FOR BIOLOGICAL APPLICATION

To expand the scope of bioactive compounds, which can be found in nature, chemists have developed many synthetic biocompatible molecules and drugs.[1] So far, many compounds have been evaluated in laboratories and have made their way into clinical application and drug approval.[2] This was feasible by structural re-design of known compounds or by *de novo* approaches, often assisted by the identification of hot spot areas by *in silico* studies.[2, 3] However, there are still many challenges to cope with. For instance, bioactive compounds such as drugs are usually delivered by diffusion control (upon uptake from the surrounding medium or, in the case of humans, after, for instance, oral or intravenous administration).[2, 4] This makes the transmission of the compound to a certain location within a complex system like a living cell, a tissue or even the human body very difficult. In some cases, selective addressing of a compound's action-domain is still impossible.[5] Moreover, the lifetime of a bioactive compound in a system depends on its metabolization and/or excretion profile and it is often still active after both processes.[5] For instance, antibiotics from excretion accumulate in our water reservoirs, possibly leading to strains of antibiotic-resistant bacteria.[6-8] Hence, there are two important issues to deal with: To discover molecules, which are bioactive, and to find ways to limit their distribution and switch them *on* and *off* when- and wherever needed.[9] A precise control of a molecule's active state would improve the impact of drugs, should thus reduce side-effects and e.g. decrease antibiotic resistance or *just* lead to exactly controllable tool compounds, helping scientists to unravel unsolved riddles of cellular processes.[10]

Bringing such a powerful instrument into a biological context depends on certain conditions: A potential substance must not be invasive, should be easy to operate, clean, and adjustable in a spatiotemporal fashion. All these criteria can be satisfied by one common mean: The usage of light, which led to the birth of the very young field of *photopharmacology*.[4, 9, 11] Whereas the stimulating properties of some plant extracts have been known since the old Egypt's days, the photochromism of the nowadays mostly used scaffold in photopharmacology, azobenzene, is by far younger.[12, 13] Its photoisomerization was first described in 1937.[13] Photocontrollable substances have even only been employed in pharmacological context within the last two decades. Hence, much has to be boldly discovered in a field where no one has gone before.[14]

However, an increase in function goes hand in hand with a higher complexity of the desired molecule. Adding photoresponsivity on the list of demands made on potential drugs, challenges the chemist once again to build complex architectures in an extremely limited space.[15]

Three different strategies using light as a tool in biology have been developed so far: optogenetics, uncaging and photoswitches.[10, 16] In optogenetics, a photosensitive actuator protein is employed as a peptidic switch, which is fused with the protein of interest. Upon irradiation with light, it undergoes structural changes which are eventually transferred onto the whole protein. In this manner, the fusion protein can be photo regulated. However, structural integration of a new peptidic section might disrupt the original function of the protein.[10] In contrast, the use of both uncaging and photoswitching is based on the manipulation of smaller molecular systems. In particular, uncaging classically describes the cleavage of a photolabile protecting group from a biological relevant structure such as a ligand or an amino acid (in a peptide). On the other hand, photoswitches are light-responsive structures, which undergo a reversible, structural isomerization between two (or more) photoisomers. This isomerization is accompanied by changes in sterical demand, dipole moment, and further electronical properties, generating two (or more) functional states from one molecule. The present work will mainly focus on this strategy of photocontrol.[10, 11, 16, 17]

Several structures have been investigated regarding their photoinduced isomerization properties: Azobenzenes,[18, 19] diarylethenes,[20] fulgides and fulgimides,[21] overcrowded alkenes,[22] spiropyrans,[23] and donor-acceptor Stenhouse complexes[24] are just a few examples. However, only a limited number of candidates have been brought into a biological context so far.[9, 19, 25] Building a drug-like molecule from a photochromic scaffold demands several properties of the switch. Integration of a photoresponsive structure is in the first place a matter of size. The photoswitch needs to be incorporated in a crafty manner into a bioactive structure to not disrupt biological relevant interactions. In addition, the photoisomerization should induce a change in the structural and/or electronic property of the compound in such a way that the mode of action of the biomolecule is inhibited or drastically altered. Therefore, reasonable photochromic properties in aqueous environment are needed, a subject which is not investigated in all photoswitches. Also, the decoration of the photochromic core with different functional groups can influence the photoswitching properties and change the isomerization behavior and hence, must be planned at the early stage of the design of a target compound.[4, 9, 11, 16, 25]

Consequently, the chemist needs to choose the most suitable photoswitch for a given problem and needs to artfully mold the compound's structure. Hence, a deep knowledge of different scaffolds, their properties and their turnability is required to design the *ideal* switch for a given problem. However, not many photochromic compounds have been investigated in a logical manner to fully understand their behavior. Hence, the first part of this thesis (Chapter I), is dedicated to the investigation of the photochromic characteristics and the

tunability of a novel class of azo photoswitches, phenyl azoindoles.[26] In the following chapters, different strategies of photocontrol are applied in biological relevant systems. In particular, Chapter II deals with the photo-electronic control of redox coenzymes. It is shown how a photoinduced redox-lock strategy can alter the redox properties of such structures and consequently facilitate redox reactions in organic and biological environment on demand.[27] Chapter III is devoted to the photoinduced allosteric regulation of multienzyme complexes, using imidazole glycerol phosphate synthase and tryptophan synthase as examples. Finally, the last part of the thesis (Chapter IV) covers the use of photocontrol *via* sterical means developing ligands towards sirtuins and as histamin H1 antagonists.

References:

1. Newman, D. J.; Cragg, G. M., Natural Products as Sources of New Drugs over the Last 25 Years. *Journal of Natural Products* **2007**, *70*, 461–477.

2. Overington, J. P.; Al-Lazikani, B.; Hopkins, A. L., How Many Drug Targets are There? *Nature Reviews Drug Discovery* **2006**, *5*, 993–996.

3. Hall, D. R.; Ngan, C. H.; Zerbe, B. S.; Kozakov, D.; Vajda, S., Hot Spot Analysis for Driving the Development of Hits into Leads in Fragment-Based Drug Discovery. *Journal of Chemical Information and Modeling* **2012**, *52*, 199–209.

4. Lerch, M. M.; Hansen, M. J.; van Dam, G. M.; Szymanski, W.; Feringa, B. L., Emerging Targets in Photopharmacology. *Angewandte Chemie International Edition* **2016**, *55*, 10978–10999.

5. Ruiz-Garcia, A.; Bermejo, M.; Moss, A.; Casabo, V. G., Pharmacokinetics in Drug Discovery. *Journal of Pharmaceutical Sciences* **2008**, *97*, 654–690.

6. Gibs, J.; Stackelberg, P. E.; Furlong, E. T.; Meyer, M.; Zaugg, S. D.; Lippincott, R. L., Persistence of Pharmaceuticals and Other Organic Compounds in Chlorinated Drinking Water as a Function of Time. *Science of The Total Environment* **2007**, *373*, 240–249.

7. Watkinson, A. J.; Murby, E. J.; Kolpin, D. W.; Costanzo, S. D., The Occurrence of Antibiotics in an Urban Watershed: From Wastewater to Drinking Water. *Science of The Total Environment* **2009**, *407*, 2711–2723.

8. Armstrong, J. L.; Shigeno, D. S.; Calomiris, J. J.; Seidler, R. J., Antibiotic-Resistant Bacteria in Drinking Water. *Applied and Environmental Microbiology* **1981**, *42*, 277–283.

9. Velema, W. A.; Szymanski, W.; Feringa, B. L., Photopharmacology: Beyond Proof of Principle. *Journal of the American Chemical Society* **2014**, *136*, 2178–2191.

10. Brieke, C.; Rohrbach, F.; Gottschalk, A.; Mayer, G.; Heckel, A., Light-Controlled Tools. *Angewandte Chemie International Edition* **2012**, *51*, 8446–8476.

11. Broichhagen, J.; Frank, J. A.; Trauner, D., A Roadmap to Success in Photopharmacology. *Accounts of Chemical Research* **2015**, *48*, 1947–1960.

12. Allen, J. P.; Art, The Art of Medicine in Ancient Egypt. *Metropolitan Museum of Art* **2005**.

13. Hartley, G. S., The Cis-form of Azobenzene. *Nature* **1937**, *140*, 281–281.

14. Goldstone, J., Where No Man Has Gone Before. In *Star Treck: The Original Series*, **1966**.

15. Trauner, D., The Chemist and the Architect. *Angewandte Chemie International Edition* **2018**, *57*, 4177–4191.

16. Szymański, W.; Beierle, J. M.; Kistemaker, H. A. V.; Velema, W. A.; Feringa, B. L., Reversible Photocontrol of Biological Systems by the Incorporation of Molecular Photoswitches. *Chemical Reviews* **2013**, *113*, 6114–6178.

17. Irie, M., Photochromism: Memories and Switches. *Chemical Reviews* **2000**, *100*, 1683–1684.

18. Bandara, H. M. D.; Burdette, S. C., Photoisomerization in Different Classes of Azobenzene. *Chemical Society Reviews* **2012**, *41*, 1809–1825.

19. Beharry, A. A.; Woolley, G. A., Azobenzene Photoswitches for Biomolecules. *Chemical Society Reviews* **2011**, *40*, 4422–4437.

20. Irie, M., Diarylethenes for Memories and Switches. *Chemical Reviews* **2000**, *100*, 1685–1716.

21. Yokoyama, Y., Fulgides for Memories and Switches. *Chemical Reviews* **2000**, *100*, 1717–1740.

22. Feringa, B.; Wynberg, H., Torsionally distorted olefins. Resolution of cis- and trans-4,4'-Bi-1,1',2,2',3,3'-hexahydrophenanthrylidene. *Journal of the American Chemical Society* **1977**, *99*, 602–603.

23. Berkovic, G.; Krongauz, V.; Weiss, V., Spiropyrans and Spirooxazines for Memories and Switches. *Chemical Reviews* **2000**, *100*, 1741–1754.

24. Lerch, M. M.; Szymanski, W.; Feringa, B. L., The (Photo)chemistry of Stenhouse photoswitches: Guiding Principles and System design. *Chemical Society Reviews* **2018**, *47*, 1910–1937.

25. Feringa, B. L., Browne, W. R., Eds., Molecular Switches. *Wiley-VCH Verlag GmbH & Co. KGaA: Weinheim*, *Germany*, **2011**.

26. Simeth, N. A.; Crespi, S.; Fagnoni, M.; König, B., Tuning the Thermal Isomerization of Phenylazoindole Photoswitches from Days to Nanoseconds. *Journal of the American Chemical Society* **2018**, *140,* 2940–2946.

27. Simeth, N. A.; Kneuttinger, A. C.; Sterner, R.; König, B., Photochromic Coenzyme Q Derivatives: Switching Redox Potentials with Light. *Chemical Science* **2017**, *8*, 6474–6483.

List of Abbreviations and Acronyms

AcOH	Acetic Acid
AICAR	5-Aminoimidazole-4-carboxamide ribotide
Ar	Aryl
ATP	Adenosintriphosphate
aq	Aqueous
AzoF	Phenylazophenylalanine
BIM	Bisindolemaleimide
$B(OBu)_3$	Tributylborane
$B(OMe)_3$	Trimethylborane
$B(O^iPr)(Opin)$	2-Isopropoxy-4,4,5,5-tetramethyl-1,3,2-dioxaborolane
Bu	Butyl
^{n}Bu	primary-Butyl
^{s}Bu	secondary-Butyl
Bu_4NBF_4	Tetrabutylammonium tetrafluoroborate
CoIn	Conical Intersection
CoQ	Coenzyme Q, Ubiquinone
C-PCM	Conductor-like polarizable continuum model
d	Days
Δ	Thermal equilibrium
DAD	Diode Array Detector
DAE	Diarylethene
DBU	1,8-Diazabicyclo(5.4.0)undec-7-ene
DCIP	2,6-Dichlorophenol indophenol
DCM	Dichloromethane
DFT	Density functional theory
DIPA	Diisopropylamine
DMF	Dimethylformamide
DMSO	Dimethylsulfoxide
DNA	Deoxyribonucleic acid
DTE	Dithienylethene
DTM	Dithienylmaleimide
E	Energy

ε	Permittivity
ε_λ	Molar attenuation coefficient at a defined wavelength λ
EPR	Electron Paramagnetic Resonance
eq	Equivalent(s)
ESI-MS	Electrospray ionization Mass Spectroscopy
Et	Ethyl
Et_2O	Diethylether
f	Oscillator Strength
FAD	Flavine adenine dinucleotide
g	Gramm
GAT	Glutamine amidotransferases
GAP	Glycerin aldehyde-3 phosphate
GPCR	G-protein coupled receptors
h	Hours
H	Enthalpy
HDAC	Histone deacetylase
HF	Hartree-Fock
HOMO	Highest Occupied Molecular Orbital
HPLC	High performance liquid chromatography
HRMS	High resolution mass spectrometry
Hz	Hertz
IC_{50}	Inhibitor concentration that causes 50% reduction in catalytic activity
IGP	Indole-3-glycerol phosphate
IGPS	Imidazole glycerol phosphate synthase
ImGP	Imidazoleglycerolphosphate
IR	Infrared
k_{cat}	Turnover number
K_i	Thermodynamic inhibitory constant
KIE	Kinetic Isotope Effect
K_m	Michaelis-Menten constant
KO^tBu	Potassium Tertbutoxyde
λ	Wavelength
LC	Liquid chromatography

LED	Light emitting diode
LUMO	Lowest Unoccupied Molecular Orbital
M	Molar
MD	Molecular Dynamic
Me	Methyl
MeCN	Acetonitrile
MeOH	Methanol
MeOD	Deuterated Methanol
mg	Millogramm
mL	Milliliter
µL	Microliter
µM	Micromolar
µs	Microseconds
min	Minutes
MPLC	Medium Pressure Liquid Chromatography
MS	Mass spectrometry
MRI	Magnetic Resonance Imaging
NAD	Nicotinamide adenine dinucleotide
*N*BS	*N*-Bromosuccinimide
Nd:YAG	Neodymium-doped yttrium aluminum garnet; Nd:Y3Al5O12
nm	Nanometer
NMR	Nuclear magnetic resonance
NPY	Nitropiperonyl tyrosine
ONBY	Tyrosine analog o-nitrobenzyl-O-tyrosine
Peppsi-^{i}Pr	[1,3-Bis(2,6-Diisopropylphenyl)imidazol-2-ylidene](3-chloropyridyl)palladium(II) dichloride
PDB ID	Protein data bank identity
$Pd(OAc)_2$	Palladium acetate
$Pd(PPh_3)_4$	Tetrakis(triphenylphosphine)palladium(0)
Ph	Phenyl
pH	Potential of hydrogen
pK_a	Acid dissociation constant
PLPG	Photolabile protecting groups
PhNNPy	Phenylazopyridine

ppm	Parts per million
PRFAR	N'-[(5'-phosphoribulosyl)formimino]-5-aminoimidazole-4-carboxamide-ribonucleotide
^{i}Pr	Isopropyl
PSS	Photo Stationary State
Py	Pyridine
QY	Quantum yield
R_f	Retardation factor
rt	Room temperature
S	Entropy
SIRT	Silent information regulator type
$SnClBu_3$	Tributyltinchloride
τ	Lifetime
TD-DFT	Time Dependent Density functional theory
TEA	Triethylamine
TFA	Trifluoroacetic acid
THF	Tetrahydrofuran
TICT	Twisted intramolecular electron transfer
TLC	Thin layer chromatography
TPPTS	3,3',3"-Phosphanetriyltris(benzenesulfonic acid) trisodium salt
TS	Tryptophan synthase
UV	Ultraviolet
Vis	Visible
X-Ray	Röntgen radiation
ZMAL	(S)-tert-Butyl (6-acetamido-1-((4-methyl-2-oxo-2H-chromen-7-yl)amino)-1-oxohexan-2-yl)carbamate

CONTENTS

I. ARYLAZOINDOLES: A NEW CLASS OF AZO SWITCHES

Chapter I

If we knew what it was we were doing, it would not be called research, would it?

Albert Einstein

I.1 Heteroarylazo Dyes as Molecular Photoswitches

Abstract:

Over 150 years after its discovery and more than 80 years since its photochromism was described for the first time, azobenzene has become one of the pillars of molecular switches. Due to its stability and reliability, the old molecule has found applications spanning all the fields of modern chemistry, material science, biology and photopharmacology. In particular, in their seek to obtain the ideal photoswitch for a given problem, scientists have tweaked the properties of azobenzenes to all the extents. Concerning this aspect, heteroaryl azo dyes have hardly been considered so far. However, exchanging a carbon atom with a heteroatom extends the range of scaffolds the chemist can rely on and most importantly brings a panoply of promising new features. Heterocyclic azo dyes are known to switch since the photochromism of azobenzene was studied. Only in the recent years, however, their use is blossoming, rising them from a bare niche of the azo switches and putting them into the limelight. Here we discuss the versatility and multifaceted characteristics of these scaffolds as molecular photoactuators, that are elevating them as a serious alternative for azobenzene derivatives. With this review, we aim to summarize the researches on heteroarylazo photoswitches, which are easily lost in the vast reaches of the azo compound literature, and to focus on the future challenges this growing field has to endeavor.

Author contributions:

Nadja A. Simeth and Stefano Crespi performed the literature research and wrote the manuscript. NAS structured the work and made the figures. Burkhard König supervised the work.

I.1.1 Introduction

The chemistry of azo dyes was founded with the discovery of diazonium salts, already in 1858.[1] Up to today, these dyes have been used manifold to treat leather, textiles and even food or are used as pigments in rubbers and plastics. Chemical derivatization of the compounds generated a wide range of colors, from the Pigment Yellow 12 to Trypan Blue (used on cotton).[2, 3] Though we come across these compounds every day since the 1860s, not before the 1930s scientists found that azo dyes actually exist in two different isomeric forms (namely, as an *E*- and *Z*-isomer) that can be interconverted using light *stimuli* disclosing the first photochemical switches (or *photoswiches*).[4-7] The mechanisms, the changes in geometry and polarity, and the molecular motion of the isomerization process itself have been employed in a broad scope of applications. For instance, azobenzenes have been used to manipulate catalytic activity,[8] material properties[9] or biological recognition,[10] used in molecular storage[11] and logic devices[12] or for real-time information transfer.[13]

Due to this enormous application potential the interest on azoswitches reached a peak in the last decades. To generate the *perfect* photoswitch for a given problem, researches extensively tuned the properties of azobenzene, the parent and most used azo compound so far. Suitable substituents have been attached to the core to alter its color, chemical and mechanical properties. In this way, red-shifted absorbing derivatives that can be switched using either visible or near-IR light have been synthesized,[14, 15] along with extremely fast[16] or thermally highly stable ones.[17, 18] In many cases, nearly quantitative photoswitching between the two isomeric forms has been achieved.[19] Whereas the characteristics of azobenzenes need to be shifted by adding substituents onto the core, heteroaromatic derivates differ in their properties due to their intrinsic electronic properties.[18, 19] Indeed, exchanging a carbon in azobenzene for one (or more) heteroatom(s) leads not only to a broader structural diversity.[19] Owing to the different electronic characteristics, the main absorption band of heteroatom-containing azo switches are shifted compared to azobenzenes (hypsochromically for π-acceptors of the azo moiety and bathochromically for π-donors).[20] This is feasible without further functionalization of the photochromic core. In addition, intra- and intermolecular interactions can be more easily taken into account. Due to the presence of the heteroatom, properties like hydrogen-bonding or coordination to metal centers can be achieved directly from the photochromic core itself. Hence, this strategy jointly ties the photochromism and secondary interactions. Moreover, the electronic structure of the aromatic ring systems bearing heteroatoms of group 15 and 16 give access to five-membered aromatic rings.

Consequently, molecules bearing novel photophysical and photochemical properties, different steric demands and geometry become accessible.[18]

Given the increasing interest on heteroaryl azo dyes as photoswitches, we believe it is about time to summarize the state-of-the-art of this fast-growing topic. Consequently, we will herein review the use of heteroaromatic azo switches, without the intent to be comprehensive, but rather aiming on providing a qualitative overview of the field. Hence, we will present different heteroarenes (and their bicyclic derivates) ordered according to the kind and number of heteroatoms in the aryl rings (Figure 1) and highlight prominent applications.

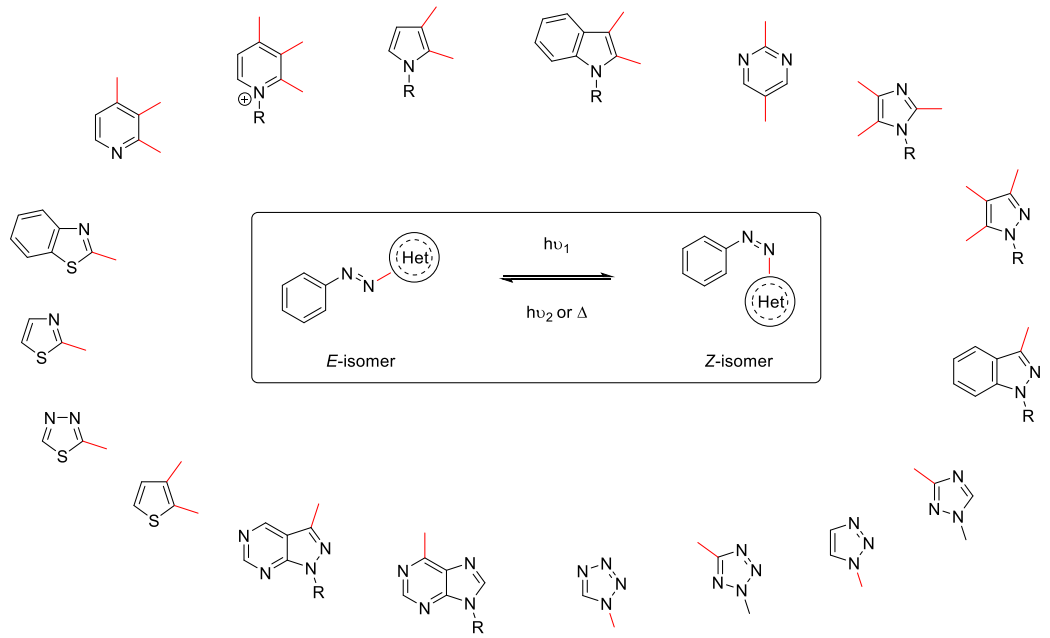

Figure 1: *E*-to-*Z*-isomerization of different heteroarylazo switches discussed here.

I.1.2 Heteroaryl Rings Bearing One Nitrogen Atom

I.1.2.1 Pyridines and Pyridinium Salts

The first explored and up to the present mostly used heterocyclic subunit is pyridine.[4] Already in the 1950s the *geometrical isomerism* of azopyridines was observed through melting point studies of isomeric mixtures and irradiation experiments combined with UV-Vis spectroscopy.[4, 6, 7] In contrast to azobenzene, which dipole moment is zero for the *E*- isomer and 3 Debye for its *Z*-isomer,[21] azopyridines exhibit a dipole moment in both forms due to the electronic perturbations induced by the presence of the nitrogen atom.[7] Moreover, the lone pair of the pyridine moiety can be employed as a junction for supramolecular interactions with other molecules.

For instance, Otsuki and coworkers used the electron-donating ability of pyridine to construct a photo-addressable ligand for zinc-porphyrins employing phenylazopyridine (PhNNPy) as labile axial ligand.[22-25] Thereby, they observed fluorescence-quenching of the metalloporphyrin upon binding of PhNNPy, which could be regenerated through protonation or reduction of the system. However, investigations on photoswitching of the labile ligand were only mentioned in a footnote and seemed to not influence the systems so far. Ten years later, Otsuki and his group could improve their system equipping PhNNPy with a shuttlecock or a bowl framework to attain sterical control over the binding properties upon photochemical *E*-to-*Z* isomerization of the ligand (Figure 2A).[25] They could further demonstrate the control of fluorescence properties upon switching.[24] The key-ingredients facilitating the photocontrol over the system was to sterically restrain the axial ligand. The group of Herges adopted this concept and synthesized a porphyrin, which exhibits a covalently bond PhNNPy group (Figure 2B). By using nickel(II) as metal center they were able to build up a powerful framework to control the magnetic properties of the complex through photoswitching.[26] In particular, the PhNNPy was embedded in such a way that only the *Z*-isomer could coordinate to the metal center. Through switching of the tethered, axial ligand from the *E*- to the *Z*-isomer, the coordination number of the Ni^{II} center was switched from $n = 4$ to 5. Hence, the square planar, low-spin complex was transformed into a pyramidal high-spin complex through irradiation with light of 500 nm. The process was reversible (*Z*-to-*E* isomerization could be triggered with 435 nm light) over several thousand cycles. Moreover, the group could point out that a potential application as switchable contrast agent for dynamic MRI studies might be feasible as photoisomerization of the presented compound led to a contrast difference of 43%. Indeed, the group of Herges could further improve the MRI contrast properties of their system modifying their design of a tethered axial ligand attaching the more electron-rich PhNN *meta*-Py derivative to the porphyrin.[27] In a later work, the group could transfer the same concept using a bulky, photo-dissociative, non-covalently bond PhNNPy, which could only coordinate to the nickel porphyrin in the sterically less hindered *E*-form, applying the same concepts used by Otsuki and coworkers (*vide supra*).[28, 29] Moreover, iron centered metal complexes have been employed to induce spin-crossover, however less successfully,[30, 31] while the *E*-to-*Z* isomerization of the PhNNPy ligands was suggested as a method to photochemically control the luminescence properties of rhenium complexes.[32-35]

Albeit the concept of photoisomerazable ligands controlling the properties of organometallic complexes is reported in several examples, it cannot be transferred as easily to every system.

For instance, Freixa and coworkers investigated photoswitchable complexes of iridium[36-38] and ruthenium.[39] In these examples, *E*-to-*Z* photoisomerization is nearly suppressed, especially when using PhNNPy as ligand. The group supports these findings with DFT calculations suggesting that the lack of reactivity can to be attributed to a low energetic and thus strong metal-to-ligand charge transfer (MLCT) interaction, quenching the π* excited state of the azo compounds formed upon irradiation.[38] However, Zhou *et al.* took advantage of the azo moiety's ^{3}MLCT to generate a metal-ligand system which's photodissociation is redox-controllable.[40] In the presence of a reducing agent, the energy acceptor property of the azo function,[38, 41, 42] which prohibits photo-dissociating of the azopyridine ligand,[43] can be quenched and the metal center can generate a new coordination site upon irradiation.[40]

The group of Broer used pyridine based azoswitches to generate motion in a photoactive film.[9] In particular, the phenylazopyridine (PhNNPy) **1** shown in Figure 2C is able to act as a hydrogen acceptor forming a hydrogen bond with the carboxylic acid **2** (Figure 2C). The increase in the push-pull character of the azo switch leads to high thermal *Z*-to-*E* isomerization rates of the polymer film doped with compounds **1** and **2** (Figure 2C). Irradiation of the film induces the photochemical formation of the *Z*-isomer accompanied by a geometrical reorganization of the film. Usually, azobenzene doped films stay in this bent condition at least until the light-stimulus is removed. However, the irradiated films experience a temperature increase that dramatically decreases the isomerization lifetime of the already fast switches. Thus, a continuous wave can be generated in the polymer through irradiation, when the film is fixed on both ends (Figure 2C). This motion can be used to transport small, macroscopic objects on the film surface or to make oscillating materials. Moreover, Velasco and coworkers used a similar pyridine-based system to generate a high-speed photoswitch for real-time transmitting systems.[44, 45] However, in this case the fast thermal relaxation mechanism is supposed to proceed through a hydrazone-mediated pathway. Curiously, Broer *et al.* tried to employ such a derivative in their photoactive film but obtained slower relaxation of the *Z*-isomer, compared to azo-push-pull system based on PhNNPy **1**.[9]

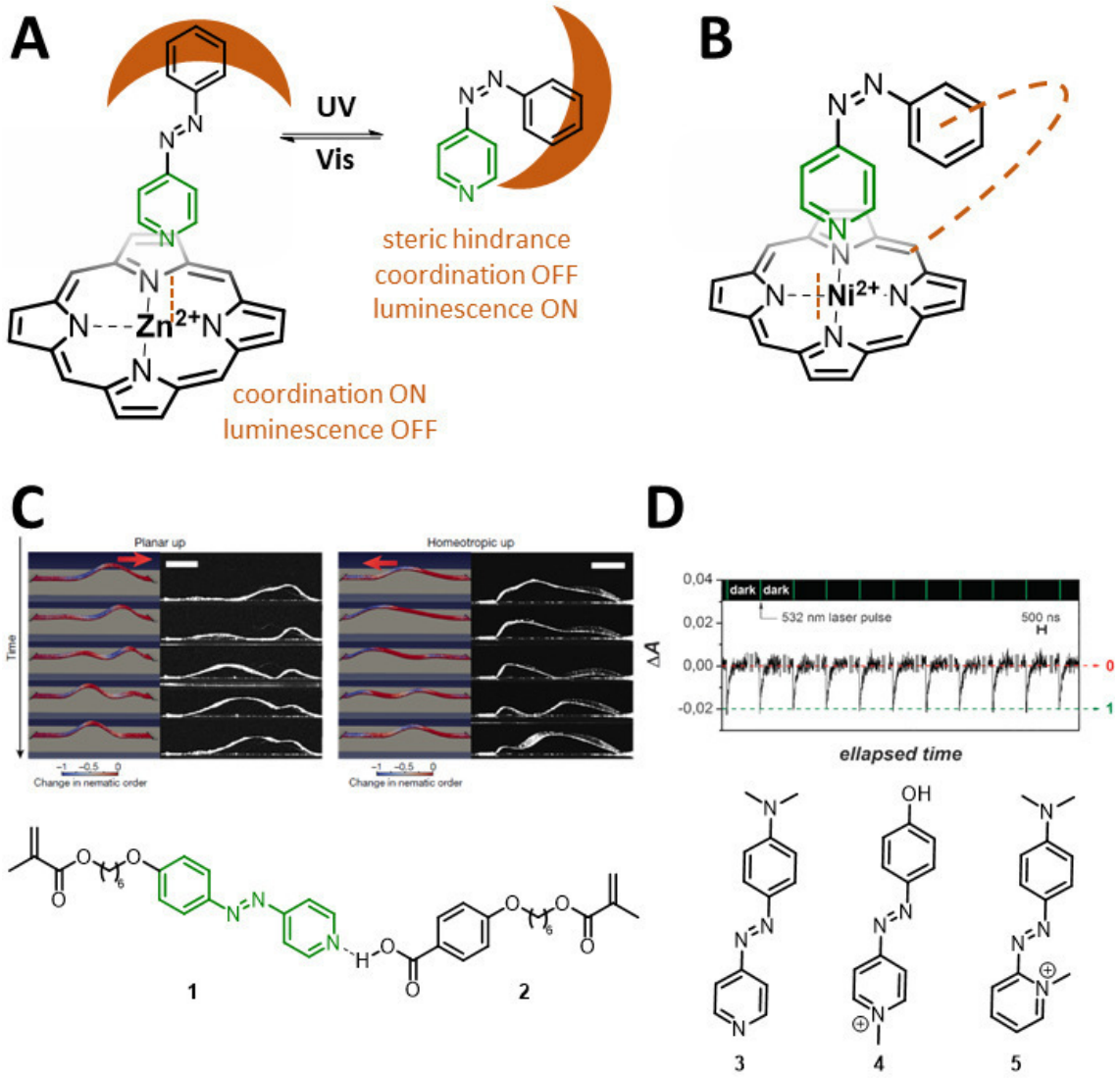

Figure 2: A**: PhNNPy with a shuttlecock or a bowl framework to attain sterical control over the binding properties towards zink porphyrin upon photochemical *E*-to-*Z* isomerization of the ligand.[25]** B**: Tethered axial PhNNPy ligand, which is geometrically only able to bind as *Z*-isomer. Upon binding the coordination number of the nickel atom changes from four to five and is accompanied by a spin-crossover of the metal center.[26]** C**: Hydrogen bonding with compound 2 leads to enhanced azo-push-pull properties of PhNNPy 1 (bottom). Hence, a photoactive polymer film containing both monomers is thermally relaxing fast enough to generate continuous waves in the fixed film upon irradiation (top). Reproduced with permission from Springer Nature.[9]** D**: Pyridine (3) and Pyridinium (4, 5) azo-push-pull systems for real-time information systems. Herein, compound 5 isomerizes thermally in the nanosecond range upon irradiation with green light (top: light-dark-cycles of compound 5). Reprinted with permission from the Royal Society of Chemistry.[49]**

The push-pull character of pyridine-based switches can be enhanced by methylation, thus generating a positive charge on the pyridine core.[46] Especially, 2- and 4- azopyridinium salts with a phenyl ring bearing an (alkylated) hydroxy or amino group in *para*-position to the azo function were used to generate thermal *Z*-to-*E* isomerizations half-lives in the ms-range (for

alkoxy) and the ns-range (for amino derivatives, *cf.* Figure 2D).[44, 45, 47] Noteworthy, the absorption profiles of these derivatives are bathochromically shifted compared to non-push-pull analogues, absorbing in the visible region (for the amino-pyridinium derivative **5** shown in Figure 2D the shift is up to 200 nm compared to azobenzene, hence, addressable with green light).[45, 47] The quick isomerization behavior was used to make fast-responding liquid crystal dopants,[47] photo-driven oscillators[44] and real-time information transmitting systems.[45] Additionally, the redox potentials of both photoisomers of azopyridiniums were found to strongly depend on the photoisomer. This could be of interest for the development of photo-regulated electron-carriers.[48]

I.1.2.2 Pyrrole and Indole

Azopyrroles and indoles have been exploited as substructures in dyes, drugs or in non-linear optics,[50-52] but the number of examples the scaffolds are used as molecular photoswitches, is limited. Similar to other electron-rich azo-compounds, their main $\pi\pi^*$ transition band is bathochromically shifted by *ca.* 50-100 nm.[16, 18, 19] Moreover, phenylazopyrroles are reported to possess very good PSS (ca. 85% *E*-to-*Z* and up to 98% in photochemical *Z*-to-*E* isomerization), high fatigue resistance and half-lives from *ca.* 20 s to *ca.* 4 days depending on the position of the azo function and the steric demand of the substituents placed onto the ring.[18, 19] Azopyrroles incorporated in azo-push-pull systems lead to fast *Z*-to-*E* relaxation kinetics (milliseconds to seconds) and switches addressable with visible light (*vide infra*).[49, 53-55] Hence, these derivatives could be employed for example as photo-oscillators and in material chemistry but only a few reports on their uses are known so far.[56]

Beyond that, the *Z*- form of the 3-phenylazoindoles exhibits an even wider span of thermal lifetimes (ns to days) and have been reported to be tunable through choice of substituents and solvent (mixture) in our recent study.[16]

I.1.3 Heteroaryl Rings Bearing Two Nitrogen Atom

I.1.3.1 Pyrimidine

The synthesis of azopyrimidines is known since the 1930s. However, their similarity with the nucleic acids, especially regarding the formation of hydrogen bonds, makes them promising candidates for applications in photopharmacology and biocompatible real-time information transmission.[57-59] Unfortunately, only very few studies focus on the photochromic properties of azopyrimidines. Representing the even more electron deficient analogue of pyridine, azopyrimidenes are suitable to be employed in azo-push-pull systems. Velasco and coworkers

report to reach thermal isomerization kinetics as fast as 40 ns in phosphate buffer on a 4-azophenol derivate.[59] [71] Besides, the rotamer distribution in differently substituted azopyrimidines could be controlled in a very recent work by Thiele and Dračínský. It was discovered that the intramolecular interactions (*viz.* H-bonding) and the electronic demand of the substituents on the heterocycle have an influence on the formation and stability of the *Z*-isomer in this class of molecules.[58]

I.1.3.2 Pyrazole and Indazole

More recently, in 2014, Fuchter and coworkers investigated the photochromic properties of phenylazopyrazoles. Some derivatives showed excellent addressable two-way-photoswitching and long thermal half-lives.[18] Similarly, also the bicyclic derivative, azoindazole, was reported to exhibit good to excellent photoisomerization characteristics and high thermal stability of the *Z*-isomer.[17] These properties make them comparable with the best-performing azobenzene derivatives[18] and consequently, could also make this class an interesting candidate for molecular storage devices, a field which is currently dominated by diarylethenes.[19] Phenylazopyrazoles have been recently applied in supramolecular complexes[60] (Figure 3A) and are used in photopharmacology.[61] Being the subject of several structure-property studies, azopyrazoles can be considered one of the better understood heteroarylazo switches (beside of the much more well-established pyridine and imidazole, *vide infra*).[18, 19, 62] Recent works of the groups of Fuchter and Venkataramani reveal the importance of steric factors on the stability of the *Z*-isomer and the thermal lifetime of the compounds. Additionally, suitable substituents on the phenyl moiety can generate azo-push-pull or tautomerizable systems (OH substituents on the phenyl unit or an unsubstituted nitrogen of the pyrazole) and hence, give access to a broad range of lifetimes *via* various thermal isomerization pathways.[18, 19, 62] Hence, we believe this scaffold can be readily employed in rational design of compounds with photo-addressable cores and will be very likely used more frequently in the future.

I.1.3.3 Imidazole

Phenylazoimidazole derivatives are, after azopyridines, the second most utilized heteroarylazo switches up to date. Moreover, many properties and mechanistic effects have been investigated experimentally and by computational means.[19, 63-65] In particular, azoimidazoles possess excellent *E*-to-*Z*-PSSs (>95% of *Z* isomer), but only decent *Z*-to-*E*-

PSSs due to the overlapping of the ππ* and nπ* bands that limits the efficiency of the photochemical back-isomerization process.[19, 66] Quantum yields of photochemical isomerization and the thermal lifetime of the *Z*-isomer are higher compared to azobenzene.[63] Unsubstituted imidazole-*N*H leads to particularly fast thermal *Z*-to-*E* relaxation, most probably due to the formation of hydrazone tautomers, as like other five-membered heteroarene photoswitches (or azobenzenes with amino- or hydroxy-substituents on the phenyl moiety).[64, 66, 67] In contrast, *N*-substituted imidazoles exhibit thermal half-lives of hours to days.[19, 65] In particular, the special features of this system are yet again to be found in the electronic nature of the photochromic core.

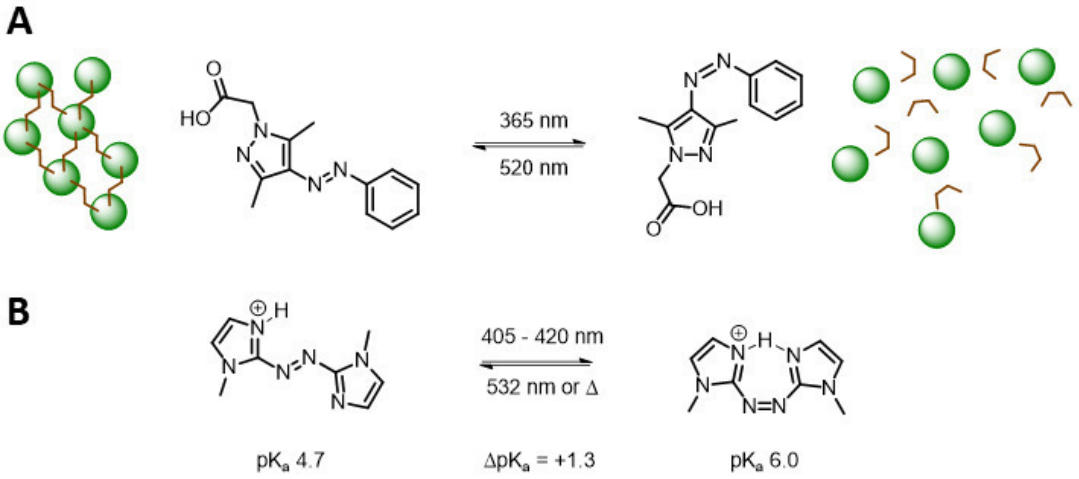

Figure 3: A: **The *E*-Azopyrazole links cyclodextrin vesicles (green), whereas the *Z*-isomer is sterically hindered, the host-guest interaction is disturbed and hence, the vesicles are released.[60]** B: **Switching protonated *E*- azobis(2-imidazole) to its *Z*-isomer, an additional proton bond can be formed and consequently, the basicity is increased.[72]**

Due to their well-investigated properties, azoimidazoles have already found several applications. For instance, they have been structurally combined with a ribofuranose unit to be potentially employed as novel photoswitchable nucleotides[68] or as ligands in copper complexes.[69] Due to their electron excess, they show improved spin crossover in a nickel^{II} porphyrin complex,[69] and can be utilized as photo-controllable bases. Previous works were either using the azo function[70] or a basic amine function was attached to one of the phenyl rings in azobenzene for proton binding.[71] Fuchter and coworkers applied an azobis(2-imidazole) where the *Z*-isomer possesses a geometry capable of forming an additional, second hydrogen bond to the bond proton (Figure 3B).[72] In this manner, the *Z*-isomer is able to provide a higher pK_a value than the *E*-isomer (ΔpK_a = 1.3). Interestingly, this structural effect is also stabilizing the *Z*-isomer itself and hence, increasing its thermal half-life.

I.1.4 Heteroaryl Rings Bearing Three Nitrogen Atoms and More

Azoswitches containing heterocycles with more than two nitrogen atoms per ring are rare. For instance, phenylazotriazoles and tetrazoles are reported scaffolds but to the best of our knowledge, their photochromic properties have only been commented on in a study regarding the photochromic behavior of five-membered heterocyclic azoswitches by Fuchter and coworkers.[19, 73] Moreover, due to their challenging synthesis and considerable instability only a limited number of nitrogen atoms can be incorporated in a photoswitch.[74-77] To our surprise, 1,1'-azobis-1,2,3-triazole (containing a stable N_8 chain)[74] and 1,1'-azobis-tetrazole (containing a N_{10} chain)[75] had been synthesized and even photoisomerized (isomerization followed by Raman spectroscopy). The N_8-containing 1,1'-azobis-1,2,3-triazole could be moreover investigated though UV-Vis spectroscopy. Indeed, upon irradiation of the red *E*-isomer the compound undergoes an untypical change in the color in the solid state, due to the formation of a blue *Z*-isomer.[74]

The groups of Szymanski and Feringa derived azoswitches from various substituted purins in the context of photopharmacology.[78] The authors report high fatigue resistance and red-shifted absorption properties of some azoadenine and azoguanine derivatives. Grøtli and coworkers incorporated the related azopyrazolpyrimidine moiety into an azo switch to obtain a photocontrollable RET-kinase inhibitor.[79] Both examples indicate that purines and related scaffolds are promising candidates for the development of novel photoswitchable nucleotides, smart drugs and further photopharmacological applications.

I.1.5 Heteroaryl Rings Bearing Other Heteroatoms and Mixed Scaffolds

Arylazothiophenes and thiazoles were already studied for their applicability in materials for non-linear optics[51, 52, 80, 81] before additional investigations regarding their photochromic behavior were performed by the group of Raposo. Whereas 5- arylazo-2,2'-bithiophenes showed photochromic properties addressable with visible light (*E*-to-*Z* isomerization was assigned to 35-50%, thermal half-lives to 18-69 s), no photochromism was found in 4-azobithiophenes.[82] Moving from purely sulfur based scaffolds to 4- and 5-thiazoles the photochromic characteristics were studied in azo dyes also possessing a second heteroaryl moiety on the other side of the azo-function (phenylazo derivatives are known in the literature, but were not studied as photoswitches[83]).[53, 54, 84] As aryl counterpart, mainly bithiophenes and thiopheno-pyrroles were used to generate an azo-push-pull system facilitating fast *Z*-to-*E* thermal relaxation *via* the fast rotation pathway[49, 85] and visible light photoswitching.[53, 54, 84] Teaming up with the group of Velasco, Raposo and coworkers

investigated the thermal relaxation process in more detail and found that such photochromic systems exhibit thermal isomerization lifetimes down to the µs-range and extremely high fatigue resistance.[49, 85] Consequently, an application as molecular photo-oscillator using the switches as dopants in liquid-crystals was considered.[49] Similar to fast-oscillating PhNNPys, arylazothiophenes and thiazoles could potentially be further developed in the direction of visible-light mediates materials or in photopharmacology due to the low-energetic electronic transitions.[49]

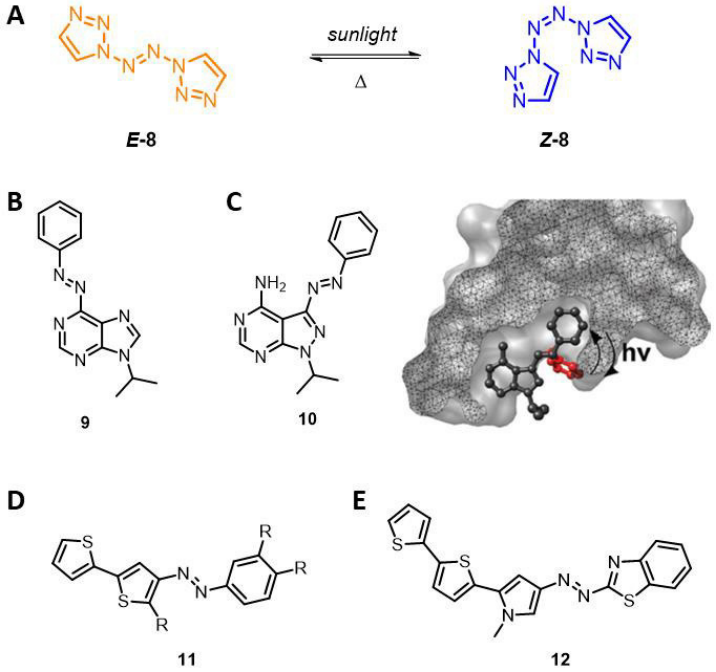

Figure 4: A**: Stable azo-N_8-chains can be isomerized with sunlight or thermal energy, respectively.** [74] B**: The purine-based azoswitch 9 can be photoisomerized with visible light.**[78] C**: The azopyrazolpyrimidine based RET-kinase inhibitor 10 only binds in its *E*-form as the *Z*-form is sterically too bulky and released from the binding site. Reprinted with permission from Springer Nature.**[79] D**: 5- Arylazo-2,2'-bithiophenes 11 can be isomerized with visible light, whereas the similar 4-arylazo derivatives do not show photochromic properties.**[84] E**: The arylazo thiazoles 12 is addressable with green laser-light and isomerized thermally from the Z-isomer in the µs-range. Hence, application as molecular photo-oscillators are considered.**

I.1.6 Conclusion and Outlook

Heteroarylazoswitches have advanced in recent years to extremely adjustable photoswitches. Indeed, they exhibit a broader range of characteristics than the parent azobenzene, owing to the special electronic features originated by the presence of the heteroatom(s). For instance, their metastable *Z*- form lifetime spans from the stable (1000 days) to the swift (tenths of ns), extremizing the characteristics of the azobenzene, with little to no functionalization. Hence, many scaffolds have already found astonishing applications such as photo-

addressable Brønsted bases, metal ligands to control luminescence or spin states or in functional materials, which are even able to transform molecular motion into macroscopic action. However, only few scaffolds are thoroughly investigated and thus, most applications are realized applying the chemistry of two specific heterocyclic azoswitches, namely azopyridine and azoimidazole. However, more and more core structures have been characterized and rationally studied. Especially, nitrogen bearing heteroarenes, such as pyrazoles, pyrroles or indoles are increasingly better understood, extremely tunable and are hence prominent scaffolds for future applications. Moreover, heteroazo switches like arylazothiazoles, are often addressable with visible light, which paves the way to the applications of selected compounds in emerging fields such as photopharmacology. In addition, many heteroarylazo dyes, such as furan-,[86] isoxazole-[87] and quinoxaline-based ones[88, 89] are known in current literature but were not (yet) investigated regarding their photochromic properties.

In conclusion, research is still at a very early stage, especially in terms of applications. However, the field is clearly moving forward, seeking deeper insight, novel scaffolds and smart issues, which will very likely have significant impact in the area of light-controlled processes.

I.1.7 References

1. Wizinger-Aust, R., Peter Griess und seine Zeit. *Angewandte Chemie* **1958**, *70*, 199–204.

2. Hunger, K.; Herbst, W., Pigments, Organic. In Ullmann's Encyclopedia of Industrial Chemistry. *Wiley-VCH* **2000**.

3. Hunger, K.; Mischke, P.; Rieper, W.; Raue, R.; Kunde, K.; Engel, A., Azo Dyes. In Ullmann's Encyclopedia of Industrial Chemistry. *Wiley-VCH* **2000**.

4. Kirpal, A.; Böhm, W., Über eine neuartige Isomerie in der Pyridin-Reihe (I. Mitteil.). *Berichte der deutschen chemischen Gesellschaft (A and B Series)* **1932**, *65*, 680–682.

5. Hartley, G. S., The Cis-form of Azobenzene. *Nature* **1937**, *140*, 281–281.

6. Le Fèvre, R. J. W.; Worth, C. V., 397. Indications of geometrical isomerism with 2 : 2'-azopyridine. *Journal of the Chemical Society (Resumed)* **1951**, 1814-1817.

7. Campbell, N.; Henderson, A. W.; Taylor, D., 257. Geometrical isomerism of azo-compounds. *Journal of the Chemical Society (Resumed)* **1953**, 1281–1286.

8. Wilson, D.; Branda, N. R., Turning "On" and "Off" a Pyridoxal 5'-Phosphate Mimic Using Light. *Angewandte Chemie International Edition* **2012**, *51*, 5431–5434.

9. Gelebart, A. H.; Jan Mulder, D.; Varga, M.; Konya, A.; Vantomme, G.; Meijer, E. W.; Selinger, R. L. B.; Broer, D. J., Making Waves in a Photoactive Polymer Film. *Nature* **2017**, *546*, 632–636.

10. Velema, W. A.; Szymanski, W.; Feringa, B. L., Photopharmacology: Beyond Proof of Principle. *Journal of the American Chemical Society* **2014**, *136*, 2178–2191.

11. Andréasson, J.; Pischel, U., Storage and Processing of Information Using Molecules: The All-Photonic Approach with Simple and Multi-Photochromic Switches. *Israel Journal of Chemistry* **2013**, *53*, 236–246.

12. Andréasson, J.; Pischel, U.; Straight, S. D.; Moore, T. A.; Moore, A. L.; Gust, D., All-Photonic Multifunctional Molecular Logic Device. *Journal of the American Chemical Society* **2011**, *133*, 11641–11648.

13. García-Amorós, J.; Velasco, D., Recent Advances Towards Azobenzene-Based Light-Driven Real-Time Information-Transmitting Materials. *Beilstein Journal of Organic Chemistry* **2012**, *8*, 1003–1017.

14. Bléger, D.; Hecht, S., Visible-Light-Activated Molecular Switches. *Angewandte Chemie International Edition* **2015**, *54*, 11338–11349.

15. Dong, M.; Babalhavaeji, A.; Samanta, S.; Beharry, A. A.; Woolley, G. A., Red-Shifting Azobenzene Photoswitches for in Vivo Use. *Accounts of Chemical Research* **2015**, *48*, 2662–2670.

16. Simeth, N. A.; Crespi, S.; Fagnoni, M.; König, B., Tuning the Thermal Isomerization of Phenylazoindole Photoswitches from Days to Nanoseconds. *Journal of the American Chemical Society* **2018**, *140*, 2940–2946.

17. Travieso-Puente, R.; Budzak, S.; Chen, J.; Stacko, P.; Jastrzebski, J. T. B. H.; Jacquemin, D.; Otten, E., Arylazoindazole Photoswitches: Facile Synthesis and Functionalization via S_NAr Substitution. *Journal of the American Chemical Society* **2017**, *139*, 3328–3331.

18. Weston, C. E.; Richardson, R. D.; Haycock, P. R.; White, A. J. P.; Fuchter, M. J., Arylazopyrazoles: Azoheteroarene Photoswitches Offering Quantitative Isomerization and Long Thermal Half-Lives. *Journal of the American Chemical Society* **2014**, *136*, 11878–11881.

19. Calbo, J.; Weston, C. E.; White, A. J. P.; Rzepa, H. S.; Contreras-García, J.; Fuchter, M. J., Tuning Azoheteroarene Photoswitch Performance through Heteroaryl Design. *Journal of the American Chemical Society* **2017**, *139*, 1261–1274.

20. Brown, E. V.; Granneman, G. R., Cis-Trans Isomerism in the Pyridyl Analogs of Azobenzene. Kinetic and Molecular Orbital Analysis. *Journal of the American Chemical Society* **1975**, *97*, 621–627.

21. Hartley, G. S.; Le Fèvre, R. J. W., 119. The Dipole Moments of Cis- and Trans-Azobenzenes and of Some Related Compounds. *Journal of the Chemical Society (Resumed)* **1939**, 531–535.

22. Otsuki, J.; Harada, K.; Araki, K., Supramolecular Electro- and Proto-Photoswitch. *Chemistry Letters* **1999**, *28*, 269–270.

23. Otsuki, J.; Narutaki, K., Photochromism of Phenylazopyridines and Its Application to the Fluorescence Modulation of Zinc–Porphyrins. *Bulletin of the Chemical Society of Japan* **2004**, *77*, 1537–1544.

24. Otsuki, J.; Narutaki, K.; Bakke, J. M., Light-triggered Luminescence Modulation Using Labile Axial Coordination to Zinc–Porphyrin. *Chemistry Letters* **2004**, *33*, 356–357.

25. Suwa, K.; Otsuki, J.; Goto, K., Syntheses of Shuttlecock- and Bowl-Equipped Phenylazopyridines and Photomodulation of their Coordination Ability to Zn-Porphyrin. *Tetrahedron Letters* **2009**, *50*, 2106–2108.

26. Venkataramani, S.; Jana, U.; Dommaschk, M.; Sonnichsen, F. D.; Tuczek, F.; Herges, R., Magnetic Bistability of Molecules in Homogeneous Solution at Room Temperature. *Science* **2011**, *331*, 445–448.

27. Dommaschk, M.; Peters, M.; Gutzeit, F.; Schütt, C.; Näther, C.; Sönnichsen, F. D.; Tiwari, S.; Riedel, C.; Boretius, S.; Herges, R., Photoswitchable Magnetic Resonance Imaging Contrast by Improved Light-Driven Coordination-Induced Spin State Switch. *Journal of the American Chemical Society* **2015**, *137*, 7552–7555.

28. Thies, S.; Sell, H.; Schütt, C.; Bornholdt, C.; Näther, C.; Tuczek, F.; Herges, R., Light-Induced Spin Change by Photodissociable External Ligands: A New Principle for Magnetic Switching of Molecules. *Journal of the American Chemical Society* **2011**, *133*, 16243–16250.

29. Thies, S.; Sell, H.; Bornholdt, C.; Schütt, C.; Köhler, F.; Tuczek, F.; Herges, R., Light-Driven Coordination-Induced Spin-State Switching: Rational Design of Photodissociable Ligands. *Chemistry - A European Journal* **2012**, *18*, 16358–16368.

30. Bannwarth, A.; Schmidt, S. O.; Peters, G.; Sönnichsen, F. D.; Thimm, W.; Herges, R.; Tuczek, F., FeIII Spin-Crossover Complexes with Photoisomerizable Ligands: Experimental and Theoretical Studies on the Ligand-Driven Light-Induced Spin Change Effect. *European Journal of Inorganic Chemistry* **2012**, *2012*, 2776–2783.

31. Ragon, F.; Yaksi, K.; Sciortino, N. F.; Chastanet, G.; Létard, J.-F. o.; D'Alessandro, D. M.; Kepert, C. J.; Neville, S. M., Thermal Spin Crossover Behaviour of Two-Dimensional Hofmann-Type Coordination Polymers Incorporating Photoactive Ligands. *Australian Journal of Chemistry* **2014**, *67*, 1563–1573.

32. Busby, M.; Matousek, P.; Towrie, M.; Vlček, A., Ultrafast Rxcited-State Dynamics of Photoisomerizing Complexes Fac-[Re(Cl)(CO)3(papy)2] and Fac-[Re(papy)(CO)3(bpy)]+ (papy=trans-4-phenylazopyridine). *Inorganica Chimica Acta* **2007**, *360*, 885–896.

33. Pourrieux, G.; Fagalde, F.; Romero, I.; Fontrodona, X.; Parella, T.; Katz, N. E., Electron-, Proton-, and Photon-Induced Spectroscopic Changes in Chromophore-Quencher Tricarbonyl(2,2'-Bipyridine)rhenium(I) Complexes with 4,4'-Azobis(pyridine). *Inorganic Chemistry* **2010**, *49*, 4084–4091.

34. Yam, V. W.-W.; Lau, V. C.-Y.; Wu, L.-X., Synthesis, Photophysical, Photochemical and Electrochemical Properties of Rhenium(I) Diimine Complexes with Photoisomerizable Pyridyl-azo, -ethenyl or -ethyl Ligands. *Journal of the Chemical Society, Dalton Transactions* **1998**, *20*, 1461–1468.

35. Wenger, O. S.; Henling, L. M.; Day, M. W.; Winkler, J. R.; Gray, H. B., Rhenium(I) Tricarbonyl Complexes with Photoisomerizable Ligands. *Polyhedron* **2004**, *23*, 2955–2958.

36. Pérez-Miqueo, J.; Telleria, A.; Muñoz-Olasagasti, M.; Altube, A.; García-Lecina, E.; de Cózar, A.; Freixa, Z., Azobenzene-Functionalized Iridium(III) Triscyclometalated Complexes. *Dalton Transactions* **2015**, *44*, 2075–2091.

37. Pérez-Miqueo, J.; Altube, A.; García-Lecina, E.; Tron, A.; McClenaghan, N. D.; Freixa, Z., Photoswitchable Azobenzene-Appended Iridium(III) Complexes. *Dalton Transactions* **2016**, *45*, 13726–13741.

38. Telleria, A.; Pérez-Miqueo, J.; Altube, A.; García-Lecina, E.; de Cózar, A.; Freixa, Z., Azobenzene-Appended Bis-Cyclometalated Iridium(III) Bipyridyl Complexes. *Organometallics* **2015**, *34*, 5513–5529.

39. Telleria, A.; van Leeuwen, P. W. N. M.; Freixa, Z., Azobenzene-Based Ruthenium(II) Catalysts for Light-Controlled Hydrogen Generation. *Dalton Transactions* **2017**, *46*, 3569–3578.

40. Zhou, Q.-X.; Zheng, Y.; Wang, T.-J.; Chen, Y.-J.; Li, K.; Zhang, Y.-Y.; Li, C.; Hou, Y.-J.; Wang, X.-S., A Novel Azopyridine-Based Ru(II) Complex with GSH-Responsive DNA Photobinding Ability. *Chemical Communications* **2015**, *51*, 10684–10686.

41. Yutaka, T.; Mori, I.; Kurihara, M.; Mizutani, J.; Tamai, N.; Kawai, T.; Irie, M.; Nishihara, H., Photoluminescence Switching of Azobenzene-Conjugated Pt(II) Terpyridine Complexes by Trans−Cis Photoisomerization. *Inorganic Chemistry* **2002**, *41*, 7143–7150.

42. Yutaka, T.; Kurihara, M.; Kubo, K.; Nishihara, H., Novel Photoisomerization Behavior of Rh Binuclear Complexes Involving an Azobenzene-Bridged Bis(terpyridine) Ligand. Strong Effects of Counterion and Solvent and the Induction of Redox Potential Shift. *Inorganic Chemistry* **2000**, *39*, 3438–3439.

43. Pinnick, D. V.; Durham, B., Photosubstitution Reactions of Ru(bpy)2XYn+ complexes. *Inorganic Chemistry* **1984**, *23*, 1440–1445.

44. Garcia-Amorós, J.; Nonell, S.; Velasco, D., Photo-Driven Optical Oscillators in the kHz Range Based on Push–Pull Hydroxyazopyridines. *Chemical Communications* **2011**, *47*, 4022–4024.

45. Garcia-Amorós, J.; Nonell, S.; Velasco, D., Light-Controlled Real Time Information Transmitting Systems Based on Nanosecond Thermally-Isomerising Amino-Azopyridinium Salts. *Chemical Communications* **2012**, *48*, 3421–3423.

46. Rockley, J.; Summers, L., Chemical Constitution and Activity of Bipyridinium Herbicides. XV. Synthesis, Reduction and Biological Activity of 4,4'-Azobis(1-methylpyridinium) bis(methyl sulfate). *Australian Journal of Chemistry* **1981**, *34*, 2683–2686.

47. Garcia-Amorós, J.; Massad, W. A.; Nonell, S.; Velasco, D., Fast Isomerizing Methyl Iodide Azopyridinium Salts for Molecular Switches. *Organic Letters* **2010**, *12*, 3514–3517.

48. Nakagawa, M.; Rikukawa, M.; Watanabe, M.; Sanui, K.; Ogata, N., Photochromic, Electrochemical, and Photoelectrochemical Properties of Novel Azopyridinium Derivatives. *Bulletin of the Chemical Society of Japan* **1997**, *70*, 737–744.

49. Garcia-Amoros, J.; Reig, M.; Castro, M. C. R.; Cuadrado, A.; Raposo, M. M. M.; Velasco, D., Molecular Photo-Oscillators Based on Highly Accelerated Heterocyclic Azo Dyes in nematic Liquid Crystals. *Chemical Communications* **2014**, *50*, 6704–6706.

50. Raposo, M. M. M.; Sousa, A. M. R. C.; Fonseca, A. M. C.; Kirsch, G., Thienylpyrrole Azo Dyes: Synthesis, Solvatochromic and Electrochemical Properties. *Tetrahedron* **2005**, *61*, 8249–8256.

51. Raposo, M. M. M.; Fonseca, A. M. C.; Castro, M. C. R.; Belsley, M.; Cardoso, M. F. S.; Carvalho, L. M.; Coelho, P. J., Synthesis and Characterization of Novel Diazenes Bearing Pyrrole, Thiophene and Thiazole Heterocycles as Efficient Photochromic and Nonlinear Optical (NLO) Materials. *Dyes and Pigments* **2011**, *91*, 62–73.

52. Raposo, M. M. M.; Castro, M. C. R.; Fonseca, A. M. C.; Schellenberg, P.; Belsley, M., Design, Synthesis, and Characterization of the Electrochemical, Nonlinear Optical Properties, and Theoretical Studies of Novel Thienylpyrrole Azo Dyes Bearing Benzothiazole Acceptor Groups. *Tetrahedron* **2011**, *67*, 5189-5198.

53. Coelho, P. J.; Castro, M. C. R.; Fonseca, A. M. C.; Raposo, M. M. M., Photoswitching in Azo Dyes Bearing Thienylpyrrole and Benzothiazole Heterocyclic Systems. *Dyes and Pigments* **2012**, *92*, 745–748.

54. Coelho, P. J.; Sousa, C. M.; Castro, M. C. R.; Fonseca, A. M. C.; Raposo, M. M. M., Fast Thermal Cis–Trans Isomerization of Heterocyclic Azo Dyes in PMMA Polymers. *Optical Materials* **2013**, *35*, 1167–1172.

55. Coelho, P. J.; Carvalho, L. M.; Fonseca, A. M. C.; Raposo, M. M. M., Photochromic Properties of Thienylpyrrole Azo Dyes in Solution. *Tetrahedron Letters* **2006**, *47*, 3711–3714.

56. Garcia-Amorós, J.; Reig, M.; Castro, M. C. R.; Cuadrado, A.; Raposo, M. M. M.; Velasco, D., Molecular Photo-Oscillators Based on Highly Accelerated Heterocyclic Azo Dyes in Nematic Liquid Crystals. *Chemical Commununications* **2014**, *50*, 6704–6706.

57. Bártová, K.; Čechová, L.; Procházková, E.; Socha, O.; Janeba, Z.; Dračínský, M., Influence of Intramolecular Charge Transfer and Nuclear Quantum Effects on Intramolecular Hydrogen Bonds in Azopyrimidines. *The Journal of Organic Chemistry* **2017**, *82*, 10350–10359.

58. Procházková, E.; Čechová, L.; Kind, J.; Janeba, Z.; Thiele, C. M.; Dračínský, M., Photoswitchable Intramolecular Hydrogen Bonds in 5-Phenylazopyrimidines Revealed By In Situ Irradiation NMR Spectroscopy. *Chemistry - A European Journal* **2018**, *24*, 492–498.

59. Garcia-Amorós, J.; Díaz-Lobo, M.; Nonell, S.; Velasco, D., Fastest Thermal Isomerization of an Azobenzene for Nanosecond Photoswitching Applications under Physiological Conditions. *Angewandte Chemie International Edition* **2012**, *51*, 12820–12823.

60. Stricker, L.; Fritz, E.-C.; Peterlechner, M.; Doltsinis, N. L.; Ravoo, B. J., Arylazopyrazoles as Light-Responsive Molecular Switches in Cyclodextrin-Based Supramolecular Systems. *Journal of the American Chemical Society* **2016**, *138*, 4547–4554.

61. Weston, C. E.; Krämer, A.; Colin, F.; Yildiz, Ö.; Baud, M. G. J.; Meyer-Almes, F.-J.; Fuchter, M. J., Toward Photopharmacological Antimicrobial Chemotherapy Using Photoswitchable Amidohydrolase Inhibitors. *ACS Infectious Diseases* **2017**, *3*, 152–161.

62. Devi, S.; Saraswat, M.; Grewal, S.; Venkataramani, S., Evaluation of Substituent Effect in *Z* -Isomer Stability of Arylazo-1 *H* -3,5-dimethylpyrazoles: Interplay of Steric, Electronic Effects and Hydrogen Bonding. *The Journal of Organic Chemistry* **2018**, *83*, 4307–4322.

63. Otsuki, J.; Suwa, K.; Narutaki, K.; Sinha, C.; Yoshikawa, I.; Araki, K., Photochromism of 2-(Phenylazo)imidazoles. *The Journal of Physical Chemistry A* **2005**, *109*, 8064–8069.

64. Otsuki, J.; Suwa, K.; Sarker, K. K.; Sinha, C., Photoisomerization and Thermal Isomerization of Arylazoimidazoles. *The Journal of Physical Chemistry A* **2007**, *111*, 1403–1409.

65. Zhao, L.; Liu, J.; Zhou, P., Effect of Methylation on the Photodynamical Behavior of Arylazoimidazoles: New Insight from Theoretical ab Initio Potential Energy Calculations and Molecular Dynamics Simulations. *The Journal of Physical Chemistry A* **2017**, *121*, 141–150.

66. Wendler, T.; Schütt, C.; Näther, C.; Herges, R., Photoswitchable Azoheterocycles via Coupling of Lithiated Imidazoles with Benzenediazonium Salts. *The Journal of Organic Chemistry* **2012**, *77*, 3284–3287.

67. Fukuda, N.; Kim, J. Y.; Fukuda, T.; Ushijima, H.; Tamada, K., Synthesis and Optical Characterization of Novel Imidazole-Based Azo Materials. *Japanese Journal of Applied Physics* **2006**, *45*, 460–464.

68. Endo, M.; Nakayama, K.; Kaida, Y.; Majima, T., Photoisomerization of 2'-Deoxyribofuranosyl and Ribofuranosyl 2-Phenylazoimidazole. *Tetrahedron Letters* **2003**, *44*, 6903–6906.

69. Heitmann, G.; Schütt, C.; Herges, R., Spin State Switching in Solution with an Azoimidazole-Functionalized Nickel(II)-Porphyrin. *European Journal of Organic Chemistry* **2016**, *2016*, 3817–3823.

70. Subhas, S.; Amirhossein, B.; Ming-xin, D.; Andrew, W. G., Photoswitching of ortho-Substituted Azonium Ions by Red Light in Whole Blood. *Angewandte Chemie International Edition* **2013**, *52*, 14127–14130.

71. V., P. M.; S., S. R.; Andreas, K.; Stefan, H., Photoswitching of Basicity. *Angewandte Chemie International Edition* **2008**, *47*, 5968–5972.

72. Weston, C. E.; Richardson, R. D.; Fuchter, M. J., Photoswitchable Basicity through the Use of Azoheteroarenes. *Chemical Communications* **2016**, *52*, 4521–4524.

73. Araki, S.; Hirose, S.; Konishi, Y.; Nogura, M.; Hirashita, T., Synthesis of 3-(Phenylazo)-1,2,4-triazoles by a Nucleophilic Reaction of Primary Amines with 5-Chloro-2,3-diphenyltetrazolium Salt via Mesoionic 2,3-Diphenyltetrazolium-5-aminides. *Beilstein Journal of Organic Chemistry* **2009**, *5*.

74. Li, Y.-C.; Qi, C.; Li, S.-H.; Zhang, H.-J.; Sun, C.-H.; Yu, Y.-Z.; Pang, S.-P., 1,1'-Azobis-1,2,3-triazole: A High-Nitrogen Compound with Stable N8 Structure and Photochromism. *Journal of the American Chemical Society* **2010**, *132*, 12172–12173.

75. Klapötke, T. M.; Piercey, D. G., 1,1'-Azobis(tetrazole): A Highly Energetic Nitrogen-Rich Compound with a N_{10} Chain. *Inorganic Chemistry* **2011**, *50*, 2732–2734.

76. Klapötke, T. M.; Krumm, B.; Martin, F. A.; Stierstorfer, J., New Azidotetrazoles: Structurally Interesting and Extremely Sensitive. *Chemistry - An Asian Journal* **2012**, *7*, 214–224.

77. Tang, Y.; Yang, H.; Wu, B.; Ju, X.; Lu, C.; Cheng, G., Synthesis and Characterization of a Stable, Catenated N $_{11}$ Energetic Salt. *Angewandte Chemie International Edition* **2013**, *52*, 4875–4877.

78. Kolarski, D.; Szymanski, W.; Feringa, B. L., Two-Step, One-Pot Synthesis of Visible-Light-Responsive 6-Azopurines. *Organic Letters* **2017**, *19*, 5090–5093.

79. Ferreira, R.; Nilsson, J. R.; Solano, C.; Andréasson, J.; Grøtli, M., Design, Synthesis and Inhibitory Activity of Photoswitchable RET Kinase Inhibitors. *Scientific Reports* **2015**, *5*, 9769–9777.

80. Raposo, M. M. M.; Ferreira, A. M. F. P.; Belsley, M.; Moura, J. C. V. P., 5'-Alkoxy-2,2'-Bithiophene Azo Dyes: a Novel Promising Series of NLO-Chromophores. *Tetrahedron* **2008**, *64*, 5878–5884.

81. Raposo, M. M. M.; Castro, M. C. R.; Belsley, M.; Fonseca, A. M. C., Push–Pull Bithiophene Azo-Chromophores Bearing Thiazole and Benzothiazole Acceptor Moieties: Synthesis and Evaluation of their Redox and Nonlinear Optical Properties. *Dyes and Pigments* **2011**, *91*, 454–465.

82. Coelho, P. J.; Carvalho, L. M.; Moura, J. C. V. P.; Raposo, M. M. M., Novel Photochromic 2,2'-Bithiophene Azo Dyes. *Dyes and Pigments* **2009**, *82*, 130–133.

83. El-Shishtawy, R. M.; Borbone, F.; Al-amshany, Z. M.; Tuzi, A.; Barsella, A.; Asiri, A. M.; Roviello, A., Thiazole Azo Dyes with Lateral Donor Branch: Synthesis, Structure and Second Order NLO Properties. *Dyes and Pigments* **2013**, *96*, 45–51.

84. Coelho, P. J.; Castro, M. C. R.; Fernandes, S. S. M.; Fonseca, A. M. C.; Raposo, M. M. M., Enhancement of the Photochromic Switching Speed of Bithiophene Azo Dyes. *Tetrahedron Letters* **2012**, *53*, 4502–4506.

85. Garcia-Amorós, J.; R. Castro, M. C.; Coelho, P.; M. Raposo, M. M.; Velasco, D., New Heterocyclic Systems to Afford Microsecond Green-Light Isomerisable Aazo Dyes and their Use as Fast Molecular Photochromic Switches. *Chemical Communications* **2013**, *49*, 11427–11429.

86. Gavkus, D. N.; Maiorova, O. A.; Borisov, M. Y.; Egorova, A. Y., Azo Coupling of 5-Substituted Furan-2(3H)-ones and 1H-pyrrol-2(3H)-ones with Arene(hetarene)diazonium salts. *Russian Journal of Organic Chemistry* **2012**, *48*, 1229–1232.

87. Hamama, W. S.; Ibrahim, M. E.; Zoorob, H. H., Synthesis and Biological Evaluation of Some Novel Isoxazole Derivatives: Isoxazole with Basic Side Chain. *Journal of Heterocyclic Chemistry* **2017**, *54*, 341–346.

88. Sherif, S.; Ekladious, L.; Abd Elmalek, G., The Synthesis of Some Azo Dyes Containing the Quinoxaline Nucleus. I. *Journal für Praktische Chemie* **1970**, *312*, 759–766.

89. Rangnekar, D. W.; Tagdiwala, P. V., Synthesis of Azo dyes from 6-Amino-2-methoxy-quinoxaline and Their use as Disperse Dyes for Polyester Fibres. *Dyes and Pigments* **1987**, *8*, 151–156.

I.2 Tuning the Thermal Isomerization of Phenylazoindole Photoswitches from Days to Nanoseconds

Abstract

The growing interest in light-driven molecular switches and optical oscillators led to the development of molecules that are able to interconvert from a stable to a metastable configuration upon photochemical triggering and to return to the thermodynamically stable form as soon as the light stimulus is removed. Controlling a wide range of back-isomerization lifetimes in the dark is a crucial goal for potential application of these compounds such as molecular machines. We herein present a novel class of easily synthesizable azo photoswitches based on the arylazoindole core. Most notably, minimal modifications of the core such as the methylation, dramatically change the Z-to-E thermal isomerization rate from days (Me in position 1) to the nanosecond range (Me in position 2). Moreover, fine tuning of the *Z*-to-*E* lifetimes can be achieved choosing a proper dimethyl sulfoxide-water (or buffered water) sol-vent mixture. The photochemical and thermal mechanisms have been elucidated by a thorough computational and spectroscopic analysis. This allowed to detect three different pathways of thermal isomerization and to identify the hydrazone tautomer of the phenylazoindole as the major actor in the fast Z-E thermal isomerization of the NH-substituted switch in protic media.

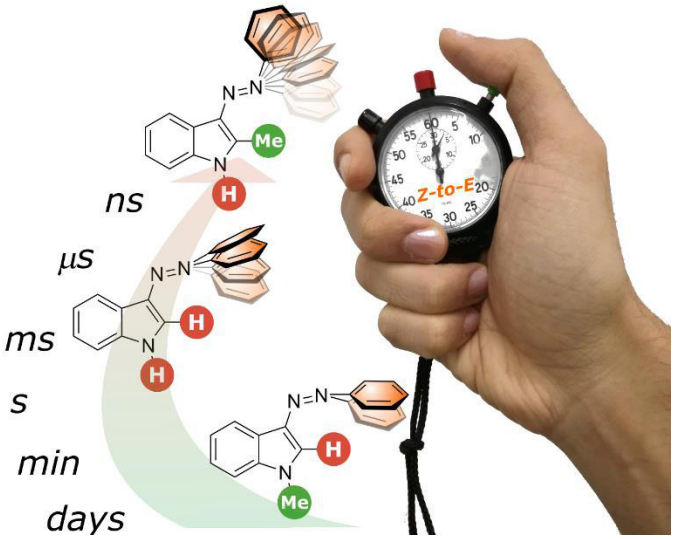

This section was published as:

Simeth, N. A.;‡ Crespi, S.; ‡ Fagnoni, M.; König, B., Tuning the Thermal Isomerization of Phenylazoindole Photoswitches from Days to Nanoseconds. *Journal of the American Chemical Society* **2018**, 140 (8), 2940-2946. Reprinted with Permission from the American Chemical Society.

Author contributions

NAS performed all synthesis and characterization of the compounds as well as UV-Vis spectroscopy. SC performed laser-flash photolysis and quantum chemical calculations. NAS and SC wrote the manuscript together (‡). MF and BK supervised the work.

I.2.1 Introduction

Photoswitches have evolved into handy tools to control molecular properties, such as magnetization, fluorescence or biological activity, or can be exploited as the centerpiece of molecular machines.[1] Thereby, light is applied as an external stimulant. It is easy to handle, unmatchable fast and precise in practical usage, and orthogonal to biological systems and most chemical transformations.[1–3] Within the many classes of photoswitches investigated, azo dyes have emerged as a popular example in the last decades including manifold applications, *e.g.* in polymers,[4,5] electronics,[6] material science,[7] protein probes and *in vivo* photocontrol of biomolecules,[8–11] or as light-controllable catalysts.[12] Among them, azobenzene (and its derivatives) is undoubtedly the most prominent scaffold investigated in both fundamental research and modern applications.[13] The planar azobenzene *E*-isomer can be efficiently converted into its meta-stable *Z*-isomer via UV irradiation, with a consequent change in the electronic as well as geometrical properties of the molecule.[14,15] The *Z*-isomer is the main component of the thus formed photostationary state (PSS) and can interconvert to the more stable *E*-isomer through visible light irradiation or through thermal relaxation.[15] Indeed, the ideal thermal lifetime of the meta-stable *Z*-isomer strongly depends on the application of interest. Highly thermal stable azoswitches are desired for applications as such as molecular storage or logic devices, respectively.[16] In contrast, fast relaxing azobenzenes are preferably employed, for instance, in real-time optical information-transmitting materials[17] or in *in vivo* applications due to their temporally limited action.[18] Thus, a lot of effort has been put to modify the thermal lifetime of azobenzenes. Most of these transformations have been achieved through the introduction of different substituents onto the azobenzene core. Ortho-fluoro[19] or ortho-thiol substituents[20] have been used to stabilize the thermal lifetime of azobenzenes, whereas 4,4′ push pull or azophenolic systems (or a combination of both) can lead to extremely fast-relaxing switches.[17,21] More recently, also heteroaromatic scaffolds were considered to broaden the range of azo dye properties, including their thermal lifetime. Notably, azopyrimidine,[21] azopyridines,[22,23] azopyrroles,[24] azoimidazole[25–29] and azopyrazoles,[30–32] or lately the bicyclic azoindazole scaffold,[33] were reported. They were used, for example, to control the assembly of supramolecular systems or as photo-controllable ligands being, depending on the scaffold and its substitution pattern, highly stable (for a pyrazole derivative, the thermal lifetime is reported to be up to 1000 days[32]) or fast-relaxing systems (40 ns, for an azopyrimidine[21]). However, a scaffold usually exhibits a certain lifetime and the tunability is mostly limited to few orders of magnitude, thus it belongs either to the thermally stable or to the fast back-isomerizing family.

Herein, we present phenylazoindoles as photochromic scaffolds with extremely tunable thermal lifetimes. Indoles are omnipresent in nature, substructures of drugs and various dyes. Though previously employed as antibacterial agents, food-dyes,[34] or metal complexing ligands,[35] arylazoindoles have not been considered as photochromic compounds so far. We investigated both minimal chemical variations of the scaffold (methylation in different positions) and solvent effects on the thermal lifetime of the compounds. We elucidated the mechanism of the isomerizations and take advantage of it to tune the properties of the here presented photoswitches from days to nanoseconds. Thereby, we focus on providing a deep and general understanding of a new class of azo photoswitches to pave the way to further rational developments, using this novel core potentially for all kinds of applications.

I.2.2 Results and Discussion

I.2.2.1 Synthesis

The phenylazoindoles **3a**-**c** were synthesized through azo coupling of diazonium salt **2** and the appropriate indoles **1a**-**c** (see Scheme 1 and Section A.I.2.1. in the Appendix).

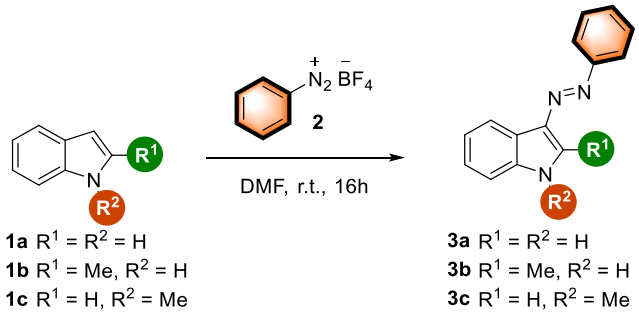

Scheme 1: Synthesis of 3a-c.

I.2.2.2 Spectroscopy

The absorption and isomerization properties of phenylazoindoles **3a**-**c** were investigated in various solvents, from non-polar (aromatic and non-aromatic) to polar aprotic and polar-protic ones. Most prominent is the broad absorption band between 359 and 380 nm. We could assign the aforementioned band to the $\pi \rightarrow \pi^*$ transition of the azo group (see Table A1; for the recorded UV/Vis spectra, see Section A.I.2.2.) owing to the similarities with azobenzene and other azoheteroarenes, and TD-DFT simulations (see Section A.I.2.4.).[15,33] By trend, methylation (**3b** and **3c**) induces a slight bathochromic shift of the band compared to **3a** (between 4 to 11 nm). The weaker $n \rightarrow \pi^*$ band is present between 400 to 500 nm as a tailing of the $\pi \rightarrow \pi^*$ transition. Due to the high variety of lifetimes (τ) of the *Z*-isomer encountered, we decided to study the different kinetics of thermal relaxation processes of

***Z*-3a-c** using three different experimental setups. In particular, for the slower kinetics, the *E*-to-*Z* isomerization was induced through irradiation with LEDs of 400 nm or 365 nm and the back isomerization from the PSS in the dark was recorded through an UV/Vis spectrometer (seconds to hours range, see for example Figure 1A) or multiplate UV/Vis reader (hours to days). The faster kinetics were studied via nanosecond laser flash photolysis with excitation provided by a Nd:YAG laser at 355 nm (full details and pictures of the various experimental setups are included in the Section A.I.1. in the Appendix). Multiple isomerization cycles can be achieved by pulsed irradiation of a single wavelength (see for example Figure 1B, concerning the pulsed irradiation with 400 nm of **3a** in DMSO).

The results are summarized in Table 1 (see Table A2 for a wider number of entries and Section A.I.2.2. for spectra and isomerization kinetics). Compounds ***Z*-3a** and ***Z*-3b** exhibited thermal isomerization lifetimes comparable with or far lower than the second range. Laser flash photolysis allowed us to describe the transient absorption signal belonging to the *Z*-form of **3a** and **3b**. In particular, in **3b** a broad absorption band appeared around 450 nm immediately after the laser shot, attributable to the n→π* transition of its *Z*-isomer (Figure 1C). On the other hand, only the bleaching of the π→π* of the *E*-isomer can be observed in **3a**. TD-DFT UV/Vis absorption simulations of the most stable Z- isomers of **3a**,**b** allowed us to conclude that the geometry of ***Z*-3b** is causing the n→π* transition to be more symmetry-allowed than the one in ***Z*-3a** (*cf.* Section A.I.2.4. in the Appendix).

Moving from apolar to polar-aprotic solvents in **3a** led to τ shifting from the millisecond to the second range (Entries 1-5, 12-13, Table 1). This trend becomes less discernible with ***Z*-3b**, which only in dioxane has a $\tau > 1$ s (entry 2, Table 1). In **3a**,**b** it seems that the increased speed of the thermal *Z*-to-*E* relaxation goes hand in hand with the proton-availability (compare entries 7 and 13 for ***Z*-3a**). A striking example is **3a** in mixtures of MeOH or DMSO with water. While the addition of water in methanol does not drastically modify the lifetime (*cf.* Table 1, entry 7, 9, 10 for ***Z*-3a**), the increased protic environment in aprotic DMSO lowers τ from seconds to microseconds (*cf.* Table 1, entry 13-15). This allowed tuning the lifetime only by changing the water-content in DMSO. Similar observations can be made for ***Z*-3b**.

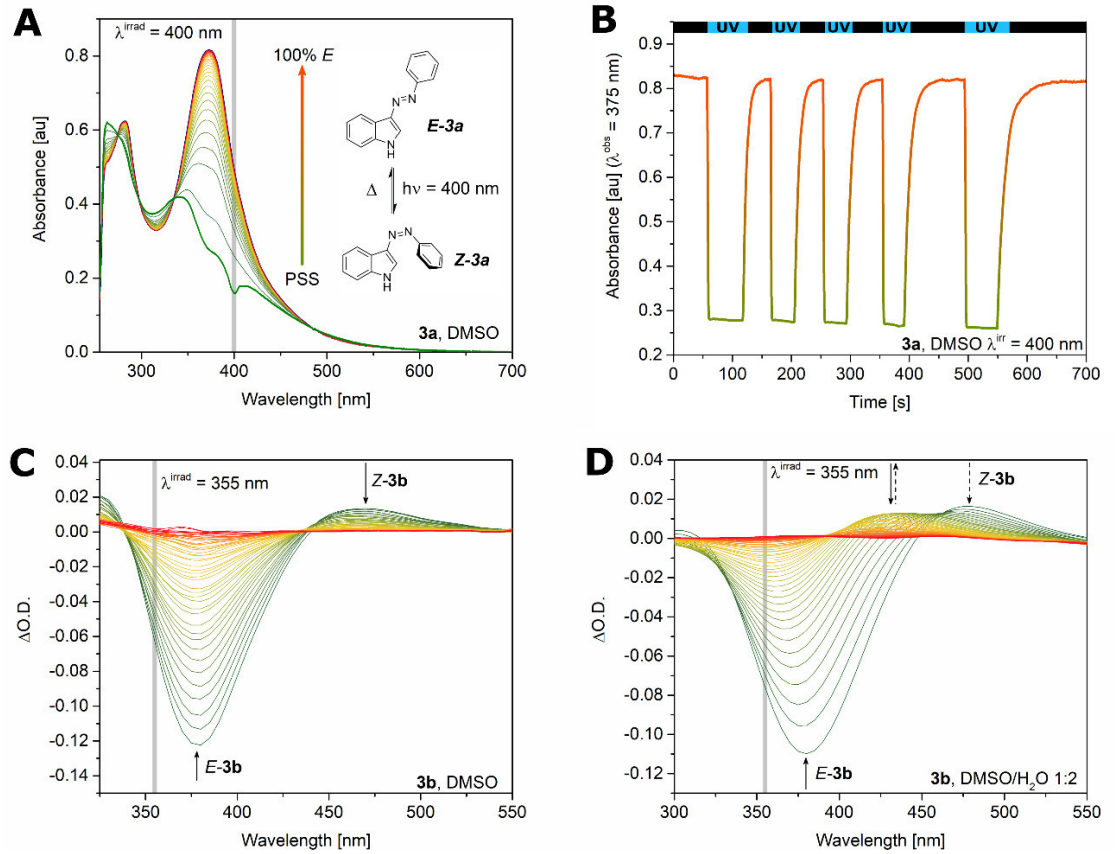

Figure 1: A: **Thermal relaxation from the PSS (τ=4.3 s) of 3a in DMSO after irradiation with λ^{irrad}=400 nm.** B: **Multiple isomerization cycles of 3a in DMSO (black bars: dark, blue bars: irradiation with λ^{irrad}=400 nm; the observed wavelength corresponds to λ^{obs}=375 nm) indicating a good fatigue resistance.** C: **Transient signal registered for 3b in DMSO. The disappearing of the n→π* band belonging to *Z*-3b is accompanied by the restoration of π →π* band of *E*-3b.** D: **Transient signal registered for 3b in a DMSO/water 1:2 mixture (detailed spectrometric data and kinetics in Section A.I.2.2.). The decay of the n→π* band of *Z*-3b is followed by the formation of a hypsochromically shifted transient signal. Then, the π →π* band of *E*-3b reappears.**

Here, 1:1 mixtures of water and MeOH or DMSO afford lifetimes of 41.4 μs or 32.1 μs, respectively. Moreover, in a mixture of acidic water and DMSO, the relaxation time decreases to 2.2 μs for ***Z*-3a** and even reaches the nano-second range (743 ns) for ***Z*-3b** (entry 16). A similar result was obtained for both **3a** and **3b** when DBU was used as additive (entry 17), suggesting a proton-transfer mechanism contributes to the speed of the thermal isomerization. Reaching the sub-microsecond scale is crucial for applications requiring real-time information transmission, and up to now, this goal was achieved in azobenzene cores only in one case by using phenolic push-pull systems.[21] The dependency on protic environment becomes more evident comparing the lifetimes of ***Z*-3a** in MeOH and MeOD, which show a significant kinetic isotope effect (entries 7 and 8 in Table 1). A KIE=5.5 indicates that a proton transfer is involved in the rate-determining step in this solvent.

Table 1. *Z*-to-*E* Isomerization Lifetimes for 3a-c.

Entry	Solvents[a]	Lifetime t		
		3a	3b	3c[c]
1	cyclohexane	42.5 ms[b]	116.8 ms[b]	1.1 h
2	dioxane	84.9 ms[b]	1.9 s[c]	17.6 h
3	mesitylene	12.3 ms[b]	3.3 ms[b]	1.13 d
4	benzene	78.5 ms[b]	167 ms[b]	6.0 min
5	toluene	47.5 ms[b]	60.2 ms[b]	17.1 min
6	aqueous toluene[d]		1.4 ms[b]	
7	MeOH	6.8 ms[b]	454 μs (51%), 78 μs (49%) [e]	2.4 h
8	MeOD	37.7 ms[b]		
9	MeOH water 9:1	14.8 ms[b]	41.9 μs[b]	
10	MeOH water 1:1	2.9 ms[b]	41.4 μs[b]	
11	MeOH[f]	4.7 ms[b]		
12	MeCN (dry)	4.3 s[c]	1.9 μs[b]	1.2 d
13	DMSO (dry)	6.5 s[c]	1.3 ms[b]	2.6 d
14	DMSO water 9:1	266 μs[b]	111.2 μs[b]	
15	DMSO water 1:1	187.9 μs[b]	32.1 μs[b]	
16	DMSO - buffered water (pH = 4)[f] 1:1	2.2 μs[b]	743 ns[b]	
17	DMSO water 1:1 + 25 mL DBU	31 ns	46 ns	

[a] The concentration was adjusted to 50 μM for all the measurements. [b] Determined *via* nanosecond laser flash photolysis. [c] Determined *via* UV/Vis spectroscopy. [d] Toluene saturated with water (15 μL of water were added to 2 mL of a 50 μM solution of **3b** in toluene. The emulsion thus formed was sonicated for 1h.) [e] The decay is biexponential. In parentheses is shown the contribution of the single lifetimes to the whole decay. [f] Concentration of **3a** = 75 μM[g] pH = 4.00 ± 0.02 (20 °C) (Citric acid = 0.056 M; NaOH = 0.11 M; HCl = 0.044 M).

Increasing the concentration of **3a** in MeOH leads to faster isomerization kinetics (entry 11). In anhydrous toluene no concentration effect on τ was found, see Table A2. The presence of an intermolecular interaction in **3a** can be followed by NMR (see Section A.I.2.6. in the Appendix). In contrast to the other experiments, ***Z*-3b** in methanol relaxes with a biexponential kinetic. This suggests, compared with the previous findings, that the presence of a protic environment modifies the mechanism of the dark reaction for ***Z*-3a** and ***Z*-3b**. Indeed, for the specific case of **3b** in MeOH, two mechanisms of thermal relaxation are in

competition (*cf.* entry 7 for **3b**). A detailed kinetic analysis of the thermal isomerization reaction is present in Section A.I.2.6. of the Appendix. In particular, both a dependency on concentration of the photoswitch and on water was found for the *N*-H containing photoswitch **3b**. The kinetic law that was derived is similar to the one obtained for the arylazoimidazoles, compounds that are supposed to isomerize through an intermolecular proton transfer leading to the formation of a hydrazone intermediate (Chart 1).[17,26,32]

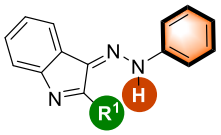

R^1 = H, Me

Chart 1: Formula of the s-trans Hydrazone Tautomer of 3a,b.

The water content dependency led to an interesting saturation kinetic, that is another evidence of a mechanism characterized by an intermolecular proton transfer that is mediated by the presence of protic medium (for more details, see Appendix).

Moreover, we observed notable differences in the transient spectra of **3a**,**b**. In the absence of protic media, the transient signal of the *Z*-isomer directly interconverts to the *E*-form (that exhibits an isosbestic point in **3b**, where the n→π* absorption band of the *Z* form can be clearly discerned, see Figure 1C). However, in protic environment, the signal of ***Z*-3b** shifts hypsochromically, giving rise to a second band, which belongs to an intermediate of the *Z*-to-*E* thermal conversion that eventually collapses with the restoration of the *E*-isomer (cf. Figure 1D). In **3a** a new band arises at a similar wavelength of the comparable one in **3b**, before the ***E*-3a** π → π * is restored).

To prove our theory and to generalize the effect of a protic medium on the isomerization reaction of **3a,b**, we saturated toluene with water (*cf.* Figure 2 and Table 1, entry 6 for **3b**). Consequently, the isomerization rate increased sixtyfold and a transient signal, similar to the intermediate signal observed above, appears. Furthermore, the importance of the *N*H moiety in the thermal *Z*-to-*E* relaxation was proven studying compound **3c**. Indeed, the methylation of the indole-nitrogen (in **3c**) causes significant changes of the relaxation properties with respect to the *N*–H containing derivatives (**3a**,**b**). Compound **3c** exhibits longer lifetimes (minutes to days, see Table 1) compared to **3a**,**b**. Moreover, in polar-aprotic solvents (DMSO and MeCN) as well as in mesitylene, **3c** shows τ larger than one day. Owing to their stable photostationary state, we were able to determine the PSS population of **3c** in DMSO (Figure 3) and MeCN applying ^{1}H-NMR-spectroscopy (85:15 and 61:39 of *Z*:*E* ratio, respectively; see Section A.I.2.3. in the Appendix).

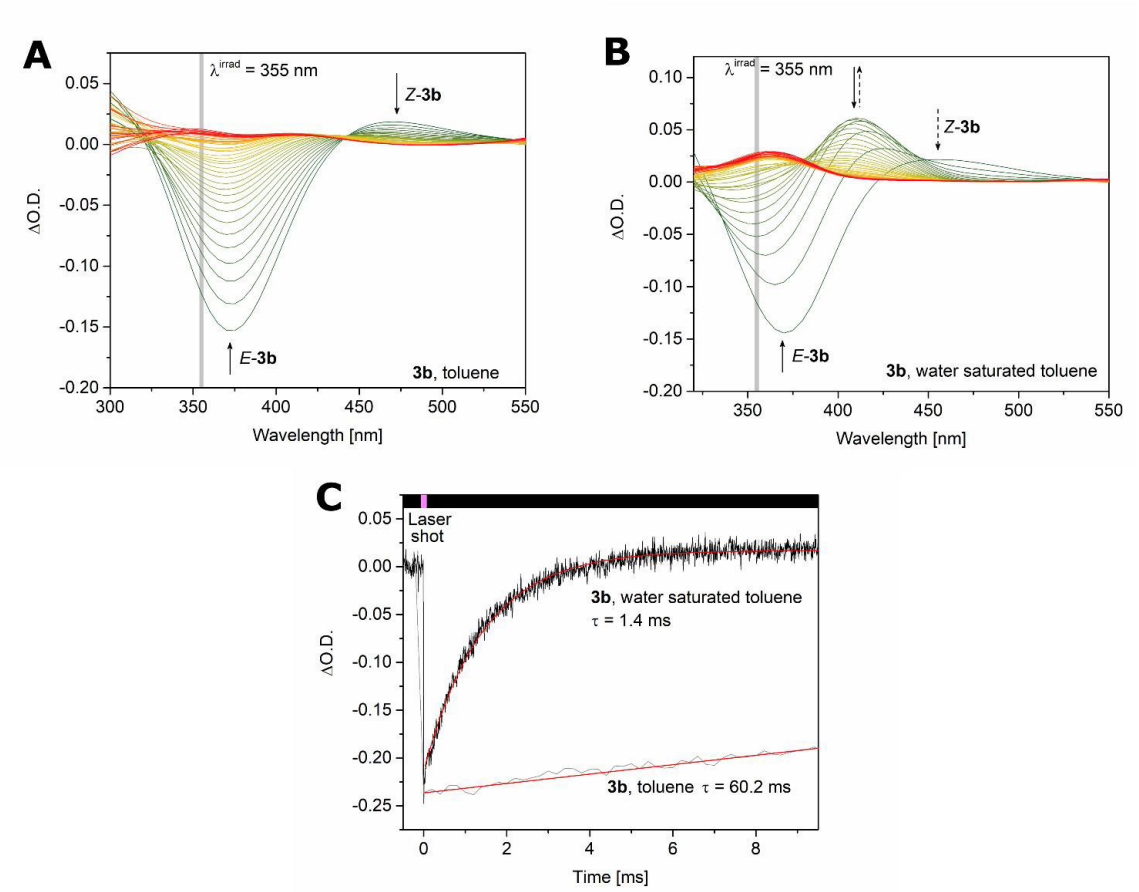

Figure 2. A: **Thermal *Z*-*E* isomerization of compound 3b in toluene. An isosbestic point can be observed, indicating the monomolecular decay of the n→π* band of *Z*-3b in favor of the formation of the π →π* of *E*-3b.** B: **The addition of water to toluene induces a change in the transient spectra. As like as in DMSO (cf. Figure 2D), a new species, blue-shifted compared to the n→π* band of *Z*-3b, can be detected by laser flash photolysis. This intermediate contributes to the restoration of the π →π* band of *E*-3b.** C: **Transient signal of the restoration of the π →π* band of *E*-3b (λ^{obs} =370 nm) in toluene and water saturated toluene. A forced protic environment inside toluene increases the overall *Z*-to-*E* isomerization rate.**

However, to the best of our knowledge, spectroscopic observations similar to the ones we witnessed have not been made so far. Phenylazoindoles themselves are known to give rise to a hydrazone tautomerism.[36] Thus, we aimed to explain the involvement of an azo-hydrazone and why minimal modifications of the indolic core lead to a surprisingly wide span of thermal relaxation rates through a detailed computational study.

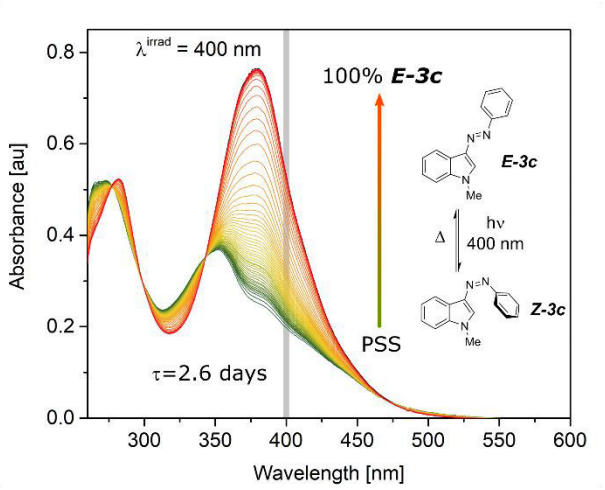

Figure 3. Thermal relaxation from the PSS (85:15 *Z:E* ratio, τ=2.6 d) of 3c in DMSO after irradiation with λ^{irrad} = 400 nm.

I.2.2.3 Computational studies

To seek for similarities with the azobenzene core, we endeavored to analyze both the photochemical *E*-to-*Z* and thermal *Z*-to-*E* interconversion pathways. Representing the most general scaffold, **3a** was selected for the study. Hence, we performed an MS CASPT2/CASSCF calculation of the *E*-to-*Z* pathway, both from the first (S1, n→π* in character; *cf.* Figure 4A) and the second excited state (S2, π→π*). The analysis of the molecular structure, its electronic distribution and the g and h vectors defining the branching space of the conical intersections (CoIns) (*cf.* Figure 4A and B), helped us to assign the photochemical decay pathways (a complete analysis of the CoIns is present in Section A.I.2.4. in the Appendix).[37] Similarly to azobenzene, population of the n→π* singlet excited state leads to a rotational conical inter-section (S0←S1, CoInA), which generates the *Z*-isomer.[14]

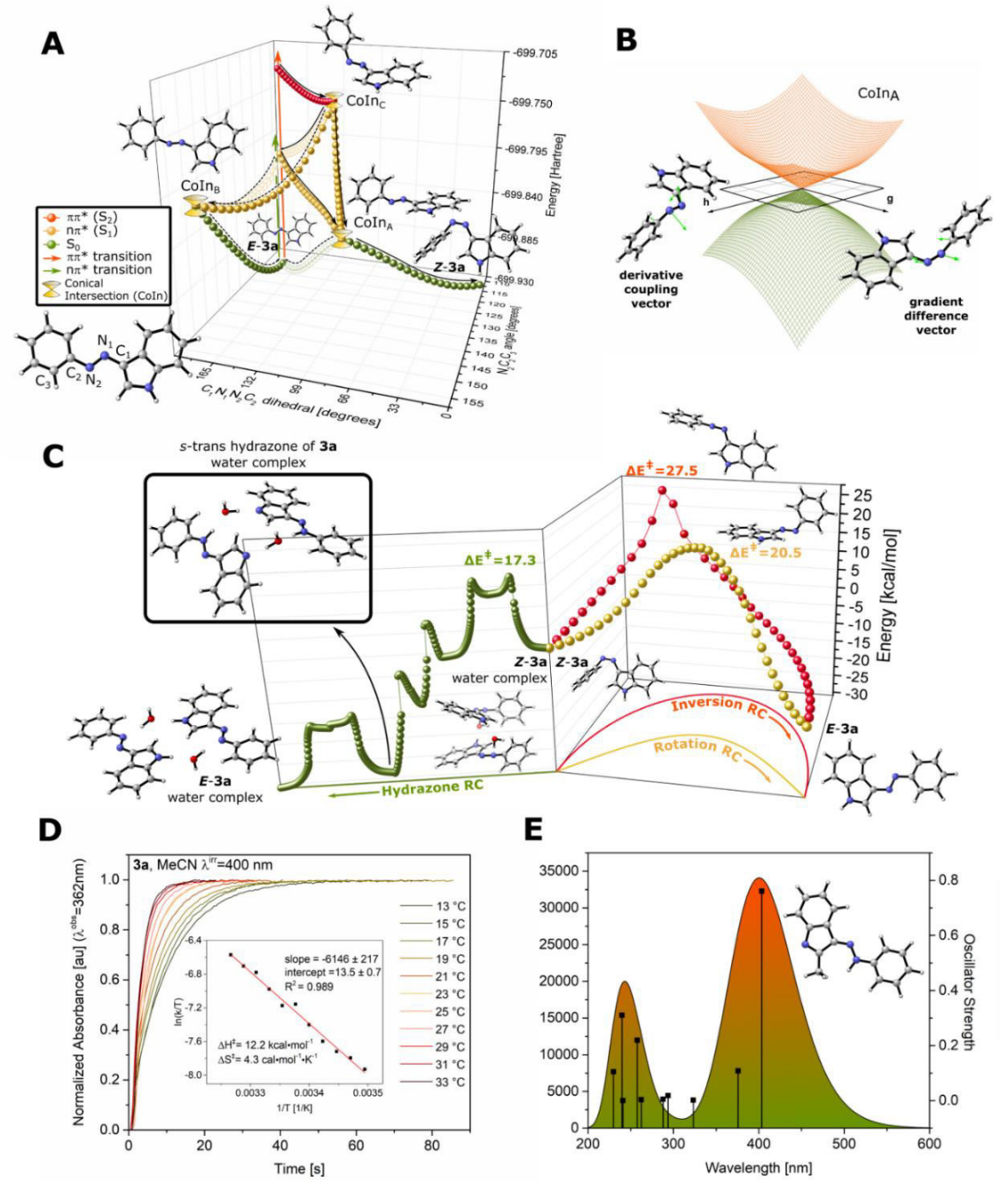

Figure 4. A: **Photochemical *E*-to-*Z* isomerization pathways (CASSCF(10,8)/6-31G(d) level of theory), showing the different pathways 3a can cover after excitation to the first or second excited state.** B: **Branching space of Conical Intersection A (CoIn$_A$) represented in figure** A. **The derivative coupling (*g*) and gradient difference vectors (*h*, green), removing the degeneracy between the S1 and S0, at which the conical intersection occurs.** C: **Thermal reaction coordinates (RC) restoring *E*-3a from *Z*-3a. In particular, the rotation, inversion and hydrazone formation mechanisms are compared. In the box, the spectroscopically detectable hydrazone of 3a is represented.** D: **Thermal relaxation kinetics of 3a in MeCN at different temperatures. The related Eyring-Polanyi plot is depicted in the inset.** E: **(TD)-PBE0/6-311+G(2d,p) simulated UV/Vis spectrum of the s-trans conformer of the azo-hydrazone of 3b in DMSO. In the inset, the optimized structure of the same species is shown.**

This process is barrierless. Excitation to the S2 level is followed by a deactivation to S1 via a conical intersection topologically similar to the S0←S1 one (CoInC). The molecule has now enough potential energy either to go through CoInA relaxing to ***Z*-3a** or to funnel through another conical intersection to the sole ***E*-3a** isomer (CoInB). CoInB is only accessible in this way, because it is located energetically uphill compared to the Franck-Condon geometry of the S1.

In accordance with our experiments, the simulated photochemical behaviour of **3a**, and in general of phenylazoindole cores, do not differ drastically compared to the parent azobenzene photoswitch.[14] In contrast, the thermal *Z*-to-*E* pathway was studied via broken symmetry (BS)-DFT taking into account three different mechanisms, *viz.* the inversion, the rotation (both of them typical of azobenzene)[38] and the intermolecular hydrazone-formation (with and without water assisting molecules). We found that the indole moiety lowers the rotational activation barrier with respect to the inversion in **3a**-**b** ($\Delta E^{\ddagger}$=20.3 and 30.7 kcal/mol for the rotation and inversion mechanism, respectively, at the ωB97XD/6-31G(d) level of theory; Figure 3C; comparable findings were recently reported on arylazoindazoles[33]), while N-Me indole (**3c**) increases it ($\Delta E^{\ddagger}$=33.8 and 30.7 kcal/mol for the rotation and inversion mechanism, respectively, at the ωB97XD/6-31G(d) level of theory). That could be an explanation for the higher lifetimes encountered in aprotic solvents for **3c** compared to **3a** and **3b**, where other pathways, apart monomolecular relaxation, were not detected. The computed thermochemical values we have in hand ($\Delta H^{\ddagger}$=14 kcal/mol at the (C-PCM)-B3LYP/6-31G(d) in MeCN) are comparable with the experimental Eyring-Polanyi plot obtained for **3a** in MeCN ($\Delta H^{\ddagger}$=12 kcal/mol; Figure 4D)

Most interestingly, using DFT calculations we proved the participation of a hydrazone intermediate in a third relaxation pathway. We reasoned that the hydrazone formation in azoindoles is only feasible intermolecularly, due to the impossibility for the indolic proton to reach the azo group intramolecularly (see Scheme 2 for a schematic overview; Section A.I.2.4. in the Appendix).

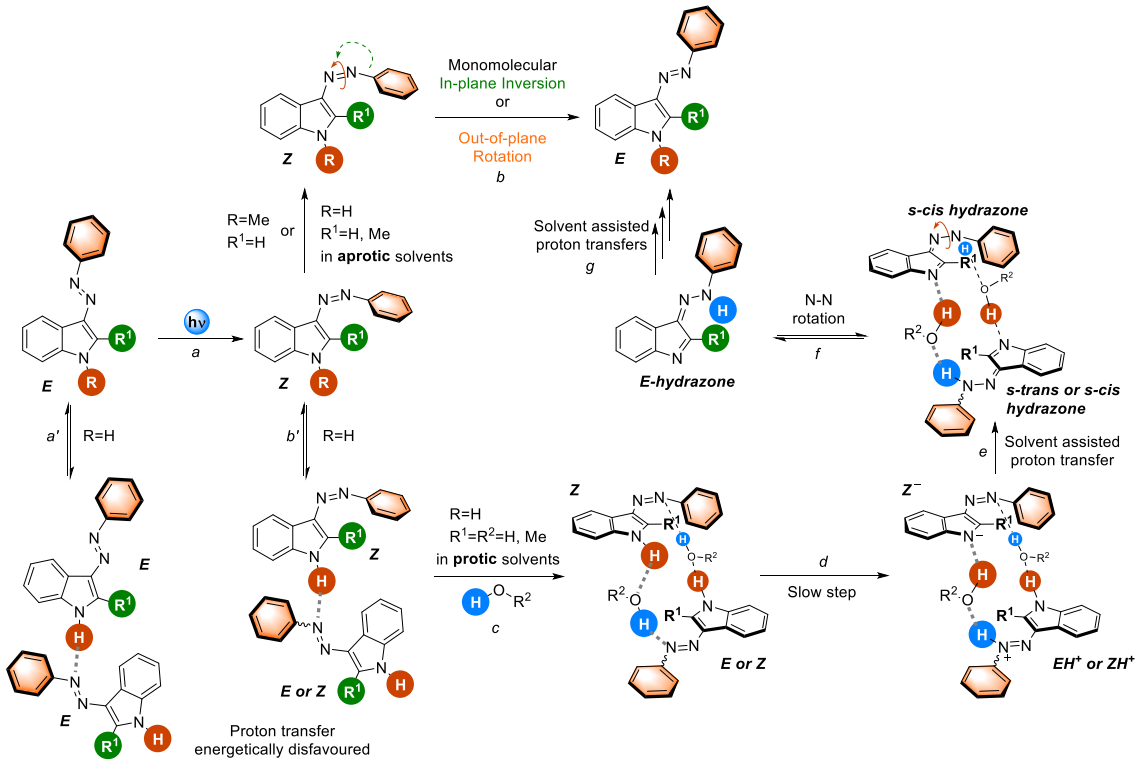

Scheme 2: Schematic, mechanistic overview of the various *Z*-to-*E* isomerization pathways in 3-phenylazoindoles.

However, without the assistance of water (representing the simplest proton donor) the interaction of two molecules of **3a** is characterized by high energy barriers, which make this pathway not competitive with the previously analyzed monomolecular thermal isomerizations. On the other hand, two explicit molecules of water bridging two *Z*-conformers of **3a** lower the energetical barriers for the hydrazone formation, thus explaining the increase of rate observed with protic solvents in *N*-H containing azoindoles (Section A.I.2.6. in the Appendix). We propose the following mechanism. The first step involves a water-mediated proton transfer from the indole nitrogen of one molecule of ***Z*-3a** onto the azo-moiety of the second one (β-nitrogen atom with respect to the indole, see Figure 4C, path *c* in Scheme 2). The barrier for the formation of this complex is only 17.3 kcal/mol due to the stabilizing action of the water molecules. The ensuing generation of the two *s*-cis hydrazones is defined by a low activation energy ($\Delta E^{\ddagger}$=3.5 kcal/mol) and results to be slightly exothermal (ca. 1 kcal/mol). After the rotation around the newly formed N-N-single bonds (characterized by ($\Delta E^{\ddagger}$= 8.6 and 10.2 kcal/mol), the *s*-trans hydrazone dimer is formed, which is located inside a potential well (ca. 30 kcal/mol more stable than the initial water-bridged ***Z*-3a** dimer; see figure 4C and path *f* in Scheme 2). Due to this fact, the transient signal of the intermediate present in protic media can be assigned to the *s*-trans hydrazone

(compare Figure 4E, showing the simulated TD-DFT UV/Vis spectra of the azohydrazone of **3b** with the experimentally observed band, figure 2D).

Then, the system undergoes two consecutive water-mediated proton-transfers leading to the *E*-isomer of **3a** (path *g* in Scheme 2). The hydrazone pathway possesses a slightly lower activation energy in protic media than the rotation or the inversion ones. This explains the surprisingly fast isomerization kinetics found with increased proton availability of the medium for **3a**,**b**. With this mechanism in hand, we also expect **3a** and **3b** to be able to switch faster at higher concentrations, nicely explaining the concentration-dependent behavior we found in our experiments (entry 11, Table 1; Section A.I.2.6. in Appendix). Moreover, the competition between the hydrazone and the rotation pathway can be recognized for **3b** in MeOH for its biexponential decay. In contrast, due to its methylated nitrogen atom, the azo-hydrazone formation is precluded to **3c**.

I.2.3 Conclusion

In summary, the photochromic properties of phenylazoindoles have been investigated for the first time. We synthesized compounds **3a**-**c** representing three very basic derivatives of this class of azo dyes. All compounds photo-isomerize applying light of 355, 365 and 400 nm wavelength. Thereby, *N*-methylated **3c** showed the typical behaviour of an azobenzene (τ between several minutes to two days). In contrast to these findings, *N*-H azoindoles exhibit shorter lifetimes, strongly dependent on the protic character of the solvent. We took further advantage of this relationship and tuned the reaction kinetics, increasing the proton content of the solvents. Best results were obtained in mixtures of DMSO and water (1:1) using DBU as an additive, giving rise to lifetimes between 33.9 and 46 ns for **3a** or **3b**, respectively. The surprisingly short lifetimes are explained by a thorough mechanistic study, assuming the intermolecular formation of a hydrazone. Such a mechanism was studied in detail for the first time, spectroscopically, kinetically and computationally. Compared to the canonical inversion and rotation pathways, this conversion is energetically favored in protic media. Thus, faster *Z*-to-*E* relaxation rates can be achieved for **3a**,**b** in contrast to **3c**. Hence, only slight changes of the substituent position or the solvent composition can drastically tune the properties of phenylazoindoles. Such extremely versatile properties render this core structure a suitable candidate for the wide range of applications of photoswitches.

I.2.4 Acknowledgments

We are grateful to Regina Hoheisel and Julia Zach for technical support and to Prof. S. M. Bonesi (University of Buenos Aires) for his help with the kinetic analysis. This work was supported by CINECA SCAI, with computer time granted by ISCRA projects (project code: HP10CBEIAU and HP10C8U1NY). N.A.S. thanks the Studienstiftung des Deutschen Volkes for a doctoral scholarship. S.C. gratefully thanks P. Sbazzeguti, Prof. S. Protti and Dr. D. Ravelli for their help and fruitful discussions.

I.2.5 References

1. Feringa, B. L., Browne, W. R., Eds., Molecular Switches. *Wiley-VCH Verlag GmbH & Co. KGaA: Weinheim*, *Germany*, **2011**.

2. Velema, W. A.; Szymanski, W.; Feringa, B. L. Photopharmacology: Beyond the Proof of Principle. *Journal of the American Chemical Society* **2014**, *136*, 2178–2191.

3. Withers, N. Molecular photoswitches: The Worm that Turned Off. *Nature Chemistry* **2010**, *2*, 11.

4. Gelebart, A. H.; Jan Mulder, D.; Varga, M.; Konya, A.; Vantomme, G.; Meijer, E. W.; Selinger, R. L. B.; Broer, D. J. Making Waves in a Photoactive Polymer. *Nature* **2017**, *546*, 632–636.

5. Camacho-Lopez, M.; Finkelmann, H.; Palffy-Muhoray, P.; Shelley, M. Fast Liquid-Crystal Elastomer Swims into the Dark. *Nature Materials* **2004**, *3*, 307–310.

6. del Valle, M.; Gutiérrez, R.; Tejedor, C.; Cuniberti, G. Tuning the Conductance of a Molecular Switch. *Nature Nanotechnology* **2007**, *2*, 176–179.

7. Baroncini, M.; d'Agostino, S.; Bergamini, G.; Ceroni, P.; Comotti, A.; Sozzani, P.; Bassanetti, I.; Grepioni, F.; Her-nandez, T. M.; Silvi, S.; Venturi, M.; Credi, A. Photoinduced Reversible Switching of Porosity in Molecular crystals Based on Star-Shaped Azobenzene Tetramers. *Nature Chemistry* **2015**, *7*, 634–640.

8. Banghart, M.; Borges, K.; Isacoff, E.; Trauner, D.; Kramer, R. H. Light-Activated Ion Channels for Remote Control of Neuronal Firing. *Nature Neuroscience* **2004**, *7*, 1381–1386.

9. Gautier, A.; Gauron, C.; Volovitch, M.; Bensimon, D.; Julli-en, L.; Vriz, S. How to Control Proteins with Light in Living Systems. *Nature Chemical Biology* **2014**, *10*, 533–541.

10. Vomasta, D.; Högner, C.; Branda, N. R.; König, B. Regulation of Human Carbonic Anhydrase I (hCAI) Activity by Using a Photochromic Inhibitor. *Angewandte Chemie International Edition* **2008**, *47*, 7644–7647.

11. Simeth, N. A.; Kneuttinger, A. C.; Sterner, R.; König, B. Photochromic Coenzyme Q Derivatives: Switching Redox Potentials with Light. *Chemical Science* **2017**, *8*, 6474–6483.

12. Neilson, B. M.; Bielawski, C. W. Illuminating Photoswitchable Catalysis. *ACS Catalysis* **2013**, *3*, 1874–1885.

13. Dürr, H., Bouas-Laurent, H., Eds.; Photochromism: Molecules and Systems. *Elsevier: Amsterdam* ; *Boston*, **2003**.

14. Conti, I.; Garavelli, M.; Orlandi, G. The Different Photoisomerization Efficiency of Azobenzene in the Lowest nπ* and ππ* Singlets: The Role of a Phantom State. *Journal of the American Chemical Society* **2008**, *130*, 5216–5230.

15. Bandara, H. M. D.; Burdette, S. C. Photoisomerization in Sifferent Classes of Azobenzene. *Chemical Society Reviews* **2012**, *41*, 1809–1825.

16. Andréasson, J.; Pischel, U.; Straight, S. D.; Moore, T. A.; Moore, A. L.; Gust, D. All-Photonic Multifunctional Molecular Logic Device. *Journal of the American Chemical Society* **2011**, *133*, 11641–11648.

17. García-Amorós, J.; Velasco, D. Recent Advances Towards Azobenzene-Based Light-Driven Real-Time Information-Transmitting Materials. *Beilstein Journal of Organic Chemisty* **2012**, *8*, 1003–1017.

18. Kienzler, M. A.; Reiner, A.; Trautman, E.; Yoo, S.; Trauner, D.; Isacoff, E. Y. A Red-Shifted, Fast-Relaxing Azobenzene Photoswitch for Visible Light Control of an Ionotropic Glutamate Receptor. *Journal of the American Chemical Society* **2013**, *135*, 17683–17686.

19. Bléger, D.; Schwarz, J.; Brouwer, A. M.; Hecht, S. *o*-Fluoroazobenzenes as Readily Synthesized Photoswitches Offering Nearly Quantitative Two-Way Isomerization with Visible Light. *Journal of the American Chemical Society* **2012**, *134*, 20597–20600.

20. Samanta, S.; McCormick, T. M.; Schmidt, S. K.; Seferos, D. S.; Woolley, G. A. Robust Visible Light Photoswitching with *ortho*-Thiol Substituted Azobenzenes *Chemical Communications* **2013**, *49*, 10314.

21. Garcia-Amorós, J.; Díaz-Lobo, M.; Nonell, S.; Velasco, D. Fastest Thermal Isomerization of an Azobenzene for Nanosecond Photoswitching Applications under Physiological Conditions. *Angewandte Chemie International Edition* **2012**, *51*, 12820–12823.

22. Venkataramani, S.; Jana, U.; Dommaschk, M.; Sonnichsen, F. D.; Tuczek, F.; Herges, R. Magnetic Bistability of Molecules in Homogeneous Solution at Rroom Temperature. *Science* **2011**, *331*, 445–448.

23. Suwa, K.; Otsuki, J.; Goto, K. Syntheses of Shuttlecock- and Bowl-Equipped Phenylazopyridines and Photomodulation of their Coordination Ability to Zn-Porphyrin. *Tetrahedron Letters* **2009**, *50*, 2106–2108.

24. Calbo, J.; Weston, C. E.; White, A. J. P.; Rzepa, H. S.; Contreras-García, J.; Fuchter, M. J. Tuning Azoheteroarene Photoswitch Performance through Heteroaryl Design. *Journal of the American Chemicals Society* **2017**, *139*, 1261–1274.

25. Zhao, L.; Liu, J.; Zhou, P. New Insight into the Photoisomerization Process of the Salicylidene Methylamine under Vacuum. *Journal of Physical Chemistry A* **2017**, *121*, 141–150.

(26) Otsuki, J.; Suwa, K.; Sarker, K. K.; Sinha, C. Photoisomerization and Thermal Isomerization of Arylazoimidazoles. *Journal of Physical Chemistry A* **2007**, *111*, 1403–1409.

27. Heitmann, G.; Schütt, C.; Herges, R. Spin State Switching in Solution with an Azoimidazole-Functionalized Nickel(II)-Porphyrin. *European Journal of Organic Chemistry* **2016**, *2016*, 3817–3823.

28. Weston, C. E.; Richardson, R. D.; Fuchter, M. J. Photoswitchable Basicity through the Use of Azoheteroarenes. *Chemical Communications* **2016**, *52*, 4521–4524.

29. Wendler, T.; Schütt, C.; Näther, C.; Herges, R. Photoswitchable Azoheterocycles via Coupling of Lithiated Imidazoles with Benzenediazonium Salts. *Journal of the Organic Chemistry* **2012**, *77*, 3284–3287.

30. Wang, Y.-T.; Liu, X.-Y.; Cui, G.; Fang, W.-H.; Thiel, W. Photoisomerization of Arylazopyrazole Photoswitches: Stereospecific Excited-State Relaxation. *Angewandte Chemie International Edition* **2016**, *55*, 14009–14013.

31. Stricker, L.; Fritz, E.-C.; Peterlechner, M.; Doltsinis, N. L.; Ravoo, B. J. Arylazopyrazoles as Light-Responsive Molecular Switches in Cyclodextrin-Based Supramolecular Systems. *Journal of the American Chemical Society* **2016**, *138*, 4547–4554.

32. Weston, C. E.; Richardson, R. D.; Haycock, P. R.; White, A. J. P.; Fuchter, M. J. Arylazopyrazoles: Azoheteroarene Photoswitches Offering Quantitative Isomerization and Long Thermal Half-Lives. *Journal of the American Chemical Society* **2014**, *136*, 11878–11881.

33. Travieso-Puente, R.; Budzak, S.; Chen, J.; Stacko, P.; Ja-strzebski, J. T. B. H.; Jacquemin, D.; Otten, E. Arylazoindazole Photoswitches: Facile Synthesis and Functionalization via S_NAr Substitution. *Journal of the American Chemical Society* **2017**, *139*, 3328–3331.

34. Barden, T. C. In Heterocyclic Scaffolds II; Gribble, G. W., Ed.; *Springer Berlin Heidelberg: Berlin, Heidelberg*, **2010**; *26*, 31–46.

35. Ding, H.; Peng, Z.; Wang, J.; Lu, P.; Wang, Y. Preparation of 3-Azoindoles and 3-Hydrazonoindolin-2-imines as well as Their Applications as NNO Pincer Ligands for Boron. *Organic & Biomolecular Chemistry* **2016**, *14*, 7114–7118.

36. Babür, B.; Seferoğlu, N.; Aktan, E.; Hökelek, T.; Şahin, E.; Seferoğlu, Z. Phenylazoindole Dyes 3: Determination of Azo-hydrazone Tautomers of New Phenylazoindole Dyes in Solution and Solid State. *Journal of Molecular Structure* **2015**, *1081*, 175–181.

37. Olivucci, M.; Bernardi, F.; Celani, P.; Ragazos, I.; Robb, M. A. Substituent Effects in Buta-1,3-diene Photochemistry: A CAS-SCF Study of 2,3-Dimethylbutadiene and 2-Cyanobutadiene Excited-State Reaction Paths. *Journal of the American Chemical Society* **1994**, *116*, 1077–1085.

38. Yu, L.; Xu, C.; Zhu, C. Probing the $\pi \rightarrow \pi^*$ photoisomerization mechanism of cis-azobenzene by multi-state ab initio on-the-fly trajectory dynamics simulation. *Physical Chemistry Chemical Physics* **2015**, *17*, 17646–17660.

I.3 Substituent Effects on 3-Phenylazoindole Photoswitches

Abstract:

The development and investigation of heteroazo switches flourished in recent years. Due to their specific photophysical and photochemical properties, they find versatile applications from material science to medicine. However, a deep mechanistic understanding is needed to be able to predict the properties of such azoswitches. Especially, the effect of different substituents on the chromophore and its characteristics is of great interest as they are often crucial to imbed the molecular switch into a system of interest. Herein, we provide a detailed spectroscopic and computational study on the influence of substituents on 3-phenylazoindoles. We will point out changes in absorption properties and analyze the photo stationary state of the thermally labile *Z*-isomers through computational means providing a general structure-property relationship guideline for further use of these compounds.

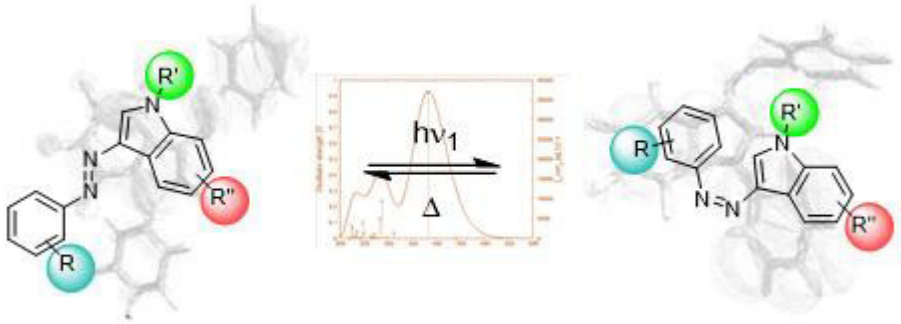

Author contributions

Nadja Simeth synthesized all compounds, characterized them, performed online UV-Vis experiments, optimized the structures using DFT, calculated TD-DFT and wrote the manuscript. Alfredo Bellisario and Stefano Crespi did the computational analysis of the PSS and coded the Math Lab based program. Stefano Crespi supervised the computational work. Maurizio Fagnoni and Burkhard König supervised the overall project.

I.3.1 Introduction

Photochromic compounds received a remarkably rising interest in the last two decades.[1-3] They found various applications as *e.g.* molecular memory and logic devices,[4-6] light-gated chemical reactions,[7, 8] molecular material science,[9, 10] drug delivery,[11, 12] modulation of biological function,[13, 14] and control of cell death.[15, 16] Molecular photoswitching is based on bi-stable systems interconverting between two distinct isomeric forms by application of light as an external stimulus.[17] Particularly, azobenzenes are popular photochromic systems due to their large geometrical changes upon isomerization,[18, 19] their synthetic accessability,[20, 21] their high fatigue resistance,[18, 19] and the tunability of their photo-physical properties.[22-25] Upon irradiation, they interconvert from a thermodynamically stable *E*- to a meta-stable *Z*-isomer. The reaction is reversible and *Z*-to-*E* isomerization can be triggered through irradiation with light of longer wavelength or thermally. To tune the properties of azobenzenes, the scaffold needs to be decorated with suitable substituents. For instance, tetra-*ortho*-fluoro-, tetra-*ortho*-methoxy- and tetra-*ortho*-chloro-azobenzenes led to red-shifted absorption properties.[22, 26-28] Moreover, *ortho*-flouro and *ortho*-thiolether substituents result in azo dyes with thermally relatively stable *Z*-isomers, whereas azo-push-pull system led to short lifetimes of the *Z*-isomer.[29-31] In contrast, scaffold hopping approaches leading to *e.g.* heterocyclic aromatic systems were rarely considered to alter the properties of azo dyes. Only in very recent years, an increasing number of studies have focused on this aspect to broaden the selection of azo switches available to the chemist. For instance, nitrogen based heteroaryls like pyridine,[32] imidazole,[33] pyrazole,[34] purine[35] and very recently, the indole scaffold[36] have been employed in arylazo switches.

We became interested in phenylazoindoles due to their highly tunable properties which are depending on the position of the azo-function and the solvent.[36] In particular, 5- and 6-phenyl azoindoles behave similarly to parent azobenzene, regarding their spectroscopic properties and the lifetimes (τ) of the *Z*-isomer. In contrast, the spectrum of 2-phenylazoindole is bathochromically shifted and the *Z*-isomer of the compound exhibits extremely short thermal lifetimes (<10 ns) due to the rotation transition state characterized by low barriers. 3-Phenylazoindoles are the most tunable scaffold of the series. Depending on the substituent on the indole nitrogen (NH or NMe) and the character of the solvent, the thermal lifetimes are varying from the nanosecond range to days.[36]

To fully understand the characteristics of azo switches like phenylazoindoles, computational approaches, especially such as time-dependent density functional theory (TD-DFT), have been shown to provide reliable predictions of both transition energies and oscillator

strengths (*f*). As those determine the electronic transitions, TD-DFT can be applied to simulate absorption spectra of the compounds of interest.[37, 38] Furthermore, the calculated transitions can be used to assign the nature of the transition type, which eventually can lead to a better understanding of the events taking place.[39] However, the availability of methods is broad and the applicability varies between compound classes.[40] Especially, dealing with compounds that are light-responsive and interconvert between two structural isomers, each exhibiting unique spectral properties, the method applied has to meet the requirements of both photoisomers.

In this work, we will focus first on probing our system, validating the performance of different functionals and basis sets in the TD-DFT framework. Subsequently, we will apply the best conditions to simulate the UV/Vis spectra of a library of 28 molecules in toluene, DMSO and methanol. Thereby, we will focus on substituent effects on the phenyl moiety of 3-phenylazoindoles and also synthesize some of the compounds for comparison. In addition, we will vary the functionalization on the indole nitrogen and the benzo-moiety of the indole unit and provide a structure-property relationship analysis of the whole library. Finally, we will apply the methods to analyze the PSS contribution of both photoisomers, which cannot be assigned *via* classical analytical methods such as NMR or HPLC due to the fast *Z*-to-*E* isomerization kinetics.

I.3.2 Results and Discussion

I.3.2.1 Scope

Chart 1 depicts the molecules which were included in this study. Specifically, we focused on varying the substituents on the phenyl moiety of the azoindoles, changing their electron demand and considering more complex moieties like cinnamic acid (**8**), morpholine (**5**) or pyrrole (**10**) for potential photopharmacological application. In doing so, we aimed to obtain a clearer picture of the effect substituents have on the UV/Vis properties of the molecules. Furthermore, we modified the substituent on the indole NH from -H (**1a–11a**) to -Me (**1b–11b**), -Ph (**1c**) and the sterically more demanding Ms (**1d**). We also investigated how perfluorination of the benzo moiety of the indole would alter the structure's characteristics (**12a-d**). Having the experimental data of **1a** and **1b** in hand,[36] we synthesized compounds **2a**-**7a** analogously to our previous work (for details see Appendix, Section A.I.3.1.).[36] During the preparation, X-Ray structures of **1b**, **2a**, **3a** and **4a** could be obtained. Moreover, we investigated the compounds **2a-7a** regarding their photochromic properties (*vide infra*).

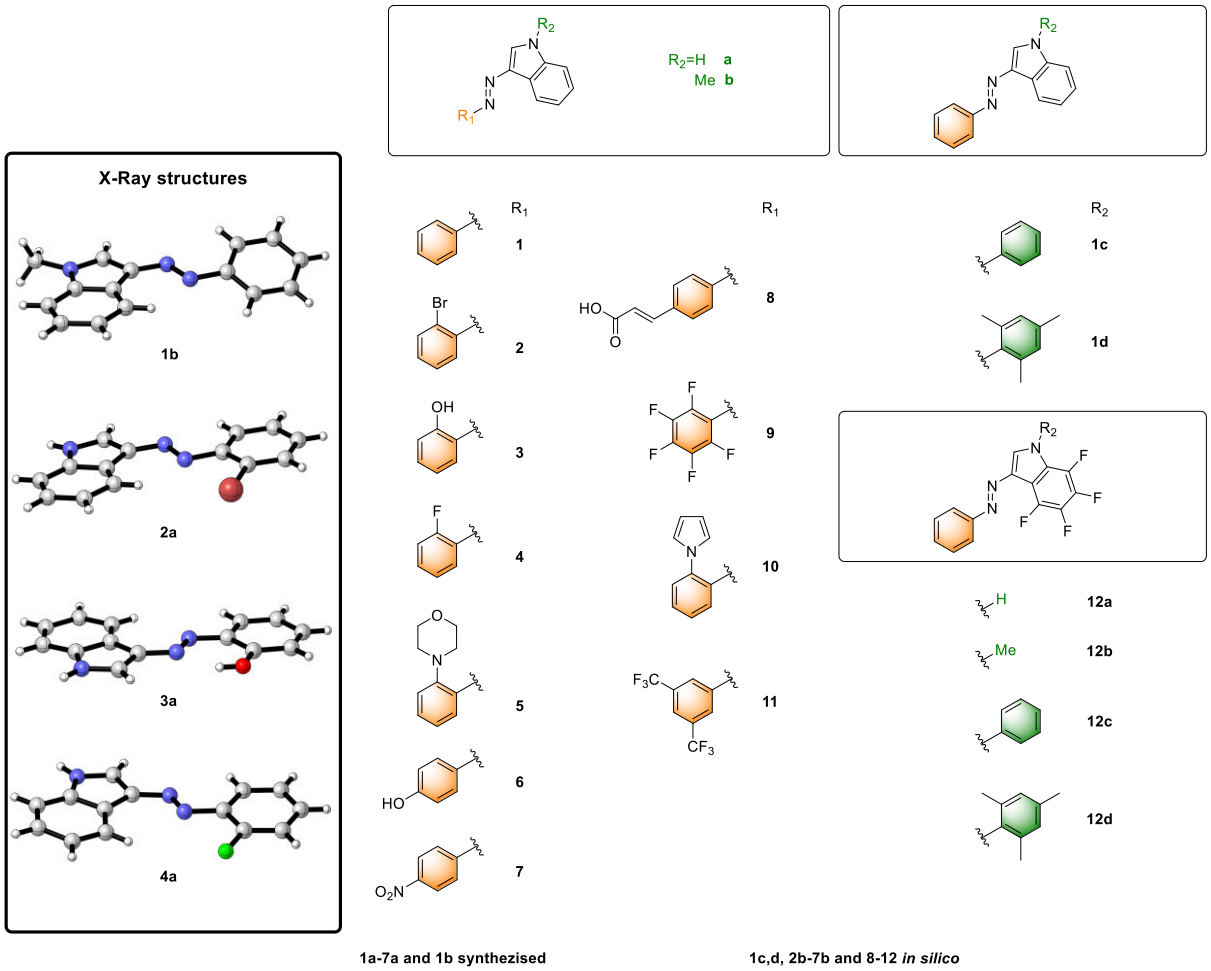

Chart 1: Scope of the computed molecules.

I.3.2.2 Benchmark Study

The computational investigation was carried out using Gaussian 09, Revision D.01 and Gaussian 16, Revision A.03 software packages. Due to the high number of structures involved, we decided to preliminarily screen the most stable conformer of each molecule in its *E*- and *Z*-configuration employing the B3LYP/3-21G level of theory (see A.I.3.6. for further details). Albeit the choice of such an old basis set should be seen merely as qualitative, it still provides decent results for a rough glimpse on the behavior of the conformers of the molecule of interest, with the advantage to be very inexpensive from a computational point of view (see the time benchmark in Section A.I.3.7.). The energetically most stable *E*- and *Z*-isomers were further optimized using the B3LYP/6-311+G(2d, p) approach and confirmed to be minima *via* the absence of imaginary normal modes of vibrations. The aforementioned level of theory is well documented in the literature for its reliability to predict the geometries of photoswitchable compounds.[41]

We decided to evaluate a wide variety of basis sets and functionals at the TD-DFT level of theory, in order to provide full insight in the simulation of the electronic spectra of this class

of azo switches. Single point calculations up to the first 25 singlet state were deemed to be sufficient in order to fully define the absorption spectra down to 200 nm. Thus, the UV/Vis spectrum of the *E*-isomer of **1a**, namely ***E*-1a**, (Figure 1 and 2) was chosen as reference model for our benchmark studies and compared with the one experimentally obtained in toluene (Figure 1 and 2). Consequently, solvent effects were taken into account applying the conductor-like polarizable continuum model (C-PCM, ε=2.379 for toluene).[42]

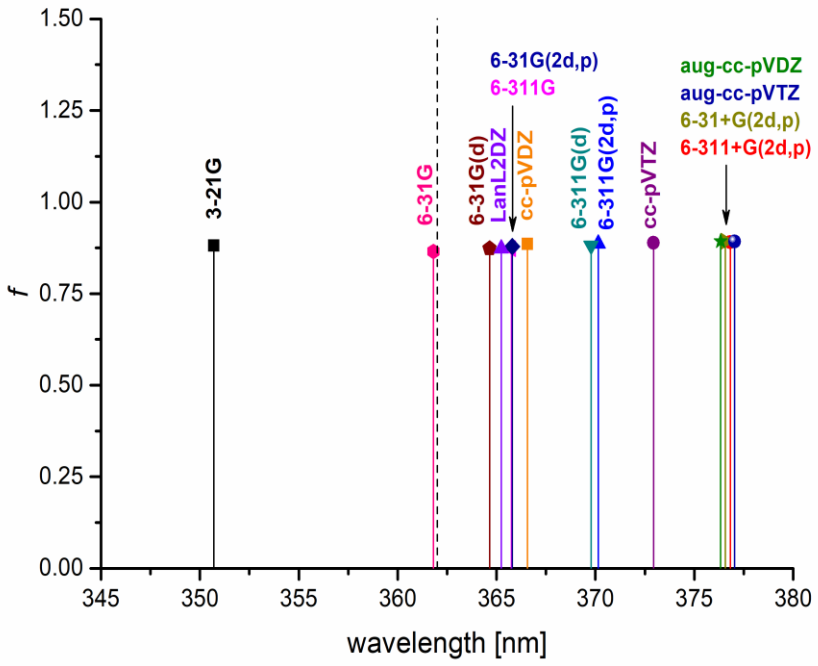

Figure 1: Basis set effect on the calculated electronic transitions (TD-B3LYP, 25 states, toluene bulk) of *E*-1a. The second transition, corresponding to the most prominent absorption band around 362 nm, is shown together with the experimental maximum obtained from the UV/Vis spectrum of *E*-1a in toluene at its thermal equilibrium (dashed line).

First tests were performed using the B3LYP functional and a different collection of basis sets. The basis set quality was found to influence the position of the main allowed transition in the TD-DFT spectra, while the value of the oscillator strength remains almost the same (see Figure 1 and Table A37 in the A.I.3.6). In particular, 3-21G overestimated the maximum by 12 nm (see Table A37). A basis set that includes the electron core potential (ECP) like LANL2DZ let the predicted absorption to deviate only 3 nm from the experiment.[43] Increasing the number of primitives in the contracted core function (see for example 6-31G basis set compared to 3-21G) induces a red-shift in the position of the maximum, as like as varying from a double ζ to a triple ζ basis (compare 6-311G with 6-31G, or cc-pVTZ and cc-pVDZ). Moreover, the addition of polarized functions transposes the transition to higher

wavelength, both in Pople's and Dunning's basis sets. Interestingly, the inclusion of a diffuse function in all the examined cases gives almost the same predicted wavelength (*ca.* 377 nm), differing about 15 nm from the experimental maximum). It is known, however, that B3LYP underestimates the transition energies with an error around 0.1-0.2 eV (*ca.* 10-20 nm).[40] Accordingly, we decided to test the functionals with the triple ζ 6-311+G(2d,p) basis set, that affords pertinent results for TD-DFT calculations[40] to a minor computational cost (see Table A37 in A.I.3.7.), considering the analogue basis aug-cc-pVTZ, herein tested.

The pure functionals based on the generalized gradient approximation (both GGA and meta-GGA, see Figure 2A and Table A38 in A.I.3.7.) have the tendency to broadly underestimate the lower allowed transition, locating the absorption between 390 and 420 nm. Moreover, they predict a lower probability compared to the other functionals examined (see Figure 3). This behavior is well known in the exact-exchange free functionals.[40] Conversely, using the Hartree-Fock method (HF, Figure 2A) results in higher transition energy (*ca.* 305 nm *vs* 362 nm of the experimental value) and higher oscillator strength, ensuing the necessity to include in a certain degree the HF exchange, as implemented by the hybrid and meta-hybrid functionals. As expected, in both cases (see Figure 2B for the hybrid functionals and 2C for the meta-hybrid) the position and intensity of the absorption can be directly related to the amount of Hartree Fock exchange present in the functional. In particular, the higher the percentage of HF exchange energy, the higher the computed values of absorption maximum and *f*. An exemplary case is furnished by the hybrids BHandH and BHandHLYP (Figure 2B) that possess the same value of HF exchange (*viz.* 50%[40]) and remarkably predict similar values in wavelength and oscillator strengths (*ca.* 339 nm with $f = 1.0$). From the results, it appeared that a Fock-exchange mixing parameter of 25 % as afforded by PBE0 was appropriate to describe in an accurate and precise way the main transition in the *E*-isomer of the phenylazoindoles, using the 6-311+G(2d,p) basis set. Even though range-separated functionals have the tendency to well behave in the simulation of UV/Vis spectra, in our particular case they tend to overshoot the lower transition energies (Figure 2D).[44] The absence of a marked charge-transfer (CT) or Rydberg lower excited state could be the reason for this caveat.[40]

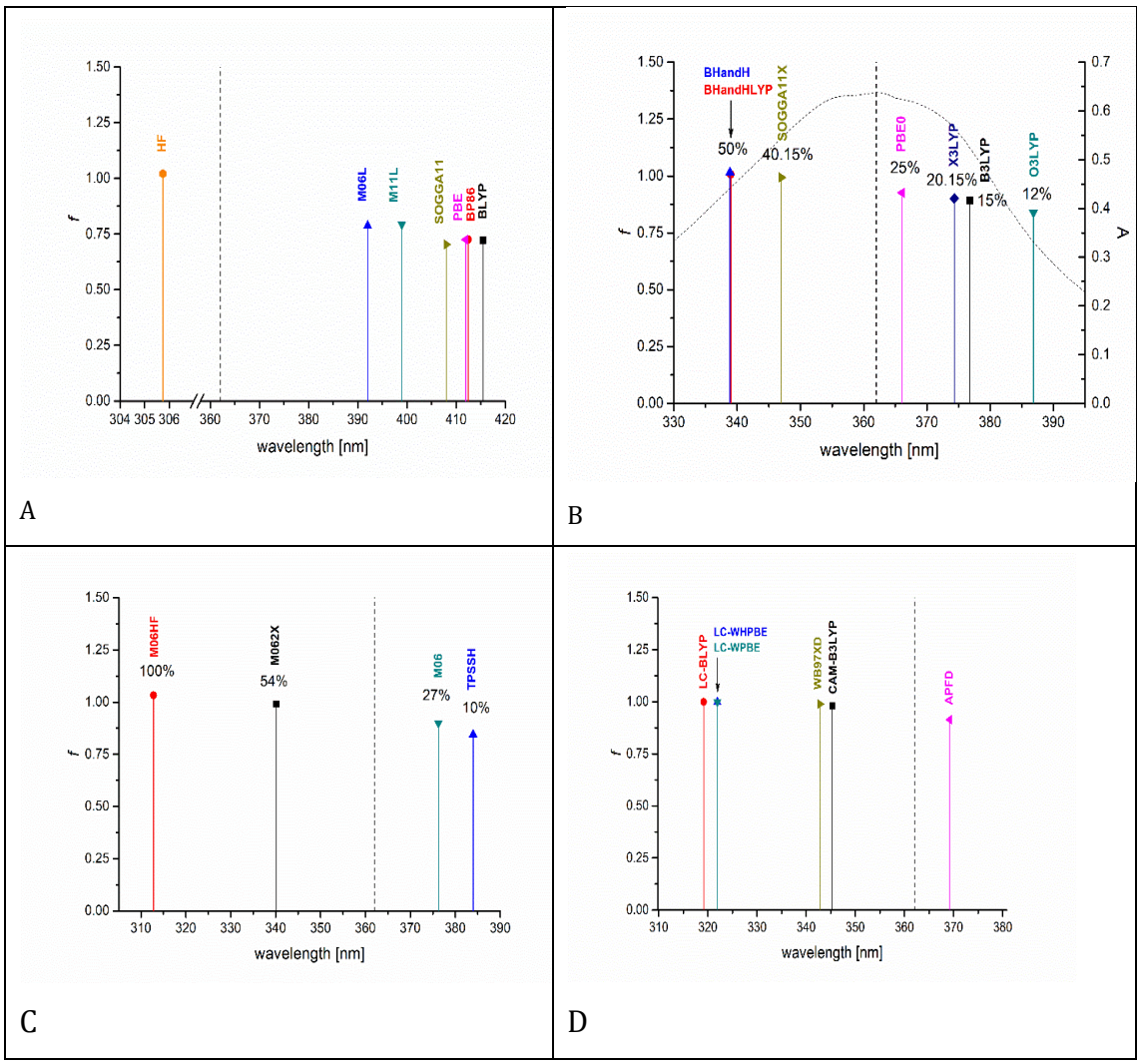

Figure 2: First allowed electronic transition of *E*-1a (6-311+G(2d,p) basis set, toluene bulk) using different functionals belonging to the following families: A**: pure HF or GGA and meta-GGA.** B**: hybrid, over every transition the percentage of Hartree-Fock exchange is explicated.** C**: meta-hybrid, over every transition the percentage of Hartree-Fock exchange is explicated.** D**: range-separated and diffusion corrected.**

I.3.2.3 Spectroscopic Analysis

I.3.2.3.1 UV-Vis Spectra

The synthesized compounds **1a**-**7a** and **1b** were investigated regarding their electronic properties using UV-Vis spectroscopy (the data of compounds **1a** and **1b** were taken from our previous study).[36] The results are summarized in Table 1 (for a wider range of solvents, see Table A1 in the Section A.I.3.3.). Additionally, the spectra of all compounds included in this study were simulated using (C-PCM)[42]-TD-PBE0/6-311+G(2d,p) as a single-point over the first 25 states (Table 1 for compounds **1a**-**7a** and **1b**, further data see A.I.3.3., Table A1).

Table 1: Overview of experimental and calculated maxima of the different synthesized compounds in Toluene, DMSO and MeOH and their PSS ratio determined through computational analysis (Values for 1a and 1b were taken from Ref. 36).

Compound	Solvent[a]	λ_{max} [nm] PBE0	λ_{max} [nm]	$\varepsilon\lambda_{max}$	τ[b]	PSS[i] [*Z*-*E*] (calc.)
1a	Toluene[a]	366	362	15151	47.5 ms	
	DMSO[a]	368	372	16447	6.5 s	
	MeOH[a]	366	365	14716	6.8 ms	
1b	Toluene[a]	373	366	14134	17.1 min	85-15
	DMSO[a]	376	380	15964	2.6 d	
	MeOH[a]	373	369	14338	2.4 h	
2a	Toluene[b]	379	373	13956	51.4 s	94-6
	DMSO[b]	380	388	13248	1.41 s	19-81
	MeOH[b]	378	377	13582	13.1 ms	28-72
3a	Toluene[c]	382	385	13890	12.1 ms	35-65
	DMSO[c]	384	389	15151	18.4 ms	45-55
	MeOH[c]	382	384	15556	7.76 ms	6-94
4a	Toluene[a]	375	367	14148	136 s	90-10
	DMSO[a]	376	379	15592	1.02 s	19-81
	MeOH[a]	374	371	15552	9 ms	6-81
5a	Toluene[a]	340 (412)	347 (388)	11018	1.49 ms	9-91
	DMSO[a]	341, 411	394	17192	--	57-43
	MeOH[a]	340, 410	384	16820	--	9-91
6a	Toluene[e]	373	373	10710	10.2 s	87-13
	DMSO[e]	375	380	12450	5.74 s	86-14
	MeOH[e]	373	374	13752	--	7-93
7a	Toluene[f]	427	399	11593	121 s	94-6
	DMSO[f]	442	422	14723	reaction	5-95
	MeOH[f]	438	407	15977	94.4 s	16-84

[a]Concentration was 50 μM. [b]Concentration was 100 μM. [c]Concentration was 100 μM. [d]Concentration was 20 μM. [e]Concentration was 40 μM. [f]Concentration was 30 μM. [g]Concentration was 15 μM. [h]Lifetimes <1s were determined using Laser-Flash Photolysis, other values using UV/Vis spectroscopy [i]Using the method as presented in section A.I.3.9.

Firstly, we compared the simulations with the experimental spectra. In particular, λ_{max} of the main transition band of the synthesized compounds, which can be attributed to the ππ* transition of the *E*-isomer (in accordance with previous reports), was compared with the main transition (*f* >0.8) in TD-DFT, the second excited state transition (as the first one, the nπ*, is formally forbidden (*f* = 0)). All compounds show a main transition band between 350 nm and 422 nm in the experiment. The calculations tend to underestimate the transition energy of **1a-6a** by 3–6 nm in toluene, while by 4–8 nm in DMSO. MeOH is more precise and the deviation found is mainly around 1-4 nm. The only negative performance was given with **7a**. The presence of the nitro chromophore makes the calculation overestimate the wavelength at which the main band will appear. However, the functional and basis sets describe robustly the electronic properties of **1a-7a** in solution. Indeed, they are not only able to distinguish the nature of the transition (either nπ* or ππ*) but, in the majority of the cases, they are extremely close to the experimentally obtained values and trends shown comparing different substituents. Hence, the TD-DFT simulations can be used to also analyze compounds, which were only part of the *in silico*-study.

Aside from per-fluoro phenylazoindole ***E*-9a**, which shows hardly any difference compared to the parent ***E*-1a**, substituents on the phenyl moiety of the switch have a bathochromic effect on the main electronic transition (ca. 10–20 nm red-shifted). The shift is especially well pronounced in the spectra of ***E*-5**, ***E*-7** and ***E*-10**, which can be reasoned through the presence of either an extended π-conjugation (lone pair of the amino group of the *ortho*-morpholino substituent in ***E*-5** or interaction of the aromatic *ortho*-pyrrole substituent in ***E*-8**) or a push-pull-azo system (*para*-nitro substituent in ***E*-7**). Moreover, compounds ***E*-5** and ***E*-10** are not only red-shifted, but also exhibit a broadening of the main absorption band, as more electronic transitions become formally allowed in the visible region of the spectrum.

Having ***E*-5a** already in hand we wanted to also synthesize ***E*-10a**. However, the ortho-pyrrole moiety only led to internal trapping of the diazonium salt formed during the reaction (details as well as characterization of the isolated compounds see Section A.I.3.1.).

Methylation of the indole's NH moiety leads to a slight red-shift of the spectrum (ca. 10–20 nm). This is strongly pronounced for azoindoles ***E*-8** and ***E*-10** (> 30 nm). Also, introduction of a phenyl- or a mesityl-group on the indole nitrogen leads in most of the examples to a red-shift of the spectrum, which is particularly prominent comparing ***E*-1a** and ***E*-1c** (ca. 50 nm). In contrast, perfluorination of the benzo moiety of the bicycle induces a blue-shift (ca. 5-50 nm) in the spectra.

I.3.2.3.2 E-to-Z Isomerization, Thermal Lifetimes and PSS Analysis

Upon irradiation with light of an appropriate wavelength (355 nm YAG laser or 400 nm LED) the azoindole switches undergo a photochemical *E*-to-*Z* isomerization, which can be followed spectroscopically by the decrease of the ππ* transition band of the *E*-isomer. Removal of the light-source leads to a quick recovery of the *E*-isomer characterized by the lifetime (τ) of the *Z*-isomer. The lifetimes of the eight synthesized compounds were determined through UV-Vis spectroscopy or laser-flash photolysis and were in the range of milliseconds to seconds for NH phenylazoindoles (only the parent compound **1a** studied previously in more detail showed faster isomerization kinetics[36]) and up to 2.6 d in *N*-methylated **1b**.[36] Probing the compounds' mechanism using protic and non-protic environment, we found that also some substituted 3-phenylazoindoles are able to relax *via* a hydrazone-intermediate already spotted in **1a** in the presence of protic environment (*cf.* Table 1 and Table A1 in A.I.3.3.).[36]

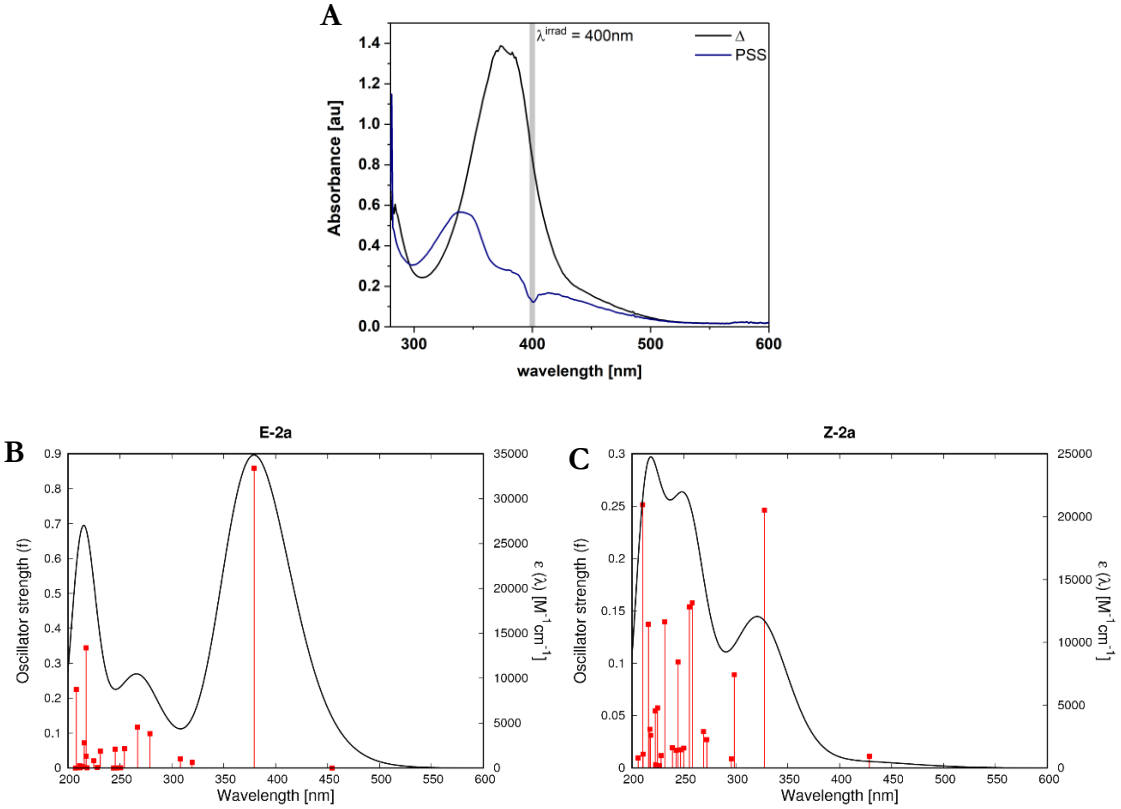

Figure 3: A: 2a in toluene at Δ (black line) and the PSS (blue line). B: Calculated spectrum of *E*-2a and C: of *Z*-2a in toluene (as C-PCM) using TD-PBE0/6-311+G(2d,p).

Figure 3A exemplarily depicts the spectrum of **2a** in toluene at the thermodynamic equilibrium (black line, mainly *E*-isomer) and their photo stationary state (PSS, blue line)

containing the maximum amount of *Z*-isomer that can be generated through irradiation at the present conditions (for further spectra see Section A.I.3.3.). Due to the fast, thermal *Z*-to-*E* isomerization of the compounds, the photo stationary state (PSS) distribution could not be assigned using classical means like NMR or HPLC analysis. Recently, the group of Fuchter reported a method calculating the PSS of thermally labile heteroaryl azo switches by calculating the spectrum of the pure *Z*-isomer from UV-Vis studies.[45] However, having a benchmark-proven *in silico* method in hand, we decided to obtain the value of the PSS comparing the spectroscopically obtained one with a simulated one generated by mixing the computed spectra of the pure *E*- and *Z*-isomers (pure spectra of ***E*-2a** and ***Z*-2a** can be found in Figure 3B and 3C, more details and further spectra see A.I.3.3.). Comparing the computed PSS of the thermally stable photoswitch **1b** in DMSO with the experimentally determined one by NMR,[36] we attributed the share of the *Z*-isomer to be 85% with both the methods. Proven the method to be significantly accurate we consequently used the same method to analyze the PSS compositions of the thermally more labile compounds. The results can be found in Table 1. Additionally, we were able to automatize this procedure developing a Matlab based code (further details see Section A.I.3.8.). Hence, the method is viable enough to be easily extended to other azo switches and photoswitchable scaffolds in general.

I.3.3 Conclusion

In summary, we performed a computational benchmark study to explore the effects of different basis sets and functionals on the calculated transition energies using the parent compound **1a** as a model. We found that PBE0/6-311+G(2d,p) gave best results with the CPCM-TD-DFT single point calculations and hence, we applied it to simulate the UV/Vis spectra of a series of substituted 3-phenylazoindoles in various solvents. For comparison, several derivatives were additionally synthesized and characterized through UV/Vis spectroscopy regarding their photophysical and photochemical behavior. Both theoretically and experimentally obtained values were in good agreement. Combining the spectroscopic and the computed results we found that all compounds exhibit an ordinary profile of arylazo-compounds with a maximum between *ca.* 350- 420 nm. Thereby, the position of the transition band strongly depends on the solvent and the substituents. Indeed, functional groups, which induce an explicit push-pull-system or extended the π-system of the switch led to strongly, bathochromically shifted spectra. In contrast, perfluorination of the benzo-moiety of the indole induced a hypsochromic shift whereas sterical demand was less important for the transitions energies. Analyzing the thermal stability of the *Z*-isomers of the

synthesized compounds, we found that the majority of them relax in the millisecond-range. Moreover, the isomerization mechanism could be tuned from an out-of-plane rotational mechanism to a hydrazone-mediated one in polar-protic solvents similar to the parent **1a**. As the fast isomerization kinetics made it impossible to determine the PSS using established methods like NMR or HPLC analysis, we used the simulated spectra of *E*- and *Z*-isomers at different ratios to compare the experimentally obtained spectra at the PSS with the simulated ones. In this manner, we were able to assign the share of the thermally labile *Z*-isomers at the PSS. Furthermore, we were able to automate the process and the method can be potentially extended to other photochromic scaffolds in future work. Together with the systematic analysis of photophysical and photochemical characteristics of the compounds our study may lead to both more rational design of novel scaffolds and better interpretation of the obtained data.

I.3.4 Acknowledgements

We thank the Consortium CINECA-SCAI for the computational hours granted on the Galileo supercomputer (project IsC48_PO-DHT). NAS thanks the Studienstiftung des Deutschen Volkes for a doctoral scholarship. We thank L. Capaldo for fruitful discussions and G. G. Visconti for providing access to his facilities.

I.3.5 References

1. Brieke, C.; Rohrbach, F.; Gottschalk, A.; Mayer, G.; Heckel, A., Light-Controlled Tools. *Angewandte Chemie International Edition* **2012**, *51*, 8446–8476.

2. Bléger, D.; Hecht, S., Visible-Light-Activated Molecular Switches. *Angewandte Chemie International Edition* **2015**, *54*, 11338–11349.

3. Russew, M.-M.; Hecht, S., Photoswitches: From Molecules to Materials. *Advanced Materials* **2010**, *22*, 3348–3360.

4. Andréasson, J.; Pischel, U.; Straight, S. D.; Moore, T. A.; Moore, A. L.; Gust, D., All-Photonic Multifunctional Molecular Logic Device. *Journal of the American Chemical Society* **2011**, *133*, 11641–11648.

5. Irie, M., Diarylethenes for Memories and Switches. *Chemical Reviews* **2000**, *100*, 1685–1716.

6. Andréasson, J.; Pischel, U., Storage and Processing of Information Using Molecules: The All-Photonic Approach with Simple and Multi-Photochromic Switches. *Israel Journal of Chemistry* **2013**, *53*, 236–246.

7. Erno, Z.; Asadirad, A. M.; Lemieux, V.; Branda, N. R., Using Light and a Molecular Switch to 'Lock' and 'Unlock' the Diels-Alder reaction. *Organic & Biomolecular Chemistry* **2012**, *10*, 2787–2792.

8. Wilson, D.; Branda, N. R., Turning "On" and "Off" a Pyridoxal 5'-Phosphate Mimic Using Light. *Angewandte Chemie International Edition* **2012**, *51*, 5431–5434.

9. Wang, Y.; Han, P.; Xu, H.; Wang, Z.; Zhang, X.; Kabanov, A. V., Photocontrolled Self-Assembly and Disassembly of Block Ionomer Complex Vesicles: A Facile Approach toward Supramolecular Polymer Nanocontainers. *Langmuir* **2010**, *26*, 709–715.

10. Asadirad, A. M.; Boutault, S.; Erno, Z.; Branda, N. R., Controlling a Polymer Adhesive Using Light and a Molecular Switch. *Journal of the American Chemical Society* **2014**, *136*, 3024–3027.

11. Göstl, R.; Hecht, S., Photoreversible Prodrugs and Protags: Switching the Release of Maleimides by Using Light under Physiological Conditions. *Chemistry – A European Journal* **2015**, *21*, 4422–4427.

12. Petriashvili, G.; Devadze, L.; Zurabishvili, T.; Sepashvili, N.; Chubinidze, K., Light Controlled Drug Delivery Containers Based on Spiropyran Doped Liquid Crystal Micro Spheres. *Biomedical Optics Express* **2016**, *7*, 442–447.

13. Reisinger, B.; Kuzmanovic, N.; Löffler, P.; Merkl, R.; König, B.; Sterner, R., Exploiting Protein Symmetry To Design Light-Controllable Enzyme Inhibitors. *Angewandte Chemie International Edition* **2014**, *53*, 595–598.

14. Broichhagen, J.; Podewin, T.; Meyer-Berg, H.; von Ohlen, Y.; Johnston, N. R.; Jones, B. J.; Bloom, S. R.; Rutter, G. A.; Hoffmann-Röder, A.; Hodson, D. J.; Trauner, D., Optical Control of Insulin Secretion Using an Incretin Switch. *Angewandte Chemie International Edition* **2015**, *54*, 15565–15569.

15. Velema, W. A.; van der Berg, J. P.; Hansen, M. J.; Szymanski, W.; Driessen, A. J. M.; Feringa, B. L., Optical Control of Antibacterial Activity. *Nature Chemistry* **2013**, *5*, 924–928.

16. Borowiak, M.; Nahaboo, W.; Reynders, M.; Nekolla, K.; Jalinot, P.; Hasserodt, J.; Rehberg, M.; Delattre, M.; Zahler, S.; Vollmar, A.; Trauner, D.; Thorn-Seshold, O., Photoswitchable Inhibitors of Microtubule Dynamics Optically Control Mitosis and Cell Death. *Cell* **2015**, *162*, 403–411.

17. Feringa, B. L., The Art of Building Small: From Molecular Switches to Molecular Motors. *The Journal of Organic Chemistry* **2007**, *72*, 6635–6652.

18. Beharry, A. A.; Woolley, G. A., Azobenzene photoswitches for biomolecules. *Chemical Society Reviews* **2011**, *40*, 4422–4437.

19. Bandara, H. M. D.; Burdette, S. C., Photoisomerization in different classes of azobenzene. *Chemical Society Reviews* **2012**, *41*, 1809–1825.

20. Hansen, M. J.; Lerch, M. M.; Szymanski, W.; Feringa, B. L., Direct and Versatile Synthesis of Red-Shifted Azobenzenes. *Angewandte Chemie International Edition* **2016**, *55*, 13514–13518.

21. Merino, E., Synthesis of Azobenzenes: the Coloured Pieces of Molecular Materials. *Chemical Society Reviews* **2011**, *40*, 3835–3853.

22. Beharry, A. A.; Sadovski, O.; Woolley, G. A., Azobenzene Photoswitching without Ultraviolet Light. *Journal of the American Chemical Society* **2011**, *133*, 19684–19687.

23. Dong, M.; Babalhavaeji, A.; Samanta, S.; Beharry, A. A.; Woolley, G. A., Red-Shifting Azobenzene Photoswitches for in Vivo Use. *Accounts of Chemical Research* **2015**, *48*, 2662–2670.

24. Timm, J.; Schürmann, U.; Kienle, L.; Bensch, W., High Azobenzene Functionalization Enhances Stability of the Cis Isomer: Periodic Mesoporous Organosilica Network on the Way to New Light Triggered Applicable Materials. *Microporous and Mesoporous Materials* **2016**, *228*, 30–36.

25. Zhao, F.; Grubert, L.; Hecht, S.; Bleger, D., Orthogonal Switching in Four-State Azobenzene Mixed-Dimers. *Chemical Communications* **2017**, *53*, 3323–3326.

26. Bléger, D.; Hecht, S., Aktivierung Molekularer Schalter mit Sichtbarem Licht. *Angewandte Chemie* **2015**, *127*, 11494–11506.

27. Samanta, S.; Babalhavaeji, A.; Dong, M.-x.; Woolley, G. A., Photoswitching of ortho-Substituted Azonium Ions by Red Light in Whole Blood. *Angewandte Chemie International Edition* **2013**, *125*, 14377–14380.

28. Rullo, A.; Reiner, A.; Reiter, A.; Trauner, D.; Isacoff, E. Y.; Woolley, G. A., Long Wavelength Optical Control of Glutamate Receptor Ion Channels Using a Tetra-*ortho*-Substituted Azobenzene Derivative. *Chemical Communications* **2014**, *50*, 14613–14615.

29. Samanta, S.; McCormick, T. M.; Schmidt, S. K.; Seferos, D. S.; Woolley, G. A., Robust Visible Light Photoswitching with *ortho*-Thiol Substituted Azobenzenes. *Chemical Communications* **2013**, *49,* 10314–10316.

30. García-Amorós, J.; Velasco, D., Recent Advances Towards Azobenzene-Based Light-Driven Real-Time Information-Transmitting Materials. *Beilstein Journal of Organic Chemistry* **2012**, *8*, 1003–1017.

31. Knie, C.; Utecht, M.; Zhao, F.; Kulla, H.; Kovalenko, S.; Brouwer, A. M.; Saalfrank, P.; Hecht, S.; Bléger, D., *ortho*-Fluoroazobenzenes: Visible Light Switches with Very Long-Lived Z Isomers. *Chemistry – A European Journal* **2014**, *20*, 16492–16501.

32. Venkataramani, S.; Jana, U.; Dommaschk, M.; Sönnichsen, F. D.; Tuczek, F.; Herges, R., Magnetic Bistability of Molecules in Homogeneous Solution at Room Temperature. *Science* **2011**, *331*, 445–448.

33. Otsuki, J.; Suwa, K.; Sarker, K. K.; Sinha, C., Photoisomerization and Thermal Isomerization of Arylazoimidazoles. *The Journal of Physical Chemistry A* **2007**, *111*, 1403–1409.

34. Weston, C. E.; Richardson, R. D.; Haycock, P. R.; White, A. J. P.; Fuchter, M. J., Arylazopyrazoles: Azoheteroarene Photoswitches Offering Quantitative Isomerization and Long Thermal Half-Lives. *Journal of the American Chemical Society* **2014**, *136*, 11878–11881.

35. Kolarski, D.; Szymanski, W.; Feringa, B. L., Two-Step, One-Pot Synthesis of Visible-Light-Responsive 6-Azopurines. *Organic Letters* **2017**, *19*, 5090–5093.

36. For 2-, 5- and 6-phenylazoindole: *unpublished work*; For 3-phenylazoindole see Simeth, N. A.; Crespi, S.; Fagnoni, M.; König, B., Tuning the Thermal Isomerization of Phenylazoindole Photoswitches from Days to Nanoseconds. *Journal of the American Chemical Society* **2018,** *140*, 2940–2946.

37. Jacquemin, D.; Wathelet, V.; Perpète, E. A.; Adamo, C., Extensive TD-DFT Benchmark: Singlet-Excited States of Organic Molecules. *Journal of Chemical Theory and Computation* **2009**, *5*, 2420–2435.

38. Jacquemin, D.; Perpète, E. A.; Scuseria, G. E.; Ciofini, I.; Adamo, C., TD-DFT Performance for the Visible Absorption Spectra of Organic Dyes: Conventional versus Long-Range Hybrids. *Journal of Chemical Theory and Computation* **2008**, *4*, 123–135.

39. Rillema, D. P.; Stoyanov, S. R.; Cruz, A. J.; Nguyen, H.; Moore, C.; Huang, W.; Siam, K.; Jehan, A.; KomReddy, V., HOMO-LUMO Energy Gap Control in Platinum(ii) Biphenyl Complexes Containing 2,2[prime or minute]-bipyridine Ligands. *Dalton Transactions* **2015,** *44*, 17075–17090.

40. Adamo, C.; Jacquemin, D., The Calculations of Excited-State Properties with Time-Dependent Density Functional Theory. *Chemical Society Reviews* **2013**, *42*, 845–856.

41. Löfås, H.; Orthaber, A.; Jahn, B. O.; Rouf, A. M.; Grigoriev, A.; Ott, S.; Ahuja, R.; Ottosson, H., New Class of Molecular Conductance Switches Based on the [1,3]-Silyl Migration from Silanes to Silenes. *The Journal of Physical Chemistry C* **2013,** *117*, 10909–10918.

42. Cossi, M.; Rega, N.; Scalmani, G.; Barone, V., Energies, Structures, and Electronic Properties of Molecules in Solution with the C-PCM Solvation Model. *Journal of Computational Chemistry* **2003**, *24*, 669–681.

43. Hay, P. J.; Wadt, W. R., Ab initio Effective Core Potentials for Molecular Calculations. Potentials for K to Au Including the Outermost Core Orbitals. *The Journal of Chemical Physics* **1985**, *82*, 299–310.

44. Peach, M. J. G.; Benfield, P.; Helgaker, T.; Tozer, D. J., Excitation Energies in Density Functional Theory: An Evaluation and a Diagnostic Test. *The Journal of Chemical Physics* **2008**, *128*, 044118.

45. Calbo, J.; Weston, C. E.; White, A. J. P.; Rzepa, H. S.; Contreras-García, J.; Fuchter, M. J., Tuning Azoheteroarene Photoswitch Performance through Heteroaryl Design. *Journal of the American Chemical Society* **2017**, *139*, 1261–1274.

II. PHOTOCHROMIC REDOX COFACTORS

Chapter II

Success was hard to come, and when it did, it was much appreciated. But the effort seemed to be out of proportion to the reward.

Y. Martel – *Life of Pi*

II.1 Photochromic Coenzyme Q Derivatives: Switching Redox Potentials with Light

Abstract

Coenzyme Q is an important redox cofactor involved in a variety of cellular processes, and thus found in several cell compartments. We report a photochromic derivative of coenzyme Q that combines the molecular structures of the redox active cofactor and a photochromic dye. Light irradiation triggers an electronic rearrangement reversibly changing the redox potential. We used this effect to control the intermolecular redox reaction of the photochromic coenzyme Q derivative with dihydropyridine in solution by light irradiation. On mitochondria, the altered redox properties showed an effect on the respiratory chain. The experiments demonstrate that the redox reactions can be initiated inside the system of interest through irradiation with light and the accompanied photoisomerization.

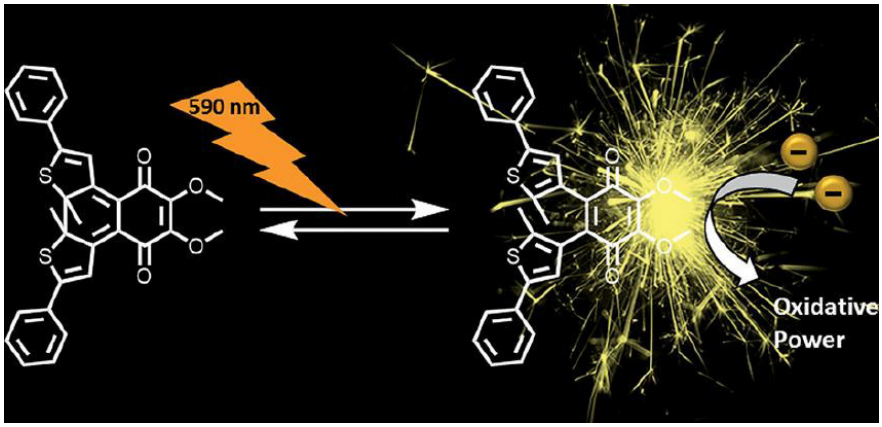

This section was published as:

Simeth, N. A.; Kneuttinger, A. C.; Sterner, R.; König, B., Photochromic coenzyme Q derivatives: switching redox potentials with light. *Chemical Science* **2017**, *8* (9), 6474–6483. Reprinted with Permission from the Royal Society of Chemistry.

Author contributions

NAS performed all synthesis and characterization of the compounds, performed light-triggered oxidation experiments, and wrote the manuscript beside of the biochemical investigations. ACK performed biochemical studies and wrote that part of the manuscript. RS and BK supervised the project.

II.1.1 Introduction

The concept of employing small, light-responsive molecules to gain a spatiotemporal control over biological processes is known for a long time.[1] However, in recent years, the field, now often termed as *photopharmacology*, expanded rapidly.[2-5] Photochromic inhibitors based on azo dyes or bridged diarylethenes (DAEs) were used to modulate enzymatic activities.[6-11] Moreover, switchable antibiotics[12-14] and molecules, which cause light-induced apoptosis of single cells in tissue[15] illustrate the potential of the approach. Using light as an external stimulant adds an extrinsic parameter determining the selectivity of the compound.[3] Furthermore, light is non-invasive, easy to apply, and offers an inimitable spatiotemporal control over the process of interest.[1] Both azobenzenes and DAEs interconvert upon light irradiation between two structural isomers, which differ strongly in their physical properties, and thus also in their activity towards biomolecules.[1, 2] DAEs generally show good photoconversion, fatigue resistance, and thermal stability. They are thus frequently used as photochromic tools in biological contexts.[1, 16]

While several analogues of DNA bases,[17, 18] fatty acids, and phospholipids[19-23] have been reported, the number of photoswitchable derivatives of enzymatic cofactors such as ATP, NAD(P)H, FAD, CoQ, is small. Recently, Wilson *et al.* presented a photochromic analogue of pyridoxal-5'-phosphate,[24] and furthermore ATP has been derivatized into a light-controllable mimetic.[25] However, redox cofactors, a likewise widely spread family of coenzymes, have not been considered so far.[26] They are involved in many cellular processes, and therefore found in various cellular compartments. They facilitate *e.g.* transhydrogenation reactions catalyzed by oxidoreductases by either accepting or providing electrons.[27] In general, they act as an activated electron carrier for the oxidation of metabolites in aerobic organisms. An important auxiliary molecule involved in this process is Coenzyme Q (CoQ), also called ubiquinone. The core part of the molecule, the benzoquinone ring, facilitates the molecule to serve as a two-electron carrier – interconverting between a ubiquinone and an ubiquinol form. Due to its large, nonpolar, poly-isoprenyl chain, the coenzyme is able to diffuse within lipophilic membranes.[28] Besides its function as an auxiliary in metabolism,[26] it also acts as an antioxidant,[29, 30] regulates the physiochemical properties of membranes,[31] and modulates the amount of β-integrins on the surface of blood monocytes.[32]

As most of the cofactors, redox cofactors are not only present in one single cellular compartment, but widely distributed. Thus, targeting them with conventional strategies of medicinal chemistry would cause an uncontrollable impact on all cells of the organism and it would be difficult to regulate the effect in the desired fashion. However, using a

photopharmacological strategy, we are able to activate the agent specifically at the favored site for a defined time.

For our CoQ mimetic, we merged a redox-active benzoquinone moiety with two substituted thiophene moieties, building a photochromic DAE. Through irradiation with light, the 6π-system formed by the three parts undergoes an electrocyclic ring-closing reaction. The ring-closure changes color, shape, and electronic properties of the molecule. Most applications of photochromic compounds aim at an altered structure with different physiological effect, but only few studies utilized the different electronic properties of both photoisomeres.[24, 33] However, we focus on changing the redox potentials of the benzoquinone moiety through electronical changes upon irradiation. This specific mode of action may allow in principle to use one cofactor mimetic to target all related enzymes even if the active site differs, as the molecule's mode of action does not rely on its spatial interaction, but its redox state. Moreover, benzoquinone motifs have been considered as a scaffold by Deng *et al.* and Katsumura *et al.* and were investigated regarding their switching behavior.[34, 35]

Light- and electronic-modulated switches have already been a subject of physical-electrochemical as well as spectroscopic studies,[36-41] but to the best of our knowledge, have never been considered as a the role of a cofactor in biological context. Thus, we present the first photochromic molecule that has the potential to serve as a redox cofactor.

II.1.2 Results and Discussion

II.1.2.1 Design

To modulate the redox properties of Coenzyme Q by light irradiation, we designed the photochromic derivatives **1a**^{o} and **1b**^{o} as depicted in Figure 1 by merging a redox-active benzoquinone with thiophene moieties to build a DAE. This allows the molecule to accept electrons for redox reactions just in one photoisometic state. Upon irradiation by light of 254 nm, the redox-switch undergoes a 6π-conrotatory electrocyclic ring closure to the closed photoisomer (**1a**^{o}**,b**^{o} to **1a**^{c}**,b**^{c}, Figure 1). The rearrangement delocalizes one double bond of the redox-active moiety in the conjugated backbone of the closed switch. The "closed photoisomer" should be thus mostly redox-inactive as the quinone system was intercepted. In contrast, the "open form" should be able to undergo oxidation reactions similar to unaltered CoQ (**1a**^{o}**,b**^{o} to **1a**^{o,red}**,b**^{o,red}, Figure 1). The methoxy groups of the benzoquinone moiety (**1b**^{o}) are known to be crucial for interaction at the binding site of CoQ-consuming proteins, and are therefore retained in the model compound (Figure 1).[42]

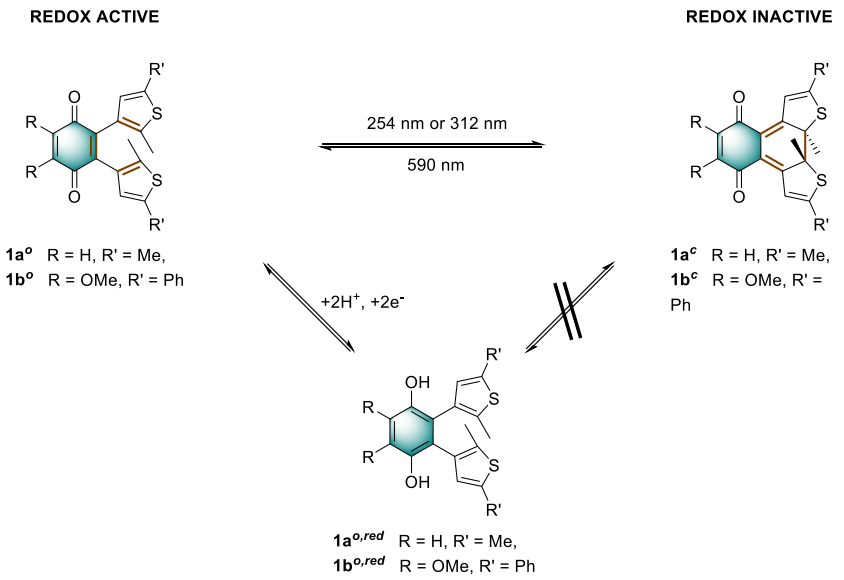

Figure 1: General principle of switchable redox potentials based on photochromic CoQ mimetics.

II.1.2.2 Synthesis of the Photochromic Coenzyme Q Derivatives

The key step of the synthesis towards compounds **1a**^{o} and **1b**^{o} was a Stille cross-coupling reaction of **5a** or **5b** onto quinone **8a** or **8b**, respectively (Scheme 1). The thiophene precursors (**5a** and **5b**) were easily synthesized from 2,5-dimethyl thiophene (**2**) or 2-methyl thiophene (**3**), respectively, partly following known protocols.[34, 43] After bromination and arylation through Suzuki-Miyaura cross-coupling the pre-functionalized thiophenes **5a** and **5b** were treated with ^{t}BuLi and subsequently $SnClBu_3$ yielding organo stannates **6a** and **6b**.[35] The quinone **8b** was synthesized through oxidation of **7** using Fenton's reagent in acetic acid.[44] Benzoquinone (**8a**) as well as 2,3-dimethoxy benzoquinone (**8b**) were then halogenated utilizing bromine under oxidative conditions.[45] The final step was performed employing $Pd(PPh_3)_4$ and elevated temperatures for 16 h to give **1a**^{o} and **1b**^{o} in acceptable yields (10% or 29%, respectively).[34]

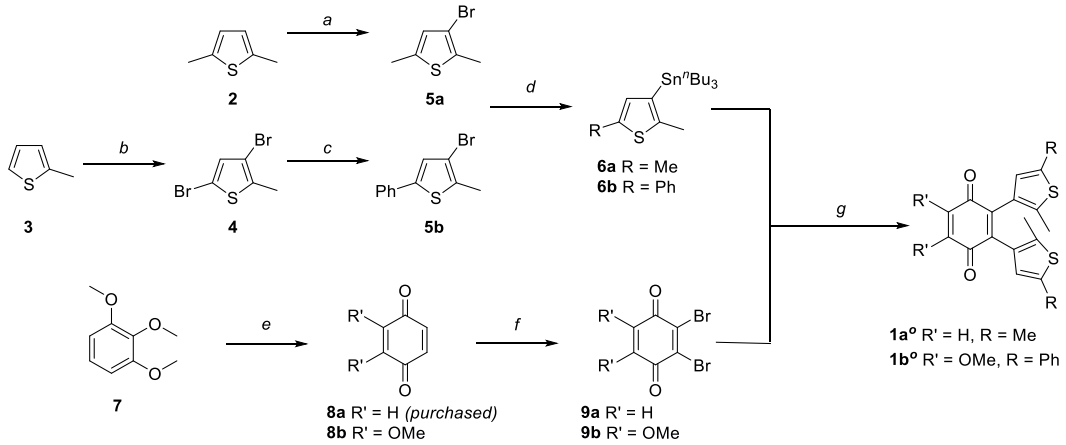

Scheme 1: Synthesis of photochromic Coenzyme Q mimetics 1a^o and 1b^o: *a*: NBS, AcOH, 2 h, 66%. *b*: Br_2, AcOH, 18 h, r.t., 69%. *c*: $PhB(OH)_2$, $Pd(PPh_3)_2Cl_2$, $AsPh_3$, Na_2CO_3 (2 M, aq), THF, 16 h, 80 °C, 80%. *d*: ^{s}BuLi, $SnBu_3Cl$, dry THF, -78 °C to r.t., quantitative. *e*: $K_3[Fe(CN)_6]$, H_2O_2, AcOH, r.t., 16 h, 28%. *f*: Br_2, H_2SO_4, Et_2O, 1 h; then Ag_2O, Et_2O, 1 h, 30% for 9a; 55% for 9b. *g*: $Pd(PPh_3)_4$, CuI, dry toluene, 85 °C (1a^o) or 115 °C (1b^o), 16 h, 10% (1a^o) or 29% (1b^o).

The open form of the photochromic quinones (**1a**^{o} and **1b**^{o}) were converted into the corresponding closed isomers (**1a**^{c} and **1b**^{c}) through irradiation with UV light (Scheme 2). Compound **1a**^{o} did not tolerate the long-term irradiation and decomposed. However, closed isomer **1b**^{c} was isolated from reversed phase column chromatography (13% yield).

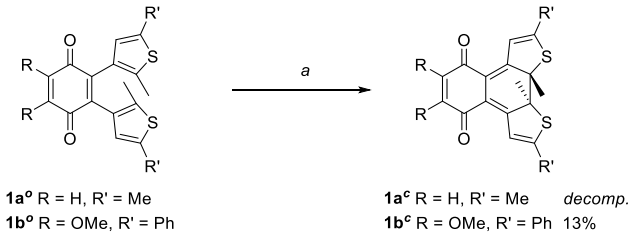

Scheme 2: Synthesis of closed isomers 1a^c and 1b^c. a: 312 nm, DMSO, r.t., 3h.

II.1.2.3 Spectroscopic, electrochemical and spectroelelectrochemical studies

The photoisomerization of compound **1a**^{o} and **1b**^{o} was investigated in toluene, DMSO, DCM, dioxane and MeCN. Unfortunately, compound **1a**^{o} did not tolerate irradiation with UV light (312 nm) and resulted in decomposition into uncharacterized products (for spectra see Appendix, Section A.II.1.1.). However, compound **1b**^{o} switches in polar and non-polar solvents (Figure 2 and in Section A.II.1.1.). Upon irradiation with UV light (312 nm or 254 nm, respectively), the color of the solution changed from bright red to blue. The photoisomerization was monitored by UV/Vis spectroscopy; associated spectra in DMSO are depicted exemplary in Figure 2 (further spectra are shown in the A.II.1.1.). New absorption maxima at 410 nm and 594 nm show the formation the photoisomer; the isosbestic point at 323 nm indicates a distinct two-compound isomerization. Photostationary

states (PSSs) were determined by HPLC measurements. The PSS for the closing reaction was determined to be 52% in DMSO, whereas the opening reaction was achieved quantitatively through irradiation with orange light (590 nm, 30µM, 2 min). A twisted intramolecular electron transfer (TICT) as reported for other DAE derivatives bearing an electron-acceptor core moiety rationalizes the generally rather low PSS for the closing reaction.[46, 47] Thus, we focused on the opening reaction for further experiments, which generates a redox active compound from a redox silent molecule upon irradiation.

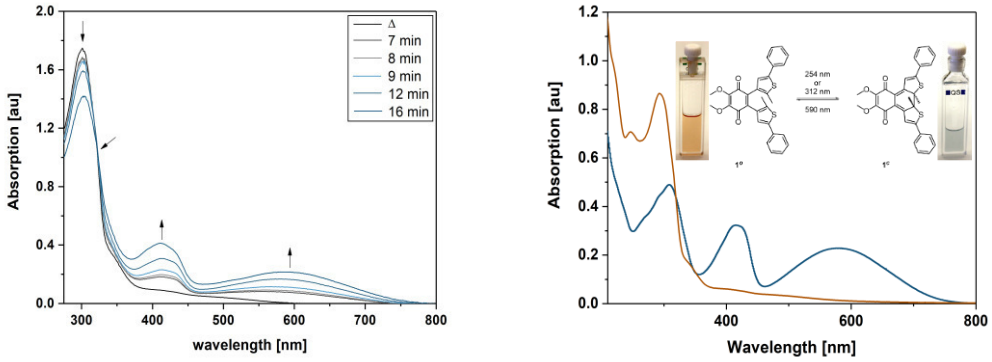

Figure 2: *left*: Photoisomerization of 1b^{o} in DMSO (30 µM, irradiation with 312 nm). *right*: Spectra of isolated photoisomers 1b^{o} (red line, maxima at 247 nm and 297 nm) and 1b^{c} (blue line, maxima at 307 nm, 415 nm and 583 nm) in MeCN (isosbestic point at 317 nm). For further details see Appendix, Section A.II.1.1.

To determine the redox potential of CoQ derivatives **1b^{o}** and **1b^{c}**, we performed cyclic voltammetric (CV) studies. The compounds included in the study are depicted in Chart 1. Compound **12** was hereby synthesized from commercially available **11** similar to **9b** in one step. All 1,4-benzoquinone derivatives (**9b**, **10**: Figure 3, C and D; **8b**, **9a**, **11**, **12**, A.II.1.2.) including the open photochromic compound **1b^{o}** (Figure 3, A) show similar behavior as CoQ_{10} (Figure 3, D). Specifically, all compounds exhibit two well-defined, fully reversible reduction signals. This finding is in agreement with previous investigations on benzoquinones. The first step corresponds to the formation of a semiquinone radical, while the second step corresponds to the formation of a dianion (or hydroquinone if protons are present).[48] The potentials of the molecules are predestined by the substitution pattern of the respective compound and are summarized in Table 1. The substituents of the benzoquinone core affect the reduction potential values. With an increasing number of electron-withdrawing bromine substituents the reductions occur at less negative potentials. In contrast to all other investigated para-benzoquinones, the closed isomer **1b^{c}** generates three – not two – cathodic waves as well as one anodic one (Figure 3, B), which are reproducible (*cf.* Section

A.II.1.2.) Also, the intensities of the respective waves differ, and hence indicate that redox steps involve a different number of electrons.

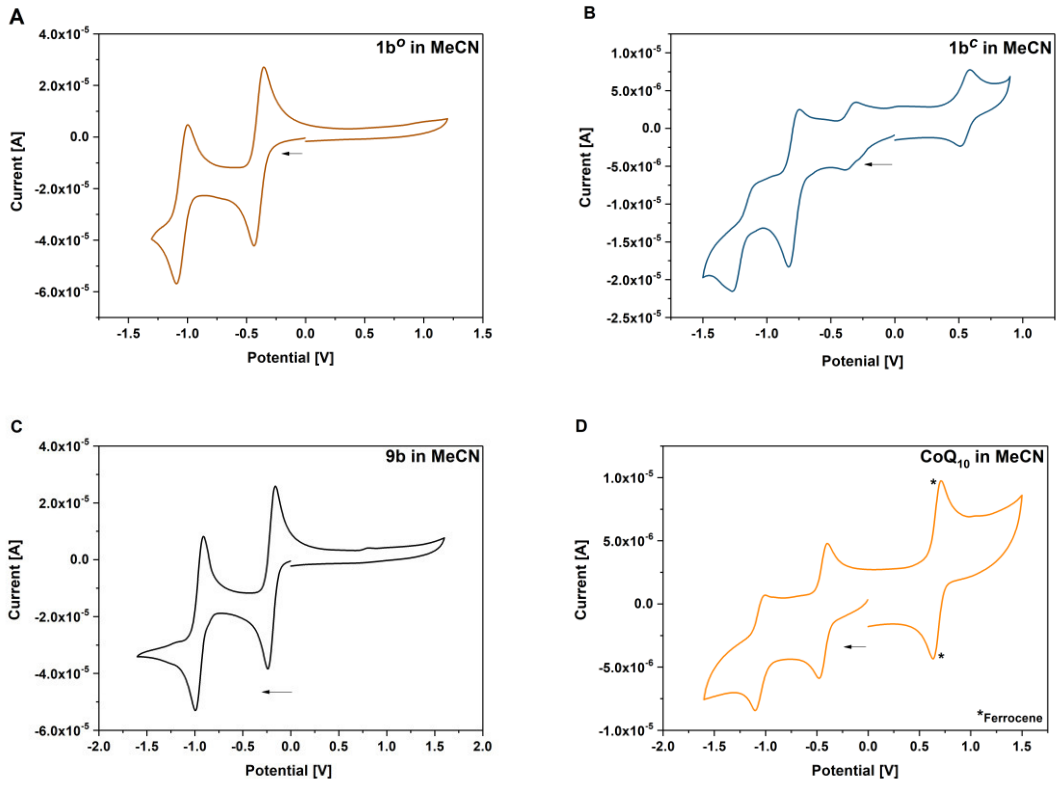

Figure 3: Cyclic voltammogram of compounds 1b^{o} (A, 30 µM), 1b^{c} (B, 2 µM), 9b (C, 30 µM), and CoQ$_{10}$ (D, 2 µM, *ferrocene (0.005M) as internal standard) in MeCN + 0.1M Bu$_4$NBF$_4$.

Next, we investigated the redox states by spectroelectrochemistry, using several different 1,4-benzoquinone derivatives for comparison (Chart 1).

Exemplary, changes of the UV/Vis spectra of compounds **1b**^{o}, **1b**^{c}, and **9b** during one cathodic potential sweep are depicted in Figure 4 (Difference spectra of **1b**^{o}, **1b**^{c}, and **9b** as well as UV/Vis spectra of **9a**, **10**, **11** and **12** can be found in the A.II.1.2.). All para-benzoquinones – besides the closed photoswitch **1b**^{c} – show similar absorption bands with the changing potential; without applying an external potential, the benzoquinones show an absorption band at around 280–300 nm depending on their substitution pattern. During the first reduction step corresponding to the formation of the semiquinone intermediate,[48] this band decreases to give rise to two new bands– one at around 310 nm and a broader one at around 410 nm exhibiting a well-defined double maximum, which is also present in the case of **1b**^{o} and CoQ$_{10}$, but not so well-defined.[50] For CoQ$_{10}$, this might be due to solubility issues in MeCN. The second cathodic wave is the formation of the dianion,[48] generating a novel band at around 370 nm, whereas the two bands of the semiquinone radical decrease again.

All spectra show clear isosbestic points indicating a distinct two-compound process. The reduction process is fully reversible and can be repeated over several cycles.

Table 1: Redox potentials of benzoquinone derivatives 8b, 9a, 9b, 1b^o, 1b^c, CoQ_{10}(10), 11, and 12 (*cf.* Chart 1) vs. SCN[49] (determined by CV measurements in MeCN + 0.1M Bu_4NBF_4 using ferrocene (0.005M) as internal standard).

Compound	Potentials vs. SCN [V][49]
1b^o	-0.58; -1.23
1b^c	+0.83; -0.24; -0.55; -1.39
8b	-0.66; -1.37
9a	-0.24; -0.97
9b	-0.35; -1.1
CoQ_{10} (**10**)	-0.77; -1.39
11	-0.69; -1.34
12	-0.54; -1,27

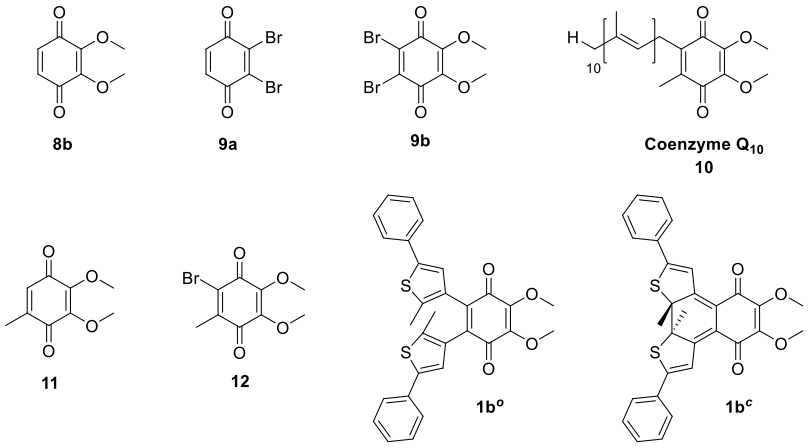

Chart 1: 1,4-Benzoquinones included in the electrochemical studies.

In contrast to the other investigated benzoquinones, the closed photoswitch **1b^c** showed a slightly different spectrum in the beginning due to the attached chromophore. The molecule exhibits maxima at 307 nm, 415 nm, and 583 nm. During the first reduction step, the maximum at 415 nm broadens, while the other maxima remain unchanged. Changes are more drastic as the second reduction occurs; the long-wave band around 580 nm fully decreases, the band at around 410 nm broadens even more and the short-wave band at around 300 nm experiences a hypsochromic shift. While the last reduction step takes place, the band around 410 nm is also hypsochromically shifted.

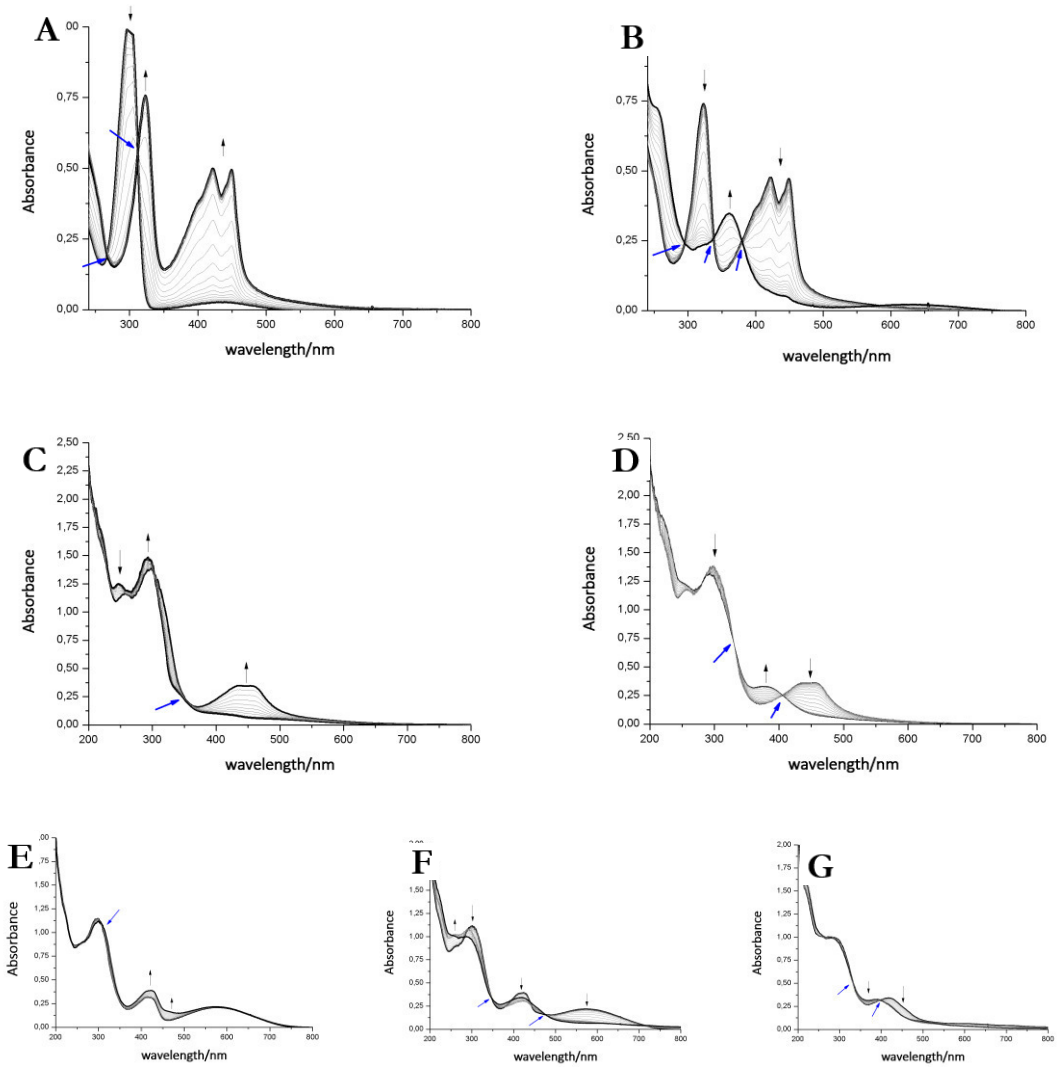

Figure 4: Spectroelectrochemical studies of compounds 9b (A**: first wave,** B**: second wave), 1b^{o} (**C**: first wave,** D**: second wave) and 1b^{c} (**E**: first wave,** F**: second wave,** G**: third wave). One spectra-set correlates with one cathodic wave. Black arrows indicate increase/decrease of maxima; blue arrows assign isosbestic points.**

Although there are similarities to the non-photochromic benzoquinones and to **1b^{o}**, the spectroelectrochemical studies clearly reveals a different behavior of **1b^{c}**. Especially, the well-pronounced decrease of the long-wave band around 580 nm, which can be assigned to the conjugated thiophene backbone in the chromophore of the photoswitch,[16] indicates a redox process in this moiety of the molecule. However, this appears rather counterintuitive, as though impaired the benzoquinone moiety still should be more prompt to reduction. Yet very recently, Saito *et al.* report EPR and computational studies on a related molecule and could show the formation of a radical anion similar to a semiquinone.[19h] A charge delocalization over the whole molecule is likely to be allowed through two nearly degenerated LUMO and LUMO+1. Thus, we suggest that the second reductive wave also has semiquinone character but delocalized over the whole molecule (loss of long-wave band

around 580 nm, which is associated with the closed ring in DAEs). The first and the third reduction potential show less prominent changes in UV/Vis and are yet to be assigned.
Overall, the cyclovoltammetric and spectroelectrochemical studies revealed a different redox behavior for both photoisomers of **1b.** Spectroscopic investigations revealed that **1b**^{o} and **1b**^{c} can be in fact interconverted into each another through light but the PSS values of the closing reaction in all investigated solvents is rather low (maximum 52% in DMSO). Also, the speed of both the opening and the closing reaction are in the minute-range. However, both characteristics are crucial for many redox mediated reactions, especially in bio-systems as *e.g.* enzymatic reactions take place in the milli-second range or are even faster. Therefore, compound **1b** can only be considered for a limited set of experiments up to now. The investigated redox reactions should also to be in the minute range or should not mind diffusion of the cofactor mimetic during irradiation. The quantitative opening reaction can be used to provide a redox partner within a system upon irradiation applying the photo-switching process in a photo-cage fashion; back-switching, however, would be not quantitative. Taking these properties into account, we investigated the applicability of the redox switch as a tool in reactions.

II.1.2.4 Photoactivated Oxidation Reactions

In the mitochondrial respiratory chain, CoQ_n oxidizes NADH to NAD^+ in Complex I (NADH-Q oxidoreductase).[26] Thus, we decided to let our photochromic CoQ mimetic **1b**^{o} react with Hantzsch ester **13**, which belongs to the same family of dihydropyridines as NADH, and hence serves as an excellent test substrate for a photoactivated oxidation reaction.

A solution of each photoisomer (5 mM, **1b**^{o}, **1b**^{c}) was treated with a solution of Hantzsch ester **13** (12 mM) in DMSO and reacted at ambient temperature in the dark. We took samples in certain time intervals and analyzed them through analytical HPLC (UV/Vis detection at 317 nm which equals PSS, HPLC traces see Appendix, Section A.II.1.5.) to follow the consumption and the generation of the respective redox pairs. The formation of **1b**^{o,red} from **1b**^{o} and **1b**^{c}, respectively, through reduction with **13** is depicted in Figure 6A (normed areas of HPLC traces). The open photoisomer **1b**^{o} is rapidly reduced by Hantzsch ester **13** (red line, Figure 6A), whereas the closed one **1b**^{c} shows almost no conversion to **1b**^{o,red} or any other product (blue, Figure 6B, minor background reaction results from thermal ring-opening). Thus, compound **1b**^{c} is unreactive before irradiation.

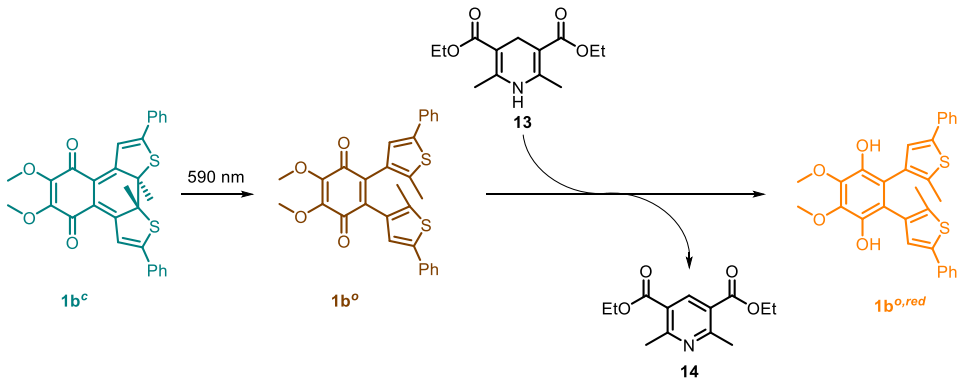

Figure 5: Photoactivated redox reaction between photochromic CoQ derivative 1b^{o} and an NADH model- Hantzsch ester 13. Compound 1b^{o} is generated in situ from closed isomer 1b^{c} via irradiation.

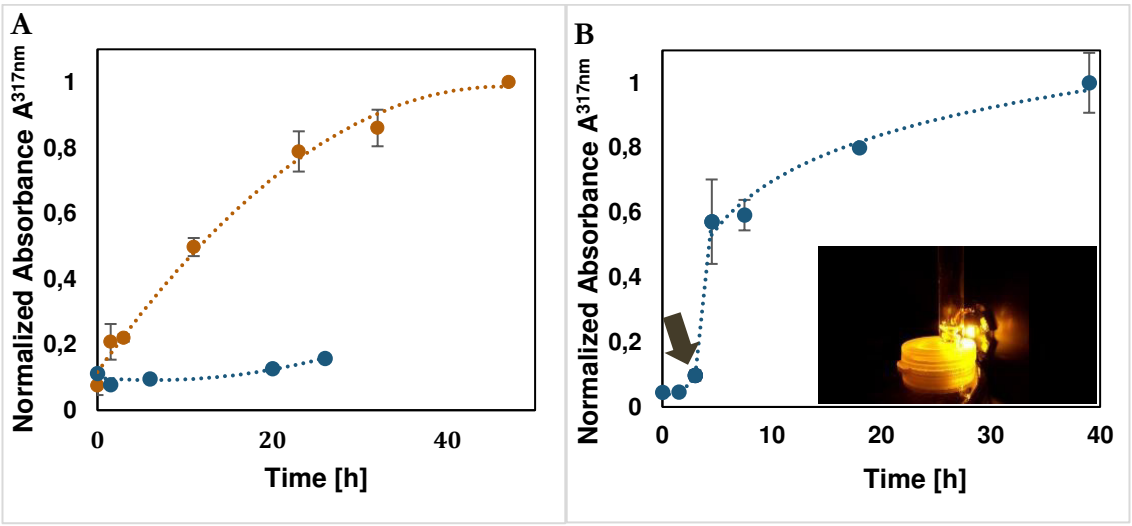

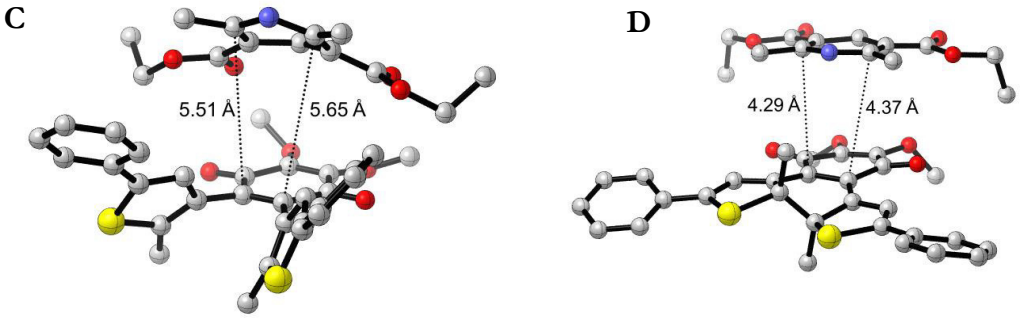

Figure 6: A**: Formation of 1b^{o,red} via reduction of 1b^{o} (5 mM, DMSO, red line) or 1b^{c} (5 mM DMSO, blue line) through dihydropyridine derivative, Hantzsch ester 13 monitored through HPLC-UV/Vis.** B**: Formation of 1b^{o,red} after photoactivation (arrow) of 1b^{c} (10 mM, DMSO) after three hours of initial reaction time with a 590 nm single-spot LED for 10 min (picture). Values are typically the means ± SEM of three individual experiments.** C**: Optimized geometry of the 1b^{o}–13 adduct.** D**: Optimized geometry of the 1b^{c}–13 adduct (All the distances are reported in Ångstroms).**

Then, we investigated whether the formation of **1b**^{o,red} can be triggered through light-activation of **1b**^{c}. The closed isomer (10 mM, DMSO) was treated with Hantzsch ester **13** (12 mM) and left stirring in the dark for three hours. Subsequently, the solution was irradiated with a 590 nm single-spot LED for 10 min (picture, Figure 6) to be quantitatively converted into **1b**^{o}. HPLC analysis confirmed a full conversion into only the open photoisomer and also an immediately initialized reduction into **1b**^{o,red} (Figure 6B, for HPLC traces see Appendix, A.II.1.5.). The initial slope of the reaction seems to be larger than utilizing **1b**^{o}. This could be due to a pre-aggregation of **1b**^{c} and the Hantzsch ester. A preliminary computational analysis was carried out in order to unravel the presence of an interaction between both photoisomers and Hantzsch ester **13**. The DFT method at the B3LYP/6-31G(d) level of theory (*cf.* Sections A.II.1.7. and A.II.1.10.).[28] We decided to follow a modification of an approach already found in the literature[29] to gain qualitative insight on the presence of a non-covalent π stacking between the two photoisomers of **1b** and **13**.

From an energetic point of view, the closed form appeared to be more stable (*ca.* 7 Kcal mol^{-1}), *cf.* Appendix, Section A.II.1.7.) due to the interaction with **13**. Moreover, the geometry of the optimized structures clearly shows the Hantzsch ester resides in closer proximity to **1b**^{o} than to **1b**^{c} (see Figure 6C and D).

In summary, we can conclude that the intermolecular reaction does relay on the respective redox potentials of the compounds indicating that we are truly able to change redox potentials of **1b** by photo-induced ring-opening of the electronically caged closed photoisomer.

II.1.2.5 Photoactivated mitochondrial reduction of 2,6-dichlorophenol indophenol

In order to test the effect of **1b**^{c} and **1b**^{o} on a natural system, mitochondria were isolated from the wildtype yeast strain BY4742.[30] CoQ_n serves as electron transmitter in the respiratory chain of mitochondria from Complex II (succinate dehydrogenase) to Complex III (cytochrome-C oxidoreductase). By using 2,6-dichlorophenol indophenol (DCIP) as electron acceptor instead of Complex III, CoQ analogues can be tested on isolated mitochondria.[31] The reduction of DCIP with **1b**^{c} and **1b**^{o} was followed spectrophotometrically (Figure 7), continuously for 30 min or interrupted by irradiation with 590 nm, in order to switch the closed **1b**^{c} into the open, more active **1b**^{o} isomer.

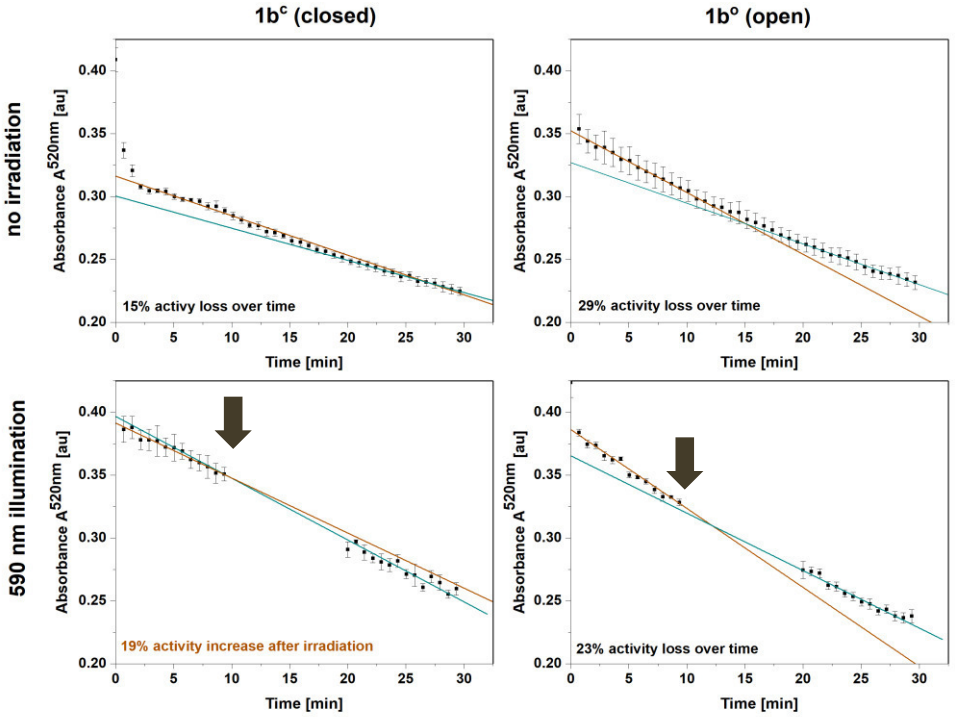

Figure 7: Reduction of 2,6-dichlorophenol indophenol (DCIP) by mitochondria over time monitored spectrophotometrically at 520 nm. 1b^c and 1b^o assays were carried out continuously (upper panels) or interrupted by irradiation at 590 nm as indicated by arrows (lower panels). The data were fitted for linear activity at 0-10 min (red) and 20-30 min (blue). Whereas activity decreases with time without irradiation of either the closed or the open form as well as after irradiation of the open form (blue slope < red slope), it increases after irradiation of the closed form (blue slope > red slope).

For both isomers of our CoQ mimetic **1b**, reduction of DCIP could be observed in the continuous assay (Figure 7, *no irradiation*) where a fast initial rate (red) was followed by a lower rate (blue). Comparing the initial rate of DCIP reduction with **1b^c** and **1b^o**, the open isomer is only approximately 70% more active than the closed isomer. We assume that this seemingly high activity of the closed isomer is due to residual activity of bound natural CoQ_n, which we cannot exclude in isolated mitochondria.

To emphasize the activity difference of **1b^c** and **1b^o**, we irradiated both isomers after 10 min reaction time (Figure 7, *590 nm irradiation*). The activity for the open isomer decreased as in the non-irradiated assay (blue slope < red slope). However, the rate for the closed isomer after irradiation increased (blue slope > red slope) indicating that the reaction was restarted. Thus, despite the complex system of mitochondria, in which CoQ is deployed in several reactions, we were able to see an activation of the DCIP reduction after irradiation of **1b^c**.

Consequently, the photochromic CoQ mimetic **1b** cannot only replace CoQ_n in a natural system, but can also activate the same after irradiation.

II.1.3 Conclusion

In conclusion, we have developed a photochromic CoQ derivative (**1b**) combining a redox active and a photochromic moiety in one molecule. We could show by cyclic voltammetry that the redox potential of both photoisomers differs, and thus can be altered through photoisomerization. In addition, the mode of action of cathodic waves in spectroelectrochemical studies was examined indicating the nature of the reductive steps. Furthermore, we could show that the closed form of the switch (**1b**^{c}) is redox inactive in a reaction with Hantzsch ester, a member of the dihydropyridine family, and has to be photoactived to its open isomer (**1b**^{o}) to be redox active. This proves that the reactivity of **1b** relies on the altered redox potentials of the two photoisomers and is thus controllable through electronic changes rather than by conformational and geometry changes as seen in most other studies. Finally, we were able to show that treatment of isolated mitochondria with both photoisomers led to a difference of approximately 70% of the velocity of DCIP reduction. We could further show that the closed isomer **1b**^{c} can restart the DCIP reduction upon activation through irradiation. Thus, we present the first photochromic redox cofactor that operates in a complex, biological context and were able to convert the formally caged closed form of the mimetic into an active redox probe inside the system. However, reversibility of the redox reaction could not yet be achieved due to low PSS values and insufficiently fast reaction rates. Optimization of both issues have to be addressed in further research to finally generate a tool facilitating the control of redox-dependent biological functions in cells by light.

II.1.4 Experimental Section

*2,3-Bis(2,5-dimethylthiophen-3-yl)cyclohexa-2,5-diene-1,4-dione (**1a**)*

A crimp top vial was equipped with **8a** (97 mg, 0.36 mmol), **6a** (591 mg, 1.47 mmol), CuI (30 mg, 0.16 mmol) and dry toluene (7 mL) under nitrogen. The vial was deaerated through argon bubbling for five minutes. Then $Pd(PPh_3)_4$ (173 mg, 0.15mmol) was added and the vial was sealed and heated to 85 °C for 16 h. The reaction mixture was cooled to room temperature and the solvent was removed *in vacuo*. The residue was dissolved in EtOAc (5 mL), a saturated KF solution (aq, 5 mL) was added and the mixture was stirred for one hour. The reaction mixture was filtered to remove precipitated Bu_3SnF and the organic layer

was isolated. The aqueous layer was extracted with EtOAc (2 x 10 mL). The combined organic layers were dried over $MgSO_4$ and the solvent was removed *in vacuo*. The crude product was purified through MPLC (0 to 20% EtOAc in petroleum ether). The pure product was isolated as brown solid.

Yield: 12 mg, 0.04 mmol, 10%. ^{1}H-NMR: (400 MHz, Chloroform-*d*) δ =6.76 (s, 2H), 6.63 (d, *J* = 1.3 Hz, 2H), 2.46 (s, 6H'), 2.34 (s, 6H).^{13}C-NMR: (101 MHz, Chloroform-*d*) δ =146.4 (s, q) , 137.6 (s, q), 134.8 (s, q), 132.3 (s, q) , 126.9 (s, +), 123.4 (s, q), 116.4 (s, +), 15.2 (s, +) , 13.8 (s, +). ESI-MS: calculated: 328.0592. found: 331.08 (reduced form; MH^+, 100%). HR-MS: found: 329.0665 (MH^+, 100%). R_f: 0.85 (30% EtOAc in petroleum ether).

*2,3-Dimethoxy-5,6-bis(2-methyl-5-phenylthiophen-3-yl)cyclohexa-2,5-diene-1,4-dione (**1b^o**)*

Compounds **5b** (1.42 g, 3.97 mmol), **8a** (522 mg, 1.59 mmol) and CuI (30 mg, 0.16 mmol) were dissolved in dry toluene (25 mL) under Argon atmosphere. The solution was deaerated through Argon bubbling for 5 min and $Pd(PPh_3)_4$ (183 mg, 0.16 mmol) was added. The vial was sealed and the reaction mixture was refluxed for 16 h. The reaction mixture was cooled to room temperature and the solvent was removed *in vacuo*. The residue was dissolved in EtOAc (10 mL), a saturated KF solution (aq, 10 mL) was added and the mixture stirred for one hour. The reaction mixture was filtered to remove precipitated Bu_3SnF and the organic layer was isolated. The aqueous layer was extracted with EtOAc (2 x 20 mL). The organic layers were combined and dried over Na_2SO_4. The volatiles were removed *in vacuo* and the crude product was purified through MPLC (0 to 55% EtOAc in petroleum ether) to give a red solid. For biological testing the sample was further purified through reversed phase MPLC (C18, 65 to 100% MeCN in H_2O/0.05% TFA).

Yield: 560 mg, 1.04 mmol, 29%. ^{1}H-NMR: (600 MHz, Chloroform-*d*): δ =7.44 – 7.40 (m, 4H, phenyl), 7.34 – 7.28 (m, 4H), 7.24 (d, *J* = 7.3 Hz, 4H, phenyl), 6.83 (s, 2H, thiophene), 4.11 (s, 6H, methoxy), 2.07 (s, 6H, methyl). ^{13}C-NMR: (151 MHz, Chloroform-*d*): δ =183.2 (+), 144.6 (+), 140.3 (+), 139.6 (+), 138.00 (+), 134.0 (+), 130.1 (+), 128.8 (+), 127.3 (+), 125.7 (+), 125.3 (+), 61.4 (+, methoxy), 14.9 (+, methyl). FTIR: $\tilde{\nu}$(cm^{-1}): 2937 (w), 1655 (s), 1592 (s), 1256 (m), 1070 (m), 757 (s), 693 (s). HR-MS: calculated: 512.1116; found: 513.1187 (MH^+, 100%). Melting point: 137 °C. R_f: 0.65 (50% EtOAc in petroleum ether).

*(10a,10b)-5,6-Dimethoxy-10a,10b-dimethyl-2,9-diphenyl-10a,10b-dihydronaphtho[2,1-b:3,4-b']dithiophene-4,7-dione (**1b^c**)*

Compound **9b^o** (29 mg, 0.06 mmol) was dissolved in DMSO (5 mL) and effused into a Petri dish. The solution was irradiated for 4 h with a 312 nm hand-lamp and then directly injected

onto a reversed phase column. The compound could be isolated through elution with MeCN in H_2O/0.05% TFA (reversed phase MPLC, C18, gradient 65 to 100%) to give a blue solid. Yield: 9 mg, 0.01 mmol, 13%. ^{1}H-NMR: (400 MHz, Chloroform-*d*) δ=8.24 (s, 2H, thiophene), 7.83 – 7.61 (m, 4H, phenyl), 7.45 (dd, *J* = 5.2, 1.9 Hz, 6H, phenyl), 4.08 (s, 6H, methoxy), 2.09 (s, 3H, methyl). HR-MS: calculated: 512.1116; found: 513.1185 (100%).

*3-Bromo-2,5-dimethylthiophene (**5a**)*

Compound **2** (2.0 mL, 17.54 mmol, 1.0 eq) was dissolved in glacial acetic acid (50 mL). NBS (3120 mg, 17.54 mmol, 1.0 eq) was added in portions. The reaction mixture was stirred for 2 h at ambient temperature. The solution was poured onto ice water (50 mL) and extracted with DCM (3 x 8 mL). The combined organic phases were dried over $MgSO_4$. The solvent was evaporated *in vacuo*. The crude product was purified through MPLC (petroleum ether). The pure product was obtained as translucent oil.

Yield: 2213 mg, 11.58 mmol, 66%. ^{1}H-NMR: (300 MHz, Chloroform-*d*) δ =2.35 (s, 3H, CH3 thiophene), 2.42 (s, 3H, CH3 thiophene), 6.57 (s, 1H, CH thiophene). R_f: 0.92 (petroleum ether). The analytical data were in agreement with published data.[51]

*3-Bromo-2-methyl-5-phenylthiophene (**5b**)*

A crimp top vial was equipped with **4** (3390 mg, 13.25 mmol), phenyl boronic acid (1651 mg, 13.52 mmol), $Pd(PPh_3)_2Cl_2$ (88 mg, 0.13 mmol), $AsPh_3$ (69 mg, 0.23 mmol), THF (39 mL) and a Na_2CO_3 solution (aq, 2M, 16 mL) and sealed. The vial was purged with argon for five minutes and the reaction mixture was heated to 80 °C for 16 h. The mixture was cooled to room temperature and extracted with EtOAc (2 x 40 mL). The organic layers were combined and dried over $MgSO_4$. The solvent was removed *in vacuo* and the crude product was purified through MPLC (petroleum ether). The pure product was isolated as white crystalline powder. Yield: 2700 mg, 10.67 mmol, 80%. The analytical data were in agreement with published data.[52]

*2,3-Dibromo-5,6-dimethoxycyclohexa-2,5-diene-1,4-dione (**9b**)*

Compound **8b** (768 mg, 4.57 mmol) was dissolved in dry Et_2O (21 mL) under nitrogen atmosphere. Bromine (2773 mg, 17.35 mmol, 0.90 mL) was dissolved in a mixture of $CHCl_3$ (10 mL) and dry Et_2O (2.3 mL) and added dropwise to the reaction mixture at 0 °C. The reaction mixture was stirred for one hour at ambient temperature; then, concentrated sulfuric acid (23 mL) was added dropwise at 0 °C. The reaction mixture was stirred at ambient

temperature for another hour and then poured onto ice. The mixture was extracted with Et_2O (3 x 50 mL). Ag_2O (5503 mg, 23.75 mmol) was added to the combined organic layers and stirred for 20 min. The solids were filtered off and the solvent was removed *in vacuo*. The crude product was purified through reversed phase MPLC (C18; 30 to 65 % MeCN in H_2O/0.05% TFA). The pure product was obtained as red powder and crystallized for analytical purpose from $CHCl_3$/petroleum ether.

Yield: 826 mg, 2.54 mmol, 55%. ^{1}H-NMR (600 MHz, Chloroform-*d*) δ =4.04 (s, 6H). ^{13}C-NMR (101 MHz, Chloroform-*d*) δ =174.7 (s, q), 145.0 (q), 137.2 (q), 61.7 (s, +). FTIR: $\tilde{\nu}$(cm^{-1}): 2948 (w), 1625 (s), 1662 (s), 1562 (s), 936 (m), 731 (s). APCI-MS: found: 324.87 (MH^+, ^{79}Br, 50%), 326.87 (MH^+, ^{79}Br/^{81}Br, 100%), 328.87 (MH^+, ^{81}Br, 50%). HR-MS: calculated: 323.8633; found: 323.8625 ($M^{+\bullet}$,^{79}Br). Melting point: 102 °C. R_f: 0.74 (50% EtOAc in petroleum ether).

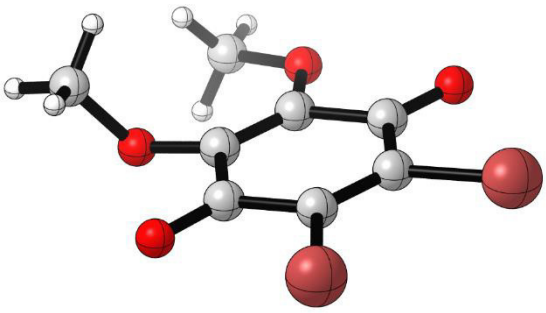

Figure 8: X-Ray structure of compound 9b.

II.1.5 Acknowledgments

We thank Regina Hoheisel for CV measurements, Antonín Králík and Morten Grøtli for fruitful discussions, and Stefano L. Crespi for assistance regarding computational studies. We thank Lisa-Marie Altmann and Lorena Oegl for technical assistance. NAS thanks the Studienstiftung des Deutschen Volkes for a doctoral scholarship.

II.1.6 References

1. Brieke, C.; Rohrbach, F.; Gottschalk, A.; Mayer, G.; Heckel, A., Light-Controlled Tools. *Angewandte Chemie International Edition* **2012**, *51*, 8446–8476.

2. Szymański, W.; Beierle, J. M.; Kistemaker, H. A. V.; Velema, W. A.; Feringa, B. L., Reversible Photocontrol of Biological Systems by the Incorporation of Molecular Photoswitches. *Chemical Reviews* **2013**, *113*, 6114–6178.

3. Velema, W. A.; Szymanski, W.; Feringa, B. L., Photopharmacology: Beyond Proof of Principle. *Journal of the American Chemical Society* **2014**, *136*, 2178–2191.

4. Lerch, M. M.; Hansen, M. J.; van Dam, G. M.; Szymanski, W.; Feringa, B. L., Emerging Targets in Photopharmacology. *Angewandte Chemie International Edition* **2016**, *55*, 10978–10999.

5. Wilson, D.; Branda, N. R., Photochromic Materials in Biochemistry. In Photochromic Materials, *Wiley-VCH Verlag GmbH & Co. KGaA* **2016**, 361–391.

6. Westmark, P. R.; Kelly, J. P.; Smith, B. D., Photoregulation of Enzyme Activity. Photochromic, Transition-State-Analog Inhibitors of Cysteine and Serine Proteases. *Journal of the American Chemical Society* **1993**, *115*, 3416–3419.

7. Falenczyk, C.; Schiedel, M.; Karaman, B.; Rumpf, T.; Kuzmanovic, N.; Grotli, M.; Sippl, W.; Jung, M.; Konig, B., Chromo-Pharmacophores: Photochromic Diarylmaleimide Inhibitors for Sirtuins. *Chemical Science* **2014**, *5*, 4794–-4799.

8. Vomasta, D.; Högner, C.; Branda, N. R.; König, B., Regulation of Human Carbonic Anhydrase I (hCAI) Activity by Using a Photochromic Inhibitor. *Angewandte Chemie International Edition* **2008**, *47*, 7644–7647.

9. Trads, J. B.; Burgstaller, J.; Laprell, L.; Konrad, D. B.; de la Osa de la Rosa, L.; Weaver, C. D.; Baier, H.; Trauner, D.; Barber, D. M., Optical Control of GIRK Channels Using Visible Light. *Organic & Biomolecular Chemistry* **2017**, *15*, 76–81.

10. Reisinger, B.; Kuzmanovic, N.; Löffler, P.; Merkl, R.; König, B.; Sterner, R., Exploiting Protein Symmetry To Design Light-Controllable Enzyme Inhibitors. *Angewandte Chemie International Edition* **2014**, *53*, 595–598.

11. Szymanski, W.; Ourailidou, M. E.; Velema, W. A.; Dekker, F. J.; Feringa, B. L., Light-Controlled Histone Deacetylase (HDAC) Inhibitors: Towards Photopharmacological Chemotherapy. *Chemistry – A European Journal* **2015**, *21*, 16517–16524.

12. Lien, L.; Jaikaran, D. C. J.; Zhang, Z.; Woolley, G. A., Photomodulated Blocking of Gramicidin Ion Channels. *Journal of the American Chemical Society* **1996**, *118*, 12222–12223.

13. Babii, O.; Afonin, S.; Berditsch, M.; Reiβer, S.; Mykhailiuk, P. K.; Kubyshkin, V. S.; Steinbrecher, T.; Ulrich, A. S.; Komarov, I. V., Controlling Biological Activity with Light: Diarylethene-Containing Cyclic Peptidomimetics. *Angewandte Chemie International Edition* **2014**, *53*, 3392–3395.

14. Velema, W. A.; van der Berg, J. P.; Hansen, M. J.; Szymanski, W.; Driessen, A. J. M.; Feringa, B. L., Optical Control of Antibacterial Activity. *Nature Chemistry* **2013**, *5*, 924–928.

15. Borowiak, M.; Nahaboo, W.; Reynders, M.; Nekolla, K.; Jalinot, P.; Hasserodt, J.; Rehberg, M.; Delattre, M.; Zahler, S.; Vollmar, A.; Trauner, D.; Thorn-Seshold, O., Photoswitchable Inhibitors of Microtubule Dynamics Optically Control Mitosis and Cell Death. *Cell* **2015**, *162*, 403–411.

16. Irie, M., Diarylethenes for Memories and Switches. *Chemical Reviews* **2000**, *100*, 1685–1716.

17. Cahová, H.; Jäschke, A., Nucleoside-Based Diarylethene Photoswitches and Their Facile Incorporation into Photoswitchable DNA. *Angewandte Chemie International Edition* **2013**, *52*, 3186–3190.

18. Singer, M.; Jäschke, A., Reversibly Photoswitchable Nucleosides: Synthesis and Photochromic Properties of Diarylethene-Functionalized 7-Deazaadenosine Derivatives. *Journal of the American Chemical Society* **2010**, *132*, 8372–8377.

19. Morgan, C. G.; Thomas, E. W.; Yianni, Y. P.; Sandhu, S. S., Incorporation of a Novel Photochromic Phospholipid Molecule into Vesicles of Dipalmitoylphosphatidyl-choline. *Biochimica et Biophysica Acta - Biomembranes* **1985**, *820*, 107–114.

20. Frank, J. A.; Moroni, M.; Moshourab, R.; Sumser, M.; Lewin, G. R.; Trauner, D., Photoswitchable Fatty Acids Enable Optical Control of TRPV1. *Nature Communications* **2015**, *6*, 7118–7129.

21. Frank, J. A.; Yushchenko, D. A.; Hodson, D. J.; Lipstein, N.; Nagpal, J.; Rutter, G. A.; Rhee, J.-S.; Gottschalk, A.; Brose, N.; Schultz, C.; Trauner, D., Photoswitchable Diacylglycerols Enable Optical Control of Protein Kinase C. *Nature Chemical Biology* **2016**, *12*, 755–762.

22. Morgan, C. G.; Yianni, Y. P.; Sandhu, S. S.; Mitchell, A. C., Liposome Fusion and Lipis Exchange on Ultraviolet Irradiation of Liposomes Containing a Photochromic Phospholipid. *Photochemistry and Photobiology* **1995**, *62*, 24–29.

23. Frank, J. A.; Franquelim, H. G.; Schwille, P.; Trauner, D., Optical Control of Lipid Rafts with Photoswitchable Ceramides. *Journal of the American Chemical Society* **2016**, *138*, 12981–12986.

24. Wilson, D.; Branda, N. R., Turning "On" and "Off" a Pyridoxal 5'-Phosphate Mimic Using Light. *Angewandte Chemie International Edition* **2012**, *51*, 5431–5434.

25. Kamei, T.; Fukaminato, T.; Tamaoki, N., A Photochromic ATP Analogue Sriving a Motor Protein with Reversible Light-Controlled Motility: Controlling Velocity and Binding Manner of a Kinesin-Microtubule System in an in vitro Motility Sssay. *Journal of the Chemical Society, Chemical Communication* **2012**, *48*, 7625–7627.

26. Berg, J. M.; Tymoczko, J. L.; Stryer, L., Biochemistry, Fifth Edition. *W.H. Freeman New York* **2002**.

27. Cantó, C.; Auwerx, J., NAD+ as a Signaling Molecule Modulating Metabolism. *Cold Spring Harbor Symposia on Quantitative Biology* **2011**, *76*, 291–298.

28. Lenaz, G.; Genova, M. L., Mobility and Function of Coenzyme Q (Ubiquinone) in the Mitochondrial Respiratory Chain. *Biochimica et Biophysica Acta - Bioenergetics* **2009**, *1787*, 563–573.

29. Bentinger, M.; Brismar, K.; Dallner, G., The Antioxidant Role of Coenzyme Q. *Mitochondrion* **2007**, *7, Supplement*, S41-S50.

30. Beyer, R. E., The Role of Ascorbate in Antioxidant Protection of Biomembranes: Interaction with vitamin E and Coenzyme Q. *Journal of Bioenergetics and Biomembranes* **1994**, *26*, 349–358.

31. Cornell, B. A.; Keniry, M. A.; Post, A.; Robertson, R. N.; Weir, L. E.; Westerman, P. W., Location and Activity of Ubiquinone 10 and Ubiquinone Analogues in Model and Biological Membranes. *Biochemistry* **1987**, *26,* 7702–7707.

32. Turunen, M.; Wehlin, L.; Sjöberg, M.; Lundahl, J.; Dallner, G.; Brismar, K.; Sindelar, P. J., β2-Integrin and Lipid Modifications Indicate a Non-Antioxidant Mechanism for the Anti-Atherogenic Effect of Dietary Coenzyme Q10. *Biochemical and Biophysicsical Research Communications* **2002**, *296*, 255–260.

33. Göstl, R.; Hecht, S., Controlling Covalent Connection and Disconnection with Light. *Angewandte Chemie International Edition* **2014**, *53*, 8784–8787.

34. Deng, X.; Liebeskind, L. S., A Contribution to the Design of Molecular Switches: Novel Acid-Mediated Ring-Closing−Photochemical Ring-Opening of 2,3-Bis(heteroaryl)quinones (Heteroaryl = Thienyl, Furanyl, Pyrrolyl). *Journal of the American Chemical Society* **2001**, *123*, 7703–7704.

35. Katsumura, S.; Yoshida, S.; Kubo, H.; Saiga, T. Preparation of 2,3-Diarylquinoline Derivatives as Electrophotographic Materials. *JP09077743A*, **1997**.

36. Vilà, N.; Royal, G.; Loiseau, F.; Deronzier, A., Photochromic and Redox Properties of Bisterpyridine Ruthenium Complexes Based on Dimethyldihydropyrene Units as Bridging Ligands. *Inorganic Chemistry* **2011**, *50*, 10581–10591.

37. Goulle, V.; Harriman, A.; Lehn, J.-M., An Electro-Photoswitch: Redox Switching of the Luminescence of a Bipyridine Metal Complex. *Journal of the Chemical Society, Chemical Communications* **1993**, *12*, 1034–1036.

38. Sánchez, R. S.; Gras-Charles, R.; Bourdelande, J. L.; Guirado, G.; Hernando, J., Light- and Redox-Controlled Fluorescent Switch Based on a Perylenediimide–Dithienylethene Dyad. *The Journal of Physical Chemistry C* **2012**, *116*, 7164–7172.

39. Goulet-Hanssens, A.; Utecht, M.; Mutruc, D.; Titov, E.; Schwarz, J.; Grubert, L.; Bléger, D.; Saalfrank, P.; Hecht, S., Electrocatalytic Z → E Isomerization of Azobenzenes. *Journal of the American Chemical Society* **2016**, *139*, 335–341.

40. Petersen, M. Å.; Andersson, A. S.; Kilså, K.; Nielsen, M. B., Redox-Controlled Dihydroazulene-Vinylheptafulvene Photoswitch Incorporating Tetrathiafulvalene. *European Journal of Organic Chemistry* **2009**, *2009*, 1855–1858.

41. Herder, M.; Utecht, M.; Manicke, N.; Grubert, L.; Patzel, M.; Saalfrank, P.; Hecht, S., Switching with Orthogonal Stimuli: Electrochemical Ring-Closure and Photochemical Ring-Opening of Bis(thiazolyl)maleimides. *Chemical Science* **2013**, *4*, 1028–1040.

42. Gao, X.; Wen, X.; Esser, L.; Quinn, B.; Yu, L.; Yu, C.-A.; Xia, D., Structural Basis for the Quinone Reduction in the bc1 Complex: A Comparative Analysis of Crystal Structures of Mitochondrial Cytochrome bc1 with Bound Substrate and Inhibitors at the Qi Site. *Biochemistry* **2003**, *42*, 9067–9080.

43. Ma, J.; Cui, X.; Wang, F.; Wu, X.; Zhao, J.; Li, X., Photoswitching of the Triplet Excited State of DiiodoBodipy-Dithienylethene Triads and Application in Photo-Controllable Triplet–Triplet Annihilation Upconversion. *The Journal of Organic Chemistry* **2014**, *79*, 10855–10866.

44. Matsumoto, M.; Kobayashi, H., Hexacyanoferrate-Catalyzed Oxidation of Trimethoxybenzenes to Dimethoxy-p-benzoquinones with Hydrogen Peroxide. *The Journal of Organic Chemistry* **1985**, *50*, 1766–1768.

45. Yu, D.; Mattern, D. L., Convenient Preparations of the Three 2,3-Dihalo-1,4-benzoquinones. *Synthetic Communications* **1999**, *29*, 821–825.

46. Yamaguchi, T.; Uchida, K.; Irie, M., Asymmetric Photocyclization of Diarylethene Derivatives. *Journal of the American Chemical Society* **1997**, *119*, 6066–6071.

47. Yamaguchi, T.; Irie, M., Photochromic Properties of Diarylethene Maleimide Derivatives in Polar Solvents. *Chemical Letters* **2004**, *33*, 1398–1399.

48. Guin, P. S.; Das, S.; Mandal, P. C., Electrochemical Reduction of Quinones in Different Media: A Review. *International Journal of Electrochemistry* **2011**, ID: 816202.

49. Pavlishchuk, V. V.; Addison, A. W., Conversion Constants for Redox Potentials Measured Versus Different Reference Electrodes in Acetonitrile Solutions at 25°C. *Inorganica Chimica Acta* **2000**, *298*, 97–102.

50. Shim, Y.-B.; Park, S.-M., Spectroelectrochemical Studies of *p*-Benzoquinone Reduction in Aqueous Media. *Journal of Electroanalytical Chemistry* **1997**, *425,* 201–207.

51. Fröhlich, J.; Hametner, C.; Kalt, W., Synthesis of Trisubstituted Thiophenesvia a Halogen Dance Reaction at 2-Bromo-5-methylthiophene. *Monatshefte für Chemie / Chemical Monthly* **1996**, *127*, 325–330.

52. Wang, R.; Pu, S.; Liu, G.; Cui, S.; Liu, W., Synthesis and Photochromism of Isomeric Unsymmetrical Diarylethenes Bearing Both Naphthalene and Thiophene Moieties. *Journal of Photochemistry and Photobiology A: Chemistry* **2012**, *243*, 47–55.

II.2 Synthesis and Characterization of Generation II Coenzyme Q Switches

Abstract

Coenzyme Q is a key player in the cellular energy production. Consequently, its function is crucial for cell survival and death. As the regulation of cellular stress is of high interest for multifaceted aspects of biochemical and pre-clinical research suitable tool compounds are desired. Recently, we reported on photochromic Coenzyme Q mimetics merging a benzoquinone with a diarylethene motif. To enhance the photophysical properties of the compounds, we herein present re-designed structures with potentially improved switching properties. Consequently, we take one step further on the pathway towards light-controllable, fully operational redox coenzymes.

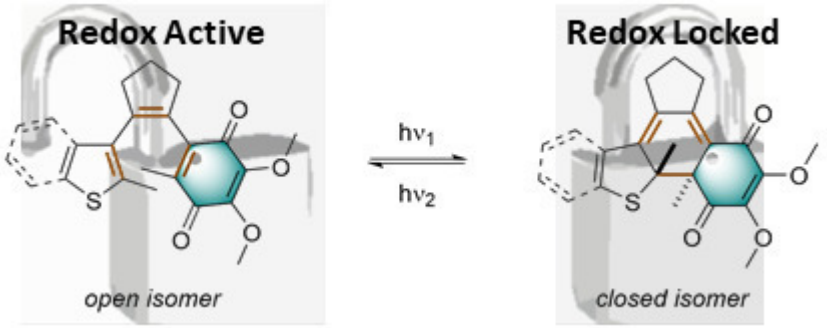

Author contributions

NAS performed all syntheses, UV/Vis and HPLC experiments and wrote the manuscript.

II.2.1 Introduction and Aim

Coenzyme Q, also called ubiquinone, is a crucial component in the mitochondrial respiratory chain (Figure 1). Hence, it plays a key role in the efficient energy production from carbohydrates and fatty acids. In particular, at complex I (NADH-CoQ reductase) of the respiratory chain, ubiquinone is reduced to ubiquinol by simultaneous oxidation of NADH and the transport of three to four protons through the membrane (matrix to intermembrane space). A similar process is present in the complex II (succinat-CoQ reductase). Here, Coenzyme Q is reduced by simultaneous oxidation of FADH. Ubiquinol is finally diffusing within the membrane to complex III ($CoQH_2$-cytochrom c reductase) where it is re-oxidized to Coenzyme Q. The generated protons are again released into the intermembrane space. The protons pumped through the membrane during the redox reactions generate a potential gradient over the inner mitochondrial membrane, which will finally be released through ATP synthase, synthesizing ATP. Consequently, ubiquinone is a key player in cellular energy production and crucial for cell survival and death. Regulation of cellular stress and surviving is an interesting point of action for multifaceted aspects of biochemical and pre-clinical research.[1-3]

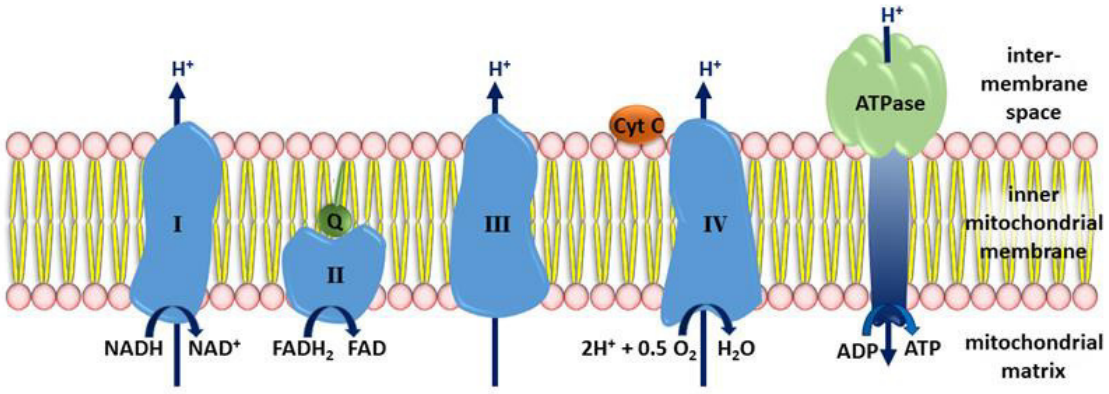

Figure 1: Schematic presentation of the respiratory chain. Coenzyme Q (green ball *Q*) is reduced at complex I and II to OH2 and transports in this manner electrons to complex III where it is re-oxidized to Q.

In Chapter III.1. we studied a photoswitchable redox cofactor inspired by Coenzyme Q, which oxidative properties could be photoregulated on mitochondria. The design involves a benzoquinone core, which was symmetrically substituted with two thiophenes to form a photochromic DTE. However, a major drawback of the compound is its limited efficiency regarding the ring-closure reaction. Whereas the opening reaction works quantitatively, the PSS of the closing reaction is not higher than 52%. Hence, switching of the molecule is only partly reversible.[4] This limits the application of the compound as redox tool in cellular and

super-cellular systems. Thus, we intended to develop a second generation of photochromic CoQ mimetics in order to enhance the PSS of the ring closure-reaction. In the same time, the fatigue resistance of the compound should be improved as we found that upon photoswitching for several times a side-product formation is triggered, and a part of the material cannot be recovered. Our new design (*cf.* Figure 2) involves an unsymmetrically substituted cyclopentene exhibiting a thiophene (or benzothiophene) moiety on one side and a redox-active benzoquinone derivative on the other. A similar concept was employed by the group of Jäschke in their work regarding photoswitchable nucleotides.[5, 6] They reported a photoactuator characterized by reliable switching behavior, even in aqueous systems, and the embedding of the switch in DNA strands. Consequently, transferring the same concept to our intentions appeared to be very promising.

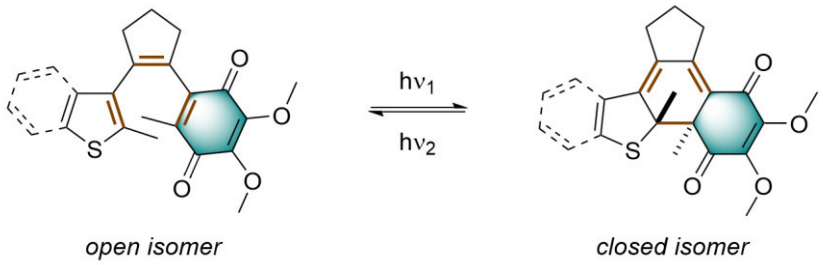

Figure 2: Design of second generation photochromic Coenzyme Q derivatives merging a photochromic 6π system (brown) and a redox-active benzoquinone (blue). A cyclopentadiene moiety constitutes the core on which the benzoquinone and a (benzo)thiophene are attached.

II.2.2 Results and Discussion

II.2.2.1 Synthesis

The key step of the reaction sequence is a Suzuki-Miyaura cross-coupling reaction of a functionalized thiophene (**5a**,**b**) onto the brominated para-benzoquinone **7** (Scheme 1). The synthesis towards **5a** and **5b** started through arylation of the brominated thiophene **1a**[4] or through methylation and subsequent bromination of benzothiophene (**1b**) to result in **2a** and **2b** (80% or 85%, respectively).[7, 8] Compounds **2a** and **2b** were then treated with ^{n}BuLi and $B(OMe)_3$ and directly subjected to a Suzuki-Miyaura cross-coupling reaction with 1,2-dibromo cyclopentadiene (**3**). The yields of the one-pot reaction were 14% or 25%, respectively. Subsequently, **4a** and **4b** were treated with ^{n}BuLi and trapped with $B(O^{i}Pr)(Opin)$ to give compounds **5a** and **5b** in quantitative yield.[5, 6] The compounds obtained in this way were then reacted with benzoquinone **7** in a Suzuki-Miyaura cross-coupling reaction.

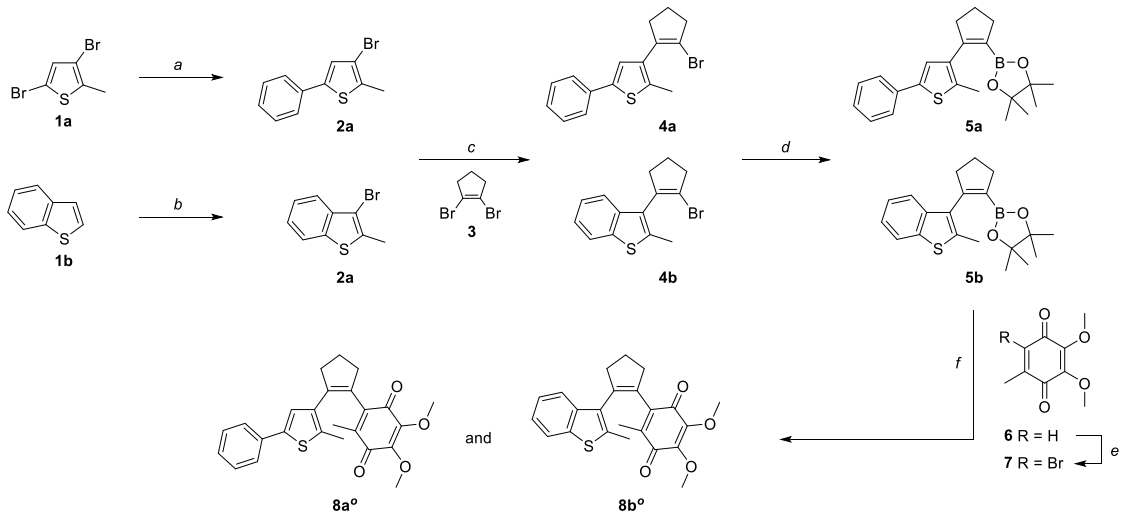

Scheme 1: Synthetic approach towards second generation of photochromic CoQ mimetics. *a*: $PhB(OH)_2$ (1.05 eq), $Pd(PPh_3)_2Cl_2$ (0.1 eq), $AsPh_3$ (0.2 eq), Na_2CO_3 (2 M, aq), THF, 80 °C, Ar, 16 h 80%. *b*: 1) ^{n}BuLi (1.6 M, 1.1 eq), MeI (1 eq), dry DCM, -78 °C to r.t., N_2, 2 h; 2) NBS (1 eq), r.t., 16 h, 85%. *c*: 1) ^{n}BuLi (1.6 M, 1.1 eq), $B(OMe)_3$ (1.1 eq), dry THF, -78 °C to r.t., N_2, 2 h; 2) compound 3 (0.8 eq), $Pd(OAc)_2$ (0.1 eq), dppf (0.2 eq), Na_2CO_3 (2 M, aq), 80 °C, Ar, 16 h (4a: 14%, 4b: 25%). *d*: ^{n}BuLi (1.6 M, 1.1 eq), $B(O^iPr)(Opin)_2$ (1.1 eq), dry THF, -78 °C to r.t., N_2, 2 h, quantitative. *e*: 1) Br_2, H_2SO_4, Et_2O, 1h; 2) Ag_2O, Et_2O, 1h, 53%. *f*: K_3PO_4 (1.2 eq), $Pd(OAc)_2$ (0.1 eq), dppf (0.2 eq), TEA (0.4 eq), THF/water (5:1), 80 °C, Ar, 16 h (8a: 1%, 8b: 0%).

However, we could only obtain compound **8a** in poor yields (1%) which was further examined spectroscopically (*vide infra*). The Suzuki-Miyaura cross-coupling reaction mainly resulted in dehalogenation or further decomposition of the starting material. Hence, we screened further conditions to find synthetic access to **8b**. The results are summarized in table 1.

Most conditions resulted in unaltered **5b** or a defunctionalized derivative (cleavage of the C-Bpin bond to give C-H), which could be isolated through chromatography (Table 1, Entry 1-5). Only in entry 6 and 7 both starting materials could be recovered. Though, in none of the investigated conditions product formation was observed. Spontaneous crystallization of the fractions collected from chromatography of the reaction mixture of entry 4 helped to unravel the reason the reaction was failing. The X-Ray structure is depicted in Figure 3 and reveals that $Pd(PPh_3)_4$ appears to form a stable organopalladium complex with **7** after oxidative addition. We thus speculate that the complex is too unreactive to undergo transmetallation under all the investigated conditions.

Table 1: Suzuki-Miyaura cross-coupling of 5b and 7 under various conditions.

Entry	Palladium Source	Ligand	Base	Conditions[1]	Results[2]
1	$PdAc_2$	dppf	K_3PO_4, NEt_3	THF, H_2O, 16h, 80 °C	**5b**, defunctionalized[3] **5b**
2	$PdAc_2$	TPPTS	Cs_2CO_3	MeCN, H_2O, 1.5h, 120 °C	**5b**, defunctionalized[3] **5b**
3	$PdAc_2$	dppf	Cs_2CO_3	dry THF, 16h, 80 °C	**5b**
4	$Pd(PPh_3)_4$	$AsPh_3$	Cs_2CO_3	dry THF, 16h, 80 °C	**5b**
5	$Pd(PPh_3)_4$	$AsPh_3$	Cs_2CO_3, CsF	dry THF, 16h, 80 °C	**5b**
6	Peppsi-^{i}Pr	as cat.	KOtBu	dry THF, 80 °C, 16h	**5b** and **7**
7	Peppsi-^{i}Pr	as cat.	KOtBu	dioxane, 80 °C, 16h	**5b** and **7**

[1]all reactions were conducted under Argon atmosphere. [2]after chromatographic isolation and MS/NMR analysis. [3] cleavage of the C-Bpin bond to give C-H.

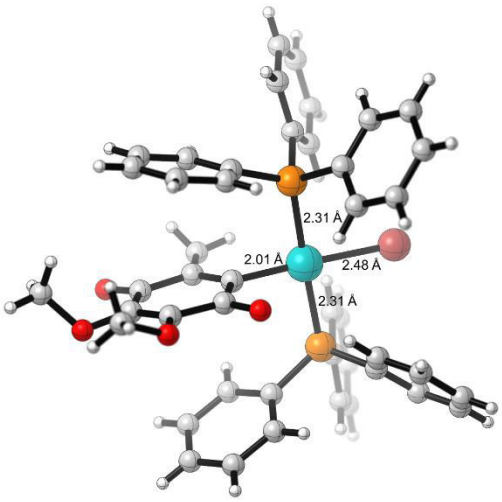

Figure 3: X-ray structure of Pd(II) complex representing a stable intermediate of oxidative addition of the Suzuki-Miyaura cross-coupling reaction (details see Appendix).

To enhance the reactivity of the cross-coupling reaction, we investigated the use of alternative precursors. As the standard Suzuki-Miyaura conditions were not successful, we tried to use the Molander variation and synthesized compound **9**, which was partly successful

(NMR analysis showed ca. 25% conversion of **5b** to **9**, Scheme 2, **A**).[9] The reaction mixture was directly subjected to cross-coupling conditions but again it resulted in no product formation. A very recently reported and more efficient dual photo and Nickel catalyzed variation of this reaction could not be employed, due to the broad absorption of the benzoquinone in the visible range.[10, 11] In addition, we examined Stille cross-coupling conditions. However, also in this case the synthesis of the starting material was challenging and resulted only in C-Br cleavage in compound **4b** (Scheme 2, **B**).

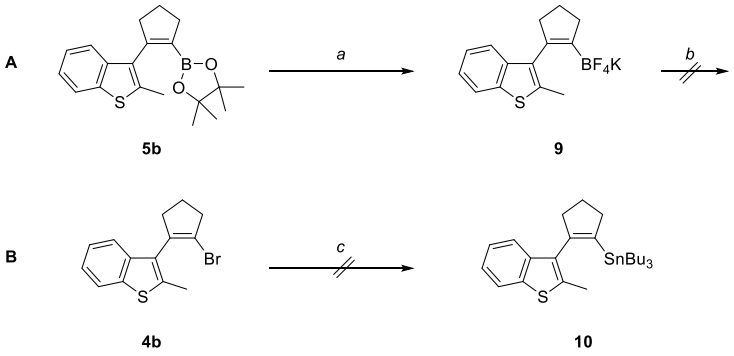

Scheme 2: Derivatization of benzothiophenes 5b and 4b. *a*: KHF_2 (4 eq), EtO_2/water, r.t., 3.5 h, 25%. *b*: 7 (1 eq), K_3PO_4 (1.2 eq), $Pd(OAc)_2$ (0.1 eq), dppf (0.2 eq), TEA (0.4 eq), THF/water (5:1), 80 °C, Ar, 16 h. *c*: 1) ^{s}BuLi (2.4 M, 1 eq), dry THF, -78 °C, N_2; 2) $SnBuCl_3$ (1 eq), -78 °C to r.t., N_2, 2 h.

As also these reactions did not give access to **8b**, we suspected that the observed low reactivity could be originated from the non-aromatic character of benzoquinone **7**. Thus, we decided to synthesize the aromatic compound **12** through reduction and subsequent protection of **7** (Scheme 3). We first reduced **7** to hydroquinone **11**, followed by TMS protection resulting in compound **12**. Unfortunately, also the aromatic derivative **12** could not be coupled to borate **5b**.

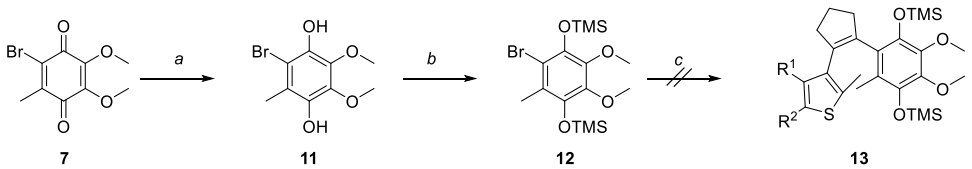

Scheme 3: Suzuki-Miyaura cross-coupling reaction after reduction and protection of 7. a: $Na_2S_2O_4$ (7.5 eq), EtO_2/water, r.t., 16 h, 69%. b: DBU (2.5 eq), TMSCl (2.2 eq), DCM, r.t., 1.5 h, 20%. c: $Pd(PPh_3)_4$, Cs_2CO_3 (3 eq), THF, Na_2CO_3 (20%, aq), 80 °C, Ar, 16h.

As the synthesis of compound **8b** remained challenging, we decided to focus on the further characterization of compound **8a**.

II.2.2.2 UV/Vis spectroscopy

The UV/Vis spectrum of compound **8a** in DMSO shows a main absorption band around 280 nm. Upon irradiation with 312 nm wavelength, a new maximum at 545 nm arises, which can be attributed to the ring closed isomer (Figure 4).[12] No clear isosbestic point can be assigned due to the spectra of the two isomers overlap over a relatively broad area (around 317 nm).

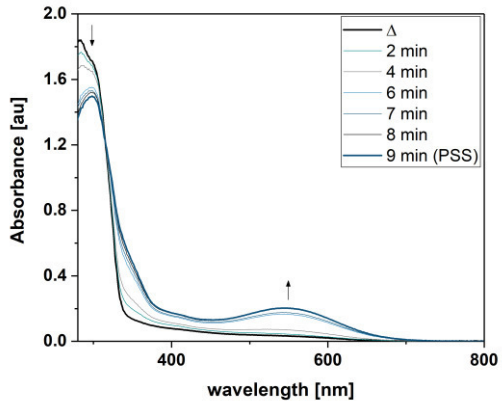

Figure 4: UV/Vis spectra of 8a in DMSO (black) and stepwise irradiation with 312 nm from the thermal equilibrium (Δ) to reach PSS after 9 min.

The PSS of the compound only contained 14% of the ring-opened isomer, indicating good photoswitching properties (HPLC trace, see Figure 5). However, two new peaks were formed according to HPLC traces. Irradiation of the sample with light of 535 nm inducing ring-opening revealed that only one of the two species could be switched reversible; *ca.* half of the isomerization product was irreversibly generated (*cf.* Table 2). Hence, already after two irradiation cycles mainly irreversible formed side-product was present in the reaction mixture (Figure 5 and Table 2). The Hecht group reported, the observed phenomenon is frequent when phenyl substituted DAEs are used.[13] This could potentially be improved using more electron with-drawing substituents on the thiophene moiety or a benzothiophene motif.[13, 14]

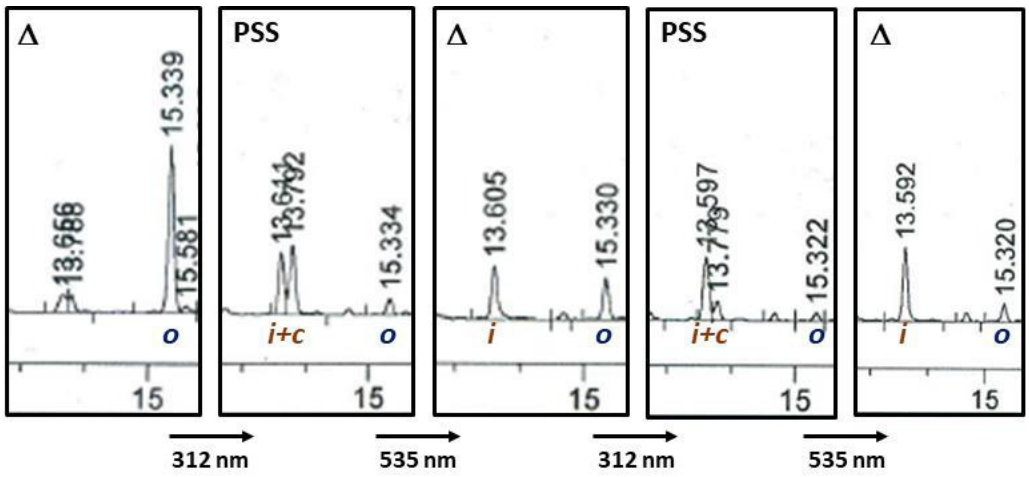

Figure 5: HPLC trace of different irradiation cycles of compound 8a in 1,4 dioxane at 317 nm.

Table 2: Distribution of photo isomers over several isomerization cycles (normalized HPLC areas, traces see Figure 4).

Entry	Cycle	**8a**^{o}	**8a**^{c}	**8a**^{i}
1	Δ	100%	0%	0%
2	PSS	14%	38%	48%
3	Δ	41%	0%	59%
4	PSS	10%	21%	69%
5	Δ	21%	0%	79%

II.2.3 Summary

In summary, we synthesized an unsymmetrical DAE as photochromic CoQ mimetic, compound **8a**. In contrast to first-generation of Coenzyme Q switches, the PSS of **8a** was significantly higher (86% instead of 52% in DMSO). However, a large amount of the formed photoisomers turned out to be an irreversible generated side-product. HPLC analysis of the photoinduced reaction showed clearly that irradiation of the compound first led to photoisomerisation and, in a second reaction step, in the quantitative formation of a by-product as reported for similar compounds. Hence, the fatigue resistance of compound **8a** is still limited. Moreover, we investigated the synthesis of a benzoquinone derivative as this molecular structure is known to enhance the fatigue resistance of photochromic compounds.[14] However, the final Suzuki-Miyaura cross-coupling reaction was challenging. X-Ray crystallography revealed that the reaction stopped after the formation of the benzoquinone-Pd(II)-Br intermediate. As this challenge could not be overcame yet, the

search for a photo-stabilizing counter moiety is still open. Having this in hand, it would probably enable to access a photochromic Coenzyme Q derivative with similar high PSS, as we found during this study, but with enhanced fatigue resistance, hence, providing a proper tool compound to modulate the redox state within the respiratory chain of cells.

II.2.4 Experimental Part

*2-Bromo-5,6-dimethoxy-3-methylcyclohexa-2,5-diene-1,4-dione (**7**)*

Compound **6** (1.5 g, 8.24 mmol) was dissolved in dry Et_2O (130 mL) under nitrogen atmosphere and cooled to 0 °C. Then, bromine (870 µL, 16.48 mmol) dissolved in $CHCl_3$ (10 mL) was added dropwise. The reaction mixture was stirred for 30 min and then, sulfuric acid (50 mL, conc.) was added. Stirring was continued at the same temperature for 1 h before the reaction was heated to ambient temperature and poured onto ice. The aqueous phase was extracted with ether (2 x 50 mL). The combined organic phases were treated with AgO_2 (5.0 g, 21.42 mmol) and stirred for 1 h at room temperature. The solids were filtered of and the organic phase dried over Na_2SO_4. The solution was concentrated *in vacuo* and the crude product was purified through automated column chromatography (25 to 50% EtOAc in PE) to give a red crystalline solid.

Yield: 1.14 g, 4.37 mmol, 53%. ^{1}H-NMR (300 MHz, Chloroform-*d*) δ =4.04 (s, 3H), 4.01 (s, 3H), 2.21 (s, 3H), 1.56 (s, 3H). CI-MS: calculated: 261.07; found: 261.1 ($M^{\bullet+}$, 100%).

*2,3-dimethoxy-5-methyl-6-(2-(2-methyl-5-phenylthiophen-3-yl)cyclopent-1-en-1-yl)cyclo-hexa-2,5-diene-1,4-dione (**8a**)*

A crimp top vial was equipped with pinacolato ester **5a** (81 mg, 0.221 mmol), benzoquinone **7** (58 mg, 0.221 mmol), K_3PO_4 (56 mg, 0.265 mmol), $PdOAc_2$ (5 mg, 0.022 mmol), dppf (13 mg, 0.022 mmol), TEA (80 µL, 0.884 mmol), THF (10 mL) and water (2 mL), purged with argon for three minutes and sealed. The vial was heated to 80 °C for 16 h, cooled to room temperature and diluted with EtOAc (10 mL) and water (10 mL). The phases were separated, and the aqueous phase was extracted with EtOAc (2 x 10 mL). The combined organic phases were dried over Na_2SO_4 and the volatiles were removed *in vacuo*. The crude compound was purified through MPLC (3 to 100% EtOAc in petroleum ether, then 40 to 100% MeCN in H_2O/0.05% TFA). The product was obtained as brown solid.

Yield: 4 mg, 0.01 mmol, 1%. ^{1}H NMR (600 MHz, Chloroform-*d*) δ =7.48 – 7.44 (m, 2H), 7.32 (t, *J* = 7.7 Hz, 2H), 7.25 – 7.20 (m, 1H), 6.90 (s, 1H), 3.98 (s, 3H), 3.93 (s, 3H), 2.21 (s, 3H), 1.70 (s, 3H). ^{13}C NMR (151 MHz, Chloroform-*d*) δ =184.4 (q), 183.7 (q), 144.5 (q),

144.4 (q), 140.7 (q), 140.4 (q), 139.3 (q), 135.8 (q), 134.5 (q), 134.2 (q), 133.4 (q), 128.8 (+), 127.2 (+), 125.4 (+), 123.2 (+), 61.1 (+, both methoxy CH_3), 38.4 (-), 38.1 (-), 23.6 (-), 14.6 (+), 13.3 (+). IR (cm^{-1}) $\tilde{\nu}$= 2922 (s), 2855 (m), 1703 (s), 1687 (s), 1439 (s), 160 (s), 1025 (s), 760 (s). ESI-MS: calculated: 420.1395found: 863.3 ($2MNa^+$, 65%), 443.1 (MNa^+, 15%), 421.1 (MH^+, 100%); HR-MS: 421.1473 (MH^+, 100%). R_f: 0.86 (40% EtOAc in petroleum ether).

*Potassium tetrafluoro(2-(2-methylbenzo[b]thiophen-3-yl)cyclopent-1-en-1-yl)-l5-borate (**9**)*

Compound **5b** (52 mg, 0.153 mmol) was dissolved in Et_2O (5 mL). KHF_2 (36 mg, 0.459 mmol) in water (0.25 mL) was added dropwise. The reaction mixture was vigorously stirred for 3.5 h, then acetone (5 mL) and water (5mL) was added. The phases were separated, and the organic phase was concentrated in high vacuum. The solids were re-dissolved in acetone and precipitated with ether.[9]

A control fluorine NMR was recorded, and the compound was directly employed for Suzuki-Miyaura cross-coupling with compound **7**.

^{19}F NMR (282 MHz, Acetone-d_6) δ =-150.8.

*2-Bromo-5,6-dimethoxy-3-methylbenzene-1,4-diol (**11**)*

Compound **7** (800 mg, 3.06 mmol) was dissolved in EtO_2 (60mL). A solution of $Na_2S_2O_4$ (4.00 g, 22.98 mmol) in water (40 mL) was added dropwise at room temperature and stirred for 16h. The phases were separated, and the aqueous phase was extracted with Et_2O (2 x 10 mL). The combined organic phases were dried over Na_2SO_4. The volatiles were evaporated *in vacuo* and the crude product was obtained as a beige crystalline solid and could be used without further purification and directly converted to compound **12**.

Yield: 560 mg, 2.13 mmol, 69%. ESI-MS: calculated: 261.98; found: 264.0 ($M^{+\cdot}$, ^{81}Br, 100%), 262.0 ($M^{+\cdot}$,^{79}Br, 98%), 249.0 ($M^{+\cdot}$, ^{81}Br, 90%), 247.0 ($M^{+\cdot}$,^{79}Br, 88%). Melting point: 144 °C. R_f: 0.96 (50% EtOAc in petroleum ether).

*((2-Bromo-5,6-dimethoxy-3-methyl-1,4-phenylene)bis(oxy))bis(trimethylsilane) (**12**)*

Compound **11** (260 mg, 0.99 mmol) was dissolved in DCM (25mL). TMSCl (2.17 mmol, 276 µL), followed by DBU (2.47 mmol, 369 µL) was added. The reaction mixture was stirred at ambient temperature for 1.5 h. After no further conversion could be observed through TLC control water (10 mL) was added and the phases were separated. The aqueous phase was extracted with DCM (2 x 10 mL). The combined organic phases were dried over Na_2SO_4.

The volatiles were evaporated *in vacuo* and the crude product was purified through MPLC (0 to 45% EtOAc in petroleum ether). The pure product was obtained as colorless solid. Yield: 82 mg, 0.2 mmol, 20%. ^{1}H-NMR: ^{1}H NMR (400 MHz, Chloroform-*d*) δ =3.78 (s, 3H), 3.77 (s, 3H), 2.24 (s, 3H), 0.27 (s, 9H), 0.22 (s, 9H). ^{13}C NMR (101 MHz, Chloroform-*d*) δ =143.6 (q), 142.7 (q), 141.6 (q), 141.2 (q), 124.7 (q), 112.8 (q), 60.2 (+), 60.0 (+), 16.7 (+), 0.1 (+), 0.0 (+). IR (cm^{-1}) $\tilde{\nu}$= 2956 (w), 1461 (m), 1428 (s), 1248 (s), 1249 (s), 1193 (w), 1133 (w), 1092 (s), 834 (s). ESI-MS: calculated: 406.06; found: 408.1 ($M^{+\cdot}$, ^{81}Br, 90%), 406.1 ($M^{+\cdot}$,^{79}Br, 85%), 378.1 ($M^{+\cdot}$, ^{81}Br, 100%), 376.1 ($M^{+\cdot}$,^{79}Br, 95%). Melting point: 55 °C. R_f: 0.89 (50% EA in petroleum ether).

II.2.5 Acknowledgments

We thank Lorena Oegl for technical support. NAS thanks the Studienstiftung des deutschen Volkes for a PhD scholarship.

II.2.6 References

1. Berg, J. M.; Tymoczko, J. L.; Stryer, L., Biochemistry, Fifth Edition. *W.H. Freeman New York* **2002**.

2. Alberts, B.; Alexander, J.; Lewis, J.; Raff, M.; Roberts, K.; Walter, P., Molecular Biology of the Cell, 4th Edition. *Garland Science New York* **2002**.

3. Jonckheere, A. I.; Smeitink, J. A. M.; Rodenburg, R. J. T., Mitochondrial ATP Synthase: Architecture, Function and Pathology. *Journal of Inherited Metabolic Disease* **2012**, *35*, 211–225.

4. Simeth, N. A.; Kneuttinger, A. C.; Sterner, R.; König, B., Photochromic Coenzyme Q Derivatives: Switching Rredox Potentials with Light. *Chemical Science* **2017**, *8*, 6474–6483.

5. Singer, M.; Jäschke, A., Reversibly Photoswitchable Nucleosides: Synthesis and Photochromic Properties of Diarylethene-Functionalized 7-Deazaadenosine Derivatives. *Journal of the American Chemical Society* **2010**, *132*, 8372–8377.

6. Cahova, H.; Jaeschke, A., Nucleoside-Based Diarylethene Photoswitches and Their Facile Incorporation into Photoswitchable DNA. *Angewewandte Chemie, International Edition* **2013**, *52*, 3186–3190.

7. Zhao, S.-m.; Zhang, W.-g., High regioselective preparation of mono-bromothiophene derivatives. *Huaxue Shiji* **2009**, *31*, 646–648.

8. Galangau, O.; Kimura, Y.; Kanazawa, R.; Nakashima, T.; Kawai, T., Enhanced Photochemical Sensitivity in Photochromic Diarylethenes Based on a Benzothiophene/thiophene Nonsymmetrical Structure. *European Journal of Organic Chemistry* **2014**, *2014*, 7165–7173.

9. Molander, G. A.; Yun, C.-S.; Ribagorda, M.; Biolatto, B., B-Alkyl Suzuki−Miyaura Cross-Coupling Reactions with Air-Stable Potassium Alkyltrifluoroborates. *The Journal of Organic Chemistry* **2003**, *68*, 5534–5539.

10. Tellis, J. C.; Primer, D. N.; Molander, G. A., Single-electron Transmetalation in Organoboron Cross-Coupling by Photoredox/Nickel Dual Catalysis. *Science* **2014**, *345*, 433–436.

11. Primer, D. N.; Karakaya, I.; Tellis, J. C.; Molander, G. A., Single-Electron Transmetalation: An Enabling Technology for Secondary Alkylboron Cross-Coupling. *Journal of the American Chemical Society* **2015**, *137*, 2195–2198.

12. Irie, M., Diarylethenes for Memories and Switches. *Chemical Reviews* **2000**, *100*, 1685–1716.

13. Herder, M.; Schmidt, B. M.; Grubert, L.; Pätzel, M.; Schwarz, J.; Hecht, S., Improving the Fatigue Resistance of Diarylethene Switches. *Journal of the American Chemical Society* **2015**, *137*, 2738–2747.

14. Hanazawa, M.; Sumiya, R.; Horikawa, Y.; Irie, M., Thermally Irreversible Photochromic Systems. Reversible Photocyclization of 1,2-Bis (2-methylbenzo[b]thiophen-3-yl)perfluorocyclocoalkene derivatives. *Journal of the Chemical Society, Chemical Communications* **1992**, *3*, 206–207.

II.3 Towards Photocontrollable NAD^+ Analogues

Abstract

Nicotinamide adenine dinucleotide is a ubiquitous cofactor in the cell that is crucially involved in energy production and many biotransformations. However, its concentration can only be regulated by enhanced biosynthesis or consummation so far. Hence, a direct interference with the system of investigation is unavoidable. To be able to stimulate the system from the outside, we suggest the use of photoswitchable derivates. Consequently, we developed photochromic nicotine amides merging the redox active structure with a photocontrollable dithienyl ethene. This structural combination links the light-mediated reaction of the photochromic part directly to the redox reaction generating two states: an unaltered and a redox-locked isomer. We will demonstrate the synthesis, spectroscopic and electrochemical investigation of the compounds and finally show their application in redox chemistry.

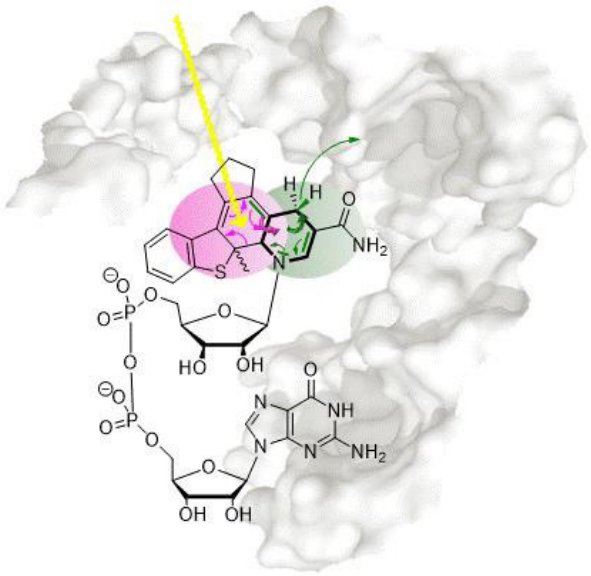

Author contributions

NAS performed all syntheses, UV/Vis and HPLC experiments and wrote the manuscript.

II.3.1 Introduction and Aim

Redox cofactors such as nicotinamide adenine dinucleotide (NAD^+) are ubiquitous in the cell and are involved in many cellular processes. They facilitate, for example, transhydrogenation reactions catalyzed by oxireductases, by either accepting or providing electrons. Moreover, they act as activated electron carriers for the oxidation of metabolites in aerobic organisms. The energy released from the digestion of carbohydrates, fatty acids or other metabolites is stored in nicotinamide adenine NAD^+ or its reduced form NADH, respectively.[1-4]

More recently, the full extent of the cellular impact of redox cofactors began to emerge with the identification of NAD^+ consuming proteins such as sirtuins. Cantó *et al.* reported that there is evidence that the activity of such enzymes is modulated by the availability of NAD^+ and therefore coherent with metabolic shifts of the NAD^+/NADH redox state.[5, 6] To investigate this correlation the NAD^+/NADH redox state has to be artificially altered.[5] This can be done through *e.g.* enhancing NAD^+ production in the organism by providing a precursor such as nicotinamide for its synthesis or by reducing NAD^+ level, stimulating the activity of NAD^+ consuming proteins.[7-9] However, all these approaches require an irreversible, external interaction with the protein system. Moreover, only few studies have described how NAD^+ precursors influence the NAD^+ level so far. Hence, the NAD^+ level will probably be changed in the whole cell as a consequence of the increased precursor concentration and could not be limited to a single cellular compartment.[5] The natural NAD^+ level, on the other hand, differs in the various compartments.[10] Hence, a controlled alteration of the NAD^+/NADH level would be beneficial to determine the impact of the redox state on the state of action of certain enzymes, such as sirtuins, and on the whole cell.

A proper tool compound, which can be easily controlled to reversibly and spatiotemporally regulate the NAD^+ level within the cell, would be essential to cope with the challenge of the investigation of the NAD^+ level. In a previous study, we reported on the use of light as an external trigger to control the redox properties of a diarylethene (DAE) derivative of Coenzyme Q.[11] The usage of light as a stimulant is particularly appealing as it is non-invasive in many chemical and biochemical systems, and easily controllable regarding space and time of action.[12] Using suitable functionalized photochromic compounds as mediators, light can be effectively utilized even in complex biological systems. In the past two decades, many studies have taken advantage of this concept, contributing to the growing field of *photopharmacology*.[13-15] In this manner, for instance microtubuli modulators,[16] photoswitchable

fatty acids,[17] photochromic enzyme ligands[18-20] and last but not least cofactor mimetics such as ATP,[21] pyridoxal-5'-phosphate and,[22] Coenzyme Q mimetics[11] have been developed.
Both our previously presented Coenzyme Q mimetic[11] and the bispyridinium DAE reported by Branda and coworkers[23] exhibit a DAE derivative as a light-controllable redox lock. Similarly, we endeavored in developing photochromic NAD^+ mimetics incorporating the redox-active nicotine amide subunit into a DAE to subject its redox properties under the control of light.

II.3.2 Results and Discussion

II.3.2.1 Design

To gain photocontrol over the pyridinium-dihydropyridine redox system, we envisioned to merge a photochromic DAE system with the heteroaromatic structure as depicted in Figure 1. Thereby, two of the six electrons, which are involved in the 3,3'-electrocyclic ring-closure reaction, are donated by the pyridinium moiety. Hence, they are part in both the photo-triggered electrocyclic reaction and the redox chemistry of the molecule. Through light-induced switching between the open and closed isomer of the molecule, we intended to alter the redox properties of the whole molecule and, in this way, subject it to photo-control.

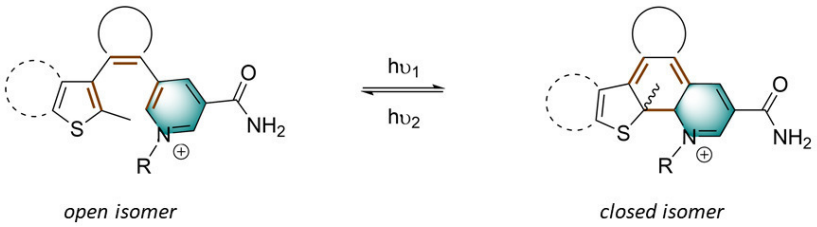

Figure 1: Structural merge of the redox-active pyridinium moiety (blue) and an 3,3'-electrocyclic system (brown). Photo-induced ring-closure leads to a change of the electronic properties in the pyridinium moiety and hence, to an altered redox-behavior of the whole compound.

II.3.2.2 Synthesis

The key reaction towards photochromic NAD^+ mimetics is a Suzuki-Miyaura cross-coupling reaction of benzoquinone **5** onto the respective pyridine or pyridinium precursor **6** (Scheme 1). The pinacolato borate **5** could be synthesized in four steps from purchased benzothiophene following a procedure of Singer *et al.*[24] As coupling partner either 5-bromo nicotinamide (**6b**) or its methylated analogue (**6a**) was employed.[25] The conditions of the final cross-coupling reaction were adapted from published procedures.[24] However, we found that the amide functionality was prone to hydrolysis (resulting in **8**, Scheme 2) using

frequently utilized carbonate bases (K_2CO_3 or Cs_2CO_3). Employing $NaNH_2$ though, led to reasonable yields of the desired nicotinamides **7a**^{o} and **7b**^{o}.

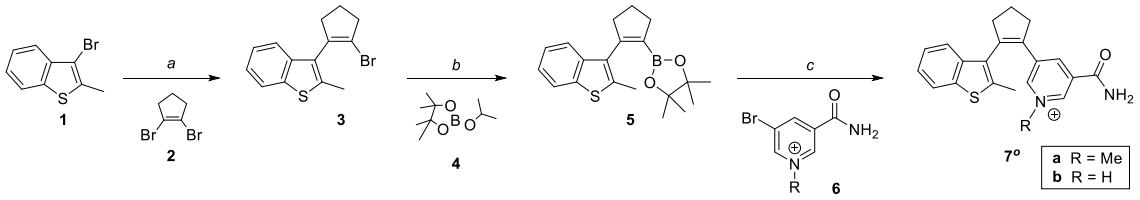

Scheme 1: Synthesis of photochromic nicotinamides 7a^o and 7b^o *via* Suzuki-Miyaura cross-coupling. *a*: 1)^{n}BuLi (1.6 M in hexane, 1.1 eq), dry THF, -78 °C, N_2; 2) $B(OBu)_3$ (1.1 eq), -78 °C to r.t.; 3) compound 2 (0.8 eq), $Pd(OAc)_2$ (0.1 eq), dppf (0.2 eq), Na_2CO_3 (2M, aq), Ar, 80 °C, 16 h; *b*: 1)^{n}BuLi (1.6 M in hexane, 1.1 eq), THF, -78 °C; 2) compound 4 (1.1 eq), -78 °C to r.t., 2 h; *c*: compound 5 (1.2 eq), compound 6 (1 eq), $Pd(OAc)_2$ (0.1 eq), TPPTS (0.2 eq), $NaNH_2$ or Cs_2CO_3 (7 eq), H_2O:MeCN (1:1), Ar, 120 °C, 2 h.

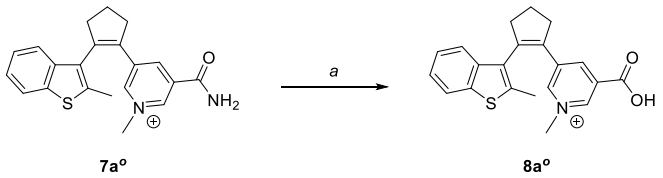

Scheme 2: Hydrolysis of 7a as side-reaction during palladium mediated cross-coupling. *a*: $Pd(OAc)_2$ (0.1 eq), TPPTS (0.2 eq), K_2CO_3 orCs_2CO_3 (7 eq), H_2O:MeCN (1:1), Ar, 120 °C, 2 h.

We continued our investigations with both **7a**^{o}, **7b**^{o} and **8a**^{o}, all of them bearing a potential redox-active core (the pyridine or pyridinium, respectively).

II.3.2.3 Spectroscopy

We studied the photochromic behavior of the compounds in various solvents. Figure 2 exemplarily depicts the spectra of the pyridine **7b** (left, in DMSO) and, **7a** and **8a**^{c} (right, in MeCN).

To trigger the electrocyclic ring-closure, UV-light of 254 nm was used in this case, as no prominent absorption band in the visible range of the UV-Vis absorption spectrum is present. Upon irradiation, the arising of a novel absorption band was observed around 486 nm (DMSO, **7b**^{c}), 489 nm (MeCN, **7a**^{c}) and 504 nm (MeCN, **8a**^{c}), corresponding to the formation of the ring-closed isomer.[26] Isosbestic points at 296 nm (DMSO, **7b**), 246 nm (MeCN, **7a**) and 267 nm (MeCN, **8a**) indicate a clean monomolecular reaction. However, the closed isomers did not appear to be thermally stable, due to the aromatic stabilization energy of the pyridine or pyridinium sub-moiety of the switches.[27, 28] Keeping the sample in the dark for several minutes resulted in the original spectrum of the ring-opened form in all

investigated molecules and solvents. Hence, determination of the contribution to the PSSs was not feasible. Even though the switching of the compounds was reversible, it was accompanied by photobleaching, especially over longer irradiation times (*vide infra* Figure 4 *right* for compound **11**). This could be due to the instability of the compounds in general or to the use of highly energetic UV-light of 254 nm.

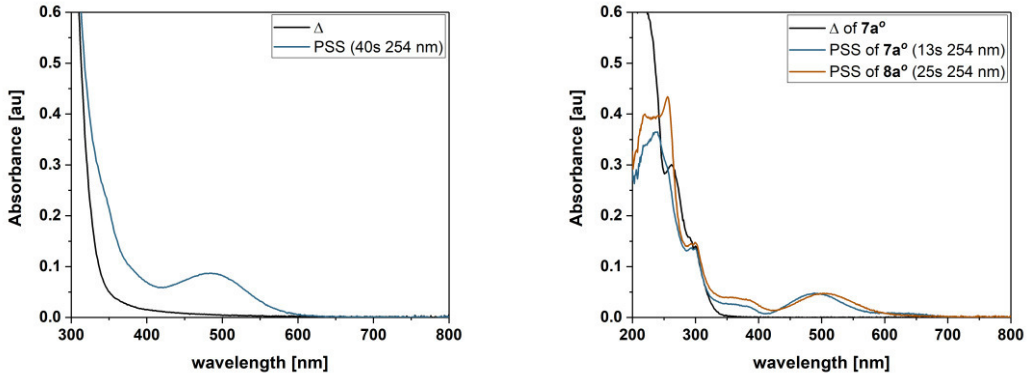

Figure 2: UV-Vis absorption spectra of *left:* 7b in DMSO (50µM) and *right:* 7a (25µM, black: open form, blue: closed form) 8a^{c} (25µM, brown) in MeCN.

II.3.2.4 Cyclic Voltammetry

To estimate the redox potentials of photoswitches **7a^{o}**, **7b^{o}** and **8a^{o}**, we performed cyclic voltammetry and compared the obtained potentials with other pyridines or pyridinium salts. The results are summarized in Table 1.

Table 1: Redox potential of various pyridines and pyridinium derivative. (determined by CV measurements in MeOH or MeOH/water + 0.1M Bu_4NBF_4 using ferrocene (0.005M) as internal standard).

Compound	Potential VS SCN [V][29]	
Vitamin C		0.58
NADH	1.23	1.72
Hantzsch ester (9)	0.76	
NAD^+	-1.20	-1.35
7a^{o}	-0.05	-1.10
7b^{o}	-1.33	
8a^{o}	-0.47	-1.12

Comparing the potentials of our synthesized pyridine and pyridinium derivatives with the parent compound, NAD^+, we found that all photochromic compounds exhibit oxidative properties. However, the three photoswitches are weaker in oxidation strength than NAD^+. Surprisingly, the nicotine amide derivative **7b^{o}**, which is more electron rich than **7a^{o}** or **8a^{o}**,

shows the lowest potential (-1.33 V) being almost equal to NAD^+ (-1.20 V and -1.34 V). Indeed, the photoswitches should be able to serve as oxidant in chemical redox reactions.

II.3.2.5 Reactions with Hantzsch ester and other reducing agents

In a preliminary screening we tried to react the obtained photoswitches with different reducing agents. Inspired by the parent compound, NAD^+, we treated the switches with its reduced form, NADH, (*i.e.* respiratory chain, or oxireductases)[5] and its natural reaction partner Vitamin C (*i.e.* Krebs Cycle),[30] and the classical chemical reductant Hantzsch ester (for the potentials, see Table 1). We analyzed the reactions using HPLC-DAD and LC-ESI-MS, but no reduction of the photoswitches was observed. However, a particular case was found in the reaction with the Hantzsch ester. Indeed, we found that the reducing agent was converted into its oxidized counterpart (the other reducing agents could not be analyzed in the same conditions, as the analytical window was not adequate, *i.e.* the compounds eluted from LC column within the dead time). Hence, we intended to investigate this reaction in more detail and incubated photoswitch **7a^o**, **7b^o** and **8b^o** with Hantzsch ester **9** in MeOH, MeCN or DMSO, respectively (Scheme 3).

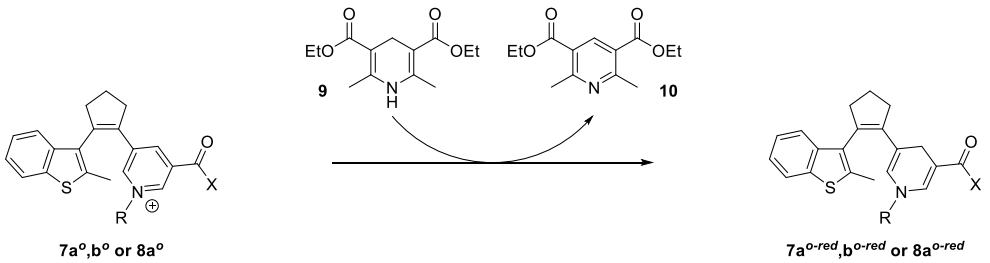

Scheme 3: Redox reaction of photoswitch 7a^o, 7b^o and 8b^o with an excess of Hantzsch ester 9.

We found that the compounds were able to oxidize Hantzsch ester **9** (*cf.* left, Figure 3 compound **8b^o** in MeOH, **7a^o**, **7b^o** and analogous reactions in MeCN and DMSO see Appendix). However, according to HPLC-DAD traces and LC-ESI-MS studies, no reduced photoswitch was found. Moreover, using an excess of Hantzsch ester (5 eq) in our study, we still saw quantitative conversion of **9** into its oxidized counterpart. Control experiments using only Hantzsch ester under these conditions did not lead to any conversion, substantiating the suspicion that the compounds could act as a catalyst in this reaction. Indeed, increasing the concentration of the switch in the reaction goes hand in hand with an increase in the rate of the reaction (*right*, Figure 3). However, formation of a sacrificial oxidant was not found in the reaction mixture (LC-ESI-MS for organic molecules, head-space GC for H_2 detection). Additionally, we investigated the influence of light on the reaction forming the presumably

unreactive closed isomer or the photobleaching product *in situ*. Comparing the conversion of **9** of samples with and without irradiation showed that irradiated samples were approximately oxidized 15-40% less (corrected for the background reaction of Hantzsch ester under irradiation, see Section A.II.3.4. in the Appendix).

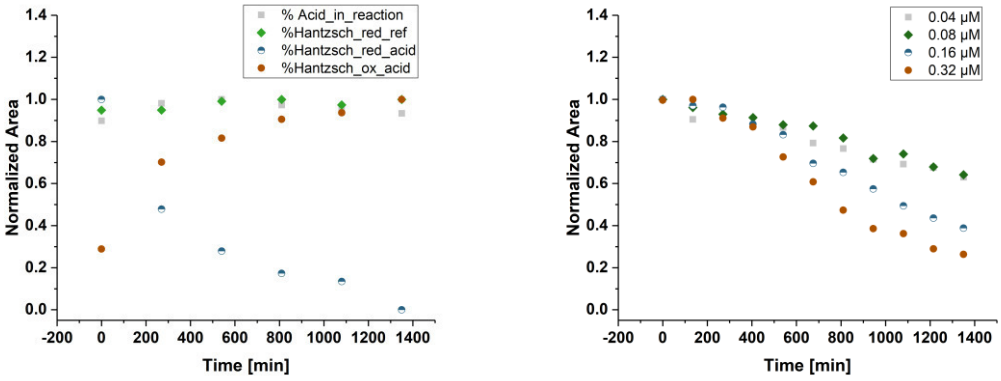

Figure 3: ***left:*** **Kinetic profile of Hantzsch ester oxidation through compound 8a^o (3.3 µM in MeOH); relative amount of 8a^o (gray) 9 (blue) and 10 (brown) in the reaction mixture and 9 without addition of 8a^o (green) under the same conditions;** ***right:*** **Kinetic profile of Hantzsch ester oxidation at different concentrations of 7a^o (in MeOH).**

To obtain more insight into the reaction, we intended to investigate which part of the molecule was crucial for the oxidation. Hence, we reacted various pyridines and substituted pyridines (Chart 1) analogous to the photoswitches **7a^o**, **7b^o** and **8a^o** with Hantzsch ester. Additionally, we synthesized compound **11** (Chart 1) applying the same procedure as for the other photoswitches (Scheme 4) and reacted the molecule with **9**. Beforehand, we tested the photochromic behavior of the compound and found similar characteristics as in **7a^o**, **7b^o** and **8a^o**, apart from its absorption maximum that was hypsochromically shifted (Figure 4).

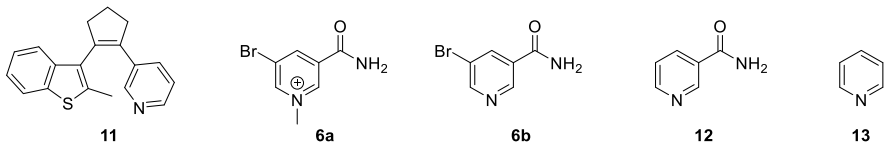

Chart 1: Pyridines and Pyridinium salt to be reacted with Hantzsch ester.

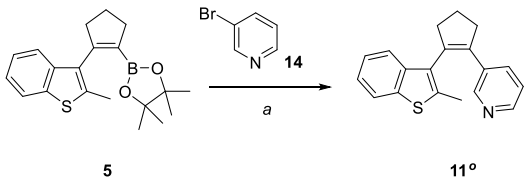

Scheme 4: Synthesis of unfunctionalized pyridine switch 11. ***a*****: compound 5 (1.2 eq), compound 14 (1 eq), Pd(OAc)$_2$ (0.1 eq), TPPTS (0.2 eq), Cs$_2$CO$_3$ (7 eq), H$_2$O:MeCN (1:1), Ar, 120 °C, 2 h.**

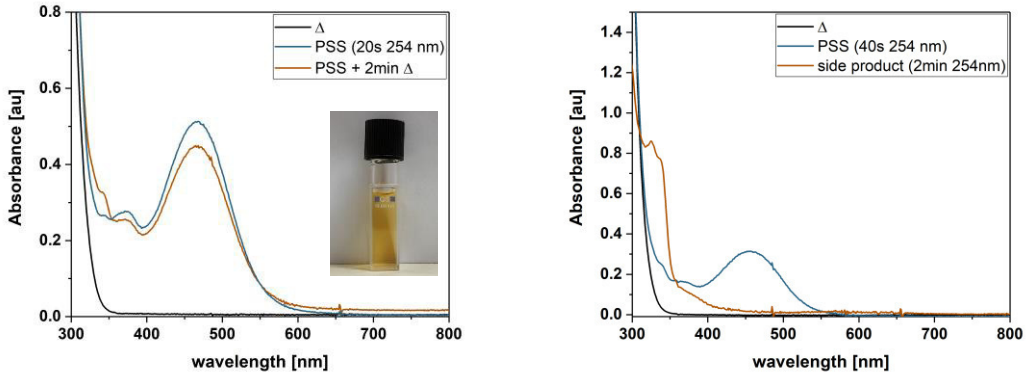

Figure 4: UV-Vis absorption spectra of 11^{o} in *left:* MeOH (100 µM) and MeCN (100 µM).

In the reaction with the Hantzsch ester (**9**) under the same conditions as prior (MeOH as solvent), we found that only bromo-pyridinium ion **6a** can undergo a reaction with the reductant. The other compounds, bromo-pyridine **6b**, nicotine amide (**12**) and pyridine (**13**) are not able to oxidize **9** under the reaction conditions. Similar behavior was found for the simplified photoswitch **11** (black stars, Figure 5, beginning and final concentration of **9** was measured).

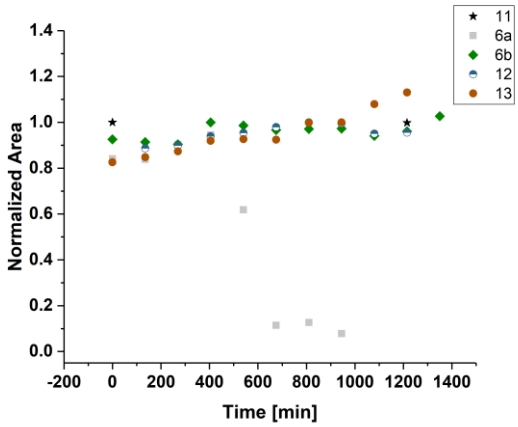

Figure 5: Kinetic profile of Hantzsch ester oxidation through compounds 11-14.

Hence, the photoswitches **7a**^{o},**b**^{o} and **8a**^{o} undergo a reaction with Hantzsch ester. Thereby, also unmethylated **7b**^{o} was reacting. Additional methylation leads to even more electron poor compounds resulting in a faster conversion. Furthermore, the reaction of compound **6a** and the inertness of **11**^{o} shows that attachment of the photoswitch is not crucial for the oxidation of **9**.

II.3.3 Conclusion

In summary, we have merged a DAE with nicotinamides and nicotinamide salts as a model for the NAD^+/NADH system. In particular, we synthesized four different photoswitches (**7a**^{o},**b**^{o}, **8a**^{o} and **11**^{o}) and investigated their photochromic behavior. All compounds could be isomerized in MeCN, MeOH and DMSO upon irradiation, or thermally. However, longer irradiation times led to the photobleaching of the compounds. The ring-closed isomer is formed *via* the electrocyclic ring-closure disrupting the aromaticity of the pyridine (or pyridinium) moiety. Thus, it is thermally not stable under ambient conditions and the PSS could not be assigned. Cyclic voltammetry allowed to determine the redox potentials of compounds **7a**^{o},**b**^{o} and **8a**^{o} and revealed that they could be feasible oxidants. Consequently, we found that the Hantzsch ester could be oxidized quantitatively in a model reaction with the photoswitches. However, according to LS-ESI-MS the photoswitch remained unaltered. Further investigations revealed that addition of only a sub-stochiometric amount of the photoswitch slows the reaction down but still facilitates full conversion of the reductant leading to the conclusion that the switches can act as catalysts. Finally, we investigated the influence of the irradiation (hence, initiating a ring-closure or rather bleaching reaction, which should result in an inactivated catalyst) of the reaction mixture on the conversion. We found that the total conversion of the Hantzsch ester was decreased upon irradiation. However, under treatment with 254 nm light, also a significant background reaction of the reductant was observed. Hence, a clear assignment of the occurrences and further structural optimizations of the presented photoswitches are indispensable to finally result in a fully photocontrollable NAD^+ mimetic.

II.3.4 Experimental

General procedure for Suzuki-Miyaura cross-coupling

A crimp top vial was equipped with functionalized Benzothiophene **5** (100 mg, 0.296 mmol, 1.2 eq), the appropriate nicotinamide **6a** or **6b** (0.246 mmol, 1 eq) and, $NaNH_2$ (28 mg, 1.722 mmol, 7 eq) and flushed with argon. An argon purged mixture of MeCN and water (1:1, 3 mL) was added and the suspension was once again purged with argon. Then, TPPTS (28 mg, 0.049 mmol, 0.2 eq) and $PdAc_2$ (6 mg, 0.025 mmol, 0.1 eq) were added and the vial was sealed. The reaction mixture was heated to 120 °C for 1.5 h. After cooling to ambient temperature, the dark yellow solution was felted and directly purified through preparative

HPLC (MeCN in water/0.05% TFA ; gradient 5 to 98% in 20 min). The products were obtained as yellow solids.

*3-Carbamoyl-1-methyl-5-(2-(2-methylbenzo[b]thiophen-3-yl)cyclopent-1-en-1-yl)pyridin-1-ium (**7a°**)*

Yield: 47 mg (0.135 mmol, 55%). ^{1}H NMR (600 MHz, Methanol-d_4) δ =8.99 (d, J = 1.5 Hz, 1H), 8.52 (t, J = 1.5 Hz, 1H), 8.50 – 8.42 (m, 1H), 7.86 – 7.76 (m, 1H), 7.41 – 7.35 (m, 1H), 7.32 – 7.23 (m, 2H), 4.20 (s, 3H), 3.16 (tq, J = 7.0, 2.1 Hz, 2H), 3.07 – 2.98 (m, 1H), 2.98 – 2.85 (m, 1H), 2.35 (s, 3H), 2.30 (ttd, J = 8.6, 6.8, 1.9 Hz, 2H). ^{13}C NMR (151 MHz, Methanol-d_4) δ = 165.5 (q), 145.5 (+), 144.6 (+), 143.8 (q), 141.4 (+), 140.5 (q), 139.1 (q), 139.0 (q), 138.5 (q), 135.1 (q), 135.0 (q), 129.7 (q), 125.8 (+), 125.6 (+), 123.5 (+), 122.9 (+), 49.3 (+, assigned through HSQC), 40.6 (-), 36.3 (-), 23.5 (-), 14.5 (+). ESI-MS: calculated: 349.4700; found: 349.1 (M^+, 100%). HR-MS: 349.1373 (M^+, 100%). IR: $\tilde{\nu}$ = 3191 (w), 3082 (w), 2363 (w), 1670 (s), 1431 (m), 1200 (m), 1126 (s), 801 (m), 723 (m). R_f: 0.05 (10% MeOH in DCM).

*5-(2-(2-Methylbenzo[b]thiophen-3-yl)cyclopent-1-en-1-yl)nicotinamide (**7b°**)*

Yield: 49 mg (0.148 mmol, 60%). ^{1}H NMR (600 MHz, Methanol-d_4) δ =8.67 (s, 1H), 8.21 (s, 1H), 8.14 (t, J = 2.1 Hz, 1H), 7.76 (d, J = 8.5 Hz, 1H), 7.42 (dd, J = 9.2, 0.7 Hz, 1H), 7.29 – 7.23 (m, 2H), 3.20 – 3.12 (m, 1H), 3.10 – 3.02 (m, 1H), 3.02 – 2.94 (m, 1H), 2.87 – 2.77 (m, 1H), 2.30 – 2.20 (m, 5H). ^{13}C NMR (151 MHz, Methanol-d_4) δ =169.3 (q), 150.0 (+), 148.6 (q), 146.2 (+), 140.3 (q), 140.1 (q), 138.8 (q), 137.8 (q), 137.0 (q), 135.5 (+), 131.2 (q), 125.5 (+), 125.2 (+), 123.2 (+), 123.0 (+), 101.2 (q), 40.2 (-), 36.8 (-), 23.7 (-), 14.3 (+). ESI-MS: calculated: 334.1100; found: 335.1 (MH^+, 100%). HR-MS: 335.1216 (MH^+, 100%). IR: $\tilde{\nu}$ = 3176 (w), 2918 (w), 2844 (w), 2356 (w), 1662 (s), 1595 (s), 1431 (m), 1394 (m), 1178 (s), 1129 (s), 731 (s), 678 (m). R_f: 0.10 (10% MeOH in DCM).

*3-Carboxy-1-methyl-5-(2-(2-methylbenzo[b]thiophen-3-yl)cyclopent-1-en-1-yl)pyridin-1-ium (**8a°**)*

Yield: 30 mg (0.086 mmol, 35%). ^{1}H NMR (600 MHz, Methanol-d_4) δ =9.09 (d, J = 1.4 Hz, 1H), 8.75 (t, J = 1.5 Hz, 1H), 8.42 (t, J = 1.7 Hz, 1H), 7.91 – 7.75 (m, 1H), 7.43 – 7.37 (m, 1H), 7.28 (ddd, J = 7.4, 5.0, 1.7 Hz, 2H), 4.30 (s, 3H), 3.15 (dd, J = 7.0, 1.5 Hz, 1H), 3.10 – 3.00 (m, 1H), 2.97 – 2.89 (m, 1H), 2.35 (s, 3H), 2.30 (dd, J = 8.1, 7.0 Hz, 1H). ^{13}C NMR (151 MHz, Methanol-d_4) δ =162.3 (+), 144.9 (+), 144.0 (+), 143.5 (q), 141.43 (q), 139.2 (q), 137.8 (q), 137.4 (q), 136.7 (q), 133.3 (q), 131.0 (q), 128.5 (q), 124.4 (+), 124.2 (+), 122.0 (+), 121.4 (+), 49.3 (-, assigned through HSQC), 39.3 (-), 34.8 (-), 22.05 (-), 13.0 (+). ESI-MS: calculated:

335.0980; found: 335.1 (M^+, 100%). HR-MS: 350.1212 (M^+, 100%). IR: $\tilde{\nu}$ = 3082 (w), 2930 (w), 1670 (m), 1394 (m), 1177 (s), 1121 (s), 764 (s), 719 (s). R_f: 0.05 (10% MeOH in DCM).

*3-(2-(2-methylbenzo[b]thiophen-3-yl)cyclopent-1-en-1-yl)pyridine (**9'**)*

The crude product was purified through MPLC (0 to 60% ethyl acetate in petroleum ether). The product was obtained as colorless powder. Yield (78 mg, 0.269 mmol, 89%).
^{1}H NMR (300 MHz, Methanol-d_4) δ =8.29 – 8.11 (m, 2H), 7.80 – 7.70 (m, 1H), 7.50 (dt, J = 8.0, 1.9 Hz, 1H), 7.48 – 7.39 (m, 1H), 7.32 – 7.21 (m, 2H), 7.14 (ddd, J = 8.1, 4.9, 0.9 Hz, 1H), 3.11 (dddd, J = 15.6, 7.7, 5.3, 2.4 Hz, 1H), 3.05 – 2.86 (m, 2H), 2.82 – 2.67 (m, 1H), 2.32 – 2.10 (m, 5H). ^{13}C NMR (75 MHz, Methanol-d_4) δ =148.3 (+), 147.8 (+), 140.4 (q), 140.3 (q), 138.6 (q), 137.4 (q), 136.6 (q), 136.0 (+), 135.1 (q), 131.7 (q), 125.4 (+), 125.1 (+), 124.9 (+), 123.2 (+), 123.1 (+), 40.2 (-), 36.9 (-), 23.8 (-), 14.3 (+). ESI-MS: calculated: 291.1082; found: 292.1 (MH^+, 100%). HR-MS: 292.1158 (MH^+, 100%).IR: $\tilde{\nu}$ = 3053 (m), 2945 (m), 2840 (m), 1562 (w), 1476 (w), 1435 (s), 1185 (w), 1148 (w), 1021 (m), 805 (m), 760 (s), 731 (s). R_f: 0.5 (40% EtOAc in petroleum ether).

II.3.5 Acknowledgments

We thank Regina Hoheisel for CV measurements and Antonin Králík for head-space-GC measurements. NAS thanks the Studienstifung des Deutschen Volkes for a PhD scholarship.

II.3.6 References

1. Ying, W., NAD+/NADH and NADP+/NADPH in Cellular Functions and Cell Death: Regulation and Biological Consequences. *Antioxid. Redox Signaling* **2008**, *10*, 179–206.

2. Mouchiroud, L.; Houtkooper, R. H.; Auwerx, J., NAD+ metabolism: A Therapeutic Target for Age-Related Metabolic Disease. *Critical Reviews in Biochemistry and Molecular Biology* **2013**, *48*, 397–408.

3. Nakamura, M.; Bhatnagar, A.; Sadoshima, J., Overview to Pyridine Nucleotides Review Series. *Circulation Research* **2012**, *111*, 604–610.

4. Li, W.; Sauve, A. A., NAD+ Content and Its Role in Mitochondria. *Methods in Molecular Biology* **2015**, *1241,* 39–48.

5. Cantó, C.; Auwerx, J., NAD+ as a Signaling Molecule Modulating Metabolism. *Cold Spring Harbor Symposia on Quantitative Biology* **2011**, *76*, 291–298.

6. Cantó, C.; Menzies, K.; Auwerx, J., NAD(+) Metabolism and the Control of Energy Homeostasis - a Balancing act Between Mitochondria and the Nucleus. *Cell metabolism* **2015**, *22*, 31–53.

7. Bieganowski, P.; Brenner, C., Discoveries of Nicotinamide Riboside as a Nutrient and Conserved NRK Genes Establish a Preiss-Handler Independent Route to NAD+ in Fungi and Humans. *Cell* **2004**, *117*, 495–502.

8. Revollo, J. R.; Grimm, A. A.; Imai, S.-i., The NAD Biosynthesis Pathway Mediated by Nicotinamide Phosphoribosyltransferase Regulates Sir2 Activity in Mammalian Cells. *Journal of Biological Chemistry* **2004**, *279*, 50754–50763.

9. Rongvaux, A.; Andris, F.; Van Gool, F.; Leo, O., Reconstructing Eukaryotic NAD Metabolism. *BioEssays* **2003**, *25*, 683–690.

10. Koch-Nolte, F.; Fischer, S.; Haag, F.; Ziegler, M., Compartmentation of NAD+-Dependent Signalling. *FEBS Letters* **2011**, *585*, 1651–1656.

11. Simeth, N. A.; Kneuttinger, A. C.; Sterner, R.; König, B., Photochromic Coenzyme Q Derivatives: Switching Redox Potentials with Light. *Chemical Science* **2017**, *8*, 6474–6483.

12. Brieke, C.; Rohrbach, F.; Gottschalk, A.; Mayer, G.; Heckel, A., Light–Controlled Tools. *Angewandte Chemie International Edition* **2012**, *51*, 8446–8476.

13. Velema, W. A.; Szymanski, W.; Feringa, B. L., Photopharmacology: Beyond Proof of Principle. *Journal of the American Chemical Society* **2014**, *136*, 2178–2191.

14. Szymański, W.; Beierle, J. M.; Kistemaker, H. A. V.; Velema, W. A.; Feringa, B. L., Reversible Photocontrol of Biological Systems by the Incorporation of Molecular Photoswitches. *Chemical Reviews* **2013**, *113*, 6114–6178.

15. Lerch, M. M.; Hansen, M. J.; van Dam, G. M.; Szymanski, W.; Feringa, B. L., Emerging Targets in Photopharmacology. *Angewandte Chemie International Edition* **2016**, *55*, 10978-10999.

16. Borowiak, M.; Nahaboo, W.; Reynders, M.; Nekolla, K.; Jalinot, P.; Hasserodt, J.; Rehberg, M.; Delattre, M.; Zahler, S.; Vollmar, A.; Trauner, D.; Thorn-Seshold, O., Photoswitchable Inhibitors of Microtubule Dynamics Optically Control Mitosis and Cell Death. *Cell* **2015**, *162*, 403–411.

17. Frank, J. A.; Moroni, M.; Moshourab, R.; Sumser, M.; Lewin, G. R.; Trauner, D., Photoswitchable fatty acids enable optical control of TRPV1. *Nature Communications* **2015**, *6*, 7118–7129.

18. Reisinger, B.; Kuzmanovic, N.; Löffler, P.; Merkl, R.; König, B.; Sterner, R., Exploiting Protein Symmetry To Design Light-Controllable Enzyme Inhibitors. *Angewandte Chemie International Edition* **2014**, *53*, 595–598.

19. Falenczyk, C.; Schiedel, M.; Karaman, B.; Rumpf, T.; Kuzmanovic, N.; Grotli, M.; Sippl, W.; Jung, M.; Konig, B., Chromo-Pharmacophores: Photochromic Diarylmaleimide Inhibitors for Sirtuins. *Chemical Science* **2014**, *5*, 4794–4799.

20. Lachmann, D.; Studte, C.; Männel, B.; Hübner, H.; Gmeiner, P.; König, B., Photochromic Dopamine Receptor Ligands Based on Dithienylethenes and Fulgides. *Chemistry – A European Journal* **2017**, *23*, 13423–13434.

21. Eisel, B.; Hartrampf, F.; Meier, T.; Trauner, D., Reversible Optical Control of F1Fo-ATP Synthase Using Photoswitchable Inhibitors. *FEBS Letters* **2018**, 592, 343–355.

22. Wilson, D.; Branda, N. R., Turning "On" and "Off" a Pyridoxal 5'-Phosphate Mimic Using Light. *Angewandte Chemie International Edition* **2012**, *51*, 5431–5434.

23. Al-Atar, U.; Fernandes, R.; Johnsen, B.; Baillie, D.; Branda, N. R., A Photocontrolled Molecular Switch Regulates Paralysis in a Living Organism. *Journal of the American Chemical Society* **2009**, *131*, 15966–15967.

24. Singer, M.; Jäschke, A., Reversibly Photoswitchable Nucleosides: Synthesis and Photochromic Properties of Diarylethene-Functionalized 7-Deazaadenosine Derivatives. *Journal of the American Chemical Society* **2010**, *132*, 8372–8377.

25. Brewster, M. E.; Simay, A.; Czako, K.; Winwood, D.; Farag, H.; Bodor, N., Reactivity of biologically important reduced pyridines. IV. Effect of Substitution on Ferricyanide-Mediated Oxidation Rates of Various 1,4-Dihydropyridines. *Journal of Organic Chemistry* **1989**, *54*, 3721–3726.

26. Irie, M., Diarylethenes for Memories and Switches. *Chemical Reviews* **2000**, *100*, 1685–1716.

27. Li, X.; Pu, S.; Li, H.; Liu, G., Photochromism of Novel Isomeric Diarylethenes with Benzofuran and Pyridine Moieties. *Dyes and Pigments* **2014**, *105*, 47–56.

28. Liu, G.; Pu, S.; Wang, R., Photochromism of Asymmetrical Diarylethenes with a Pyrrole Unit: Effects of Aromatic Stabilization Energies of Aryl Rings. *Organic Letters* **2013**, *15*, 980–983.

29. Pavlishchuk, V. V.; Addison, A. W., Conversion Constants for Redox Potentials Measured Versus Different Reference Electrodes in Acetonitrile Solutions at 25 o C. *Inorganica Chimica Acta* **2000**, *298*, 97–102.

30. Wiskich, J. T., 6 - Control of the Krebs Cycle* A2 - Davies, David D. In Metabolism and Respiration, *Academic Press* **1980**, 243–278.

III. PHOTOCHROMIC TOOLS FOR MULTIENZYME COMPLEXES

Chapter III

It's a dangerous business, Frodo, going out your door. You step onto the road, and, if you don't keep your feet, there's no knowing where you might be swept off.

J.R:R. Tolkien – *The Lord of the Rings*

III.1 Allosteric Regulation of the Imidazole Glycerol Phosphate Synthase Multienzyme Complexe with Light-Controllable Ligands

Abstract:

Imidazole glycerol phosphate synthase is a bienzyme complex involved in the bifurcation step of the histidine and the *de novo* purine biosynthetic pathways. Therefore, a tightly allosterically regulated cooperation between both subunits of the multienzyme complex is crucial. Though being investigated for decades, the mechanism of the catalytical coupling has not been fully understood yet. We envisioned to subject the catalytic activity of one subunit to photocontrol, mimicking the binding mode of the parent ligand applying a photoswitchable analogue. In this manner, control of the coupled reaction would be feasible with spatiotemporal resolution. This could give crucial clues about the delicate interplay of both subunits and lead to novel insights into the mechanistic interactions of multienzyme complexes in general. Here, we describe the development of photo regulable ligands towards imidazole glycerol phosphate synthase based on both the diarylethene and the azo motif. We will focus on the synthesis of the target structures, highlight first results in biological testing and give insight in the mode of action of the presented ligand through molecular dynamic simulations.

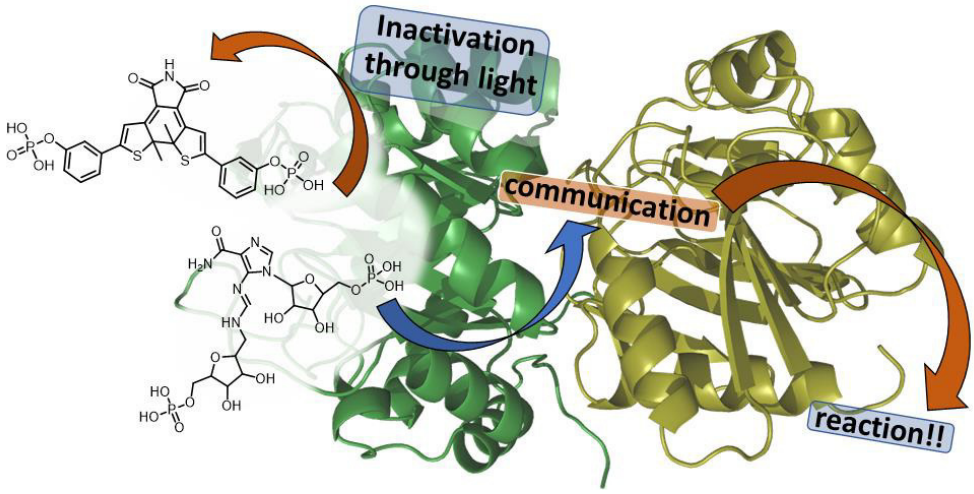

A part of this section was published as:
Kneuttinger, A. C.; Winter, M.; Simeth, N. A.; Heyn, K.; Merkl, R.; König, B.; Sterner, R., Artificial light-regulation of an allosteric bi-enzyme complex by a photosensitive ligand. *ChemBioChem* **2018**, doi: 10.1002/cbic.201800219.

Author contributions

NAS synthesized and characterized all compounds, performed UV/Vis spectroscopic studies and wrote that part of the manuscript as well as introduction and conclusion. ACK and MW studied the compounds in enzyme assays and ACK wrote that part of the manuscript. KH performed MD simulations and wrote that part of the manuscript. RM, RS and BK supervised the project and helped with interpreting the data.

III.1.1 Introduction

Imidazole glycerol phosphate synthase (IGPS) is a bienzyme complex and belongs to the family of glutamine amidotransferases (GATs). In particular, IGPS is involved in the bifurcation step of the histidine and *de novo* purine biosynthetic pathways.[1] The enzyme complex consists of two subunits (Figure 1): the glutaminase subunit (HisH, a representative of the dyad glutaminases) hydrolyzes glutamine to glutamate and ammonia. The synthase subunit (HisF, also called cyclase subunit) catalyzes the addition of an amino group (originating from the cleaved ammonia of the HisH reaction) onto N'-[(5'-phosphoribulosyl)formimino]-5-aminoimidazole-4-carboxamide-ribonucleotide (PRFAR), which is subsequently cleaved into 5-aminoimidazole-4-carboxamide ribotide (AICAR) and imidazoleglycerolphosphate (ImGP).[2] To effectively use the ammonia molecule, which is transported through an intermolecular tunnel from the HisH to the HisF moiety, both subunits need to work in a concerted manner.[1] Indeed, IGPS is one of the most tightly regulated GATs known up to now using a mainly allosteric activation pathway.[3] A crucial element of the allosteric regulation process, is binding of PRFAR to the active site of HisF, which stimulates HisH activity approximately 300-fold.[2] Moreover, without presence of HisF the HisH subunit shows no measurable activity.[3] To cooperate, the glutaminase has to dock onto the N-terminal face of the cyclase to form IGPS and become catalytically functional.[4] However, the detailed mechanism of the allosteric coupling has not been fully understood yet.[2]

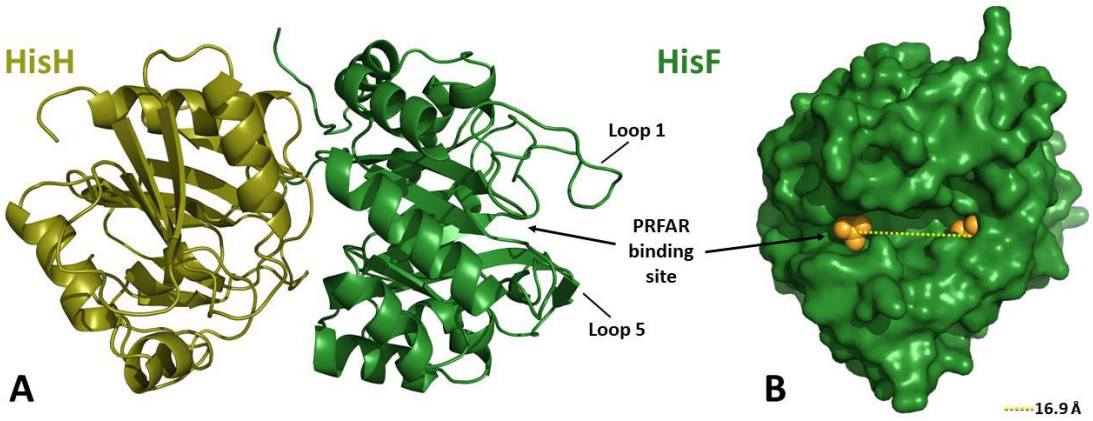

Figure 1: Imidazole glycerol phosphate synthase (IGPS) is a bienzyme complex. A**: It consist of the HisH moiety (olive) and the HisF moiety (green).** B**: PRFAR binds in a deep groove in the HisF moiety. The two phosphate anchoring groups span a distance of 16.9Å,[5] shown in the crystal structure of IGPS obtained from *Thermotoga maritima* (protein data bank (pdb)-id: 1gpw).**

The application of light-mediated tools in biochemical, biological, and even medicinal contexts has expanded rapidly in the past two decades.[6, 7] Astonishing examples in the

growing field of *photopharmacology* have demonstrated that light is a powerful tool in the inhibition of enzymes,[8-11] the assemble of lipid structures[12] or the control of cell survival,[13] as a few examples among many. Using light is especially appealing as it is easy to operate, incomparably fast and precise, and not interfering with most biotransformations. In general, two different approaches can be applied to photocontrol a system of interest.[14] In order to photoregulate enzyme activity, some of the studies focused on the use of small molecular photo responsive structures such as photolabile protecting groups (PLPGs) and photoswitches.[15] These structures can be incorporated into unnatural amino acids as well as into synthetical ligands. In order to light regulate IGPS activity, we set out to use these small molecular structures not only to control one of the two active sites directly, but also to control the second site allosterically.

The first strategy, which we will use to light regulate the allosteric communication of HisF and HisH, is based on the structural integration of photo addressable unnatural amino acids. In particular, amino acids, which have been shown previously to be crucially involved in the enzymes' interactions[2] or were identified through molecular dynamic (MD) simulations, respectively, will be exchanged (introduced *via* genetically adapted ^{t}RNAs following known strategies)[16, 17] with either photolabile protected analogous (ONBY or NPY)[16] or photoswitchable aminoacids (AzoF, Figure 2).[17] In this manner, either the *wildtype* structure will be disturbed by the presence of the PLPG, allowing its recovery after irradiation and photo-induced cleavage of the protecting group, or through conformational change affecting the *wildtype* structure of the photochromic amino acid side chain, respectively. The unnatural amino acids were either purchased (ONBY) or synthesized following known protocols (NPY, AzoF),[16, 17] hence they will not be discussed further within the scope of this thesis.

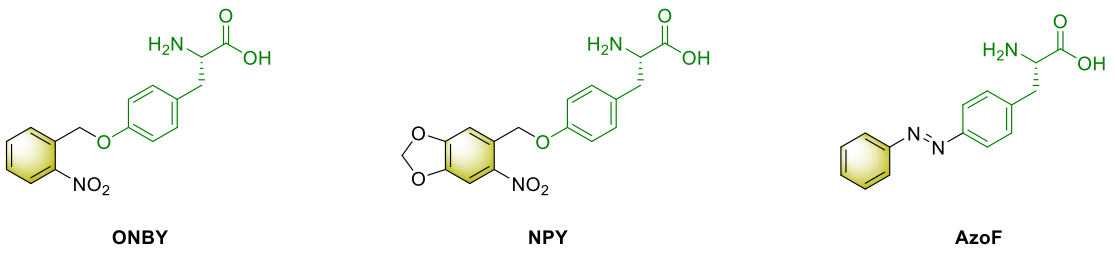

Figure 2: The unnatural amino acids, which will be integrated into the enzyme's primary structure bearing either a PLPG (olive in ONBY and NPY) or a photochromic extension (olive in AzoF) on a natural amino acid (green: tyrosin for ONBY and NPY, phenylalanine for AzoF).

Our second strategy is based on photochromic ligands towards IGPS. Whereas unnatural amino acids need to be introduced through genetical modifications, photochromic ligands

can lead to photocontrol through binding towards the *wildtype* of the enzyme of interest.[15] Indeed, good binding affinities of one photoisomer of the ligands and weaker binding of the other photoisomer is crucial to photoactivate or inactivate the target enzyme. Thus, the compounds must be well designed and need to possess strong interaction sites towards the biomolecule of interest.[6] In the IGPS system, the HisF substrate PRFAR is most suitable as a template to design photochromic ligands. Mainly two advantages favor PRFAR over glutamine: its binding constant is in the μM instead of the mM range, and it activates HisH activity allosterically, whereas glutamine has none such effect. Furthermore, the structure of ProFAR, the precursor molecule of PRFAR in histidine biosynthesis, had already been used previously to build a photochromic ligand.[18] Consequently, we decided to re-synthesize dithienylethenes (DTEs) **DTE1–4** (Figure 3) and investigate their binding modes as a starting point for our search of a photo addressable ligand, which should finally not only address its target enzyme, HisF, but also its coupled partner enzyme, HisH, through induction of allosteric interactions.

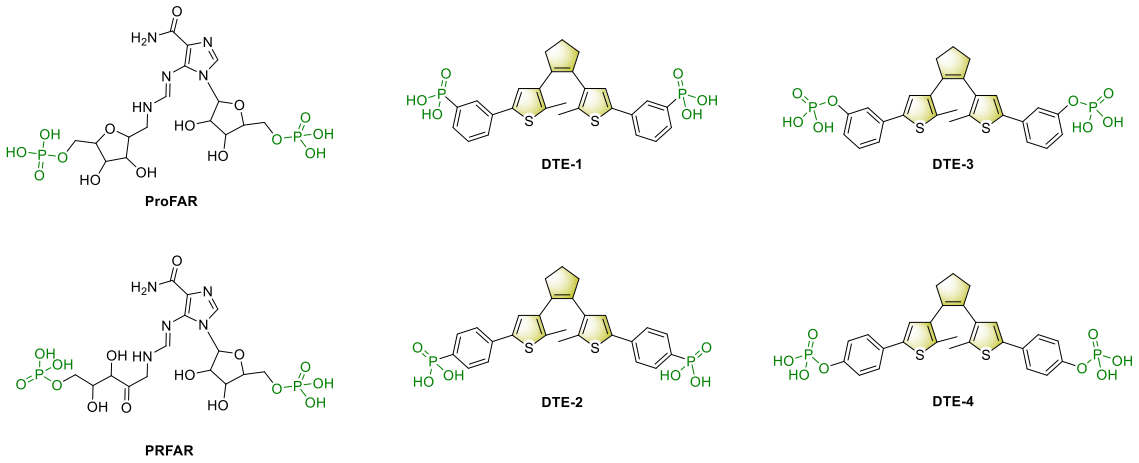

Figure 3: The bisphosphates DTE1-4 were previously designed to mimic the binding mode of ProFAR, the precursor molecule of PRFAR, and will hence be the starting point of this study. They combine the bisphosphate motif of the parent ligand (green) with a photochromic DTE core (olive).

III.1.2 Results and Discussion

III.1.2.1 Results of **DTE1-4**

III.1.2.1.1 Inhibition of HisF by DTE1–4

We first analyzed the binding of the ligands to HisF by determining IC_{50} values (which is the inhibitor concentration that causes 50% reduction in catalytic activity). For this purpose, activity measurements were performed where concentrations of **DTE1–4** in their ring-open and ring-closed states, respectively, were gradually increased, while PRFAR concentration

was kept constant at 7 μM (about twofold of the Michaelis-Menten constant K_m).[2] All ligands inhibited HisF with IC_{50} values in the low micro-molar range (see Table 1 and Appendix). However, **DTE3** stood out with an IC_{50} of only 0.5 μM for the ring-opened form. Furthermore, all compounds showed modestly lower IC_{50} values (ranging between 1.2-fold and 2.7-fold) for the closed states compared to the open states.

In order to characterize the inhibitory effect of the DTE ligands on HisF further, thermodynamic inhibitory constants K_i were determined. For this purpose, PRFAR saturation curves were monitored in the presence of different ligand concentrations (see Appendix). For each substrate saturation curve, an apparent Michaelis-Menten constant K_m^{app} was determined (see Appendix), which was then used to calculate K_i assuming competitive inhibition. For comparison, K_i values were also calculated from the IC_{50} values. All ligands showed inhibition constants in the low micro-molar range (Table 1), similar or up to 18-fold lower than the K_m of PRFAR (3.6 μM).[2] Moreover, in agreement with IC_{50} measurements, **DTE3** showed the best inhibitory effect with a K_i of 0.2 μM for the open form. Furthermore, for **DTE3** a 2.5-fold difference between open and closed state could be measured. The other ligands showed either much higher K_i values (**DTE2**) or no significant K_i differences between their open and closed forms (compounds **DTE1** and **DTE4**). As expected for competitive inhibition, the turnover numbers k_{cat} in the presence of ligand were the same as without inhibitor (Table 1).

Table 1: Inhibition values (IC_{50} and K_i) and k_{cat} values of the HisF reaction with compounds DTE1-4 in their ring-open and ring-closed states.

Compound	IC_{50} [μM]	K_i [μM][a]	K_i [μM][b]	k_{cat} [s]$^{-1}$
DTE1 – open	4.0 ± 0.2	2.0 ± 0.3	1.4	1.3 ± 0.1
DTE1 – closed	7.9 ± 0.9	1.8 ± 0.1	2.7	1.4 ± 0.0
DTE2 – open	4.6 ± 0.2	2.5 ± 0.6	1.6	1.5 ± 0.0
DTE2 – closed	10.4 ± 0.8	6.0 ± 1.5	3.5	1.2 ± 0.1
DTE3 – open	0.5 ± 0.0	0.2 ± 0.0	0.2	1.4 ± 0.1
DTE3 – closed	1.2 ± 0.1	0.5 ± 0.1	0.4	1.5 ± 0.1
DTE4 – open	5.4 ± 0.5	3.1 ± 0.2	1.8	1.4 ± 0.0
DTE4 – closed	14.4 ± 0.8	3.1 ± 0.2	4.9	1.2 ± 0.1

[a]Calculated using the Km^{app} values listed in Table A1 in the Section A.III.1.3. in the Appendix as described in III.1.4.4.. [b]Calculated using the IC_{50} values as described in the Appendix.

Altogether, **DTE3** (exhibiting phosphate groups in *meta*-position) was identified as the most effective competitive inhibitor of HisF. It showed not only a high inhibition capacity, but this property was also affected threefold by irradiation: switching from its flexible ring-opened to its rigid ring-closed state lowered its binding affinity for the active site of HisF.

III.1.2.1.2 Binding modes of DTE3 at the active site of HisF

We performed molecular dynamics simulations to further analyze how **DTE3** interacts with the active site of HisF and why the open conformation exhibits a stronger inhibitory effect than the closed one. For this purpose, PRFAR (as a reference; structure from pdb: 1ox5) and **DTE3** in its ring-open and ring-closed states were placed in the HisF active site of the IGPS complex (pdb-id 1gpw). To reach equilibration, movements were constrained to the various ligands in a 100 ps MD simulation, which led to the three conformations indicated in blue in Figure 4A–C. In order to reveal binding modes, the poses of the ligands resulting from an unconstrained 100 ns MD simulation were compared. then revealed the various binding modes of each ligand. Ligand conformations from the middle and the end of the MD simulation are shown in green and yellow in Figure 4D–F. In the following, the symbol "~" indicates similar, and "≠" dissimilar conformations.

PRFAR showed minimal movements during the simulation and stayed firmly bound in the active site, mainly due to interactions of its two phosphate moieties with the side chains and backbones of various residues (Figure 4A, 4D: blue ~ green ~ yellow). These results are in agreement with published MD simulations.[19] Similar to PRFAR, ring-opened **DTE3** interacted at the start of the simulation with both phosphate binding sites. However, unlike PRFAR, one phosphate group of **DTE3** moved side- and upwards during the simulation, eventually interacting with residues G20 and F23 from loop 1 of HisF (Figure 4B, 4E: blue ≠ green ~ yellow). Hence, the ligand remained permanently attached to one phosphate binding site. In contrast, ring-closed **DTE3** turned out to be so rigid, that it could not be forced to continuously interact with either phosphate binding sites. One phosphate group formed contacts to A224 and S225 residues equally to PRFAR, but did not stay at this position during the MD simulation. Instead, this phosphate group moved towards the base of loop 1 interacting with K19 and D11, a catalytic residue of HisF, while the second phosphate group rested at a position that usually forms contacts to the carboxamide group of PRFAR, *e.g.* residue S144. Altogether, ring-closed **DTE3** moved itself in a position crossway to PRFAR, held by only loose interactions (Figure 4C, 4F: blue ≠ green ≠ yellow). In summary, the MD simulation can explain the different behavior of ring-opened and ring-closed **DTE3** in the inhibitory studies of HisF. Upon irradiation, the ligand stiffens and loses its original interactions, building completely new ones. The threefold less inhibitory effect

suggests that these new interactions are weaker or more unspecific than the initial ones, respectively.

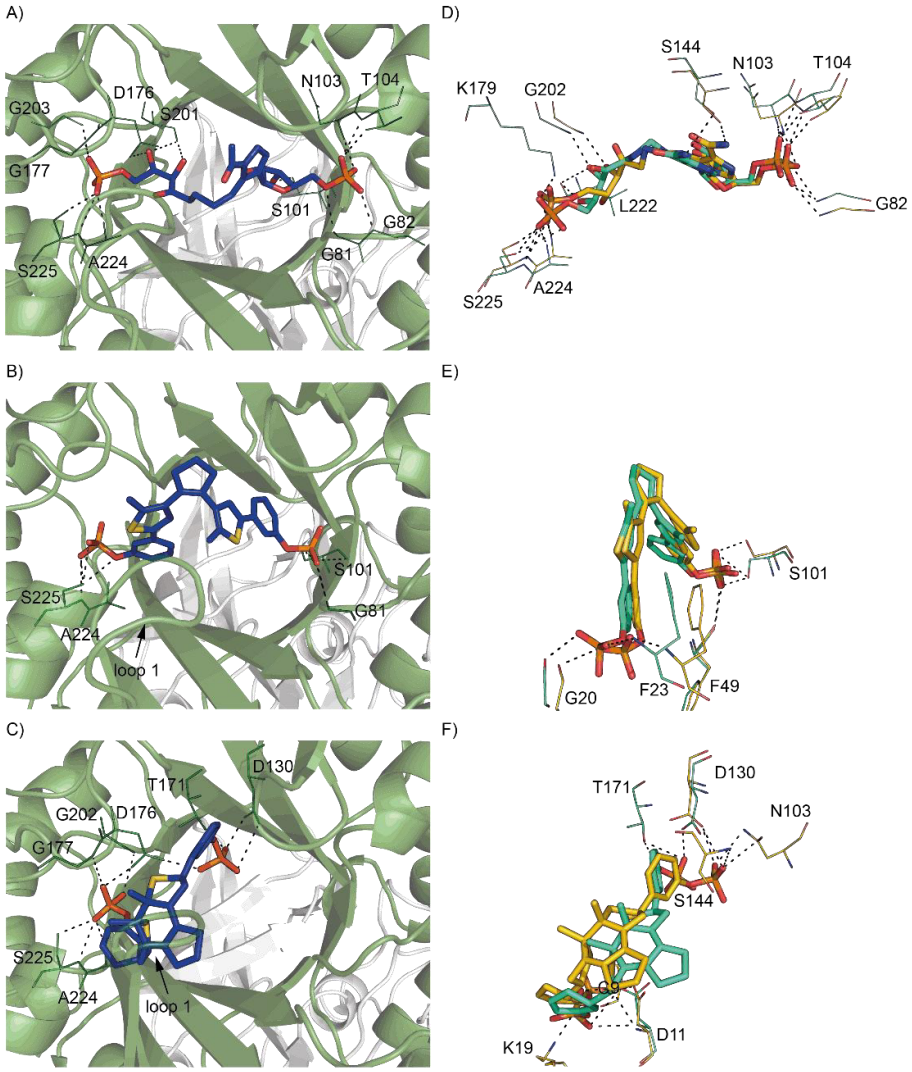

Figure 4: MD simulations of IGPS (ribbon diagram with HisF in green and HisH in white) with bound PRFAR (A, D**) and DTE3 in its open (**B, E**) and closed (**C, F**) states.** A–C: **Each ligand (depicted as blue sticks) was placed in accordance with the known phosphate binding sites into the HisF active site (pdb-id 1gpw) and subjected to a 100 ps MD simulation during which only movements of the ligand were allowed.** D–F: **A subsequent 100 ns MD simulation with the entire ligand-bound IGPS complex revealed the binding modes of each ligand. Shown are two snapshots of the ligands after 50 ns (green sticks) and after 100 ns (yellow sticks). Polar contacts of the phosphate groups of the ligands with the protein backbone and with side chains are indicated by dashed lines.**

III.1.2.1.3 Inhibition of allosteric stimulation of HisH by DTE ligands

HisF and HisH form the allosterically controlled IGPS complex. HisH exhibits significant activity, only upon binding of PRFAR to the active site of HisF .[3, 20, 21] Similary, ProFAR, which is the more stable precursor of PRFAR in histidine biosynthesis, binds to HisF and

activates HisH.[3] Moreover, even a structurally quite dissimilar compound such as NAD^+ shows a modest binding affinity for HisF, which leads to measurable glutamine hydrolysis by HisH.[2] However, the different binding modes of **DTE3** and PRFAR for HisF as revealed by our MD simulations suggested to us that the DTE ligands are unable to activate HisH. In order to verify this assumption, we used two previously established assays: 1) A continuous assay measuring glutamate production photometrically by a coupled glutamate dehydrogenase (GDH) reaction that makes use of NAD^+ as a cofactor (Appendix Section A.III.1.3., Figure A4A),[3] and 2) a discontinuous assay in which the glutamate production step is separated from the GDH reaction, in order to keep NAD^+ separate from activating HisH by binding to HisF (A.III.1.3., Figure A4B).[2]

We compared HisH glutaminase activity in presence of ProFAR, NAD^+, ligands **DTE1–4** in their ring-open and ring-closed state, as well as the basic activity without any ligand (A.III.1.3., Figure A4C). In both assays, ProFAR exhibited the strongest activation resulting in turnover rates of 4.7 min^{-1} (continuous assay) and 2.8 min^{-1} (discontinuous assay), well matching the previously determined k_{cat} value of 4.8 min^{-1}.[2] The second-best activation of HisH was caused by NAD^+ with turnover rates of 1.3 min^{-1} (continuous assay) and 0.23 min^{-1} (discontinuous assay). The basic turnover rate of HisH as detected with the discontinuous assay was 0.05 min^{-1}, again matching the published value of 0.03 min^{-1}.[2] For the DTE ligands, only activities below the ones for NAD^+ were found in both assays. The activities in the discontinuous assay ranged from low basic activity of 0.02–0.03 min^{-1} for compound **DTE4**, to no detectable activities for compounds **DTE1**, **DTE2** and **DTE3**, the activities in the continuous assay were somewhat higher.

Taken together, these results show that the DTE ligands were not able to activate HisH. Just in contrast, they inhibited the activation caused by NAD^+ in the continuous assay.

In the next step, we further analyzed the inhibition capacity of the DTE ligands towards HisH. For this purpose, we chose to compare our best candidate, **DTE3**, with **DTE1**, which exhibited weaker inhibition of HisF in general and no significant difference between its ring-open and ring-closed state in particular (Table 1). In the following IC_{50} experiments, ProFAR was taken as HisH activator in the continuous assay and kept constant at 40 μM, whereas the concentration of the DTE ligands was stepwise increased (A.III.1.3., Figure A5). In these experiments, compound **DTE1** showed in both conformations an IC_{50} of about 33 μM. **DTE3** inhibited HisH about two-fold more efficiently, with its ring-open state being more efficient (IC_{50} = 12.3 μM) than its ring-closed state (IC_{50} = 16.2 μM).

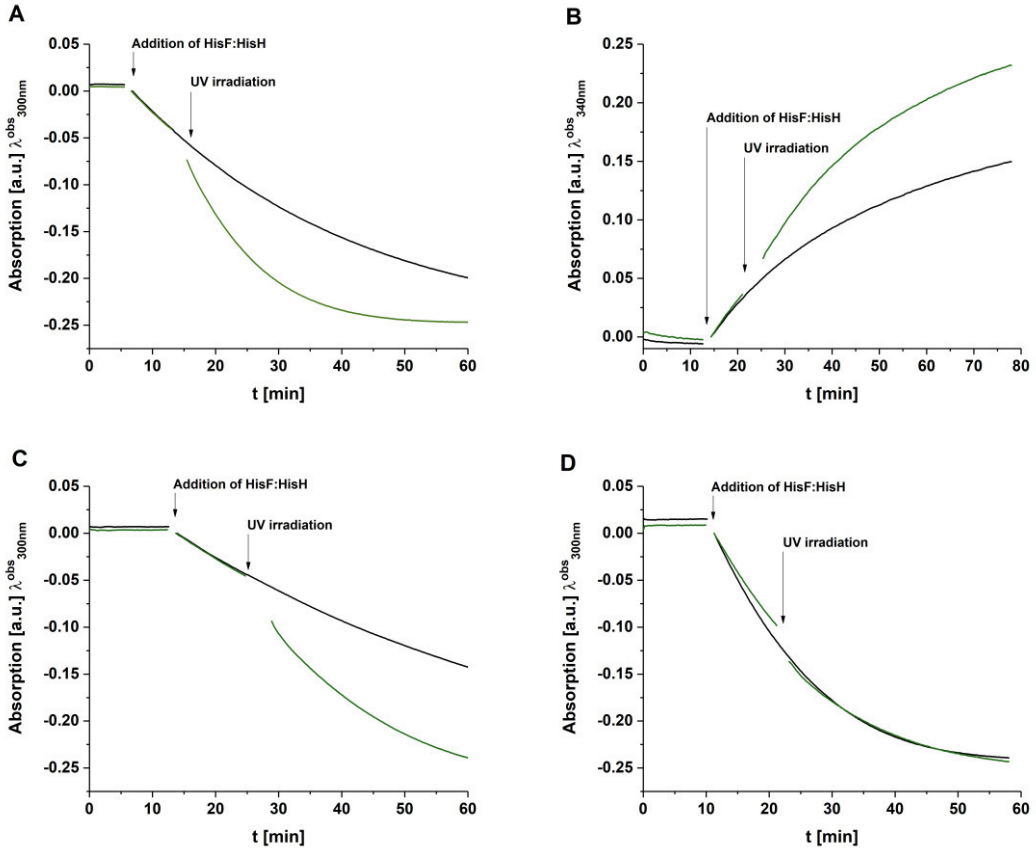

Figure 5: Increase in activity of HisF (A), HisH (B), and IGPS (C, D) upon ring-closure of DTE3 (A, B, C). For comparison, IGPS activity was also followed upon ring-closure of compound 2 (D). Reaction conditions: (A) 50 mM Tris acetate pH 8.5, 0.1 µM HisF:HisH, 100 mM ammonium acetate, 50 µM PRFAR, 7.5 µM DTE3 (open); (B) 50 mM Tricine/KOH pH 8.0, 1 µM HisF:HisH, 10 mM NAD^+, 8 mM glutamine, 1g/L GDH, 40 µM ProFAR, 20 µM DTE3(open); (C, D) 50 mM Tris acetate pH 8.5, 0.1 µM HisF:HisH, 5 mM glutamine, 50 µM ProFAR, 7.5 µM DTE3 (open) and 40 µM DTE1 (open). After initial substrate turnover, the reaction mixture was either left in the spectrophotometer (black transition curve) or removed and irradiated with 312 nm light for 2 min (DTE3) or 1.5 min (DTE1) (green transition curves), respectively, correlating irradiation times determined for complete ring-closure. The baseline shift resulting from different absorption values of the open and closed isomer at 300 nm was corrected with a reference solution without enzymes. See Appendix for turnover numbers prior and after UV irradiation.

III.1.2.1.4 Direct DTE-based light-control of catalysis and allostery of IGPS

Finally, we tested whether the activity of IGPS can be controlled by irradiation with light during catalysis. We started by measuring the turnover of PRFAR by HisF in presence of **DTE3**. In the reaction setup, we compared two samples of identical composition, in which one was taken out and irradiated after the initial reaction phase, whereas the other was kept in the dark. By starting off with the strongly inhibiting, ring-open state of **DTE3**, we were able to enhance the reaction rate about threefold upon irradiation to the ring-closed state (Figure 5A). A similar effect could be observed when HisH activity was tracked with the

continuous assay where the irradiation with UV-light of ring-open **DTE3** led to a two-fold increase of glutamine turnover (Figure 5B). Furthermore, when we monitored the rate of the total IGPS reaction by following PRFAR turnover, we consistently determined a roughly threefold acceleration of the reaction upon irradiation (Figure 5C). If **DTE1** was used instead of **DTE3**, though, no enhancement of the reaction rate could be observed (Figure 5D).

In summary, we have shown that photochromic ligands can be applied for the indirect regulation of an enzyme *via* allowing or hindering the access of an allosteric ligand. In the next step, we wanted to further improve the structure to achieve allosteric activation directly upon ligand binding.

III.1.2.2 Re-Design and MD Simulations

Our investigations revealed that the allosteric communication of IGPS is not triggered upon phosphate binding only (open form of **DTE3**). Another not yet identified interaction of the native ligand PRFAR seems to be necessary. To be able to further address the allosteric communication through a stable and potentially photo-controllable ligand, we re-investigated the binding mode of the parent ligand *in silico* through MD simulations. We found that the amide functionality in PRFAR (Figure 3) is in close proximity to the loop 1 and loop 5 region (Figure 1), potentially exhibiting additional polar interactions to the enzyme's backbone or AA side chains. Especially, loop 1 is highly flexible and seems to play a role in allosteric communication.[19, 22] Hence, we tried to mimic these potential interactions by introducing polar moieties into photochromic ligands.

This assumption led to three novel distinctive designs of generation II ligands (Chart 1). Like **DTE1–4** (*vide supra*), all generation II ligands exhibit a bisphosphate motif mediating binding towards HisF. To attach further functional groups potentially interacting with the loop region, we replaced the cyclopentene ring with a maleimide moiety to generate dithienylmaleimide (DTM) **1a** (4–5 Å distance to the loops), which can be elongated with an additional carbamide function (**1b**, around 3–4 Å distance to the loops). In accordance with our MD simulations this functionality should be capable of directing hydrogen donor-acceptor interactions towards the loop 1 and loop 5 region of HisF. In addition, DTEs and DTMs are very similar regarding their spatial dimensions. Consequently, the high affinity towards HisF is very likely maintained.

The second and third designs (molecules **2**-**4**, Chart 1) are structurally less related with **DTE1–4**. Here, we intended to modify the photochromic core, too. We planned to replace the diarylethene (DAE) switch with a phenylazopyrazole derivative, which could be potentially elongated with carbamide moieties. Azopyrazoles were firstly investigated regarding their photochromic properties by the group of Fuchter in 2014.[23, 24] The authors

reported an extremely robust, synthetically easily accessible dye with a thermally highly stable *Z*-isomer and excellent two-way photoswitching properties. In contrast to DAEs, azo dyes undergo larger geometrical changes upon photo-induced isomerization which could be of advantage in the context of allosteric regulation. However, to position the phosphate groups in the appropriate distance both to each another and to the photoactive core, alkyl chains need to be attached. This makes the molecule overall more flexible and possibly more difficult to be positioned correctly at the binding site, compared to the rigid, aryl-elongated, DTM scaffold. However, the phosphate groups are a rather strong binding motif and the synthesis is easier by the usage of alkyl chains as linker.

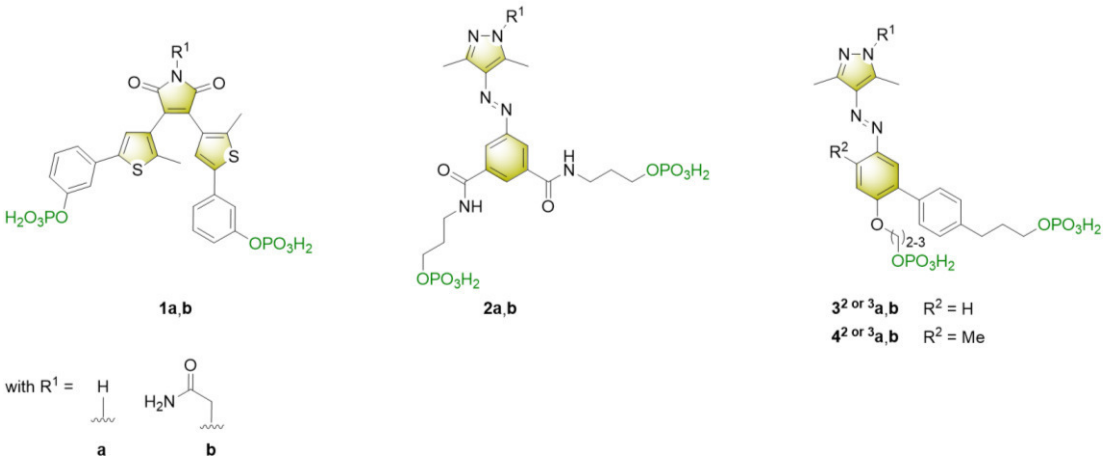

Chart 1: Generation II of photoactive HisF ligands. Design 1 (1a,b) is very similar to previously investigated generation I ligands and is based on a DTM core. Designs 2 (2a,b) and 3 (3a,b and 4a,b exhibiting a C^2 or a C^3-linker, respectively) are based on an azopyrazole scaffold as photochrome. All ligands exhibit a bisphosphate motif as recognition element and can be elongated through a carbamide function for improved interactions with the HisF loop1 and loop5 region.

III.1.2.3 Synthesis and spectroscopic characterization

III.1.2.3.1 Maleimide based Inhibitors

Retrosynthetic Analysis. The retrosynthetic analysis of molecule **1a**,**b** results in two different synthetic strategies. The photochromic core structure is assembled firstly following published procedures[10] and is subsequently functionalized *via* Suzuki-Miyaura cross-coupling (Scheme 1, red dashed line). Another possibility is to firstly perform the palladium mediated arylation reaction of both halves of the molecule and then merge them *via* a Perkin condensation reaction (Scheme 1, blue dashed line). Both approaches will be investigated in the following.

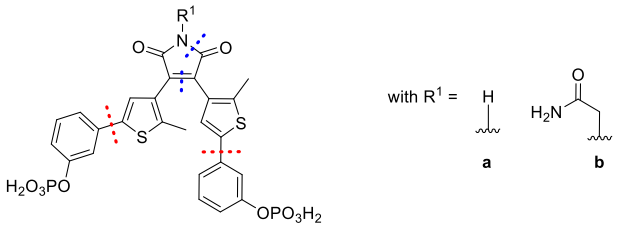

1a,b

Scheme 1: Retrosynthetic analysis of 1a,b. The molecular can be build up either *via* Suzuki-Miyaura cross-coupling (red) or Perking condensation (blue).

Synthesis *via* Suzuki-Miyaura cross-coupling. Analogously to the synthesis of **DTE1-4**, we envisioned the synthesis of similarly functionalized DTMs through Suzuki-Miyaura cross-coupling onto the respective bischloro-DTE (*cf.* table 1) and subsequent aminolysis. Indeed, this approach is especially appealing as the variation of both the core and the functionalized groups would be easily accessible. Hence, bischloro DTE **5** was synthesized according to known procedures.[10] Subsequently, we screened various conditions for Suzuki-Miyaura cross-coupling, varying the palladium catalyst (both Pd(II) and Pd(0) precursors were explored), base, solvent and temperature (Table 1).

Albeit the strategy appears to be very straightforward, the Suzuki-Miyaura cross-coupling onto the bischloro-dithienyl maleimide turned out to be extremely challenging. In accordance with previous investigations of Studte regarding the coupling of phenyl boronic acid,[25] the investigated conditions resulted mainly in dehalogenation of the starting material and none generated the desired product. In addition, using 3-methoxy boronic acid (Entry 8, Table 1) or a Molander-type derivative (Entry 7, Table 1) could not improve the results.

Table 1: Various conditions of Pd–mediated cross-coupling of functionalized aryl borates onto DTM 5.

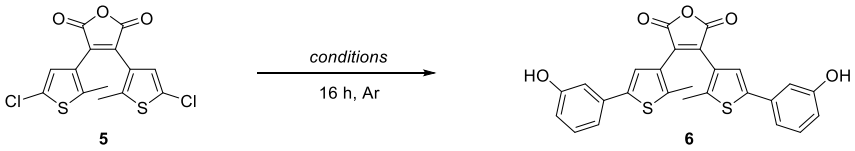

Entry	Boronic Acid/Borate[a]	Catalyst[b]	Base[c]	Solvent[d]	Temperature [°C]	Result[e]
1	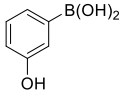	$Pd(PPh_3)_4$	Na_2CO_3	H_2O/THF	80	d.h.
2	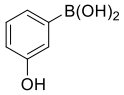	$Pd(PPh_3)_4$	Na_2CO_3	H_2O/THF	60	d.h.
3	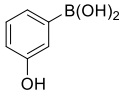	PEPPSI-Ipr	KOtBu	iPrOH	80	d.h.
4	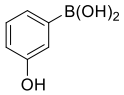	PEPPSI-Ipr	KOtBu	iPrOH	60	d.h.
5	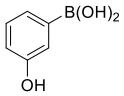	$Pd(OAc)_2$, dppf	Na_2CO_3	H_2O/THF	80	d.h.
6	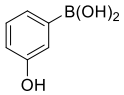	$Pd_2(dba)_3$, Xphos	K_3PO_4	dioxane	100	d.h.
7	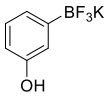	$Pd_2(dba)_3$, Xphos	K_3PO_4	dioxane	100	d.h.
8	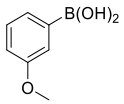	$Pd_2(dba)_3$, Xphos	K_3PO_4	dioxane	100	d.h.

[a]2.2 eq with respect to maleic anhydride **5** (0.1 mmol). [b]0.1 eq. [c]3 eq. [d]0.5 M. [e]d.h. dehalogenation of maleic anhydride **5**.

Synthesis *via* Perkin condensation. We intended to adapt a synthetic approach developed by Falencyk *et al.* to obtain compound **1a** (Scheme 2).[10] Hence, we performed a Suzuki-Miyaura cross-coupling on **7** and **10** to obtain the arylated precursors **8** and **11** (58% or 72% yield, respectively). Direct synthesis of **11** through reduction of **8** as previously reported for similar 2-oxoacetate indoles was not successful.[26]

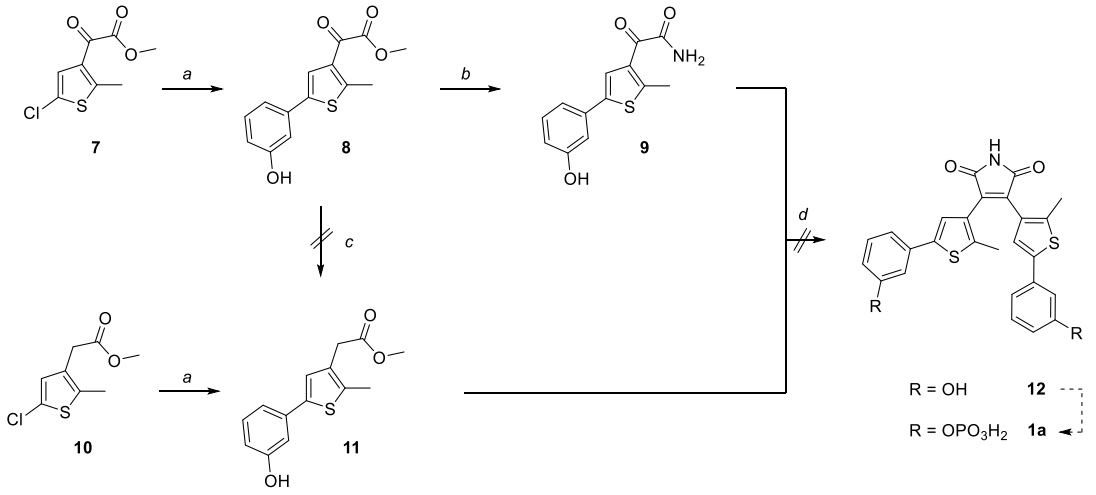

Scheme 2: Synthesis and Perkin condensation of 3-hydroxy thiophenes 9 and 11. *a:* 3-hydroxy boronic acid (1.2 eq), XPhos (0.2 eq), $Pd(OAc)_2$ (0.1 eq), K_3PO_4 (3 eq), dioxane, Ar, 110 °C, 16 h (8: 58%, 11: 72%). *b*: NH_3 (2M in MeOH), MeOH, 2h (*quant.*). *c*: triethylsilane (2.7 eq), TFA, 0 °C to r.t., 16h. *d*: KO^{t}Bu (1.2 eq, 1M in THF), dry THF, N_2, 0 °C to r.t., 16 h.

Then, a Perkin condensation of **9** and **11** was performed. However, the reaction did not give the desired product **12**. The reaction requires strongly basic conditions (KO^{t}Bu) and upon treatment of **9** with the base we observed a coloration of the reaction mixture. We suppose, that this was a consequence of the deprotonation of the phenol moiety. The so formed anionic intermediate might be in competition with the enolate intermediate, which is crucial to start the ring closure of the Perkin condensation.

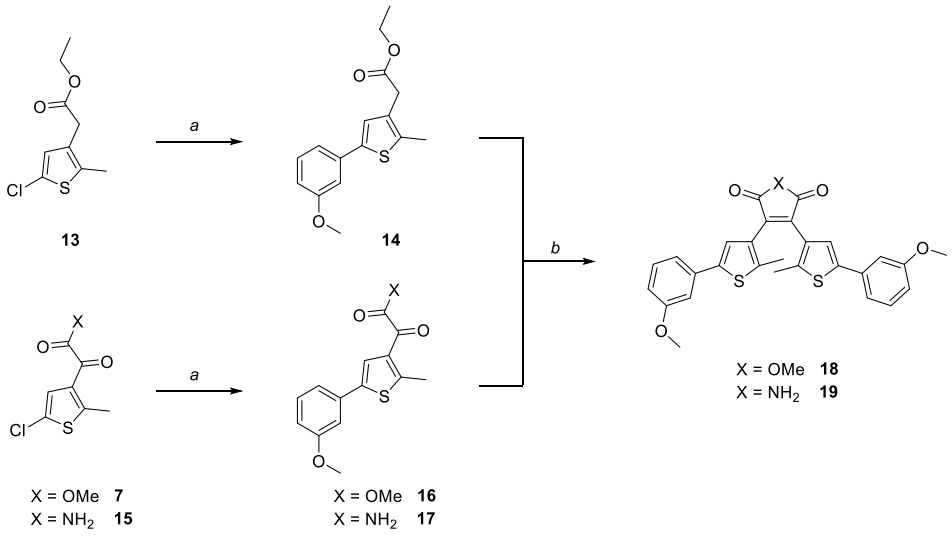

Scheme 3: Synthesis methoxy protected precursors 14 and 17 and Perkin condensation towards 19. *a*: 3-methoxy boronic acid (1.2 eq), XPhos (0.2 eq), $Pd(OAc)_2$ (0.1 eq), K_3PO_4 (3 eq), dioxane, Ar, 110 °C, 16 h (14: 14%, 16: 0%, 17: 65%). *b*: KO^{t}Bu (1.2 eq, 1M in THF), dry THF, N_2, 0 °C to r.t., 16 h (44%).

To circumvent a potential competing side reaction, we protected the phenolic group by using the corresponding 3-methoxy boronic acid in the palladium mediated cross-coupling. Whereas compound **14** could be isolated (14%), the synthesis of **16** was unsuccessful (Scheme 3). In contrast, the amino analogue **17** was accessible in good yields (65%). Hence, we employed **17** and **14** under classical Perkin conditions and were able to isolate **19** (44% yield).

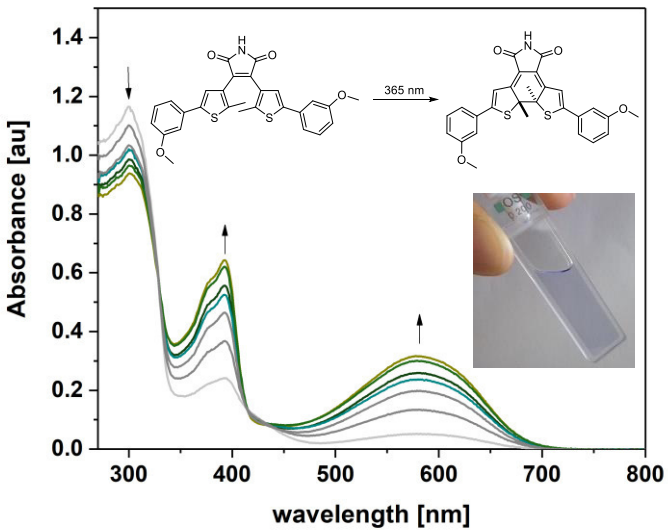

Figure 6: UV-Vis spectrum of compound 19 (100µM in DMSO) after 3 s, 5 s, 7 s, 10 s, 15 s, 25 s and 35 s, and a picture of the cuvette at the PSS.

Additionally, the photochromic behavior of the compound **19** was investigated in DMSO (Figure 6). Upon irradiation with light of 365 nm (Nichia NCSU033B, 700 mA) we observed two novel bands arising at 392 nm and 581 nm, together with a coloration of the DMSO solution in the cuvette (colorless to purple). The newly formed bands can be attributed to the formation of the closed isomer (which has a conjugated π-system) *via* an electrocyclic ring-closure.[27]

The methoxy protected DTM **19** was subsequently deprotected using BBr_3 in DCM at -78 °C resulting in compound **12** (17% after isolation via preparative HPLC) followed by a phosphorylation with $POCl_3$ (Scheme4). Finally, compound **1a** could be isolated through preparative HPLC in low yields (<1%). Identification of the obtained compound could only be performed *via* NMR analysis due to the very low amount of material obtained (0.3 mg, see Experimental Section).

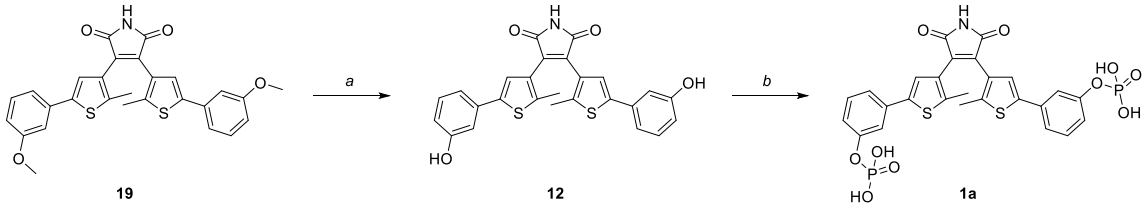

Scheme 4: Synthesis of target molecule 1a from methoxy protected 19. *a*: BBr_3 (1M in DCM), dry DCM, -78 °C to r.t., 16 h (17%). *b*: $POCl_3$, pyridine, dry THF, 0 °C to r.t., 2 h (<1%).

Synthesis of a carboxylic acid analogue. We considered to simplify the structure of the target compound, as the access to the phosphorylated DTMs turned out to be quite tedious and up to now low yielding. To provide a potentially negatively charged anchoring group under physiological conditions, we planned to functionalize the DTM core with carboxy groups. This approach would more quickly result in compounds, which could be evaluated in a biological context.

As the precursors discussed above, compounds **20** and **21** were obtained *via* palladium mediated cross-coupling (35% or 20% yield, respectively). Subsequently, the compounds were subjected to Perkin condensation. However, the COOH-group seemed to undergo deprotonation, preventing the formation of the maleimide ring in a similar way to the unprotected OH-functionalities. Hence, no product could be isolated. ESI-MS analysis showed that only starting material and degradation products (of lower mass) were obtained.

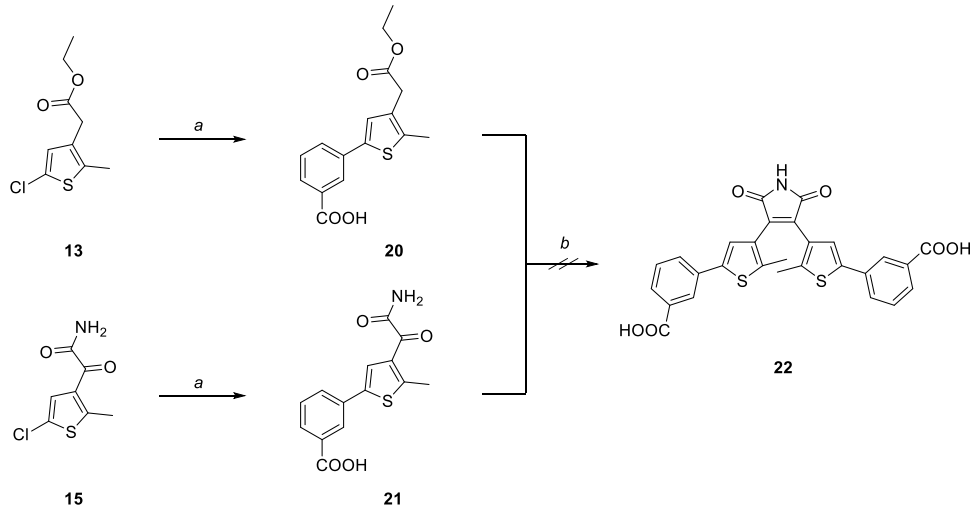

Scheme 5: Synthesis of carboxy substituted analogue 22 *via* Perkin condensation of 20 and 21. *a*: 3-carboxy boronic acid (1.2 eq), XPhos (0.2 eq), $Pd(OAc)_2$ (0.1 eq), K_3PO_4 (3 eq), dioxane, Ar, 110 °C, 16 h (20: 35%, 21: 20%). *b*: KO^{t}Bu (1.2 eq, 1M in THF), dry THF, N_2, 0 °C to r.t., 16 h.

III.1.2.3.2 Aryl azopyrazole based inhibitors

Retrosynthetic Analysis. In the retrosynthetic analysis of both compound **2a**,**b** and **3a**,**b** and **4a**,**b** we identified the benzene ring as central piece of both structural designs (Scheme 6). Starting from a suitable aniline derivative, the azo group can be installed *via* an azo coupling reaction (red dashed line Scheme 6). Likewise, the alkyl and aryl substituents can be condensed onto it (blue dashed lines Scheme 6).

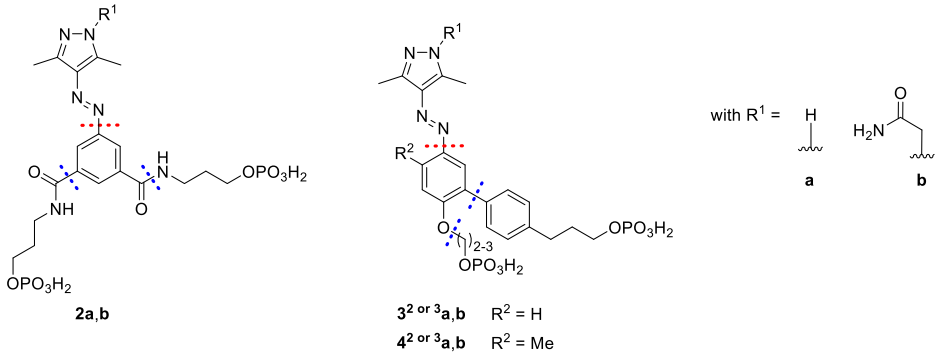

Scheme 6: Retrosynthetic Analysis of arylazopyrazoles 2, 3 and 4. Using the benzene ring as center piece both the azo function (red dashed lines) and the alkyl/aryl substituents (blue dashed lines) can be attached.

Synthesis of compound 2a and 2b. In the first step of the reaction sequence towards target molecules **2a** and **2b**, dicarboxy aniline **23** was treated with $NaNO_2$ in HCl applying a procedure reported by Strecker *et al.* (Scheme 7).[28] The so formed diazonium salt was trapped with acetylacetone to result in compound **24** (83% yield). Ring closure to the corresponding pyrazole was achieved through reaction of **24** with hydrazine (92% yield).[28] The biscarboxylic acid **25** was subsequently activated with thionyl chloride, upon which amino alcohol **26** reacted with the so formed compound to give **27** in low yields (8%). The last step towards target molecule **2a** involved $POCl_3$ in a phosphorylation reaction under basic conditions. However, the reaction conditions appeared to be too harsh. HPLC-DAD and ESI-MS analysis revealed that diverse smaller molecules were formed upon degradation.

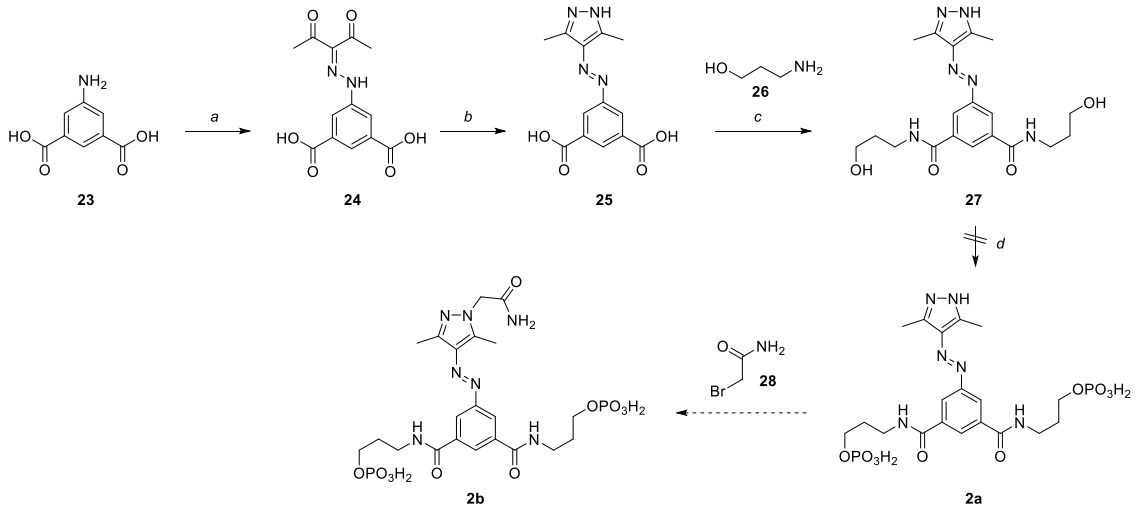

Scheme 7: Synthesis towards aryl azopyrazoles 2a and 2b. *a*: $NaNO_2$ (1.2 eq), acetyl acetone (1.3 eq), NaOAc (3 eq), HCl/water/EtOH, 1 h, r.t. (83%). *b*: hydrazine hydrate (1 eq), EtOH, 70 °C, 3h (92%). *c*: 1) $SOCl_2$, 80 °C, 2h; 2) 26 (2.2 eq), pyridine, dry DMSO, r.t. 16 h (8%). *d*: $POCl_3$, pyridine, dry THF, 0 °C to r.t., 2h.

As the phosphorylation of **27** only led to decomposition of the starting material, we further simplified the target structure replacing the phosphate as hydrogen acceptor moiety with a carboxy group (Scheme 8). Analogously to the main reaction sequence, compound **25** was activated with $SOCl_2$ and then reacted with a suitably functionalized amine. Purification *via* preparative HPLC gave compound **29** in low yields (4%).

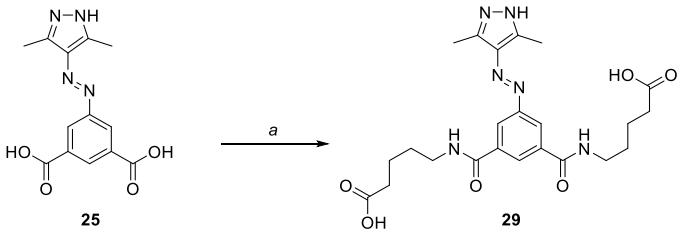

Scheme 8: Activation of 25 with $SOCl_2$ and subsequent reaction with 5-amino valeric acid resulted in functionalized azopyrazole 29. *a:* 1) $SOCl_2$, 80 °C, 2h; 2) 26 (2.2 eq), pyridine, dry DMSO, r.t. 16 h (4%).

Photochemistry. After successful isolation, compound **29** was investigated regarding its photophysical properties. The high density of functional groups led to a good solubility in saline buffer, which will be of advantage in a following biological evaluation. The compound exhibits an absorption maximum at 332 nm, attributable to the ππ* transition of the *E*-isomer (black line, Figure 7 left), in accordance with the behavior of known azopyrazole derivates.[23] Upon irradiation with 365 nm (Nichia NCSU033B, 700 mA) or 400 nm (Edison Edixeaon, 700 mA) the *E*-isomer is interconverted into its corresponding *Z*-form, reaching the PSS (green line, Figure 7 left). Although the parent phenylazopyrazole reported by Fuchter is known to isomerize almost quantitatively to the *Z*-isomer, the dicarboxy derivative

we synthesized appears to have overlapping ππ* and nπ* transitions. Consequently, no clean two-way photoswitching can be observed. Possibly, the alkylated carboxy substituents could destabilize the T-shaped transition state this class of azopyrazole usually exhibits and hence, leads to a thermally labile *Z*-isomer (Figure 7, right, τ=1 s).

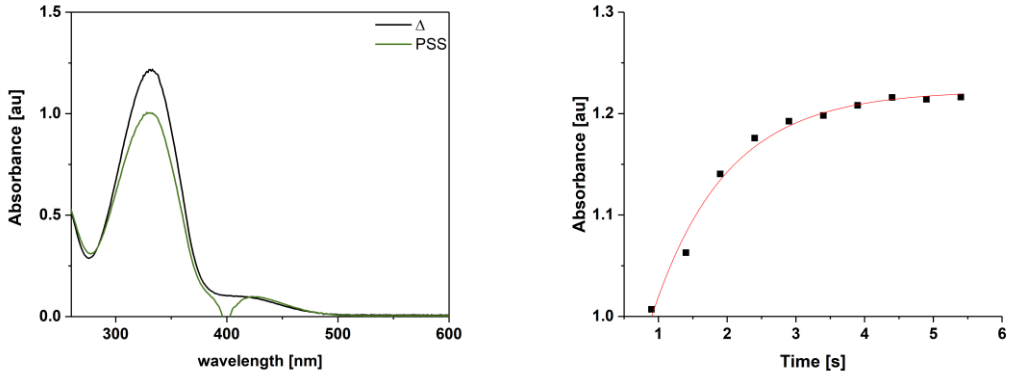

Figure 7: UV-Vis absorption spectrum (left) of compound 29 in saline buffer (67 µM, 0.001% DMSO, black: thermal equilibrium, green: PSS upon irradiation with 400 nm) and its lifetime (right, τ= 1 s).

Synthesis of biarylazopyrazole based inhibitors. We envisioned to synthesize an azopyrazole derivative based on a biaryl moiety to have access to more rigid azo–based ligands. Consequently, an amino cresol **30** was treated with $NaNO_2$ and trapped with acetylacetone to result in compound **31** (78% yield, Scheme 9, path *a*). Compound **32** could be formed following a classical Williamson ether synthesis. However, we found that compound **31** was quite unreactive. Only 9% of desired product with a C^2-linker (11% of the C^3 analogue) could be isolated after 72 h reaction time (path *b*). Adapting a published procedure, we tried to attach the second aryl moiety with a Ti^{III} mediated coupling.[29]

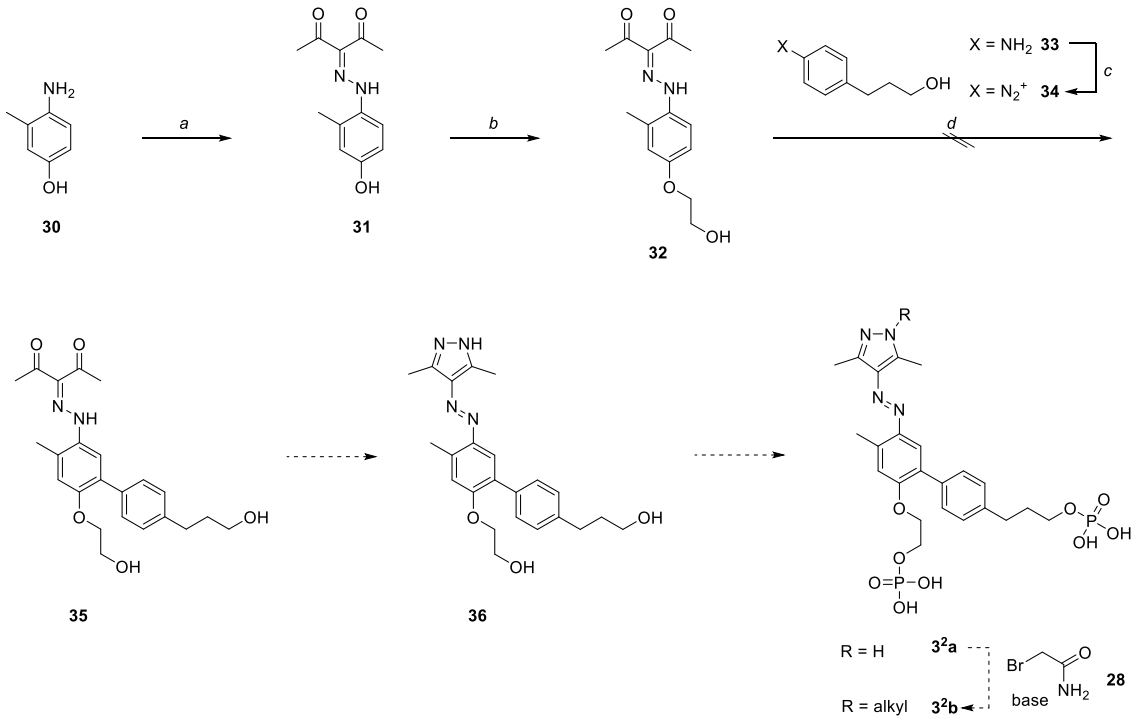

Scheme 9: Synthesis of biaryl based azopyrazoles 3^2a and 3^2b. *a*: $NaNO_2$ (1.2 eq), acetyl acetone (1.3 eq), NaOAc (3 eq), HCl/water/EtOH, 1 h, r.t. (78%). *b*: 2-chloro ethanol (1.2 eq), KCl (0.1 eq), K_2CO_3 (2.5 eq), DMF, 80 °C, 72 h (9%). *c*: $NaNO_2$ (1.2 eq), HCl/water, 1 h, r.t. *d*: $TiCl_3$ (1.2M in HCl), HCl/water, 1 h, r.t.

In particular, aniline **33** was treated with $NaNO_2$ in HCl to form the corresponding diazonium salt **34**. A trapping experiment with 5-hydroxy indole confirmed its formation (ESI-MS, Scheme 10). The diazonium salt solution was then added to **32**. Complexation of Ti^{III} to the ether function and reaction with the diazo compound should lead to the release of nitrogen and the subsequent oxidative bond formation. However, the product could only be observed in small amounts using HPLC-DAD and LC-MS analysis. Isolation did not appear worthwhile, due to the large number of steps needed to synthesize the target structure (Scheme 9).

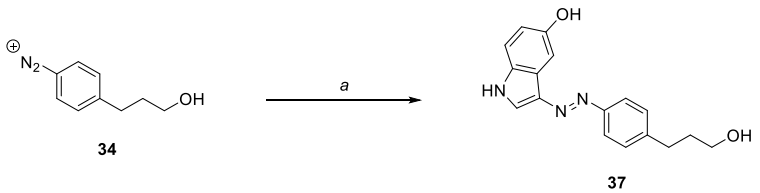

Scheme 10: Diazonium salt 34 could be trapped with 5-hydroxy indole. *a*: 1) $NaNO_2$ (1.2 eq), HCl/water, 1 h, r.t.; 2) 5-hydroxy indole (1.2 eq), DMF, 1 h r.t.

Alternative route *via* Suzuki-Miyaura cross-coupling. As the Ti^{III} mediated arylation turned out to be ineffective, we modified our strategy and intended to employ classical Suziki-Miyaura cross-coupling conditions, by using a pre-functionalized phenol. Hence,

ortho-bromo phenol (**38**) was converted into the corresponding ether *via* Williamson's strategy to give **39**[3] in reasonable yields (ca. 25%). However, the product could not be completely separated from the alkylating agents (neither through column chromatography nor *via* distillation) and was hence converted with a purity of only 70%. The subsequent nitration with HNO_3 in sulfuric acid gave **40**[3] (ESI-MS) and was directly reduced to the corresponding aniline using $SnCl_2$ (ESI-MS). Yet again, isolation through chromatography (reversed phase MPLC) turned out to be challenging and no pure product could be isolated. In addition, direct reaction of the crude mixture to result in **42**[3] was not successful (only traces were found with ESI-MS). Hence, this route did not give access to the desired product **3**[3]**a**.

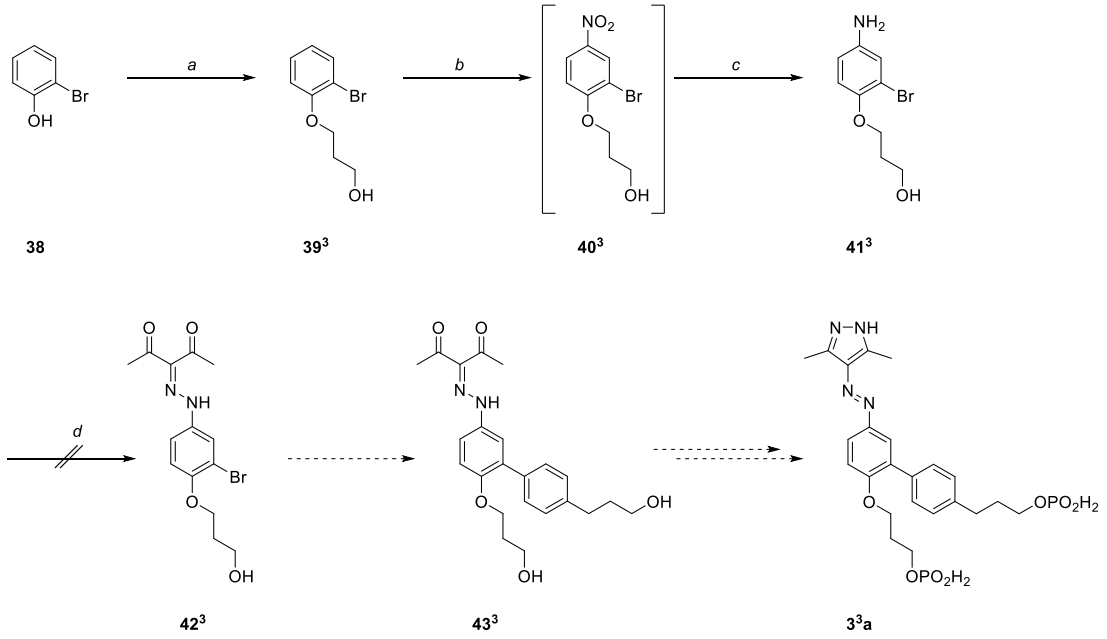

Scheme 11: Synthesis of 3[3]a *via* palladium mediated cross-coupling. *a*: 3-chloro ethanol (1.2 eq), KCl (0.1 eq), K_2CO_3 (2.5 eq), DMF, 80 °C, 72 h. b: H_2SO_4, HNO_3, 0 °C to r.t., 2 h. c: $SnCl_2$ (4 eq), HCl, EtOH, 80 °C, 16h. d: $NaNO_2$ (1.2 eq), acetyl acetone (1.3 eq), NaOAc (3 eq), HCl/water/EtOH, 1 h, r.t.

III.1.3 Conclusion and Outlook

In summary, **DTE1–4** were investigated regarding their binding properties towards HisF in both of their photoisomers. Thereby, all photochromic ligands showed binding with IC_{50} values in the low micromolar range. In particular, **DTE3** exhibited additionally an approximately two- to three-fold difference of both photoisomers in their IC_{50} value. Hence, the compound was also studied in the IGPS overall reaction, where photo-induced ring-closure of **DTE3** reduced its inhibitory affinity and hence, accelerated both the HisF and the HisH reaction. However, no allosteric effects directly upon binding or dissociation of the

switch could be observed. MD simulations indicated that interaction sites in addition to the phosphoate binding sites (*i.e.* hydrogen donor-acceptor moieties) have to be provided by the ligand. Hence, we re-designed the structures proposing the maleimide based analogue (**1a**,**b**) of **DTE3** and highly decorated phenyl azopyrazoles (**2a**,**b**, **3a**,**b** and **4a**,**b**). To access compound **1a**, we investigated both a Suzuki-Miyaura cross-coupling based strategy and a route having a Perkin condensation as the key step. The palladium mediated cross-coupling turned out to be unsuccessful in this case. However, the Perkin condensation afforded (**1a**) in low yield after applying a suitable protection group strategy. The azopyrazoles we designed were either based on a symmetrical biscarboxy aniline (**2a**,**b**) or should exhibit a more rigid biaryl core-structure (**3a**,**b** and **4a**,**b**). Whereas the biaryl core could not be assembled using either Ti^{III} or palladium-mediated coupling reactions so far, biscarboxy phenylazopyrazole was accessible in good yields. Further functionalization *via* the corresponding bisacid chloride and subsequent bisamide formation could be performed in low yields. However, the finial phosphorylation of the alcohol functionality of **27** only resulted in decomposition. Hence, we decided to simplify the structure and synthesized the corresponding carboxy derivative (**29**) moving from a bisphosphate as hydrogen acceptor to a biscarboxy functionality. The compound was successfully synthesized and showed photochromic properties in aqueous buffer, which are promising indications that the compound will also be photocontrollable under enzyme assay conditions.

Both the maleimide based ligand **1a** and the azopyrazole based ligand **29** and their photoisomers will be investigated regarding the binding properties to HisF. Subsequently, their effect on HisH *via* allosteric communication will be evaluated to go one step further in understanding the complex cooperation mechanism in IGPS and GATs in general.

III.1.4 Experimental Section

III.1.4.1 Synthesis

General Procedure I: Suzuki-Miyaura cross-coupling[10]

The appropriate chloro-thiophene (1 eq), the respective phenyl boronic acid (1.2 eq), $Pd(OAc)_2$ (0.1 eq), XPhos (0.2 eq) and K_3PO_4 (3 eq) were dissolved in 1,4-dioxane (5 mL per 1 mmol of thiophene). The resulting suspension was deareated through argon purge (10 min) and heated to 110 °C for 16h. The reaction mixture was cooled to ambient temperature and diluted with water (10 mL per 1 mmol of thiophene) and ethyl acetate (5 mL per 1 mmol of thiophene). The phases were separated and the aqueous phase was extracted with ethyl acetate (5 mL per 1 mmol of thiophene) and the organic phases were combined

and dried over Na_2SO_4. The volatiles were removed *in vacuo* and the crude product was purified through MPLC. The conditions are specified for each compound.

General Procedure II: Aminolysis

The appropriate ester was dissolved in a solution of ammonia (2M in MeOH) and stirred at room temperature for two hours. Usually, the product precipitated already after a few minutes. The volatiles were removed *in vacuo* and the typically pure compound was dried on high vacuum.

General Procedure III: Perkin Condensation[10]

The appropriate amide (1 eq) was dissolved in dry THF (2 mL per 0.5 mmol) under nitrogen atmosphere and cooled to 0 °C. The reaction mixture was treated with KO^{t}Bu (1.2 eq, 1M in THF) and stirred for one hour. Then, the corresponding ester (1 eq) was added and the reaction mixture was stirred for 16 hours at ambient temperature. The reaction was quenched with HCl (aq, 2M) and the mixture was diluted with water (2 mL per 0.5 mmol) and ethyl acetate (2 mL per 0.5 mmol). The phases were separated and the aqueous phase was extracted with ethyl acetate (2x2 mL per 0.5 mmol). The combined organic phases were dried over Na_2SO_4 and the volatiles were removed *in vacuo*. The crude product was purified through MPLC. The conditions are specified for each compound.

General Procedure IV: Deprotection of Methoxy-groups

The appropriate DTM (1 eq) was dissolved in dry DCM (2 mL per 0.1 mmol) under nitrogen and cooled to -78 °C. Then, the reaction mixture was treated with BBr_3 (2 eq per methoxy group, 1M in DCM) dropwise. The reaction mixture was allowed to slowly warm to ambient temperature for 16 h. The reaction mixture was quenched through addition of water (2 mL per 0.1 mmol) and the phases were separated. The aqueous phase was extracted with DCM (2x2 mL per 0.1 mmol). The combined organic phases were dried over Na_2SO_4 and the volatiles were removed *in vacuo*. The product was isolated through preparative HPLC.

General Procedure V: Acetylation of primary amines

The appropriate bis-amide (1 eq) was dissolved in $SOCl_2$ (0.5 mL per 0.15 mmol) and heated to 80 °C until the yellow suspension turned into a bright red solution (depending on the amount from 3h for *ca.* 0.4 mmol to 18h for larger amounts). Then, the solvent was evaporated *in vacuo*. The solids were co-evaporated with DCM (3x 2 mL per 0.15 mmol) and

dissolved in dry DMSO (1 mL per 0.15 mmol). Then, the corresponding primary amine (2.2 eq) and subsequently dry pyridine (0.2 mL per 0.15 mmol) was added. The reaction mixture was stirred at 50 °C for 16h. The reaction mixture was poured onto water (10 mL per 0.15 mmol), neutralized and extracted with ethyl acetate (3x10 mL per 0.15 mmol). The combined organic phases were dried over Na_2SO_4 and the volatiles were removed *in vacuo*. The crude product was purified as specified for each compound.

General Procedure VI: Phenol Ether Formation

The appropriate phenol (1 eq), the corresponding n-chloro alcohol (1.2 eq), KCl (0.1 eq) and K_2CO_3 (2.5 eq) were dissolved in DMF (1 mL per 1 mmol). The suspension was heated to 80 °C for 72h. The reaction mixture was poured onto cold water (10 mL per 1 mmol) and the aqeous phase was extracted with DCM (3x10 mL per 1 mmol). The combined organic phases were dried over Na_2SO_4 and the volatiles were removed *in vacuo*. The crude product was purified through MPLC (first 0 to 20% MeOH in DCM, then 5 to 100% MeCN in H_2O with 0.05% TFA).

*3-(5-Methyl-4-(4-(2-methyl-5-(3-(phosphonooxy)phenyl)thiophen-3-yl)-2,5-dioxo-2,5-dihydro-1H-pyrrol-3-yl)thiophen-2-yl)phenyl dihydrogen phosphate (**1a**)*

Compound **12** (6 mg, 0.013 mmol) was dissolved in dry THF (1 mL) and cooled to 0 °C under nitrogen atmosphere. Then, dry pyridine (0.5 mL) and $POCl_3$ (0.3 mL) were added and the reaction mixture was stirred while warming to ambient temperature for two hours. The compound was purified through preparative HPLC (MeCN in H_2O/0.05% TFA 5 to 98% in 20 min).

The compound was obtained as colorless solid (0.3 mg, 0.00047 mmol, <1%). ^{1}H NMR (400 MHz, Methanol-d_4) δ =7.61 (s, 2H), 7.48 (s, 2H), 7.28 (d, J = 7.7 Hz, 4H), 7.15 (d, J = 7.3 Hz, 2H), 2.72 (s, 6H). ^{31}P NMR (162 MHz, Methanol-d_4) δ =-3.05. R_t: 8.4 min.

*Methyl 2-(5-(3-hydroxyphenyl)-2-methylthiophen-3-yl)-2-oxoacetate (**8**)*

The compound was synthesized according general procedure I using 3-hydroxy phenyl boronic acid. Conditions for MPLC was 15-100% EA in PE. The pure product was obtained as beige powder (2.65 g, 9.60 mmol, 58%).

^{1}H NMR (400 MHz, Chloroform-*d*) δ =7.65 (s, 1H), 7.23 (d, J = 7.9 Hz, 1H), 7.11 (ddd, J = 7.7, 1.7, 0.9 Hz, 1H), 7.03 (t, J = 2.1 Hz, 1H), 6.78 (ddd, J = 8.2, 2.5, 0.9 Hz, 1H), 3.96 (s, 3H), 2.78 (s, 3H). ^{13}C NMR (101 MHz, Chloroform-*d*) δ =180.2 (-), 164.1 (-), 156.2 (-), 154.0 (-), 140.0 (-), 134.5 (-), 132.1 (-), 130.3 (+), 124.9 (+), 118.3 (+), 115.2 (+), 112.7 (+), 52.9

(+), 16.4 (+). ESI-MS: calculated: 276.0456; found: 575.1 ($2MNa^+$, 100%), 299.0 (MNa^+. 90%), 277.1 (MH^+, 100%), 217.0 (MH^+-HCOOMe). HR-MS: 277.0530 (MH^+, 100%). IR: $\tilde{\nu}$ = 3403 (w), 2922 (w), 1733 (s), 1651 (s), 1450 (m), 1323 (m), 1182 (s), 1134 (s), 999 (m), 775 (s), 749 (s). R_f: 0.8 (80% ethyl acetate in petroleum ether). Melting point: 112 °C.

*2-(5-(3-Hydroxyphenyl)-2-methylthiophen-3-yl)-2-oxoacetamide (**9**)*

The compound was synthesized following general procedure II. The product was obtained as light brown powder (921 mg, 3.53 mmol, 98%).

^{1}H NMR (400 MHz, Chloroform-*d*) δ =8.24 (s, 1H), 7.23 (t, *J* = 7.9 Hz, 1H), 7.12 (ddd, *J* = 7.7, 1.7, 1.0 Hz, 1H), 7.07 (t, *J* = 2.1 Hz, 1H), 6.75 (ddd, *J* = 8.1, 2.5, 1.0 Hz, 1H), 2.78 (s, 3H). ^{13}C NMR (101 MHz, Chloroform-*d*) δ =182.0 (q), 164.1 (q), 156.3 (q), 154.9 (q), 139.2 (q), 134.8 (q), 132.0 (q), 130.2 (+), 126.4 (+), 118.2 (+), 115.0 (+), 112.7 (+), 16.9 (+). ESI-MS: calculated: 261.0460; found: 545.1 ($2MNa^+$, 60%), 284.0 (MNa^+, 75%), 262.0 (MH^+, 70%), 217.0 (MH^+-$HCONH_2$, 100%). HR-MS: 262.0531 (MH^+, 100%). IR: $\tilde{\nu}$ = 3388 (w), 3228 (w), 2952 (w), 1707 (w), 1648 (s), 1584 (s), 1454 (m), 1178 (w), 1017 (m), 779 (s). R_f: 0.4 (80% ethyl acetate in petroleum ether). Melting point: 127 °C.

*Methyl 2-(5-(3-hydroxyphenyl)-2-methylthiophen-3-yl)acetate (**11**)*

The compound was synthesized according general procedure I using 3-hydroxy phenyl boronic acid. Conditions for MPLC was 15-100% EA in PE. The pure product was obtained as beige powder (1.83 g, 6.99 mmol, 72%).

^{1}H NMR (400 MHz, Chloroform-*d*) δ =7.36 (t, *J* = 7.9 Hz, 1H), 7.28 – 7.24 (m, 2H), 7.17 (t, *J* = 2.0 Hz, 1H), 6.88 (ddd, *J* = 8.0, 2.5, 0.9 Hz, 1H), 3.90 (s, 3H), 3.73 (s, 2H), 2.58 (s, 3H). ^{13}C NMR (101 MHz, Chloroform-*d*) δ =172.0 (q), 156.1 (q), 139.7 (q), 135.7 (q), 135.5 (q), 130.0 (+), 125.2 (+), 117.8 (+), 114.3 (+), 112.3 (+), 52.3 (+), 34.1 (-), 13.3 (+). GC-MS: calculated: 262.0664; found: 262.0 ($M^{+\cdot}$, 80%), 203.1 ($M^{+\cdot}$-$CH_3CO_2^{\cdot}$, 100%). IR: $\tilde{\nu}$ = 3355 (w), 3179 (w), 2952 (w), 1715 (m), 1648 (m), 1591 (s), 1443 (s), 1271 (s), 835 (s). 782 (s). R_f: 0.8 (80% ethyl acetate in petroleum ether). Melting point: 238 °C.

*3,4-Bis(5-(3-hydroxyphenyl)-2-methylthiophen-3-yl)-1H-pyrrole-2,5-dione (**12**)*

The reaction was performed according to general procedure IV. The product was obtained as purple solid (6 mg, 0.013 mmol, 17%) after purification through preparative HPLC. Due to the small amount of compound obtained, only a limited characterization was performed, and the compound converted in the next step.

^{1}H NMR (400 MHz, Acetone-d_6) δ =7.59 (s, 2H), 7.23 (t, J = 7.8 Hz, 2H), 7.13 – 7.06 (m, 4H), 6.80 (ddd, J = 8.1, 2.4, 1.0 Hz, 2H), 2.73 (s, 6H). ESI-MS: calculated: 473.0755; found: 472.1 ($(M-H)^-$, 100%). HR-MS: 474.0838 (MH^+, 100%). R_f: 0.26 (40% ethyl acetate in petroleum ether).

*Methyl 2-(5-(3-methoxyphenyl)-2-methylthiophen-3-yl)acetate (**14**)*

The compound was synthesized according general procedure I using 3-methoxy phenyl boronic acid. Conditions for MPLC were 5% EA in PE. The pure product was obtained as colorless highly viscous liquid (385 mg, 1.33 mmol, 14%).

^{1}H NMR (400 MHz, Chloroform-d) δ =7.44 – 7.35 (m, 2H), 7.30 – 7.23 (m, 1H), 7.20 (dd, J = 2.5, 1.7 Hz, 1H), 6.93 (ddd, J = 8.2, 2.6, 0.9 Hz, 1H), 4.30 (q, J = 7.1 Hz, 2H), 3.97 (s, 3H), 3.67 (s, 2H), 2.55 (s, 3H), 1.41 (t, J = 7.1 Hz, 3H). ^{13}C NMR (101 MHz, Chloroform-d) δ =171.0 (q), 159.9 (q), 139.8 (q), 135.7 (q), 135.4 (q), 130.4 (q), 129.8 (+), 125.3 (+), 118.1 (+), 112.7 (+), 111.0 (+), 60.9 (-), 55.3 (+), 34.3 (-), 14.2 (+), 13.3 (+). ESI-MS: calculated: 290.0977; found: 308.1 (MNH_4^+, 85%), 291.1 (MH^+, 100%). HR-MS: 291.1053 (MH^+, 100%). IR: $\tilde{\nu}$ = 2982 (w), 2837 (w), 1730 (s), 1599 (m), 1464 (m), 1431 (m), 1263 (m), 1163 (s), 1028 (s), 775 (s). R_f: 0.9 (80% ethyl acetate in petroleum ether).

*2-(5-(3-Methoxyphenyl)-2-methylthiophen-3-yl)-2-oxoacetamide (**17**)*

The compound was synthesized according general procedure I using 3-methoxy phenyl boronic acid. Conditions for MPLC were 30-100% EA in PE. The pure product was obtained as beige powder (879 mg, 3.20 mmol, 65%).

^{1}H NMR (300 MHz, Chloroform-d) δ =8.26 (s, 1H), 7.30 (t, J = 7.9 Hz, 1H), 7.20 – 7.16 (m, 1H), 7.13 – 7.07 (m, 1H), 6.92 – 6.81 (m, 1H), 3.86 (s, 3H), 2.79 (s, 3H). ^{13}C NMR (101 MHz, Chloroform-d) δ =186.7 (q), 163.9 (q), 158.4 (q), 143.3 (q), 138.5 (q), 136.1 (q), 133.9 (+), 130.0 (+), 122.3 (+), 117.3 (+), 115.2 (+), 59.2 (+), 20.5 (+). ESI-MS: calculated: 275.0616; found: 573.1 ($2MNa^+$, 40%), 298.1 (MNa^+, 30%), 276.1 (MH^+, 80%), 231.0 (MH^+-$HCONH_2$, 100%). HR-MS: 298.0502 (MNa^+, 30%), 276.0684 (MH+, 80%) 231.0471 (MH^+-$HCONH_2$, 100%). IR: $\tilde{\nu}$ = 3407 (m), 3217 (m), 2922 (m), 2848 (w), 1715 (s), 1654 (s), 1465 (m), 1353 (m), 1148 (m), 768 (s). R_f: 0.7 (80% ethyl acetate in petroleum ether). Melting point: 152 °C.

*3,4-bis(5-(3-methoxyphenyl)-2-methylthiophen-3-yl)-1H-pyrrole-2,5-dione (**19**)*

The compound was synthesized according to general procedure III. The compound was purified through MPLC (30-65% EtOAc in petroleum ether). The product was obtained as yellow to green solid (120 mg, 0.239 mmol, 44%)

^{1}H NMR (400 MHz, Chloroform-*d*) δ =8.09 (*b*s, 1H), 7.48 (s, 2H), 7.48 – 7.43 (m, 2H), 7.33 (ddd, *J* = 7.6, 1.8, 1.0 Hz, 2H), 7.08 (d, *J* = 5.4 Hz, 2H), 7.02 (ddd, *J* = 8.2, 2.6, 1.0 Hz, 2H), 4.02 (d, *J* = 1.5 Hz, 6H), 2.59 (d, *J* = 1.1 Hz, 6H). ^{13}C NMR (101 MHz, Chloroform-*d*) δ =170.4 (q), 160.0 (q), 141.5 (q), 141.4 (q), 134.9 (q), 134.1 (q), 133.9 (q), 130.0 (+), 129.9 (+), 127.4 (q), 124.4 (+), 122.7 (+), 118.3 (+), 113.2 (+), 111.3 (+), 109.4 , 55.3 (+), 15.1 (+), 14.6 (+). ESI-MS: calculated: 501.1068; found: 502.1 (MH^+, 95%), 501.1 ($M^{+\cdot}$, 100%). HR-MS: 502.1138. IR: $\tilde{\nu}$ = 3243 (w), 3001 (w), 2914 (w), 1707 (s), 1599 (m), 1431 (m), 1167 (s), 1044 (m), 775 (m), 656 (s). R_f: 0.8 (80% ethyl acetate in petroleum ether).

*3-(4-(2-Ethoxy-2-oxoethyl)-5-methylthiophen-2-yl)benzoic acid (**20**)*

The compound was synthesized according general procedure I using 3-carboxy phenyl boronic acid. Conditions for MPLC were 25 to 100% EA in PE to 20% MeOH in EA. The pure product was obtained as light brown highly viscous liquid (113 mg, 0.39 mmol, 35%).
^{1}H NMR (400 MHz, Acetone-d_6) δ =8.20 (t, *J* = 1.8 Hz, 1H), 7.92 (dt, *J* = 7.8, 1.4 Hz, 1H), 7.82 (ddd, *J* = 7.8, 2.0, 1.1 Hz, 1H), 7.55 – 7.49 (m, 1H), 7.35 (s, 1H), 4.12 (q, *J* = 7.1 Hz, 2H), 3.60 (s, 2H), 2.42 (s, 3H), 1.22 (t, *J* = 7.1 Hz, 3H). ^{13}C NMR (101 MHz, Acetone-d_6) δ =170.2 (q), 166.4 (q), 138.0 (q), 135.8 (q), 134.7 (q), 131.8 (q), 131.3 (q), 129.3 (+), 129.2 (+), 128.0 (+), 126.5 (+), 125.8 (+), 60.3 (-), 33.5 (-), 13.6 (+), 12.3 (+). ESI-MS: calculated: 304.0769; found: 303.1 ($(M-H)^-$, 100%). HR-MS: 303.0701 ($(M-H)^-$, 100%). IR: $\tilde{\nu}$ = 2982 (w), 2941 (w), 2572 (w), 1737 (m), 1681 (s), 1443 (w), 1297 (m), 1200 (m), 947 (m), 753 (s). R_f: 0.8 (20% MeOH in ethyl).

*3-(4-(2-Amino-2-oxoacetyl)-5-methylthiophen-2-yl)benzoic acid (**21**)*

The compound was synthesized according general procedure I using 3-carboxy phenyl boronic acid. Conditions for MPLC were 25 to 100% EA in PE to 25% MeOH in EA. The pure product was obtained as a mixture with the 3-carboxy boronic acid and could not be separated. The crude NMR showed that 20% product were formed. Expecting that only the amide functionality could react in the subsequent Perkin condensation, a test reaction using this mixture was performed.
^{1}H NMR (300 MHz, Acetone-d_6) δ =7.85 (ddd, *J* = 7.8, 2.0, 1.1 Hz, 1H), 7.71 (d, *J* = 5.5 Hz, 2H), 7.61 – 7.57 (m, 2H), 7.21 (s, 1H), 2.70 (s, 3H). ESI-MS: calculated: 289.0409; found: 579.1 ($2MH^+$, 30%), 307.1 (MNH_4^+, 15%), 290.0 (MH^+, 55%), 245.0 (MH^+-$HCONH_2$, 100%). HR-MS: 288.0338 ($(M-H)^-$, 100%).

*5-(2-(2,4-Dioxopentan-3-ylidene)hydrazineyl)isophthalic acid (**24**)*

The reaction was performed according to the procedure reported by Stricker *et al.* [28]

The product was obtained as yellow powder (13.81 g, 47. 29 mmol, 83%).

^{1}H NMR (300 MHz, DMSO-d_6) δ =13.68 (s, 1H), 13.38 (*b*s, 1H), 8.21 (d, *J* = 1.5 Hz, 2H), 8.17 (t, *J* = 1.5 Hz, 1H), 2.45 (s, 3H), 2.39 (s, 3H). ^{13}C NMR (75 MHz, DMSO-d_6) δ =197.0 (q), 196.0 (q), 166.0 (q), 142.6 (q), 134.3 (q), 132.4 (q), 125.6 (+), 120.2 (+), 31.1 (+), 26.0 (+). ESI-MS: calculated: 292.0695; found: 315.1 (MNa^+, 5%), 293.1 (MH^+, 100%). HR-MS: 293.0768 (MH^+, 100%). IR: $\tilde{\nu}$ = 1726 (m), 1636 (m), 1502 (m), 1174 (s), 805 (m), 671 (s). R_f: 0.1 (10% MeOH in DCM). Melting point: 272 °C.

*(E)-5-((3,5-Dimethyl-1H-pyrazol-4-yl)diazenyl)isophthalic acid (**25**)*

The reaction was performed according to the procedure reported by Stricker *et al.* [28]

The product was obtained as bright yellow powder (1.05 g, 3.64 mmol, 92%).

^{1}H NMR (300 MHz, DMSO-d_6) δ =8.48 (d, *J* = 1.6 Hz, 1H), 8.39 (d, *J* = 1.6 Hz, 2H), 2.47 (s, 6H). ^{13}C NMR (75 MHz, DMSO-d_6) δ =167.1 (q), 166.3 (q), 153.0 (q), 149.1 (q), 141.1 (q), 134.3 (q), 132.6 (q)s, 131.6 (q), 13 0.0 (+), 125.4 (+), 118.0 (+), 11.9 (+), 9.6 (+). ESI-MS: calculated: 288.0859; found: 289.1 (MH^+, 100%). HR-MS: 289.0931 (MH^+, 100%). IR: $\tilde{\nu}$ = 3191 (m), 1722 (s), 1565 (w), 1431 (m), 1249 (s), 839 (m), 783 (s). R_f: 0.1 (10% MeOH in DCM). Melting point: 227 °C.

*(E)-5-((3,5-Dimethyl-1H-pyrazol-4-yl)diazenyl)-N1,N3-bis(3-hydroxypropyl)isophthalamide (**27**)*

The compound was synthesized according to general procedure V. The product was obtained as yellow solid (642 mg, 1.60 mmol, 8%) after purification through preparative HPLC.

^{1}H NMR (400 MHz, Methanol-d_4) δ =8.33 (d, *J* = 1.7 Hz, 2H), 8.29 (t, *J* = 1.7 Hz, 1H), 3.67 (t, *J* = 6.3 Hz, 4H), 3.52 (t, *J* = 6.9 Hz, 4H), 1.86 (p, *J* = 6.6 Hz, 4H). ^{13}C NMR (101 MHz, Methanol-d_4) δ =167.6 (q), 153.7 (q), 141.9 (q), 135.9 (q), 134.4 (q), 126.3 (+), 122.6 (+), 59.2 (-), 36.9 (-), 31.8 (-), 10.7 (+). ESI-MS: calculated: 402.2016; found: 403.2 (MH^+, 100%). R_f: 0.2 (80% ethyl acetate in petroleum ether).

*(E)-5,5'-((5-((3,5-Dimethyl-1H-pyrazol-4-yl)diazenyl)isophthaloyl)bis(azanediyl))dipentanoic acid (**29**)*

The compound was synthesized according to general procedure V. The compound was purified though preparative HPLC (MeCN in H_2O/0.05% TFA, 5-98% in 13 min). The product was obtained as yellow solid (14 mg, 0.03 mmol, 4%). ^{1}H NMR (400 MHz, Methanol-d_4) δ =8.49 (dt, *J* = 4.2, 1.7 Hz, 2H), 8.42 (t, *J* = 1.8 Hz, 1H), 3.44 (q, *J* = 4.7, 3.7

Hz, 2H), 2.56 (s, 6H), 2.37 (td, *J* = 6.5, 3.2 Hz, 2H), 1.70 (p, *J* = 3.2 Hz, 4H). ^{13}C NMR (101 MHz, Methanol-d_4) δ =176.0 (q), 167.4 (q), 167.1 (q), 153.7 (q), 141.9 (q), 135.9 (q), 134.4 (q), 132.1 (q), 128.5 (+), 124.6 (+), 124.4 (+), 39.4 (-), 33.1 (-), 28.5 (-), 22.1 (-), 10.6 (+). ESI-MS: calculated: 486.2227; found: 487.2 (MH^+, 25%), 388.2 (100%), 289.1 (50%). HR-MS: 487.2296 (MH^+). IR: $\tilde{\nu}$ = 3340 (w), 3176 (w), 3094 (m), 2960 (m), 1715 (s), 1625 (s), 1558 (s), 1409 (s), 1290 (s), 1241 (s), 1185 (s), 760 (s), 678 (s). R_f: 4.8 min.

*3-(2-(4-Hydroxy-2-methylphenyl)hydrazineylidene)pentane-2,4-dione (**31**)*

The reaction was performed according to the procedure reported by Stricker *et al.* [28]

The product was obtained as yellow powder (1.43 g, 6.10 mmol, 78%).

^{1}H NMR (400 MHz, DMSO-d_6) δ =15.11 (s, 1H), 9.71 (s, 1H), 7.68 (d, *J* = 8.7 Hz, 1H), 6.86 (dd, *J* = 8.8, 2.7 Hz, 1H), 6.80 (d, *J* = 2.6 Hz, 1H), 2.59 (s, 3H), 2.49 (s, 3H), 2.38 (s, 3H). ^{13}C NMR (101 MHz, DMSO-d_6) δ =196.7 (q), 196.4 (q), 156.3 (q), 133.1 (q), 132.1 (q), 127.8 (q), 117.7 (+), 117.1 (+), 115.0 (+), 31.5 (+), 26.9 (+), 17.0 (+). ESI-MS: calculated: 234.1004; found: 235.1 (MH^+, 100%). HR-MS: 235.1077 (MH^+, 100%). IR: $\tilde{\nu}$ = 3138 (m), 2110 (w), 1629 (m), 1595 (m), 1368 (m), 1327 (s), 1197 (s), 931 (m), 816 (s). R_f: 0.6 (80% ethyl acetate in petroleum ether). Melting point: 231 °C.

*3-(2-(4-(2-Hydroxyethoxy)-2-methylphenyl)hydrazineylidene)pentane-2,4-dione (**32**^{2})*

The compound was synthesized according to general procedure VI. The product was obtained as obtained as red oily solid (106 mg, 0.38 mmol, 9%) after MPLC (C18, 5-100% MeCN in H_2O/0.05% TFA).

^{1}H NMR (400 MHz, Methanol-d_4) δ =7.69 (d, *J* = 8.9 Hz, 1H), 6.92 (dd, *J* = 8.9, 2.8 Hz, 1H), 6.86 (d, *J* = 2.7 Hz, 1H), 4.05 (dd, *J* = 5.3, 4.2 Hz, 2H), 3.86 (dd, *J* = 5.3, 4.1 Hz, 2H), 2.54 (s, 3H), 2.45 (s, 3H), 2.35 (s, 3H). ^{13}C NMR (101 MHz, Methanol-d_4) δ =197.7 (q), 197.1 (q), 157.4 (q), 133.2 (q), 132.8 (q), 127.4 (+), 116.3 (+), 113.6 (+), 69.5 (-), 60.3 (-), 30.1 (+), 25.2 (+), 15.7 (+). ESI-MS: calculated: 278.1267; found: 301.1 (MNa^+, 10%), 279.1 (MH^+, 100%). The corresponding hydrazone derivative could be formed following Strecker *et al.*[28] and was confirmed by ESI-MS.

ESI-MS: calculated: 274.1430; found: 275.2 (MH^+, 10 0%).

*3-(2-(4-(3-Hydroxypropoxy)-2-methylphenyl)hydrazineylidene)pentane-2,4-dione (**32**[3])*

The compound was synthesized according to general procedure VI. The product was obtained as red oily solid (139 mg, 0.476 mmol, 11%) after MPLC (C18, 5-100% MeCN in H_2O/0.05% TFA).

^{1}H NMR (400 MHz, Methanol-*d*$_4$) δ =7.64 (d, *J* = 8.9 Hz, 1H), 6.87 (dd, *J* = 8.9, 2.8 Hz, 1H), 6.84 – 6.66 (m, 1H), 4.06 (t, *J* = 6.3 Hz, 2H), 3.73 (t, *J* = 6.3 Hz, 2H), 2.52 (s, 3H), 2.42 (s, 3H), 2.32 (s, 3H), 1.97 (p, *J* = 6.3 Hz, 2H). ^{13}C NMR (101 MHz, Methanol-*d*$_4$) δ =197.5 (q), 196.9 (q), 157.5 (q), 133.0 (q), 132.7 (q), 127.3 (q), 116.2 (+), 116.2 (+), 113.5 (+), 64.6 (-), 58.1 (-), 32.0 (-), 30.1 (+), 25.2 (+), 15.7 (+). ESI-MS: calculated: 292.1423; found: 315.1 (MNa^+, 10%), 293.1 (MH^+, 100%). HR-MS: 293.1496 (MH^+, 100%).

*(E)-3-((4-(3-Hydroxypropyl)phenyl)diazenyl)-1H-indol-5-ol (**37**)*

ESI-MS: calculated: 281.1164; found: 282.2 (MH^+, 100%).

*3-(2-Bromophenoxy)propan-1-ol (**39**[3])*

Ortho-bromo phenol (4.0 g, 23.12 mmol) was dissolved in acetone (150 mL). K_2CO_3 (9.6 g, 69.36 mmol) and 3-chloro propan-1-ol (1.9 mL, 23.12 mmol) were added and the reaction mixture was heated to 70 °C for 72h. Silica gel was added to the cooled reaction mixture and the solvent was evaporated. The dry load was chromoragraphed through MPLC (EA in PE, 30 to 50%). The desired product was obtained as colorless oil. The alkylation agent could not be fully removed through chromatography or distillation. Hence, the compound was converted as a mixture.

^{1}H NMR (400 MHz, Chloroform-*d*) δ =7.53 (dd, *J* = 7.9, 1.6 Hz, 1H), 7.29 – 7.23 (m, 1H), 6.91 (dd, *J* = 8.3, 1.4 Hz, 1H), 6.85 (td, *J* = 7.7, 1.4 Hz, 1H), 4.20 (t, *J* = 5.8 Hz, 2H), 3.97 – 3.88 (m, 2H), 2.11 (p, *J* = 5.7 Hz, 2H). ^{13}C NMR (101 MHz, Chloroform-*d*) δ =155.0 (q), 133.3 (+), 128.5 (+), 122.1 (+), 112.9 (+), 112.1 (q), 67.6 (-), 61.0 (-), 31.8 (-). APCI-MS: 250.0 ($MNH4^+Br^{81}$, 100%), 248.0282 ($MNH4^+Br^{79}$, 100%), 232.9997 (MH^+Br^{81}, 90%), 231.0016 (MH^+Br^{79}, 90%). HR-MS: 250.0264 ($MNH4^+Br^{81}$, 100%), 248.0 ($MNH4^+Br^{79}$, 100%), 233.0 (MH^+Br^{81}, 90%), 231.0 (MH^+Br^{79}, 90%). IR: $\tilde{\nu}$ = 3325 (w), 2881 (w), 1588 (m), 1669 (s), 1274 (s), 1245 (s), 1051 (s), 746 (s). R_f: 0.6 (80% ethyl acetate in petroleum ether).

*3-(2-Bromo-4-nitrophenoxy)propan-1-ol (**40**[3])*

The starting material (14.72 mmol) was dissolved in H_2SO_4 (conc, 6 mL) and cooled to 0 °C. HNO_3 (2 mL) was added dropwise. The reaction mixture was stirred at this temperature for two hours and subsequently, poured onto crushed ice. The aqueous phase was extracted with

DCM (3x20 mL) and the combined organic phases were dried over Na_2SO_4. The volatiles were removed *in vacuo* and the crude product directly converted in the next step.
ESI-MS: calculated: 274-9793; found: 295.0 ($MHH_4^+Br^{81}$, 100%), 293.0 ($MHH_4^+Br^{79}$, 95%), 276.0 ($MHH_4^+Br^{79}$, 100%), 298.0 ($MHH_4^+Br^{81}$, 100%).

*3-(4-Amino-2-bromophenoxy)propan-1-ol (**41**[3])*

The starting material (14.72 mmol) was dissolved in EtOH (100 mL) and HCl (12M, aq, 60 mL). $SnCl_2$ (9.96 g, 44.16 mmol) was added and the reaction mixture was refluxed for 16h. The mixture was cooled to ambient temperature and EA (100 mL) was added. The phases were separated, and the volatiles were removed *in vacuo*. ESI-MS confirmed that the residues of the aqueous phase contained the desired product. The crude, beige solid was directly used for the next step.
ESI-MS: calculated: 245.0051; found: 248.0 (MH^+ Br^{81}, 100%)246.0 (MH^+ Br^{79}, 100%).

III.1.4.2 Strains, expression vectors, enzymes, and chemicals

Expression strains used for production of HisF and HisH were purchased from Agilent Technologies (*E. coli* BL21 Gold (DE3)) and Qiagen (*E. coli* M15). Both expression vectors were taken from previously published works: pET-11c for HisF expression[3] and pQE-70 for HisH expression.[2] The synthesis of ProFAR and PRFAR was performed as previously described.[30] Glutamate dehydrogenase (GDH) was purchased from Roche. All other chemicals were purchased from commercial sources and were of analytical grade or higher.

III.1.4.3 Expression and purification of ImGP synthase from *T. maritima*

HisF and HisH were produced by heterologous gene expression adapted from previously published work.[2] The *E. coli* strains containing the respective expression vectors were grown in two to four liter of Luria-Bertani medium at 37 °C to an optical density of OD_{600} = 0.6. After 30 min at 30 °C, protein expression was induced with 0.5 mM IPTG, followed by incubation of the cultures over night at 30 °C. Bacterial pellets were harvested and resuspended in either 50 mM Tris/HCl pH 7.5 (HisF) or 50 mM KP pH 7.8 (HisH). Sonification and repeated centrifugation yielded the protein-containing supernatant, which was subjected to a heat step (15 min 75 °C for HisF and 15 min 70 °C for HisH) followed by ion exchange chromatography with a MonoQ column (HR 16/10, 20 mL, Pharmacia). Proteins were eluted with a linear gradient of 0-2.25 M NaCl and fractions containing the proteins were pooled and dialyzed against the previously used buffers without NaCl. In order remove DNA contaminations, ammonia sulfate precipitation was applied to the proteins.

Finally, the proteins were further purified with a size exclusion chromatography column (Superdex 75 HiLoad 26/600, GE Healthcare) using 50 mM HEPES, 100 mM NaCl pH 7.5 as running buffer. Fractions were checked on SDS-PAGE analysis for > 90% purity, pooled, concentrated, and dripped into liquid nitrogen for storage at −80°C.

III.1.4.4 Steady-state kinetics

Measurements were in general performed at constant 25 °C in a spectrophotometer (Jasco V650-UV/Vis spectrophotometer) and activities were deduced from the initial slopes of transition curves. Exact reaction conditions are given under each Figure describing the respective experiment. The ammonia-dependent HisF activity and the glutamine-dependent total reaction of IGPS were measured at 300 nm following PRFAR turnover ($\Delta\varepsilon_{300}$(PRFAR−AICAR) = 5637 $M^{-1}cm^{-1}$.[3] HisH activity was determined in a coupled enzymatic assay with glutamate dehydrogenase (GDH) as helper enzyme and NAD^+ as co-substrate. Activity was detected at 340 nm according to NAD^+ turnover ($\Delta\varepsilon_{340}$(NADH−NAD^+) = 6300 $M^{-1}cm^{-1}$). This assay was regularly performed continuously, however, in order to circumvent the stimulating effect of NAD^+ on HisH activity, it was performed discontinuously as described previously in detail.[2] All reactions were started by the addition of the IGPS complex.

III.1.4.5 Inhibition studies

IC_{50} measurements were performed by keeping the substrate concentration constant while the inhibitor concentration was varied in an at least 100-fold range. For HisF, PRFAR was kept constant at twofold K_m (7 μM) and for HisH, ProFAR as stimulator and glutamine as substrate were kept constant at saturating conditions (40 μM and 8 mM, respectively). Determined initial velocities (v_i) were then normalized to the initial velocity without inhibitor (v_0) and half-logarithmically plotted against each inhibitor concentration *[I]*. In order to identify IC_{50}, the data were then fitted with the dose-response equation based on the Hill model, with *H* as Hill coefficient:[31]

$$\frac{v_i}{v_0} = \frac{1}{1 + \left(\frac{[I]}{IC_{50}}\right)^H}$$

Using the IC_{50} curves, three inhibitor concentrations in the range of 30-70% inhibition were chosen for K_i measurements.[31] In presence of each chosen concentration of inhibitor, substrate saturation curves with increasing concentrations of PRFAR were recorded for HisF in at least duplicates. By fitting the resulting data with the Michaelis-Menten equation, v_{max} and apparent Michaelis constants K_m^{app} were determined for each inhibitor concentration.

Finally, the inhibition constant K_i of each DTE compound was calculated with the following equation:[31]

$$K_i = \frac{K_m \cdot [I]}{K_m^{app} - K_m}$$

The K_m of PRFAR turnover in HisF is 3.6 µM (List et al., 2012) . Via the Cheng and Prusoff relationship[32] the quality of the inhibition data was checked by converting the IC_{50} values, involving the used substrate concentration [S] and the K_m value, into K_i values:

$$K_i = \frac{IC_{50}}{1 + \frac{[S]}{K_m}}$$

III.1.4.6 MD simulations

MD simulations were conducted with Yasara[33] version 16.9 and force field AMBER03, based on the IGPS complex (pdb-id 1gpw, chain CD). Prior to MD simulations, the ligands were added to the complex in open and closed conformations by superposition of the ligand to the phosphates of the native ligand PRFAR bound in the crystal structure of IGPS from *Saccharomyces cerevisiae* (pdb-id 1ox5). A simulation cell was created, which was 5 Å larger than the protein along each axis and filled with water to a density of 0.997 g/mL, and counterions were added to a final concentration of 0.9 % NaCl. The simulation was conducted at 25 °C adjusted by the Berendsen thermostat. For each temperature, three independent simulation runs of length 100 ns were performed with slightly different temperatures (± 0.1 °C) to alter starting conditions. Each minimization consisted of an initial equilibration step of length 14 ps. A short MD simulation of 100ps was conducted to adjust the ligand in the binding pocket by allowing only ligand movement. During the next 100 ns of simulation, movement of all the whole protein was allowed and a snapshot was recorded every 20 ps. All figures with molecular structures were generated with PyMOL.[34]

III.1.5 Acknowledgments

We thank Thomas Kinateder and Elisabeth Bauer for technical support. NAS thanks the Studienstiftung des Deutschen Volkes for a PhD scholarship.

III.1.6 References

1. Korolev, S.; Skarina, T.; Evdokimova, E.; Beasley, S.; Edwards, A.; Joachimiak, A.; Savchenko, A., Crystal Structure of Glutamine Amidotransferase from Thermotoga maritima. *Proteins* **2002**, *49*, 420–422.

2. List, F.; Vega, M. C.; Razeto, A.; Häger, Michaela C.; Sterner, R.; Wilmanns, M., Catalysis Uncoupling in a Glutamine Amidotransferase Bienzyme by Unblocking the Glutaminase Active Site. *Chemistry & Biology* **2012**, *19*, 1589–1599.

3. Beismann-Driemeyer, S.; Sterner, R., Imidazole Glycerol Phosphate Synthase from *Thermotoga Maritima*: Quarterney Structure, Steady-State Kinetics, and Reaction Mechanism of the Bienzyme Complex. *Journal of Biological Chemistry* **2001**, *276*, 20387–20396.

4. Chaudhuri, B. N.; Lange, S. C.; Myers, R. S.; Davisson, V. J.; Smith, J. L., Toward Understanding the Mechanism of the Complex Cyclization Reaction Catalyzed by Imidazole Glycerolphosphate Synthase: Crystal Structures of a Ternary Complex and the Free Enzyme. *Biochemistry* **2003**, *42*, 7003–7012.

5. Lang, D.; Thoma, R.; Henn-Sax, M.; Sterner, R.; Wilmanns, M., Structural Evidence for Evolution of the Beta/Alpha Barrel Scaffold by Gene Duplication and Fusion. *Science* **2000**, *289*, 1546–1550.

6. Velema, W. A.; Szymanski, W.; Feringa, B. L., Photopharmacology: Beyond Proof of Principle. *Journal of the American Chemical Society* **2014**, *136*, 2178–2191.

7. Lerch, M. M.; Hansen, M. J.; van Dam, G. M.; Szymanski, W.; Feringa, B. L., Emerging Targets in Photopharmacology. *Angewandte Chemie International Edition* **2016**, *55*, 10978–10999.

8. Bliman, D.; Nilsson, J. R.; Kettunen, P.; Andréasson, J.; Grøtli, M., A Caged Ret Kinase Inhibitor and its Effect on Motoneuron Development in Zebrafish Embryos. *Scientific Reports* **2015**, *5*, 13109–13118.

9. Lachmann, D.; Studte, C.; Männel, B.; Hübner, H.; Gmeiner, P.; König, B., Photochromic Dopamine Receptor Ligands Based on Dithienylethenes and Fulgides. *Chemistry – A European Journal* **2017**, *23*, 13423–13434.

10. Falenczyk, C.; Schiedel, M.; Karaman, B.; Rumpf, T.; Kuzmanovic, N.; Grotli, M.; Sippl, W.; Jung, M.; Konig, B., Chromo-pharmacophores: photochromic diarylmaleimide inhibitors for sirtuins. *Chemical Science* **2014**, *5*, 4794–4799.

11. Broichhagen, J.; Podewin, T.; Meyer-Berg, H.; von Ohlen, Y.; Johnston, N. R.; Jones, B. J.; Bloom, S. R.; Rutter, G. A.; Hoffmann-Röder, A.; Hodson, D. J.; Trauner, D., Optical Control of Insulin Secretion Using an Incretin Switch. *Angewandte Chemie International Edition* **2015**, *54*, 15565–15569.

12. Frank, J. A.; Moroni, M.; Moshourab, R.; Sumser, M.; Lewin, G. R.; Trauner, D., Photoswitchable Fatty Acids Enable Optical Control of TRPV1. *Nature Communications* **2015**, *6*, 7118–7129.

13. Borowiak, M.; Nahaboo, W.; Reynders, M.; Nekolla, K.; Jalinot, P.; Hasserodt, J.; Rehberg, M.; Delattre, M.; Zahler, S.; Vollmar, A.; Trauner, D.; Thorn-Seshold, O., Photoswitchable Inhibitors of Microtubule Dynamics Optically Control Mitosis and Cell Death. *Cell* **2015**, *162*, 403–411.

14. Szymański, W.; Beierle, J. M.; Kistemaker, H. A. V.; Velema, W. A.; Feringa, B. L., Reversible Photocontrol of Biological Systems by the Incorporation of Molecular Photoswitches. *Chemical Reviews* **2013**, *113*, 6114–6178.

15. Brieke, C.; Rohrbach, F.; Gottschalk, A.; Mayer, G.; Heckel, A., Light-Controlled Tools. *Angewandte Chemie International Edition* **2012**, *51*, 8446–8476.

16. Luo, J.; Torres-Kolbus, J.; Liu, J.; Deiters, A., Genetic Encoding of Photocaged Tyrosines with Improved Light-Activation Properties for the Optical Control of Protease Function. *ChemBioChem* **2017**, *18*, 1442–1447.

17. Bose, M.; Groff, D.; Xie, J.; Brustad, E.; Schultz, P. G., The Incorporation of a Photoisomerizable Amino Acid into Proteins in *E. coli*. *Journal of the American Chemical Society* **2006**, *128*, 388–389.

18. Reisinger, B.; Kuzmanovic, N.; Löffler, P.; Merkl, R.; König, B.; Sterner, R., Exploiting Protein Symmetry To Design Light-Controllable Enzyme Inhibitors. *Angewandte Chemie International Edition* **2014**, *53*, 595–598.

19. Rivalta, I.; Sultan, M. M.; Lee, N.-S.; Manley, G. A.; Loria, J. P.; Batista, V. S., Allosteric Pathways in Imidazole Glycerol Phosphate Synthase. *Proceedings of the National Academy of Sciences of the United States of America* **2012**, *109*, E1428–E1436.

20. Myers, R. S.; Amaro, R. E.; Luthey-Schulten, Z. A.; Davisson, V. J., Reaction Coupling through Interdomain Contacts in Imidazole Glycerol Phosphate Synthase. *Biochemistry* **2005**, *44*, 11974–11985.

21. Myers, R. S.; Jensen, J. R.; Deras, I. L.; Smith, J. L.; Davisson, V. J., Substrate-Induced Changes in the Ammonia Channel for Imidazole Glycerol Phosphate Synthase. *Biochemistry* **2003**, *42*, 7013–7022.

22. Lisi, G. P.; East, K. W.; Batista, V. S.; Loria, J. P., Altering the Allosteric Pathway in IGPS Suppresses Millisecond Motions and Catalytic Activity. *Proceedings of the National Academy of Sciences* **2017**, *114*, E3414-E3423.

23. Weston, C. E.; Richardson, R. D.; Haycock, P. R.; White, A. J. P.; Fuchter, M. J., Arylazopyrazoles: Azoheteroarene Photoswitches Offering Quantitative Isomerization and Long Thermal Half-Lives. *Journal of the American Chemical Society* **2014**, *136*, 11878–11881.

24. Calbo, J.; Weston, C. E.; White, A. J. P.; Rzepa, H. S.; Contreras-García, J.; Fuchter, M. J., Tuning Azoheteroarene Photoswitch Performance through Heteroaryl Design. *Journal of the American Chemical Society* **2017**, *139*, 1261–1274.

25. Studte, C. Synthesis and Application of Photochromic Dithienylethenes with Biological Relevamce. Univerisity of Regensburg, *Regensburg*, **2016**.

26. Fleming, C.; Remón, P.; Li, S.; Simeth, N. A.; König, B.; Grøtli, M.; Andréasson, J., On the Use of Diarylmaleimide Derivatives in Biological Contexts: An Investigation of the Photochromic Properties in Aqueous Solution. *Dyes and Pigments* **2017**, *137*, 410–420.

27. Irie, M., Diarylethenes for Memories and Switches. *Chemical Reviews* **2000**, *100*, 1685-1716.

28. Stricker, L.; Fritz, E.-C.; Peterlechner, M.; Doltsinis, N. L.; Ravoo, B. J., Arylazopyrazoles as Light-Responsive Molecular Switches in Cyclodextrin-Based Supramolecular Systems. *Journal of the American Chemical Society* **2016**, *138*, 4547–4554.

29. Fürst, M. C. D.; Bock, L. R.; Heinrich, M. R., Regioselective Radical Arylation of 3-Hydroxypyridines. *The Journal of Organic Chemistry* **2016,** *81*, 5752–5758.

30. Davisson, V. J.; Deras, I. L.; Hamilton, S. E.; Moore, L. L., A plasmid-based approach for the synthesis of a histidine biosynthetic intermediate. *The Journal of Organic Chemistry* **1994**, *59*, 137–143.

31. Copeland, R. A., Reversible Inhibitors. In Enzymes, 2nd Edition. *Wiley-VCH* **2002**.

32. Yung-Chi, C.; Prusoff, W. H., Relationship Between the Inhibition Constant (KI) and the Concentration of Inhibitor which Causes 50 per cent Inhibition (I50) of an Enzymatic reaction. *Biochemical Pharmacology* **1973**, *22*, 3099–3108.

33. Krieger, E.; Darden, T.; Nabuurs, S. B.; Finkelstein, A.; Vriend, G., Making Optimal Use of Empirical Energy Functions: Force-field Parameterization in Crystal Space. *Proteins: Structure, Function, and Bioinformatics* **2004**, *57*, 678–683.

34. Schrodinger, The PyMOL Molecular Graphics System (LLC.). **2015**.

III.2 Photochromic Ligands for the Trp-Synthase Multienzyme complex

Abstract:
In recent years, more and more chemists are developing light-addressable, bioactive molecules in the growing field of *photopharmacology*. Many processes have already been subjected to photoregulation to either elucidate mechanistic relationships or limit drug-activity in a spatiotemporal manner. In particular, many examples show that the catalytic activity of enzymes can be modulated using photoswitchable ligands. Thereby, the active center is usually blocked by a competitive inhibitor. However, many enzymes are allosterically coupled in multienzyme complexes such as the well-investigated heterotetrameric tryptophan synthase. Hence, the subunit's interplay is tightly regulated and coordinated. Developing photocontrollable tools for such processes would allow to probe the allosteric communication of the subunits spatiotemporally through light and, consequently, open a novel approach to study such complex processes.

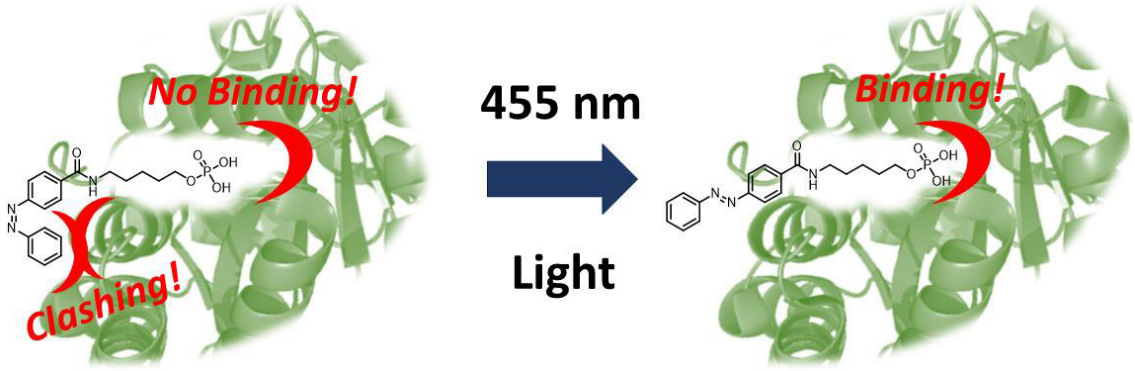

Author contributions

N. A. Simeth synthesized and characterized all compounds, performed UV/Vis spectroscopic studies and wrote the manuscript. B. König supervised the work.

III.2.1 Introduction

The usage of light to generate energy, motion and transport information is known to biology since cellular life is existing. Energy production through photosynthesis or the transport of visual information through isomerization of retinal in our eye are only two of the many admirable examples where nature is exploiting light.[1] In recent years, more and more chemists are mimicking these strategies and developing light-addressable, bioactive molecules in the growing field of *photopharmacology*.[2, 3] Thereby, potential photocontrollable drugs,[4] antibiotics[5, 6] and tool compounds for *e.g.* many enzymatic processes[7-9] have been developed. These photocontrollable tools are very often photoswitchable ligands inhibiting the catalytic reaction of a single enzyme.[10] However, many biological processes are performed by several cooperating enzymes or multienzyme complexes.

Tryptophan synthase (TS) is a multienzyme complex involved in the last two steps of tryptophan biosynthesis in bacteria, plants and fungi.[11] The structure consists of two different monomers: α (TrpA) and β (TrpB) which are building a heterotetrameric, linear multienzyme complex in an αββα conformation (Figure 1).[12, 13]

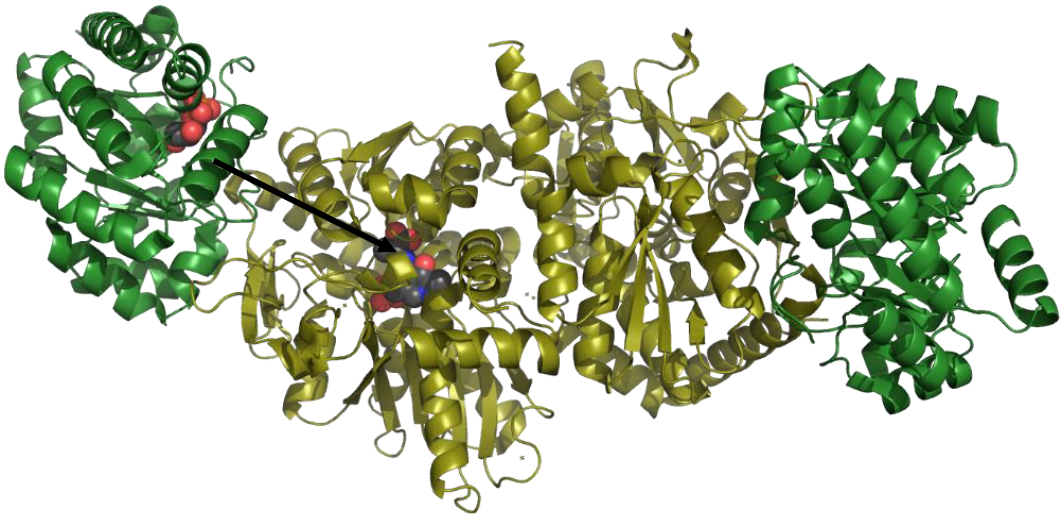

Figure 1: The linear multienzyme complex TS in its αββα conformation (green: α, olive: β). The TrpA-TrpB unit on the left side displays additionally IGP bound to the α subunit and PLP to the β subunit. The black arrow indicated the way of the indole through the intramolecular protein tunnel to the active site of TrpB [13]

In particular, each αβ dimer is forming a functional unit. TrpA is catalyzing the retro-aldol cleavage of indole-3-glycerol phosphate (IGP) to glycerin aldehyde-3 phosphate (GAP).[11] Thereby, one molecule of indole is cleaved off and transported through an intramolecular protein tunnel to the active site of TrpB. There, it is used to synthesize tryptophan (trp) from serin using pyridoxal phosphate (PLP) as a cofactor. Similar but more complex as in IGPS

(see Chapter III.1), both reactions, indole synthesis in TrpA and tryptophan (trp) synthesis in TrpB, require a tight allosteric regulation of both subunits:[11, 12] Upon binding of IGP in the TrpA active site, binding of serine in the TrpB active site is enhanced facilitating the initial reaction of serine with the PLP cofactor. The resulting formation of an intermediate aminoacrylate in turn enhances the turnover of IGP to indole, which is then transported to the TrpB active site where it reacts with the aminoacrylate to form tryptophan.[11]

In contrast to IGPS, TS has been well investigated and the mechanism of the bidirectional allosteric communication between the alpha and beta subunit is significantly understood.[11] However, probing of the multienzyme complex has never been realized *via* a photoactuator.

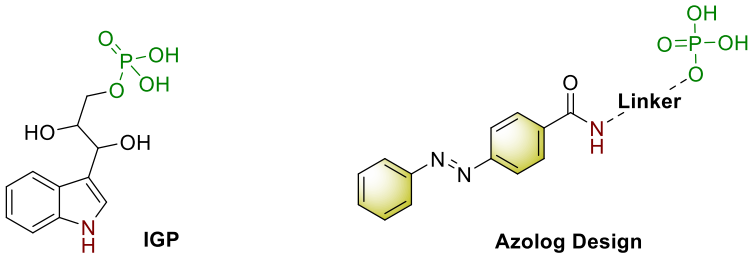

Figure 2: Design of azologs: the main interaction site of IGP (left), the phosphate (green), should be installed in varying distance (dashed line) to the *N*H-function (brown) and the azo moiety (olive) to find a ligand with a geometry that mediates high affinity binding of one photoisomer and lower affinity binding of the other.

In order to achieve this goal, we attempted to employ a known *photopharmacological* strategy.[14] Analyzing the binding mode of IGP towards the Trp subunit, we identified the phosphate motif (green, Figure 2) as the main and the NH function of the indole ring (brown, Figure 2) as an additional interaction site.[11, 12] Consequently, we intended to mimic the binding sites in our synthetical ligand and designed appropriate azo-analogues (*azologs*, Figure 2).[14] In particular, the phosphate motif is attached in varying distances to the azo moiety, which is equipped with an amide group, through linkers with different lengths (dashed green line, Figure 2). In this way, we intended to find a ligand exhibiting the optimal geometry to bind the enzyme in one photoisomer and to show weaker binding properties in the other, potentially due to steric clashes of the changed geometry of the azo moiety (*cf.* Figure 2). This would eventually generate a photocontrollable ligand, allowing to probe the allosteric communication of TS in a spatiotemporal manner through light.

III.2.2 Results and Discussion

III.2.2.1 Synthesis

To synthetize a small library of azologs of IGP, we started from commercially available 4-carboxy azobenzene (**1**, Scheme 1). We converted the carboxylic acid, by treatment with $SOCl_2$, into the corresponding acyl chloride **2**, which was directly reacted with differently functionalized amines to give **3a–f** (3–31% yield). In the last step, the compounds were reacted with $POCl_3$ using 1,8-bis(dimethylamino)naphthalene (*proton sponge*) as a base to functionalize the alcohol group. Upon aqueous workup, the phosphorus chloride was hydrolyzed, resulting into the corresponding phosphate derivatives **4a–f**. After preparative HPLC purification, the compounds were isolated as orange solids. The yields were highly substrate dependent on the substrate and varied from low (0.2%) to moderate (37%).

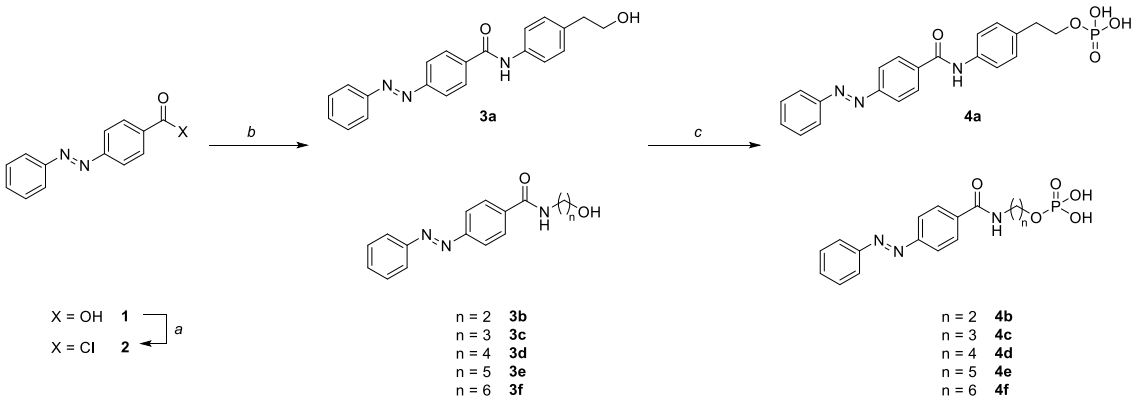

Scheme 1: Synthetic approach towards photochromic TS ligands. *a*: $SOCl_2$, 80 °C, 2h (not isolated). *b*: 4-(2-hydroxyethyl)aniline or suitable amino alcohol (1 eq), dry pyridine/dry $CHCl_3$ (1:5), r.t., 16 h, 3-31%. *c*: method I: 1) *proton sponge* (3 eq), $POCl_3$, dry THF/dry $CHCl_3$, 0 °C to r.t., 2h; 2) acetone/water (1:1), 0.2-7% (4a,b,d,f); method II: 1) *proton sponge* (3 eq), $POCl_3$, $PO(OMe)_3$, 0 °C to r.t., 2h; 2) acetone/water (1:1), 0.5-37% (4c,e).

III.2.2.2 Photophysical Characterization

To investigate the photophysical properties of compounds **4a–f**, we characterized them through UV/Vis spectroscopy. Figure 3 exemplarily depicts the spectra of **4e** and **4f** in phosphate saline buffer (further spectra and a tabular overview can be found in the Appendix, Section A.III.2.3.).

All compounds exhibited a main absorption maximum between 324 nm to 335 nm depending on the substitution and the amount of DMSO (to enhance the solubility) in the solution. This absorption band could be attributed to the $\pi\pi^*$ transition present in all classical azobenzenes.[15] Upon irradiation with 400 nm light, the band decreased and simultaneously the band around 420 nm arose, which was attributed to formation of the $n\pi^*$ of the *Z*-isomer, reaching the PSS.[15]

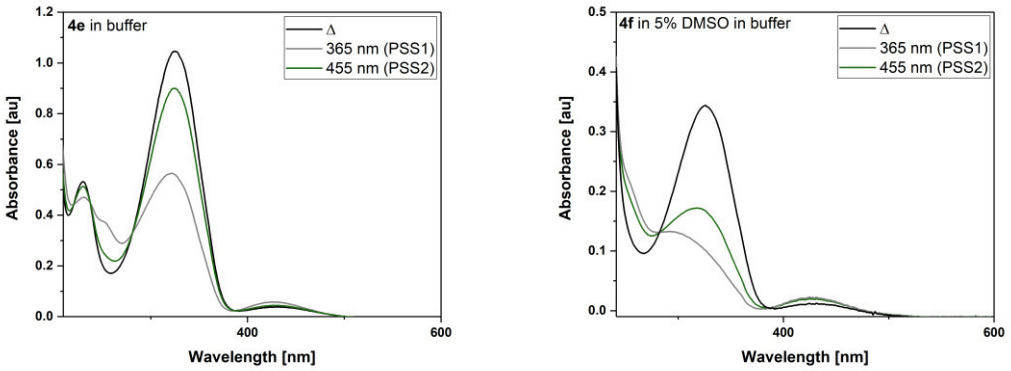

Figure 3: UV/Vis spectra of compounds 4e (68 µM) and 4f (22µM). The individual solvents are specified in the spectrum. Black lines depict the absorption spectrum at the thermal equilibrium (Δ), grey lines at the PSS1 (irradiation with 365 nm LED), green lines at the PSS2 (irradiation of PSS1 with a 455 nm LED).

The metastable *Z*-isomer was found to have a thermal lifetime in the range of a few days (for compound **4e** in buffer 3.76 d, see Appendix, Section A.III.2.3.). However, the *Z*-to-*E* isomerization could also be induced photochemically through irradiation with light of 455 nm (green lines, Figure 3). However, the composition of the thermal equilibrium (D) could not be regenerated, probably due to overlap of the nπ* band of the *E*-isomer and the nπ* band of the *Z*-isomer. Summing up, compounds **4a–f** exhibited two-way photoswitching in aqueous environment and the *Z*-isomers possessed lifetimes in the range of a few days.

III.2.3 Conclusion and Outlook

In conclusion, we designed a series of six photochromic ligands to study the allosteric cooperation mechanism in TPS. In particular, the two main interaction sites (the phosphate group and the indolic NH) of the parent ligand, IGP, was chosen to be mimicked in the synthetic ligands. To find the optimum distance between the phosphate function and the azo moiety and to be able to modulate the immersion of the phosphate motif into the enzyme towards the binding site, we varied the distance between both anchoring groups with different linkers. All the compounds were synthetically accessible from 4-carboxy benzene *via* formation of a corresponding amide bearing an alcoholic function, which was subsequently phosphorylated. Subsequently, the phosphate azo switches were characterized regarding their photophysical properties. All compounds showed two-way photoswitching with purple (400 nm) or blue light (455 nm), respectively. The thermal lifetime was exemplarily determined for compound **4e** and resulted to be in the range of a few days.

Hence, all requirements are fulfilled to investigate the compounds in an enzyme assay and use them as light-controllable tools to deepen the insight into the mechanism of TS.

III.2.4 Experimental Section

General procedure for amide formation

A crimp top vial was equipped with (E)-4-(phenyldiazenyl) benzoic acid (1 eq) and dissolved in $SOCl_2$ (1 mL per 200 mg). The suspension was heated to 80 °C for two hours to give a clear, red solution. The reaction mixture was cooled to ambient temperature and the solvent was removed *in vacuo*. The vial was flushed with vacuum/nitrogen for three times and dry $CHCl_3$ (5 mL) was added under nitrogen atmosphere. To this, a solution of the respective aniline (1 eq) or amino alcohol (1eq), respectively, in dry pyridine (1 mL) was added dropwise through a syringe. The solution was stirred for 16 h and the solvent was removed *in vacuo*. The crude product was purified through MPLC (20 → 100% EA in PE).

Analytical samples were purified through HPLC (MeCN in H_2O/0.05% TFA 5-100% over 20 min) to give all compounds as orange solids. Proton-NMR could be recorded using a Bruker Avance 400 MHz NMR. However, due to low solubility of the compounds, carbon NMRs had to be recorded on a Bruker Avance 600 Kryo. Unfortunately, the compounds decomposed partly during measuring. Thus, carbon signals were assigned using HSQC measurements.

*(E)-N-(4-(2-Hydroxyethyl)phenyl)-4-(phenyldiazenyl)benzamide (**3a**)*

(E)-4-(Phenyldiazenyl) benzoic acid (4.42 mmol) was employed. **3a** was obtained in 8 % yield (0.37 mmol). ^{1}H NMR (300 MHz, 10% MeOD-*d4* in Chloroform-*d*): δ =8.03 (d, *J* = 8.5 Hz, 2H), 7.98 – 7.93 (m, 2H), 7.92–7.89 (m, 2H), 7.57 (d, *J* = 8.3 Hz, 2H), 7.53 – 7.45 (m, 3H), 7.19 (d, *J* = 8.4 Hz, 2H), 3.76 (t, *J* = 6.9 Hz, 2H), 2.80 (t, *J* = 6.9 Hz, 2H). ^{13}C NMR (151 MHz, Acetone-d_6): δ = 132.0 (+), 130.3 (+), 130.1 (+), 129.6 (+), 123.8 (+), 123.4 (+), 121.1 (+), 64.0 (-), 30.4 (-). Assignment was based on HSQC measurements due to low concentrations and lability of the compound. Thus, quaternary carbons could not be assigned. ESI-MS: calculated: 345.1477, found: 713.3 ($2MNa^+$, 5%; 368.1 MNa^+, 10%; 346.2 MH^+, 100%). HR-MS (ESI): found: 368.1373 (MNa^+, 15%), 346.1559 (MH^+, 100%). IR (cm^{-1}) $\tilde{\nu}$= 3351(m), 3045 (w), 2926 (w), 2863 (w), 1648 (s), 1520 (s), 1051 (m), 861 (m), 820 (m), 771 (m), 686 (m). R_f (10%MeOH in DCM): 0.6.

*(E)-N-(2-Hydroxyethyl)-4-(phenyldiazenyl)benzamide (**3b**)*

(E)-4-(Phenyldiazenyl) benzoic acid (4.42 mmol) was employed. **3b** was obtained in 31 % yield (1.39 mmol). ^{1}H NMR (400 MHz, Acetone-d_6) δ =8.10 – 8.05 (m, 2H), 7.98 – 7.90 (m, 4H), 7.60 – 7.51 (m, 3H), 3.68 (t, J = 5.7 Hz, 2H), 3.50 (q, J = 5.6 Hz, 2H). ^{13}C NMR (151 MHz, Acetone-d_6) δ =129.5 (+), 129.2 (+), 128.2 (+), 122.7 (+), 122.3 (+), 60.8 (-), 42.5 (-). Assignment was based on HSQC measurements due to low concentrations and decomposition of the compound during the extended measuring time. Thus, quaternary carbons could not be assigned. ESI-MS: calculated. ESI-MS: calculated: 269.1164, found: 561.2 (2MNa$^+$, 20%), 292.1 (MNa$^+$, 20%), 270.1 (MH$^+$, 100%). HR-MS (ESI): found: 292.1062 (MNa$^+$, 20%), 270.1242 (MH$^+$, 100%). IR (cm^{-1}) $\tilde{\nu}$= 3258 (w), 3064 (w), 3926 (w), 1722 (m), 1626 (m), 1268 (s), 1092 (m), 857 (m), 686 (s). R_f (10%MeOH in DCM): 0.5.

*E)-N-(3-Hydroxypropyl)-4-(phenyldiazenyl)benzamide (**3c**)*

(E)-4-(Phenyldiazenyl) benzoic acid (2.10 mmol) was employed. **3c** was obtained in 10 % yield (0.22 mmol). ^{1}H NMR (400 MHz, Acetone-d_6) δ =8.16 – 8.06 (m, 2H), 8.03 – 7.87 (m, 4H), 7.75 – 7.47 (m, 3H), 3.64 (t, J = 6.0 Hz, 2H), 3.55 (q, J = 6.5 Hz, 2H), 1.80 (p, J = 6.3 Hz, 2H). ^{13}C NMR (101 MHz, Acetone-d_6) δ =166.1 (q), 153.9 (q), 152.5 (q), 137.1 (q), 131.7 (+), 129.3 (+), 128.3 (+), 122.8 (+), 122.5 (+), 59.1 (-), 36.9 (-), 32.5 (-). ESI-MS: calculated: 283.1324, found: 306.1 (MNa$^+$, 20%), 284.1 (MH$^+$, 100%). HR-MS (ESI): found: 306.1215 (MNa$^+$, 20%), 284.1401 (MH$^+$, 100%). IR (cm^{-1}) $\tilde{\nu}$= 3368 (w), 3291 (m), 3060 (w), 2937 (w), 2881 (w), 1627 (s), 1536 (s), 1073 (m), 775 (m), 686 (s). R_f (10%MeOH in DCM): 0.5.

*(E)-N-(4-Hydroxybutyl)-4-(phenyldiazenyl)benzamide (**3d**)*

(E)-4-(Phenyldiazenyl) benzoic acid (2.21 mmol) was employed. **3d** was obtained in 3 % yield (0.06 mmol). ^{1}H NMR (400 MHz, Acetone-d_6) δ =8.11 – 8.06 (m, 2H), 7.99 – 7.93 (m, 4H), 7.63 – 7.55 (m, 3H), 3.59 (t, J = 6.2 Hz, 2H), 3.51 – 3.39 (m, 2H), 1.78 – 1.66 (m, 2H), 1.66 – 1.55 (m, 2H). ^{13}C NMR (101 MHz, Acetone-d_6) δ =165.5 (q), 153.8 (q), 152.5 (q), 137.4 (q), 131.7 (+), 130.8 (+), 129.3 (+), 128.2 (+), 122.8 (+), 122.4 (+), 61.3 (-), 39.6 (-), 30.2 (-), 26.2 (-). ESI-MS: calculated: 297.1477, found: 617.3 (MNa$^+$, 40%), 320.1 (MNa$^+$, 20%), 298.2 (MH$^+$, 100%). HR-MS: 320.1376 (MNa$^+$, 40%), 298.1559 (MH$^+$, 100%). IR (cm^{-1}) $\tilde{\nu}$= 3321 (w), 3045 (w), 2926 (w), 2862 (w), 1647 (s), 1521 (s), 861 (m), 820 (s), 771 (s), 865 (s). R_f (10%MeOH in DCM): 0.5.

*(E)-N-(5-Hydroxypentyl)-4-(phenyldiazenyl)benzamide (**3e**)*

(E)-4-(Phenyldiazenyl) benzoic acid (1.33 mmol) was employed. **3e** was obtained in 5 % yield (0.07 mmol). ^{1}H NMR (400 MHz, Acetone-d_6) ^{1}H NMR (400 MHz, Acetone-d_6) δ =8.11 – 8.05 (m, 2H), 7.99 – 7.94 (m, 4H), 7.63 – 7.56 (m, 3H), 3.54 (t, J = 6.3 Hz, 2H), 3.47 – 3.40 (m, 2H), 1.65 (p, J = 7.2 Hz, 2H), 1.59 – 1.51 (m, 2H), 1.51 – 1.42 (m, 2H). ^{13}C NMR (151 MHz, Acetone-d_6) δ =130.2 (+), 129.3 (+), 128.2 (+), 122.8 (+), 122.4 (+), 62.3 (-), 40.5 (-), 33.4 (-), 29.4 (-), 24.1 (-). Assignment was based on HSQC measurements due to low concentrations and decomposition of the compound during the extended measuring time. Thus, quaternary carbons could not be assigned. ESI-MS: calculated: 311.1634, found: 312.2 (MH^+, 100%). HR-MS: 334.1531 (MNa^+, 40%), 312.1712 (MH^+, 100%). IR (cm^{-1}) $\tilde{\nu}$= 3295 (w), 3052 (w), 2933 (w), 2870 (w), 1714 (s), 1629 (s), 1536 (s), 1271 (s), 1119 (m), 775 (s), 686 (s). R_f (10%MeOH in DCM): 0.8.

*(E)-N-(6-Hydroxyhexyl)-4-(phenyldiazenyl)benzamide (**3f**)*

(E)-4-(Phenyldiazenyl) benzoic acid (4.32 mmol) was employed. **3a** was obtained in 2 % yield (0.07 mmol). ^{1}H NMR (400 MHz, Acetone-d_6) δ =8.10 – 8.06 (m, 2H), 8.00 – 7.93 (m, 4H), 7.65 – 7.53 (m, 3H), 3.53 (t, J = 6.4 Hz, 2H), 3.43 (td, J = 7.2, 5.8 Hz, 2H), 1.64 (p, J = 7.1 Hz, 2H), 1.56 – 1.48 (m, 2H), 1.45 – 1.36 (m, 4H). ^{13}C NMR (151 MHz, Acetone-d_6) δ 152.8 (+), 152.5 (+), 131.7 (+), 129.3 (+), 128.3 (+), 122.8 (+), 122.4 (+), 62.4 (-), 40.6 (-), 33.8 (-), 30.7 (-), 30.6 (-), 27.2 (-). Assignment was based on HSQC measurements due to low concentrations and decomposition of the compound during the extended measuring time. Thus, quaternary carbons could not be assigned. ESI-MS: calculated: 325.1790, found: 673.3 ($2MNa^+$, 25%), 348.2 (MNa^+, 35%), 326.2 (MH^+, 100%). HR-MS: 348.1687 (MNa^+, 20%), 326.1869 (MH^+, 100%). IR (cm^{-1}) $\tilde{\nu}$= 3384 (w), 3295 (m), 2937 (m), 2855 (m), 1627 (s), 1531 (s), 1297 (m), 858 (m), 775 (s), 686 (s). R_f (10%MeOH in DCM): 0.5.

General procedure I for phosphorylation

An oven-dried crimp top vial was equipped with compound **3a**,**b**,**d**,**f** (1 eq), *proton sponge* (3 eq) and a stirring bar, and sealed. The vial was purged with vacuum/nitrogen (three times each) before dry $CHCl_3$ (1 mL per 0.15 mmol) was added. The reaction mixture was cooled to 0 °C and $POCl_3$ in dry THF (1:2, 0.5 mL per 0.15 mmol) was added dropwise *via* syringe. Then, the mixture was allowed to warm to ambient temperature and was stirred for two hours. After quenching with acetone/water (1:1), the solvent was removed *in vacuo* and the

crude product was purified through preparative HPLC (MeCN in H_2O/0.05% TFA, 5→95%). The products were obtained as orange powder after lyophilization.

General procedure II for phosphorylation

An oven-dried crimp top vial was equipped with compound **3c**,**e** (1 eq), *proton sponge* (3 eq) and a stirring bar, and sealed. The vial was purged with vacuum/nitrogen (three times each) before $PO(OMe)_3$ (1 mL per 0.15 mmol) was added. The reaction mixture was cooled to 0 °C and $POCl_3$ (0.5 mL per 0.15 mmol) was added dropwise *via* syringe. Then, the mixture was allowed to warm to ambient temperature and was stirred for two hours. After quenching with acetone/water (1:1), the solvent was removed *in vacuo* and the crude product was purified through preparative HPLC (MeCN in H_2O/0.05% TFA, 5→95%). The products were obtained as orange powders after lyophilization. Due to the low reaction yields, Carbon NMR was not feasible in case of **4a**-**d**,**f**.

*(E)-4-(4-(Phenyldiazenyl)benzamido)phenethyl dihydrogen phosphate (**4a**)*

Compound **3a** (125 mg, 0.36 mmol) was employed. **4a** was obtained in 0.5% yield (0.8 mg, 0.002 mmol). ^{1}H NMR (400 MHz, Methanol-d_4) δ =8.11 (d, J = 8.5 Hz, 2H), 8.02 (d, J = 8.5 Hz, 2H), 7.96 (dd, J = 7.9, 1.9 Hz, 2H), 7.65 (d, J = 8.3 Hz, 2H), 7.60–7.54 (m, 3H), 7.30 (d, J = 8.4 Hz, 2H), 4.14 (q, J = 7.0 Hz, 2H), 2.98 (t, J = 7.0 Hz, 2H). ^{31}P NMR (162 MHz, Methanol-d_4) δ =0.01. ESI-MS: calculated: 425.1141, found: 426.1 (MH^+, 55%), 380.1 (50%), 346.2 (100%), 309.1 (50%), 224.1 (30%); found: 424.1 ($(M-H)^-$, 100%), 344.1 (30%). HR: 426.1210 (MH^+, 100%), 424.1079 ($(M-H)^-$, 100%). IR (cm^{-1}) $\tilde{\nu}$= HPLC: 2922 (w), 2662 (w), 1647 (m), 1524 (m), 1062 (s), 771 (s), 686 (s). R_t=15.7 min, >99% purity (220nm), 96% purity (254 nm trace).

*(E)-2-(4-(Phenyldiazenyl)benzamido)ethyl dihydrogen phosphate (**4b**)*

Compound **3b** (374 mg, 1.38 mmol) was employed. **4b** was obtained in 0.2% yield (1.2 mg, 0.003 mmol). ^{1}H NMR (400 MHz, Methanol-d_4) δ=8.07 – 7.89 (m, 6H), 7.62 – 7.48 (m, 6H), 3.79 – 3.69 (m, 4H). ^{31}P NMR (162 MHz, Methanol-d_4) δ=-0.01. ESI-MS: calculated: 349.0828. found: 348.1 ($(M-H)^-$, 100%). IR (cm^{-1}) $\tilde{\nu}$= 3299 (w), 2963 (w), 2930 (w), 1629 (s), 1536 (s), 861 (s), 775 (s), 686 (s). HPLC: R_t= 16.2 min, 95% purity (220nm), 96% purity (254 nm trace).

*(E)-3-(4-(Phenyldiazenyl)benzamido)propyl dihydrogen phosphate (**4c**)*

Compound **3c** (63 mg, 0.22 mmol) was employed. **4c** was obtained in 7% yield (5.3 mg, 0.02 mmol). ^{1}H NMR (400 MHz, Methanol-d_4) δ=8.69 (s, 0H), 8.08 – 7.89 (m, 1H), 7.69 – 7.41 (m, 1H), 3.67 (t, J = 6.5 Hz, 0H), 3.56 (tt, J = 6.9, 2.9 Hz, 0H), 2.10 (p, J = 6.7 Hz, 0H). ^{31}P NMR (162 MHz, Methanol-d_4). δ =0.00. ESI-MS: calculated: 347.3108. found: 346.1 (MH^-, 100%). IR (cm^{-1}) $\tilde{\nu}$= 3317 (w), 3079 (w), 2937 (w), 2463 (w), 1625 (m), 1543 (m), 1442 (m), 1286 (m), 857 (m), 775 (s), 686 (s). HPLC: R_t= 18.1 min, 95% purity (220 nm and 254 nm).

*(E)-4-(4-(Phenyldiazenyl)benzamido)butyl dihydrogen phosphate (**4d**)*

Compound **3d** (293 mg, 0.99 mmol) was employed. **4d** was obtained in 4% yield (14.7 mg, 0.04 mmol). ^{1}H NMR (400 MHz, Methanol-d_4) δ =8.18 – 8.06 (m, 4H), 8.03 – 7.96 (m, 2H), 7.63 – 7.56 (m, 3H), 4.90 (t, J = 5.4 Hz, 2H), 3.80 (t, J = 6.0 Hz, 2H), 2.46 – 2.32 (m, 2H). ^{31}P NMR (162 MHz, Methanol-d_4) δ =0.01. ESI-MS: calculated: 377.1141, found: 378.1 (MH^+, 100%), 247.3 (80%), 223.1 (30%); found: 376.1 ($(M-H)^-$, 100%). HR: 378.1215 (MH^+, 100%), 376.1078 (MH^-, 100%). IR (cm^{-1}) $\tilde{\nu}$= 3414 (w), 3029 (w), 1662 (s), 1275 (m), 1178 (s), 1115 (s), 690 (s). HPLC: R_t= 18.7 min, 97% purity (220 nm), 95% purity (254 nm).

*(E)-5-(4-(Phenyldiazenyl)benzamido)pentyl dihydrogen phosphate (**4e**)*

Compound **3e** (184mg, 0.59 mmol) was employed. **4e** was obtained in 37% yield (86.7 mg, 0.22 mmol). ^{1}H NMR (400 MHz, Methanol-d_4) δ =8.04 – 7.73 (m, 6H), 7.51 – 7.12 (m, 3H), 3.89 (q, J = 6.5 Hz, 2H), 3.30 (t, J = 7.1 Hz, 2H), 1.70 – 1.48 (m, 4H), 1.40 – 1.28 (m, 2H). ^{13}C NMR (101 MHz, Methanol-d_4) δ =168.0 (q), 154.1 (q), 152.5 (q), 136.4 (q), 131.5 (+), 129.0 (+), 128.0 (+), 122.6 (+), 122.4 (+), 66.2 (-), 39.6 (-), 29.8 (-), 28.6 (-), 22.7 (-).^{31}P NMR (162 MHz, Methanol-d_4) δ =0.16. ESI-MS: calculated: 391.1297, found: 390.1 ($(M-H)^-$, 90%), 269.1 (100%). HR-MS: 392.1372 (MH^+, 100%). IR (cm^{-1}) $\tilde{\nu}$= 3313 (w), 3049 (w), 2930 (w), 2860 (w), 1643 (m), 1525 (m), 1010 (s), 771 (s), 686 (s). HPLC: R_t= 13.4 min, 98% purity (220 nm), <99% purity (254 nm).

*(E)-6-(4-(Phenyldiazenyl)benzamido)hexyl dihydrogen phosphate (**4f**)*

Compound **3f** (24 mg, 0.074 mmol) was employed. **4f** was obtained in 7% yield (1.9 mg, 0.005 mmol). ^{1}H NMR (400 MHz, Methanol-d_4) δ =8.02 – 7.92 (m, 6H), 7.60 – 7.51 (m, 3H), 3.97 (q, J = 6.6 Hz, 2H), 3.41 (t, J = 7.1 Hz, 2H), 1.68 (dp, J = 13.7, 6.8 Hz, 4H), 1.46 (dd, J = 7.9, 4.4 Hz, 4H). ^{31}P NMR (162 MHz, Methanol-d_4) δ =0.30. ESI-MS: calculated: 405.1454,

found: 406.2 (MH^+, 25%), 274.3 (100%), 214.1 (90%); found: 404.1 ($(M-H)^-$, 100%). HR: 406.1526 (MH^+, 100%), 404.1388 ($(M-H)^-$, 100%). IR (cm^{-1}) $\tilde{\nu}$= 3314 (w), 2930 (m), 2855 (m), 1625 (m), 1536 (m), 1014 (s), 775 (s). HPLC: R_t= 14.0 min, 95% purity (220 nm), <99% purity (254 nm).

III.2.5 Acknowledgements

We thank Elisabeth Bauer for technical assistance and Karin Rustler and Andrea C. Kneuttinger for fruitful discussions. We are grateful to Thomas Kinateder who will carry out the biological evaluation under the guidance of Reinhard Sterner. We thank Kristina Heyn (group of Rainer Merkl) for the reproduction of the crystal structure of the TS (2j9x).

III.2.6 References

1. Berg, J. M.; Tymoczko, J. L.; Stryer, L., Biochemistry, Fifth Edition. *W.H. Freeman New York* **2002**.

2. Velema, W. A.; Szymanski, W.; Feringa, B. L., Photopharmacology: Beyond Proof of Principle. *Journal of the American Chemical Society* **2014**, *136*, 2178–2191.

3. Lerch, M. M.; Hansen, M. J.; van Dam, G. M.; Szymanski, W.; Feringa, B. L., Emerging Targets in Photopharmacology. *Angewandte Chemie International Edition* **2016**, *55*, 10978–10999.

4. Polosukhina, A.; Litt, J.; Tochitsky, I.; Nemargut, J.; Sychev, Y.; De Kouchkovsky, I.; Huang, T.; Borges, K.; Trauner, D.; Van Gelder, R. N.; Kramer, R. H., Photochemical Restoration of Visual Responses in Blind Mice. *Neuron* **2012**, *75*, 271–282.

5. Velema, W. A.; van der Berg, J. P.; Hansen, M. J.; Szymanski, W.; Driessen, A. J. M.; Feringa, B. L., Optical Control of Antibacterial Activity. *Nature Chemistry* **2013**, *5*, 924–928.

6. Wegener, M.; Hansen, M. J.; Driessen, A. J. M.; Szymanski, W.; Feringa, B. L., Photocontrol of Antibacterial Activity: Shifting from UV to Red Light Activation. *Journal of the American Chemical Society* **2017**, *139*, 17979–17986.

7. Falenczyk, C.; Schiedel, M.; Karaman, B.; Rumpf, T.; Kuzmanovic, N.; Grotli, M.; Sippl, W.; Jung, M.; Konig, B., Chromo-Pharmacophores: Photochromic Diarylmaleimide Inhibitors for Sirtuins. *Chemical Science* **2014**, *5*, 4794–4799.

8. Reisinger, B.; Kuzmanovic, N.; Löffler, P.; Merkl, R.; König, B.; Sterner, R., Exploiting Protein Symmetry To Design Light-Controllable Enzyme Inhibitors. *Angewandte Chemie International Edition* **2014**, *53*, 595–598.

9. Simeth, N. A.; Kneuttinger, A. C.; Sterner, R.; König, B., Photochromic Coenzyme Q Derivatives: Switching Redox Potentials with Light. *Chemical Science* **2017**, *8*, 6474–6483.

10. Brieke, C.; Rohrbach, F.; Gottschalk, A.; Mayer, G.; Heckel, A., Light-Controlled Tools. *Angewandte Chemie International Edition* **2012**, *51*, 8446–8476.

11. Raboni, S.; Bettati, S.; Mozzarelli, A., Tryptophan Synthase: a Mine for Enzymologists. *Cellular and Molecular Life Sciences* **2009**, *66*, 2391–2403.

12. Dunn, M. F.; Aguilar, V.; Brzovic, P.; Drewe, W. F.; Houben, K. F.; Leja, C. A.; Roy, M., The Tryptophan Synthase Bienzyme Complex Transfers Indole Between the Alpha- and Beta-Sites via a 25-30 Å Long Tunnel. *Biochemistry* **1990**, *29*, 8598–8607.

13. Ngo, H.; Kimmich, N.; Harris, R.; Niks, D.; Blumenstein, L.; Kulik, V.; Barends, T. R.; Schlichting, I.; Dunn, M. F., Allosteric Regulation of Substrate Channeling in Tryptophan Synthase: Modulation of the L-Serine Reaction in Stage I of the Beta-Reaction by Alpha-Site Ligands. *Biochemistry* **2007**, *46*, 7740–53.

14. Broichhagen, J.; Frank, J. A.; Trauner, D., A Roadmap to Success in Photopharmacology. *Accounts of Chemical Research* **2015**, *48*, 1947–1960.

15. Bandara, H. M. D.; Burdette, S. C., Photoisomerization in Different Classes of Azobenzene. *Chemical Society Reviews* **2012**, *41*, 1809–1825.

IV. PHOTOCHROMIC SMALL MOLECULAR ENZYME INHIBITORS ADDRESSABLE WITH VISIBLE LIGHT

Chapter IV

Our scars have the power to remined us that the past was real.

Hannibal Lecter

IV.1 Photochromic Indolyl Fulgimides as Chromo-Pharmacophores Targeting Sirtuins

Abstract:

Sirtuins are involved in epigenetic regulation, the pathogenesis of cancer and, several metabolic and neurodegenerative diseases. Though being a promising drug target, only one small molecule passed class II clinical trials so far. Deriving a better mechanistic understanding is hence crucial to find new modulators. We previously reported on a series of dithienylmaleimides as photochromic tools compounds. However, their photochromic behavior was limited. To improve the interconversion and stability of both photoisomers, we replaced the dithienylmaleimide with a fulgimide as photochromic core to result in biologically active compounds reversibly addressable with purple and orange light. We characterize the obtained compounds regarding their spectroscopic properties, their photostability and binding characteristics towards sirtuins resulting in a fully remote-controllable Sirtuin modulator using visible light as the external stimulant.

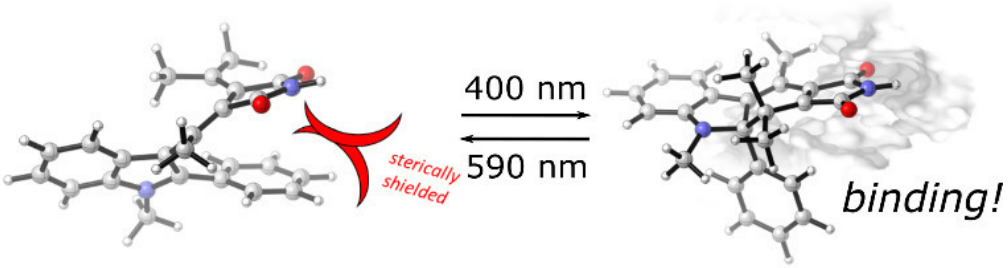

This section was published as:

Nadja A. Simeth, Lisa-Marie Altmann, Nathalie Wössner, Elisabeth Bauer, Manfred Jung and Burkhard Königa. Photochromic Indolyl Fulgimides as Chromo-Pharmacophores Targeting Sirtuins. *The Journal of Organic Chemistry*, **2018**, *83* (15), 7919–7927. Reprinted with Permission from the American Chemical Society.

Author contributions

NAS synthesized compounds 1b and 1c and their precursors and characterized them. NAS performed all UV/Vis spectroscopic studies and HPLC analysis and wrote the manuscript. LMA synthesized compound **1a** and **7d-f** and their precursors. EB assisted with synthesis. NW performed enzymatic studies and wrote that part of the manuscript. MJ and BK supervised the work.

IV.1.1 Introduction

Histone deacetylases (HDACs) are an enzyme family involved in epigenetic regulation but have also been associated with the pathogeneses of cancer and several further human illnesses, like metabolic or neurodegenerative diseases. Hence, HDACs became an interesting target in both anticancer research and epigenetics. The enzyme family is dived in four subclasses. Class I, II and IV are zinc-dependent amidohydrolases. The members of class III (sirtuins) require NAD^+ as a co-substrate.[1-5] In the human genome seven different sirtuin isotypes are encoded (Sirt1-7).[6] HDACs became an interesting target in both anticancer research and epigenetics. Indeed, several anticancer drugs targeting HDAC class I and II are already in clinical trial or approved therapeutics.[7] However, for sirtuins only one small molecule inhibitor passed class II clinical trials so far, the indole-based inhibitor Selisistat (EX-527).[8] The most promising classes of small molecule inhibitors towards sirtuins up to this date include their endogenous inhibitor, namely nicotinamide and its analogues, splitomicins,[3] suramins,[9] chromon-4-ones, chromones,[10, 11] the human Sirt2 (hSirt2) selective SirReals, that induce a rearrangement in the active site of hSirt2,[12] thienopyrimidinones[13] and bisindolylmaleimides(BIMs).[2] To find new modulators of the sirtuins, a deeper mechanistic insight regarding their bioactivity is needed.

In the last decade, the development of small photochromic molecules in biological research has increased rapidly due to their highly diverse applicability. Moreover, the usage of light as an external control element in a biological context is very appealing as it is orthogonal to most cellular processes and can be easily regulated regarding dose, space and time.[14, 15] Especially for the investigation of enzymatic processes, photoswitches have been incorporated into larger biomolecules as non-natural amino-acids or have been used as photo-controllable enzyme ligands.[16] In this fashion, photoswitchable modulators for *e.g.* ATP synthase,[17] the respiratory chain,[18] kinases,[19, 20] proteasomes,[21] acetylcholinesterase,[22] the dopamine receptor,[23] and, HDACs[24, 25]are reported.

Diarylethenes (DAEs), fulgides and fulgimides are frequently employed as photochromic moiety since they usually form thermally very stable photoisomers. The pivotal photo-reaction of both photoswitches is a reversible ring closure and ring opening electrocyclization, interconverting a flexible open (less colored) and a rigid closed (more colored) photo-isomer (*cf.* Scheme 1).[16]

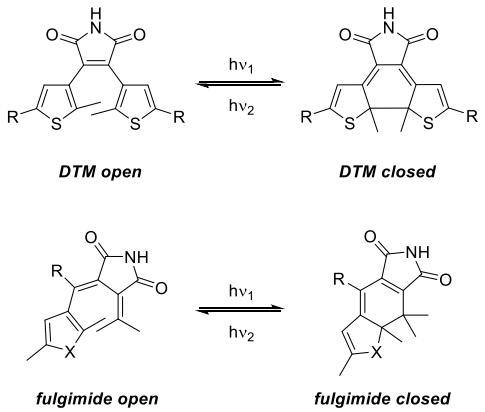

Scheme 1: Light-induced photo-isomerization of dithienylmaleimides (DTMs) and fulgimides: Irradiation with $h\nu_1$ triggers the ring-closure reaction to result in the more colored, rigid closed form. Through the application of suitable lower-energetic light ($h\nu_2$) the reaction can be reversed.

In order to control a biochemical process by means of a photoswitchable ligand, the photochromic moiety of the modulator should be in close proximity to a site that interacts strongly with the biomolecule.[26] Optimally, the interaction is fully intact in one photoisomeric state, but not in the other. We intended to fully exploit this concept by merging the biochemically interacting and the photochromic site in the same moiety, to form a so-called *chromo-pharmacophore*,[25] where the photochemical changes influence the bio interaction the most.

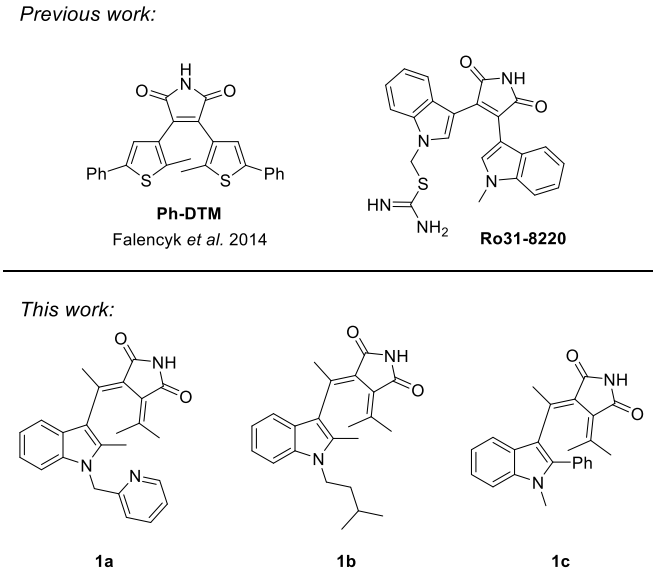

Chart 1: <u>Top</u>: Previously developed dithienylmaleimide switch by Falencyk *et al.* inspired by the sirtuin bisindolylmaleimide (BIM) inhibitor Ro31-8220 (Published by the Royal Society of Chemistry).[25] <u>Bottom</u>: Indolyl fulgimides investigated in this work regarding improved photochromic behavior.

Previously, we reported the synthesis and biological evaluation of dithienylmaleimides (DTMs) as photo-controllable inhibitors for sirtuins (**Ph-DTM**, Chart 1).[25] The structure was inspired by Ro31-8220, which has been identified as a hSirt2 inhibitor.[2] Indeed, both molecules have in common a maleimide core. Whereas the parent inhibitor exhibits two indole substituents, the photoswitch has two thiophene groups attached to the core. It can be photoisomerized with light of 312 nm and 530 nm exhibiting selectivity towards hSirt2 with one photoisomer showing a 22-fold better affinity than the other. Although being a promising starting point in the development of photochromic sirtuin ligands, **Ph-DTM** faced two main limitations: 1) photo-isomerization has to be triggered applying highly energetic UV-light, which can be tolerated in enzyme assays, but could be a serious drawback for future application in more complex cellular- or tissue-based- assays; 2) photoinduced ring closure could only be facilitated in non-polar solvents due to a twisted intramolecular electron charge transfer within the photoswitch in polar environment (*e.g.* buffered aqueous systems). Thus, under assay conditions photoswitching was only feasible in one direction.[25, 27-29]

Here, we envisioned to replace the DTM core through an indolyl fulgimide (**1a**-**c**, Chart 1) that are known to photoisomerize in aqueous systems.[23, 24] The indole moiety causes a bathochromic shift in the absorption spectrum of the molecule, allowing to trigger the ring-closing reaction of the switch with purple light (400 nm). In addition, indole allows further substitutions through functionalized alkyl chains as present in Ro31-8220 and many other BIMs.[2] Hence, we report the development of a small series of indolyl fulgimides as chromo-pharmacophores. We will investigate the compounds regarding their spectroscopic characteristics as well as their activity towards sirtuins.

IV.1.2 Results and Discussion

IV.1.2.1 Design and Synthesis

We sought to synthesize a small library of indolyl based fulgimides as the indole core is known to induce a bathochromic shift in the compound's absorption profile and can be *N*-alkylated with various side-chains (**1a**-**f**, Scheme 1).[30] Position 2 of the indole core is substituted with either a methyl group (**1a**, **b**, **d**-**f**) or a phenyl group (**1c**) to prevent oxidation upon ring-closure. As this substituent is involved in the electrocyclic ring-closure, usually a methyl group is used representing the smallest possible choice.[1] However, we envisioned a

larger geometrical difference upon isomerization if a phenyl ring is part of the rearrangement. Hence, we designed compound **1c** bearing this novel feature.

The synthesis towards fulgimides **1a**-**f** involved a Stobbe-condensation as key step.[24] We started from commercially available 2-Me or 2-Ph indole (**2** and **4**, Scheme 2). An acetyl group was installed in position 3 (83% or 64% yield, respectively) *via* a Vilsmeier-Haack reaction (path *a,* Scheme 2).[31] Compound **3** was treated with KOH and alkylated using various functionalized alkyl chlorides to generate substituted indoles **6a**, **b**, **d**-**f** (path *b*, 15-79% yield). Similarly, compound **5** was treated with NaH and MeI to obtain derivative **6c** (path *c*, 79%). Subsequently, compounds **6a**-**f** were employed in a Stobbe condensation with diethyl 2-(propan-2-ylidene)succinate, resulting in fulgides **7a**-**c** (*d*, 16-19%). Additionally, **7a** and **7c** were successfully crystallized and their X-Ray structure was measured (Figure 1). Compounds **7d**-**f** turned out to be highly unstable during the isolation attempts (see Experimental Section), probably due to the tertiary aliphatic amine in the side chain. Thus, we decided to use the crude mixtures of **7d-f** in the last reaction step, involving the aminolysis of the fulgides with NH_3 and a subsequent ring-closure to the form the central pyrrolin-2,5 dinone ring using (trimethylsilyl)diazomethane and NaH (*e*, Scheme 2).[32] Fulgimides **1a**-**c** could be isolated after column chromatography and subsequent preparative HPLC (2-10% yield). However, the formation of compounds **1d**-**f** was not observed.

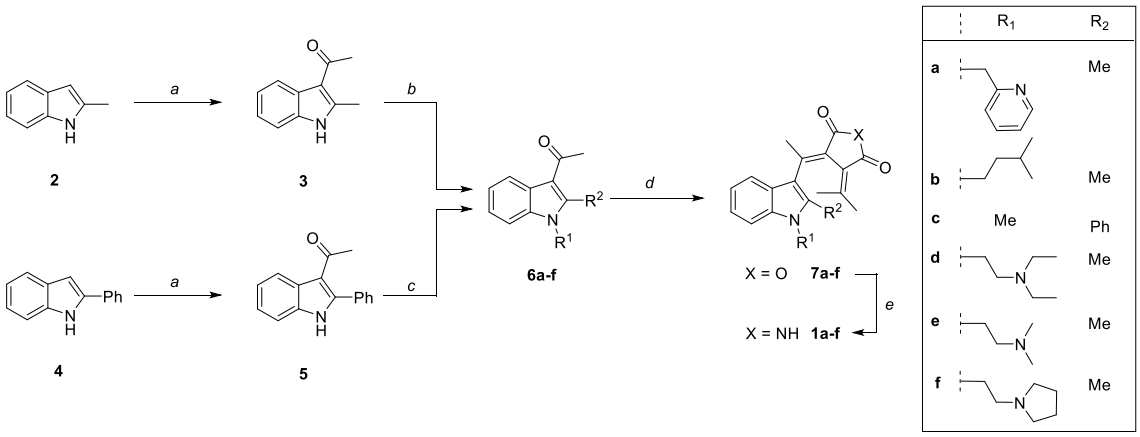

Scheme 2: Synthesis of fulgimides 1a-f: *a*: $POCl_3$, DMA, 80 °C, 2h (3: 83%, 5: 64%). *b*: alkyl chloride, KOH, DMF, 80 °C, 20h (15-79%). *c*: MeI, NaH, DMF, 0→r.t., 16h, 79%. *d*: diethyl 2-(propan-2-ylidene)succinate, LDA, THF, N_2, -105 °C→r.t., 18h; then, KOH, EtOH, 70 °C, 24h; then, AcCl, 40 °C, 18h (16-19%, 7d-f directly converted). *e*: NH_3 (2M in MeOH), N_2, 18h; then, (trimethylsilyl)diazomethane, MeOH; then, NaH, THF (2-10%, 1d-f decomposed during the preparation).

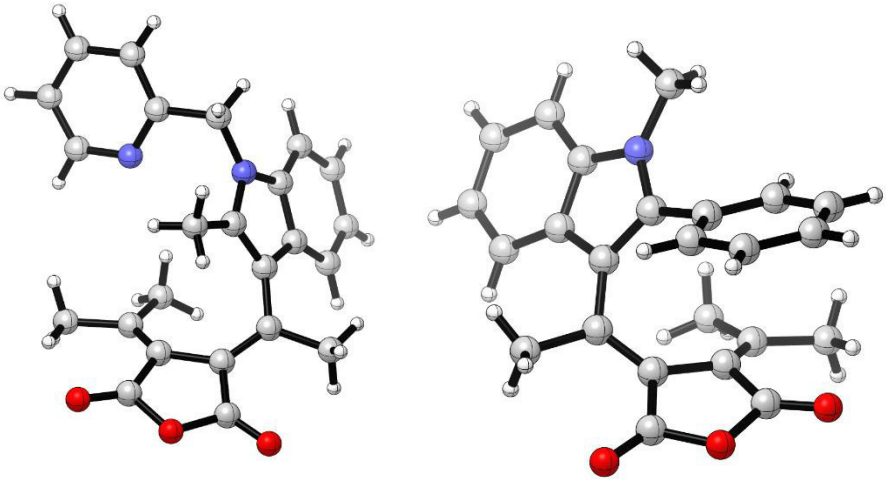

Figure 1: X-Ray structures of compounds 7a (left) and 7c (right).

IV.1.2.2 Photochromic Properties

Fulgimides exhibit three distinct photoisomers: the two ring-opened isomers (in their *E* and *Z configuration*) and the ring-closed isomer (*C*). Scheme 3 exemplary shows the light-triggered isomerizations of compound **1a**. The open photoisomers interconvert between each another through irradiation with light of 400 nm.[30] However, only the *E*-isomer can cyclize under these conditions to form the closed isomer ***C*-1a**. The ring-closed photoisomer ***C*-1a** is thermally stable (stability test at 37 °C showed hardly any ring-opening of compounds ***C*-1a** and ***C*-1c** over four hours, which are comparable to assay conditions, but ***C*-1b** resulted in decomposition; *vide infra* and A.IV.1.2.) and can be re-opened photochemically through irradiation with light of 590 nm.

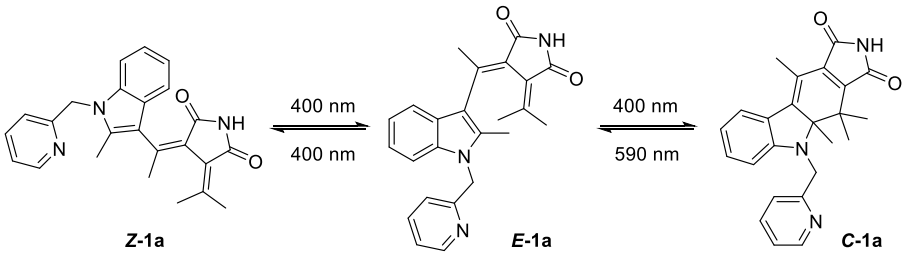

Scheme 3: Photoisomers of compound 1a: *Z*-1a can isomerize to *E*-1a under irradiation with 400 nm light reversibly. The same wavelength triggers the ring-closure reaction to form *C*-1a, which can be back-isomerized to its open form *E*-1a through irradiation with 590 nm light.

The photochemical behavior of fulgimides **1a**-**c** was investigated in DMSO and buffered aqueous solutions (ZMAL assay buffer,[33] *vide infra* and A.IV.1.4.). The spectra of **1a** are shown exemplarily in Figure 2. The open isomers of **1a**-**c** exhibit the main absorption band around 380 nm, which is tailing into the visible region giving the compounds a bright yellow color at the thermodynamic equilibrium (see Figure 2 and A.IV.1.3. for further spectra as

well as composition of the thermodynamic equilibrium). Upon irradiation with light of 400 nm, the band around 380 nm decreases and a new, broad absorption band around 580 nm arises. The new band can be attributed to the ring-closed isomer, which UV/Vis spectrum is bathochromically shifted due to its extended π-conjugation throughout the scaffold.[33] Hence, the solution at the photostationary state (PSS) appears violet in color.

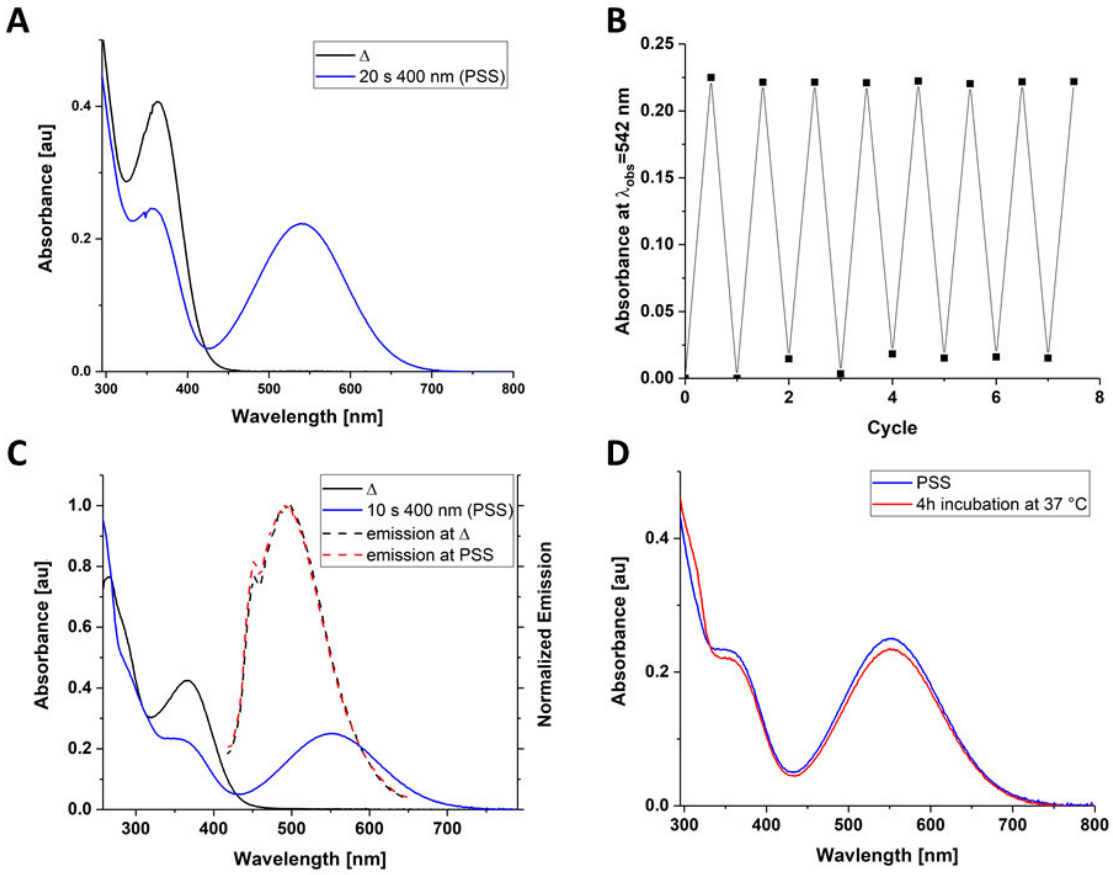

Figure 2: Spectroscopic properties of compound 1a in various solvents. A: UV/Vis spectrum of 1a 100µM in DMSO (black: open form, blue: PSS). B: Fatigue resistance of 1a 100µM in DMSO over eight cycles (λ_{obs}= 542 nm). C: Spectra of 1a 100µM in assay buffer/DMSO 1:2 (solid black: UV/Vis spectrum of open form, solid blue: UV/Vis spectrum of PSS, dashed black: fluorescence emission spectrum of open form, dashed red: fluorescence emission spectrum at PSS). D: Temperature stability of *C*-1a at 37 °C.

Table 1 summarizes the photochromic properties of fulgimides **1a**-**c**. The PSS of the compounds was reached in 10-35 seconds and contained 19-73% of the closed isomer (determined through analytical HPLC, see A.IV.1.2. for traces and Table A1 in the respective section for a wider range of measurements). The quality of the PSS appears to strongly depend on the substitution pattern of the indole moiety. Indeed, the phenyl substituent in position 2 of **1c** seems to sterically hinder the ring-closure reaction. All fulgimides show excellent fatigue resistance in repetitive cycle performance (alternated irradiation with light

of 400 nm and 590 nm, A.IV.1.2.). Noteworthy, the behavior of **1a-c** can be photoisomerizaed similar in DMSO and aqueous systems, which is an important characteristic for application in a biological environment.

Table 1: Photochromic properties of fulgimides 1a-c (concentration of 100 µM).

Compound	Solvent	λ_{max}^{Δ} [nm]	λ_{max}^{closed} [nm]	$\varepsilon\lambda_{max}^{closed}$	Isosbestic Point [nm]	PSS[a] E/Z/C [%]
1a	DMSO	363	542	7446	420	n.d.[b]
	Buffer/DMSO (2:1)	366	552	n.d.[b]	431	n.d.[b]
	Buffer (5% DMSO)[c]	261	564	7284	421	62:19:19[d]
1b	DMSO	366	563	10714	421	23:10:66
	Buffer/DMSO (2:1)	274, 375	588	4447	335, 416	23:4:73
1c	DMSO	296, 364	583	4914	408	45:24:31
	Buffer/DMSO (2:1)	296, 372	606	5148	272, 436	53:18:29
	Buffer (5% DMSO)	n.d.[b]	n.d.[b]	n.d.[b]	n.d.[b]	65:3:32[d]

[a]after irradiation with λ=400 nm determined by HPLC. [b]n.d. = not determined. [c]the concentration was 25µM. [d]The solution was irradiated with 400 nm for one minute.

Another interesting spectroscopic characteristic was observed. While irradiating the samples at 400 nm we found that the compounds exhibit fluorescence. Hence, we recorded the emission spectra of compounds **1a**-**c** in a mixture of the assay buffer and DMSO (2:1) exciting the sample at 390 nm (*cf.* assay read-out, *vide infra*). All compounds showed fluorescence maxima around 480 nm in both photoisomers. Additionally, compounds **1a** and **1b** exhibit a second maximum at 450 nm.

IV.1.2.3 Biological Evaluation

The inhibition of three human sirtuin isoforms (hSirt1-3) by **1a** and **c** was tested with the fluorescence based ZMAL assay (Compound **1b** did not appear to be thermally stable and was hence excluded from biological evaluation).[34] The photoswitches were incubated in a 96-well plate and tested at the thermodynamic equilibrium and at the PSS. Therefore, photoisomerization to the PSS was initiated directly in the assay mixture using a 96-LED irradiation setup (400 nm for 15 min, setup see A.I.1.). Comparison of the maximum activity of the sirtuins without inhibitor showed that irradiation alone did not have any influence on

the enzymatic activity. Since the compounds are fluorescent, the intrinsic fluorescence under assay conditions was measured and subtracted from the total fluorescence intensity detected. Table 2 shows the inhibition of the three sirtuin isotypes at 100 μM in percent and the IC_{50} values for the most active compounds **1a** and **1c**.

Table 2: Percentage inhibition of sirtuins at 100 μM or IC_{50} in μM.

	hSirt1		hSirt2		hSirt3	
Compound	Δ	PSS	Δ	PSS	Δ	PSS
1a	20.7 %	20.0 %	19.9 ± 1.6 μM	30.4 ± 3.5 μM	22.6 %	n.i.*
1c	n.i.*	n.i.*	28.8 %	29.6 ± 4.8 μM	4.7 %	n.i.*

*n.i. = no inhibition at 100 μM

For **1a** a 1.5-fold difference in inhibition towards hSirt 2 between the thermodynamic equilibrium and the PSS was detected. The 2-phenyl group in **1c** is untypical in classical fulgimides and was expected to result in a greater steric demand difference of the two photoisomers. Indeed, exhibiting an IC_{50} value of 29.6 μM a higher inhibition of hSirt2 was detected at the PSS as compared to the thermodynamic equilibrium. Considering that at the PSS only around 30 % of the closed isomer can be achieved (*vide supra*), the closed form of **1c** appears to be a significantly better inhibitor of hSirt2 than the open one. Indeed, it was not possible to calculate an IC_{50} value for the open isomer, since the maximum inhibition for concentrations up to 500 μM was too low (<50 %).

To visualize these findings, we optimized the structures of both photoisomers of **1a** and **1c** at the M06-2x/def2TZVP level of theory (Figure 3, see A.IV.1.6. for details). Like in the X-ray structure of its precursor (**7c** in Figure 1) the phenyl substituent in ***O*-1c** is orientated parallel to the succimimide moiety. As latter is essential for binding towards the enzyme, we suppose that the phenyl-ring could shield this interaction. In contrast, in ***C*-1c** the phenyl ring is orientated in an approximately 90-degree angle with respect to the succinimide moiety, hence, facilitating an interaction towards the active site. In both ***O*-1a** and ***C*-1a**, an interaction is possible. Changes in geometry take place mainly in the photochromic moiety of the compound leading to slightly altered binding properties.

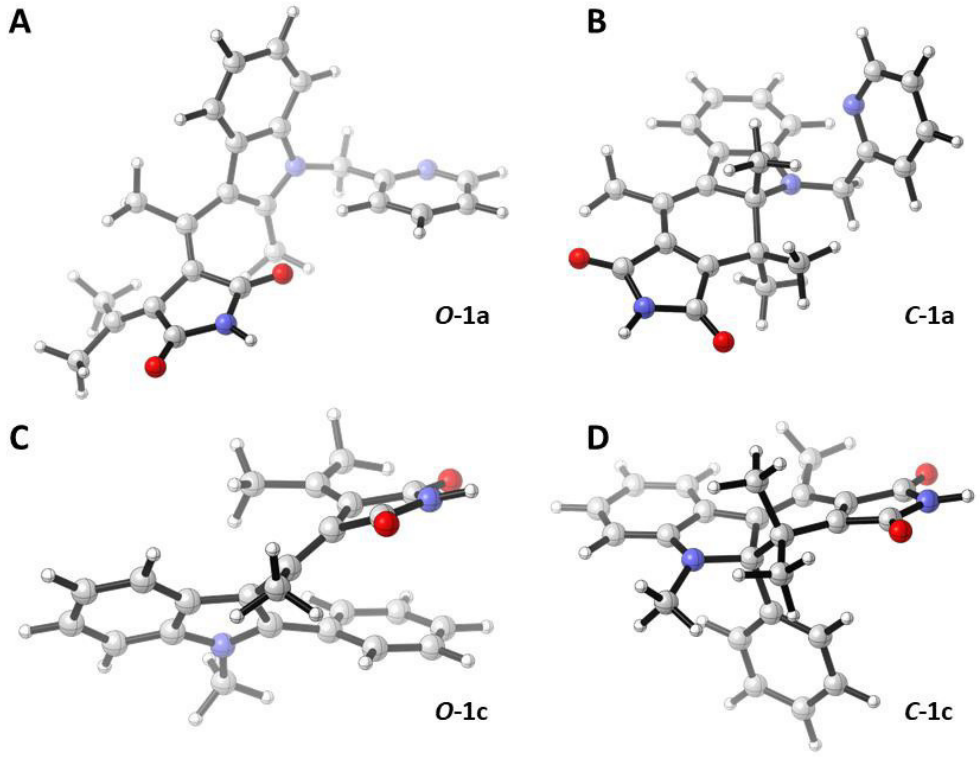

Figure 3: Simulated structures of 1a (A: open isomer, B: closed isomer) and 1c (C: open isomer, D: closed isomer) at the M06-2x/def2TZVP level of theory.

IV.1.3 Summary

In summary, we attempted to improve the photochromic properties, *i.e.* the reversible photo-isomerization in aqueous environment and bathochromic shift of the irradiation wavelength, of previously developed chromo-pharmacophores. Thus, we replaced the previously used DTM-based scaffold with a fulgimide. Spectroscopic characterization of three novel fulgimides showed good photoisomerization properties in both DMSO and DMSO buffer mixtures. Photoisomerization cycles could be induced with purple (400 nm) and orange (590 nm) light several times, without significant loss of performance. Moreover, the fulgimides exhibit fluorescence emission when irradiated with 390 nm or 400 nm light. Testing of **1a** and **c** towards hSirt1-3 in the well-established ZMAL-assay showed inhibition of hSirt2. For compound **1a** an IC_{50} value of 19.9 µM was obtained at the thermodynamic equilibrium. Inhibition at the PSS was approximately 1.5-fold lower. Also, **1c** showed a difference in affinity. At the thermodynamic equilibrium, the maximum inhibition by **1c** at the highest concentration tested (500 µM) was still below 50 % and only the IC_{50} value at the PSS could be determined to be 29.6 µM. This behavior could be visualized simulating the structures of both photoisomers. We found that the parallelly oriented phenyl moiety in the ***O*-1c** is shielding the succimide moiety and consequently preventing binding to the active

site. Hence, we could improve the photochromic properties of chromo-pharmacophores towards sirtuins as desired. Albeit succeeding in our goal, we partially lost affinity and difference in inhibition of both photoisomers compared to our previously reported series. Further structural optimizations of the presented compounds could finally lead to a fully reversibly controllable sirtuin ligand using visible light.

IV.1.4 Experimental Section

IV.1.4.1 Synthesis

General procedure for fulgimide formation

Fulgide **7** (1.0 eq.) was dissolved in NH_3 (2M in MeOH, 1 mL per 0.2 mmol) under nitrogen atmosphere and stirred at ambient temperature for 18 h. The solvent was removed under reduced pressure. The residue was dissolved in toluene (1 mL per 0.4 mmol). MeOH (1 mL per 0.2 mmol) and (trimethylsilyl)diazomethane (2M in hexane, 1.5 eq.) were added and the reaction mixture was stirred for 1.5 h at ambient temperature. Then, the solvent was removed *in vacuo*. The crude mixture was dissolved in dry THF (1 mL per 0.4 mmol) and added to a stirred suspension of NaH (60% in paraffin, 5.4 eq.) in dry THF (1 mL per 0.4 mmol) at 0 °C. The mixture was stirred for 24 h at room temperature and quenched with water. The mixture was extracted with EA (three times, *ca.* 2 mL per 0.1 mmol). The combined organic layers were washed with water (*ca.* 2 mL per 0.1 mmol) and brine (*ca.* 2 mL per 0.1 mmol) and dried over Na_2SO_4. The solvent was removed under reduced pressure. Compound **1a**-**1c** were purified through MPLC (NH-capped column, 20-100% EA in PE) and preparative HPLC (MeCN in 0.05% TFA/water 5-95% over 20 min). Compounds **1d**-**f** decomposed during the purification process and could not be isolated.

*3-(1-(2-Methyl-1-(pyridin-2-ylmethyl)-1H-indol-3-yl)ethylidene)-4-(propan-2-ylidene)pyrrolidine-2,5-dione (**1a**)*

The product was obtained as yellow powder (6.9 mg, 0.018 mmol, 3% yield). ^{1}H NMR (300 MHz, Methanol-d_4) δ =8.51 (ddd, J = 4.9, 1.8, 0.9 Hz, 1H), 7.71 (td, J = 7.7, 1.8 Hz, 1H), 7.51 – 7.42 (m, 1H), 7.40 – 7.33 (m, 1H), 7.29 (ddd, J = 7.7, 4.9, 1.1 Hz, 1H), 7.18 – 7.08 (m, 2H), 6.88 (dd, J = 7.8, 1.1 Hz, 1H), 3.63 (s, 2H), 2.75 (s, 3H), 2.15 (s, 3H), 2.08 (s, 3H), 0.96 (s, 3H). ^{13}C NMR (151 MHz, Methanol-d_4) δ =170.2 (q), 169.9 (q), 157.2 (q), 148.9 (q), 147.7 (q), 143.5 (q), 137.5 (+), 137.1 (q), 134.1 (q), 125.7 (q), 124.7 (+), 124.2 (+), 122.7 (+), 121.6 (+), 120.9 (+), 120.2 (+), 119.1 (q), 117.4 (q), 109.3 (+), 70.2 (-), 25.1 (+), 21.3 (+), 20.3

(+), 10.8 (+). ESI-MS: calculated: 385.1790. found: 386.2 (MH^+, 100%) HR-MS: 386.1861(MH^+, 100%). IR was not performed due to the small amount of compound obtained. HPLC: purity: >99%. R_t= 5.67 min and 6.14 min (73% E and 27% Z isomer).

*3-(1-(1-Isopentyl-2-methyl-1H-indol-3-yl)ethylidene)-4-(propan-2-ylidene)pyrrolidine-2,5-dione (**1b**)*

The compound was obtained as yellow solid (19 mg, 0.052 mmol, 10% yield). ^{1}H NMR (300 MHz, Methanol-d_4) δ =7.36 (ddt, J = 10.8, 8.0, 1.0 Hz, 2H), 7.16 (ddd, J = 8.2, 7.0, 1.3 Hz, 1H), 7.10 – 7.01 (m, 1H), 4.15 (s, 2H), 2.72 (s, 3H), 2.19 (s, 3H), 2.11 (s, 3H), 1.70 – 1.60 (m, 1H), 1.60 – 1.51 (m, 2H), 1.01 (d, J = 6.4 Hz, 6H), 0.88 (s, 3H). ^{13}C NMR (75 MHz, Methanol-d_4) δ =171.7 (q), 171.4 (q), 148.6 (q), 145.5 (q), 137.9 (q), 135.0 (q), 126.9 (q), 126.4 (q), 125.2 (q), 122.6 (+), 121.2 (+), 120.4 (+), 118.3 (q), 110.5 (+), 42.6 (-), 40.1 (-), 27.2 (+), 26.3 (+), 23.0 (+), 22.9 (+), 21.8 (+), 12.1 (+). ESI-MS: calculated: 364.2151 found: 387.2 (MNa^+, 15%), 365.2 (MH^+, 100). HR-MS: 387.2048(MNa^+, 15%), 365.2224 (MH^+, 100%). IR (neat, cm^{-1}) $\tilde{\nu}$ = 2956 (w), 2318 (w), 1737 (m), 1684 (m), 1580 (m), 1316 (m), 1245 (m), 734 (m). HPLC: purity: >99%. Rt= 5.75 min and 6.49 min (94% E and 6% Z isomer).

*(E)-3-(1-(1-Methyl-2-phenyl-1H-indol-3-yl)ethylidene)-4-(propan-2-ylidene)pyrrolidine-2,5-dione (**1c**)*

The compound was obtained as yellow powder (10.5 mg, 0.028 mmol, 2 % yield). ^{1}H NMR (400 MHz, Acetonitrile-d_3) δ =7.58 (dd, J = 8.0, 1.0 Hz, 1H), 7.45 (dd, J = 8.2, 0.9 Hz, 2H), 7.42 – 7.34 (m, 1H), 7.27 (ddt, J = 8.1, 7.0, 1.0 Hz, 1H), 7.22 (dt, J = 7.0, 1.4 Hz, 2H), 7.16 (ddt, J = 8.0, 7.0, 1.0 Hz, 1H), 3.61 (s, 3H), 2.69 (s, 3H), 1.89 (s, 3H), 0.91 (s, 3H). ^{13}C NMR (151 MHz, Acetonitrile-d_3) δ =170.4 (q), 168.8 (q), 147.5 (q), 143.4 (q), 139.4 (q), 139.1 (q), 132.7 (+), 130.8 (+), 129.4 (+), 129.4 (+), 126.7 (q), 125.8 (q), 125.4 (q), 123.3 (+), 121.5 (+), 121.0 (+), 117.9 (q), 111.3 (+), 31.9 (+), 26.1 (+), 22.7 (+), 21.7 (+). ESI-MS: calculated: 370.1681 found: 371.2 (MH^+, 100%) HR-MS: 371.1754 (MH^+, 100%). IR (neat, cm^{-1}) $\tilde{\nu}$ = 3168 (w), 3053 (w), 2952 (w), 1737 (s), 1689 (s), 1364 (s), 1326 (m), 1200 (m), 734 (s), 701 (s). HPLC: purity: >99%. Rt=3.41 min and 3.77 min (98% E and 2% Z iso-mer).

Acetylation of Compound **4**

*1-(2-Phenyl-1H-indol-3-yl)ethan-1-one (**5**)*

N,N-Dimethyl acetamide (DMA, 4.9 mL) was cooled to 0 °C. Then, $POCl_3$ (2.4 mL, 13.45 mmol) and 2-phenyl indole (2.0 g, 10.35 mmol) in DMA (2.6 mL) were added via syringe. The reaction mixture was heated to 80 °C for two hours. The cooled solution was then poured onto water (500 mL) and washed with diethyl ether (3x200 mL). The aqueous

phase was treated with NaOH (2M, aq) to precipitate the product. The solids were isolated through vacuum filtration over a Büchner funnel and then dried at high vacuum. The product was obtained as beige powder (2.02 mg, 8.60 mmol, 64% yield). ^{1}H NMR (400 MHz, Acetone-d_6) δ =10.92 (*b*s, 1H), 8.37 – 8.25 (m, 1H), 7.67 – 7.59 (m, 2H), 7.57 – 7.46 (m, 3H), 7.45 – 7.40 (m, 1H), 7.26 – 7.07 (m, 1H), 2.04 (s, 3H). ^{13}C NMR (101 MHz, Acetone-d_6) δ =193.4 (q), 144.6 (q), 135.8 (q), 133.3 (q), 130.0 (+), 129.3 (+), 128.5 (+), 127.7 (q), 123.0 (+), 122.2 (+), 121.8 (+), 115.1 (q), 111.2 (+), 29.5 (+). GC-MS: calculated: 235.0997, found: 235.1 ($M^{+\cdot}$, 50%), 220.1 (100%). HR-MS: found 235.09908 ($M^{+\cdot}$, 50%). IR (neat, cm^{-1}) $\tilde{\nu}$ = 3176 (w), 3041 (w), 1610 (m), 1580 (m), 1408 (m), 1197 (m), 957 (m), 745 (s), 701 (s). R_f: 0.45 (40% EA in PE). Melting Point: 224 °C.

General procedure for alkylation of indole derivatives (**6a**, **b**, **d**-**f**):

The acetylated indole **3** (1.0 eq.), KOH (5.0 eq.) and the appropriate alkylation reagent (1.5 eq.) were dissolved in DMF (1.5 ml per mmol). The reaction mixture was stirred for 20 h at 80 °C. The reaction mixture was diluted with water and extracted with EA (three times, each *ca.* 2 mL per mmol). The solution was washed with water (*ca.* 2mL per mmol). The combined organic layers were dried over $MgSO_4$ and the solvent was removed under reduced pressure. The crude product was purified through automated flash column chromatography (conditions specified for each compound).

*1-(2-Methyl-1-(pyridin-2-ylmethyl)-1H-indol-3-yl)ethan-1-one (**6a**)*

Purification through automated flash column chromatography (35-100% EA in PE). The product was obtained as yellowish powder (1014 mg, 3.84 mmol, 31% yield). ^{1}H-NMR (400 MHz, Chloroform-*d*) δ =8.60 (ddd, *J* = 4.9, 1.8, 0.9 Hz, 1H), 8.05-7.99 (m, 1H), 7,52 (td, *J* = 7.7, 1.8 Hz, 1H), 7.31-7.28 (m, 1H), 7,24 (dd, *J* = 13.5, 1.1 Hz, 1H), 7.22-7.19 (m, 1H), 7.19-7.15 (m, 1H), 6.59 (d, 7.9 Hz, 1H), 5.48 (s, 2H), 2.76 (s, 3H), 2.71 (s, 3H). ^{13}C-NMR (101 MHz, Chloroform-*d*) δ =194.8 (q), 156.0 (q), 149.7 (+), 144.8 (q), 137.2 (+), 136.3 (q), 126.5 (q), 122.7 (+), 122.4 (+), 122.2 (+), 120.9 (+), 120.1 (+), 114.9 (q), 109.8 (+), 48.39 (-), 31.8 (+), 12.7 (+). ESI-MS: calculated: 264.1263, found: 265.1 (MH^+, 100%). HR-MS: found 265.1339 (MH^+, 100%). IR (neat, cm^{-1}) $\tilde{\nu}$ = 2922 (m), 1625 (s), 1416 (s), 752 (s). R_f: 0.29 (50% EA in PE). Melting Point: 187 °C.

*1-(1-Isopentyl-2-methyl-1H-indol-3-yl)ethan-1-one (**6b**)*

Purification through automated flash column chromatography (35-100% EA in PE, then up to 10% MeOH in EA). The product was obtained as beige solid (2141 mg, 8.80 mmol, 63% yield). ^{1}H-NMR (400 MHz, Chloroform-*d*) δ =8.09 – 7.76 (m, 1H), 7.33 (ddt, *J* = 6.3, 4.0, 2.0 Hz, 1H), 7.29 – 7.05 (m, 2H), 4.28 – 3.82 (m, 2H), 2.78 (s, 3H), 2.69 (s, 3H), 1.78 – 1.70 (m, 1H), 1.67 – 1.54 (m, 2H), 1.03 (d, *J* = 6.5 Hz, 6H). ^{13}C-NMR (101 MHz, Chloroform-*d*) δ =194.6 (q), 144.5 (q), 135.8 (q), 126.5 (q), 121.9 (+), 121.8 (+), 120.7 (+), 114.2 (q), 109.6 (+), 41.5 (-), 38.4 (-), 31.7 (+), 26.3 (+), 22.5 (q), 12.6 (+). ESI-MS: calculated: 243.1623, found: 243.2 ($M^{+\cdot}$, 60%), 228.1 (100%). HR-MS: found 243.1615 ($M^{+\cdot}$). IR (neat, cm^{-1}) $\tilde{\nu}$ = 2956 (m), 2870 (m), 1638 (s), 1513 (m), 1461 (s), 1409 (s), 1372 (s), 1107 (m), 138 (s). R_f: 0.83 (EA). Melting Point: 152 °C.

*1-(1-Methyl-2-phenyl-1H-indol-3-yl)ethan-1-one (**6c**)*

Compound **5** (886 mg, 5.0 mmol) was dissolved in DMF (12.5 mL) and cooled to 0 °C. NaH (210 mg, 5.25 mmol, 60% on paraffin oil) and MeI (342 µL, 5.50 mmol) were added in portions. The reaction was stirred at ambient temperature for 16h. Then, the reaction mixture was poured onto water (100 mL) and extracted with ethyl acetate (3x50 mL). The combined organic phases were washed with NaOH (2M, aq, 50 mL) and dried over Na_2SO_4. The volatiles were removed *in vacuo*. Purification through automated flash column chromatography (25-85% EA in PE) efforted the product as pink powder (985 mg, 3.94 mmol, 79% yield). ^{1}H-NMR (400 MHz, Acetone-d_6) δ =8.64 (ddd, *J* = 7.7, 1.5, 0.8 Hz, 1H), 7.85 – 7.78 (m, 3H), 7.79 – 7.70 (m, 2H), 7.67 (dt, *J* = 8.1, 0.9 Hz, 1H), 7.55 – 7.38 (m, 2H), 3.72 (s, 3H), 2.04 (s, 3H).^{13}C-NMR (101 MHz, Acetone-d_6) δ =192.7 (q), 146.4 (q), 136.8 (q), 132.4 (q), 130.5 (+), 129.6 (+), 128.8 (+), 126.9 (q), 123.0 (+), 122.4 (+), 122.1 (+), 115.4 (q), 109.9 (+), 30.3 (+), 29.3(+). ECI-MS: calculated: 249.1154, found: 249.1 ($M^{+\cdot}$, 30%), 234.1 (100%). HR-MS: found 249.1155 ($M^{+\cdot}$). IR (neat, cm^{-1}) $\tilde{\nu}$ = 3063 (w), 2922 (m), 2855 (m), 1617 (m), 1577 (w), 1461 (m), 1386 (m), 1100 (m), 932 (m), 701 (s), 742 (s). R_f: 0.58 (40% EA in PE). Melting Point: 103 °C.

*1-(1-(2-(Diethylamino)ethyl)-2-methyl-1H-indol-3-yl)ethan-1-one (**6d**)*

Purification through automated flash column chromatography (35-100% EA in PE, 0-20% MeOH in EA). The product was obtained as brown oil (463 mg, 1.70 mmol, 15%). ^{1}H-NMR (300 MHz, Chloroform-*d*) δ =8.04-7.88 (m, 1H), 7.40-7.28 (m, 1H), 7.27-7.18 (m, 2H), 4.21 (t, *J* = 7.4 Hz, 2H), 2.79 (s, 3H), 2.75-2.65 (m, 5H), 2.58 (q, *J* = 7.1 Hz, 4H), 1.00 (t, *J* = 7.1

Hz, 6H). ^{13}C-NMR (75 MHz, Chloroform-*d*) δ =194.6 (q), 144.9 (q), 135.9 (q), 126.5 (q), 121.9 (+), 121.8 (+), 120.7 (+), 114.2 (q), 109.5 (+), 51.9 (+), 47.7 (+), 42.1 (+), 31.7 (-), 12.7 (-), 12.0 (-). ESI-MS: calculated: 272.1889, found: 273.1 (MH^+, 100%). HR-MS: found 273.1967 (MH^+, 100%). IR (neat, cm^{-1}) $\tilde{\nu}$ = 2967 (m), 2806 (m), 1636 (s), 1408 (s), 738 (s). R_f: 0.29 (80% EA in PE).

*1-(1-(2-(Dimethylamino)ethyl)-2-methyl-1H-indol-3-yl)ethan-1-one (**6e**)*

Purification by automated flash column chromatography (35-100% EA in PE, 0-20% MeOH in EA) the ptoduct as brown oil (1180 mg, 4.83 mmol, 42%). ^{1}H-NMR (400 MHz, Chloroform-*d*) δ =8.00-7.90 (m, 1H), 7.36-7.27 (m), 7.28-7.18 (m), 4.20 (t, *J* = 7.5 Hz, 2H), 2.75 (s, 3H), 2.64 (s, 3H), 2.59 (t, *J* = 7.5 Hz, 2H), 2.31 (s, 6H). ^{13}C-NMR (101 MHz, Chloroform-*d*) δ =194.6 (q), 144.6 (q), 135.9 (q), 126.5 (q), 122.0 (+), 121.9 (+), 120.8 (+), 114.4 (q), 109.5 (+), 58.0 (-), 45.8 (+), 41.4 (-), 31.6 (+), 12.5 (+). ESI-MS: calculated: 244.1576, found: 245.1 (MH^+, 100%). HR-MS: found 245.1652 (MH^+, 100%). IR (neat, cm^{-1}) $\tilde{\nu}$ = 2784 (m), 1613 (s), 1408 (s), 752 (s). R_f:0.16 (50% EA in PE).

*1-(2-Methyl-1-(2-(pyrrolidin-1-yl)ethyl)-1H-indol-3-yl)ethan-1-one (**6f**)*

Purification through automated flash column chromatography (35-100% EA in PE, 0-20% MeOH in EA). The product was obtained as brown oil (697 mg, 2.58 mmol, 22%). ^{1}H-NMR (400 MHz, Chloroform-*d*) δ =8.04-7.93 (m), 7.40-7.35 (m), 7.28-7.23 (m), 4.31 (t, *J* = 7.8 Hz, 2H), 2.84-2.76 (m), 2.67 (s), 2.63 (t, *J* = 6.7 Hz), 1.83 (quintet, *J* = 3.3 Hz). ^{13}C-NMR (101 MHz, Chloroform-*d*) δ =194.6 (q), 144.6 (q), 135.9 (q), 126.5 (q), 122.0 (+), 121.9 (+), 120.8 (+), 114.4 (q), 109.6 (+), 54.8 (-), 54.5 (-), 42.3 (-), 31.7 (+), 23.5 (-), 12.6 (+). ESI-MS: calculated: 270.1732, found: 271.1 (MH^+, 100%). HR-MS: found: 271.1809 (MH^+, 100%). IR (neat, cm^{-1}) $\tilde{\nu}$ = 2959 (m), 1628 (s), 1405 (s), 741 (s). R_f: 0.14 (80% EA in PE).

General procedure for fulgide formation

A solution of diethyl 2-(propan-2-ylidene)succinate (1.0 eq.) in dry THF (1.25 mL per mmol) was cooled to -105 °C under nitrogen atmosphere. A solution of LDA (1.0 eq.) was freshly prepared by adding a solution of ^{n}BuLi (1.0 eq.) to a solution of diisopropylamine (1.0 eq.) in anhydrous THF (0.5 mL per mmol) at -78 °C. The LDA-solution was added dropwise to the succinate -105 °C and was stirred for 30 min at the same temperature. A precooled (-78 °C) solution of compound **4** (1.0 eq.) in dry THF (0.4 mL per mmol) was added dropwise. The reaction mixture was warmed to room temperature for 18 hours. The reaction was

acidified with aqueous HCl (2M) and the aqueous layer was extracted with EA (three times, *ca.* 4 mL per mmol). The combined organic layers were washed with brine (*ca.* 4 mL per mmol), dried over $MgSO_4$ and the solvent was removed *in vacuo*. The residue was dissolved in EtOH (5 mL per mmol)) and a saturated aqueous solution of KOH (0.4 mlL per mmol) was added. The mixture was stirred at 70 °C for 24 h, poured onto ice and acidified with aqueous HCl (2M). The aqueous layer was extracted with EA (three times, *ca.* 4 mL per mmol) and the solvent was removed under reduced pressure. The residue was dissolved in acetyl chloride (1.7 mL per mmol) and the solution was stirred at 40 °C for 18 hours. The solvent was evaporated *in vacuo* and the crude product was purified by automated flash column chromatography (35-100% EA in PE, 0-25% MeOH in EA) and preparative HPLC (in the case of **7a**-**b**; **7c** crystallized after normal phase chromatography which used for structure determination and the compound was converted after that; **7d**-**f** turned out to be highly instable under HPLC conditions, NEt_3 treated silica gel or NH-caped silica gel. Thus, they were converted directly after identification through ESI-MS).

*(E)-3-(1-(2-Methyl-1-(pyridin-2-ylmethyl)-1H-indol-3-yl)ethylidene)-4-(propan-2-ylidene)dihydro-furan-2,5-dione (**7a**)*

The pure product was obtained as yellow solid (245 mg, 0.63 mmol 19%). ^{1}H-NMR (400 MHz, Chloroform-*d*) δ =8.58 (d, *J* = 5.0 Hz, 1H), 7.63 (td, *J* = 7.7, 1.8 Hz), 7.44 (dd, *J* = 7.1, 1.6 Hz), 7.30-7.26 (m, 1H), 7.25-7.13 (m), 6.78 (d, *J* = 7.9 Hz, 1H), 5.45 (s, 2H), 2.83 (s, 3H), 2.18 (d, *J* = 1.3 Hz, 6H), 1.02 (s, 3H). A set of small signals from closed photoisomer could not be avoided. ^{13}C-NMR (101 MHz, Chloroform-*d*) δ =164.0 (q), 163.7 (q), 156.1(q), 153.8 (q), 149.2 (+), 149.1 (q), 137.6 (+), 136.8 (q), 135.1 (q), 125.2 (q), 123.0 (+), 122.5 (+), 121.3 (q), 121.1 (+), 120.7 (+), 119.7 (+), 119.5 (q), 117.3 (q), 109.6 (+), 48.3 (-), 26.4 (+), 23.6 (+), 22.7 (+), 12.3 (+). ESI-MS: calculated: 386.1630, found: 387.1 (MH^+, 100%). HR-MS: found 387.1712 (MH^+, 100%, closed form), 387.1706 (MH^+, 100%, opened form). IR (neat, cm^{-1}) $\tilde{\nu}$ = 2922 (w), 1800 (s), 1748 (s), 1408 (s), 1222 (s), 920 (s), 745 (s). R_f: 0.41 (50% EA in PE).

*(E)-3-(1-(1-Isopentyl-2-methyl-1H-indol-3-yl)ethylidene)-4-(propan-2-ylidene)dihydrofuran-2,5-dione (**7b**)*

The pure product was obtained as yellow solid (182 mg, 0.498 mmol, 16%). ^{1}H-NMR (400 MHz, Chloroform-*d*) δ =7.42 – 7.37 (m, 1H), 7.31 – 7.27 (m, 1H), 7.22 (ddd, *J* = 8.3, 7.0, 1.2 Hz, 1H), 7.14 (ddd, *J* = 8.0, 6.9, 1.1 Hz, 2H), 4.18 – 3.92 (m, 2H), 2.81 (s, 3H), 2.20 (d, *J* = 0.9 Hz, 6H), 1.63 – 1.50 (m, 3H), 1.02 (dd, *J* = 6.6, 1.4 Hz, 8H), 0.93 (s, 3H). A set of signals from closed photoisomer could not be avoided. Assignment was done through ppm

calculation and comparison with the precursor. Due to the complexity a carbon NMR was not recoded of this intermediate. ESI-MS: calculated: 365.1991, found: 753.4 ($2MNa^+$, 45%), 388.2 (MNa^+, 20%), 366.2 (MH^+, 100%). HR-MS: found 366.2065 (MH^+, 100%,). IR (neat, cm^{-1}) $\tilde{\nu}$ = 2982 (w), 1804 (w), 1737 (s), 1712 (s), 1367 (m), 1282 (m), 1223 (m), 1175 (s), 1077 (s), 1029 (s). R_f: 0.85 (40% EA in PE).

*(E)-3-(1-(1-Methyl-2-phenyl-1H-indol-3-yl)ethylidene)-4-(propan-2-ylidene)dihydrofuran-2,5-dione (**7c**)*

The product was obtained as crystalline solid (498 mg, 1.348 mmol, 16% yield). The structure was confirmed through X-Ray analysis and converted directly.

ESI-MS: calculated: 371.1521, found: 165-3 ($2M+Na^+$, 25%), 394.1 (M^+Na^+, 20%), 372.2 (MH^+, 100%). HR-MS: 372.1594 (MH^+, 100%).

*(E)-3-(1-(1-(2-(Diethylamino)ethyl)-2-methyl-1H-indol-3-yl)ethylidene)-4-(propan-2-ylidene)dihydrofuran-2,5-dione (**7d**)*

The product was obtained as yellow oil and was directly converted to fulgimide **1d**.

ESI-MS: calculated: 394.2256, found: 395.2 (MH+, 100%). HR-MS: 395.2335 (MH+, 100%).

*(E)-3-(1-(1-(2-(Dimethylamino)ethyl)-2-methyl-1H-indol-3-yl)ethylidene)-4-(propan-2-ylidene)dihydrofuran-2,5-dione (**7e**)*

The product was obtained as yellow oil and directly converted to fulgimide **1e**.

ESI-MS: calculated: 366.1943, found: 367.2 (MH+, 100%). HR-MS: found 367.2021 (MH+, 100%).

*(E)-3-(1-(2-Methyl-1-(2-(pyrrolidin-1-yl)ethyl)-1H-indol-3-yl)ethylidene)-4-(propan-2-ylidene)dihydrofuran-2,5-dione (**7f**)*

The product was obtained as yellow solid and directly converted to fulgimide **1f**.

ESI-MS: calculated: 392.2100, found: 393.2 (MH+, 100%). HR-MS: found 393.2177.

IV.1.4.2 Biological evaluation

The biological activity of compounds **1a-c** were tested employing an *in vitro* activity assay based on the deacetylation of the substrate Z-Lys(Ac-AMC) (ZMAL).[34] A detailed description of the procedure can be found in the Appendix. To determine the influence of the intrinsic fluorescence of the compounds a no-conversion control was performed. For preliminary testing each compound was diluted to 100 μM final assay concentration. For

compounds scoring an inhibition higher that 50 % at 100 μM for either of the isomers an IC_{50} value was determined.

IV.1.5 Acknowledgments

We thank Stefano Crespi (University of Pavia) for his help with computational calculations and Julian Nazet (University of Regensburg) for preliminary *in silico* binding experiments. Computing time was granted by CINECA (HPC-SCAI project HP10C8U1NY). NAS thanks the Studienstiftung des Deutschen Volkes for a PhD fellowship. M.J. and N.W. thank the Deutsche Forschungsgemeinschaft (DFG, Ju295/14-1) for funding.

IV.1.6 References

1. North, B. J.; Verdin, E., Sirtuins: Sir2-Related NAD-Dependent Protein Deacetylases. *Genome Biology* **2004**, *5*, 224–224.

2. Trapp, J.; Jochum, A.; Meier, R.; Saunders, L.; Marshall, B.; Kunick, C.; Verdin, E.; Goekjian, P.; Sippl, W.; Jung, M., Adenosine Mimetics as Inhibitors of NAD+-Dependent Histone Deacetylases, from Kinase to Sirtuin Inhibition. *Journal of Medicinal Chemistry* **2006**, *49*, 7307–7316.

3. Freitag, M.; Schemies, J.; Larsen, T.; El Gaghlab, K.; Schulz, F.; Rumpf, T.; Jung, M.; Link, A., Synthesis and Bological Activity of Splitomicin Analogs Targeted at Human NAD+-Dependent Histone Deacetylases (Sirtuins). *Bioorganic & Medicinal Chemistry* **2011**, *19*, 3669–3677.

4. Lawson, M.; Uciechowska, U.; Schemies, J.; Rumpf, T.; Jung, M.; Sippl, W., Inhibitors to Understand Molecular Mechanisms of NAD+-Dependent Deacetylases (Sirtuins). *Biochimica et Biophysica Acta - Gene Regulatory Mechanisms* **2010**, *1799*, 726–739.

5. Xie, H. J.; Jung, K. H.; Nam, S. W., Overexpression of SIRT2 Contributes Tumor Cell Growth in Hepatocellular Carcinomas. *Molecular & Cellular Toxicology* **2011**, *7*, 367–374.

6. Frye, R. A., Phylogenetic Classification of Prokaryotic and Eukaryotic Sir2-Like Proteins. *Biochemical and Biophysical Research Communications* **2000**, *273*, 793–798.

7. Slingerland, M.; Guchelaar, H.-J.; Gelderblom, H., Histone Deacetylase Inhibitors: an Overview of the Clinical Studies in Solid Tumors. *Anticancer Drugs* **2014**, *25*, 140–149.

8. Sussmuth, S. D.; Haider, S.; Landwehrmeyer, G. B.; Farmer, R.; Frost, C.; Tripepi, G.; Andersen, C. A.; Di Bacco, M.; Lamanna, C.; Diodato, E.; Massai, L.; Diamanti, D.; Mori, E.; Magnoni, L.; Dreyhaupt, J.; Schiefele, K.; Craufurd, D.; Saft, C.; Rudzinska, M.;

Ryglewicz, D.; Orth, M.; Brzozy, S.; Baran, A.; Pollio, G.; Andre, R.; Tabrizi, S. J.; Darpo, B.; Westerberg, G., An Exploratory Double-Blind, Randomized Clinical Trial with Selisistat, a SirT1 Inhibitor, in Patients with Huntington's Disease. *British Journal of Clinical Pharmacology* **2015**, *79*, 465–476.

9. Trapp, J.; Meier, R.; Hongwiset, D.; Kassack, M. U.; Sippl, W.; Jung, M., Structure–Activity Studies on Suramin Analogues as Inhibitors of NAD+-Dependent Histone Deacetylases (Sirtuins). *ChemMedChem* **2007**, *2*, 1419–1431.

10. Fridén-Saxin, M.; Seifert, T.; Landergren, M. R.; Suuronen, T.; Lahtela-Kakkonen, M.; Jarho, E. M.; Luthman, K., Synthesis and Evaluation of Substituted Chroman-4-one and Chromone Derivatives as Sirtuin 2-Selective Inhibitors. *Journal of Medicinal Chemistry* **2012**, *55*, 7104–7113.

11. Seifert, T.; Malo, M.; Kokkola, T.; Engen, K.; Fridén-Saxin, M.; Wallén, E. A. A.; Lahtela-Kakkonen, M.; Jarho, E. M.; Luthman, K., Chroman-4-one- and Chromone-Based Sirtuin 2 Inhibitors with Antiproliferative Properties in Cancer Cells. *Journal of Medicinal Chemistry* **2014**, *57*, 9870–9888.

12. Rumpf, T.; Schiedel, M.; Karaman, B.; Roessler, C.; North, B. J.; Lehotzky, A.; Oláh, J.; Ladwein, K. I.; Schmidtkunz, K.; Gajer, M.; Pannek, M.; Steegborn, C.; Sinclair, D. A.; Gerhardt, S.; Ovádi, J.; Schutkowski, M.; Sippl, W.; Einsle, O.; Jung, M., Selective Sirt2 Inhibition by Ligand-Induced Rearrangement of the Active Site. *Nature Communications* **2015**, *6*, 6263–6276.

13. Sundriyal, S.; Moniot, S.; Mahmud, Z.; Yao, S.; Di Fruscia, P.; Reynolds, C. R.; Dexter, D. T.; Sternberg, M. J. E.; Lam, E. W. F.; Steegborn, C.; Fuchter, M. J., Thienopyrimidinone Based Srtuin-2 (Sirt2)-Selective Inhibitors Bind in the Ligand Induced Selectivity Pocket. *Journal of Medicinal Chemistry* **2017**, *60*, 1928–1945.

14. Velema, W. A.; Szymanski, W.; Feringa, B. L., Photopharmacology: Beyond Proof of Principle. *Journal of the American Chemical Society* **2014**, *136*, 2178–2191.

15. Lerch, M. M.; Hansen, M. J.; van Dam, G. M.; Szymanski, W.; Feringa, B. L., Emerging Targets in Photopharmacology. *Angewandte Chemie International Edition* **2016**, *55*, 10978–10999.

16. Brieke, C.; Rohrbach, F.; Gottschalk, A.; Mayer, G.; Heckel, A., Light-Controlled Tools. *Angewandte Chemie International Edition* **2012**, *51*, 8446–8476.

17. Eisel, B.; Hartrampf, F.; Meier, T.; Trauner, D., Reversible Optical Control of F1Fo-ATP Synthase Using Photoswitchable Inhibitors. *FEBS Letters* **2018**, *592*, 343–355.

18. Simeth, N. A.; Kneuttinger, A. C.; Sterner, R.; König, B., Photochromic Coenzyme Q Derivatives: Switching Redox Potentials with Light. *Chemical Science* **2017**, *8*, 6474–6483.

19. Wilson, D.; Li, J. W.; Branda, N. R., Visible-Light-Triggered Activation of a Protein Kinase Inhibitor. *ChemMedChem* **2017**, *12*, 284–287.

20. Ferreira, R.; Nilsson, J. R.; Solano, C.; Andréasson, J.; Grøtli, M., Design, Synthesis and Inhibitory Activity of Photoswitchable RET Kinase Inhibitors. *Scientific Reports* **2015**, *5*, 9769–9776.

21. Hansen, M. J.; Velema, W. A.; de Bruin, G.; Overkleeft, H. S.; Szymanski, W.; Feringa, B. L., Proteasome Inhibitors with Photocontrolled Activity. *ChemBioChem* **2014,** *15*, 2053–2057.

22. Broichhagen, J.; Jurastow, I.; Iwan, K.; Kummer, W.; Trauner, D., Optical Control of Acetylcholinesterase with a Tacrine Switch. *Angewandte Chemie International Edition* **2014,** *53*, 7657–7660.

23. Lachmann, D.; Studte, C.; Männel, B.; Hübner, H.; Gmeiner, P.; König, B., Photochromic Dopamine Receptor Ligands Based on Dithienylethenes and Fulgides. *Chemistry – A European Journal* **2017**, *23*, 13423–13434.

24. Wutz, D.; Gluhacevic, D.; Chakrabarti, A.; Schmidtkunz, K.; Robaa, D.; Erdmann, F.; Romier, C.; Sippl, W.; Jung, M.; Konig, B., Photochromic Histone Deacetylase Inhibitors Based on Dithienylethenes and Fulgimides. *Organic & Biomolecular Chemistry* **2017**, *15*, 4882–4896.

25. Falenczyk, C.; Schiedel, M.; Karaman, B.; Rumpf, T.; Kuzmanovic, N.; Grotli, M.; Sippl, W.; Jung, M.; Konig, B., Chromo-Pharmacophores: Photochromic Diarylmaleimide Inhibitors for Sirtuins. *Chemical Science* **2014**, *5*, 4794–4799.

26. Szymański, W.; Beierle, J. M.; Kistemaker, H. A. V.; Velema, W. A.; Feringa, B. L., Reversible Photocontrol of Biological Systems by the Incorporation of Molecular Photoswitches. *Chemical Reviews* **2013**, *113*, 6114–6178.

27. Yamaguchi, T.; Uchida, K.; Irie, M., Asymmetric Photocyclization of Diarylethene Derivatives. *Journal of the American Chemical Society* **1997**, *119*, 6066–6071.

28. Irie, M.; Sayo, K., Solvent Effects on the Photochromic Reactions of Diarylethene Derivatives. *The Journal of Physical Chemistry* **1992**, *96*, 7671–7674.

29. Fleming, C.; Remón, P.; Li, S.; Simeth, N. A.; König, B.; Grøtli, M.; Andréasson, J., On the Use of Diarylmaleimide Derivatives in Biological Contexts: An Investigation of the Photochromic Properties in Aqueous Solution. *Dyes and Pigments* **2017**, *137*, 410–420.

30. Strübe, F.; Siewertsen, R.; Sönnichsen, F. D.; Renth, F.; Temps, F.; Mattay, J., Photochromism of Rotation-Hindered Furylfulgides Influenced by Steric Modifications. *European Journal of Organic Chemistry* **2011**, *2011*, 1947–1955.

31. Dietrich, S. Synthese und Photochrome Eigenschaften Funktionalisierter Indolylfulgimide. *Dissertation, Berlin* **2006**.

32. Okuyama, T.; Yokoyama, Y.; Yokoyama, Y., Control of the Association of Indolylfulgimide with Bis(acylamino)pyridine by Photochromism. *Bulletin of the Chemical Society of Japan* **2001**, *74*, 2181–2187.

33. Irie, M., Diarylethenes for Memories and Switches. *Chemical Reviews* **2000**, *100*, 1685–1716.

34. Heltweg, B.; Trapp, J.; Jung, M., In vitro Assays for the Setermination of Histone Deacetylase Activity. *Methods* **2005**, *36*, 332–337.

IV.2 Design and Synthesis of Photochromic Histamin H1 Antagonists Addressable with Visible Light

Abstract:

The human histamine H_1 receptor belongs to the family of G protein coupled receptors and is involved in allergic reactions. Hence, many antagonists such as desloratadine, levocetirizine, fexofenadine or rupatadine are used in the clinic as drugs for the treatment of allergic diseases. Though structural re-design has improved the properties of the nowadays-used pharmaceuticals, they are still not free from side effects. A novel strategy to limit the activity in space and time and therefore lower side effects is to use light-triggered drugs. Hence, we envisioned that combining the crucial biological interaction motifs of the drug fexofenadine into an azo-based *chromo-pharmacophore* could be the starting point for the development of photocontrollable histamine H_1R antagonists.

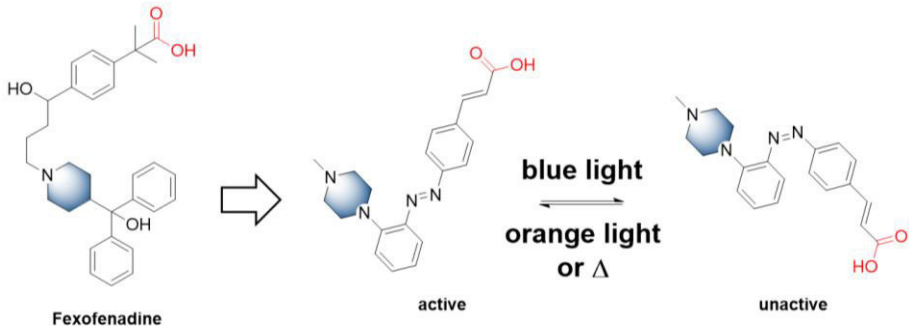

Author contributions

N. A. Simeth designed, synthesized and characterized all compounds and performed UV/Vis spectroscopic studies and wrote the manuscript. Burkhard König supervised the work.

IV.2.1 Introduction

The four histamine receptors (H_1R, H_2R, H_3R, H_4R) belong to the family A of G-protein coupled receptors (GPCRs) and accept the biogenic amine histamine as endogenous ligand. They are widely expressed throughout the body in epithelial, vascular, smooth vascular, neuronal, glial, and immune cells.[1-3] The human histamine H_1 receptor (hH_1R) is particularly interesting as a subject of study as it is involved, for instance, in allergic diseases. Hence, many hH_1R antagonists such as desloratadine, levocetirizine, fexofenadine or rupatadine are used in the clinic as drugs for the treatment of allergic reactions.[4, 5] Moreover, highly selective H_1R antagonists and (partial) agonists are of great interests as small molecular tool compounds to facilitate full pharmacological characterization of the receptor.[6] However, the development of highly selective ligands is traditionally relaying on excellent synthetic design. For example, first-generation drugs for treatment of allergic reactions had significant side effects like sedation, dry mouth and arrhythmia, as a consequence of crossing the blood-brain barrier.[3] In contrast, second- and third-generation drugs are less likely to penetrate the blood-brain barrier, due to the introduction of polar groups like carboxylic acid moieties that limit this considerable side-effect.[7] Albeit exhibiting improved properties compared to first-generation compounds, second-generation pharmaceuticals, like the over-the-counter drug cetirizine, are still not free from unwanted effects.[8] Moreover, tool compounds are required to have a high specificity towards their receptor, a property most compounds belonging to the hH_1R-interacting ones cannot fulfill so far.[6, 7]

A novel strategy to circumvent these challenges is to use light-triggered pharmaceuticals. Indeed, the activity of a biologically relevant tool compound (or drug) is coupled to the possibility to achieve a structural change upon irradiation with light of a certain wavelength. In this manner, enhanced spatiotemporal control can be obtained without further structural optimization. In the very young field of *photopharmacology* different strategies of light-controlled molecules are under investigation.[9-12] A particularly successful photoactive scaffold is azobenzene. Azobenzenes undergo an *E*-to-*Z* isomerization of the central N=N double bond, which is accompanied by substantial changes in geometry and its dipole moment. The isomerization can be reversed upon treatment with light of longer wavelength or thermally. [13] Many scientists have focused on tuning the properties of azobenzenes. The lifetime of the meta-stable *Z*-isomer can be tuned from nanoseconds to years.[14-17] Also, the irradiation wavelengths have been shifted to the red introducing ortho-methoxy, ortho-methyl sulfane, ortho-piperazine, otho-piperidine substituents and azo-push-pull systems.[18-20] We found the piperidine feature especially interesting as it is part of the structure of

fexofenadine, a second-generation H_1R drug (blue, Figure 1).[7, 18] Hence, we envisioned that combining the tertiary amine and the carboxylic acid motif, which are present in fexofenadine and responsible for crucial hydrogen interactions to amino acids in the active site, into an azo-based *chromo-pharmacophore* could be a good starting point in the development of photocontrollable histamine H_1R antagonists.[7, 21]

IV.2.2 Results and Discussion

IV.2.2.1 Design

The design of the photochromic H_1R antagonists is inspired by the second-generation drug fexofenadine (left, Figure 1). Two functional groups, namely the carboxylic acid (red, Figure 1) and the piperidine (blue, Figure 1), are reported to exhibit crucial hydrogen binding interactions to K191 and D107 in the ligand binding pocket.[7] To mimic the distance between both functionalities optimally, we designed a short- (**1a**, Figure 1) and a long-linker (**1b**, Figure 1) derivative. Additionally, the piperazine moiety was attached in ortho-position to the azo function to generate a red-shifted azobenzene.[18, 19] Hence, the switches can be expected to isomerize upon visible-light irradiation. This is of great advantage, as visible light is causing less cell damage than UV-light and can also penetrate deeper into the tissue.[19] Consequently, it would allow us to employ the frequently used guinea pig ileum-based assay for biological evaluation.[3]

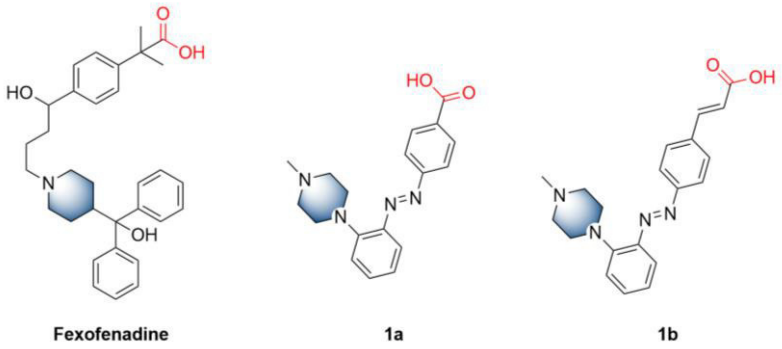

Figure 1: Potential photochromic H_1R inhibitors. The chromo-pharmacophore exhibits two interaction moieties, the tertiary amine (blue) and the carboxylic acid (red), on different sides of the azo switch varying between a short- and a long-distance structure.

IV.2.2.2 Synthesis

The key reaction to the synthesis towards photochromic inhibitors **1a** and **1b** is a Mills reaction of precursor **4**, which could be synthesized from ortho-fluoro aniline (**2**),[22] and nitroso carboxy acids **6a** or **6b**, respectively, following a known procedure (Scheme 1). Both

nitroso compounds were obtained through treatment of the corresponding anilines (**5a** and **5b**) with OXONE and subsequent precipitation. The final Mills reaction gave **1a** and **1b** in acceptable yields after isolation through preparative HPLC (10% and 16%, respectively).

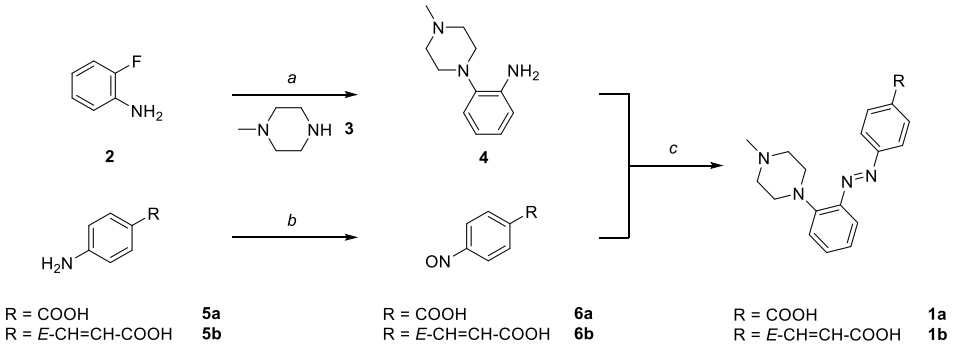

Scheme 1: Synthesis of photochromic H_1R inhibitors 1a and 1b *via* Mills reaction of 4 and 6a or 6b, respectively. *a*: K_2CO_3 (1.1 eq), DMF, 120 °C, 16h, 90%. *b*: OXONE (2 eq), DCM/water (2:3), r.t., 1 h, directly converted. *c*: HOAc, r.t., 16 h, (1a: 10%, 1b: 16%).

IV.2.2.3 Spectroscopy

Both compounds were investigated regarding their photochromic properties in DMSO (Figure 2) and DMSO-buffer mixtures (spectra see Appendix, Section A.IV.2.3.). The results are summarized in Table 1. Both compounds exhibit two distinct maxima in their *E*-form (black line, Figure 2).[23] Exhibiting a piperazine moiety in ortho-position of the azo group, the spectra are red-shifted compared to classical azobenzenes (as reported previously for this substitution pattern).[19, 23]

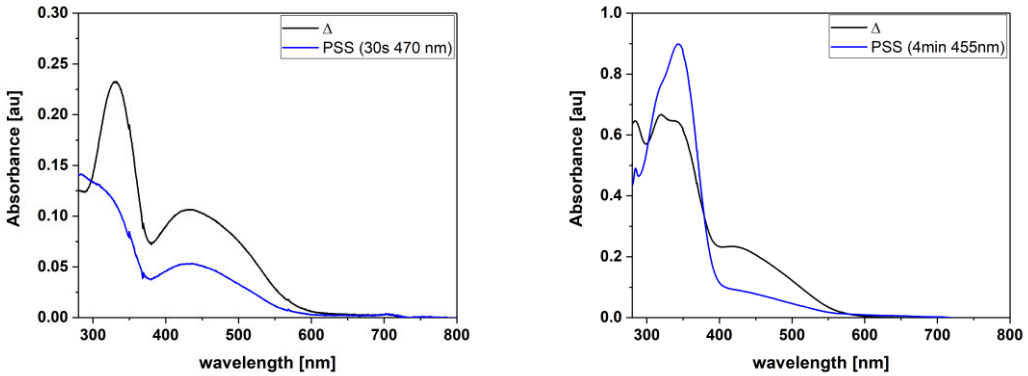

Figure 2: Absorption spectra of compound 1a (100 µM, left) and 1b (250 µM, right) in DMSO.

Table 1: UV/Vis properties of compounds 1a and 1b.

Compound	solvent mixture	λ_{max} [nm][a]	$\varepsilon\lambda_{max}$[$M^{-1}cm^{-1}$][b]	concentration [μM]
1a	DMSO	330 (434)	11329	100
1a	buffer (5% DMSO)[c]	327	11169	250
1b	DMSO	320 (422)	11742	300
1b	buffer (5% DMSO)[c]	347	11665	400

[a]the main absorption maximum is reported, the second maximum or shoulder is indicated in brackets (cuvette width was 0.2 cm). [b]molar attenuation coefficient at the individual absorption maximum of the compound in the used solvent. [c]used buffer: Dulbecco's Phosphate buffered Saline.

Due to the broad absorption properties in the visible range of the spectrum, photoinduced *E*-to-*Z* isomerization was feasible with 455 nm and 470 nm, respectively. However, using 365 nm for *E*-to-*Z* isomerization resulted in higher PSS for both compounds (*cf.* Appendix). Exact PSS values could not be assigned due to short thermal lifetime of both compounds. In agreement with previous reports, the compounds relax in the minute-range (76 min for **1a** and 44 min for **1b** in DMSO at 25 °C, respectively, see Appendix).[19, 23]

IV.2.3 Conclusion and Outlook

In conclusion, we designed two azoswitches inspired by the anti-histamine drug fexofenadine. The compounds combine the two major binding features, *i.e.* the carboxy moiety and the piperidine moiety, as a chromo-pharmacophore. Moreover, we positioned the tertiary nitrogen in ortho-position to the azo function to result in a red-shifted azobenzene derivative. We could synthesize both compounds and characterize them regarding their photochromic properties using UV-Vis spectroscopy. Indeed, both compounds show red-shifted absorption profiles and *E*-to-*Z* isomerization can be induced using visible light (455 nm or 470 nm, respectively). The *Z*-isomer is relaxing back thermally (τ= 76 min for **1a** and 44 min for **1b** in DMSO at 25 °C, respectively). The compound is soluble in DMSO and DMSO-buffer-mixtures. Testing of the compounds regarding their activity towards H_1R using a guinea pig ileum assay is content of ongoing research.

IV.2.4 Experimental Section

*(E)-3-(4-Nitrosophenyl)acrylic acid (**5b**)*

4-Amino cinnamic acid (2.00 g, 12.26 mmol) was dissolved in DCM (20 mL) and treated with a solution of OXONE (3.73 g, 24.51 mmol) in water (30 mL). The reaction mixture was stirred for an hour and the formed precipitate sucked off over a Büchner funnel and died *in vacuo*. The product was directly converted to **1b**.

*(E)-4-((2-(4-Methylpiperazin-1-yl)phenyl)diazenyl)benzoic acid (**1a**)*

4-Nitroso benzoic acid (613 mg, 5.22 mmol) and 2-(4-methylpiperazin-1-yl)aniline (998 mg, 5.22 mmol) were dissolved in HOAc (6 mL) and stirred at ambient temperature for 16 h. The reaction mixture was poured onto crushed ice and extracted with EA (2x20 mL). The organic phases were combined, dried over Na_2SO_4 and the volatiles were removed under reduced pressure. The crude product was purified through preparative HPLC. Compound **1a** was obtained as red solid (184 mg, 0.54 mmol, 10 % yield). ^{1}H-NMR (300 MHz, Methanol-*d4*) δ =8.21 (d, *J* = 8.5 Hz, 2H), 7.96 (d, *J* = 8.6 Hz, 2H) 7.71 (dd, *J* = 8.1, 1.6 Hz, 1H), 7.52 (ddd, *J* = 8.7, 7.3, 1.6 Hz, 1H), 7.25 (dd, *J* = 8.2, 1.2 Hz, 1H), 7.15 (ddd, *J* = 8.4, 7.3, 1.2 Hz, 1H), 3.93 – 3.34 (m, 8H), 3.01 (s, 3H). ^{13}C-NMR (75 MHz, Methanol-*d4*) δ =169.0 (q), 156.9 (q), 150.6 (q), 146.2 (q), 134.4 (+), 134.0 (q), 132.0 (+), 124.5 (+), 123.8 (+), 120.8 (+), 118.0 (+), 55.1 (-), 51.2 (-), 43.7 (+). IR [cm^{-1}]$\tilde{\nu}$ = 3004 (w), 2919 (w), 2840 (w), 2609 (w), 2482 (w), 1674 (s), 1595 (m), 1405 (m), 1267 (m), 1197 (s), 1125 (s), 1010 (s), 719 (s), 779 (s). ESI-MS: calculated: 324.1586 found: 325.1 (MH^+, 100%) HR-MS: 325.1659. HPLC: 10.98 min and 11.20 min (both isomers), purity >97%.

*(E)-3-(4-((E)-(2-(4-Methylpiperazin-1-yl)phenyl)diazenyl)phenyl)acrylic acid (**1b**)*

Compound **1b** was synthesized analogous to compound **1a** employing **5b** (1.00 g, 5.64 mmol) and 2-(4-methylpiperazin-1-yl)aniline (1.08 g, 5.64 mmol) in HOAc (6 mL). The compound was obtained as a red solid (316 mg, 0.90 mmol, 16 % yield). ^{1}H-NMR (300 MHz, Methanol-*d4*) δ =7.94 (d, *J* = 8.6 Hz, 1H), 7.81 (d, *J* = 8.6 Hz, 1H), 7.75 (d, *J* = 16.0 Hz, 1H), 7.69 (dd, *J* = 8.1, 1.6 Hz, 1H), 7.50 (ddd, *J* = 8.7, 7.2, 1.6 Hz, 1H), 7.23 (dd, *J* = 8.2, 1.3 Hz, 1H), 7.15 (ddd, *J* = 8.2, 7.2, 1.3 Hz, 1H), 6.60 (d, *J* = 16.0 Hz, 1H), 3.87–3.86 (m, 2H), 3.57–3.68 (m, 2H), 3.30–3.50 (m, 2H), 3.01 (s, 3H). ^{13}C-NMR (75 MHz, Methanol-*d4*) δ =170.0 (q), 155.1 (q), 150.4 (q), 146.3 (q), 144.9 (+), 138.6 (+), 134.0 (+), 130.4 (+), 124.5 (two signals, +), 121.2 (+), 120.7 (+), 118.0 (+), 55.1 (-), 51.2 (-), 43.7 (+). IR [cm^{-1}]$\tilde{\nu}$ = 3403 (w), 3004 (w), 2918 (w), 1677 (s), 1598 (s), 1483 (w), 1413 (w), 1286 (w), 1177 (s), 1129 (s), 1021

(s), 1021 (s), 954 (m), 834 (m), 719 (m). ESI-MS: calculated: 350.1743 found: 351.18 (MH^+, 100%). HR-MS: 351.1815. R_t: 11.69 min, purity >99% (DAD 220 nm).

IV.2.5 Acknowledgments

We thank Karin Rustler for fruitful discussions and her ongoing research in the project and Dr. Steffen Pockes (Elz group, University of Regensburg) for the biological evaluation of the compounds.

IV.2.6 References

1. Foord, S. M.; Bonner, T. I.; Neubig, R. R.; Rosser, E. M.; Pin, J.-P.; Davenport, A. P.; Spedding, M.; Harmar, A. J., International Union of Pharmacology. XLVI. G Protein-Coupled Receptor List. *Pharmacological Reviews* **2005**, *57*, 279–288.

2. Panula, P.; Chazot, P. L.; Cowart, M.; Gutzmer, R.; Leurs, R.; Liu, W. L. S.; Stark, H.; Thurmond, R. L.; Haas, H. L., International Union of Basic and Clinical Pharmacology. XCVIII. Histamine Receptors. *Pharmacological Reviews* **2015**, *67*, 601–655.

3. Seifert, R.; Strasser, A.; Schneider, E. H.; Neumann, D.; Dove, S.; Buschauer, A., Molecular and cellular analysis of human histamine receptor subtypes. *Trends in Pharmacological Sciences 34*, 33–58.

4. Hammer, S. G.; Gobleder, S.; Naporra, F.; Wittmann, H.-J.; Elz, S.; Heinrich, M. R.; Strasser, A., 2,4-Diaminopyrimidines as Dual Ligands at the Histamine H1 and H4 receptor—H1/H4-Receptor Selectivity. *Bioorganic & Medicinal Chemistry Letters* **2016**, *26*, 292–300.

5. Simons, F. E. R.; Simons, K. J., Peripheral H1-Blockade Effect of Fexofenadine. *Annals of Allergy, Asthma & Immunology 79*, 530–532.

6. Striegl, B. Synthese und Funktionelle in-vitro-Pharmakologie neuer Histamin-H1-Rezeptoragonisten aus der Suprahistaprodifen-Reihe. *Dissertation*, *Regensburg*, **2006**.

7. Shimamura, T.; Shiroishi, M.; Weyand, S.; Tsujimoto, H.; Winter, G.; Katritch, V.; Abagyan, R.; Cherezov, V.; Liu, W.; Han, G. W.; Kobayashi, T.; Stevens, R. C.; Iwata, S., Structure of the Human Histamine H1 Receptor Complex with Doxepin. *Nature* **2011**, *475*, 65.

8. Tashiro, M.; Kato, M.; Miyake, M.; Watanuki, S.; Funaki, Y.; Ishikawa, Y.; Iwata, R.; Yanai, K., Dose Dependency of Brain Histamine H1 Receptor Occupancy Following Oral

Administration of Cetirizine Hydrochloride Measured using PET with [11C]Doxepin. *Human Psychopharmacology: Clinical and Experimental* **2009**, *24*, 540–548.

9. Szymański, W.; Beierle, J. M.; Kistemaker, H. A. V.; Velema, W. A.; Feringa, B. L., Reversible Photocontrol of Biological Systems by the Incorporation of Molecular Photoswitches. *Chemical Reviews* **2013**, *113*, 6114–6178.

10. Velema, W. A.; Szymanski, W.; Feringa, B. L., Photopharmacology: Beyond Proof of Principle. *Journal of the American Chemical Society* **2014**, *136*, 2178–2191.

11. Lerch, M. M.; Hansen, M. J.; van Dam, G. M.; Szymanski, W.; Feringa, B. L., Emerging Targets in Photopharmacology. *Angewandte Chemie International Edition* **2016**, *55*, 10978–10999.

12. Brieke, C.; Rohrbach, F.; Gottschalk, A.; Mayer, G.; Heckel, A., Light-Controlled Tools. *Angewandte Chemie International Edition* **2012**, *51*, 8446–8476.

13. Bandara, H. M. D.; Burdette, S. C., Photoisomerization in Different Classes of Azobenzene. *Chemical Society Reviews* **2012**, *41*, 1809–1825.

14. García-Amorós, J.; Velasco, D., Recent Advances towards Azobenzene-Based Light-Driven Real-Time Information-Transmitting Materials. *Beilstein Journal of Organic Chemistry* **2012**, *8*, 1003–1017.

15. Simeth, N. A.; Crespi, S.; Fagnoni, M.; König, B., Tuning the Thermal Isomerization of Phenylazoindole Photoswitches from Days to Nanoseconds. *Journal of the American Chemical Society* **2018**, *140*, 2940–2946.

16. Weston, C. E.; Richardson, R. D.; Haycock, P. R.; White, A. J. P.; Fuchter, M. J., Arylazopyrazoles: Azoheteroarene Photoswitches Offering Quantitative Isomerization and Long Thermal Half-Lives. *Journal of the American Chemical Society* **2014**, *136*, 11878–11881.

17. Calbo, J.; Weston, C. E.; White, A. J. P.; Rzepa, H. S.; Contreras-García, J.; Fuchter, M. J., Tuning Azoheteroarene Photoswitch Performance through Heteroaryl Design. *Journal of the American Chemical Society* **2017**, *139*, 1261–1274.

18. Beharry, A. A.; Sadovski, O.; Woolley, G. A., Azobenzene Photoswitching without Ultraviolet Light. *Journal of the American Chemical Society* **2011**, *133*, 19684–19687.

19. Dong, M.; Babalhavaeji, A.; Samanta, S.; Beharry, A. A.; Woolley, G. A., Red-Shifting Azobenzene Photoswitches for in Vivo Use. *Accounts of Chemical Research* **2015**, *48*, 2662–2670.

20. Hansen, M. J.; Lerch, M. M.; Szymanski, W.; Feringa, B. L., Direct and Versatile Synthesis of Red-Shifted Azobenzenes. *Angewandte Chemie International Edition* **2016**, *55*, 13514–13518.

21. Falenczyk, C.; Schiedel, M.; Karaman, B.; Rumpf, T.; Kuzmanovic, N.; Grotli, M.; Sippl, W.; Jung, M.; Konig, B., Chromo-Pharmacophores: Photochromic Diarylmaleimide Inhibitors for Sirtuins. *Chemical Science* **2014**, *5*, 4794–4799.

22. Sun, X.; Lv, X.-H.; Ye, L.-M.; Hu, Y.; Chen, Y.-Y.; Zhang, X.-J.; Yan, M., Synthesis of Benzimidazoles via Iridium-Catalyzed Acceptorless Dehydrogenative Coupling. *Organic & Biomolecular Chemistry* **2015**, *13*, 7381–7383.

23. Sadovski, O.; Beharry, A. A.; Zhang, F.; Woolley, G. A., Spectral Tuning of Azobenzene Photoswitches for Biological Applications. *Angewandte Chemie International Edition* **2009**, *48*, 1484–1486.

V. SUMMARY

This Thesis focusses on the design, synthesis, and properties of small photochromic molecules and their application as tool compounds in a biological context. Specifically, **Chapter I** deals with an investigation of a new class of heteroaryl azoswitches, namely phenylazoindoles. Reviewing recent advances in the seek towards novel azo photoswitches, it became clear that heteroaryl scaffolds offer electronic properties not observed for classical azobenzenes. Indeed, we found that 3-phenylazoindoles exhibit fast photochemical *E*-to-*Z* isomerization and extremely tunable thermal *Z*-to-*E* isomerization. Depending on both the substitution of the indole nitrogen and the character of the solvent, *Z*-to-*E* relaxation can be finetuned in a range from nanoseconds to days through accessing either a rotation or intermolecular, hydrazone-mediated pathway. These results were confirmed though laser flash photolysis and quantum-chemical methods. Presence of substituents on the phenyl moiety does not largely influence the behavior found in parent phenylazoindole. However, as with *N*-arylation of the indole, the main absorption band is bathochromically shifted. Analysis of the photostationary state was not feasible through classical means like HPLC or NMR due to the fast isomerization kinetics of the *Z*-isomer. Hence, we developed a strategy based on TD-DFT simulations of the *E*- and *Z*-isomers.

In **Chapter II**, photocontrol of redox-coenzyme mimetics is reported. Through structural merge of a redox-active benzoquinone or pyridine moiety with a diarylethene motif, we were able to couple the 3,3'-electrocyclic ring-closure reaction of the photoswitch to a conjugated system crucial for the redox-active part of the molecule. After successful synthesis, both isolated photoisomers of a ditienylbenzoquinone were independently investigated regarding their properties. Initial analysis *via* cyclic voltammetry and spectro-electrochemical measurements exposed classical redox behavior of the open isomer and unusual properties of the closed one. Oxidation of Hantzsch ester – chosen as a model – proved that this reaction can be facilitated only with the open isomer. Also, *in situ* irradiation of the closed, redox-locked isomer with orange light regenerated the open form of the switch and initiated the redox reaction. The same behavior was successfully transferred onto the respiratory chain in isolated mitochondria. However, the switch could be only used in one way, specifically to unlock the redox-reaction and attempts to improve the photochromic properties to generate a bidirectional switch were unsuccessful so far. Likewise, expanding the concept to other

redox-active scaffolds like pyridines, the redox motif in NAD^+, was challenging, as the obtained compounds proved to be both thermally and photochemically unstable. Hence, the structures have yet to be improved in this regard.

Chapter III deals with the development of tool compounds for multienzyme complexes. Aim of the project was to investigate allosteric communications in two multienzyme complexes, namely imidazole glycerol phosphate synthase and tryptophan synthase. Thereby, we focused on the design and investigation of photoswitchable ligands. In contrast to many previous reports, we did not intend to provide a photo-regulable competitive inhibitor, but to facilitate an allosteric reaction addressable with light. We synthesized dithienylcyclopentenebisphosphates exhibiting the phosphate functions in varying distances to find a suitable ligand for the HisF subunit of imidazole glycerol phosphate synthase. Here, the meta-bisphosphate derivative of the series showed the best binding properties. Investigating the overall imidazole-glycerol-phosphate-synthase-catalyzed reaction, we found that the allosteric reaction could be photocontrolled indirectly through blockage of the HisF binding site depending of the present photoisomer. However, a direct allosteric response upon ligand binding was not observed. Hence, we synthesized the corresponding dithienylmaleimidebisphosphate derivative as well as substituted phenyl azopyrazoles, which were identified as adequate candidates through molecular-dynamic simulations. The biological evaluation of the novel compounds is still ongoing. Similarly, we designed a series of six azobenzene-based ligands bearing a phosphate function in different distances with respect to the photoswitch. In this way, the binding mode of indole-3-glycerol phosphate should be mimicked, and tryptophan synthase subjected to photocontrol. UV-Vis spectroscopic studies revealed good photochromic properties of the molecule in aqueous environment. A detailed investigation on the tryptophan synthase multienzyme complex is still a subject of current research.

In **Chapter IV**, we developed photochromic enzyme ligands which undergo structural changes upon irradiation with visible light. Thus, we focused on the use of indolylfulgimides and red-shifted azobenzenes as photochromic scaffolds. In particular, the structural similarity of the succimide motif in indolylfulgimides with maleimide-based, NAD^+-competitive inhibitors motivated us to produce photochromic analogues. They were reversibly switchable under enzymatic-assay conditions using purple and orange light. Two compounds showed IC_{50} values in the micromolar range towards the Sirt2 isoform of sirtuins, a DNA-regulating, NAD^+-consuming enzyme class. One compound exhibited a 1.5-fold difference in the IC_{50} of both photoisomers. As mentioned before, red-shifted azobenzenes were also used as photochromic core structures to design potential Histamin

H1 antagonists. The azo function was positioned in between two important interaction groups to alter their relative geometry upon photoswitching. Moreover, a piperazine moiety was installed in *ortho*-position to the azo function to induce a red-shift of the chromophor's absorption profile through electron donation. Two compounds have been successfully synthesized and switched with blue light (455 nm or 470 nm, respectively) to the *Z*-form and thermally back to the *E*-isomer.

Covering the development of biological relevant photoswitches and investigating mechanistic relationships, the findings in this Thesis may pave the way to further development of photochromic molecular tools towards clinical research and drug development.

VI. ZUSAMMENFASSUNG

Gegenstand dieser Dissertation ist das Design, die Synthese und die Erforschung photochromer Moleküle und deren Anwendung als pharmakologische Wirkstoffe. In **Kapitel I** wird eine neue Klasse von Heteroarylazophotoschaltern untersucht, die 3-Phenylazoindole. Neuere Erkenntnisse zeigen, dass das Vorhandensein von Heteroarylstrukturen in Azophotoschaltern neuartige elektronische Eigenschaften bewirkt und so ein für Azobenzol sonst nicht zugängliches photochemisches Verhalten eröffnen. Daher untersuchten wir die Merkmale von 3-Phenylazoindolen als Vertreter dieser Gruppe. 3-Phenylazoindole weisen eine sehr schnelle photochemische *E*-zu-*Z*-Isomerisierung auf, wohingegen die Geschwindigkeit der thermischen Rückisomerisierung von verschiedenen Faktoren, z.B. der Methylierung des Indolstickstoffs, dem Vorhandensein eines freien NHs und den Eigenschaften des Lösungsmittels abhängt und daher zwischen Nanosekunden und Tagen variiert werden kann. Grund dieses ungewöhnlichen Verhaltens ist der Zugang zu verschiedenen Relaxationswegen, dem Rotationsweg und einer *Z*-zu-*E*-Isomerisierung über die Bildung eines intermolekularen Hydrazones. Diese Erkenntnisse wurden durch Laser-Flash-Photolyse sowie durch quantenchemische Rechnungen unterstützt. Weitere Untersuchungen zum Einfluss verschiedener Substituenten am Phenylring der 3-Phenylazoindeole ergaben, dass diese ebenso wie eine Arylierung des Indolstickstoffes zu einer bathochromen Verschiebung der Absorptionsbande führten. Da sowohl die substituierten als auch die unsubstituierten Verbindungen extrem schnelle thermische Isomerisierungsraten aufweisen, kann der photostationäre Zustand nicht durch klassische Methoden wie NMR oder HPLC erfasst werden und wurde daher durch quantenchemische Berechnungen approximiert.

Kapitel II beschäftigt sich mit der Photokontrolle von Redoxcoenzymmimetika. Durch eine strukturelle Verschmelzung eines redoxaktiven Benzochinons oder eines Pyridins mit einem Diarylethen konnten wir die 3,3'-elektrozyklische Ringschlussreaktion des Photoschalters an die Elektronenverfügbarkeit der redoxaktiven Teilstrukturen kuppeln. Die Charakterisierung der beiden isolierten Photoisomere eines Dithienylbenzochinons zeigte, dass das offene Isomer das klassische Verhalten eines Benzochinones aufweist, wohingegen sich das geschlossene Isomer sowohl in Cyclovoltammetrie als auch in Spektroelektochemie untypisch verhält. Darüber hinaus untersuchten wir die Reaktion beider Photoisomere mit Hantzschester und konnten lediglich eine Oxidationsreaktion durch das offene Isomer

beobachten. Das geschlossene Isomer ist unreaktiv, solange es nicht mit orangem Licht bestrahlt und dadurch *in situ* in seine offene Isoform überführt wurde. Derselbe Effekt konnte in isolierten Mitochondrien beobachtet werden. Doch die Photoreaktion war nur bedingt umkehrbar. Daher versuchten wir durch ein neues Design die Photoeigenschaften des Schalters zu verbessern, allerdings erfolglos. Ähnlich schwierig gestaltete sich eine Erweiterung des Konzeptes auf die Verwendung von Pyridin, dem Redoxzentrum in NAD^+, als redoxaktive Struktureinheit, da sich das geschlossene Isomer als thermisch labil erwies und die Photostabilität bislang unzureichend ist.

Kapitel III befasst sich mit der Entwicklung pharmakologischer Werkzeuge für die Multienzymkomplexe Imidazolglyzerolphosphat-Synthase und Tryptophan-Synthase. Dabei stand die Erforschung der allosterischen Wechselwirkung innerhalb der Multienzymkomplexe mittels photoregulierbarer Liganden im Mittelpunkt. Die Besonderheit der Arbeit besteht darin, dass nicht, wie sonst üblich photochrome, kompetitive Inhibitoren für einzelne Enzyme entwickelt werden, sondern, dass nun eine allosterischen Reaktion in einem Enzymverbund mit Licht bewirkt werden soll. Daher wurden Dithienylcyclopentenbisphosphate synthetisiert, welche Bisphosphateeinheiten in verschiedenen Abständen aufweisen, um einen geeigneten photochromen Liganden für die HisF-Untereinheit in Imidazolglyzerolphosphat-Synthase zu finden. Hierbei war das Meta-Bisphosphoderivat der aktivste Ligand. Zudem konnte die allosterisch regulierte Imidazolglyzerolphosphat-Synthase-Gesamtreaktion photoreguliert werden, nicht aber durch direkte allosterische Regulation des Multienzymkomplexes, sondern durch die unterschiedlich starke Inhibition des photochromen Liganden. Daher wurde als Nächstes das entsprechende Bisphosphodithienylmaleimidederivat sowie Phenylazopyrazole synthetisiert, die zuvor mittels Molekulardynamik-Simulationen als geeignet identifiziert wurden und zusätzliche biologisch relevante Interaktionsgruppen besitzen. Die biochemische Untersuchung dieser Liganden dauert noch an. Parallel dazu wurden azobenzolbasierte Liganden für den Tryptophansynthasekomplex dargestellt. Die kleine Bibliothek aus sechs Liganden, die eine Phosphatgruppe als Bindungseinheit in variierenden Abständen zum Azobenzolteil besitzen, verfügen alle über ausgezeichnete photochrome Eigenschaften in DMSO und Puffersystemen. Die biochemische Evaluierung dieser Substanzen ist noch nicht abgeschlossen.

In **Kapitel IV** wird die Regulation von Enzymaktivität durch lichtinduzierte sterische Änderungen berichtet. Dabei wurden Indolylfulgimide und rot-verschobene Azobenzolderivate verwendet, zwei photochrome Gruppen, die mit sichtbarem Licht

angeregt werden können. Da die Succimidyntereinheit des Fulgimides eine strukturelle Ähnlichkeit zu maleimidebasierten NAD^+-kompetitiver Inhibitoren aufweist, wurde diese Struktur ausgewählt, um einen fulgimidbasierten Inhibitor zu synthetisieren. Drei Verbindungen wurden isoliert und können reversibel mit violettem beziehungsweise orangem Licht unter Enzymassaybedingungen geschaltet werden. Zudem weisen die Moleküle an Sirt2 IC_{50}-Werte im mikromolaren Bereich auf. Die beste Verbindung zeigte dabei einen 1,5-fachen Unterschied zwischen den IC_{50}-Werten beider Photoisomere. Die rot-verschobenen Azobenzole bilden das photochrome Kernstück potentieller Histamin H1-Antagonisten. Dazu wurde die Azogruppe im Liganden so designt, dass die Photoisomerisierung die Geometrie zweier biologisch relevanter funktioneller Gruppen stark beeinflusst. Eine der beiden Funktionalitäten, eine Piperizineinheit, ist dabei in ortho-Position zur Azobrücke positioniert, um durch die erhöhte Elektronendichte ein rot-verschobenes Azobenzolderivat zu erzeugen. Tatsächlich ist es möglich, beide Verbindungen mit blauem Licht vom *E*- in das *Z*-Isomer zu überführen und das *E*-Isomer anschließend thermisch zu regenerieren. Eine biologische Untersuchung ist noch ausstehend.

Die gewonnenen Erkenntnisse in der Entwicklung neuer biologisch relevanter Photoschalter sowie die Erforschung ihrer (photo)chemischen Mechanismen tragen dazu bei, zukünftig photoschaltbare pharmakologische Werkzeuge auch für klinisch relevante Anwendungen zu erhalten.

APPENDIX

The Appendix can be found on the attached data storage medium.

Appendix

A.I.3. Substituent Effects on 3-Phenylazoindole Photoswitches A234

A.I.1. General Preliminary Remarks

a) General working methods

All reactions were performed under magnetic stirring at room temperature unless otherwise specified. All reagents and solvents were obtained from commercial suppliers and used without further purification, if not otherwise stated.

For TLC, silica coated aluminum plates (Merck $60F^{254}$ silica gel, 0.2 mm) were utilized. Visualization was carried out with a UV lamp at 254 or 366 nm or through suitable staining.

b) Isolation of compounds

For MPLC, a Biotage Isolera One Flash Purification System with manually packed columns using Merck Geduran SI 60 (70-230 grain diameter) or Macherey- Nagel GmbH & Co. KG 60M (0.04-0.063 mm, 230-400 grain diameter) was utilized. For preparative HPLC, a 1260 Infinity LC System from Agilent with a reverse phase Phenomenex Luna® 10µ C18(2) column (250 × 21.2 mm, 100 Å) was utilized. HPLC conditions were the following: solvent A = water (Millipore), solvent B = MeCN (Fisher scientific, gradient grade); flow rate = 22 mL/min.

c) Analysis

Nuclear magnetic resonance spectroscopy (NMR) was carried out using a Bruker Avance 400 MHz spectrometer (^{1}H: 400 MHz, ^{13}C: 101 MHz, T = 300K). Chemical shifts are reported in δ [ppm] relative to an internal standard (solvent residual peak). The solvents used are indicated for each spectrum. Coupling constants are reported in Hertz [Hz]. Characterization of the signals: s = singlet, d = doublet, t = triplet, q = quartet, m = multiplet, bs = broad singlet, dd = doublet of doublet, dt = doublet of triplet. Integration is directly proportional to the number of the protons. Characterization of the ^{13}C-NMR signals: (+) for CH_3 or CH, (-) for CH_2 and (q) for quaternary C-atoms. The latter assignment resulted from DEPT135.

CV measurements and spectroelectrochemical studies were carried out under argon atmosphere. All measurements were performed in MeCN containing 0.1 M tertra ^{n}butylammonium tertra fluoroborate using ferrocene/ferrocenium (Fc/Fc+) as an internal reference. A glassy carbon electrode (working electrode), platinum wire counter electrode, and Ag quasi-reference electrode were employed for CV measurements. The scan rate was 50 mV/s, a step potential of 5.0 mV was applied. Spectroelectrochemical studies were carried out in an optically transparent thin layer electrochemical cell (OTTLE). The scan rate was 2 mV/s, a step potential of 0.02 V was applied.

d) Spectroscopy

UV/Vis Spectra. For UV/Vis measurements, an Agilent 8453 spectrometer was employed. The signal was processed with an in-house developed software. For temperature control, a Varian Cary Single cell peltier apparatus was used.

Kinetic Measurements. Method 1 (for isomerization between 1s and few minutes). The aforementioned Agilent 8453 UV/Vis apparatus is used. Irradiation was carried out in a 90-degree angle with respect to UV/Vis recording (see following pictures), so that irradiation could be performed online during the measurement. For irradiation a 365 nm Nichia NCSU033B (700 mA) or a 400 nm Edison Edixeon EDEV-SL-C1-03 (700 mA) was used.

For the experiment, a fluorescence cuvette was equipped with a solution of the appropriate arylazoindole (50 μM, 3 mL) and a stirring bar. The cuvette was placed in the cuvette holder and stirred there for ca. ten minutes to adjust to the set temperature (standard was 23 °C). Then, the UV/Vis spectrum of the sample was recorded for a total time of 60 minutes (one scan per second from 150 nm – 1100 nm). After one minute, the sample was irradiated with UV light (365 nm LED or 400 nm LED, respectively) for one minute. Afterwards, the thermal back-isomerization was recorded for further 58 minutes if not otherwise stated. For clarity, only excerpts of the experiments are shown.

Method 2 (longer isomerization periods). Thermal cis-to-trans-isomerization was recorded using a Thermo Scientific Multiskan Spectrum (18 °C, see the following picture). Irradiation prior to measuring was performed using a home-built 96-well plate irradiation setup. a solution of the appropriate arylazoindoles (50 μM, 250 μL) was pipetted in a 96-well microtiter plate (Greiner®). The wells were covered with a foil to avoid evaporation of the solvent. Then, the plate was

irradiated with a 96-365 nm-LED irradiation setup for 10 min to assure that the PSS was reached. The thermal cis-to-trans isomerization was recorded.

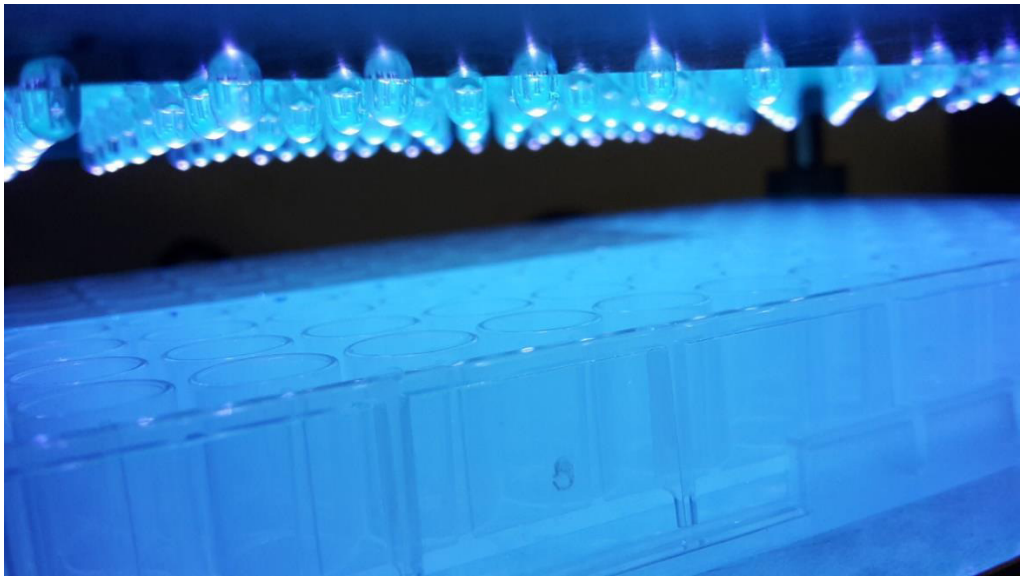

Method 3 (Laser-Flash-Photolysis, for isomerization between ns and seconds). The laser pulse photolysis apparatus consisted of a Flashlamp pumped Q-switched SpitLight-100 Nd:YAG laser from InnoLas, used at the third harmonic of its fundamental wavelength. It delivered a maximum power of 10 mJ at 355 nm with 6 ns pulse duration. The LP920-K monitor system (supplied by Edinburgh Instruments), arranged in a cross-beam configuration, consisted of a high-intensity 450 W ozone free Xe arc lamp (operating both in pulsed and in continuous wave), a Czerny-Turner with Triple Grating Turret monochromator, and a five-stage dynode photomultiplier.

The signals were captured by means of a Tektronix TDS 3012C digital phosphor oscilloscope, and the data was processed with the L900 software supplied by Edinburgh Instruments. The solutions to be analyzed were placed in a fluorescence cuvette (d = 10 mm) without any further treatment (all the signals are thus registered in the presence of the atmospheric oxygen). All the decays reported are an average of either 10 (for the single wavelength acquisition) or 3 (for the transient maps) signals.

A.I.2. Tuning the Thermal Isomerization of Phenylazoindole Photoswitches from Days to Nanoseconds

TABLE OF CONTENTS

1 Synthesis of compounds 3a-c

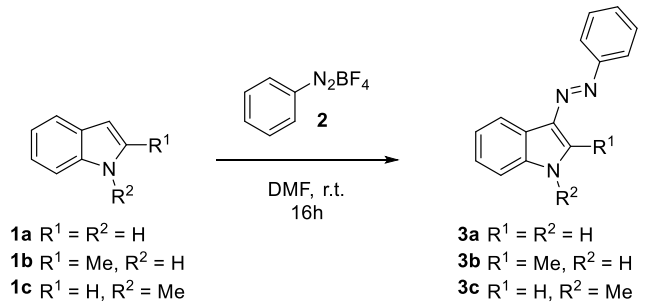

Scheme A1 Synthesis of phenyl-azoindoles **3a-c** from the appropriate indoles **1a-c**.

Diazonium-salt formation:

Aniline (3000 mg, 23.22 mmol) was dissolved in HBF_4 (15 mL, 32% aq) and cooled to -15 °C (NaCl/crushed ice). Then, $NaNO_2$ (2222 mg, 23.22 mmol) in water (3 mL) was added dropwise. The reaction mixture was stirred for 30 minutes, then the white precipitate was sucked off and washed with ice-cold Et_2O (10 mL) and Et_2O/MeOH (1:1, 5 mL). After washing, vacuum was applied for 15 more minutes, in order to dry the diazonium salt (**2**) crystalline powder, before it was employed directly in the azo-coupling or stored in the freezer (-18 °C, up to 10 days).

Azo-coupling:

The appropriate indole (1000 mg, 1 eq.) was dissolved in DMF (5 mL). Diazonium salt **2** (1 eq) was added in small portions. The color immediately changed to red. The reaction mixture was stirred at ambient temperature for 16h and then poured into water (200 mL). The organic compounds usually formed red droplets which were collected through extraction of the aqueous solution with DCM (3 x 100 mL). The combined organic phase was dried over Na_2SO_4, filtered and the solvent was removed *in vacuo*. The crude material was purified through MPLC (Ethyl Acetate in Petrol Ether 35 → 100%). The compounds were identified through NMR and EI-MS analysis. The spectroscopic data are in accordance with the literature.[S1]

In order to exclude that impurities not detected by NMR could affect the signals registered using the laser-flash photolysis, the product was further purified through preparative HPLC (MeCN in H_2O: 40 → 100%, only the fraction furnishing a signal greater than 60% of the peak of the analyte was collected).

3-(Phenyldiazenyl)-1H-indole (**3a**)

Indole (1000 mg, 8.54 mmol) and diazonium salt **2** (1641 mg, 8.54 mmol) were employed. The product was obtained as a dark red solid after HPLC (112 mg, 0.51 mmol, 6 %). ^{1}H NMR (400 MHz, Methanol-d_4) δ 8.48 – 8.40 (m, 1H), 8.13 (s, 1H), 7.86 – 7.78 (m, 2H), 7.54 – 7.42 (m, 3H),

7.40 – 7.33 (m, 1H), 7.31 – 7.14 (m, 2H). ^{13}C NMR (101 MHz, Methanol-d_4) δ =153.0 (q), 137. 2 (q), 136.0 (q), 133.0 (+), 128.7 (+), 128.5 (+), 123.9 (+), 122.4 (+), 122.2 (+), 121.0 (+), 118.6 (q), 111.6 (+). EI-MS: calculated: 221,10 found: 221.1 ($M^{+\bullet}$).

2-Methyl-3-(phenyldiazenyl)-1H-indole (**3b**)

2-Methyl indole (1000 mg, 7.61 mmol) and diazonium salt **2** (1465 mg, 7.61 mmol) were employed. The product was obtained as a dark red solid after HPLC (430 mg, 1.83 mmol, 24 %). ^{1}H NMR (400 MHz, Acetone-d_6) δ=8.51 – 8.45 (m, 1H), 7.90 – 7.82 (m, 2H), 7.53 – 7.44 (m, 2H), 7.43 – 7.38 (m, 1H), 7.38 – 7.31 (m, 1H), 7.23 – 7.14 (m, 2H), 2.83 (s, 3H). ^{13}C NMR (101 MHz, Acetone-d_6) δ=154.0 (q), 144.8 (q), 135.8 (q), 132.4 (q), 128.9 (+), 128.2 (+), 123.3 (+), 122.4 (+), 122.1 (+), 121.3 (+), 119.4 (q), 111.1 (+), 10.5 (+). EI-MS: calculated: 235,11 found: 235.1 ($M^{+\bullet}$).

1-Methyl-3-(phenyldiazenyl)-1H-indole (**3c**)

1-Methyl indole (1000 mg, 7.61 mmol) and diazonium salt **2** (1465 mg, 7.61 mmol) were employed. The product was obtained as a dark red solid after HPLC (340 mg, 1.45 mmol, 19 %). ^{1}H NMR (400 MHz, Acetone-d_6) δ=8.46 –8.49 (m, 1H), 8.13 (s, 1H), 7.83 – 7.83 (m, 2H), 7.44 – 7.50 (m, 3H), 7.22 – 7.36 (m, 2H), 3.95 (s, 3H). ^{13}C NMR (101 MHz, Acetone-d_6) δ=153.9 (q), 137.7 (q), 136.2 (+), 135.1 (q), 128.9 (+), 128.7 (+), 123.8 (+), 122.76 (+), 122.6 (+), 121.5 (+), 119.2 (q), 110.0 (+), 32.7 (+). EI-MS: calculated: 235,11 found: 235.1 ($M^{+\bullet}$).

2 Spectroscopic analysis

2.2 Absorption properties in different solvents of compounds 3a-c

Compound		Cyclohexane	Dioxane	Benzene	PhMe	Mesitylene	MeCN	MeOH	DMSO
3a	λ_{max} [nm]	350	361	361	362	359	362	365	372
	$\varepsilon_{\lambda max}$ [$cm^{-1}M^{-1}$]	12242	13777	12916	15151	15713	14654	14716	16447
3b	λ_{max} [nm]	359	369	370	373	373	371	373	379
	$\varepsilon_{\lambda max}$ [$cm^{-1}M^{-1}$]	15518	12590	15821	15998	15751	12957	12537	14658
3c	λ_{max} [nm]	359	369	368	366	367	371	369	380
	$\varepsilon_{\lambda max}$ [$cm^{-1}M^{-1}$]	14450	15545	15849	14134	13604	15936	14338	15964

Table A1 Overview of the absorption maxima and molar extinction coefficient of **3a-c** in different solvents.

2.3 Lifetimes in different solvents of compounds 3a-c

Entry	Solvents[a]	Lifetime τ		
		3a	**3b**	**3c**[c]
1	cyclohexane	42.5 ms[b]	116.8 ms[b]	1.1 h
2	dioxane	84.9 ms[b]	1.9 s[c]	17.6 h
3	benzene	78.5 ms[b]	167 ms[b]	6.0 min
4	mesitylene	12.3 ms[b]	3.3 ms[b]	1.13 d
5	toluene	47.5 ms[b]	60.2 ms[b]	17.1 min
6	toluene[d]	45.7 ms		
7	aqueous toluene[e]		1.4 ms[b]	
8	MeOH	6.8 ms[b]	454 µs (51%), 78 µs (49%)[f]	2.4 h
9	MeOH[e]	4.7 ms[b]		
10	MeOD	37.7 ms[b]		
11	MeOH water 9:1	14.8 ms[b]	41.9 µs[b]	
12	MeOH water 1:1	2.9 ms[b]	41.4 µs[b]	
13	MeOH - buffered water (pH = 4)[h] 1:1	9.5 µs	1.2 µs	
14	MeOH water 1:2	2.9 ms	574 µs	
15	MeCN (dry)	4.3 s[c]	1.9 ms[b]	1.2 d
16	MeCN water 95:5		256 µs (32%), 59µs (68%)[f]	
17	MeCN water 9:1		1.5 ms	
18	DMSO (dry)	6.5 s[c]	1.3 ms[b]	2.6 d
19	DMSO water 9:1	266 µs[b]	111.2 µs[b]	
20	DMSO water 1:1	187.9 µs[b]	32.1 µs[b]	
21	DMSO - buffered water (pH = 4)[g] 1:1	2.2 µs[b]	743 ns[b]	
22	DMSO - buffered water (pH = 7)[h] 1:1	676 µs	224 µs	
23	DMSO - buffered water (pH = 9)[i] 1:1	842 µs	250 µs	
24	DMSO water 1:2	201 µs	31 µs	
25	DMSO water 1:1 + 25 µL DBU	31 ns	46 ns	

Table A2 Table resuming the *Z*-to-*E* thermal isomerization lifetimes of **3a-c**. [a] The concentration was adjusted to 50 µM for all the measurements. [b] Determined via nanosecond laser flash photolysis. [c] Determined via UV/Vis spectroscopy. [d] Concentration of **3a** = 75 µM [e] Solvent saturated with water (15 µL of water were added to 2 mL of a 50 µM solution of **3b** in toluene. The emulsion thus formed was sonicated for 1h.). [f] The decay is biexponential. In parentheses is shown the contribution of the single lifetimes to the whole decay. [g] pH = 4.00 ± 0.02 (20 °C) (Citric acid; NaOH; HCl) [h] pH = 6.87-6.89 ± 0.02 (20 °C) (Na_2HPO_4; KH_2PO_4). [i] pH = 8.99-9.01 ± 0.01 (20 °C) (H_3BO_3; KCl; NaOH)

In the following sections, spectra of all compounds in all investigated solvents at the thermal equilibrium and the PSS are presented; the transient signal maps of the compounds with thermal kinetics studied with Laser Flash Photolysis are depicted. The kinetics of the thermal *Z*-to-*E* isomerization with the fitting of the experimental signal are also given. The traces were fitted using a mono-exponential decay function (except for the specific case where a bi-exponential kinetic was found), using a Levenberg-Marquardt iteration algorithm. In case of multiple transient appearing, the lifetime was evaluated considering the kinetic of the π-π* band formation of the *E*-isomer.

The experiments were conducted on 50 μM solutions of the specified compound at room temperature (23 °C). All the variations of temperature, concentration or other settings are specified in the specific cases.

The solvents are reported in the order shown in Table A2 for every compound.

Either the LED irradiation time or the laser shot are represented with a magenta-coloured line on top of the picture. Black lines indicate periods where no irradiation took place.

2.3.1 3a

Cyclohexane

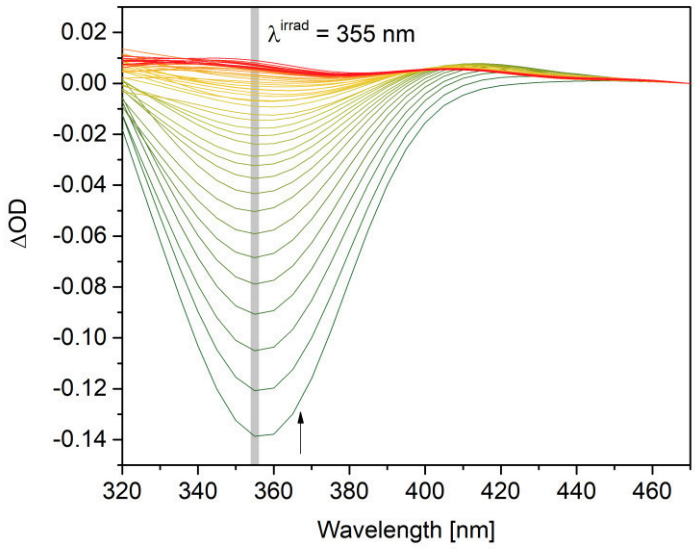

Figure A1 Transient signal map for **3a** in cyclohexane.

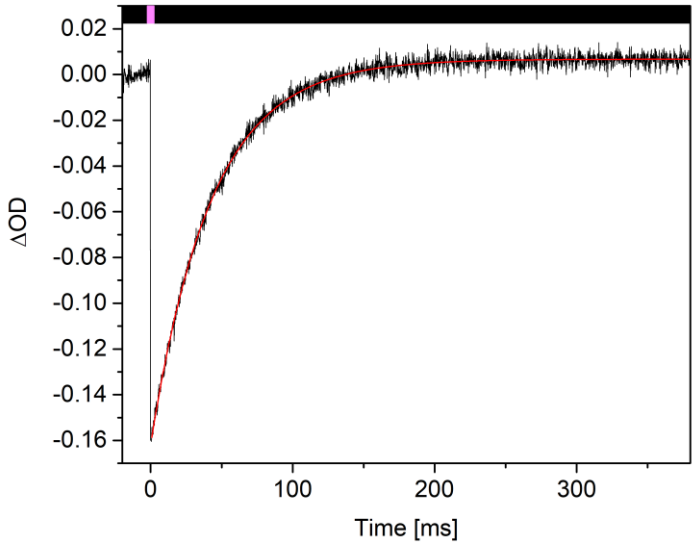

Figure A2 Transient signal detected at 355 nm for **3a** in cyclohexane.

Equation	y = A1·exp(-x/τ) + y0
y0	0.00672 ± 8.15787E-5
A1	-0.16852 ± 3.74172E-4
τ	42.54594 ± 0.15571
R-Square(COD)	0.99421
Adj. R-Square	0.99421

Table A3 Fitting of the signal shown in Figure A2

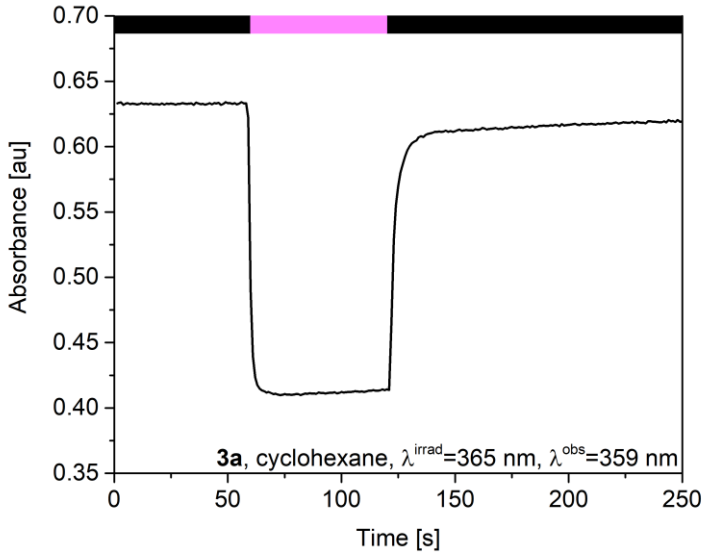

Figure A3 Absorbance variation of **3a** in cyclohexane, irradiation with a 365 nm LED, λ^{obs}=359 nm.

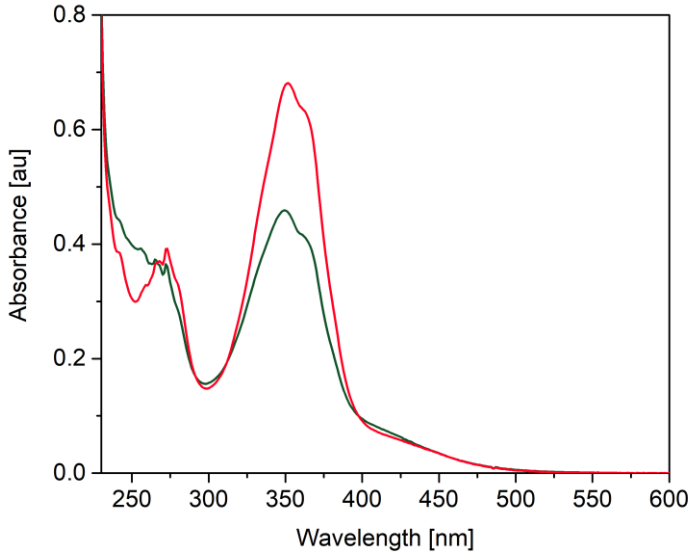

Figure A4 UV/vis of ***E*-3a** in cyclohexane (red), and of the PSS (green) after irradiation with a 365 nm LED.

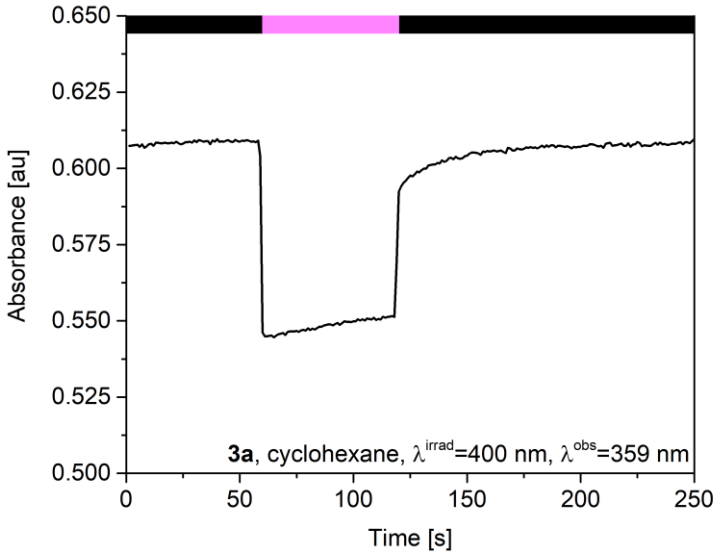

Figure A5 Absorbance variation of **3a** in cyclohexane, irradiation with a 400 nm LED, λ^{obs}=359 nm.

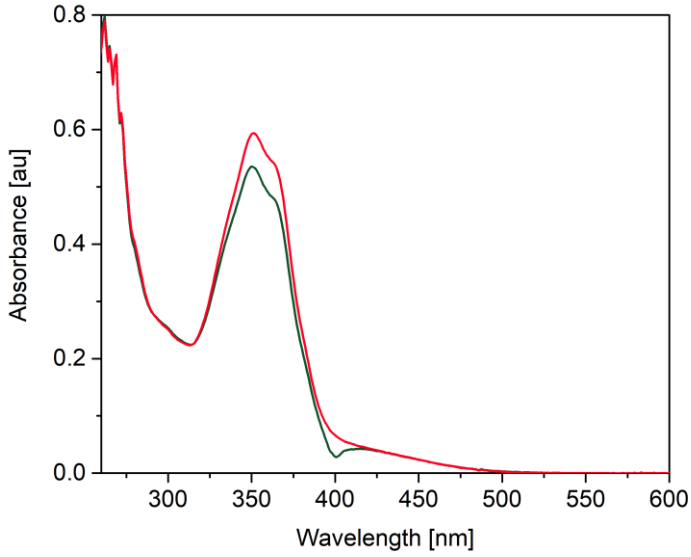

Figure A6 UV/vis of ***E*-3a** in cyclohexane (red), and of the PSS (green) after irradiation with a 400 nm LED.

Dioxane

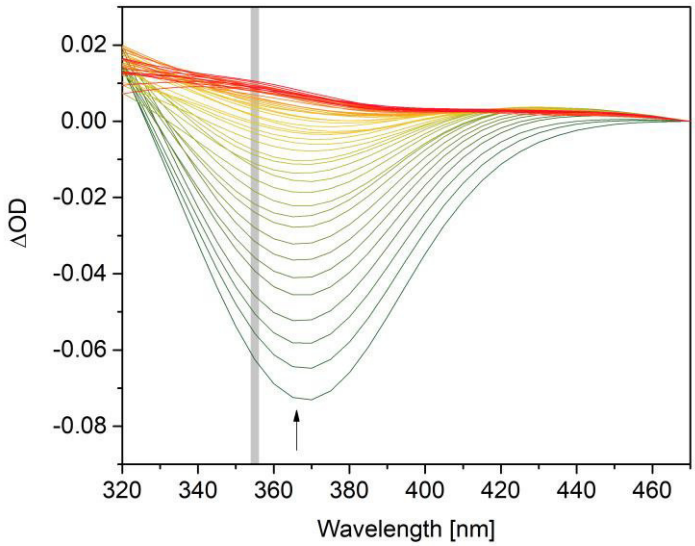

Figure A7 Transient signal map for **3a** in dioxane.

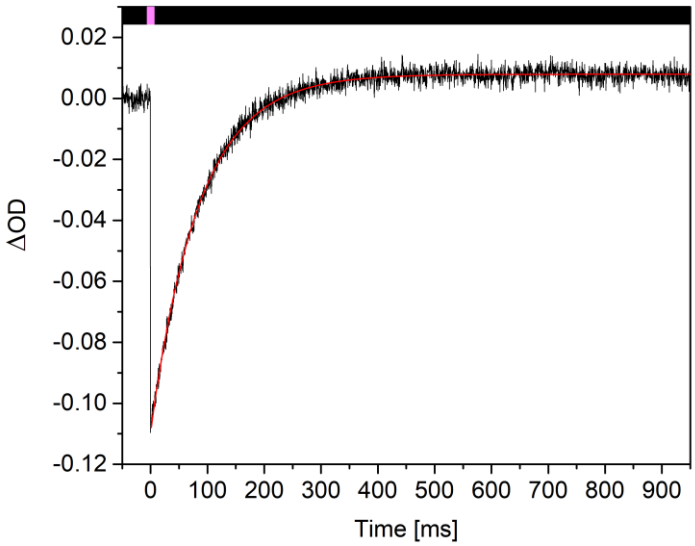

Figure A8 Transient signal detected at 365 nm for **3a** in dioxane.

Equation	y = A1·exp(-x/τ) + y0
y0	0.00793 ± 6.2276E-5
A1	-0.11718 ± 3.39595E-4
τ	84.92804 ± 0.3901
R-Square(COD)	0.99057
Adj. R-Square	0.99056

Table A4 Fitting of the signal shown in Figure A8.

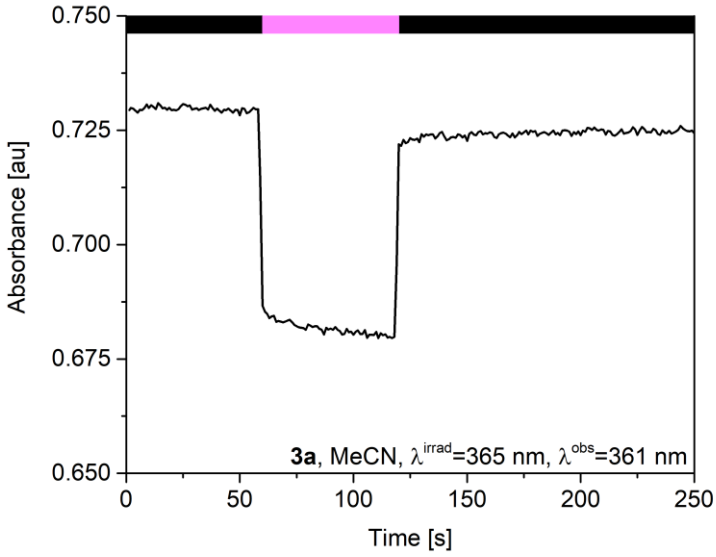

Figure A9 Absorbance variation of **3a** in dioxane, irradiation with a 365 nm LED, λ^{obs}=361 nm.

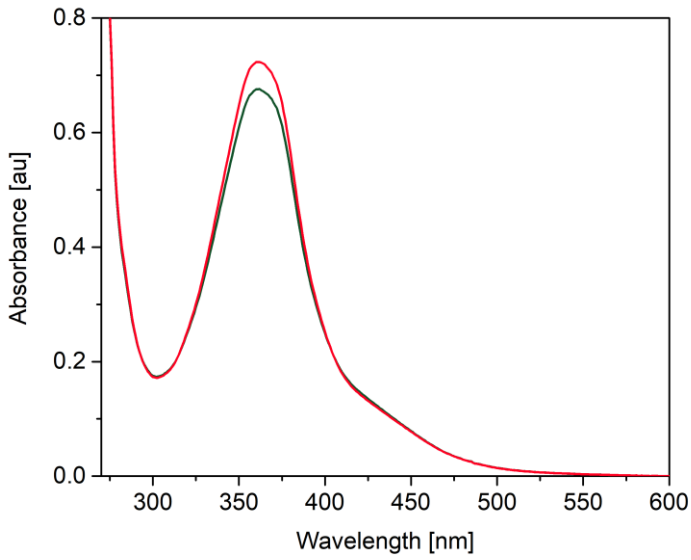

Figure A10 UV/vis of ***E*-3a** in dioxane (red), and of the PSS (green) after irradiation with a 365 nm LED.

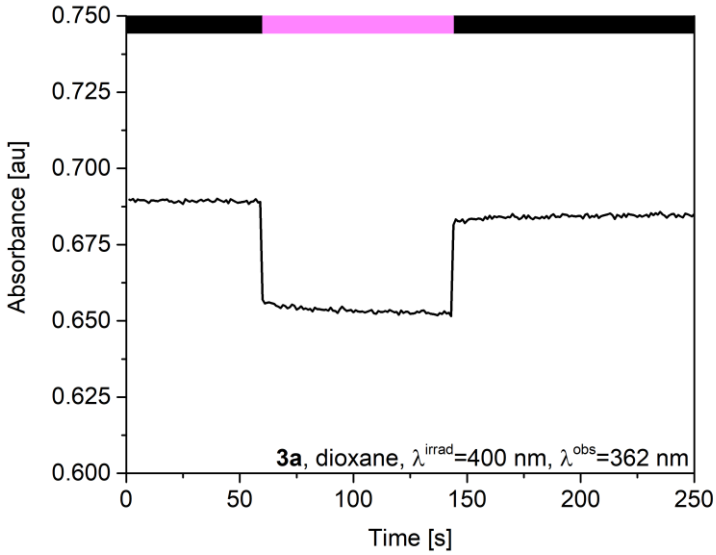

Figure A11 Absorbance variation of **3a** in dioxane, irradiation with a 400 nm LED, λ^{obs}=361 nm.

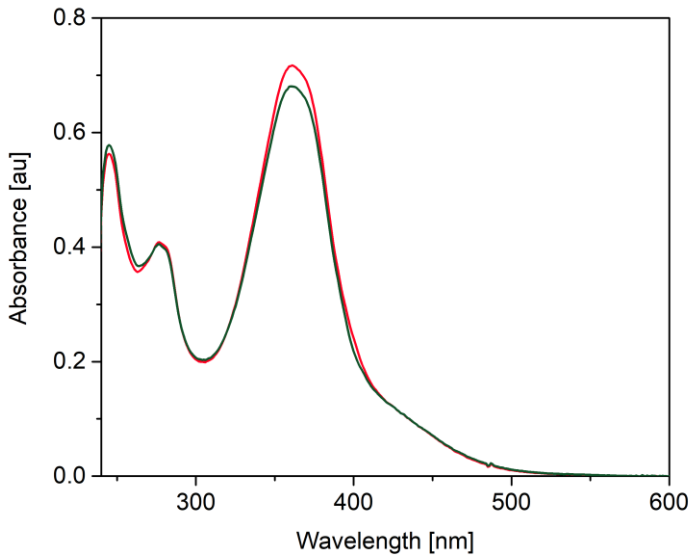

Figure A12 UV/vis of ***E*-3a** in dioxane (red), and of the PSS (green) after irradiation with a 400 nm LED.

Benzene

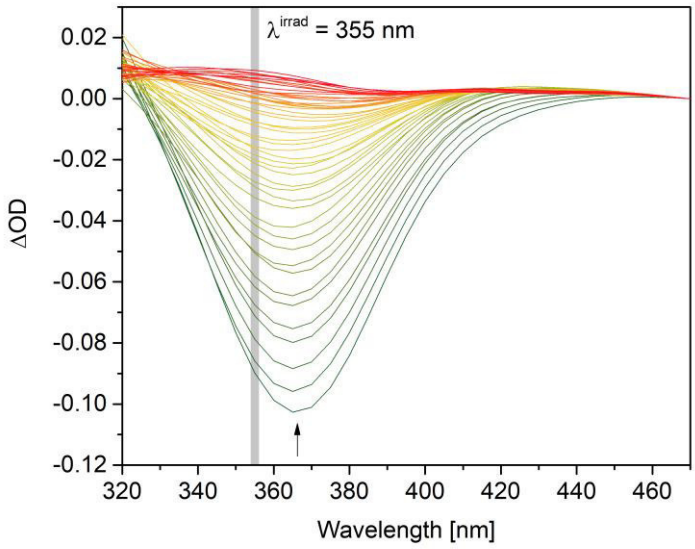

Figure A13 Transient signal map for **3a** in benzene.

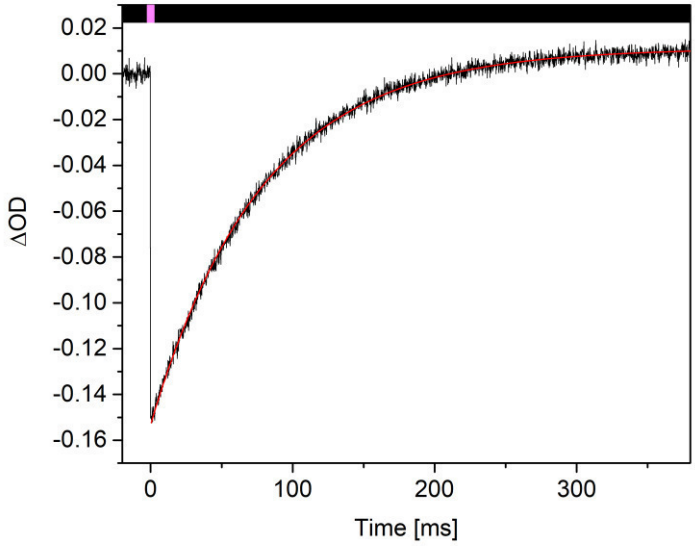

Figure A14 Transient signal detected at 360 nm for **3a** in benzene.

Equation	y = A1·exp(-x/τ) + y0
y0	0.01119 ± 1.03066E-4
A1	-0.16437 ± 2.26246E-4
τ	78.50249 ± 0.23735
R-Square(COD)	0.99702
Adj. R-Square	0.99702

Table A5 Fitting of the signal shown in Figure A14

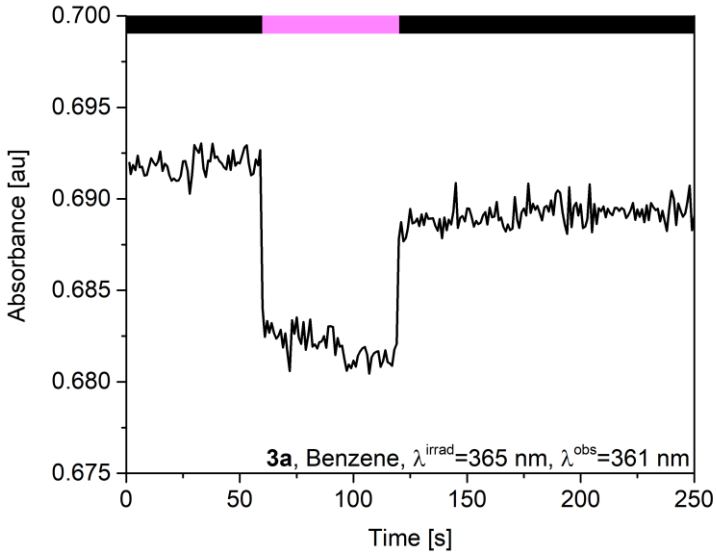

Figure A15 Absorbance variation of **3a** in benzene, irradiation with a 365 nm LED, λ^{obs}=361 nm.

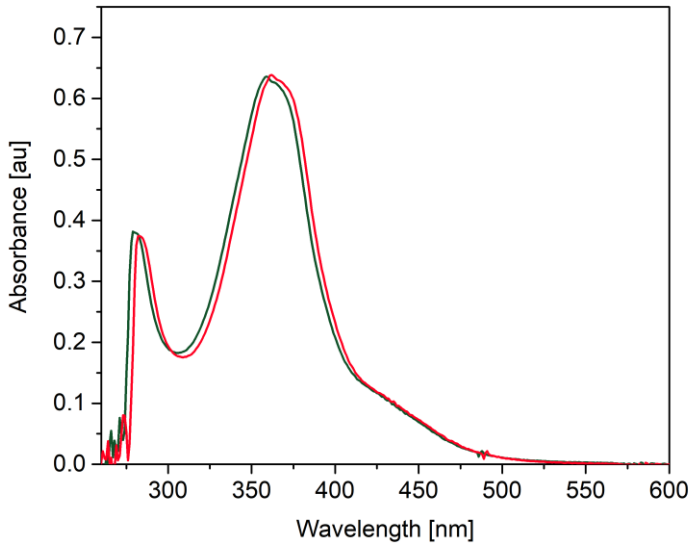

Figure A16 UV/vis of ***E*-3a** in benzene (red), and of the PSS (green) after irradiation with a 365 nm LED.

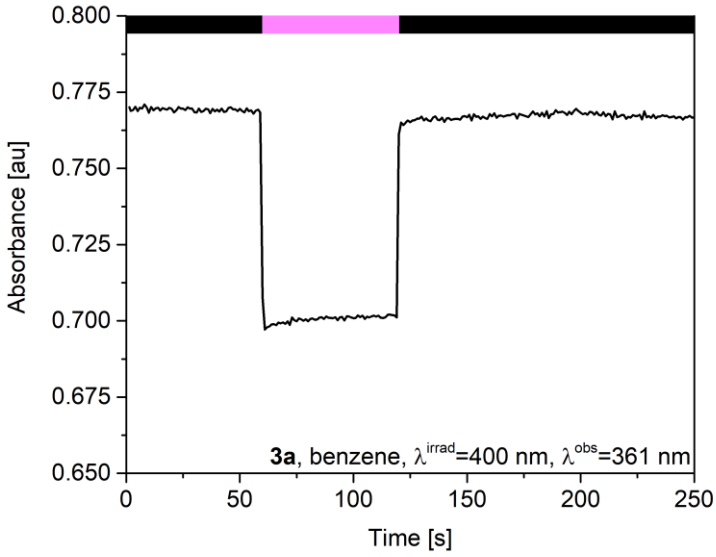

Figure A17 Absorbance variation of **3a** in benzene, irradiation with a 400 nm LED, λ^{obs}=361 nm.

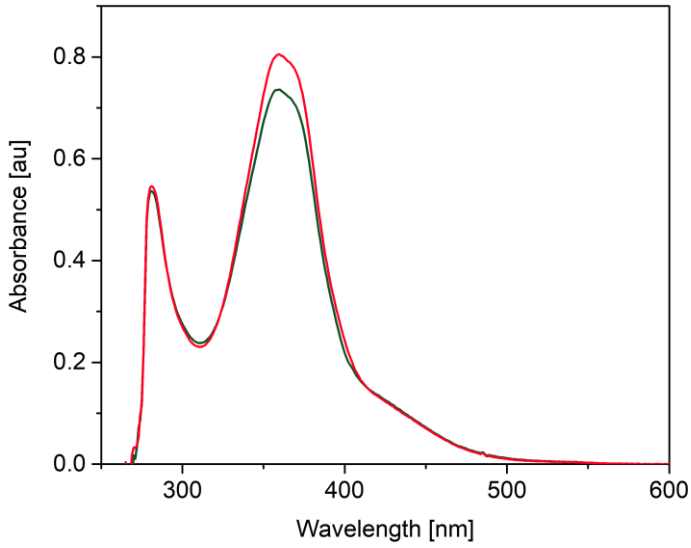

Figure A18 UV/vis of ***E*-3a** in benzene (red), and of the PSS (green) after irradiation with a 400 nm LED.

Mesitylene

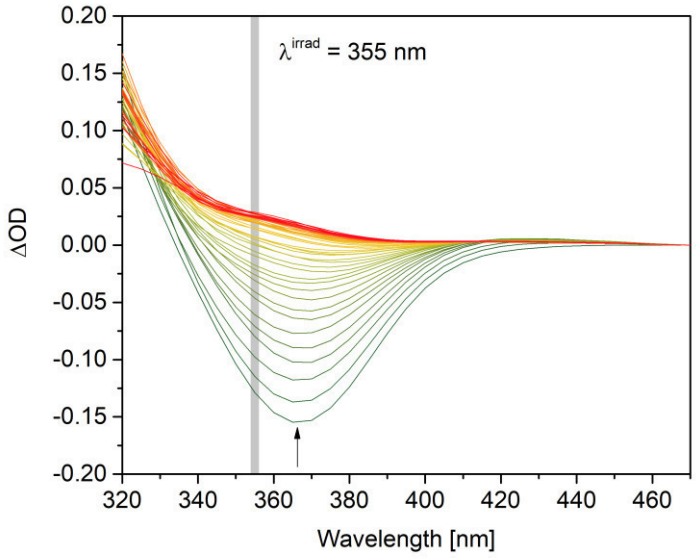

Figure A19 Transient signal map for **3a** in mesitylene.

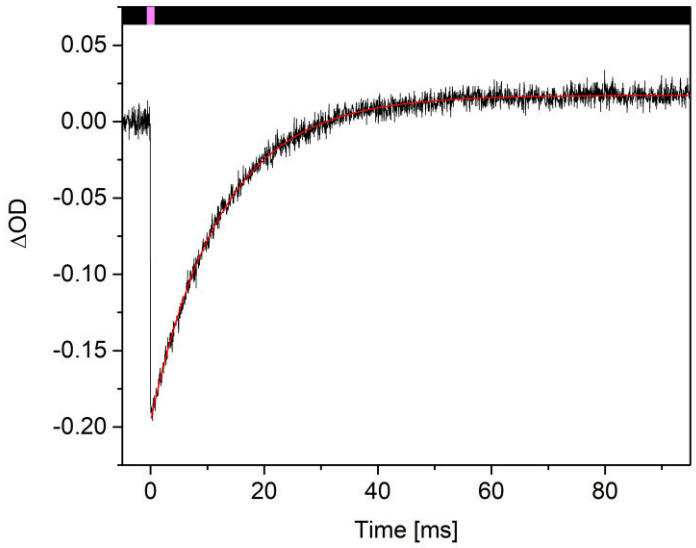

Figure A20 Transient signal detected at 365 nm for **3a** in mesitylene.

Equation	y = A1·exp(-x/τ) + y0
y0	0.01732 ± 1.42407E-4
A1	-0.21315 ± 5.55734E-4
τ	12.35036 ± 0.05599
R-Square(COD)	0.99147
Adj. R-Square	0.99147

Table A6 Fitting of the signal shown in Figure A20.

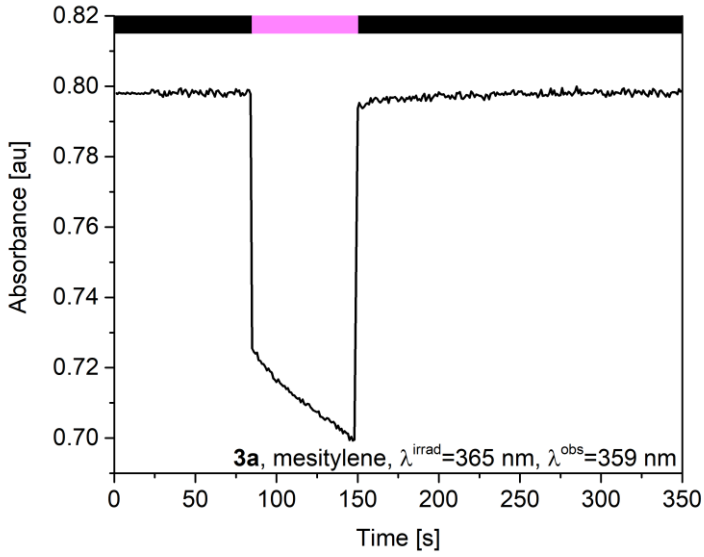

Figure A21 Absorbance variation of **3a** in mesitylene, irradiation with a 365 nm LED, λ^{obs}=359 nm.

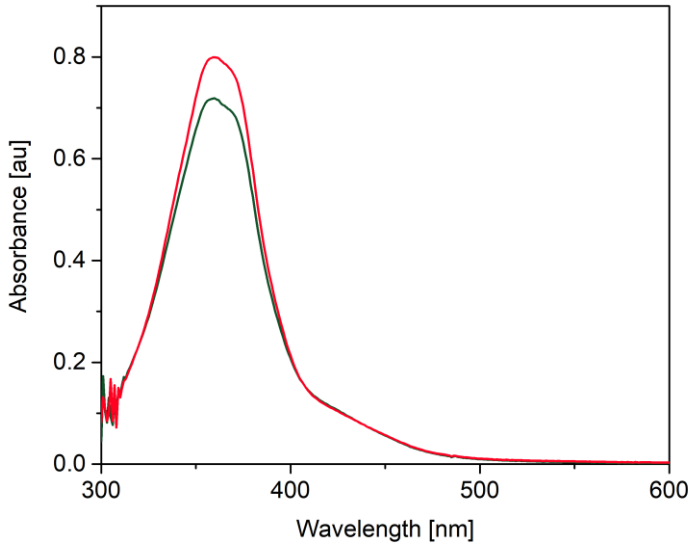

Figure A22 UV/vis of ***E*-3a** in mesitylene (red), and of the PSS (green) after irradiation with a 365 nm LED.

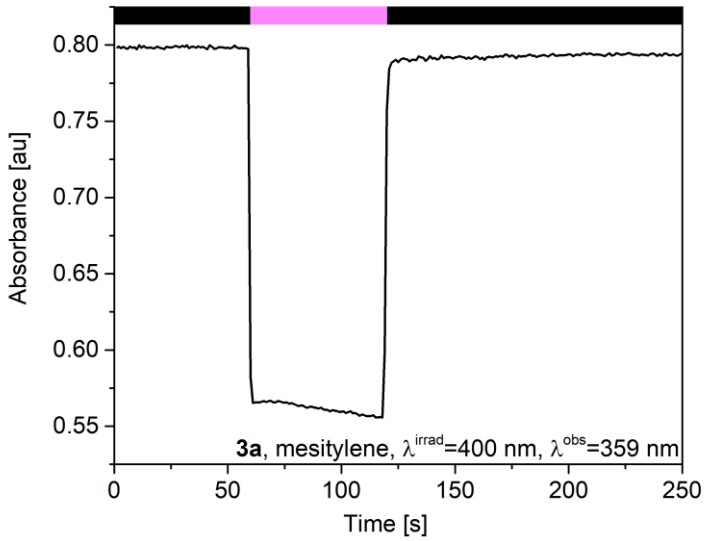

Figure A23 Absorbance variation of **3a** in mesitylene, irradiation with a 400 nm LED, λ^{obs}=359 nm.

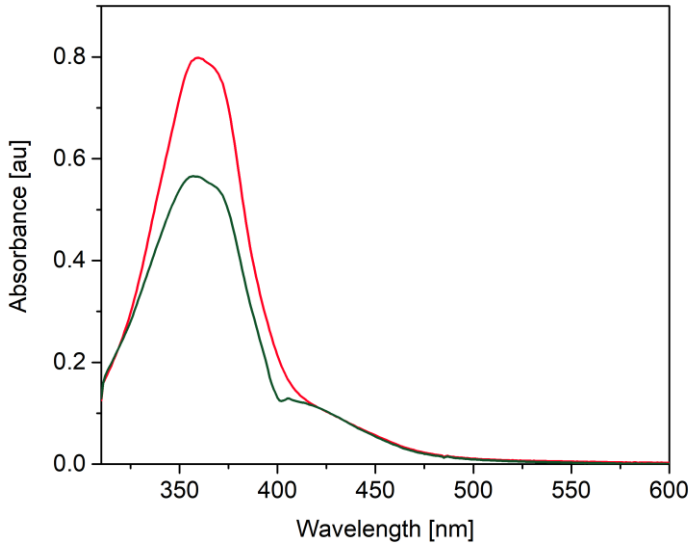

Figure A24 UV/vis of ***E*-3a** in mesitylene (red), and of the PSS (green) after irradiation with a 400 nm LED.

Toluene

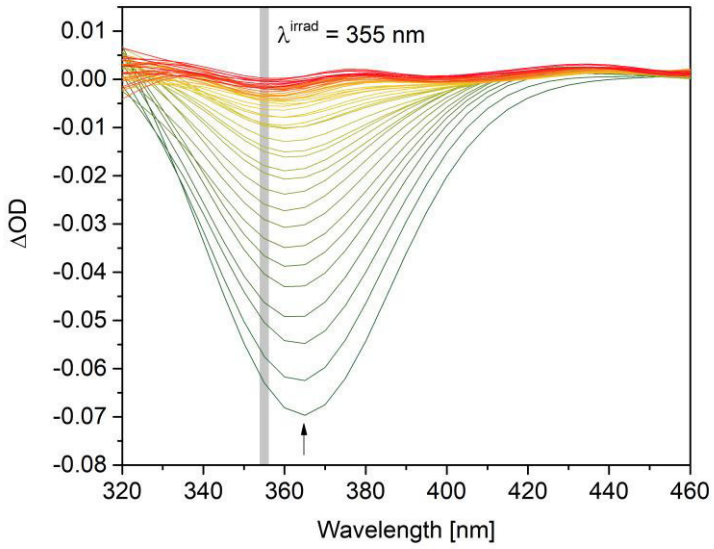

Figure A25 Transient signal map for **3a** in toluene.

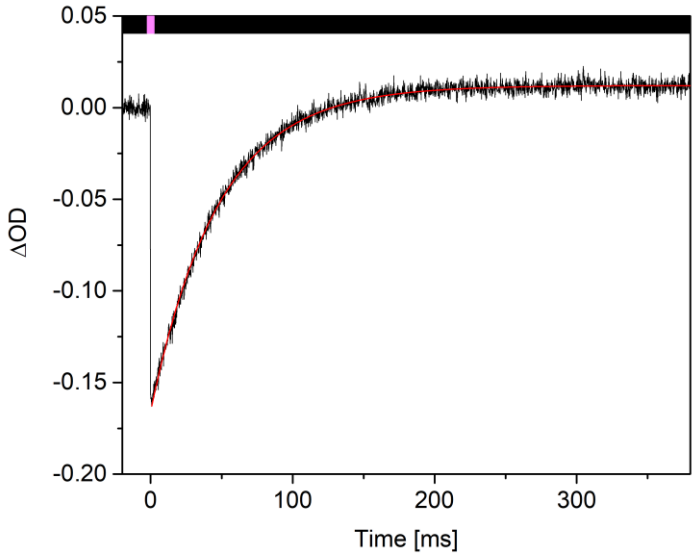

Figure A26 Transient signal detected at 365 nm for **3a** in toluene.

Equation	y = A1·exp(-x/τ) + y0
y0	0.0121 ± 1.01167E-4
A1	-0.17783 ± 4.17185E-4
τ	47.50156 ± 0.18976
R-Square(COD)	0.9933
Adj. R-Square	0.99329

Table A7 Fitting of the signal shown in Figure A26.

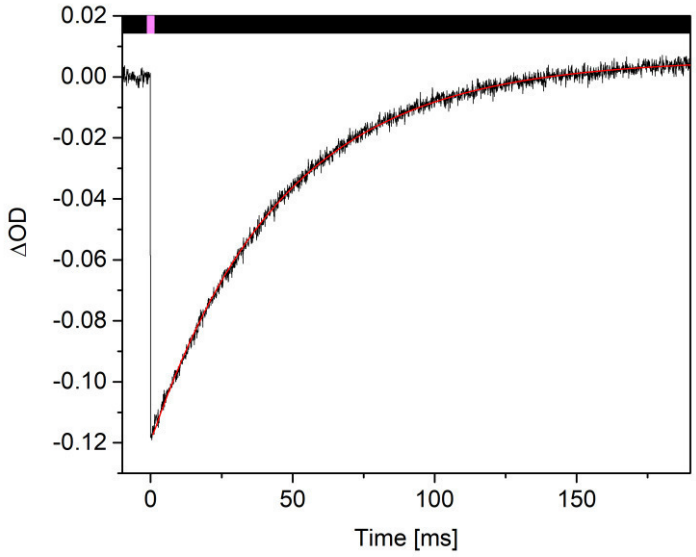

Figure A27 Transient signal detected at 365 nm for **3a** in toluene (0.75 μM).

Equation	y = A1·exp(-x/τ) + y0
y0	0.0059 ± 8.47125E-5
A1	-0.12556 ± 1.49611E-4
τ	45.77156 ± 0.13301
R-Square(COD)	0.99762
Adj. R-Square	0.99761

Table A8 Fitting of the signal shown in Figure A27.

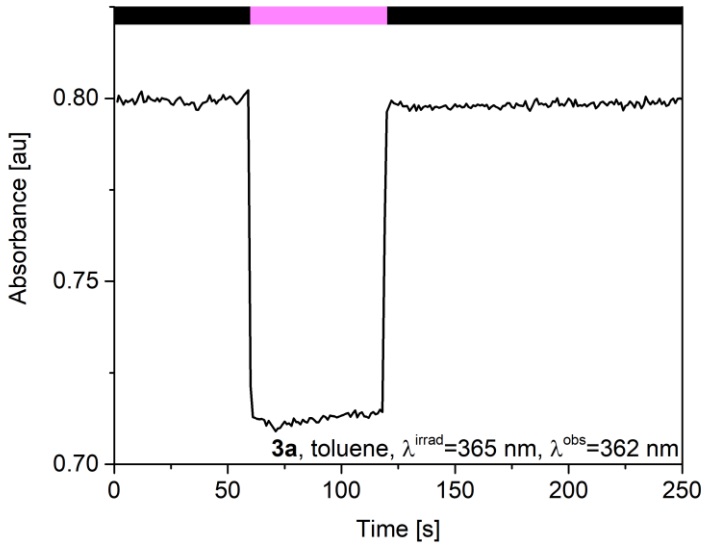

Figure A28 Absorbance variation of **3a** in toluene, irradiation with a 365 nm LED, λ^{obs}=362 nm.

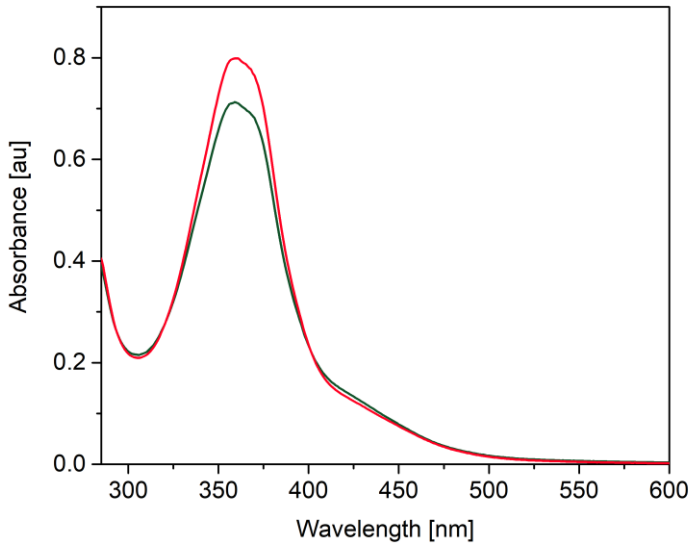

Figure A29 UV/vis of ***E*-3a** in toluene (red), and of the PSS (green) after irradiation with a 365 nm LED.

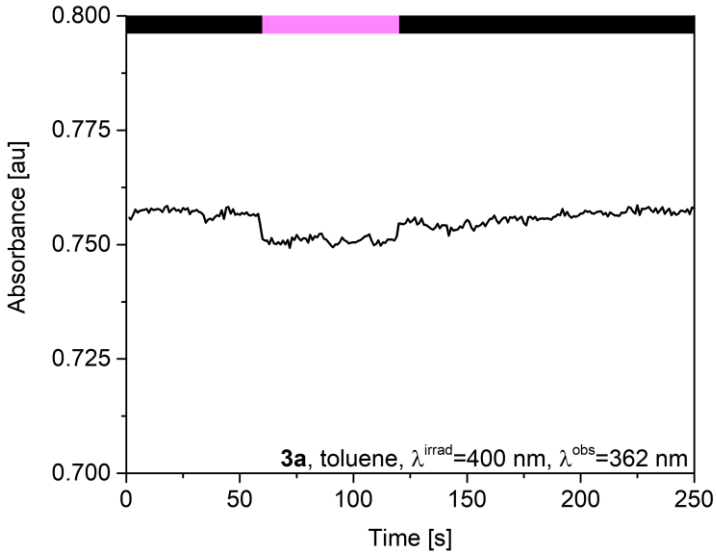

Figure A30 Absorbance variation of **3a** in toluene, irradiation with a 400 nm LED, λ^{obs}=362 nm.

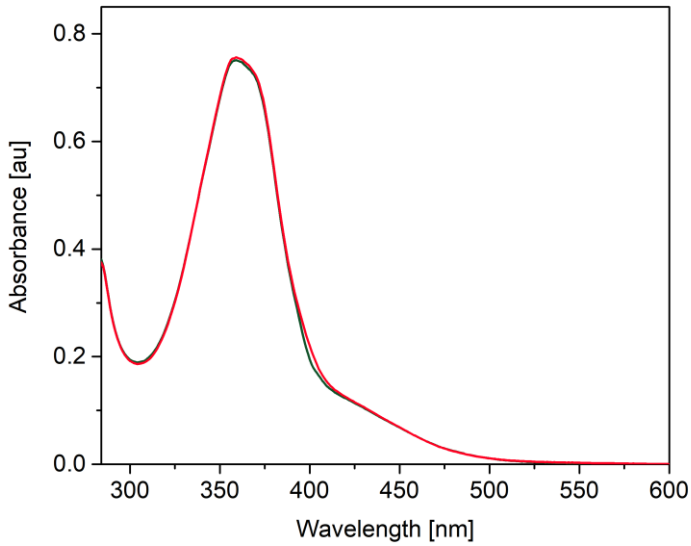

Figure A31 UV/vis of ***E*-3a** in toluene (red), and of the PSS (green) after irradiation with a 400 nm LED.

Methanol

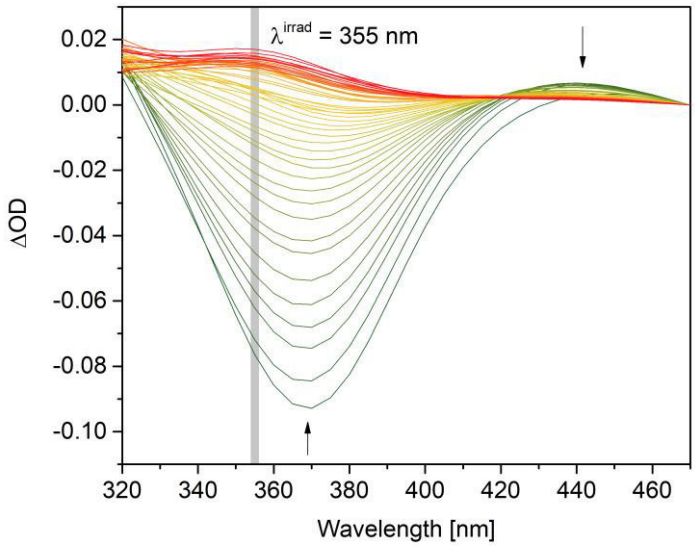

Figure A32 Transient signal map for **3a** in methanol.

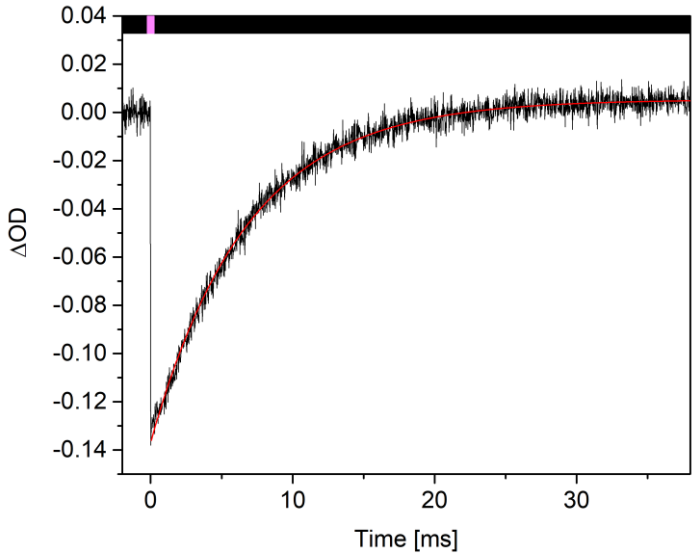

Figure A33 Transient signal detected at 365 nm for **3a** in methanol.

Equation	y = A1·exp(-x/τ) + y0
y0	0.00539 ± 1.46491E-4
A1	-0.14222 ± 3.96414E-4
τ	6.76588 ± 0.03773
R-Square(COD)	0.98885
Adj. R-Square	0.98884

Table A9 Fitting of the signal shown in Figure A33.

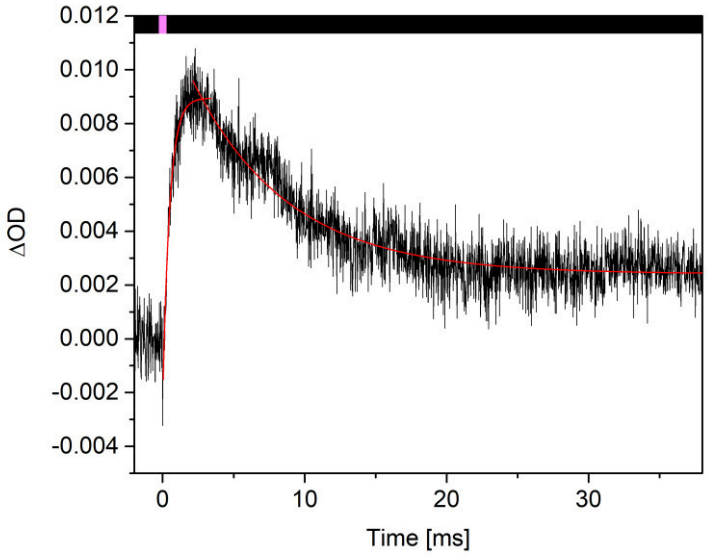

Figure A34 Transient signal detected at 420 nm for **3a** in methanol.

Equation	y = A1·exp(-x/τ) + y0
y0	0.00895 ± 9.52894E-5
A1	-0.01136 ± 3.74204E-4
τ	0.48446 ± 0.0272
R-Square(COD)	0.90037
Adj. R-Square	0.89917

Table A10 Fitting of the growth of the signal shown in Figure A34.

Equation	y = A1·exp(-x/τ) + y0
y0	0.00241 ± 3.5326E-5
A1	0.00984 ± 1.71875E-4
τ	6.74508 ± 0.17172
R-Square(COD)	0.82341
Adj. R-Square	0.82321

Table A11 Fitting of the decay of the signal shown in Figure A34.

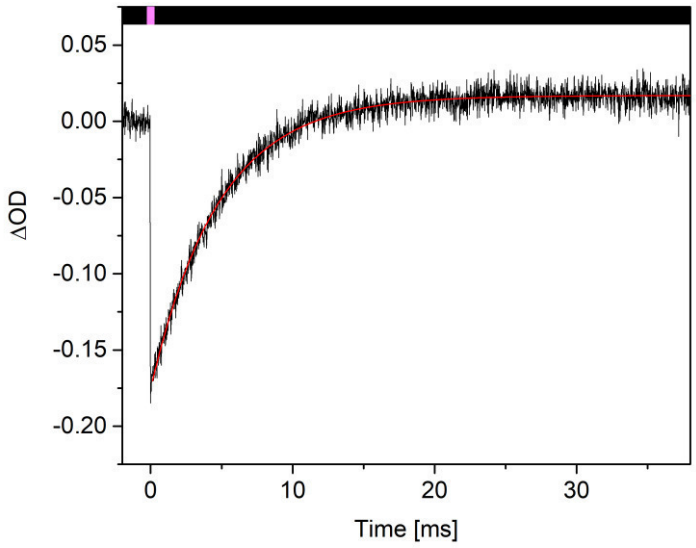

Figure A35 Transient signal detected at 365 nm for **3a** in methanol (0.75 μM).

Equation	$y = A1 \cdot \exp(-x/\tau) + y0$
y0	0.01689 ± 2.01817E-4
A1	-0.19253 ± 8.50475E-4
τ	4.75812 ± 0.03538
R-Square(COD)	0.97724
Adj. R-Square	0.97721

Table A12 Fitting of the decay of the signal shown in Figure A35.

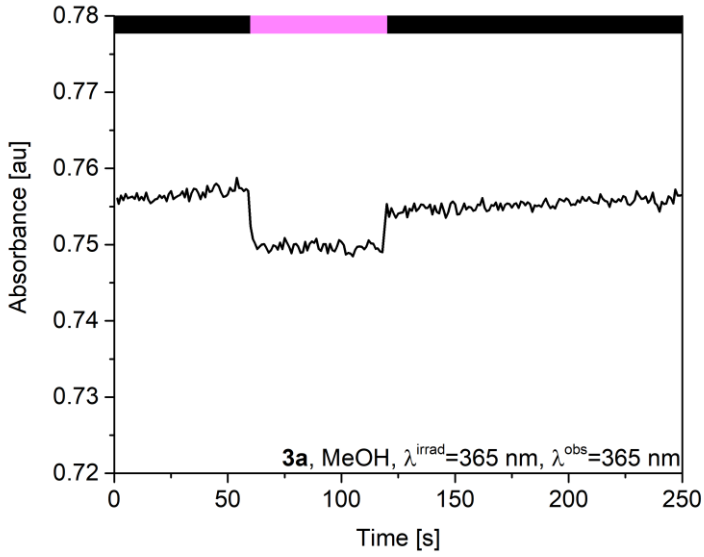

Figure A36 Absorbance variation of **3a** in MeOH, irradiation with a 365 nm LED, λ^{obs}=365 nm.

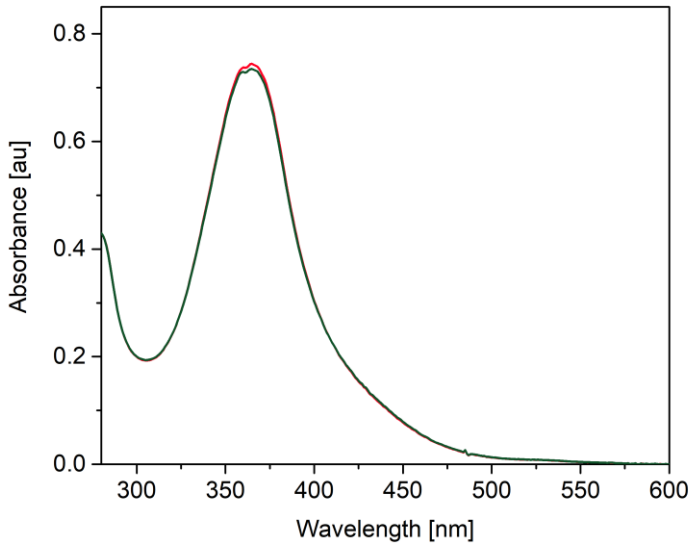

Figure A37 UV/vis of ***E*-3a** in MeOH (red), and of the PSS (green) after irradiation with a 365 nm LED.

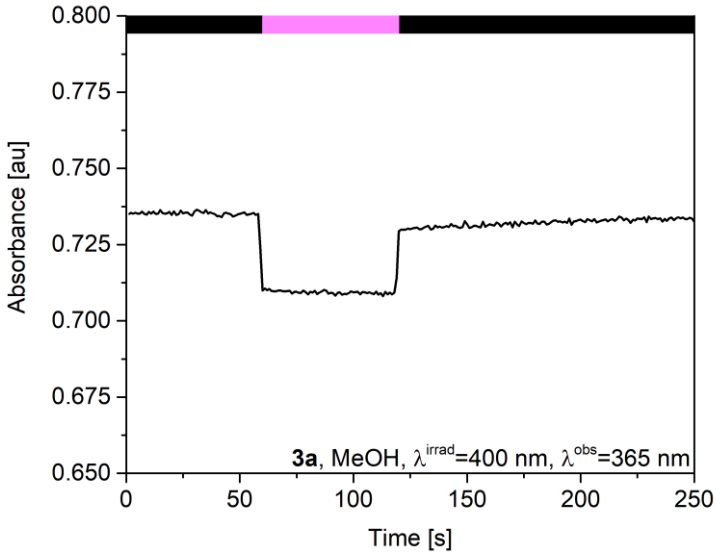

Figure A38 Absorbance variation of **3a** in MeOH, irradiation with a 365 nm LED, λ^{obs}=400 nm.

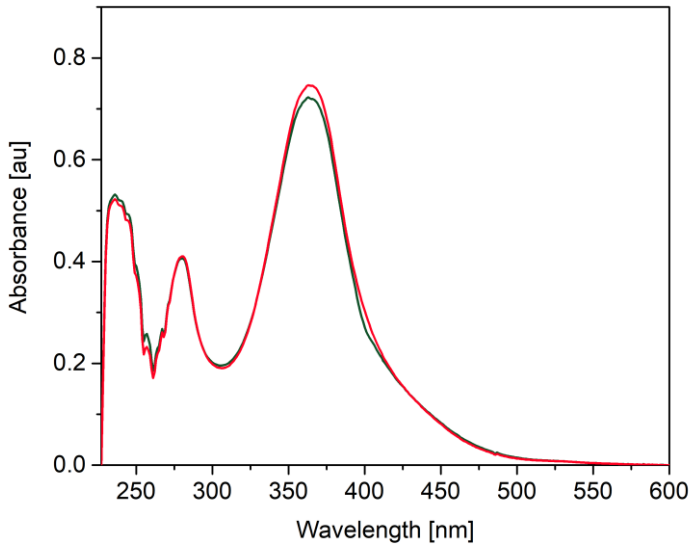

Figure A39 UV/vis of ***E*-3a** in MeOH (red), and of the PSS (green) after irradiation with a 400 nm LED.

MeOD

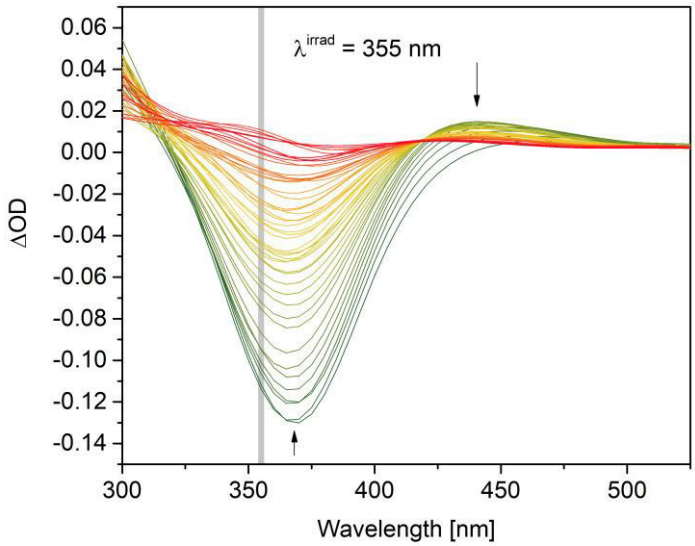

Figure A40 Transient signal map for **3a** in MeOD.

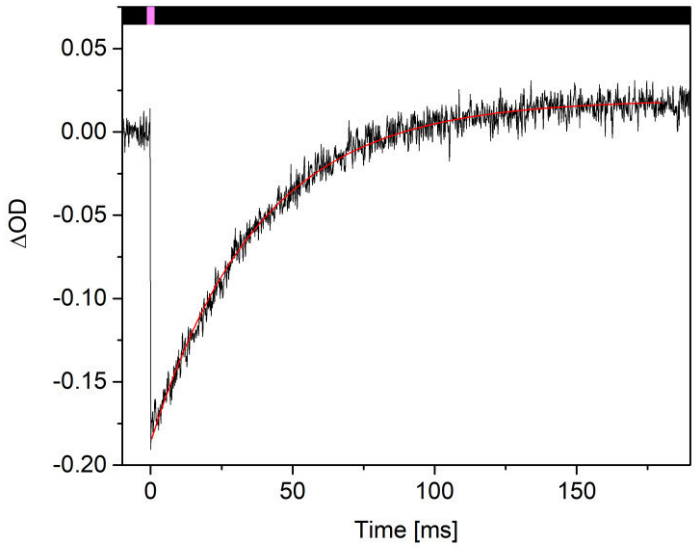

Figure A41 Transient signal detected at 365 nm for **3a** in MeOD.

Equation	y = A1·exp(-x/τ) + y0
y0	0.01942 ± 2.84414E-4
A1	-0.20566 ± 6.16329E-4
τ	37.72755 ± 0.24983
R-Square(COD)	0.98679
Adj. R-Square	0.98677

Table A13 Fitting of the signal shown in Figure A41.

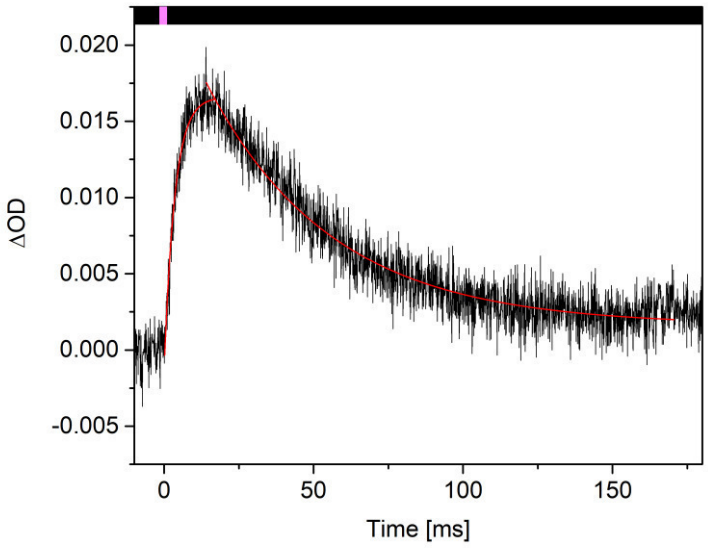

Figure A42 Transient signal detected at 440 nm for **3a** in MeOD.

Equation	y = A1·exp(-x/τ) + y0
y0	0.0166 ± 1.94495E-4
A1	-0.01793 ± 4.55863E-4
τ	3.5394 ± 0.1914
R-Square(COD)	0.92274
Adj. R-Square	0.92182

Table A14 Fitting of the growth of the signal shown in Figure A42.

Equation	y = A1·exp(-x/τ) + y0
y0	0.00162 ± 8.76195E-5
A1	0.02232 ± 2.64102E-4
τ	41.66609 ± 0.89513
R-Square(COD)	1.62896E-6
Adj. R-Square	0.91084

Table A15 Fitting of the decay of the signal shown in Figure A42.

Methanol - Water 9:1

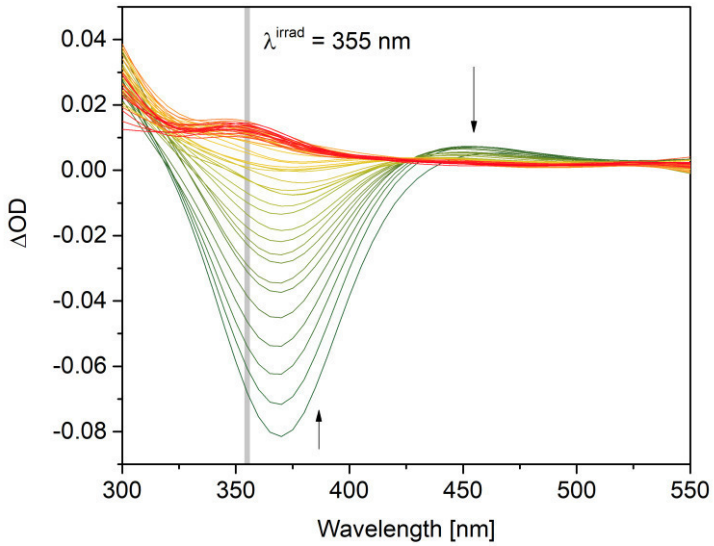

Figure A43 Transient signal map for **3a** in MeOH-H_2O 9:1.

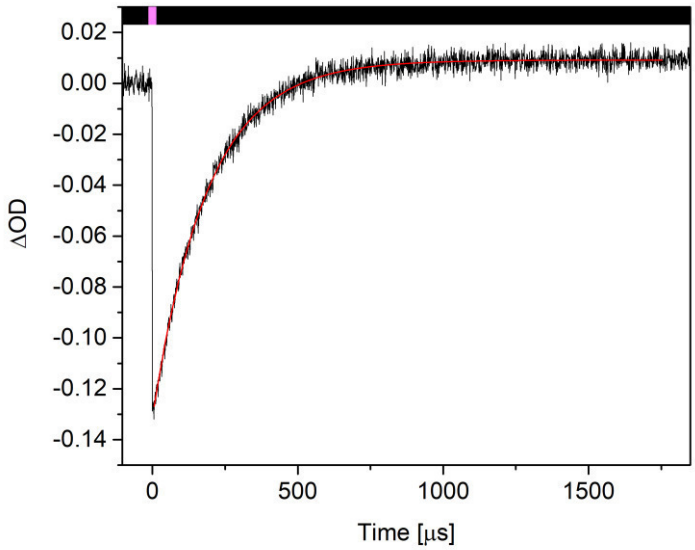

Figure A44 Transient signal detected at 370 nm for **3a** in MeOH-H_2O 9:1.

Equation	y = A1·exp(-x/τ) + y0
y0	0.00894 ± 1.33486E-4
A1	-0.13116 ± 4.11548E-4
τ	14.82742 ± 0.0879
R-Square(COD)	0.98759
Adj. R-Square	0.98757

Table A16 Fitting of the signal shown in Figure A44.

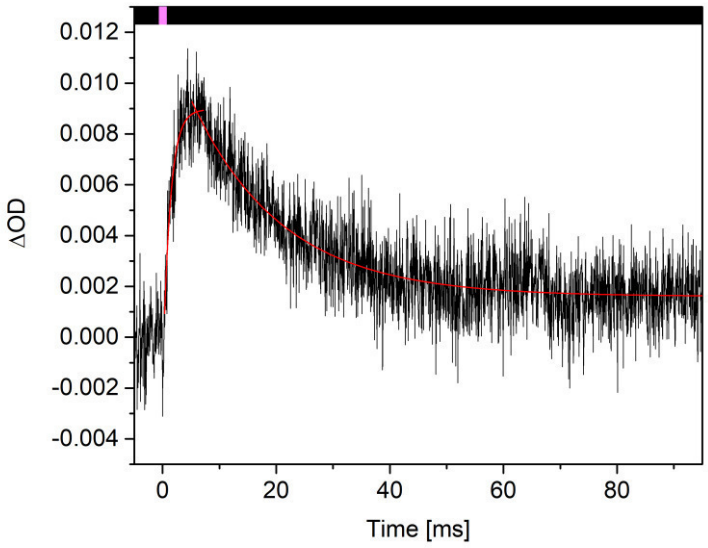

Figure A45 Transient signal detected at 440 nm for **3a** in MeOH-H_2O 9:1.

Equation	y = A1·exp(-x/τ) + y0
y0	0.00897 ± 1.65031E-4
A1	-0.01055 ± 7.11154E-4
τ	1.27848 ± 0.13426
R-Square(COD)	0.78465
Adj. R-Square	0.78144

Table A17 Fitting of the growth of the signal shown in Figure A45.

Equation	y = A1·exp(-x/τ) + y0
y0	0.00161 ± 4.85678E-5
A1	0.01062 ± 2.61403E-4
τ	15.87205 ± 0.54545
R-Square(COD)	0.71054
Adj. R-Square	0.71022

Table A18 Fitting of the decay of the signal shown in Figure A45.

Methanol - Water 1:1

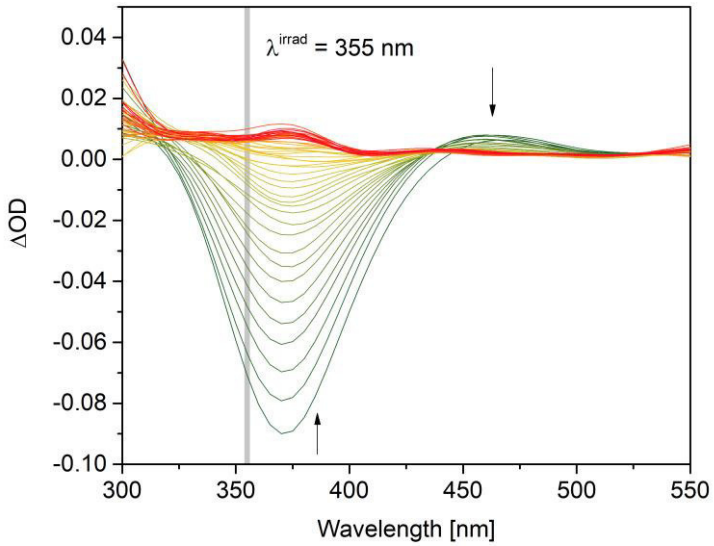

Figure A46 Transient signal map for **3a** in MeOH-H_2O 1:1.

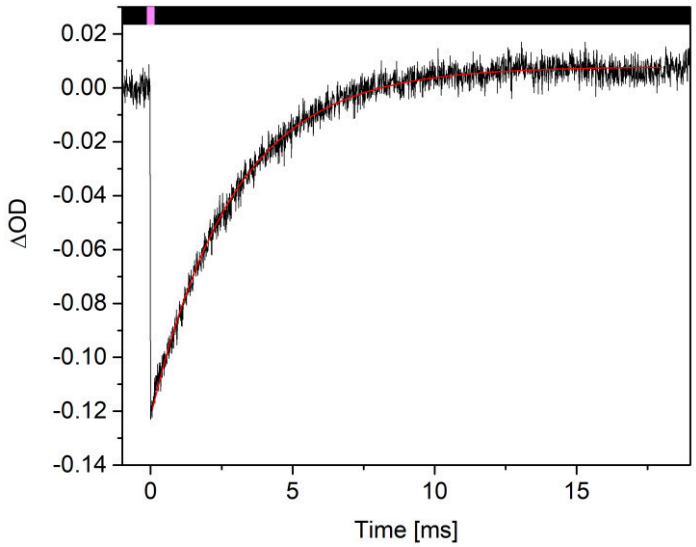

Figure A47 Transient signal detected at 370 nm for **3a** in MeOH-H_2O 1:1.

Equation	y = A1·exp(-x/τ) + y0
y0	0.00791 ± 1.31759E-4
A1	-0.12991 ± 4.18322E-4
τ	2.89774 ± 0.01742
R-Square(COD)	0.98709
Adj. R-Square	0.98707

Table S19 Fitting of the signal shown in Figure A47.

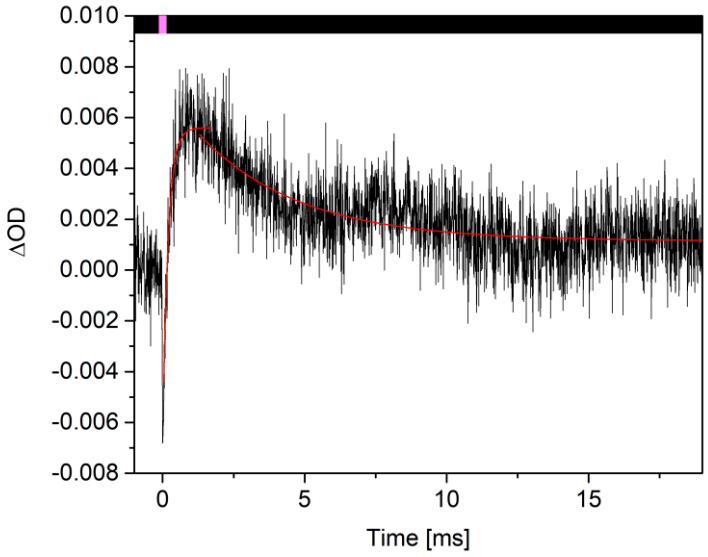

Figure A48 Transient signal detected at 440 nm for **3a** in MeOH-H_2O 1:1.

Equation	y = A1·exp(-x/τ) + y0
y0	0.0056 ± 1.23826E-4
A1	-0.01225 ± 7.55371E-4
τ	0.19599 ± 0.01704
R-Square(COD)	0.78162
Adj. R-Square	0.77894

Table A20 Fitting of the growth of the signal shown in Figure A48.

Equation	y = A1·exp(-x/τ) + y0
y0	0.00114 ± 5.46594E-5
A1	0.00605 ± 2.72628E-4
τ	3.53921 ± 0.22747
R-Square(COD)	0.43661
Adj. R-Square	0.43597

Table A21 Fitting of the decay of the signal shown in Figure A48.

MeOH - buffered water (pH = 4) 1:1

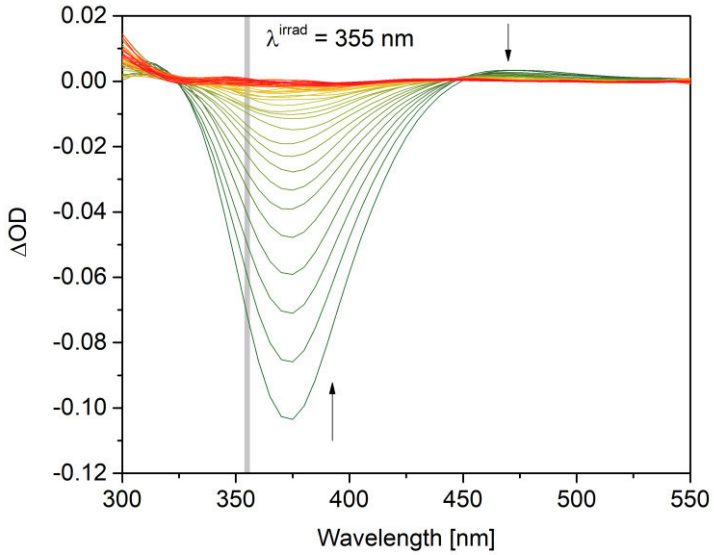

Figure A49 Transient signal map for **3a** in MeOH- buffered H_2O (pH=4) 1:1.

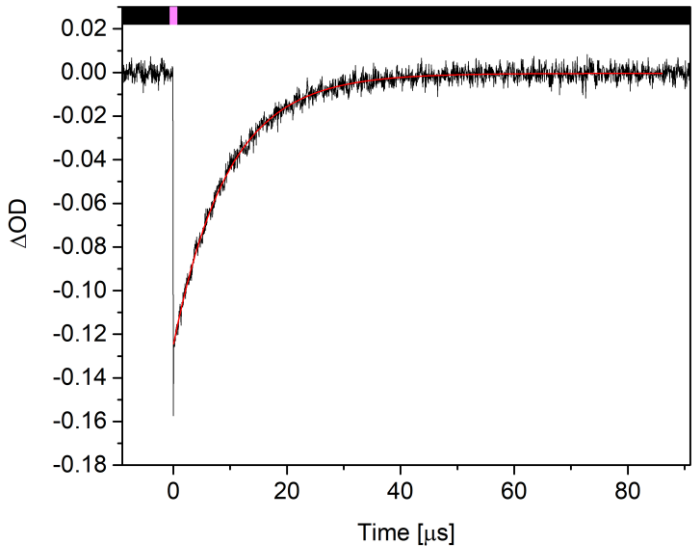

Figure A50 Transient signal detected at 375 nm for **3a** in MeOH- buffered H_2O (pH=4) 1:1.

Equation	y = A1·exp(-x/τ) + y0
y0	-3.91634E-4 ± 9.40343E-5
A1	-0.12466 ± 4.24688E-4
τ	9.52264 ± 0.05404
R-Square(COD)	0.98742
Adj. R-Square	0.98741

Table A22 Fitting of the signal shown in Figure A50.

Methanol - Water 1:2

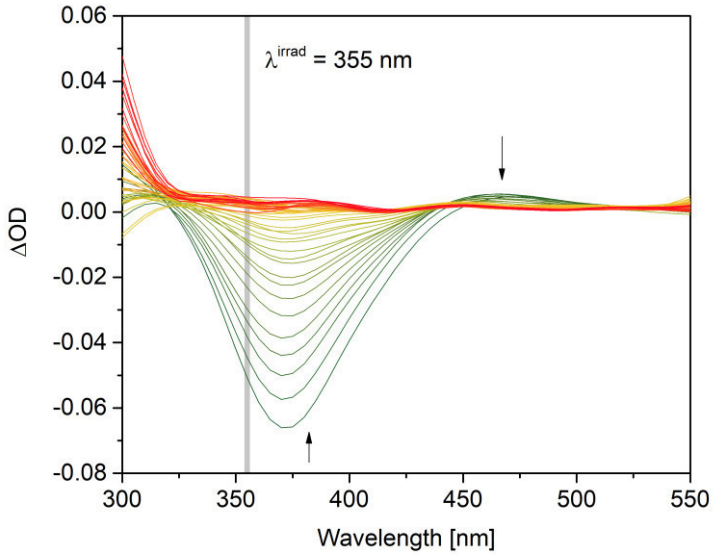

Figure A51 Transient signal map for **3a** in MeOH-H_2O 1:2.

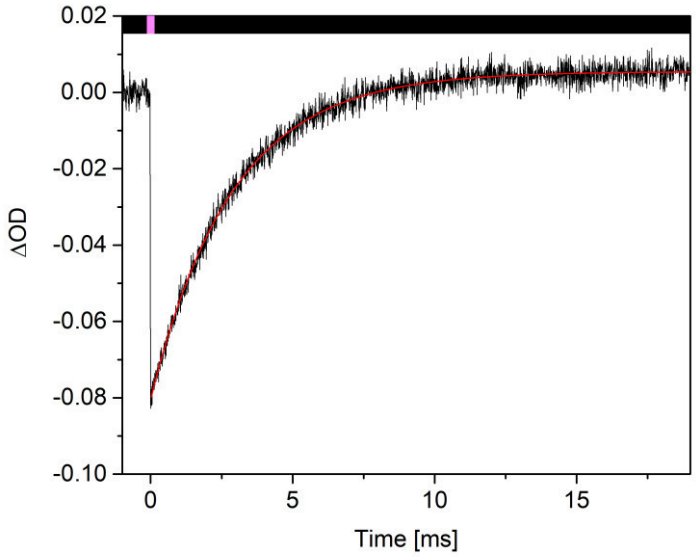

Figure A52 Transient signal detected at 375 nm for **3a** in MeOH-H_2O 1:2.

Equation	y = A1·exp(-x/τ) + y0
y0	0.00546 ± 7.84826E-5
A1	-0.08581 ± 2.59824E-4
τ	2.87345 ± 0.01604
R-Square(COD)	0.98784
Adj. R-Square	0.98783

Table A23 Fitting of the signal shown in Figure A52.

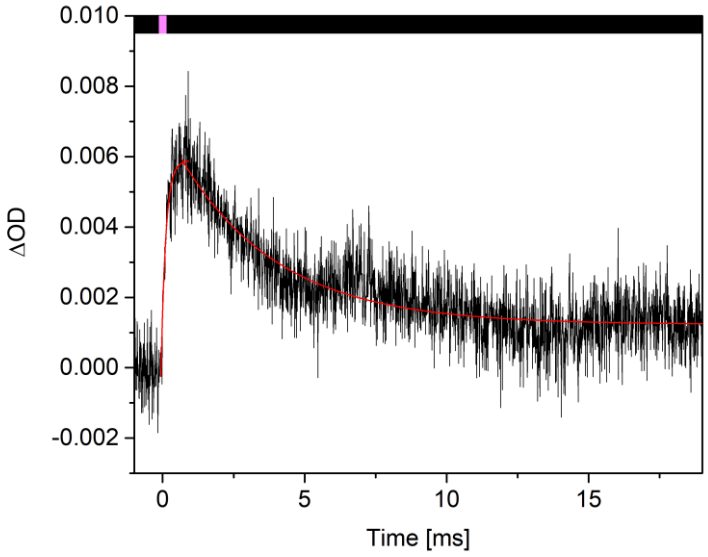

Figure A53 Transient signal detected at 465 nm for **3a** in MeOH-H_2O 1:2.

Equation	y = A1·exp(-x/τ) + y0
y0	0.00589 ± 1.36293E-4
A1	-0.00427 ± 2.39947E-4
τ	0.16579 ± 0.02006
R-Square(COD)	0.78486
Adj. R-Square	0.78033

Table A24 Fitting of the growth of the signal shown in Figure A53.

Equation	y = A1·exp(-x/τ) + y0
y0	0.00123 ± 3.26719E-5
A1	0.00572 ± 1.23106E-4
τ	3.42852 ± 0.12344
R-Square(COD)	0.69456
Adj. R-Square	0.69422

Table A25 Fitting of the decay of the signal shown in Figure A53.

Acetonitrile

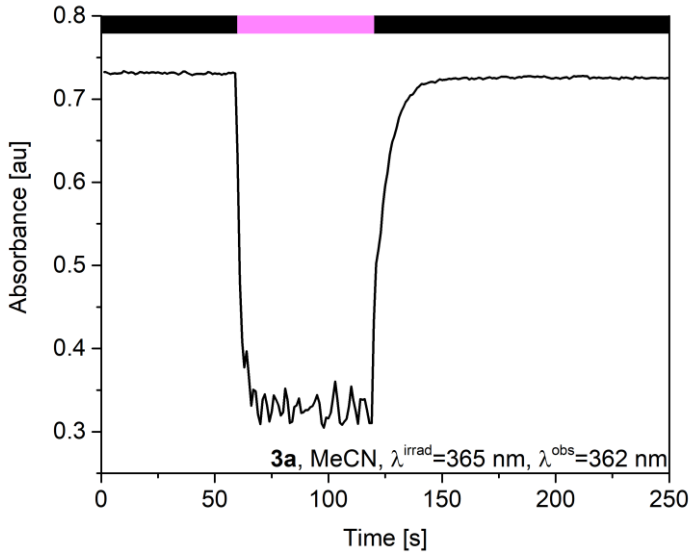

Figure A54 Absorbance variation of **3a** in MeCN, irradiation with a 365 nm LED, λ^{obs}=362 nm.

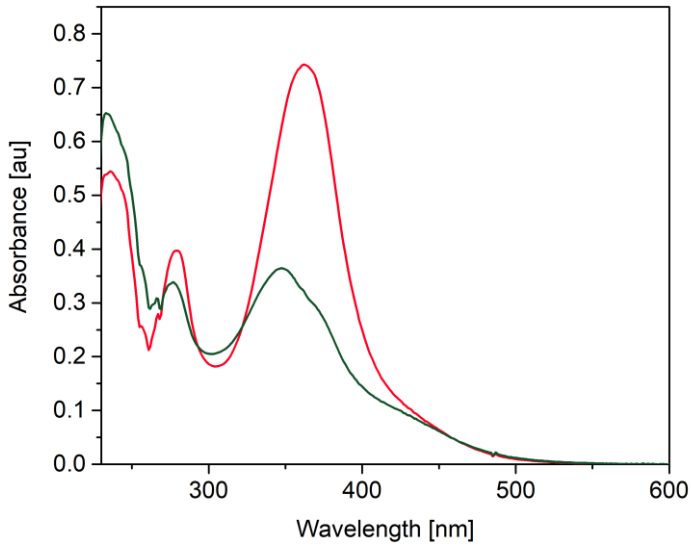

Figure A55 UV/vis of ***E*-3a** in MeCN (red), and of the PSS (green) after irradiation with a 365 nm LED.

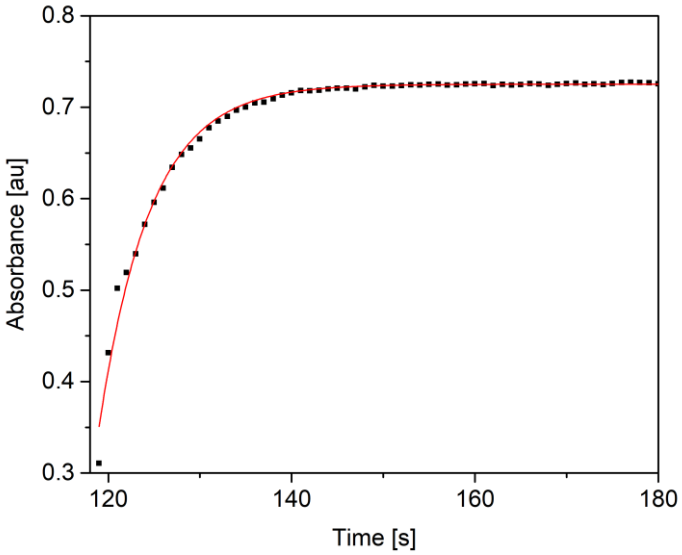

Figure A56 PSS-to-*E* kinetic of **3a** in MeCN, irradiation with 365 nm LED, λ^{obs}=362 nm.

Equation	y = A1·exp(-x/τ) + y0
y0	0.72522 ± 5.15549E-4
A1	-6.7543E8 ± 2.49744E8
τ	5.58327 ± 0.09518
R-Square(COD)	0.99054
Adj. R-Square	0.99039

Table A26 Fitting of the growth of the signal shown in Figure A56.

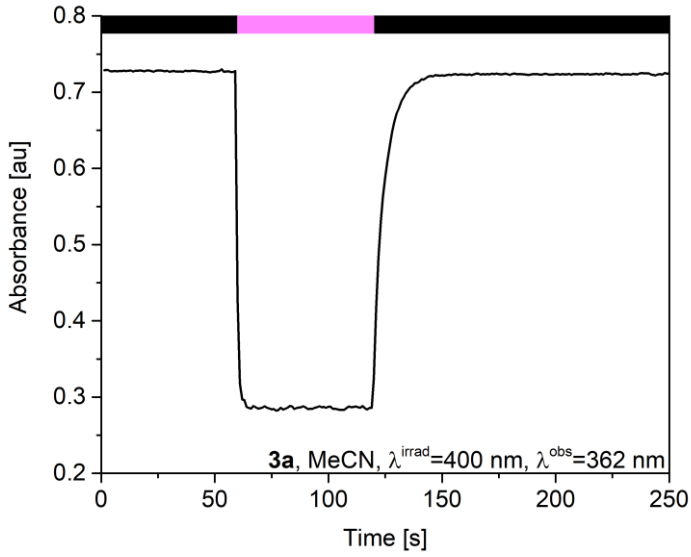

Figure A57 Absorbance variation of **3a** in MeCN, irradiation with a 400 nm LED, λ^{obs}=362 nm.

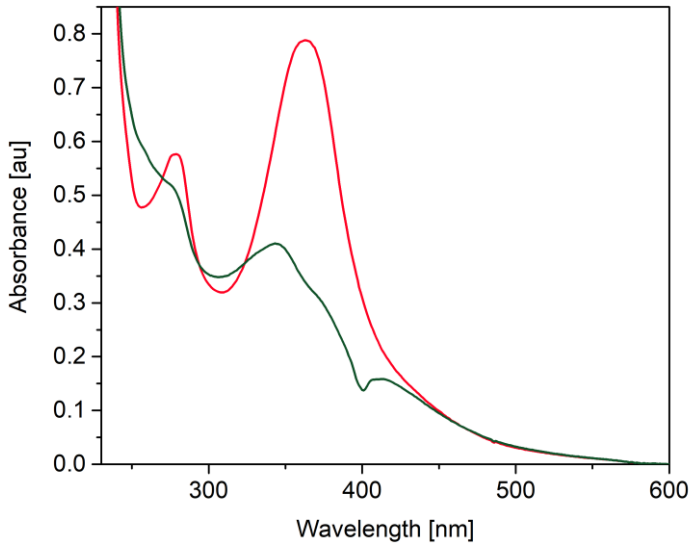

Figure A58 UV/vis of ***E*-3a** in MeCN (red), and of the PSS (green) after irradiation with a 400 nm LED.

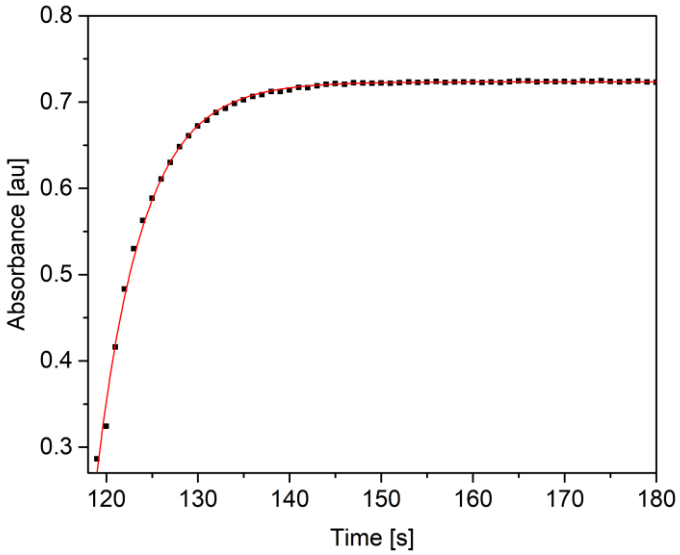

Figure A59 PSS-to-*E* kinetic of **3a** in MeCN, irradiation with 400 nm LED, λ^{obs}=362 nm.

Equation	y = A1·exp(-x/τ) + y0
y0	0.72522 ± 5.15549E-4
A1	-6.7543E8 ± 2.49744E8
τ	5.58327 ± 0.09518
R-Square(COD)	0.99054
Adj. R-Square	0.99039

Table A27 Fitting of the growth of the signal shown in Figure A59.

DMSO

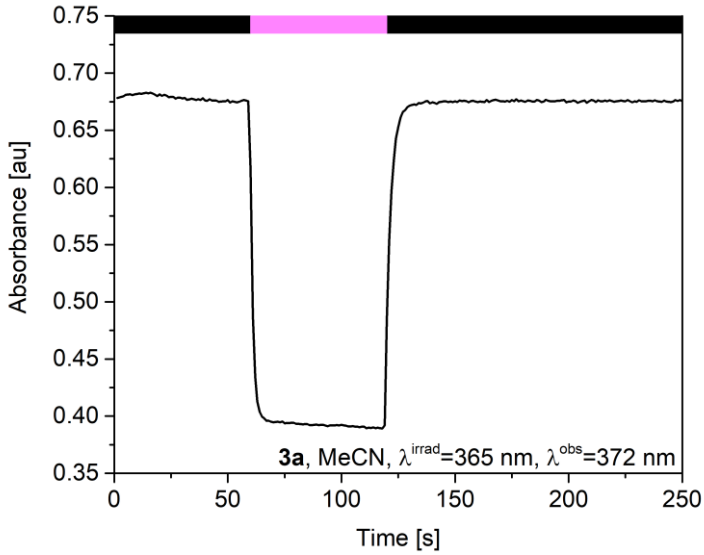

Figure A60 Absorbance variation of **3a** in DMSO, irradiation with a 365 nm LED, λ^{obs}=372 nm.

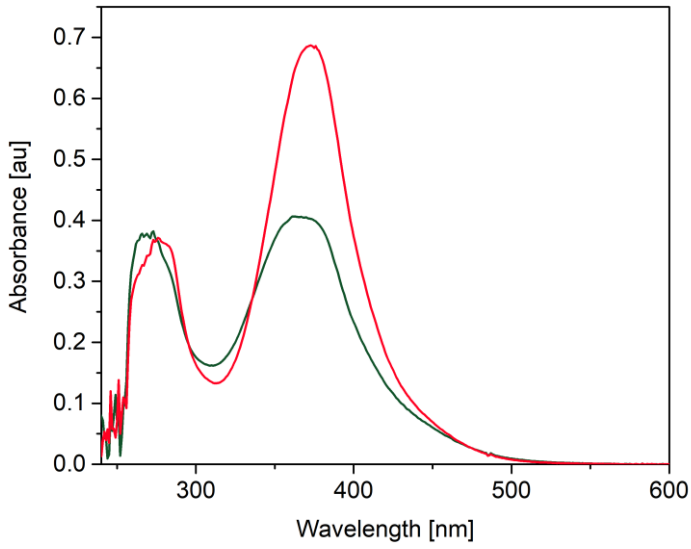

Figure A61 UV/vis of ***E*-3a** in DMSO (red), and of the PSS (green) after irradiation with a 365 nm LED.

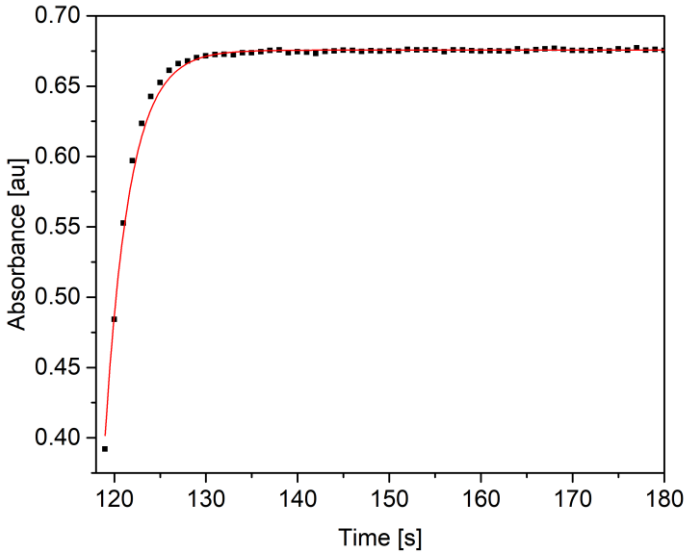

Figure A62 PSS-to-*E* kinetic of **3a** in DMSO, irradiation with 365 nm LED, λ^{obs}=372 nm.

Equation	y = A1·exp(-x/τ) + y0
y0	0.67564 ± 1.39536E-4
A1	-5.85659E18 ± 2.63998E18
τ	2.67363 ± 0.02688
R-Square(COD)	0.99571
Adj. R-Square	0.99566

Table A28 Fitting of the growth of the signal shown in Figure A62.

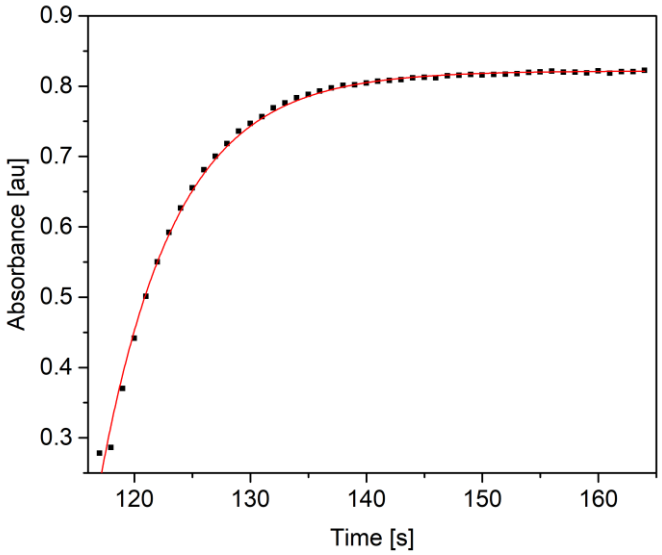

Figure A63 PSS-to-*E* kinetic of **3a** in DMSO, irradiation with 400 nm LED, λ^{obs}=372 nm.

Equation	y = A1·exp(-x/τ) + y0
y0	0.82168 ± 0.00194
A1	-4.24216E7 ± 1.58E7
τ	6.46568 ± 0.13126
R-Square(COD)	0.996
Adj. R-Square	0.99582

Table A29 Fitting of the growth of the signal shown in Figure A63.

DMSO - H_2O 9:1

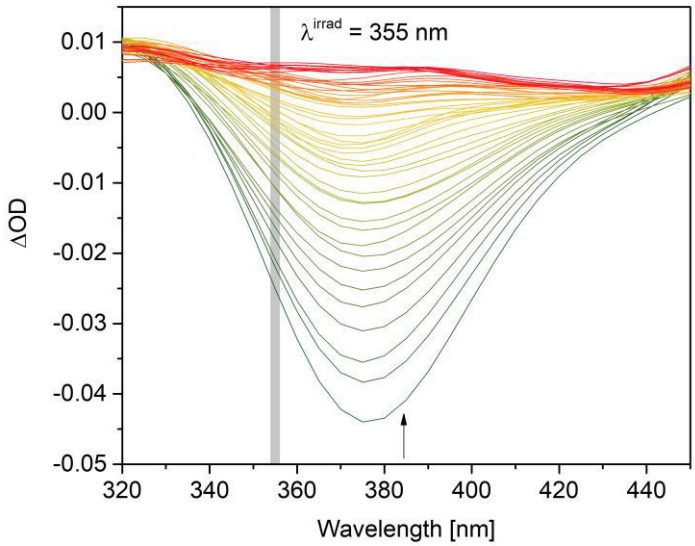

Figure A64 Transient signal map for **3a** in DMSO-H_2O 9:1.

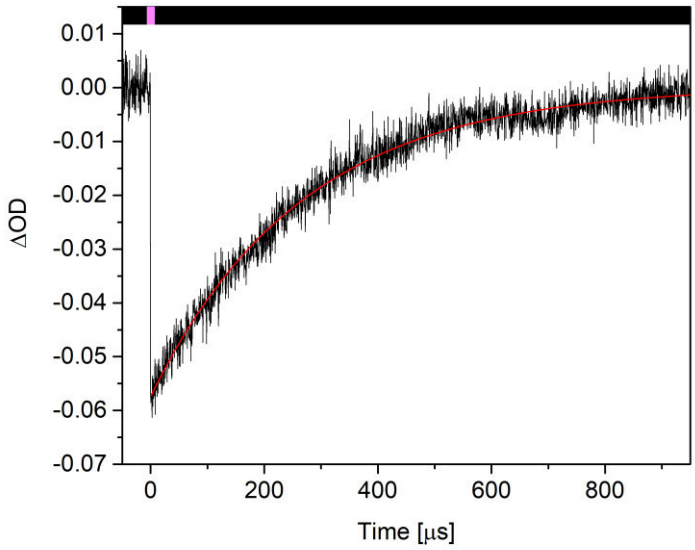

Figure A65 Transient signal detected at 375 nm for **3a** in DMSO-H_2O 9:1.

Equation	y = A1·exp(-x/τ) + y0
y0	2.65734E-4 ± 1.62744E-4
A1	-0.05768 ± 2.19927E-4
τ	266.5882 ± 2.81684
R-Square(COD)	0.97367
Adj. R-Square	0.97365

Table A30 Fitting of the signal shown in Figure A65.

DMSO - H_2O 1:1

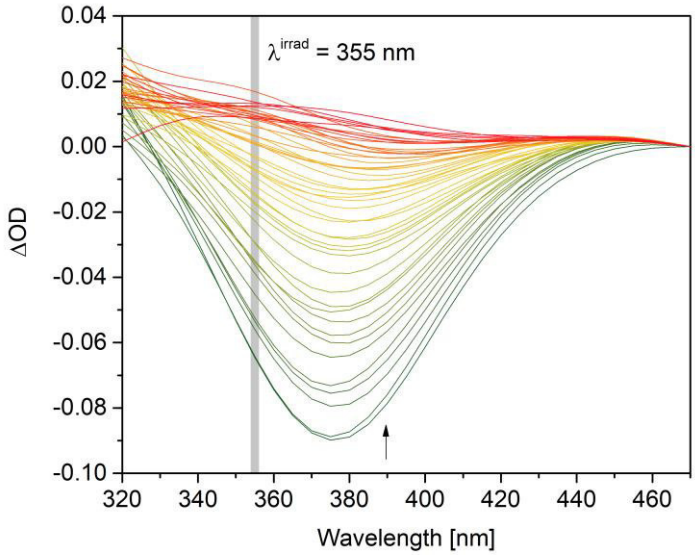

Figure A66 Transient signal map for **3a** in DMSO-H_2O 1:1.

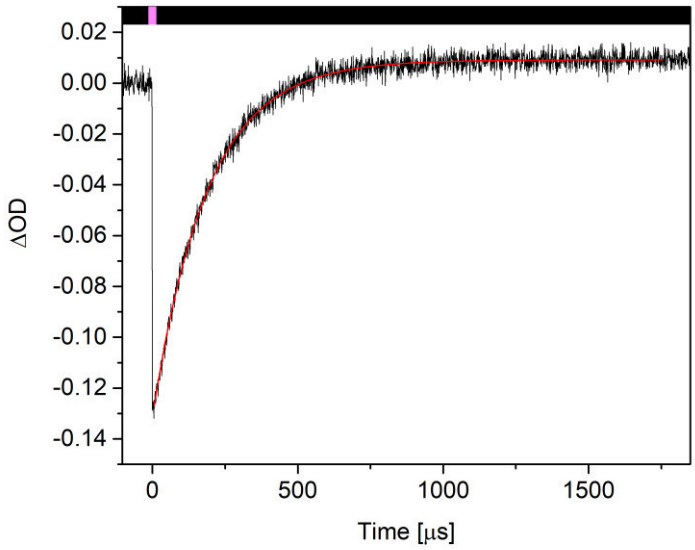

Figure A67 Transient signal detected at 375 nm for **3a** in DMSO-H_2O 1:1.

Equation	y = A1·exp(-x/τ) + y0
y0	0.00916 ± 8.49466E-5
A1	-0.14047 ± 4.15299E-4
τ	187.8634 ± 0.89429
R-Square(COD)	0.99093
Adj. R-Square	0.99092

Table A31 Fitting of the signal shown in Figure A67.

DMSO - buffered H_2O (pH = 4) 1:1

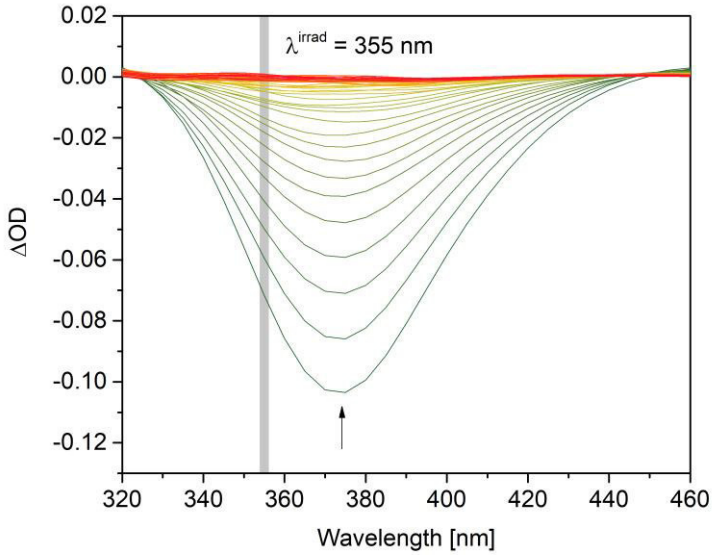

Figure A68 Transient signal map for **3a** in DMSO-buffered H_2O (pH = 4) 1:1.

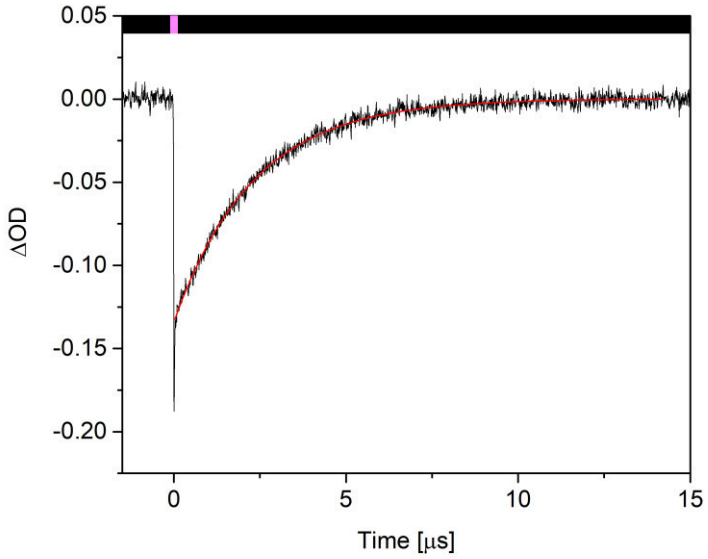

Figure A69 Transient signal detected at 370 nm for **3a** in DMSO-buffered H_2O (pH = 4) 1:1.

Equation	y = A1·exp(-x/τ) + y0
y0	0.00916 ± 8.49466E-5
A1	-0.14047 ± 4.15299E-4
τ	187.8634 ± 0.89429
R-Square(COD)	0.99093
Adj. R-Square	0.99092

Table A32 Fitting of the signal shown in Figure A69.

DMSO - buffered H_2O (pH = 7) 1:1

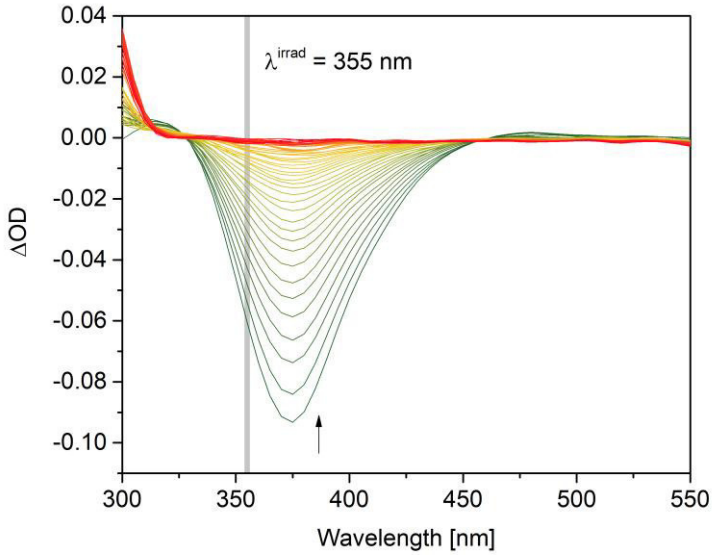

Figure A70 Transient signal map for **3a** in DMSO-buffered H_2O (pH = 7) 1:1.

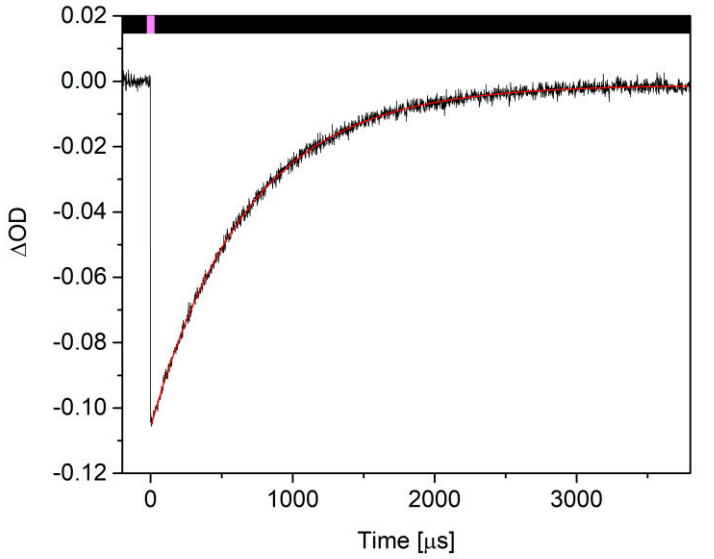

Figure A71 Transient signal detected at 375 nm for **3a** in DMSO-buffered H_2O (pH = 7) 1:1.

Equation	y = A1·exp(-x/τ) + y0
y0	-0.00106 ± 5.2087E-5
A1	-0.10486 ± 1.4199E-4
τ	675.95522 ± 1.82404
R-Square(COD)	1.63279E-6
Adj. R-Square	0.99738

Table A33 Fitting of the signal shown in Figure A71.

DMSO - buffered H_2O (pH = 9) 1:1

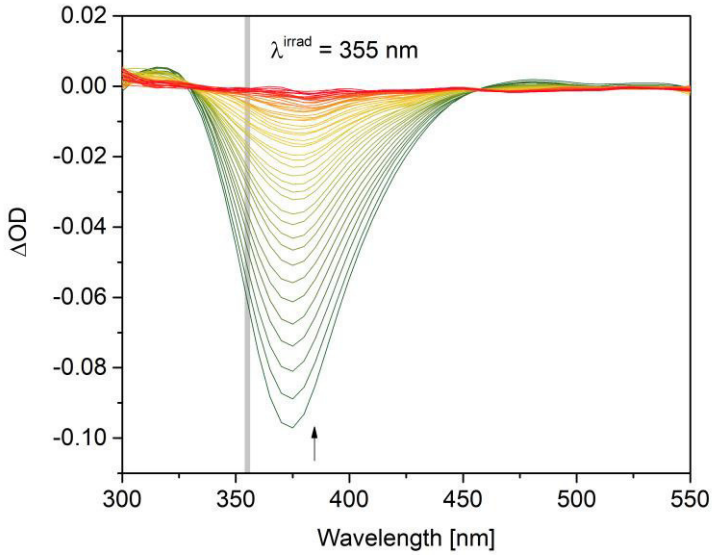

Figure A72 Transient signal map for **3a** in DMSO-buffered H_2O (pH = 9) 1:1.

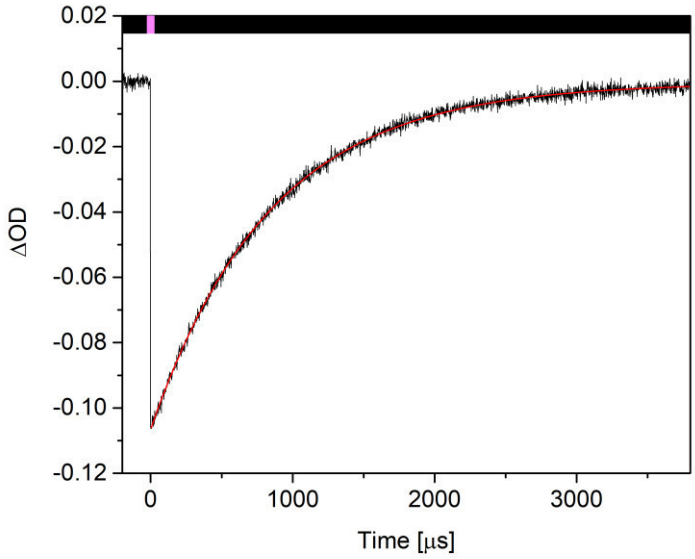

Figure A73 Transient signal detected at 375 nm for **3a** in DMSO-buffered H_2O (pH = 9) 1:1.

Equation	y = A1·exp(-x/τ) + y0
y0	-4.40005E-4 ± 6.1301E-5
A1	-0.10612 ± 1.20826E-4
τ	841.80537 ± 2.21454
R-Square(COD)	0.99788
Adj. R-Square	0.99787

Table A34 Fitting of the signal shown in Figure A73.

DMSO - H_2O 1:1 + 25 µL DBU

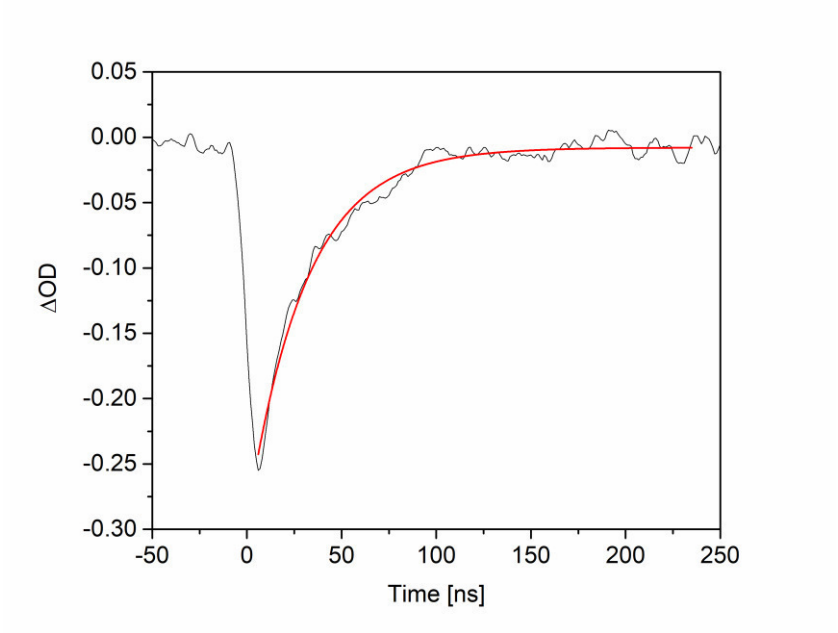

Figure A74 Transient signal detected at 375 nm for **3a** in DMSO-H_2O 1:1 + 25 µL DBU.

Equation	y = A1·exp(-x/τ) + y0
y0	-0.0079 ± 6.8694E-4
A1	-0.28573 ± 0.00376
τ	30.51079 ± 0.58498
R-Square(COD)	0.98203
Adj. R-Square	0.98187

Table A35 Fitting of the signal shown in Figure A74.

DMSO - H_2O 1:2

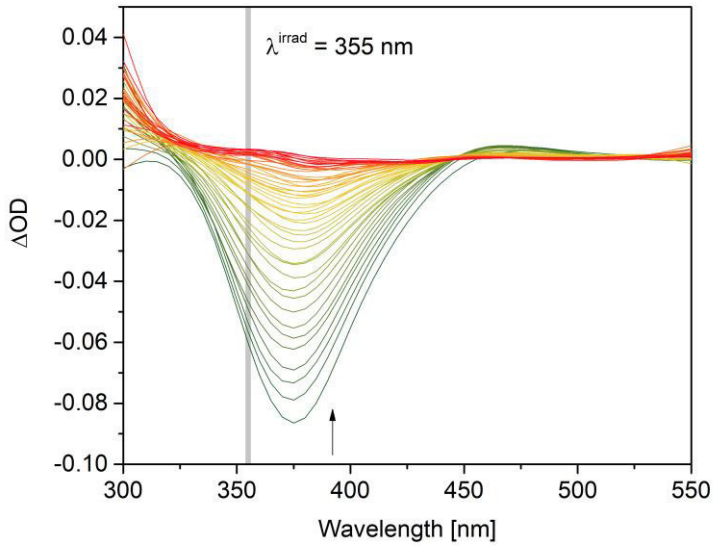

Figure A75 Transient signal map for **3a** in DMSO-H_2O 1:2.

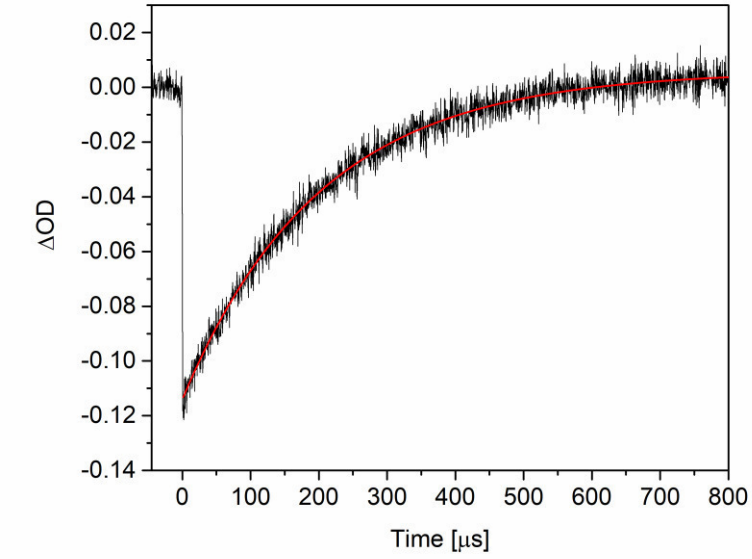

Figure A76 Transient signal detected at 371 nm for **3a** in DMSO-H_2O 1:2.

Equation	y = A1·exp(-x/τ) + y0
y0	0.00593 ± 2.06987E-4
A1	-0.12001 ± 3.80031E-4
τ	200.99355 ± 1.5217
R-Square(COD)	0.98339
Adj. R-Square	0.98337

Table A36 Fitting of the signal shown in Figure A76.

2.3.2 3b

Cyclohexane

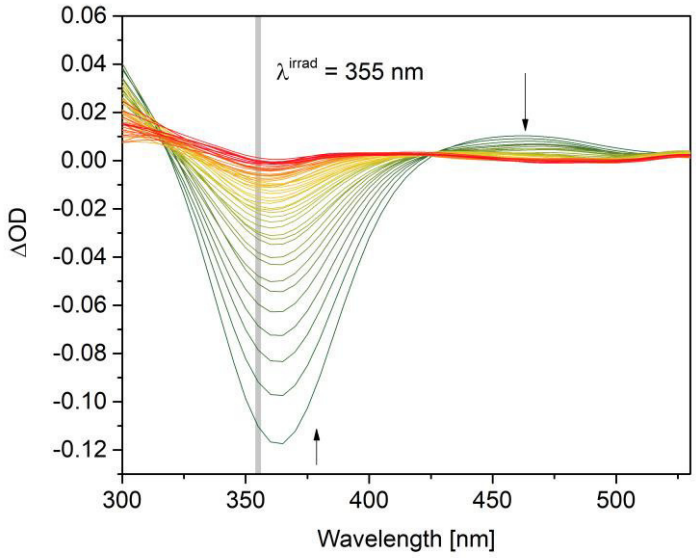

Figure A77 Transient signal map for **3b** in cyclohexane.

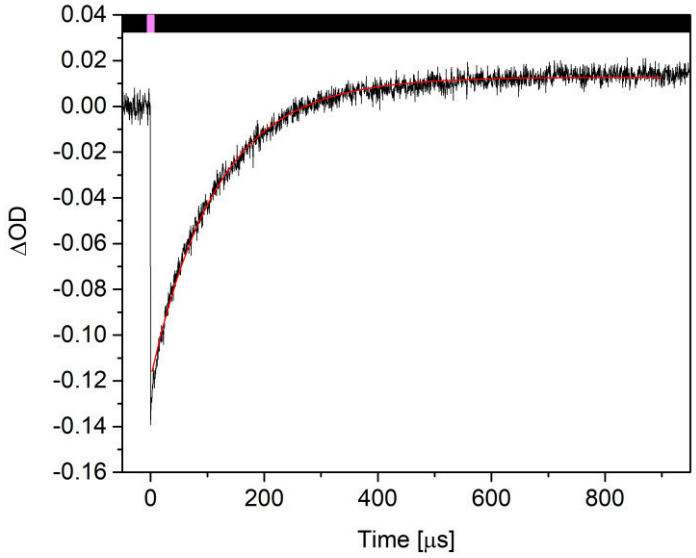

Figure A78 Transient signal detected at 365 nm for **3b** in cyclohexane.

Equation	y = A1·exp(-x/τ) + y0
y0	0.01284 ± 1.00686E-4
A1	-0.13157 ± 4.03427E-4
τ	116.81379 ± 0.61459
R-Square(COD)	0.98917
Adj. R-Square	0.98916

Table A37 Fitting of the signal shown in Figure A78.

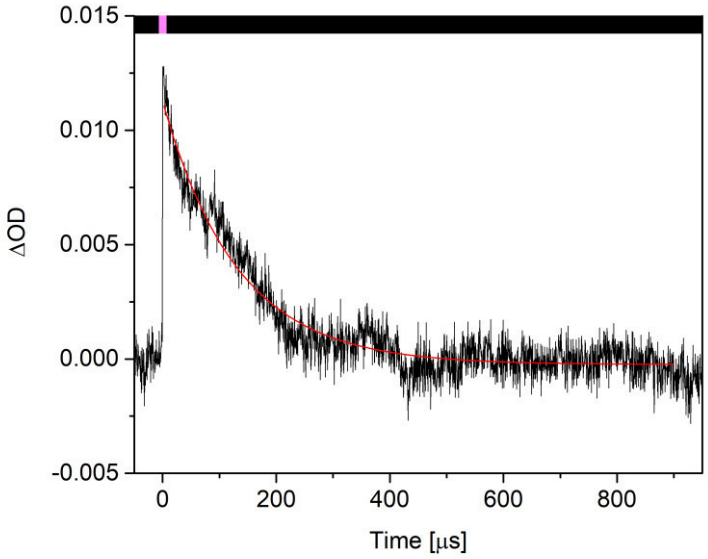

Figure A79 Transient signal detected at 465 nm for **3b** in cyclohexane.

Equation	y = A1·exp(-x/τ) + y0
y0	-2.47464E-4 ± 2.81514E-5
A1	0.01152 ± 9.94026E-5
τ	131.14277 ± 2.03112
R-Square(COD)	0.91657
Adj. R-Square	0.91647

Table A38 Fitting of the signal shown in Figure A79.

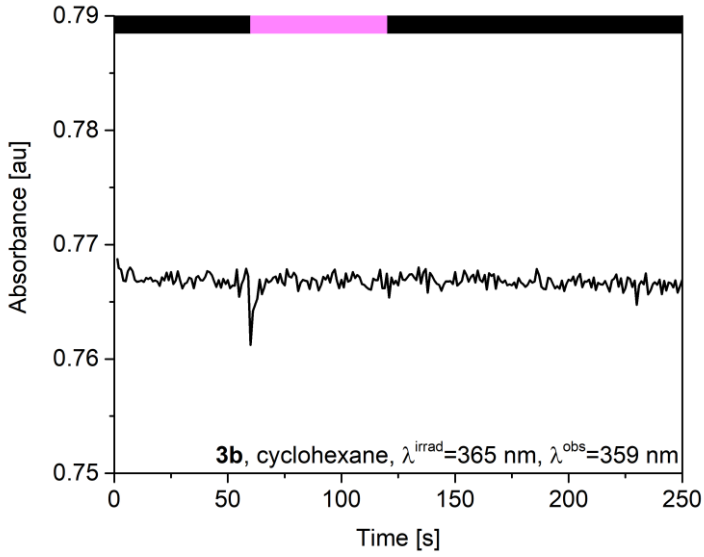

Figure A80 Absorbance variation of **3b** in cyclohexane, irradiation with a 365 nm LED, λ^{obs}=359 nm.

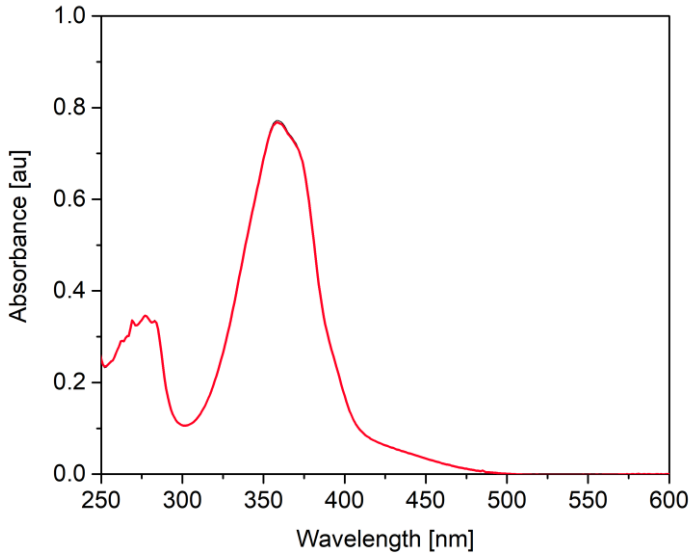

Figure A81 UV/vis of ***E*-3b** in cyclohexane (red), and of the PSS (green) after irradiation with a 365 nm LED.

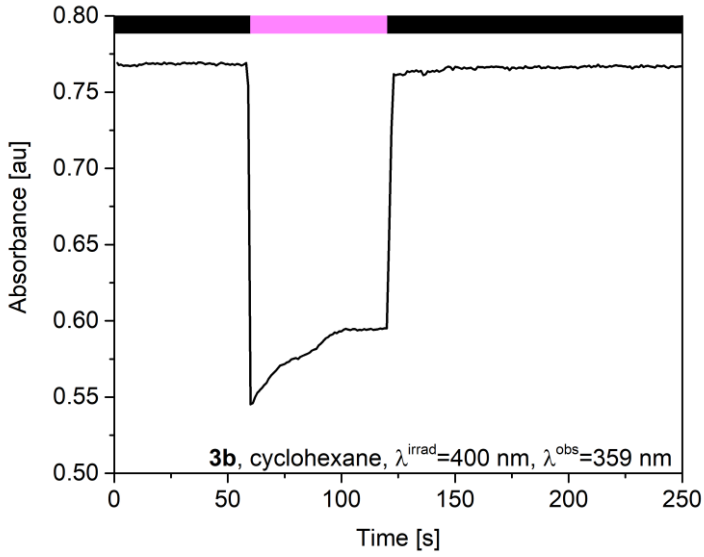

Figure A82 Absorbance variation of **3b** in cyclohexane, irradiation with a 400 nm LED, λ^{obs}=359 nm.

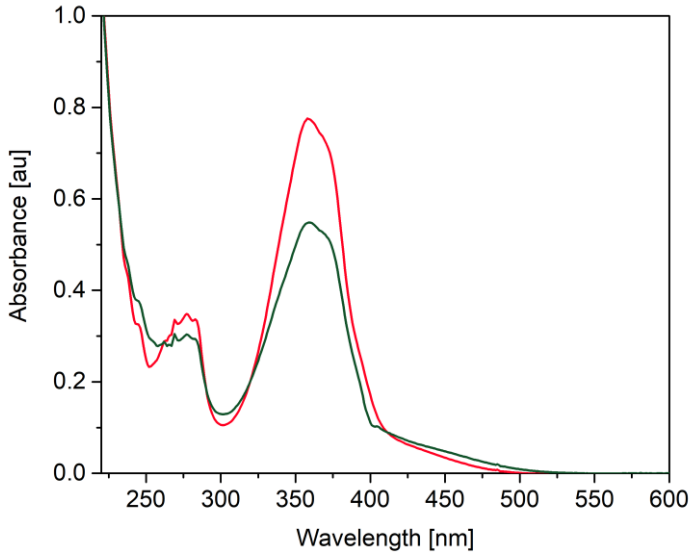

Figure A83 UV/vis of ***E*-3b** in cyclohexane (red), and of the PSS (green) after irradiation with a 400 nm LED.

Dioxane

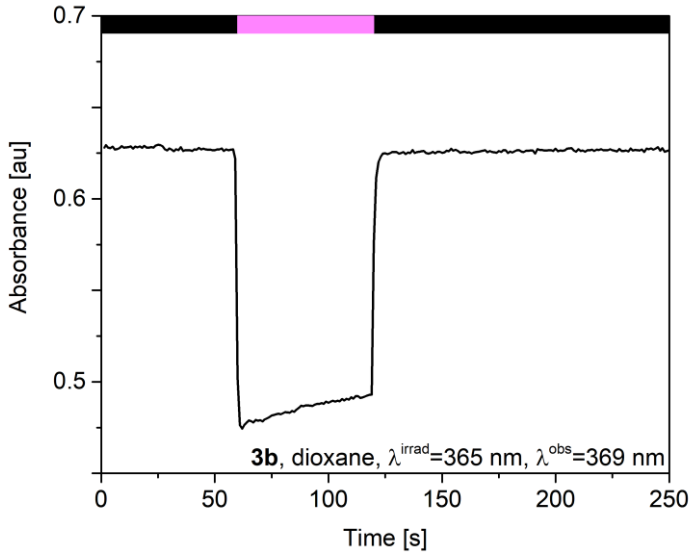

Figure A84 Absorbance variation of **3b** in dioxane, irradiation with a 365 nm LED, λ^{obs}=369 nm.

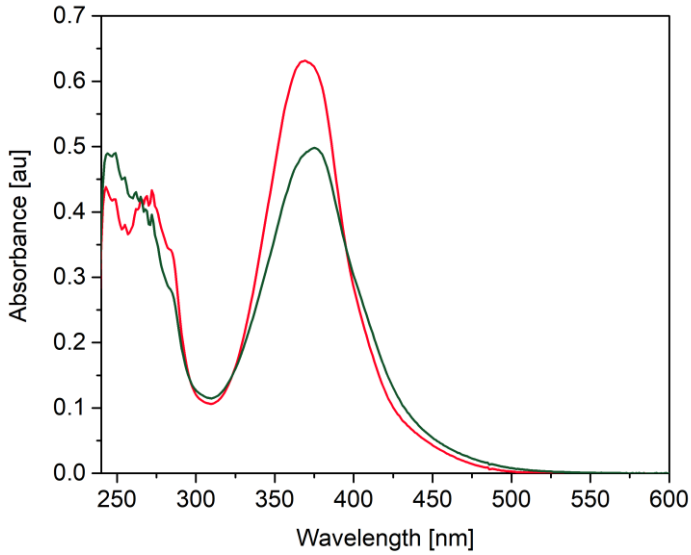

Figure A85 UV/vis of ***E*-3b** in dioxane (red), and of the PSS (green) after irradiation with a 365 nm LED.

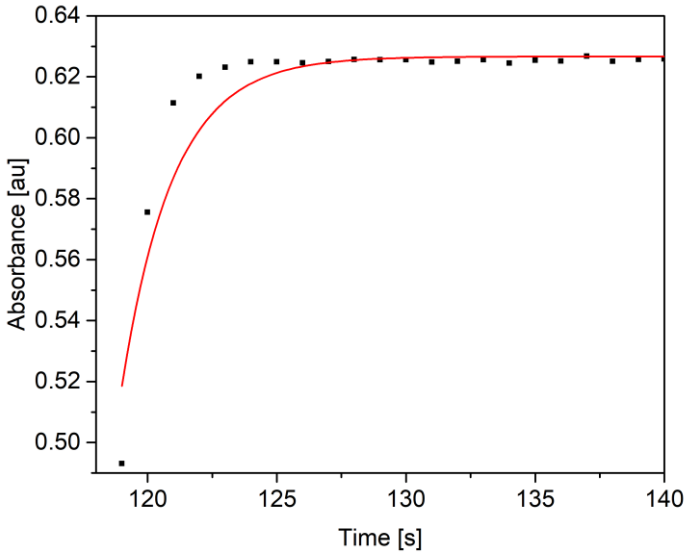

Figure A86 PSS-to-*E* kinetic of **3b** in dioxane, irradiation with 365 nm LED, λ^{obs}=369 nm.

Equation	y = A1·exp(-x/τ) + y0
y0	0.62666 ± 2.56962E-4
A1	-7.5447E24 ± 2.36983E25
τ	1.99975 ± 0.10506
R-Square(COD)	0.89957
Adj. R-Square	0.89845

Table A39 Fitting of the growth of the signal shown in Figure A86.

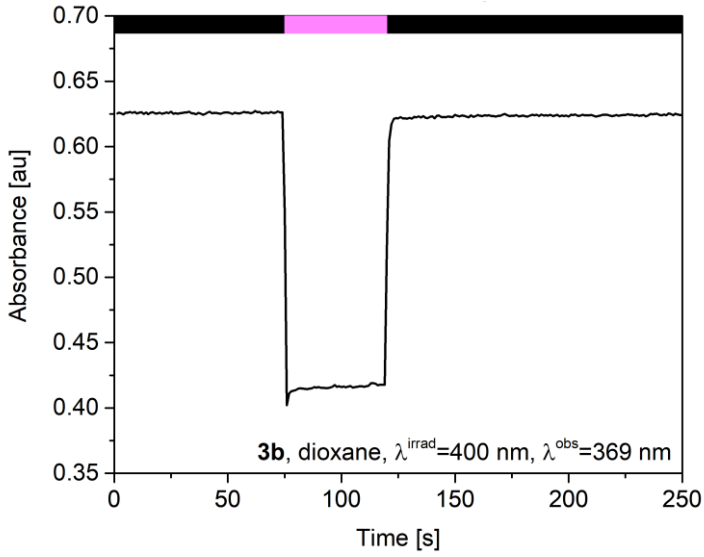

Figure A87 Absorbance variation of **3b** in dioxane, irradiation with a 400 nm LED, λ^{obs}=369 nm.

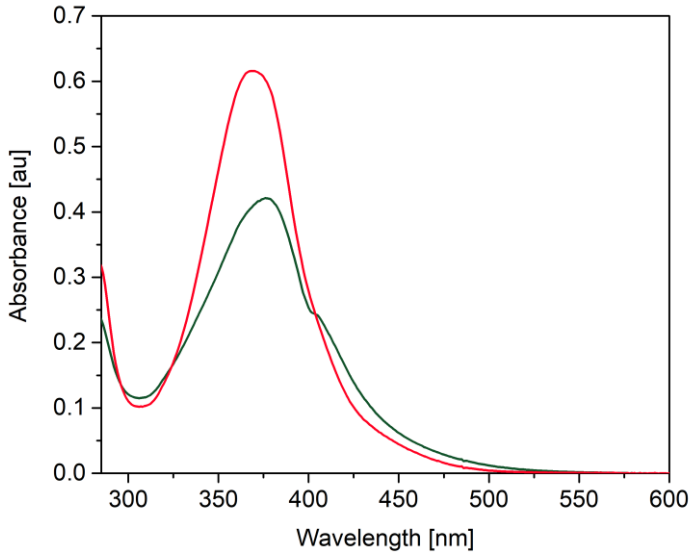

Figure A88 UV/vis of ***E*-3b** in dioxane (red), and of the PSS (green) after irradiation with a 400 nm LED.

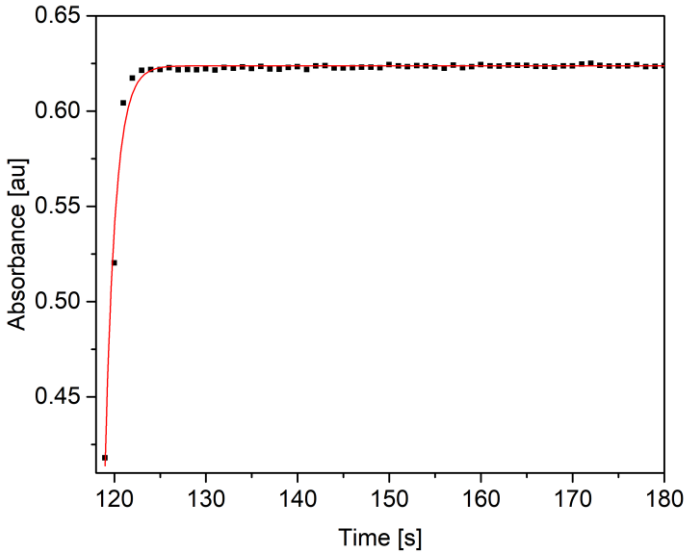

Figure A89 PSS-to-*E* kinetic of **3b** in dioxane, irradiation with 400 nm LED, λ^{obs}=369 nm.

Equation	y = A1·exp(-x/τ) + y0
y0	0.62443 ± 5.17491E-4
A1	-8.46096E25 ± 2.8789E26
τ	1.9373 ± 0.10684
R-Square(COD)	0.91866
Adj. R-Square	0.9174

Table A40 Fitting of the growth of the signal shown in Figure A89.

Benzene

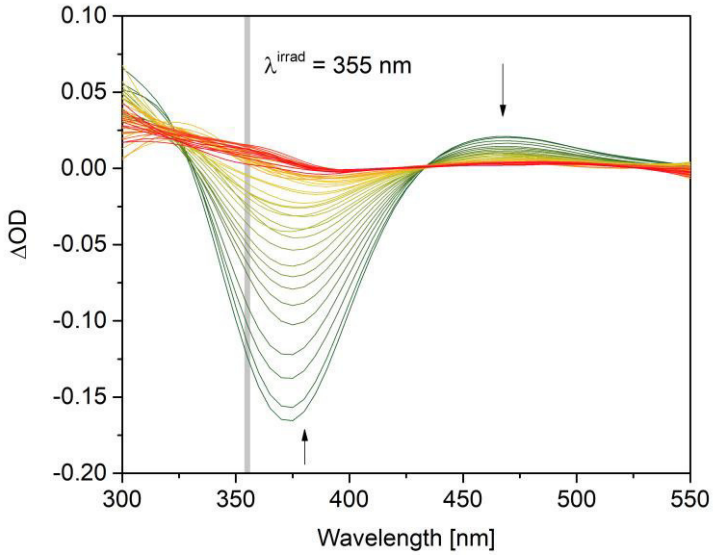

Figure A90 Transient signal map for **3b** in benzene.

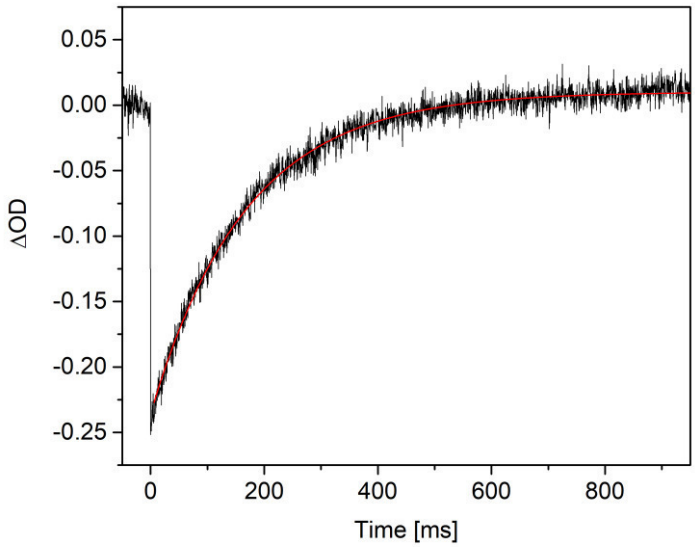

Figure A91 Transient signal detected at 370 nm for **3b** in benzene.

Equation	y = A1·exp(-x/τ) + y0
y0	0.01016 ± 2.80694E-4
A1	-0.24583 ± 8.15417E-4
τ	166.86256 ± 1.06959
R-Square(COD)	0.98532
Adj. R-Square	0.9853

Table A41 Fitting of the signal shown in Figure A91.

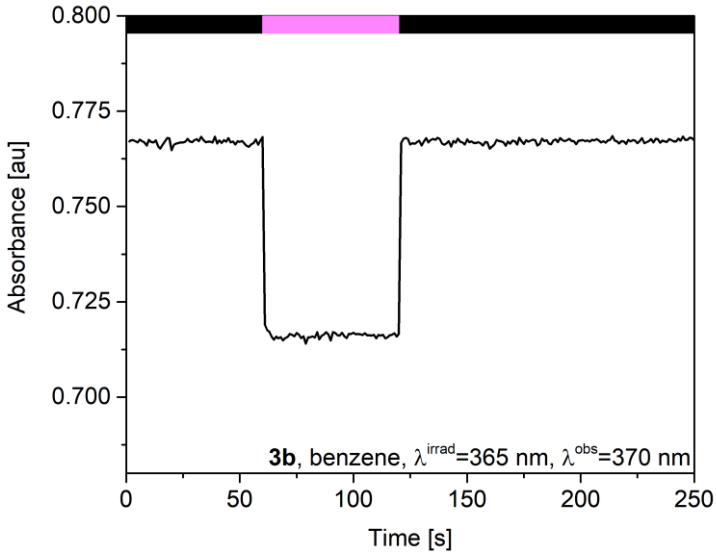

Figure A92 Absorbance variation of **3b** in benzene, irradiation with a 365 nm LED, λ^{obs}=370 nm.

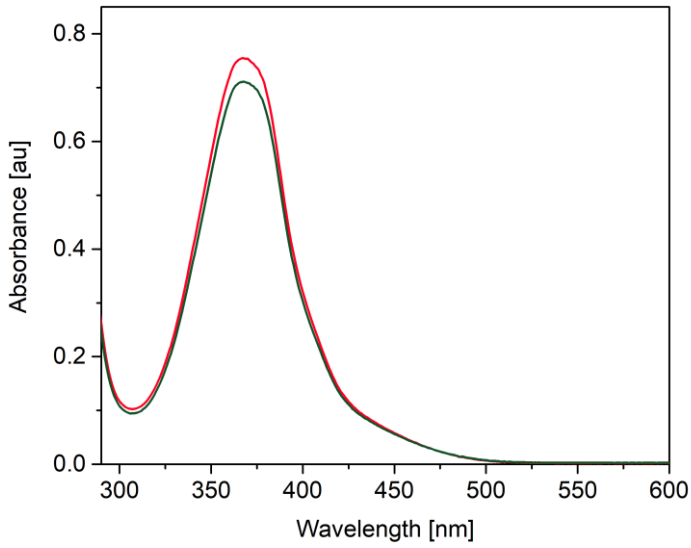

Figure A93 UV/vis of ***E*-3b** in benzene (red), and of the PSS (green) after irradiation with a 365 nm LED.

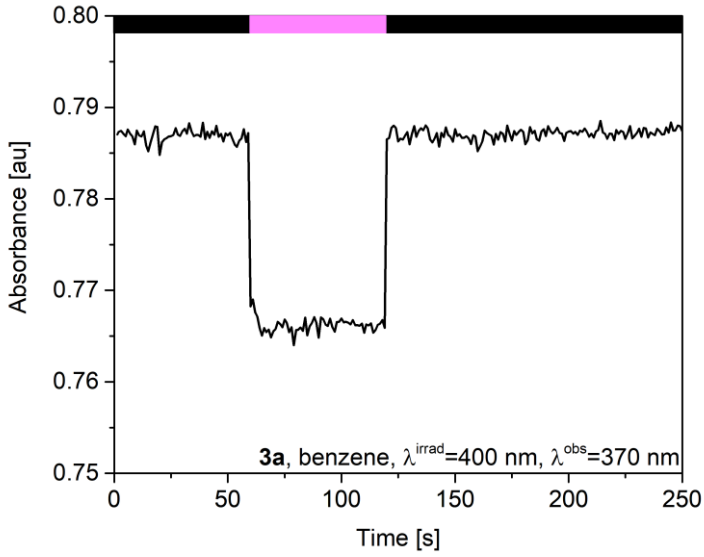

Figure A94 Absorbance variation of **3b** in benzene, irradiation with a 400 nm LED, λ^{obs}=370 nm.

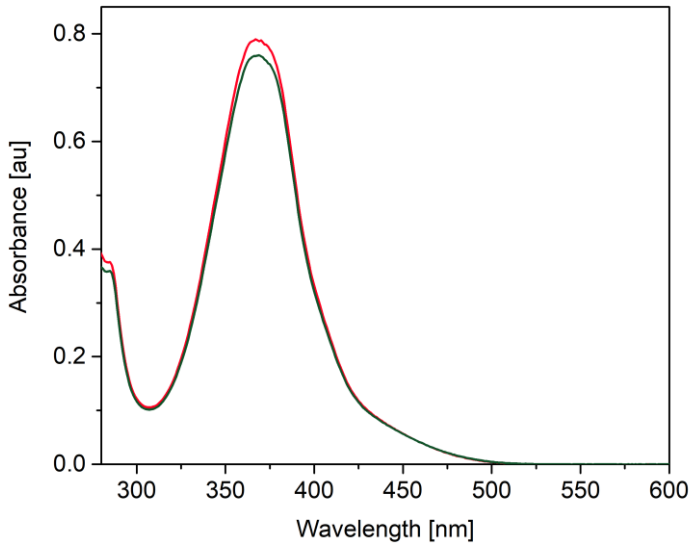

Figure A95 UV/vis of ***E*-3b** in benzene (red), and of the PSS (green) after irradiation with a 400 nm LED.

Mesitylene

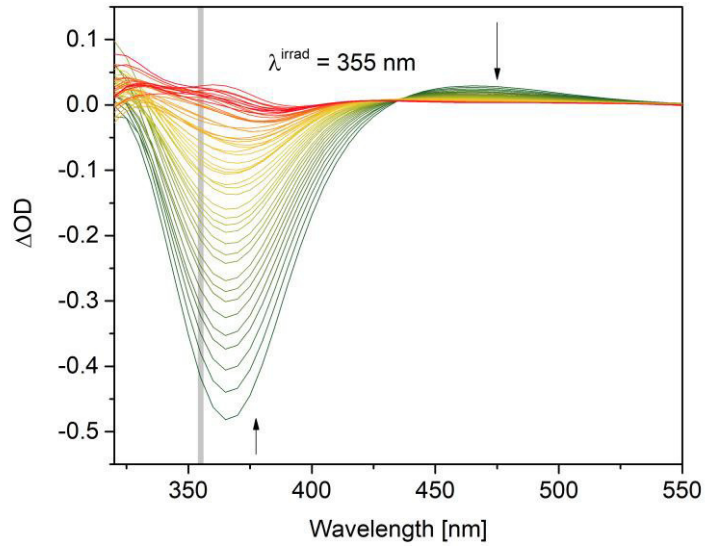

Figure A96 Transient signal map for **3b** in mesitylene.

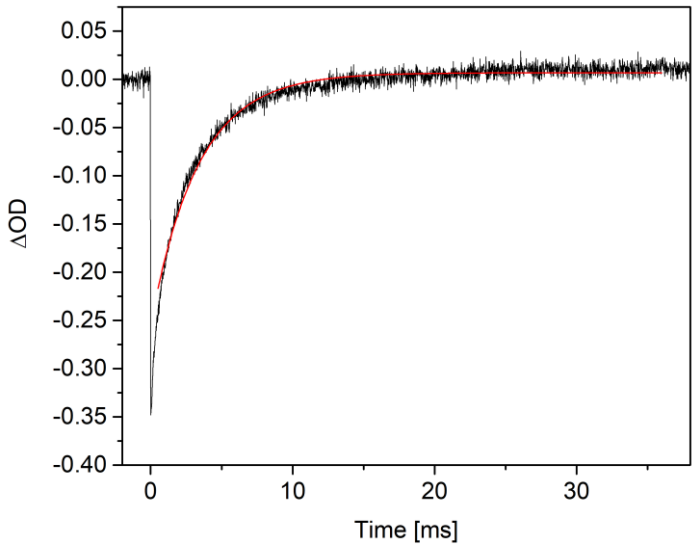

Figure A97 Transient signal detected at 365 nm for **3b** in mesitylene.

Equation	y = A1·exp(-x/τ) + y0
y0	0.00688 ± 2.02732E-4
A1	-0.261 ± 0.00142
τ	3.34546 ± 0.02511
R-Square(COD)	0.97694
Adj. R-Square	0.97691

Table A42 Fitting of the signal shown in Figure A97.

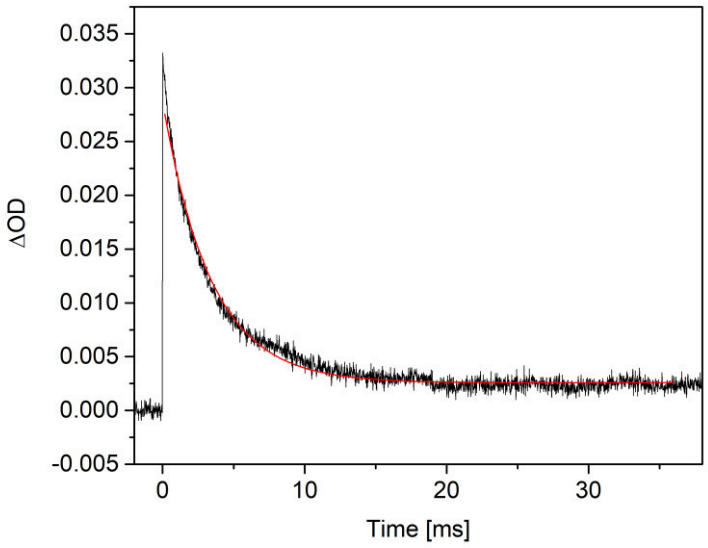

Figure A98 Transient signal detected at 465 nm for **3b** in mesitylene.

Equation	y = A1·exp(-x/τ) + y0
y0	0.00257 ± 1.9344E-5
A1	0.02614 ± 1.08164E-4
τ	3.39945 ± 0.02173
R-Square(COD)	0.98301
Adj. R-Square	0.98299

Table A43 Fitting of the signal shown in Figure A98.

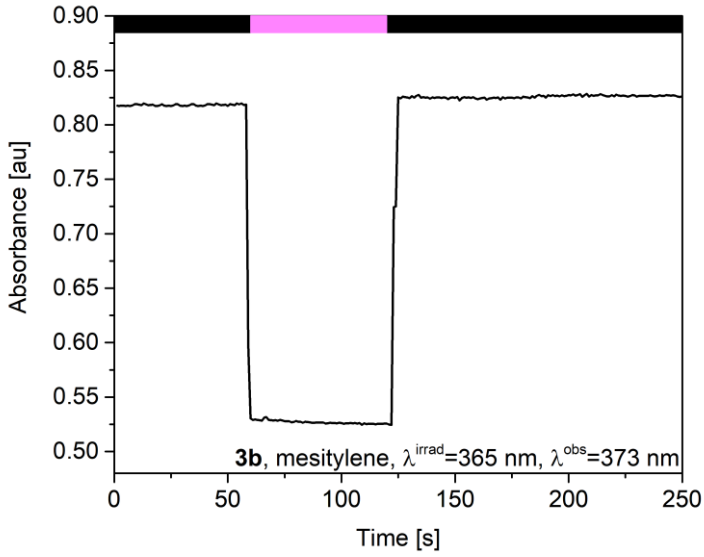

Figure A99 Absorbance variation of **3b** in mesitylene, irradiation with a 365 nm LED, λ^{obs}=373 nm.

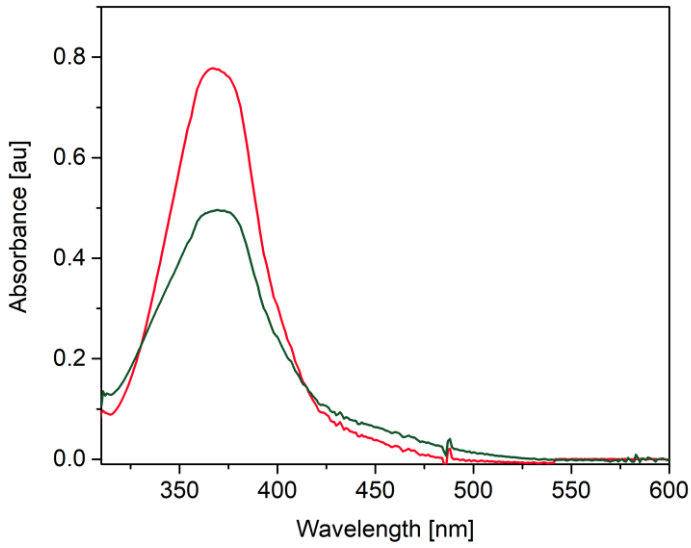

Figure A100 UV/vis of ***E*-3b** in mesitylene (red), and of the PSS (green) after irradiation with a 365 nm LED.

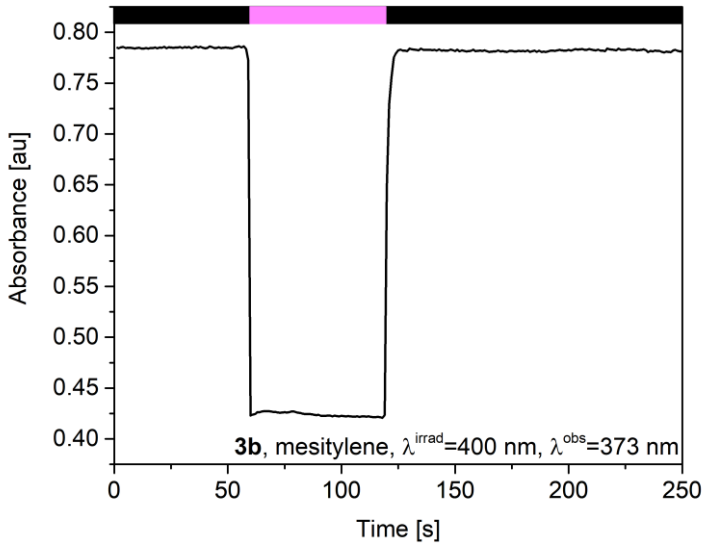

Figure A101 Absorbance variation of **3b** in mesitylene, irradiation with a 400 nm LED, λ^{obs}=373 nm.

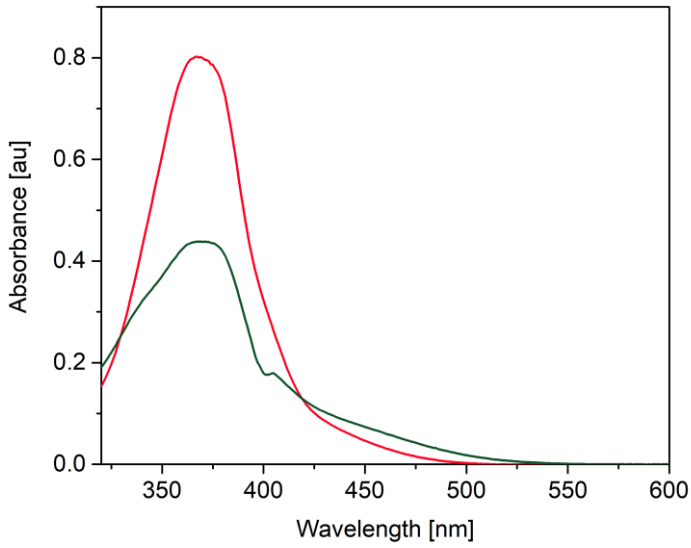

Figure A102 UV/vis of ***E*-3b** in mesitylene (red), and of the PSS (green) after irradiation with a 400 nm LED.

Toluene

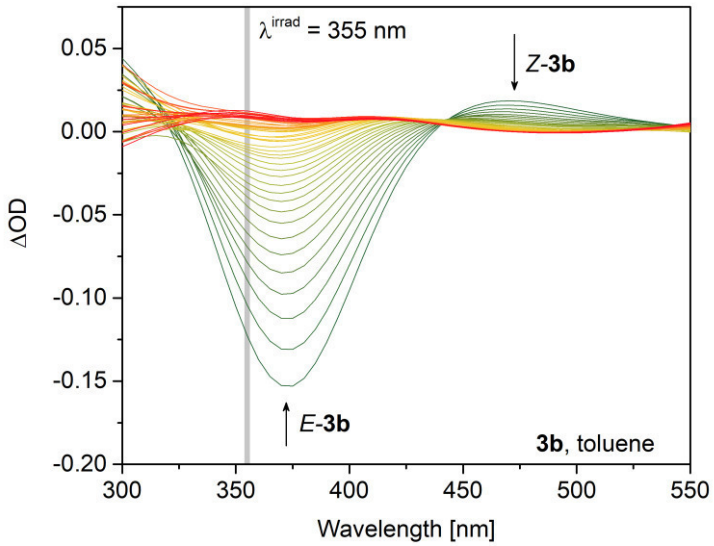

Figure A103 Transient signal map for **3b** in toluene.

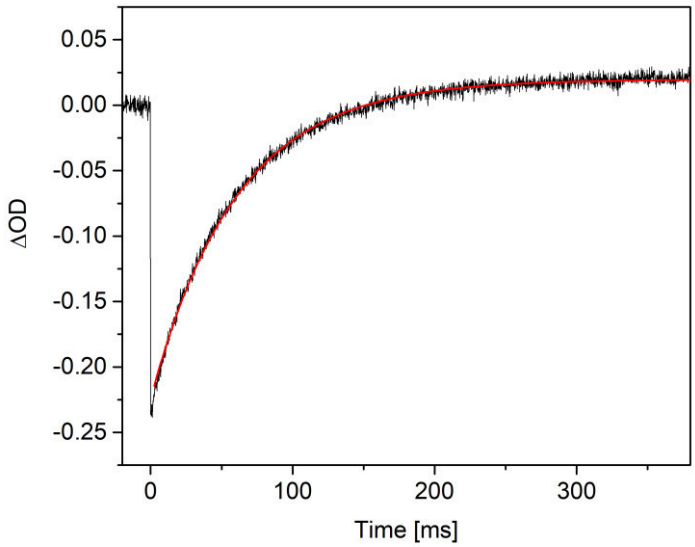

Figure A104 Transient signal detected at 370 nm for **3b** in toluene.

Equation	y = A1·exp(-x/τ) + y0
y0	0.01974 ± 1.3165E-4
A1	-0.24378 ± 4.38331E-4
τ	60.23915 ± 0.19773
R-Square(COD)	0.99588
Adj. R-Square	0.99588

Table A44 Fitting of the signal shown in Figure A104.

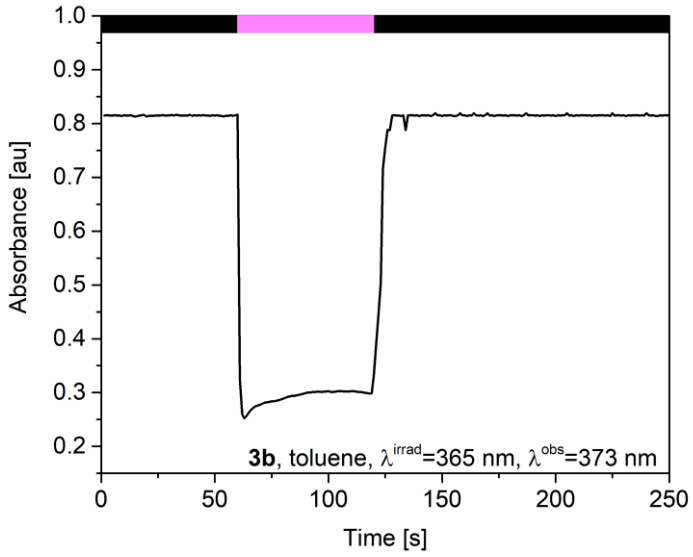

Figure A105 Absorbance variation of **3b** in toluene, irradiation with a 365 nm LED, λ^{obs}=373 nm.

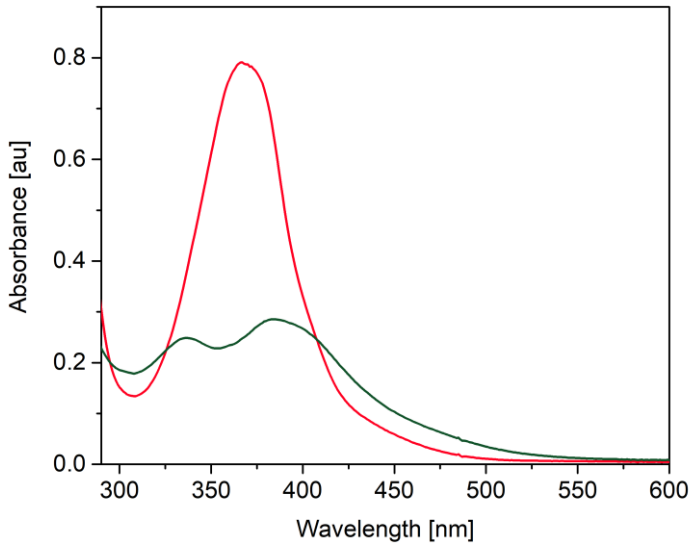

Figure A106 UV/vis of ***E*-3b** in toluene (red), and of the PSS (green) after irradiation with a 365 nm LED.

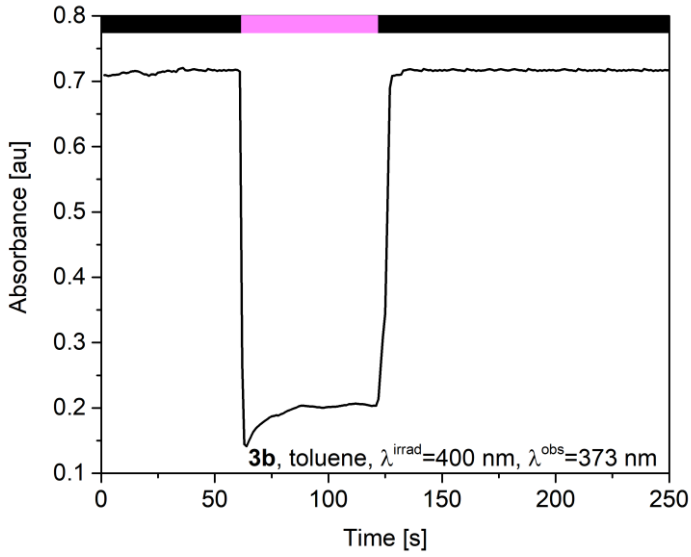

Figure A107 Absorbance variation of **3b** in toluene, irradiation with a 365 nm LED, λ^{obs}=400 nm.

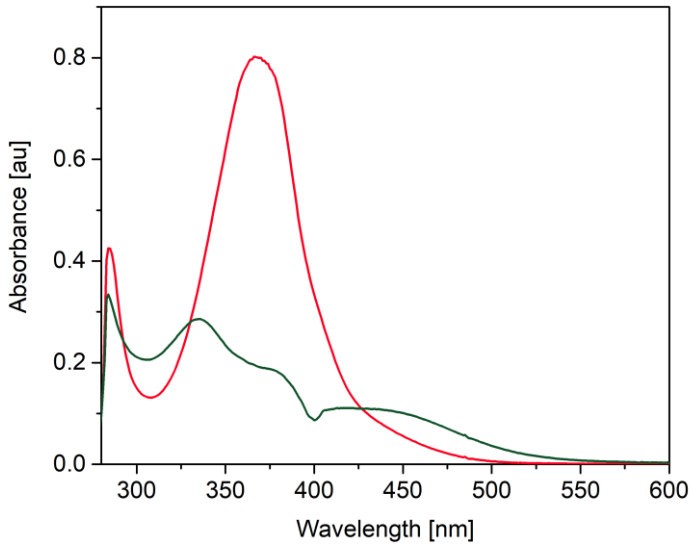

Figure A108 UV/vis of ***E*-3b** in toluene (red), and of the PSS (green) after irradiation with a 400 nm LED.

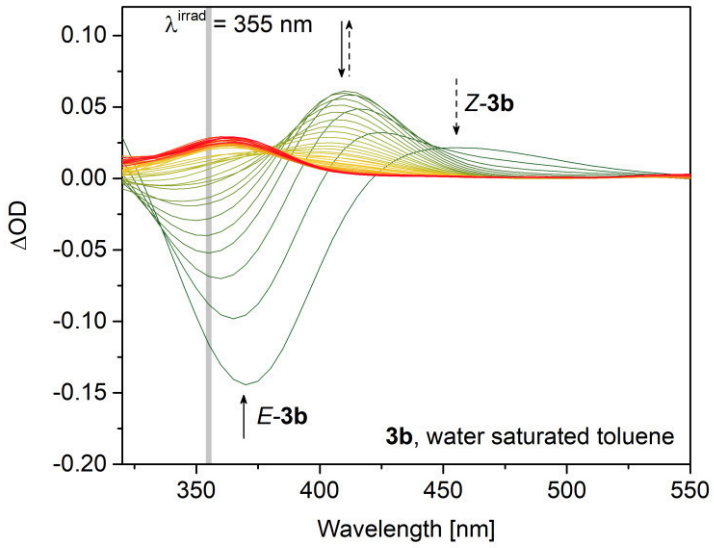

Figure A109 Transient signal map for **3b** in aqueous toluene.

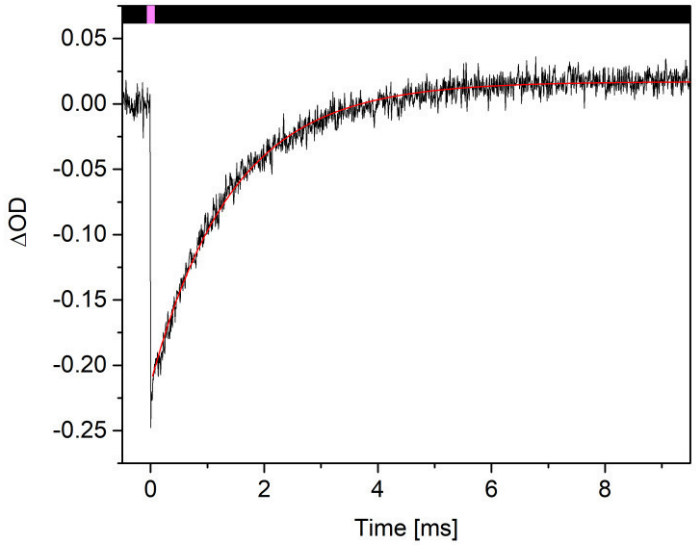

Figure A110 Transient signal detected at 370 nm for **3b** in aqueous toluene.

Equation	y = A1·exp(-x/τ) + y0
y0	0.01704 ± 3.34834E-4
A1	-0.23091 ± 0.00116
τ	1.41961 ± 0.01287
R-Square(COD)	0.96849
Adj. R-Square	0.96846

Table A45 Fitting of the signal shown in Figure A110.

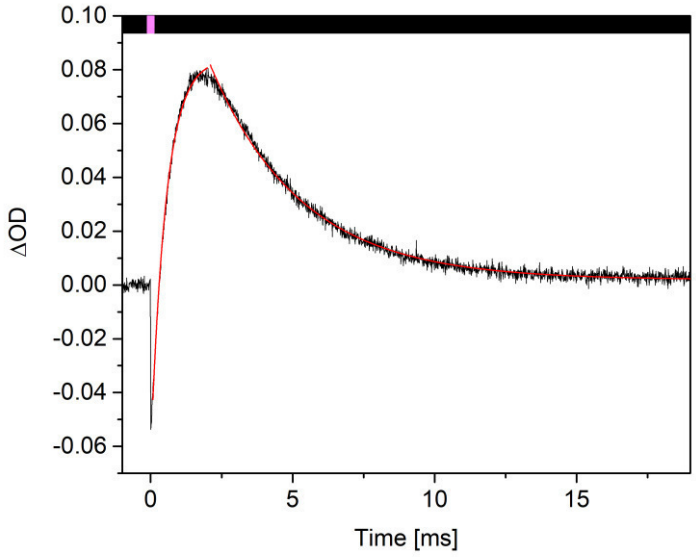

Figure A111 Transient signal detected at 410 nm for **3b** in aqueous toluene.

Equation	y = A1·exp(-x/τ) + y0
y0	0.08411 ± 4.25734E-4
A1	-0.14729 ± 7.62566E-4
τ	0.53045 ± 0.00669
R-Square(COD)	0.9961
Adj. R-Square	0.99606

Table A46 Fitting of the growth of the signal shown in Figure A111.

Equation	y = A1·exp(-x/τ) + y0
y0	0.00191 ± 7.2463E-5
A1	0.15382 ± 6.95465E-4
τ	3.20247 ± 0.01493
R-Square(COD)	0.9933
Adj. R-Square	0.9933

Table A47 Fitting of the decay of the signal shown in Figure A111.

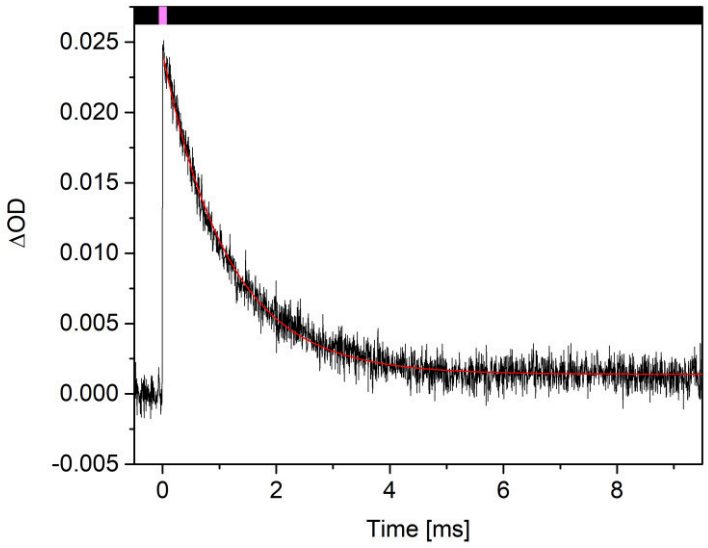

Figure A112 Transient signal detected at 455 nm for **3b** in aqueous toluene.

Equation	$y = A1 \cdot \exp(-x/\tau) + y0$
y0	0.0014 ± 2.64662E-5
A1	0.02283 ± 1.1358E-4
τ	1.14004 ± 0.00954
R-Square(COD)	0.97097
Adj. R-Square	0.97094

Table A48 Fitting of the of the signal shown in Figure A112.

MeOH

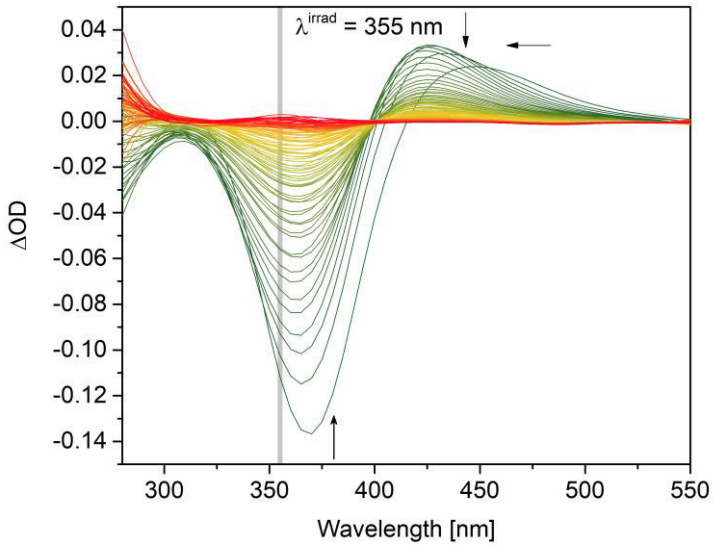

Figure A113 Transient signal map for **3b** in MeOH.

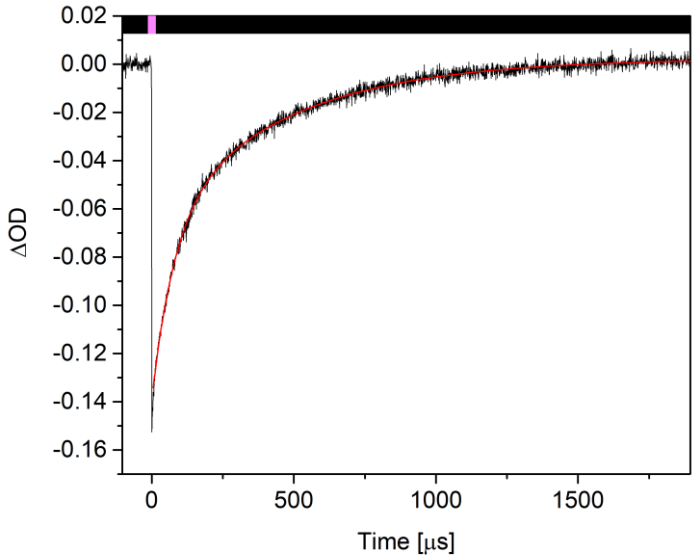

Figure A114 Transient signal detected at 370 nm for **3b** in MeOH.

Equation	y = A1·exp(-x/τ1) + A2·exp(-x/τ2) + y0
y0	0.00242 ± 1.38774E-4
A1	-0.07249 ± 8.68397E-4
τ1	78.31507 ± 1.61082
A2	-0.06936 ± 8.56456E-4
τ2	454.54435 ± 6.73901
R-Square(COD)	0.99475
Adj. R-Square	0.99474

Table A49 Fitting of the signal shown in Figure A114.

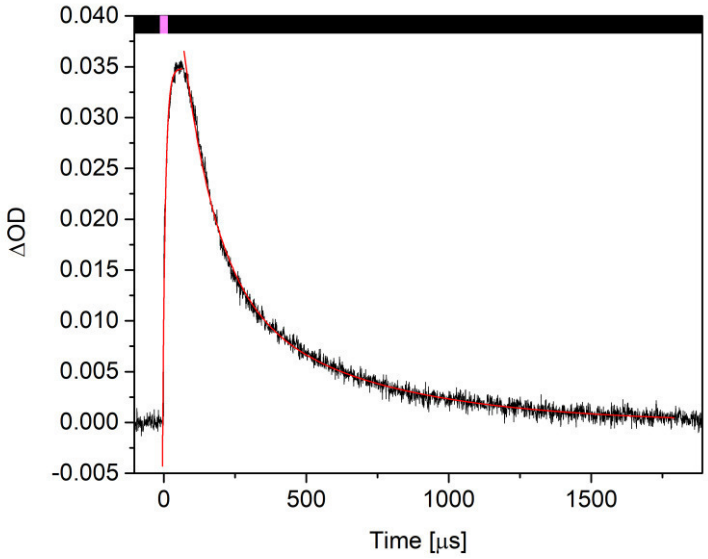

Figure A115 Transient signal detected at 435 nm for **3b** in MeOH.

Equation	y = A1·exp(-x/τ) + y0
y0	0.03483 ± 3.28579E-4
A1	-0.02337 ± 6.33304E-4
τ	9.70259 ± 0.49635
R-Square(COD)	0.96433
Adj. R-Square	0.96325

Table A50 Fitting of the growth of the signal shown in Figure A115.

Equation	y = A1·exp(-x/τ1) + A2·exp(-x/τ2) + y0
y0	-5.93471E-5 ± 8.29798E-5
A1	0.04173 ± 4.82366E-4
τ1	115.87332 ± 2.74481
A2	0.01598 ± 6.01915E-4
τ2	524.00544 ± 20.74432
R-Square(COD)	0.99388
Adj. R-Square	0.99387

Table A51 Fitting of the decay of the signal shown in Figure A115.

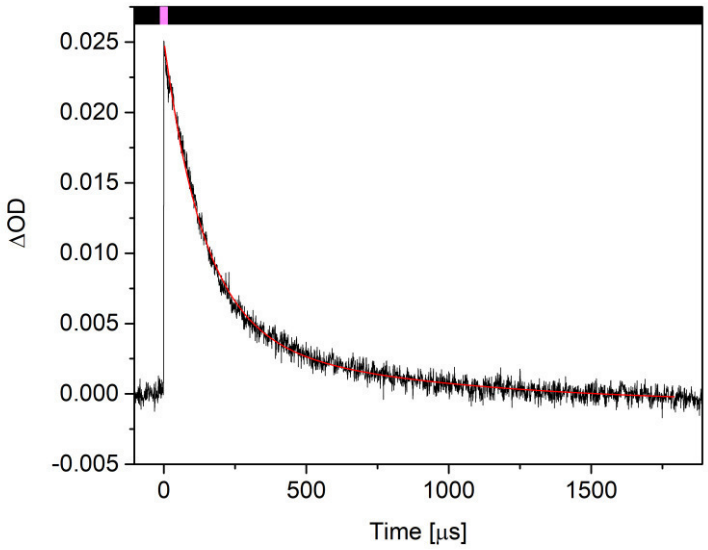

Figure A116 Transient signal detected at 465 nm for **3b** in MeOH.

Equation	y = A1·exp(-x/τ1) + A2·exp(-x/τ2) + y0
y0	-7.21337E-4 ± 1.53219E-4
A1	0.02052 ± 3.86966E-4
τ1	139.81865 ± 3.11489
A2	0.00536 ± 2.93072E-4
τ2	767.28335 ± 94.02381
R-Square(COD)	0.98905
Adj. R-Square	0.98902

Table A52 Fitting of the decay of the signal shown in Figure A116.

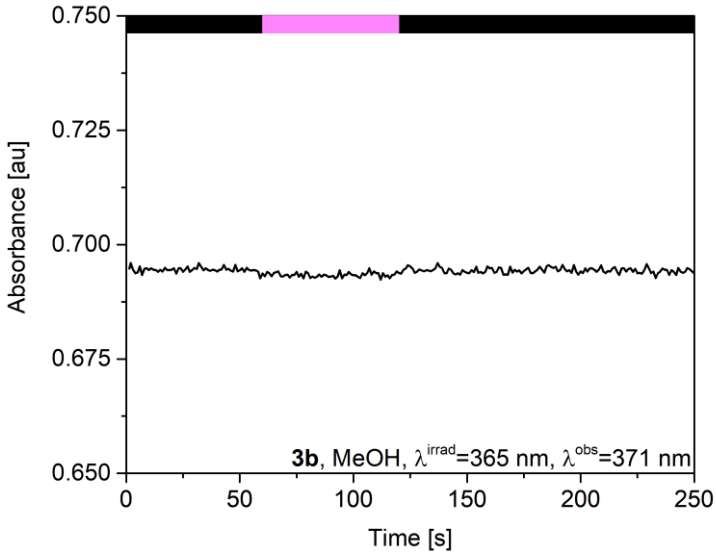

Figure A117 Absorbance variation of **3b** in MeOH, irradiation with a 365 nm LED, λ^{obs}=371 nm.

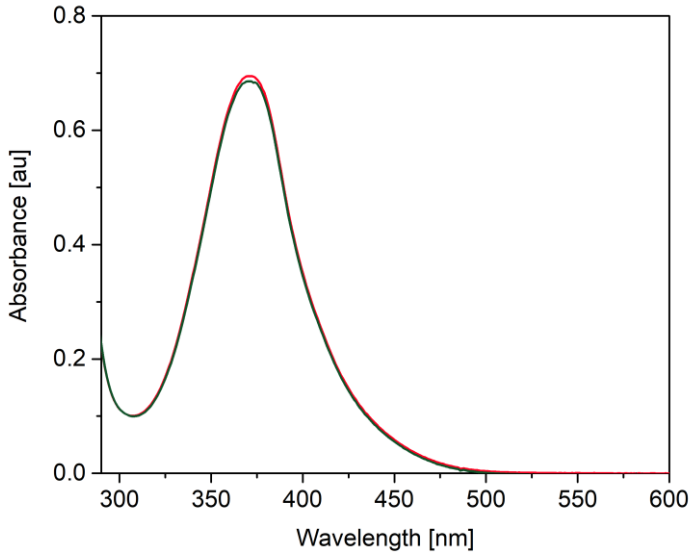

Figure A118 UV/vis of ***E*-3b** in MeOH (red), and of the PSS (green) after irradiation with a 365 nm LED.

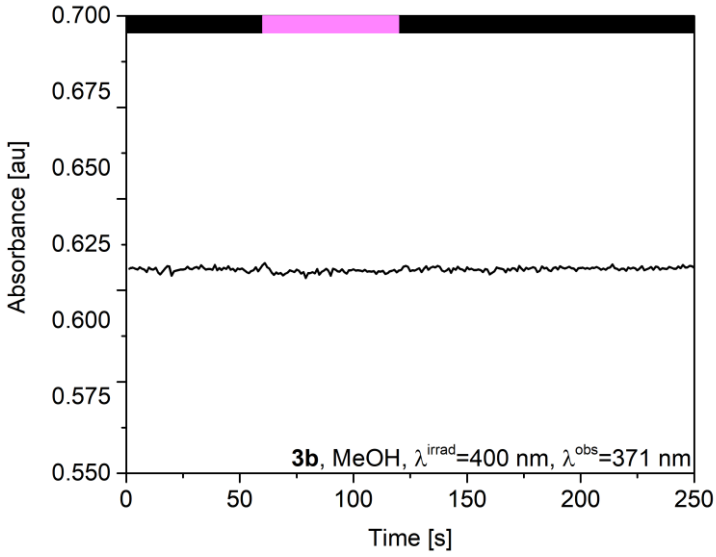

Figure A119 Absorbance variation of **3b** in MeOH, irradiation with a 400 nm LED, λ^{obs}=371 nm.

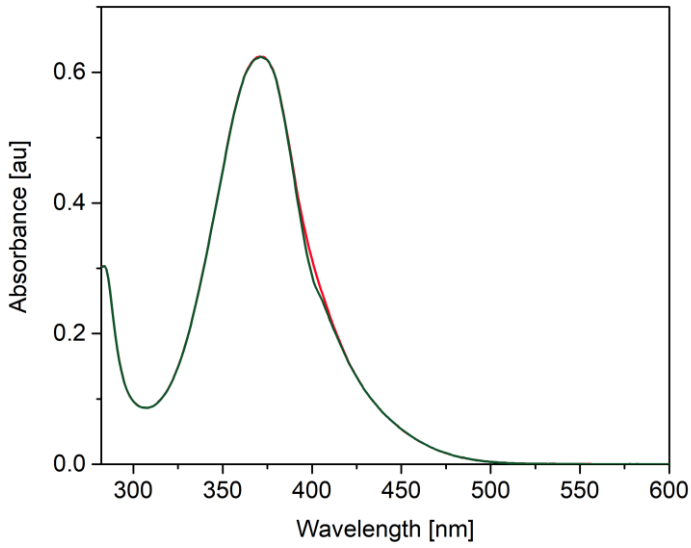

Figure A120 UV/vis of ***E*-3b** in MeOH (red), and of the PSS (green) after irradiation with a 400 nm LED.

MeOH - H_2O 9:1

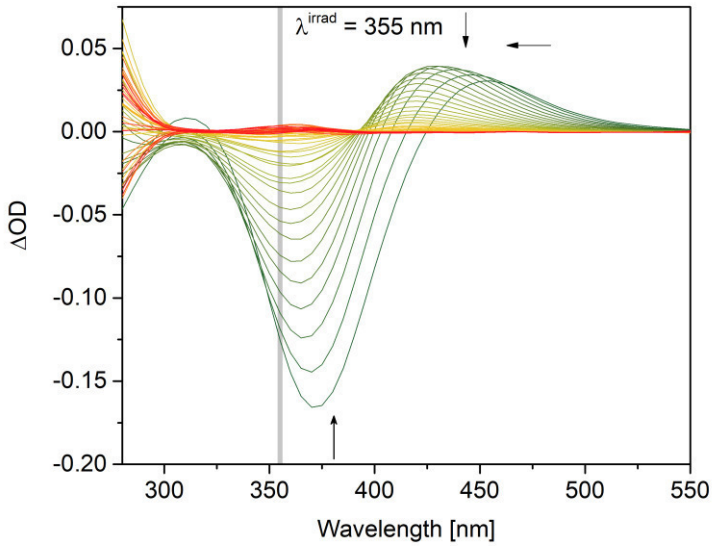

Figure A121 Transient signal map for **3b** in MeOH-H_2O 9:1.

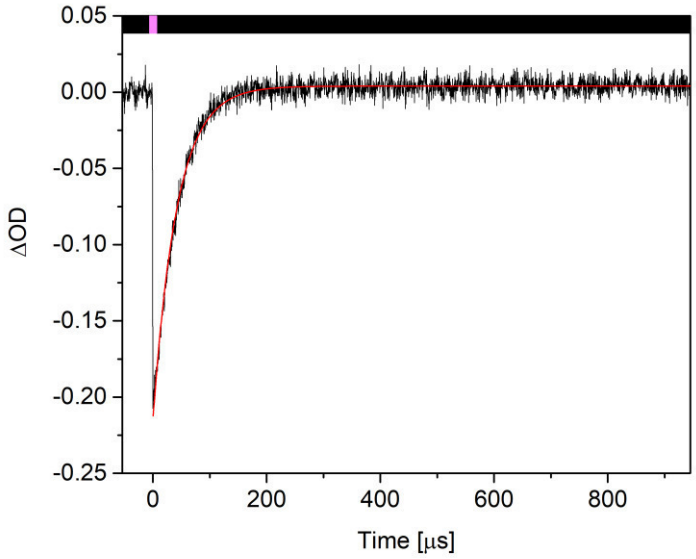

Figure A122 Transient signal detected at 370 nm for **3b** in MeOH-H_2O 9:1.

Equation	y = A1·exp(-x/τ) + y0
y0	0.00401 ± 1.28297E-4
A1	-0.21888 ± 0.00112
τ	41.85969 ± 0.31679
R-Square(COD)	0.97392
Adj. R-Square	0.97389

Table A53 Fitting of the signal shown in Figure A122.

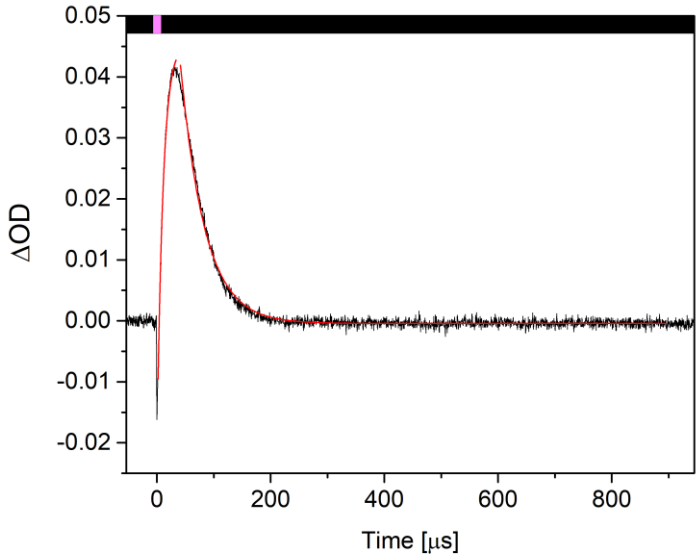

Figure A123 Transient signal detected at 420 nm for **3b** in MeOH-H_2O 9:1.

Equation	y = A1·exp(-x/τ) + y0
y0	0.04546 ± 4.00564E-4
A1	-0.06655 ± 5.48822E-4
τ	10.47096 ± 0.24499
R-Square(COD)	0.99649
Adj. R-Square	0.99637

Table A54 Fitting of the growth of the signal shown in Figure A123.

Equation	y = A1·exp(-x/τ) + y0
y0	-4.33514E-4 ± 1.81469E-5
A1	0.11198 ± 8.56481E-4
τ	42.68898 ± 0.21829
R-Square(COD)	0.98911
Adj. R-Square	0.98909

Table A55 Fitting of the decay of the signal shown in Figure A123.

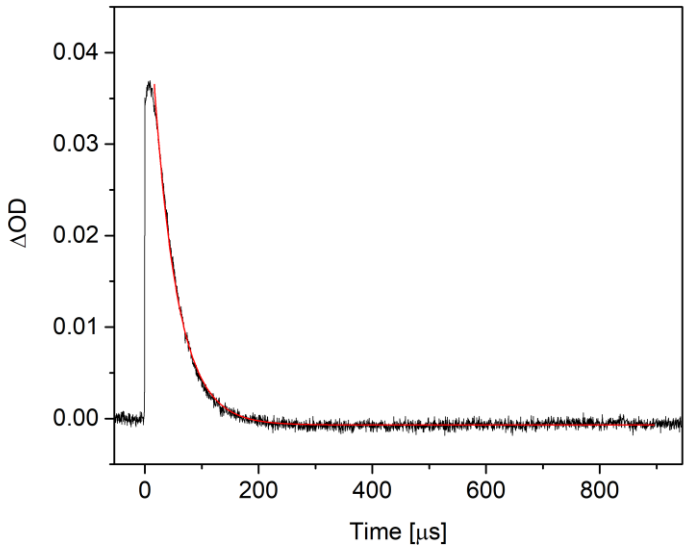

Figure A124 Transient signal detected at 450 nm for **3b** in MeOH-H_2O 9:1.

Equation	y = A1·exp(-x/τ) + y0
y0	-7.0269E-4 ± 1.15272E-5
A1	0.05532 ± 2.0506E-4
τ	41.6676 ± 0.15854
R-Square(COD)	0.99375
Adj. R-Square	0.99375

Table A56 Fitting of the growth of the signal shown in Figure A124.

MeOH - H_2O 1:1

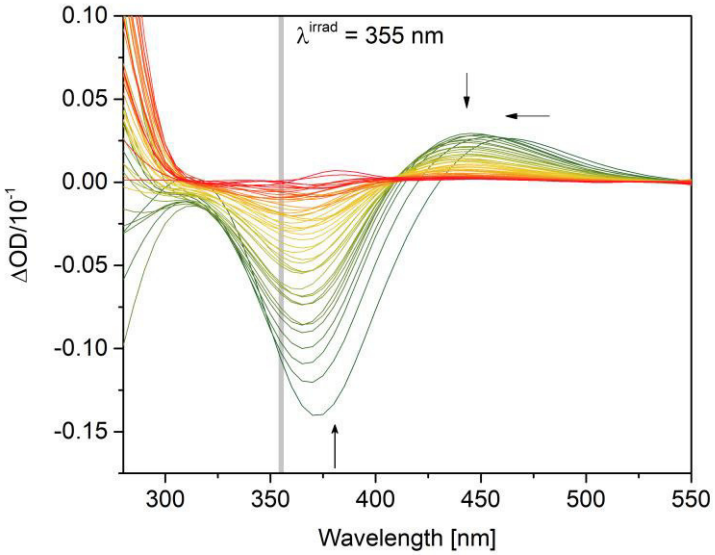

Figure A125 Transient signal map for **3b** in MeOH-H_2O 1:1.

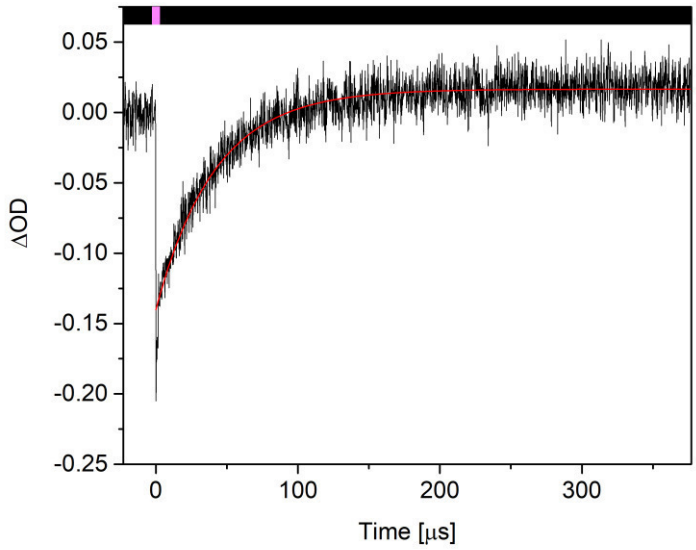

Figure A126 Transient signal detected at 370 nm for **3b** in MeOH-H_2O 1:1.

Equation	y = A1·exp(-x/τ) + y0
y0	0.01659 ± 3.55252E-4
A1	-0.15671 ± 0.0016
τ	41.41825 ± 0.70536
R-Square(COD)	0.88842
Adj. R-Square	0.8883

Table A57 Fitting of the signal shown in Figure A126.

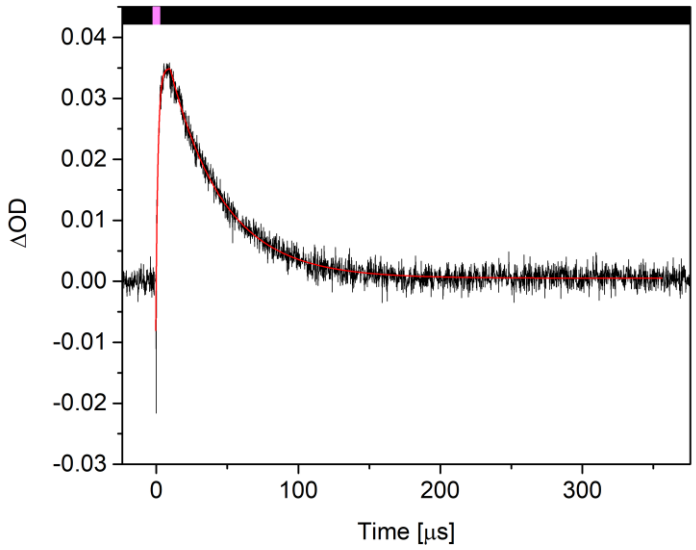

Figure A127 Transient signal detected at 440 nm for **3b** in MeOH-H_2O 1:1.

Equation	y = A1·exp(-x/τ) + y0
y0	0.03495 ± 8.83047E-4
A1	-0.03306 ± 0.00176
τ	1.52324 ± 0.17794
R-Square(COD)	0.88297
Adj. R-Square	0.87799

Table A58 Fitting of the growth of the signal shown in Figure A127.

Equation	y = A1·exp(-x/τ) + y0
y0	5.13411E-4 ± 4.23198E-5
A1	0.04459 ± 3.31698E-4
τ	37.44588 ± 0.35261
R-Square(COD)	0.96575
Adj. R-Square	0.96572

Table A59 Fitting of the decay of the signal shown in Figure A127.

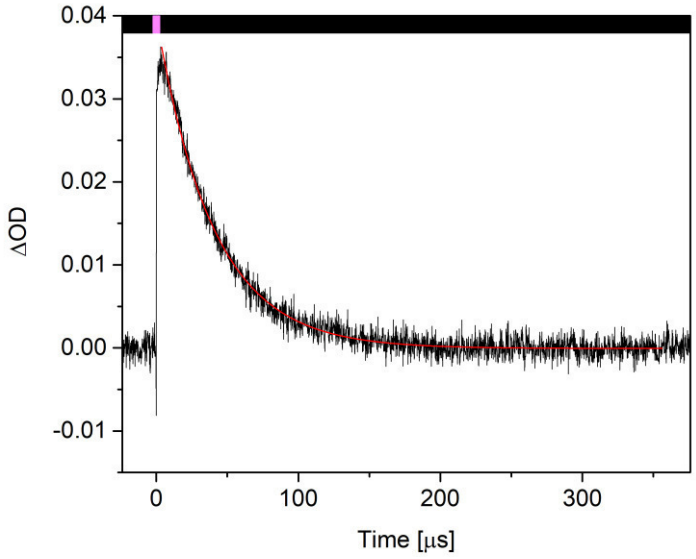

Figure A128 Transient signal detected at 450 nm for **3b** in MeOH-H_2O 1:1.

Equation	y = A1·exp(-x/τ) + y0
y0	-6.33017E-5 ± 3.54999E-5
A1	0.03991 ± 1.891E-4
τ	39.81169 ± 0.28785
R-Square(COD)	0.97935
Adj. R-Square	0.97932

Table A60 Fitting of the signal shown in Figure A128

MeOH - buffered H_2O (pH=4) 1:1

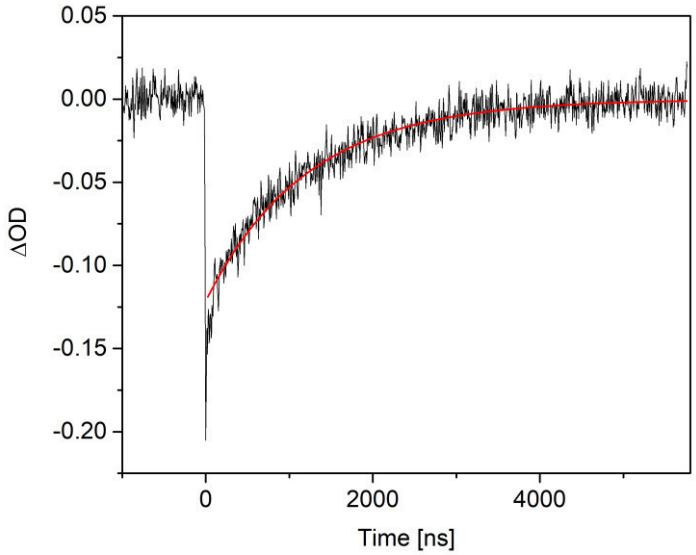

Figure A129 Transient signal detected at 370 nm for **3b** in MeOH-buffered H_2O (pH=4) 1:1.

Equation	$y = A1 \cdot \exp(-x/\tau) + y0$
y0	-6.33017E-5 ± 3.54999E-5
A1	0.03991 ± 1.891E-4
τ	39.81169 ± 0.28785
R-Square(COD)	0.97935
Adj. R-Square	0.97932

Table A61 Fitting of the signal shown in Figure A129.

MeOH - H_2O 1:2

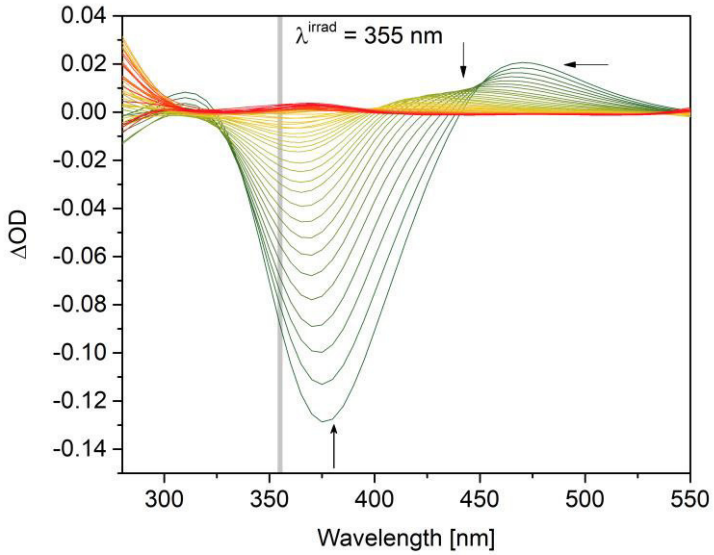

Figure A130 Transient signal map for **3b** in MeOH-H_2O 1:2.

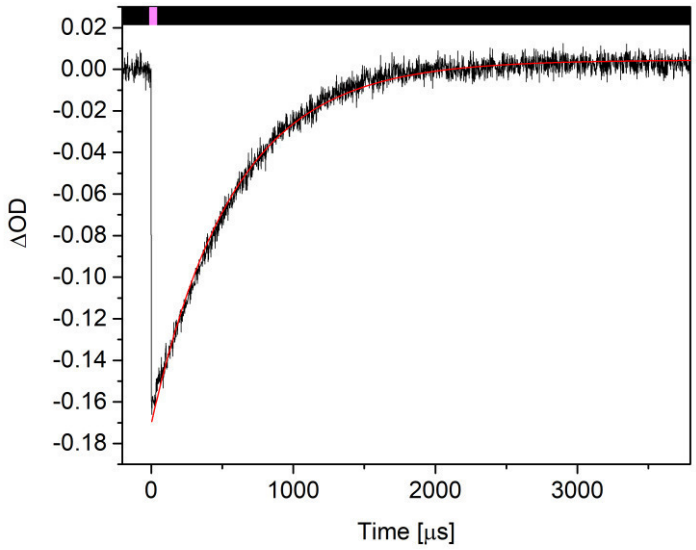

Figure A131 Transient signal detected at 375 nm for **3b** in MeOH-H_2O 1:2.

Equation	y = A1·exp(-x/τ) + y0
y0	0.00447 ± 1.36646E-4
A1	-0.17507 ± 4.52332E-4
τ	574.43952 ± 2.7365
R-Square(COD)	0.99112
Adj. R-Square	0.99111

Table A62 Fitting of the signal shown in Figure A131.

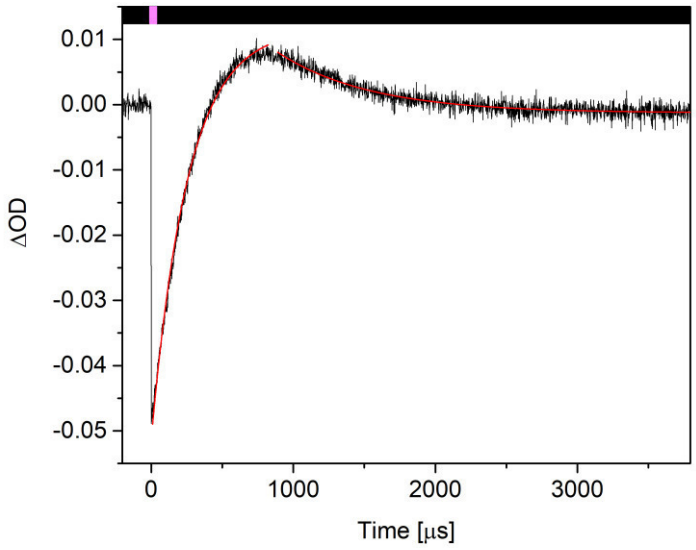

Figure A132 Transient signal detected at 420 nm for **3b** in MeOH-H_2O 1:2.

Equation	y = A1·exp(-x/τ) + y0
y0	0.01168 ± 1.84683E-4
A1	-0.06305 ± 2.1826E-4
τ	255.41296 ± 2.63815
R-Square(COD)	0.99521
Adj. R-Square	0.99519

Table A63 Fitting of the growth of the signal shown in Figure A132.

Equation	y = A1·exp(-x/τ) + y0
y0	-0.00126 ± 5.35427E-5
A1	0.03657 ± 0.00149
τ	650.26317 ± 16.84683
R-Square(COD)	0.86425
Adj. R-Square	0.86407

Table A64 Fitting of the decay of the signal shown in Figure A132.

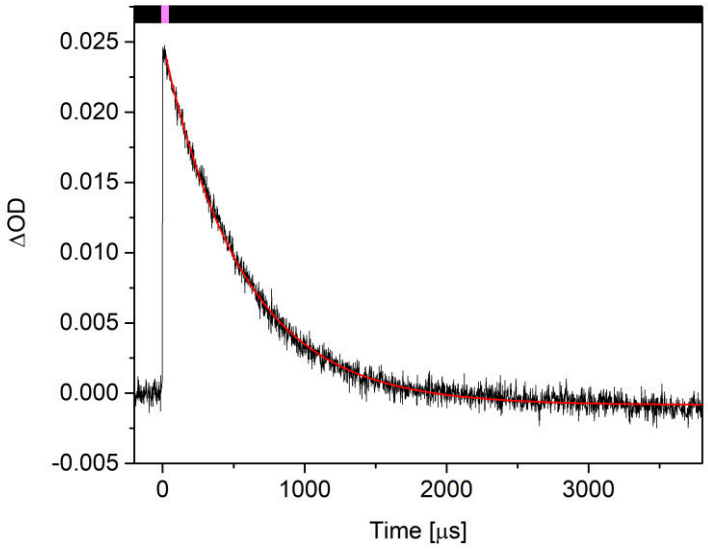

Figure A133 Transient signal detected at 470 nm for **3b** in MeOH-H_2O 1:2.

Equation	y = A1·exp(-x/τ) + y0
y0	-8.44099E-4 ± 1.95972E-5
A1	0.02581 ± 7.12636E-5
τ	560.58025 ± 2.72926
R-Square(COD)	0.9907
Adj. R-Square	0.99069

Table A65 Fitting of the signal shown in Figure A133.

MeCN

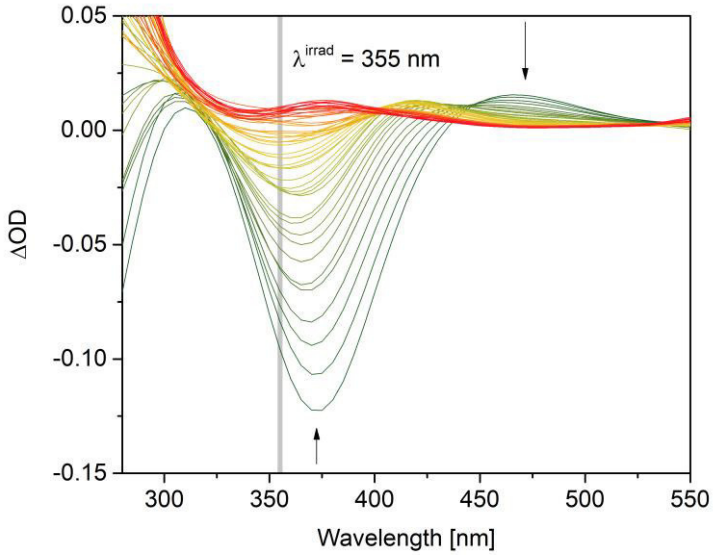

Figure A134 Transient signal map for **3b** in MeCN.

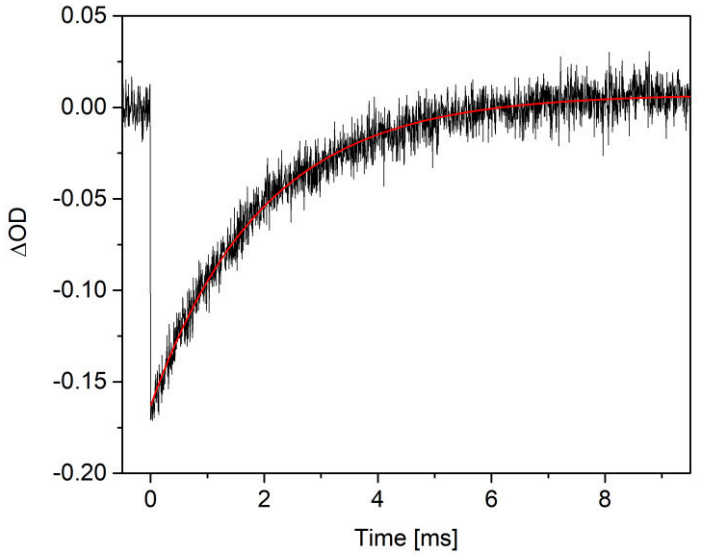

Figure A135 Transient signal detected at 370 nm for **3b** in MeCN.

Equation	y = A1·exp(-x/τ) + y0
y0	0.0073 ± 3.81747E-4
A1	-0.17039 ± 8.34589E-4
τ	1.96155 ± 0.02115
R-Square(COD)	0.9634
Adj. R-Square	0.96336

Table A66 Fitting of the signal shown in Figure A135.

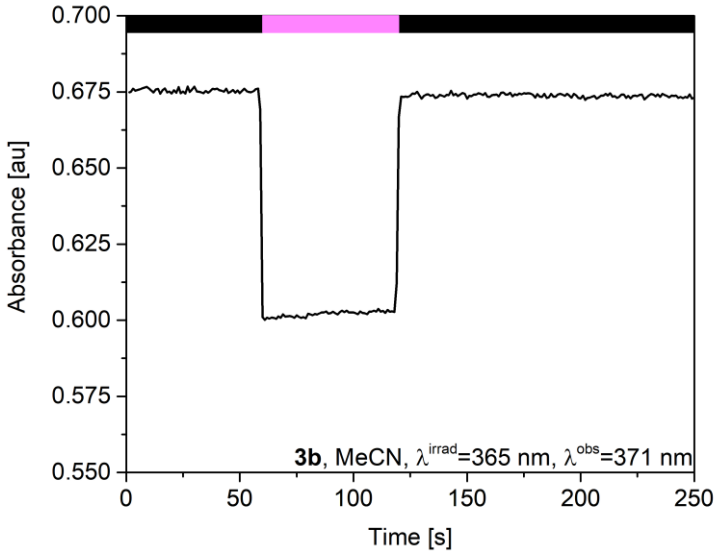

Figure A136 Absorbance variation of **3b** in MeCN, irradiation with a 365 nm LED, λ^{obs}=371 nm.

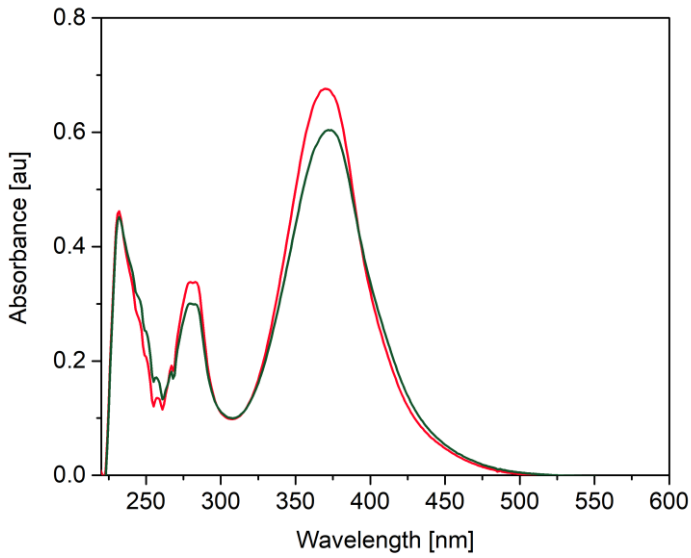

Figure A137 UV/vis of ***E*-3b** in MeCN (red), and of the PSS (green) after irradiation with a 365 nm LED.

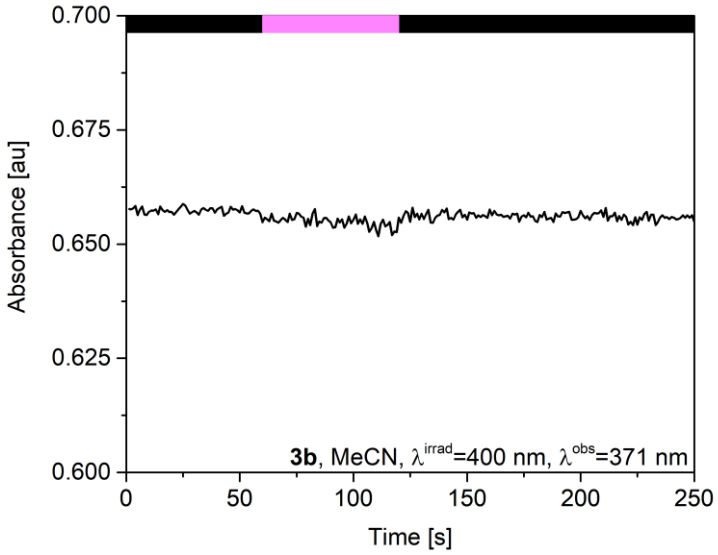

Figure A138 Absorbance variation of **3b** in MeCN, irradiation with a 400 nm LED, λ^{obs}=371 nm.

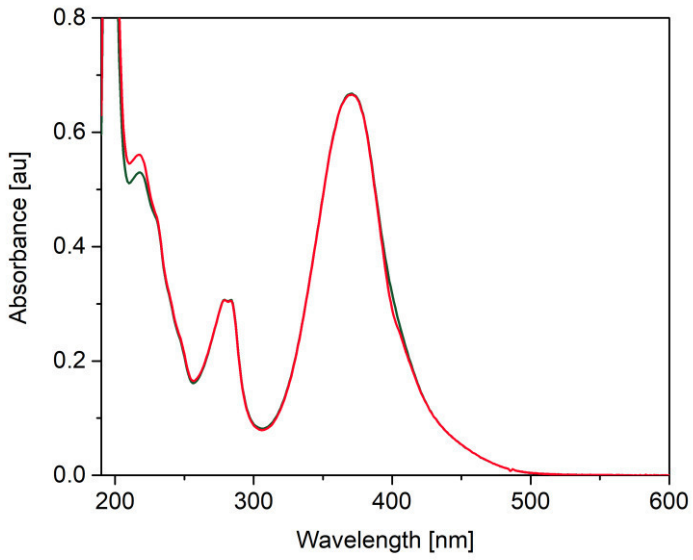

Figure A139 UV/vis of ***E*-3b** in MeCN (red), and of the PSS (green) after irradiation with a 400 nm LED.

MeCN-H_2O 95:5

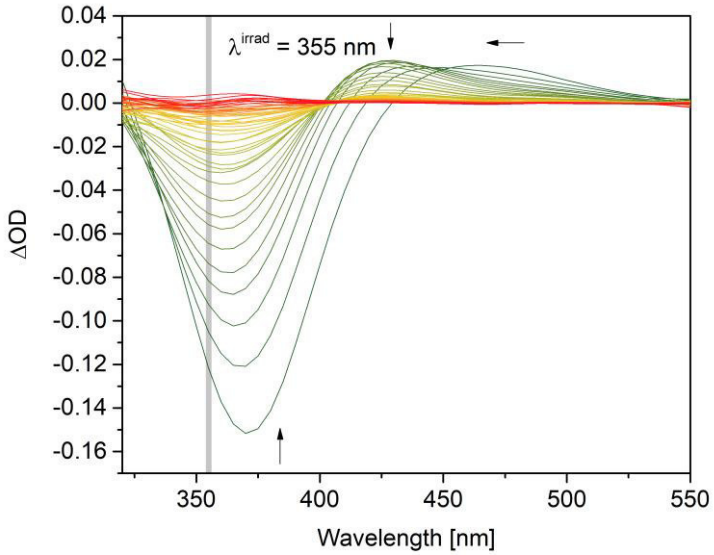

Figure A140 Transient signal map for **3b** in MeCN-H_2O 95:5.

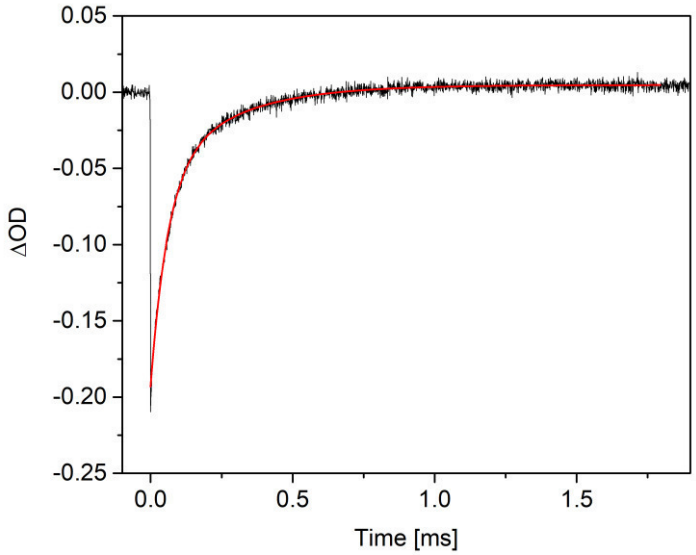

Figure A141 Transient signal detected at 370 nm for **3b** in MeCN-H_2O 95:5.

Equation	y = A1·exp(-x/τ1) + A2·exp(-x/τ2) + y0
y0	0.00469 ± 1.07451E-4
A1	-0.1352 ± 0.00196
τ1	0.05929 ± 0.00114
A2	-0.0627 ± 0.00208
τ2	0.25631 ± 0.00644
R-Square(COD)	0.99253
Adj. R-Square	0.99252

Table A67 Fitting of the signal shown in Figure A141.

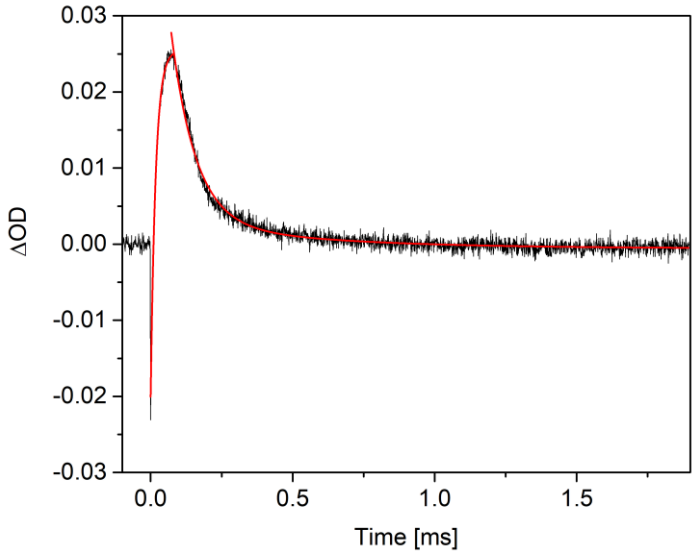

Figure A142 Transient signal detected at 420 nm for **3b** in MeCN-H_2O 95:5.

Equation	y = A1·exp(-x/τ) + y0
y0	0.02548 ± 1.98674E-4
A1	-0.04554 ± 3.83935E-4
τ	0.01755 ± 3.44587E-4
R-Square(COD)	0.99504
Adj. R-Square	0.99491

Table A68 Fitting of the growth of the signal shown in Figure A142.

Equation	y = A1·exp(-x/τ1) + A2·exp(-x/τ2) + y0
y0	-5.73982E-4 ± 7.4209E-5
A1	0.05851 ± 8.69393E-4
τ1	0.08532 ± 0.00195
A2	0.00405 ± 4.60652E-4
τ2	0.50412 ± 0.0673
R-Square(COD)	0.97176
Adj. R-Square	0.9717

Table A69 Fitting of the decay of the signal shown in Figure A142.

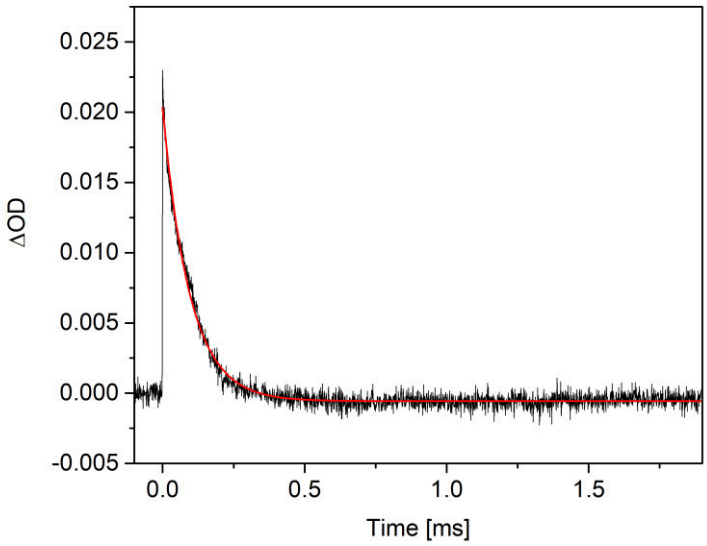

Figure A143 Transient signal detected at 460 nm for **3b** in MeCN-H_2O 95:5.

Equation	y = A1·exp(-x/τ) + y0
y0	-5.65393E-4 ± 1.27278E-5
A1	0.0209 ± 1.00631E-4
τ	0.09499 ± 6.89737E-4
R-Square(COD)	0.97595
Adj. R-Square	0.97593

Table A70 Fitting of the signal shown in Figure A143.

MeCN - H_2O 9:1

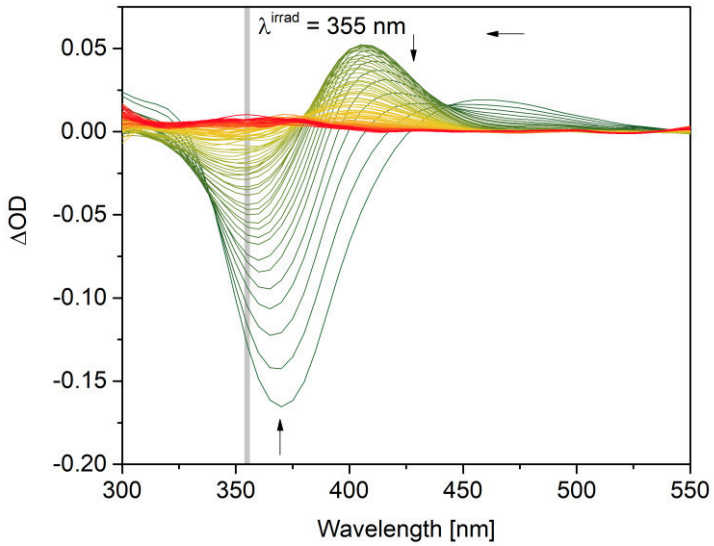

Figure A144 Transient signal map for **3b** in MeCN-H_2O 9:1.

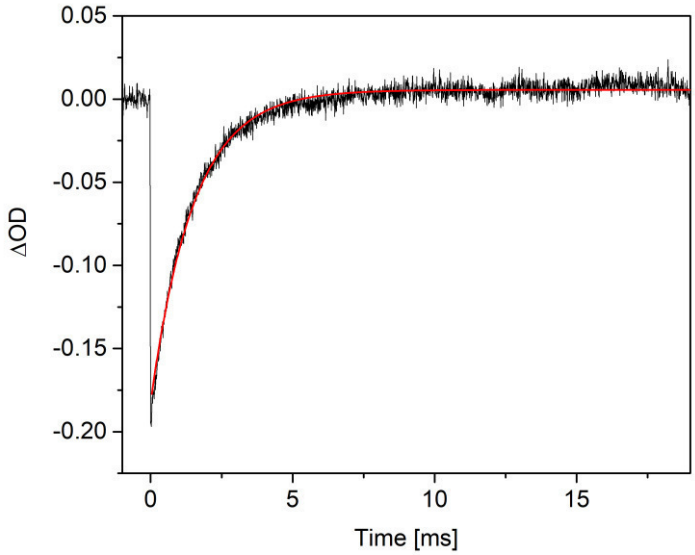

Figure A145 Transient signal detected at 370 nm for **3b** in MeCN-H_2O 9:1.

Equation	y = A1·exp(-x/τ) + y0
y0	0.00554 ± 1.24868E-4
A1	-0.18787 ± 7.66967E-4
τ	1.505 ± 0.00942
R-Square(COD)	0.98243
Adj. R-Square	0.98241

Table A71 Fitting of the signal shown in Figure A145.

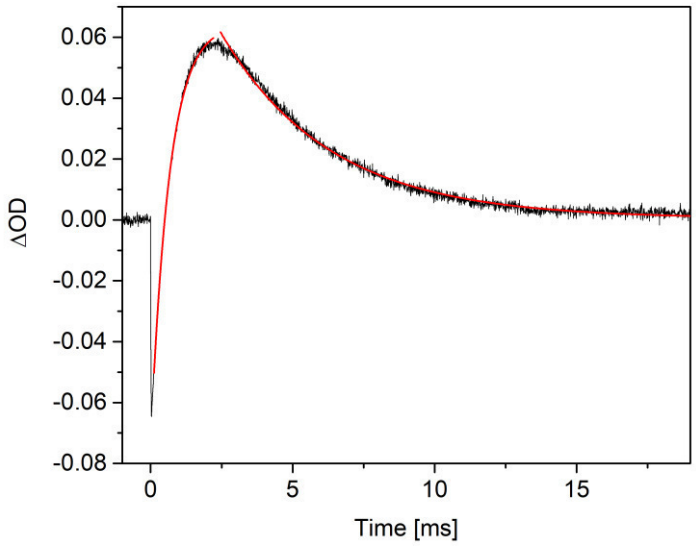

Figure A146 Transient signal detected at 405 nm for **3b** in MeCN-H_2O 9:1.

Equation	y = A1·exp(-x/τ) + y0
y0	0.06436 ± 3.26054E-4
A1	-0.13786 ± 5.09923E-4
τ	0.64932 ± 0.00632
R-Square(COD)	0.99778
Adj. R-Square	0.99775

Table A72 Fitting of the growth of the signal shown in Figure A146.

Equation	y = A1·exp(-x/τ) + y0
y0	4.69351E-4 ± 7.47029E-5
A1	0.11606 ± 5.36968E-4
τ	3.84483 ± 0.02049
R-Square(COD)	1.75246E-6
Adj. R-Square	0.99273

Table A73 Fitting of the decay of the signal shown in Figure A146.

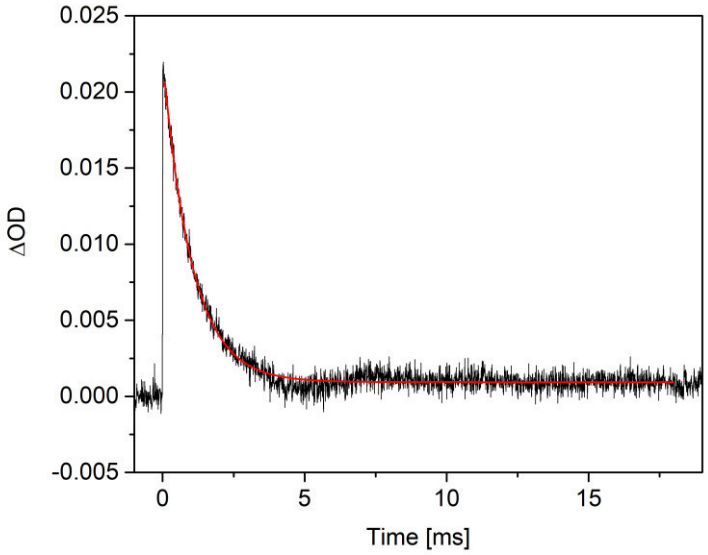

Figure A147 Transient signal detected at 460 nm for **3b** in MeCN-H_2O 9:1.

Equation	y = A1·exp(-x/τ) + y0
y0	9.3751E-4 ± 1.52177E-5
A1	0.02132 ± 1.29487E-4
τ	1.02444 ± 0.00876
R-Square(COD)	0.96886
Adj. R-Square	0.96882

Table A74 Fitting of the signal shown in Figure A147.

DMSO

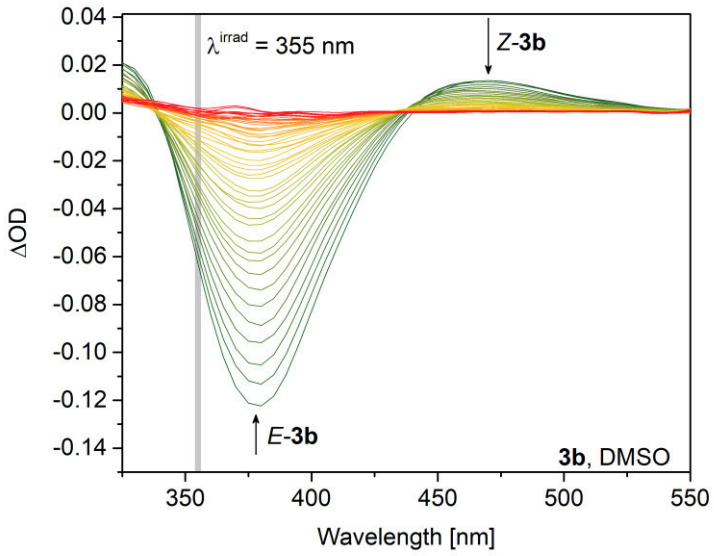

Figure A148 Transient signal map for **3b** in DMSO.

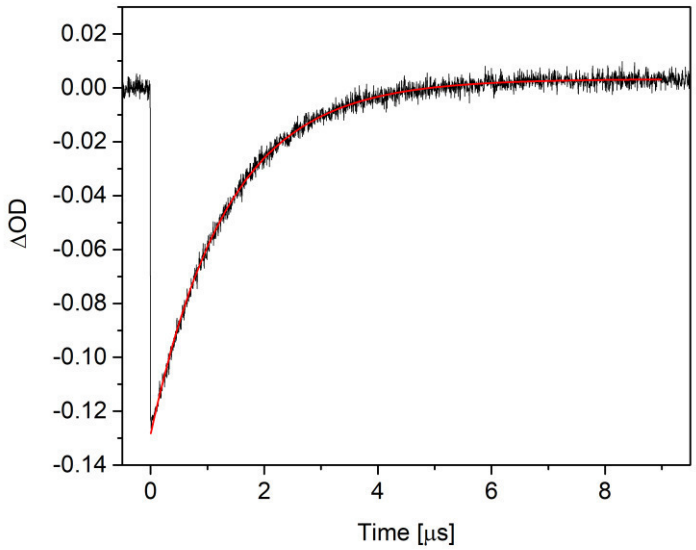

Figure A149 Transient signal detected at 380 nm for **3b** in DMSO.

Equation	y = A1·exp(-x/τ) + y0
y0	0.00327 ± 7.73427E-5
A1	-0.13205 ± 2.6093E-4
τ	1.33139 ± 0.00482
R-Square(COD)	0.99507
Adj. R-Square	0.99506

Table A75 Fitting of the signal shown in Figure A149.

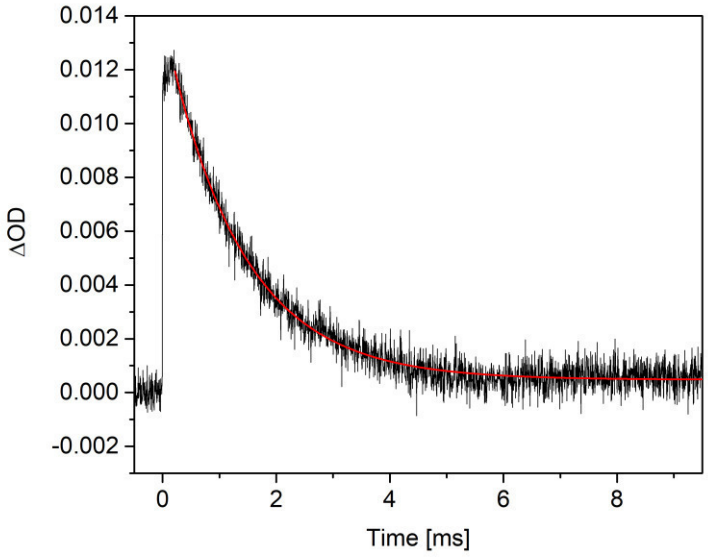

Figure A150 Transient signal detected at 465 nm for **3b** in DMSO.

Equation	y = A1·exp(-x/τ) + y0
y0	4.79046E-4 ± 1.67091E-5
A1	0.01347 ± 7.9873E-5
τ	1.34164 ± 0.01223
R-Square(COD)	0.96827
Adj. R-Square	0.96824

Table A76 Fitting of the signal shown in Figure A150.

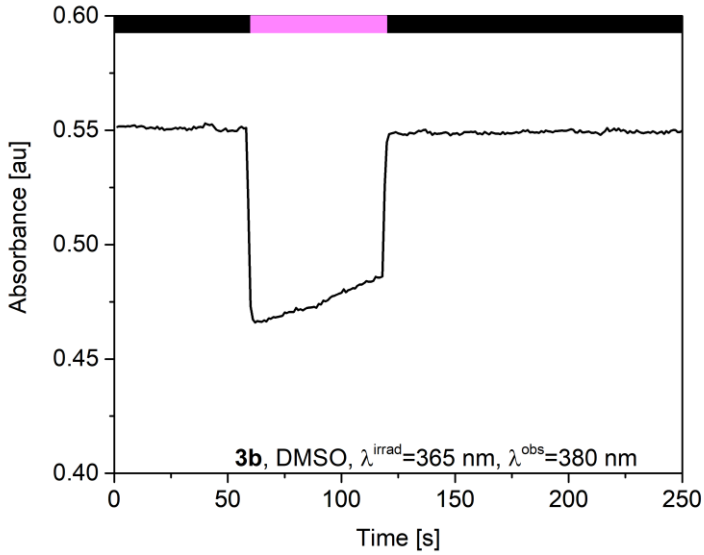

Figure A151 Absorbance variation of **3b** in DMSO, irradiation with a 365 nm LED, λ^{obs}=380 nm.

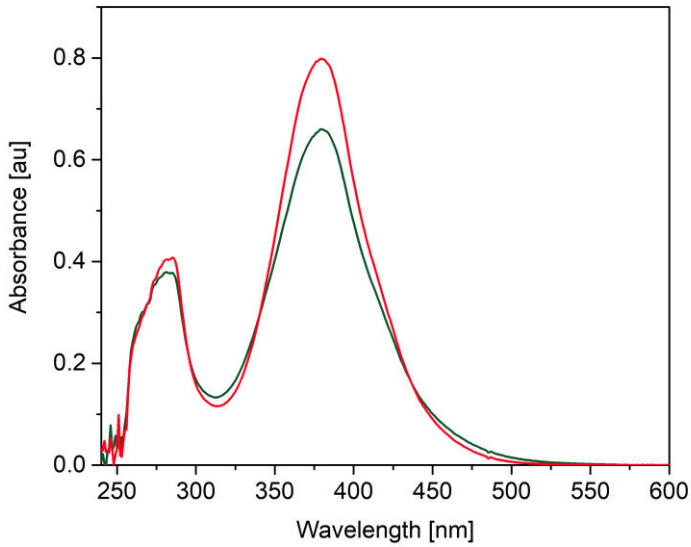

Figure A152 UV/vis of ***E*-3b** in DMSO (red), and of the PSS (green) after irradiation with a 365 nm LED.

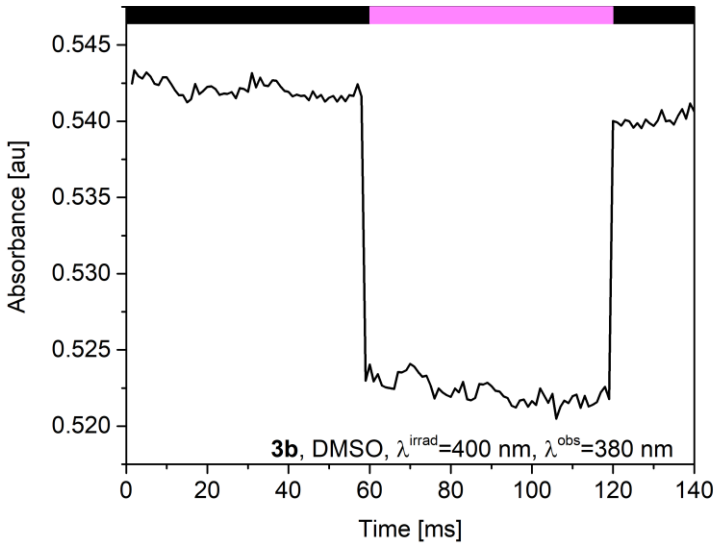

Figure A153 Absorbance variation of **3b** in DMSO, irradiation with a 400 nm LED, λ^{obs}=380 nm.

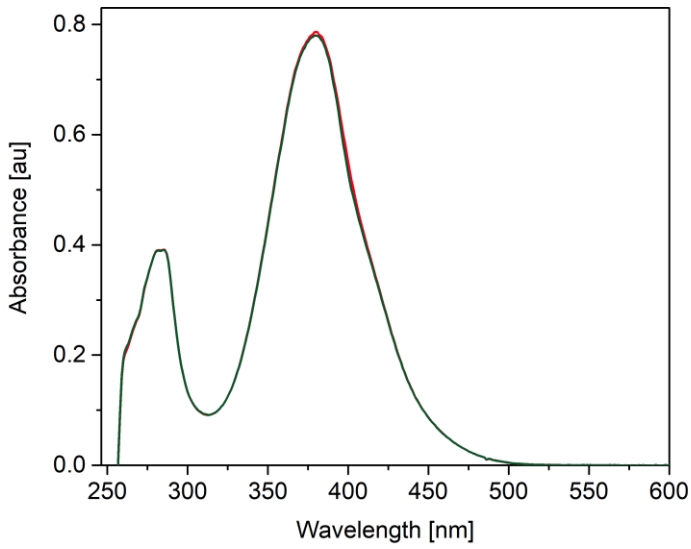

Figure A154 UV/vis of ***E*-3b** in DMSO (red), and of the PSS (green) after irradiation with a 400 nm LED.

DMSO - H_2O 9:1

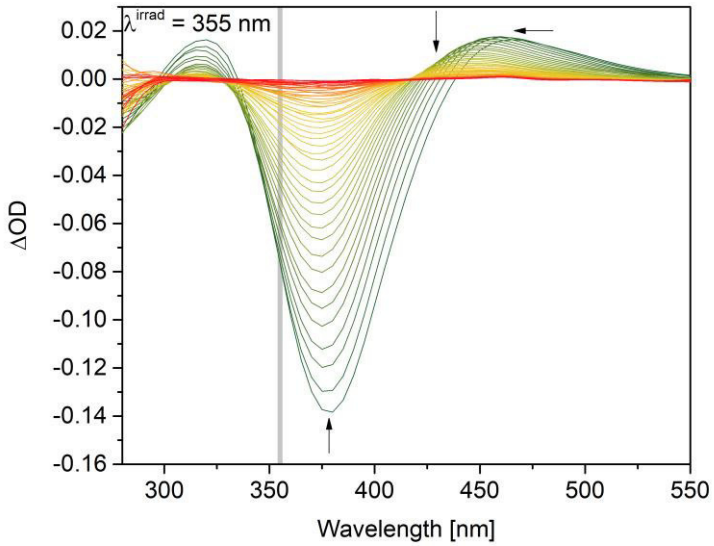

Figure A155 Transient signal map for **3b** in DMSO-H_2O 9:1.

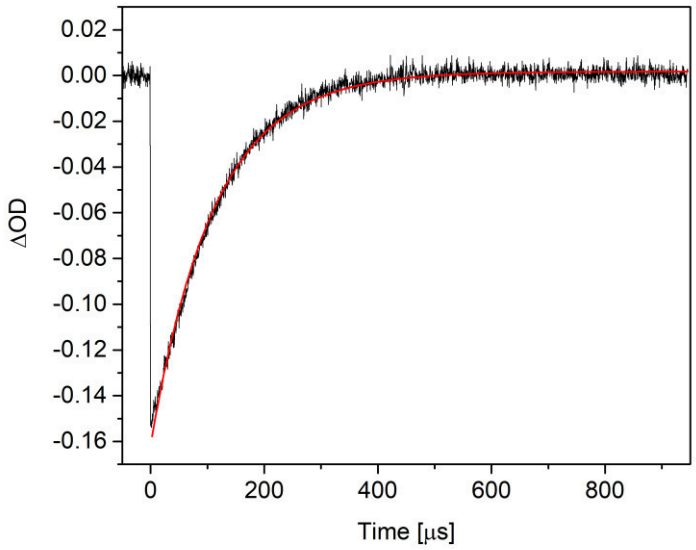

Figure A156 Transient signal detected at 375 nm for **3b** in DMSO-H_2O 9:1.

Equation	y = A1·exp(-x/τ) + y0
y0	0.00175 ± 8.86875E-5
A1	-0.16326 ± 3.9182E-4
τ	111.21788 ± 0.44405
R-Square(COD)	0.99323
Adj. R-Square	0.99322

Table A77 Fitting of the signal shown in Figure A156.

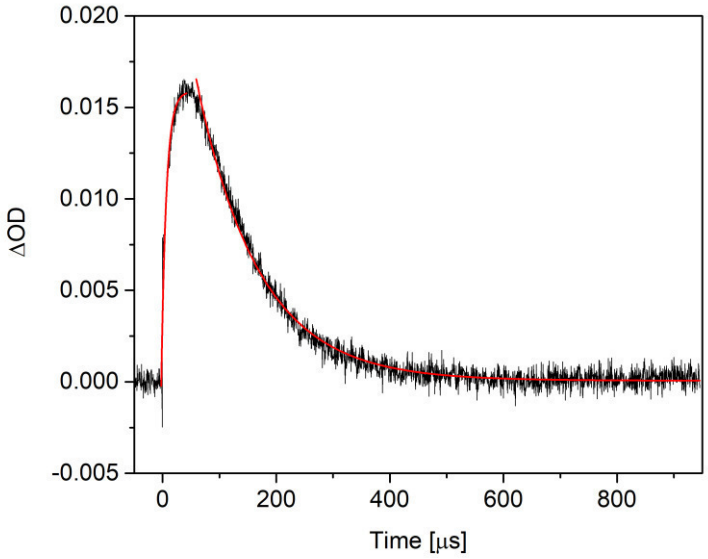

Figure A157 Transient signal detected at 445 nm for **3b** in DMSO-H_2O 9:1.

Equation	y = A1·exp(-x/τ) + y0
y0	0.01586 ± 2.13401E-4
A1	-0.01206 ± 3.46624E-4
τ	8.67905 ± 0.56806
R-Square(COD)	0.93666
Adj. R-Square	0.93521

Table A78 Fitting of the growth of the signal shown in Figure A157.

Equation	y = A1·exp(-x/τ) + y0
y0	6.2609E-5 ± 1.5453E-5
A1	0.02826 ± 1.83405E-4
τ	109.51581 ± 0.71539
R-Square(COD)	0.98334
Adj. R-Square	0.98332

Table A79 Fitting of the decay of the signal shown in Figure A157.

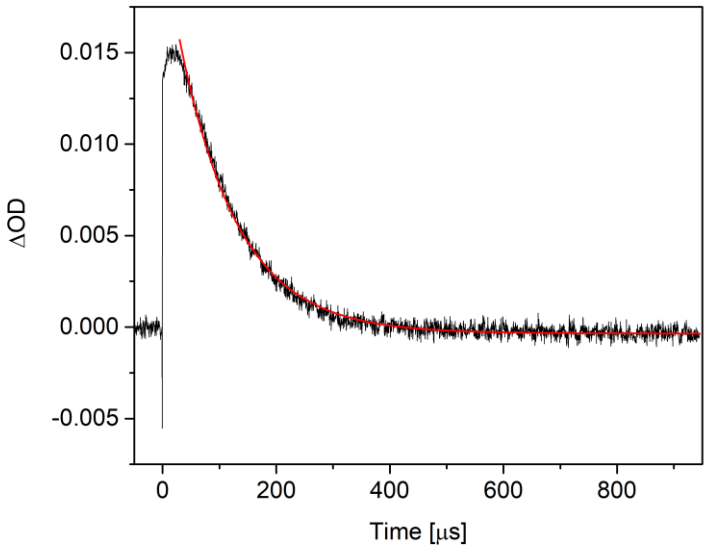

Figure A158 Transient signal detected at 460 nm for **3b** in DMSO-H_2O 9:1.

Equation	y = A1·exp(-x/τ) + y0
y0	-3.493E-4 ± 1.06587E-5
A1	0.02151 ± 8.51372E-5
τ	102.73277 ± 0.50598
R-Square(COD)	0.98992
Adj. R-Square	0.98991

Table A80 Fitting of the signal shown in Figure A158.

DMSO - H_2O 1:1

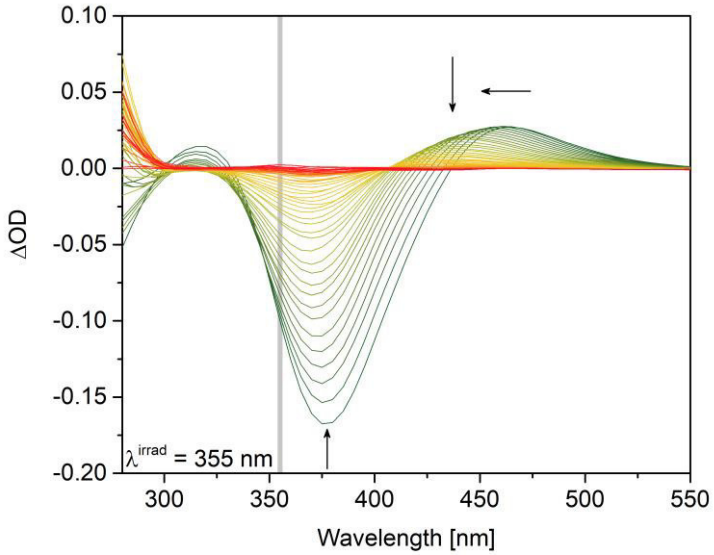

Figure A159 Transient signal map for **3b** in DMSO-H_2O 1:1.

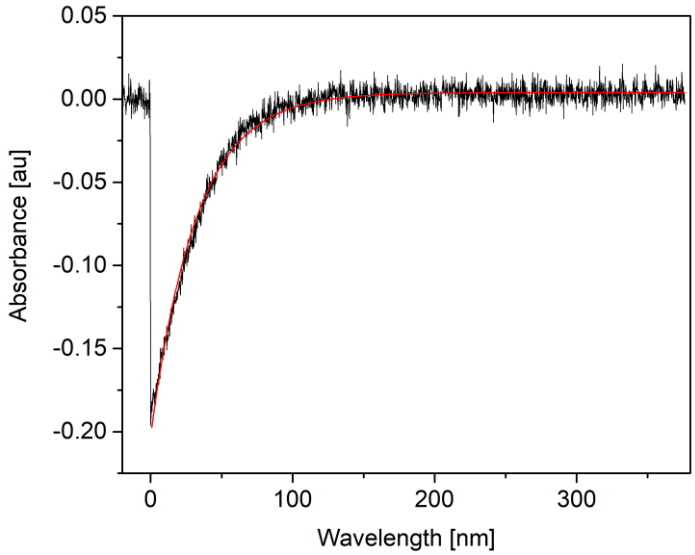

Figure A160 Transient signal detected at 375 nm for **3b** in DMSO-H_2O 1:1.

Equation	y = A1·exp(-x/τ) + y0
y0	0.00394 ± 1.49854E-4
A1	-0.20645 ± 8.68704E-4
τ	32.09446 ± 0.20971
R-Square(COD)	0.98121
Adj. R-Square	0.98119

Table A81 Fitting of the signal shown in Figure A160.

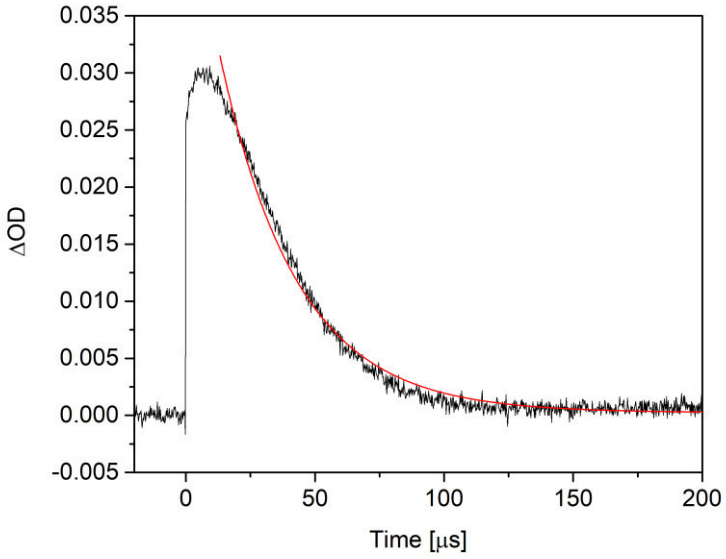

Figure A161 Transient signal detected at 455 nm for **3b** in DMSO-H_2O 1:1.

Equation	y = A1·exp(-x/τ) + y0
y0	2.36944E-4 ± 3.72932E-5
A1	0.04858 ± 3.236E-4
τ	29.91279 ± 0.22723
R-Square(COD)	0.98706
Adj. R-Square	0.98703

Table A82 Fitting of the signal shown in Figure A161.

DMSO - buffered H_2O (pH=4) 1:1

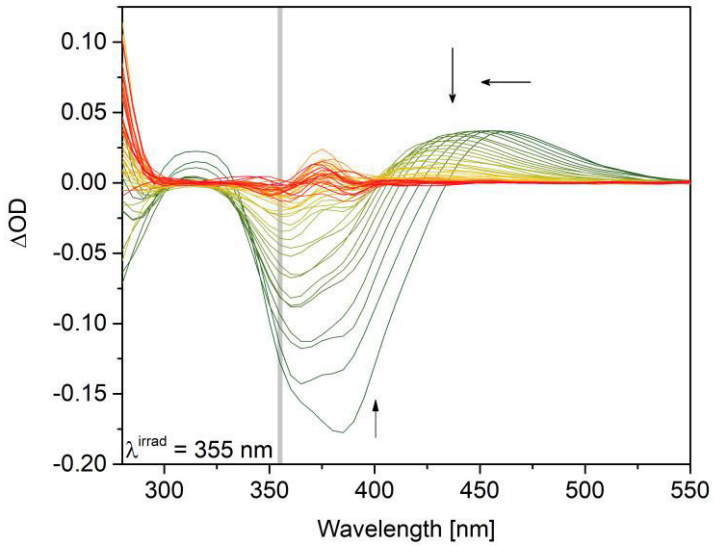

Figure A162 Transient signal map for **3b** in DMSO-buffered H_2O (pH=4) 1:1.

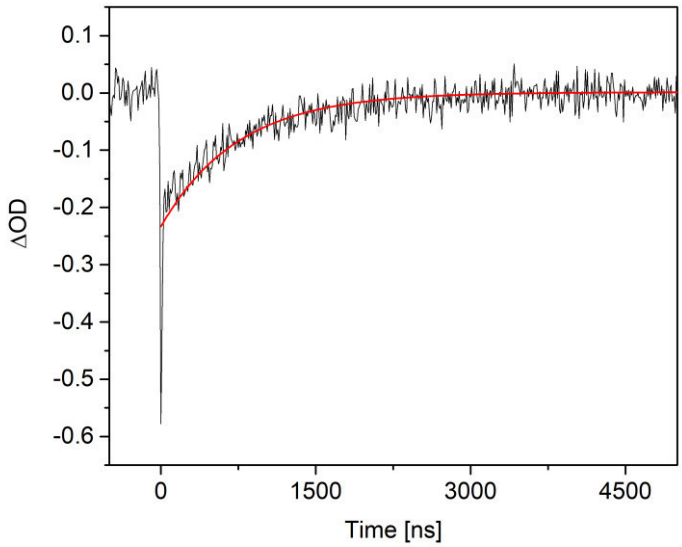

Figure A163 Transient signal detected at 380 nm for **3b** in DMSO- buffered H_2O (pH=4) 1:1.

Equation	y = A1·exp(-x/τ) + y0
y0	0.00131 ± 6.47261E-4
A1	-0.23486 ± 0.0052
τ	743.25708 ± 24.78394
R-Square(COD)	0.70488
Adj. R-Square	0.70449

Table A83 Fitting of the signal shown in Figure A163.

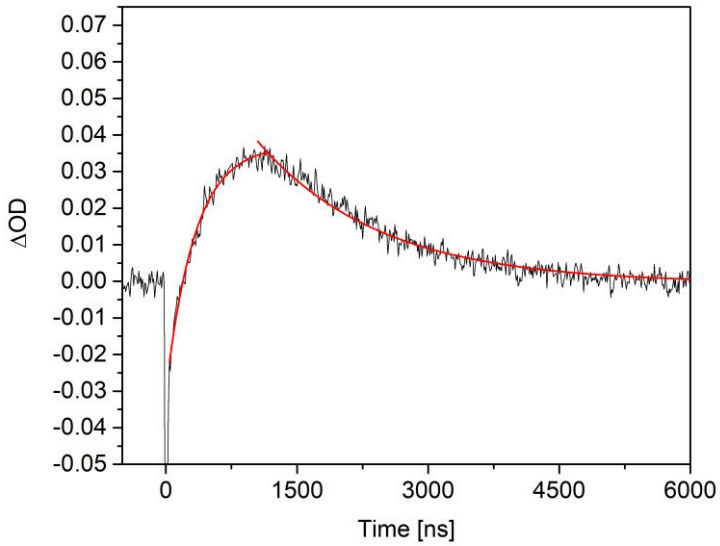

Figure A164 Transient signal detected at 430 nm for **3b** in DMSO- buffered H_2O (pH=4) 1:1.

Equation	y = A1·exp(-x/τ) + y0
y0	-4.9642E-4 ± 6.88459E-5
A1	0.08273 ± 0.00146
τ	1387.13548 ± 19.92213
R-Square(COD)	0.93554
Adj. R-Square	0.93544

Table A84 Fitting of the decay of the signal shown in Figure A164.

Equation	y = A1·exp(-x/τ) + y0
y0	0.03723 ± 6.07849E-4
A1	-0.0671 ± 9.04948E-4
τ	328.89001 ± 11.92738
R-Square(COD)	0.98292
Adj. R-Square	0.98261

Table A85 Fitting of the growth of the signal shown in Figure A164.

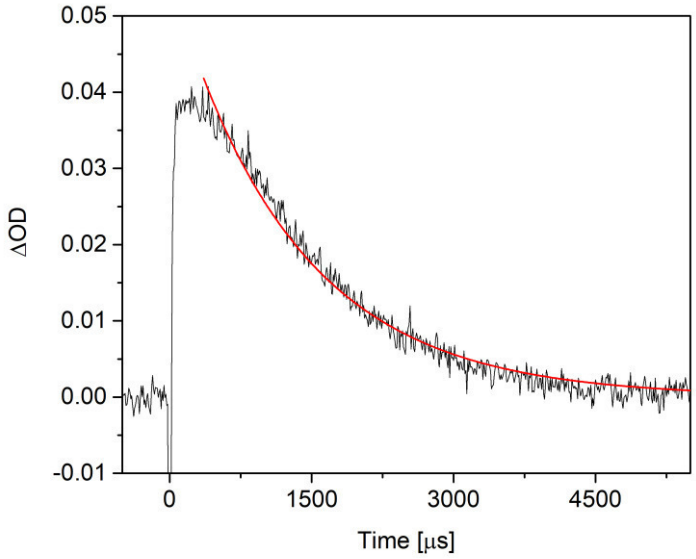

Figure A165 Transient signal detected at 460 nm for **3b** in DMSO- buffered H_2O (pH=4) 1:1.

Equation	y = A1·exp(-x/τ) + y0
y0	4.23526E-5 ± 4.17151E-5
A1	0.05499 ± 3.9103E-4
τ	1309.45975 ± 11.289
R-Square(COD)	1.68336E-6
Adj. R-Square	0.97428

Table A86 Fitting of the signal shown in Figure A165.

DMSO - buffered H_2O (pH=7) 1:1

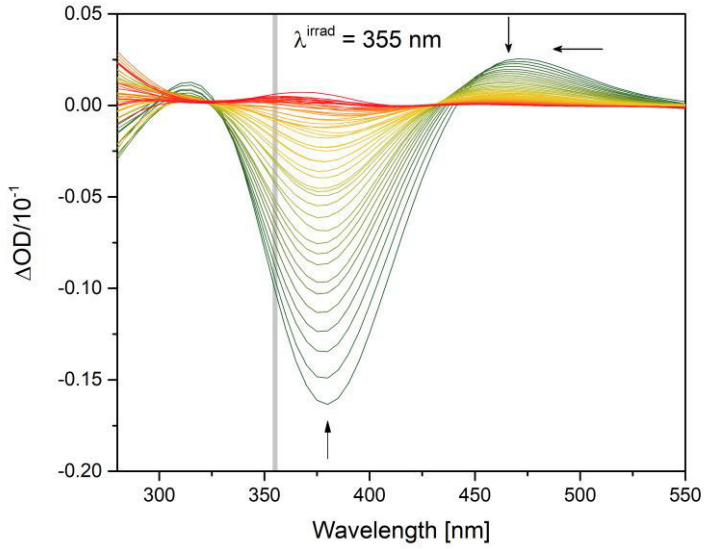

Figure A166 Transient signal map for **3b** in DMSO-buffered H_2O (pH=7) 1:1.

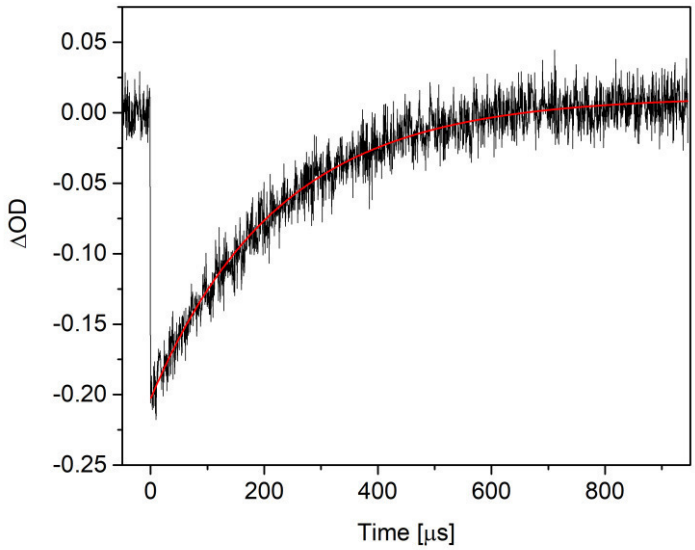

Figure A167 Transient signal detected at 375 nm for **3b** in DMSO- buffered H_2O (pH=7) 1:1.

Equation	y = A1·exp(-x/τ) + y0
y0	0.01143 ± 6.66874E-4
A1	-0.21423 ± 0.00118
τ	224.54167 ± 3.00536
R-Square(COD)	0.95088
Adj. R-Square	0.95082

Table A87 Fitting of the signal shown in Figure **A167**.

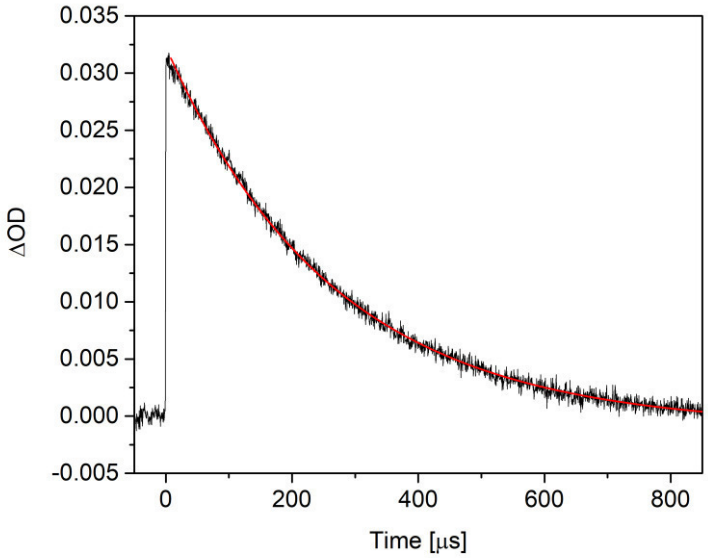

Figure A168 Transient signal detected at 465 nm for **3b** in DMSO- buffered H_2O (pH=7) 1:1.

Equation	y = A1·exp(-x/τ) + y0
y0	-9.6101E-4 ± 3.30026E-5
A1	0.03327 ± 4.57811E-5
τ	265.5033 ± 1.00643
R-Square(COD)	0.9966
Adj. R-Square	0.9966

Table A88 Fitting of the signal shown in Figure A168.

DMSO - H_2O 1:1 + 25 µL DBU

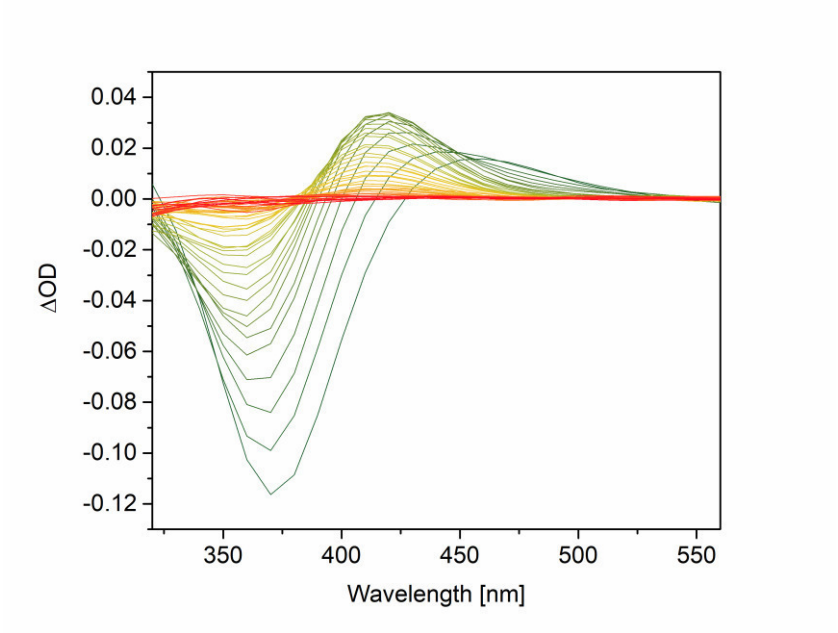

Figure A169 Transient signal map for **3b** in DMSO-H_2O 1:1 + 25 µL DBU.

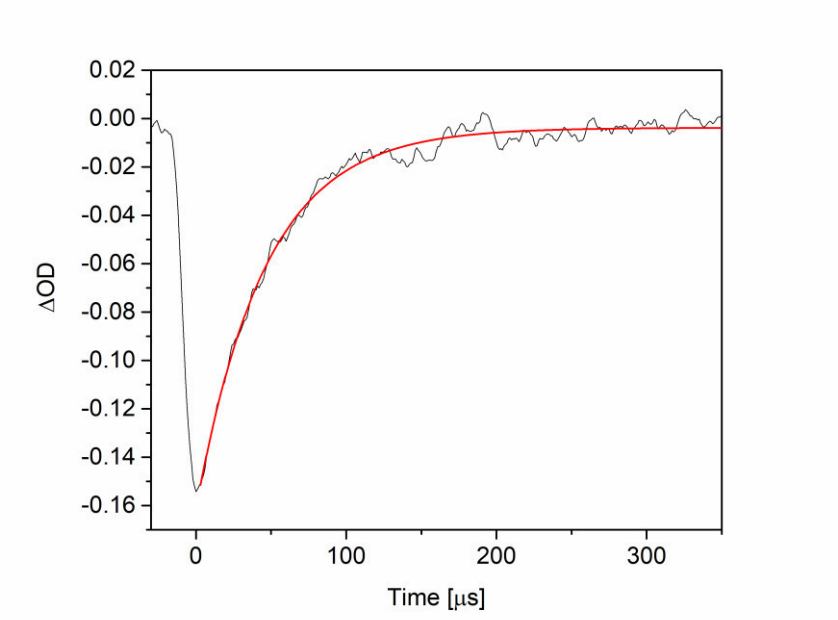

Figure A170 Transient signal detected at 381 nm for **3b** in DMSO-H_2O 1:1 + 25 µL DBU.

Equation	y = A1·exp(-x/τ) + y0
y0	-0.00376 ± 2.69006E-4
A1	-0.15776 ± 0.00116
τ	45.80947 ± 0.55644
R-Square(COD)	0.98876
Adj. R-Square	0.9887

Table A89 Fitting of the signal shown in Figure A170.

DMSO - H_2O 1:2

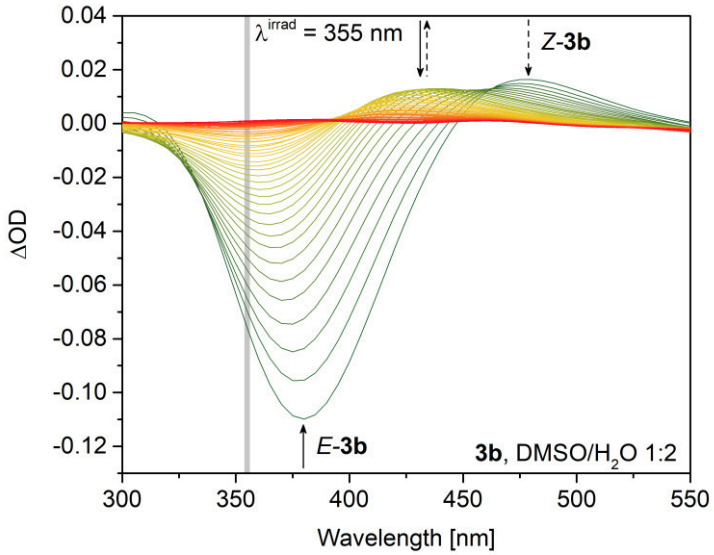

Figure A171 Transient signal map for **3b** in DMSO-H_2O 1:2.

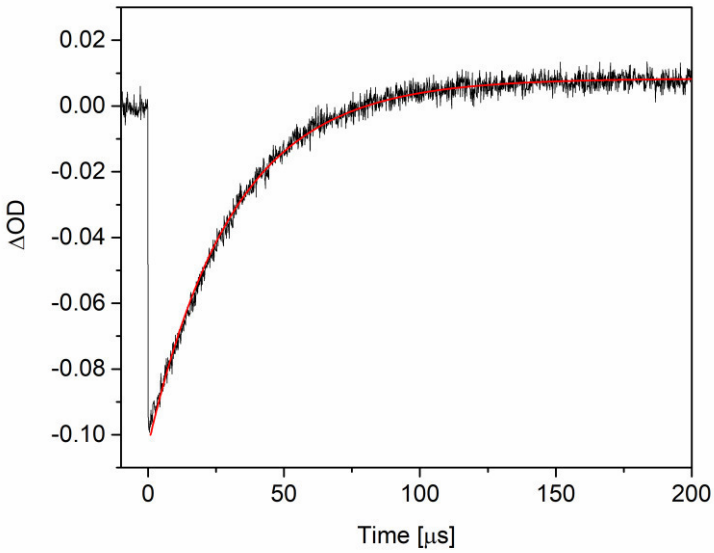

Figure A172 Transient signal detected at 381 nm for **3b** in DMSO-H_2O 1:2.

Equation	y = A1·exp(-x/τ) + y0
y0	0.00838 ± 7.81655E-5
A1	-0.11156 ± 2.94799E-4
τ	31.00774 ± 0.14322
R-Square(COD)	0.99184
Adj. R-Square	0.99183

Table A90 Fitting of the signal shown in Figure A172.

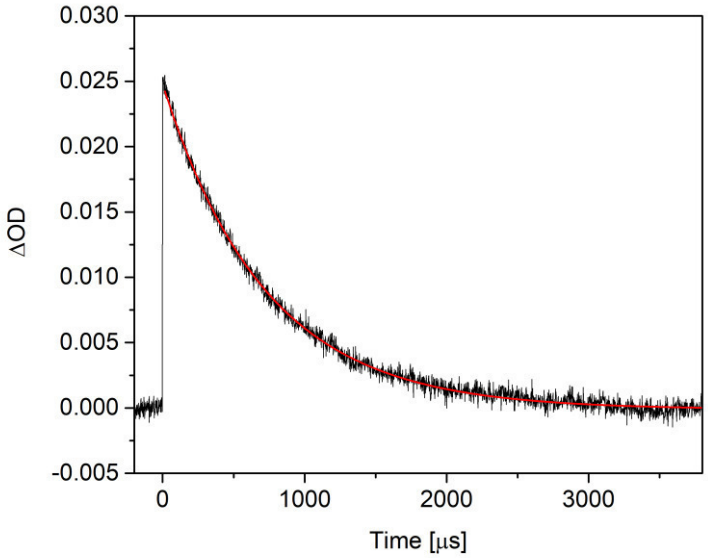

Figure A173 Transient signal detected at 465 nm for **3b** in DMSO-H_2O 1:2.

Equation	y = A1·exp(-x/τ) + y0
y0	-1.11283E-4 ± 2.03398E-5
A1	0.0249 ± 5.18701E-5
τ	720.79356 ± 3.07685
R-Square(COD)	0.99374
Adj. R-Square	0.99374

Table A91 Fitting of the signal shown in Figure A173.

2.3.3 3c

Cyclohexane

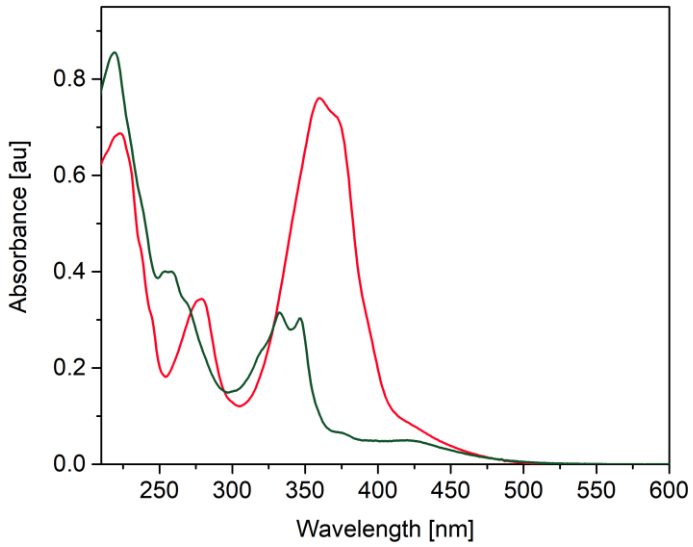

Figure A174 UV/vis of ***E*-3c** in cyclohexane (red), and of the PSS (green) after irradiation with a 365 nm LED.

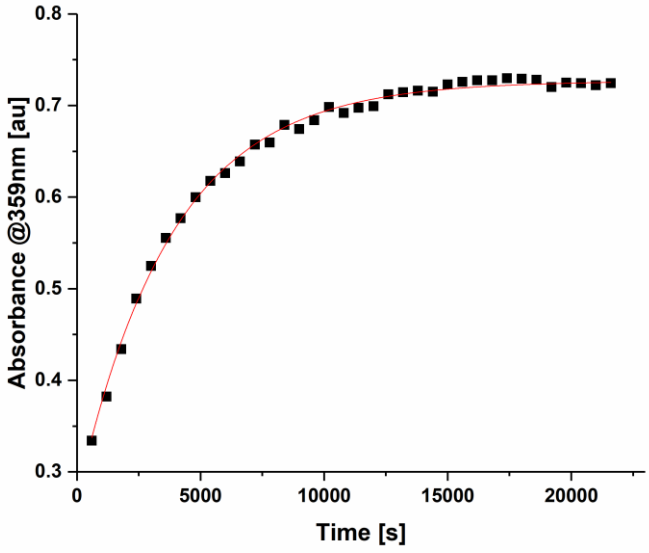

Figure A175 PSS-to-*E* kinetic of **3c** in cyclohexane, irradiation with 365 nm LED, λ^{obs}=359 nm.

Equation	y = A1·exp(-x/τ) + y0
y0	0.72683 ± 0.0017
A1	-0.45576 ± 0.00545
τ	3818.61938 ± 84.15608
R-Square(COD)	0.99703
Adj. R-Square	0.99685

Table A92 Fitting of the growth of the signal shown in Figure A175.

Dioxane

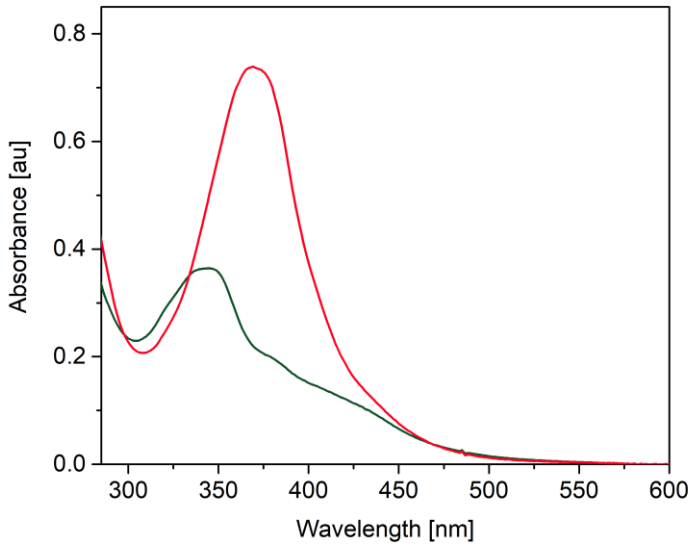

Figure A176 UV/vis of ***E*-3c** in dioxane (red), and of the PSS (green) after irradiation with a 365 nm LED.

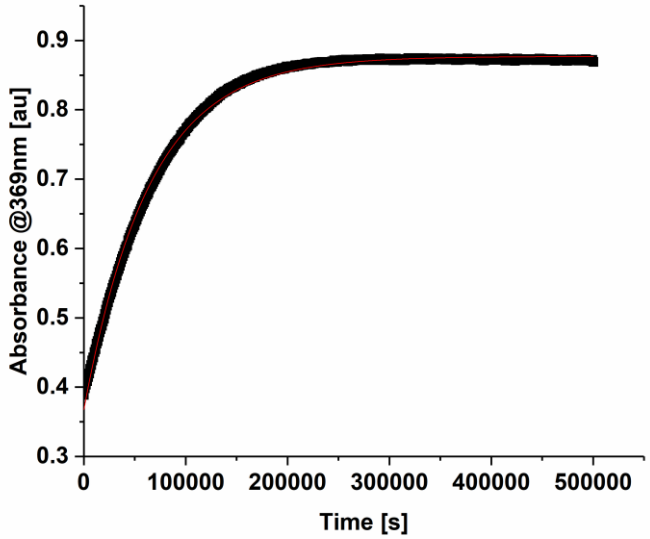

Figure A177 PSS-to-*E* kinetic of **3c** in dioxane, irradiation with 365 nm LED, λ^{obs}=369 nm.

Equation	y = A1·exp(-x/τ) + y0
y0	0.87699 ± 3.42385E-4
A1	-0.51034 ± 0.00133
τ	63764.54785 ± 291.09162
R-Square(COD)	0.99778
Adj. R-Square	0.99777

Table A93 Fitting of the growth of the signal shown in Figure A177.

Benzene

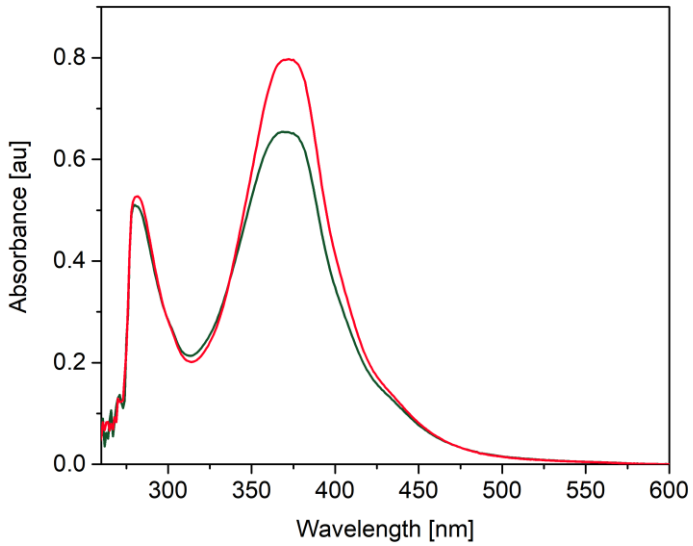

Figure A178 UV/vis of ***E*-3c** in benzene (red), and of the PSS (green) after irradiation with a 365 nm LED.

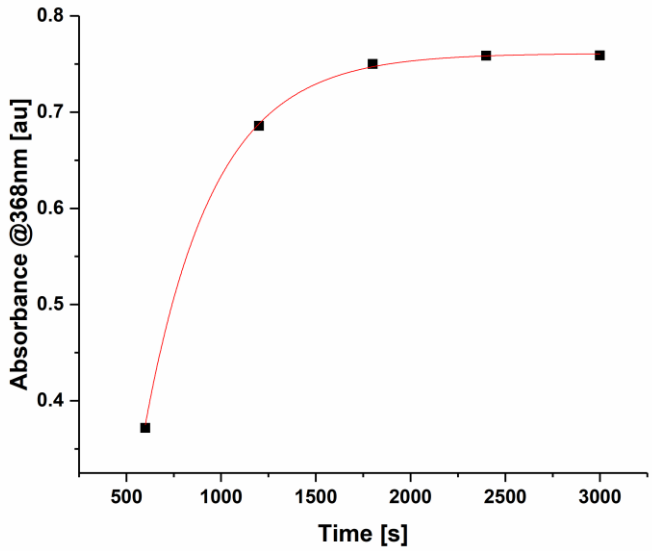

Figure A179 PSS-to-*E* kinetic of **3c** in benzene, irradiation with 365 nm LED, λ^{obs}=368 nm.

Equation	y = A1·exp(-x/τ) + y0
y0	0.76098 ± 0.00255
A1	-2.03277 ± 0.1223
τ	361.13518 ± 13.4427
R-Square(COD)	0.99976
Adj. R-Square	0.99951

Table A94 Fitting of the growth of the signal shown in Figure A179.

Mesitylene

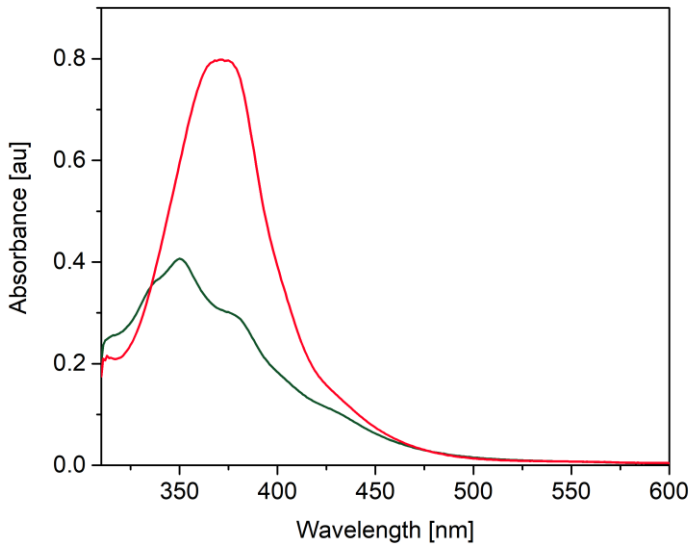

Figure A180 UV/vis of ***E*-3c** in mesitylene (red), and of the PSS (green) after irradiation with a 365 nm LED.

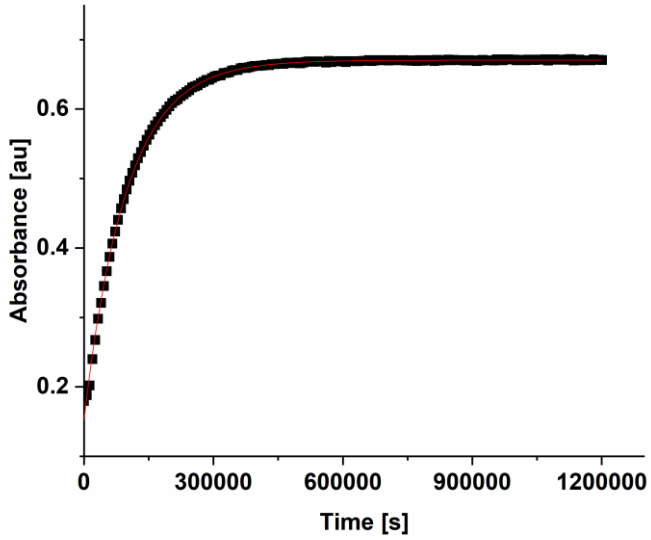

Figure A181 PSS-to-*E* kinetic of **3c** in mesitylene, irradiation with 365 nm LED, λ^{obs}=367 nm.

Equation	y = A1·exp(-x/τ) + y0
y0	0.67036 ± 2.39673E-4
A1	-0.51769 ± 0.0013
τ	97696.50478 ± 398.58729
R-Square(COD)	0.99928
Adj. R-Square	0.99927

Table A95 Fitting of the growth of the signal shown in Figure A181.

Toluene

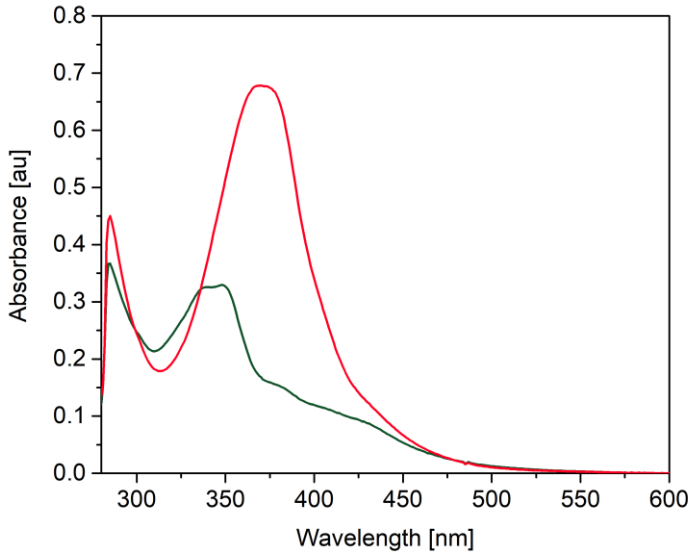

Figure A182 UV/vis of ***E*-3c** in toluene (red), and of the PSS (green) after irradiation with a 365 nm LED.

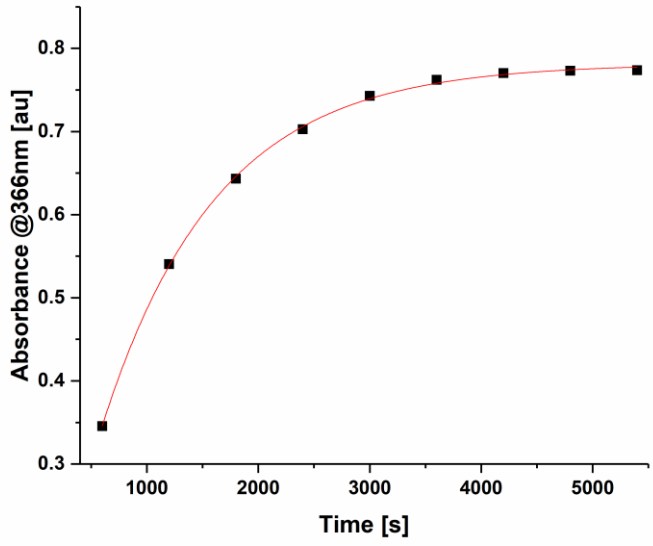

Figure A183 PSS-to-*E* kinetic of **3c** in toluene, irradiation with 365 nm LED, λ^{obs}=366 nm.

Equation	y = A1·exp(-x/τ) + y0
y0	0.78154 ± 0.00219
A1	-0.78153 ± 0.01123
τ	1027.22227 ± 21.31498
R-Square(COD)	0.99959
Adj. R-Square	0.99945

Table A96 Fitting of the growth of the signal shown in Figure A183.

MeOH

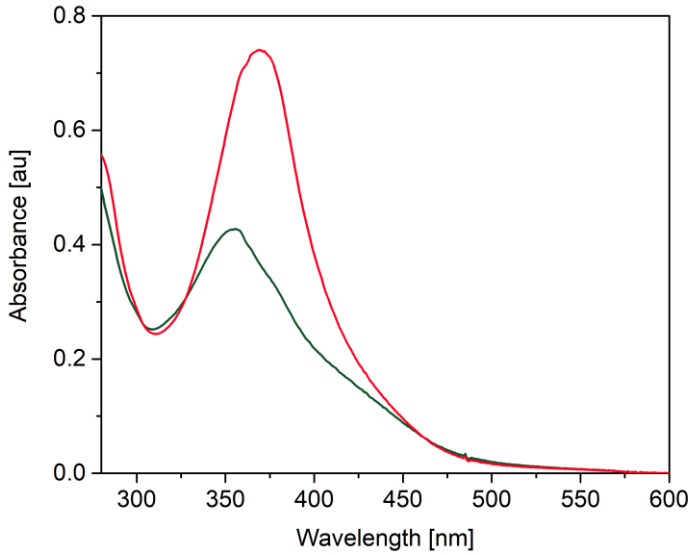

Figure A184 UV/vis of ***E*-3c** in MeOH (red), and of the PSS (green) after irradiation with a 365 nm LED.

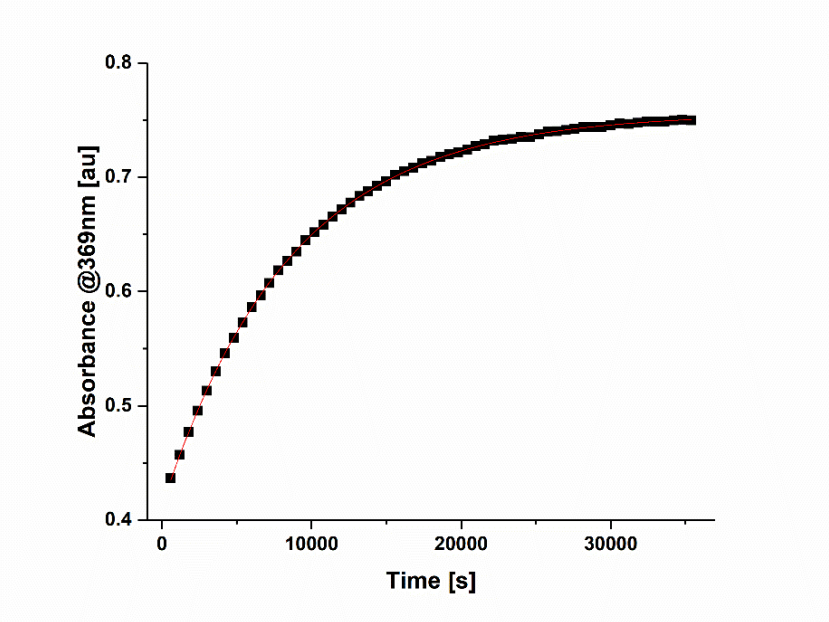

Figure A185 PSS-to-*E* kinetic of **3c** in MeOH, irradiation with 365 nm LED, λ^{obs}=369 nm.

Equation	y = A1·exp(-x/τ) + y0
y0	0.75577 ± 2.06828E-4
A1	-0.3442 ± 3.80659E-4
τ	8517.57591 ± 22.55011
R-Square(COD)	0.99994
Adj. R-Square	0.99994

Table A97 Fitting of the growth of the signal shown in Figure A185.

MeCN

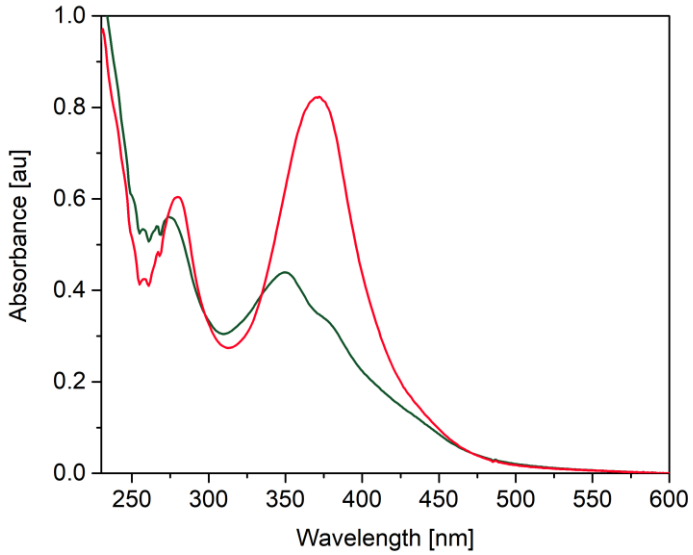

Figure A186 UV/vis of ***E*-3c** in MeCN (red), and of the PSS (green) after irradiation with a 365 nm LED.

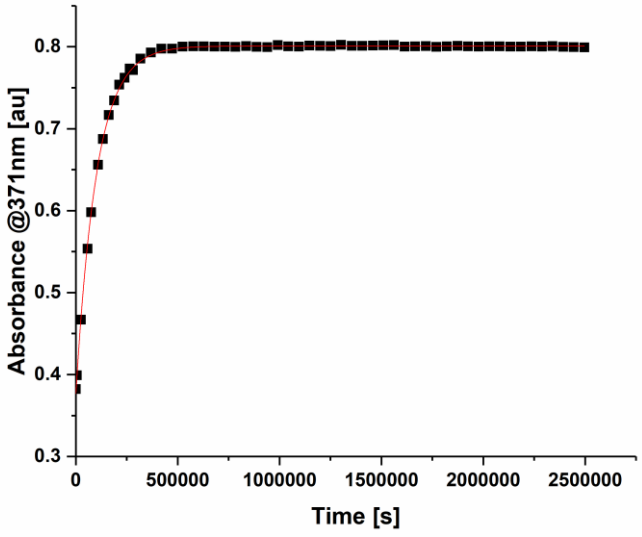

Figure A187 PSS-to-*E* kinetic of **3c** in MeCN, irradiation with 365 nm LED, λ^{obs}=371 nm.

Equation	y = A1·exp(-x/τ) + y0
y0	0.801 ± 2.99777E-4
A1	-0.42437 ± 0.00128
τ	101479.69866 ± 613.50362
R-Square(COD)	0.99961
Adj. R-Square	0.9996

Table A98 Fitting of the growth of the signal shown in Figure A187.

DMSO

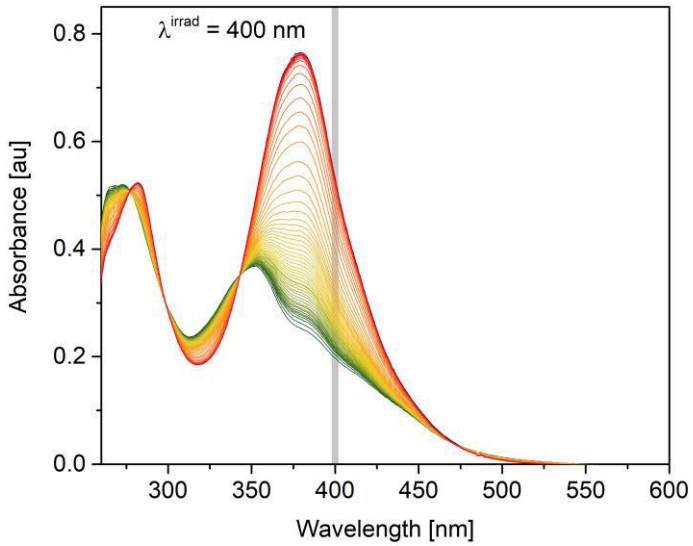

Figure A188 UV/vis of ***E*-3c** in MeCN (red), and of the PSS (green) after irradiation with a 365 nm LED.

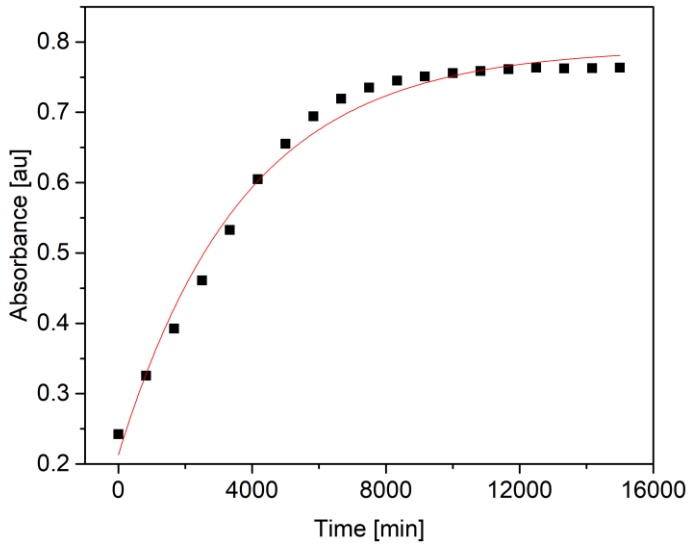

Figure A189 PSS-to-*E* kinetic of **3c** in DMSO, irradiation with 365 nm LED, λ^{obs}=370 nm.

Equation	y = A1·exp(-x/τ) + y0
y0	0.79133 ± 0.01078
A1	-0.57819 ± 0.01635
τ	3734.66995 ± 271.99886
R-Square(COD)	0.98743
Adj. R-Square	0.98585

Table A99 Fitting of the growth of the signal shown in Figure A189.

2.4 Thermal isomerization kinetics of 3a at various temperatures

Temperature [°C]	Temperature [K]	τ [s]
13	286.15	9.7
15	288.15	8.42
17	290.15	7.75
19	292.15	6.81
21	294.15	5.56
23	296.15	4.33
25	298.15	4.37
27	300.15	3.57
29	302.15	2.91
31	304.15	2.68
33	306.15	2.33

Table A100 Overview of the different lifetimes at different temperatures registered for **3a** in MeCN

13 °C

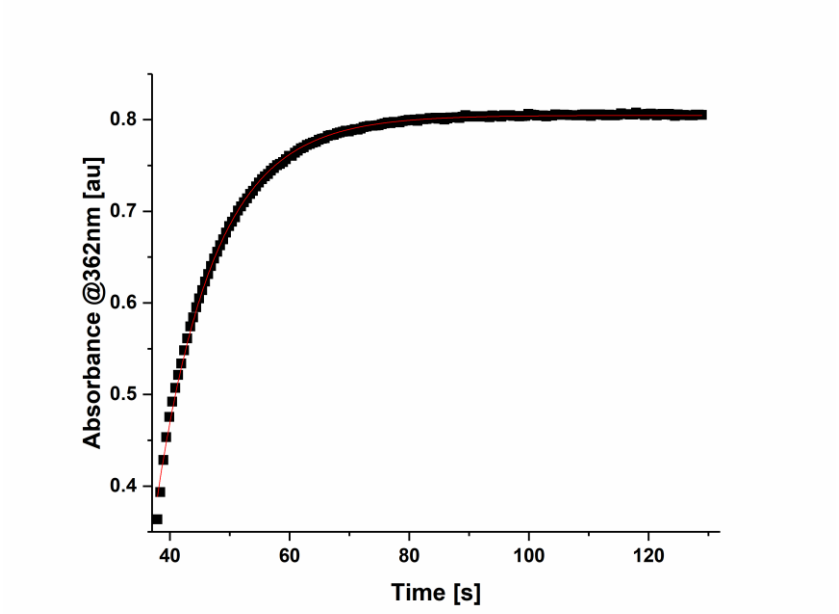

Equation	y = A1·exp(-x/τ) + y0
y0	0.8048 ± 2.86615E-4
A1	-20.66538 ± 0.45671
τ	9.70688 ± 0.05022
R-Square(COD)	0.99888
Adj. R-Square	0.99887

15 °C

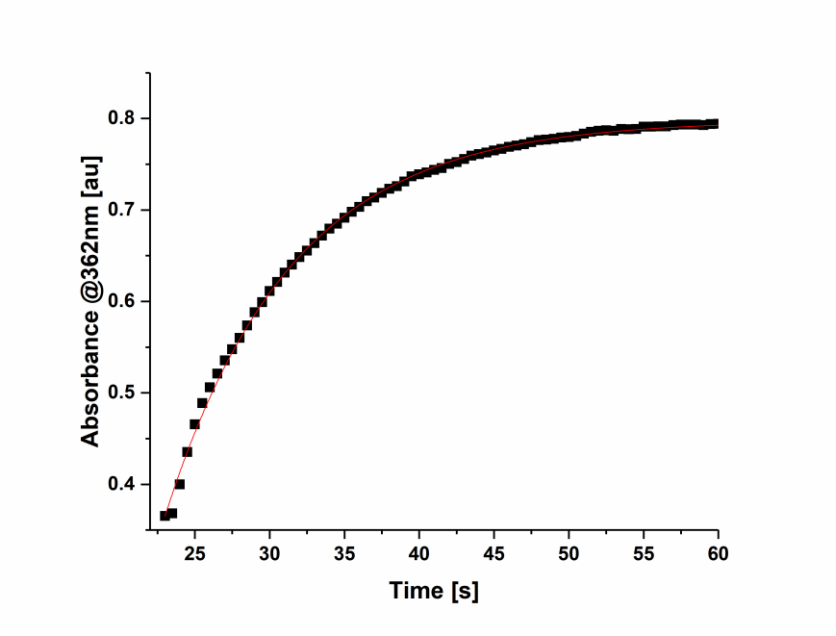

Equation	y = A1·exp(-x/τ) + y0
Plot	Absorbance (AU)
y0	0.79805 ± 0.00109
τ	8.42492 ± 0.09327
R-Square(COD)	0.99855
Adj. R-Square	0.99851

17 °C

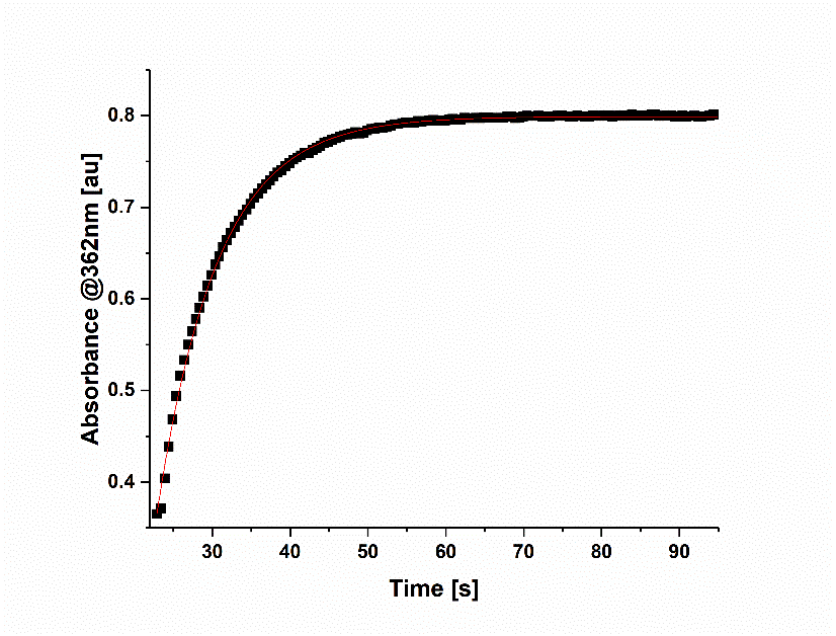

Equation	y = A1·exp(-x/τ) + y0
y0	0.79912 ± 3.69601E-4
A1	-8.33469 ± 0.17562
τ	7.74667 ± 0.04911
R-Square(COD)	0.99868
Adj. R-Square	0.99866

19 °C

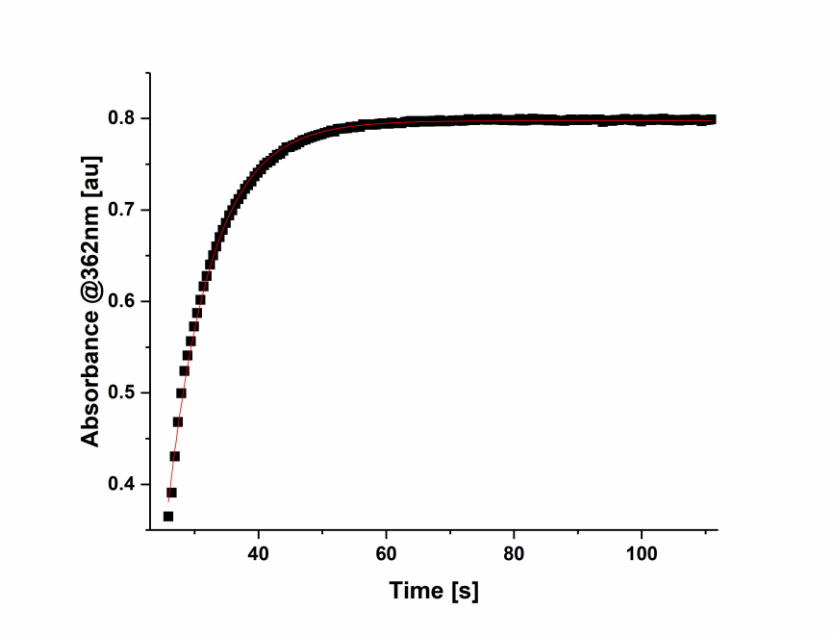

Equation	y = A1*exp(-x/τ) + y0
y0	0.79764 ± 3.09178E-4
A1	-18.74842 ± 0.51846
τ	6.80558 ± 0.04477
R-Square(COD)	0.99825
Adj. R-Square	0.99823

21 °C

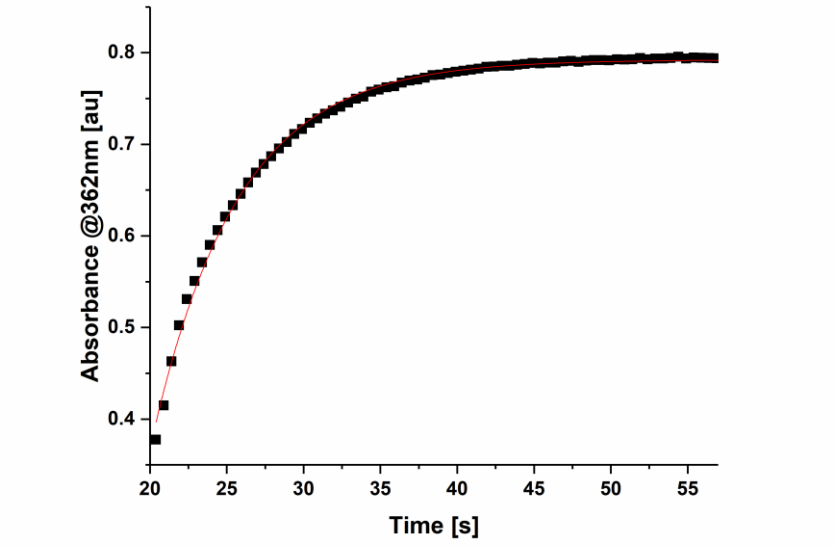

Equation	y = A1·exp(-x/τ) + y0
y0	0.79228 ± 8.91028E-4
A1	-15.45017 ± 0.80979
τ	5.56549 ± 0.07401
R-Square(COD)	0.99734
Adj. R-Square	0.99726

25 °C

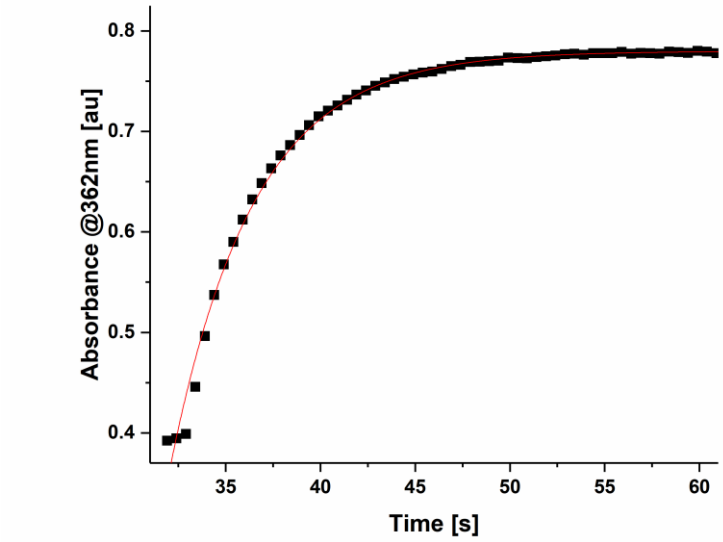

Equation	y = A1·exp(-x/τ) + y0
y0	0.77987 ± 0.00177
A1	-632.15364 ± 115.92526
τ	4.37466 ± 0.10627
R-Square(COD)	0.99296
Adj. R-Square	0.99271

27 °C

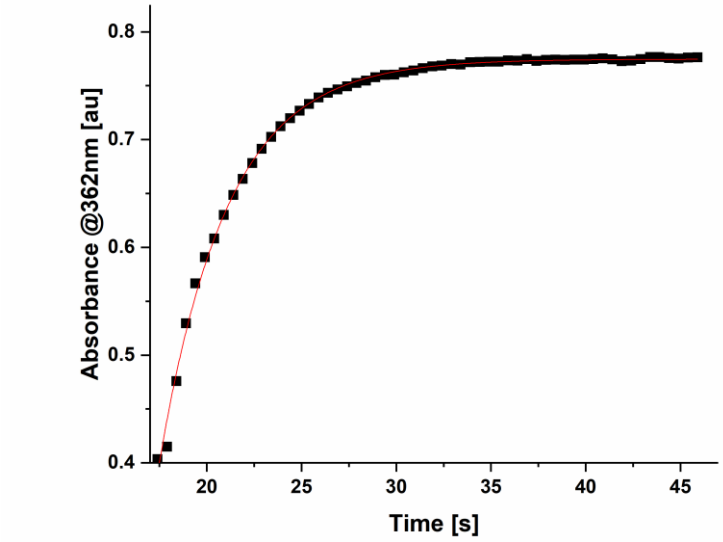

Equation	y = A1·exp(-x/τ) + y0
y0	0.77469 ± 8.57862E-4
A1	-50.00092 ± 3.76478
τ	3.57548 ± 0.05218
R-Square(COD)	0.9974
Adj. R-Square	0.9973

29 °C

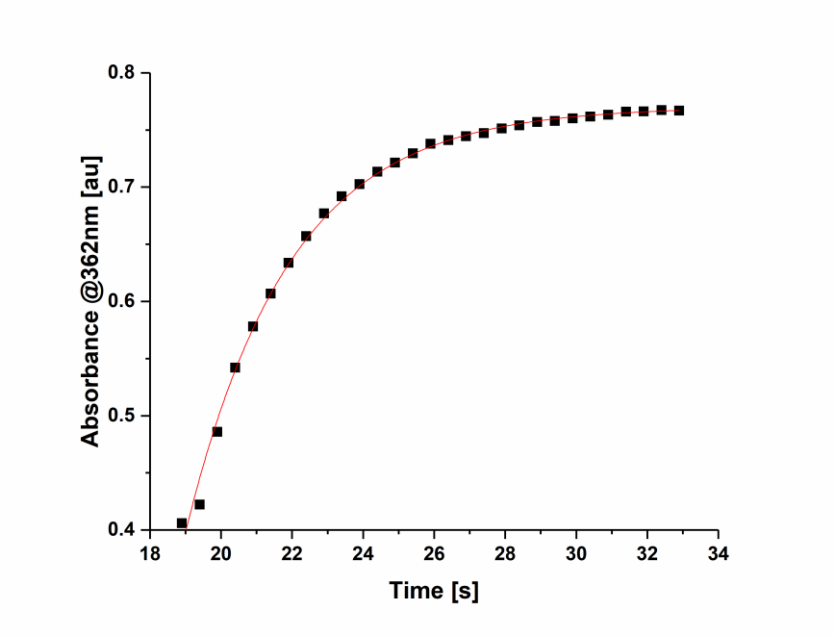

Equation	y = A1*exp(-x/τ) + y0
y0	0.77028 ± 0.00249
A1	-253.08752 ± 49.06239
τ	2.9137 ± 0.08541
R-Square(COD)	0.99613
Adj. R-Square	0.99583

31 °C

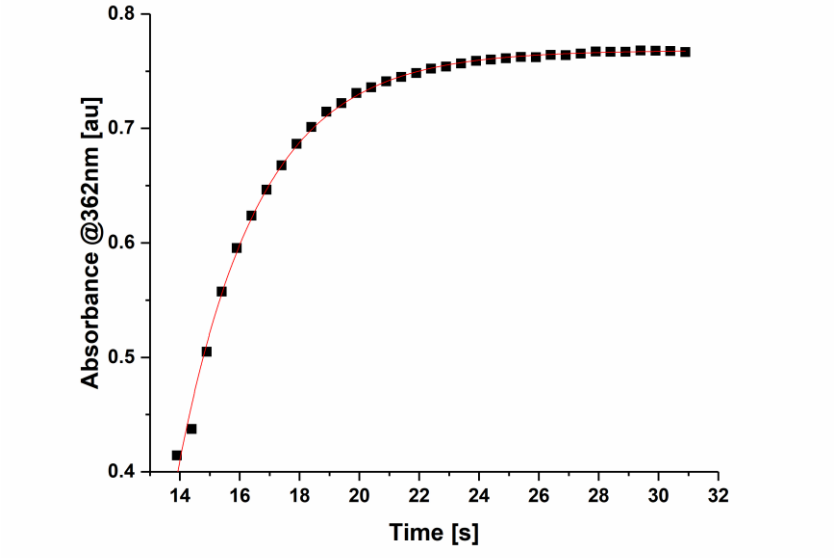

Equation	y = A1*exp(-x/τ) + y0
y0	0.76819 ± 0.00145
A1	-66.70308 ± 7.77401
τ	2.67878 ± 0.05776
R-Square(COD)	0.99696
Adj. R-Square	0.99677

33 °C

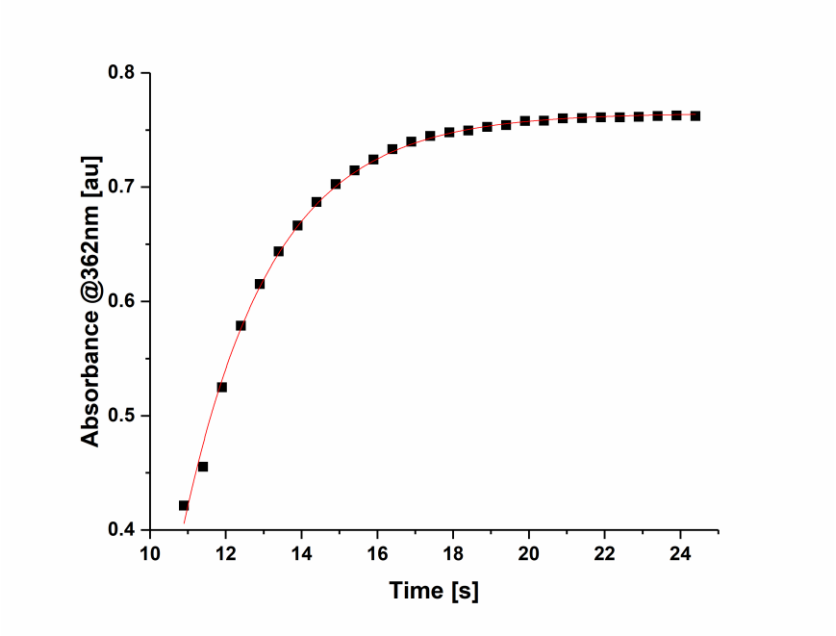

Equation	y = A1*exp(-x/s) + y0
y0	0.76476 ± 0.00171
A1	-38.90982 ± 4.65234
τ	2.32631 ± 0.05716
R-Square(COD)	0.99706
Adj. R-Square	0.99682

2.5 UV/Vis titration of 3b with HCl

We titrated compound **3b** in MeCN (2 mL of a 59 μM solution) with one equivalent of a concentrated solution of HCl (54 μL of a 2.2 mM solution, added in 1.5 μL portions). Doing so we quantitatively protonated *E*-**3b**, forming product *E*-**3b**H$^+$ (see Scheme S2). This equilibrium is known for azo-compounds to happen in acidic medium.[S2] *E*-**3b**H$^+$ can undergo a more facile rotation around the N-N bond in respect of *E*-**3b**, due to its partial single bond character furnished by the resonance structure *E*-**3b**H$^{+\prime}$. Thus, we cannot exclude *a priori* the role of the protonated azoindole in the *Z*-to-*E* conversion of *Z*-**3b**. The arising peak has a maximum of absorbance at 435 nm, while the intermediate detected in aqueous MeCN for **3b** has a maximum at 405 nm (see for instance MeCN-water 9:1 mixtures in the section above). Consequently, we can safely exclude the protonated species to be the intermediate detected with Laser Flash Photolysis.

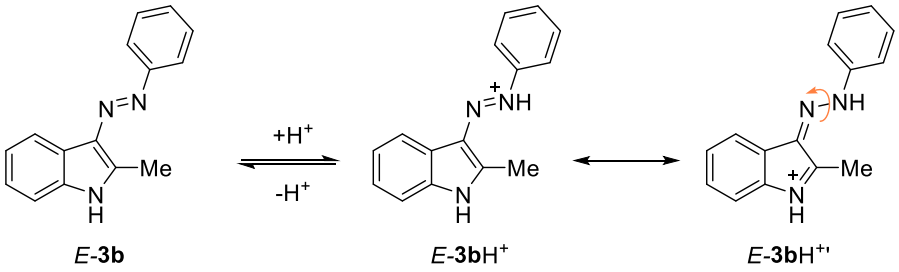

Scheme S2

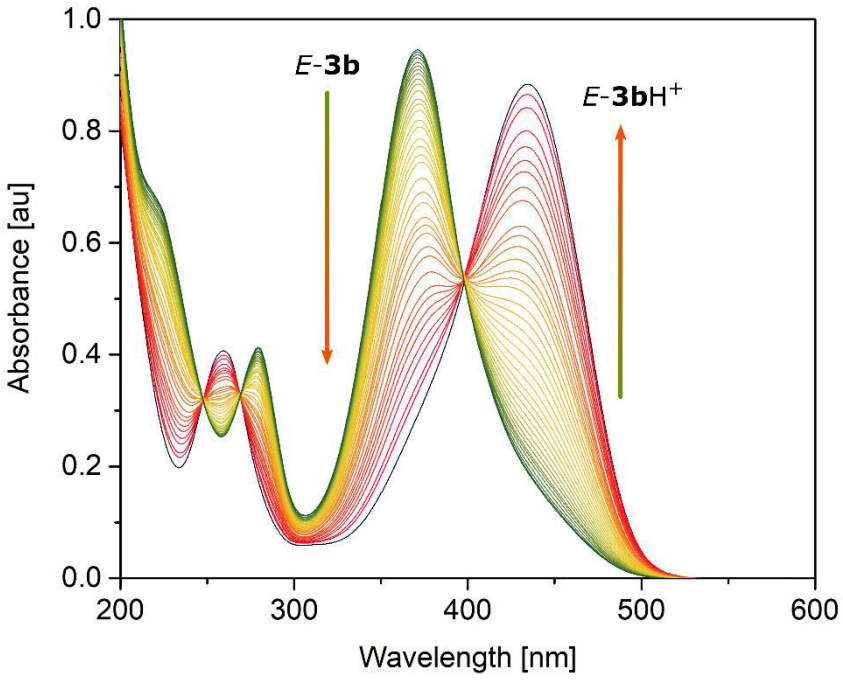

Figure A190 UV/Vis titration of **3c** with HCl in MeCN

3 ^{1}H and ^{13}C NMR Experiments

3.2 NMR spectra of compounds 3a-c

3a – ^{1}H-NMR, 400 MHz methanol-*d*

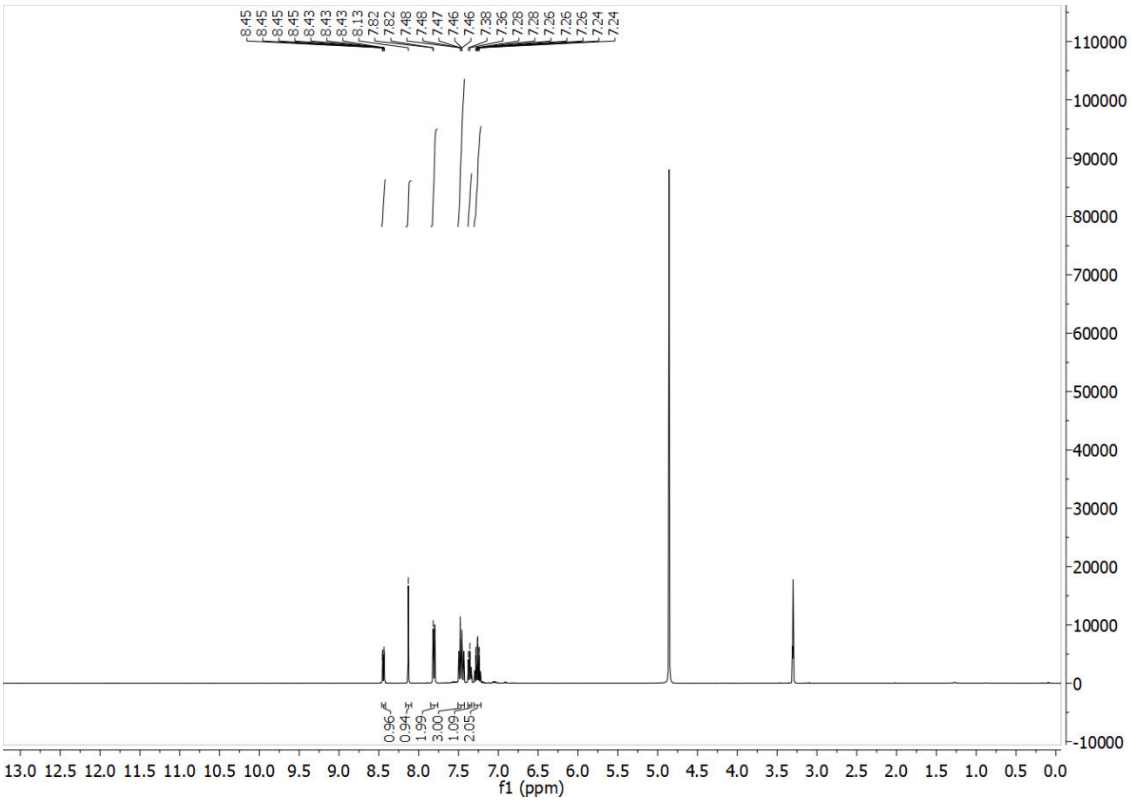

3a – ^{13}C-NMR, 101 MHz, methanol-*d*

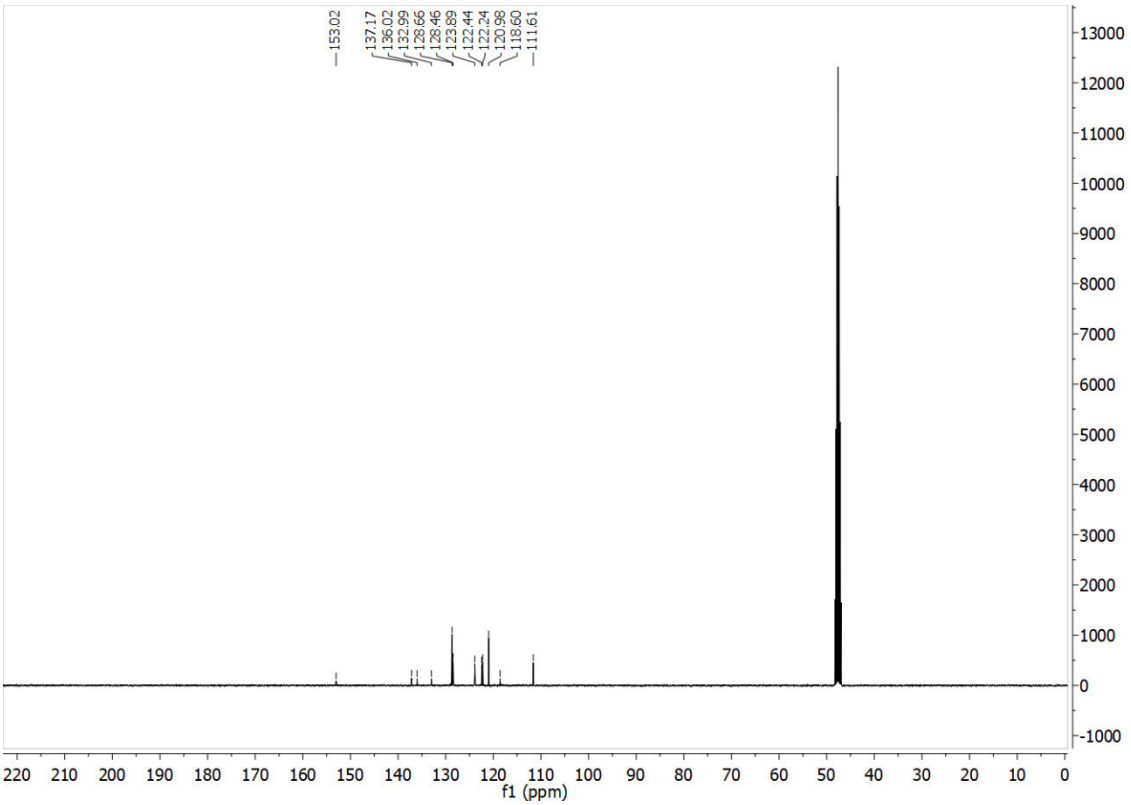

3b – ^{1}H-NMR, 400 MHz, acetone-*d6*

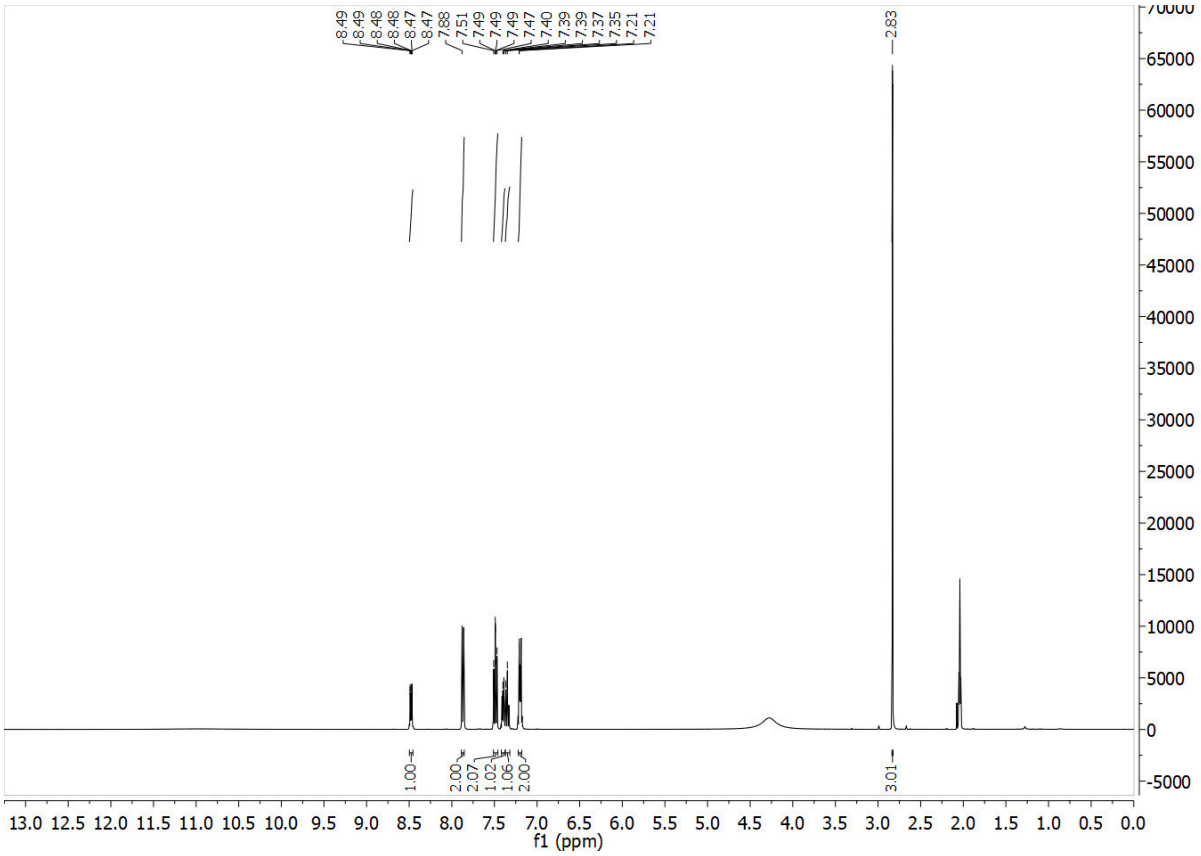

3b – ^{13}C-NMR, 101 MHz, acetone-*d6*

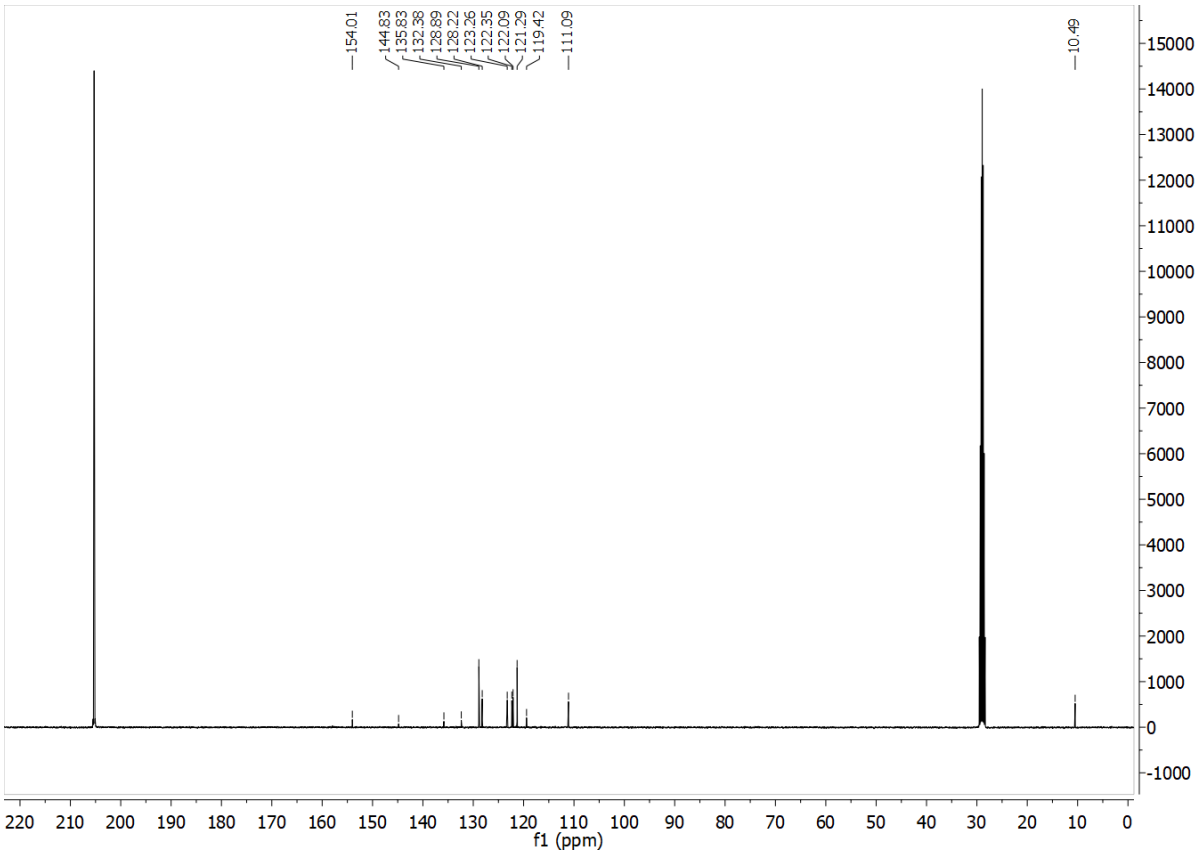

3c – ^{1}H-NMR, 400 MHz, acetone-*d6*

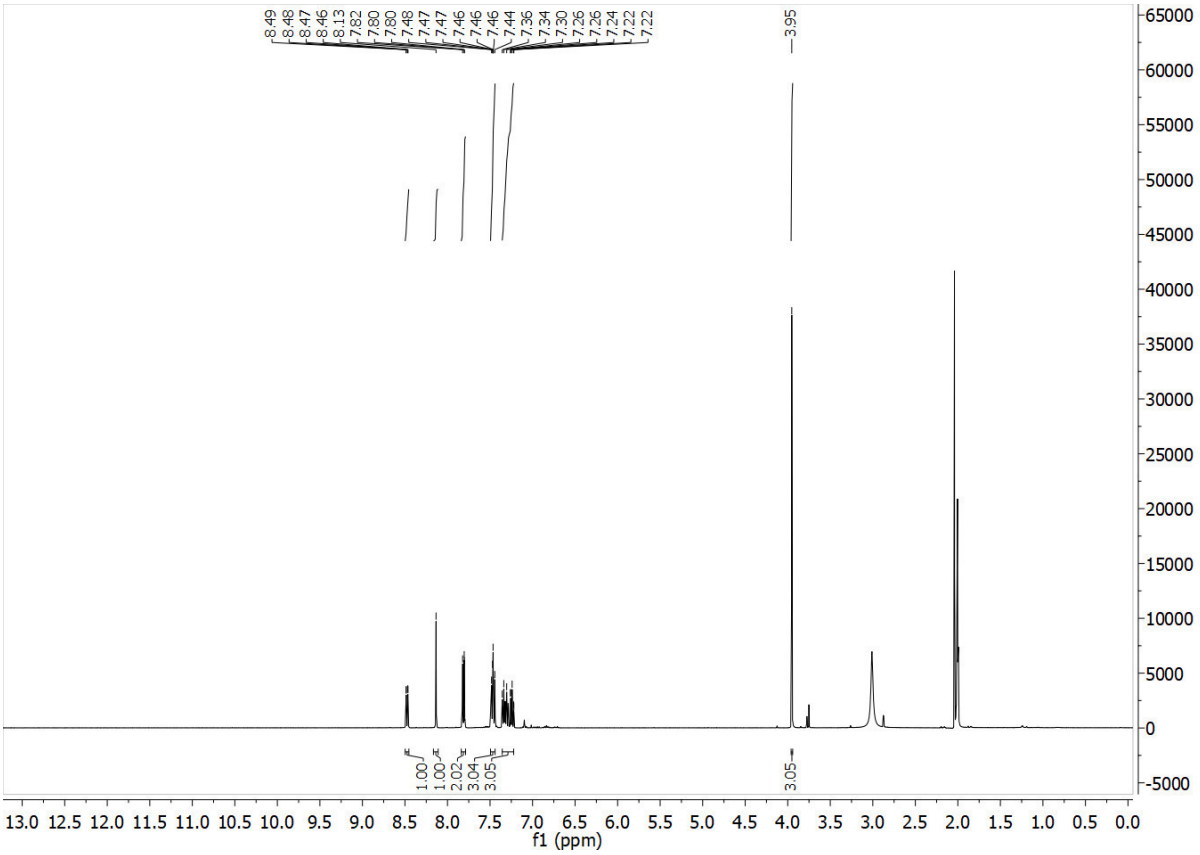

3c – ^{13}C-NMR, 101 MHz, acetone-*d6*

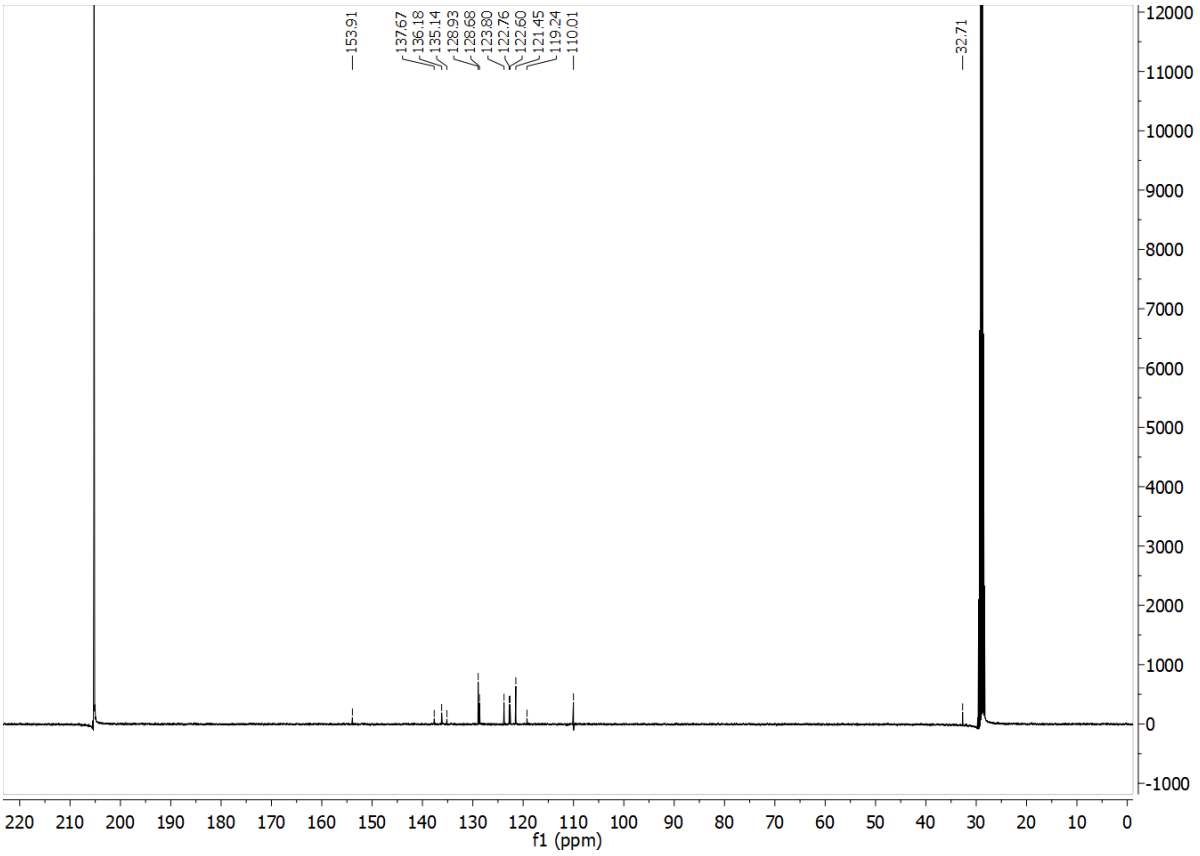

3.3 3a ^{1}H-NMR dilution experiment

In order to support the presence of an intermolecular interaction between the NH containing azoindoles studied, we decided to measure the ^{1}H-NMR spectra of compound **3a** at different concentrations. It is indeed reported in the literature that the intermolecular interactions between nitrogen heterocycles can be followed by a deviation of their NMR signals, taken at different concentrations.[S3] All the experiments were conducted using non-anhydrous DMSO-*d6*. Interestingly, the proton signal of the indolic N-H undergoes a slight high-field shift at higher dilution (ca. 0.05 ppm, from entry 1 to 10 in Table A101). This spectral variation can be ascribed to the formation of intermolecular hydrogen bonds between different molecules of **3a**, that results to be easier at higher concentrations. Thus, these experiments confirm that higher concentrations of NH-bearing azoindole lead to easier intermolecular interactions. Consequently, higher concentrations favour the intermolecular hydrazone mechanism we have proposed, as can be stated by the concentration-dependent results present in Table 1 in the main text (entries 7 and 11).

Entry	**3a** [mg]	Volume(DMSO-*d6*) [mL]	Concentration(**3a**) [mM]
1	70.100	0.007	45.293
2	35.050	0.007	22.647
3	17.525	0.007	11.323
4	8.763	0.007	5.662
5	4.381	0.007	2.831
6	2.191	0.007	1.415
7	1.095	0.007	0.708
8	0.548	0.007	0.354
9	0.274	0.007	0.177
10	0.137	0.007	0.088

Table A101 Concentration of the solutions of 3a analysed by means of ^{1}H-NMR spectroscopy.

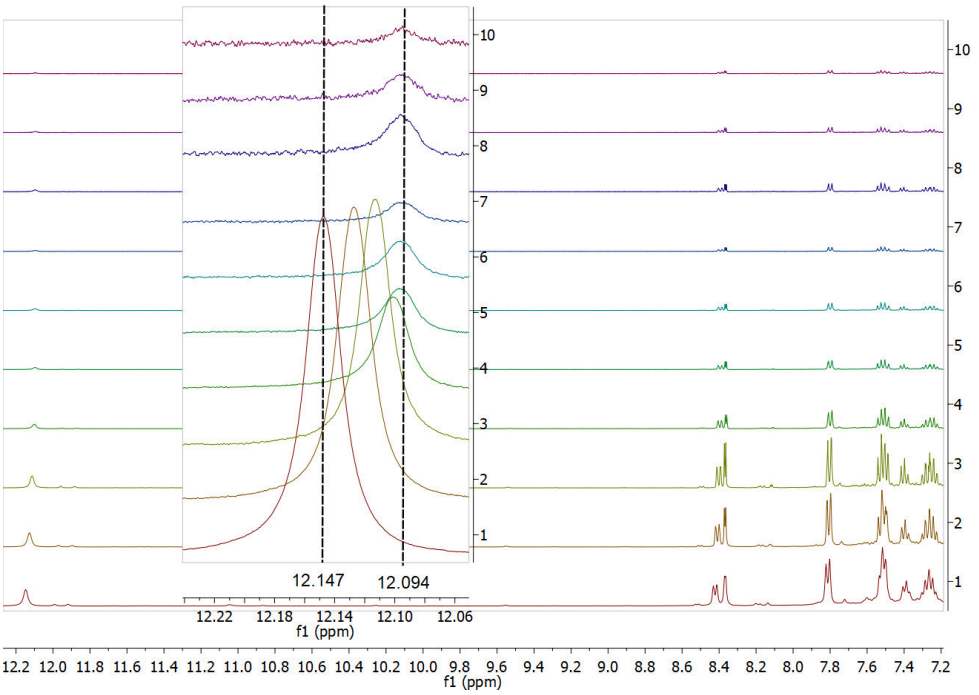

Figure A191 ^{1}H-NMR signals of the aromatic signals of **3a** at different concentrations (referred to Table A101). The inset corresponds to the shift of the NH proton signal of **3a**.

3.4 3c Photostationary State evaluation *via* ^{1}H-NMR

The evaluation of the *Z:E* Photostationary State relative population was done by means of ^{1}H-NMR spectroscopy in MeCN-*d3* and DMSO-*d6*. In order to achieve better accuracy, the *Z:E* ratio was estimated by comparing the integrals referred to the N-CH_3 protons of *E*-**3c** (3.73 ppm in MeCN-*d3*, 3.94 ppm in DMSO-*d6*) with the one of *Z*-**3c** (3.37 ppm in MeCN-*d3*, 3.61 ppm in DMSO-*d6*). The samples were irradiated for 15 min inside the NMR tube with the 96-365 nm LEDs furnished by the multi-plate setup (to assure maximal irradiation surface and total conversion of the *E* isomer to the PSS; for details of the setup see Section **Fehler! Verweisquelle konnte nicht gefunden werden.**) at the distance of 1 cm.

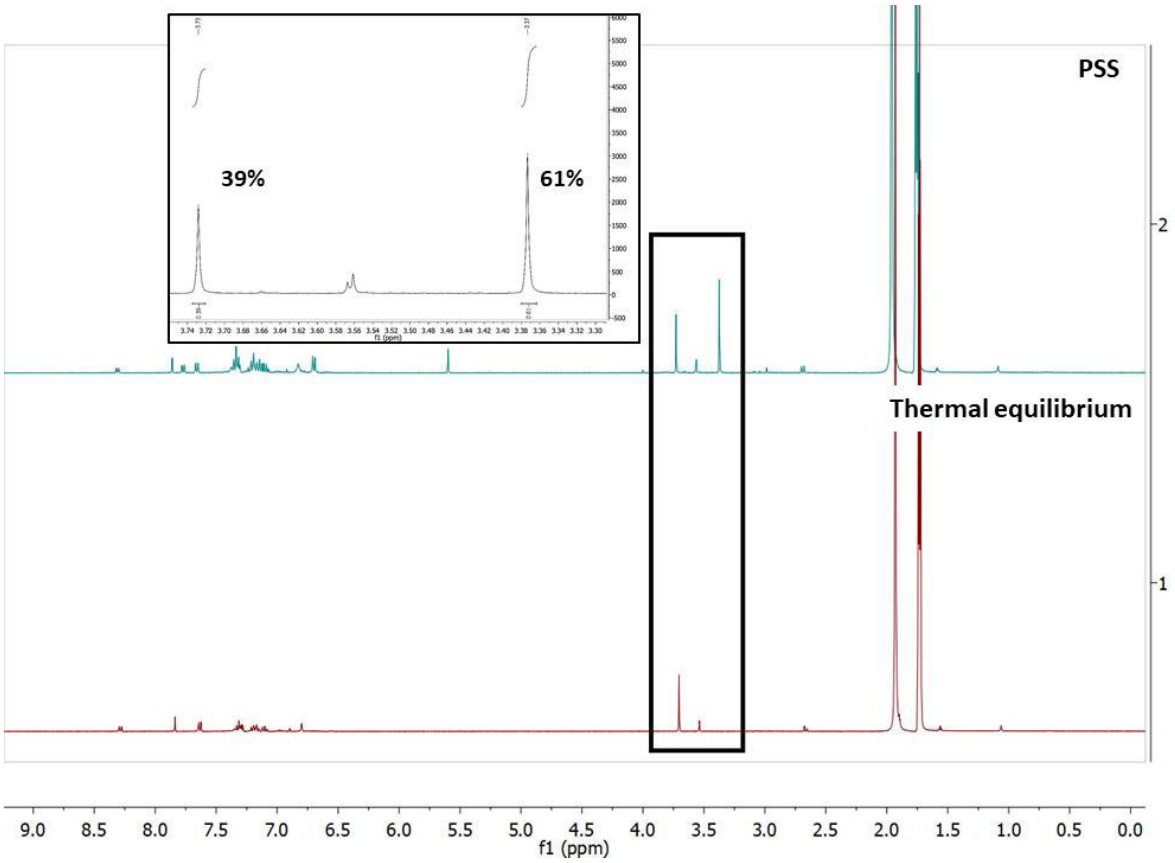

Figure A192 3c in MeCN-*d3* at the PSS and at the thermal equilibrium. In the inset the PSS ratio is given.

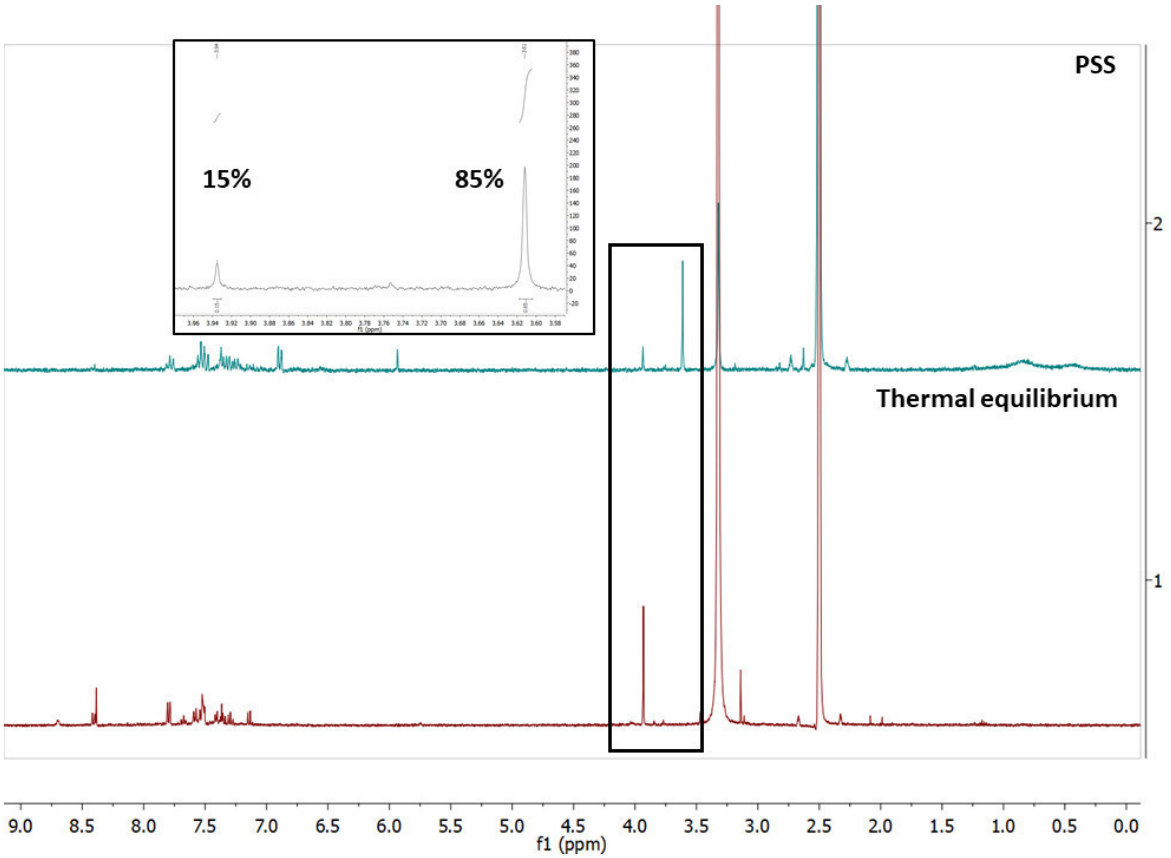

Figure A193 3c in DMSO-*d6* at the PSS and at the thermal equilibrium. In the inset the PSS ratio is given.

4 Computational details

4.2 Photochemical pathway

In order to clarify the photochemistry of the phenylazindoles and to find a relationship, if any, with the parent azobenzene core, we decided to study the photochemical deactivation pathways of our molecules through computational chemistry. In order to simplify the task and generalize the problem, we focused our attention on the photochemical behaviour of **3a**, taken as a reference model. The procedure used for the calculations is CASSCF, a multiconfigurational ab initio method (MCSCF) which make use of all the configurations involving a set of molecular orbitals (MOs, the so–called active space) and a given number of electrons. Hence, this set of configurations is dubbed CASSCF(n,m) where n is the number of electrons and m the number of orbitals involved (both occupied and virtual).[S4] We found that the minimal active space to achieve an acceptable quality/cost ratio was CASSCF(10,8), as a modification of active spaces proven to be effective for azobenzene.[S5] In particular, the n_+, n_-, π and π^* orbitals of the azo group are included, along with two additional π and two π^* orbitals, to obtain a more appropriated model of the substituent effects on the –N=N– group.

We applied the State–Averaged (SAx) CASSCF calculation, in which a single set of molecular orbitals is defined for all the x states that are averaged. The method has the advantage that all the orbitals in SA–CASSCF are orthogonal to each another, allowing faster calculations, even though every state possesses its own set of optimized CI (Configuration Interaction) indices.[S6]

SA3–CASSCF(6,6)/6–31G* based on the three lower singlet roots was applied for stationary points optimization, as implemented in MOLCAS version v8.0.15-06-18[S7]. No symmetry constraints were imposed to the structures investigated. Analytical frequency calculations to evaluate the nature of minima and saddle points were carried out at the same level of theory.

The Conical Intersections (CoIns) between S2-S1 and S1-S0 of **3a** were optimized using the POLYHES method based on the Newton-Raphson formalism developed by Manaa and Yarkony as implemented in COLUMBUS version COL_7.0_beta suite. [S8–11] This method allowed the analysis of the non-adiabatic coupling vectors defining the branching space of the conical intersection. The conical inersections and minimum geometries were then connected via a Linear Interpolation of Internal Coordinate (LIIC) approach.

A multistate second–order perturbation CASPT2 treatment (MS–CASPT2) was followed to account for dynamical correlation,[S12,13] hence, employing a MS–CASPT2//SA3–CASSCF(10,8)/6–31G* level of theory. The aforementioned method applies a perturbation on the energies of the CASSCF eigenvectors and afterward mixes the perturbed states, preventing artifacts near conical intersections (CoIn) or avoided crossing to arise, as observed by Serrano–Andrés *et al.*.[S14] To avoid the intruder states (mostly Rydberg ones) to cause singularities in the CASPT2 computed energies, an Imaginary Level Shift of 0.25 Hartree was introduced.[S15]

The visualization of the structures and orbitals generated by Molcas and COLUMBUS was achieved using Avogadro[S16] and Multiwfn.[S17]

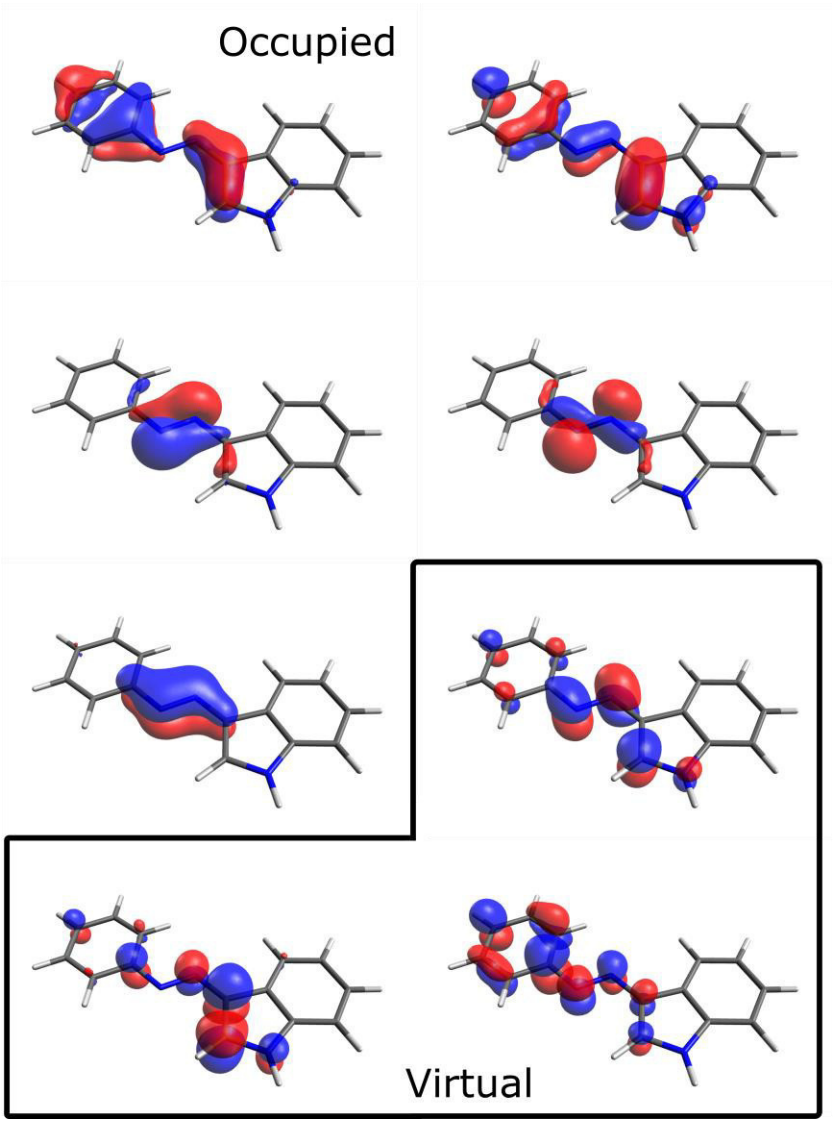

Figure A194 Active space of ***E-3a***. The occupied (in the upper part of the figure) and virtual (in the lower part) orbitals for ***E-3a*** that are taken into account into the active space are depicted.

It has to be noted that the considered pathways and the conical intersections found were limited to the photochemical Trans→Cis isomerization pathway, in which we are interested for the aim of this work. A more complete and accurate analysis of all the pathways and conical intersections, comprehending the photochemical Cis→Trans conversion, are currently ongoing and will be the matter of future works.

4.2.1 Cartesian coordinates

Geometries optimized at the SA3-CASSCF(10,8)/6-31G* level of theory.

***E*-3a**

	X	Y	Z
C	-9.01779041	-4.90011336	-0.88770925
C	-9.54644506	-4.33709676	0.26455185
C	-8.80085605	-3.40880677	0.98482361
C	-7.54181504	-3.04145432	0.56611261
C	-7.00581402	-3.60840891	-0.59741717
C	-7.75757412	-4.54001206	-1.31715332
N	-5.72907233	-3.31132050	-1.12485645
N	-5.06430854	-2.47539120	-0.47352534
C	-3.80583530	-2.18686080	-0.99909776
C	-2.88605938	-1.24238668	-0.38653404
C	-1.74675663	-1.22370606	-1.19179581
N	-1.94484388	-2.09650325	-2.23320191
C	-3.18810893	-2.67769964	-2.11633486
C	-2.94539097	-0.43783690	0.74979600
C	-1.86740170	0.36300479	1.05189495
C	-0.72941114	0.37068480	0.23263323
C	-0.65046486	-0.41567227	-0.89326958
H	-9.58938244	-5.61818139	-1.44810814
H	-10.52873805	-4.61622144	0.60099284
H	-9.21082225	-2.97258530	1.87836060
H	-6.96638127	-2.32634587	1.12010307
H	-7.33244780	-4.96593202	-2.20737094
H	-1.29623001	-2.28356449	-2.95995590
H	-3.53925793	-3.39104085	-2.82943426
H	-3.81935957	-0.44636435	1.37539692
H	-1.89315041	0.99115432	1.92409192
H	0.09956888	1.00557939	0.49079726
H	0.22451723	-0.40667113	-1.51895413

***Z*-3a**

	X	Y	Z
C	-7.92147348	-4.48854291	-2.01019020
C	-8.23594463	-5.17245473	-0.84545242
C	-8.15252507	-4.52160384	0.37611011
C	-7.74396083	-3.20078694	0.44025239
C	-7.38684241	-2.53537080	-0.72691180
C	-7.51092875	-3.16803685	-1.95873593
N	-7.06277144	-1.14182830	-0.67489023
N	-5.88282091	-0.73790043	-0.57163397
C	-4.73140643	-1.54867273	-0.49099679
C	-3.43750503	-0.88720825	-0.39912228
C	-2.47294853	-1.88906190	-0.32416401
N	-3.12275079	-3.09817928	-0.36506881
C	-4.47890826	-2.89710374	-0.46537063
C	-3.05154104	0.45186941	-0.37694684
C	-1.71070835	0.75011663	-0.28081728
C	-0.75247871	-0.27053339	-0.20675343
C	-1.11394742	-1.59857525	-0.22694693
H	-8.00279514	-4.98195437	-2.96231235
H	-8.55831903	-6.19703112	-0.89084326
H	-8.41373397	-5.04055651	1.28113717
H	-7.68988272	-2.68829538	1.38382550
H	-7.27695597	-2.63070515	-2.86006141
H	-2.68847179	-3.98957170	-0.32825078
H	-5.13346123	-3.73648923	-0.50671475
H	-3.79177905	1.22813875	-0.43386580
H	-1.38973562	1.77599683	-0.26188876
H	0.28831796	-0.00955571	-0.13236124
H	-0.37577143	-2.37882309	-0.16975527

Coin$_A$

	X	Y	Z
C	-9.01496	-4.64038	-1.27118
C	-8.98641	-5.08259	0.05194
C	-8.10178	-4.48975	0.93478
C	-7.24867	-3.47894	0.52921
C	-7.28033	-3.03786	-0.80459
C	-8.18581	-3.63650	-1.70452
C	-4.26084	-1.66137	-0.87184
C	-3.14430	-0.82505	-0.46160
C	-1.99149	-1.58472	-0.66113
C	-3.73147	-2.85572	-1.29881
C	-3.04705	0.46764	0.04662
C	-1.79786	0.96910	0.34119
C	-0.64929	0.19383	0.13589
C	-0.72549	-1.08746	-0.36457
N	-6.46141	-2.05065	-1.23473
N	-5.58127	-1.25666	-0.80144
N	-2.36584	-2.80984	-1.16576
H	-9.70021	-5.08906	-1.96861
H	-9.64315	-5.86745	0.37856
H	-8.06922	-4.81411	1.96008
H	-6.56669	-3.02432	1.22319
H	-8.21621	-3.29427	-2.72234
H	-1.74522	-3.53624	-1.43304
H	-4.22425	-3.71583	-1.69769
H	-3.93160	1.05755	0.20170
H	-1.69880	1.96511	0.73272
H	0.31383	0.60823	0.37449
H	0.15954	-1.67832	-0.51959

Coin$_B$

	X	Y	Z
C	4.797464	-0.783890	-0.010816
C	5.293287	0.518780	0.009855
C	4.381277	1.576345	0.023400
C	3.029363	1.364719	0.017430
C	2.532897	0.033703	-0.004293
C	3.452958	-1.049241	-0.019012
C	-1.045551	-1.063696	-0.031979
C	-2.031976	0.020753	-0.015585
C	-3.287070	-0.596011	-0.029053
C	-1.758699	-2.269545	-0.054775
C	-1.926850	1.401871	0.008204
C	-3.082675	2.160780	0.018297
C	-4.330579	1.537220	0.004527
C	-4.453165	0.161634	-0.019245
N	1.227799	-0.182518	-0.010442
N	0.258275	-0.902614	-0.024588
N	-3.122606	-1.953656	-0.051412
H	5.483239	-1.613027	-0.021715
H	6.350500	0.704735	0.015481
H	4.743225	2.589512	0.039688
H	2.340894	2.189542	0.027954
H	3.085557	-2.058365	-0.034684
H	-3.855412	-2.619974	-0.067147
H	-1.408589	-3.276533	-0.069440
H	-0.963461	1.880377	0.018578
H	-3.021747	3.233316	0.036773
H	-5.220220	2.141395	0.012583
H	-5.420332	-0.308105	-0.029688

Coin$_C$

	X	Y	Z
C	-8.658424	-5.074750	-0.715895
C	-9.189390	-4.433338	0.405980
C	-8.693808	-3.190189	0.804503
C	-7.682137	-2.584487	0.106593
C	-7.122284	-3.227477	-1.029049
C	-7.647065	-4.484877	-1.424076
C	-4.312711	-1.763472	-1.483400
C	-3.345093	-1.141117	-0.610178
C	-2.069345	-1.612821	-0.959431
C	-3.525709	-2.682600	-2.384434
C	-3.501577	-0.200620	0.395014
C	-2.376385	0.278049	1.048314
C	-1.118702	-0.191798	0.685421
C	-0.940025	-1.135673	-0.319028
N	-6.142356	-2.718109	-1.819637
N	-5.650847	-1.519983	-1.389851
N	-2.184661	-2.542541	-1.961041
H	-9.047528	-6.029030	-1.021430
H	-9.986257	-4.894666	0.960401
H	-9.116424	-2.701665	1.663946
H	-7.306338	-1.625731	0.399162
H	-7.225408	-4.954913	-2.292864
H	-1.432223	-3.080323	-2.316811
H	-3.854288	-3.655781	-2.681986
H	-4.485196	0.142647	0.656378
H	-2.471562	1.006208	1.832211
H	-0.251578	0.186141	1.197821
H	0.043138	-1.480178	-0.583811

SA3-CASSCF/6-31G* [Hartree]			
	S_0	S_1	S_2
E-**3a**	-699.92876149	-699.81064407	-699.72608296
Z-**3a**	-699.90776790	-699.78488785	-699.70643530
$Coin_A$	-699.84265720	-699.84260168	-699.77698629
$Coin_B$	-699.80591456	-699.80513083	-699.75139670
$Coin_C$	-699.85035057	-699.75476638	-699.75462444
MS-CASPT2//SA3-CASSCF/6-31G* [Hartree]			
	S_0	S_1	S_2
E-**3a**	-702.10460284	-701.99885899	-701.93663368
Z-**3a**	-702.08628627	-701.97472257	-701.89834876
$Coin_A$	-702.02922684	-702.01878944	-701.95908857
$Coin_B$	-701.98672907	-701.98128933	-701.93192274
$Coin_C$	-702.03582954	-701.96101351	-701.94309758

Table A102 Energies of the optimized geometries regarding the photochemical pathway.

4.2.2 Topological analysis of the conical intersections.

It is known that the topography of the region around the conical intersection influences the dynamics of the system.[11,18] The inclination and symmetry of the conical provide hints on the probability of the molecule to return on the upper state or choosing one pathway in respect of another. The topography of the region around the conical intersection is defined by a set of four parameters: σ_x, σ_y, Δ_{gh} and d_{gh}.[S11] Thereby, σ_i controls the tilt of the cone away from the vertical direction along the direction of the gradient difference (**g**, i=x) and derivative coupling (**h**, i=y) vectors, Δ_{gh} determines the deviation from cylindrical symmetry, and d_{gh} controls the pitch of the cone. The energies describing the upper (E_{sup}) and lower (E_{inf}) parts of the branching space are the following:

$$E_{sup} = d_{gh}\left(\sigma_x x + \sigma_y y + \sqrt{\left(\frac{x^2+y^2}{2} + \Delta_{gh}\frac{x^2-y^2}{2}\right)}\right) \quad (1)$$

$$E_{inf} = d_{gh}\left(\sigma_x x + \sigma_y y - \sqrt{\left(\frac{x^2+y^2}{2} + \Delta_{gh}\frac{x^2-y^2}{2}\right)}\right) \quad (2)$$

The energies given in the following tables regarding the energy surfaces of the branching space of the CoIns are expressed in eV.

S_0←S_1 ($CoIn_A$)

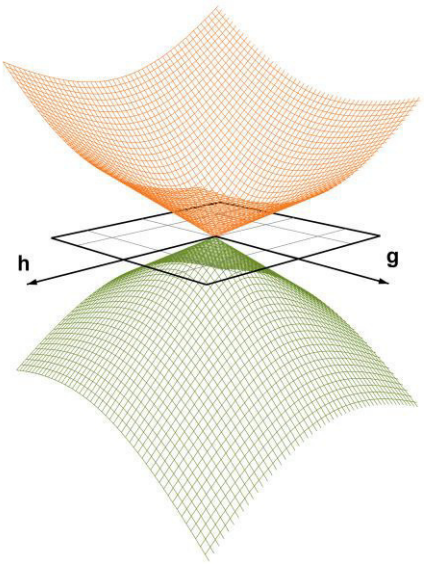

Figure A195 Branching space of the Conical Intersection $CoIn_A$, connecting S_1 and S_0.

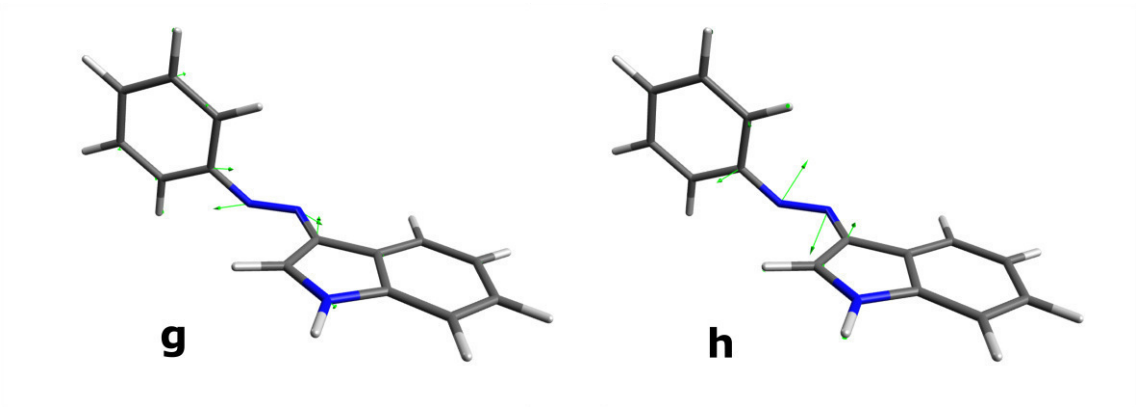

Figure A196 Normalized gradient difference (**g**) and Derivative Coupling (**h**) non-orthogonalized vectors of $CoIn_A$.

σ_x	-0.271
σ_y	0.147
Δ_{gh}	-0.06
d_{gh}(eV/Å)	5.44

Table A103 Parameters defining the topology of $Coin_A$

The *g*–*h* space is defined by the distortion of the geometry towards either *E*-**3a** (**g** vector) or *Z*-**3a** (**h** vector). This CoIn resembles the rotational conical intersection typical of azobenzene.[S19] The slightly negative Δ_{gh} value corresponds to a minimal asymmetry of the otherwise cylindrical double cone towards x (**g**, direction of the *E*-**3a** formation). The conical is pitched, due to the high value of d_{gh}. The topology of the conical and its symmetry suggest that the transition from S_1 to S_0 is extremely efficient (due to its peaked shape)[S20] and slightly favours the formation of *E* in respect to *Z*. Anyways, both of the isomers can be accessed.

S_0←S_1 ($CoIn_B$)

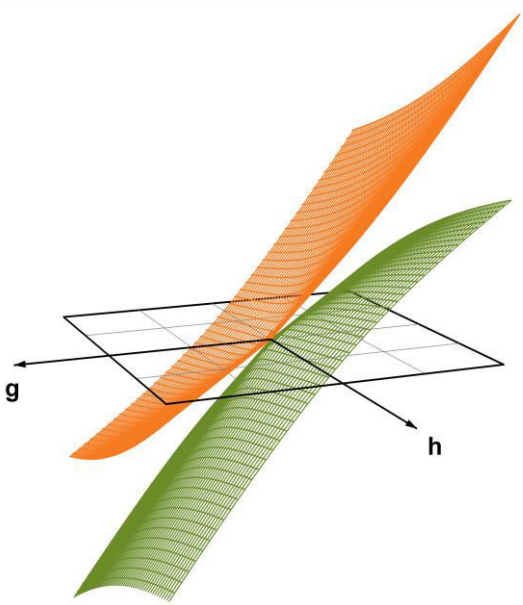

Figure A197 Branching space of the Conical Intersection $CoIn_B$, connecting S_1 and S_0.

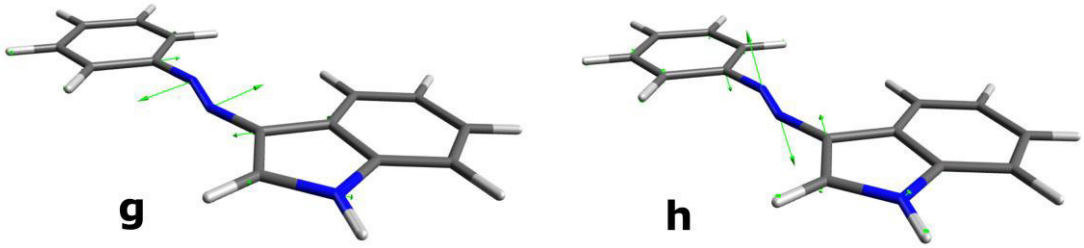

Figure A198 Normalized gradient difference (**g**) and Derivative Coupling (**h**) non-orthogonalized vectors of $CoIn_B$.

σ_x	2.041
σ_y	0.837
Δ_{gh}	0.34
d_{gh} (eV/Å)	4.97

Table A104 Parameters defining the topology of $CoIn_B$

The degeneracy of this conical intersection can be lifted by falling into the *E*-**3a** isomer geometry, both from the distortion depicted by **g** and **h**. $CoIn_B$ resembles the elongated conical intersection of azobenzene that connects S_0 and S_1. Due to its position compared to the Franck-Condon geometry of S_1 (see Table A102), this geometry is accessible only after populating S_2 and funnelling through $CoIn_C$. Due to the impossibility to form *Z*-**3a**, $CoIn_B$ lowers the quantum efficiency of the *E*-to-*Z* photochemical isomerization from S_2. A parallel of this point, regarding the topology and behaviour, can be found in the parent azobenzene.[S21] The conical intersection is elongated toward y, shifting from the cylindrical symmetry. Moreover, it is extremely tilted toward the x direction, and possesses a peaked shape of the two cones.

S_1←S_2 ($CoIn_C$)

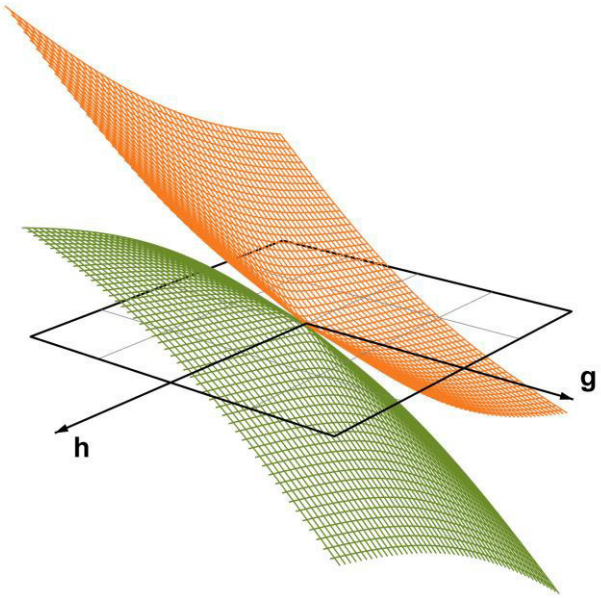

Figure A199 Branching space of the Conical Intersection $CoIn_C$, connecting S_2 and S_1.

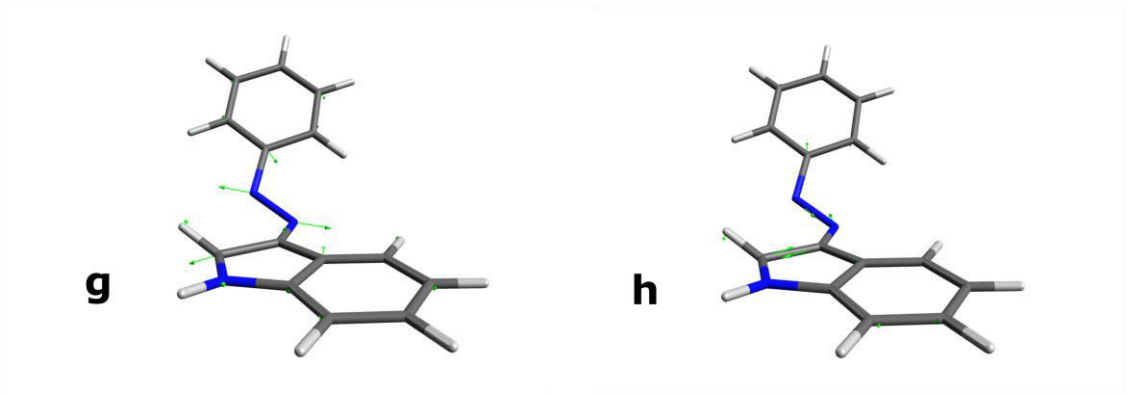

Figure A200 Normalized gradient difference (**g**) and Derivative Coupling (**h**) non-orthogonalized vectors of $CoIn_C$.

σ_x	1.115
σ_y	-0.939
Δ_{gh}	0.06
d_{gh} (eV/Å)	5.56

Table A105 Parameters defining the topology of $CoIn_C$

The **g** vector of $CoIn_C$ deforms the molecule toward the rotation coordinate, favouring the population of geometries similar to the one belonging to $CoIn_A$. On the other hand, **h** lifts the degeneracy in the direction of either the trans isomer on the S_1 surface (that will eventually funnel through $CoIn_A$) or $CoIn_B$ (that will deactivate the molecule reforming the *E* starting reagent). $CoIn_C$ is characterized by a cylindrical geometry slightly deformed toward y (Δ_{gh}=0.06). The conical is overall tilted both in the x and y direction, letting the two aforementioned pathways to be equally probable. The efficiency of the S_1←S_2 funnelling is mirrored by the peaked shape of the double-cone (d_{gh}=5.56).

4.2.3 Linear Interpolation of Internal Coordinates (LIIC) Pathways

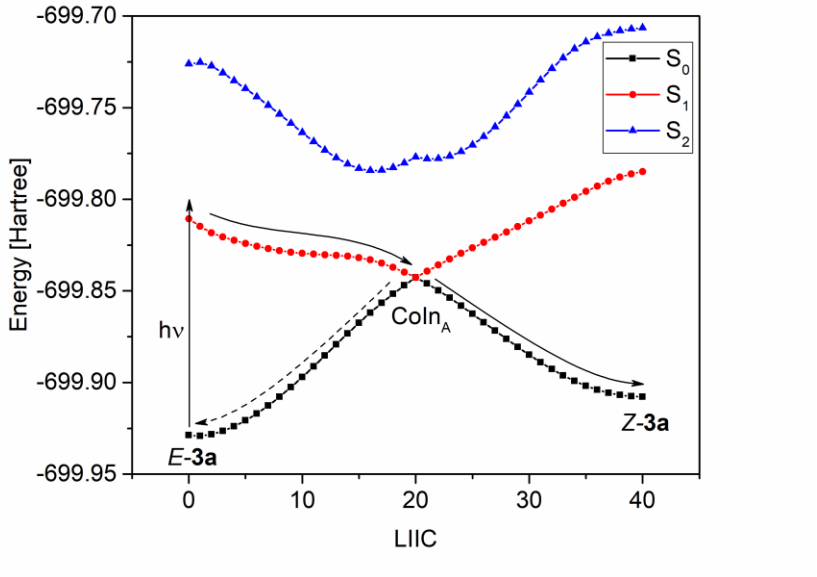

Figure A201 LIIC pathway connecting the Franck-Condon geometry of *E*-**3a** at the S_1 (after vertical n→π* excitation) with the geometry of $CoIn_A$ (in red, from point 0 to point 20. The corresponding energies at the S_0 and S_2 are also shown.) and LIIC pathway connecting $CoIn_A$ to *Z*-**3a** (in black, from point 20 to point 40. The corresponding energies at the S_1 and S_2 are also shown.). This trajectory is barrierless.

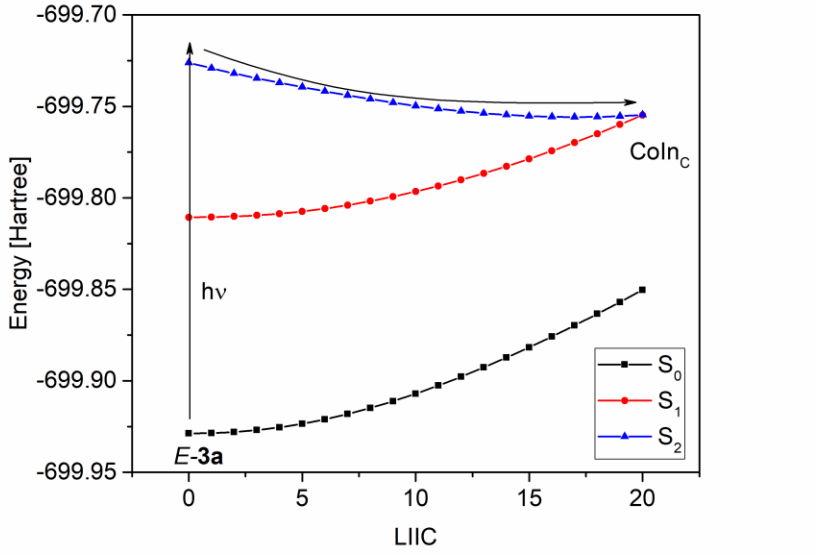

Figure A202 LIIC pathway (in blue) connecting the Franck-Condon geometry of *E*-**3a** at the S_2 (after vertical π→π* excitation) with the geometry of $CoIn_C$. This trajectory is barrierless. The corresponding energies at the S_0 and S_1 are also shown.

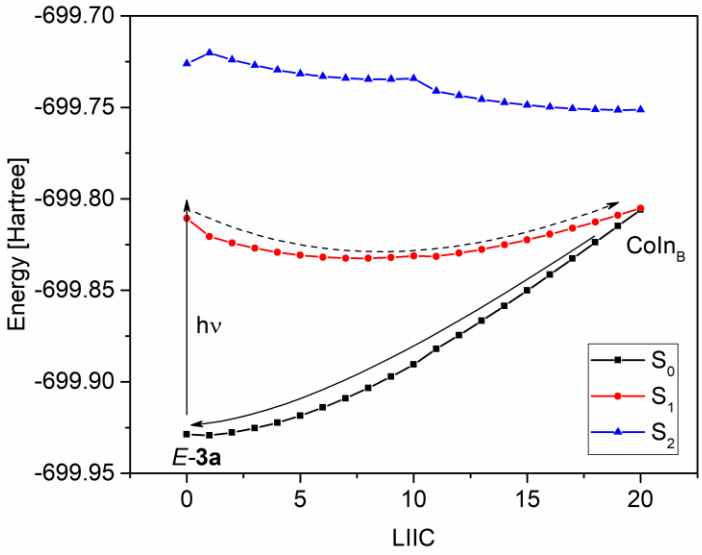

Figure A203 LIIC pathway (in red) connecting the Franck-Condon geometry of *E*-**3a** at the S_1 (after vertical n→π* excitation) with the geometry of $CoIn_B$. The trajectory describes an endergonic pathway (ΔE=+11 kcal/mol at the MS-CASPT2). The corresponding energies at the S_0 and S_2 are also shown.

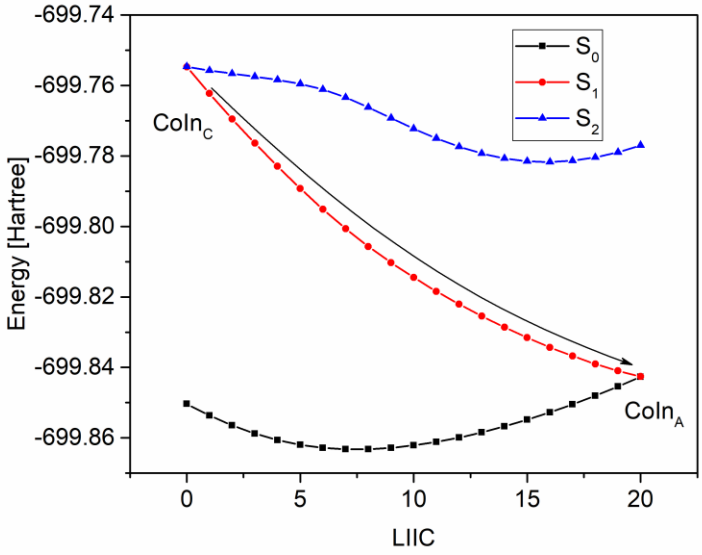

Figure A204 LIIC pathway connecting $CoIn_C$ to $CoIn_A$. This trajectory is barrierless. The corresponding energies at the S_0 and S_2 are also shown.

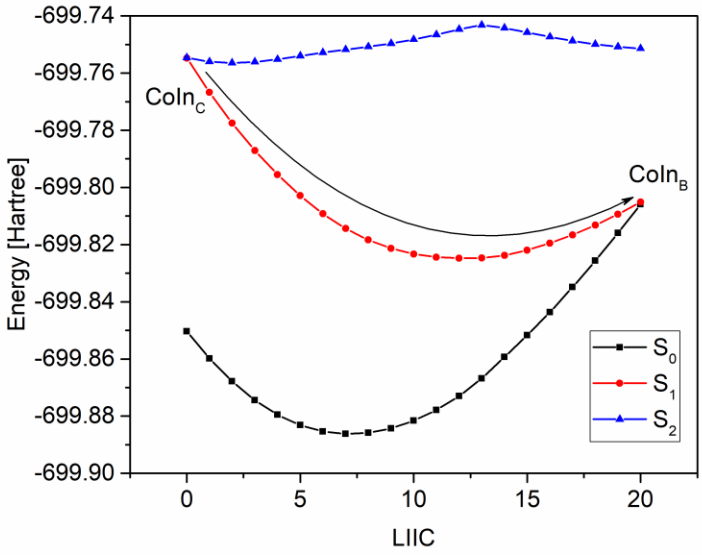

Figure A205 LIIC pathway connecting $CoIn_C$ to $CoIn_B$. This trajectory is globally exergonic (ΔE=-13kcal/mol at the MS-CASPT2 level of theory). The corresponding energies at the S_0 and S_2 are also shown.

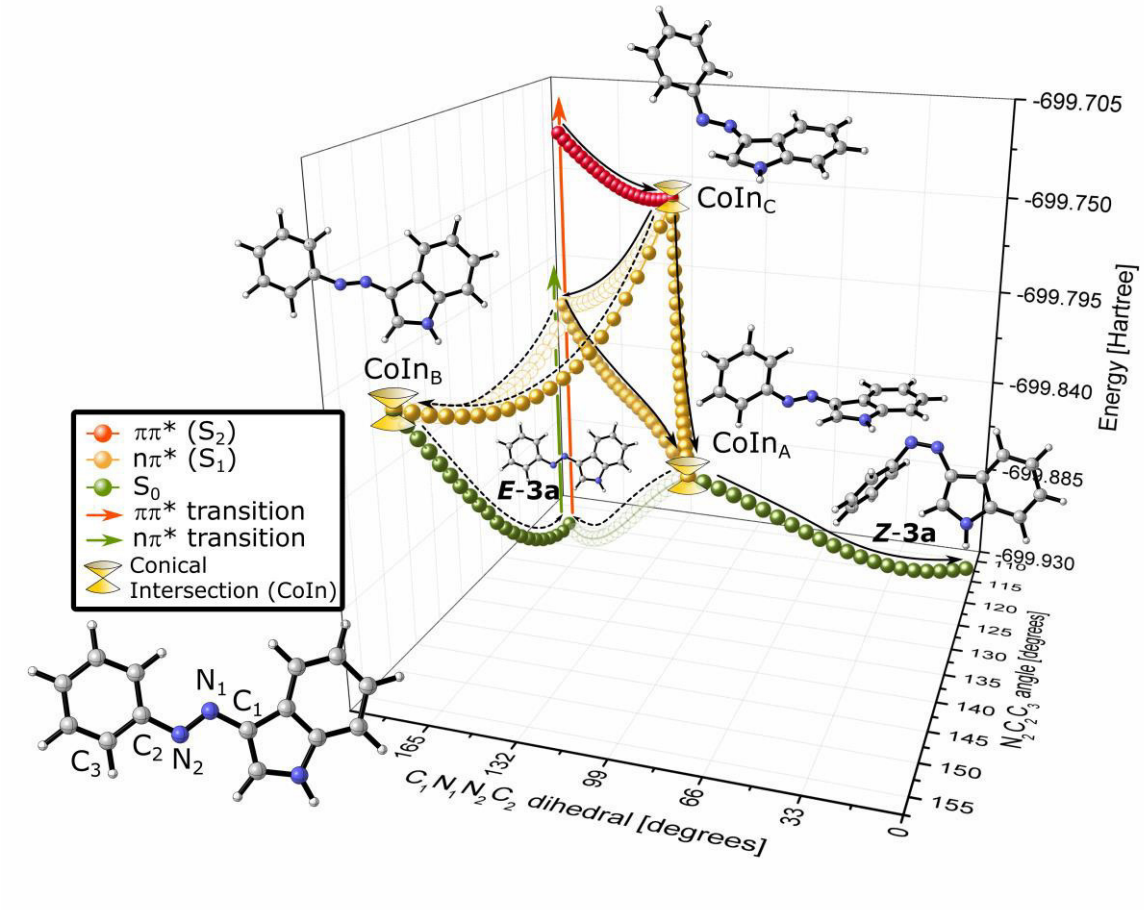

Figure A206 LIIC pathways describing the photochemical *E*-to-*Z* isomerization (bold arrows. The dashed arrows represent the pathways that lead to the formation of the *E* reagent). In order to depict in a single picture the LIIC shown in the previous figures, the energy of the system (in Hartree) is plotted as a function of the $C_1N_1N_2C_2$ (see inset) dihedral and $N_2C_2C_3$ angle.

4.3 TD-DFT UV/Vis simulations

The TD-DFT simulation was carried out using Gaussian 09, Revision D.01 and Gaussian 16, Revision A.03 software packages.[22] The most stable trans- and cis-isomers (between the different ones screened with the B3LYP/3-21G approach) were further optimised using the B3LYP/6-311+G(2d,p) level of theory. The UV/Vis spectra were simulated at the (C)-PCM-PBE0/6-311+G(2d,p) level (solvent: DMSO), computing the lowest 25 singlet transitions. We found, after a peculiar benchmark, that this approach gives better results in terms of accuracy of the position of the predicted bands, compared to the experimental ones. The benchmark and an in-deep analysis of the spectroscopic properties of the arylazoindoles will be the subject of a future publication.

The UV/Vis band was plotted as ε vs λ (excitation wavelength in nm) with the peaks, furnished by the calculation, assuming a gaussian band shape (characterized by a standard deviation σ=0.4eV). The equation for the simulated spectra follows the one described in the Gaussian White Papers[1]:

$$\varepsilon(\lambda) = \sum_{i=1}^{n} \varepsilon_i(\lambda) = \sum_{i=1}^{n} \left\{ 1.3062974 \times 10^8 \frac{f_i}{\frac{10^7}{3099.6}} \exp\left[-\left(\frac{1/\lambda - 1/\lambda_i}{\frac{1}{3099.6}} \right)^2 \right] \right\} \qquad (3)$$

with f_i the computed oscillator strengths, referred to a specific wavelength λ_i.

We are interested in the nature of the two lowest transitions, to seek a comparison, if any, with azobenzene and unravel the nature of the intermediate we have found using laser flash photolysis. Hence, the calculations were made on the optimized structures of *E*-**3a-c**, *Z*-**3a-c** and the two most stable rotational isomers (*s*-trans and *s*-cis) of the hydrazone form of **3b**.

[1] http://dev.gaussian.com/uvvisplot/

4.3.1 Cartesian coordinates

***E*-3a**

	X	Y	Z
C	-9.6872703203	0.7975455704	1.0134847347
C	-9.8379456993	2.1621515239	0.762393773
C	-8.7515754188	2.9057112926	0.3137552264
C	-7.5220904316	2.2891308025	0.117233506
C	-7.3679126933	0.9235936823	0.3676346424
C	-8.4637242361	0.1762593514	0.819602174
N	-6.0712841141	0.399629475	0.133374074
N	-5.9491057746	-0.8337725713	0.3649581614
C	-4.6935501683	-1.3618494747	0.1425003584
C	-3.4451711152	-0.7819741024	-0.31557527
C	-2.506002377	-1.8398500951	-0.3396663213
N	-3.1559658262	-2.9924226619	0.0813202506
C	-4.4563906063	-2.7038928623	0.3670986547
C	-3.0286261039	0.497805502	-0.7014713999
C	-1.7110423241	0.6810714808	-1.0930589799
C	-0.7977304597	-0.3842661032	-1.1086666807
C	-1.1832100805	-1.6616969831	-0.7315549021
H	-10.5339016809	0.2178338383	1.3631573414
H	-10.7983062914	2.6396194693	0.9167472723
H	-8.861671055	3.9655181788	0.1168934218
H	-6.6634491826	2.8497223328	-0.2316534885
H	-8.3372470726	-0.8803796584	1.011418721
H	-2.7327231829	-3.9012770656	0.1633739032
H	-5.1466290504	-3.4558389838	0.7129988428
H	-3.7304558308	1.3183363651	-0.6898412966
H	-1.3771431935	1.6668153173	-1.3938167736
H	0.2245719623	-0.2070683317	-1.4200203961
H	-0.4799914216	-2.4864542851	-0.7426215639

***Z*-3a**

C	-7.9285757895	-4.5072081977	-2.0056470992
C	-8.2435623858	-5.1888100993	-0.8328382243
C	-8.1486984277	-4.5306464671	0.3906365538
C	-7.7301878352	-3.2058655279	0.4471140797
C	-7.3891928669	-2.5356721049	-0.7284683119
C	-7.5084427926	-3.1826768238	-1.9592723262
N	-7.0626781979	-1.1439734054	-0.684484859
N	-5.8876028941	-0.7260258575	-0.5870795168
C	-4.7372171097	-1.5184846961	-0.5030078489
C	-3.4488852407	-0.8667468945	-0.4047398234
C	-2.472932749	-1.880259718	-0.3298713443
N	-3.1443060361	-3.0918816828	-0.3798174205
C	-4.4883356693	-2.8863902653	-0.482949545
C	-3.0466586111	0.4727050351	-0.3751144183
C	-1.6949478596	0.7550094278	-0.2728209233
C	-0.7368272163	-0.271673095	-0.1995899798
C	-1.1111456167	-1.6053357101	-0.2269575196
H	-8.0169381706	-5.0064434296	-2.9636266214
H	-8.5765174061	-6.2187143138	-0.8734843206
H	-8.4090574785	-5.0481820969	1.3066769295
H	-7.6663406997	-2.6843694724	1.3945996913
H	-7.2731534593	-2.6434596607	-2.8690167371
H	-2.7096987248	-3.9994469737	-0.3452693332
H	-5.1598600788	-3.7236611954	-0.5327649742
H	-3.7849814568	1.2619439553	-0.431571067
H	-1.3643519114	1.7863498293	-0.2483972328
H	0.3126134064	-0.0154049884	-0.1203422385
H	-0.3735409194	-2.3973657723	-0.1706052003

***E*-3b**

C	4.610185	0.869655	0.000027
C	5.279741	-0.36034	0.000028
C	4.546188	-1.548086	0.000001
C	3.153034	-1.506483	-0.00003
C	2.478393	-0.277168	-0.000029
C	3.220665	0.917479	-0.000001
N	1.063048	-0.355277	-0.000055
N	0.476929	0.773123	0.000039
C	-0.899833	0.724933	0.000003
C	-1.846244	-0.376625	0.
C	-3.13586	0.212651	0.000009
N	-2.965311	1.593487	0.000104
C	-1.633995	1.910083	0.000024
C	-1.742684	-1.776079	0.000005
C	-2.910586	-2.53391	-0.00001
C	-4.179467	-1.9259	-0.000007
C	-4.310312	-0.53964	0.000014
H	5.180552	1.795383	0.000045
H	6.366155	-0.389005	0.000049
H	5.058914	-2.506355	0.000003
H	2.560899	-2.416892	-0.000053
H	2.688563	1.8622	-0.000001
H	-3.713598	2.270633	-0.000358
H	-0.765062	-2.241538	0.000014
H	-2.842684	-3.618424	-0.000014
H	-5.071983	-2.545473	-0.000016
H	-5.288206	-0.064878	0.000027
C	-1.152458	3.324452	-0.00005
H	-0.532765	3.52704	0.879743
H	-0.534232	3.527504	-0.880781
H	-1.989824	4.030335	0.000823

***Z*-3c**

C	-2.837559	-0.125215	1.942392
C	-4.096456	0.277406	1.4857
C	-4.414071	0.144331	0.131996
C	-3.481763	-0.388343	-0.756558
C	-2.202914	-0.750314	-0.30896
C	-1.88955	-0.631494	1.055563
N	-1.361244	-1.432777	-1.245431
N	-0.119659	-1.256287	-1.339518
C	0.592771	-0.20707	-0.730122
C	1.93923	-0.399757	-0.240643
C	2.430281	0.877077	0.124964
N	1.434475	1.793474	-0.170017
C	0.328576	1.158701	-0.699099
C	2.752887	-1.527747	-0.059771
C	4.025867	-1.351989	0.471
C	4.494735	-0.073752	0.834768
C	3.703889	1.059315	0.669163
H	-2.592755	-0.047973	2.998656
H	-4.828517	0.674918	2.183185
H	-5.396314	0.437022	-0.229585
H	-3.726452	-0.53498	-1.80471
H	-0.917308	-0.950811	1.416038
H	1.539154	2.796489	-0.12637
H	2.391538	-2.512273	-0.340662
H	4.673192	-2.213527	0.609437
H	5.492232	0.030475	1.252567
H	4.065185	2.045029	0.950555
C	-0.836082	1.950906	-1.19341
H	-1.309477	1.450995	-2.042504
H	-1.605564	2.073857	-0.420703
H	-0.518959	2.947569	-1.523043

S-trans hydrazone of 3a

C	4.222142581	-1.7932552063	0.
C	5.3003279164	-0.9026173824	0.
C	5.0536870585	0.4725631171	0.
C	3.7467220115	0.9563956755	0.
C	2.6721240886	0.0550628309	0.
C	2.909165547	-1.3271498927	0.
N	1.3688945773	0.5784438918	0.
N	0.3068487236	-0.1978863827	0.
C	-0.8982604347	0.3106795422	0.
C	-2.1195002882	-0.4940035797	0.
C	-3.1738807565	0.4467220656	0.
N	-2.6887492297	1.7791164213	0.
C	-1.3865592428	1.6986375345	0.
C	-2.385410602	-1.8609129826	0.
C	-3.7237897415	-2.2732157114	0.
C	-4.7685969559	-1.3375418929	0.
C	-4.5045537543	0.0378297958	0.
H	4.4022942917	-2.8646728076	0.
H	6.3197826934	-1.2763909439	0.
H	5.8805302831	1.1769383455	0.
H	3.5587102313	2.027100912	0.
H	2.0719028607	-2.0147140315	0.
H	1.2712175317	1.5924687961	0.
H	-1.5791852276	-2.5893501509	0.
H	-3.9564317729	-3.3345419055	0.
H	-5.7978390514	-1.6855096833	0.
H	-5.3088519591	0.7679820164	0.
H	-0.7763488993	2.5976208987	0.

S-cis hydrazone of 3a

C	-3.7392273976	0.3916102563	1.710032121
C	-4.3164045868	0.9795482001	0.5811165283
C	-3.9046985453	0.596678328	-0.6984110791
C	-2.9104838862	-0.3708143543	-0.8533624662
C	-2.3305010679	-0.947470245	0.2805878673
C	-2.744408334	-0.5765802315	1.5634984132
N	-1.3142359658	-1.9528901301	0.1252149276
N	-0.0089528408	-1.8006331651	0.04850632
C	0.6211682625	-0.6541703341	0.1027608746
C	2.0839069976	-0.5883690632	0.0079553598
C	2.4001621218	0.7839079048	0.1029415575
N	1.2375359142	1.5780526227	0.2503379076
C	0.2212115276	0.7586989033	0.2504101623
C	3.0901711647	-1.5397581037	-0.1420176991
C	4.4172244514	-1.0970781954	-0.1954767519
C	4.7287001328	0.2679243	-0.1007847173
C	3.7202357164	1.226505818	0.0499470895
H	-4.0647971871	0.6830447116	2.7042558136
H	-5.090698094	1.7321948051	0.6983869934
H	-4.3589152886	1.0474591266	-1.5758481861
H	-2.5809700727	-0.6794693481	-1.8407567202
H	-2.2873719962	-1.0430718234	2.430854149
H	-1.6009943958	-2.9217422241	0.0625761343
H	2.853224299	-2.5977359412	-0.2157039945
H	5.2187685258	-1.8215333825	-0.3120940098
H	5.767354121	0.5841507287	-0.1451901816
H	3.9528493275	2.2852399617	0.1240191919
H	-0.7895136035	1.1323766145	0.3516851551

S-trans hydrazone of 3b

C	4.178308	-1.813667	0.000519
C	5.275987	-0.948493	-0.000065
C	5.058718	0.430496	-0.000572
C	3.76264	0.940558	-0.000563
C	2.667189	0.065248	-0.000001
C	2.876017	-1.320825	0.000579
N	1.377547	0.61685	0.00008
N	0.293978	-0.143569	0.000007
C	-0.905313	0.365677	0.000179
C	-2.112171	-0.462555	0.000015
C	-3.18394	0.453168	0.000116
N	-2.730514	1.793782	0.000044
C	-1.428828	1.764574	0.000161
C	-2.345448	-1.833634	-0.000198
C	-3.674024	-2.275535	-0.000315
C	-4.737355	-1.363162	-0.000229
C	-4.503902	0.017554	0.000004
H	4.335303	-2.888967	0.000931
H	6.287173	-1.344282	-0.000114
H	5.900607	1.117331	-0.001008
H	3.598672	2.01631	-0.000954
H	2.020933	-1.985782	0.001092
H	1.302249	1.629877	-0.000453
H	-1.52055	-2.540679	-0.00021
H	-3.883534	-3.341836	-0.000469
H	-5.759064	-1.733434	-0.000327
H	-5.320255	0.733548	0.000032
C	-0.634363	3.037176	0.00031
H	0.007124	3.121694	0.889414
H	0.006606	3.122084	-0.889141
H	-1.323428	3.885209	0.00066

S-cis hydrazone of 3b

C	-3.131024	0.327606	1.801526
C	-4.43482	0.373105	1.305302
C	-4.689685	-0.097727	0.015435
C	-3.653896	-0.597398	-0.770152
C	-2.345031	-0.642338	-0.267956
C	-2.086528	-0.179922	1.02818
N	-1.352001	-1.2297	-1.107783
N	-0.022871	-1.346157	-0.810223
C	0.708452	-0.311703	-0.536731
C	2.109105	-0.459788	-0.119137
C	2.600183	0.852533	0.00545
N	1.627795	1.815036	-0.367578
C	0.528832	1.183319	-0.655381
C	2.908727	-1.556777	0.175927
C	4.225603	-1.317382	0.591238
C	4.711682	-0.01053	0.716281
C	3.901616	1.09597	0.423853
H	-2.918351	0.681901	2.806576
H	-5.240799	0.771403	1.914356
H	-5.698156	-0.06841	-0.388226
H	-3.849929	-0.949069	-1.780182
H	-1.082222	-0.221422	1.43449
H	-1.666825	-2.121072	-1.474575
H	2.522723	-2.567925	0.082854
H	4.877129	-2.156218	0.820323
H	5.734927	0.149207	1.045796
H	4.271144	2.112681	0.516796
C	-0.658543	1.908942	-1.203858
H	-1.049435	1.404084	-2.095056
H	-1.480008	1.95601	-0.480849
H	-0.358701	2.927114	-1.463066

***E*-3c**

C	-9.6850260798	1.2503518998	1.0224026778
C	-9.8474941729	2.6111641289	0.7586442349
C	-8.7703378731	3.3565613649	0.2910417334
C	-7.5389453608	2.7458300505	0.0883735208
C	-7.3726207829	1.3838942088	0.3515154055
C	-8.4594223428	0.6348708072	0.8225518554
N	-6.0754601689	0.8659596111	0.109441071
N	-5.9428972559	-0.3647666898	0.355222013
C	-4.6891619187	-0.8889337022	0.1264453001
C	-3.4487987149	-0.3136790794	-0.3516334538
C	-2.5096447937	-1.3734979774	-0.3692086699
N	-3.1446744493	-2.5287180231	0.0737479512
C	-4.439905736	-2.2280824693	0.3653552708
C	-3.0386959334	0.9601593778	-0.7593722187
C	-1.7247581952	1.1400814287	-1.167009606
C	-0.8108748035	0.0763093562	-1.1766315823
C	-1.1904567444	-1.1973545534	-0.7774613744
C	-2.5207858526	-3.8298234945	0.1997374207
H	-10.5242233472	0.668775281	1.386768239
H	-10.8093287882	3.0841034498	0.9177609694
H	-8.8891909688	4.4135476255	0.0840905552
H	-6.6876745449	3.3083203533	-0.2752730886
H	-8.3242386267	-0.4188669833	1.0241703096
H	-5.1248112275	-2.9775057914	0.7288323753
H	-3.7419570053	1.7796401427	-0.7521563794
H	-1.395525889	2.1220332396	-1.4849753112
H	0.2080894278	0.250227154	-1.5007011456
H	-0.4825807291	-2.0171549467	-0.7859722003
H	-1.6857815895	-3.7925156544	0.9032796276
H	-3.2563489704	-4.5420890829	0.5686244774

***Z*-3c**

C	-7.3900739999	-4.1687446702	-2.4541260978
C	-7.7711618679	-4.8749921114	-1.3159531573
C	-7.8592855901	-4.2122777298	-0.0942901782
C	-7.5566572925	-2.858208589	-0.0041065625
C	-7.1488158651	-2.1604682324	-1.1421133581
C	-7.0853924418	-2.8145321488	-2.3735493052
N	-6.9418753487	-0.7475544533	-1.0748050914
N	-5.8217322378	-0.237314141	-0.8437369359
C	-4.63165757	-0.933277874	-0.6210329871
C	-3.4212604334	-0.1858250735	-0.3678438134
C	-2.3866292006	-1.1251237216	-0.1797704136
N	-2.9402516998	-2.3911851518	-0.3121859021
C	-4.2726876424	-2.277970979	-0.5741025199
C	-3.1308411325	1.1791344688	-0.2855406262
C	-1.8266675288	1.5634109735	-0.0199728046
C	-0.8081923831	0.6127084793	0.1647116235
C	-1.0719092908	-0.7462315473	0.0877515698
C	-2.2089008697	-3.6371728637	-0.1889322121
H	-7.3368923252	-4.6723699774	-3.4124689902
H	-8.0147900815	-5.9282447622	-1.3838154143
H	-8.1730534384	-4.7499623799	0.7930297468
H	-7.6352690543	-2.3342452341	0.9409361954
H	-6.8001714285	-2.2568670373	-3.2575649138
H	-4.8658233595	-3.1644239566	-0.7075355855
H	-3.9161140198	1.9101404871	-0.4279354407
H	-1.5826996151	2.6167779318	0.0475371046
H	0.2011922712	0.9473537656	0.3709566507
H	-0.2842499138	-1.4757568114	0.2307601622
H	-1.7630379803	-3.724893284	0.804373835
H	-2.8945292066	-4.4683955734	-0.3405633132
H	-1.4159149864	-3.6934348365	-0.9380145974

4.3.2 Computed electronic transitions

For the seek of simplicity only the lowest five transitions are reported. For each transition the excitation energy in eV, the associated wavelength in nm and the value of the oscillator strength (f) are given. Moreover, the index of the orbitals involved in the transition (dubbed as Occupied → Unoccupied) with their largest coefficient in the CI expansion are reported. Pictures of the orbitals of the two lowest transitions are also given.

An interesting feature of the azoindoles studied is the oscillator strength associated with the lowest transition, that is always of n→π* nature (*vide infra*). All the *E*- isomers of **3a-c** possess f=0 for the lowest transition, due to the n→π* excitation is symmetry forbidden in azo-compounds.[S23] On the other hand, the *Z*- configuration in azobenzene breaks the symmetry limitations, due to its non-planar geometry. However, *Z*-**3a,b** most stable conformer is characterized by C_{2v} symmetry, because the phenyl ring is preferably positioned in an orthogonal fashion compared to the indole ring. Probably, the minor sterical demands of the five-membered cycle inside the indole, in respect to benzene in azobenzene, allows the twist of the phenyl moiety to its symmetrical shape. Only *Z*-**3b** shows a non-symmetric geometry, due to the presence of the methyl, preventing the full rotation of the phenyl ring. Thus, the n→π* band is (slightly) allowed in this configuration. Due to the calculated spectra, we can assume the continuum of absorption bands that are bathocromically shifting in the transient spectra of **3b** are derived from the sequential appearance of the *Z*- isomer, the *s*-cis hydrazone and the *s*-trans hydrazone. The latter is characterized by a "fingerprint" absorption around 410 nm.

The second transition is always of π→π* nature for **3a**-**c**. Interestingly, the electrons come from an occupied orbital delocalized on the entire π core, with larger coefficients on the indole ring.

***E*-3a**

Excited State 1: 2.8587 eV 433.70nm f=0.0000
57 → 59 0.70082
Excited State 2: 3.3669 eV 368.24nm f=0.9057
58 → 59 0.70159
Excited State 3: 3.9627 eV 312.88nm f=0.0133
56 → 59 0.68747
58 → 60 0.13311
Excited State 4: 4.3954 eV 282.08nm f=0.0073
54 → 59 0.59009
55 → 59 0.27378
55 → 61 0.11041
58 → 61 0.23934
Excited State 5: 4.5237 eV 274.08nm f=0.1079
54 → 59 -0.24792
55 → 59 0.62365
56 → 60 0.14891

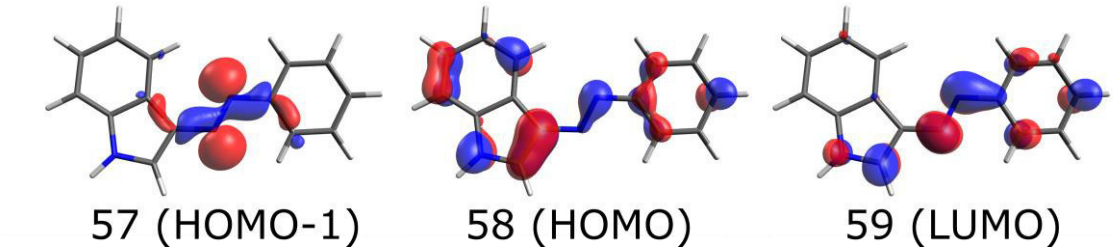

Figure S207 Orbitals involved in the two lowest transitions for *E*-**3a**.

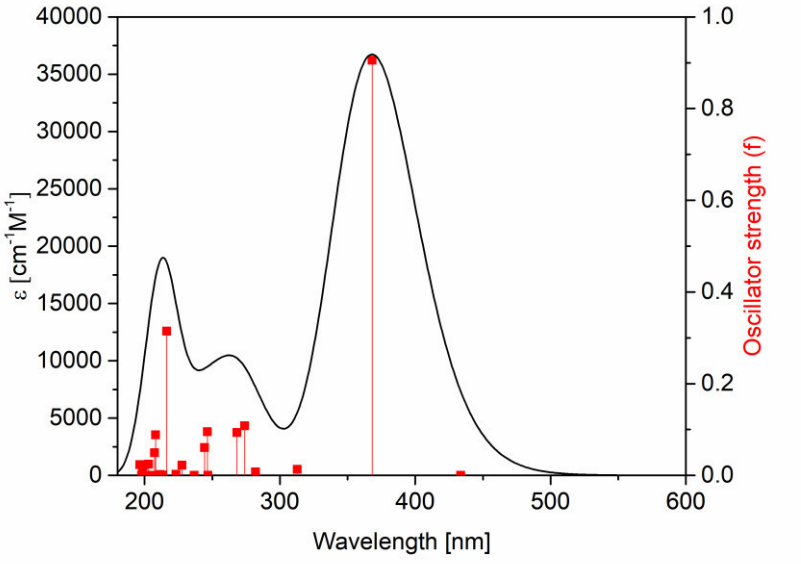

Figure A208 Simulated UV/Vis spectrum of *E*-**3a**.

***Z*-3a**

Excited State 1: 2.9657 eV 418.06nm f=0.0025
55 → 59 -0.16858
57 → 59 0.67837
Excited State 2: 3.8265 eV 324.02nm f=0.2449
58 → 59 0.69470
Excited State 3: 4.1815 eV 296.51nm f=0.0916
56 → 59 0.69369
58 → 60 -0.10603
Excited State 4: 4.2588 eV 291.12nm f=0.0006
55 → 59 0.67472
57 → 59 0.17144
Excited State 5: 4.6888 eV 264.43nm f=0.0038
54 → 59 0.70272

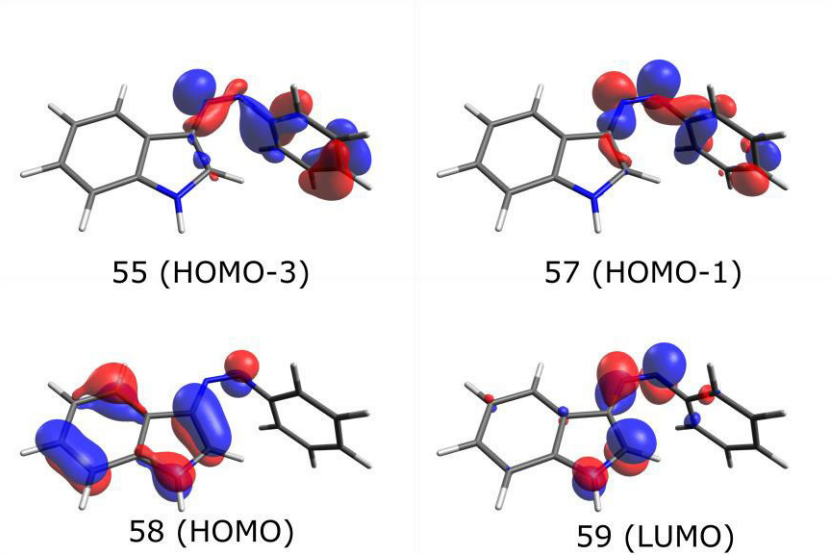

Figure A209 Orbitals involved in the two lowest transitions for *Z*-**3a**.

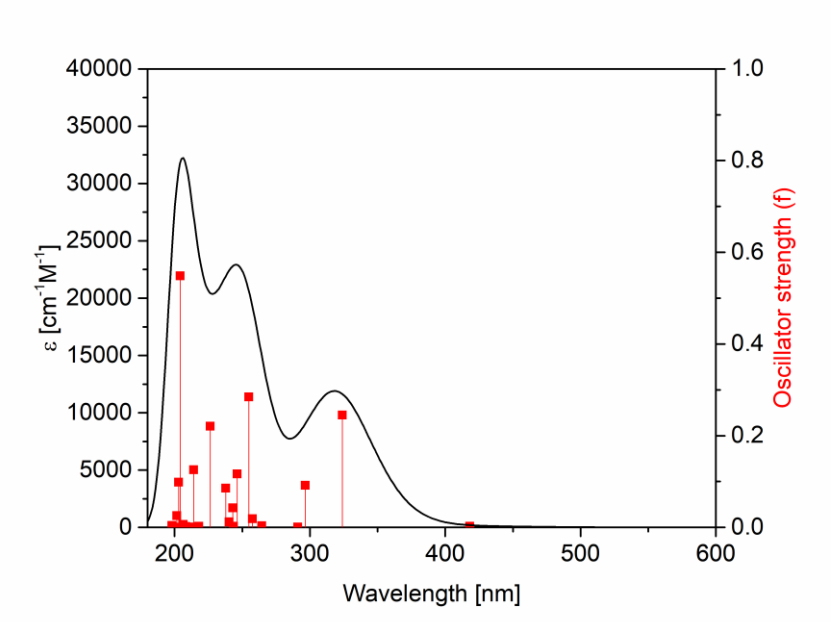

Figure A210 Simulated UV/Vis spectrum of *Z*-**3a**.

E-3b

Excited State 1: 2.8626 eV 433.12 nm f=0.0000
61 → 63 0.70096
Excited State 2: 3.2319 eV 383.63 nm f=0.8734
62 → 63 0.70376
Excited State 3: 3.8402 eV 322.86 nm f=0.0238
60 → 63 0.69304
62 → 64 0.11886
Excited State 4: 4.3533 eV 284.80 nm f=0.0056
58 → 63 0.58041
59 → 63 0.25052
59 → 65 0.10838
62 → 65 0.28783
Excited State 5: 4.4681 eV 277.48 nm f=0.0904
58 → 63 -0.20702
59 → 63 0.59764
60 → 64 0.14065
62 → 64 0.23300

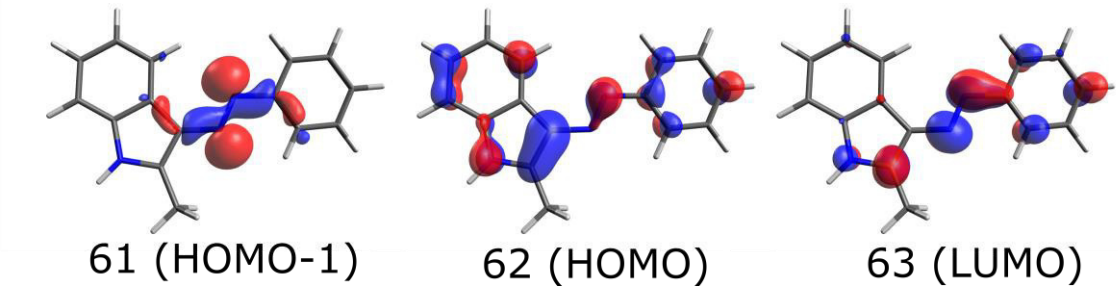

Figure A211 Orbitals involved in the two lowest transitions for *E*-**3b**.

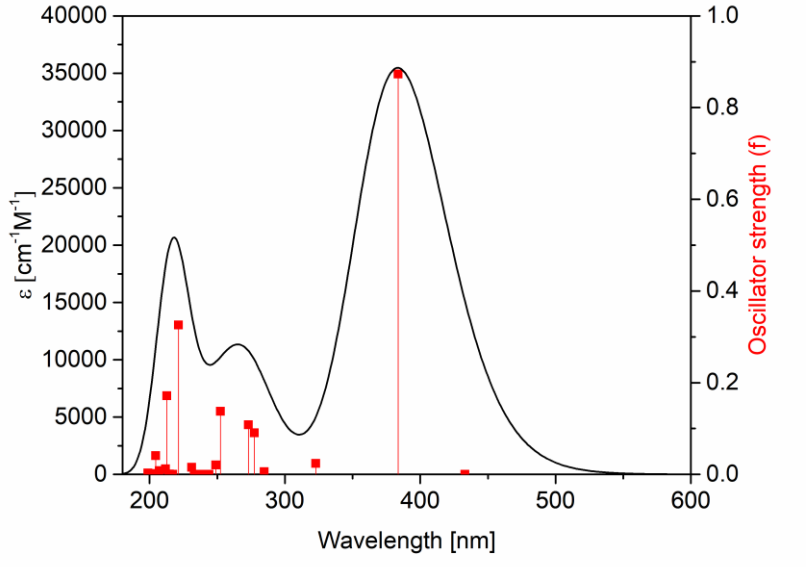

Figure A212 Simulated UV/Vis spectrum of *E*-**3b**.

Z-3b

Excited State 1: 2.5759 eV 481.32 nm f=0.1040
58 → 63 -0.13090
60 → 63 0.24429
61 → 63 0.10508
62 → 63 0.63667
Excited State 2: 3.5576 eV 348.51 nm f=0.0848
58 → 63 -0.15244
60 → 63 0.50008
61 → 63 0.34753
62 → 63 -0.28921
Excited State 3: 3.8758 eV 319.89 nm f=0.0373
60 → 63 -0.35781
61 → 63 0.59184
Excited State 4: 4.3395 eV 285.71 nm f=0.0264
58 → 63 -0.41660
59 → 63 0.16745
60 → 63 -0.12276
62 → 64 0.49276
62 → 65 0.12721
Excited State 5: 4.4147 eV 280.85 nm f=0.0097
58 → 63 0.15050
59 → 63 0.43370
60 → 65 0.10475
62 → 64 -0.13508
62 → 65 0.49578

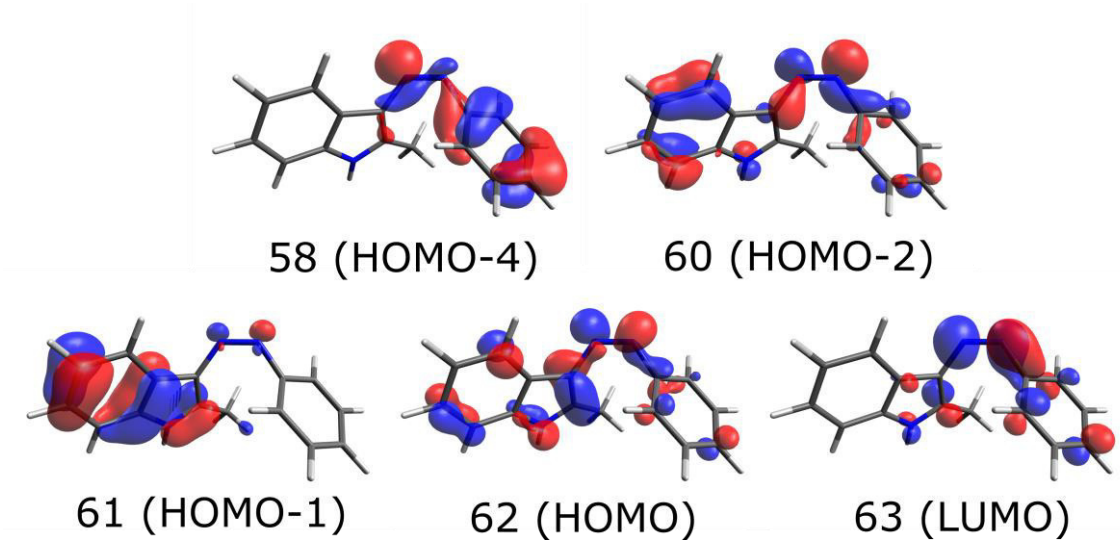

Figure A213 Orbitals involved in the two lowest transitions for *Z*-**3b**.

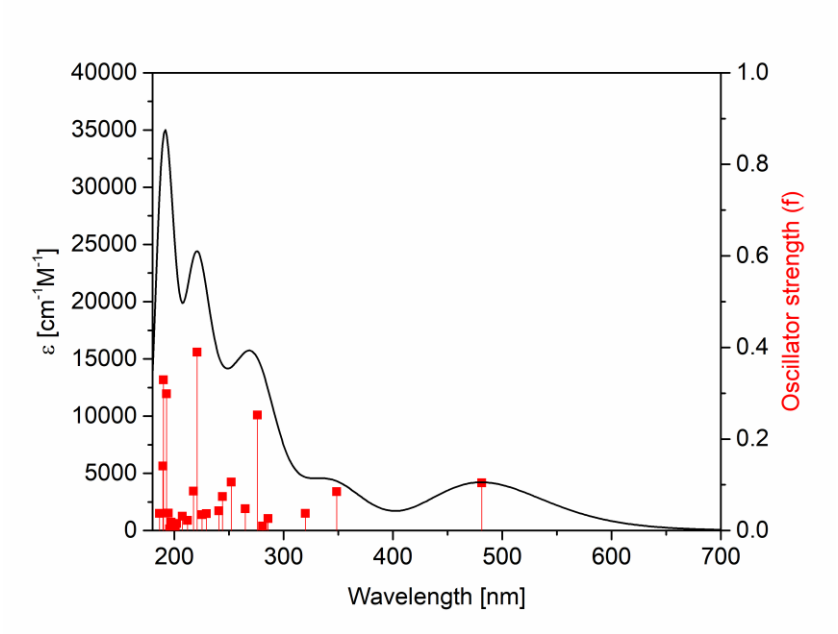

Figure A214 Simulated UV/Vis spectrum of *Z*-**3b**.

E-3c

Excited State 1: 2.8681 eV 432.28nm f=0.0000
61 -> 63 0.70053
Excited State 2: 3.2992 eV 375.80nm f=0.9697
62 -> 63 0.70222
Excited State 3: 3.9567 eV 313.35nm f=0.0116
60 -> 63 0.68102
62 -> 64 0.16346
Excited State 4: 4.4010 eV 281.72nm f=0.0026
58 -> 63 0.57493
59 -> 63 0.26062
59 -> 65 0.11092
62 -> 64 -0.10003
62 -> 65 0.26835
Excited State 5: 4.4867 eV 276.34nm f=0.1000
60 -> 63 -0.15732
62 -> 64 0.66599

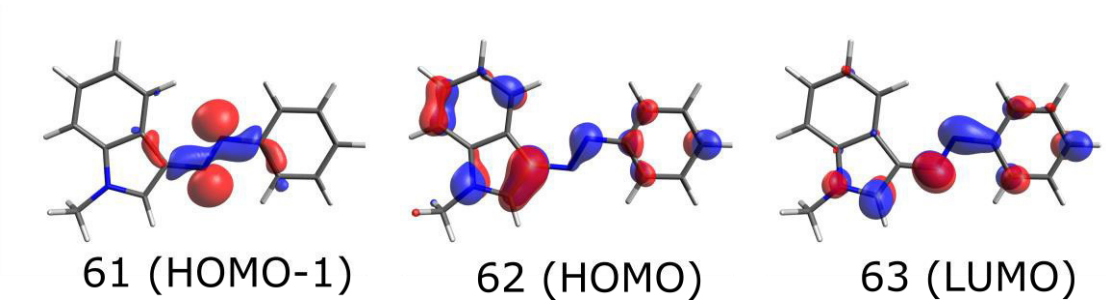

Figure A215 Orbitals involved in the two lowest transitions for *E*-**3c**.

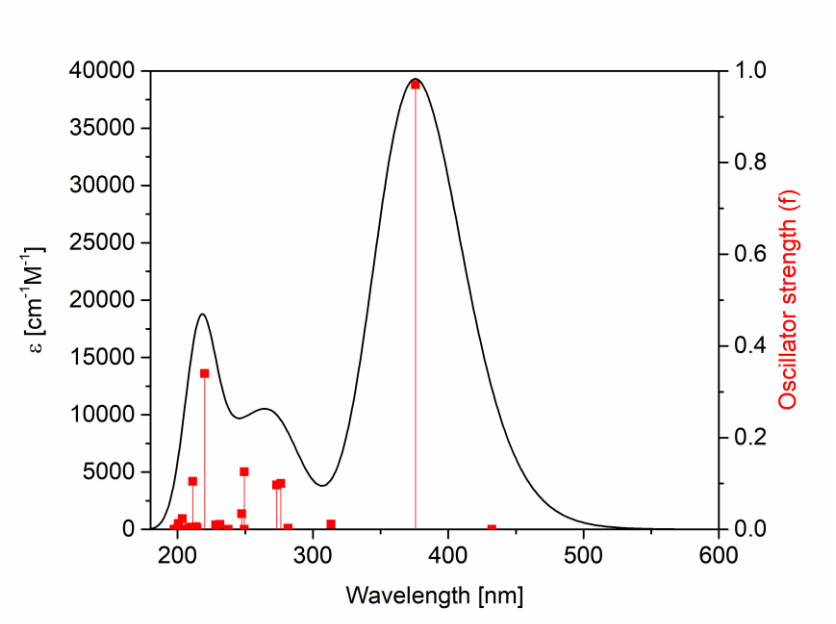

Figure A216 Simulated UV/Vis spectrum of *E*-**3c**.

Z-3c

Excited State 1: 2.9900 eV 414.66nm f=0.0025
59 -> 63 -0.16413
61 -> 63 0.68004
Excited State 2: 3.7798 eV 328.02nm f=0.3076
62 -> 63 0.69692
Excited State 3: 4.1761 eV 296.89nm f=0.0723
60 -> 63 0.68810
62 -> 64 -0.13411
Excited State 4: 4.2826 eV 289.51nm f=0.0005
59 -> 63 0.67473
61 -> 63 0.16861
Excited State 5: 4.7183 eV 262.78nm f=0.0255
58 -> 63 0.67589
62 -> 64 0.18577

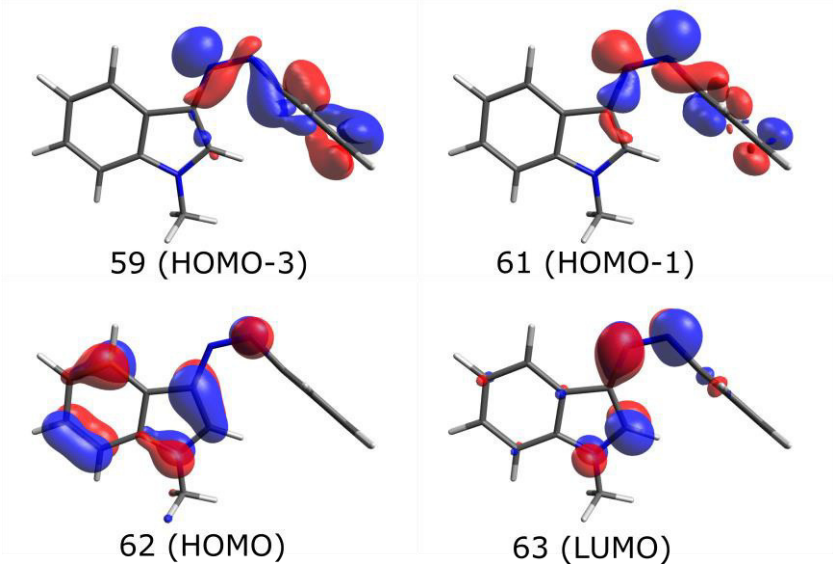

Figure A217 Orbitals involved in the two lowest transitions for *Z*-**3c**.

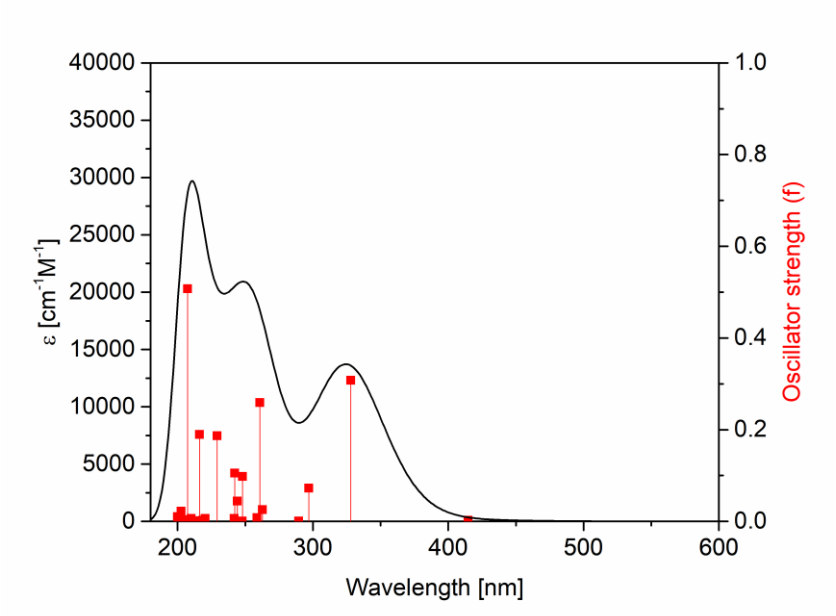

Figure A218 Simulated UV/Vis spectrum of *Z*-**3c**.

***s*-trans hydrazone of 3b**

Excited State 1: 3.0538 eV 406.00 nm f=0.7947
61 -> 63 -0.10872
62 -> 63 0.69755
Excited State 2: 3.2977 eV 375.97 nm f=0.0990
61 -> 63 0.69447
62 -> 63 0.10909
Excited State 3: 3.8365 eV 323.17 nm f=0.0023
58 -> 63 0.69938
Excited State 4: Singlet-A 4.2200 eV 293.80 nm f=0.0191
60 -> 63 0.67336
61 -> 64 -0.14082
Excited State 5: 4.3041 eV 288.06 nm f=0.0054
59 -> 63 0.63829
62 -> 64 -0.16781
62 -> 65 0.22666

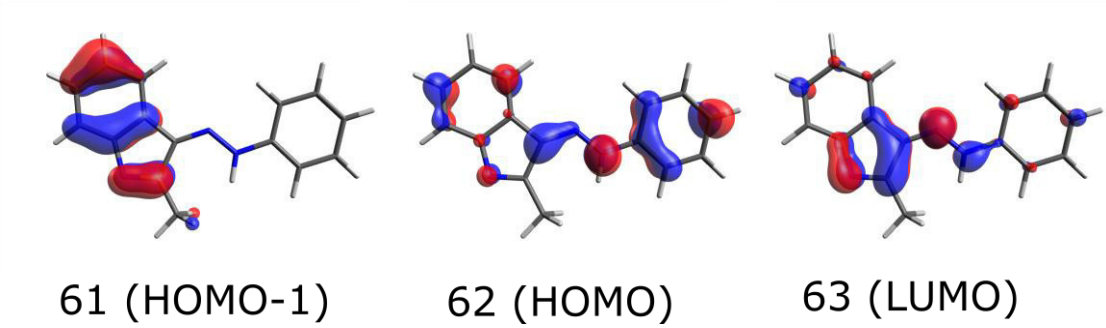

Figure A219 Orbitals involved in the two lowest transitions for the *s*-trans hydrazone of-**3b**.

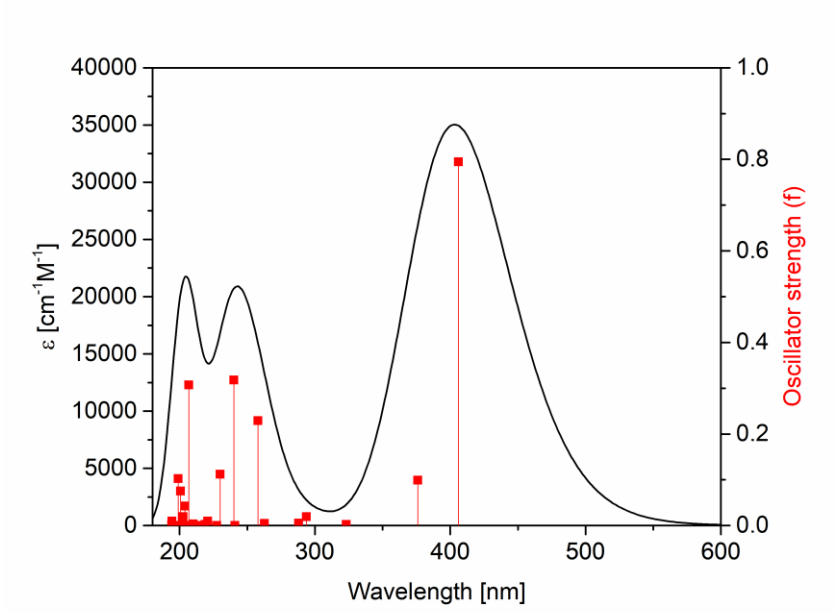

Figure A220 Simulated UV/Vis spectrum of the *s*-trans hydrazone of-**3b**.

***s*-cis hydrazone of 3b**

Excited State 1: 2.7294 eV 454.25 nm f=0.2662
58 -> 63 -0.14815
62 -> 63 0.68604
Excited State 2: 3.1913 eV 388.51 nm f=0.0211
61 -> 63 0.70167
Excited State 3: 3.7872 eV 327.38 nm f=0.1101
58 -> 63 0.67685
62 -> 63 0.15265
Excited State 4: 4.0882 eV 303.28 nm f=0.0414
57 -> 63 0.10725
60 -> 63 0.66582
61 -> 64 -0.14571
Excited State 5: 4.1819 eV 296.48 nm f=0.0031
59 -> 63 0.68712
62 -> 65 -0.13561

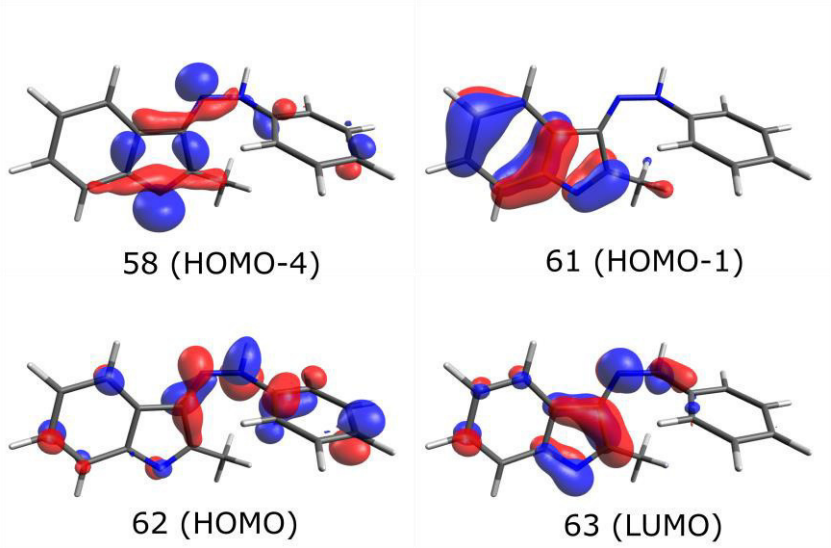

Figure A221 Orbitals involved in the two lowest transitions for the *s*-cis hydrazone of-**3b**.

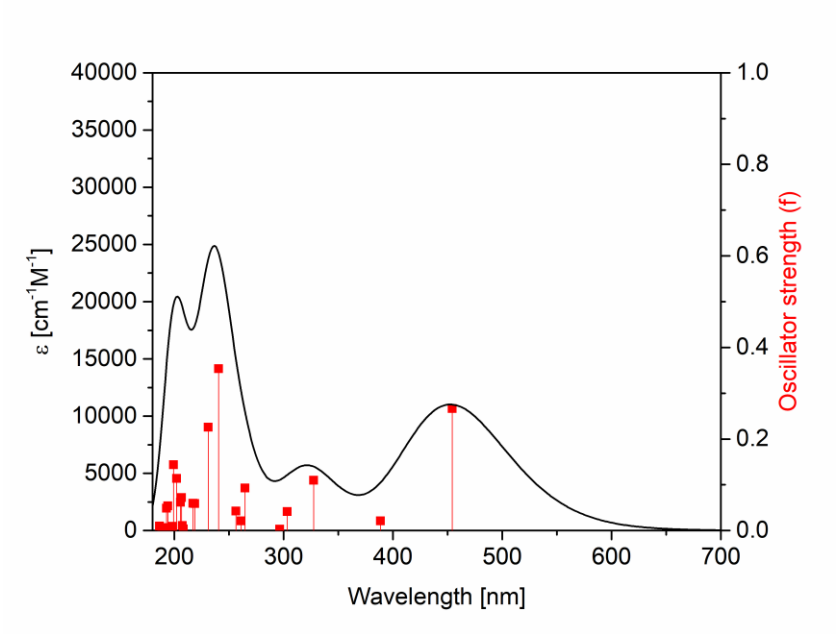

Figure A222 Simulated UV/Vis spectrum of the *s-cis* hydrazone of-**3b**.

4.4 Thermal Pathway

The thermal pathway of *Z*-to-*E* isomerization was studied using the Density Functional Theory approach. B3LYP/6-31G(d) was used to optimize the transition states for the monomolecular isomerization of **3a** taken as a model. All the minima and saddle points were optimized and their nature tested by frequency calculations. The rotational and inversion TSs, similar to the one typical of azobenzene,[S23] were found. In order to characterize the rotational transition state, that is diradicalic in nature, the broken symmetry BS-DFT model was used.

The hydrazone pathway was studied using B3LYP/6-31G(d), considering two *Z*-**3a** molecules with two bridging water molecules (this complex will be abbreviated in *Z*-dimer, for simplicity). No concerted mechanism, where two protons are exchanged simultaneously, could be found in the ground state. Water was crucial to lower the energy of the transition states to the formation of the hydrazone. The rate-determining-step of the reaction was found to be the migration of one NH proton of *Z*-**3a** to the β nitrogen (compared to the indole ring) of the other *Z*-**3a** molecule (**TS1**). The ensuing intermediate (**Int1**) is characterized by a charged separated nature, because it is formed by an anion and a cation, generated from a water mediated proton shift. A second proton transfer (**TS2**) facilitated by the second water molecule forms two *s*-cis hydrazones. Two rotations of the newly formed N-N bonds of the hydrazones (associated with transition states **TS3** and **TS4**) generate firstly an *s*-cis/*s*-**t**rans-water-bridged complex and finally a *s*-trans hydrazone dimer. Two water mediated proton transfer (**TS5** and **TS6**) restore the *E*-**3a** water bridged dimer, after populating the charged intermediate **Int2**.

The wavefunction was not stable enough at the B3LYP level to optimize a transition state of proton transfer between two *Z*-**3a** molecules without water. To have a hint of the energies involved in the non-water mediated process, the ωB97XD functional was used with the 6-31G(d) basis set. Even though the results cannot be formally compared, the difference in energy greater than 15 kcal/mol gives a qualitative grasp of the role of water in stabilizing the transition state of proton transfer.

Differences in the energetical barriers of intramolecular rotation between **3a** and **3c**, paralleling the experimental results, can be found applying the ωB97XD/6-31G(d) level of theory. Interestingly in this case B3LYP fails to give a result comparable with the observed behaviour of the molecule. It is probably necessary to include the long-range and dispersion contribution in the functional to model the energetical differences in the transition state of the differently substituted phenylazoindoles.

4.4.1 Cartesian Coordinates and thermochemical data

Z-dimer (B3LYP/6-31G(d))

C	-4.025496	1.109032	1.580816
C	-4.445115	2.308472	1.004224
C	-3.533746	3.360103	0.856589
C	-2.209633	3.210731	1.259674
C	-1.783023	1.99733	1.824206
C	-2.704791	0.958248	2.007047
N	-0.478545	1.860356	2.40007
N	0.600543	2.033533	1.755869
C	0.721246	2.154549	0.385186
C	1.986844	2.53774	-0.212135
C	1.853984	2.344284	-1.606674
N	0.574604	1.854959	-1.844327
C	3.197613	3.017774	0.304092
C	4.234414	3.288048	-0.582312
C	4.082219	3.091397	-1.970076
C	2.889332	2.616047	-2.504363
H	-4.726784	0.289302	1.710337
H	-5.476709	2.431909	0.686568
H	-3.859125	4.304879	0.428867
H	-1.502345	4.026893	1.149214
H	-2.375312	0.04361	2.491802
H	0.241359	1.466877	-2.738798
H	3.316382	3.163396	1.373241
H	5.183237	3.655253	-0.200612
H	4.913176	3.312144	-2.63429
H	2.766306	2.454064	-3.571155
C	-0.1005	1.744319	-0.676949
H	-1.097347	1.332329	-0.662307
H	0.238506	-1.466494	2.738314
C	-4.028052	-1.102501	-1.580641
C	-4.449881	-2.300833	-1.003353
C	-3.540528	-3.354162	-0.855386
C	-2.216233	-3.20758	-1.258884
C	-1.787378	-1.995303	-1.824137
C	-2.707154	-0.954496	-2.007253
N	-0.482733	-1.861243	-2.40035
N	0.596146	-2.036128	-1.756251
C	0.716883	-2.156499	-0.385508
C	1.982062	-2.541059	0.211813
C	1.849781	-2.346356	1.606233
N	0.571196	-1.854957	1.843776
C	3.192063	-3.023128	-0.304312
C	4.228679	-3.294166	0.582073
C	4.077059	-3.096246	1.969726
C	2.88496	-2.618829	2.503909
H	-4.727769	-0.28147	-1.710408
H	-5.481642	-2.422105	-0.685402
H	-3.867645	-4.298085	-0.427105
H	-1.510515	-4.02507	-1.148189
H	-2.37597	-0.040727	-2.492487
H	3.310398	-3.169703	-1.373379
H	5.176909	-3.662966	0.200442
H	4.907853	-3.317631	2.633932
H	2.762375	-2.455819	3.570597
C	-0.104054	-1.744303	0.676503
H	-1.100345	-1.330986	0.661759
O	-0.222351	0.362341	-4.092974
H	-0.952552	0.391953	-4.72765
H	-0.248001	-0.54883	-3.702384
O	-0.2218	-0.362539	4.093849
H	-0.953277	-0.391009	4.727131
H	-0.24576	0.548543	3.70282

Energy= -1561.4995619 (Hartrees)

Sum of electronic and zero-point Energies= -1561.006952 (Hartrees)

Sum of electronic and thermal Energies= -1560.974261 (Hartrees)

Sum of electronic and thermal Enthalpies= -1560.973316 (Hartrees)

Sum of electronic and thermal Free Energies= -1561.074981 (Hartrees)

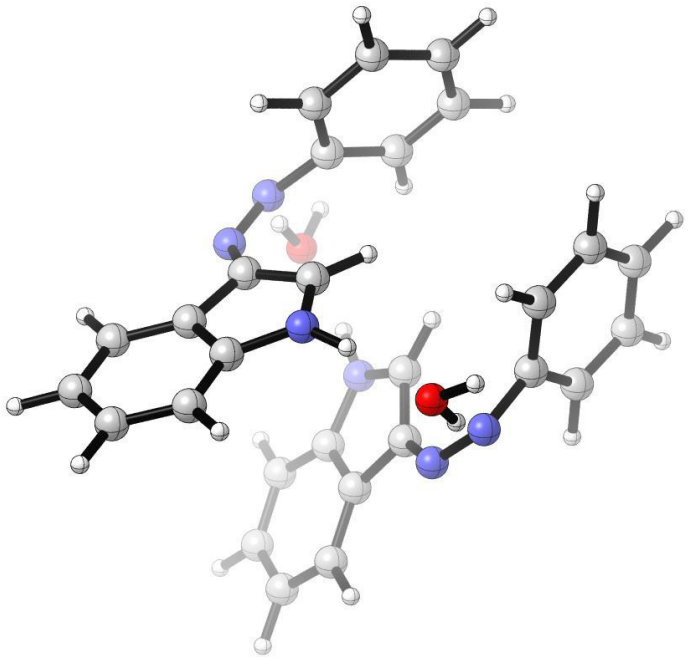

Figure A223 Dimer of two *Z*-**3a** molecules with two molecules of water (dubbed as *Z*-dimer) at the B3LYP/6-31G(d) level of theory.

TS1 (B3LYP/6-31G(d))

C	-4.137223	0.666222	1.746598
C	-4.621939	1.866124	1.225727
C	-3.751838	2.953712	1.081424
C	-2.410099	2.84105	1.432259
C	-1.911621	1.627208	1.940468
C	-2.795672	0.551221	2.115321
N	-0.593815	1.511912	2.471932
N	0.472684	1.818996	1.830397
C	0.58843	2.055564	0.492934
C	1.860462	2.460822	-0.079762
C	1.702756	2.377459	-1.484556
N	0.414853	1.934491	-1.785417
C	3.085135	2.86929	0.460752
C	4.122767	3.184172	-0.412856
C	3.954473	3.098396	-1.809242
C	2.743355	2.69272	-2.363119
H	-4.80454	-0.181685	1.878762
H	-5.668795	1.962803	0.951223
H	-4.125944	3.900057	0.698659
H	-1.738937	3.687162	1.322739
H	-2.418987	-0.366381	2.560115
H	0.075104	1.379762	-2.898814
H	3.216367	2.930591	1.537188
H	5.0826	3.501141	-0.01255
H	4.784843	3.351601	-2.463348
H	2.605221	2.614716	-3.437874
C	-0.238748	1.763478	-0.631046
H	-1.252796	1.388725	-0.630413
H	0.35993	-1.635214	2.70073
C	-4.067645	-1.068848	-1.788926
C	-4.382845	-2.343271	-1.318707
C	-3.370198	-3.297642	-1.165943
C	-2.049155	-2.980001	-1.464052
C	-1.733311	-1.689546	-1.917048
C	-2.7475	-0.741977	-2.100955
N	-0.417775	-1.36022	-2.362462
N	0.702069	-1.588775	-1.777806
C	0.85745	-1.939656	-0.485345
C	2.164705	-2.283965	0.059094
C	2.029087	-2.273155	1.463141
N	0.707629	-1.92747	1.7627
C	3.40326	-2.587526	-0.51214
C	4.469539	-2.868439	0.339355
C	4.31465	-2.854043	1.738035
C	3.087752	-2.554284	2.325256
H	-4.846614	-0.322994	-1.91556
H	-5.41141	-2.599083	-1.081425
H	-3.614163	-4.299246	-0.822936
H	-1.266079	-3.723953	-1.359292
H	-2.491726	0.240069	-2.484377
H	3.526827	-2.590214	-1.590398
H	5.443487	-3.098229	-0.083264
H	5.168356	-3.075679	2.371777
H	2.959921	-2.528867	3.402954
C	0.009025	-1.745645	0.63763
H	-1.013051	-1.400788	0.676756
O	-0.155774	0.643808	-3.833751
H	-0.917721	0.956953	-4.343801
H	-0.326616	-0.566028	-3.200073
O	-0.124647	-0.685162	4.05683
H	-0.87216	-0.82097	4.65672
H	-0.2596	0.227396	3.660688

Energy= -1561.472055 (Hartrees)

Sum of electronic and zero-point Energies= -1560.985599 (Hartrees)

Sum of electronic and thermal Energies= -1560.954445 (Hartrees)

Sum of electronic and thermal Enthalpies= -1560.953501 (Hartrees)

Sum of electronic and thermal Free Energies= -1561.050684 (Hartrees)

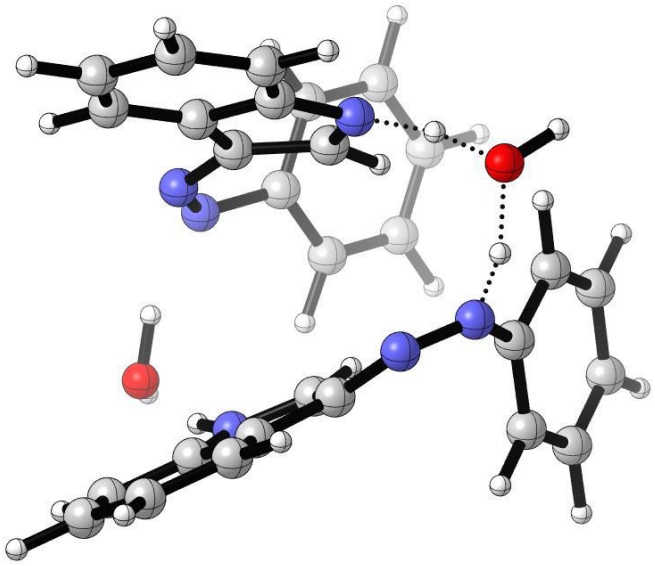

Figure A224 Transition state for the water-mediated proton transfer to form the intermediate **Int1** at the B3LYP/6-31G(d) level of theory.

Int1 (B3LYP/6-31G(d))

C	-4.352728	0.425891	1.712586
C	-4.879442	1.605605	1.186098
C	-4.045308	2.719501	1.029833
C	-2.699518	2.654195	1.377077
C	-2.157223	1.462218	1.894106
C	-3.006663	0.358522	2.075205
N	-0.838173	1.386873	2.416177
N	0.22654	1.711678	1.763664
C	0.347747	1.942149	0.43703
C	1.636213	2.308015	-0.127535
C	1.462775	2.27523	-1.533079
N	0.154636	1.903798	-1.864067
C	2.878824	2.643403	0.419672
C	3.927019	2.942115	-0.44897
C	3.748618	2.908896	-1.84552
C	2.51606	2.573669	-2.402466
H	-4.990946	-0.443296	1.85211
H	-5.929856	1.665648	0.914577
H	-4.451542	3.649813	0.640226
H	-2.056638	3.520823	1.257752
H	-2.597233	-0.546901	2.518059
H	-0.116978	1.154723	-3.394178
H	3.016093	2.66634	1.497199
H	4.901009	3.205792	-0.043505
H	4.585707	3.147924	-2.496879
H	2.369776	2.536324	-3.478946
C	-0.49315	1.73098	-0.717662
H	-1.531667	1.425916	-0.71914
H	0.522034	-1.347855	2.753681
C	-3.895675	-1.324436	-1.890914
C	-4.154832	-2.518917	-1.218775
C	-3.099299	-3.378494	-0.894992
C	-1.789766	-3.043867	-1.226442
C	-1.535191	-1.829705	-1.879307
C	-2.588119	-0.978171	-2.231572
N	-0.222909	-1.494355	-2.331751
N	0.922424	-1.565968	-1.73351
C	1.10031	-1.75292	-0.42674
C	2.434172	-1.914785	0.148239
C	2.27907	-1.829822	1.545393
N	0.920292	-1.614195	1.81611
C	3.703477	-2.117501	-0.393996
C	4.782782	-2.226061	0.482942
C	4.607914	-2.139322	1.875094
C	3.346163	-1.937745	2.433018
H	-4.709807	-0.653918	-2.148767
H	-5.173791	-2.786347	-0.954792
H	-3.298737	-4.321482	-0.393881
H	-0.972766	-3.718907	-0.992929
H	-2.367192	-0.060878	-2.766197
H	3.842309	-2.17482	-1.468765
H	5.781482	-2.374343	0.082456
H	5.471371	-2.224866	2.528131
H	3.198984	-1.855914	3.505255
C	0.219575	-1.576886	0.689575
H	-0.835215	-1.348739	0.704303
O	-0.200336	0.505076	-4.165753
H	-0.851134	0.882681	-4.774399
H	-0.173724	-0.97893	-3.235246
O	-0.085882	-0.578228	4.102204
H	-0.855621	-0.897525	4.595631
H	-0.388673	0.278589	3.652891

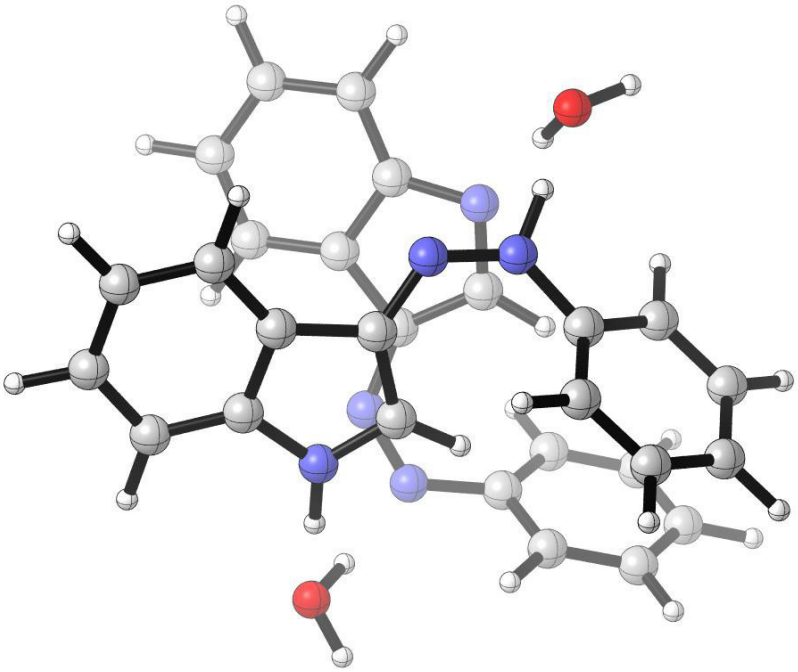

Figure A225 Charge-separated intermediate **Int1** at the B3LYP/6-31G(d) level of theory.

TS2 (B3LYP/6-31G(d))

C	4.2895841566	0.0163048969	-1.9282477295
C	4.8174383977	1.2836190933	-1.6826496592
C	3.9636134379	2.3932053645	-1.6822039051
C	2.5996700166	2.2420775773	-1.909424331
C	2.0581131093	0.9634893621	-2.1404742412
C	2.9236097474	-0.1433374256	-2.1630108419
N	0.7108834774	0.7613120729	-2.5268913889
N	-0.3478749133	1.3050330271	-1.9978110848
C	-0.4391669476	1.9222147517	-0.8187079982
C	-1.708104318	2.4790037634	-0.3618793984
C	-1.5136076081	2.8038965854	1.0001185667
N	-0.2130275981	2.467773256	1.4149712333
C	-2.9404312458	2.7134211386	-0.9732705048
C	-3.9627282692	3.2759608905	-0.2069187285
C	-3.7630788221	3.6006953422	1.1461703022
C	-2.5354180146	3.3655417404	1.7665506286
H	4.9407904376	-0.8539979013	-1.9429011517
H	5.881653051	1.4113629668	-1.5054127496
H	4.3679525118	3.3880625789	-1.5129613864
H	1.9455362253	3.1079065935	-1.9172298664
H	2.5134505445	-1.1264764343	-2.3783896134
H	0.0459545616	1.9172990363	3.0793635062
H	-3.0945229283	2.4585560087	-2.0179693899
H	-4.9312277894	3.4664201481	-0.662698611
H	-4.5778474844	4.0391709401	1.7166955169
H	-2.3738815569	3.6046776469	2.8143201493
C	0.4132329924	1.9900137115	0.3554656455
H	1.4344804104	1.6389987949	0.4340639305
H	-0.4226040385	-1.9056556276	-2.5090720892
C	3.9146588291	-0.6959876667	2.1631463102
C	4.2659966244	-1.9790718096	1.743982938
C	3.273870383	-2.9521959765	1.582629638
C	1.9376798964	-2.6459492442	1.8222854829
C	1.5886520127	-1.3463882408	2.2166283086
C	2.579182932	-0.3755218221	2.407278419
N	0.2492532121	-1.0116611666	2.5741382264
N	-0.8858108541	-1.3213863386	2.0186003005
C	-1.0370076225	-1.816051738	0.7979974554
C	-2.3518300161	-2.1865710373	0.2744464415
C	-2.181324275	-2.3768345085	-1.1114761604
N	-0.8378519084	-2.1301732457	-1.4422456819
C	-3.6096940227	-2.3598408423	0.8499865954
C	-4.6705452331	-2.7166183297	0.0151546981
C	-4.48523578	-2.9005629146	-1.3651902918
C	-3.2312998062	-2.7310927251	-1.9537180912
H	4.6790864964	0.0633796386	2.2987231154
H	5.3062286523	-2.2257346773	1.5527018471
H	3.5437368094	-3.9603062272	1.2806696038
H	1.1719037304	-3.407061453	1.7139007219
H	2.2872053091	0.6101508073	2.7533984442
H	-3.7571965485	-2.2097669698	1.914900812
H	-5.6615029861	-2.8496489257	0.4399510085
H	-5.3333021782	-3.1744161554	-1.98604278
H	-3.0766649674	-2.8567631217	-3.0206995871
C	-0.1621373625	-1.8299912032	-0.3499300512
H	0.8765733145	-1.538087565	-0.4083312361
O	0.1434608373	1.3878373941	3.9262522738
H	0.6847405512	1.9243259064	4.5223491194
H	0.1481574838	-0.3160253221	3.3334958607
O	0.0186687282	-1.338285403	-3.6614637696
H	0.7565565014	-1.7957059222	-4.0921465694
H	0.3965227136	-0.2734520936	-3.2566192122

Energy= -1561.4731533 (Hartrees)

Sum of electronic and zero-point Energies= -1560.986873 (Hartrees)

Sum of electronic and thermal Energies= -1560.955394 (Hartrees)

Sum of electronic and thermal Enthalpies= -1560.954450 (Hartrees)

Sum of electronic and thermal Free Energies= -1561.053174 (Hartrees)

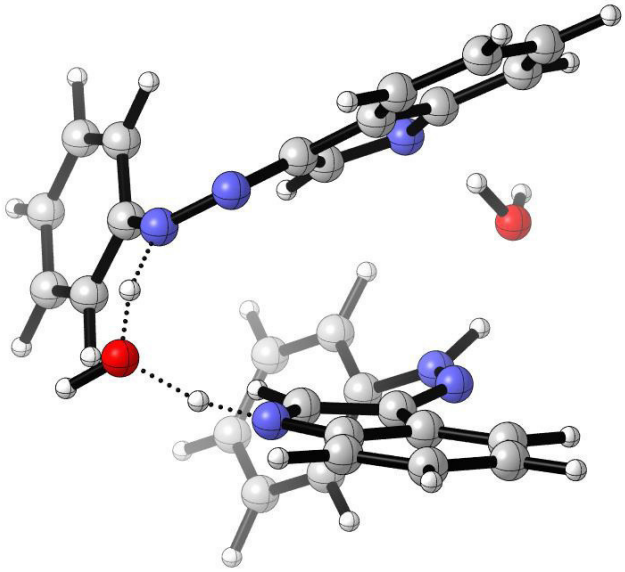

Figure A226 Transition state for the water-mediated proton transfer to form the water-complexed *s*-cis hydrazone intermediate from **Int1** at the B3LYP/6-31G(d) level of theory.

s-cis hydrazone dimer (B3LYP/6-31G(d))

C	4.1621339476	-0.0838985877	-2.0112375441
C	4.7597333672	1.0854121945	-1.539162566
C	3.9762591588	2.226588872	-1.3427644241
C	2.6083123633	2.2039783033	-1.6017340974
C	2.0061828304	1.019820666	-2.053491807
C	2.7932739497	-0.1210770781	-2.2716299166
N	0.6434928638	0.957790439	-2.4398153489
N	-0.4354903861	1.5459367374	-1.9630455978
C	-0.5500717414	2.1149385574	-0.7859845887
C	-1.7979805153	2.7611662243	-0.3705567499
C	-1.6364598536	3.0489805818	1.0001352826
N	-0.3770717114	2.6047193435	1.4655295578
C	-2.9756803583	3.0996940824	-1.0304670749
C	-3.9851793153	3.7295596698	-0.295084738
C	-3.8182054509	4.016763385	1.0674950107
C	-2.6374565682	3.6767132866	1.7351029288
H	4.7608954029	-0.9753863999	-2.1761752831
H	5.8259877744	1.1123667378	-1.3339657231
H	4.4353095843	3.1488500153	-0.9968896217
H	2.0123234336	3.1001402062	-1.4671645618
H	2.3183451187	-1.0168372153	-2.6597768572
H	-0.0493360437	1.9420475908	3.1518259451
H	-3.1048847805	2.8744372091	-2.0850568747
H	-4.9155843036	4.0002017607	-0.7871418929
H	-4.6196533973	4.5077688539	1.6128044953
H	-2.5014320024	3.8877910413	2.7919237002
C	0.2584285931	2.1008916468	0.439465719
H	1.2403485386	1.6602392648	0.5575097114
H	-0.2655676339	-1.9020325507	-3.1504956791
C	4.008832441	-0.6773148309	2.2117252892
C	4.398734693	-1.9396398901	1.7625319822
C	3.4258853909	-2.9152670046	1.5250324916
C	2.0757429894	-2.6364714492	1.7206061943
C	1.6851394368	-1.3587824687	2.1493329596
C	2.6604467533	-0.3840035561	2.4087622897
N	0.3415413155	-1.0418033919	2.4724420013
N	-0.8050234037	-1.4197640617	1.9433643924
C	-0.9691900231	-1.9622014782	0.7596533945
C	-2.2953073256	-2.3652096065	0.2837718003
C	-2.127016814	-2.6837443291	-1.07929011
N	-0.7864922407	-2.4850126823	-1.4836542262
C	-3.5449174897	-2.4746813018	0.886729181
C	-4.619171972	-2.9074651342	0.1023364024
C	-4.4457824819	-3.2263552744	-1.2523750056
C	-3.192546297	-3.1160110068	-1.8628790855
H	4.7552783931	0.0873388015	2.4081814996
H	5.4495287172	-2.1661157536	1.6067251815
H	3.7201398434	-3.9084950486	1.1966494355
H	1.3297425292	-3.4061285837	1.5546776977
H	2.3436667672	0.5862727968	2.7786509468
H	-3.6785513699	-2.2249332176	1.935234448
H	-5.6056230273	-2.9972031999	0.5494173665
H	-5.2987477504	-3.5608832553	-1.8365901878
H	-3.0494632232	-3.3530519411	-2.913241606
C	-0.1162905423	-2.1048008706	-0.4268640676
H	0.9351704909	-1.8562992723	-0.4971247215
O	0.1331530451	1.3701149769	3.9429321735
H	0.6987515943	1.8965320385	4.5253419378
H	0.2162270175	-0.3519700899	3.2235024295
O	0.0548955323	-1.3777554984	-3.9307337021
H	0.5440809122	-2.0014795918	-4.4856341659
H	0.4264171138	0.2998445274	-3.1986528009

Energy= -1561.5011243 (Hartrees)

Sum of electronic and zero-point Energies= -1561.008167 (Hartrees)

Sum of electronic and thermal Energies= -1560.975078 (Hartrees)

Sum of electronic and thermal Enthalpies= -1560.974134 (Hartrees)

Sum of electronic and thermal Free Energies= -1561.077681 (Hartrees)

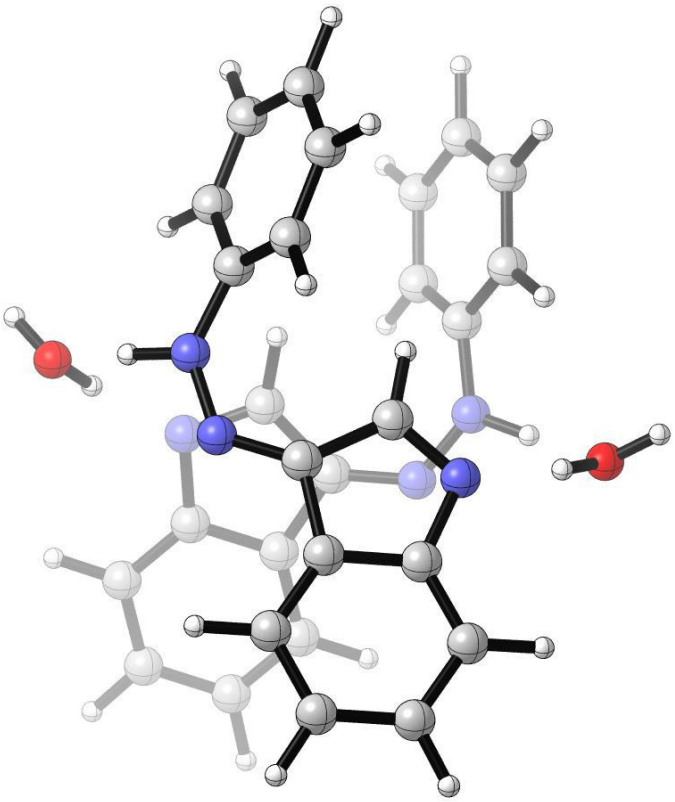

Figure A227 *s*-cis hydrazone water-complexed dimer at the B3LYP/6-31G(d) level of theory.

TS3 (B3LYP/6-31G(d))

C	3.8393511234	1.0250682457	-4.0434286306
C	4.0039297469	2.4116157955	-4.122328306
C	2.9954814965	3.2384140696	-3.6294103402
C	1.840173905	2.7022523529	-3.0573304937
C	1.6770324589	1.3112421988	-2.9754658113
C	2.6906527683	0.477484495	-3.482988477
N	0.5698326409	0.6986614432	-2.343918508
N	-0.6350990832	1.4820061037	-2.3336414864
C	-0.8964173089	1.9937445168	-1.1877370547
C	-2.0691370317	2.8222238209	-0.856576238
C	-1.9530039869	3.0998114178	0.517350799
N	-0.7759493479	2.5008155312	1.0726734723
C	-3.1415324944	3.3028810287	-1.593025315
C	-4.1041968633	4.0741930512	-0.9242023706
C	-3.9839787175	4.3455678286	0.4416867056
C	-2.8992352856	3.8573481552	1.1876501386
H	4.6109273484	0.3621132495	-4.427467611
H	4.90082076	2.8364589292	-4.56371182
H	3.1004173953	4.3190018418	-3.6901601815
H	1.0629602422	3.3638268825	-2.6913625097
H	2.5645772023	-0.6002985183	-3.4261004725
H	-0.325108691	2.092877486	2.8733094144
H	-3.2299180378	3.0840275838	-2.6528465069
H	-4.9555568118	4.4635639446	-1.4749106332
H	-4.743897056	4.943567801	0.9368154211
H	-2.8039435946	4.0605287351	2.249911029
C	-0.1679556933	1.8816866636	0.1142245207
H	0.7505629332	1.3269194073	0.259431843
H	-0.4193755579	-2.3069307177	-2.872560957
C	3.9840663048	0.0468065451	1.8258394424
C	4.5272931697	-1.1712825049	1.4167470643
C	3.7061737582	-2.3009418851	1.3512468065
C	2.3545687872	-2.2201381441	1.6751392619
C	1.8050576271	-0.9883076529	2.0624315513
C	2.6318273971	0.1425760705	2.1509185628
N	0.4649493072	-0.8537148011	2.5051649187
N	-0.6432423047	-1.494455471	2.1774911222
C	-0.8280716128	-2.1764768119	1.0733125716
C	-2.0758622286	-2.9002720285	0.8145838971
C	-1.9971400606	-3.3166543006	-0.5306158263
N	-0.7953908039	-2.8709020017	-1.1293533457
C	-3.1875617383	-3.216714976	1.5896378354
C	-4.2179340232	-3.9526657566	0.9942360326
C	-4.1333910347	-4.3668353852	-0.3427701385
C	-3.0175679119	-4.0515012742	-1.1253729071
H	4.6118020299	0.9312950144	1.8894609115
H	5.578978791	-1.2431929826	1.1559822586
H	4.1228493383	-3.2594501462	1.0540097729
H	1.7321161605	-3.1072334367	1.6385251696
H	2.2022613901	1.0800963298	2.490194179
H	-3.2513377351	-2.8966117428	2.625619629
H	-5.0985440327	-4.2084177047	1.5774267681
H	-4.9478180578	-4.9398043829	-0.7776575786
H	-2.9447858842	-4.3635629657	-2.1631665975
C	-0.1104168822	-2.2496053329	-0.2068519742
H	0.8315096821	-1.7717644227	-0.4453602061
O	-0.0171559613	1.6820677027	3.7171489963
H	0.5405307571	2.3485992198	4.143146187
H	0.2972153587	-0.1270009763	3.2076286648
O	-0.0833963213	-1.7888023231	-3.6458788653
H	0.630507982	-2.3300680682	-4.0133612669
H	0.3356730126	-0.1939634172	-2.8110022079

Energy= -1561.4874216 (Hartrees)

Sum of electronic and zero-point Energies= -1560.995180 (Hartrees)

Sum of electronic and thermal Energies= -1560.962700 (Hartrees)

Sum of electronic and thermal Enthalpies= -1560.961756 (Hartrees)

Sum of electronic and thermal Free Energies= -1561.064134 (Hartrees)

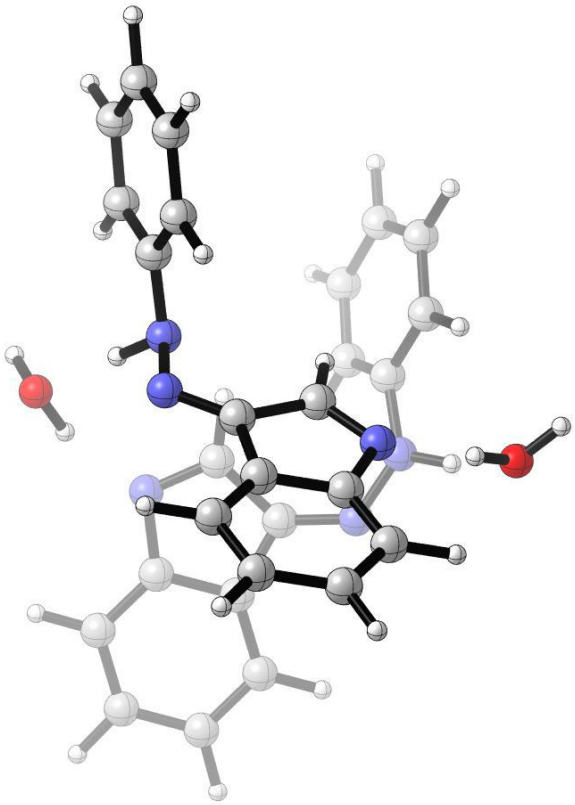

Figure A228 Transition state for the rotation around the single N-N bond of a *s*-cis hydrazone belonging to the water-complexed *s*-cis hydrazone intermediate at the B3LYP/6-31G(d) level of theory.

s-cis/*s*-trans hydrazone (B3LYP/6-31G(d))

C	-5.151028	-3.372721	-1.607458
C	-6.44071	-2.877762	-1.405501
C	-6.607413	-1.569963	-0.940824
C	-5.506644	-0.758621	-0.680619
C	-4.215068	-1.264657	-0.886685
C	-4.036677	-2.576714	-1.3509
N	-3.068806	-0.484776	-0.640348
N	-3.183522	0.717642	-0.133228
C	-2.144306	1.480267	0.112145
C	-2.263124	2.806761	0.714089
C	-0.939277	3.278275	0.831008
N	-0.013657	2.336937	0.322765
C	-3.33048	3.585674	1.154152
C	-3.048984	4.836937	1.711628
C	-1.729004	5.296297	1.834025
C	-0.65339	4.51863	1.395343
H	-5.006574	-4.388842	-1.964833
H	-7.306206	-3.502582	-1.60629
H	-7.606676	-1.174147	-0.779665
H	-5.628498	0.25595	-0.321354
H	-3.030446	-2.957539	-1.497028
H	1.731338	2.966779	0.512902
H	-4.352645	3.228024	1.068885
H	-3.866057	5.462143	2.061652
H	-1.540258	6.268546	2.281057
H	0.375001	4.851916	1.502245
C	-0.703145	1.300634	-0.085165
H	-0.218985	0.432178	-0.521291
H	-0.050587	-2.469259	-0.930543
C	3.389985	1.413547	-3.597734
C	4.180691	0.381852	-4.103463
C	4.836824	-0.484207	-3.221361
C	4.704559	-0.323101	-1.845517
C	3.89153	0.702875	-1.341049
C	3.23967	1.5763	-2.21903
N	3.809184	0.931462	0.062255
N	3.476398	0.096217	1.031632
C	2.925513	-1.078527	0.836327
C	2.582484	-1.975968	1.941441
C	1.730359	-2.95204	1.381647
N	1.510626	-2.704292	0.006228
C	2.912868	-2.016556	3.293077
C	2.378744	-3.048998	4.071043
C	1.536417	-4.019437	3.508886
C	1.198426	-3.981207	2.152527
H	2.880677	2.09372	-4.275007
H	4.293262	0.254799	-5.176357
H	5.467853	-1.279587	-3.608265
H	5.226597	-0.981592	-1.158203
H	2.620878	2.368241	-1.811316
H	3.563043	-1.263514	3.728735
H	2.619889	-3.100587	5.129361
H	1.138886	-4.811283	4.137861
H	0.543082	-4.725183	1.708927
C	2.235332	-1.66407	-0.316243
H	2.198166	-1.256977	-1.318049
O	2.610341	3.421039	0.602216
H	2.5621	4.167835	-0.012613
H	3.756239	1.910547	0.365342
O	-0.766109	-2.023328	-1.455689
H	-0.524474	-2.154397	-2.383965
H	-2.155927	-0.910206	-0.864268

Energy= -1561.5166968 (Hartrees)

Sum of electronic and zero-point Energies= -1561.023300 (Hartrees)

Sum of electronic and thermal Energies= -1560.990441 (Hartrees)

Sum of electronic and thermal Enthalpies= -1560.989497 (Hartrees)

Sum of electronic and thermal Free Energies= -1561.093611 (Hartrees)

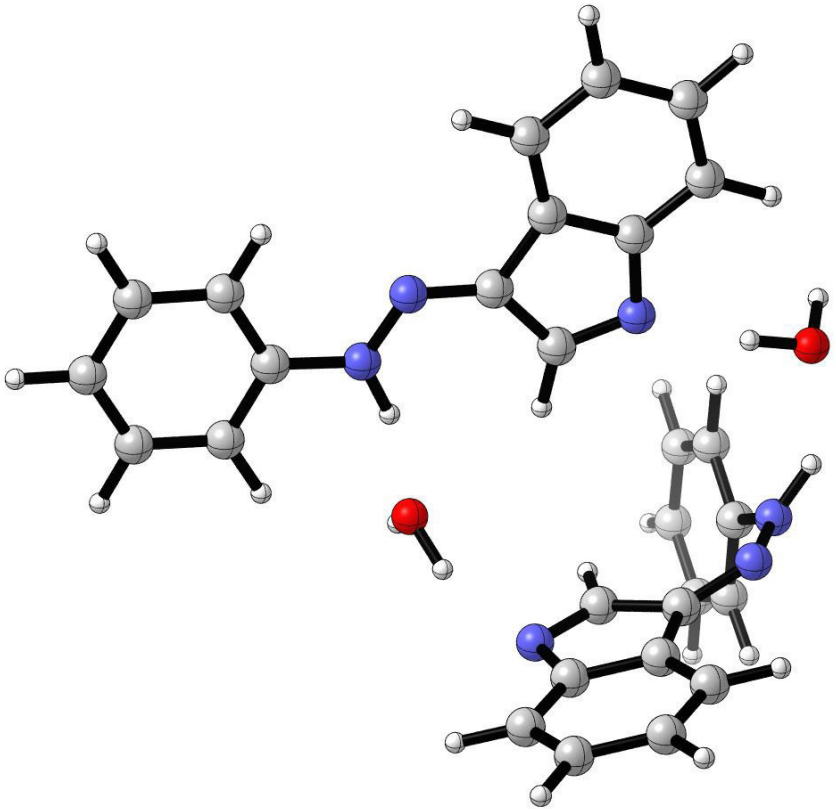

Figure A229 Water-complexed *s*-cis/*s*-trans hydrazone intermediate at the B3LYP/6-31G(d) level of theory.

TS4 (B3LYP/6-31G(d))

C	-4.656389764	-3.5086014216	-2.0359101508
C	-5.9846269914	-3.0933863976	-1.9225458829
C	-6.2642654129	-1.8181386054	-1.4226774028
C	-5.2372871366	-0.9600419299	-1.0395976762
C	-3.9066031794	-1.3860919848	-1.1575316094
C	-3.6147456715	-2.6648390636	-1.6564556769
N	-2.8291497839	-0.5612562651	-0.7875680608
N	-3.0386173685	0.623698602	-0.2685243865
C	-2.0429396452	1.4035885509	0.0837533036
C	-2.2272345365	2.723239965	0.6817760791
C	-0.9217812654	3.2081620838	0.9146644451
N	0.0523186997	2.2726442575	0.4954383877
C	-3.3378289267	3.4907984021	1.0236476793
C	-3.1217549516	4.7468527616	1.5987266599
C	-1.8231374241	5.2248332725	1.8278665298
C	-0.70496484	4.4580318189	1.487331736
H	-4.4251161515	-4.4980011773	-2.4213337488
H	-6.793360482	-3.7547064443	-2.2197070534
H	-7.2946351772	-1.4850846007	-1.3305853032
H	-5.4459718222	0.0300517242	-0.6527025102
H	-2.5795838022	-2.9841389036	-1.7359771507
H	1.8727916424	2.5202248335	0.604420917
H	-4.3441141911	3.1216835352	0.8473370431
H	-3.9734282581	5.3634722211	1.8729946426
H	-1.6847447959	6.2047648338	2.2762948464
H	0.3033117428	4.8232206358	1.6623520962
C	-0.5906196157	1.2376366703	0.017574796
H	-0.0640838176	0.3750085634	-0.3761836547
H	0.3595547987	-2.0924523184	-0.6401960233
C	5.8454182001	0.6241675424	-2.3108644679
C	6.5415485526	-0.5834118439	-2.4101095127
C	6.6262672938	-1.4054375821	-1.2845603837
C	6.0323519653	-1.0371104173	-0.0785849426
C	5.3282147928	0.1780203965	0.0200021567
C	5.2377498824	1.0061640765	-1.1171886306
N	4.7893056438	0.6279876412	1.2325000579
N	4.3427393424	-0.3176024113	2.2135846364
C	3.405089449	-1.1135337462	1.8468105855
C	2.7926104156	-2.1586287012	2.6875728323
C	1.761678268	-2.7137786702	1.9096853885
N	1.6832114987	-2.078404609	0.6287593545
C	3.0421520359	-2.6199762708	3.9713611421
C	2.234349494	-3.65591385	4.4651869239
C	1.2115667145	-4.2036630199	3.6856726501
C	0.9576825226	-3.7358006069	2.3861780048
H	5.7627539174	1.2769079822	-3.176830923
H	7.0093570632	-0.8770271153	-3.3453278238
H	7.1692775436	-2.3461253304	-1.3383404032
H	6.1252983468	-1.6783171445	0.7921210951
H	4.680251396	1.9360415475	-1.0491587282
H	3.8376831711	-2.1886721206	4.5712303298
H	2.406016483	-4.0370173354	5.4676513992
H	0.6006039891	-5.005041148	4.091245792
H	0.1634128692	-4.1561268756	1.7768894571
C	2.6185380051	-1.1888426275	0.5735510951
H	2.7715887975	-0.5586641544	-0.2945524059
O	2.8561848142	2.6539605036	0.6632489535
H	2.9682434438	3.4952163034	1.1286209967
H	4.1134798175	1.4026386803	1.1499208498
O	-0.3325848769	-1.8942875255	-1.3233406991
H	0.1482938512	-1.7961736926	-2.1583948991
H	-1.8781903857	-0.9351809543	-0.9378371327

Energy= -1561.5166968 (Hartrees)

Sum of electronic and zero-point Energies= -1561.023300 (Hartrees)

Sum of electronic and thermal Energies= -1560.990441 (Hartrees)

Sum of electronic and thermal Enthalpies= -1560.989497 (Hartrees)

Sum of electronic and thermal Free Energies= -1561.093611 (Hartrees)

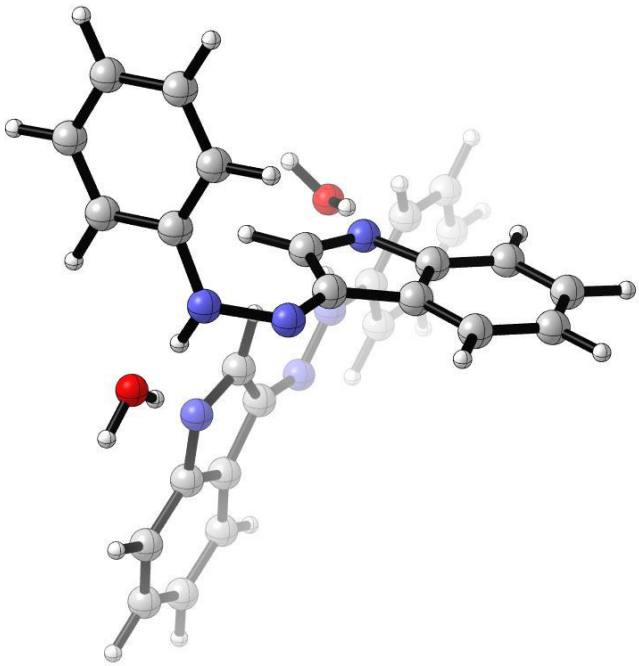

Figure A230 Transition state for the rotation around the single N-N bond of the*s*-cis hydrazone belonging to the water-complexed *s*-cis/*s*-trans hydrazone intermediate at the B3LYP/6-31G(d) level of theory.

s-trans hydrazone dimer (B3LYP/6-31G(d))

C	6.4656743608	2.7974122699	-0.1298519567
C	7.6003109745	2.1454029704	0.3571718249
C	7.5329701829	0.7815824432	0.6572393765
C	6.3516991983	0.0680457026	0.475206557
C	5.2181327176	0.7319925487	-0.0146667714
C	5.2739455988	2.1009950729	-0.3178490202
N	3.9976095017	0.064483485	-0.2206430656
N	3.8632633236	-1.2012438904	0.0849803503
C	2.7230268589	-1.8284300854	-0.1025073254
C	2.4996983945	-3.2302361386	0.2400832277
C	1.1519567689	-3.4834672426	-0.0992231799
N	0.5391529313	-2.3276712765	-0.6331025208
C	3.2901272083	-4.2394507231	0.7853029382
C	2.712713355	-5.4973500894	0.9824556039
C	1.373296997	-5.7422927217	0.6441521263
C	0.5739096236	-4.7342523212	0.0975979119
H	6.5042198131	3.8577951431	-0.3643002605
H	8.5271041338	2.6927997322	0.5026366525
H	8.4105818836	0.265382102	1.0372421122
H	6.2911657022	-0.9890092933	0.7047366436
H	4.3848307766	2.6017635782	-0.6903850027
H	-2.0184864333	-1.8817738563	-2.3613685242
H	4.3267569938	-4.0519944917	1.0502269988
H	3.3109005487	-6.2994603724	1.406360667
H	0.9515427887	-6.7296450636	0.8109846333
H	-0.4650814855	-4.9123459142	-0.1650819869
C	1.4413363058	-1.3775367031	-0.6357774182
H	1.2212679623	-0.382468948	-1.0075335573
H	1.1478956242	2.0731751417	-1.0785554046
C	-6.4666079776	-2.7962368087	-0.1325929621
C	-7.6015077513	-2.1439553856	0.3534803486
C	-7.5342711258	-0.7800180242	0.6530041823
C	-6.3528720515	-0.0665903695	0.4713191898
C	-5.2190565838	-0.7307849484	-0.0175909361
C	-5.2747626886	-2.0999231101	-0.3202055662
N	-3.9984867687	-0.0633454203	-0.2234330358
N	-3.86357041	1.2019105155	0.0839637137
C	-2.7233089968	1.829040614	-0.1035259444
C	-2.4993579744	3.2302989144	0.2410193584
C	-1.1518510105	3.4837157173	-0.0990022855
N	-0.5397493556	2.3285916621	-0.6351713066
C	-3.2891840969	4.2388248335	0.7883857067
C	-2.711387132	5.4963284154	0.9869069123
C	-1.3721966034	5.741497631	0.6478307236
C	-0.5734371657	4.7341277539	0.0991274955
H	-6.5050058524	-3.8567593903	-0.366419364
H	-8.5284393708	-2.691216041	0.4985789436
H	-8.412132511	-0.2635839103	1.0321157538
H	-6.2924523063	0.9905457677	0.7005068892
H	-4.3854021885	-2.6008915573	-0.6918944736
H	-4.3255807521	4.0510689357	1.0540047072
H	-3.3090745565	6.2979654254	1.4124102835
H	-0.9501613335	6.7285751377	0.8155872726
H	0.4653865887	4.9125008711	-0.1640074994
C	-1.4421810891	1.3787030166	-0.6386044256
H	-1.2227902231	0.384141347	-1.0121310279
O	-2.0650605885	-1.820649659	-1.3957742376
H	-1.1474676068	-2.0725627011	-1.077488527
H	-3.2206941285	-0.6198070947	-0.6202287692
O	2.0656555503	1.8216505122	-1.3964202557
H	2.0186653519	1.8811288278	-2.3621152573
H	3.2198440987	0.620941464	-0.6174482365

Energy= -1561.5468584 (Hartrees)

Sum of electronic and zero-point Energies= -1561.052645 (Hartrees)

Sum of electronic and thermal Energies= -1561.020284 (Hartrees)

Sum of electronic and thermal Enthalpies= -1561.019340 (Hartrees)

Sum of electronic and thermal Free Energies= -1561.121707 (Hartrees)

Figure A231 Water-complexed *s*-trans hydrazone dimer intermediate at the B3LYP/6-31G(d) level of theory.

TS5 (B3LYP/6-31G(d))

C	6.397432	2.874202	0.103239
C	7.562931	2.153183	0.369523
C	7.504408	0.756983	0.435058
C	6.303145	0.084228	0.23702
C	5.129065	0.811088	-0.028996
C	5.186534	2.214274	-0.095654
N	3.875582	0.200999	-0.245913
N	3.82086	-1.081982	-0.07484
C	2.682176	-1.751679	-0.273429
C	2.533063	-3.17059	0.004234
C	1.175486	-3.46618	-0.276758
N	0.496837	-2.321248	-0.724026
C	3.38671	-4.17484	0.467412
C	2.870954	-5.459748	0.637964
C	1.523022	-5.747012	0.357048
C	0.660107	-4.752444	-0.103083
H	6.428339	3.959745	0.051454
H	8.506192	2.670261	0.523041
H	8.406902	0.185974	0.63935
H	6.250491	-0.997011	0.282445
H	4.274211	2.768303	-0.294397
H	-1.963379	-2.463014	0.787042
H	4.42748	-3.955797	0.689237
H	3.521244	-6.254802	0.994115
H	1.151019	-6.758514	0.49844
H	-0.382154	-4.965819	-0.328272
C	1.380941	-1.334394	-0.722427
H	1.117608	-0.335958	-1.047659
H	0.681501	1.89873	-0.37983
C	-6.664629	-2.665514	-0.146841
C	-7.808728	-1.900856	0.088815
C	-7.690862	-0.523597	0.304192
C	-6.444257	0.093561	0.287086
C	-5.303167	-0.684638	0.049139
C	-5.407134	-2.066281	-0.168814
N	-4.010833	-0.119636	0.016161
N	-3.837227	1.156731	0.124805
C	-2.623953	1.698214	0.077584
C	-2.389184	3.137311	0.142454
C	-0.997111	3.30622	-0.003684
N	-0.401313	2.043592	-0.139499
C	-3.206867	4.258215	0.294213
C	-2.604436	5.517144	0.296753
C	-1.214239	5.665846	0.148463
C	-0.383553	4.556332	-0.005849
H	-6.747885	-3.73491	-0.31756
H	-8.786799	-2.372627	0.10489
H	-8.578248	0.075157	0.488937
H	-6.340525	1.159052	0.453923
H	-4.509444	-2.647866	-0.358077
H	-4.281369	4.151067	0.406436
H	-3.222427	6.402594	0.415487
H	-0.780169	6.66128	0.155122
H	0.691799	4.648192	-0.121816
C	-1.327771	1.100301	-0.091248
H	-1.07354	0.050534	-0.160645
O	-2.100232	-2.129256	-0.113764
H	-1.170239	-2.211729	-0.527816
H	-3.21209	-0.789894	-0.092904
O	2.05255	1.829158	-0.826458
H	2.095643	1.932405	-1.790343
H	2.889467	1.00029	-0.546128

Energy= -1561.5214421 (Hartrees)

Sum of electronic and zero-point Energies= -1561.033206 (Hartrees)

Sum of electronic and thermal Energies= -1561.002191 (Hartrees)

Sum of electronic and thermal Enthalpies= -1561.001247 (Hartrees)

Sum of electronic and thermal Free Energies= -1561.099539 (Hartrees)

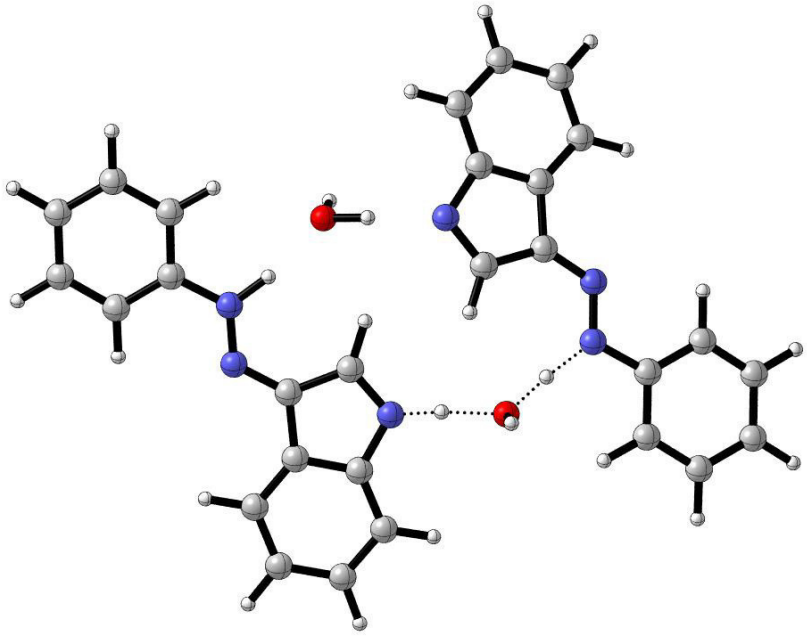

Figure A232 Transition state for the water-mediated proton transfer to form the intermediate **Int2** at the B3LYP/6-31G(d) level of theory.

Int2 (B3LYP/6-31G(d))

C	6.6836421167	-2.7218647265	-0.010595501
C	7.8176978908	-1.9324971224	-0.2091321975
C	7.682814661	-0.5402642046	-0.2553229968
C	6.4372622859	0.0598060052	-0.1059544981
C	5.290185924	-0.7328251892	0.090801369
C	5.4305301455	-2.1308496026	0.1400445584
N	3.9873077529	-0.2095781277	0.2583401584
N	3.894788693	1.0627453365	0.0755586292
C	2.7032777876	1.673911636	0.2394275348
C	2.4827624994	3.0722828145	-0.0681611245
C	1.1079133146	3.3048725669	0.1984220555
N	0.4902300447	2.1406279797	0.6658452628
C	3.2867361243	4.1119964315	-0.548628362
C	2.7079021852	5.3632106756	-0.7508314617
C	1.343152365	5.5876668634	-0.4845211129
C	0.5296932324	4.5620318049	-0.0076805213
H	6.7729940167	-3.8049372947	0.0263928908
H	8.7952097052	-2.3931990706	-0.3241203955
H	8.5609472862	0.0835077892	-0.4056251131
H	6.3247551719	1.1371490342	-0.1369723477
H	4.5459687992	-2.7438216965	0.286834053
H	-1.9474181755	2.4371931691	-0.7700471309
H	4.3390300739	3.9413762795	-0.7586829833
H	3.3190192662	6.1831233759	-1.1203089061
H	0.9216703068	6.5760266482	-0.650274971
H	-0.5232860714	4.7285333029	0.2090949787
C	1.4329803975	1.1968836538	0.6847348329
H	1.2128730117	0.1970601981	1.0378324527
H	0.5502669649	-2.022565907	0.2581055923
C	-6.6004160515	2.7773118087	0.2402704703
C	-7.7686048365	2.0462792453	0.0163892596
C	-7.6942303931	0.6683225344	-0.2161850541
C	-6.4655911944	0.0170388831	-0.2278917497
C	-5.2999490958	0.7620063292	-0.0018109512
C	-5.3598333316	2.1435844708	0.2332903272
N	-4.021986831	0.1627222554	0.001818887
N	-3.8863911389	-1.1118569902	-0.1176051224
C	-2.6834193084	-1.6914492679	-0.0984427503
C	-2.5060093505	-3.137165251	-0.1791489413
C	-1.1201648132	-3.3669276174	-0.0649615067
N	-0.4832193065	-2.1263256041	0.0685878826
C	-3.3723256648	-4.2230780468	-0.3228858165
C	-2.8226797051	-5.5044728599	-0.3498933697
C	-1.4361726378	-5.7119951888	-0.2342665263
C	-0.5566741621	-4.6407425974	-0.0883433898
H	-6.6515923122	3.8463943149	0.4241731579
H	-8.7333045356	2.5450210273	0.0226306193
H	-8.6014702775	0.0974345612	-0.3918298604
H	-6.3940688901	-1.0488407239	-0.4087350472
H	-4.4423184147	2.6963885907	0.4133116833
H	-4.4433921303	-4.070298618	-0.4106166562
H	-3.4787467694	-6.3627400332	-0.4628042586
H	-1.0440503201	-6.7242337215	-0.2603540615
H	0.5160112633	-4.7807461373	0.001074489
C	-1.37250648	-1.138714115	0.0477790968
H	-1.0698137056	-0.1021467731	0.1200047559
O	-2.0791960025	2.0771589798	0.1216751252
H	-1.1173482618	2.0829461747	0.5095116671
H	-3.1988917892	0.8191098296	0.0945018204
O	2.114322745	-2.098460462	0.7748765589
H	2.1995908884	-2.1859744385	1.7372543919
H	2.782270037	-1.3552831824	0.5364981248

Energy= -1561.5247819 (Hartrees)

Sum of electronic and zero-point Energies= -1561.031644 (Hartrees)

Sum of electronic and thermal Energies= -1561.000149 (Hartrees)

Sum of electronic and thermal Enthalpies= -1560.999205 (Hartrees)

Sum of electronic and thermal Free Energies= -1561.099067 (Hartrees)

Figure A233 Charge-separated intermediate **Int2** at the B3LYP/6-31G(d) level of theory.

TS6 (B3LYP/6-31G(d))

C	-6.7594300003	2.5459744012	-0.7541373952
C	-7.8909592503	1.7301323162	-0.699092278
C	-7.736109766	0.3486069847	-0.5355277163
C	-6.469985672	-0.2163573358	-0.4279270309
C	-5.327585844	0.6043628242	-0.4755825716
C	-5.4859898981	1.9901608602	-0.6459596938
N	-4.0013862179	0.1214410139	-0.3805967306
N	-3.9027683675	-1.120865664	-0.0688557697
C	-2.6629211497	-1.6727484405	-0.0523439272
C	-2.3667118673	-2.9771672052	0.5009981024
C	-0.9760170174	-3.1747709933	0.2942037302
N	-0.4385744011	-2.0778897125	-0.3754158108
C	-3.1198259084	-3.9616441243	1.1529128556
C	-2.4750502047	-5.1204630782	1.5764863098
C	-1.0937874852	-5.3064923472	1.3668276165
C	-0.3283379379	-4.3371003292	0.7250118711
H	-6.8671758019	3.6199699617	-0.8837159089
H	-8.8839028365	2.1626290333	-0.7881095326
H	-8.6130376118	-0.2932687673	-0.4981205417
H	-6.3381701336	-1.2854505653	-0.3075243609
H	-4.6009497545	2.6187025464	-0.6841213655
H	1.8583633713	-1.6701600022	-2.1156920133
H	-4.1840938039	-3.8198016635	1.3185807747
H	-3.0451257433	-5.8979188097	2.0789148395
H	-0.620212267	-6.2218604537	1.7122960391
H	0.7371831263	-4.471998297	0.5588243261
C	-1.4320227704	-1.1991503836	-0.5707209881
H	-1.266908285	-0.286852859	-1.1308634714
H	-0.54178124	2.1432509334	0.1501590218
C	6.2855061288	-2.9327242411	-0.8278164323
C	7.5082273513	-2.305586679	-0.5803875242
C	7.539538784	-0.9465239142	-0.2470621925
C	6.3625290177	-0.2111995348	-0.1600169947
C	5.1405201051	-0.8509331231	-0.4128520331
C	5.0955064844	-2.2133627682	-0.7459100901
N	3.9059270872	-0.1725024073	-0.34284308
N	3.8626405988	1.0719575238	-0.0255783815
C	2.6891600642	1.7151196818	0.06795575
C	2.5808333134	3.1330627659	0.3847367849
C	1.1995442103	3.4220570396	0.4166684545
N	0.5035803482	2.2380200886	0.1432948607
C	3.5018063317	4.1546263452	0.6310155939
C	3.0144935561	5.4320942656	0.902259718
C	1.6336626745	5.7003754652	0.9270615684
C	0.6998186353	4.6953694185	0.6829459402
H	6.2548485503	-3.9877754893	-1.0839393025
H	8.4336545091	-2.8705651325	-0.6444302421
H	8.4897831456	-0.4570974432	-0.0530274994
H	6.3723511225	0.8411288899	0.0980968971
H	4.1320383844	-2.6806574579	-0.9292526177
H	4.568440062	3.9539201243	0.6108751901
H	3.714515319	6.2394575908	1.0973562799
H	1.2892202892	6.7083787231	1.1382271029
H	-0.3682836232	4.8896254662	0.693024791
C	1.355811274	1.2353188061	-0.0638883031
H	1.0245116425	0.2327004399	-0.2969337696
O	1.8963024889	-1.66511281	-1.1466742591
H	0.7977876458	-1.913539665	-0.7732781659
H	3.025327524	-0.7495570582	-0.6271292967
O	-2.2168626296	2.1091667199	0.2814336927
H	-2.4828411736	2.1361375533	1.2139208833
H	-2.7762984835	1.3550989723	-0.0920977032

Energy= -1561.52457 (Hartrees)

Sum of electronic and zero-point Energies= -1561.036378 (Hartrees)

Sum of electronic and thermal Energies= -1561.005071 (Hartrees)

Sum of electronic and thermal Enthalpies= -1561.004127 (Hartrees)

Sum of electronic and thermal Free Energies= -1561.103833 (Hartrees)

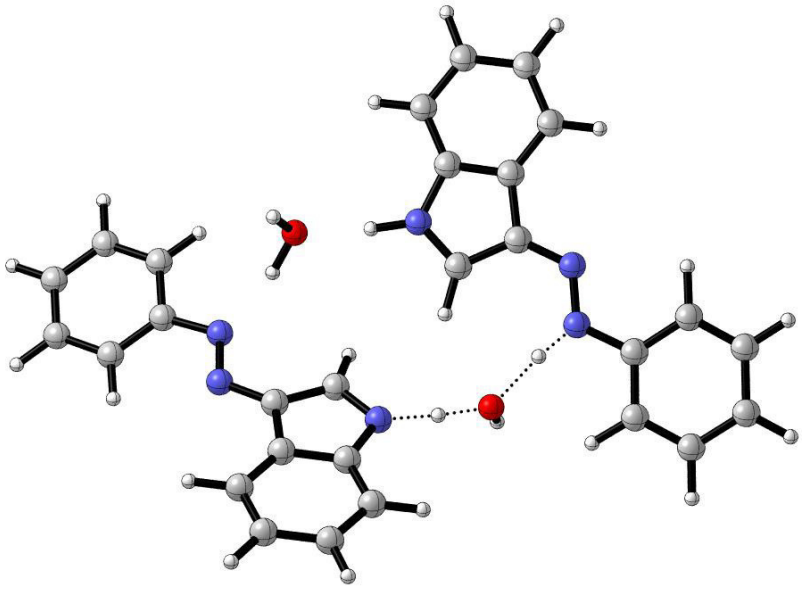

Figure A234 Transition state for the water-mediated proton transfer to form the *E*- dimer of **3a** from the intermediate **Int2** at the B3LYP/6-31G(d) level of theory.

E-dimer (B3LYP/6-31G(d))

C	-6.6828079386	2.6137493194	-0.0625348466
C	-7.8667209948	1.8789720808	-0.1385749843
C	-7.8142180977	0.4798793555	-0.1617910108
C	-6.5938297894	-0.1832372954	-0.1094226018
C	-5.3997633076	0.5559971449	-0.0318061765
C	-5.4536532243	1.9583371747	-0.0094355038
N	-4.1070365807	-0.0261014337	0.0257200782
N	-4.092582345	-1.2989978979	0.0076997976
C	-2.8745175309	-1.9310548192	0.0457370621
C	-2.7436865089	-3.3739641391	0.0304579749
C	-1.3553278617	-3.6527113742	0.0534519402
N	-0.6820694003	-2.4372830451	0.0862000937
C	-3.6561853724	-4.4371970592	-0.003178661
C	-3.1624191258	-5.7369895409	-0.0141231685
C	-1.7763551202	-5.9942883939	0.0078124185
C	-0.8515345998	-4.9560866287	0.041927179
H	-6.7141185858	3.6998158001	-0.0456695019
H	-8.8251721918	2.3891163212	-0.1806059752
H	-8.7346338627	-0.0952521846	-0.2219110322
H	-6.5395006575	-1.2654549423	-0.1273166645
H	-4.5265514087	2.5210179217	0.0481849298
H	2.0927239189	-1.9257854693	-1.4572706825
H	-4.7238925208	-4.2413209592	-0.0209489988
H	-3.8557773626	-6.573207415	-0.039916855
H	-1.4242169013	-7.0220047169	-0.0009269262
H	0.2176876347	-5.1471208786	0.0611690706
C	-1.5731766368	-1.4172004671	0.0792044064
H	-1.2452499988	-0.3887087131	0.1077877672
H	-0.3503098064	2.2907312148	-0.0558090521
C	6.6683064103	-2.6318838649	0.0421314463
C	7.8522681287	-1.8972706566	0.1189232879
C	7.799910398	-0.4981798533	0.1426426495
C	6.5796141429	0.1650860823	0.0900238081
C	5.385497268	-0.5739888463	0.0116413432
C	5.4392382865	-1.9763218187	-0.0112211144
N	4.092856058	0.0083082398	-0.0461940071
N	4.078547884	1.2811933344	-0.027821294
C	2.8605478304	1.9133640199	-0.0661338002
C	2.7298042009	3.3562713286	-0.0505949467
C	1.3414682539	3.6351168452	-0.0739693428
N	0.6681466201	2.4197323219	-0.1071359482
C	3.6423525358	4.4194480254	-0.0164661762
C	3.1486567474	5.7192666562	-0.0054218176
C	1.7626171008	5.9766557707	-0.0277401059
C	0.8377435923	4.9385149628	-0.0623478355
H	6.699500492	-3.7179478861	0.0248781801
H	8.8106451677	-2.4075377077	0.1611549007
H	8.7203636788	0.0768288525	0.2033594287
H	6.5253957237	1.2473017576	0.1083005205
H	4.5121105426	-2.5388984283	-0.0694016689
H	4.7100445979	4.2235163324	0.0015940405
H	3.8420595452	6.555435902	0.0207500878
H	1.4105393699	7.0043916537	-0.0189054885
H	-0.2314609872	5.129614722	-0.0818786409
C	1.5591866197	1.3995931799	-0.1000937307
H	1.2312080591	0.3711263477	-0.1289495197
O	2.0413238585	-1.9044011142	-0.4890909582
H	0.3363919487	-2.3082647118	0.0345259581
H	2.7207213396	-1.2212017288	-0.2307754157
O	-2.0553694286	1.886627145	0.4677001434
H	-2.1067384189	1.9082468968	1.4358803707
H	-2.734874169	1.2034022103	0.2096181292

Energy= -1561.5496587

Sum of electronic and zero-point Energies= -1561.055474

Sum of electronic and thermal Energies= -1561.022996

Sum of electronic and thermal Enthalpies= -1561.022052

Sum of electronic and thermal Free Energies= -1561.125441

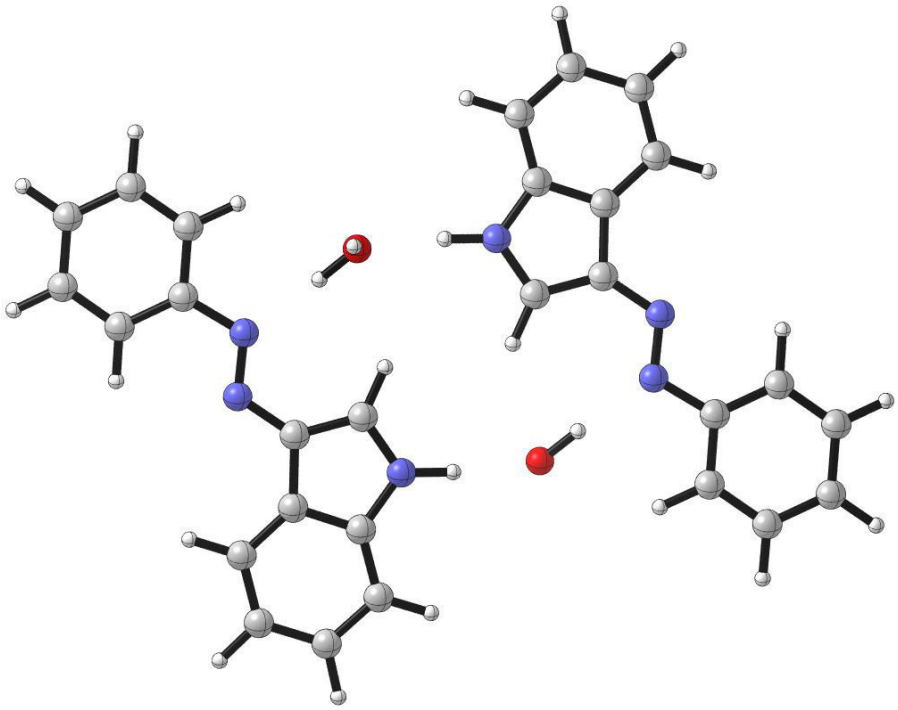

Figure A235 Dimer of two *E*-**3a** molecules with two molecules of water (dubbed as *E*-dimer) at the B3LYP/6-31G(d) level of theory.

Z-dimer (non-water-complexed) (ωB97XD/6-31G(d))

C	4.397867	0.863773	-0.79926
C	4.910027	1.759416	0.13487
C	4.181434	2.90146	0.467783
C	2.943059	3.13934	-0.114795
C	2.422648	2.223515	-1.032825
C	3.158979	1.095651	-1.390454
N	1.189887	2.496044	-1.699339
N	0.092205	2.37836	-1.105317
C	-0.089953	1.868348	0.182361
C	-1.435738	1.787439	0.701149
C	-1.373959	1.062081	1.900377
N	-0.046245	0.734377	2.110941
C	-2.676664	2.225436	0.223436
C	-3.80603	1.924215	0.960609
C	-3.722456	1.194026	2.162356
C	-2.507762	0.749313	2.651489
H	4.963574	-0.019885	-1.078046
H	5.879626	1.580358	0.589292
H	4.58202	3.612796	1.18403
H	2.366231	4.023124	0.140022
H	2.761398	0.406725	-2.130274
H	0.275151	0.097477	2.823619
H	-2.738214	2.765682	-0.714866
H	-4.780438	2.237167	0.599016
H	-4.632614	0.963872	2.707734
H	-2.439727	0.166575	3.564401
C	0.7214	1.19373	1.088892
H	1.777838	0.979332	1.070368
H	-0.444756	0.156934	-2.68265
C	3.610653	-2.093152	0.678939
C	3.728112	-2.980985	-0.386136
C	2.625889	-3.743757	-0.773125
C	1.408917	-3.604523	-0.118931
C	1.286171	-2.688879	0.930567
C	2.39648	-1.956292	1.345376
N	0.076556	-2.596333	1.684585
N	-0.98399	-2.160364	1.178719
C	-1.107519	-1.591552	-0.090745
C	-2.422387	-1.252976	-0.586339
C	-2.240639	-0.53843	-1.781925
N	-0.876777	-0.45497	-2.006855
C	-3.716506	-1.474038	-0.10599
C	-4.78319	-0.976627	-0.834747
C	-4.581001	-0.264982	-2.031356
C	-3.307546	-0.034963	-2.525242
H	4.466298	-1.509046	1.0028
H	4.67838	-3.096749	-0.898537
H	2.71698	-4.455954	-1.587959
H	0.544425	-4.188541	-0.419077
H	2.309227	-1.289822	2.19862
H	-3.864665	-2.006724	0.827099
H	-5.796147	-1.129887	-0.474765
H	-5.439865	0.114279	-2.576872
H	-3.146361	0.518828	-3.444996
C	-0.199965	-1.064257	-0.999133
H	0.878249	-1.040309	-0.981291

Energy= -1408.1696248 (Hartrees)

Sum of electronic and zero-point Energies= -1407.721294 (Hartrees)

Sum of electronic and thermal Energies= -1407.695403 (Hartrees)

Sum of electronic and thermal Enthalpies= -1407.694459 (Hartrees)

Sum of electronic and thermal Free Energies= -1407.778325 (Hartrees)

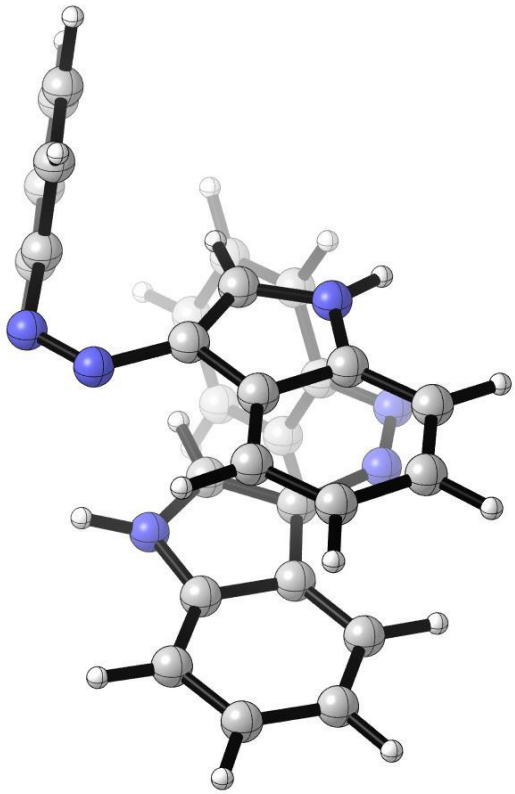

Figure A236 Dimer of two *Z*-**3a** molecules at the ωB97XD/6-31G(d) level of theory.

TS-dimer (non-water-complexed) (ωB97XD/6-31G(d))

C	-4.12073	-0.940661	-1.161144
C	-4.640915	-1.84232	-0.238574
C	-3.863251	-2.922352	0.182326
C	-2.566746	-3.081562	-0.286602
C	-2.028818	-2.152889	-1.184406
C	-2.825745	-1.105458	-1.646791
N	-0.715817	-2.325076	-1.711641
N	0.299471	-2.202685	-0.963926
C	0.314033	-1.731947	0.331756
C	1.578149	-1.552185	1.005552
C	1.293482	-0.8133	2.173141
N	-0.065844	-0.52669	2.254539
C	2.898049	-1.895184	0.693033
C	3.902961	-1.494979	1.55721
C	3.613364	-0.759596	2.723371
C	2.31218	-0.410751	3.042807
H	-4.721609	-0.105559	-1.508931
H	-5.652046	-1.718349	0.137501
H	-4.269943	-3.642336	0.886638
H	-1.947656	-3.905709	0.053928
H	-2.430382	-0.424067	-2.396412
H	-0.287619	0.911771	2.267716
H	3.11901	-2.443654	-0.217418
H	4.936403	-1.74242	1.330759
H	4.425492	-0.461188	3.380486
H	2.080974	0.163585	3.935318
C	-0.627934	-1.080243	1.160351
H	-1.684339	-0.944949	0.980452
H	0.433236	-0.265704	-2.880482
C	-3.967723	1.775335	0.99202
C	-4.128092	2.74633	0.009264
C	-3.011912	3.429044	-0.475022
C	-1.743553	3.129583	0.000384
C	-1.582422	2.122807	0.958326
C	-2.701594	1.470953	1.479378
N	-0.315754	1.850483	1.543295
N	0.820363	1.829085	0.938043
C	1.003643	1.622198	-0.375697
C	2.34504	1.364713	-0.877307
C	2.199405	0.606757	-2.044717
N	0.828667	0.43845	-2.267617
C	3.617178	1.625507	-0.374545
C	4.707667	1.127135	-1.072034
C	4.542648	0.378247	-2.247703
C	3.281046	0.101403	-2.75576
H	-4.829683	1.246041	1.384765
H	-5.117458	2.982024	-0.36997
H	-3.131431	4.207438	-1.222367
H	-0.877321	3.666543	-0.372817
H	-2.577515	0.727371	2.260636
H	3.738531	2.169832	0.555281
H	5.709356	1.303519	-0.693313
H	5.418086	-0.003735	-2.763074
H	3.145623	-0.497657	-3.650077
C	0.119675	1.021968	-1.300973
H	-0.951828	0.900927	-1.25334

Energy= -1408.1161479 (Hartrees)

Sum of electronic and zero-point Energies= -1407.671814 (Hartrees)

Sum of electronic and thermal Energies= -1407.645996 (Hartrees)

Sum of electronic and thermal Enthalpies= -1407.645052 (Hartrees)

Sum of electronic and thermal Free Energies= -1407.729030 (Hartrees)

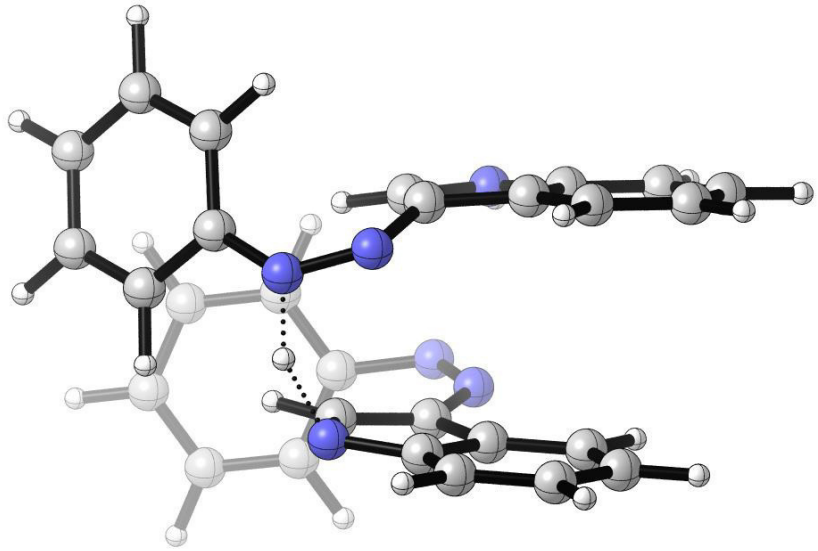

Figure A237 TS of the intermolecular proton transfer between two *Z*-**3a** molecules at the ωB97XD/6-31G(d) level of theory.

Inversion TS for 3a (B3LYP/6-31G(d))

C	4.637269644	0.1111458223	1.2054852713
C	5.3295839401	0.3139920516	0.0080803068
C	4.637786699	0.1454534068	-1.1949291839
C	3.2951329954	-0.2099593598	-1.2238105625
C	2.5915544079	-0.4133130409	-0.0028958757
C	3.294615739	-0.2449781894	1.223626133
N	1.306587212	-0.7608347473	-0.0081701929
N	0.120410145	-1.0980229731	-0.0136174576
C	-0.8488369079	-0.0715746727	0.0003716424
C	-2.2667329032	-0.335737756	-0.0043264048
C	-2.9101105448	0.9268193474	0.0131193143
N	-1.9132794059	1.8956296444	0.0275833724
C	-0.6821429091	1.3038641992	0.0199739436
C	-3.0453271108	-1.5028746689	-0.0214410438
C	-4.4287536194	-1.3772160315	-0.0206701855
C	-5.0501363822	-0.1111357425	-0.003174095
C	-4.3012989026	1.0600733682	0.0139890978
H	5.1514685266	0.2304822163	2.1566966177
H	6.3788558219	0.5912326477	0.0122672462
H	5.1523909661	0.2919204891	-2.1421238752
H	2.771020445	-0.3432332487	-2.1645355058
H	2.7701124277	-0.405108986	2.1599350396
H	-2.0731102598	2.8923394334	0.0412455502
H	0.2279300049	1.8863812584	0.0288237762
H	-2.5676362996	-2.4773728988	-0.0349224081
H	-5.0477417648	-2.2698829816	-0.0337850197
H	-6.1346240793	-0.0491149062	-0.0030979748
H	-4.7790289288	2.0360059403	0.0274713795

Energy= -704.2663695 (Hartrees)

Sum of electronic and zero-point Energies= -704.048151 (Hartrees)

Sum of electronic and thermal Energies= -704.035232 (Hartrees)

Sum of electronic and thermal Enthalpies= -704.034288 (Hartrees)

Sum of electronic and thermal Free Energies= -704.089836 (Hartrees)

Inversion TS for 3c (B3LYP/6-31G(d))

C	-4.6384967987	0.1304974893	-1.2001328748
C	-5.3303285512	0.3181423438	0.0001512176
C	-4.638493591	0.1307332934	1.2004703495
C	-3.2967970563	-0.2282292882	1.223960356
C	-2.592767057	-0.4157275304	0.0002201248
C	-3.2968001471	-0.2284687627	-1.2235554485
N	-1.3089560595	-0.7645828068	0.000251155
N	-0.1221780486	-1.1032290495	0.0002604154
C	0.8476501081	-0.081278407	0.0001362035
C	2.2642024087	-0.3439977663	0.0001329965
C	2.9025834981	0.9214456534	-0.0000099611
N	1.9111913366	1.9006694564	-0.000080988
C	0.6864555312	1.2959466464	-0.0000014341
C	3.0449441221	-1.5088293476	0.0002326309
C	4.4286359955	-1.3800466268	0.0001832627
C	5.0465707536	-0.1128962871	0.0000373901
C	4.2942820503	1.0571317368	-0.0000619481
H	-5.1527119768	0.2643027122	-2.1494740138
H	-6.379051852	0.5975602677	0.0001253067
H	-5.1527065473	0.2647253478	2.1497863373
H	-2.772902679	-0.3761373418	2.1626674171
H	-2.7729079209	-0.3765612582	-2.1622346731
H	-0.2244271488	1.878357446	-0.0000433998
H	2.5693438211	-2.4844829035	0.0003436949
H	5.049527234	-2.271542144	0.0002575747
H	6.1309310943	-0.048023641	0.0000004989
H	4.7735087504	2.0318538443	-0.0001778179
C	2.1549578044	3.3320998378	-0.0002930369
H	2.7201117389	3.6268647767	0.8905188623
H	2.7197759037	3.6266673063	-0.8913832899
H	1.1976457228	3.8561888625	-0.0001664478

Solv.	ε	ΔG‡
gas	0	24.23
cyclohexane	2.0165	24.91
dioxane	2.2099	24.99
mesitylene	2.265	25.01
benzene	2.2706	25.01
toluene	2.3741	25.05
methanol	32.613	26.06
acetonitrile	35.688	26.07

Table A Activation energies for the inversion TS of **3c** in different solvents (the value of ε for each solvent is the one implemented in Gaussian).

Rotational TS for 3a (B3LYP/6-31G(d))

C	-3.3518938335	-0.4094484566	1.7213658113
C	-4.5913876668	0.0435717179	1.2487397298
C	-4.759052278	0.3113621097	-0.1172385192
C	-3.7046655216	0.1330045538	-0.9999098703
C	-2.4387103407	-0.3060949922	-0.5309863558
C	-2.2829596542	-0.585399963	0.8539371803
N	-1.4516809681	-0.4483360052	-1.4730948818
N	-0.2408489412	-0.8366703812	-1.1057105227
C	0.655298705	0.0528113291	-0.6444118853
C	2.0153540482	-0.290874534	-0.2474200067
C	2.6459557952	0.9096926602	0.1534294
N	1.7235875918	1.9394018285	0.005245619
C	0.5343358644	1.4452656197	-0.4728422127
C	2.7257948205	-1.4938187165	-0.199270018
C	4.0452719748	-1.4729376496	0.245622158
C	4.6568936924	-0.2690766349	0.6419735693
C	3.9675469287	0.9407564947	0.602494932
H	-3.225901428	-0.6315387935	2.7781314208
H	-5.4211648365	0.1770687963	1.9370738326
H	-5.7209861019	0.6549764871	-0.4884504057
H	-3.8137428239	0.3265827423	-2.06262715
H	-1.3281292457	-0.9519706448	1.2148552074
H	1.9094795706	2.9134217258	0.1895027767
H	-0.3068023286	2.0893749265	-0.6784603187
H	2.2496040891	-2.4194187074	-0.5083652709
H	4.6136808974	-2.3976916249	0.2875738825
H	5.6876039335	-0.2812096694	0.9854103446
H	4.4418270571	1.8694827816	0.9084095533

Energy= -704.2814127

Sum of electronic and zero-point Energies= -704.064224

Sum of electronic and thermal Energies= -704.051584

Sum of electronic and thermal Enthalpies= -704.050640

Sum of electronic and thermal Free Energies= -704.104342

4.4.2 Reaction coordinates for the intramolecular *Z*-to-*E* pathways

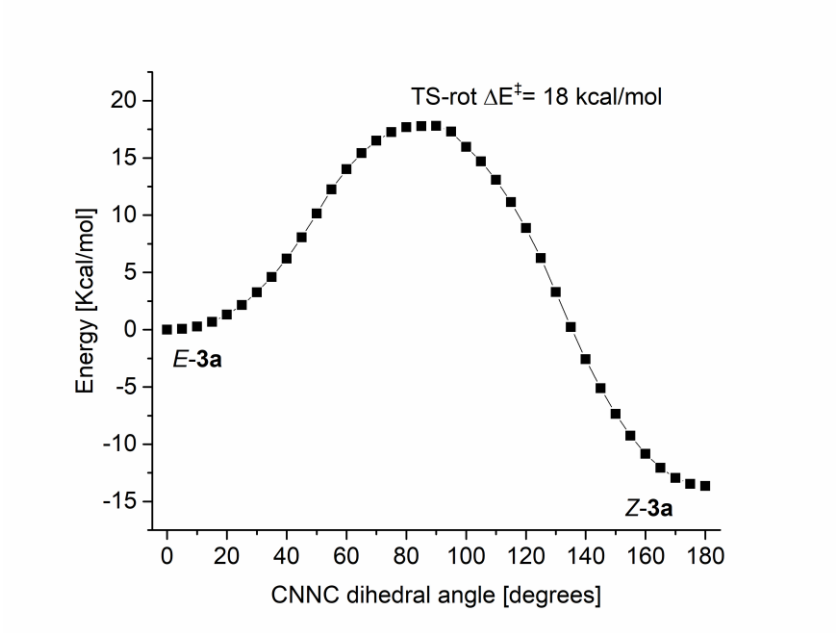

Figure A238 Energy barrier for the constrained rotation around the azo group, describing the rotational transition state. The data are obtained at the (BS)-B3LYP/6-31G(d) level of theory.

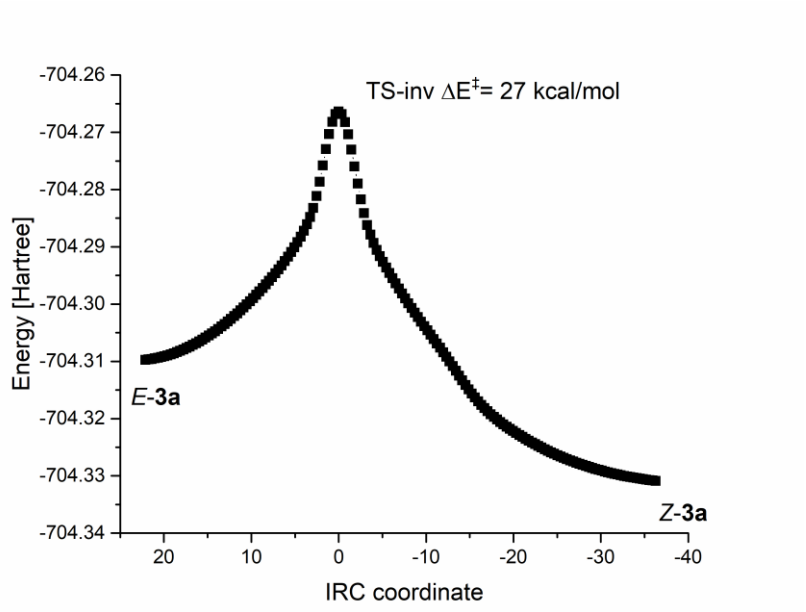

Figure A239 Intrinsic reaction coordinate regarding the inversion mechanism at the B3LYP/6-31G(d) level of theory.

4.4.3 Reaction coordinates for the intermolecular hydrazone *Z*-to-*E* pathway

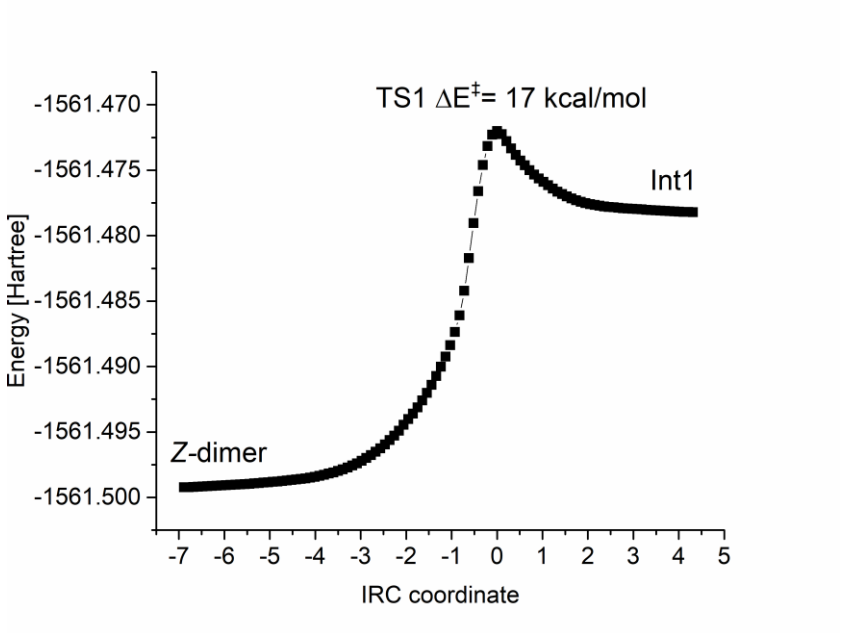

Figure A240 Intrinsic reaction coordinate for the formation of the charge-separated dimer **Int1** from the *Z*-dimer of **3a** complexed with two water molecules at the B3LYP/6-31G(d) level of theory.

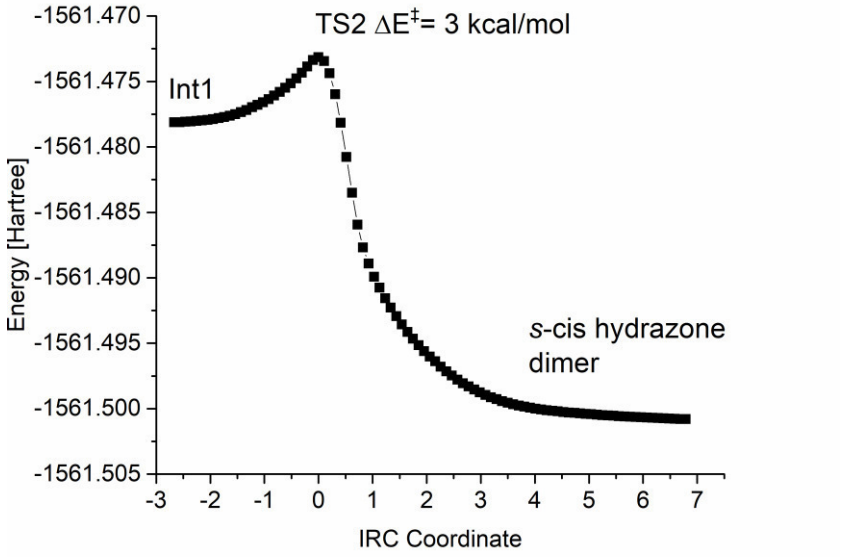

Figure A241 Intrinsic reaction coordinate for the formation of the *s*-cis hydrazone dimer from **Int1** at the B3LYP/6-31G(d) level of theory.

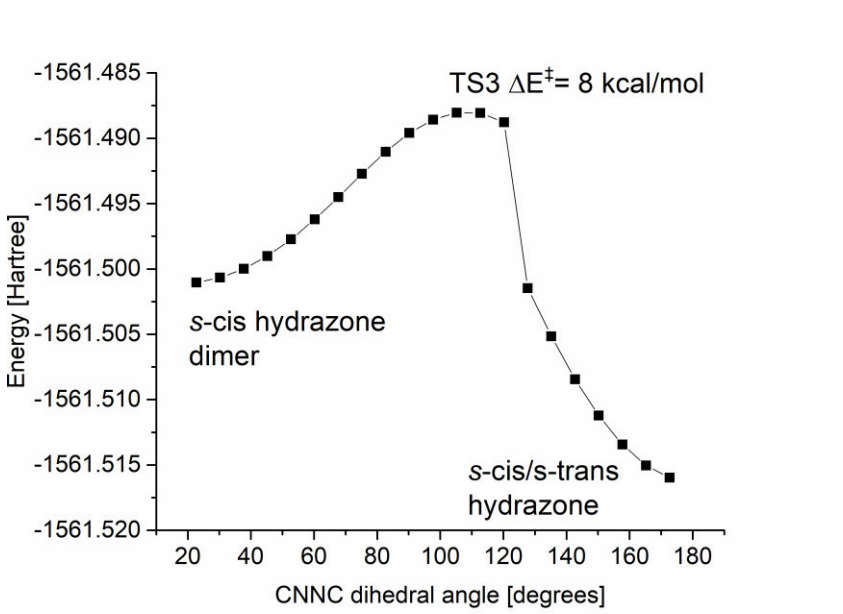

Figure A242 Energy barrier for the constrained rotation around the azo group of one of the two *s*-cis hydrazones. The outcome of the reaction is a water complex of an *s*-trans and *s*-cis hydrazone. The data are obtained at the B3LYP/6-31G(d) level of theory. The discontinuity is due to the "umbrella" inversion of the pyramidalized protonated nitrogen of the rotating hydrazone. This pathway was not investigated further.

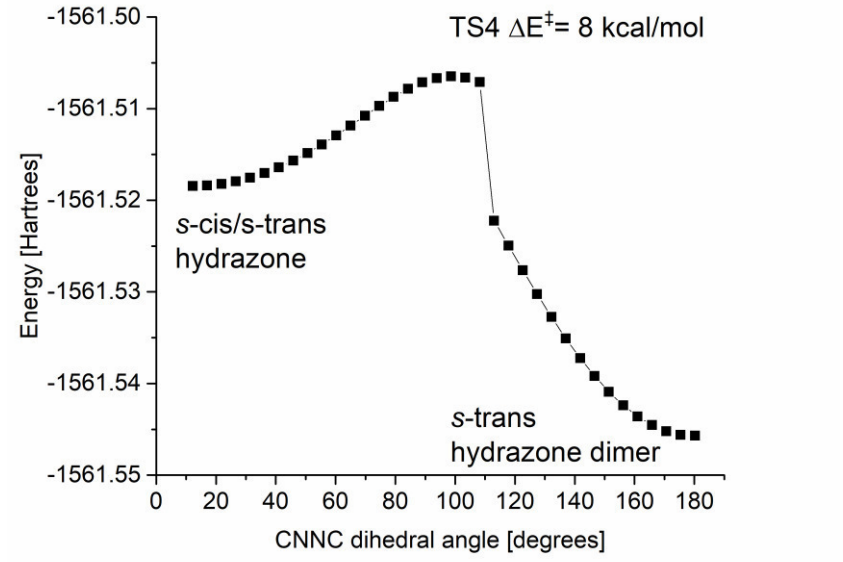

Figure A243 Energy barrier for the constrained rotation around the azo group, of the *s*-cis hydrazone in the *s*-cis/*s*-trans hydrazone complez. The outcome of the reaction is a water complex of two *s*-trans hydrazones. The data are obtained at the B3LYP/6-31G(d) level of theory. The discontinuity is due to the "umbrella" inversion of the pyramidalized protonated nitrogen of the rotating hydrazone. This pathway was not investigated further.

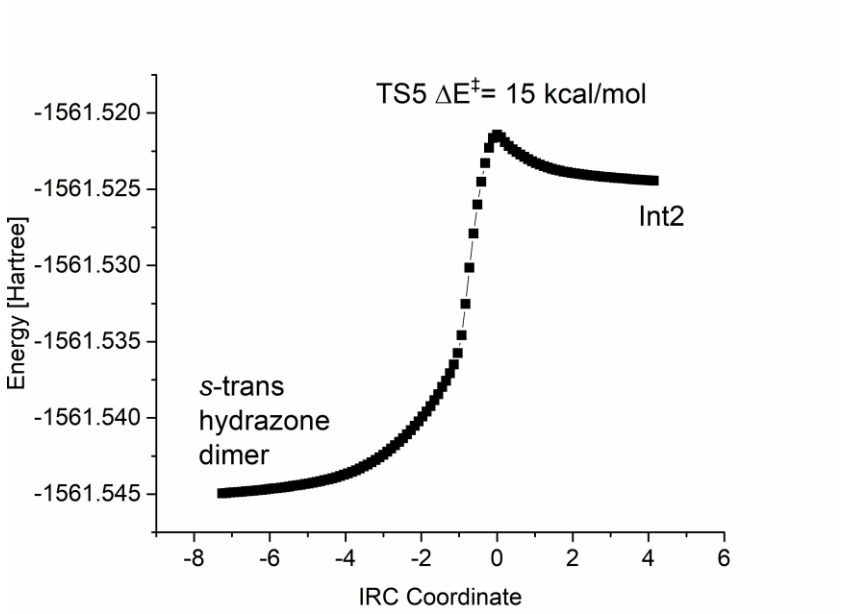

Figure A244 Intrinsic reaction coordinate for the formation of **Int2** from the *s*-trans hydrazone dimer at the B3LYP/6-31G(d) level of theory.

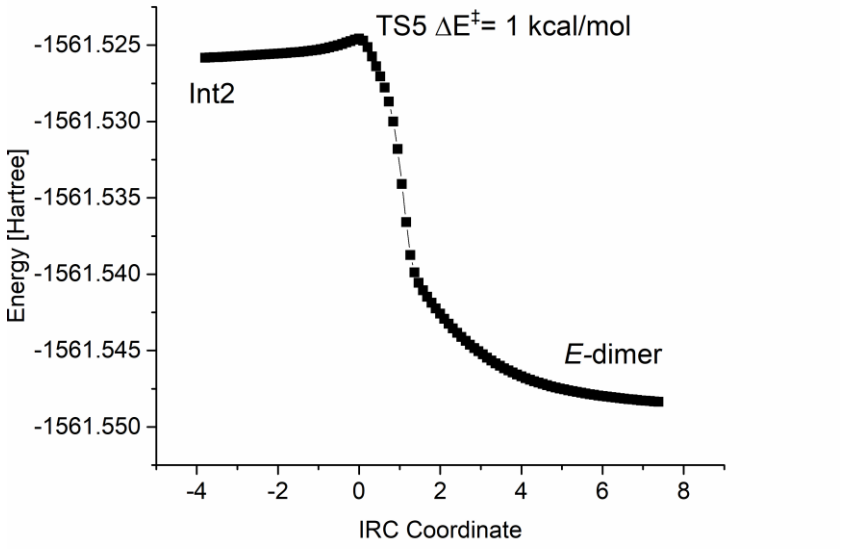

Figure A245 Intrinsic reaction coordinate for the formation of the *E*-dimer of **3a** from **Int2** at the B3LYP/6-31G(d) level of theory.

6 Kinetic analysis

6.1 Analysis

In order to have more insights on the different mechanisms involved in the reaction of the *Z*- form of compound **3**, we designed a series of kinetic experiments.

All the experiments presented (with the exception of **3b** in MeOH, discussed more thoroughly in the main text) are characterised by mono-exponential decays and evidence a first-order (or pseudo first-order) kinetic. In particular, we monitored the disappearance of the *Z*-isomer following the formation of the ππ* band of the *E*- isomer, immediately after its conversion to its *Z*- form by means of irradiation. Consequently, the kinetic involved can be summarized as:

$$v = -\frac{\partial[Z\text{-}\mathbf{3}]}{\partial t} = k_{obs}[Z\text{-}\mathbf{3}] \qquad (4)$$

where k_{obs} is the kinetic constant observed in the experiment. We tested the dependency of the rate constant on the presence of the indolic proton and on the presence of a protic solvent. In particular, the absence of the N-H in the structure of the compound as in **3c** leads to the results summarized in Table A106.

3c [μM]	τ [h]	k_{obs} [10^{-4} s^{-1}]
6	2.5	1.1
30	2.2	1.3
50	2.4	1.2
50[a]	2.2	1.3
70	2.5	1.1
100	2.3	1.2
135	2.3	1.2

[a]100 μL of water added to a 3 mL solution.

Table A106 Lifetimes and k_{obs} for different concentrations of **3c** in MeOH.

The k_{obs} is independent from both the initial concentration and the water content, therefore it can be stated that **3c** follows a first-order kinetic mechanism of *Z*-to-*E* interconversion. However, in order to rule out the possibility that the protic solvent neutralizes the effect of the addition of water, we repeated the previous experiment using dry MeCN as solvent (see Table A107).

3c [μM]	τ [d]	k_{obs} [10^{-5} s^{-1}]
25	1.18	0.99
50	1.17	0.98
50[a]	1.23	0.94
80	0.93	1.24
130	1.11	1.04

[a]100 μL of water added to a 3 mL solution

Table A107 Lifetimes and k_{obs} for different concentrations of **3c** in MeCN.

Only limited variations, attributable more likely to experimental factors, can be found in the experiment. Hence, the N-Me switch seems not affected neither by the concentration, nor by the presence of a protic solvent.

The case of **3b**, here representing the N-H indole class of switches, is more interesting. In particular, no concentration dependency was found in dry DMSO, as reported in Table A108. Since

the rate constant k_{obs} is not varied upon changes of the concentration, also in this case we have a first-order mechanism.

3b [μM]	**τ [ms]**	k_{obs} **[s^{-1}]**
6	1.4	721
30	1.4	717
50	1.3	779
70	1.3	792
100	1.4	740
135	1.4	711

Table A108 Lifetimes and k_{obs} for different concentrations of **3b** in dry DMSO.

However, the addition of a minimal amount of water in the solvent mixture (50 μL of water in 3 mL of dry DMSO solutions, 1.67% v/v) leads to a concentration dependency on the rate of the reaction. The value of ΔOD measured after the laser shot remains almost constant (ca. -0.1), hence the amount of *Z*-**3b** generated results constant (if we suppose the ε of the *Z* isomer is negligible compared to the ε of the *E* isomer measured at the ππ* peak of the latter, we can approximate the concentration of the *Z*-form generated after the laser shot to be 6μM). The results measured with the laser flash photolysis are summarized in Table A109 and plotted in Figure A246.

3b [μM]	**τ [μs]**	k'_{obs} **[$10^3 s^{-1}$]**
6	503	1.99
12	435	2.30
18	361	2.77
24	306	3.27
30	283	3.53
36	278	3.60
42	269	3.72
46.8	257	3.89
54	237	4.22
66	221	4.52
81	210	4.76
90	203	4.92

Table A109 Lifetimes and k'_{obs} for different concentrations of **3b** in DMSO with fixed water content (1.67% v/v).

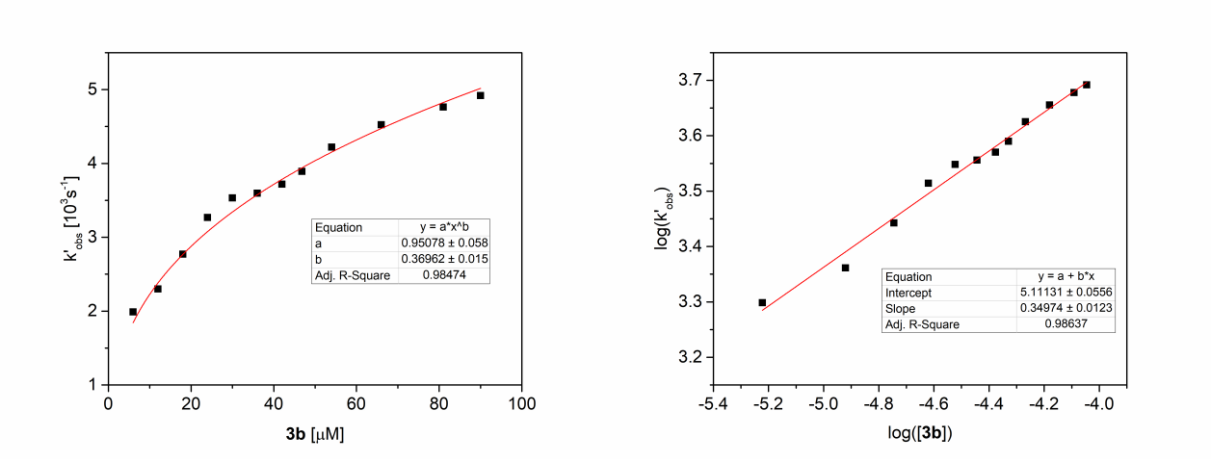

Figure A246 Plot of the observed kinetic constant k'_{obs} *vs* the concentration of **3b** in DMSO with fixed water content (1.67% v/v) (left). Double logarithmic linearization of the previous plot (right).

The kinetic constants k'_{obs} observed at different concentrations of **3b** (to be more precise, here we consider the sum [**3b**]=([*Z*-**3b**]+[*E*-**3b**]) that over time remains constant to the initial value of *E*-**3b** dissolved in solution before irradiation) are fitted using an allometric function, as reported for the case of the arylazomidazoles (see Ref. (26) in the main text):

$$k'_{obs} = k'[\mathbf{3b}]^n \tag{5}$$

and linearized in its logarithmic form:

$$\log_{10} k'_{obs} = \log_{10} k' + n \log_{10}[3b] \tag{6}$$

Thus, for Equation (5) k'=1.3·10^5 M$^{-0.35}$s^{-1} while n=0.35, producing a rate equation expressed as

$$v = k'[\mathbf{3b}]^{0.35}[Z\text{-}\mathbf{3b}] \tag{7}$$

similar to the one shown in Ref. (26).

This kinetic was indeed explained by Otsuki *et al.* considering that "the isomerization reaction is self-catalysed through intermolecular interactions, most likely through intermolecular hydrogen bonding."[26]

On the other hand, the dependence of the observed kinetic constant to water concentration can be verified fixing the total concentration of [**3b**] ([**3b**]=50 μM) while the amount of water in DMSO is varied. Again, an apparent first order kinetic $v = k''_{obs}$[*Z*-**3b**] as Eqn. (4) is found at each point. However, the value of k''_{obs} becomes greater when the water concentration is increased, following a saturation kinetic as expressed by Table A110.

H_2O [% v/v]	H_2O [M]	τ [μs]	k''_{obs} [$10^4 s^{-1}$]
0	0	1300	0.0769
0.33	0.185	1261	0.0793
0.67	0.37	559	0.1789
1	0.555	437	0.2288
1.33	0.74	392	0.2551
1.67	0.925	230	0.4348
3.33	1.85	180	0.5556
6.67	3.7	83.4	1.199
10	5.55	72	1.389
16.66	9.25	47	2.128
20	11.1	35	2.857
23.33	12.95	43.9	2.278
30	16.65	37.9	2.638
33.33	18.5	33.3	3.003
40	22.2	35	2.857
50	27.75	32.1	3.115
66	36.63	31	3.226

Table A110 Lifetimes and k''_{obs} for different concentrations of water in DMSO, with fixed [**3b**] content.

The data are fitted using a rectified hyperbole function with formula:

$$k''_{obs} = \frac{\alpha[H_2O]}{\beta + [H_2O]} \tag{8}$$

which can be linearized with a Lineweaver-Burk plot (see Figure S247).

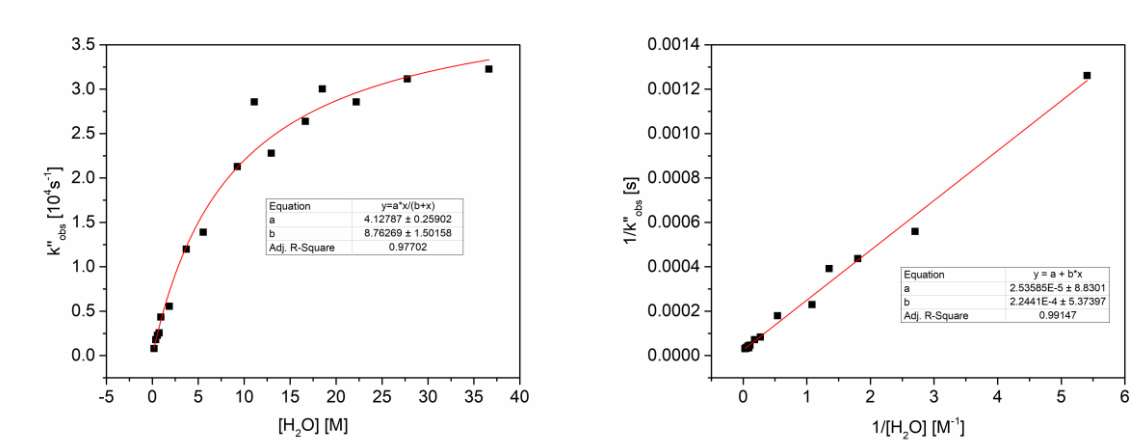

Figure S247 Plot of the observed kinetic constant k''_{obs} *vs* the concentration of H_2O in DMSO (left). Double inverse linearization of the previous plot (right).

The parameters defining the hyperbolic behaviour of the kinetic constant are $\alpha = 4 \cdot 10^4$ s^{-1} and $\beta = 8.96$ M. α corresponds to the value of k''_{obs} at saturation, while β defines the water concentration at which k''_{obs} is equal to $\frac{\alpha}{2}$.

Thus, the rate equation can be rewritten as:

$$v = \frac{\alpha[H_2O]}{\beta + [H_2O]}[Z\text{-}\mathbf{3b}] \tag{9}$$

A similar saturation kinetic can be related to the increased solvent ability to promote the intermolecular proton transfer. In particular, water can alter the short-range solvation between the molecules of **3b** involved in the proton transfer, in a way similar to the DMSO in benzene in the example of Berman *et al.*[S24]

To generalize, we can explicate the total concentration of **3b** that was kept fixed for the experiment and rewrite α as $\alpha = k'''[\mathbf{3b}]^{0.35}$

$$v = \frac{k'''[H_2O]}{\beta + [H_2O]}[\mathbf{3}\boldsymbol{b}]^{0.35}[Z\text{-}\mathbf{3}\boldsymbol{b}] \qquad (10)$$

and $k''' = 1.4 \cdot 10^6\ M^{-1.35}s^{-1}$.

6.2 Lifetimes of the measurements reported in 6.1

6.2.1 3c

MeOH

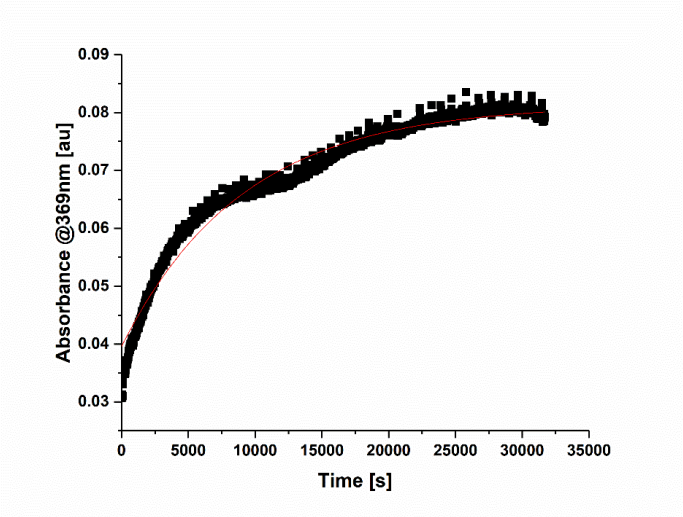

Figure A248: PSS-to-*E* kinetic of **3c** in MeOH (6 μM), irradiation with 400 nm LED, λ^{obs}=369 nm.

Equation	y = A1*exp(-x/τ) + y0
y0	0.08138 ± 1.23834E-4
A1	-0.04181 ± 1.60898E-4
τ	9106.15387 ± 98.82725
R-Square(COD)	0.97155
Adj. R-Square	0.97152

Table A111 Fitting of the growth of the signal shown in Figure A248.

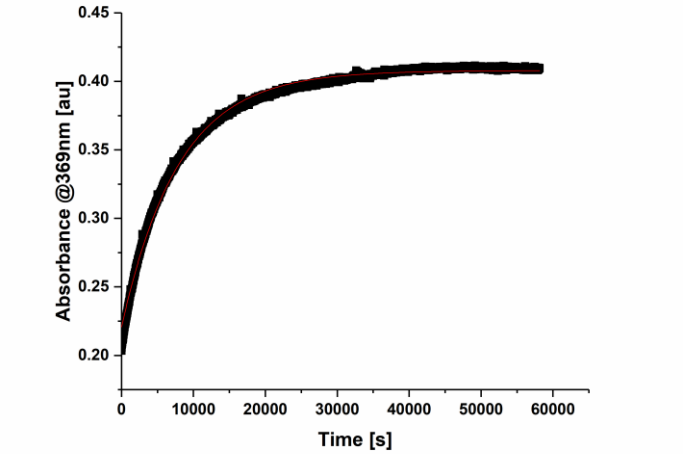

Figure A249: PSS-to-*E* kinetic of **3c** in MeOH (30 μM), irradiation with 400 nm LED, λ^{obs}=369 nm.

Equation	y = A1*exp(-x/τ) + y0
y0	0.40788 ± 1.0445E-4
A1	-0.18734 ± 3.84315E-4
τ	7905.40629 ± 28.8313
R-Square(COD)	0.99454
Adj. R-Square	0.99453

Table A112 Fitting of the growth of the signal shown in Figure A249.

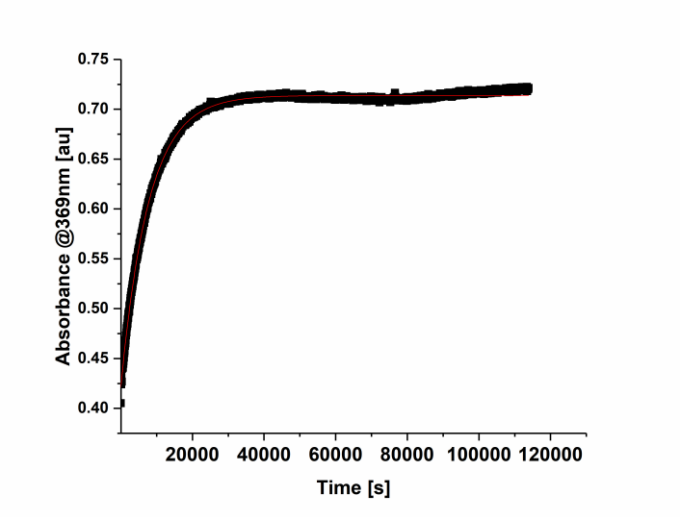

Figure A250: PSS-to-*E* kinetic of **3c** in MeOH (3 mL 50 μM solution with 100 μL water), irradiation with 400 nm LED, λ^{obs}=369 nm.

Equation	y = A1*exp(-x/τ) + y0
y0	0.71382 ± 9.59142E-5
A1	-0.2931 ± 6.21859E-4
τ	7740.7039 ± 25.42772
R-Square(COD)	0.99696
Adj. R-Square	0.99695

Table A113 Fitting of the growth of the signal shown in Figure A250.

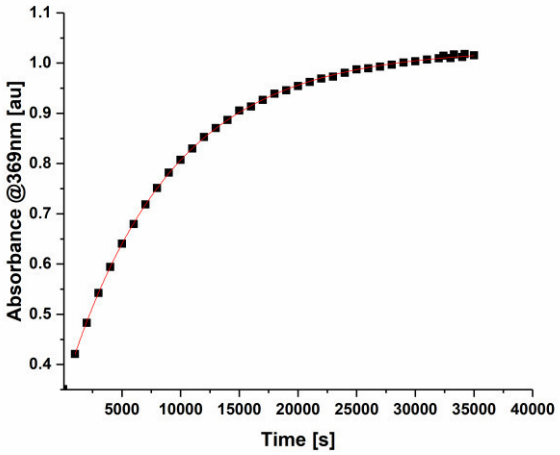

Figure A251: PSS-to-*E* kinetic of **3c** in MeOH (70 μM), irradiation with 400 nm LED, λ^{obs}=369 nm.

Equation	y = A1*exp(-x/τ) + y0
y0	1.02812 ± 7.70044E-4
A1	-0.6798 ± 0.0015
τ	8917.80976 ± 46.17369
R-Square(COD)	0.99986
Adj. R-Square	0.99985

Table A114 Fitting of the growth of the signal shown in Figure A251.

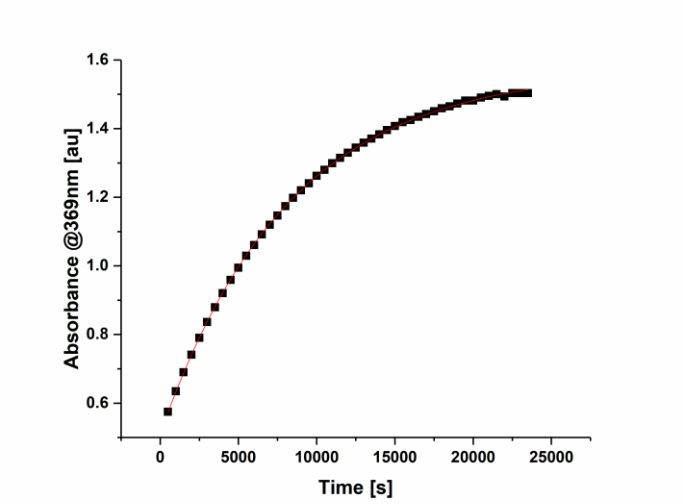

Figure A252: PSS-to-*E* kinetic of **3c** in MeOH (100 μM), irradiation with 400 nm LED, λ^{obs}=369 nm.

Equation	y = A1*exp(-x/τ) + y0
y0	1.57385 ± 0.00179
A1	-1.06434 ± 0.00181
τ	8164.62797 ± 44.40198
R-Square(COD)	0.99987
Adj. R-Square	0.99987

Table A115 Fitting of the growth of the signal shown in Figure A252.

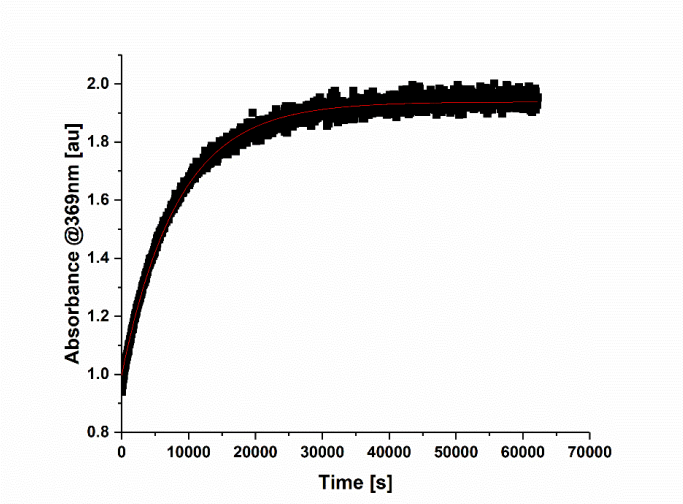

Figure A253: PSS-to-*E* kinetic of **3c** in MeOH (135 μM), irradiation with 400 nm LED, λ^{obs}=369 nm.

Equation	y = A1*exp(-x/τ) + y0
y0	1.93841 ± 7.46717E-4
A1	-0.94056 ± 0.00278
τ	8365.32144 ± 43.74776
R-Square(COD)	0.99098
Adj. R-Square	0.99097

Table A116 Fitting of the growth of the signal shown in Figure A253.

MeCN

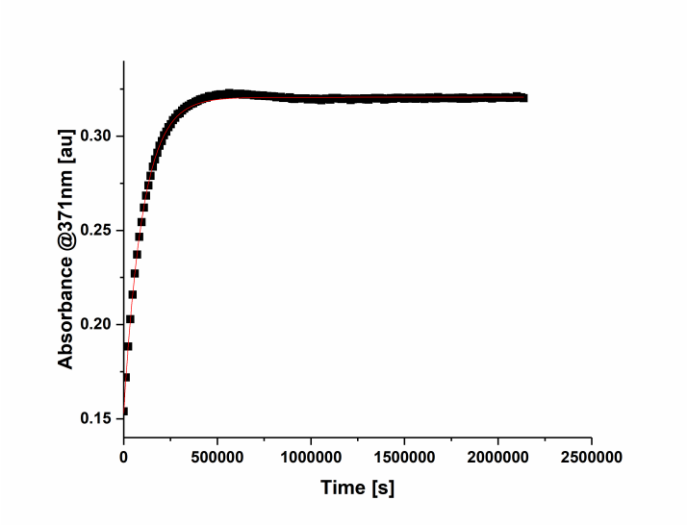

Figure A254: PSS-to-*E* kinetic of **3c** in MeCN (25 μM), irradiation with 400 nm LED, λ^{obs}=371 nm.

Equation	y = A1*exp(-x/τ) + y0
y0	0.32067 ± 8.59956E-5
A1	-0.16782 ± 6.35096E-4
τ	101840.70954 ± 610.08646
R-Square(COD)	0.99845
Adj. R-Square	0.99843

Table A117 Fitting of the growth of the signal shown in Figure A254.

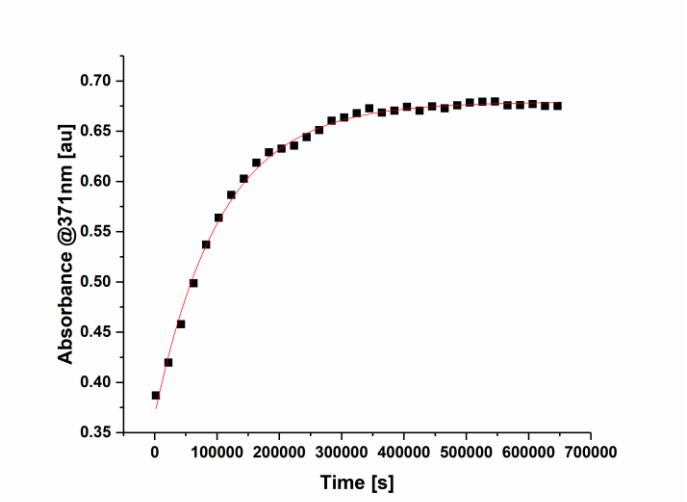

Figure A255: PSS-to-*E* kinetic of **3c** in MeCN (3 mL 50 μM solution with 100μL water), irradiation with 400 nm LED, λ^{obs}=371 nm.

Equation	y = A1*exp(-x/τ) + y0
y0	0.67917 ± 0.0014
A1	-0.3116 ± 0.00377
τ	106052.0137 ± 2607.87334
R-Square(COD)	0.99637
Adj. R-Square	0.99613

Table A118 Fitting of the growth of the signal shown in Figure A255.

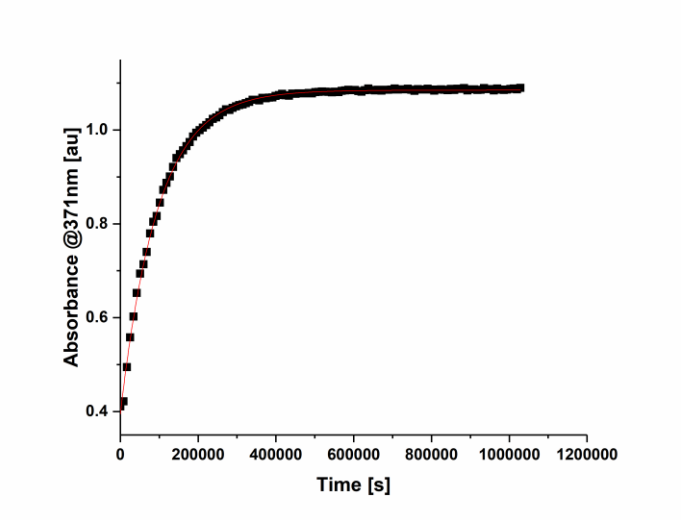

Figure A256: PSS-to-*E* kinetic of **3c** in MeCN (130 μM), irradiation with 400 nm LED, λ^{obs}=371 nm.

Equation	y = A1*exp(-x/τ) + y0
y0	1.08494 ± 5.42677E-4
A1	-0.69046 ± 0.00259
τ	96251.17347 ± 607.56613
R-Square(COD)	0.99888
Adj. R-Square	0.99886

Table A119 Fitting of the growth of the signal shown in Figure A256.

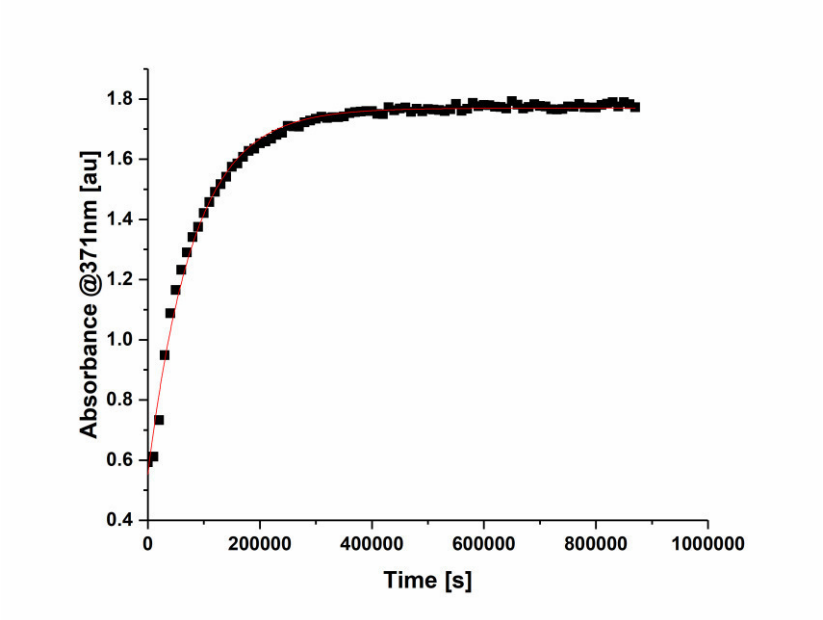

Figure A257: PSS-to-*E* kinetic of **3c** in MeCN (80 μM), irradiation with 400 nm LED, λ^{obs}=371 nm.

Equation	y = A1*exp(-x/τ) + y0
y0	1.76956 ± 0.0027
A1	-1.21734 ± 0.01259
τ	80712.91789 ± 1422.88285
R-Square(COD)	0.9938
Adj. R-Square	0.99365

Table A120 Fitting of the growth of the signal shown in Figure A257.

6.2.2 3b

Dry DMSO

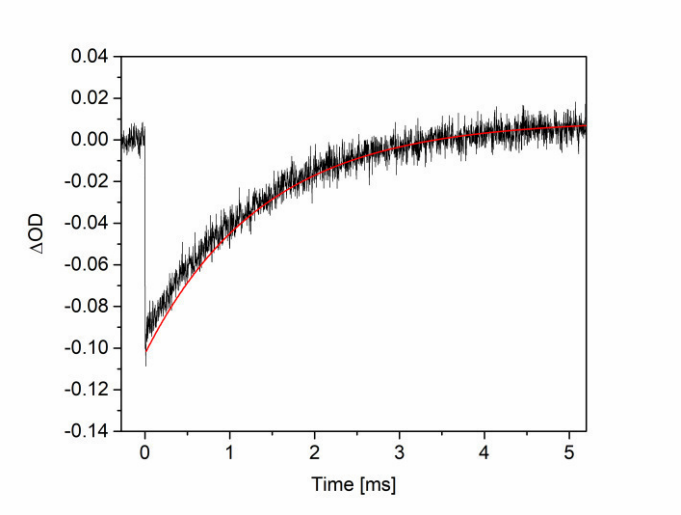

Figure A258: Transient signal detected at 381 nm for **3b** (6 μM) in dry DMSO.

Equation	y = A1*exp(-x/τ) + y0
y0	0.0095 ± 3.09994E-4
A1	-0.11218 ± 4.77653E-4
τ	1.38691 ± 0.01538
R-Square(COD)	0.96866
Adj. R-Square	0.96863

Table A121 Fitting of the growth of the signal shown in Figure A258.

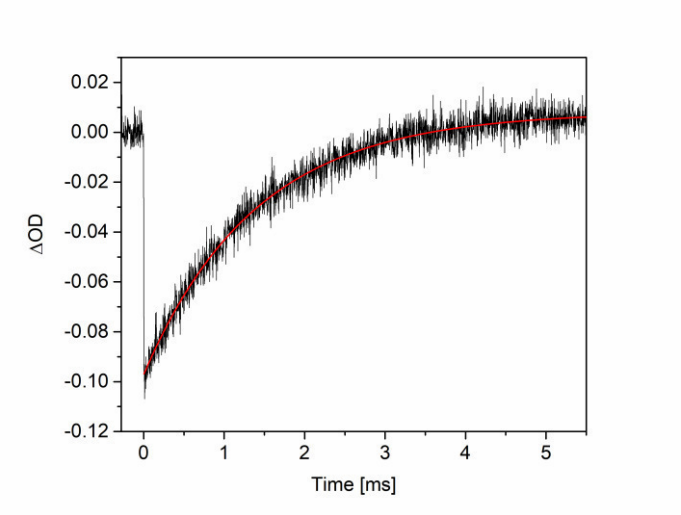

Figure A259: Transient signal detected at 381 nm for **3b** (30 μM) in dry DMSO.

Equation	y = A1*exp(-x/τ) + y0
y0	0.00816 ± 2.61882E-4
A1	-0.1053 ± 4.26703E-4
τ	1.39491 ± 0.01431
R-Square(COD)	0.97181
Adj. R-Square	0.97178

Table A122 Fitting of the growth of the signal shown in Figure A259.

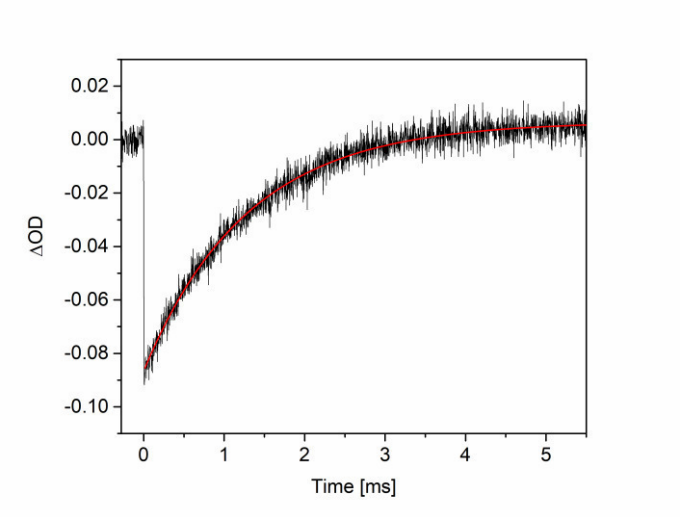

Figure A260: Transient signal detected at 381 nm for **3b** (50 μM) in dry DMSO.

Equation	y = A1*exp(-x/τ) + y0
y0	0.00677 ± 1.86797E-4
A1	-0.09334 ± 3.56708E-4
τ	1.28398 ± 0.01151
R-Square(COD)	0.97646
Adj. R-Square	0.97644

Table A123 Fitting of the growth of the signal shown in Figure A260.

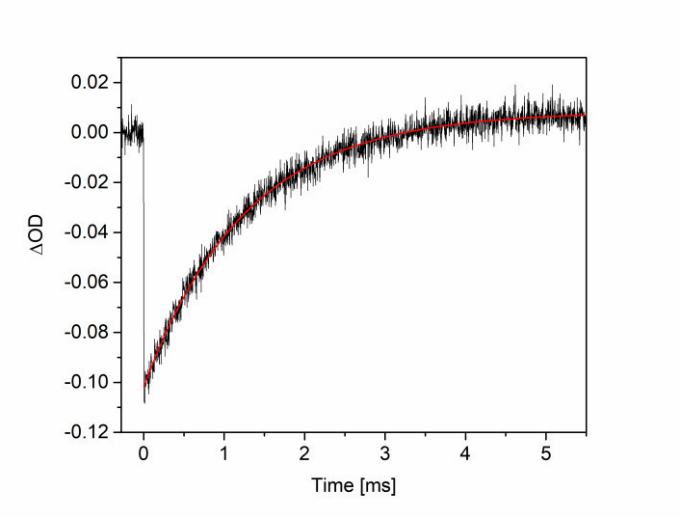

Figure A261: Transient signal detected at 381 nm for **3b** (70 μM) in dry DMSO.

Equation	y = A1*exp(-x/τ) + y0
y0	0.00841 ± 1.77403E-4
A1	-0.11027 ± 3.73462E-4
τ	1.263 ± 0.00958
R-Square(COD)	0.98189
Adj. R-Square	0.98187

Table A124 Fitting of the growth of the signal shown in Figure A261.

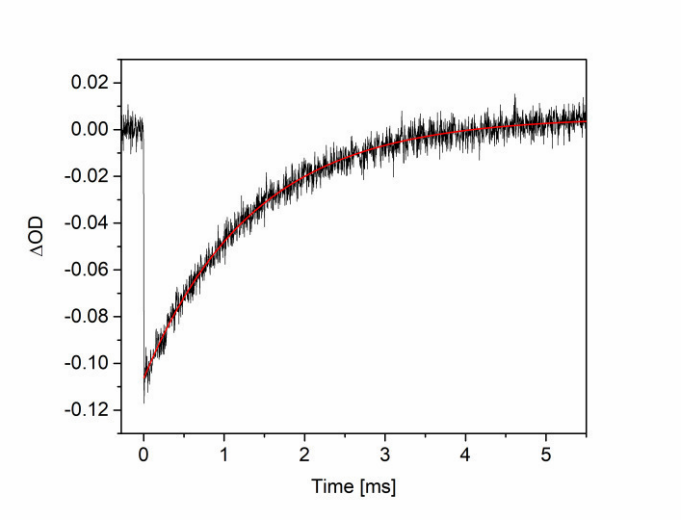

Figure A262: Transient signal detected at 381 nm for **3b** (100 μM) in dry DMSO.

Equation	y = A1*exp(-x/τ) + y0
y0	0.00542 ± 2.26047E-4
A1	-0.11182 ± 4.00456E-4
τ	1.35098 ± 0.01176
R-Square(COD)	0.9803
Adj. R-Square	0.98027

Table A125 Fitting of the growth of the signal shown in Figure A262.

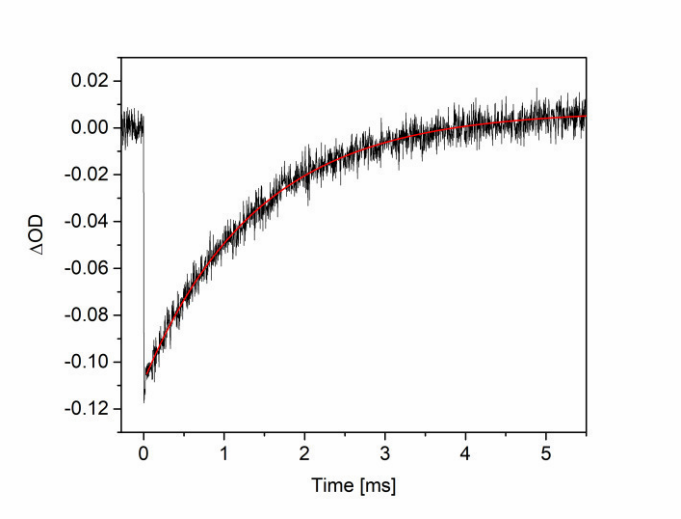

Figure A263: Transient signal detected at 381 nm for **3b** (130 μM) in dry DMSO.

Equation	y = A1*exp(-x/τ) + y0
y0	0.0074 ± 2.32971E-4
A1	-0.11547 ± 4.33389E-4
τ	1.40598 ± 0.01255
R-Square(COD)	0.97747
Adj. R-Square	0.97744

Table A126 Fitting of the growth of the signal shown in Figure A263.

DMSO (water 1.67% v/v)

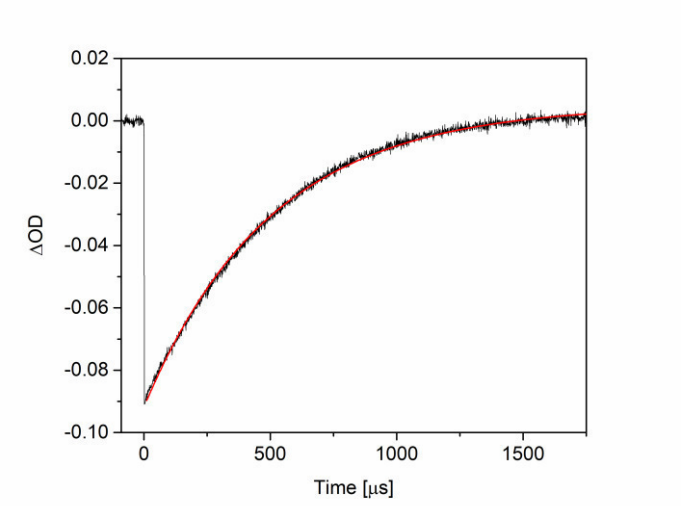

Figure A264: Transient signal detected at 381 nm for **3b** (6 μM) in DMSO with fixed water content (1.67% v/v).

Equation	y = A1*exp(-x/τ) + y0
y0	0.00515 ± 7.32628E-5
A1	-0.09702 ± 9.97736E-5
τ	501.17785 ± 1.42994
R-Square(COD)	0.99807
Adj. R-Square	0.99807

Table A127 Fitting of the growth of the signal shown in Figure A264.

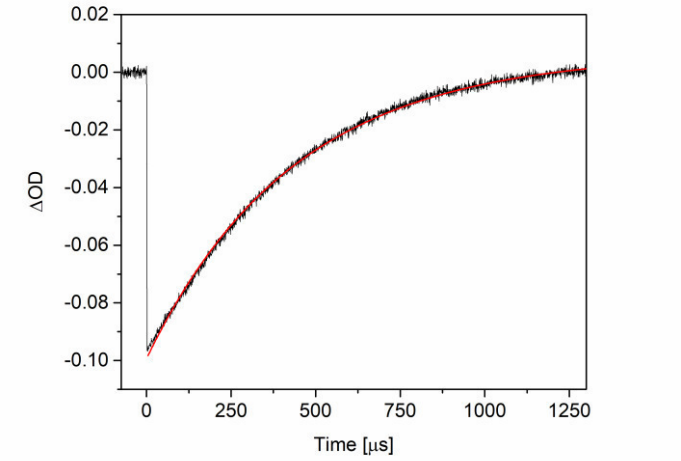

Figure A265: Transient signal detected at 381 nm for **3b** (12 μM) in DMSO with fixed water content (1.67% v/v).

Equation	y = A1*exp(-x/τ) + y0
y0	0.00654 ± 9.57518E-5
A1	-0.10585 ± 1.041E-4
τ	435.19562 ± 1.31042
R-Square(COD)	0.99818
Adj. R-Square	0.99818

Table A128 Fitting of the growth of the signal shown in Figure A265.

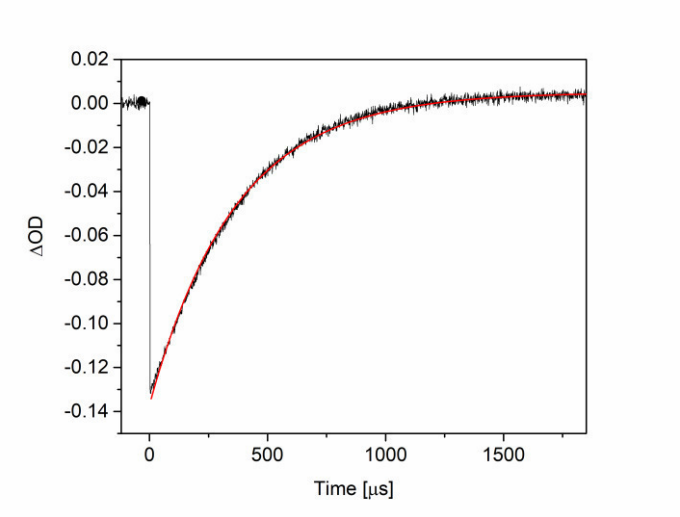

Figure A266: Transient signal detected at 381 nm for **3b** (18 μM) in DMSO with fixed water content (1.67% v/v).

Equation	y = A1*exp(-x/τ) + y0
y0	0.00513 ± 6.09471E-5
A1	-0.14211 ± 1.93941E-4
τ	361.03527 ± 0.91983
R-Square(COD)	0.99751
Adj. R-Square	0.99751

Table A129 Fitting of the growth of the signal shown in Figure A266.

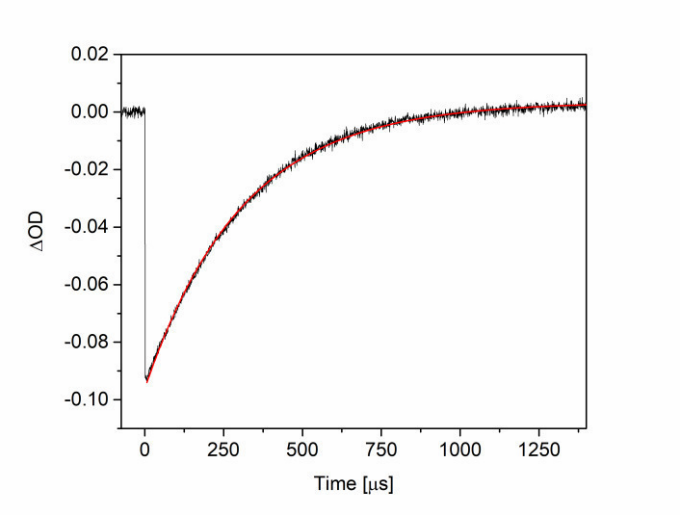

Figure A267: Transient signal detected at 381 nm for **3b** (24 μM) in DMSO with fixed water content (1.67% v/v).

Equation	y = A1*exp(-x/τ) + y0
y0	0.00355 ± 5.25016E-5
A1	-0.09971 ± 1.08831E-4
τ	306.56132 ± 0.75496
R-Square(COD)	0.99812
Adj. R-Square	0.99812

Table A130 Fitting of the growth of the signal shown in Figure A267.

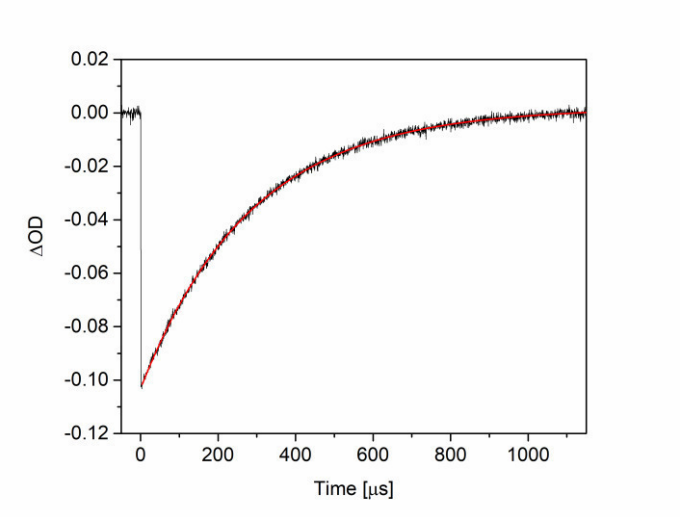

Figure A268: Transient signal detected at 381 nm for **3b** (30 μM) in DMSO with fixed water content (1.67% v/v).

Equation	y = A1*exp(-x/τ) + y0
y0	0.00197 ± 5.79784E-5
A1	-0.10518 ± 1.03369E-4
τ	283.1641 ± 0.67535
R-Square(COD)	0.99837
Adj. R-Square	0.99837

Table A131 Fitting of the growth of the signal shown in Figure A268.

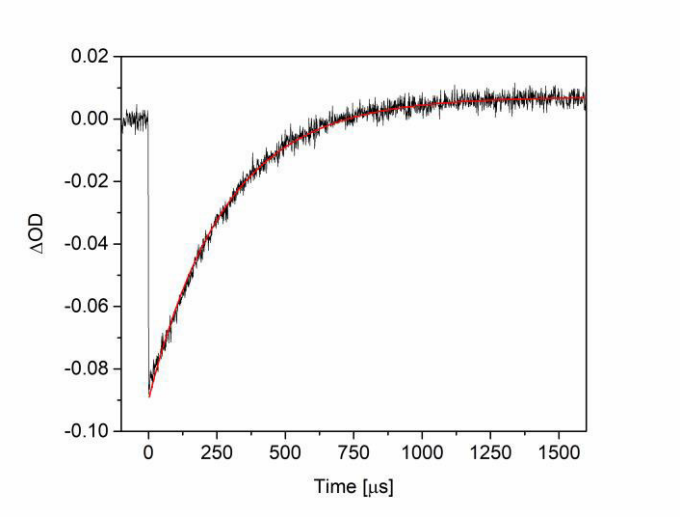

Figure A269: Transient signal detected at 381 nm for **3b** (36 μM) in DMSO with fixed water content (1.67% v/v).

Equation	y = A1*exp(-x/τ) + y0
y0	0.00712 ± 6.72961E-5
A1	-0.09698 ± 2.59501E-4
τ	278.35376 ± 1.30019
R-Square(COD)	0.99146
Adj. R-Square	0.99145

Table A132 Fitting of the growth of the signal shown in Figure A269.

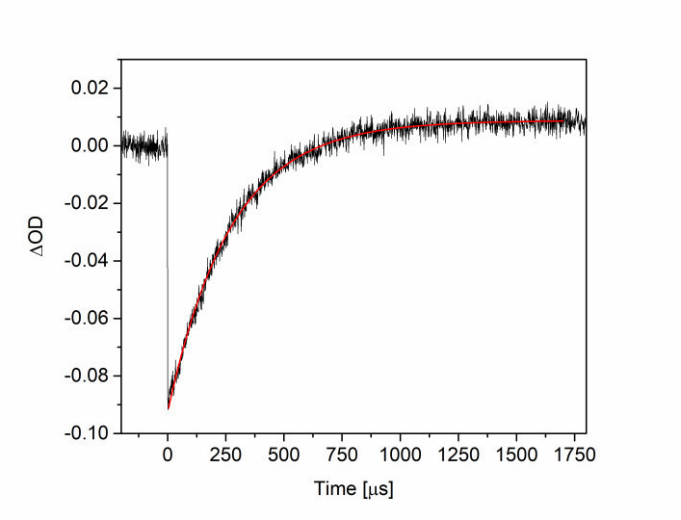

Figure A270: Transient signal detected at 381 nm for **3b** (42 μM) in DMSO with fixed water content (1.67% v/v).

Equation	y = A1*exp(-x/τ) + y0
y0	0.00879 ± 1.03844E-4
A1	-0.10134 ± 3.27684E-4
τ	270.45961 ± 1.64064
R-Square(COD)	0.98915
Adj. R-Square	0.98913

Table A133 Fitting of the growth of the signal shown in Figure A270.

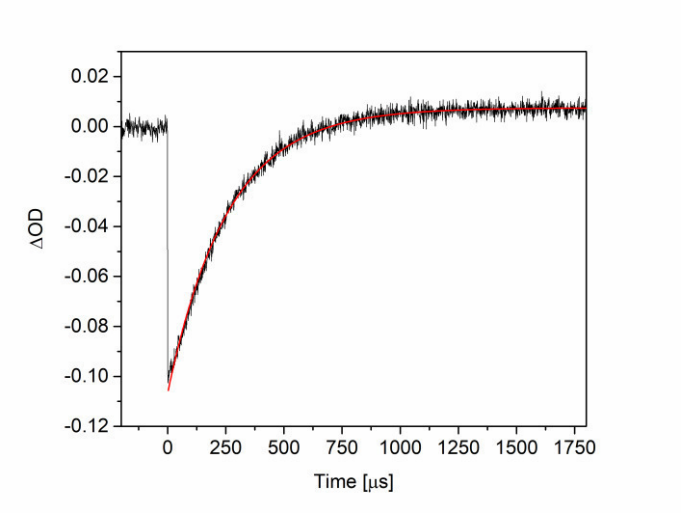

Figure A271: Transient signal detected at 381 nm for **3b** (46.8 μM) in DMSO with fixed water content (1.67% v/v).

Equation	y = A1*exp(-x/τ) + y0
y0	0.00749 ± 7.47382E-5
A1	-0.11408 ± 2.9895E-4
τ	257.30597 ± 1.16286
R-Square(COD)	0.99191
Adj. R-Square	0.9919

Table A134 Fitting of the growth of the signal shown in Figure A271.

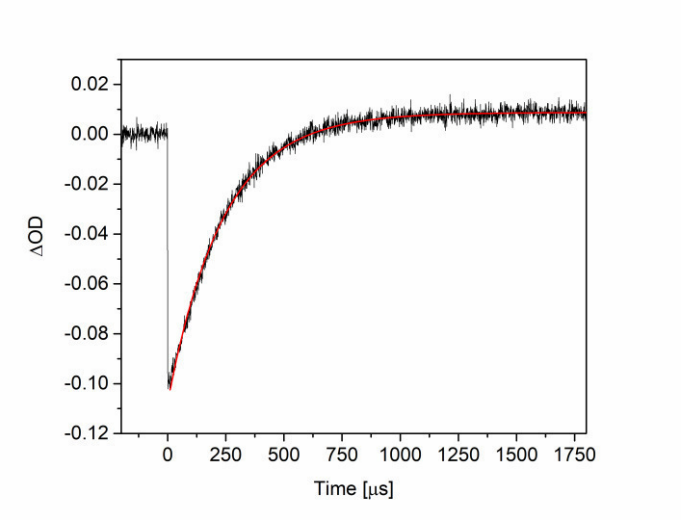

Figure A272: Transient signal detected at 381 nm for **3b** (54 μM) in DMSO with fixed water content (1.67% v/v).

Equation	y = A1*exp(-x/τ) + y0
y0	0.00874 ± 7.46523E-5
A1	-0.11624 ± 3.20942E-4
τ	236.96419 ± 1.08825
R-Square(COD)	0.99169
Adj. R-Square	0.99168

Table A135 Fitting of the growth of the signal shown in Figure A272.

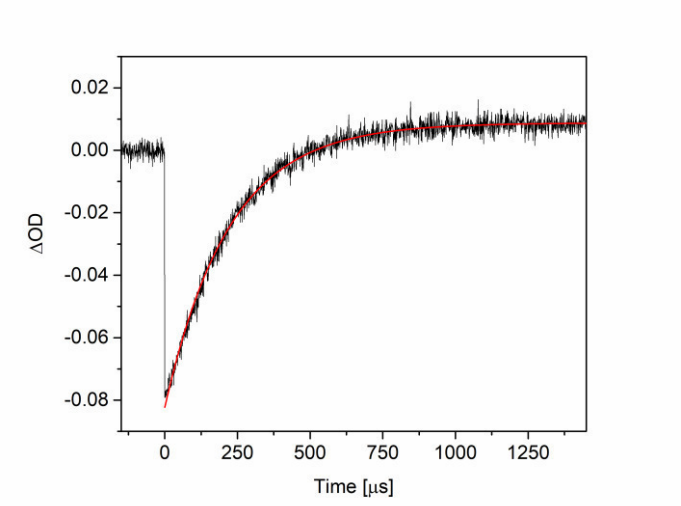

Figure A273: Transient signal detected at 381 nm for **3b** (66 μM) in DMSO with fixed water content (1.67% v/v).

Equation	y = A1*exp(-x/τ) + y0
y0	0.00877 ± 7.61047E-5
A1	-0.09107 ± 3.00779E-4
τ	221.07004 ± 1.26804
R-Square(COD)	0.987
Adj. R-Square	0.98699

Table A136 Fitting of the growth of the signal shown in Figure A273.

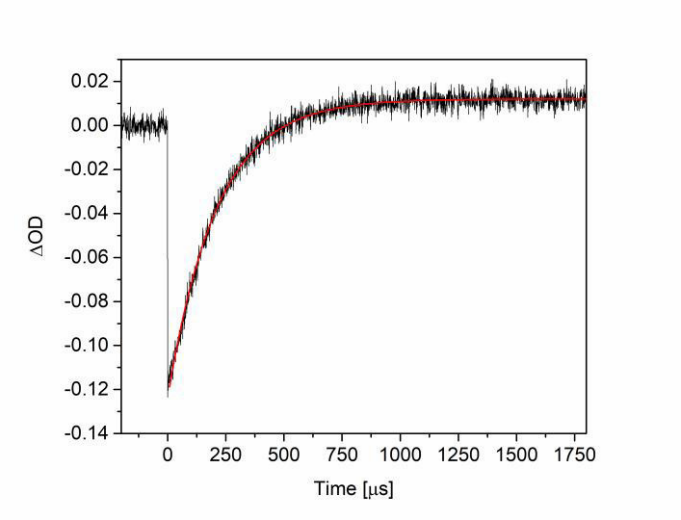

Figure A274: Transient signal detected at 381 nm for **3b** (81 μM) in DMSO with fixed water content (1.67% v/v).

Equation	y = A1*exp(-x/τ) + y0
y0	0.01209 ± 1.01579E-4
A1	-0.13612 ± 4.76026E-4
τ	209.94236 ± 1.19216
R-Square(COD)	0.98699
Adj. R-Square	0.98698

Table A137 Fitting of the growth of the signal shown in Figure A274.

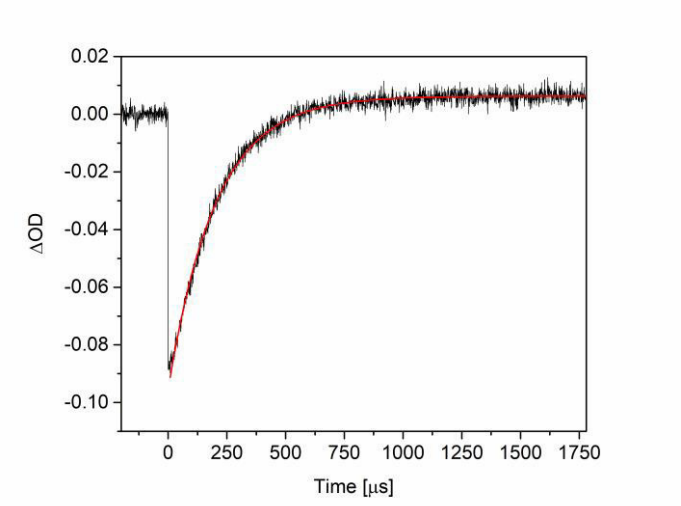

Figure A275: Transient signal detected at 381 nm for **3b** (90 μM) in DMSO with fixed water content (1.67% v/v).

Equation	y = A1*exp(-x/τ) + y0
y0	0.00629 ± 6.14478E-5
A1	-0.10184 ± 3.12334E-4
τ	200.61959 ± 0.97556
R-Square(COD)	0.99026
Adj. R-Square	0.99025

Table A138 Fitting of the growth of the signal shown in Figure A275.

DMSO (3b 50 μM)

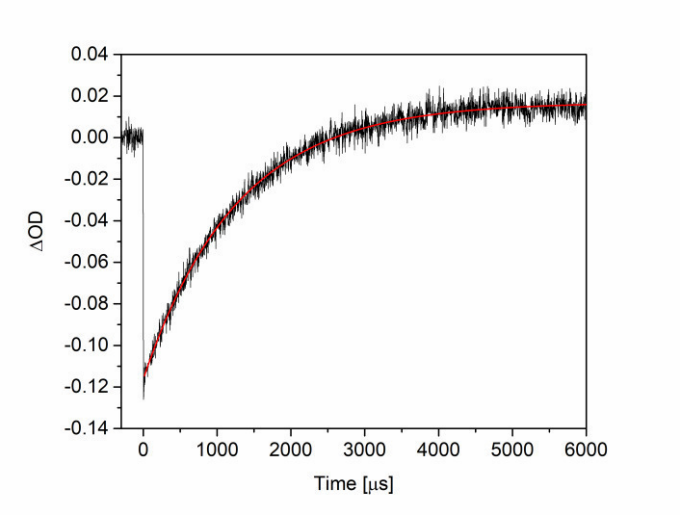

Figure A276: Transient signal detected at 381 nm for **3b** (50 μM) in DMSO with 0.185 M of water.

Equation	y = A1*exp(-x/τ) + y0
y0	0.01704 ± 1.78623E-4
A1	-0.13318 ± 4.17074E-4
τ	1260.6513 ± 8.42795
R-Square(COD)	0.98523
Adj. R-Square	0.98522

Table A139 Fitting of the growth of the signal shown in Figure A276.

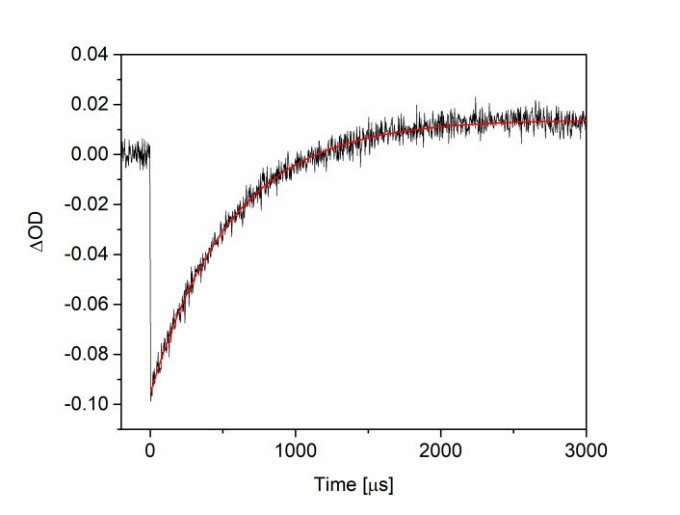

Figure A277: Transient signal detected at 381 nm for **3b** (50 μM) in DMSO with 0.37 M of water.

Equation	y = A1*exp(-x/τ) + y0
y0	0.01407 ± 9.80025E-5
A1	-0.10985 ± 4.29241E-4
τ	556.49034 ± 3.65395
R-Square(COD)	0.98166
Adj. R-Square	0.98164

Table A140 Fitting of the growth of the signal shown in Figure A277.

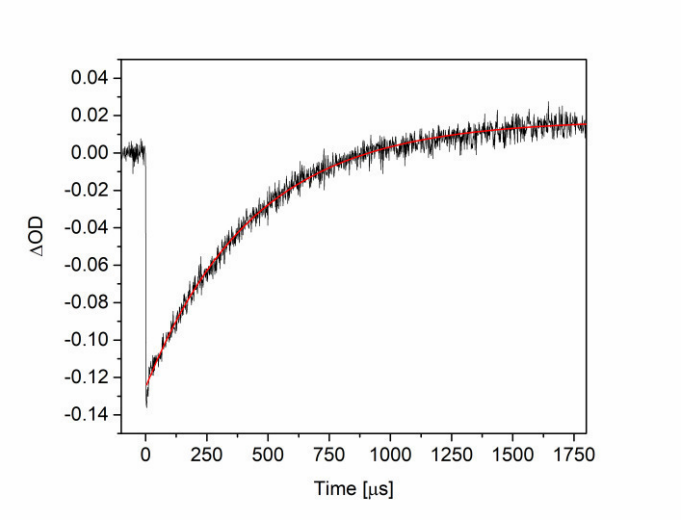

Figure A278: Transient signal detected at 381 nm for **3b** (50 μM) in DMSO with 0.555 M of water.

Equation	y = A1*exp(-x/τ) + y0
y0	0.01776 ± 1.5511E-4
A1	-0.14308 ± 4.71074E-4
τ	436.62033 ± 2.73973
R-Square(COD)	0.98524
Adj. R-Square	0.98522

Table A141 Fitting of the growth of the signal shown in Figure A278.

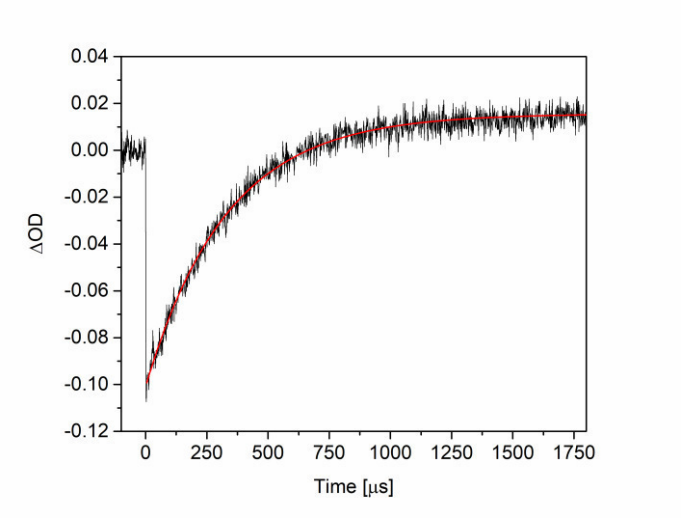

Figure A279: Transient signal detected at 381 nm for **3b** (50 μM) in DMSO with 0.74 M of water.

Equation	y = A1*exp(-x/τ) + y0
y0	0.01563 ± 1.18815E-4
A1	-0.11644 ± 4.91234E-4
τ	392.15937 ± 2.37344
R-Square(COD)	0.97854
Adj. R-Square	0.97852

Table A142 Fitting of the growth of the signal shown in Figure A279.

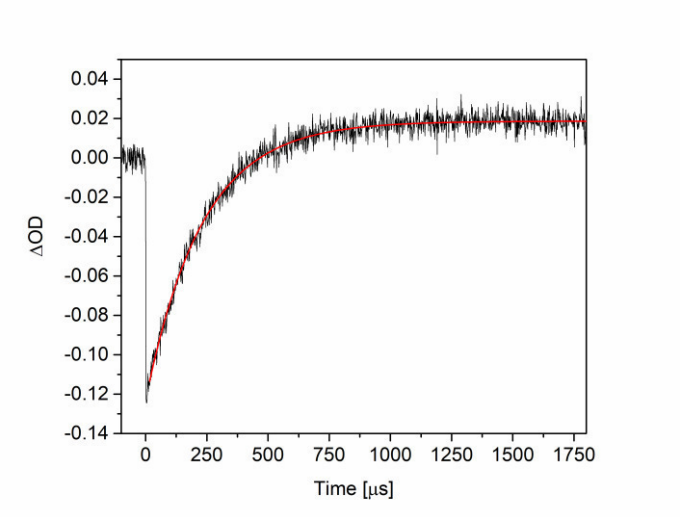

Figure A280: Transient signal detected at 381 nm for **3b** (50 μM) in DMSO with 0.925 M of water.

Equation	y = A1*exp(-x/τ) + y0
y0	0.01868 ± 1.1935E-4
A1	-0.14183 ± 8.31063E-4
τ	230.11471 ± 1.96561
R-Square(COD)	0.96774
Adj. R-Square	0.9677

Table A143 Fitting of the growth of the signal shown in Figure A280.

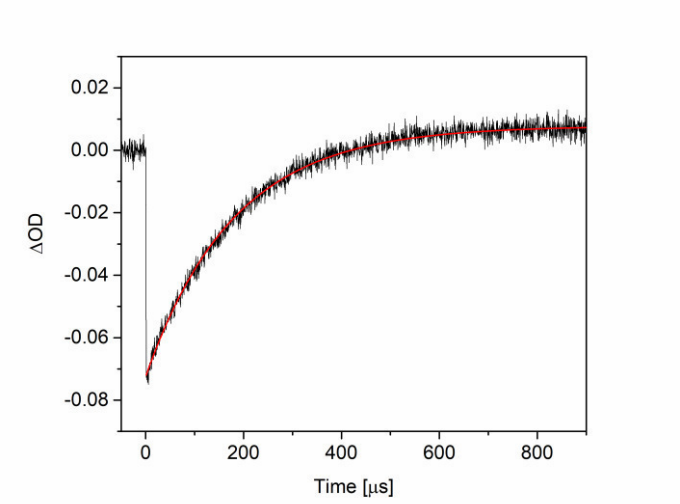

Figure A281: Transient signal detected at 381 nm for **3b** (50 μM) in DMSO with 1.85 M of water.

Equation	y = A1*exp(-x/τ) + y0
y0	0.0078 ± 8.34638E-5
A1	-0.08026 ± 2.28657E-4
τ	179.78271 ± 1.01932
R-Square(COD)	0.98841
Adj. R-Square	0.9884

Table A144 Fitting of the growth of the signal shown in Figure A281.

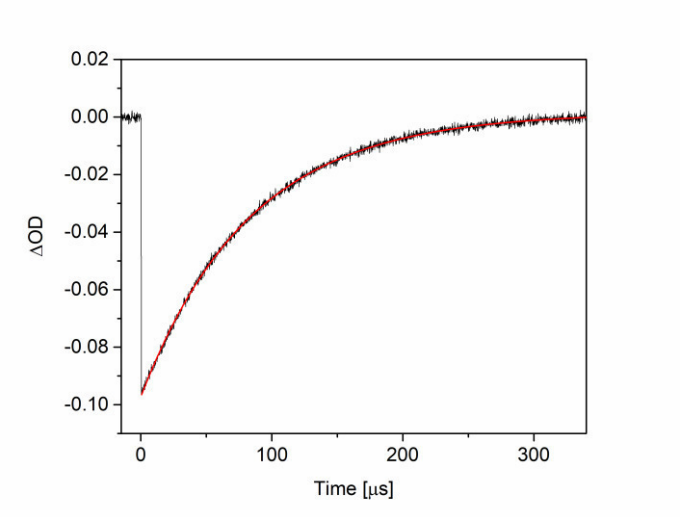

Figure A282: Transient signal detected at 381 nm for **3b** (50 μM) in DMSO with 3.7 M of water.

Equation	y = A1*exp(-x/τ) + y0
y0	0.00155 ± 5.15272E-5
A1	-0.09874 ± 8.71626E-5
τ	83.39322 ± 0.18312
R-Square(COD)	0.99865
Adj. R-Square	0.99865

Table A145 Fitting of the growth of the signal shown in Figure A282.

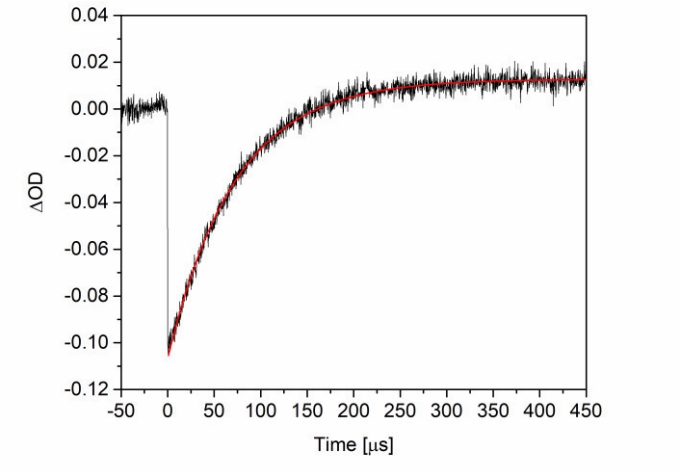

Figure A283: Transient signal detected at 381 nm for **3b** (50 μM) in DMSO with 5.55 M of water.

Equation	y = A1*exp(-x/τ) + y0
y0	0.0128 ± 9.91698E-5
A1	-0.11961 ± 3.64231E-4
τ	71.97025 ± 0.38853
R-Square(COD)	0.98884
Adj. R-Square	0.98883

Table A146 Fitting of the growth of the signal shown in Figure A283.

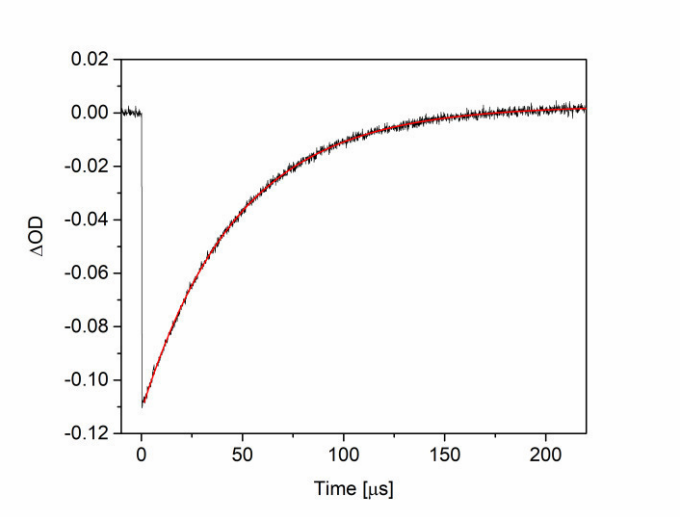

Figure A284: Transient signal detected at 381 nm for **3b** (50 μM) in DMSO with 9.25 M of water.

Equation	y = A1*exp(-x/τ) + y0
y0	0.00274 ± 4.43618E-5
A1	-0.11435 ± 1.12607E-4
τ	47.00296 ± 0.09499
R-Square(COD)	0.99861
Adj. R-Square	0.9986

Table A147 Fitting of the growth of the signal shown in **Figure A284**.

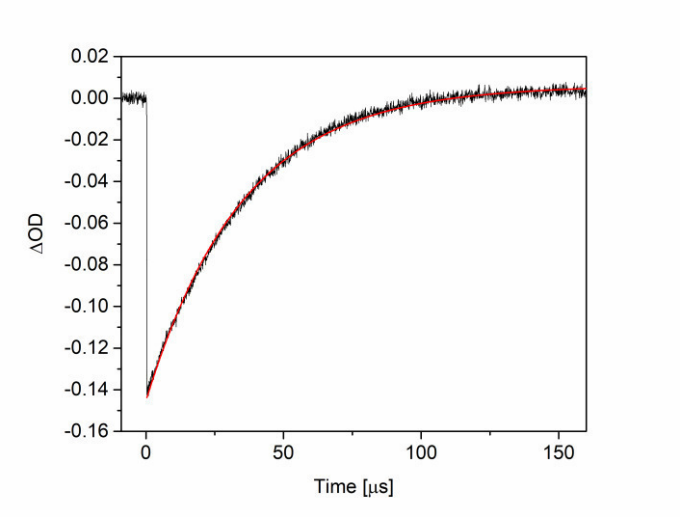

Figure A285: Transient signal detected at 381 nm for **3b** (50 μM) in DMSO with 11.1 M of water.

Equation	y = A1*exp(-x/τ) + y0
y0	0.00619 ± 8.66845E-5
A1	-0.15156 ± 1.94971E-4
τ	34.94613 ± 0.09763
R-Square(COD)	0.99744
Adj. R-Square	0.99744

Table A148 Fitting of the growth of the signal shown in Figure A285.

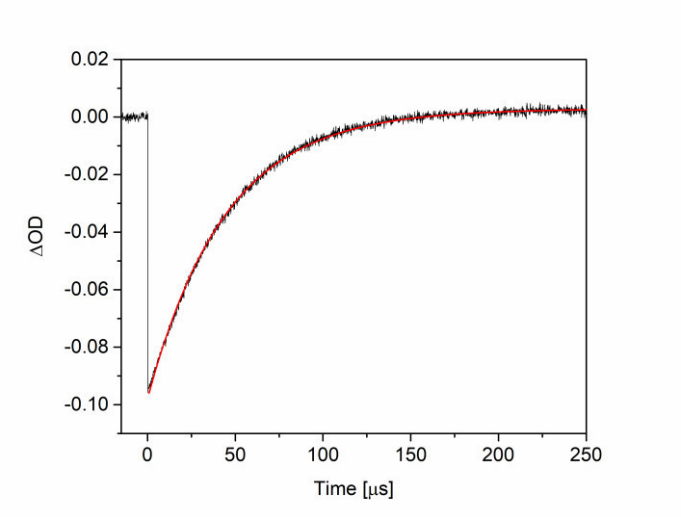

Figure A286: Transient signal detected at 381 nm for **3b** (50 μM) in DMSO with 12.95 M of water.

Equation	y = A1*exp(-x/τ) + y0
y0	0.00284 ± 3.56626E-5
A1	-0.10089 ± 1.18635E-4
τ	44.01684 ± 0.09495
R-Square(COD)	0.99818
Adj. R-Square	0.99818

Table A149 Fitting of the growth of the signal shown in Figure A286.

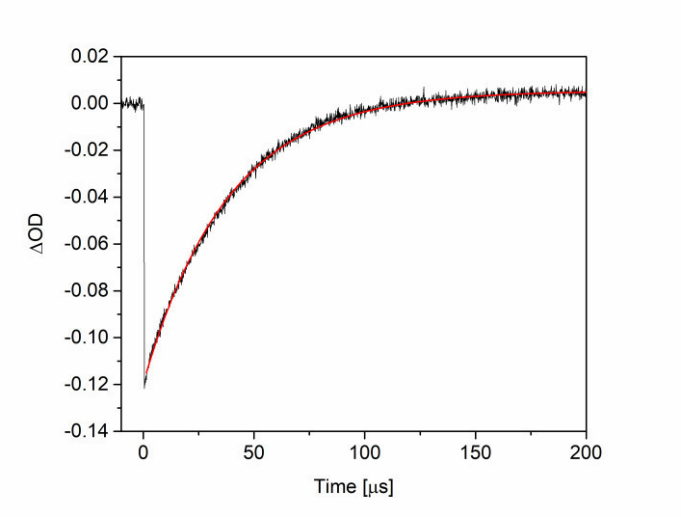

Figure A287: Transient signal detected at 381 nm for **3b** (50 μM) in DMSO with 16.65 M of water.

Equation	y = A1*exp(-x/τ) + y0
y0	0.00544 ± 6.19276E-5
A1	-0.12491 ± 2.02492E-4
τ	37.97394 ± 0.11328
R-Square(COD)	0.99661
Adj. R-Square	0.99661

Table A150 Fitting of the growth of the signal shown in Figure A287.

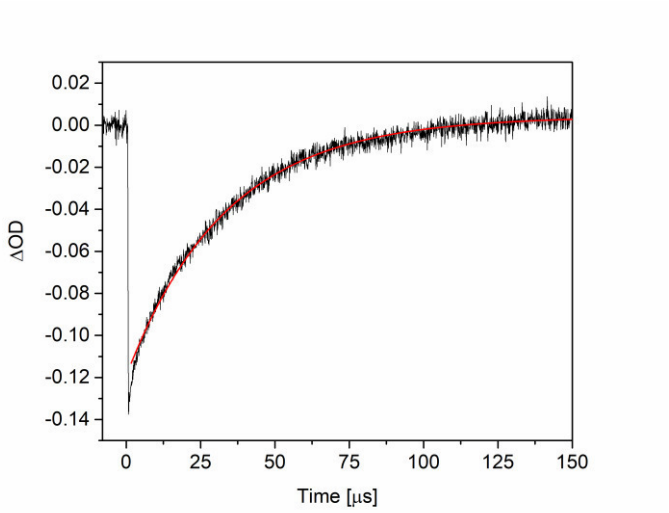

Figure A288: Transient signal detected at 381 nm for **3b** (50 μM) in DMSO with 18.5 M of water.

Equation	y = A1*exp(-x/τ) + y0
y0	0.00418 ± 1.39142E-4
A1	-0.12342 ± 3.43782E-4
τ	33.37975 ± 0.19285
R-Square(COD)	0.98914
Adj. R-Square	0.98913

Table A151 Fitting of the growth of the signal shown in Figure A288.

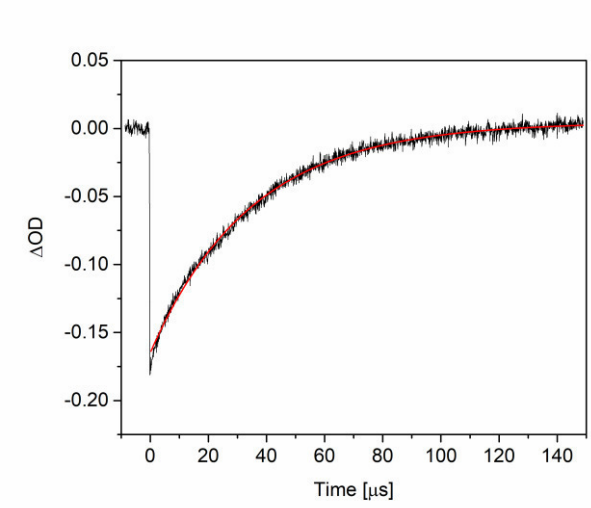

Figure A289: Transient signal detected at 381 nm for **3b** (50 μM) in DMSO with 22.2 M of water.

Equation	y = A1*exp(-x/τ) + y0
y0	0.00467 ± 1.77817E-4
A1	-0.1696 ± 3.25069E-4
τ	34.73048 ± 0.15947
R-Square(COD)	0.99387
Adj. R-Square	0.99387

Table A152 Fitting of the growth of the signal shown in Figure A289.

7 Mechanistic proposal

The findings reported in Section 6 suggest that the *Z*- form of **3** is converted into the more stable *E*- isomer via a monomolecular mechanism both when the indolic nitrogen is not present and, if present, when the solvent is aprotic. With N-H substituted molecules, in the presence of protic solvents (also as additives) the mechanism changes. In the latter case the rate depends both on the concentration of the starting material, as previously found by Otsuki *et al.*[26] and on the concentration of protic medium. This strongly supports the contribution of a protic-solvent-mediated proton transfer between the *Z*-isomer of an N-H indole photoswitch and another molecule of the azo compound (it is irrelevant for the reaction mechanism if in its *Z*- or *E*- form). Moreover, the kinetic data are in accordance with the following mechanistic evidences:

- A proton transfer mediated by protic solvent is involved in the rate determining step of the reaction, as found with the relevant Kinetic Isotope Effect in MeOD (Entry 3, Table A2).
- At high concentration it is possible to have an intermolecular interaction between different molecules of the N-H containing photoswitch, as reported in Section 3.3.[S25]
- The calculated barriers of proton transfer between two molecules of **3a** in the absence of a protic molecule bridging them are too high (>30 kcal mol^{-1} see Section 4.4).
- Quantum chemistry confirms that water bridging two **3a** molecules lowers the proton transfer energetic barrier, acting as a proton carrier (see Section 4.4).
- The intermediate of the *E*-to-*Z* isomerization appears only in the presence of protic solvents (see Section 2).
- The UV spectrum of the intermediate seen in the presence of protic medium matches the computed one for the hydrazone tautomer of the starting material (see Section 4.3).
- Both acidic (with acid buffer) and basic (with DBU) conditions greatly enhance the rate of the reaction (see Section 4.3), probing a proton transfer is present in the rate determining step of the reaction.

In view of the above, the following scheme, representing the proposed mechanism, can be drawn.

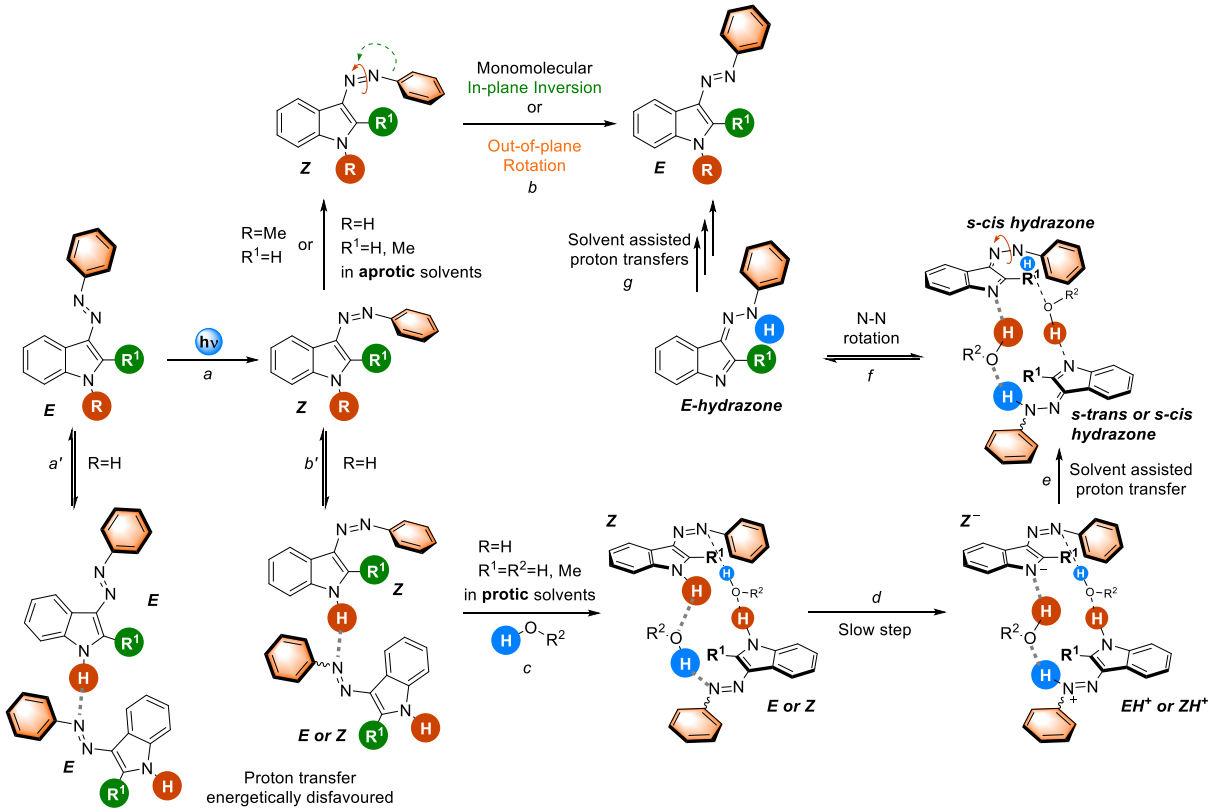

Scheme A3

The azoindole photoswitch is isolated as its *E*-isomer. In solution the switches possessing an N-H indolic moiety are characterized by intermolecular interactions involving the aforementioned proton (path *a'*). After irradiation (path *a*), the *E*-to-*Z* isomerization of the N=N bond occurs, affording the *Z*- isomer. If the indolic nitrogen is substituted with a methyl as in **3c**, the *Z*- form will interconvert *via* an in-plane inversion of the azo group, or *via* an out-of-plane rotation (path *b*). This pathway is monomolecular and it is typical of the reactivity of the metastable *Z*- configuration of the azo-switches. A similar reactivity is described for **3a** and **3b** when dissolved in aprotic solvent. In this case, however, we cannot rule out the possibility of an intermolecular interaction between the *Z*- form and another switch (either *Z*- or *E*-). This pathway (path *b'*), if present, can be assigned to a parasitic equilibrium, ultimately leading to path *b*, because of the high proton transfer energy (between the proton and the nitrogen marked with a dashed bond). On the other hand, in protic solvents this interaction can be helped by bridging solvent molecules, forming a short-range solvation shell[S24] (path *c*). This system was computationally represented in its simpler case, where two water molecules are bridging two *Z*-phenylazoindoles. Increased concentrations of starting material make the formation of these clusters more probable. Moreover, the amount of protic solvent present will influence the formation of a more complex short-range solvation shell, eventually giving rise to a saturation of the speed that can be reached by the ensuing proton transfer step (path *d*). The formation of an ionic couple (Z^- and EH^+ or ZH^+) is predicted to occur by quantum chemical calculations and to be the slow step of the reaction. A second, faster, solvent assisted proton transfer (path *e*) will form the *s*-cis hydrazone of the first switch (and either the *s*-cis or *s*-trans hydrazone of the second azo, depending on the nature of the reagent, if starting as *Z*- or *E*-). The hydrazone tautomer of the azo compound is able to rotate freely around the N-N single bond, generating the more stable *s*-trans conformer (path *f*). The hydrazone lies in a well of the potential energy curve connecting reagents and products, thus it lives long enough to be spotted at the laser flash photolysis. A series of solvent assisted proton transfers similar to the ones reported in path *d* and *e* leads ultimately to the restoration of the *E*-phenylazoindole (path *g*).

8 References

(A1) Albar, H. A.; Shawali, A. S.; Abdaliah, M. A. *Can. J. Chem.* **1993**, *71*, 2144–2149.

(A2) Babür, B.; Seferoğlu, N.; Aktan, E.; Hökelek, T.; Şahin, E.; Seferoğlu, Z. *J. Mol. Struct.* **2015**, *1081*, 175–181.

(A3) Mitra, A.; Seaton, P. J.; Ali Assarpour, R.; Williamson, T. *Tetrahedron* **1998**, *54*, 15489–15498.

(A4) Roos, B. O.; Taylor, P. R.; Siegbahn, P. E. M. *Chem. Phys.* **1980**, *48*, 157–173.

(A5) Wei-Guang Diau, E. *J. Phys. Chem. A* **2004**, *108* (6), 950–956.

(A6) Stålring, J.; Bernhardsson, A.; Lindh, R. *Mol. Phys.* **2001**, *99*, 103–114.

(A7) Aquilante, F.; Autschbach, J.; Carlson, R. K.; Chibotaru, L. F.; Delcey, M. G.; De Vico, L.; Fdez. Galván, I.; Ferré, N.; Frutos, L. M.; Gagliardi, L.; Garavelli, M.; Giussani, A.; Hoyer, C. E.; Li Manni, G.; Lischka, H.; Ma, D.; Malmqvist, P. Å.; Müller, T.; Nenov, A.; Olivucci, M.; Pedersen, T. B.; Peng, D.; Plasser, F.; Pritchard, B.; Reiher, M.; Rivalta, I.; Schapiro, I.; Segarra-Martí, J.; Stenrup, M.; Truhlar, D. G.; Ungur, L.; Valentini, A.; Vancoillie, S.; Veryazov, V.; Vysotskiy, V. P.; Weingart, O.; Zapata, F.; Lindh, R. *J. Comput. Chem.* **2016**, *37*, 506–541.

(A8) Manaa, M. R.; Yarkony, D. R. *J. Chem. Phys.* **1993**, *99*, 5251–5256.

(A9) Yarkony, D. R. *J. Chem. Phys.* **2001**, *114*, 2614–2622.

(A10) Yarkony, D. R. *J. Chem. Phys.* **2000**, *112*, 2111–2120.

(A11) Barbatti, M.; Aquino, A. J. A.; Lischka, H. *J. Phys. Chem. A* **2005**, *109*, 5168–5175.

(A12) Andersson, K.; Malmqvist, P. A.; Roos, B. O.; Sadlej, A. J.; Wolinski, K. *J. Phys. Chem.* **1990**, *94*, 5483–5488.

(A13) Finley, J.; Malmqvist, P.-Å.; Roos, B. O.; Serrano-Andrés, L. *Chem. Phys. Lett.* **1998**, *288*, 299–306.

(A14) Serrano-Andrés, L.; Merchán, M.; Lindh, R. *J. Chem. Phys.* **2005**, *122*, 104107.

(A15) Forsberg, N.; Malmqvist, P.-Å. *Chem. Phys. Lett.* **1997**, *274*, 196–204.

(A16) Hanwell, M. D.; Curtis, D. E.; Lonie, D. C.; Vandermeersch, T.; Zurek, E.; Hutchison, G. R. *J. Cheminformatics* **2012**, *4*, 17.

(A17) Lu, T.; Chen, F. *J. Comput. Chem.* **2012**, *33*, 580–592.

(A18) Jasper, A. W.; Truhlar, D. G. *J. Chem. Phys.* **2005**, *122*, 044101.

(A19) Conti, I.; Garavelli, M.; Orlandi, G. *J. Am. Chem. Soc.* **2008**, *130*, 5216–5230.

(A20) Barbatti, M.; Ruckenbauer, M.; Lischka, H. *J. Chem. Phys.* **2005**, *122*, 174307.

(A21) Yu, L.; Xu, C.; Zhu, C. *Phys Chem Chem Phys* **2015**, *17*, 17646–17660.

(A22) Frisch, M.; Trucks, G.; Schlegel, H.; Scuseria, G.; Robb, M.; Cheeseman, J.; Scalmani, G.; Barone, V.; Mennucci, B.; Petersson, G.; Nakatsuji, H.; Caricato, M.; Li, X.; Hratchian, H.; Izmaylov, A.; Bloino, J.; Zheng, G.; Sonnenberg, J.; Hada, M.; Ehara, M.; Toyota, K.; Fukuda, R.; Hasegawa, J.; Ishida, M.; Nakajima, T.; Honda, Y.; Kitao, O.; Nakai, H.; Vreven, T.; Montgomery, J.; Peralta, J.; Ogliaro, F.; Bearpark, M.; Heyd, J.; Brothers, E.; Kudin, K.; Staroverov, V.; Kobayashi, R.; Normand, J.; Raghavachari, K.; Rendell, A.; Burant, J.; Iyengar, S.; Tomasi, J.; Cossi, M.; Rega, N.; Millam, J.; Klene, M.; Knox, J.; Cross, J.; Bakken, V.; Adamo, C.; Jaramillo, J.; Gomperts, R.; Stratmann, R.; Yazyev, O.; Austin, A.; Cammi, R.; Pomelli, C.; Ochterski, J.; Martin, R.; Morokuma, K.; Zakrzewski, V.; Voth, G.; Salvador, P.; Dannenberg, J.; Dapprich, S.; Daniels, A.; Farkas; Foresman, J.; Ortiz, J.; Cioslowski, J.; Fox, D. *Gaussian 09 Revis. D01 Gaussian Inc Wallingford CT* **2009**.

(A23) Bandara, H. M. D.; Burdette, S. C. *Chem Soc Rev* **2012**, *41*, 1809–1825.

(A24) Berman, E. D.; Thomas, R.; Thal, P.; Scott, R. *Can. J. Chem.* **1987**, *65*, 1594–1598.

(A25) Mitra, A.; Seaton, P. J.; Assarpour, R. A.; Williamson, T *Tetrahedron* **1998**, *54*, 15489–l5498

A.I.3. Substituent Effects on 3-Phenylazoindole Photoswitches

Contents

1. Synthesis

General procedure I for diazonium salt formation

Aniline (3000 mg, 23.22 mmol) was dissolved in HBF_4 (15 mL, 32% aq) and cooled to -15 °C (NaCl/crushed ice). Then, $NaNO_2$ (2222 mg, 23.22 mmol) in water (3 mL) was added dropwise. The reaction mixture was stirred for 30 minutes, then the white precipitate was sucked off and washed with ice-cold Et_2O (10 mL) and Et_2O/MeOH (1:1, 5 mL). After washing, vacuum was applied for 15 more minutes, in order to dry the diazonium salt (**2**) crystalline powder, before it was employed directly in the azo-coupling or stored in the freezer (-18 °C, up to 10 days).

General procedure II for diazonium salt formation

The appropriate aniline (2 mmol) was dissolved in HBF_4 (4 mL, aq, 32%) and cooled to -15 °C using a bath of NaCl/crushed ice. Then, $NaNO_2$ (1 eq) in water (1 mL) was added dropwise. The salt was filtered off (using pre-cold equipment as some of the salts turned out be extremely sensitive to temperature)

General procedure for azo-coupling

The appropriate indole (1000 mg, 1 eq.) was dissolved in DMF (5 mL). Diazonium salt **2** (1 eq) was added in small portions. The color immediately changed to red. The reaction mixture was stirred at ambient temperature for 16h and then poured into water (200 mL). The organic compounds usually formed red droplets which were collected through extraction of the aqueous solution with DCM (3 x 100 mL). The combined organic phase was dried over Na_2SO_4, filtered and the solvent was removed *in vacuo*. The crude material was purified through MPLC (Ethyl Acetate in Petrol Ether 35 → 100% for **2a**, **3a**, **4a**, **6a**; MeOH in DCM 0 → 20% for **7a**). For spectroscopic purity, the product was further purified in preparative HPLC (MeCN in H_2O: 40 → 100%).

*((E)-3-((2-Bromophenyl)diazenyl)-1H-indole) (**2a**)*

The compound was prepared following the *general procedure I* for the synthesis of diazonium salts (using 1000 mg of 2-bromo aniline) and the general procedure for azo-coupling.

The compound was obtained as brown solid (251 mg, 0.84 mmol, 42%). ^{1}H-NMR (300 MHz, acetone-*d6*) δ =11.28 (s, 1H), 8.85 – 8.71 (m, 1H), 8.37 (s, 1H), 7.82 (ddd, *J* = 9.0, 8.1, 1.5 Hz, 2H), 7.61 – 7.52 (m, 1H), 7.47 – 7.39 (m, 1H), 7.28 (td, *J* = 7.6, 1.7 Hz, 1H). ^{13}C-NMR (75 MHz, acetone-*d6*) δ =151.5 (s, q), 138.3 (s, q), 138.0 (s, q), 135.4 (s, +), 134.4 (s, +), 131.0 (s, +), 129.1 (s, +), 125.3 (s, +), 125.0 (s, q), 124.2 (s, +), 124.1 (s, +), 119.3 (s, q), 118.0 (s, +), 113.0 (s, +). IR [cm^{-1}] $\tilde{\upsilon}$ = 3392 (m), 2922 (s), 2855 (s), 1513 (m), 1379 (m), 1200 (m), 1099 (m), 738 (s). ESI-MS: calculated: 300.0131 (MH^+), found: 300.0 (MH^+,^{79}Br, 100%), 302.0 (MH^+, ^{81}Br, 98%). HR-MS: found: 300.0132 (MH^+,^{79}Br, 100%), 301.0163 (MH^+,^{79}Br, 14%), 302.0114 (MH^+, ^{81}Br, 97%), 302.0144 (MH^+,^{81}Br, 13%). Melting point: 187 C. R_f: 0.45 (DCM). The structure was confirmed through X-ray analysis. The compound was previously reported and characterized through elemental analysis.[1]

*((E)-2-((1H-Indol-3-yl)diazenyl)phenol) (**3a**)*

The compound was prepared following the *general procedure II* for the synthesis of diazonium salts (using 1000 mg of 2-hydroxy aniline) and the general procedure for azo-coupling.

The compound was obtained as brown solid (43 mg, 0.18 mmol, 9%). ^{1}H-NMR (300 MHz, acetone-*d6*) δ =12.57 (s, 1H), 11.23 (*b*s, 1H), 8.70 – 8.47 (m, 1H), 8.33 (d, *J* = 3.1 Hz, 1H), 7.91 (dd, *J* = 7.8, 1.7 Hz, 1H), 7.69 – 7.51 (m, 1H), 7.38 – 7.22 (m, 3H), 7.06 (td, *J* = 7.6, 1.4 Hz, 1H), 6.96 (dd, *J* = 8.2, 1.3 Hz, 1H). ^{13}C-NMR (75 MHz, acetone-*d6*) δ =153.2 (s, q), 138. 8 (s, q), 138.1 (s, q), 134.6 (s, q), 132.2 (s, +), 131.5 (s, +), 131.4 (s, +), 125.2 (s, +), 123.6 (s, +), 123.5 (s, +), 120.5 (s, +), 119.7 (s, q), 118.6 (s, +), 113.1 (s, +). IR [cm^{-1}] $\tilde{\upsilon}$ = 3064 (m), 2743 (m), 2106 (w), 1610 (m), 1539 (m), 1487 (m),

1051 (s), 973 (s), 749 (s), 678 (s). ESI-MS: calculated: 238.0975 (MH^+), found: 238.1 (MH^+, 100%). HR-MS: 238.0975 (MH^+, 100%), 239.1008 (MH^+, 15%). Melting point: decomposition >195 °C. R_f: 0.40 (DCM). The structure was confirmed through X-ray analysis.

*((E)-3-((2-Fluorophenyl)diazenyl)-1H-indole) (**4a**)*

The compound was prepared following the *general procedure II* for the synthesis of diazonium salts (using 1000 mg of 2-fluoro aniline) and the general procedure for azo-coupling.

The compound was obtained as red-brown solid (796 mg, 3.34 mmol, 37%). ^{1}H-NMR (400 MHz, Acetone-d_6) δ =11.21 (*b*s, 1H), 8.79 – 8.53 (m, 1H), 8.31 (s, 1H), 7.82 (td, J = 8.0, 1.8 Hz, 1H), 7.62 – 7.45 (m, 1H), 7.43 – 7.28 (m, 4H), 7.28 – 7.22 (m, 1H). ^{3}C NMR (101 MHz, Acetone-d_6) δ =159.2 (q, d, J = 252.9 Hz), 141.6 (q, d, J = 7.2 Hz), 137.2 (q), 136.9 (q), 133.5 (+), 130.2 (+, d, J = 8.0 Hz), 124.4 (+, d, J = 3.8 Hz), 124.2 (+), 122.8 (+, d, J = 8.3 Hz), 118.5 (q), 116.9 (+), 116.7 (+), 116.5 (+), 112.0 (+). ^{19}F NMR (377 MHz, Acetone-d_6) δ =-126.38 (ddd, J = 11.2, 7.8, 5.1 Hz). IR [cm^{-1}] $\tilde{\nu}$ = 3381 (w), 3214 (w), 2963 (w), 2922 (w), 1521 (m), 1484 (m), 1387 (m), 1260 (w), 1092 (s), 1014 (s), 742 (s). ESI-MS: calculated: 239.0859 found: 240.1 (MH^+, 100%). HR-MS: found: 240.0938 (MH^+, 100%). R_f: 0.7 (20% EA in petroleum ether). The structure was confirmed through X-ray analysis.

*(E)-4-(2-((1H-Indol-3-yl)diazenyl)phenyl)morpholine) (**5a**)*

Compound **4a** (104 mg, 0.43 mmol) and morpholine (1515 mg, 1.5 mL, 17.40 mmol) were dissolved DMSO (3 mL). K_2CO_3 (60 mg, 0.43 mmol) was added. The suspension was stirred at ambient temperature for 72 h. The reaction process was followed by TLC and the reaction mixture was poured onto water (30 mL) after no further conversion was observed. The aqueous phase was extracted with EtOAc (3x30 mL) and the combined organic phases were dried over Na_2SO_4. The volatiles were removed *in vacuo*. The compound was directly purified *via* preparative HPLC.

The compound was obtained as yellow-brown viscous oil (112 mg, 0.37 mmol, 84%). ^{1}H NMR (400 MHz, Acetone-d_6) δ =8.63 – 8.47 (m, 1H), 8.29 (s, 1H), 7.70 (dd, J = 8.0, 1.6 Hz, 1H), 7.37 (ddd, J = 8.6, 7.1, 1.6 Hz, 1H), 7.30 (ddd, J = 6.9, 3.9, 2.3 Hz, 3H), 7.15 (ddd, J = 8.3, 7.1, 1.4 Hz, 1H), 3.99 – 3.91 (m, 5H), 3.47 – 3.32 (m, 4H). ^{13}C NMR (101 MHz, Acetone-d_6) δ =147.11 (q), 145.93 (q), 137.10 (q), 136.87 (q), 133.08 (+), 129.65 (+), 124.09 (+), 123.48 (+), 122.61 (+), 122.51 (+), 118.86 (+), 118.41 (q), 116.75 (+), 112.06 (+), 66.57 (-), 53.21 (-). IR [cm^{-1}] $\tilde{\nu}$ = 3191 (w), 2960 (w), 2851 (w), 1730 (m), 1614 (m), 1461 (m), 1331 (w), 1200 (m), 1115 (s), 932 (m), 749 (s). ESI-MS: calculated: 306.1481 found: 307.2 (MH^+, 100). HR-MS: found: 307.1554 (MH^+, 100). R_f: 0.1 (DCM).

*((E)-4-((1H-Indol-3-yl)diazenyl)phenol) (**6a**)*

The compound was prepared following the *general procedure II* for the synthesis of diazonium salts (using 1000 mg of 4-hydroxy aniline) and the general procedure for azo-coupling.

The compound was obtained as brown solid (4 mg, 0.017 mmol, 1%). ^{1}H-NMR (600 MHz, acetone-d6) δ =10.97 (*b*s, 1H), 8.54 – 8.43 (m, 1H), 8.12 (s, 1H), 7.78 (d, J = 8.7 Hz, 6H), 7.49 (dt, J = 8.1, 1.0 Hz, 2H), 7.24 (ddd, J = 8.1, 7.0, 1.4 Hz, 1H), 7.20 (ddd, J = 8.1, 7.0, 1.1 Hz, 1H), 6.99 – 6.93 (m, 2H). ^{13}C-NMR (151 MHz, acetone-d6) δ =158.6 (s, q), 147.3 (s, q), 136.8 (s, +), 136.0 (s, +), 130.7 (2 Signals, s, +), 123.5 (s, +), 123.2 (s, +), 122.6 (s, +), 122.0 (s, +), 119.0 (s, q), 115.5 (s, q), 111.8 (2 Signals, s, +). ESI-MS: calculated: 238.238.09751 (MH^+), found: 238.1 (MH^+, 100%). HR-MS: 238.0977 (MH^+, 100%), 239.1066 (MH^+, 16%). R_f: 0.50 (10% MeOH in DCM). Further analytical data could not be obtained due to limited material.

*(E)-3-((4-Nitrophenyl)diazenyl)-1H-indole (**7a**)*

The compound was prepared following the *general procedure II* for the synthesis of diazonium salts (using 1000 mg of 4-nitro aniline) and the general procedure for azo-coupling.

The compound was obtained as dark red highly viscous oil (327 mg, 1.23 mmol, 17%). ^{1}H NMR (600 MHz, Acetone-d_6) δ =8.55 – 8.48 (m, 1H), 8.42 (s, 1H), 8.41 – 8.35 (m, 2H), 8.09 – 7.95 (m, 2H), 7.61 – 7.49 (m, 1H), 7.37 – 7.19 (m, 2H).^{13}C NMR (151 MHz, Acetone-d_6) δ =158.6 (q), 148.2 (+, only visible in HMBC), 138.1 (q), 138.0 (q), 136.6 (+), 125.6 (q), 125.4 (+), 124.2 (+), 123.7 (+), 122.9 (+), 119.2 (q), 113.1 (+). IR [cm^{-1}] $\tilde{\upsilon}$ = 3690 (w), 2960 (m), 2922 (m), 2855 (m), 1446 (m) 1375 (m), 1092 (s), 1033 (s), 682 (s). ESI-MS: calculated: 266.0804 found: 267.1 (MH^+, 100%). HR-MS: found: 267.0881 (MH^+, 100%). R_f: 0.3 (DCM).

*Side-products of the synthesis of **10a***

The compounds were prepared following the *general procedure II* for the synthesis of diazonium salts (using 300 mg of 2-pyrrolo aniline) and the general procedure for azo-coupling.

However, the desired compound, **10a**, was not observed analyzing the crude mixture. Instead, two other molecules could be isolation through HPLC.

10a' is the internal trapped product. The yellow product could be isolated as a yellow solid in 12% yield (38 mg, 0.23 mmol). The structure was confirmed through NMR and X-ray analysis. ^{1}H NMR (300 MHz, Chloroform-*d*) δ =8.45 (dd, *J* = 8.2, 1.4 Hz, 1H), 7.87 (ddd, *J* = 5.8, 2.8, 1.4 Hz, 2H), 7.75 (ddd, *J* = 8.4, 7.2, 1.5 Hz, 1H), 7.60 (ddd, *J* = 8.3, 7.1, 1.3 Hz, 1H), 7.45 (dd, *J* = 4.2, 1.4 Hz, 1H), 7.13 (dd, *J* = 4.2, 2.8 Hz, 1H). ^{13}C NMR (75 MHz, Chloroform-*d*) δ =141.1 (q), 136.2 (q), 132.2 (+), 130.5 (+), 125.8 (+), 124.8 (q), 116.4 (+), 113.4 (+), 111.1 (+), 109.1 (+). ESI-MS: calculated: 169.0604 found: 170.1 (100%, MH^+).

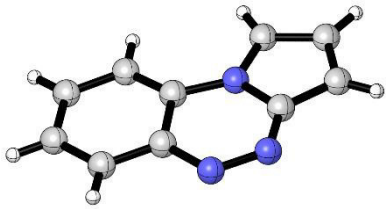

10a'' is an adduct of 8a' and indole, probably trough oxidative coupling. The compound was isolated as pink solid from preparative HPLC (38 mg, 0.13 mmol, 7% yield). The structure was confirmed through NMR and X-Ray analysis. ^{1}H NMR (300 MHz, Methanol-d_4) δ =8.02 (dd, *J* = 8.3, 1.4 Hz, 1H), 7.98 (s, 1H), 7.97 – 7.92 (m, 2H), 7.73 (d, *J* = 4.9 Hz, 1H), 7.65 (ddd, *J* = 8.3, 7.3, 1.2 Hz, 1H), 7.58 (dt, *J* = 8.3, 0.9 Hz, 1H), 7.39 (ddd, *J* = 8.7, 7.3, 1.5 Hz, 1H), 7.27 (ddd, *J* = 8.2, 7.0, 1.2 Hz, 1H), 7.19 (dt, *J* = 8.0, 1.1 Hz, 1H), 7.06 (ddd, *J* = 8.1, 7.0, 1.1 Hz, 1H). ESI-MS: calculated: 284.1064 found: 285.1 (100%, MH^+).

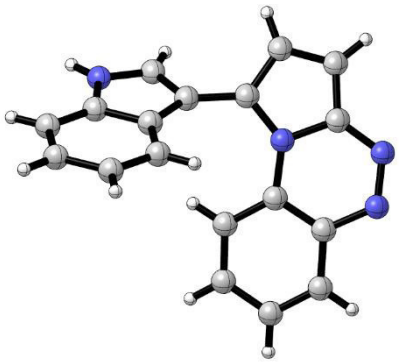

2. NMR Spectra

2a: ^{1}H NMR (400 MHz, Chloroform-*d*)

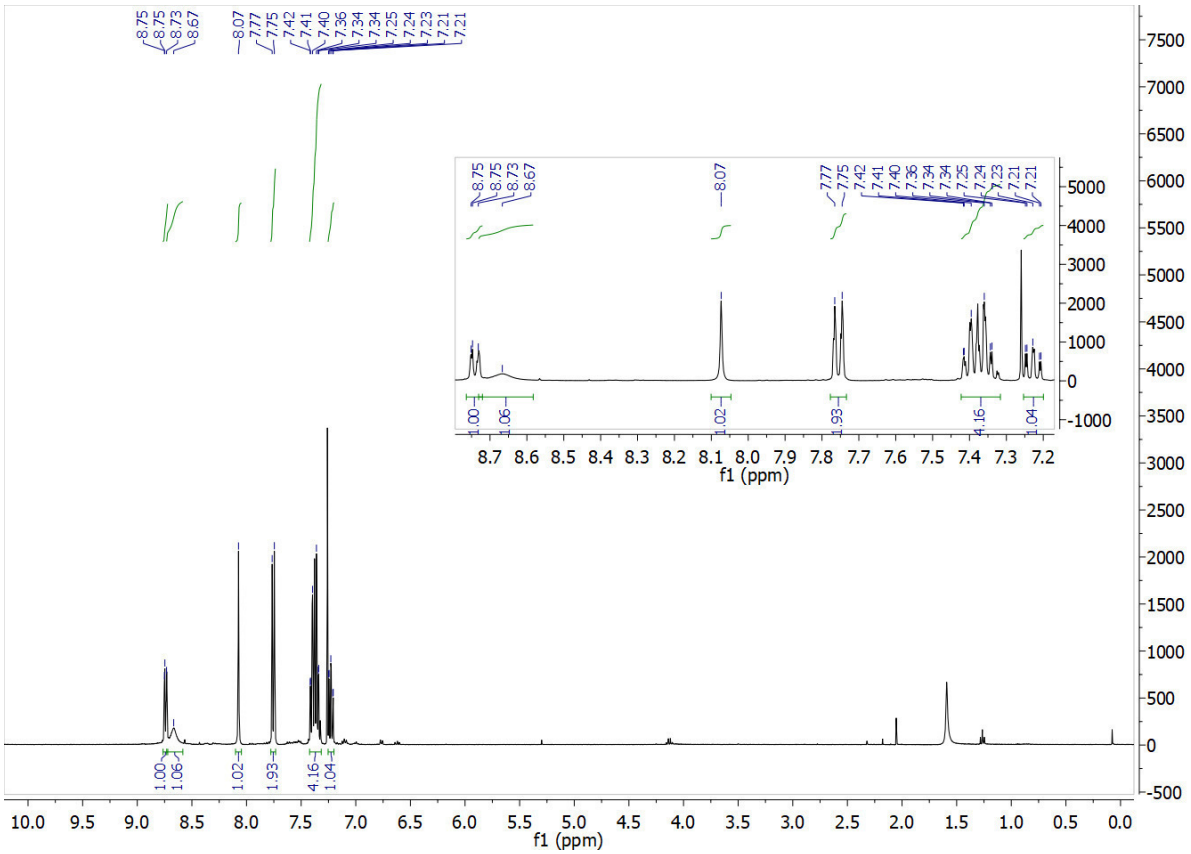

^{13}C NMR (101 MHz, Chloroform-*d*)

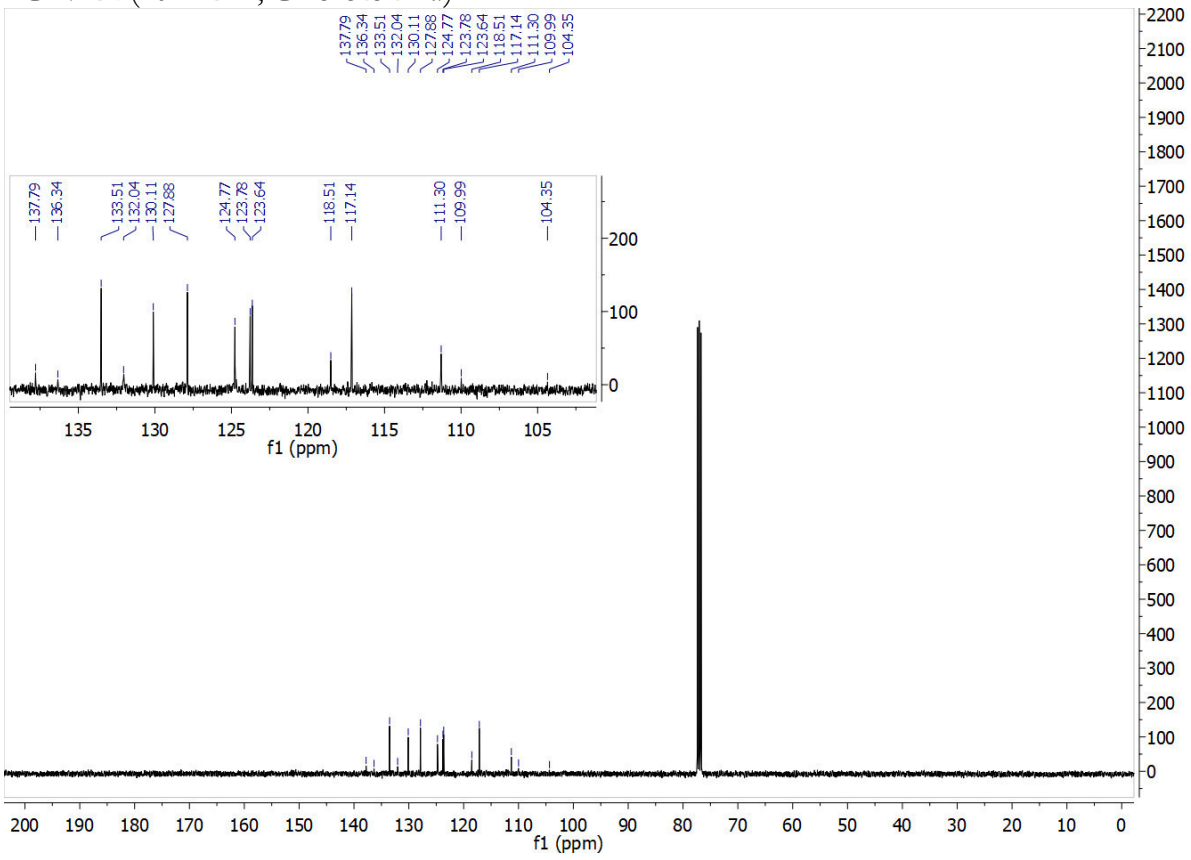

3a: ^{1}H-NMR (300 MHz, methanol-*d4*)

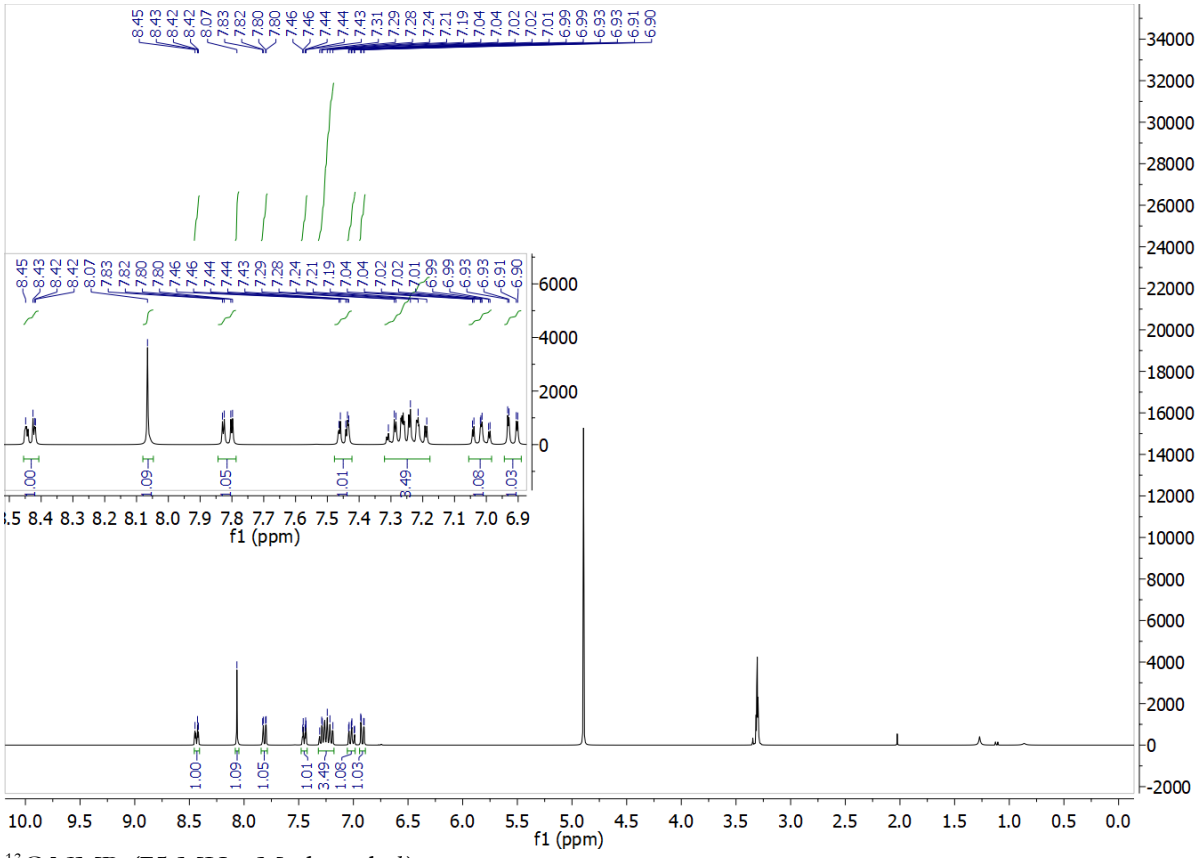

^{13}C NMR (75 MHz, Methanol-d_4)

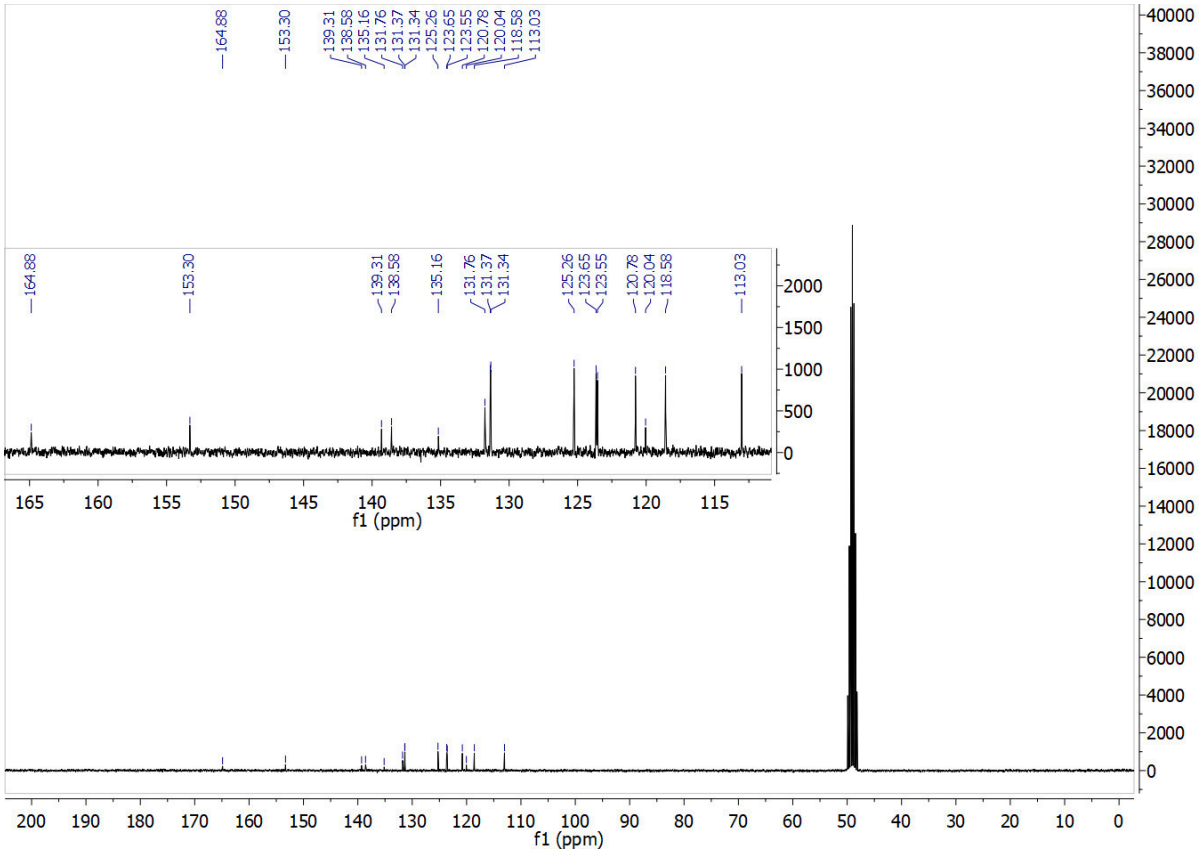

4a: ^{1}H-NMR (400 MHz, Acetone-d_6)

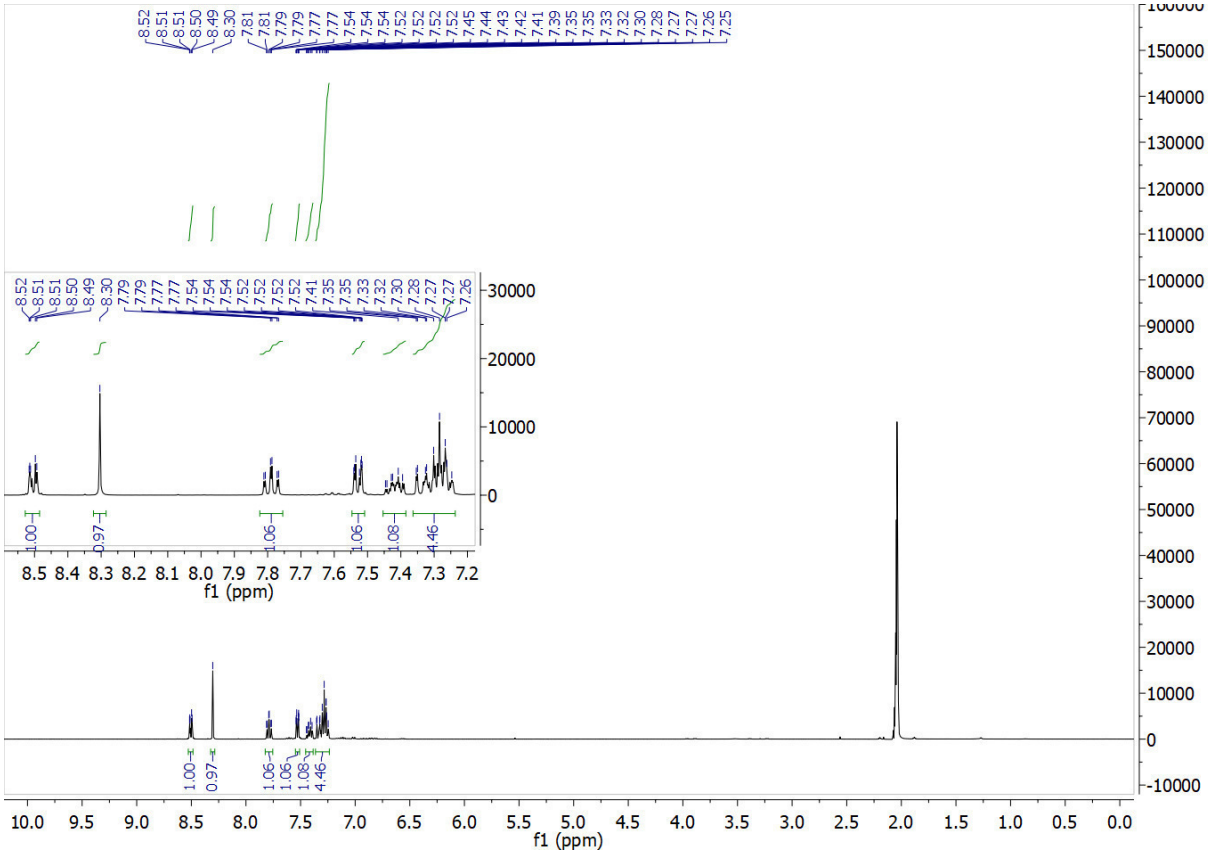

^{13}C NMR (101 MHz, Acetone-d_6)

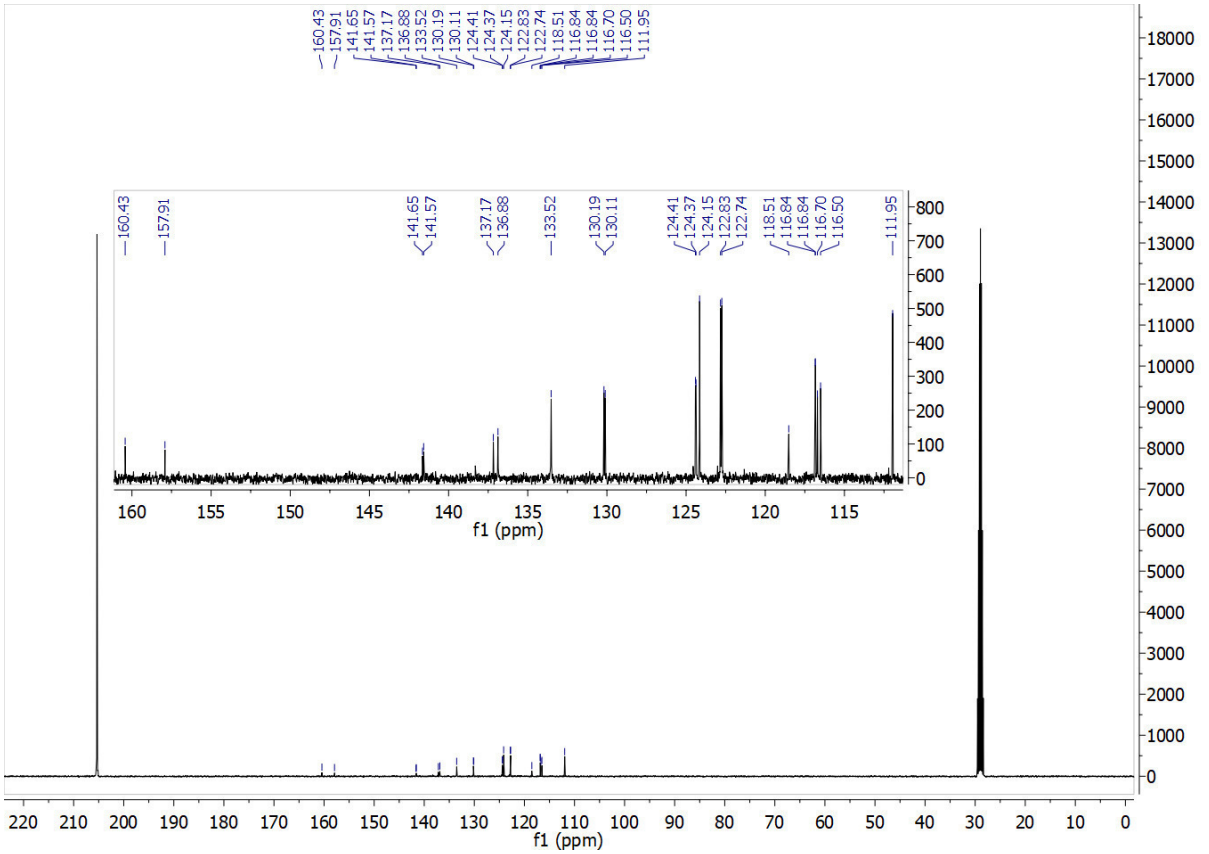

^{19}F NMR (377 MHz, Acetone-d_6)

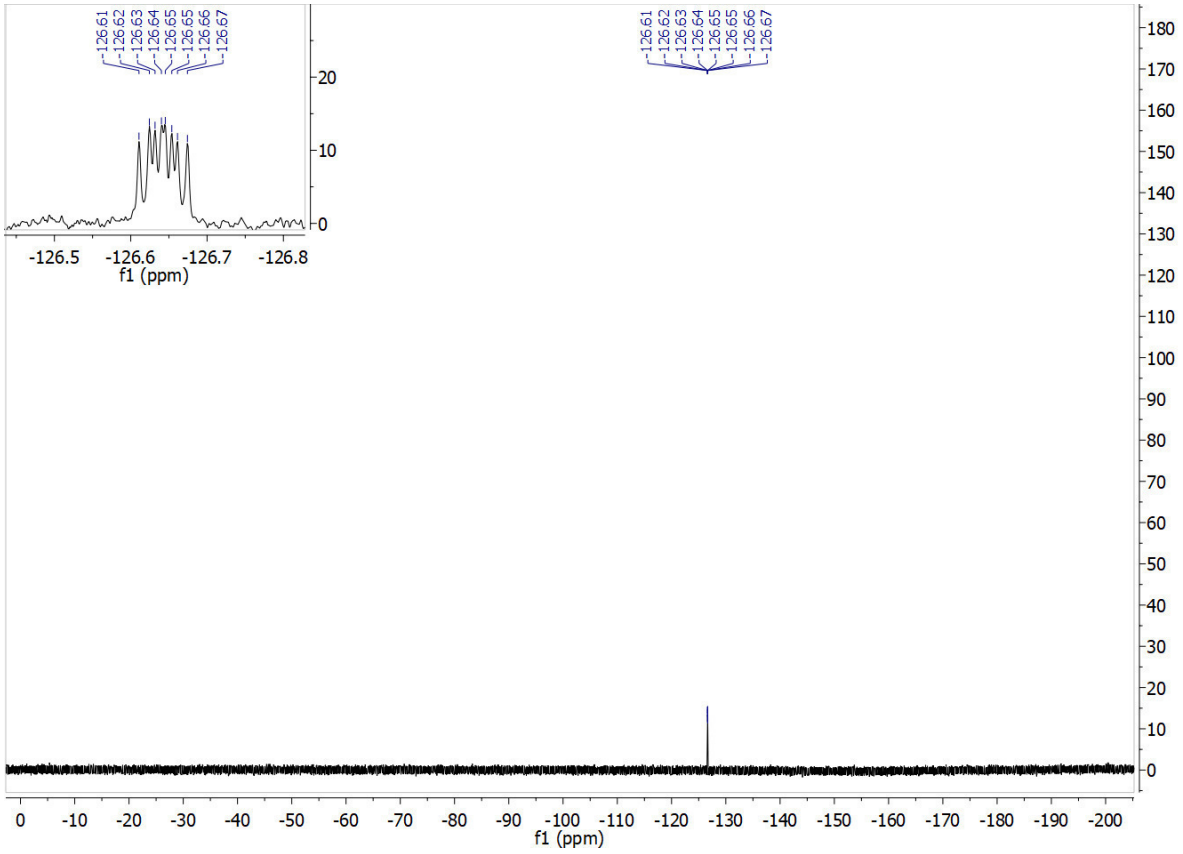

5a: ^{1}H NMR (400 MHz, Acetone-d_6)

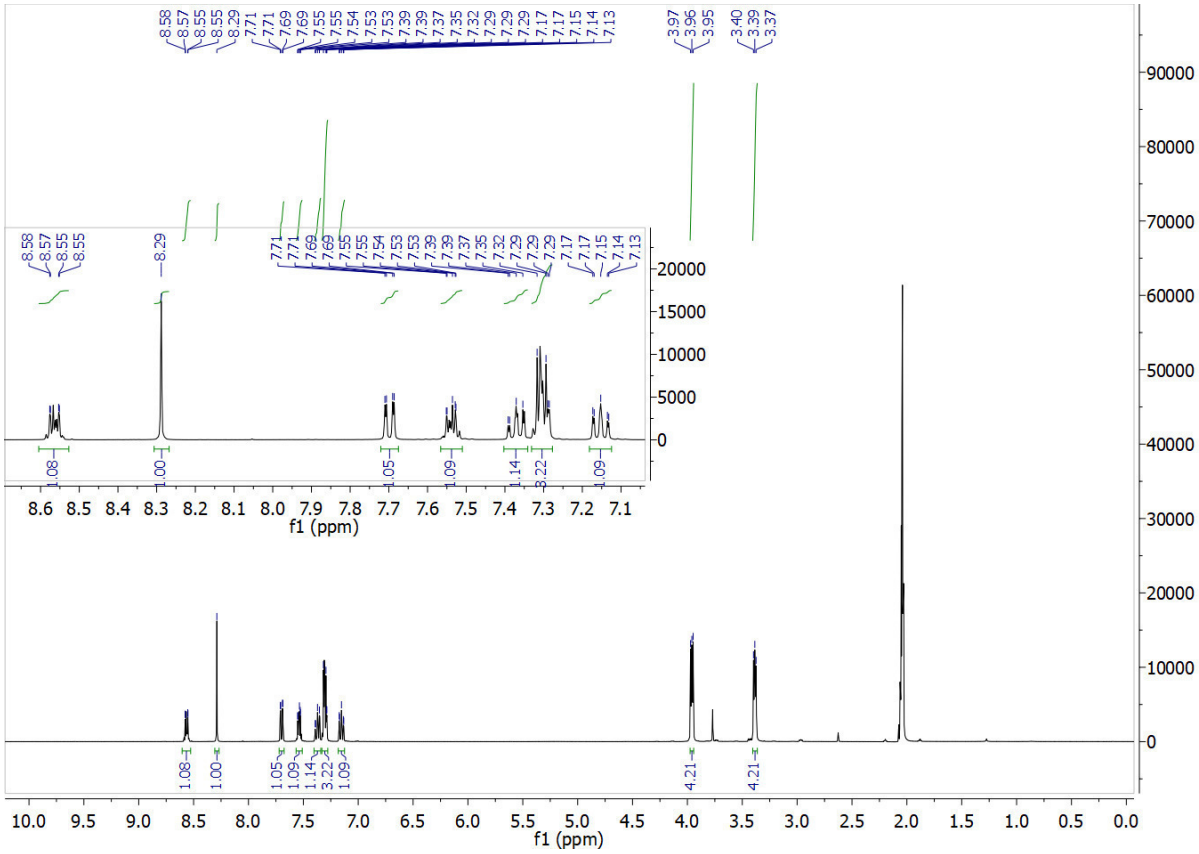

^{13}C NMR (101 MHz, Acetone-d_6)

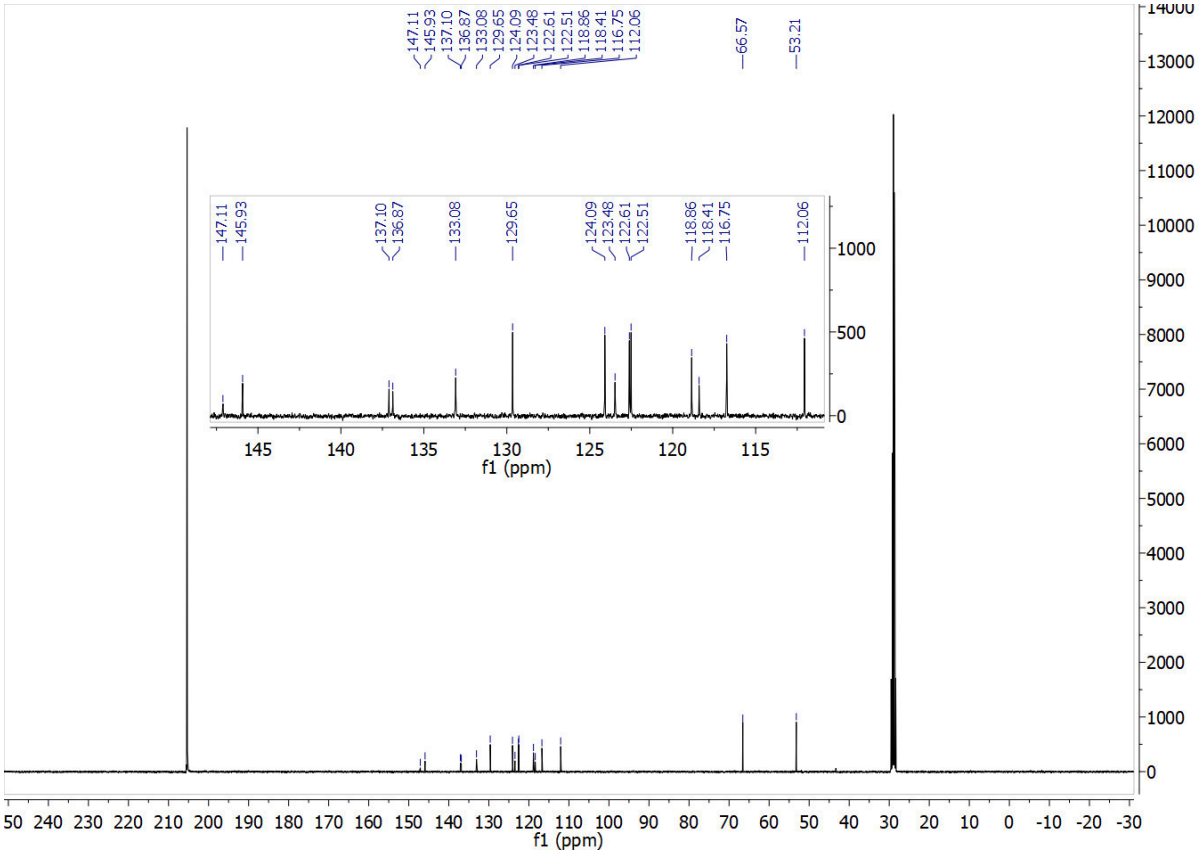

6a: ^{1}H NMR (300 MHz, methanol-*d4*)

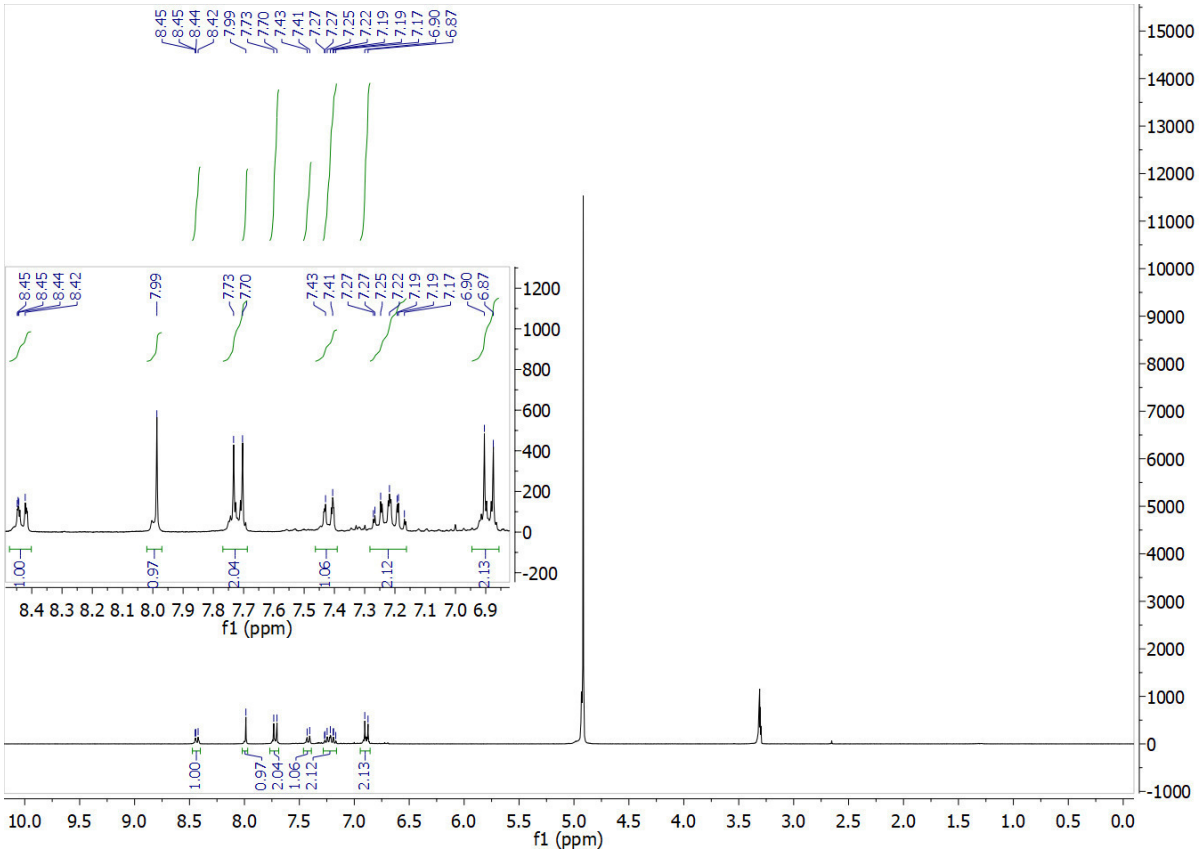

^{13}C NMR (75 MHz, methanol-*d4*)

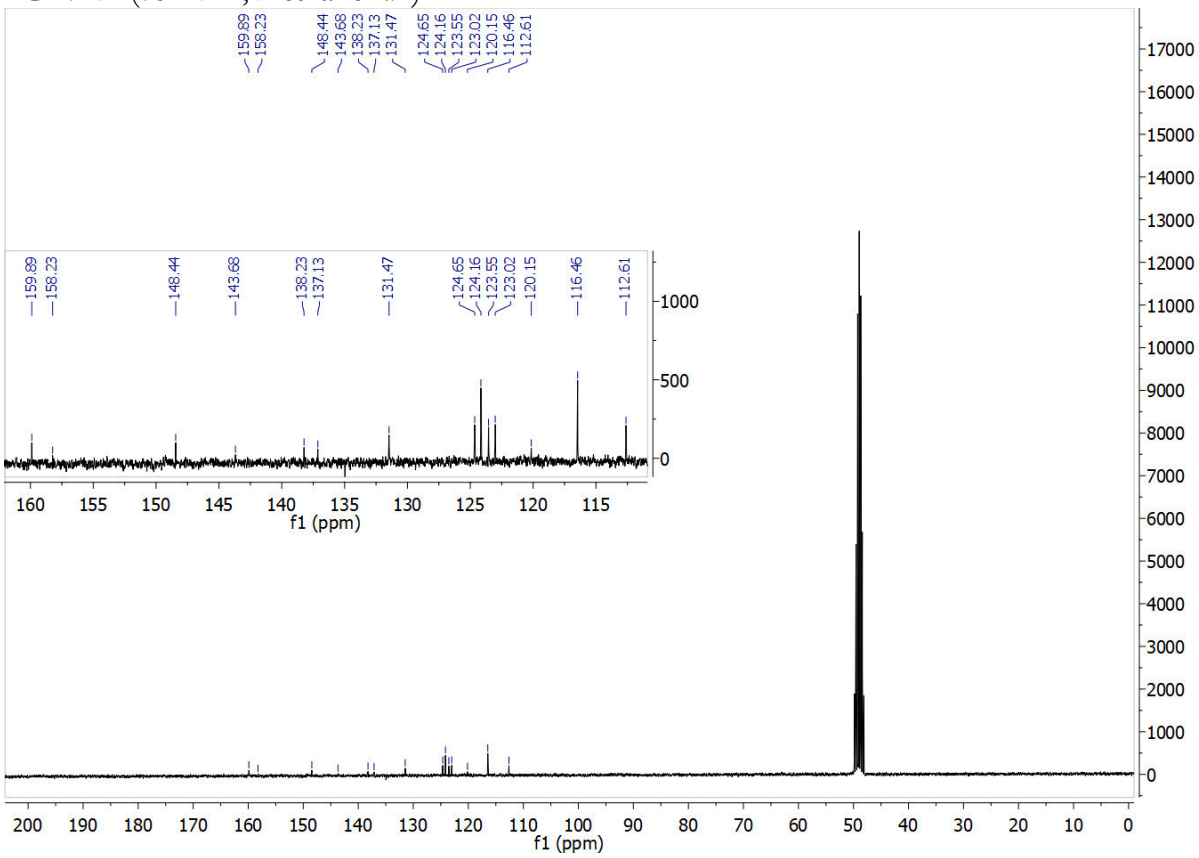

7a ^{1}H-NMR (600 MHz, Acetone-*d6*):

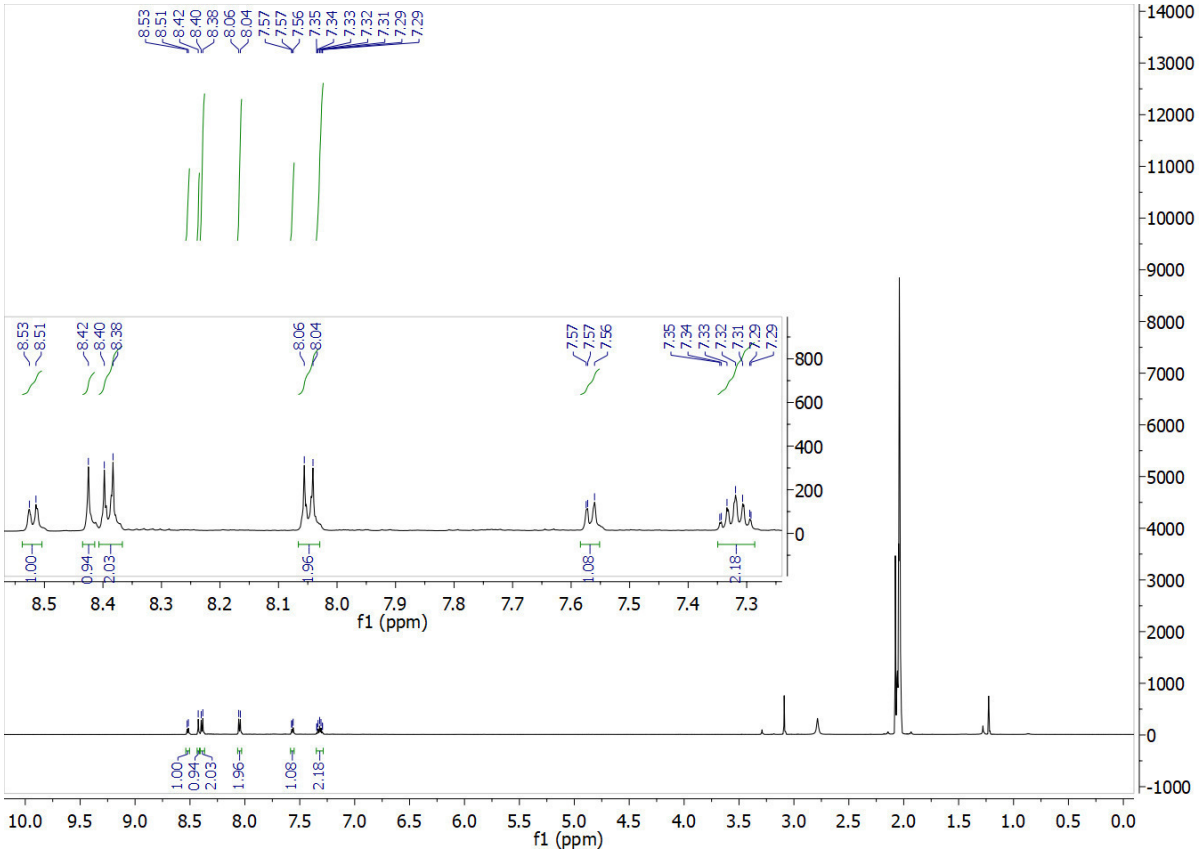

HSQC:

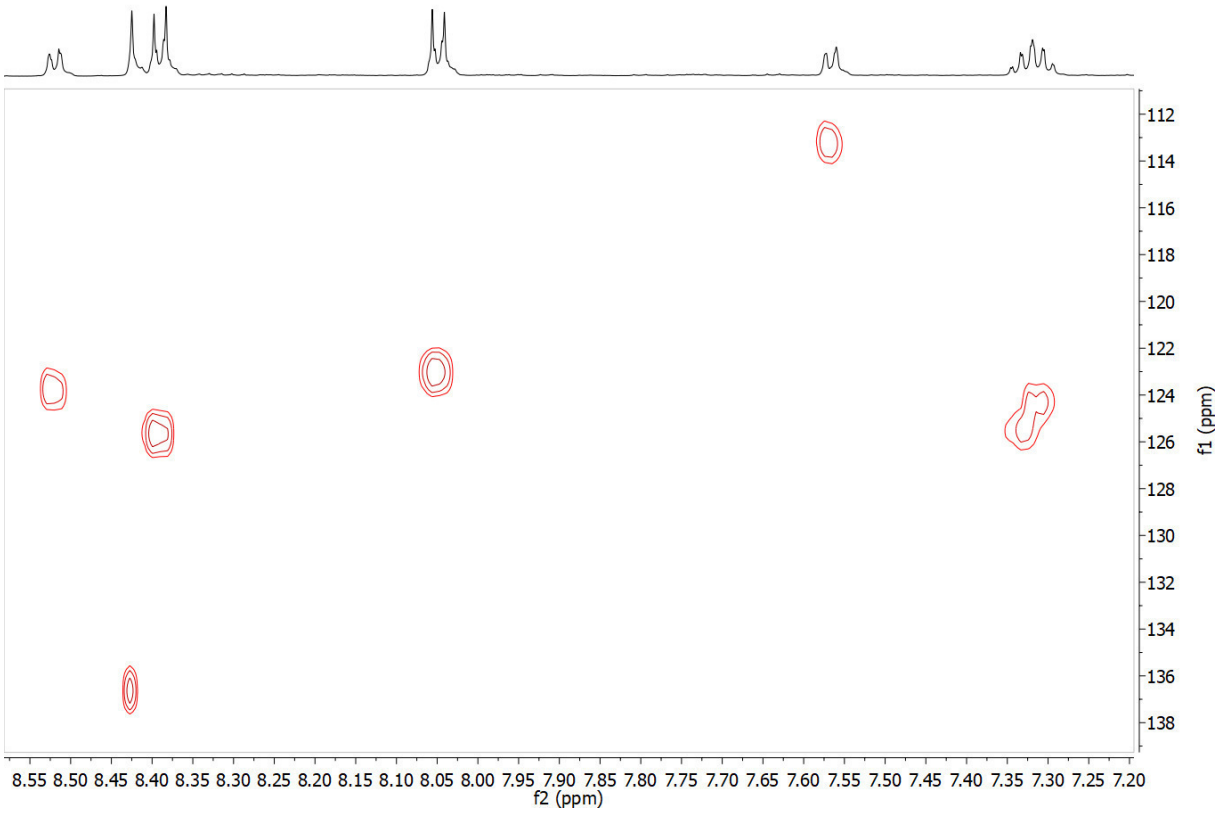
112
114
116
118
120
122
124
126
128
130
132
134
136
138
f1 (ppm)
8.55 8.50 8.45 8.40 8.35 8.30 8.25 8.20 8.15 8.10 8.05 8.00 7.95 7.90 7.85 7.80 7.75 7.70 7.65 7.60 7.55 7.50 7.45 7.40 7.35 7.30 7.25 7.20
f2 (ppm)

HMBC:

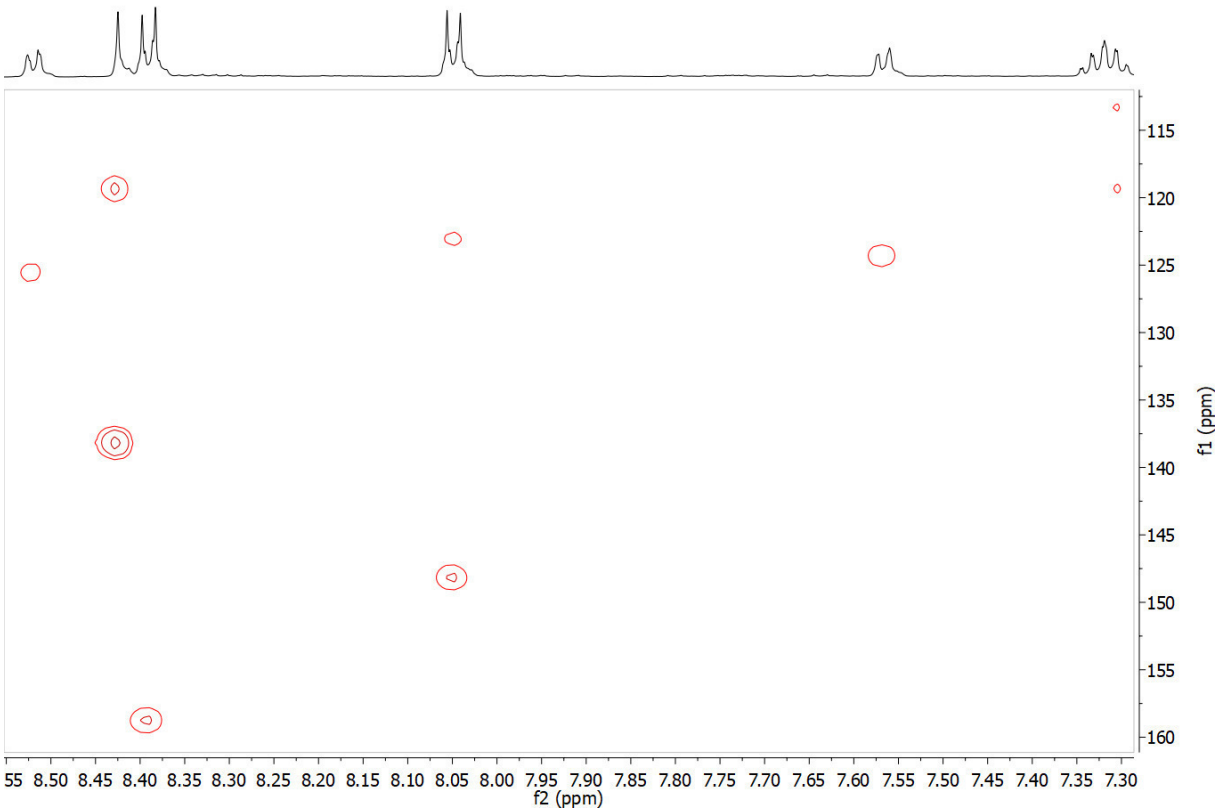
115
120
125
130
135
140
145
150
155
160
f1 (ppm)
55 8.50 8.45 8.40 8.35 8.30 8.25 8.20 8.15 8.10 8.05 8.00 7.95 7.90 7.85 7.80 7.75 7.70 7.65 7.60 7.55 7.50 7.45 7.40 7.35 7.30
f2 (ppm)

10a' ^{1}H NMR (300 MHz, Chloroform-*d*)

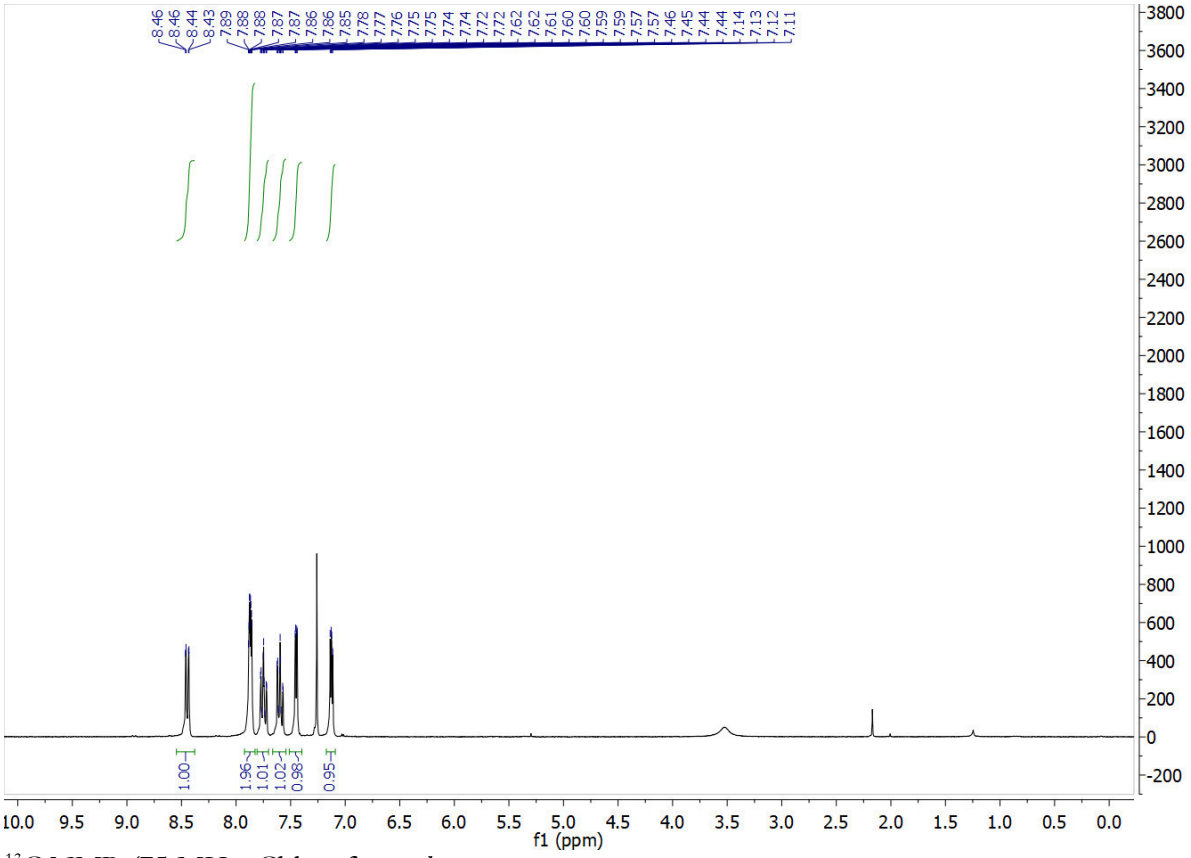

^{13}C NMR (75 MHz, Chloroform-*d*)

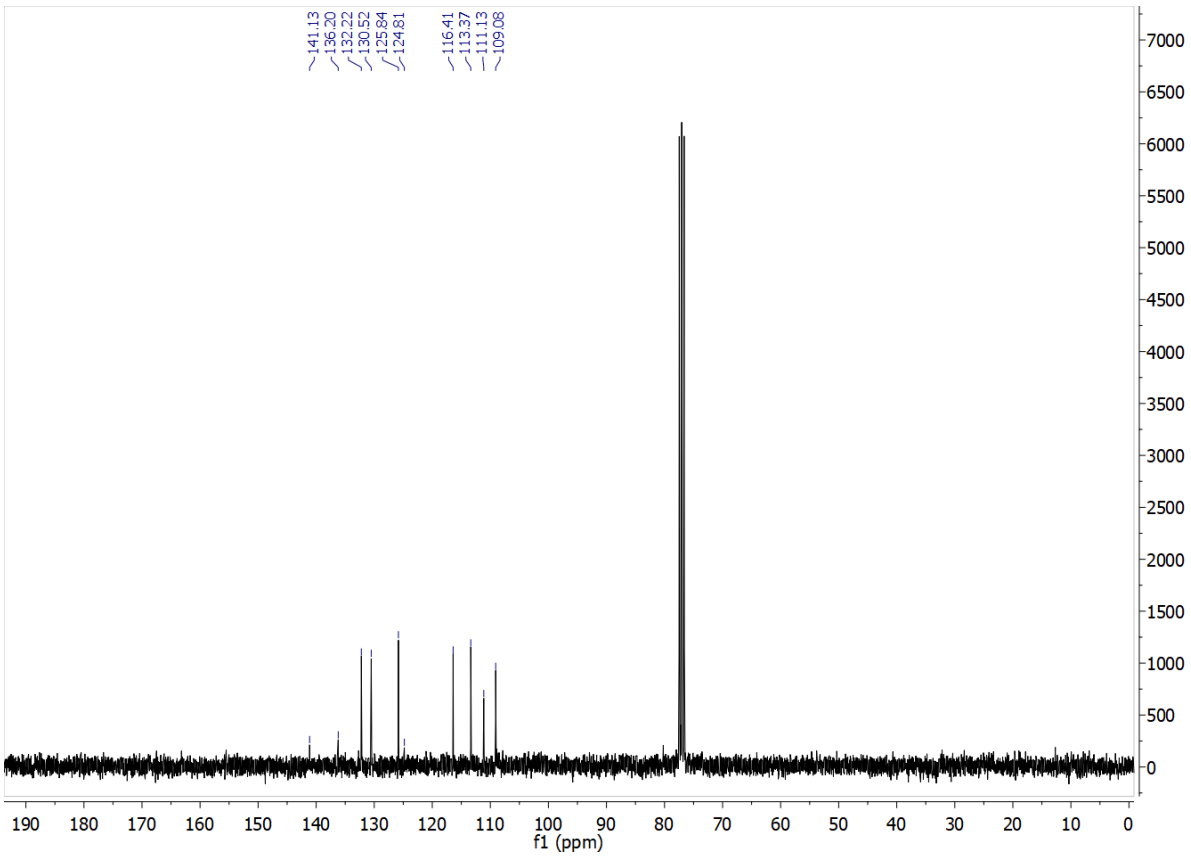

10a'' ^{1}H NMR (300 MHz, Methanol-d_4)

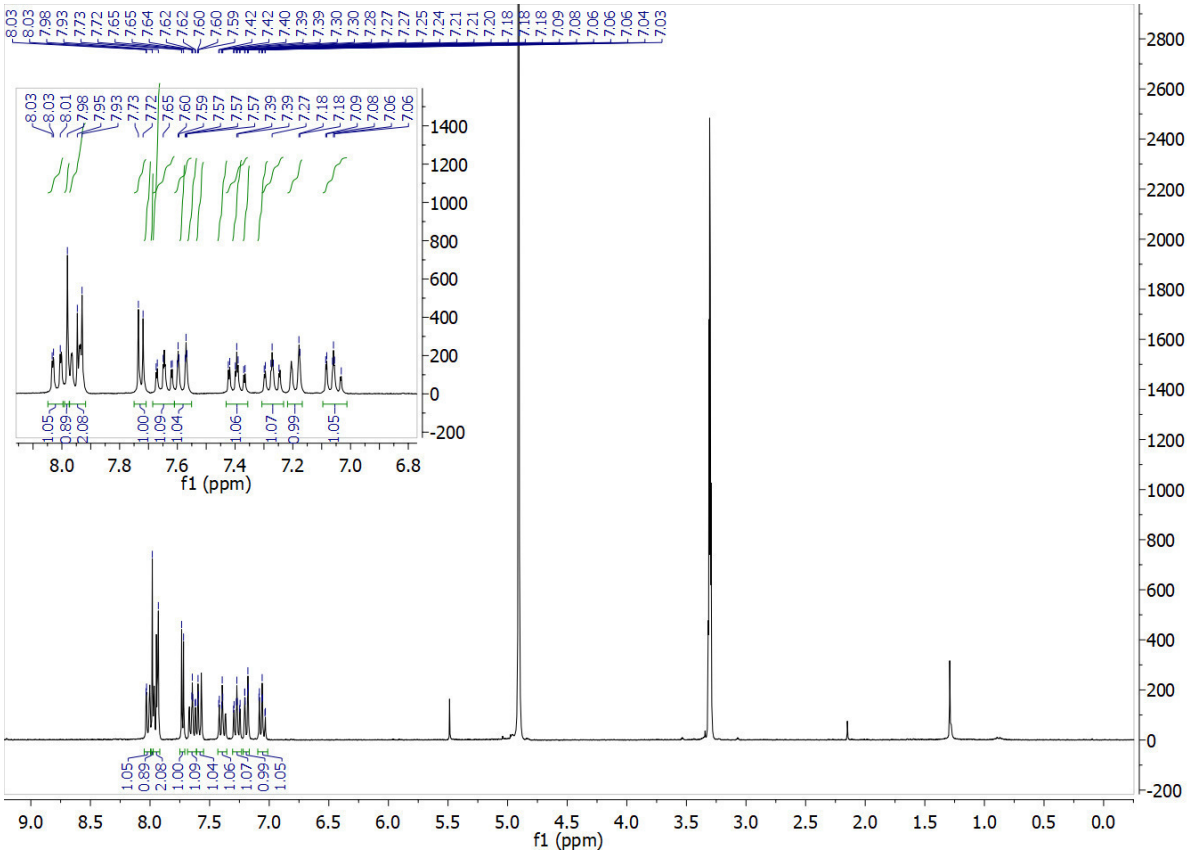

3. UV-Vis Absorption Spectra

Table A1: Overview over calculated and experimental absorption maxima, molar attenuation coefficient, lifetimes of the Z-isomer and calculated PSS distribution. Values for **1a** and **1b** were taken from our previous study.[2]

Compound	Solvent	λ_{max} [nm] PBE0	λ_{max} [nm]	$\varepsilon\lambda_{max}$	τ^b	PSS[i] E-Z (%, calc.)
1a	Toluene[a]	366	362	15151	47.5 ms	--
	DMSO[a]	368	372	16447	6.5 s	--
	DMSO/water[a]	--	--	--	187.9 µs	--
	MeOH[a]	366	365	14716	6.8 ms	--
	MeCN[a]		362	14654	4.3 s	--
	cyclohexane[a]		350	12242	42.5 ms	--
1b	Toluene[a]	373	366	14134	17.1 min	85-15
	DMSO[a]	376	380	15964	2.6 d	--
	DMSO/water[a]		--	--	--	--
	MeOH[a]	373	369	14338	2.4 h	--
	MeCN[a]	--	371	15936	1.2 d	--
	cyclohexane[a]	--	359	14450	1.1 h	--
2a	Toluene[b]	379	373	13956	51.4 s	94-6
	DMSO[b]	380	388	13248	1.41 s	19-81
	DMSO/water[b]	--	386	12513	--	--
	MeOH[b]	378	377	13582	13.1 ms	28-72
	MeCN[b]	--	377	13582	--	--
	Cyclohexane[b]	--	367	12354	--	--
3a	Toluene[c]	382	385	13890	12.1 ms	35-65
	DMSO[c]	384	389	15151	18.4 ms	45-55
	DMSO/water[c]	--	386	15086	--	--
	MeOH[c]	382	384	15556	7.76 ms	6-94
	MeCN[c]	--	384	15370	--	--
	Cyclohexane[c]	--	389	15207	--	--
4a	Toluene[a]	375	367	14148	136 s	90-10
	DMSO[a]	376	379	15592	1.02 s	19-81
	DMSO/water[a]	--	378	14408	--	--
	MeOH[a]	374	371	15552	9 ms	6-81
	MeCN[a]	--	371	14844	--	--
	cyclohexane[a]	--	357	16820	--	--
5a	Toluene[a]	340 (412)	347 (388)	11018	1.49 ms	9-91
	DMSO[a]	341, 411	394	17192	--	57-43
	DMSO/water[a]	--	375	16100	--	--
	MeOH[a]	340, 410	384	16820	--	9-91
	MeCN[a]	--	353 (385)	15812	--	--
	Cyclohexane[d]	--	342 (386)	13655	--	--
6a	Toluene[e]	373	373	10710	10.2 s	87-13
	DMSO[e]	375	380	12450	5.74 s	86-14

	DMSO/water[e]	--	377	10378	--	--
	MeOH[a]	373	374	13752	--	7-93
	MeCN[e]	--	372	11355	--	--
	cyclohexane[a]	--	358	15523	--	--
7a	Toluene[f]	427	399	11593	121 s	94-6
	DMSO[f]	442	422	14723	reaction	5-95
	DMSO/water[f]	--	417	12426	--	--
	MeOH[f]	438	407	15977	94.4 s	16-84
	MeCN[g]	--	403	12193	--	--
	Cyclohexane[g]	--	385	12913	--	--

[a]Concentration was 50 μM. [b]Concentration was 100 μM. [c]Concentration was 100 μM. [d]Concentration was 20 μM. [e]Concentration was 40 μM. [f]Concentration was 30 μM. [g]Concentration was 15 μM. [h]Lifetimes <1s were determined using Laser-Flash Photolysis, other values using UV/Vis spectroscopy [i]Using the method as presented in section A.I.3.9.

UV/Vis spectra at the thermal equilibrium (Δ, black line) and the PSS (blue line) under constant irradiation.

*Compound **2a***

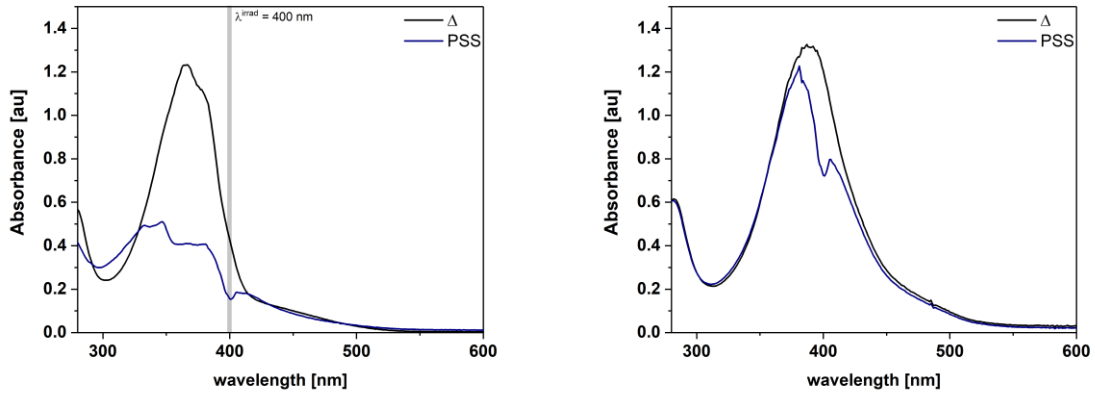

Figure A1: *left*: **2a** in cyclohexane (100 μM), *right*: in DMSO (100 μM).

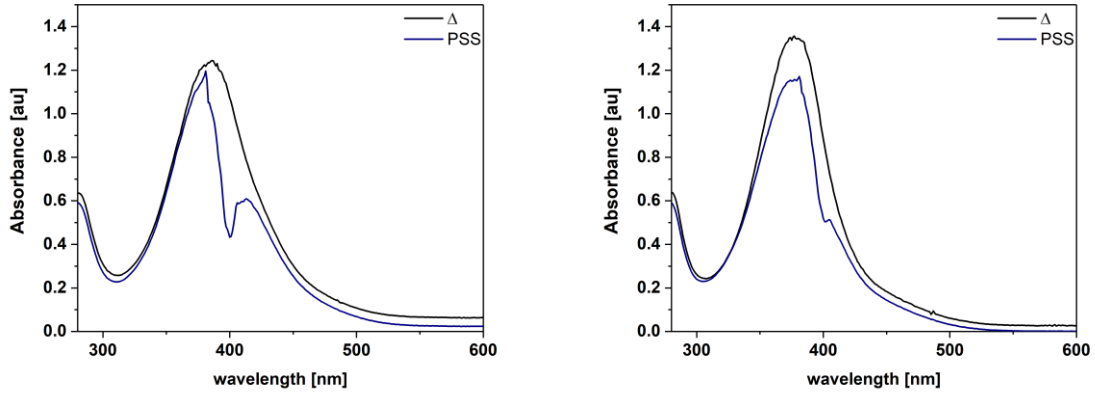

Figure A2: *left*: **2a** in DMSO/water (1:1) (100 μM), *right*: in MeCN (100 μM).

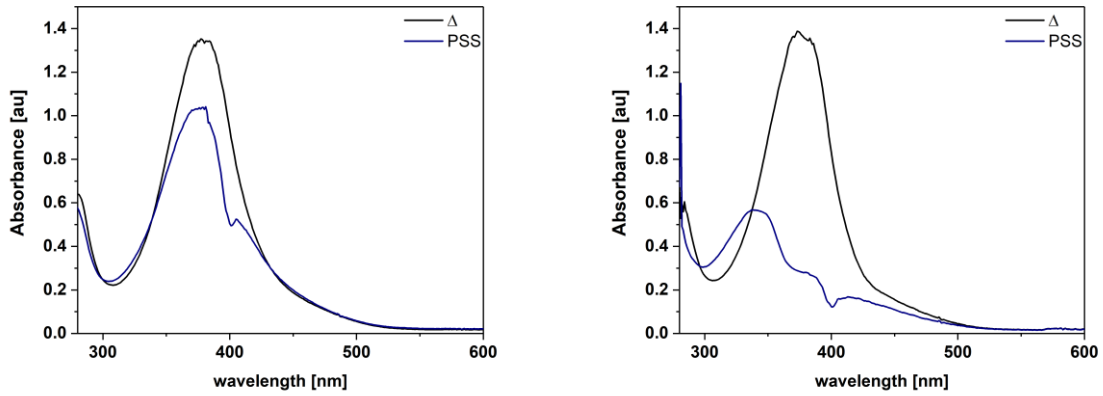

Figure A3: *left*: **2a** in MeOH (100 μM), *right*: in toluene (100 μM).

*Compound **3a***

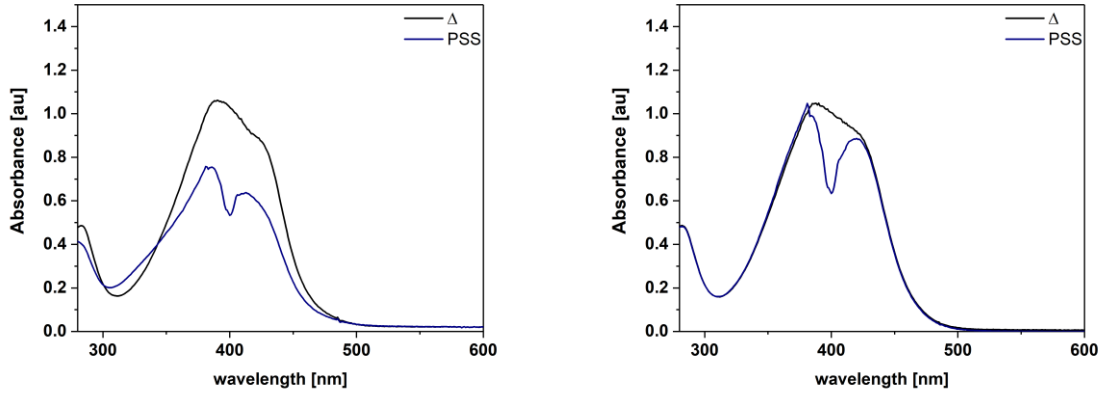

Figure A4: *left*: **3a** in DMSO (70 μM), *right*: in DMSO/water (1:1) (70 μM).

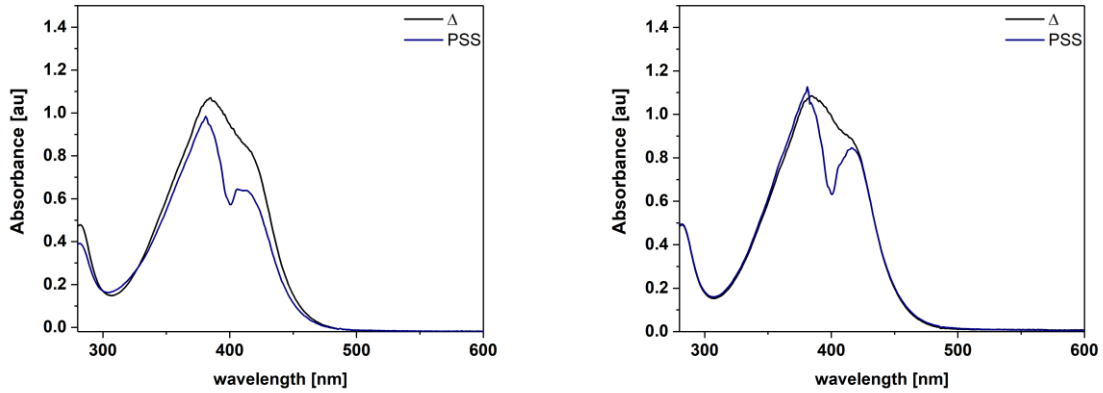

Figure A5: *left*: **3a** in MeCN (70 μM), *right*: in MeOH (70 μM).

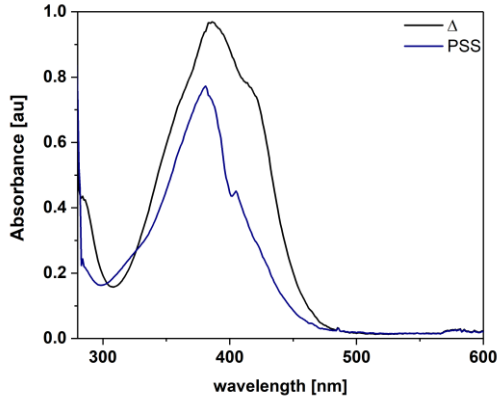

Figure A6: **3a** in toluene (70 μM).

*Compound **4a***

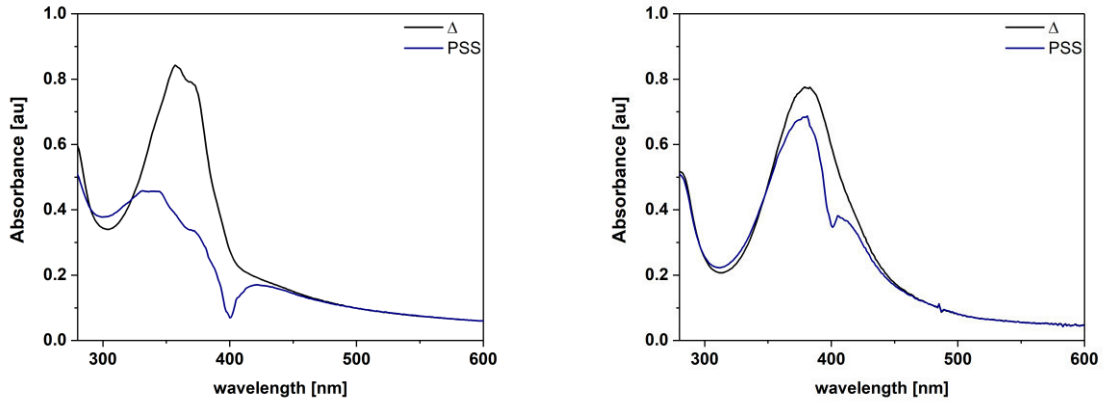

Figure A7: *left*: **4a** in cyclohexane (50 μM), *right*: in DMSO (50 μM).

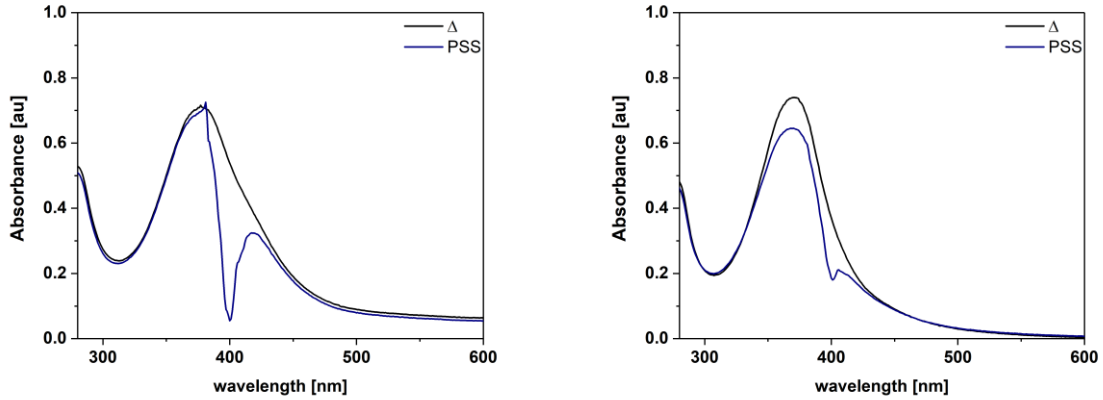

Figure A8: *left*: **4a** in DMSO/water (1:1) (50 μM), *right*: in MeCN (50 μM).

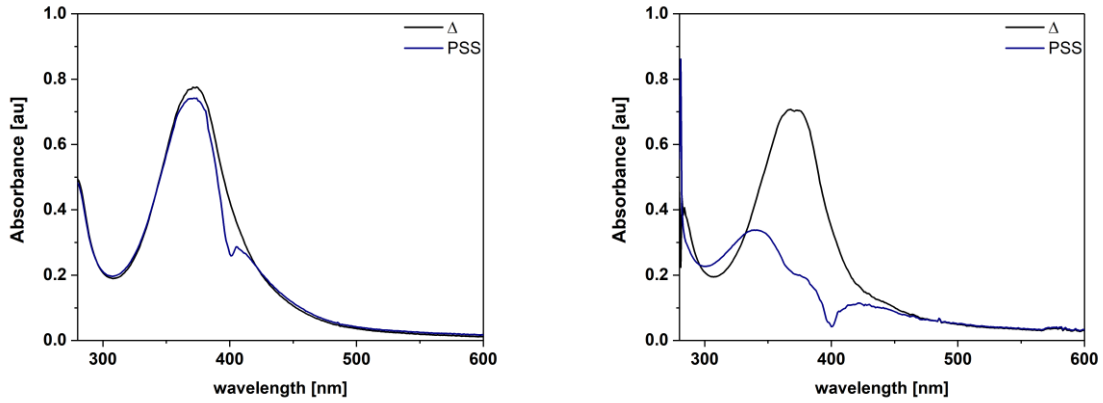

Figure A9: *left*: **4a** in MeOH (50 μM), *right*: in toluene (50 μM).

*Compound **5a***

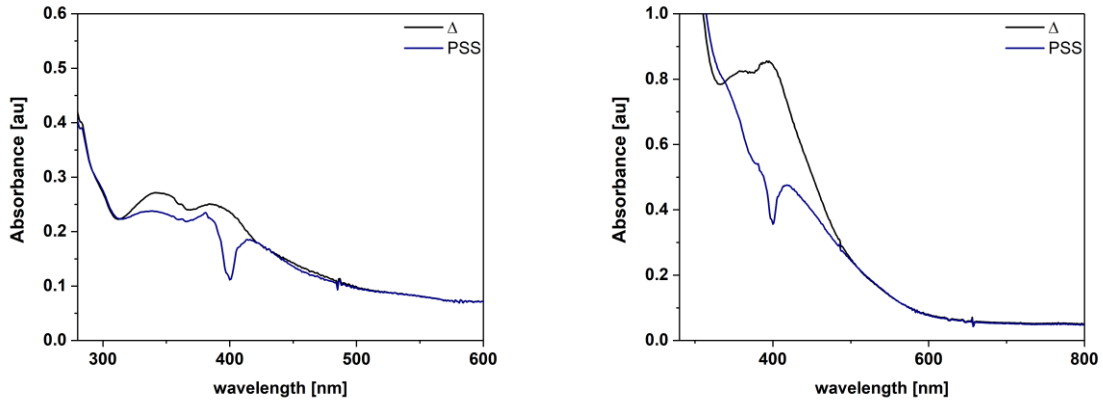

Figure A10: *left*: **5a** in cyclohexane (50 μM), *right*: in DMSO (50 μM).

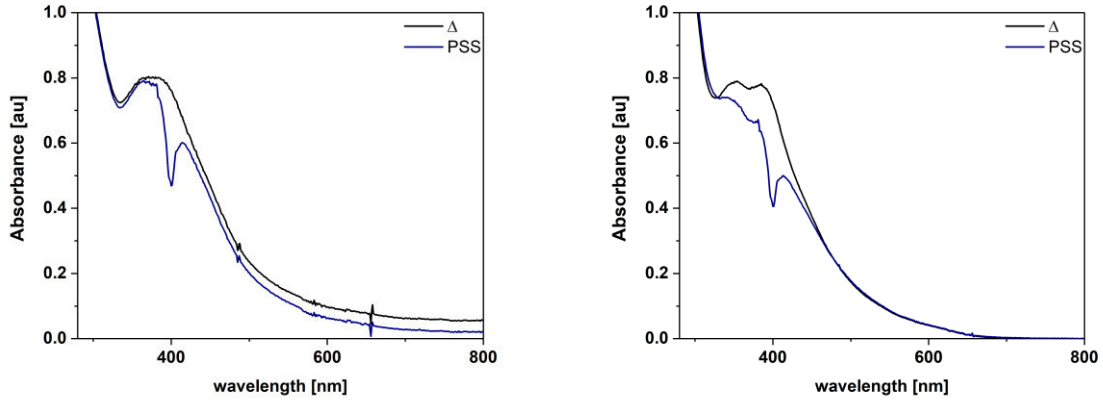

Figure A11: *left*: **5a** in DMSO/water (1:1) (50 μM), *right*: in MeCN (50 μM).

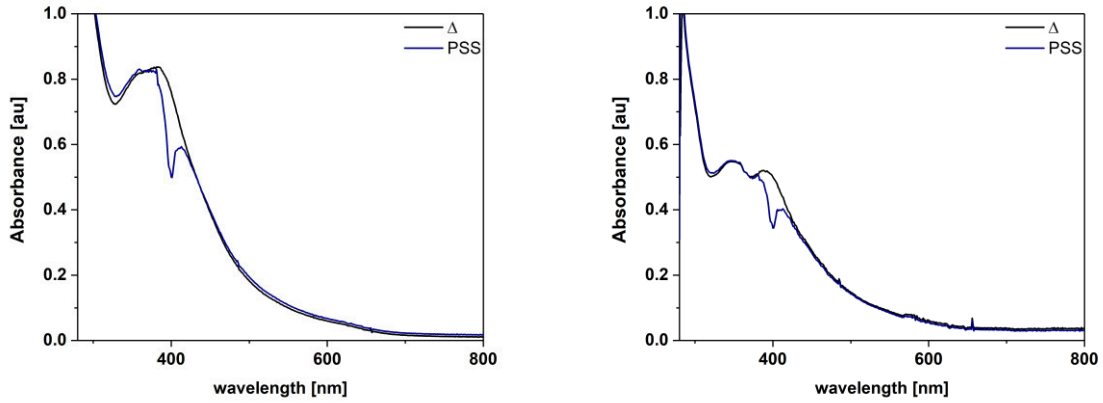

Figure A12: *left*: **5a** in MeOH (50 μM), *right*: in toluene (50 μM).

*Compound **6a***

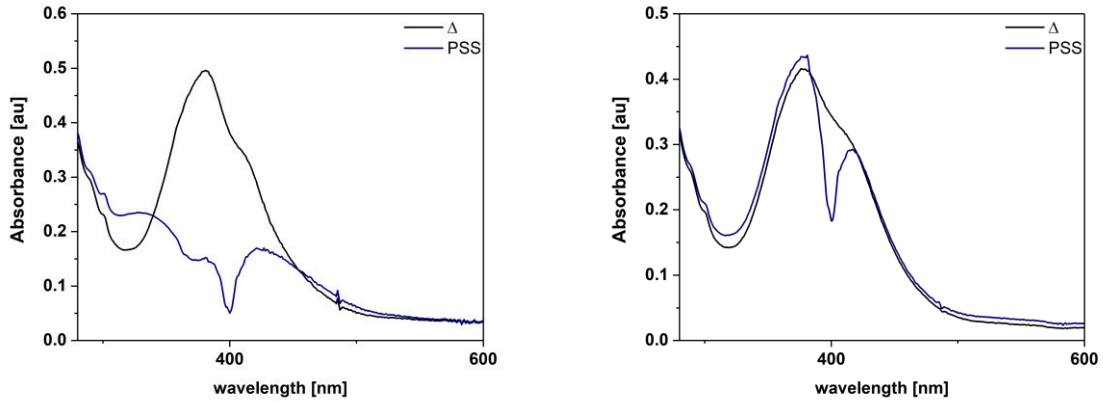

Figure A13: *left*: **6a** in DMSO (40 μM), *right*: in DMSO/water (1:1) (40 μM).

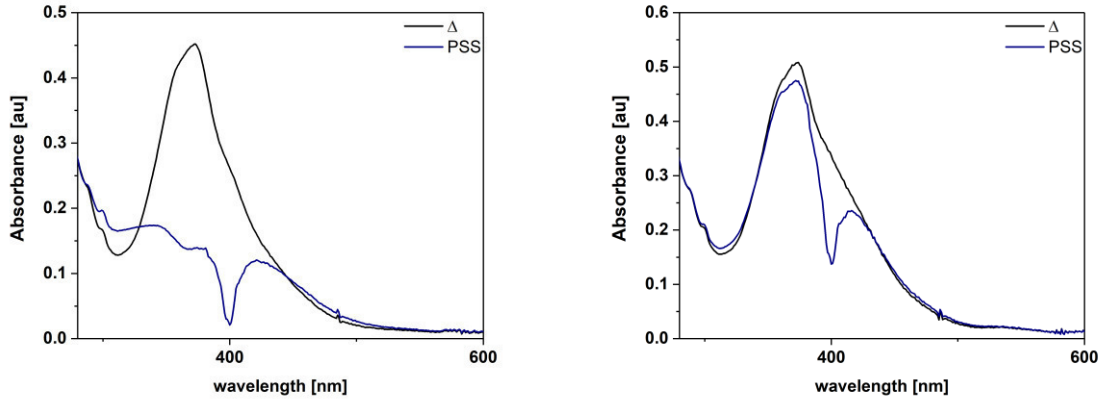

Figure A14: *left*: **6a** in MeCN (40 μM), *right*: in MeOH (40 μM).

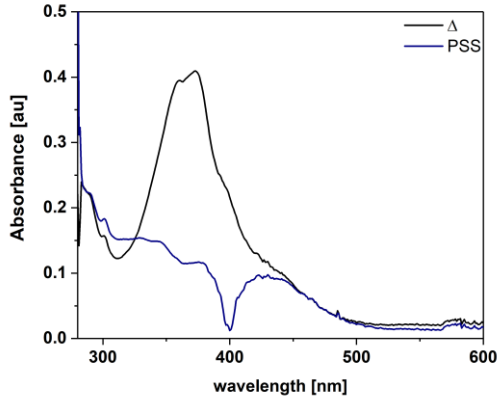

Figure A15: *left*: **6a** in toluene (40 μM).

*Compound **7a***

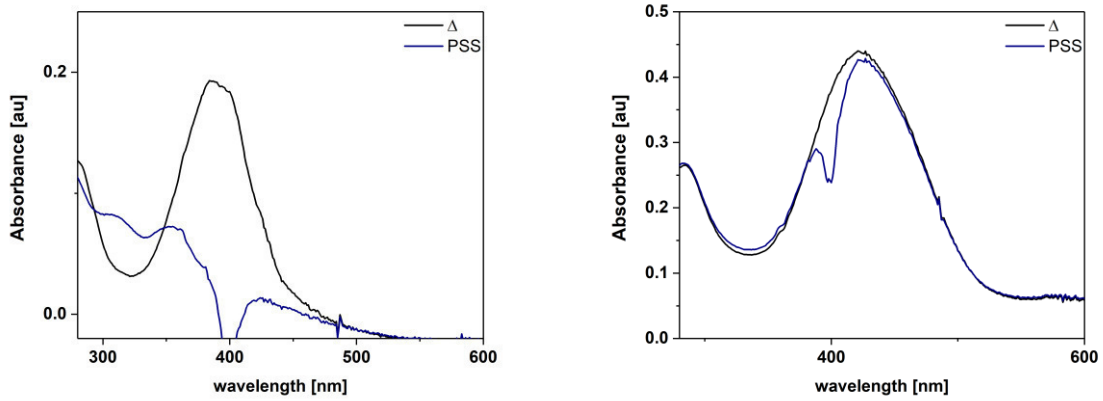

Figure A16: *left*: **7a** in cyclohexane (30 μM), *right*: in DMSO (30 μM).

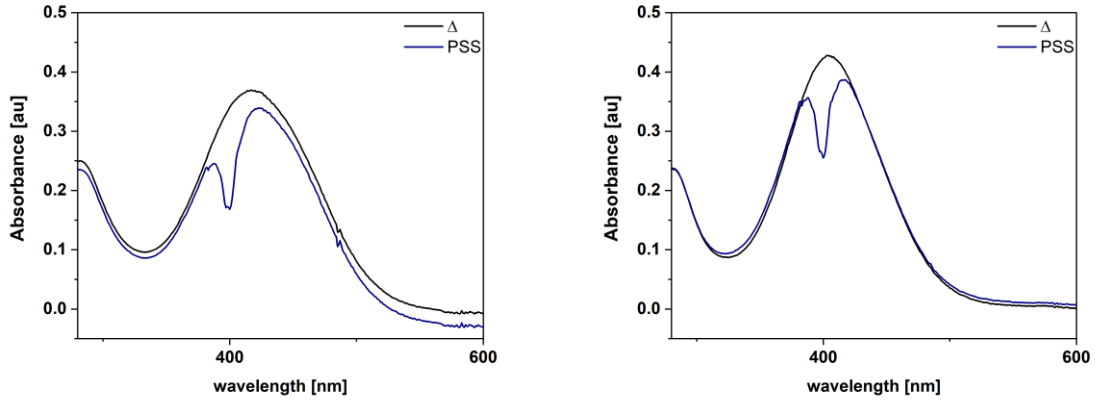

Figure A17: *left*: **7a** in DMSO/water (30 μM), *right*: in MeCN (30 μM).

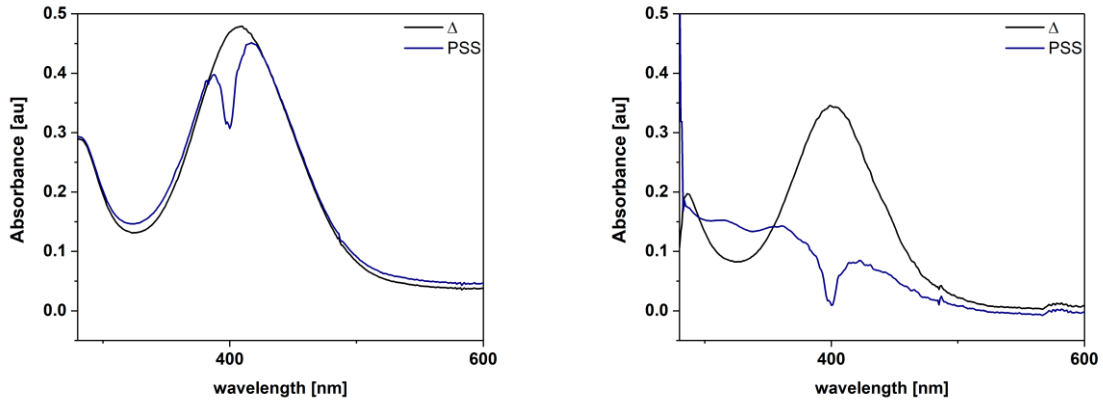

Figure A18: *left*: **7a** in MeOH (30 μM), *right*: in toluene (15 μM).

4. Lifetimes: UV/Vis Spectroscopy and Laser-Flash Photolysis

*Compound **2a***

Table A1:

	Toluene[a]	DMSO[a]	MeOH[b]
Equation	y = A1*exp(-x/t1) + y0	y = A1*exp(-x/t1) + y0	y = A1*exp(-x/t1) + y0
y0	0.72676 ± 1.60274E-5	0.65685 ± 6.84179E-5	0.00827 ± 1.37117E-4
A1	-0.61532 ± 7.60707E-5	-12.9504 ± 0.15075	-0.02986 ± 1.84396E-4
t1	51.40237 ± 0.01048	1.41193 ± 0.00405	6.24581E7 ± 1.10538E6
R-Square(COD)	0.99999	0.99817	0.94145
Adj. R-Square	0.99999	0.99816	0.94139

[a]t1 in seconds [b]t1 in nanoseconds.

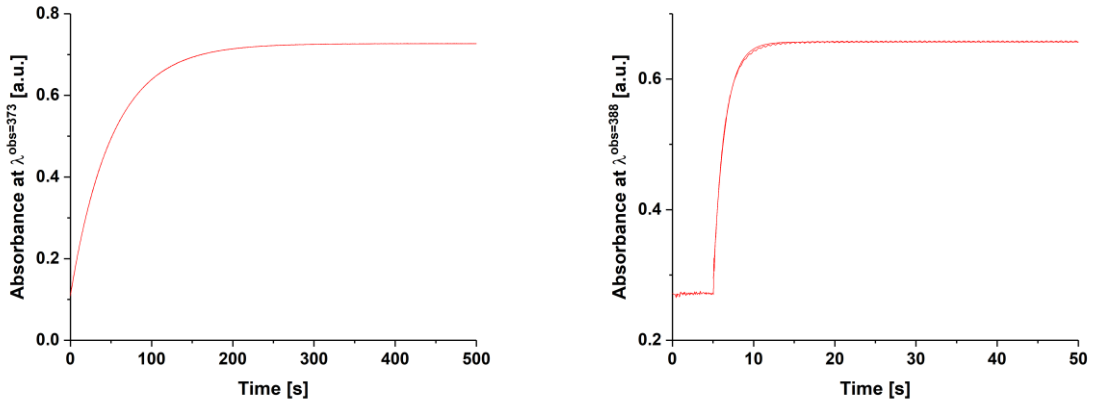

Figure A19: *left*: **2a** in Toluene (70 μM), *right*: in DMSO (70 μM).

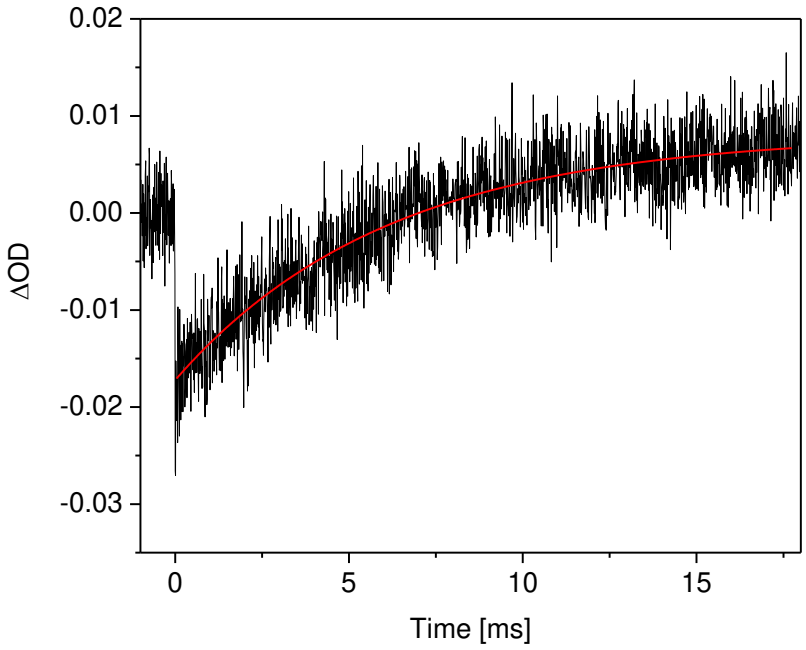

Figure A20: **2a** in MeOH (70 μM).

*Compound **3a***

Table A2:

	Toluene[a]	DMSO[a]	MeOH[a]
Equation	y = A1*exp(-x/t1) + y0	y = A1*exp(-x/t1) + y0	y = A1*exp(-x/t1) + y0
y0	-0.00134 ± 7.61332E-5	0.00415 ± 7.78229E-5	0.00679 ± 1.16768E-4
A1	-0.07992 ± 7.59232E-4	-0.19818 ± 0.00474	-0.15179 ± 0.00239
t1	1.21726E7 ± 125353.53505	1.84068E7 ± 268635.26259	7.76131E6 ± 104491.43775
R-Square(COD)	0.95767	0.90935	0.92375
Adj. R-Square	0.95763	0.90926	0.92367

[a]t1 in nanoseconds.

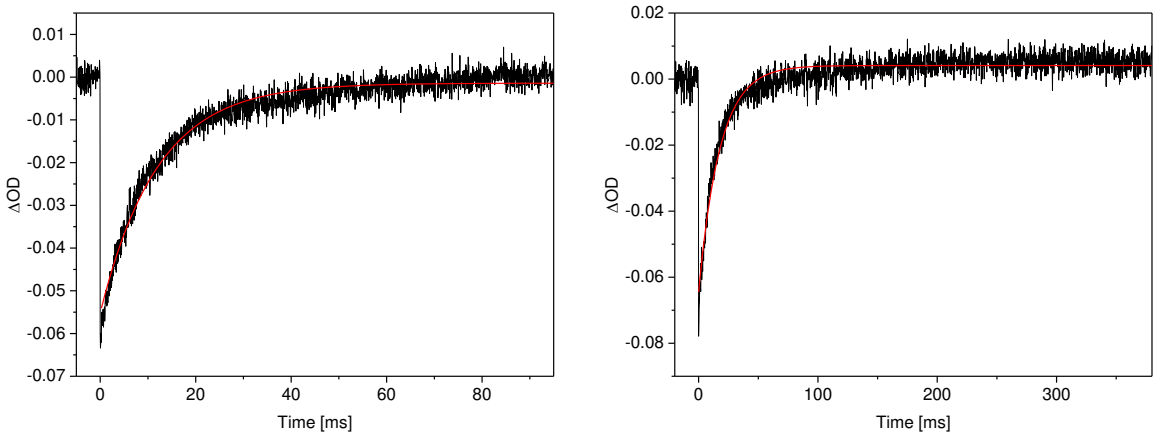

Figure A21: *left*: **3a** in Toluene (70 μM), *right*: in DMSO (70 μM).

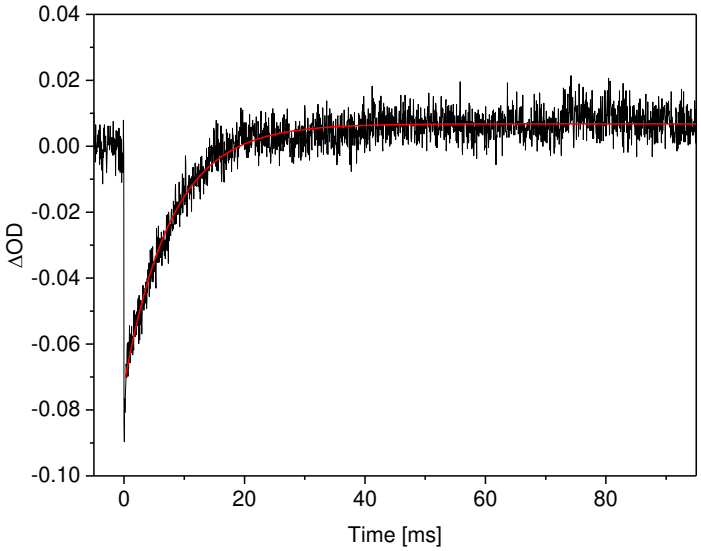

Figure A22: **3a** in MeOH (70 μM).

Compound ***4a***

Table A3:

	Toluene[a]	DMSO[b]	MeOH[b]
Equation	y = A1*exp(-x/t1) + y0	y = A1*exp(-x/t1) + y0	y = A1*exp(-x/t1) + y0
y0	0.70155 ± 2.20771E-4	0.72712 ± 0.00159	0.00751 ± 6.51539E-5
A1	-0.4909 ± 9.75198E-4	-2.23962 ± 0.09364	-0.16743 ± 0.00102
t1	136.46438 ± 0.45418	1.01625 ± 0.0216	9.00743E6 ± 51149.25507
R-Square(COD)	0.99698	0.98902	0.98577
Adj. R-Square	0.99697	0.98884	0.98576

[a]t1 in seconds [b]t1 in nanoseconds.

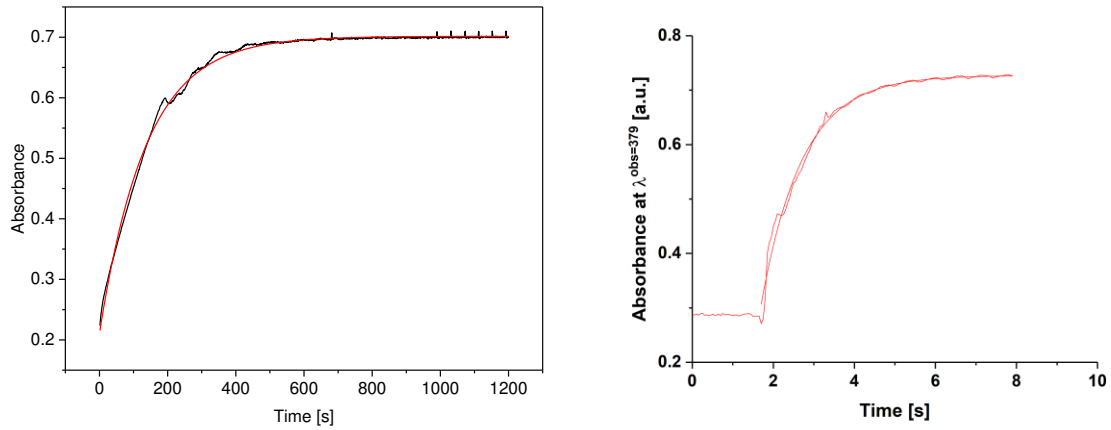

Figure A23: *left*: **4a** in Toluene (70 μM), *right*: in DMSO (70 μM).

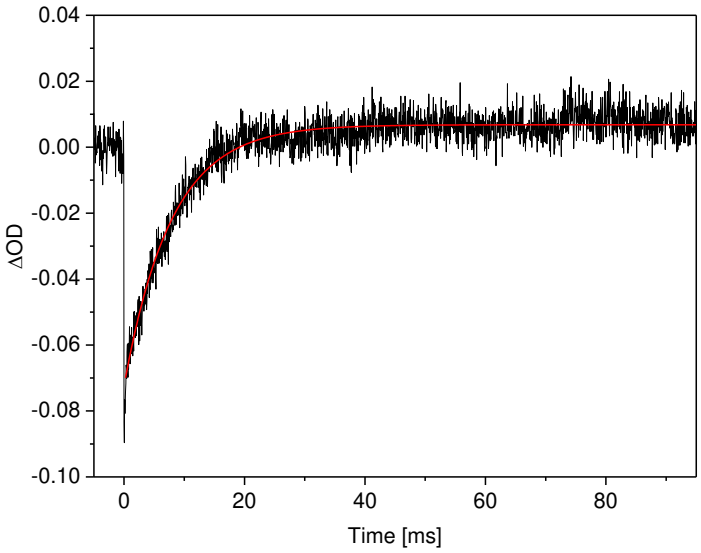

Figure A24: **4a** in MeOH (70 μM).

Compound ***5a***

Table A4:

	Toluene[a]	DMSO[a]	MeOH[a]
Equation	y = A1*exp(-x/t1) + y0	y = A1*exp(-x/t1) + y0	y = A1*exp(-x/t1) + y0
y0	0.0014 ± 5.1317E-5	0.00439 ± 5.37689E-5	0.00309 ± 3.67529E-5
A1	-0.01036 ± 4.78701E-5	-0.0132 ± 2.14566E-4	-0.01119 ± 2.96278E-4
t1	1.49372E6 ± 24233.21589	7.74428E6 ± 201634.3993	1.311E7 ± 412238.27235
R-Square(COD)	0.9615	0.81792	0.71166
Adj. R-Square	0.96146	0.81772	0.71136

[a]t1 in nanoseconds.

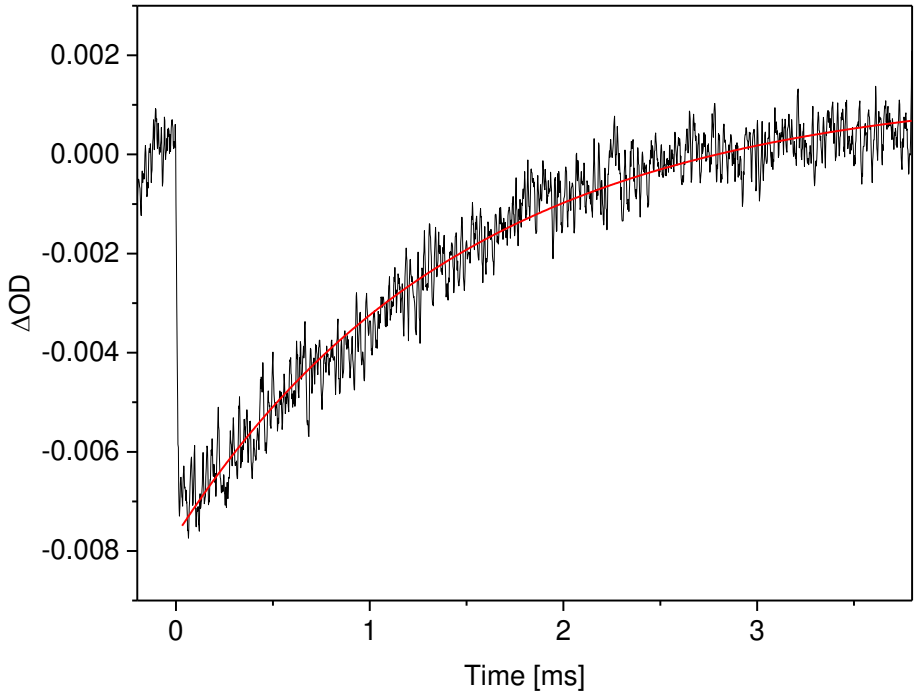

Figure A25:**5a** in Toluene (70 μM).

Compound ***6a***

Table A5:

	Toluene[a]	DMSO[a]	
Equation	y = A1*exp(-x/t1) + y0	y = A1*exp(-x/t1) + y0	
y0	0.40598 ± 4.37519E-4	0.34426 ± 5.77706E-4	
A1	-0.35436 ± 0.00228	-0.29178 ± 0.00324	
t1	10.22239 ± 0.10315	5.74329 ± 0.09553	
R-Square(COD)	0.99789	0.99722	
Adj. R-Square	0.99784	0.9971	

[a]t1 in seconds

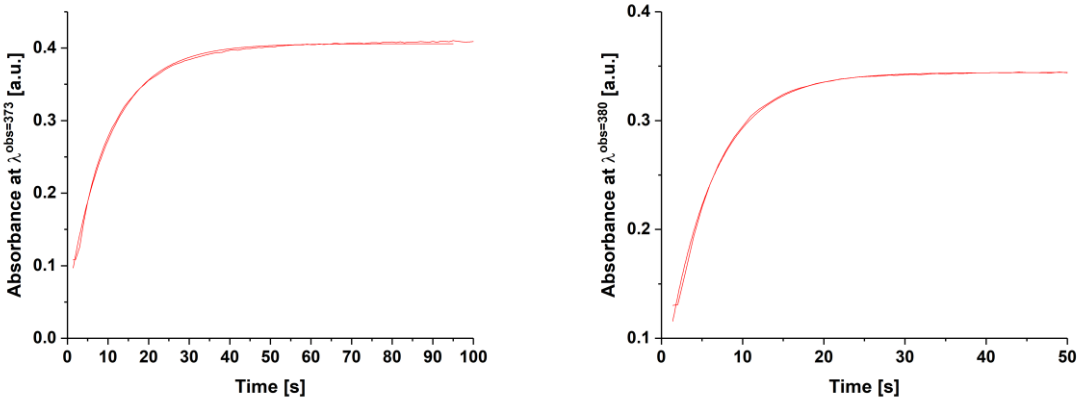

Figure A26: *left*: **6a** in Toluene (70 μM), *right*: in DMSO (70 μM).

*Compound **7a***

Table A6:

	Toluene[a]	MeOH[a]
Equation	y = A1*exp(-x/t1) + y0	y = A1*exp(-x/t1) + y0
y0	0.32757 ± 1.60002E-4	0.74051 ± 9.99735E-6
A1	-0.22143 ± 7.96921E-4	-0.0025 ± 3.60544E-5
t1	121.14833 ± 0.70449	94.43379 ± 2.44385
R-Square(COD)	0.99062	0.90967
Adj. R-Square	0.9906	0.90941

[a]t1 in seconds.

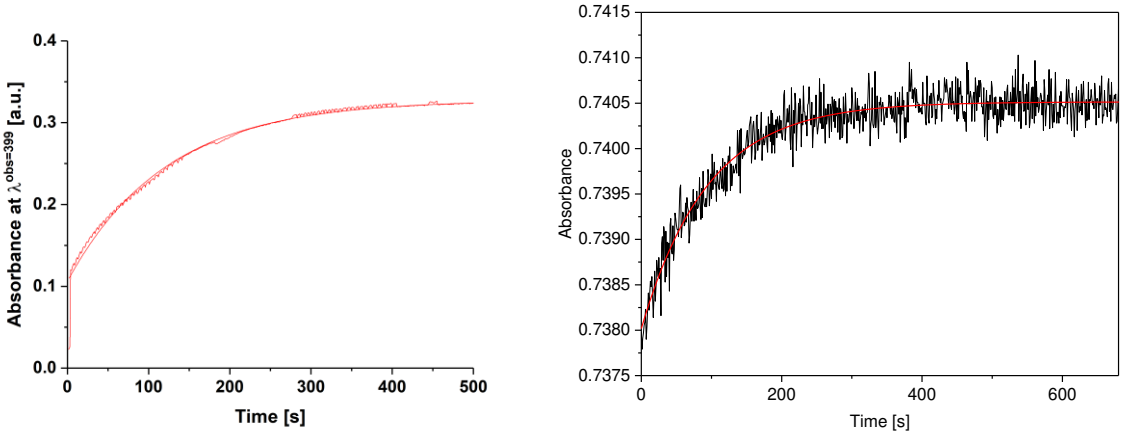

Figure A27: *left*: **7a** in Toluene (35 μM), *right*: in MeOH (70 μM).

5. X-Ray

*Compound **1b***

Experimental. Single clear orange block-shaped crystals of **1b** were obtained by recrystallisation from chloroform/heptane. A suitable crystal (0.20×0.16×0.07) was selected and mounted on a MITIGEN holder oil on a GV1000, TitanS2 diffractometer. The crystal was kept at T = 123.00(11) K during data collection. Using **Olex2**,[3] the structure was solved with the **ShelXT** structure solution program, using the Intrinsic Phasing solution method.[4] The model was refined with ShelXL using Least Squares minimisation.[5]

Crystal Data. $C_{15}H_{13}N_3$, M_r = 235.28, monoclinic, $P2_1/n$ (No. 14), a = 7.87750(10) Å, b = 8.93220(10) Å, c = 17.6085(3) Å, α = 99.1020(10)°, $\beta = \gamma$ = 90°, V = 1223.39(3) Å^3, T = 123.00(11) K, Z = 4, Z' = 1, μ(CuK□) = 0.613, 14385 reflections measured, 2463 unique (R_{int} = 0.0199) which were used in all calculations. The final wR_2 was 0.0874 (all data) and R_1 was 0.0344 (I > 2(I)).

Table A7:

Formula	$C_{15}H_{13}N_3$
$D_{calc.}$/ g cm^{-3}	1.277
m/mm^{-1}	0.613
Formula Weight	235.28
Colour	clear orange
Shape	block
Size/mm^3	0.2
T/K	0.16
Crystal System	0.07
Space Group	123.00(11)
a/Å	monoclinic
b/Å	$P2_1/n$
c/Å	7.87750(10)
a/°	8.93220(10)
b/°	17.6085(3)
g/°	90
V/Å^3	99.1020(10)
Z	90
Z'	1223.39(3)
Wavelength/Å	4
Radiation type	1
Q_{min}/°	5.088
Q_{max}/°	74.295
Measured Refl.	14385
Independent Refl.	2463
Reflections Used	2349
R_{int}	0.0199
Parameters	164

Restraints	0
Largest Peak	0.239
Deepest Hole	-0.245
GooF	1.042
wR_2 (all data)	0.0874
wR_2	0.0864
R_1 (all data)	0.0356
R_1	0.0344

*Compound **2a***

Experimental. Single clear brown prism-shaped crystals of **2a** were obtained by recrystallisation from chloroform/heptane. A suitable crystal (0.18×0.16×0.09) mm^3 was selected and mounted on a MITIGEN holder with inert oil on a SuperNova, Single source at offset, Atlas diffractometer. The crystal was kept at T = 123.01(10) K during data collection. Using **Olex2**,[3] the structure was solved with the **ShelXT** structure solution program,[5] using the Intrinsic Phasing solution method. The model was refined with version 2014/7 of **ShelXL** using Least Squares minimisation.[4]

Crystal Data. $C_{14}H_{10}BrN_3$, M_r = 300.16, orthorhombic, Pbca (No. 61), a = 13.7408(2) Å, b = 10.8233(2) Å, c = 16.5350(2) Å, $a = b = g = 90^\circ$, V = 2459.10(7) $Å^3$, T = 123.01(10) K, Z = 8, Z' = 1, m(CuK$_a$) = 4.419, 40174 reflections measured, 2577 unique (R_{int} = 0.0373) which were used in all calculations. The final wR_2 was 0.0726 (all data) and R_1 was 0.0261 (I > 2(I)).

Table A8:

Formula	$C_{14}H_{10}BrN_3$
$D_{calc.}$/ g cm^{-3}	1.621
m/mm^{-1}	4.419
Formula Weight	300.16
Colour	clear brown
Shape	prism
Size/mm^3	0.18×0.16×0.09
T/K	123.01(10)
Crystal System	orthorhombic
Space Group	Pbca
a/Å	13.7408(2)
b/Å	10.8233(2)
c/Å	16.5350(2)
a/°	90
b/°	90
g/°	90
V/$Å^3$	2459.10(7)
Z	8
Z'	1

Wavelength/Å	1.54184
Radiation type	CuK_a
$\Theta_{min}/^\circ$	5.35
$\Theta_{max}/^\circ$	76.464
Measured Refl.	40174
Independent Refl.	2577
Reflections Used	2390
R_{int}	0.0373
Parameters	163
Restraints	0
Largest Peak	0.399
Deepest Hole	-0.809
GooF	1.083
wR_2 (all data)	0.0726
wR_2	0.0708
R_1 (all data)	0.0283
R_1	0.0261

Figure A28: Images of the crystal on the diffractometer.

Table A9: Fractional Atomic Coordinates ($\times 10^4$) and Equivalent Isotropic Displacement Parameters ($Å^2 \times 10^3$) for **2a**. U_{eq} is defined as 1/3 of the trace of the orthogonalised U_{ij}.

Atom	x	y	z	U_{eq}
Br(1)	5458.2(2)	1696.5(2)	5760.6(2)	30.77(9)
N(2)	3722.6(10)	4571.6(13)	4641.3(8)	22.1(3)
N(1)	4187.2(10)	3661.6(14)	4943.0(8)	20.8(3)
N(3)	2166.6(12)	6728.9(13)	5593.9(10)	24.0(3)
C(8)	3168.4(12)	5231.1(15)	6072.6(10)	20.5(3)
C(1)	4725.9(13)	2976.3(17)	4362.1(10)	20.6(3)
C(2)	4690.1(13)	3193.6(16)	3527.1(11)	23.5(3)
C(7)	3209.1(12)	5259.2(16)	5195.9(10)	21.4(3)
C(9)	3635.8(12)	4555.2(15)	6684.2(10)	22.1(3)
C(13)	2503.8(12)	6167.4(16)	6296.2(10)	21.6(3)
C(14)	2588.7(13)	6192.5(17)	4943.5(10)	24.5(3)
C(6)	5325.5(13)	2023.7(18)	4639.6(11)	23.3(3)
C(10)	3408.6(13)	4813.2(16)	7482.6(10)	24.6(3)
C(3)	5228.1(14)	2473.9(19)	2998.5(11)	27.8(4)
C(11)	2729.8(13)	5728.1(16)	7689.2(10)	25.0(3)

Atom	x	y	z	U_{eq}
C(12)	2273.8(13)	6425.4(17)	7097.3(11)	23.8(3)
C(5)	5863.5(14)	1297.8(19)	4110.7(12)	28.6(4)
C(4)	5812.3(14)	1523.7(19)	3287.2(12)	29.9(4)

Table A10: Anisotropic Displacement Parameters ($\times 10^4$) **2a**. The anisotropic displacement factor exponent takes the form: $-2p^2[h^2a^{*2} \times U_{11} + ... + 2hka^* \times b^* \times U_{12}]$

Atom	U_{11}	U_{22}	U_{33}	U_{23}	U_{13}	U_{12}
Br(1)	33.42(14)	39.09(14)	19.80(13)	6.72(7)	0.43(6)	7.87(8)
N(2)	22.6(7)	25.2(7)	18.5(6)	0.6(5)	-1.0(5)	-1.1(5)
N(1)	20.3(6)	24.6(7)	17.5(6)	0.3(5)	0.2(5)	-0.8(5)
N(3)	26.1(7)	23.4(7)	22.4(7)	1.7(5)	-3.4(6)	4.1(6)
C(8)	20.7(7)	21.4(7)	19.5(8)	-1.3(6)	-0.1(6)	-2.1(6)
C(1)	20.0(7)	25.5(8)	16.4(7)	-0.8(6)	1.5(6)	-4.3(7)
C(2)	24.4(8)	28.7(8)	17.4(8)	1.0(6)	-1.2(6)	-4.4(6)
C(7)	22.4(7)	22.3(8)	19.5(8)	0.1(6)	-1.4(6)	-1.9(6)
C(9)	23.2(8)	21.0(7)	22.2(8)	-0.4(6)	-1.9(6)	1.1(6)
C(13)	21.0(7)	21.1(7)	22.7(8)	0.6(6)	-2.4(6)	-1.4(6)
C(14)	27.1(8)	25.8(8)	20.7(8)	2.2(7)	-3.2(6)	-1.0(7)
C(6)	22.1(8)	29.4(8)	18.5(8)	0.5(7)	1.4(6)	-1.7(7)
C(10)	27.4(8)	25.5(8)	20.8(8)	2.0(6)	-3.7(6)	-0.2(7)
C(3)	29.3(8)	38.1(10)	16.1(8)	-3.6(7)	1.2(7)	-9.6(8)
C(11)	28.2(8)	28.0(8)	18.7(7)	-2.7(6)	0.5(6)	-1.4(7)
C(12)	23.6(8)	23.7(8)	24.2(8)	-1.9(6)	1.0(6)	0.9(7)
C(5)	25.8(9)	30.6(9)	29.4(9)	-1.0(8)	2.4(7)	3.2(7)
C(4)	24.8(9)	38.2(10)	26.6(9)	-10.1(7)	6.6(7)	-1.9(7)

Table A11: Bond Lengths in Å for **2a**.

Atom	Atom	Length/Å
Br(1)	C(6)	1.8959(18)
N(2)	N(1)	1.275(2)
N(2)	C(7)	1.376(2)
N(1)	C(1)	1.422(2)
N(3)	C(13)	1.390(2)
N(3)	C(14)	1.353(2)
C(8)	C(7)	1.451(2)
C(8)	C(9)	1.404(2)
C(8)	C(13)	1.413(2)
C(1)	C(2)	1.401(2)
C(1)	C(6)	1.397(3)
C(2)	C(3)	1.385(3)
C(7)	C(14)	1.386(2)
C(9)	C(10)	1.385(2)
C(13)	C(12)	1.390(2)
C(6)	C(5)	1.389(3)
C(10)	C(11)	1.403(3)
C(3)	C(4)	1.389(3)
C(11)	C(12)	1.386(3)
C(5)	C(4)	1.385(3)

Table 12: Bond Angles in ° for **2a**.

Atom	Atom	Atom	Angle/°
N(1)	N(2)	C(7)	114.44(14)
N(2)	N(1)	C(1)	113.53(14)
C(14)	N(3)	C(13)	109.49(15)
C(9)	C(8)	C(7)	135.48(16)
C(9)	C(8)	C(13)	118.74(15)
C(13)	C(8)	C(7)	105.73(14)
C(2)	C(1)	N(1)	124.05(17)
C(6)	C(1)	N(1)	118.04(15)
C(6)	C(1)	C(2)	117.91(16)
C(3)	C(2)	C(1)	120.58(17)
N(2)	C(7)	C(8)	132.40(15)
N(2)	C(7)	C(14)	120.59(15)
C(14)	C(7)	C(8)	107.00(15)
C(10)	C(9)	C(8)	118.59(16)
N(3)	C(13)	C(8)	108.07(15)
C(12)	C(13)	N(3)	129.23(16)
C(12)	C(13)	C(8)	122.70(16)
N(3)	C(14)	C(7)	109.70(15)
C(1)	C(6)	Br(1)	121.04(13)
C(5)	C(6)	Br(1)	117.31(14)
C(5)	C(6)	C(1)	121.64(17)
C(9)	C(10)	C(11)	121.63(16)
C(2)	C(3)	C(4)	120.54(17)
C(12)	C(11)	C(10)	120.88(16)
C(11)	C(12)	C(13)	117.44(16)
C(4)	C(5)	C(6)	119.48(18)
C(5)	C(4)	C(3)	119.85(17)

Table A13: Torsion Angles in ° for **2a**.

Atom	Atom	Atom	Atom	Angle/°
Br(1)	C(6)	C(5)	C(4)	-178.20(15)
N(2)	N(1)	C(1)	C(2)	-5.5(2)
N(2)	N(1)	C(1)	C(6)	174.73(15)
N(2)	C(7)	C(14)	N(3)	179.77(15)
N(1)	N(2)	C(7)	C(8)	7.4(3)
N(1)	N(2)	C(7)	C(14)	-173.04(16)
N(1)	C(1)	C(2)	C(3)	-179.15(16)
N(1)	C(1)	C(6)	Br(1)	-2.5(2)
N(1)	C(1)	C(6)	C(5)	178.95(17)
N(3)	C(13)	C(12)	C(11)	-179.10(17)
C(8)	C(7)	C(14)	N(3)	-0.5(2)
C(8)	C(9)	C(10)	C(11)	-0.1(3)
C(8)	C(13)	C(12)	C(11)	0.4(3)
C(1)	C(2)	C(3)	C(4)	0.0(3)
C(1)	C(6)	C(5)	C(4)	0.4(3)

Atom	Atom	Atom	Atom	Angle/°
C(2)	C(1)	C(6)	Br(1)	177.76(13)
C(2)	C(1)	C(6)	C(5)	-0.8(3)
C(2)	C(3)	C(4)	C(5)	-0.4(3)
C(7)	N(2)	N(1)	C(1)	-178.99(14)
C(7)	C(8)	C(9)	C(10)	178.88(18)
C(7)	C(8)	C(13)	N(3)	-0.18(18)
C(7)	C(8)	C(13)	C(12)	-179.81(16)
C(9)	C(8)	C(7)	N(2)	2.5(3)
C(9)	C(8)	C(7)	C(14)	-177.14(19)
C(9)	C(8)	C(13)	N(3)	177.87(15)
C(9)	C(8)	C(13)	C(12)	-1.8(3)
C(9)	C(10)	C(11)	C(12)	-1.2(3)
C(13)	N(3)	C(14)	C(7)	0.4(2)
C(13)	C(8)	C(7)	N(2)	-179.92(18)
C(13)	C(8)	C(7)	C(14)	0.43(18)
C(13)	C(8)	C(9)	C(10)	1.6(2)
C(14)	N(3)	C(13)	C(8)	-0.1(2)
C(14)	N(3)	C(13)	C(12)	179.45(18)
C(6)	C(1)	C(2)	C(3)	0.6(3)
C(6)	C(5)	C(4)	C(3)	0.2(3)
C(10)	C(11)	C(12)	C(13)	1.0(3)

Table A14: Hydrogen Fractional Atomic Coordinates ($\times 10^4$) and Equivalent Isotropic Displacement Parameters ($Å^2 \times 10^3$) for **2a**. U_{eq} is defined as 1/3 of the trace of the orthogonalised U_{ij}.

Atom	x	y	z	U_{eq}
H(3)	1753	7325	5576	29
H(2)	4301	3827	3326	28
H(9)	4088	3947	6556	27
H(14)	2479	6416	4408	29
H(10)	3714	4369	7892	29
H(3A)	5198	2628	2446	33
H(11)	2584	5869	8231	30
H(12)	1831	7042	7231	29
H(5)	6255	665	4308	34
H(4)	6168	1040	2928	36

*Compound **3a***

Experimental. Single dull yellow needle-shaped crystals of **3a** were obtained by recrystallisation from chloroform/heptane. A suitable crystal (0.21×0.05×0.03) mm^3 was selected and mounted on a MITIGEN holder with inert oil on a SuperNova, Single source at offset, Atlas diffractometer. The crystal was kept at T = 123.00(10) K during data collection. Using **Olex2**,[3] the structure was solved with the **ShelXT** structure solution program, using the Intrinsic Phasing solution method.[5] The model was refined with version 2016/6 of **ShelXL** using Least Squares minimisation.[4]

Crystal Data. $C_{14}H_{11}N_3O$, M_r = 237.26, monoclinic, P2/c (No. 13), a = 13.1456(4) Å, b = 5.1912(2) Å, c = 16.5884(5) Å, b = 90.411(2)°, a = g = 90°, V = 1131.99(7) Å^3, T = 123.00(10) K, Z = 4, Z' = 1, m(Cu K$_a$) = 0.738, 10991 reflections measured, 2269 unique (R_{int} = 0.0314) which were used in all calculations. The final wR_2 was 0.1042 (all data) and R_1 was 0.0368 (I > 2(I)).

Table A15:

Formula	$C_{14}H_{11}N_3O$
$D_{calc.}$/ g cm^{-3}	1.392
m/mm^{-1}	0.738
Formula Weight	237.26
Colour	dull yellow
Shape	needle
Size/mm^3	0.21×0.05×0.03
T/K	123.00(10)
Crystal System	monoclinic
Space Group	P2/c
a/Å	13.1456(4)
b/Å	5.1912(2)
c/Å	16.5884(5)
a/°	90
b/°	90.411(2)
g/°	90
V/Å^3	1131.99(7)
Z	4
Z'	1
Wavelength/Å	1.54184
Radiation type	Cu K$_a$
Q_{min}/°	3.362
Q_{max}/°	73.496
Measured Refl.	10991
Independent Refl.	2269
Reflections Used	1878
R_{int}	0.0314
Parameters	164
Restraints	0
Largest Peak	0.258
Deepest Hole	-0.204
GooF	1.048
wR_2 (all data)	0.1042
wR_2	0.0959
R_1 (all data)	0.0469
R_1	0.0368

Figure A29: Images of the crystal on the diffractometer.

Table A16: Fractional Atomic Coordinates ($\times 10^4$) and Equivalent Isotropic Displacement Parameters ($Å^2 \times 10^3$) for **3a**. U_{eq} is defined as 1/3 of the trace of the orthogonalised U_{ij}.

Atom	x	y	z	U_{eq}
O(1)	5261.7(7)	6316(2)	6317.3(6)	30.8(3)
N(1)	7307.6(8)	6769(2)	7059.9(6)	24.9(3)
N(2)	6599.2(8)	8280(2)	7297.8(6)	24.6(3)
N(3)	6755.6(9)	13445(2)	8693.6(7)	28.0(3)
C(7)	6905.3(10)	10052(3)	7875.3(8)	24.7(3)
C(1)	7021.3(10)	4987(3)	6462.3(7)	24.0(3)
C(8)	7886.3(10)	10472(3)	8255.8(7)	24.2(3)
C(14)	6254.1(10)	11902(3)	8165.4(8)	26.9(3)
C(9)	7756.2(10)	12625(3)	8763.1(8)	26.0(3)
C(2)	6048.8(10)	4772(3)	6102.9(8)	25.1(3)
C(3)	5877.7(10)	2898(3)	5515.9(8)	28.7(3)
C(6)	7789.6(10)	3292(3)	6223.2(8)	27.8(3)
C(4)	6654.1(11)	1254(3)	5285.7(8)	29.7(3)
C(13)	8838(1)	9273(3)	8224.8(8)	28.5(3)
C(10)	8539.7(11)	13603(3)	9243.3(8)	31.0(3)
C(5)	7615.8(11)	1441(3)	5641.7(9)	30.3(3)
C(12)	9617.5(11)	10236(3)	8703.8(9)	33.9(3)
C(11)	9468.0(11)	12367(3)	9204.7(9)	34.9(4)

Table A17: Anisotropic Displacement Parameters ($\times 10^4$) **3a**. The anisotropic displacement factor exponent takes the form: $-2p^2[h^2a^{*2} \times U_{11} + ... + 2hka^* \times b^* \times U_{12}]$

Atom	U_{11}	U_{22}	U_{33}	U_{23}	U_{13}	U_{12}
O(1)	24.7(5)	33.1(6)	34.6(5)	-8.7(4)	-3.5(4)	0.7(4)
N(1)	26.2(6)	27.0(6)	21.5(5)	0.5(4)	-1.1(4)	-1.8(4)
N(2)	25.9(6)	26.6(6)	21.3(5)	1.0(4)	-0.5(4)	-1.8(4)
N(3)	31.9(6)	26.8(6)	25.4(6)	-2.2(5)	1.4(5)	2.1(5)
C(7)	26.4(6)	27.1(7)	20.5(6)	1.8(5)	-0.7(5)	-1.2(5)
C(1)	26.2(6)	25.7(7)	20.2(6)	2.5(5)	0.4(5)	-3.5(5)
C(8)	26.7(7)	25.3(7)	20.6(6)	0.8(5)	-0.2(5)	-4.3(5)
C(14)	27.4(7)	30.4(8)	23.0(6)	2.3(5)	-1.5(5)	0.7(5)
C(9)	29.7(7)	26.2(7)	22.2(6)	3.6(5)	1.7(5)	-2.2(5)
C(2)	24.7(6)	26.4(7)	24.3(6)	1.6(5)	0.9(5)	-1.9(5)
C(3)	27.4(7)	31.5(8)	27.2(7)	-1.4(6)	-2.4(5)	-5.3(5)
C(6)	24.8(7)	32.1(8)	26.7(6)	1.8(6)	0.3(5)	-1.0(5)
C(4)	35.3(7)	28.3(8)	25.6(6)	-3.9(6)	2.6(5)	-5.4(6)
C(13)	28.5(7)	29.8(8)	27.1(7)	-2.1(6)	0.8(5)	-2.1(5)
C(10)	36.2(8)	30.0(8)	26.9(7)	-3.3(6)	1.1(6)	-7.5(6)

Atom	U_{11}	U_{22}	U_{33}	U_{23}	U_{13}	U_{12}
C(5)	29.7(7)	31.0(8)	30.3(7)	-1.4(6)	4.2(5)	2.3(6)
C(12)	25.6(7)	41.5(9)	34.7(7)	-3.7(6)	-1.6(6)	-1.7(6)
C(11)	30.8(7)	42.2(9)	31.6(7)	-4.2(7)	-4.6(6)	-9.9(6)

Table A18: Bond Lengths in Å for **3a**.

Atom	Atom	Length/Å
O(1)	C(2)	1.3580(17)
N(1)	N(2)	1.2819(16)
N(1)	C(1)	1.4055(17)
N(2)	C(7)	1.3857(17)
N(3)	C(14)	1.3548(18)
N(3)	C(9)	1.3865(18)
C(7)	C(8)	1.4482(18)
C(7)	C(14)	1.3758(19)
C(1)	C(2)	1.4112(19)
C(1)	C(6)	1.3992(19)
C(8)	C(9)	1.410(2)
C(8)	C(13)	1.399(2)
C(9)	C(10)	1.393(2)
C(2)	C(3)	1.394(2)
C(3)	C(4)	1.386(2)
C(6)	C(5)	1.379(2)
C(4)	C(5)	1.395(2)
C(13)	C(12)	1.386(2)
C(10)	C(11)	1.380(2)
C(12)	C(11)	1.398(2)

Table A19: Bond Angles in ° for **3a**.

Atom	Atom	Atom	Angle/°
N(2)	N(1)	C(1)	115.38(11)
N(1)	N(2)	C(7)	114.27(11)
C(14)	N(3)	C(9)	109.23(12)
N(2)	C(7)	C(8)	130.87(12)
C(14)	C(7)	N(2)	121.80(12)
C(14)	C(7)	C(8)	107.28(12)
N(1)	C(1)	C(2)	125.95(12)
C(6)	C(1)	N(1)	115.09(11)
C(6)	C(1)	C(2)	118.96(13)
C(9)	C(8)	C(7)	105.53(12)
C(13)	C(8)	C(7)	135.32(13)
C(13)	C(8)	C(9)	119.14(12)
N(3)	C(14)	C(7)	109.74(12)
N(3)	C(9)	C(8)	108.22(12)
N(3)	C(9)	C(10)	129.25(14)
C(10)	C(9)	C(8)	122.52(13)
O(1)	C(2)	C(1)	122.17(12)
O(1)	C(2)	C(3)	118.39(12)
C(3)	C(2)	C(1)	119.44(13)
C(4)	C(3)	C(2)	120.46(13)
C(5)	C(6)	C(1)	121.34(13)
C(3)	C(4)	C(5)	120.49(13)
C(12)	C(13)	C(8)	118.45(14)
C(11)	C(10)	C(9)	117.01(14)
C(6)	C(5)	C(4)	119.32(13)
C(13)	C(12)	C(11)	121.32(14)
C(10)	C(11)	C(12)	121.56(13)

Table A20: Hydrogen Fractional Atomic Coordinates ($\times 10^4$) and Equivalent Isotropic Displacement Parameters ($Å^2 \times 10^3$) for **3a**. U_{eq} is defined as 1/3 of the trace of the orthogonalised U_{ij}.

Atom	x	y	z	U_{eq}
H(1)	5460.84	7383.85	6646.65	46
H(3)	6494.62	14729.87	8945.8	34
H(14)	5572.43	12068.95	8020.69	32
H(3A)	5238.25	2749.41	5276.99	34
H(6)	8430.5	3414.91	6461.14	33
H(4)	6532.87	17.26	4890.9	36
H(13)	8945.1	7861.85	7890.56	34
H(10)	8441.71	15024.28	9575.1	37
H(5)	8134.41	329.34	5488.49	36
H(12)	10252.88	9449.87	8691.98	41
H(11)	10006.55	12966.23	9519.19	42

Compound ***4a***

Experimental. Single clear intense brown prism-shaped crystals of (**Q152**) were obtained by recrystallisation from .... A suitable crystal (0.23×0.20×0.14) mm^3 was selected and mounted on a MITIGEN holder oil on a SuperNova, Single source at offset, Atlas diffractometer. The crystal was kept at T = 122.99(10) K during data collection. Using **Olex2**,[3] the structure was solved with the **ShelXT** structure solution program, using the Intrinsic Phasing solution method.[4] The model was refined with version 2016/6 of **ShelXL** using Least Squares minimisation.[5]

Crystal Data. $C_{14}H_{10}FN_3$, M_r = 239.25, triclinic, *P*-1 (No. 2), a = 7.4944(3) Å, b = 11.0027(4) Å, c = 14.0513(5) Å, a = 91.900(3)°, b = 90.732(3)°, g = 101.377(3)°, V = 1135.04(7) $Å^3$, T = 122.99(10) K, Z = 4, Z' = 2, m(CuK$_a$) = 0.804, 27447 reflections measured, 4724 unique (R_{int} = 0.0528) which were used in all calculations. The final wR_2 was 0.1177 (all data) and R_1 was 0.0410 (I > 2(I)).

Table A21:

Formula	$C_{14}H_{10}FN_3$
$D_{calc.}$/ g cm^{-3}	1.4
m/mm^{-1}	0.804
Formula Weight	239.25
Colour	clear intense brown
Shape	prism
Size/mm^3	0.23×0.20×0.14
T/K	122.99(10)
Crystal System	triclinic
Space Group	*P*-1
a/Å	7.4944(3)
b/Å	11.0027(4)
c/Å	14.0513(5)
a/°	91.900(3)
b/°	90.732(3)
g/°	101.377(3)
V/$Å^3$	1135.04(7)
Z	4
Z'	2
Wavelength/Å	1.54184
Radiation type	CuK$_a$
Q_{min}/°	4.101
Q_{max}/°	76.55
Measured Refl.	27447
Independent Refl.	4724
Reflections Used	4186
R_{int}	0.0528
Parameters	325
Restraints	0
Largest Peak	0.243

Deepest Hole	-0.242
GooF	1.065
wR_2 (all data)	0.1177
wR_2	0.1126
R_1 (all data)	0.0468
R_1	0.041

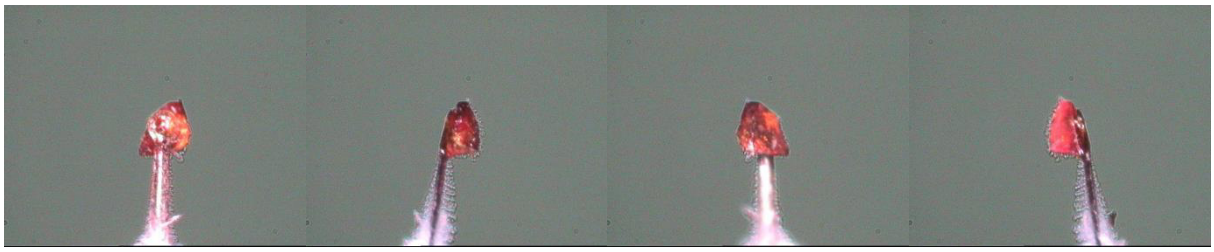

Figure A30: Images of the crystal on the diffractometer.

Table A22: Fractional Atomic Coordinates ($\times 10^4$) and Equivalent Isotropic Displacement Parameters ($Å^2 \times 10^3$) for **4a**. U_{eq} is defined as 1/3 of the trace of the orthogonalised U_{ij}.

Atom	x	y	z	U_{eq}
F1	3699.1(12)	1750.9(9)	-86.2(7)	41.2(2)
F2	7007.5(12)	10128.6(9)	2334.1(7)	41.9(2)
N4	8273.4(14)	8967.8(10)	3777.8(8)	25.6(2)
N1	5447.2(14)	3904.4(10)	795.9(8)	26.2(2)
N3	5324.7(14)	7268.7(10)	2639.1(8)	27.9(2)
N2	6412.1(14)	4933.7(10)	1080.3(8)	26.0(2)
N5	8996.1(14)	8189.3(10)	4212.9(8)	26.8(2)
N6	7047.2(17)	5921.3(11)	5820.5(9)	33.6(3)
C8	3664.3(16)	5496.1(11)	1974.4(9)	23.8(2)
C9	3609.0(16)	6521.2(11)	2597.8(9)	25.1(3)
C7	5519.1(16)	5659.6(12)	1654.6(9)	24.6(2)
C22	6042.0(16)	7507.7(12)	5148.7(9)	25.1(3)
C13	2067.0(17)	4614.5(12)	1790.0(9)	26.4(3)
C1	6460.4(17)	3178.6(12)	241.3(9)	25.9(3)
C14	6455.2(17)	6752.2(12)	2079.6(9)	27.2(3)
C23	4831.9(18)	8306.5(12)	5028.8(9)	27.8(3)
C12	494.5(17)	4762.9(13)	2248.7(9)	28.6(3)
C15	9533.9(18)	9764.8(12)	3213.0(9)	26.9(3)
C21	7841.9(17)	7445.4(12)	4809.0(9)	26.6(3)
C27	5618.0(18)	6539.2(12)	5793.5(9)	28.9(3)
C2	8341.6(18)	3493.0(13)	107.2(9)	28.2(3)
C10	2027.9(17)	6674.9(12)	3061.9(9)	28.1(3)
C11	481.6(17)	5775.7(13)	2881.8(10)	29.2(3)
C16	11423.8(18)	10025.9(12)	3366(1)	29.8(3)
C28	8378.7(19)	6468.6(13)	5248.2(10)	31.9(3)
C3	9233.6(19)	2722.0(14)	-422.5(10)	33.0(3)
C6	5524.0(19)	2071.6(13)	-186.7(10)	31.0(3)
C24	3255.7(18)	8129.3(14)	5551.8(10)	33.0(3)
C20	8833.8(19)	10361.8(13)	2483.1(10)	31.5(3)
C26	4028.3(19)	6354.8(14)	6318.1(10)	33.9(3)
C5	6385(2)	1289.8(14)	-720.9(11)	37.6(3)

Atom	x	y	z	U_{eq}
C25	2862.1(19)	7165.1(15)	6190.7(10)	36.1(3)
C17	12544(2)	10827.6(13)	2787.9(11)	35.5(3)
C19	9927(2)	11160.2(14)	1896.5(11)	38.5(3)
C4	8256(2)	1618.4(15)	-834.1(10)	38.0(3)
C18	11799(2)	11389.9(13)	2052.7(11)	38.6(3)

Table A23: Anisotropic Displacement Parameters ($\times 10^4$) **4a**. The anisotropic displacement factor exponent takes the form: $-2p^2[h^2a^{*2} \times U_{11} + ... + 2hka^* \times b^* \times U_{12}]$

Atom	U_{11}	U_{22}	U_{33}	U_{23}	U_{13}	U_{12}
F1	34.4(4)	39.3(5)	45.4(5)	-5.9(4)	9.6(4)	-3.3(4)
F2	36.0(5)	44.9(5)	46.7(5)	10.8(4)	-1.5(4)	11.8(4)
N4	24.6(5)	24.0(5)	28.0(5)	0.3(4)	3.6(4)	4.6(4)
N1	26.3(5)	27.6(5)	25.8(5)	1.0(4)	3.8(4)	7.7(4)
N3	24.6(5)	25.0(5)	33.7(6)	-3.6(4)	3.3(4)	4.4(4)
N2	25.1(5)	27.9(5)	26.7(5)	0.9(4)	2.6(4)	8.9(4)
N5	25.4(5)	26.3(5)	28.7(5)	1.1(4)	3.6(4)	5.3(4)
N6	33.8(6)	30.8(6)	37.3(6)	10.2(5)	2.5(5)	7.5(5)
C8	23.1(6)	24.7(6)	25.3(5)	2.6(4)	2.2(4)	8.5(4)
C9	23.4(6)	24.2(6)	28.4(6)	1.7(5)	1.7(5)	6.4(5)
C7	22.4(6)	26.2(6)	26.6(6)	1.8(5)	2.5(4)	7.9(4)
C22	23.2(6)	25.9(6)	25.2(6)	0.6(5)	1.8(4)	2.7(4)
C13	26.1(6)	26.3(6)	27.1(6)	1.2(5)	1.3(5)	5.7(5)
C1	29.2(6)	27.3(6)	22.9(5)	2.4(5)	4.3(5)	9.2(5)
C14	21.7(5)	28.9(6)	31.4(6)	1.1(5)	3.1(5)	5.8(5)
C23	27.1(6)	29.1(6)	27.5(6)	1.9(5)	3.3(5)	5.8(5)
C12	23.0(6)	31.2(6)	31.0(6)	4.0(5)	0.7(5)	3.5(5)
C15	28.9(6)	22.9(6)	28.4(6)	-1.9(5)	7.3(5)	4.0(5)
C21	23.7(6)	26.7(6)	29.3(6)	0.6(5)	2.6(5)	5.3(5)
C27	28.4(6)	28.1(6)	29.1(6)	3.5(5)	-0.2(5)	2.6(5)
C2	28.7(6)	31.5(6)	25.5(6)	0.4(5)	2.9(5)	8.4(5)
C10	27.3(6)	28.1(6)	30.9(6)	0.6(5)	3.8(5)	10.3(5)
C11	23.2(6)	34.8(7)	31.5(6)	3.9(5)	5.1(5)	9.8(5)
C16	28.5(6)	27.8(6)	32.4(6)	-1.4(5)	5.5(5)	4.1(5)
C28	28.4(6)	33.4(7)	35.6(7)	5.1(5)	2.6(5)	9.8(5)
C3	31.9(7)	42.4(8)	27.6(6)	1.8(5)	5.9(5)	14.4(6)
C6	32.0(7)	30.8(7)	29.6(6)	2.2(5)	7.2(5)	4.2(5)
C24	27.1(6)	39.7(7)	33.8(7)	2.3(6)	4.1(5)	10.1(5)
C20	31.8(6)	28.7(6)	34.9(7)	0.4(5)	5.9(5)	7.8(5)
C26	30.4(7)	36.5(7)	32.8(7)	8.9(5)	3.1(5)	0.4(5)
C5	48.3(8)	29.7(7)	34.0(7)	-4.1(5)	7.4(6)	6.0(6)
C25	25.9(6)	45.8(8)	35.3(7)	5.2(6)	7.5(5)	3.1(6)
C17	33.0(7)	30.0(7)	40.8(7)	-4.6(6)	11.4(6)	-0.3(5)
C19	52.2(9)	30.5(7)	35.4(7)	7.6(6)	10.1(6)	13.0(6)
C4	47.2(8)	38.6(8)	32.1(7)	-2.9(6)	11.3(6)	17.5(6)
C18	45.2(8)	28.4(7)	41.3(8)	2.8(6)	19.0(6)	4.0(6)

Table A24: Bond Lengths in Å for **4a**.

Atom	Atom	Length/Å
F1	C6	1.3538(16)
F2	C20	1.3542(17)
N4	N5	1.2689(17)
N4	C15	1.4247(16)

Atom	Atom	Length/Å
N1	N2	1.2668(16)
N1	C1	1.4264(15)
N3	C9	1.3824(16)
N3	C14	1.3551(16)
N2	C7	1.3852(16)
N5	C21	1.3800(17)
N6	C27	1.3780(19)
N6	C28	1.3493(18)
C8	C9	1.4125(17)
C8	C7	1.4454(16)
C8	C13	1.3994(17)
C9	C10	1.3962(17)
C7	C14	1.3794(18)
C22	C23	1.3941(19)
C22	C21	1.4502(17)
C22	C27	1.4125(18)
C13	C12	1.3853(18)
C1	C2	1.4005(18)
C1	C6	1.3933(19)
C23	C24	1.3835(18)
C12	C11	1.4043(19)
C15	C16	1.4009(19)
C15	C20	1.388(2)
C21	C28	1.381(2)
C27	C26	1.3931(19)
C2	C3	1.3839(18)
C10	C11	1.3818(19)
C16	C17	1.3839(19)
C3	C4	1.392(2)
C6	C5	1.3813(19)
C24	C25	1.402(2)
C20	C19	1.380(2)
C26	C25	1.380(2)
C5	C4	1.390(2)
C17	C18	1.387(2)
C19	C18	1.389(2)

Table A25: Bond Angles in ° for **4a**.

Atom	Atom	Atom	Angle/°
N5	N4	C15	112.82(11)
N2	N1	C1	112.08(10)
C14	N3	C9	109.26(10)
N1	N2	C7	114.71(10)
N4	N5	C21	114.54(11)
C28	N6	C27	109.71(12)
C9	C8	C7	105.93(10)
C13	C8	C9	119.12(11)
C13	C8	C7	134.94(11)
N3	C9	C8	108.06(10)
N3	C9	C10	129.41(12)
C10	C9	C8	122.53(12)
N2	C7	C8	132.61(11)
C14	C7	N2	120.52(11)
C14	C7	C8	106.80(10)
C23	C22	C21	135.36(12)
C23	C22	C27	119.15(12)
C27	C22	C21	105.32(12)
C12	C13	C8	118.55(12)
C2	C1	N1	124.49(12)
C6	C1	N1	117.96(11)
C6	C1	C2	117.54(12)
N3	C14	C7	109.94(11)
C24	C23	C22	118.81(13)
C13	C12	C11	121.31(12)
C16	C15	N4	124.61(13)
C20	C15	N4	117.63(12)
C20	C15	C16	117.70(12)
N5	C21	C22	131.85(12)
N5	C21	C28	120.93(12)
C28	C21	C22	107.12(12)
N6	C27	C22	108.28(11)
N6	C27	C26	129.45(13)
C26	C27	C22	122.19(13)
C3	C2	C1	120.99(13)
C11	C10	C9	117.03(12)
C10	C11	C12	121.43(12)
C17	C16	C15	120.62(14)
N6	C28	C21	109.54(12)
C2	C3	C4	119.91(13)
F1	C6	C1	119.08(12)
F1	C6	C5	118.45(13)
C5	C6	C1	122.47(13)
C23	C24	C25	121.19(14)
F2	C20	C15	118.33(12)
F2	C20	C19	119.11(14)
C19	C20	C15	122.55(14)
C25	C26	C27	117.43(13)
C6	C5	C4	118.78(13)
C26	C25	C24	121.23(13)
C16	C17	C18	120.12(14)
C20	C19	C18	118.69(15)
C5	C4	C3	120.31(13)
C17	C18	C19	120.30(13)

Table A26: Hydrogen Fractional Atomic Coordinates ($\times 10^4$) and Equivalent Isotropic Displacement Parameters ($Å^2 \times 10^3$) for **4a**. U_{eq} is defined as 1/3 of the trace of the orthogonalised U_{ij}.

Atom	x	y	z	U_{eq}
H3	5627.01	7953.54	2968.05	33
H6	7084.78	5283.37	6152.01	40
H13	2061.16	3943.61	1368.79	32
H14	7680.75	7085.05	1994.64	33
H23	5079.63	8946.96	4604.94	33
H12	-573.75	4180.23	2135.06	34
H2	9001.18	4230.94	378.24	34
H10	2016.03	7352.24	3473.98	34
H11	-590.92	5842.71	3186.53	35
H16	11930.57	9657.16	3860.8	36
H28	9487.56	6225.26	5162.8	38
H3A	10484.3	2941.02	-503.26	40
H24	2442.72	8659.48	5478.19	40
H26	3763.19	5710.61	6737.81	41
H5	5724.5	557.18	-999.75	45
H25	1795.15	7069.6	6535.24	43
H17	13797.61	10989.66	2892.38	43
H19	9420.95	11537.04	1406.28	46
H4	8858.29	1098.27	-1186.59	46
H18	12557.44	11922.98	1662.65	46

*Compound **8a'***

Experimental. Single clear orange prism-shaped crystals of **8a'** were obtained by recrystallisation from chloroform/heptane. A suitable crystal ($0.28 \times 0.12 \times 0.11$) mm^3 was selected and mounted on a MITIGEN holder oil on a SuperNova, Single source at offset, Atlas diffractometer. The crystal was kept at T = 296.95(10) K during data collection. Using **Olex2**,[3] the structure was solved with the **ShelXT** structure solution program, using the Intrinsic Phasing solution method.[4] The model was refined with version 2016/6 of **ShelXL** using Least Squares minimisation.[5]

Crystal Data. $C_{10}H_7N_3$, M_r = 169.19, monoclinic, C2/c (No. 15), a = 9.5514(3) Å, b = 9.5468(2) Å, c = 17.8087(5) Å, □ = 105.517(3)°, □ = □ = 90°, V = 1564.70(8) $Å^3$, T = 296.95(10) K, Z = 8, Z' = 1, □ ($CuK_□$) = 0.727, 14499 reflections measured, 1590 unique (R_{int} = 0.0270) which were used in all calculations. The final wR_2 was 0.1093 (all data) and R_1 was 0.0473 (I > 2(I)).

Table A27:

Formula	$C_{10}H_7N_3$
$D_{calc.}$/ g cm^{-3}	1.436
m/mm^{-1}	0.727
Formula Weight	169.19
Colour	clear orange
Shape	prism
Size/mm^3	$0.28 \times 0.12 \times 0.11$
T/K	296.95(10)

Crystal System	monoclinic
Hooft Parameter	0.4(2)
Space Group	C2/c
a/Å	9.5514(3)
b/Å	9.5468(2)
c/Å	17.8087(5)
a/°	90
b/°	105.517(3)
g/°	90
V/Å^3	1564.70(8)
Z	8
Z'	1
Wavelength/Å	1.54184
Radiation type	CuK$_a$
Θ_{min}/°	5.155
Θ_{max}/°	73.833
Measured Refl.	14499
Independent Refl.	1590
Reflections Used	1524
R_{int}	0.027
Parameters	182
Restraints	0
Largest Peak	0.174
Deepest Hole	-0.262
GooF	1.201
wR_2 (all data)	0.1093
wR_2	0.1086
R_1 (all data)	0.0486
R_1	0.0473

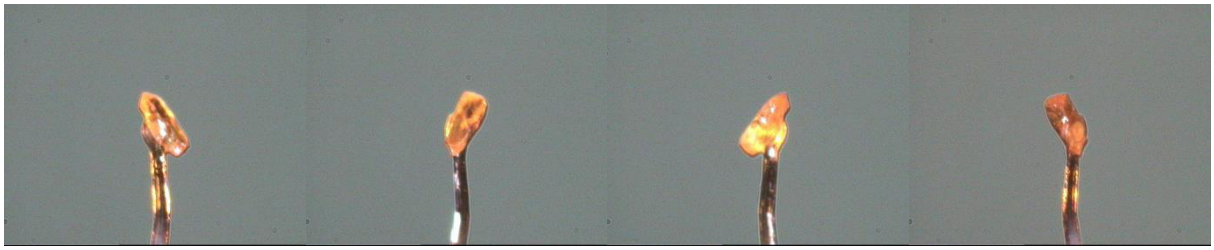

Figure A31: Images of the crystal on the diffractometer.

Table A28: Bond Angles in ° for **8a'**.

Atom	**Atom**	**Atom**	**Angle/°**
C002	N001	C003	125.49(14)
C004	N001	C002	125.89(14)
C004	N001	C003	108.62(13)
N001	C002	C009	107.8(2)

Atom	Atom	Atom	Angle/°
N001	C002	C00A	107.1(2)
C1	C002	N001	132.1(2)
C1	C002	C009	120.1(3)
C4	C002	N001	132.9(3)
C4	C002	C00A	120.0(3)
N001	C003	C006	107.87(14)
N00B	C003	N001	122.38(18)
N00B	C003	C006	129.76(18)
N001	C004	C005	108.01(14)
N00C	C004	N001	122.36(18)
N00C	C004	C005	129.63(19)
C004	C005	C006	107.75(15)
C003	C006	C005	107.75(15)
C1	C007	C3	120.4(7)
C4	C008	C1AA	120.0(7)
N00D	C009	C002	123.6(3)
C0AA	C009	C002	118.0(3)
C0AA	C009	N00D	118.4(4)
N00E	C00A	C002	124.1(4)
N00E	C00A	C2	118.4(4)
C2	C00A	C002	117.5(4)
C003	N00B	N00D	120.9(2)
C004	N00C	N00E	120.7(2)
N00B	N00D	C009	119.9(3)
N00C	N00E	C00A	119.9(3)
C002	C1	C007	121.0(5)
C1AA	C2	C00A	120.1(4)
C002	C4	C008	121.9(5)
C3	C0AA	C009	119.9(4)
C2	C1AA	C008	120.5(5)
C0AA	C3	C007	120.6(5)

Table A29: Hydrogen Fractional Atomic Coordinates ($\times 10^4$) and Equivalent Isotropic Displacement Parameters ($Å^2 \times 10^3$) for **8a'**. U_{eq} is defined as 1/3 of the trace of the orthogonalised U_{ij}.

Atom	x	y	z	U_{eq}
H003	4540.47	2268.13	3619.5	27
H004	1578.23	5233.93	3620.14	27
H005	1449.38	4672.87	2242.9	31
H006	3290.21	2830.12	2241.7	31
H007	3394.28	4800.84	6387.54	28
H008	5497.87	2699.84	6384.4	27
H1	2405.29	5136.64	5073.54	28
H2	2347.02	5640.42	5962.46	29
H4	5164.65	2373.98	5076.38	28
H0AA	6117.08	1868.52	5960.98	31
H1AA	4082.82	4332.36	6834.25	30
H3	5241.68	3161.46	6832.56	31

Table A30: Atomic Occupancies for all atoms that are not fully occupied in **8a'**.

Atom	Occupancy
H003	0.486(2)
H004	0.514(2)
C007	0.514(2)
H007	0.514(2)
C008	0.486(2)
H008	0.486(2)
C009	0.514(2)
C00A	0.486(2)
N00B	0.514(2)
N00C	0.486(2)
N00D	0.514(2)
N00E	0.486(2)
C1	0.514(2)
H1	0.514(2)
C2	0.486(2)
H2	0.486(2)
C4	0.486(2)
H4	0.486(2)
C0AA	0.514(2)
H0AA	0.514(2)
C1AA	0.486(2)
H1AA	0.486(2)
C3	0.514(2)
H3	0.514(2)

*Compound **8a''***

Experimental. Single clear intense brown prism-shaped crystals of **8a''** were obtained by recrystallisation from chloroform/methanol/heptane. A suitable crystal (0.42×0.19×0.12) mm^3 was selected and mounted on a MITIGEN holder oil on a GV1000, TitanS2 diffractometer. The crystal was kept at T = 123.0(2) K during data collection. Using **Olex2**,[3] the structure was solved with the **ShelXT** structure solution program, using the Intrinsic Phasing solution method.[4] The model was refined with version 2016/6 of **ShelXL** using Least Squares minimisation.[5]

Crystal Data. $C_{18}H_{12}N_4$, M_r = 284.32, monoclinic, $P2_1/n$ (No. 14), a = 14.4932(3) Å, b = 10.3321(2) Å, c = 19.1214(4) Å, □ = 108.602(2)°, □ = □ = 90°, V = 2713.75(10) $Å^3$, T = 123.0(2) K, Z = 8, Z' = 2, □ (CuK□) = 0.683, 66316 reflections measured, 5432 unique (R_{int} = 0.0802) which were used in all calculations. The final wR_2 was 0.1131 (all data) and R_1 was 0.0401 (I > 2(I)).

Table A31:

Formula	$C_{18}H_{12}N_4$
$D_{calc.}$/ g cm^{-3}	1.392
m/mm^{-1}	0.683
Formula Weight	284.32
Colour	clear intense brown
Shape	prism
Size/mm^3	0.42×0.19×0.12

T/K	123.0(2)
Crystal System	monoclinic
Space Group	$P2_1/n$
a/Å	14.4932(3)
b/Å	10.3321(2)
c/Å	19.1214(4)
a/°	90
b/°	108.602(2)
g/°	90
V/Å^3	2713.75(10)
Z	8
Z'	2
Wavelength/Å	1.54184
Radiation type	CuK_a
Q_{min}/°	3.361
Q_{max}/°	73.966
Measured Refl.	66316
Independent Refl.	5432
Reflections Used	4822
R_{int}	0.0802
Parameters	397
Restraints	0
Largest Peak	0.199
Deepest Hole	-0.326
GooF	1.05
wR_2 (all data)	0.1131
wR_2	0.1084
R_1 (all data)	0.0444
R_1	0.0401

Figure 32: Images of the crystal of the diffractometer.

Table A32: Fractional Atomic Coordinates (×10^4) and Equivalent Isotropic Displacement Parameters (Å^2×10^3) for **8a''**. U_{eq} is defined as 1/3 of the trace of the orthogonalised U_{ij}.

Atom	**x**	**y**	**z**	U_{eq}
N(6)	4915.7(7)	2364.8(9)	3468.6(5)	25.3(2)
N(2)	7526.8(7)	4907.4(9)	4024.8(5)	26.0(2)

Atom	x	y	z	U_{eq}
N(5)	4770.5(7)	6909.7(10)	3172.6(6)	33.0(2)
N(7)	5056.0(7)	126.5(10)	3881.4(6)	33.2(2)
N(8)	5031.6(8)	-275(1)	3231.9(6)	34.3(2)
N(3)	7330.2(8)	2686.8(10)	3581.7(6)	35.5(2)
N(4)	7407.7(8)	2257.3(10)	4238.9(6)	36.6(3)
N(1)	7721.3(8)	9442.2(10)	4360.5(7)	40.2(3)
C(19)	4980.7(8)	1974.9(11)	2787.2(6)	25.4(2)
C(1)	7489.3(8)	4493.1(11)	4711.4(6)	26.4(2)
C(29)	4667.8(8)	4788.6(11)	3389.6(6)	26.8(2)
C(10)	7561.4(8)	6108.3(11)	3719.8(6)	27.7(2)
C(31)	3974.1(8)	6463.2(11)	2620.5(7)	29.7(3)
C(25)	5010.2(8)	1401.0(11)	4011.3(7)	29.2(3)
C(30)	3877.7(8)	5130.6(11)	2740.1(6)	26.9(2)
C(28)	4844.3(8)	3548.4(11)	3777.5(6)	27.7(2)
C(20)	5005.1(8)	626.2(12)	2685.4(7)	29.8(3)
C(11)	7786.5(8)	7323.6(11)	4125.3(6)	28.3(2)
C(24)	5051.0(8)	2810.1(12)	2232.6(6)	29.7(3)
C(12)	8601.5(8)	7639.4(12)	4764.2(6)	29.3(3)
C(2)	7434.6(8)	5313.8(12)	5276.6(6)	30.0(3)
C(36)	5175.2(9)	5912.5(11)	3631.9(7)	29.6(3)
C(7)	7359.2(9)	3968.2(12)	3460.9(7)	30.4(3)
C(6)	7462.4(9)	3141.7(12)	4800.9(7)	31.5(3)
C(13)	8528.6(9)	8974.0(12)	4895.4(7)	34.9(3)
C(35)	3085.7(9)	4457.9(13)	2267.1(7)	33.5(3)
C(17)	9392.0(9)	6946.9(14)	5226.3(7)	36.1(3)
C(9)	7398.6(9)	5912.7(13)	2967.7(7)	34.4(3)
C(26)	5010.2(9)	1999.2(12)	4658.7(7)	34.8(3)
C(18)	7286.2(9)	8462.2(12)	3903.6(7)	33.9(3)
C(23)	5113.5(9)	2302.9(13)	1583.6(7)	35.0(3)
C(27)	4908(1)	3312.4(12)	4508.7(7)	34.8(3)
C(32)	3324.6(9)	7125.9(13)	2033.7(8)	38.3(3)
C(3)	7374.8(9)	4785.6(13)	5923.6(7)	35.2(3)
C(8)	7271.8(9)	4606.5(13)	2807.1(7)	35.9(3)
C(21)	5046.4(9)	141.3(13)	2013.5(8)	37.8(3)
C(5)	7430.3(10)	2638.7(13)	5472.9(8)	39.9(3)
C(34)	2433.4(9)	5117.8(14)	1694.8(8)	39.7(3)
C(4)	7385.3(10)	3452.3(14)	6028.1(8)	40.2(3)
C(22)	5098(1)	970.9(14)	1467.9(8)	39.9(3)
C(33)	2556.9(10)	6434.3(15)	1574.8(8)	43.0(3)
C(16)	10067.3(10)	7590.1(16)	5793.5(8)	45.3(3)
C(14)	9200.5(11)	9616.8(15)	5476.5(9)	48.8(4)
C(15)	9968.6(12)	8904.4(17)	5921.3(9)	52.4(4)

Table A33: Anisotropic Displacement Parameters ($\times 10^4$) **8a''**. The anisotropic displacement factor exponent takes the form: $-2\pi^2[h^2a^{*2} \times U_{11} + ... + 2hka^* \times b^* \times U_{12}]$

Atom	U_{11}	U_{22}	U_{33}	U_{23}	U_{13}	U_{12}
N(6)	29.5(5)	19.2(5)	27.1(5)	1.7(4)	8.9(4)	0.0(4)
N(2)	30.2(5)	21.3(5)	27.5(5)	-0.5(4)	10.5(4)	1.7(4)
N(5)	36.5(5)	17.7(5)	44.8(6)	0.6(4)	12.8(4)	-2.2(4)
N(7)	36.9(5)	21.6(5)	40.7(6)	4.3(4)	11.9(4)	1.6(4)
N(8)	39.1(6)	20.7(5)	44.8(6)	1.1(4)	15.7(5)	0.6(4)

Atom	U_{11}	U_{22}	U_{33}	U_{23}	U_{13}	U_{12}
N(3)	38.7(6)	25.3(5)	43.7(6)	-4.8(5)	14.9(5)	-0.2(4)
N(4)	41.8(6)	22.8(5)	47.2(6)	1.1(5)	16.9(5)	2.2(4)
N(1)	45.8(6)	20.0(5)	53.4(7)	0.7(5)	13.8(5)	2.7(4)
C(19)	24.8(5)	22.4(6)	29.4(6)	-1.1(4)	9.0(4)	0.8(4)
C(1)	26.5(5)	24.1(6)	30.0(6)	2.6(5)	10.9(4)	0.5(4)
C(29)	33.4(6)	19.8(5)	29.7(6)	-0.3(4)	13.5(5)	0.6(4)
C(10)	30.4(5)	22.6(6)	31.2(6)	3.3(5)	11.5(4)	1.6(4)
C(31)	32.1(6)	23.4(6)	37.1(6)	1.1(5)	16.3(5)	2.6(4)
C(25)	32.1(6)	22.4(6)	31.8(6)	6.4(5)	8.5(5)	-0.7(4)
C(30)	31.4(6)	22.6(6)	30.5(6)	-1.3(4)	15.1(5)	1.7(4)
C(28)	33.5(6)	20.6(6)	30.0(6)	-1.4(4)	11.4(5)	-1.4(4)
C(20)	28.5(5)	22.6(6)	39.3(6)	-1.5(5)	12.3(5)	0.0(4)
C(11)	31.7(6)	23.7(6)	31.6(6)	2.7(5)	13.0(5)	0.0(4)
C(24)	32.7(6)	25.1(6)	33.4(6)	1.9(5)	13.4(5)	3.4(4)
C(12)	32.2(6)	27.4(6)	31.8(6)	2.9(5)	14.8(5)	-1.9(5)
C(2)	32.3(6)	27.8(6)	32.2(6)	-0.3(5)	13.4(5)	-1.5(5)
C(36)	33.3(6)	22.9(6)	33.4(6)	-1.3(5)	11.5(5)	-0.2(4)
C(7)	32.6(6)	25.5(6)	33.8(6)	-5.1(5)	11.6(5)	0.7(5)
C(6)	31.8(6)	24.3(6)	39.7(7)	3.5(5)	13.1(5)	2.3(5)
C(13)	39.3(6)	26.5(6)	41.4(7)	-0.7(5)	16.4(5)	-5.4(5)
C(35)	35.4(6)	28.4(6)	38.9(6)	-6.0(5)	15.1(5)	-2.4(5)
C(17)	36.0(6)	36.5(7)	38.0(7)	8.1(5)	14.9(5)	2.0(5)
C(9)	41.2(6)	32.0(7)	30.7(6)	3.8(5)	12.8(5)	-0.8(5)
C(26)	45.7(7)	30.3(6)	28.0(6)	4.5(5)	11.0(5)	-2.9(5)
C(18)	35.3(6)	25.7(6)	39.7(7)	3.3(5)	10.8(5)	1.0(5)
C(23)	36.7(6)	37.4(7)	33.9(6)	3.9(5)	15.4(5)	5.1(5)
C(27)	48.6(7)	27.0(6)	29.7(6)	-2.2(5)	13.9(5)	-3.0(5)
C(32)	39.9(7)	28.8(6)	48.2(8)	9.3(6)	17.1(6)	9.1(5)
C(3)	36.5(6)	38.9(7)	32.9(6)	-1.0(5)	14.7(5)	-3.0(5)
C(8)	42.5(7)	36.1(7)	29.9(6)	-5.7(5)	12.6(5)	-2.1(5)
C(21)	42.1(7)	26.1(6)	49.3(8)	-9.5(6)	20.4(6)	-1.9(5)
C(5)	45.4(7)	28.3(7)	49.1(8)	12.6(6)	19.5(6)	4.2(5)
C(34)	31.6(6)	44.2(8)	41.4(7)	-8.8(6)	8.8(5)	2.0(5)
C(4)	43.2(7)	44.1(8)	36.7(7)	12.3(6)	17.3(6)	1.4(6)
C(22)	43.8(7)	41.2(8)	38.9(7)	-9.9(6)	19.0(6)	-0.3(6)
C(33)	37.9(7)	46.3(8)	42.5(7)	6.2(6)	9.6(6)	12.8(6)
C(16)	34.7(7)	58.6(9)	40.0(7)	12.4(7)	8.2(6)	-4.9(6)
C(14)	55.7(8)	37.2(8)	53.3(9)	-9.0(7)	16.9(7)	-15.4(7)
C(15)	48.9(8)	58.1(10)	45.7(8)	-4.6(7)	8.7(6)	-21.1(7)

Table 34: Bond Lengths in Å for **8a''**.

Atom	Atom	Length/Å
N(6)	C(19)	1.3954(14)
N(6)	C(25)	1.4130(14)
N(6)	C(28)	1.3762(15)
N(2)	C(1)	1.3984(14)
N(2)	C(10)	1.3787(15)
N(2)	C(7)	1.4129(15)
N(5)	C(31)	1.3720(16)
N(5)	C(36)	1.3594(16)
N(7)	N(8)	1.2991(15)
N(7)	C(25)	1.3456(16)
N(8)	C(20)	1.3911(16)
N(3)	N(4)	1.3035(16)
N(3)	C(7)	1.3469(16)
N(4)	C(6)	1.3934(17)
N(1)	C(13)	1.3733(17)
N(1)	C(18)	1.3545(17)
C(19)	C(20)	1.4091(16)
C(19)	C(24)	1.3957(16)
C(1)	C(2)	1.3956(16)
C(1)	C(6)	1.4087(16)

Atom	Atom	Length/Å
C(29)	C(30)	1.4392(16)
C(29)	C(28)	1.4617(16)
C(29)	C(36)	1.3735(16)
C(10)	C(11)	1.4570(17)
C(10)	C(9)	1.3957(17)
C(31)	C(30)	1.4099(16)
C(31)	C(32)	1.3928(17)
C(25)	C(26)	1.3837(18)
C(30)	C(35)	1.3987(16)
C(28)	C(27)	1.3930(17)
C(20)	C(21)	1.3979(18)
C(11)	C(12)	1.4400(17)
C(11)	C(18)	1.3759(17)
C(24)	C(23)	1.3765(17)
C(12)	C(13)	1.4116(17)
C(12)	C(17)	1.3999(17)

Atom	Atom	Length/Å
C(2)	C(3)	1.3800(17)
C(7)	C(8)	1.3830(17)
C(6)	C(5)	1.4007(18)
C(13)	C(14)	1.3905(19)
C(35)	C(34)	1.3769(19)
C(17)	C(16)	1.378(2)
C(9)	C(8)	1.3833(18)
C(26)	C(27)	1.3848(18)
C(23)	C(22)	1.3929(19)
C(32)	C(33)	1.377(2)
C(3)	C(4)	1.391(2)
C(21)	C(22)	1.3705(19)
C(5)	C(4)	1.372(2)
C(34)	C(33)	1.400(2)
C(16)	C(15)	1.395(2)
C(14)	C(15)	1.379(2)

Table 35: Bond Angles in ° for **8a''**.

Atom	Atom	Atom	Angle/°
C(19)	N(6)	C(25)	117.56(10)
C(28)	N(6)	C(19)	133.95(10)
C(28)	N(6)	C(25)	108.30(9)
C(1)	N(2)	C(7)	117.23(10)
C(10)	N(2)	C(1)	133.65(10)
C(10)	N(2)	C(7)	108.41(9)
C(36)	N(5)	C(31)	109.03(10)
N(8)	N(7)	C(25)	120.07(10)
N(7)	N(8)	C(20)	119.36(10)
N(4)	N(3)	C(7)	120.14(11)
N(3)	N(4)	C(6)	119.11(10)
C(18)	N(1)	C(13)	109.13(10)
N(6)	C(19)	C(20)	115.26(10)
N(6)	C(19)	C(24)	125.02(10)
C(24)	C(19)	C(20)	119.69(11)
N(2)	C(1)	C(6)	115.36(10)
C(2)	C(1)	N(2)	124.74(11)
C(2)	C(1)	C(6)	119.84(11)
C(30)	C(29)	C(28)	127.98(10)
C(36)	C(29)	C(30)	106.05(10)
C(36)	C(29)	C(28)	125.58(11)
N(2)	C(10)	C(11)	125.64(10)
N(2)	C(10)	C(9)	106.77(10)
C(9)	C(10)	C(11)	127.49(11)
N(5)	C(31)	C(30)	107.82(10)
N(5)	C(31)	C(32)	129.87(11)
C(32)	C(31)	C(30)	122.30(12)
N(7)	C(25)	N(6)	123.58(11)
N(7)	C(25)	C(26)	128.04(11)
C(26)	C(25)	N(6)	108.34(10)
C(31)	C(30)	C(29)	106.68(10)
C(35)	C(30)	C(29)	134.34(11)

Atom	Atom	Atom	Angle/°
C(35)	C(30)	C(31)	118.93(11)
N(6)	C(28)	C(29)	125.88(10)
N(6)	C(28)	C(27)	106.58(10)
C(27)	C(28)	C(29)	127.41(11)
N(8)	C(20)	C(19)	123.65(11)
N(8)	C(20)	C(21)	116.85(11)
C(21)	C(20)	C(19)	119.45(11)
C(12)	C(11)	C(10)	129.09(11)
C(18)	C(11)	C(10)	124.50(11)
C(18)	C(11)	C(12)	106.06(11)
C(23)	C(24)	C(19)	119.43(11)
C(13)	C(12)	C(11)	106.53(11)
C(17)	C(12)	C(11)	134.78(12)
C(17)	C(12)	C(13)	118.66(12)
C(3)	C(2)	C(1)	119.29(11)
N(5)	C(36)	C(29)	110.40(11)
N(3)	C(7)	N(2)	123.47(11)
N(3)	C(7)	C(8)	128.67(11)
C(8)	C(7)	N(2)	107.83(10)
N(4)	C(6)	C(1)	123.60(11)
N(4)	C(6)	C(5)	116.99(11)
C(5)	C(6)	C(1)	119.31(12)
N(1)	C(13)	C(12)	107.82(11)
N(1)	C(13)	C(14)	129.79(13)
C(14)	C(13)	C(12)	122.39(13)
C(34)	C(35)	C(30)	118.79(12)
C(16)	C(17)	C(12)	118.89(13)
C(8)	C(9)	C(10)	109.68(11)
C(25)	C(26)	C(27)	106.43(11)
N(1)	C(18)	C(11)	110.45(11)
C(24)	C(23)	C(22)	121.13(12)
C(26)	C(27)	C(28)	110.35(11)

Atom	Atom	Atom	Angle/°
C(33)	C(32)	C(31)	117.35(12)
C(2)	C(3)	C(4)	121.28(12)
C(7)	C(8)	C(9)	107.29(11)
C(22)	C(21)	C(20)	120.27(12)
C(4)	C(5)	C(6)	120.41(12)
C(35)	C(34)	C(33)	121.33(12)
C(5)	C(4)	C(3)	119.78(12)
C(21)	C(22)	C(23)	119.94(12)
C(32)	C(33)	C(34)	121.28(13)
C(17)	C(16)	C(15)	121.37(14)
C(15)	C(14)	C(13)	117.38(14)
C(14)	C(15)	C(16)	121.29(14)

Table A36: Hydrogen Fractional Atomic Coordinates ($\times 10^4$) and Equivalent Isotropic Displacement Parameters ($Å^2 \times 10^3$) for **8a''**. U_{eq} is defined as 1/3 of the trace of the orthogonalised U_{ij}.

Atom	x	y	z	U_{eq}
H(5)	4979.92	7694.04	3220.52	40
H(1)	7523.45	10231.75	4321.75	48
H(24)	5055.49	3701.47	2301.07	36
H(2)	7438.4	6207.05	5217.73	36
H(36)	5718.76	5981.61	4050.91	36
H(35)	3001.23	3580.89	2337.78	40
H(17)	9460.35	6067.34	5151.74	43
H(9)	7378.36	6562.07	2626.32	41
H(26)	5067.36	1598.64	5106.1	42
H(18)	6727.99	8546.91	3497.27	41
H(23)	5167.09	2859.03	1216.07	42
H(27)	4885.23	3946.55	4847.93	42
H(32)	3406.28	8000.66	1955.05	46
H(3)	7326.54	5331.49	6297.06	42
H(8)	7150.4	4227.75	2345.24	43
H(21)	5038.75	-747.87	1936.34	45
H(5A)	7439.44	1747.51	5543.27	48
H(34)	1900.04	4680.44	1381.77	48
H(4)	7362.01	3113.85	6472.77	48
H(22)	5122.63	644.88	1020.88	48
H(33)	2111.81	6849.51	1177.38	52
H(16)	10599.83	7138.74	6097.53	54
H(14)	9134.26	10492.79	5561.65	59
H(15)	10430.1	9307.88	6314.16	63

6. Optimized Structures

6.1. Selection of most stable conformers

Due to the high number of structures involved in the study, we decided to preliminary screen the most stable conformer of each molecule in its *E*- and *Z*-configuration at the computational cheap B3LYP/3-21G level of theory. In particular, through rotation around single bonds (*cf.* Figure A33) different conformers were optimized using the Gaussian 16, Revision A.03 software package.[6]

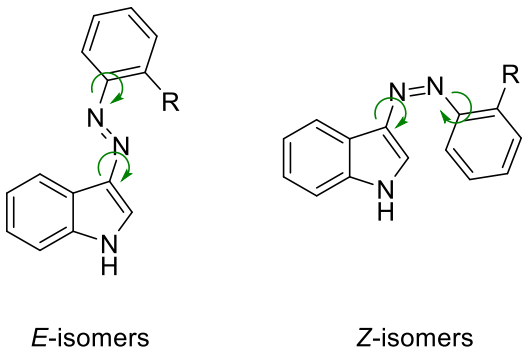

Figure A33: Rotation around single-bonds generates different conformers of both photoisomers.

The energies of the obtained, ground-state optimized structures were compared and the thermodynamically most stable one was further optimized at the B3LYP/6-311+G(2d,p) level of theory. The cartesian coordinates and optimized minimum energies are provided in the following section.

The UV/Vis spectra are printed using gnuplot as ε vs λ (excitation wavelength in nm) with the peaks, furnished by the calculation, assuming a gaussian band shape (characterized by a standard deviation s=0.4eV). The equation for the simulated spectra follows the one described in the Gaussian White Papers[1]:

$$\varepsilon(\lambda) = \sum_{i=1}^{n} \varepsilon_i(\lambda) = \sum_{i=1}^{n} \left\{ 1.3062974 \times 10^8 \frac{f_i}{\frac{10^7}{3099.6}} \exp\left[-\left(\frac{{}^1\!/\!_\lambda - {}^1\!/\!_{\lambda_i}}{\frac{1}{3099.6}} \right)^2 \right] \right\}$$

with f_i the computed oscillator strengths, referred to a specific wavelength λ_i.

[1] http://dev.gaussian.com/uvvisplot/

6.2. Cartesian Coordinates of the optimizes structures

6.2.1. *E*-isomers

***E*-1a**

C	-9.6872703203	0.7975455704	1.0134847347
C	-9.8379456993	2.1621515239	0.762393773
C	-8.7515754188	2.9057112926	0.3137552264
C	-7.5220904316	2.2891308025	0.117233506
C	-7.3679126933	0.9235936823	0.3676346424
C	-8.4637242361	0.1762593514	0.819602174
N	-6.0712841141	0.399629475	0.133374074
N	-5.9491057746	-0.8337725713	0.3649581614
C	-4.6935501683	-1.3618494747	0.1425003584
C	-3.4451711152	-0.7819741024	-0.31557527
C	-2.506002377	-1.8398500951	-0.3396663213
N	-3.1559658262	-2.9924226619	0.0813202506
C	-4.4563906063	-2.7038928623	0.3670986547
C	-3.0286261039	0.497805502	-0.7014713999
C	-1.7110423241	0.6810714808	-1.0930589799
C	-0.7977304597	-0.3842661032	-1.1086666807
C	-1.1832100805	-1.6616969831	-0.7315549021
H	-10.5339016809	0.2178338383	1.3631573414
H	-10.7983062914	2.6396194693	0.9167472723
H	-8.861671055	3.9655181788	0.1168934218
H	-6.6634491826	2.8497223328	-0.2316534885
H	-8.3372470726	-0.8803796584	1.011418721
H	-2.7327231829	-3.9012770656	0.1633739032
H	-5.1466290504	-3.4558389838	0.7129988428
H	-3.7304558308	1.3183363651	-0.6898412966
H	-1.3771431935	1.6668153173	-1.3938167736
H	0.2245719623	-0.2070683317	-1.4200203961
H	-0.4799914216	-2.4864542851	-0.7426215639

Energy= -704.5323516

Zero-point correction= 0.219034 (Hartree/Particle)

Sum of electronic and zero-point Energies= -704.313318

Sum of electronic and thermal Energies= -704.300447

Sum of electronic and thermal Enthalpies= -704.299503

Sum of electronic and thermal Free Energies= -704.354217

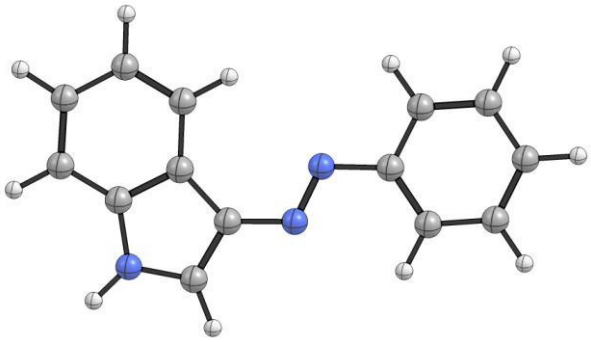

***E*-1b**

C	-9.6850260581	1.2503519004	1.0224026794
C	-9.8474941478	2.611164129	0.7586442324
C	-8.7703378908	3.3565613627	0.2910417335
C	-7.5389453615	2.7458300486	0.0883735206
C	-7.3726207846	1.3838942101	0.3515154054
C	-8.4594223675	0.6348708046	0.8225518567
N	-6.0754601742	0.865959613	0.109441071
N	-5.9428972636	-0.3647666898	0.3552220131
C	-4.6891619191	-0.8889337017	0.1264453004
C	-3.4487987152	-0.3136790792	-0.3516334539
C	-2.5096447919	-1.3734979759	-0.3692086697
N	-3.1446744496	-2.5287180228	0.0737479512
C	-4.4399057355	-2.2280824686	0.3653552709
C	-3.0386959308	0.9601593773	-0.7593722175
C	-1.7247581945	1.1400814284	-1.1670096036
C	-0.8108748053	0.076309356	-1.1766315799
C	-1.1904567459	-1.197354556	-0.7774613728
C	-2.5207858535	-3.8298234952	0.1997374209
H	-10.5242233489	0.6687752786	1.3867682377
H	-10.8093287881	3.0841034496	0.9177609691
H	-8.8891909907	4.413547624	0.0840905553
H	-6.6876745373	3.3083203546	-0.2752730888
H	-8.3242386231	-0.4188669831	1.0241703075
H	-5.1248112265	-2.9775057937	0.7288323755
H	-3.7419570069	1.7796401411	-0.7521563778
H	-1.395525889	2.1220332408	-1.4849753111
H	0.2080894281	0.250227154	-1.5007011435
H	-0.4825807292	-2.0171549491	-0.7859722017
H	-1.6857815906	-3.7925156532	0.9032796296
H	-3.2563489721	-4.5420890828	0.5686244793
H	-2.1511527063	-4.1773717019	-0.7678179093

Energy= -743.8530277

Zero-point correction= 0.246823 (Hartree/Particle)

Sum of electronic and zero-point Energies= -743.606205

Sum of electronic and thermal Energies= -743.591674

Sum of electronic and thermal Enthalpies= -743.590730

Sum of electronic and thermal Free Energies= -743.649373

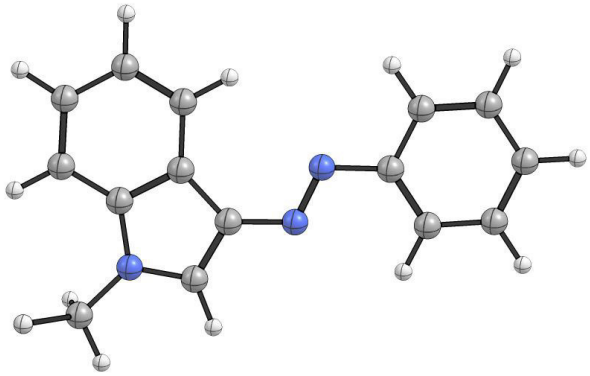

***E*-1c**

C	-3.5321924371	1.5055976947	-0.096208515
C	-2.5359051484	0.5044270998	-0.0640786947
N	-3.1837819541	-0.7350663059	-0.0240505625
C	-4.5390442757	-0.5259201142	-0.0413433855
C	-4.80383431	0.8286248368	-0.0804163343
C	-3.1542069918	2.8506401575	-0.1545028865
C	-1.8054188109	3.1614374928	-0.1887862078
C	-0.8281602164	2.1523854518	-0.1767801954
C	-1.1773552398	0.8119717957	-0.1175520347
N	-6.0201645199	1.4927301374	-0.0879342302
N	-7.0405830657	0.7546098855	-0.0899703785
C	-8.279693687	1.4387410791	-0.0939675918
C	-9.4168319906	0.6270220825	-0.1020439051
C	-10.685049904	1.1945432225	-0.1066065197
C	-10.8267392769	2.5780371278	-0.1028862481
C	-9.6923227216	3.3917113519	-0.0943745615
C	-8.4246130647	2.8329297741	-0.089741705
C	-2.5683367443	-2.0163312722	0.0083106376
C	-2.9735680877	-3.0004881013	-0.8926824151
C	-2.3948264824	-4.263037791	-0.8445666512
C	-1.4015473424	-4.5451189868	0.0874996428
C	-0.9952695467	-3.5587669335	0.9808858932
C	-1.57919465	-2.2982053672	0.9500904243
H	-5.2278908996	-1.3513967846	0.0078370183
H	-3.9085168832	3.6266618872	-0.1779976586
H	-1.4947074232	4.1983195258	-0.233290716
H	0.2193957435	2.4249956571	-0.2182905703
H	-0.4197177162	0.039718947	-0.1221139389
H	-9.2821942692	-0.447753694	-0.1044317521
H	-11.5617306337	0.5578198932	-0.1128354076
H	-11.8141345585	3.0242555391	-0.1062138316
H	-9.8034006436	4.4699660937	-0.0910159838
H	-7.5396588346	3.4542027882	-0.0826039537
H	-2.7137186724	-5.0235214747	-1.5470052608
H	-0.2297898402	-3.7738860373	1.7166408902
H	-1.2866833367	-1.5393212597	1.6640786092
H	-0.9474312473	-5.527859674	0.1184688351
H	-3.728734297	-2.7689695148	-1.6335009844

Energy= -935.638957

Sum of electronic and zero-point Energies= -935.339836

Sum of electronic and thermal Energies= -935.322258

Sum of electronic and thermal Enthalpies= -935.321314

Sum of electronic and thermal Free Energies= -935.387998

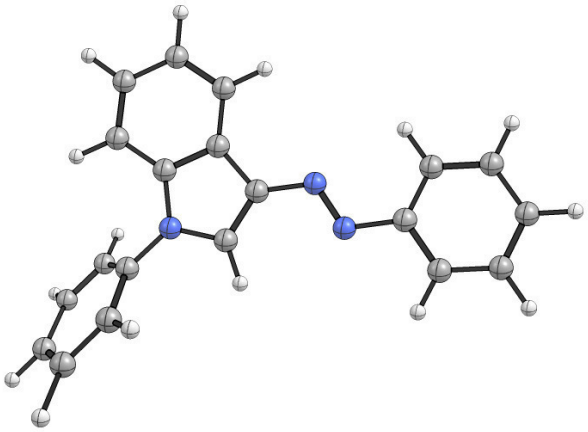

***E*-1d**

C	-3.5437745459	1.5269543566	0.5878631307
C	-2.6054369311	0.4722271924	0.685143512
N	-3.169493065	-0.6721900782	0.1185707625
C	-4.4218050164	-0.3606261931	-0.324702314
C	-4.7083175401	0.9669090056	-0.0669856717
C	-3.2001514585	2.7862337513	1.0934478525
C	-1.9509126423	2.955104117	1.6721752032
C	-1.0364583838	1.8944216449	1.757439248
C	-1.3508330652	0.6361891023	1.264527904
N	-5.927049232	1.4970739755	-0.4332982487
N	-6.0990479456	2.7164244371	-0.1577895111
C	-7.3587217937	3.2404895916	-0.5432892409
C	-7.5691656917	4.5893867941	-0.2468331192
C	-8.7693225784	5.2044880052	-0.5810896395
C	-9.7706542647	4.4765426389	-1.2151176245
C	-9.5638543404	3.1287990268	-1.5127774295
C	-8.3691074369	2.5090199617	-1.1821178607
C	-2.5414982776	-1.9580865766	0.0172334355
C	-2.6943350142	-2.8756585268	1.0642020321
C	-2.0703325822	-4.1160293673	0.9443892099
C	-1.3120172717	-4.4546329735	-0.1750464807
C	-1.1781048551	-3.5123267933	-1.1926391231
C	-1.7823879462	-2.2579912084	-1.1202102119
C	-3.5069789285	-2.5380700524	2.2882152999
C	-1.6175434559	-1.259199979	-2.2372793498
C	-0.6733421193	-5.8155640579	-0.2915188634
H	-5.0466298907	-1.0989157298	-0.8010141387
H	-3.9040309247	3.602595998	1.0276289359
H	-1.6734984921	3.9251198813	2.0670490506
H	-0.0685454667	2.0593034133	2.2153950916
H	-0.649000038	-0.1863510381	1.3273057039
H	-6.7767226735	5.1383420449	0.247117057
H	-8.9229605892	6.2512640683	-0.3469124878
H	-10.7078825027	4.9529721593	-1.4773111182
H	-10.3439313186	2.5608681491	-2.0069243737
H	-8.199895722	1.4653224889	-1.4087335894
H	-2.1786348024	-4.8345947205	1.7501230414
H	-0.5845346797	-3.7557197311	-2.0675958381
H	-3.1297826237	-1.6413815643	2.7851258367
H	-4.5519882596	-2.3435322134	2.0346217338
H	-3.4816442358	-3.3596375282	3.004135194
H	-0.9545843701	-1.6518785845	-3.0082825302
H	-2.5754287986	-1.0203838329	-2.7060957265
H	-1.1990433688	-0.3175875285	-1.8749386883
H	-0.3735608426	-6.1998509968	0.6851563785

H	-1.3712760238	-6.537959812	-0.7262058061
H	0.2096051731	-5.7878826446	-0.9321556486

Energy= -1053.6263029

Sum of electronic and zero-point Energies= -1053.245231

Sum of electronic and thermal Energies= -1053.222176

Sum of electronic and thermal Enthalpies= -1053.221232

Sum of electronic and thermal Free Energies= -1053.301295

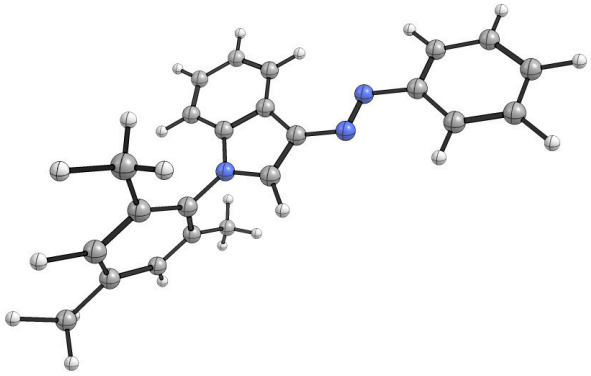

***E*-2a**

C	-9.6727900423	0.9936740948	0.8859935073
C	-9.748904728	2.3701547719	0.7196925331
C	-8.6102919126	3.0913208769	0.3625596923
C	-7.4068553027	2.4364248098	0.1743395444
C	-7.3052291517	1.0460084041	0.3367606388
C	-8.4615498195	0.3417024464	0.6955000863
N	-6.1075019096	0.3175746975	0.1587802587
N	-5.1061754889	1.0179095123	-0.1578540533
C	-3.931383699	0.3228074428	-0.3359375918
C	-3.5946060064	-1.0845494407	-0.2334687398
C	-2.2163899565	-1.180341883	-0.5342945578
N	-1.751257909	0.1020188189	-0.8029374302
C	-2.7726512848	0.9924790735	-0.6841399956
C	-4.3030969733	-2.251249355	0.0759166316
C	-3.6232416428	-3.4603115418	0.0752276891
C	-2.2548612387	-3.5311609134	-0.2266288547
C	-1.5301617006	-2.3898568048	-0.5363614189
Br	-8.4218235118	-1.5594170734	0.9403126974
H	-10.549463887	0.4239687018	1.1628449052
H	-10.6954411542	2.8753306037	0.8689531526
H	-8.6661399068	4.1654152305	0.2317631473
H	-6.5126877825	2.9778948527	-0.1029538681
H	-0.804031048	0.3369100399	-1.047542979
H	-2.6342125505	2.0484056337	-0.8497427837
H	-5.3566580227	-2.1985929378	0.3087498206
H	-4.158978413	-4.37137844	0.3128208835
H	-1.7550932456	-4.4922025188	-0.2179512051
H	-0.4730212577	-2.4417339446	-0.7698480517

Energy= -3278.06792

Sum of electronic and zero-point Energies= -3277.859032

Sum of electronic and thermal Energies= -3277.844679

Sum of electronic and thermal Enthalpies= -3277.843734

Sum of electronic and thermal Free Energies= -3277.903434

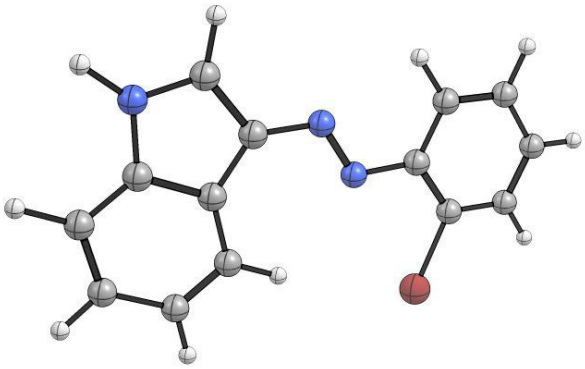

***E*-2b**

C	-9.6417089921	1.4552704556	0.9268141541
C	-9.7742426884	2.8093700611	0.6490119987
C	-8.6765600283	3.5341689506	0.1866836306
C	-7.4581807931	2.9055272972	0.0049264126
C	-7.2994609994	1.5378388298	0.2786329285
C	-8.4156618836	0.8298846294	0.7425520854
N	-6.0839443198	0.8372971238	0.115896344
N	-5.1253402753	1.537700829	-0.3169683537
C	-3.9336651818	0.8732097835	-0.4803718672
C	-3.5311604048	-0.4997781724	-0.2541902945
C	-2.163606706	-0.5669275707	-0.6118402145
N	-1.7576720959	0.6972398379	-1.0323289158
C	-2.8171618768	1.5442175797	-0.9501837239
C	-4.1716287711	-1.6554412047	0.203959675
C	-3.4384281784	-2.8305603238	0.2911938172
C	-2.0838882807	-2.8760290205	-0.0682817807
C	-1.4250695666	-1.7432318684	-0.5259592609
Br	-8.2980090534	-1.0416683634	1.1436884474
C	-0.4238122128	1.0387968743	-1.4830966147
H	-10.4859360417	0.8824452578	1.285960835
H	-10.7320457524	3.2940835402	0.7942234293
H	-8.7758202425	4.5909984237	-0.0307709773
H	-6.5952965944	3.4507142996	-0.3526011904
H	-2.7327568154	2.5828303617	-1.227773467
H	-5.2153589626	-1.6216911048	0.4808285646
H	-3.9215916355	-3.7335325554	0.6444422171
H	-1.5410404099	-3.8100736431	0.0118644093
H	-0.3786930641	-1.7815174606	-0.8030614003
H	-0.1518210297	0.4533271393	-2.3643640315
H	-0.3961549887	2.0952480394	-1.7428702428
H	0.3095530809	0.8518733829	-0.6953930253

Energy= -3317.3887289

Sum of electronic and zero-point Energies= -3317.152005

Sum of electronic and thermal Energies= -3317.136005

Sum of electronic and thermal Enthalpies= -3317.135060

Sum of electronic and thermal Free Energies= -3317.198395

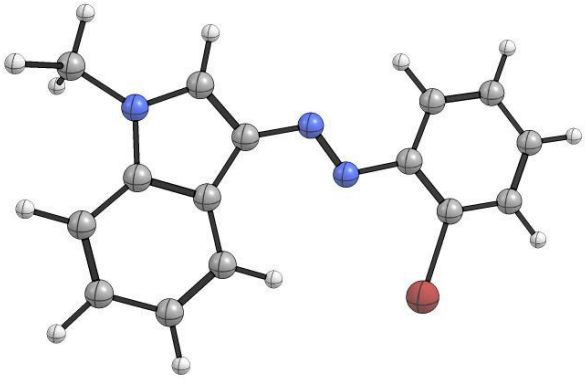

***E*-3a**

C	-9.6206241155	0.9925589806	0.9211547729
C	-9.7551900057	2.3496606242	0.6670219696
C	-8.6611763281	3.0885092945	0.2172866676
C	-7.4425140219	2.4603812397	0.026380002
C	-7.2837941692	1.0910089636	0.2766512996
C	-8.3948497715	0.3550251288	0.7303884974
N	-6.0801491575	0.3763193632	0.1082513848
N	-5.1040401412	1.0649949348	-0.3001374218
C	-3.9268078664	0.3634192161	-0.4641475661
C	-3.5820597728	-1.0300413951	-0.257563969
C	-2.2141779285	-1.1512316352	-0.5969458087
N	-1.7623560361	0.1028485085	-0.9864565589
C	-2.7846278786	1.0014714703	-0.9060157845
C	-4.2772482208	-2.167285273	0.1717566916
C	-3.5953612493	-3.3727147867	0.2479801696
C	-2.2375585222	-3.4693097316	-0.093900845
C	-1.5265262099	-2.3582267384	-0.521924049
O	-8.2376239192	-0.977285439	0.9732218131
H	-10.4708788416	0.41515005	1.2714050396
H	-10.7143048599	2.8296590222	0.8203238983
H	-8.7639243571	4.1481759561	0.0182775378
H	-6.5800289669	3.012329557	-0.3216903052
H	-0.8252604311	0.3168034643	-1.2827162787
H	-2.6545331222	2.0398991667	-1.1633906503
H	-5.3224741714	-2.0917339821	0.4345926616
H	-4.1203982625	-4.2608941232	0.5785112565
H	-1.7355727316	-4.426712666	-0.0227777697
H	-0.4778428408	-2.430419279	-0.7865412536
H	-9.0775816529	-1.3415187078	1.2755451455

Energy= -779.7775544

Sum of electronic and zero-point Energies= -779.554722

Sum of electronic and thermal Energies= -779.540468

Sum of electronic and thermal Enthalpies= -779.539524

Sum of electronic and thermal Free Energies= -779.597594

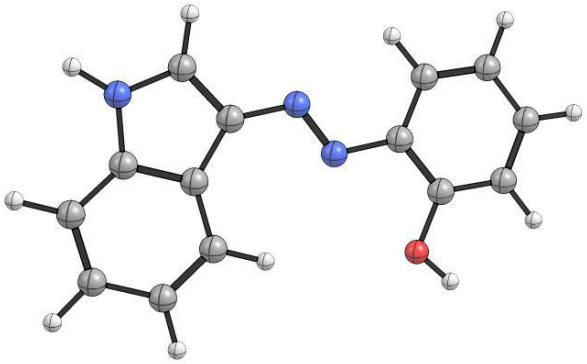

***E*-3b**

C	-9.6057957546	1.4266235374	0.9225524244
C	-9.7790868716	2.7734901035	0.6382807666
C	-8.7111346231	3.5278369144	0.1534921201
C	-7.4798945196	2.9257925503	-0.0419191629
C	-7.2820376635	1.5672732596	0.2382966714
C	-8.3674801877	0.8155578401	0.7273294829
N	-6.0639715636	0.8786569471	0.0669611521
N	-5.1103079145	1.583670375	-0.3691258846
C	-3.9192231049	0.9111839532	-0.5376447499
C	-3.5314281169	-0.4655924494	-0.3120149544
C	-2.1646828016	-0.5492246389	-0.6722601573
N	-1.745385201	0.7080970248	-1.093552389
C	-2.7981093995	1.5687990164	-1.009014341
C	-4.1850973635	-1.6138702783	0.1481846699
C	-3.4661144277	-2.7976851184	0.2348509754
C	-2.1123926448	-2.8596773741	-0.1270070079
C	-1.4407974671	-1.7353042416	-0.5864054433
O	-8.173154134	-0.5065737859	0.9998568661
C	-0.4092067494	1.0356661798	-1.5453087411
H	-10.4355392788	0.836735867	1.3002770855
H	-10.7476074134	3.2329554392	0.7953868939
H	-8.8437137135	4.5794621069	-0.0693887336
H	-6.6372713593	3.4904975173	-0.4171160919
H	-2.7014858557	2.6061378938	-1.2872791377
H	-5.2279587887	-1.564199492	0.4264886229
H	-3.9592000901	-3.6948822655	0.5894933233
H	-1.5806053095	-3.8002132796	-0.0471527174
H	-0.3952682594	-1.7865979897	-0.8649772035
H	-8.9996824012	-0.8838403921	1.3223265398
H	-0.1412523932	0.4448271693	-2.4245074707
H	-0.3722940962	2.0907731336	-1.8097909996
H	0.323804268	0.8464595767	-0.7574353586

Energy= -819.0981322

Sum of electronic and zero-point Energies= -818.847439

Sum of electronic and thermal Energies= -818.831561

Sum of electronic and thermal Enthalpies= -818.830617

Sum of electronic and thermal Free Energies= -818.892268

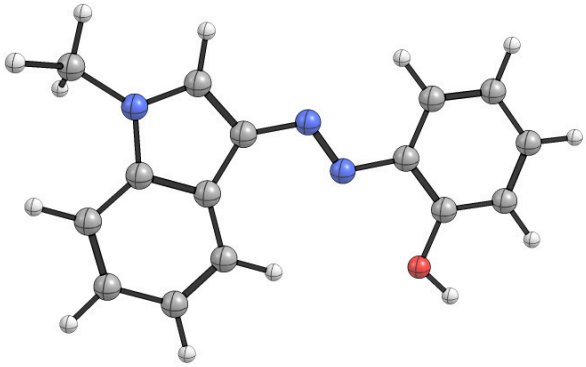

***E*-4a**

C	4.3627101268	-1.3086163421	0.0003882088
C	5.0390140198	-0.0881538969	0.0003423699
C	4.3236549424	1.1025232831	0.0000151106
C	2.9406840145	1.0546499651	-0.0002556556
C	2.2322451036	-0.1514717782	-0.0002175584
C	2.9783703848	-1.3391532037	0.0001106094
N	0.8240401700	-0.0677513224	-0.0005520104
N	0.2328886597	-1.1837331465	-0.0004896225
C	-1.1434212940	-1.1168406238	-0.0002658511
C	-2.0721309979	-0.0025060584	-0.0000788130
C	-3.3668240198	-0.5713482575	0.0000582128
N	-3.2220398247	-1.9535899859	-0.0000342646
C	-1.8990816485	-2.2741305231	-0.0001950241
C	-1.9452274230	1.3917414818	-0.0000295965
C	-3.0976038837	2.1636096049	0.0001539671
C	-4.3721347776	1.5766077130	0.0002892435
C	-4.5253314124	0.1982123556	0.0002395392
H	4.9217866215	-2.2364551438	0.0006373755
H	6.1218209530	-0.0630567517	0.0005568051
H	4.8166907663	2.0661293788	-0.0000318296
H	2.4398782759	-2.2769426144	0.0001319738
H	-1.5577187317	-3.2963968359	-0.0002853316
H	-0.9644499827	1.8443613898	-0.0001320712
H	-3.0140034889	3.2436605955	0.0001948707
H	-5.2514503654	2.2092871698	0.0004325312
H	-5.5087158104	-0.2575996905	0.0003398709
F	2.2643179648	2.2204112572	-0.0005698300
H	-3.9784190746	-2.6168907843	0.0000890851

Energy= -803.7999416

Zero-point correction= 0.210902 (Hartree/Particle)

Sum of electronic and zero-point Energies= -803.589040

Sum of electronic and thermal Energies= -803.575335

Sum of electronic and thermal Enthalpies= -803.574391

Sum of electronic and thermal Free Energies= -803.631125

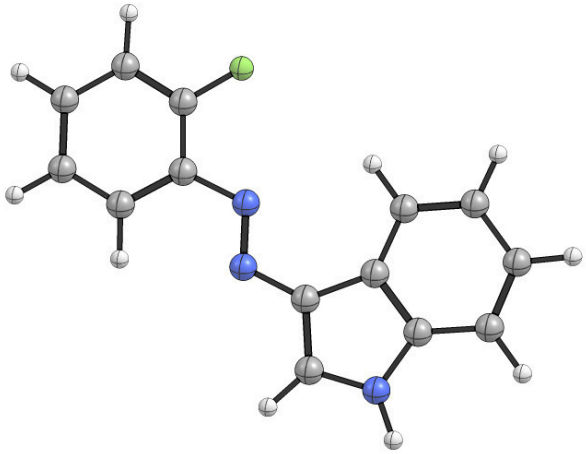

***E*-4b**

C	-4.5071925431	-1.5559599486	0.0000008336
C	-5.2982914740	-0.4067249365	0.0000158074
C	-4.7004978385	0.8472564934	0.0000118760
C	-3.3194503469	0.9328119913	-0.0000063601
C	-2.4971769269	-0.1990729012	-0.0000200394
C	-3.1262093010	-1.4529011044	-0.0000170853
N	-1.1041367571	0.0199452503	-0.0000442123
N	-0.4078812968	-1.0352510171	-0.0000244721
C	0.9537017719	-0.8391392418	-0.0000107743
C	1.7752004092	0.3538140734	-0.0000061989
C	3.1163683724	-0.0985496328	0.0000185238
N	3.1093816254	-1.4906065923	0.0000457728
C	1.8187386087	-1.9194187218	0.0000188278
C	1.5220858088	1.7296004087	-0.0000209098
C	2.6000207225	2.6035850565	-0.0000193944
C	3.9216082264	2.1346235908	-0.0000047670
C	4.1999875341	0.7748559615	0.0000128533
H	-4.9740484909	-2.5335152663	0.0000019037
H	-6.3784836630	-0.4860520187	0.0000293863
H	-5.2839450678	1.7589926888	0.0000228327
H	-2.5000561562	-2.3345516304	-0.0000303455
H	1.5729757506	-2.9694100934	0.0000286710
H	0.5040365270	2.0908765300	-0.0000357193
H	2.4185785358	3.6716047243	-0.0000326043
H	4.7401298519	2.8442777867	-0.0000094025
H	5.2218960019	0.4158459860	0.0000167513
F	-2.7588266618	2.1588945315	-0.0000097699
C	4.2888016473	-2.3317421562	-0.0000238955
H	4.8964809837	-2.1457363031	-0.8886160193
H	4.8968882221	-2.1452551322	0.8881840586
H	3.9807457351	-3.3755333280	0.0003385746

Energy= -843.1207187

Zero-point correction= 0.238709 (Hartree/Particle)

Sum of electronic and zero-point Energies= -842.882010

Sum of electronic and thermal Energies= -842.866654

Sum of electronic and thermal Enthalpies= -842.865709

Sum of electronic and thermal Free Energies= -842.926266

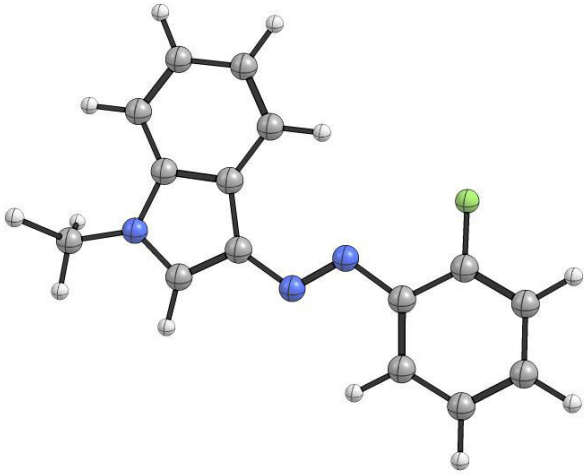

***E*-5a**

C	3.01210919	-3.33788226	-0.43436208
C	4.05769938	-2.42085994	-0.48014016
C	3.8092025	-1.06454369	-0.31501487
C	2.51035167	-0.57605066	-0.11310821
C	1.44723472	-1.51574259	-0.0933801
C	1.7197735	-2.88005919	-0.24069005
N	0.12481071	-1.01980384	-0.04397046
N	-0.7417852	-1.85032802	0.34830779
C	-2.04999001	-1.40806088	0.30478588
C	-2.66157813	-0.19160567	-0.19494069
C	-4.05076632	-0.32440907	0.03880138
N	-4.26137226	-1.55451055	0.64615349
C	-3.06921189	-2.19865968	0.79766884
C	-2.19033562	0.96798555	-0.82258293
C	-3.10225351	1.94790165	-1.18482975
C	-4.4751484	1.79748043	-0.93475376
C	-4.96936259	0.65687094	-0.32049066
H	3.20171846	-4.39604007	-0.56767729
H	5.07510041	-2.75970888	-0.63760091
H	4.64365324	-0.37770604	-0.32783302
H	0.88249309	-3.56490899	-0.23898132
H	-3.00023661	-3.1760333	1.24656868
H	-1.13396161	1.08186267	-1.01825447
H	-2.75060542	2.84926213	-1.6722752
H	-5.16071025	2.58301821	-1.22864123
H	-6.02982328	0.53605842	-0.1315429
C	1.63750497	1.22267961	1.31376144
C	3.3058384	1.73290961	-0.34935532
C	1.1269199	2.64997909	1.19788589
H	2.37517251	1.1662836	2.13089306
H	0.80707516	0.56248623	1.55065909
C	2.73540836	3.14359218	-0.4289006
H	4.14851114	1.73252767	0.36183666
H	3.68861419	1.44783262	-1.33132752
H	0.7638447	3.00231956	2.16413482
H	0.30343548	2.69274503	0.47333213
H	3.52817094	3.85954053	-0.65081497
H	1.98064839	3.19212556	-1.22614397
N	2.25448816	0.80014302	0.04685824
O	2.1604744	3.54787974	0.80524098
H	-5.15600862	-1.91853352	0.92711967

Energy= -991.2090818

Zero-point correction= 0.333671 (Hartree/Particle)

Sum of electronic and zero-point Energies= -990.875411

Sum of electronic and thermal Energies= -990.857040

Sum of electronic and thermal Enthalpies= -990.856095

Sum of electronic and thermal Free Energies= -990.922951

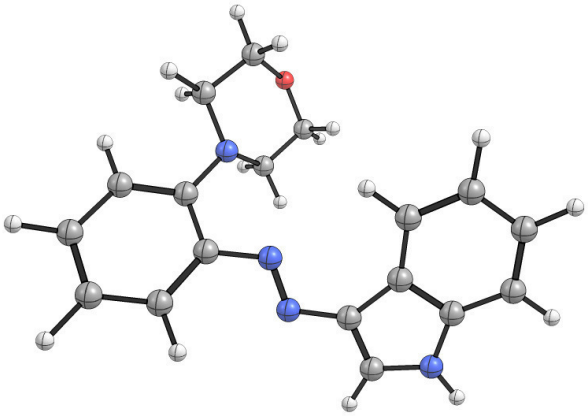

***E*-5b**

C	2.95507822	-3.53852309	-0.46933661
C	4.08912063	-2.73250419	-0.45763915
C	3.97302414	-1.3616608	-0.26714923
C	2.72394826	-0.74784254	-0.09662711
C	1.57068071	-1.57401983	-0.13503311
C	1.70949123	-2.95548642	-0.3072329
N	0.30448363	-0.94702848	-0.11512127
N	-0.65482264	-1.69448139	0.22868069
C	-1.9087996	-1.12398125	0.15592542
C	-2.38291904	0.15612858	-0.32727333
C	-3.78649485	0.14887163	-0.13786652
N	-4.14513824	-1.06888011	0.42824504
C	-3.0204742	-1.81973045	0.59362211
C	-1.78337093	1.27947125	-0.90705904
C	-2.58553251	2.35227312	-1.26853906
C	-3.97297576	2.32820732	-1.06371299
C	-4.5943771	1.22454129	-0.49686317
H	3.04112977	-4.60748015	-0.62249577
H	5.07198232	-3.16983509	-0.58979255
H	4.872547	-0.76321649	-0.23535897
H	0.80776875	-3.55141507	-0.34999109
H	-3.06134485	-2.81065682	1.01701418
H	-0.71512269	1.29570448	-1.06798861
H	-2.13363194	3.22766854	-1.71938072
H	-4.57074725	3.18337857	-1.35506766
H	-5.66674321	1.20692627	-0.34523021
C	-5.49432815	-1.46413313	0.77669397
H	-5.91751564	-0.78521745	1.52078716
H	-6.13790226	-1.46453668	-0.10616527
H	-5.47336738	-2.46927452	1.19342348
C	1.98686286	1.10077712	1.34266469
C	3.75702761	1.47252989	-0.24992663
C	1.6276063	2.57470421	1.24425107
H	2.68483462	0.95263761	2.1829279
H	1.08582008	0.52382045	1.53469598
C	3.33544655	2.93532366	-0.31470732
H	4.56928944	1.371559	0.48902873
H	4.14420387	1.17041017	-1.22507174
H	1.26737657	2.94222833	2.20591484
H	0.83931518	2.7159407	0.49350742
H	4.20393341	3.57129991	-0.49242508
H	2.61864115	3.07637448	-1.1356298
N	2.60319292	0.64409501	0.08764597
O	2.75987125	3.37087619	0.90846654

Energy= -1030.5297255

Zero-point correction= 0.361468 (Hartree/Particle)

Sum of electronic and zero-point Energies= -1030.168257

Sum of electronic and thermal Energies= -1030.148225

Sum of electronic and thermal Enthalpies= -1030.147281

Sum of electronic and thermal Free Energies= -1030.218017

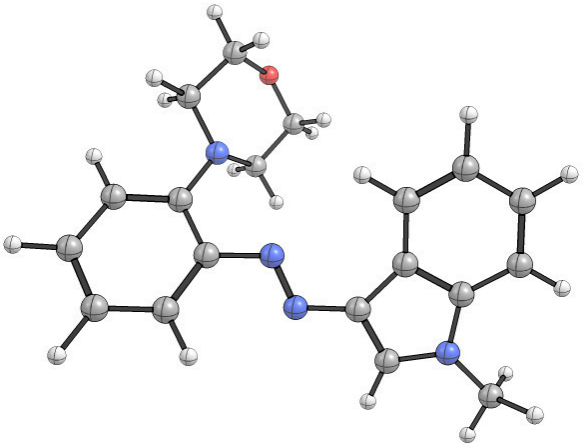

***E*-6a**

C	-9.4427810939	0.6835342764	0.9876779638
C	-9.5836987749	2.0501481091	0.7309807825
C	-8.4943881288	2.7906571519	0.2788056304
C	-7.2712481301	2.1641298555	0.0852564271
C	-7.1170761987	0.8001330512	0.337805585
C	-8.2227378475	0.0654838427	0.7931559319
N	-5.8284721759	0.2688957262	0.1060418588
N	-5.7100997485	-0.9650351318	0.340354797
C	-4.4548771136	-1.4975605442	0.1178341596
C	-3.2057858771	-0.9211210647	-0.3423374167
C	-2.2678933583	-1.9807857711	-0.3656376867
N	-2.9185576932	-3.1308607808	0.0575306643
C	-4.2197296103	-2.838863192	0.3442628781
C	-2.786882944	0.3573363982	-0.7309393821
C	-1.4695520645	0.5382394247	-1.1241376915
C	-0.5577776109	-0.5286457992	-1.1388902888
C	-0.9450713154	-1.8046574189	-0.7592876557
O	-10.8157920476	2.6033000198	0.9426717658
H	-10.3032481082	0.1273031648	1.3386951983
H	-8.6024817611	3.8520472394	0.0790859471
H	-6.4142593627	2.7255174142	-0.2659908611
H	-8.1050936511	-0.9914437597	0.9893550678
H	-2.4969102068	-4.0401914219	0.1407759133
H	-4.9105244894	-3.5893882941	0.6920307091
H	-3.4873534386	1.1790357721	-0.7200060005
H	-1.1344379051	1.5230253403	-1.4268475757
H	0.4645441207	-0.3536152815	-1.4515277283
H	-0.2430969706	-2.6305440145	-0.7696858465
H	-10.7901781031	3.5439256889	0.7329668579

Energy= -779.7825319

Sum of electronic and zero-point Energies= -779.559460

Sum of electronic and thermal Energies= -779.545346

Sum of electronic and thermal Enthalpies= -779.544402

Sum of electronic and thermal Free Energies= -779.601611

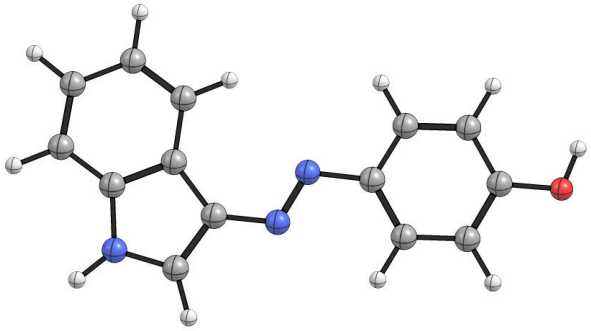

***E*-6b**

C	-9.4550224642	1.1285337367	0.9410860411
C	-9.5988919262	2.4972269038	0.698802305
C	-8.5085618799	3.2463023591	0.2638083893
C	-7.281570832	2.6262440283	0.0729839566
C	-7.1241058157	1.2599059947	0.3111094652
C	-8.2311017859	0.5168329317	0.7492887132
N	-5.8318613818	0.7358208555	0.0837502782
N	-5.7121662582	-0.5015363124	0.3039138376
C	-4.4560881817	-1.0292745761	0.0867723654
C	-3.2036536856	-0.4505122418	-0.3536889887
C	-2.2693999485	-1.5152377305	-0.3787593731
N	-2.9179721759	-2.6760562228	0.0240370473
C	-4.2185784825	-2.3742717488	0.2983122303
C	-2.7784501522	0.8302897595	-0.7231713196
C	-1.4562073023	1.0127278284	-1.1014494304
C	-0.5477196933	-0.055781473	-1.1192073303
C	-0.9416051542	-1.3362263072	-0.7578255857
O	-10.8349869206	3.0442209052	0.9069000466
C	-2.3042922513	-3.9833003547	0.1310135115
H	-10.3161691902	0.5652133012	1.2790078161
H	-8.6187334596	4.3095657386	0.0752279375
H	-6.4238624557	3.1946778608	-0.2649779973
H	-8.1114156213	-0.541844791	0.9345309919
H	-4.9137854126	-3.128579143	0.6306971831
H	-3.4773534389	1.6534124627	-0.7097078412
H	-1.1158737525	2.0001404564	-1.3895735817
H	0.4781760863	0.1199825733	-1.4196717273
H	-0.2379266512	-2.1595988142	-0.7724684486
H	-10.8102057232	3.9870982074	0.7077981433
H	-1.9188576053	-4.3114419336	-0.8373010817
H	-1.4820756919	-3.9683453738	0.8504527904
H	-3.0507940519	-4.6991936905	0.469760136

Energy= -819.1030929

Sum of electronic and zero-point Energies= -818.852232

Sum of electronic and thermal Energies= -818.836457

Sum of electronic and thermal Enthalpies= -818.835513

Sum of electronic and thermal Free Energies= -818.896643

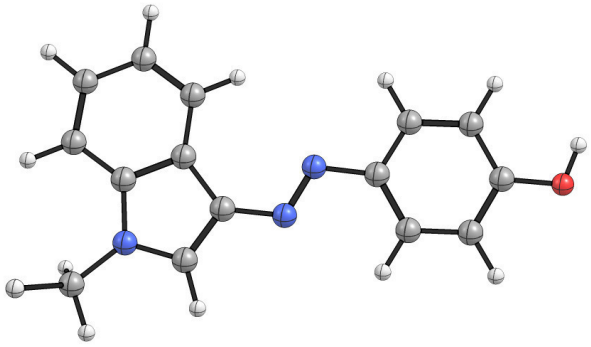

***E*-7a**

C	-3.3407072375	1.2902039454	0.0001603178
C	-4.0468364356	0.0937495123	-0.0000036973
C	-1.2819453845	0.0199072408	0.0000986821
C	-1.9567866924	1.2456974077	0.0002092604
N	0.1295305612	0.0996499689	0.0001739941
N	0.7151712108	-1.0213262973	0.0001810789
C	2.0871057051	-0.9792596464	0.0001053605
C	3.0455792180	0.1109681031	0.0000056830
C	4.3238002231	-0.4924308187	-0.0000190548
N	4.1413238340	-1.8720592395	0.0000679175
C	2.8148738359	-2.1579393571	0.0001184032
C	2.9589759830	1.5075385072	-0.0000602478
C	4.1322688392	2.2474867311	-0.0001492536
C	5.3893937401	1.6253284085	-0.0001727304
C	5.5034485983	0.2429826223	-0.0001060338
H	-3.8777147956	2.2276092675	0.0002452070
H	-1.3736290875	2.1575846541	0.0003367304
H	2.4456512688	-3.1705543456	0.0001806279
H	1.9923054293	1.9886103005	-0.0000413000
H	4.0790107474	3.3293668070	-0.0002011342
H	6.2860041265	2.2329274095	-0.0002425089
H	6.4733118231	-0.2405490290	-0.0001215760
H	4.8804943371	-2.5551814543	0.0000090461
C	-2.0171001870	-1.1758768848	-0.0000746239
H	-1.4903368813	-2.1194349631	-0.0001648441
C	-3.3982303865	-1.1395541823	-0.0001289163
H	-3.9858085514	-2.0465110240	-0.0002679582
N	-5.5145784072	0.1295615632	-0.0001055911
O	-6.1131321164	-0.9419762152	-0.0002578935
O	-6.0604798016	1.2287187956	0.0000372850

Energy= -909.1036203

Zero-point correction= 0.221536 (Hartree/Particle)

Sum of electronic and zero-point Energies= -908.882084

Sum of electronic and thermal Energies= -908.866694

Sum of electronic and thermal Enthalpies= -908.865750

Sum of electronic and thermal Free Energies= -908.927341

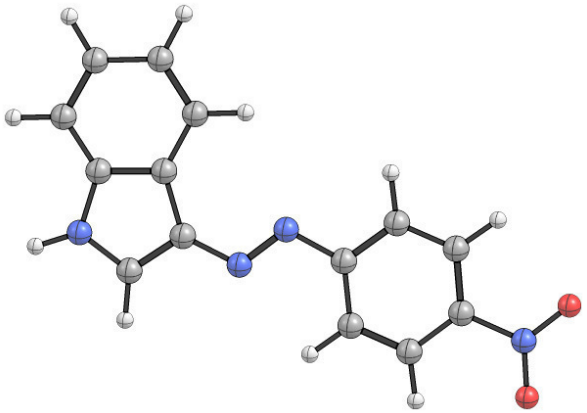

***E*-7b**

C	-3.7174301338	1.2302325913	-0.0000927083
C	-4.3474418306	-0.0082555015	0.0000905472
C	-1.5821295718	0.0917764812	-0.0001675086
C	-2.3335942025	1.2727337309	-0.0002201186
N	-0.1795912767	0.2600309639	-0.0003276928
N	0.4755432780	-0.8238817673	-0.0002935130
C	1.8396552002	-0.6987348465	-0.0001729060
C	2.7320396412	0.4435135141	-0.0000598804
C	4.0425041035	-0.0892671046	0.0000234250
N	3.9509044186	-1.4806977796	-0.0000126769
C	2.6415785048	-1.8308534876	-0.0001289117
C	2.5653709518	1.8316453492	-0.0000285651
C	3.6947797560	2.6382485567	0.0000763444
C	4.9844138619	2.0889957645	0.0001498719
C	5.1778576914	0.7143998377	0.0001222330
H	-4.3123385097	2.1319635251	-0.0001324700
H	-1.8089129413	2.2194850733	-0.0003645747
H	2.3316820594	-2.8637936612	-0.0001807633
H	1.5723910713	2.2559602660	-0.0000881573
H	3.5795683562	3.7153328980	0.0001000407
H	5.8450689939	2.7466130237	0.0002273158
H	6.1754123548	0.2928003607	0.0001725796
C	-2.2416404784	-1.1477871052	0.0000125690
H	-1.6565442558	-2.0562983721	0.0000450181
C	-3.6222644313	-1.1983019516	0.0001439927
H	-4.1517572003	-2.1403164181	0.0002838824
N	-5.8136903207	-0.0647045382	0.0002150803
O	-6.3445306963	-1.1715330645	0.0003538558
O	-6.4283379387	0.9977037922	0.0001452669
C	5.0795187074	-2.3909568607	-0.0000373477
H	5.6958044043	-2.2392867063	-0.8887579411
H	5.6960740324	-2.2389553468	0.8884357382
H	4.7102587211	-3.4144984843	0.0002177116

Energy= -948.4247881

Zero-point correction= 0.249326 (Hartree/Particle)

Sum of electronic and zero-point Energies= -948.175462

Sum of electronic and thermal Energies= -948.158403

Sum of electronic and thermal Enthalpies= -948.157459

Sum of electronic and thermal Free Energies= -948.222963

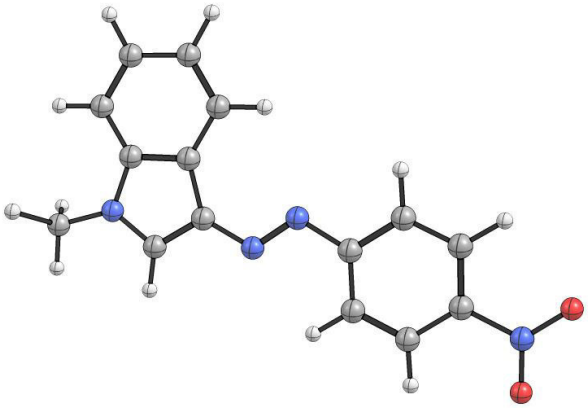

***E*-8a**

C	-6.1784418265	0.0573074757	0.7742034997
C	-6.3169316582	1.4327898826	0.5148413804
C	-5.1877764562	2.1325400414	0.0608201038
C	-3.9818213639	1.4833866905	-0.1229994593
C	-3.8574452647	0.1130478522	0.1389724272
C	-4.975650089	-0.5984999392	0.5925770243
C	-7.6164449501	2.0566047045	0.7293816999
C	-7.9422358099	3.3451596403	0.5381722407
C	-9.2783529845	3.8974395752	0.7780145522
O	-9.5727572735	5.0597979845	0.6055038474
O	-10.1913232788	2.9886604617	1.2205136503
N	-2.5774916795	-0.4415289723	-0.0848791332
N	-2.4901906633	-1.6790131103	0.1573243063
C	-1.2526877119	-2.2421136448	-0.0529389092
C	0.0157369926	-1.7028772806	-0.5076379328
C	0.9222686527	-2.7881794709	-0.5171137761
N	0.2344359568	-3.9184342037	-0.0908652035
C	-1.0562637809	-3.5909566597	0.1838872748
C	0.4725267263	-0.4395641175	-0.9005875984
C	1.7978150452	-0.2995644622	-1.2847724601
C	2.6782926063	-1.3918333364	-1.2858155387
C	2.2520136042	-2.6542229878	-0.9011954074
H	-7.0412538807	-0.4980826473	1.1257129404
H	-5.2533483203	3.1924388833	-0.1499831226
H	-3.1093266642	2.0209986292	-0.4730902055
H	-4.8823077692	-1.6562358967	0.7956000834
H	-8.3981261808	1.3921195193	1.0833731975
H	-7.2314335578	4.0818124229	0.1875396916
H	-11.0194601063	3.4779118816	1.337299492
H	0.6302944344	-4.8389162277	0.0009499592
H	-1.7708235547	-4.3192490732	0.5311253403
H	-0.2038376658	0.4021357869	-0.9002786678
H	2.1633386086	0.6730909997	-1.5910244545
H	3.7073975414	-1.2480808965	-1.591657552
H	2.9298758778	-3.4998924937	-0.9009762691

Energy= -970.5996923

Sum of electronic and zero-point Energies= -970.332504

Sum of electronic and thermal Energies= -970.314396

Sum of electronic and thermal Enthalpies= -970.313452

Sum of electronic and thermal Free Energies= -970.381754

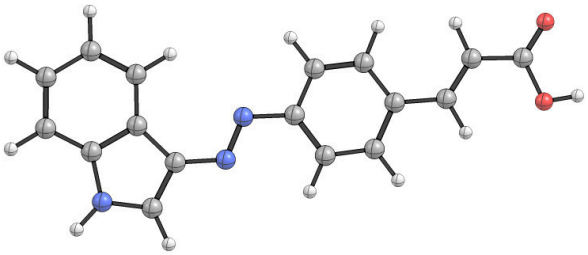

***E*-8b**

C	-6.2272203632	0.3585515207	0.802892128
C	-7.2754204638	-0.4518973158	1.2762527871
C	-7.0011009487	-1.8081272868	1.5136293435
C	-5.7392212095	-2.3233349089	1.2868276545
C	-4.7041128872	-1.5052922087	0.81489461
C	-4.9630264754	-0.1492200817	0.5736030556
C	-8.5826612207	0.1535511348	1.4941771058
C	-9.6972019255	-0.452512104	1.9347455825
C	-10.9796410309	0.2293514942	2.128557398
O	-11.985165847	-0.317128055	2.52614651
O	-10.9629315532	1.556398693	1.8222379296
N	-3.4606850357	-2.1409188221	0.6208758306
N	-2.5384718997	-1.3899332897	0.1943177113
C	-1.3156592713	-1.9960183088	-0.0008757332
C	-0.1478786094	-1.3017087954	-0.4826573649
C	0.8900064212	-2.2588428526	-0.5457373334
N	0.372214393	-3.4769285899	-0.1209176861
C	-0.9399562725	-3.3165147002	0.2022466035
C	0.1165618799	0.0175143278	-0.8613641752
C	1.3941127348	0.3431821191	-1.2878572043
C	2.4130604879	-0.6223031319	-1.3437862649
C	2.1765087885	-1.9377176788	-0.9736389541
C	1.120599438	-4.7160673835	-0.0392445325
H	-6.4224350275	1.4087304576	0.614618799
H	-7.7808197834	-2.4646348542	1.8785931151
H	-5.5240006968	-3.369032169	1.4689224379
H	-4.1660451429	0.4840466373	0.2096791613
H	-8.6469661179	1.2136365916	1.2706485513
H	-9.7306934113	-1.505225735	2.1827548236
H	-11.8599960007	1.8805915676	1.9924183434
H	-1.5347150831	-4.1414512134	0.5570440829
H	-0.6655412742	0.7647558823	-0.8199067092
H	1.6155062149	1.361181863	-1.5848410328
H	3.4010373684	-0.3346846776	-1.6819118829
H	2.9651755133	-2.6786955274	-1.0183620198
H	1.9621340531	-4.6125378708	0.6492995936
H	0.4644542538	-5.5040479528	0.3246263205
H	1.5015278575	-5.0009762307	-1.0224686559

Energy= -1009.9178731

Sum of electronic and zero-point Energies= -1009.623199

Sum of electronic and thermal Energies= -1009.603315

Sum of electronic and thermal Enthalpies= -1009.602371

Sum of electronic and thermal Free Energies= -1009.674926

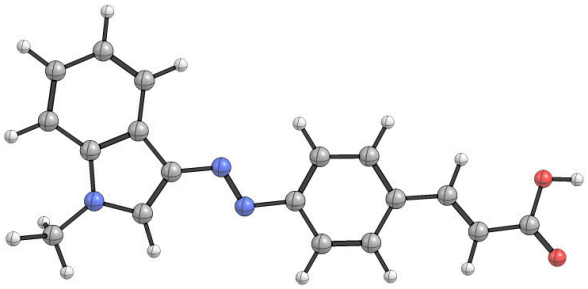

***E*-9a**

C	-9.6176832885	2.1901655119	0.794671419
C	-8.6425125758	2.7853230131	0.007669056
C	-7.4384892362	2.1347091772	-0.2017404646
C	-7.1650104144	0.8707830422	0.3418125759
C	-8.1695776463	0.2978072685	1.139865744
C	-9.3732554213	0.9492634033	1.3648640602
N	-5.8817890848	0.3534804728	0.0976540652
F	-7.9879735367	-0.8702678901	1.7586688768
F	-10.3039461893	0.3864089851	2.1421593515
F	-10.7801376365	2.808268018	1.0058942489
F	-8.8720136607	3.9790950015	-0.5468246639
F	-6.5247523189	2.7405307965	-0.9650086044
N	-5.7911225272	-0.9074824953	0.1667123123
C	-4.5314803359	-1.4136168868	-0.0383445186
C	-3.2499421916	-0.7963184058	-0.3258878638
C	-2.3214357857	-1.8569527751	-0.4290534347
N	-3.0112855134	-3.0468666121	-0.2144879481
C	-4.3216793029	-2.7811520065	0.016082002
C	-2.8004528756	0.5163010406	-0.5079381205
C	-1.4566620413	0.7262847507	-0.7809697067
C	-0.5534178564	-0.3425712325	-0.87656386
C	-0.9738123525	-1.6529001356	-0.7021005281
H	-2.6009112609	-3.9657941403	-0.2260510653
H	-5.0419010736	-3.5593240961	0.2096366406
H	-3.4941173076	1.3412031324	-0.4381239542
H	-1.0951355034	1.7371786122	-0.9246877109
H	0.489317492	-0.1428752033	-1.0909950453
H	-0.2783481337	-2.4806823754	-0.7769118876

Energy= -1200.8431698

Sum of electronic and zero-point Energies= -1200.664597

Sum of electronic and thermal Energies= -1200.647258

Sum of electronic and thermal Enthalpies= -1200.646313

Sum of electronic and thermal Free Energies= -1200.711551

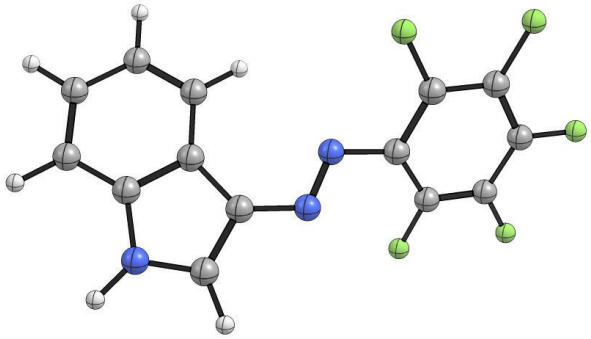

***E*-9b**

C	-9.6370605036	2.6371698208	0.7620813068
C	-8.6913252488	3.1977928537	-0.0839399828
C	-7.4806124585	2.5559780933	-0.2813574429
C	-7.1702743475	1.3337918786	0.3334509833
C	-8.1456519734	0.7959643799	1.1901314592
C	-9.3559651682	1.4393155652	1.4027582671
N	-5.8840781597	0.8240979913	0.0928182909
F	-7.9276352816	-0.3269642557	1.8780045334
F	-10.2577123016	0.9105959553	2.2367131673
F	-10.8061597756	3.2474941509	0.9621355876
F	-8.9558675398	4.3501479297	-0.7070109878
F	-6.5963993267	3.1281698512	-1.1037138978
N	-5.7727944446	-0.4312919912	0.2296445247
C	-4.5128249724	-0.9314075425	0.0301793656
C	-3.2447075161	-0.319741974	-0.3126349852
C	-2.3096012943	-1.3793526186	-0.3733390488
N	-2.975489369	-2.5700856103	-0.082820322
C	-4.2807959499	-2.2929310633	0.1537751407
C	-2.8116914702	0.9838472697	-0.5736148705
C	-1.4742115295	1.1906527832	-0.8815083144
C	-0.5634484492	0.1264050784	-0.9343928064
C	-0.9682532428	-1.1771261428	-0.6811187105
C	-2.3591017473	-3.8817866463	-0.0422701288
H	-4.989909695	-3.0665852819	0.4020378158
H	-3.5124111325	1.8050218376	-0.5365809992
H	-1.1250369876	2.195354986	-1.0864672415
H	0.4736340164	0.3226842484	-1.1776997406
H	-0.262563117	-1.997521728	-0.7241727528
H	-1.5707418851	-3.9129879357	0.712845492
H	-3.1157676921	-4.6220084497	0.2097754244
H	-1.9289420614	-4.1346924294	-1.0137061222

Energy= -1240.1643407

Sum of electronic and zero-point Energies= -1239.957995

Sum of electronic and thermal Energies= -1239.938985

Sum of electronic and thermal Enthalpies= -1239.938041

Sum of electronic and thermal Free Energies= -1240.007040

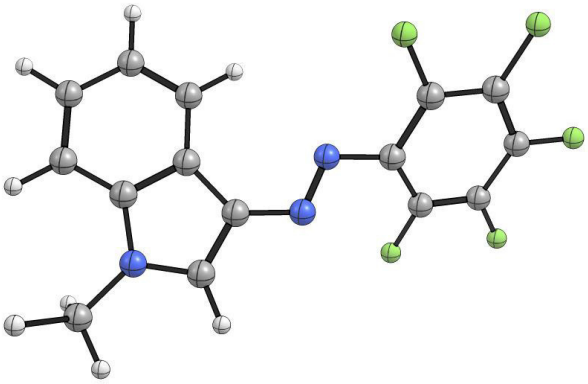

***E*-10a**

C	-9.6074375241	-0.05578863	1.0337198376
C	-9.6963465599	1.3355670227	1.0490937287
C	-8.5579627881	2.1024909086	0.8520138237
C	-7.32171337	1.4978839833	0.6200619108
C	-7.2285063082	0.0927466766	0.5920539566
C	-8.386424173	-0.6667246688	0.8107020715
N	-5.9792522496	-0.4771109575	0.2583230365
N	-6.1875095584	2.3229092876	0.4189378901
C	-4.982839755	2.2420782661	1.0875864358
C	-4.1850601579	3.2736865544	0.6655822647
C	-4.9222344732	4.0145170923	-0.301241102
C	-6.1487325461	3.4149693999	-0.4268207944
N	-5.8793274613	-1.7107569557	0.5084574403
C	-4.6926501813	-2.2994516613	0.1278904455
C	-3.5062142758	-1.7915249629	-0.5359660728
C	-2.627375908	-2.8924112165	-0.6627230758
N	-3.2523218521	-4.0004822538	-0.1030678476
C	-4.4793931781	-3.6444706397	0.3654496505
C	-3.1028855071	-0.543936481	-1.0269242533
C	-1.8552062916	-0.4366309249	-1.6230288968
C	-1.0008186651	-1.5436371353	-1.7391043799
C	-1.3749693263	-2.7896793697	-1.2588741268
H	-10.4935449418	-0.6596601559	1.1889752064
H	-10.6480288434	1.8217725384	1.2259935437
H	-8.6090873902	3.1829606921	0.8956638522
H	-8.3008833487	-1.7440522517	0.7744041998
H	-4.8079810127	1.4651747662	1.8104083784
H	-3.1846861826	3.4759844755	1.0135704574
H	-4.5868926626	4.880286864	-0.8497243223
H	-6.9854364386	3.6442019293	-1.064684319
H	-2.8589865693	-4.9250322974	-0.0520791303
H	-5.1392154266	-4.3527374931	0.8393467425
H	-3.7525048497	0.3138313942	-0.9319027546
H	-1.5314900009	0.5234477572	-2.0061697762
H	-0.0326046938	-1.4240744018	-2.2100628741
H	-0.7166573425	-3.6463471418	-1.345862121

Energy= -913.5554916

Sum of electronic and zero-point Energies= -913.274098

Sum of electronic and thermal Energies= -913.257199

Sum of electronic and thermal Enthalpies= -913.256255

Sum of electronic and thermal Free Energies= -913.320442

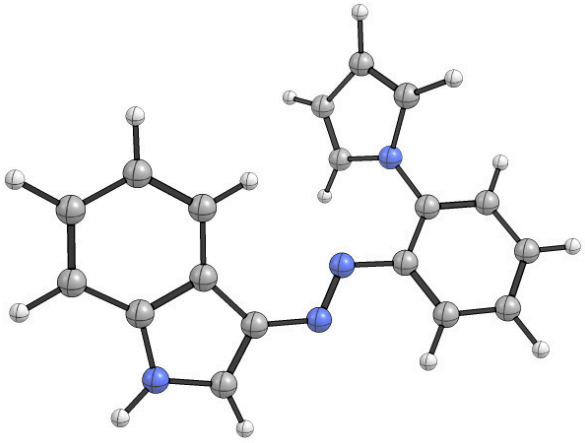

***E*-10b**

C	-9.7141592749	0.3107088409	0.7271622313
C	-10.7306780307	-0.4669068018	1.2810978815
C	-10.4610704901	-1.7611256277	1.7005474796
C	-9.1836646337	-2.3040619016	1.5584215749
C	-8.1561367035	-1.5264554773	0.988914149
C	-8.4419326936	-0.2140779109	0.5868283357
N	-6.9093985029	-2.1481863681	0.7777414699
N	-8.9506945175	-3.6311712852	1.9966500121
C	-7.9409147491	-4.0533326072	2.8375231127
C	-8.1139251365	-5.3911397907	3.0821318291
C	-9.268156529	-5.8099939373	2.3616992823
C	-9.7653470052	-4.7097654925	1.7119161019
N	-5.9480516773	-1.3627843922	0.5511075424
C	-4.7389077681	-1.9757786564	0.2817359209
C	-3.5157352952	-1.2587324394	0.027108705
C	-2.5192953295	-2.2359116681	-0.200271968
N	-3.1151104178	-3.4858493602	-0.0874447893
C	-4.4371244624	-3.3266546744	0.1993908337
C	-3.1694646017	0.0946244335	-0.0284325314
C	-1.855381524	0.4339682229	-0.3077279566
C	-0.8792081573	-0.5512648218	-0.5321718138
C	-1.1963680216	-1.9003893175	-0.4815589046
C	-2.4310584352	-4.753143217	-0.2539715495
H	-9.9203602794	1.3227218305	0.3997676408
H	-11.728457225	-0.0615022021	1.3969871008
H	-11.234323153	-2.3607862611	2.1636686261
H	-7.6452434238	0.3649010496	0.140143274
H	-7.2024642777	-3.3594489337	3.1979654817
H	-7.4870982725	-6.0004150447	3.7136661855
H	-9.6803107252	-6.8055054601	2.31741423
H	-10.6054333273	-4.6018623093	1.0470228866
H	-5.0905496525	-4.1733448535	0.3302997274
H	-3.9180344386	0.857082753	0.1455268
H	-1.5709975414	1.4782965472	-0.3543290877
H	0.1392334086	-0.2522584401	-0.748120475
H	-0.4403327396	-2.6564247463	-0.6546775819
H	-1.6267807575	-4.8557378432	0.4780126784
H	-3.1433407565	-5.5625689183	-0.1079386527
H	-2.0073813014	-4.8334332114	-1.2576267553

Energy= -952.8738303

Sum of electronic and zero-point Energies= -952.564978

Sum of electronic and thermal Energies= -952.546296

Sum of electronic and thermal Enthalpies= -952.545352

Sum of electronic and thermal Free Energies= -952.614041

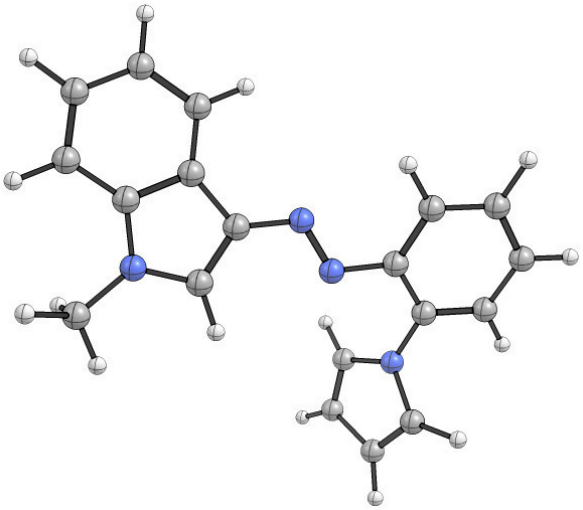

***E*-11a**

C	-8.707624882	1.7845734075	0.6268549604
C	-7.5833112717	2.5417596933	0.3404478712
C	-6.35049198	1.9274904075	0.1333332193
C	-6.2356141034	0.5431604602	0.2122332524
C	-7.3701983342	-0.2289446066	0.5016472525
C	-8.5872658706	0.3942808301	0.7049200097
N	-4.9402927823	0.0162891864	-0.0141277131
N	-4.8716885153	-1.2423187258	0.0661211248
C	-3.6307107624	-1.7911669494	-0.1472902156
C	-2.3340316453	-1.2175639261	-0.4563445381
C	-1.4393636277	-2.3073571446	-0.5577317354
N	-2.1621105688	-3.4725884596	-0.3218348011
C	-3.4612745593	-3.1635905025	-0.0787270203
C	-1.8442308115	0.0782423185	-0.6542997767
C	-0.497772172	0.2442905598	-0.9427624894
C	0.3705533858	-0.8532427993	-1.0381207224
C	-0.0888744476	-2.1477644082	-0.8465286377
C	-9.8219576097	-0.4083325813	1.018492703
F	-9.5833358129	-1.7322435027	1.0550645283
F	-10.7955471603	-0.2044236738	0.1015932052
F	-10.3484170376	-0.0656827016	2.216793386
C	-7.6651942939	4.0414374309	0.2468503842
F	-8.9110589358	4.5044043199	0.460605786
F	-7.2778841128	4.4872661369	-0.9698009976
F	-6.8567924284	4.6425137757	1.1492863244
H	-9.6635732598	2.2631979345	0.786932077
H	-5.4665539667	2.5106369317	-0.0911249739
H	-7.2766398413	-1.3030060822	0.5615301623
H	-1.7807547478	-4.4039524858	-0.3298438007
H	-4.2016590004	-3.9185856526	0.1299894723
H	-2.5103553059	0.9249443305	-0.5814957587
H	-0.1060669194	1.242131669	-1.0981570235
H	1.4167047268	-0.6882785231	-1.2649367678
H	0.5796668624	-2.9975756658	-0.9195697318

Energy= -1378.8466351

Sum of electronic and zero-point Energies= -1378.618914

Sum of electronic and thermal Energies= -1378.598628

Sum of electronic and thermal Enthalpies= -1378.597684

Sum of electronic and thermal Free Energies= -1378.673638

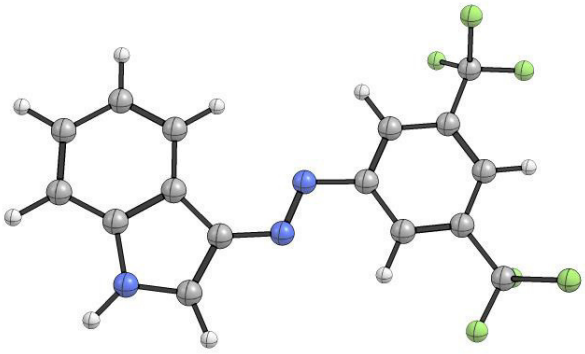

***E*-11b**

C	-8.7323023672	2.1613516351	0.6358933108
C	-7.6634675656	2.907017985	0.1654911316
C	-6.4226605993	2.3107952199	-0.0459817756
C	-6.2423725223	0.9554533755	0.2135781959
C	-7.3210108273	0.1953160233	0.689919746
C	-8.5468318148	0.8005427962	0.8952488259
N	-4.9453238551	0.445202204	-0.0333623232
N	-4.818504739	-0.7886287648	0.213627423
C	-3.5764362072	-1.3230387826	-0.0121607801
C	-2.3279949972	-0.7638823074	-0.4900892292
C	-1.4044461033	-1.8355615897	-0.5031697025
N	-2.0575441395	-2.9835612329	-0.05706755
C	-3.3442823115	-2.6682884169	0.231128668
C	-1.9013640561	0.5030085299	-0.899960358
C	-0.5840371485	0.6633858743	-1.3057835452
C	0.3145998183	-0.4125047657	-1.3109334724
C	-0.0829411569	-1.6802086895	-0.9090218673
C	-1.4486531164	-4.2930427758	0.0724850977
C	-9.721411419	0.0092227523	1.4057086302
F	-9.4212329122	-1.2855706411	1.617592576
F	-10.7591084812	0.039828817	0.5378954543
F	-10.1876283806	0.5056535813	2.5749347785
C	-7.8155831322	4.3751162931	-0.1270194982
F	-9.0625521207	4.8227661906	0.1124856229
F	-7.5321834888	4.6590352745	-1.4187359729
F	-6.9737123428	5.1234884985	0.6218941067
H	-9.6944966312	2.6260626737	0.7992740267
H	-5.5822366167	2.8856960387	-0.4133845005
H	-7.1775914809	-0.8559870758	0.8901125826
H	-4.0403251059	-3.4070544175	0.5955260875
H	-2.5920454011	1.3330877777	-0.8966818448
H	-0.2408658431	1.6397244574	-1.6257094801
H	1.3362504393	-0.2534692787	-1.6336278063
H	0.6135173071	-2.509539755	-0.9140733126
H	-0.6144369347	-4.261400887	0.7765801377
H	-2.1928370571	-4.9956697444	0.4419603602
H	-1.0825303696	-4.6443478754	-0.8945727438

Energy= -1418.1677688

Sum of electronic and zero-point Energies= -1417.912262

Sum of electronic and thermal Energies= -1417.890310

Sum of electronic and thermal Enthalpies= -1417.889366

Sum of electronic and thermal Free Energies= -1417.969038

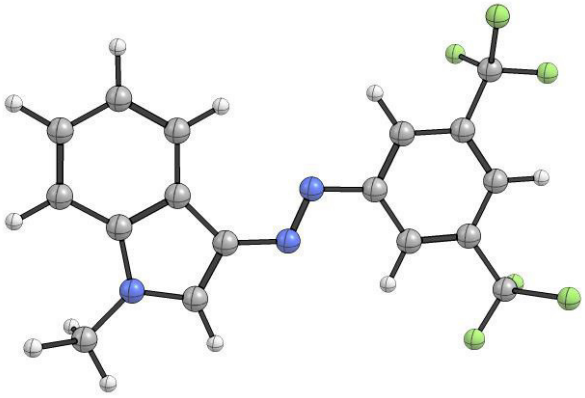

***E*-12a**

C	-3.6578415484	1.4973950308	-0.903602008
C	-2.6837249051	0.4665285477	-0.904486751
N	-3.0916051924	-0.5292242291	-0.0440748304
C	-4.2869958173	-0.1783826827	0.5080042617
C	-4.689997352	1.0485502194	0.0261286784
C	-3.4127109247	2.6038248849	-1.7275816195
C	-2.260967607	2.6536015875	-2.4933647511
C	-1.3185522211	1.618717015	-2.4712622239
C	-1.5300009599	0.5171411444	-1.671953485
N	-5.8893814373	1.5761471726	0.4746873057
N	-6.2160503078	2.6958189069	0.0105117656
C	-7.4472062556	3.21010925	0.4868679292
C	-7.8107699822	4.4570528654	-0.026601186
C	-8.9989247341	5.0576438421	0.3709552029
C	-9.8297511951	4.4157670949	1.2829514381
C	-9.468000566	3.1692403745	1.7970182783
C	-8.284851464	2.563996328	1.4055967117
F	-4.2458666228	3.6414636409	-1.8212299518
F	-2.0271741207	3.711405588	-3.2807452258
F	-0.2211356221	1.711342038	-3.2280345314
F	-0.6409627091	-0.4934972038	-1.6303255273
H	-4.7977558706	-0.8102287714	1.2151768268
H	-7.1460954424	4.9352602469	-0.7352975848
H	-9.2759626064	6.025015238	-0.0304482479
H	-10.7570615482	4.8814409279	1.5949246379
H	-10.1172397225	2.670873066	2.507573722
H	-7.9950460692	1.5986571542	1.7975006705
H	-2.5794516758	-1.3758328571	0.138437935

Energy= -1101.5825893

Sum of electronic and zero-point Energies= -1101.395993

Sum of electronic and thermal Energies= -1101.379375

Sum of electronic and thermal Enthalpies= -1101.378431

Sum of electronic and thermal Free Energies= -1101.441949

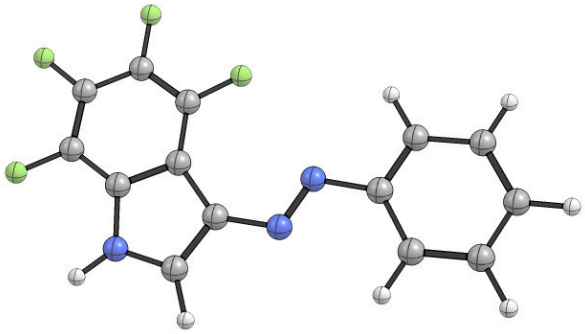

***E*-12b**

C	-3.6500713778	1.4826028076	-0.921577194
C	-2.6856453277	0.4357347758	-0.9266743706
N	-3.1087712296	-0.569743244	-0.0744711384
C	-4.3007433483	-0.1949703462	0.4637931163
C	-4.6918862008	1.0414034745	-0.0052903862
C	-3.3998208962	2.5999151995	-1.7275205545
C	-2.2486994062	2.658008257	-2.491744356
C	-1.3159249088	1.617048247	-2.4805882974
C	-1.5301667233	0.5025620097	-1.6986362159
N	-5.8874276756	1.5714130074	0.445447063
N	-6.2114112311	2.699033185	-0.0031048226
C	-7.441542187	3.2079983814	0.4815439925
C	-7.804617578	4.4627920412	-0.0131429078
C	-8.991742804	5.0590719768	0.3938773441
C	-9.8231169877	4.4054699532	1.2971318585
C	-9.4621731521	3.1512894622	1.7925922935
C	-8.279906413	2.5503166327	1.3914955615
F	-4.2296336232	3.6417837939	-1.8050222853
F	-2.0082907711	3.7258538981	-3.2631247609
F	-0.2152785339	1.7115592562	-3.2339430378
F	-0.6222849893	-0.4940220026	-1.6970442056
H	-4.8246958326	-0.8266143588	1.1623723393
H	-7.1399553154	4.95057836	-0.7153451843
H	-9.2676331428	6.0325413583	0.0065251209
H	-10.749623568	4.8677855954	1.6164376356
H	-10.1113615186	2.6432597632	2.4964233217
H	-7.991150925	1.5790544418	1.769307365
C	-2.4166247973	-1.8198853025	0.2070453615
H	-2.2992139905	-2.411046199	-0.701293421
H	-1.4323657703	-1.6297095927	0.6348683977
H	-3.0115649748	-2.383538612	0.9227392768

Energy= -1140.9015523

Sum of electronic and zero-point Energies= -1140.687148

Sum of electronic and thermal Energies= -1140.668853

Sum of electronic and thermal Enthalpies= -1140.667909

Sum of electronic and thermal Free Energies= -1140.735332

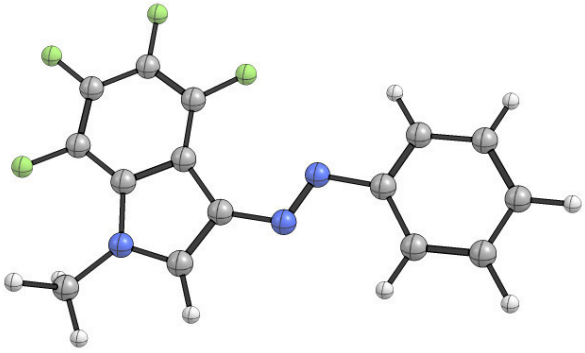

***E*-12c**

C	-3.6229597595	1.4770233014	-0.9396383321
C	-2.6624421809	0.4263847489	-0.971266768
N	-3.1226353579	-0.6223356614	-0.1817703524
C	-4.3376374898	-0.2645567943	0.3313584062
C	-4.6993785033	0.996431831	-0.083615604
C	-3.3588808599	2.6270472006	-1.6924743498
C	-2.1972242024	2.714761902	-2.4371862768
C	-1.2762768412	1.6655148136	-2.4658859278
C	-1.5056177373	0.5144294586	-1.7411265886
N	-5.9002251246	1.5181552213	0.3662175906
N	-6.1826139864	2.6857322434	0.0005952573
C	-7.417939752	3.1842078955	0.4827674526
C	-7.7371053633	4.4819842071	0.0765779699
C	-8.9247220368	5.072596291	0.4901935361
C	-9.8000624942	4.3703081628	1.3117280916
C	-9.4829068023	3.0731702029	1.7187548641
C	-8.300538964	2.4774239644	1.3103602644
C	-2.4713508378	-1.8639345927	0.1090085792
C	-3.0987625162	-3.0566941195	-0.238385239
C	-2.4962745659	-4.2685028568	0.0809105075
C	-1.2684512551	-4.2877006239	0.7333952543
C	-0.645511213	-3.0908136788	1.0744983651
C	-1.2472631933	-1.8763303996	0.77086231
F	-4.1879903383	3.6714668669	-1.741835838
F	-1.9416365333	3.8150050813	-3.1561902234
F	-0.1707464851	1.7816193153	-3.2090121449
F	-0.6139302592	-0.4884891055	-1.8065042882
H	-4.8757167522	-0.921772554	0.9937168611
H	-7.0385020794	5.0068805649	-0.5631409924
H	-9.1667788835	6.0794567334	0.1717594667
H	-10.7270558738	4.828129871	1.6360596505
H	-10.1663418012	2.5275484561	2.3591339455
H	-8.0451743898	1.4732366222	1.6199943766
H	-2.9834783931	-5.1966489919	-0.1915052458
H	0.3086259009	-3.1009023547	1.5868089109
H	-0.7740191536	-0.94263166	1.0464881159
H	-0.7972906298	-5.2323737911	0.9754874269
H	-4.0452214215	-3.0311742213	-0.7642856317

Energy= -1332.688157

Sum of electronic and zero-point Energies= -1332.421534

Sum of electronic and thermal Energies= -1332.400201

Sum of electronic and thermal Enthalpies= -1332.399256

Sum of electronic and thermal Free Energies= -1332.474683

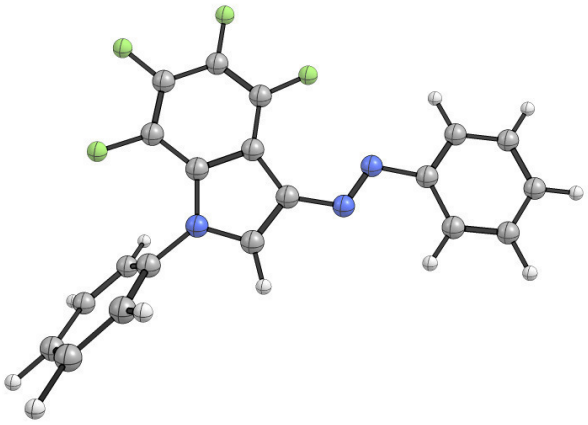

***E*-12d**

C	-3.696689486	1.4299895255	-0.5460693592
C	-2.6502927774	0.474980791	-0.5832119227
N	-3.1157430312	-0.697277308	-0.0057811446
C	-4.4118291111	-0.502663238	0.387329267
C	-4.8187451403	0.7813970334	0.0811917436
C	-3.4674333207	2.7015155337	-1.0743792598
C	-2.2366281142	3.0049655348	-1.6192051316
C	-1.2110701842	2.0497173161	-1.6487703863
C	-1.4084626183	0.7847321419	-1.1341709617
N	-6.043533159	1.3991254073	0.3006392661
N	-6.908614816	0.6781450919	0.8609451276
C	-8.1574382457	1.3057064381	1.0859595772
C	-9.1268682263	0.5147787209	1.7070455455
C	-10.3878028252	1.0333929022	1.9744408313
C	-10.6868742721	2.3452101849	1.6227218181
C	-9.7190447311	3.1372963784	1.0018533112
C	-8.4595989442	2.6278124291	0.731741241
C	-2.3891612819	-1.9290387508	0.1704297443
C	-2.4432497236	-2.8973796102	-0.8373436351
C	-1.7492880624	-4.088369879	-0.6332922253
C	-1.0161982048	-4.324927192	0.5278648814
C	-0.9909967436	-3.3344067242	1.5077204264
C	-1.6676194186	-2.1263286597	1.3523689979
F	-4.4188904984	3.643367335	-1.0665503647
F	-1.9994833181	4.2198189497	-2.130476231
F	-0.0297863614	2.3797078319	-2.1852905322
F	-0.4076848621	-0.1112062648	-1.175903956
C	-3.216212457	-2.6672244472	-2.1107574078
C	-1.6095535232	-1.0697276858	2.4258133582
C	-0.2474784753	-5.609148665	0.7080432473
H	-4.9671681095	-1.2928725341	0.8627389691
H	-8.8703041913	-0.5037753101	1.971525228
H	-11.1355783723	0.415043286	2.4563957686
H	-11.6691315981	2.7531017722	1.8297089214
H	-9.9540350477	4.1593960885	0.7285228702
H	-7.7018012622	3.2315913848	0.2512994997
H	-1.7840318462	-4.8505309109	-1.4044798415
H	-0.4292954291	-3.503612449	2.4202444767
H	-4.2643584565	-2.4316952386	-1.9130177188
H	-2.8030110049	-1.8321365848	-2.6823927742
H	-3.183088009	-3.553498926	-2.7440682651
H	-1.0425964186	-1.427663405	3.2849452227
H	-1.1269871966	-0.1586269889	2.0627013813
H	-2.6062471934	-0.7872276156	2.7722814775
H	-0.7202750846	-6.4350077813	0.1739026463
H	0.7714337628	-5.5094323731	0.321232455
H	-0.1713138554	-5.8836206143	1.7615336599

Energy= -1450.6750302

Sum of electronic and zero-point Energies= -1450.326679

Sum of electronic and thermal Energies= -1450.299725

Sum of electronic and thermal Enthalpies= -1450.298780

Sum of electronic and thermal Free Energies= -1450.387798

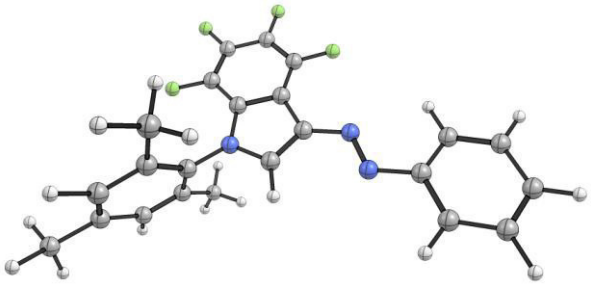

6.2.2. *Z*-isomers

***Z*-1a**

C	-7.9285757789	-4.5072081994	-2.0056471014
C	-8.2435623776	-5.1888100982	-0.8328382234
C	-8.148698432	-4.5306464679	0.3906365541
C	-7.7301878524	-3.2058655288	0.4471140794
C	-7.3891928826	-2.5356721042	-0.7284683099
C	-7.508442792	-3.1826768228	-1.9592723276
N	-7.0626781983	-1.1439734076	-0.6844848616
N	-5.8876028925	-0.7260258571	-0.5870795156
C	-4.7372171085	-1.5184846956	-0.5030078492
C	-3.4488852401	-0.8667468954	-0.4047398235
C	-2.4729327514	-1.8802597205	-0.3298713444
N	-3.144306038	-3.0918816844	-0.3798174205
C	-4.4883356667	-2.8863902679	-0.482949545
C	-3.0466586093	0.4727050351	-0.3751144185
C	-1.6949478583	0.7550094304	-0.2728209232
C	-0.7368272185	-0.2716730949	-0.1995899799
C	-1.1111456186	-1.6053357115	-0.2269575194
H	-8.0169381746	-5.0064434276	-2.9636266193
H	-8.5765173897	-6.2187142922	-0.8734843189
H	-8.4090575035	-5.048182098	1.3066769298
H	-7.6663407243	-2.6843694745	1.3945996929
H	-7.2731534347	-2.6434596603	-2.8690167375
H	-2.7096987259	-3.9994469743	-0.3452693331
H	-5.1598600792	-3.7236611962	-0.5327649755
H	-3.7849814556	1.2619439571	-0.4315710671
H	-1.3643519107	1.7863498276	-0.2483972329
H	0.3126134066	-0.0154049885	-0.1203422385
H	-0.3735409194	-2.3973657735	-0.1706052005

Energy= -704.5077845

Zero-point correction= 0.218810 (Hartree/Particle)

Sum of electronic and zero-point Energies= -704.288974

Sum of electronic and thermal Energies= -704.276117

Sum of electronic and thermal Enthalpies= -704.275173

Sum of electronic and thermal Free Energies= -704.330227

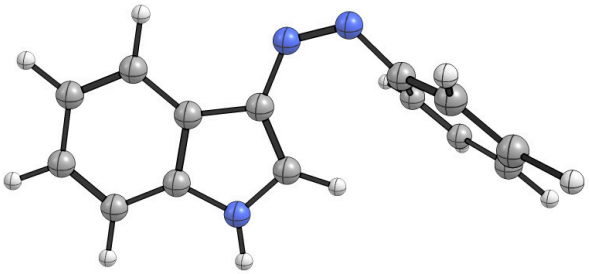

***Z*-1b**

C	-7.3900740216	-4.1687446714	-2.4541260998
C	-7.7711618438	-4.874992109	-1.3159531564
C	-7.8592855801	-4.2122777306	-0.0942901781
C	-7.5566573136	-2.8582085872	-0.0041065625
C	-7.1488158869	-2.1604682331	-1.142113357
C	-7.0853924169	-2.8145321468	-2.3735493068
N	-6.9418753642	-0.747554452	-1.0748050903
N	-5.8217322552	-0.237314141	-0.8437369349
C	-4.6316575715	-0.9332778722	-0.6210329855
C	-3.4212604317	-0.1858250737	-0.3678438132
C	-2.3866292003	-1.1251237218	-0.1797704134
N	-2.9402516978	-2.3911851543	-0.3121859021
C	-4.2726876435	-2.2779709798	-0.5741025209
C	-3.1308411317	1.1791344695	-0.2855406261
C	-1.8266675283	1.5634109719	-0.0199728046
C	-0.8081923811	0.6127084806	0.1647116236
C	-1.0719092929	-0.7462315493	0.0877515698
C	-2.2089008708	-3.6371728626	-0.188932212
H	-7.3368922994	-4.6723699776	-3.4124689886
H	-8.014790078	-5.9282447853	-1.3838154157
H	-8.1730534241	-4.7499623773	0.7930297494
H	-7.6352690644	-2.334245236	0.9409361969
H	-6.8001714075	-2.2568670392	-3.2575649126
H	-4.8658233579	-3.1644239551	-0.7075355844
H	-3.9161140211	1.9101404897	-0.4279354405
H	-1.5826996157	2.6167779313	0.0475371046
H	0.2011922713	0.9473537679	0.3709566507
H	-0.284249914	-1.4757568122	0.2307601622
H	-1.7630379818	-3.7248932841	0.8043738336
H	-2.8945292061	-4.4683955748	-0.3405633134
H	-1.4159149866	-3.6934348361	-0.938014595

Energy= -743.8287926

Zero-point correction= 0.246576 (Hartree/Particle)

Sum of electronic and zero-point Energies= -743.582217

Sum of electronic and thermal Energies= -743.567694

Sum of electronic and thermal Enthalpies= -743.566750

Sum of electronic and thermal Free Energies= -743.625565

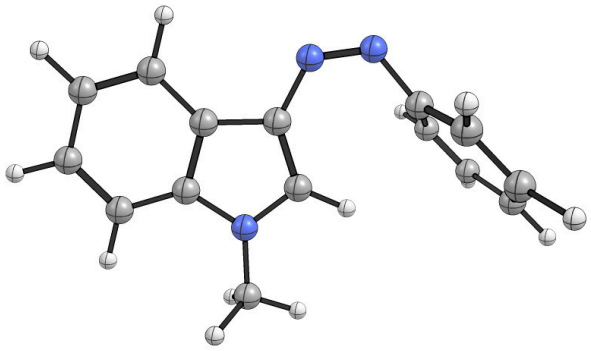

***Z*-1c**

C	-6.9248030795	0.9274129845	-1.1406221081
C	-7.7767246366	0.1820929261	-0.3018329972
N	-7.0155449093	-0.2484045116	0.7894200391
C	-5.6195709515	0.9471910587	-0.5206361539
C	-7.4330221807	1.4931761478	-2.3138786833
C	-8.7725687358	1.3088804131	-2.6108075947
C	-9.6131565296	0.5800357178	-1.7525910635
C	-9.1307305984	0.0083472229	-0.5856796329
N	-4.571692944	1.601552288	-1.1770507969
N	-3.4085710799	1.7498321161	-0.739642997
C	-2.9941596027	1.2701422912	0.5423026436
C	-2.3286293803	0.0478504191	0.6420017144
C	-1.8300596156	-0.3696160738	1.8711867508
C	-1.9748096177	0.4323440111	3.0000302057
C	-2.6144677369	1.6644493444	2.8896682575
C	-3.1200190813	2.0885706744	1.6660866829
C	-7.470005647	-1.0356693256	1.8848446456
C	-8.1465743459	-2.2329006475	1.6547453376
C	-8.5748045962	-3.0000304009	2.7313126236
C	-8.3203611732	-2.5867556161	4.0354294002
C	-7.6373469141	-1.3961601388	4.2602252554
C	-7.2184977697	-0.6149210157	3.1897250179
H	-2.2060451516	-0.5647779781	-0.2431397679
H	-1.3193109775	-1.3227156313	1.9446778273
H	-1.578189717	0.1073838112	3.9541074579
H	-2.7144418171	2.3034660631	3.7595038669
H	-3.6082513869	3.0511154768	1.571508181
H	-9.0973631715	-3.9311384048	2.5483760992
H	-7.438755707	-1.0653802882	5.2723990503
H	-6.7067370103	0.3239873083	3.3602617886
H	-8.3178001986	-2.5659086599	0.6392951935
H	-8.6517311561	-3.1901265497	4.8715507421
H	-9.7853508061	-0.5413972728	0.0773928586
H	-10.6602413879	0.464241569	-2.0048947159
H	-9.1852512813	1.7382166404	-3.5157701279
H	-6.7832190485	2.0642169146	-2.964162741
C	-5.7342870311	0.2184148649	0.6549122287
H	-4.9989813056	-0.0391086688	1.3945762114

Energy= -935.6169514

Zero-point correction= 0.299075 (Hartree/Particle)

Sum of electronic and zero-point Energies= -935.317876

Sum of electronic and thermal Energies= -935.300376

Sum of electronic and thermal Enthalpies= -935.299432

Sum of electronic and thermal Free Energies= -935.366022

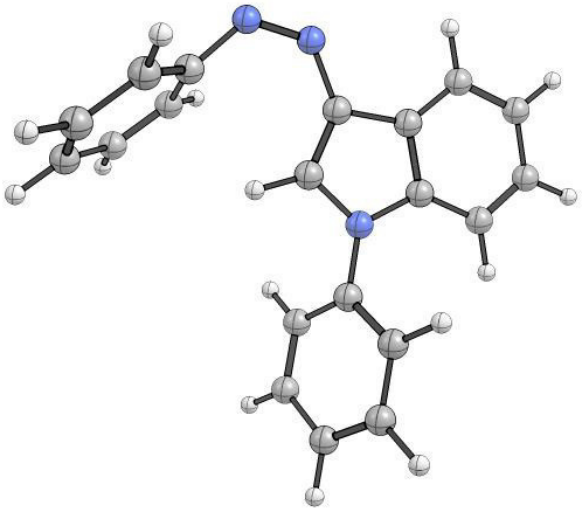

***Z*-1d**

C	-3.3686226302	1.5778956696	-0.3362130559
C	-2.4458600085	0.5314220797	-0.1400681149
N	-3.1133908768	-0.6685008816	-0.3745104937
C	-4.4116595838	-0.4029969477	-0.7080398151
C	-4.62883971	0.9717368208	-0.7008303121
C	-2.9507692461	2.9013409297	-0.1621687568
C	-1.6348427072	3.137555675	0.1993659198
C	-0.728965656	2.0793390642	0.390287779
C	-1.1199730327	0.7599480002	0.2236223522
N	-5.7262953214	1.8000812323	-0.9524482485
N	-6.8748773931	1.4240406857	-1.2789869278
C	-7.2217773101	0.0467931798	-1.4434311447
C	-7.7775841855	-0.6616891614	-0.377123276
C	-8.2143387358	-1.967937818	-0.567402665
C	-8.1137914031	-2.5700969792	-1.818857939
C	-7.5839218666	-1.850100927	-2.8864562133
C	-7.1442676494	-0.5435060332	-2.705765862
C	-2.5344580378	-1.9793453309	-0.2818123656
C	-1.9474752889	-2.5461983898	-1.419436544
C	-1.3903702853	-3.8185529078	-1.3031515757
C	-1.4027061771	-4.5214231117	-0.0998621395
C	-1.9983191364	-3.9236620275	1.0091480961
C	-2.5692274527	-2.6537212984	0.9445383885
C	-1.9224927683	-1.8126174727	-2.736124222
C	-3.2106057404	-2.0357581415	2.160757843
C	-0.7637478301	-5.8830633459	0.0061866846
H	-5.0780118	-1.218212663	-0.9237936119
H	-3.6498673563	3.7142965775	-0.3097386543
H	-1.2928550729	4.1560683547	0.3387522057
H	0.2935532616	2.2989394302	0.672836592
H	-0.4256445538	-0.0582275493	0.3696032095
H	-7.8657791115	-0.1828245894	0.5907686169
H	-8.6420793138	-2.5150840773	0.2647828902
H	-8.4600820076	-3.5859673347	-1.9646008787
H	-7.5187609045	-2.30505975	-3.8681085021
H	-6.7435047211	0.0265073631	-3.5354500612
H	-0.9358704644	-4.2709281706	-2.1783367646
H	-2.0220259148	-4.4587807253	1.9526754829
H	-2.9322017341	-1.643669153	-3.1187779961
H	-1.4507426177	-0.8321618907	-2.6405307173
H	-1.3712718334	-2.3839147315	-3.4830464584
H	-3.0875059586	-2.6824769071	3.0295075573
H	-2.7725732563	-1.0630767215	2.3953005255
H	-4.2809327803	-1.8743331047	2.009773874
H	-0.8097526895	-6.4197228322	-0.9429986407
H	0.2917402319	-5.7981566545	0.2830880306
H	-1.252435891	-6.4942604262	0.7668756634

Energy= -1053.6016995

Zero-point correction= 0.380714 (Hartree/Particle)

Sum of electronic and zero-point Energies= -1053.220986

Sum of electronic and thermal Energies= -1053.197875

Sum of electronic and thermal Enthalpies= -1053.196931

Sum of electronic and thermal Free Energies= -1053.277781

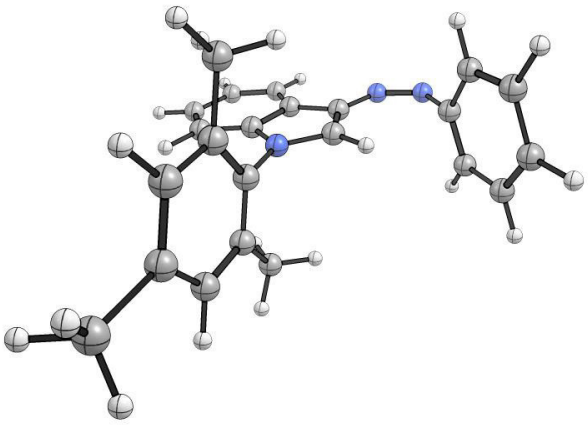

***Z*-2a**

C	-6.4266941375	-2.9853760101	4.6812743676
C	-7.1053018653	-4.0134911273	4.0372813916
C	-7.462742465	-3.8758447899	2.6981459984
C	-7.1357683042	-2.719048093	2.0063780915
C	-6.4398946382	-1.6830498956	2.6382795927
C	-6.1056094131	-1.8275076621	3.9834897348
N	-6.2585144333	-0.444162136	1.9502501603
N	-5.3397951	-0.2443679153	1.1267164601
C	-4.3107442941	-1.1339335585	0.81410568
C	-3.3827094496	-0.7977211399	-0.2435835963
C	-2.4226663328	-1.8275639889	-0.2968236444
N	-2.7525640012	-2.7401011086	0.6937837511
C	-3.8729811301	-2.3370603958	1.3557387495
C	-3.2868666354	0.2733647651	-1.1379387687
C	-2.2454004242	0.2808163406	-2.0503514488
C	-1.2995744222	-0.7589593506	-2.0894209592
C	-1.3735259474	-1.8294227973	-1.2130413798
Br	-5.1695902476	-0.421301858	4.8882320921
H	-6.1505245454	-3.0755969494	5.7235656526
H	-7.3626919593	-4.9111794317	4.5855364972
H	-8.0032545283	-4.6678725	2.1940455972
H	-7.4202852223	-2.5940077349	0.9685453721
H	-2.2344702349	-3.5759648838	0.91004406
H	-4.2610021118	-2.9238426865	2.1682704043
H	-4.0142990717	1.0740396572	-1.1062608725
H	-2.1531819388	1.1028997258	-2.7497288324
H	-0.4980114666	-0.7218078546	-2.8169521933
H	-0.6443412601	-2.6306273096	-1.2414670215

Energy= -3278.04394

Sum of electronic and zero-point Energies= -3277.835298

Sum of electronic and thermal Energies= -3277.820973

Sum of electronic and thermal Enthalpies= -3277.820029

Sum of electronic and thermal Free Energies= -3277.879519

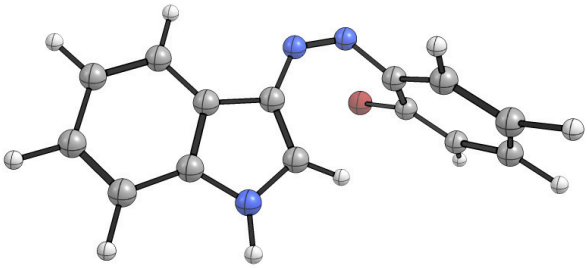

***Z*-2b**

C	-10.8012911396	0.2912235061	0.9619408252
C	-10.7725505878	-0.8161330699	1.8018318445
C	-9.6193663929	-1.5929785491	1.8845782426
C	-8.5002746002	-1.2582951887	1.136635164
C	-8.509829238	-0.1374845423	0.2992844089
C	-9.6772861417	0.6192509614	0.2137888404
N	-7.4014981754	0.0886527375	-0.5722767341
N	-6.3589994977	0.6823077643	-0.216373392
C	-6.1377625467	1.2809431714	1.0211312067
C	-4.8457389532	1.8605265389	1.3076115724
C	-4.9292905511	2.4395277547	2.5903161277
N	-6.2186516412	2.2308635536	3.0625494443
C	-6.9347457587	1.540827579	2.1331365121
C	-3.6440477723	1.9367145821	0.5978423067
C	-2.5685297456	2.581892142	1.1860811264
C	-2.6692413302	3.1504008928	2.4673498198
C	-3.8510176109	3.088593366	3.1896399884
Br	-9.7376459263	2.1511326126	-0.9365111233
C	-6.7206201541	2.6900061303	4.3434627468
H	-11.6935442372	0.8979458567	0.8806789882
H	-11.6528163244	-1.0753990854	2.3768710765
H	-9.5946602938	-2.4652409749	2.5266329062
H	-7.6022444826	-1.8627695762	1.1806597599
H	-7.9644386245	1.2992426278	2.3262417299
H	-3.5679969112	1.5000162706	-0.3894900761
H	-1.6294105869	2.6525363987	0.6507032656
H	-1.8084943954	3.6471398186	2.8982322087
H	-3.9250234702	3.5293310794	4.1761752458
H	-6.143722242	2.2524916858	5.1611581453
H	-6.6609101446	3.7784320095	4.4111762735
H	-7.7608522317	2.3881615121	4.4468965172

Energy= -3317.3650824

Zero-point correction= 0.236402 (Hartree/Particle)

Sum of electronic and zero-point Energies= -3317.128680

Sum of electronic and thermal Energies= -3317.112680

Sum of electronic and thermal Enthalpies= -3317.111736

Sum of electronic and thermal Free Energies= -3317.175022

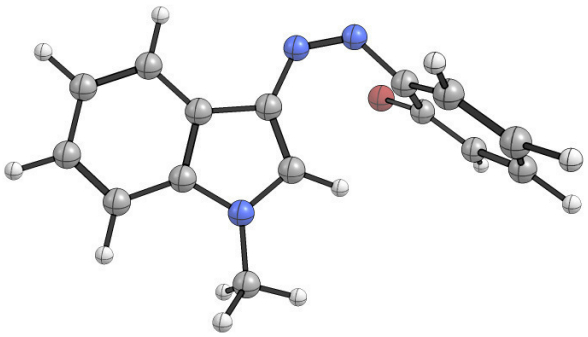

***Z*-3a**

C	-7.6927064143	-4.3049664894	-2.1387621295
C	-8.2399044213	-5.0452733552	-1.0947553661
C	-8.3500586062	-4.4825637214	0.1715294522
C	-7.9110963356	-3.1795461126	0.3850972733
C	-7.331490367	-2.4408758905	-0.6431413383
C	-7.239721121	-3.0071378947	-1.9230375818
N	-7.0144316188	-1.0613677069	-0.4232426583
N	-5.842775721	-0.641244271	-0.3101902702
C	-4.6876991072	-1.4275143137	-0.3128111571
C	-3.3929096909	-0.7848182339	-0.354235849
C	-2.4204289515	-1.8012725436	-0.2662684188
N	-3.1006185465	-3.0041175697	-0.1615202498
C	-4.4482422006	-2.7896113225	-0.1900547702
C	-2.9813281035	0.5475614478	-0.463156231
C	-1.6240601978	0.8212252359	-0.4801122817
C	-0.6696023086	-0.2078955543	-0.394343827
C	-1.0531544382	-1.5349307688	-0.2865032419
O	-6.6904955711	-2.2418768259	-2.9132154957
H	-7.6154247501	-4.7368505873	-3.1321678115
H	-8.5884613365	-6.053950254	-1.2795564795
H	-8.7876102755	-5.0460670656	0.9861327234
H	-8.0132918822	-2.713616148	1.3581106638
H	-2.6705548213	-3.9079157	-0.0539814668
H	-5.130362666	-3.6152546129	-0.0972248338
H	-3.7168616045	1.3386432439	-0.5298907314
H	-1.2862069874	1.847311837	-0.561288677
H	0.3844460994	0.0411425735	-0.4124782617
H	-0.3180241453	-2.3285771698	-0.2204542074
H	-6.7350005021	-2.7164317925	-3.7508410215

Energy= -779.753408

Sum of electronic and zero-point Energies= -779.530654

Sum of electronic and thermal Energies= -779.516507

Sum of electronic and thermal Enthalpies= -779.515563

Sum of electronic and thermal Free Energies= -779.573311

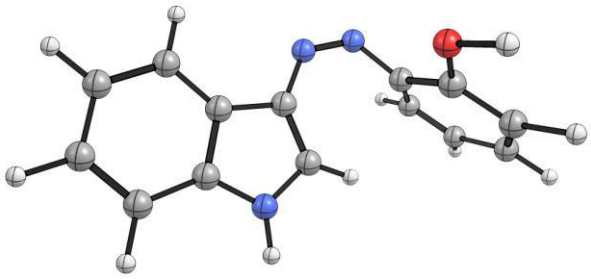

***Z*-3b**

C	-5.7078635315	0.4899076164	-1.7316179671
C	-5.527468243	0.2967218564	-3.0982981458
C	-6.0285300184	-0.8472095597	-3.7089080217
C	-6.7077066045	-1.7924353803	-2.9463123203
C	-6.8681532517	-1.6253029675	-1.5731050376
C	-6.3758128122	-0.4608803537	-0.9659039587
N	-7.6854514038	-2.544526623	-0.8407671207
N	-7.212420582	-3.4291105243	-0.0929695912
C	-5.8581786272	-3.6935636571	0.1092559563
C	-5.4681704988	-4.6702697951	1.0991042244
C	-4.062795004	-4.7749929893	1.0450304991
N	-3.6150957605	-3.9094422735	0.0568898659
C	-4.6816971961	-3.2654896723	-0.497250213
C	-6.1786956129	-5.4507001202	2.0156951718
C	-5.4717112697	-6.3059474046	2.8450396351
C	-4.0706564542	-6.3952475726	2.7787556247
C	-3.3442504697	-5.6314056986	1.8780900668
O	-6.5718506926	-0.3208955597	0.3797844118
C	-2.2295349751	-3.7335514619	-0.3311268279
H	-5.327786781	1.3872603272	-1.2522746944
H	-5.0071089323	1.0471039265	-3.6807715446
H	-5.9054806744	-0.9990563058	-4.7740383409
H	-7.1275573798	-2.6780269861	-3.4086656186
H	-4.5241611628	-2.5635509782	-1.2963867689
H	-7.2575144085	-5.3804534392	2.0660563718
H	-6.0055405242	-6.9198175983	3.5605064512
H	-3.5485689573	-7.0732961613	3.4429300032
H	-2.2645907693	-5.7034182852	1.8299282147
H	-6.2468076157	0.540247505	0.6653819315
H	-1.6350995923	-3.378309981	0.513719439
H	-1.8068164402	-4.6754556856	-0.6882433892
H	-2.1748242956	-2.9984732931	-1.1316433481

Energy= -819.0743077

Zero-point correction= 0.250527 (Hartree/Particle)

Sum of electronic and zero-point Energies= -818.823781

Sum of electronic and thermal Energies= -818.807961

Sum of electronic and thermal Enthalpies= -818.807016

Sum of electronic and thermal Free Energies= -818.868679

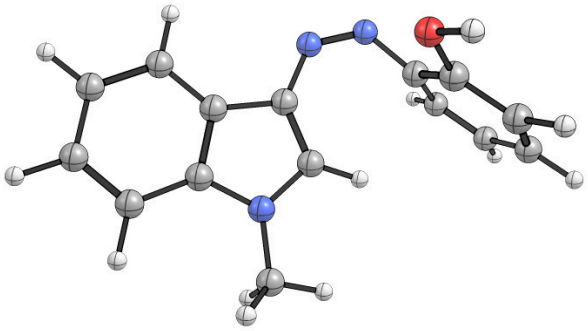

***Z*-4a**

C	3.48204213	1.00391187	1.03598337
C	4.28849334	1.03517072	-0.09846664
C	4.06570375	0.12993127	-1.13181716
C	3.0418899	-0.80557412	-1.03307243
C	2.20433927	-0.83194002	0.08313012
C	2.45796287	0.07850844	1.10772488
N	1.25119666	-1.88727931	0.23207263
N	0.01594232	-1.70981803	0.15002265
C	-0.62173352	-0.50990761	-0.16464116
C	-2.06096418	-0.4196402	-0.05122605
C	-2.434008	0.86096695	-0.5051932
N	-1.27051304	1.50896403	-0.8905923
C	-0.19019116	0.70271186	-0.68882119
C	-3.04983377	-1.30172743	0.39612251
C	-4.36867262	-0.88055444	0.37621008
C	-4.71974771	0.40330743	-0.07739328
C	-3.75773843	1.29422521	-0.52481161
H	3.63457778	1.68496352	1.86385566
H	5.09362873	1.75609528	-0.16490038
H	4.69817301	0.14130963	-2.01093135
H	0.79481517	1.04160039	-0.95450558
H	-2.77873097	-2.28913406	0.74647288
H	-5.14902496	-1.55021023	0.71688964
H	-5.76111715	0.7012505	-0.07691895
H	-4.0272959	2.28413112	-0.87391655
F	1.67238401	0.05768101	2.20701485
H	2.87663802	-1.53344257	-1.81835034
H	-1.22302642	2.43716943	-1.2777319

Energy= -803.7755786

Zero-point correction= 0.210562 (Hartree/Particle)

Sum of electronic and zero-point Energies= -803.565017

Sum of electronic and thermal Energies= -803.551296

Sum of electronic and thermal Enthalpies= -803.550352

Sum of electronic and thermal Free Energies= -803.607501

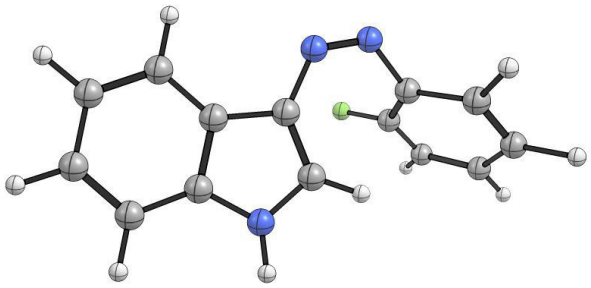

***Z*-4b**

C	3.57502648	0.7390687	1.2157562
C	4.32153517	1.02234864	0.0750569
C	4.07661594	0.32392956	-1.1035767
C	3.09045764	-0.6554874	-1.14403064
C	2.31278905	-0.93340052	-0.01858159
C	2.58790756	-0.2262968	1.15084214
N	1.40386725	-2.03609124	-0.03318459
N	0.16003823	-1.89583423	-0.06368551
C	-0.52918264	-0.68989209	-0.15127992
C	-1.9700056	-0.68642679	-0.04615553
C	-2.39398522	0.64463038	-0.23605621
N	-1.26296048	1.41798738	-0.46162735
C	-0.15594848	0.62672438	-0.40811157
C	-2.92153641	-1.68176909	0.19343259
C	-4.25842187	-1.32157225	0.2368719
C	-4.66247555	0.01128273	0.04871947
C	-3.73704118	1.01545557	-0.19048412
C	-1.2680271	2.84516561	-0.71847127
H	3.74651349	1.25415659	2.15267492
H	5.09800635	1.77597365	0.11510254
H	4.66283814	0.53091004	-1.99048765
H	0.81483225	1.05720836	-0.57723103
H	-2.60911132	-2.7075709	0.33970958
H	-5.01068212	-2.07927385	0.42007375
H	-5.71612688	0.25891724	0.09145302
H	-4.05253077	2.04148823	-0.33438489
H	-1.69713196	3.38635239	0.12766266
H	-0.24478807	3.18358362	-0.8683235
H	-1.84961316	3.07200671	-1.61472915
F	1.85919212	-0.49020319	2.25813693
H	2.90928367	-1.22418276	-2.04822107

Energy= -843.096668

Zero-point correction= 0.238337 (Hartree/Particle)

Sum of electronic and zero-point Energies= -842.858331

Sum of electronic and thermal Energies= -842.842940

Sum of electronic and thermal Enthalpies= -842.841996

Sum of electronic and thermal Free Energies= -842.903006

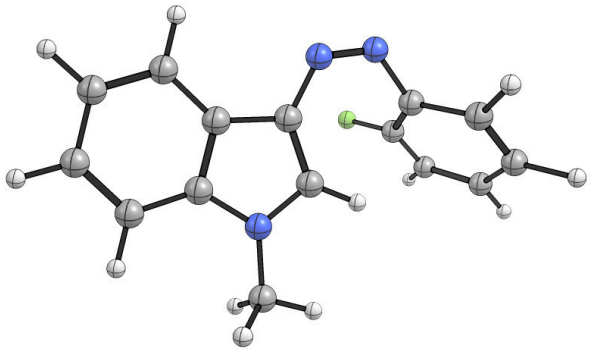

***Z*-5a**

C	-1.7836216	3.59862247	0.32531178
C	-2.6353366	3.08448042	-0.64313
C	-2.79122388	1.70782564	-0.7803615
C	-2.08225204	0.80409217	0.02218743
C	-1.17874003	1.34502581	0.96688189
C	-1.06699356	2.7215188	1.13251235
N	-0.4417269	0.49642477	1.85699971
N	0.72317557	0.11270935	1.60553225
C	1.4586426	0.41057056	0.45522489
C	2.78813976	-0.14461113	0.31616906
C	3.29755481	0.29658354	-0.9212592
N	2.31695193	1.08446671	-1.50359524
C	1.22355645	1.15944792	-0.69236503
C	3.57795609	-0.96867417	1.12473802
C	4.83997791	-1.32166936	0.6771442
C	5.32961907	-0.86981812	-0.5610953
C	4.56554161	-0.05363156	-1.37952055
H	-1.67566656	4.66837411	0.45585097
H	-3.20434106	3.75040822	-1.2809726
H	-3.48836089	1.3333893	-1.51735803
H	-0.38923734	3.09651079	1.89051714
H	0.36967921	1.7402041	-0.9895948
H	3.20068491	-1.31549317	2.07795977
H	5.4661749	-1.95850279	1.29026193
H	6.32154365	-1.1649099	-0.88091181
H	4.94171917	0.29507583	-2.33423803
C	-2.66094022	-1.33968587	1.05689059
C	-2.83771254	-1.09564952	-1.33873988
C	-2.42681225	-2.8278653	0.85647953
H	-3.73426972	-1.15592966	1.22237476
H	-2.11368828	-1.00059406	1.93570831
C	-2.58684663	-2.59360722	-1.46673777
H	-3.92563213	-0.91616715	-1.33528724
H	-2.41288899	-0.58815517	-2.20781323
H	-2.85918095	-3.39440967	1.68186295
H	-1.34876415	-3.03192395	0.8120078
H	-3.12503988	-2.99420901	-2.32714001
H	-1.51189866	-2.77614744	-1.60403483
N	-2.1970296	-0.59491704	-0.12652593
O	-3.05534775	-3.30378853	-0.33057938
H	2.39900581	1.5540139	-2.39047019

Energy= -991.1872217

Zero-point correction= 0.333506 (Hartree/Particle)

Sum of electronic and zero-point Energies= -990.853716

Sum of electronic and thermal Energies= -990.835382

Sum of electronic and thermal Enthalpies= -990.834438

Sum of electronic and thermal Free Energies= -990.902001

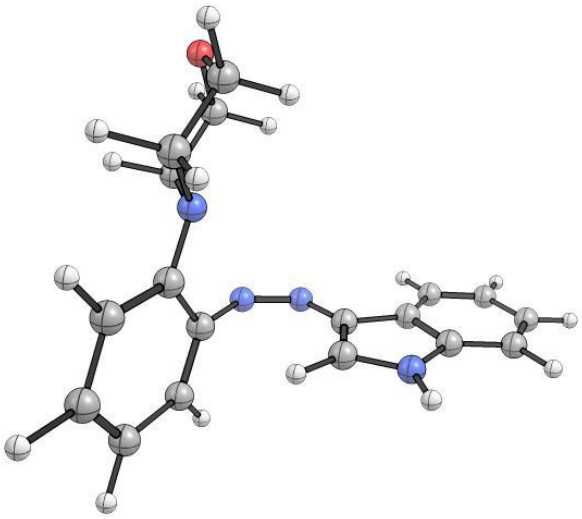

***Z*-5b**

C	1.82465323	3.4990982	-0.78289548
C	2.62782435	3.13274787	0.28875011
C	2.81203225	1.78798627	0.599034
C	2.17859845	0.77209899	-0.12911337
C	1.32135308	1.16551445	-1.18388569
C	1.18395127	2.50845169	-1.5195916
N	0.66346135	0.193501	-2.00638903
N	-0.50276374	-0.20172965	-1.7723429
C	-1.31059599	0.19978826	-0.7089291
C	-2.62578423	-0.38321831	-0.57080179
C	-3.21303626	0.18780333	0.57697209
N	-2.29787334	1.0820676	1.11530439
C	-1.16912909	1.09028645	0.35205451
C	-3.34444075	-1.32772295	-1.30943319
C	-4.61787423	-1.67095803	-0.88521417
C	-5.1870418	-1.09065533	0.26118206
C	-4.49373806	-0.15213031	1.01012721
H	1.69660985	4.5415953	-1.04745
H	3.13844244	3.88851296	0.87376684
H	3.47252032	1.52740652	1.41469625
H	0.54519787	2.76751941	-2.35594149
H	-0.35094797	1.73448805	0.61896291
H	-2.90569598	-1.7735261	-2.19267012
H	-5.18980868	-2.40065115	-1.44569538
H	-6.18521743	-1.38135972	0.56533717
H	-4.93580891	0.29300994	1.89305038
C	2.87387022	-1.46019538	-0.86211647
C	2.89915293	-0.92674648	1.49234269
C	2.66298269	-2.92025975	-0.49724315
H	3.95070293	-1.26464717	-0.98637164
H	2.37289022	-1.24511588	-1.80524533
C	2.67692694	-2.40587271	1.78606509
H	3.98065835	-0.71494945	1.52986553
H	2.41018922	-0.33293265	2.26802266
H	3.15766401	-3.56786255	-1.22184599
H	1.58925541	-3.15000757	-0.49018129
H	3.17162558	-2.68415585	2.71790796
H	1.60020616	-2.6034658	1.88290006
N	2.32137374	-0.59458635	0.19396936
O	3.22947931	-3.23200322	0.7728721
C	-2.52057814	1.89074952	2.29796084
H	-3.37914615	2.55114269	2.15659814
H	-2.70288023	1.25687898	3.16866405
H	-1.63742566	2.49846754	2.48440962

Energy= -1030.5082166

Zero-point correction= 0.361249 (Hartree/Particle)

Sum of electronic and zero-point Energies= -1030.146967

Sum of electronic and thermal Energies= -1030.126957

Sum of electronic and thermal Enthalpies= -1030.126013

Sum of electronic and thermal Free Energies= -1030.197337

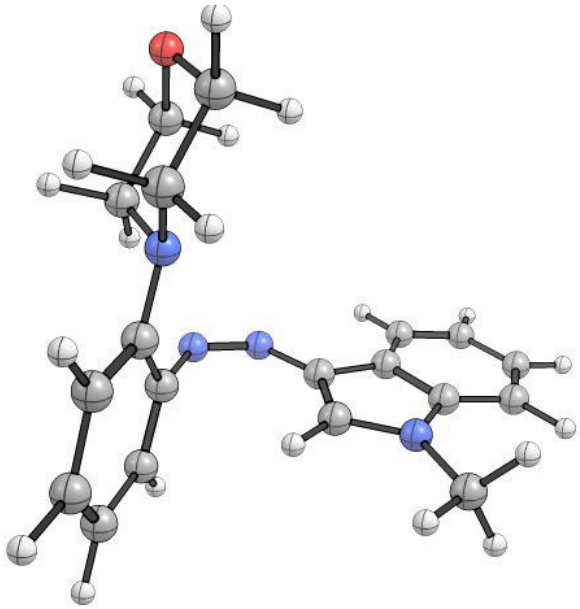

***Z*-6a**

C	-7.6540545632	-4.3645855376	-2.2568343101
C	-8.1202959157	-5.1450584136	-1.2004526112
C	-8.1486187006	-4.6187747494	0.0884339084
C	-7.7084844865	-3.3192882958	0.3211253018
C	-7.211252352	-2.5481971792	-0.7255395637
C	-7.2048987512	-3.0737804835	-2.0191771526
N	-6.8577678768	-1.1777176361	-0.4934058372
N	-5.6685405286	-0.7993285159	-0.4021901812
C	-4.5352210751	-1.6210229803	-0.4474549331
C	-3.2266523961	-1.0045033051	-0.4100083409
C	-2.2749571329	-2.0437831044	-0.4053641192
N	-2.97968987	-3.236800624	-0.4289308843
C	-4.3219487641	-2.9944148739	-0.4574246778
C	-2.7881110257	0.3236001866	-0.3822860533
C	-1.4258371294	0.5698433035	-0.3532135456
C	-0.4924329791	-0.4819450544	-0.3524248682
C	-0.902716935	-1.8050195884	-0.3783207103
O	-8.5477070809	-6.4146285	-1.4930590786
H	-7.6580701983	-4.7773477605	-3.2580056175
H	-8.5274210584	-5.216177047	0.9120006057
H	-7.7494502302	-2.901293331	1.3197144484
H	-6.8491782973	-2.4639073134	-2.8408564625
H	-2.5681062189	-4.1556248333	-0.4283125287
H	-5.0177614368	-3.8130455021	-0.4733976552
H	-3.507440257	1.1321878252	-0.3824561253
H	-1.0674104063	1.5918946784	-0.3305427633
H	0.566235248	-0.2537956519	-0.3306435717
H	-0.1841400032	-2.6163342848	-0.377123715
H	-8.8878725028	-6.8343928748	-0.6949948727

Energy= -779.7557139

Sum of electronic and zero-point Energies= -779.532985

Sum of electronic and thermal Energies= -779.518828

Sum of electronic and thermal Enthalpies= -779.517884

Sum of electronic and thermal Free Energies= -779.576275

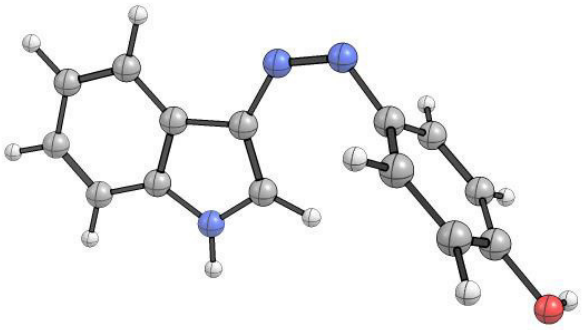

***Z*-6b**

C	-7.0620008212	-4.1537872199	-2.7187529255
C	-7.5213973484	-4.9040804641	-1.6384591894
C	-7.6890471681	-4.2970799805	-0.3962187148
C	-7.3900132134	-2.9481123285	-0.2326662536
C	-6.9037947272	-2.2012665583	-1.3025223548
C	-6.7616745337	-2.8090639218	-2.550916296
N	-6.6955355502	-0.7897560983	-1.1567575542
N	-5.5738762466	-0.3066585264	-0.8782585524
C	-4.3963373571	-1.0264111162	-0.658788492
C	-3.183771187	-0.3017878124	-0.3539900873
C	-2.1643021107	-1.2584628877	-0.1702498034
N	-2.7287643197	-2.5130468786	-0.3531644603
C	-4.0535646334	-2.3759463762	-0.6435434045
C	-2.8802587301	1.0565656853	-0.2230222393
C	-1.5785971202	1.4173270623	0.084497235
C	-0.5752182589	0.4495649299	0.2633721268
C	-0.8520269655	-0.9032215142	0.1388451228
O	-7.8024165968	-6.2283094134	-1.8610070352
C	-2.0140476956	-3.7706693245	-0.2536351804
H	-6.9562715692	-4.6316636947	-3.6847994195
H	-8.0646320997	-4.8727175448	0.4442565929
H	-7.5342784934	-2.4719586593	0.7296664419
H	-6.4155951203	-2.2213430389	-3.3927054622
H	-4.6522486994	-3.2513841565	-0.8179304594
H	-3.6540059192	1.8005579631	-0.3611675728
H	-1.3246918296	2.4652251431	0.1899859639
H	0.4327403318	0.7659482921	0.5028234062
H	-0.0759500753	-1.6459088772	0.2774737521
H	-8.1602603481	-6.6227885123	-1.0578262972
H	-1.5918868825	-3.895462174	0.7460798079
H	-2.7048770028	-4.588649234	-0.4478616495
H	-1.2047901626	-3.8123143799	-0.9860994051

Energy= -819.0766895

Zero-point correction= 0.250506 (Hartree/Particle)

Sum of electronic and zero-point Energies= -818.826184

Sum of electronic and thermal Energies= -818.810361

Sum of electronic and thermal Enthalpies= -818.809417

Sum of electronic and thermal Free Energies= -818.871489

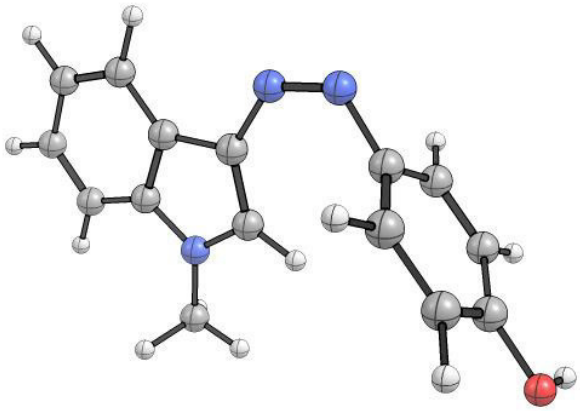

***Z*-7a**

C	-2.94951755	0.32171768	1.21407947
C	-3.52463521	-0.03932395	5.6141E-05
C	-1.16093875	1.39259111	8.48E-05
C	-1.7683328	1.04448869	1.21215706
N	-0.02831648	2.24671469	0.00011905
N	1.15750553	1.84964051	8.1774E-05
C	1.5726522	0.5189975	-4.7078E-05
C	2.98933124	0.22281367	7.0633E-06
C	3.11995985	-1.17943909	-0.00018783
N	1.83639335	-1.70607059	-0.00035941
C	0.91279459	-0.70714073	-0.00027759
C	4.1403202	1.0173766	0.00020486
C	5.37452926	0.39007215	0.00020158
C	5.48305121	-1.01193072	7.1914E-06
C	4.35729248	-1.81905805	-0.00019043
H	-3.43263313	0.03619897	2.13763937
H	-1.30943196	1.34833506	2.14447457
H	-0.13558665	-0.94245641	-0.00040018
H	4.05637026	2.09630073	0.00035428
H	6.27783992	0.98781648	0.00035158
H	6.46485264	-1.46915137	1.1899E-05
H	4.43970822	-2.89950027	-0.00033999
H	1.61102476	-2.68781193	-0.0005318
C	-1.76852006	1.04484726	-1.21199543
H	-1.30976405	1.34897215	-2.14429349
C	-2.94970267	0.32207132	-1.21394905
H	-3.43295822	0.03682104	-2.13751864
N	-4.77129146	-0.81260468	3.8471E-05
O	-5.25612885	-1.11610977	-1.08556444
O	-5.25596535	-1.11642261	1.08562689

Energy= -909.078677

Zero-point correction= 0.221168 (Hartree/Particle)

Sum of electronic and zero-point Energies= -908.857509

Sum of electronic and thermal Energies= -908.842100

Sum of electronic and thermal Enthalpies= -908.841156

Sum of electronic and thermal Free Energies= -908.903448

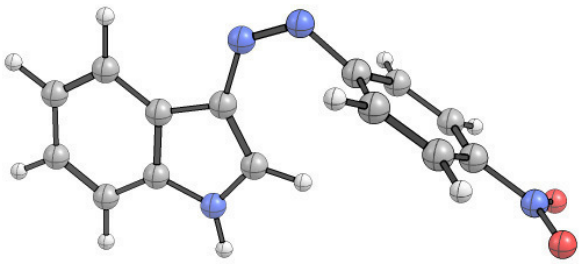

***Z*-7b**

C	-3.0411951996	0.4337349378	1.2141297292
C	-3.6068366487	0.0572764150	0.0000772002
C	-1.2797620287	1.5503774216	0.0000913778
C	-1.8790890865	1.1865325605	1.2120213438
N	-0.1691106784	2.4310009329	0.0001171325
N	1.0272070608	2.0613432505	0.0000940876
C	1.4736168783	0.7443104404	-0.0000142022
C	2.8939907117	0.4777636670	0.0000490437
C	3.0493611300	-0.9228585628	-0.0001308897
N	1.7795021430	-1.4876532501	-0.0003082468
C	0.8448999254	-0.5007365723	-0.0002400427
C	4.0284466699	1.2942161750	0.0002441275
C	5.2754784576	0.6913532917	0.0002550639
C	5.4111435197	-0.7074744414	0.0000774899
C	4.3006554271	-1.5370813890	-0.0001181971
H	-3.5169387572	0.1361639387	2.1377316358
H	-1.4281288517	1.5023109161	2.1442722020
H	-0.1989260527	-0.7573462560	-0.0003683310
H	3.9232386466	2.3713190732	0.0003813936
H	6.1667796089	1.3069488693	0.0004038088
H	6.4016079096	-1.1457277840	0.0000938718
H	4.4094397613	-2.6145174416	-0.0002536426
C	-1.8792963993	1.1868796754	-1.2118388619
H	-1.4284965170	1.5029277322	-2.1440759599
C	-3.0414001584	0.4340767126	-1.2139639963
H	-3.5172986152	0.1367652302	-2.1375696540
N	-4.8316570102	-0.7490437977	0.0000669484
O	-5.3083809892	-1.0661191894	-1.0855238049
O	-5.3081948161	-1.0664292497	1.0856488578
C	1.5025284196	-2.9124722847	-0.0005267410
H	1.9264154232	-3.3846680937	0.8880738362
H	0.4255050541	-3.0664820569	-0.0006721075
H	1.9266208372	-3.3844313669	-0.8891546050

Energy= -948.4000773

Zero-point correction=	0.248921 (Hartree/Particle)
Sum of electronic and zero-point Energies=	-948.151157
Sum of electronic and thermal Energies=	-948.134069
Sum of electronic and thermal Enthalpies=	-948.133125
Sum of electronic and thermal Free Energies=	-948.199042

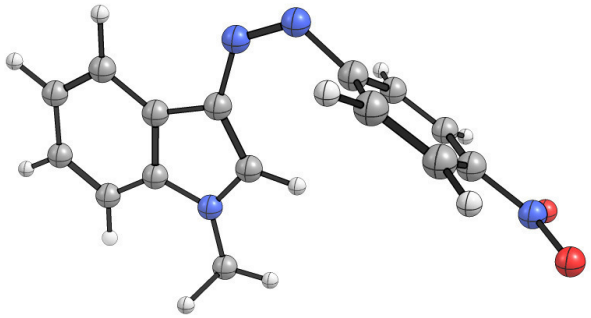

***Z*-8a**

C	-2.65298866	-3.06340662	4.83985164
C	-3.3312629	-4.26132639	4.56904857
C	-3.84337852	-4.44421412	3.27309366
C	-3.67074378	-3.48403571	2.29325116
C	-2.96646785	-2.3073415	2.57688043
C	-2.4764696	-2.09280375	3.86543586
C	-3.47977149	-5.24217427	5.63792182
C	-4.08108431	-6.44018011	5.56704632
C	-4.18322512	-7.37417825	6.69190703
O	-4.72030712	-8.45785494	6.62660416
O	-3.61547903	-6.92730247	7.84650492
N	-2.89915334	-1.26748204	1.60788292
N	-2.00217474	-1.18222145	0.74036874
C	-0.92373779	-2.05671905	0.59071182
C	0.01112594	-1.8392685	-0.49236519
C	0.9967308	-2.84133535	-0.39847984
N	0.67204242	-3.62702181	0.69719385
C	-0.46597164	-3.16952156	1.28934756
C	0.09305525	-0.8935401	-1.5196658
C	1.14763271	-0.97861119	-2.41275268
C	2.12066872	-1.98773439	-2.30200632
C	2.06043828	-2.93501859	-1.29297197
H	-2.26284111	-2.89212486	5.83708828
H	-4.38947683	-5.34683183	3.02850116
H	-4.08046179	-3.63069024	1.30132892
H	-1.96334516	-1.16673918	4.09388925
H	-3.04746193	-4.95742395	6.59190959
H	-4.54096358	-6.81121937	4.66046933
H	-3.75354607	-7.62854463	8.50082887
H	1.19751143	-4.4244425	1.01687449
H	-0.85795059	-3.6636918	2.15924808
H	-0.6561626	-0.11722152	-1.6043401
H	1.22860387	-0.255096	-3.21485123
H	2.93205155	-2.02508243	-3.01851056
H	2.80973229	-3.71312062	-1.20673534

Energy= -970.5744404

Zero-point correction= 0.266888 (Hartree/Particle)

Sum of electronic and zero-point Energies= -970.307552

Sum of electronic and thermal Energies= -970.289458

Sum of electronic and thermal Enthalpies= -970.288513

Sum of electronic and thermal Free Energies= -970.357591

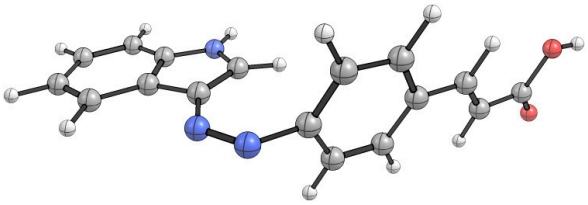

***Z*-8b**

C	-3.70332341	-4.34237671	-3.50254007
C	-4.13335232	-5.3314137	-2.6048463
C	-4.2870317	-4.96761261	-1.25597364
C	-4.00869307	-3.68363348	-0.82493694
C	-3.55299995	-2.71858077	-1.73198584
C	-3.42241351	-3.05182038	-3.08091006
C	-4.40818967	-6.67017198	-3.11272852
C	-4.81142926	-7.7417439	-2.41164239
C	-5.06103891	-9.06010805	-3.00054369
O	-5.4181217	-10.0292047	-2.36752211
O	-4.85636323	-9.12268297	-4.34587
N	-3.38795037	-1.37016375	-1.31177963
N	-2.31578277	-0.90948954	-0.85753272
C	-1.12422613	-1.61478981	-0.70198337
C	0.02592961	-0.94115952	-0.14388372
C	1.07760795	-1.87920685	-0.11191552
N	0.59214918	-3.07311368	-0.62983947
C	-0.71373315	-2.91734961	-0.97973781
C	0.24993962	0.35662231	0.32464818
C	1.50800217	0.67674449	0.80789741
C	2.54451405	-0.27205207	0.83268168
C	2.34609087	-1.56486385	0.37333357
C	1.36358133	-4.29358274	-0.77199144
H	-3.59354376	-4.59442819	-4.55162564
H	-4.63528636	-5.69634057	-0.53448571
H	-4.14345623	-3.41104572	0.21472163
H	-3.10446501	-2.29583241	-3.78837727
H	-4.26304806	-6.7997594	-4.18055987
H	-4.98360563	-7.7110787	-1.34371713
H	-5.05682775	-10.034873	-4.60400469
H	-1.25341001	-3.74505565	-1.40297247
H	-0.54890928	1.08650106	0.30523065
H	1.70099053	1.67743151	1.17515949
H	3.51635802	0.01169778	1.21768235
H	3.1474561	-2.2930561	0.39416856
H	1.7232071	-4.63540087	0.20086884
H	0.73113785	-5.06646249	-1.20386643
H	2.22077868	-4.13115498	-1.4288792

Energy= -1009.8956438

Zero-point correction= 0.294657 (Hartree/Particle)

Sum of electronic and zero-point Energies= -1009.600987

Sum of electronic and thermal Energies= -1009.581223

Sum of electronic and thermal Enthalpies= -1009.580279

Sum of electronic and thermal Free Energies= -1009.652887

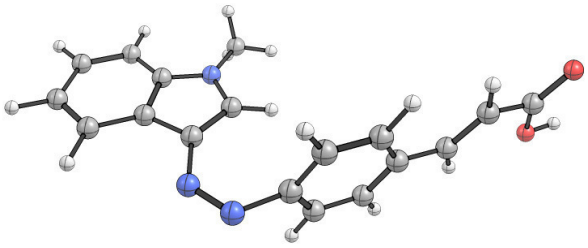

***Z*-9a**

C	-6.80122881	-3.80116641	4.41825437
C	-7.50977778	-3.82444262	3.22482016
C	-7.29823665	-2.83183858	2.27855111
C	-6.37813511	-1.80790363	2.48765906
C	-5.68002371	-1.80529417	3.69386119
C	-5.88416885	-2.78500131	4.65349139
N	-6.34015841	-0.68067322	1.60065379
F	-4.78946973	-0.83701403	3.9433072
F	-5.1995462	-2.76158537	5.80049074
F	-7.00077522	-4.74963283	5.3357768
F	-8.38814808	-4.80365428	2.99273543
F	-7.99343313	-2.87566989	1.13531179
N	-5.40061881	-0.47164903	0.80384288
C	-4.30669971	-1.29401758	0.5749911
C	-3.22583361	-0.82779887	-0.26688378
C	-2.30051843	-1.88359955	-0.37416869
N	-2.80966023	-2.94585004	0.35970384
C	-3.99671184	-2.60478057	0.92745164
C	-2.96696871	0.37937997	-0.92317726
C	-1.8002866	0.49109858	-1.66010904
C	-0.88730676	-0.57439496	-1.75191369
C	-1.12262253	-1.77899058	-1.10991605
H	-2.37598107	-3.85062577	0.44890899
H	-4.5407252	-3.32459387	1.51171499
H	-3.66923468	1.19961659	-0.85166701
H	-1.58216561	1.41703975	-2.17800684
H	0.0166098	-0.45097971	-2.33554391
H	-0.4196243	-2.60056988	-1.17950345

Energy= -1200.8215568

Zero-point correction= 0.178150 (Hartree/Particle)

Sum of electronic and zero-point Energies= -1200.643406

Sum of electronic and thermal Energies= -1200.626007

Sum of electronic and thermal Enthalpies= -1200.625063

Sum of electronic and thermal Free Energies= -1200.691433

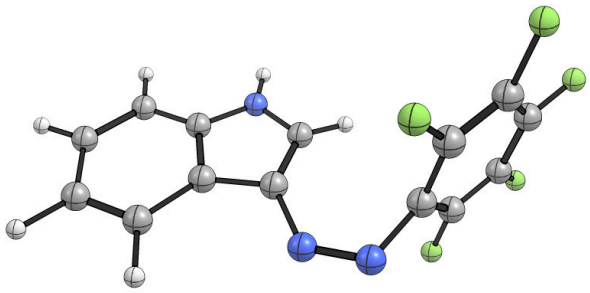

***Z*-9b**

C	-7.89209885	-4.69663651	-1.46463563
C	-7.84091242	-4.08418781	-0.21950298
C	-7.37969193	-2.78058336	-0.11128764
C	-6.96039676	-2.05894229	-1.22661127
C	-7.02569895	-2.69294625	-2.46479374
C	-7.48210352	-3.99700682	-2.59146811
N	-6.69893464	-0.65132065	-1.13925426
F	-6.63410461	-2.03991865	-3.56636651
F	-7.52507787	-4.58541424	-3.79039447
F	-8.33374915	-5.9515691	-1.57748789
F	-8.23093677	-4.756615	0.86744489
F	-7.33715209	-2.2129302	1.10097969
N	-5.56969557	-0.18346259	-0.87230173
C	-4.40461264	-0.89517332	-0.64564337
C	-3.19108488	-0.18489261	-0.31037604
C	-2.17830137	-1.15170587	-0.15759463
N	-2.74678019	-2.39858579	-0.39377925
C	-4.06488148	-2.2484514	-0.68177096
C	-2.8842887	1.16616529	-0.12861633
C	-1.58261544	1.50800478	0.19867585
C	-0.58502883	0.5294606	0.34816587
C	-0.86635956	-0.81632147	0.17255386
C	-2.0320777	-3.66093578	-0.34078911
H	-4.66150193	-3.11599325	-0.89880037
H	-3.65316845	1.91895176	-0.24364151
H	-1.32409235	2.54988413	0.34335491
H	0.4225369	0.83228421	0.60532029
H	-0.0949092	-1.56730014	0.28867036
H	-1.61568129	-3.82209426	0.65552596
H	-2.72114527	-4.47127109	-0.56935556
H	-1.22043041	-3.67077479	-1.07095616

Energy= -1240.1431275

Zero-point correction= 0.205914 (Hartree/Particle)

Sum of electronic and zero-point Energies= -1239.937213

Sum of electronic and thermal Energies= -1239.918132

Sum of electronic and thermal Enthalpies= -1239.917188

Sum of electronic and thermal Free Energies= -1239.987546

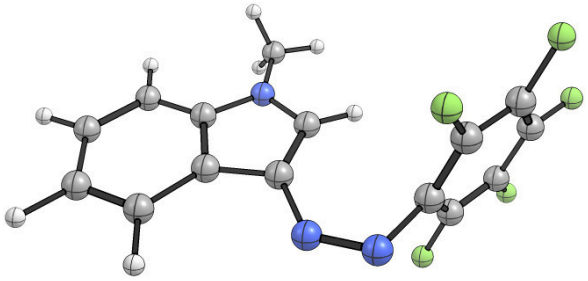

***Z*-10a**

C	-8.16401064	-0.50038676	-2.83386836
C	-6.89381108	-0.45777195	-3.40011243
C	-5.97914768	-1.46431957	-3.12069627
C	-6.32073752	-2.54351963	-2.30165475
C	-7.61442537	-2.59834845	-1.75525094
C	-8.51211499	-1.55982812	-2.00789857
N	-7.9972194	-3.60587661	-0.8119868
N	-5.36440179	-3.56166246	-2.06169632
C	-4.4759235	-4.04836512	-3.00526271
C	-3.64301844	-4.9455194	-2.3914269
C	-4.02199404	-5.00725274	-1.02047846
C	-5.07784995	-4.15274761	-0.84447177
N	-8.64359824	-4.62799595	-1.13324695
C	-9.03589911	-4.98244486	-2.42446849
C	-9.8055206	-6.19341984	-2.61451516
C	-10.0385841	-6.32619183	-3.99734129
N	-9.43205725	-5.24307887	-4.61531321
C	-8.83662321	-4.44029057	-3.68982332
C	-10.3080992	-7.16269848	-1.74047826
C	-11.0231215	-8.22328607	-2.27071378
C	-11.2463616	-8.33612348	-3.65443463
C	-10.7571852	-7.38915785	-4.53952392
H	-8.87734267	0.29216761	-3.02453058
H	-6.6026726	0.37062183	-4.03402425
H	-4.97442795	-1.41213582	-3.5202295
H	-9.49274718	-1.60446195	-1.54948578
H	-4.53645099	-3.73434676	-4.03322349
H	-2.86008211	-5.50806336	-2.87443512
H	-3.57234185	-5.61323834	-0.25034087
H	-5.65474581	-3.91234673	0.03098005
H	-9.42564369	-5.0684443	-5.60696609
H	-8.31706478	-3.55238654	-4.00029011
H	-10.1341455	-7.07592225	-0.6758937
H	-11.4195595	-8.98450344	-1.60975267
H	-11.8099279	-9.17901676	-4.03540202
H	-10.9273663	-7.47579482	-5.60628129

Energy= -913.5310383

Zero-point correction= 0.281106 (Hartree/Particle)

Sum of electronic and zero-point Energies= -913.249932

Sum of electronic and thermal Energies= -913.233049

Sum of electronic and thermal Enthalpies= -913.232104

Sum of electronic and thermal Free Energies= -913.297008

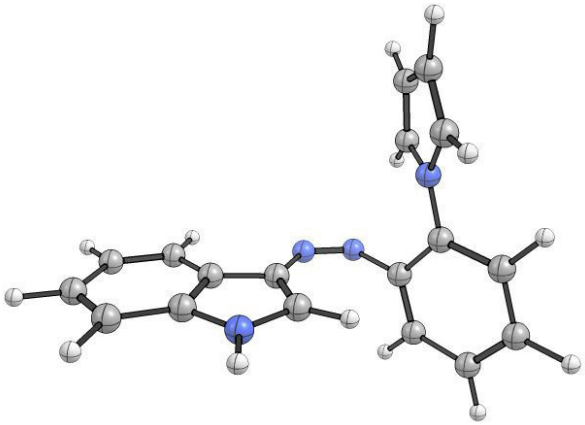

***Z*-10b**

C	-5.00904397	-0.10456067	1.66809032
C	-4.27116525	-0.07888337	2.84743519
C	-4.4403205	-1.0849039	3.78940726
C	-5.31905032	-2.14713297	3.56184486
C	-6.04208633	-2.1851762	2.35697167
C	-5.89588988	-1.14638112	1.43594451
N	-7.04851665	-3.17172903	2.10567557
N	-5.44162554	-3.16618905	4.53957548
C	-4.39309027	-3.66990889	5.29012305
C	-4.90056383	-4.5622391	6.19665634
C	-6.31100826	-4.60336753	6.00755257
C	-6.61670967	-3.741762	4.98759837
N	-6.83572472	-4.20184184	1.42515817
C	-5.61850068	-4.58273567	0.86699978
C	-5.55097326	-5.79947951	0.09015356
C	-4.21195161	-5.95163168	-0.32302602
N	-3.49192331	-4.87663605	0.18182248
C	-4.32587178	-4.06347333	0.88608596
C	-6.49671094	-6.75840972	-0.28342764
C	-6.08117918	-7.83164054	-1.05447875
C	-4.74194705	-7.96579643	-1.4587732
C	-3.78599679	-7.02825408	-1.09927745
C	-2.07104429	-4.66182897	-0.01348425
H	-4.90433587	0.68812698	0.93724245
H	-3.5877971	0.73646563	3.05022511
H	-3.90469409	-1.04494196	4.72927984
H	-6.48753929	-1.17717327	0.52883483
H	-3.37855912	-3.36953875	5.09155784
H	-4.32354764	-5.13462975	6.90532701
H	-7.0214603	-5.20089931	6.5559538
H	-7.55876507	-3.4872899	4.53509792
H	-3.93592329	-3.17644786	1.3516526
H	-7.52740318	-6.65498109	0.02995097
H	-6.79965615	-8.58542545	-1.35312459
H	-4.45071487	-8.81759731	-2.06121067
H	-2.75452116	-7.13597643	-1.41142112
H	-1.49626371	-5.49031596	0.40618338
H	-1.83878969	-4.5733508	-1.07703645
H	-1.77807977	-3.74142026	0.48751207

Energy= -952.8521563

Zero-point correction= 0.308874 (Hartree/Particle)

Sum of electronic and zero-point Energies= -952.543282

Sum of electronic and thermal Energies= -952.524729

Sum of electronic and thermal Enthalpies= -952.523784

Sum of electronic and thermal Free Energies= -952.592378

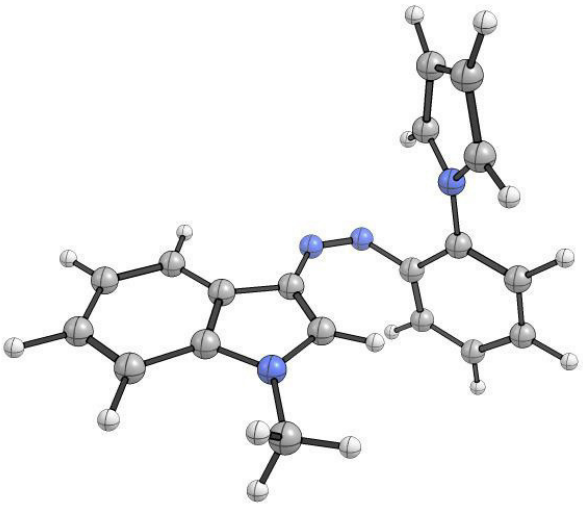

***Z*-11a**

C	-7.25233423	-5.09038798	-2.49381064
C	-7.36852275	-4.61163957	-1.19307168
C	-6.87440186	-3.35941998	-0.84614156
C	-6.24386426	-2.57431403	-1.81052831
C	-6.14168794	-3.03494201	-3.12240484
C	-6.64146156	-4.28954168	-3.4527419
N	-5.86607477	-1.23503616	-1.49779983
N	-4.72451383	-0.91952367	-1.09318083
C	-3.65588374	-1.78828149	-0.88024568
C	-2.39712021	-1.24752059	-0.41229904
C	-1.50382735	-2.32796493	-0.28051433
N	-2.19438599	-3.4721331	-0.65275276
C	-3.46972059	-3.16303176	-1.00970153
C	-1.96050828	0.0437298	-0.09922684
C	-0.65572292	0.21181241	0.3320039
C	0.22056722	-0.88090323	0.45675216
C	-0.18959014	-2.16844902	0.15239817
C	-6.47342773	-4.7972772	-4.86050387
F	-5.23827192	-5.32515754	-5.04915766
F	-6.61600407	-3.81614857	-5.77302527
F	-7.3593843	-5.76404146	-5.16524296
C	-7.99517643	-5.47383281	-0.12926263
F	-8.83108954	-6.39508539	-0.64425246
F	-8.69480156	-4.74786115	0.76445575
F	-7.05300046	-6.15071228	0.57371164
H	-7.65177233	-6.05799974	-2.76033962
H	-6.98614033	-2.98171093	0.16205248
H	-5.68602225	-2.40617746	-3.87652077
H	-1.8134045	-4.4046129	-0.66032871
H	-4.14109916	-3.94010734	-1.32507808
H	-2.63535178	0.88420738	-0.19541797
H	-0.29828277	1.20389641	0.57950952
H	1.23490312	-0.71270399	0.79706815
H	0.48466546	-3.01125303	0.24806937

Energy= -1378.8205369

Zero-point correction= 0.227377 (Hartree/Particle)

Sum of electronic and zero-point Energies= -1378.593160

Sum of electronic and thermal Energies= -1378.572855

Sum of electronic and thermal Enthalpies= -1378.571911

Sum of electronic and thermal Free Energies= -1378.649561

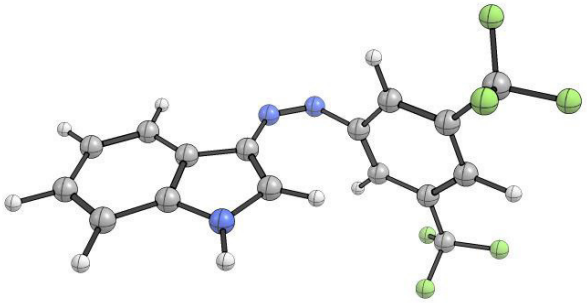

***Z*-11b**

C	-6.36226582	-3.34747212	-0.61973692
C	-6.76176694	-4.63362721	-0.97007549
C	-6.68437755	-5.07162335	-2.28652461
C	-6.20894914	-4.20996973	-3.2754794
C	-5.78558664	-2.92722112	-2.93150826
C	-5.86994861	-2.50421031	-1.60926996
N	-5.99255591	-4.69846105	-4.59683791
N	-6.8494142	-4.6170506	-5.50777546
C	-8.11676548	-4.055936	-5.39897069
C	-8.98380187	-4.04799103	-6.55563628
C	-10.1864496	-3.4267119	-6.16481102
N	-10.0608021	-3.06974492	-4.82759621
C	-8.83578622	-3.44165026	-4.37245904
C	-8.84351199	-4.50793316	-7.86797186
C	-9.90184672	-4.33456944	-8.74448361
C	-11.0943363	-3.71253384	-8.33675456
C	-11.2561173	-3.24859675	-7.04065838
C	-11.0848293	-2.40234477	-4.04456559
C	-5.46174812	-1.09640866	-1.264865
F	-6.45027435	-0.21276977	-1.55318243
F	-4.37714298	-0.69918473	-1.95885606
F	-5.17991771	-0.94954814	0.04337652
C	-7.33291952	-5.5473117	0.08160062
F	-8.68210912	-5.42408301	0.16061227
F	-6.84843614	-5.27833038	1.30923559
F	-7.07886244	-6.84418618	-0.17783479
H	-6.41072107	-3.01820684	0.40803565
H	-6.97667242	-6.07952389	-2.55102784
H	-5.38188578	-2.2748476	-3.69519323
H	-8.56800675	-3.23983029	-3.35140331
H	-7.92487277	-4.98678745	-8.18096192
H	-9.81269803	-4.68406538	-9.76588859
H	-11.9021349	-3.59328225	-9.04832262
H	-12.1765371	-2.76983298	-6.73037209
H	-11.9893986	-3.01215998	-3.9996144
H	-10.7152466	-2.24617286	-3.03331343
H	-11.3309944	-1.43365735	-4.48408772

Energy= -1418.1420183

Zero-point correction= 0.255107 (Hartree/Particle)

Sum of electronic and zero-point Energies= -1417.886911

Sum of electronic and thermal Energies= -1417.864915

Sum of electronic and thermal Enthalpies= -1417.863971

Sum of electronic and thermal Free Energies= -1417.945283

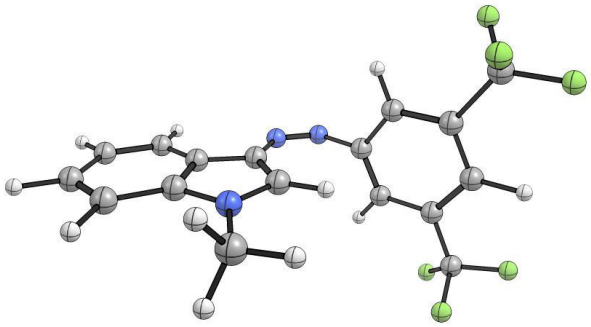

***Z*-12a**

C	-6.89064829	0.95770493	-1.14635207
C	-7.7718171	0.35393719	-0.22512767
N	-7.01887906	-0.11896146	0.82697853
C	-5.55975335	0.83756633	-0.58817342
C	-7.43281492	1.51405098	-2.30843357
C	-8.79719615	1.4553743	-2.52009487
C	-9.65325641	0.84841227	-1.58810057
C	-9.14290262	0.29530116	-0.43366462
N	-4.44867262	1.26350287	-1.33802215
N	-3.28126867	1.35385927	-0.90566435
C	-2.93005596	1.10961541	0.45984205
C	-2.23725081	-0.056159	0.78569151
C	-1.80599553	-0.25965648	2.09237116
C	-2.03612752	0.7059159	3.06840041
C	-2.6958337	1.88462116	2.7282817
C	-3.14320922	2.09154819	1.42906862
H	-2.04179476	-0.79195631	0.01486299
H	-1.2766249	-1.17103449	2.34447368
H	-1.68793334	0.54973881	4.08199313
H	-2.85957169	2.65012583	3.47773191
H	-3.65087382	3.00927694	1.1578902
C	-5.70135475	0.17038645	0.61980096
H	-4.96119871	-0.13712898	1.33551411
F	-6.66919913	2.11009406	-3.22656814
F	-9.33156176	1.98296997	-3.62750279
F	-10.9667341	0.81530055	-1.83320283
F	-9.94885337	-0.2890203	0.47207354
H	-7.38829323	-0.61099299	1.62423897

Energy= -1101.5592166

Zero-point correction= 0.186460 (Hartree/Particle)

Sum of electronic and zero-point Energies= -1101.372756

Sum of electronic and thermal Energies= -1101.356187

Sum of electronic and thermal Enthalpies= -1101.355243

Sum of electronic and thermal Free Energies= -1101.419063

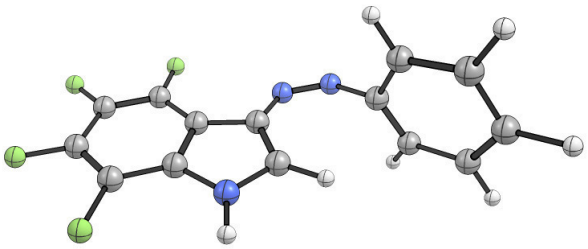

***Z*-12b**

C	-6.90918356	0.97843766	-1.14772033
C	-7.76766032	0.29943388	-0.25241181
N	-7.02391729	-0.07321031	0.85324468
C	-5.60170237	1.0055419	-0.53208843
C	-7.43744652	1.45532713	-2.3504463
C	-8.77374362	1.25472821	-2.63571751
C	-9.61054022	0.57947996	-1.73644242
C	-9.11469572	0.09950319	-0.54311057
N	-4.53118496	1.60521954	-1.21095338
N	-3.36598478	1.71752344	-0.77297753
C	-2.9676111	1.2525215	0.51924634
C	-2.36879552	-0.00122791	0.64856086
C	-1.89077821	-0.41307737	1.88778256
C	-1.99024183	0.42433837	2.99589757
C	-2.56062181	1.68695283	2.85419123
C	-3.04417021	2.1069662	1.62023887
H	-2.2804029	-0.64143171	-0.22097545
H	-1.42991397	-1.38917789	1.98496794
H	-1.60890713	0.10344576	3.95750552
H	-2.6228969	2.35286155	3.70701873
H	-3.47780892	3.09257785	1.50090068
C	-5.73980528	0.3483198	0.68498017
H	-5.01204946	0.14324166	1.4482703
F	-6.68683961	2.10591905	-3.24169447
F	-9.29626922	1.7045267	-3.78233981
F	-10.8992654	0.40551529	-2.04885372
F	-9.93338662	-0.54673495	0.30998228
C	-7.51550809	-0.79991329	2.01743447
H	-8.30487485	-0.23760067	2.51608284
H	-7.90559949	-1.77474219	1.72503019
H	-6.68652962	-0.93966096	2.70777414

Energy= -1140.8789479

Zero-point correction= 0.214259 (Hartree/Particle)

Sum of electronic and zero-point Energies= -1140.664689

Sum of electronic and thermal Energies= -1140.646427

Sum of electronic and thermal Enthalpies= -1140.645483

Sum of electronic and thermal Free Energies= -1140.713407

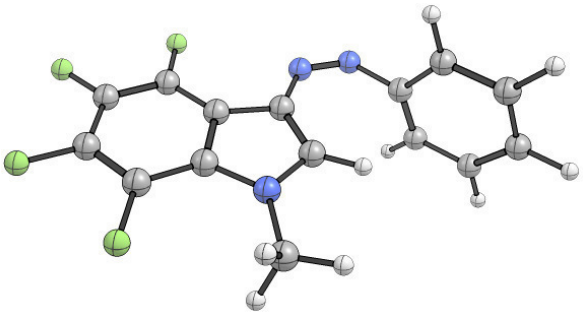

***Z*-12c**

C	-6.88839432	0.86973291	-1.14688974
C	-7.77825274	0.24102147	-0.24333841
N	-7.01776649	-0.35253826	0.75723025
C	-5.55404203	0.65886257	-0.63801254
C	-7.40938097	1.55792964	-2.24424053
C	-8.7761859	1.61494235	-2.42771548
C	-9.64595135	1.00285664	-1.51636013
C	-9.15882545	0.32325816	-0.41839206
N	-4.42958871	1.02674946	-1.3985987
N	-3.2689652	1.12898558	-0.95056402
C	-2.95012788	1.0085308	0.43980485
C	-2.15711958	-0.05949905	0.85848493
C	-1.74811268	-0.13761094	2.18555125
C	-2.09513572	0.86284304	3.08881411
C	-2.85369513	1.9481495	2.65585283
C	-3.28481295	2.02473681	1.33750986
C	-7.47420094	-1.16490139	1.84413304
C	-8.21357789	-2.31772276	1.59588813
C	-8.62189798	-3.11080411	2.66042173
C	-8.28221233	-2.7648733	3.96495814
C	-7.53463036	-1.61718464	4.20485876
C	-7.13330892	-0.81022399	3.14624644
H	-1.86732171	-0.81843396	0.14162174
H	-1.14329832	-0.97619356	2.51004374
H	-1.76142633	0.80754254	4.11773289
H	-3.10725662	2.74299266	3.34770338
H	-3.86939617	2.86998497	0.99513439
H	-9.19956693	-4.00643559	2.46794793
H	-7.27081701	-1.34034539	5.21814141
H	-6.56681542	0.09518264	3.32525777
H	-8.46211127	-2.59139263	0.57865077
H	-8.59990702	-3.38843206	4.79151299
C	-5.69406043	-0.08546142	0.51768539
H	-4.94570029	-0.49957452	1.16911251
F	-6.61698853	2.17947205	-3.1217869
F	-9.29499195	2.26758326	-3.4741038
F	-10.9655836	1.0916497	-1.71608207
F	-10.0244238	-0.22646294	0.44895967

Energy= -1332.6654735

Zero-point correction= 0.266451 (Hartree/Particle)

Sum of electronic and zero-point Energies= -1332.399022

Sum of electronic and thermal Energies= -1332.377730

Sum of electronic and thermal Enthalpies= -1332.376786

Sum of electronic and thermal Free Energies= -1332.452056

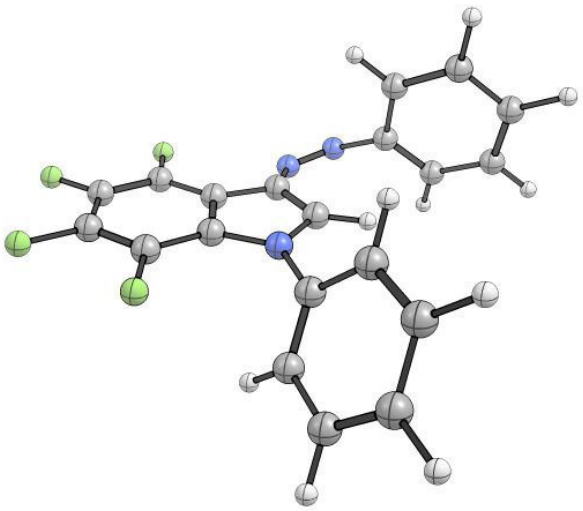

***Z*-12d**

C	-3.53451655	1.56324559	-0.32948393
C	-2.64785474	0.48956094	-0.57748441
N	-2.92563431	-0.5154342	0.33723845
C	-3.96302965	-0.11148577	1.13056857
C	-4.38089588	1.16073657	0.77032847
C	-3.44837629	2.70578092	-1.12870134
C	-2.50512363	2.76463356	-2.1351907
C	-1.63461902	1.69143268	-2.36819072
C	-1.69946431	0.54994912	-1.59630748
N	-5.29422874	2.07314486	1.32381054
N	-6.18367898	1.78809348	2.15322572
C	-6.45475528	0.45088197	2.58339342
C	-7.19780873	-0.41219199	1.77534313
C	-7.55451445	-1.66715548	2.25303744
C	-7.17589506	-2.06934391	3.53176686
C	-6.45510403	-1.19652957	4.34174042
C	-6.10636474	0.06776019	3.87850218
C	-2.24469519	-1.7784972	0.4762354
C	-2.73956367	-2.89326673	-0.20867991
C	-2.07505426	-4.10623439	-0.04258607
C	-0.9503065	-4.22541671	0.77181302
C	-0.49224278	-3.09050821	1.43751072
C	-1.12063712	-1.85372368	1.30478283
F	-4.26114098	3.75098497	-0.9523168
F	-2.40695953	3.85121994	-2.91076219
F	-0.73566877	1.78420453	-3.35502919
F	-0.85578391	-0.46663726	-1.84234992
C	-3.94693815	-2.7947796	-1.10551054
C	-0.58937263	-0.64120135	2.02547161
C	-0.23279546	-5.54422607	0.9071015
H	-4.30828338	-0.76053721	1.91486891
H	-7.49669126	-0.09098304	0.78481669
H	-8.13551133	-2.33280022	1.62528325
H	-7.45575548	-3.0486656	3.90001915
H	-6.17242854	-1.49517751	5.34441916
H	-5.56703584	0.76233289	4.51143619
H	-2.44833419	-4.98076248	-0.5648029
H	0.37876898	-3.16619226	2.07964
H	-4.82668433	-2.4410884	-0.5629203
H	-3.77636001	-2.09747931	-1.92971232
H	-4.18468687	-3.76773999	-1.53500708
H	0.21491005	-0.92134199	2.70546866

H	-0.19024445	0.09566366	1.32321583
H	-1.3662394	-0.14058466	2.60724561
H	-0.92543942	-6.38418383	0.83026846
H	0.51403336	-5.66286492	0.11599214
H	0.28843408	-5.6184629	1.86282914

Energy= -1450.6510327

Zero-point correction= 0.348276 (Hartree/Particle)

Sum of electronic and zero-point Energies= -1450.302757

Sum of electronic and thermal Energies= -1450.275894

Sum of electronic and thermal Enthalpies= -1450.274950

Sum of electronic and thermal Free Energies= -1450.363554

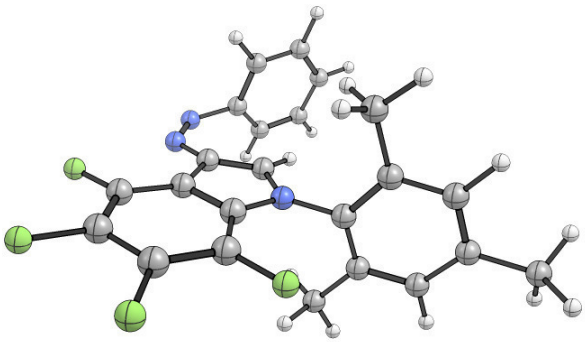

7. Simulated UV-Vis Spectra

7.1. Benchmark Study

Table A37: Overview of the performance of different basis sets in TD-DFT simulations using the B3LYP functional in comparison with the experimental electronical transition.

Basis set	**Maximum [nm]**	**Oscillator strength (*f*)**	**time**[a]
Experimental[b]	362.00		
3-21G	350.70	0.8815	0d 0h 18m 39.2s
LANL2DZ	365.24	0.8733	0d 0h 29m 53.5
6-31G	361.81	0.8655	0d 0h 25m 5.4s
6-31G(d)	364.64	0.8738	0d 1h 0m 42.0s
6-31G(2d,p)	365.80	0.8792	0d 2h 31m 4.3s
6-31+G(2d,p)	376.56	0.8929	0d 6h 3m 55.3s
6-311G	365.75	0.8730	0d 0h 48m 37.6s
6-311G(d)	369.78	0.8816	0d 1h 49m 51.9s
6-311G(2d,p)	370.15	0.8866	0d 4h 30m 0.6s
6-311+G(2d,p)	376.82	0.8908	0d 9h 54m 4.1s
cc-pVDZ	366.57	0.8862	0d 1h 23m 34.7s
aug-cc-pVDZ[c]	376.33	0.8933	0d 12h 3m 26.7s
cc-pVTZ	372.94	0.8889	0d 11h 41m 19.2s
aug-cc-pVTZ[c]	377.04	0.8926	5 d 11h 12m 37.3s

[a] CPU time using four Intel® Xeon® CPU E5-2650 0 @ 2.00GHz processors with 1GB of shared memory. [b] UV/Vis spectrum registered in toluene, 50μM.[2] [c] The transitions were computed for the ten lower states.

Table 38: Overview of the performance of different functionals in TD-DFT simulations using the 6-311+G(2d,p) basis set in comparison.

	Functional[a]	Maximum [nm]	Oscillator strength (*f*)	time[b]
Hartree-Fock and (meta-) GGA functionals	HF	305.74	1.0210	6 h 9 m 4.2 s[c]
	M06L	392.00	0.7876	5 h 56 m 25.4 s
	M11L	398.95	0.7937	5 h 41 m 21.8 s
	SOGGA11	407.98	0.7036	4 h 14 m 49.1 s
	PBE	411.96	0.7250	3 h 23 m 19.9 s
	BP86	412.43	0.7254	3 h 25 m 0.0 s
	BLYP	415.45	0.7226	3 h 13 m 52.7 s
Hybrid functionals	BHANDH (50)	338.85	1.0154	5 h 8 m 37.7 s
	BHandHLYP (50)	339.00	1.0067	4 h 58 m 49.7 s
	SOGGA11X (40.15)	346.95	0.9932	4 h 23 m 46.9 s
	PBE0 (25)	366.08	0.9261	9 h 21 m 56.0 s
	X3LYP (20.15)	374.33	0.9012	3 h 55 m 44.6 s
	B3LYP (15)	376.82	0.8908	4 h 8 m 55.7 s
	O3LYP (12)	386.85	0.8387	4 h 12 m 27.4 s
Meta-Hybrid	M06HF (100)	312.82	1.0331	8 h 52 m 12.8 s
	M062X (54)	340.13	0.9907	7 h 6 m 4.4 s
	M06 (27)	376.25	0.8990	6 h 30 m 42.1 s
	TPSSH (10)	383.96	0.8454	5 h 11 m 37.3 s
Range separated and dispersion corrected	LC-BLYP	319.15	0.9993	7 h 19 m 49.4 s
	LC-WHPBE	321.92	0.9986	6 h 26 m 46.6 s
	LC-WPBE	321.93	0.9986	6 h 44 m 10.5 s
	ωB97XD	342.80	0.9890	6 h 31 m 41.4 s
	CAM-B3LYP	345.30	0.9798	5 h 46 m 28.8 s
	APFD	369.23	0.9144	4 h 11 m 53.0 s

[a] The percentage of Hartree Fock exchange in the hybrid and meta-hybrid functionals is reported in brackets. [b] CPU time using four Intel® Xeon® CPU E5-2630 v3 @ 2.40GHz with 1GB of shared memory. [c] CPU time using four Intel® Xeon® CPU E5-2650 0 @ 2.00GHz processors with 1GB of shared memory.

7.2. TD-DFT calculations using PBE0/6-311+G(2d,p) level of theory

7.2.1. Vacuum

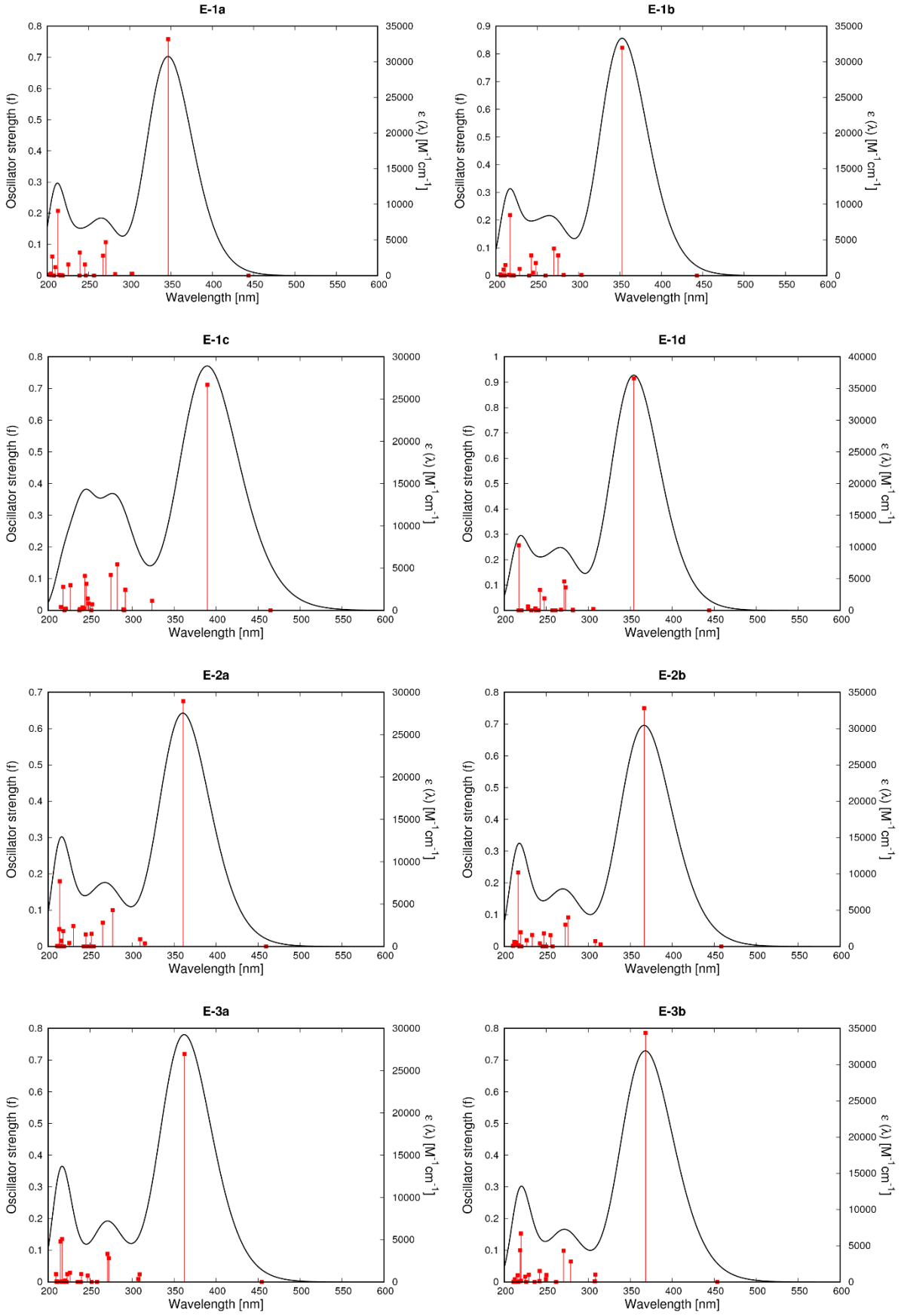

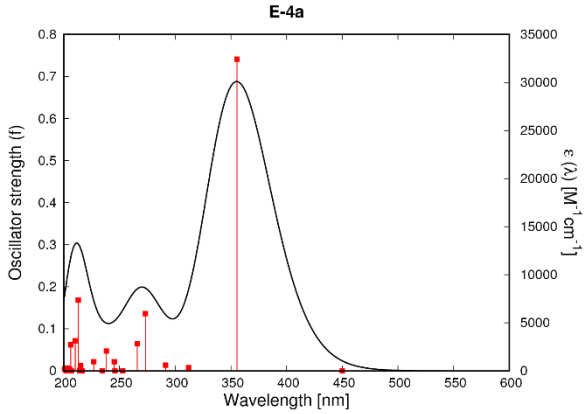
E-4a
Oscillator strength (f)
ε (λ) [M-1cm-1]
Wavelength [nm]

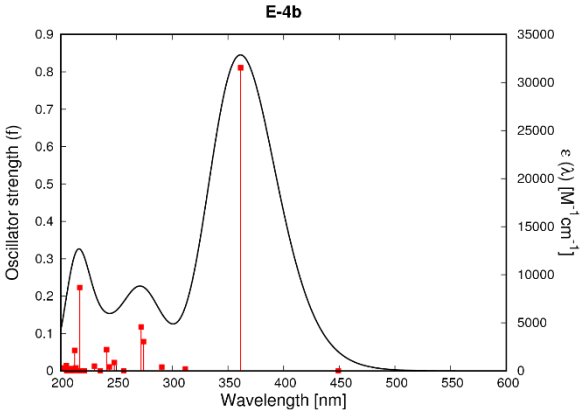
E-4b
Oscillator strength (f)
ε (λ) [M-1cm-1]
Wavelength [nm]

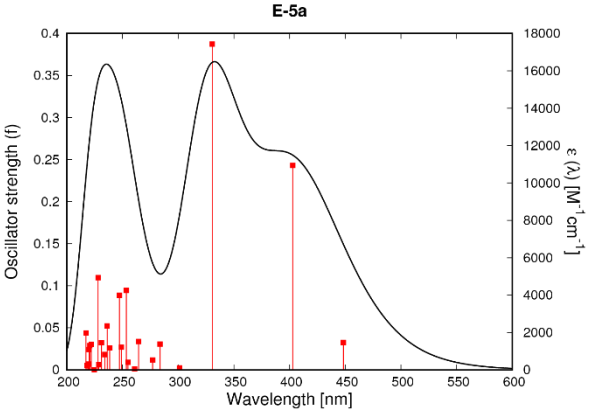
E-5a
Oscillator strength (f)
ε (λ) [M-1cm-1]
Wavelength [nm]

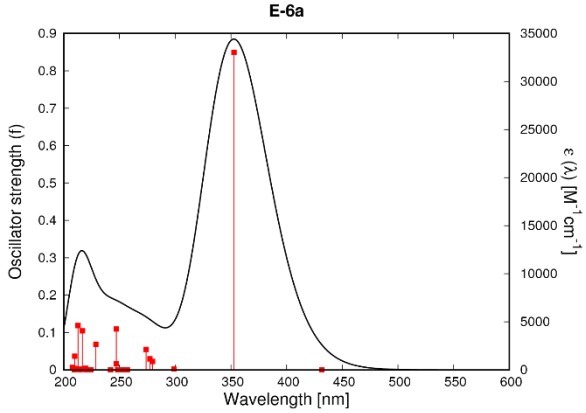
E-6a
Oscillator strength (f)
ε (λ) [M-1cm-1]
Wavelength [nm]

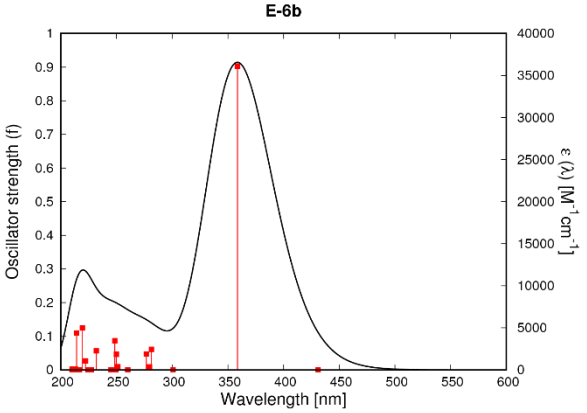
E-6b
Oscillator strength (f)
ε (λ) [M-1cm-1]
Wavelength [nm]

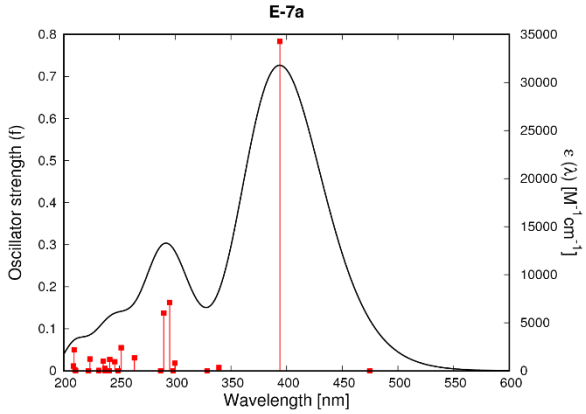
E-7a
Oscillator strength (f)
ε (λ) [M-1cm-1]
Wavelength [nm]

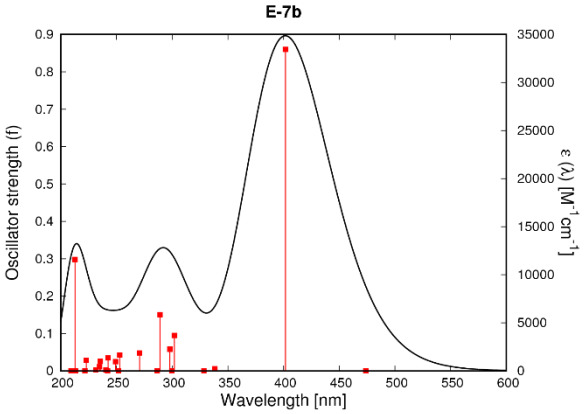
E-7b
Oscillator strength (f)
ε (λ) [M-1cm-1]
Wavelength [nm]

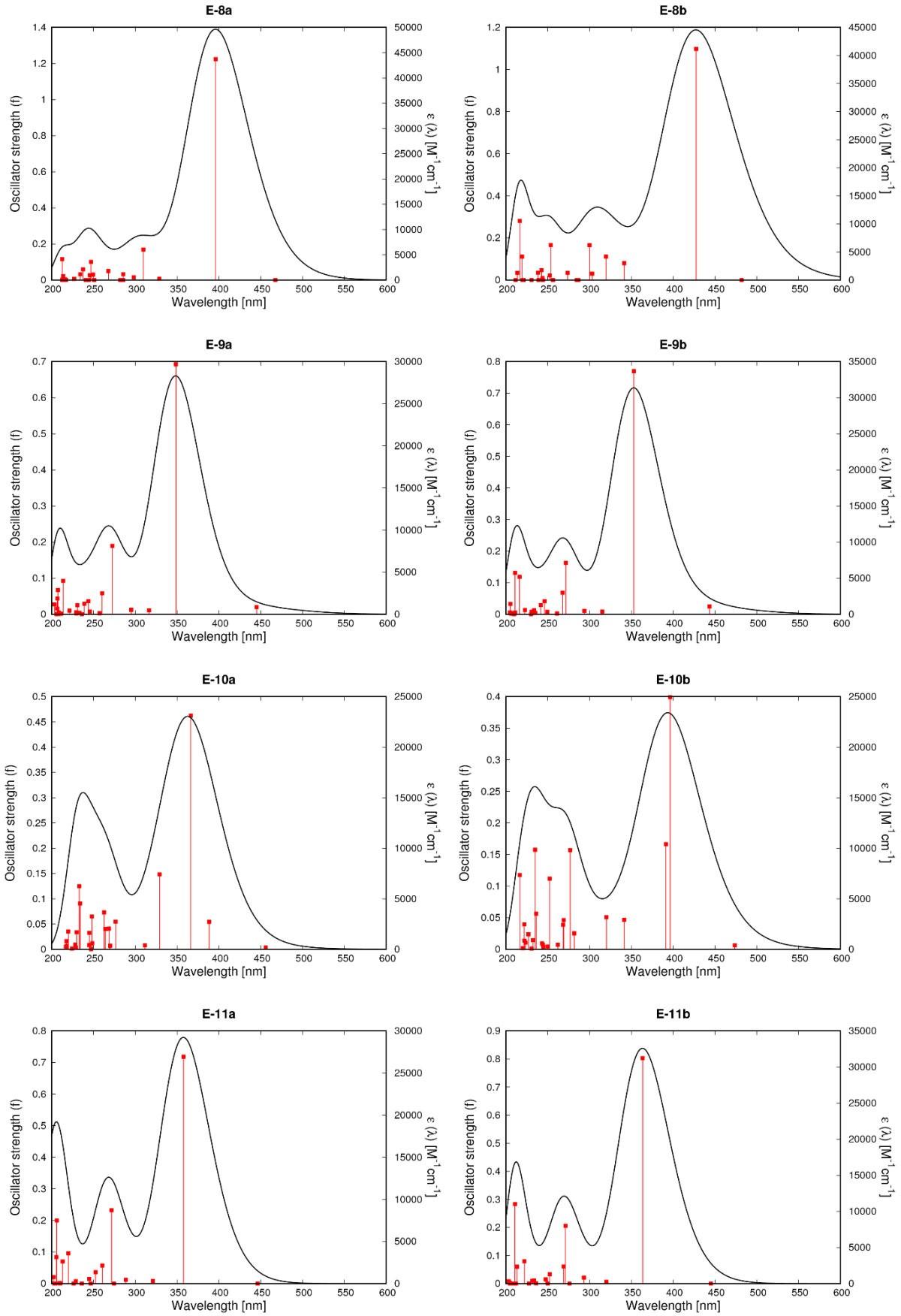
E-8a
E-8b
E-9a
E-9b
E-10a
E-10b
E-11a
E-11b
Oscillator strength (f)
ε (λ) [M-1cm-1]
Wavelength [nm]

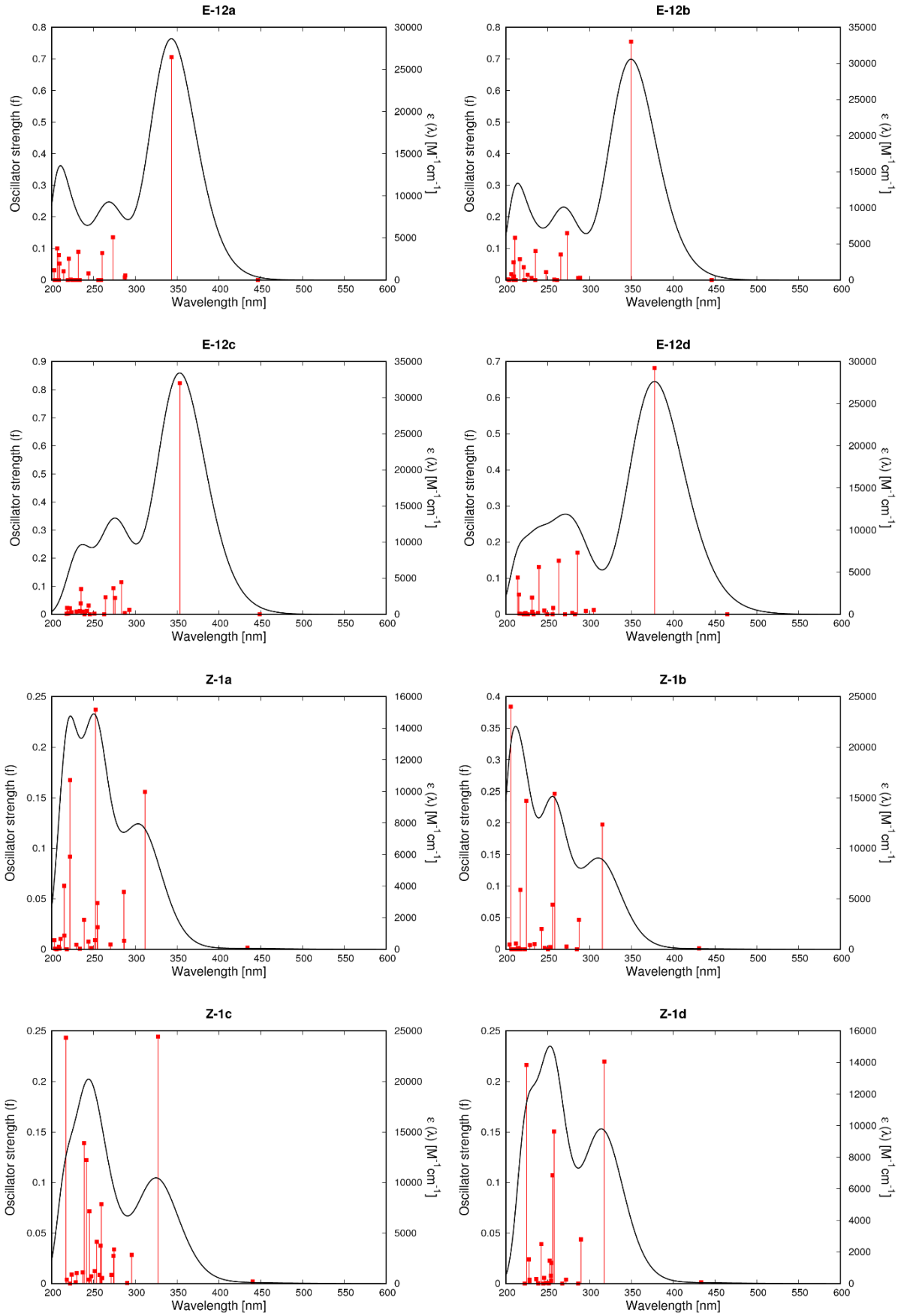
E-12a
E-12b
E-12c
E-12d
Z-1a
Z-1b
Z-1c
Z-1d
Oscillator strength (f)
ε (λ) [M-1cm-1]
Wavelength [nm]

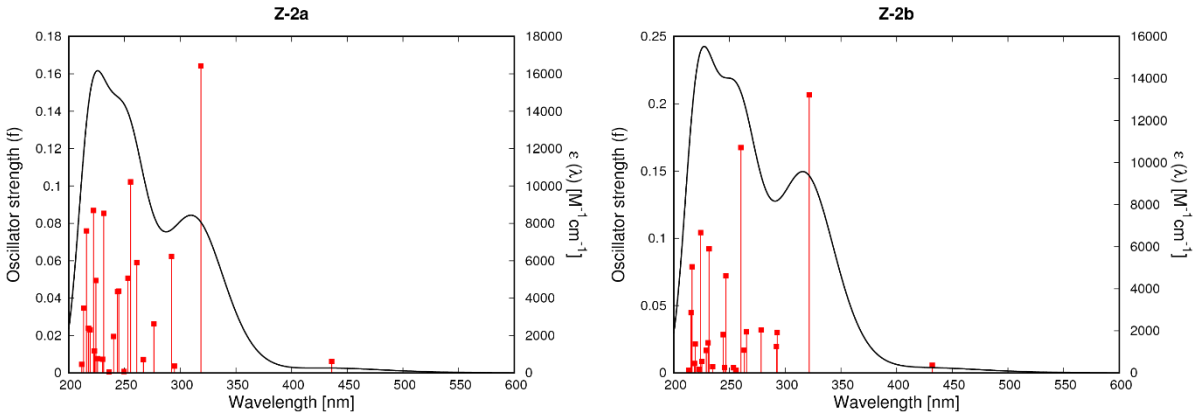
Z-2a
Oscillator strength (f)
ε (λ) [M-1cm-1]
Wavelength [nm]

Z-2b
Oscillator strength (f)
ε (λ) [M-1cm-1]
Wavelength [nm]

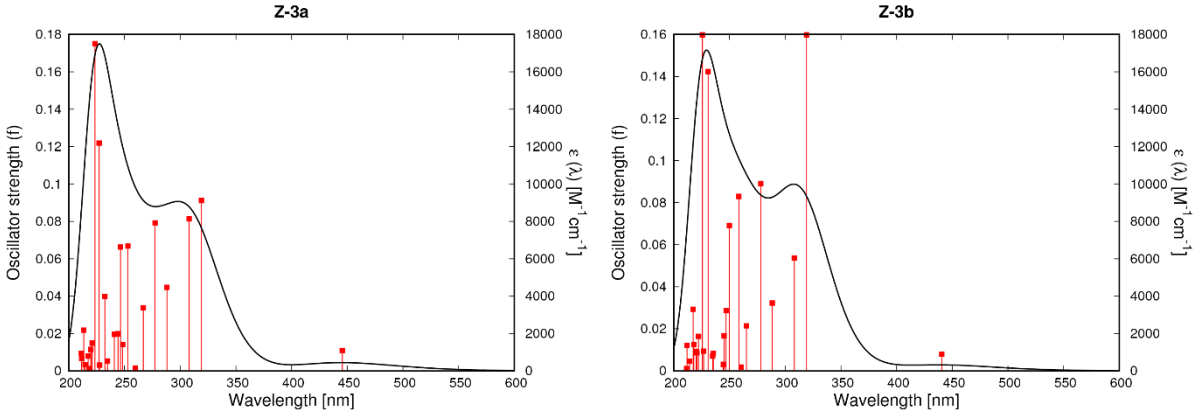
Z-3a
Oscillator strength (f)
ε (λ) [M-1cm-1]
Wavelength [nm]

Z-3b
Oscillator strength (f)
ε (λ) [M-1cm-1]
Wavelength [nm]

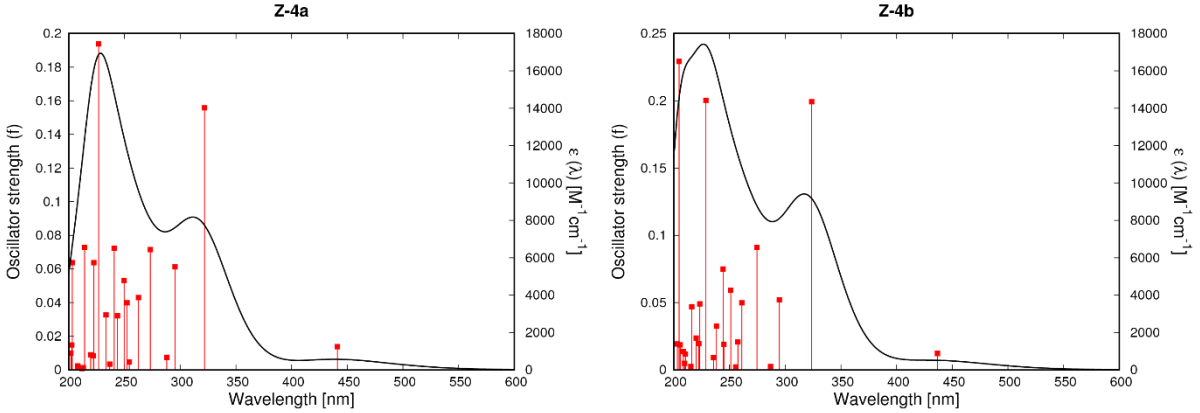
Z-4a
Oscillator strength (f)
ε (λ) [M-1cm-1]
Wavelength [nm]

Z-4b
Oscillator strength (f)
ε (λ) [M-1cm-1]
Wavelength [nm]

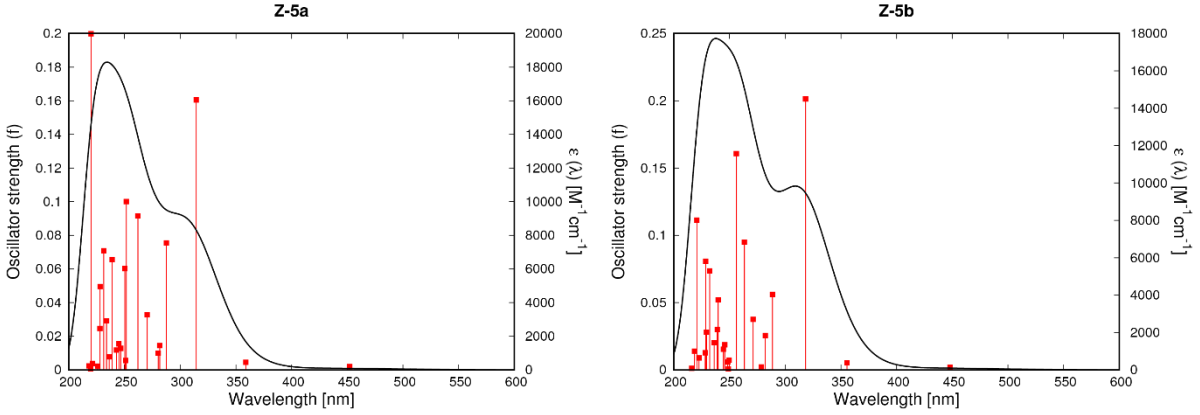
Z-5a
Oscillator strength (f)
ε (λ) [M-1cm-1]
Wavelength [nm]

Z-5b
Oscillator strength (f)
ε (λ) [M-1cm-1]
Wavelength [nm]

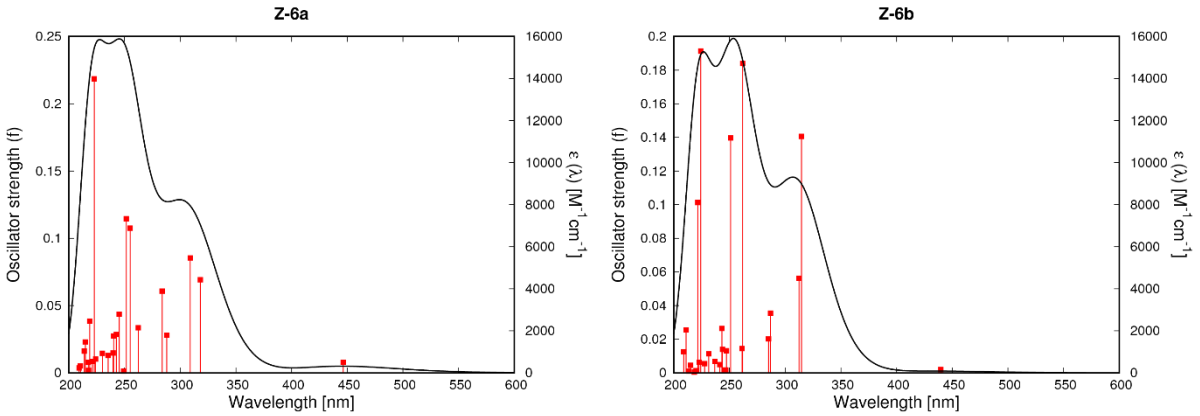
Z-6a
Oscillator strength (f)
ε (λ) [M-1cm-1]
Wavelength [nm]

Z-6b
Oscillator strength (f)
ε (λ) [M-1cm-1]
Wavelength [nm]

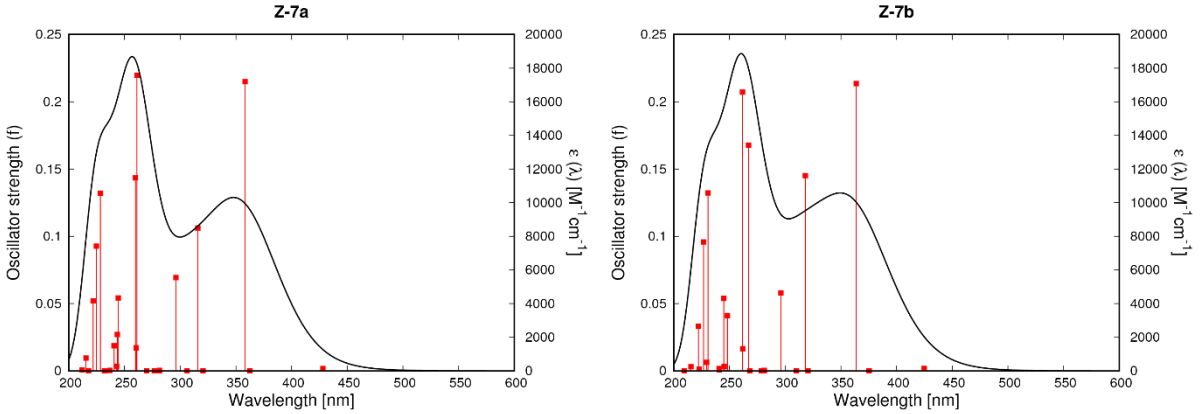
Z-7a
Oscillator strength (f)
ε (λ) [M-1cm-1]
Wavelength [nm]

Z-7b
Oscillator strength (f)
ε (λ) [M-1cm-1]
Wavelength [nm]

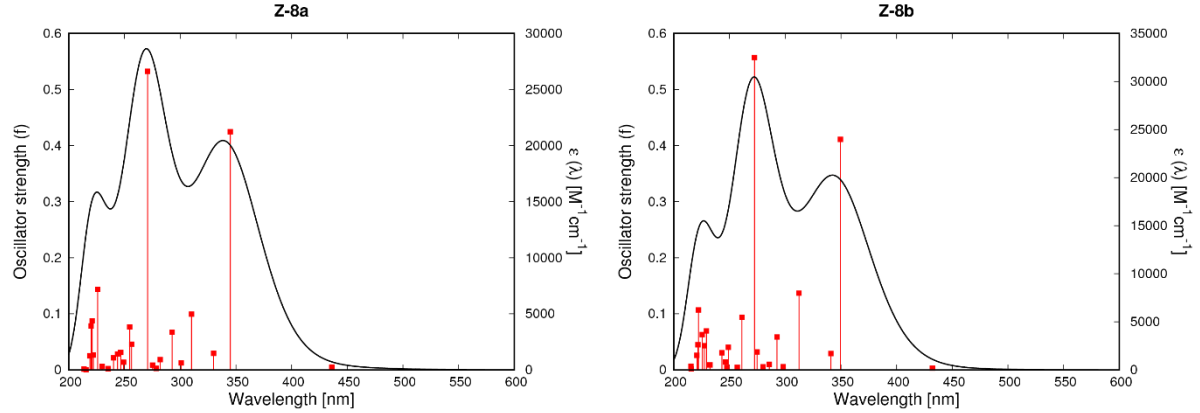
Z-8a
Oscillator strength (f)
ε (λ) [M-1cm-1]
Wavelength [nm]

Z-8b
Oscillator strength (f)
ε (λ) [M-1cm-1]
Wavelength [nm]

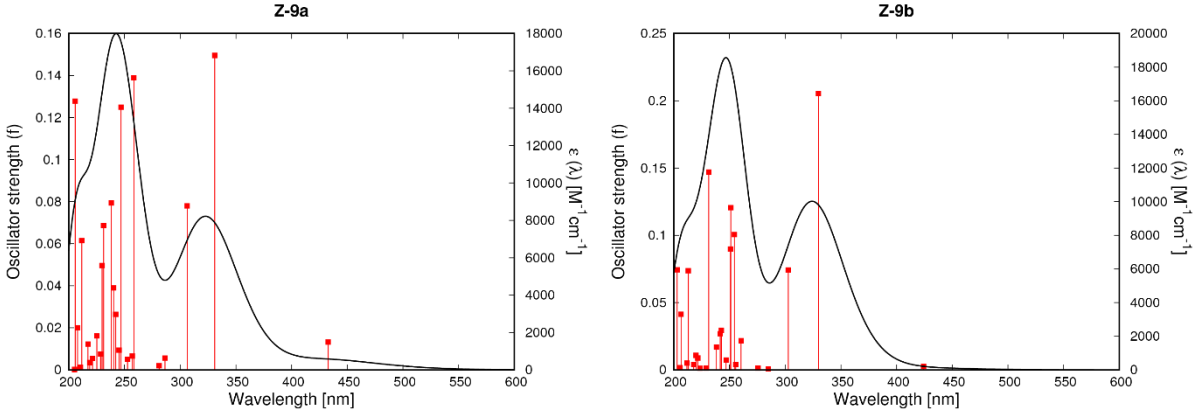
Z-9a
Oscillator strength (f)
ε (λ) [M-1cm-1]
Wavelength [nm]

Z-9b
Oscillator strength (f)
ε (λ) [M-1cm-1]
Wavelength [nm]

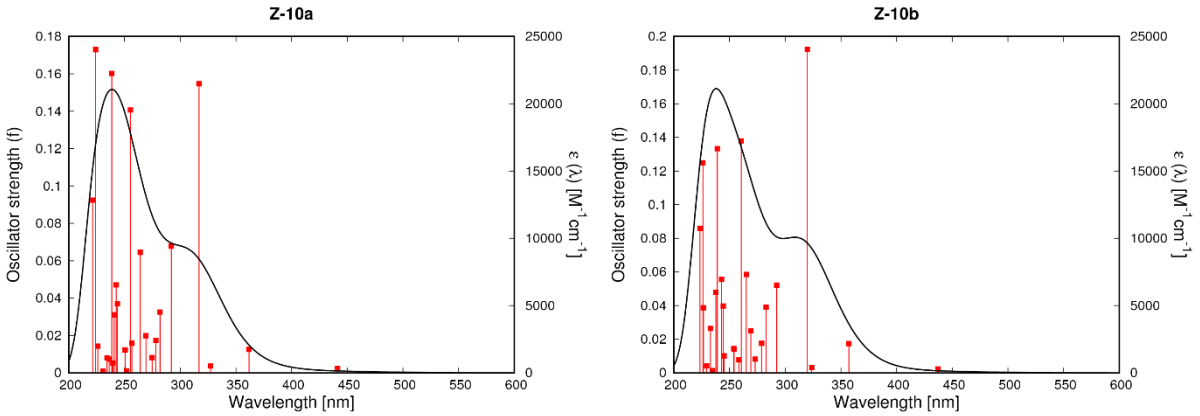
Z-10a
Oscillator strength (f)
ε (λ) [M-1cm-1]
Wavelength [nm]

Z-10b
Oscillator strength (f)
ε (λ) [M-1cm-1]
Wavelength [nm]

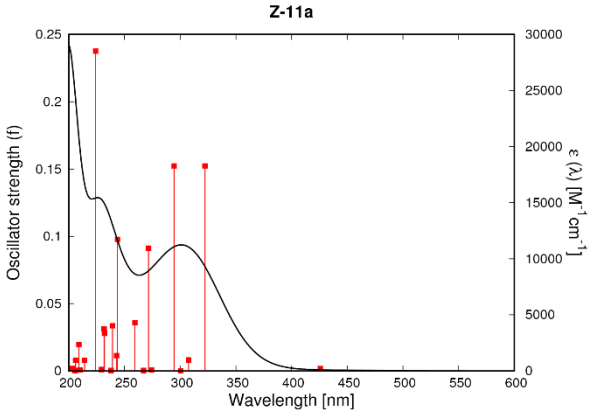
Z-11a
Oscillator strength (f)
ε (λ) [M-1cm-1]
Wavelength [nm]

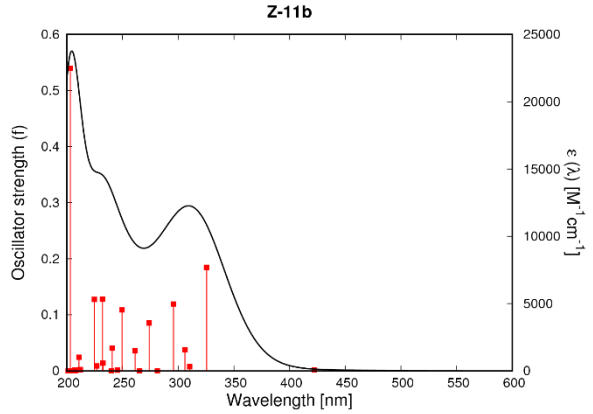
Z-11b
Oscillator strength (f)
ε (λ) [M-1cm-1]
Wavelength [nm]

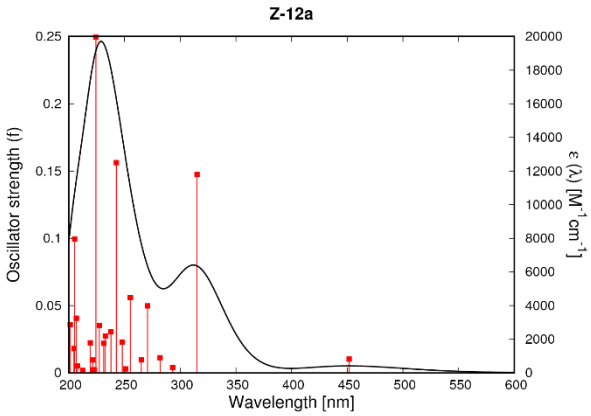
Z-12a
Oscillator strength (f)
ε (λ) [M-1cm-1]
Wavelength [nm]

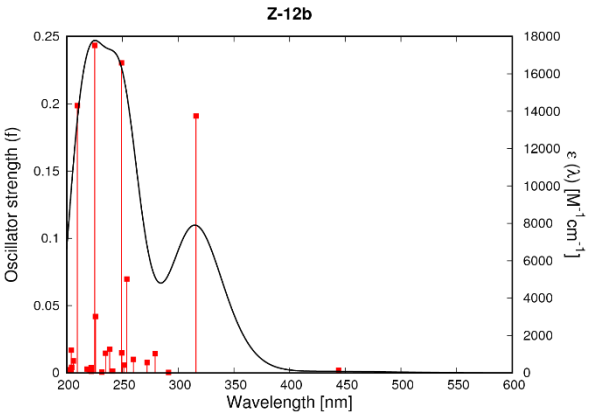
Z-12b
Oscillator strength (f)
ε (λ) [M-1cm-1]
Wavelength [nm]

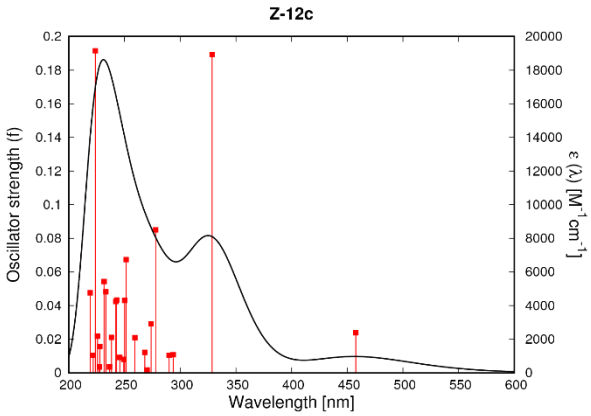
Z-12c
Oscillator strength (f)
ε (λ) [M-1cm-1]
Wavelength [nm]

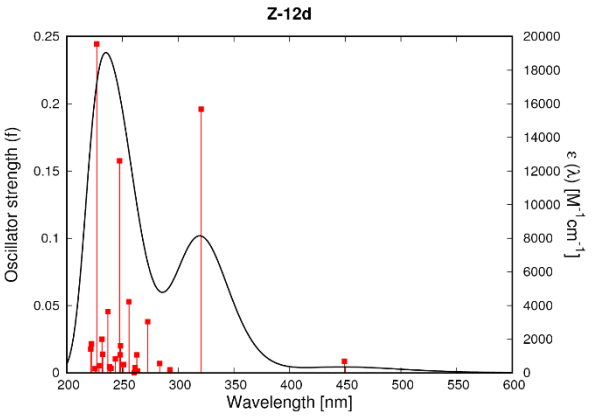
Z-12d
Oscillator strength (f)
ε (λ) [M-1cm-1]
Wavelength [nm]

7.2.2. Toluene

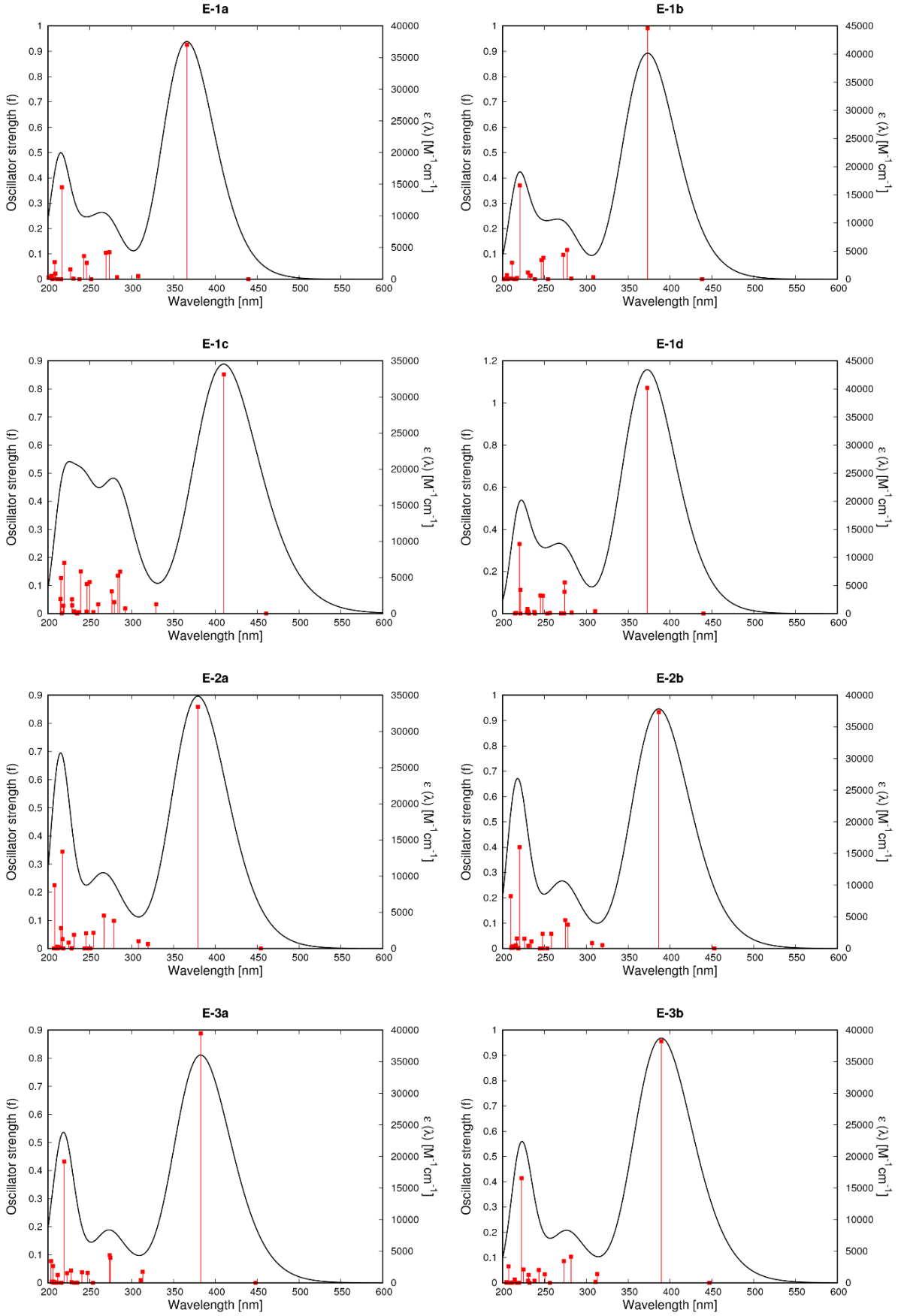
E-1a
E-1b
E-1c
E-1d
E-2a
E-2b
E-3a
E-3b
Oscillator strength (f)
ε (λ) [M⁻¹cm⁻¹]
Wavelength [nm]

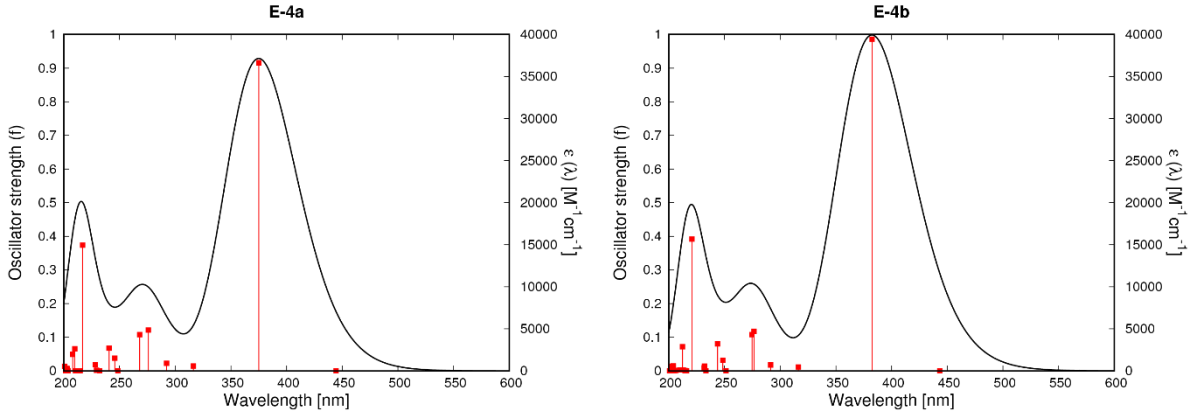
E-4a
Oscillator strength (f)
ε (λ) [M-1cm-1]
Wavelength [nm]

E-4b
Oscillator strength (f)
ε (λ) [M-1cm-1]
Wavelength [nm]

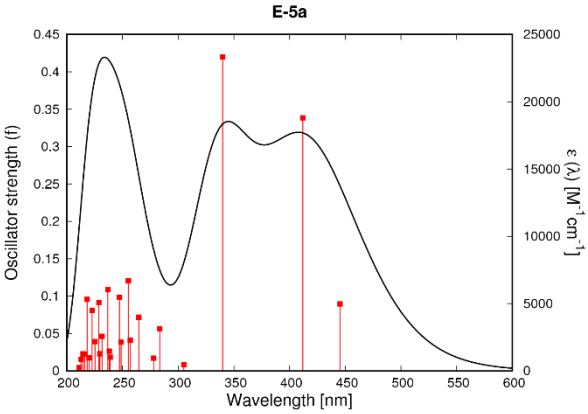
E-5a
Oscillator strength (f)
ε (λ) [M-1cm-1]
Wavelength [nm]

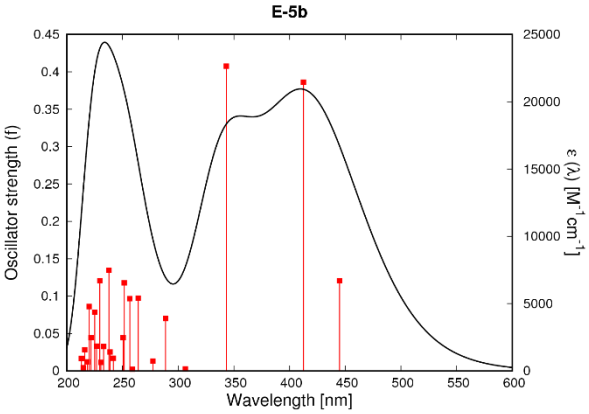
E-5b
Oscillator strength (f)
ε (λ) [M-1cm-1]
Wavelength [nm]

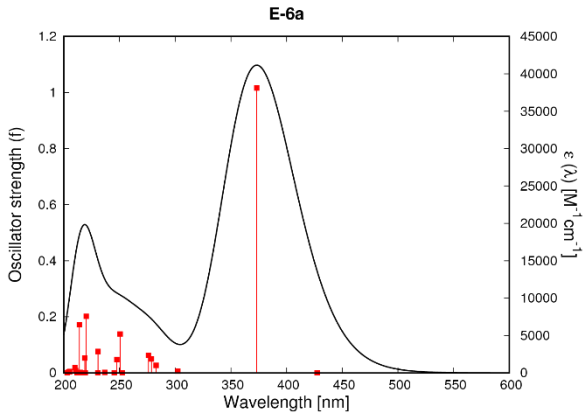
E-6a
Oscillator strength (f)
ε (λ) [M-1cm-1]
Wavelength [nm]

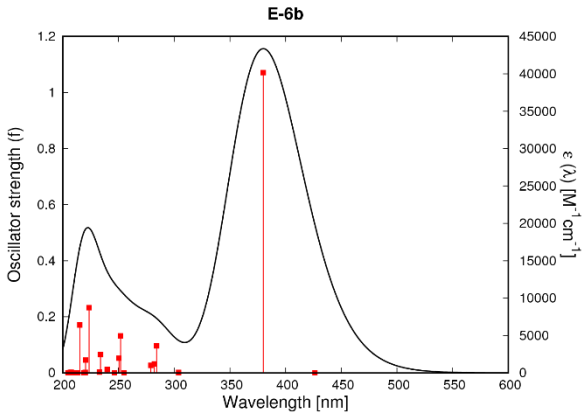
E-6b
Oscillator strength (f)
ε (λ) [M-1cm-1]
Wavelength [nm]

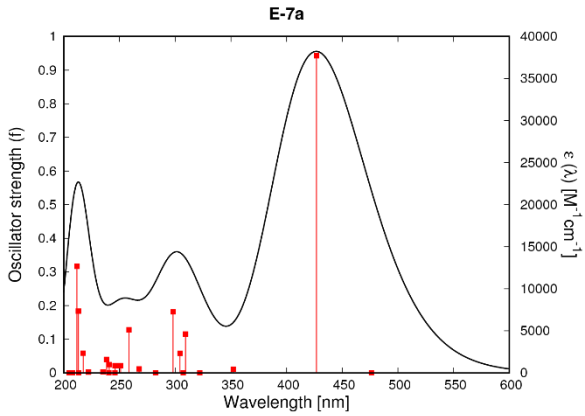
E-7a
Oscillator strength (f)
ε (λ) [M-1cm-1]
Wavelength [nm]

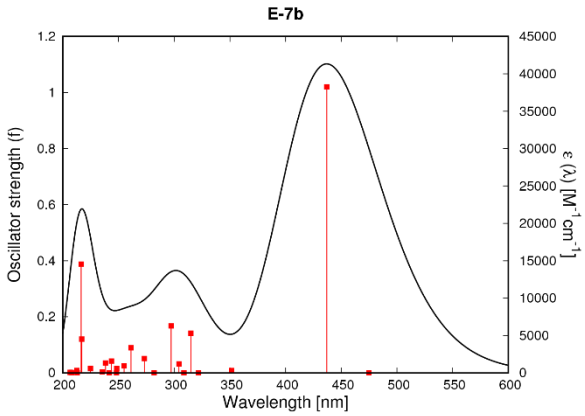
E-7b
Oscillator strength (f)
ε (λ) [M-1cm-1]
Wavelength [nm]

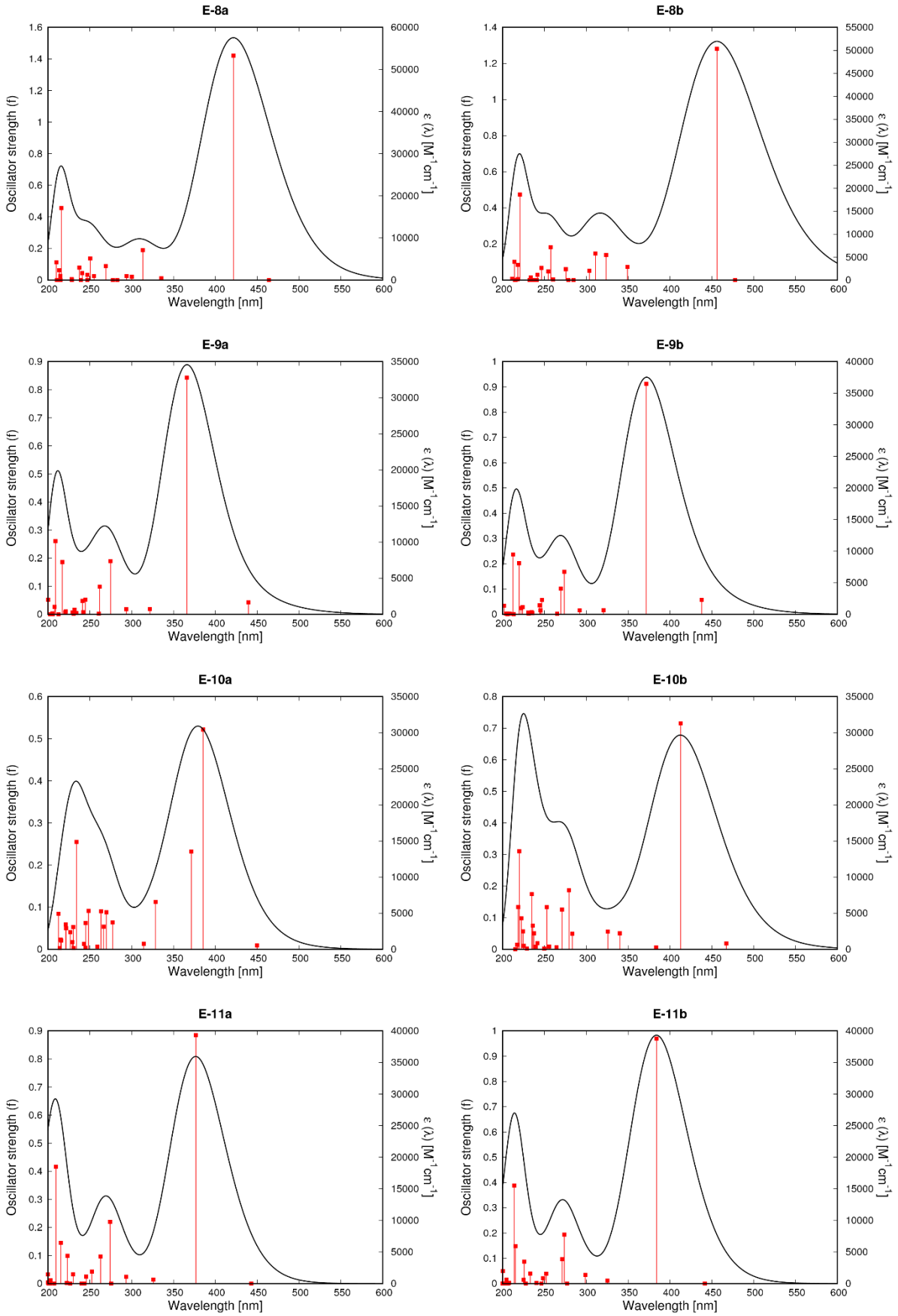
E-8a
E-8b
E-9a
E-9b
E-10a
E-10b
E-11a
E-11b
Oscillator strength (f)
ε (λ) [M-1cm-1]
Wavelength [nm]

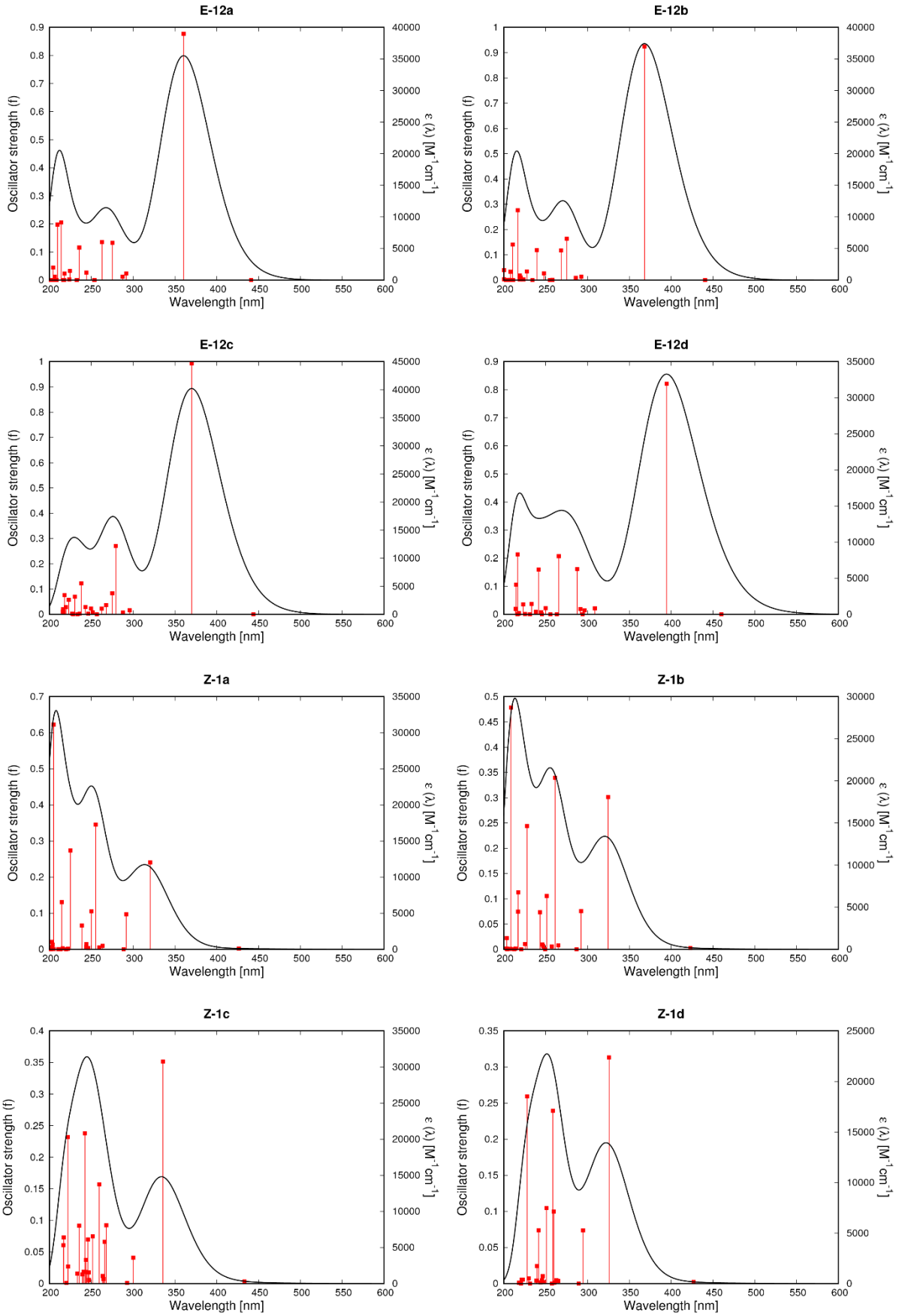
E-12a
E-12b
E-12c
E-12d
Z-1a
Z-1b
Z-1c
Z-1d
Oscillator strength (f)
ε (λ) [M-1cm-1]
Wavelength [nm]

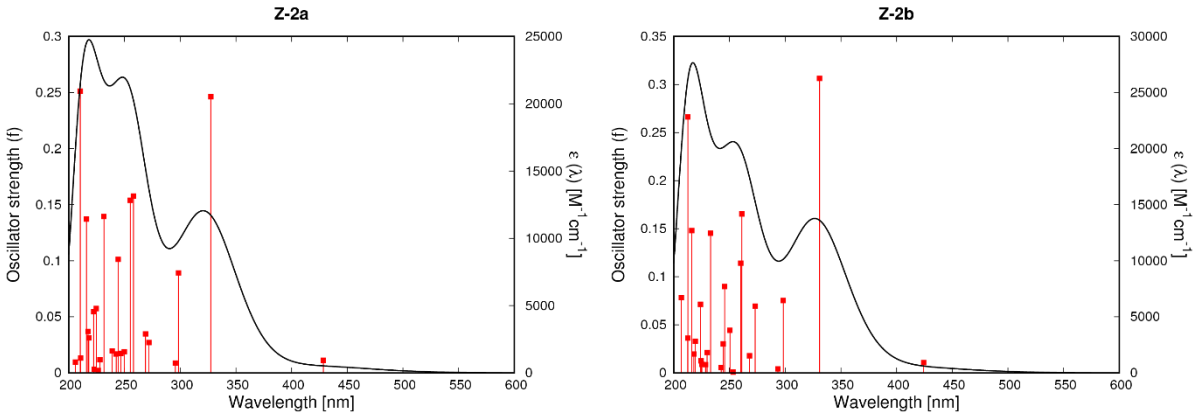
Z-2a
Oscillator strength (f)
ε (λ) [M-1cm-1]
Wavelength [nm]

Z-2b
Oscillator strength (f)
ε (λ) [M-1cm-1]
Wavelength [nm]

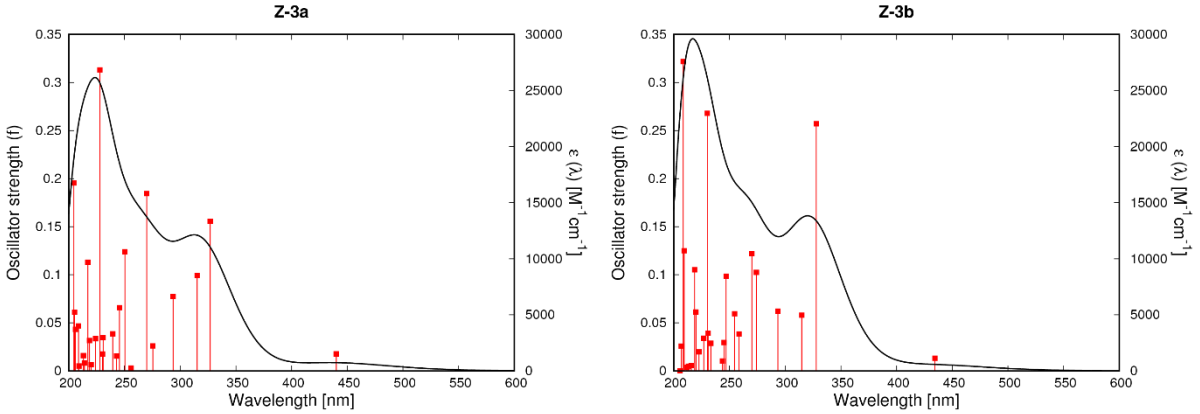
Z-3a
Oscillator strength (f)
ε (λ) [M-1cm-1]
Wavelength [nm]

Z-3b
Oscillator strength (f)
ε (λ) [M-1cm-1]
Wavelength [nm]

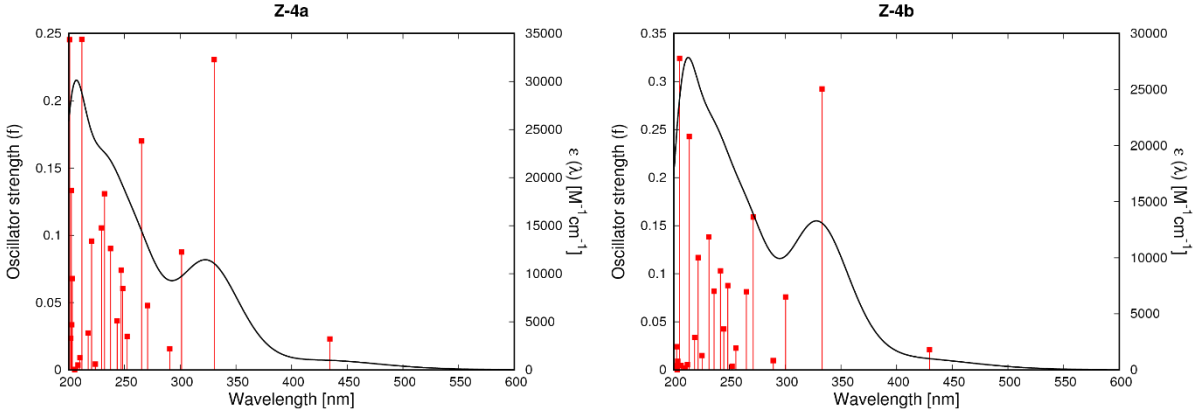
Z-4a
Oscillator strength (f)
ε (λ) [M-1cm-1]
Wavelength [nm]

Z-4b
Oscillator strength (f)
ε (λ) [M-1cm-1]
Wavelength [nm]

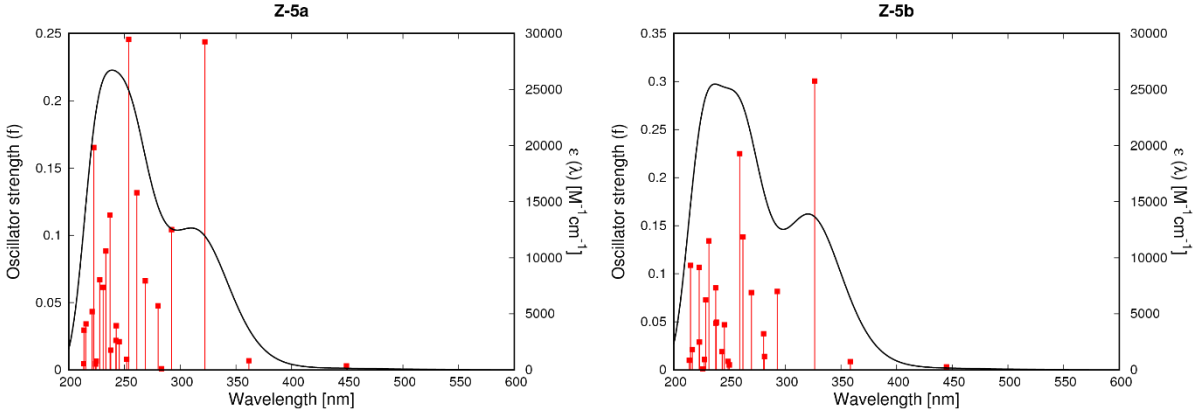
Z-5a
Oscillator strength (f)
ε (λ) [M-1cm-1]
Wavelength [nm]

Z-5b
Oscillator strength (f)
ε (λ) [M-1cm-1]
Wavelength [nm]

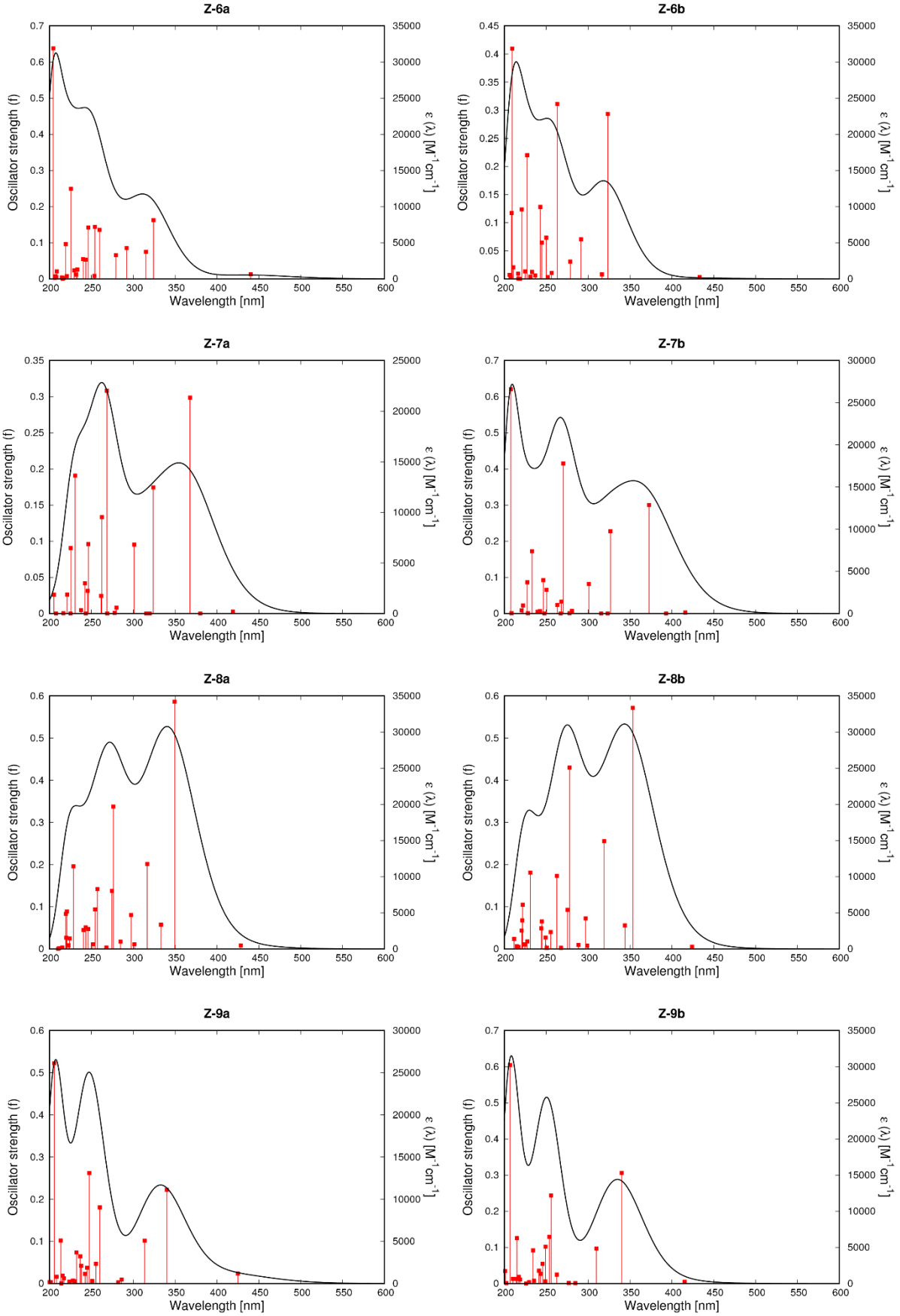
Z-6a
Z-6b
Z-7a
Z-7b
Z-8a
Z-8b
Z-9a
Z-9b
Oscillator strength (f)
ε (λ) [M-1cm-1]
Wavelength [nm]

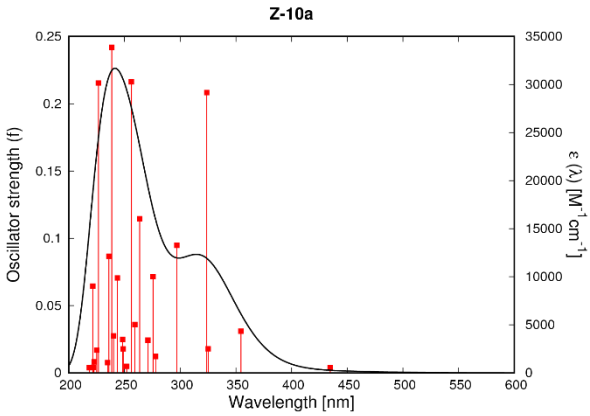
Z-10a
Oscillator strength (f)
ε (λ) [M-1cm-1]
Wavelength [nm]

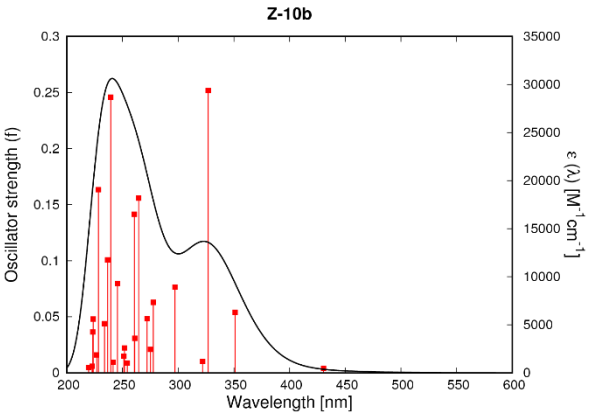
Z-10b
Oscillator strength (f)
ε (λ) [M-1cm-1]
Wavelength [nm]

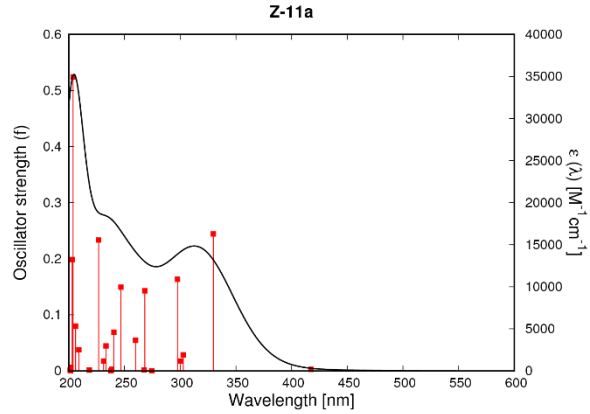
Z-11a
Oscillator strength (f)
ε (λ) [M-1cm-1]
Wavelength [nm]

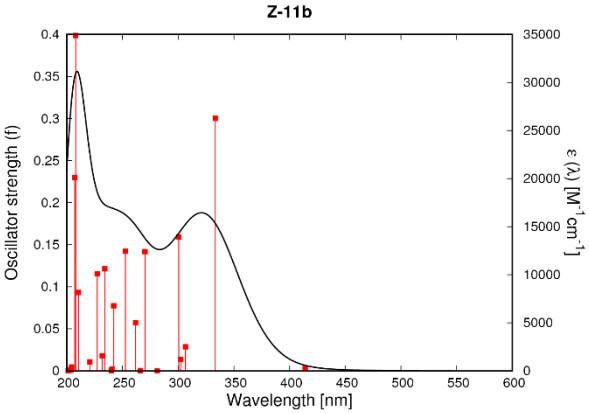
Z-11b
Oscillator strength (f)
ε (λ) [M-1cm-1]
Wavelength [nm]

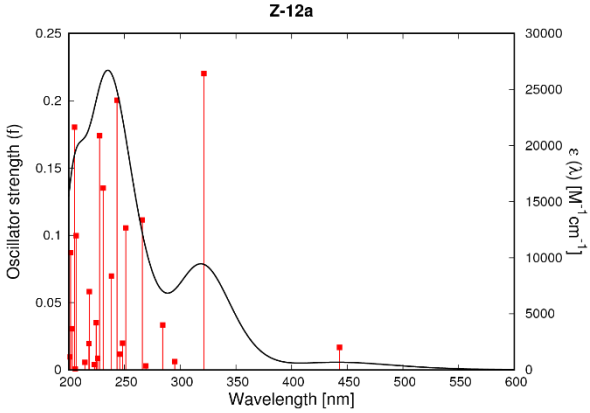
Z-12a
Oscillator strength (f)
ε (λ) [M-1cm-1]
Wavelength [nm]

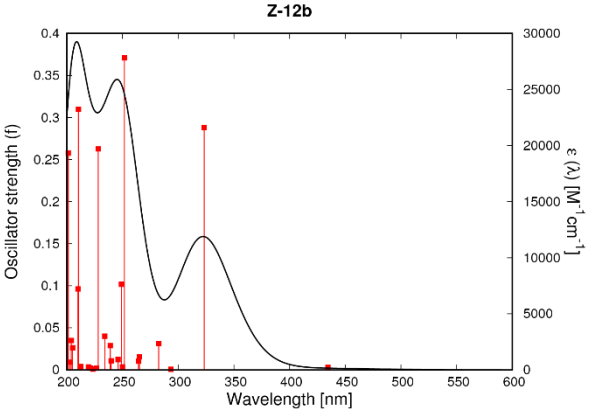
Z-12b
Oscillator strength (f)
ε (λ) [M-1cm-1]
Wavelength [nm]

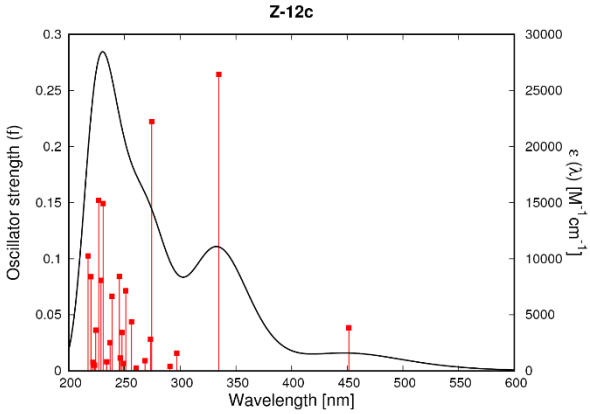
Z-12c
Oscillator strength (f)
ε (λ) [M-1cm-1]
Wavelength [nm]

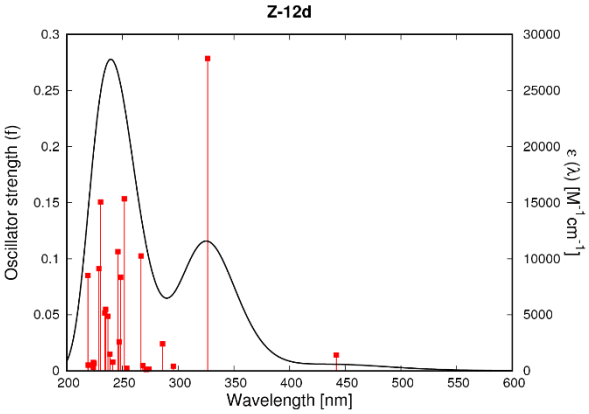
Z-12d
Oscillator strength (f)
ε (λ) [M-1cm-1]
Wavelength [nm]

7.2.3. DMSO

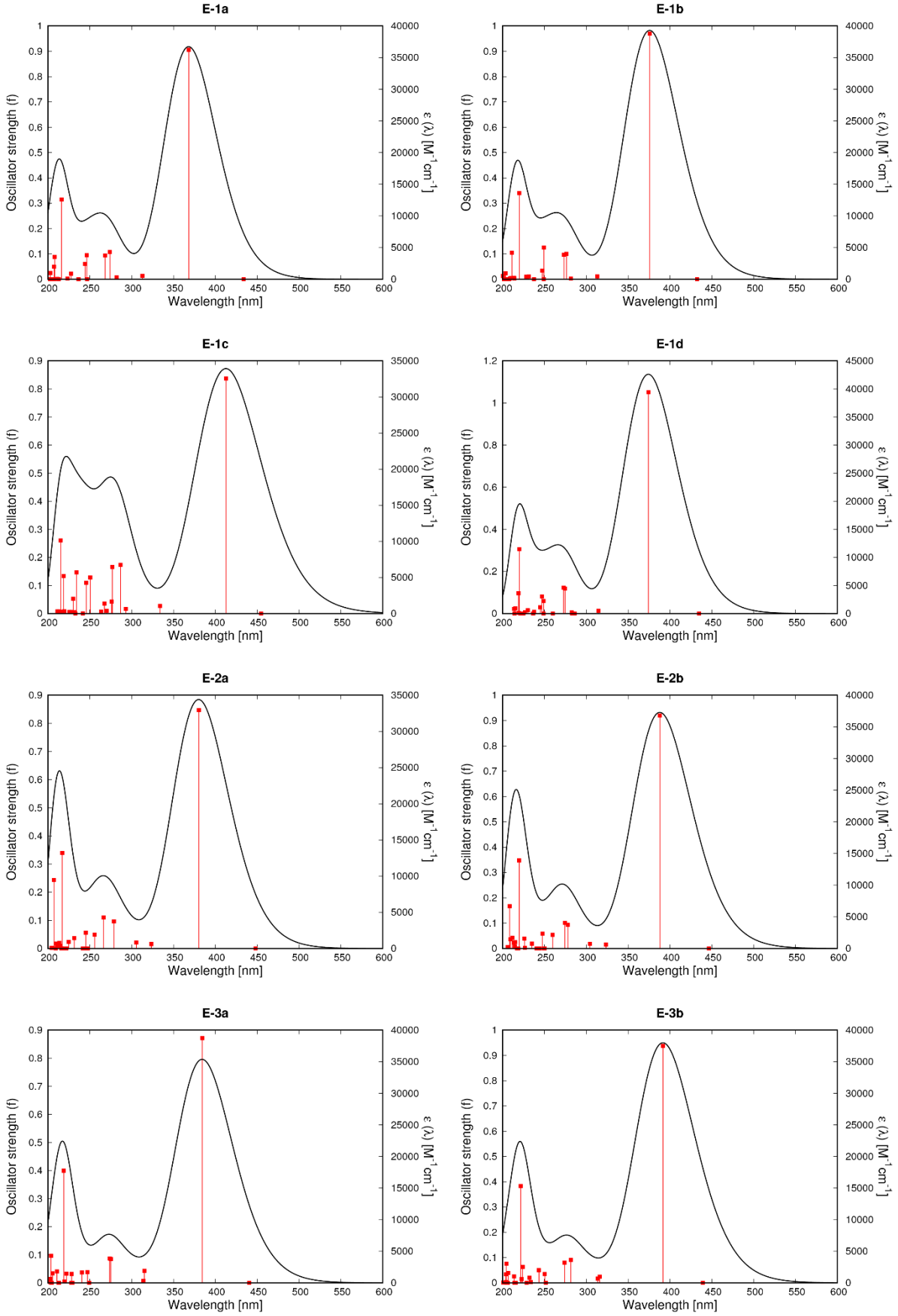
E-1a
E-1b
E-1c
E-1d
E-2a
E-2b
E-3a
E-3b
Oscillator strength (f)
ε (λ) [M-1cm-1]
Wavelength [nm]

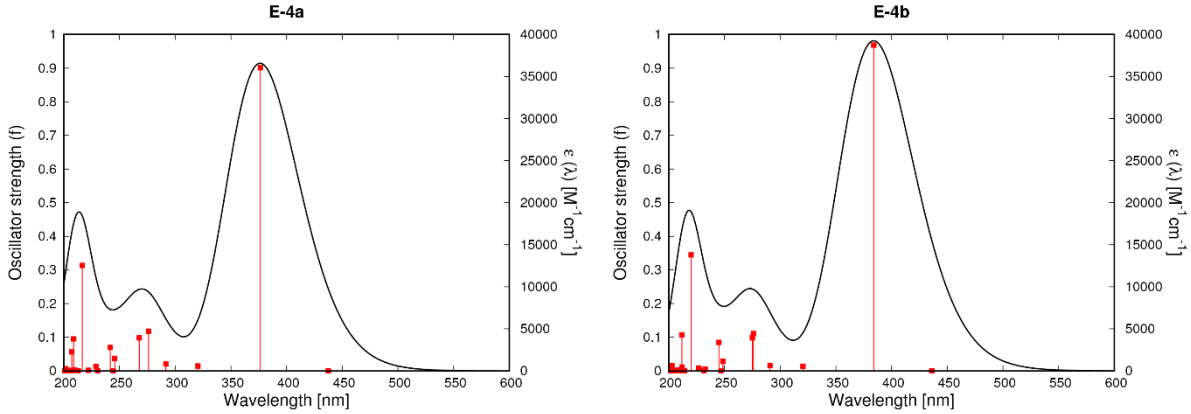
E-4a
Oscillator strength (f)
ε (λ) [M-1cm-1]
Wavelength [nm]

E-4b
Oscillator strength (f)
ε (λ) [M-1cm-1]
Wavelength [nm]

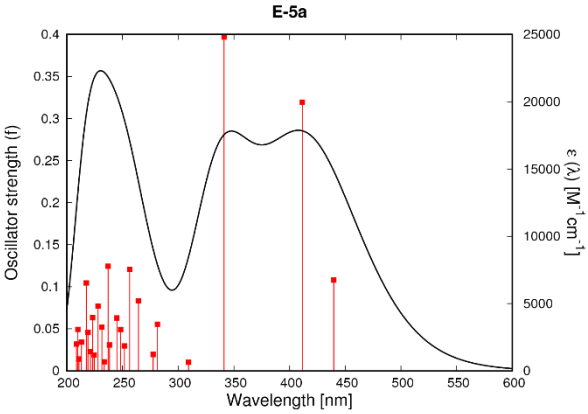
E-5a
Oscillator strength (f)
ε (λ) [M-1cm-1]
Wavelength [nm]

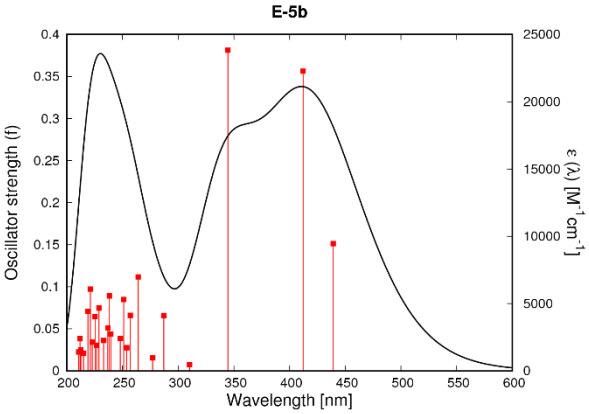
E-5b
Oscillator strength (f)
ε (λ) [M-1cm-1]
Wavelength [nm]

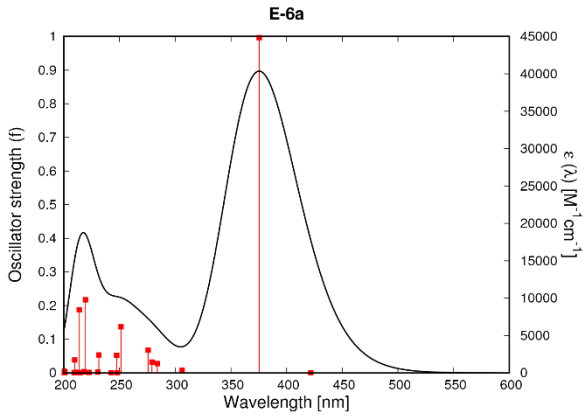
E-6a
Oscillator strength (f)
ε (λ) [M-1cm-1]
Wavelength [nm]

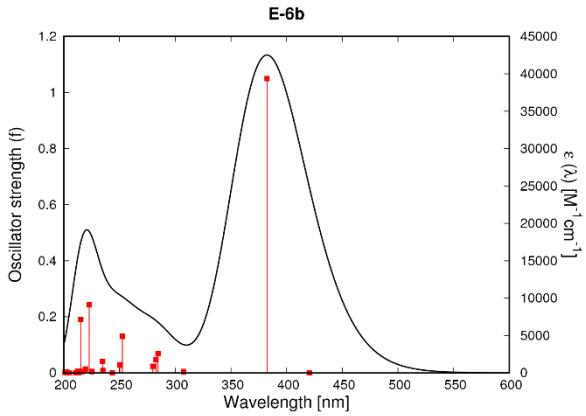
E-6b
Oscillator strength (f)
ε (λ) [M-1cm-1]
Wavelength [nm]

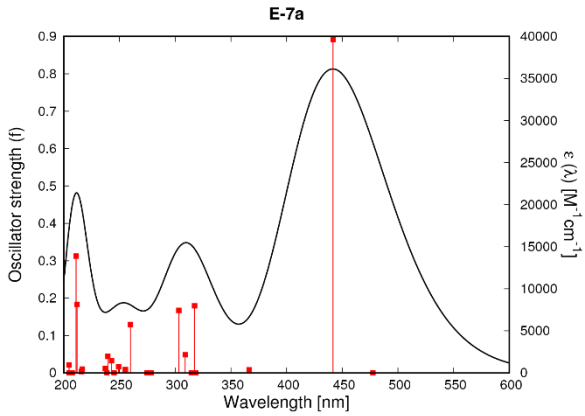
E-7a
Oscillator strength (f)
ε (λ) [M-1cm-1]
Wavelength [nm]

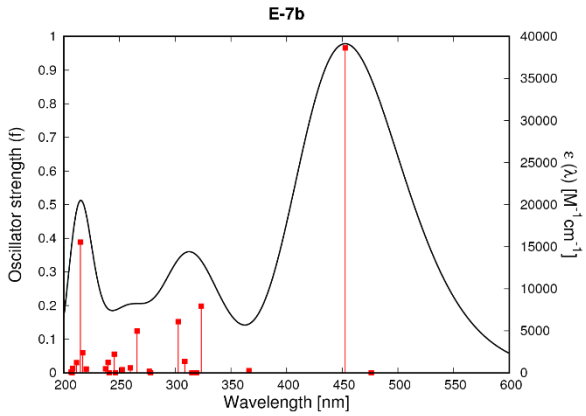
E-7b
Oscillator strength (f)
ε (λ) [M-1cm-1]
Wavelength [nm]

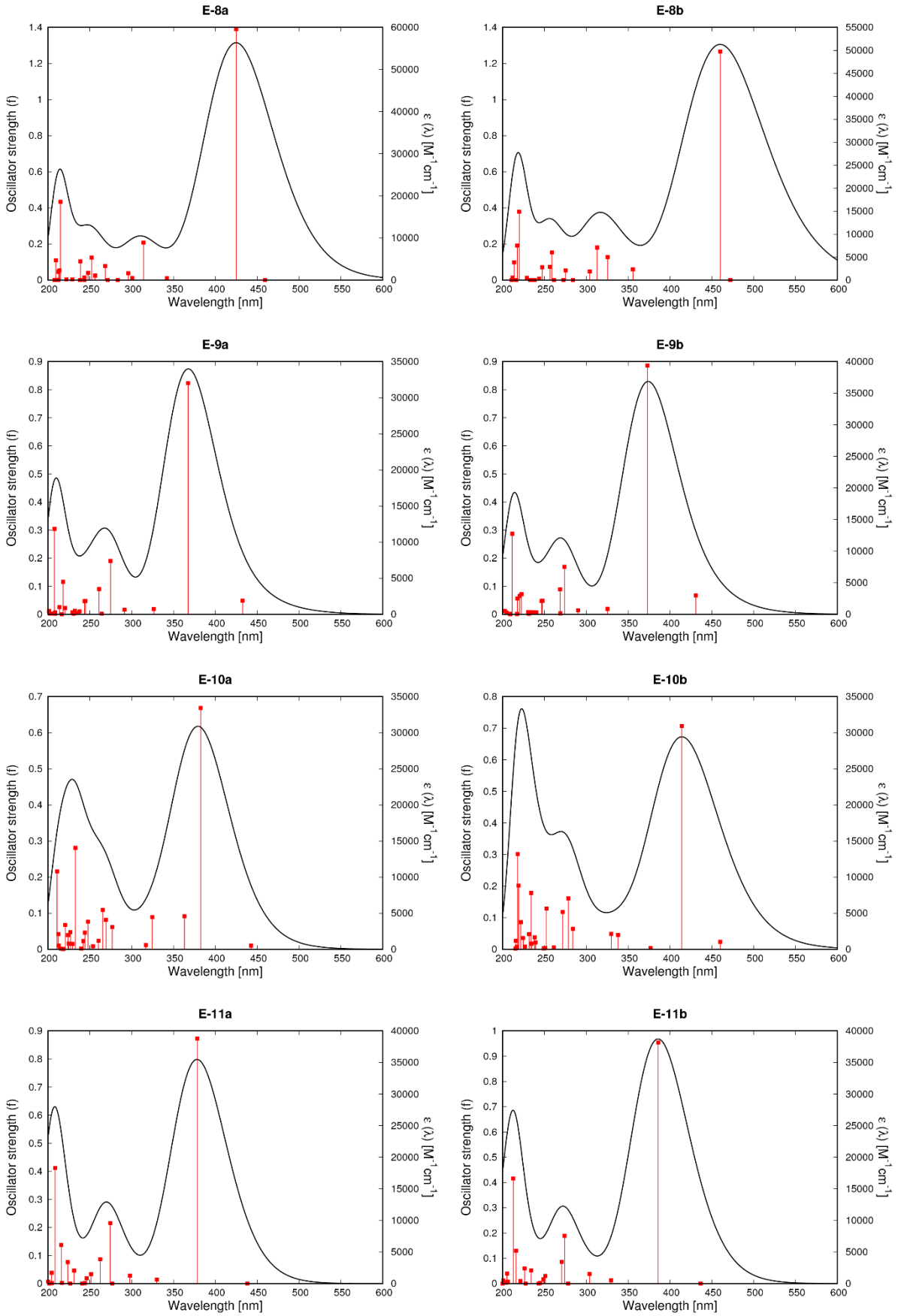
E-8a
E-8b
E-9a
E-9b
E-10a
E-10b
E-11a
E-11b
Oscillator strength (f)
ε (λ) [M-1cm-1]
Wavelength [nm]

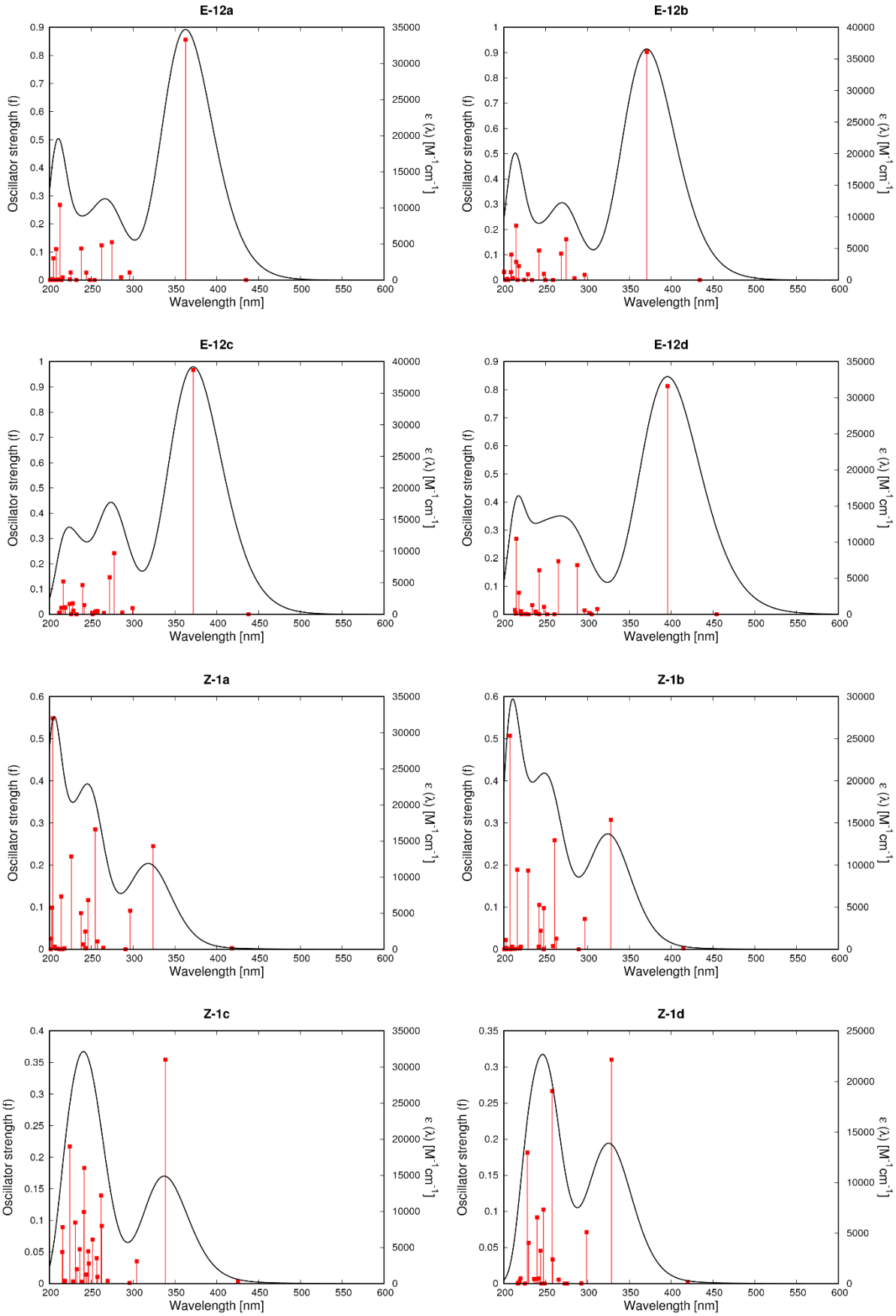
E-12a
E-12b
E-12c
E-12d
Z-1a
Z-1b
Z-1c
Z-1d
Oscillator strength (f)
ε (λ) [M-1cm-1]
Wavelength [nm]

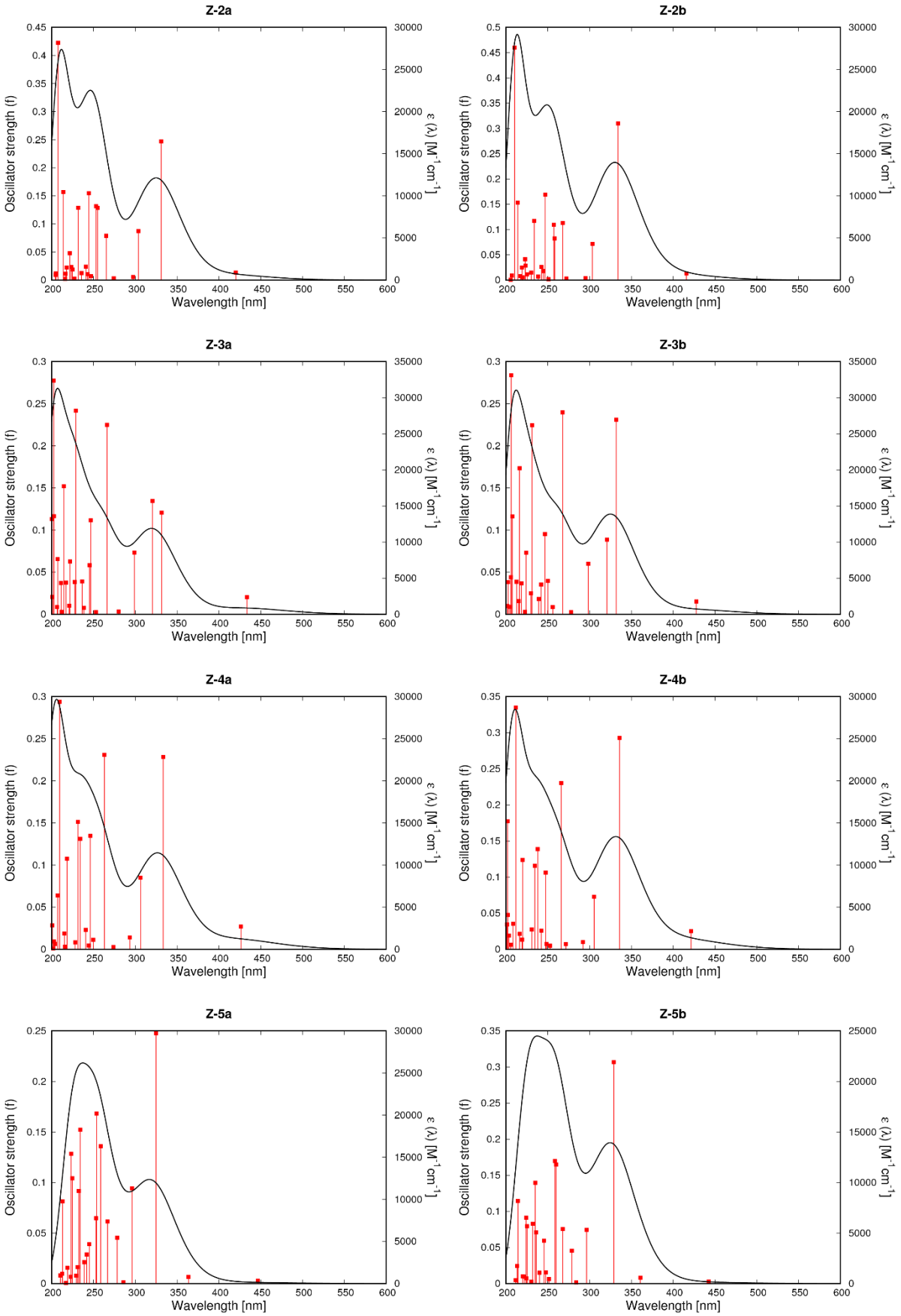
Z-2a
Z-2b
Z-3a
Z-3b
Z-4a
Z-4b
Z-5a
Z-5b
Oscillator strength (f)
ε (λ) [M-1cm-1]
Wavelength [nm]

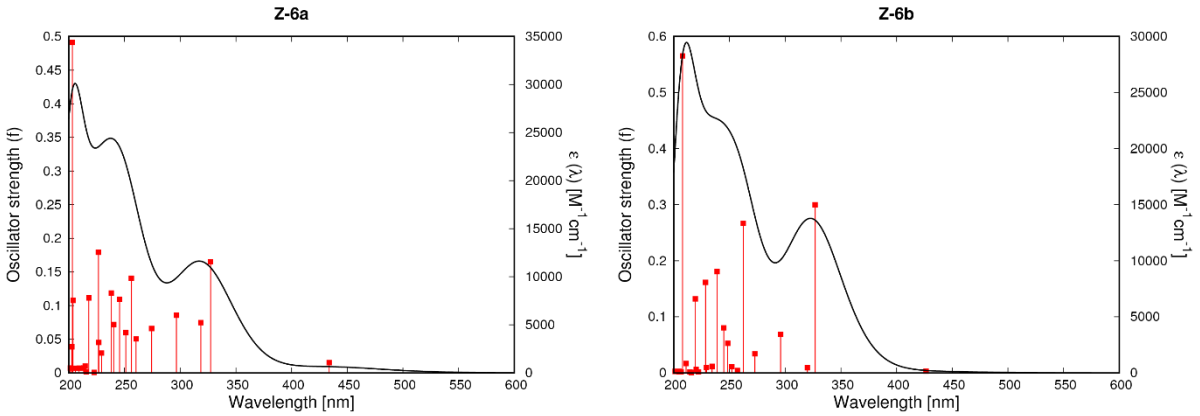
Z-6a
Oscillator strength (f)
ε (λ) [M-1cm-1]
Wavelength [nm]

Z-6b
Oscillator strength (f)
ε (λ) [M-1cm-1]
Wavelength [nm]

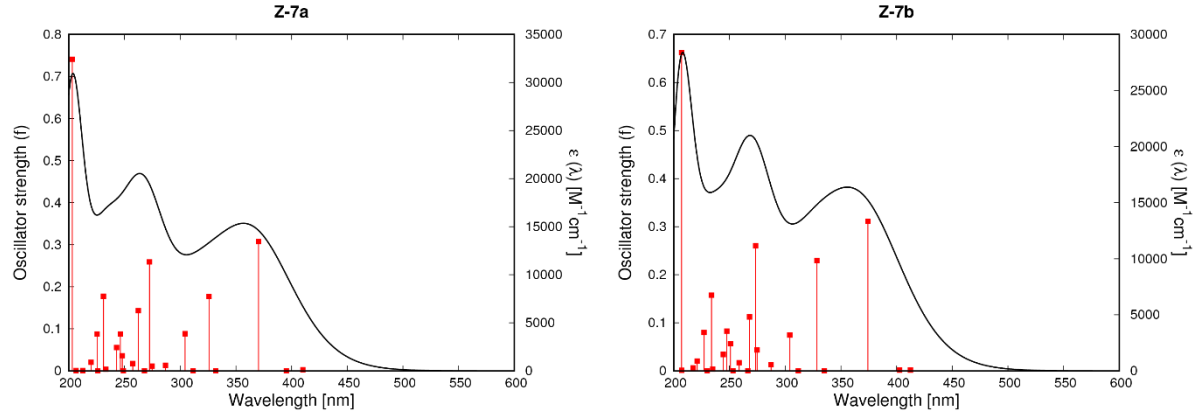
Z-7a
Oscillator strength (f)
ε (λ) [M-1cm-1]
Wavelength [nm]

Z-7b
Oscillator strength (f)
ε (λ) [M-1cm-1]
Wavelength [nm]

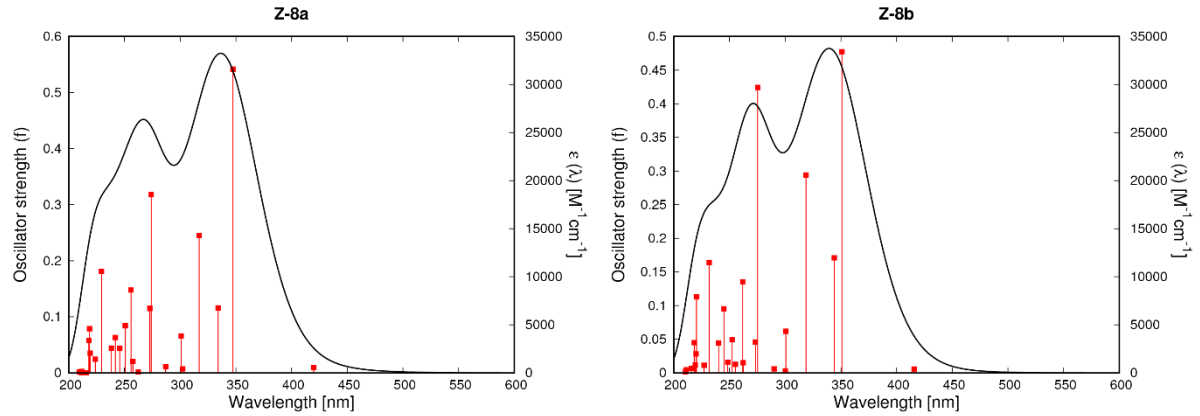
Z-8a
Oscillator strength (f)
ε (λ) [M-1cm-1]
Wavelength [nm]

Z-8b
Oscillator strength (f)
ε (λ) [M-1cm-1]
Wavelength [nm]

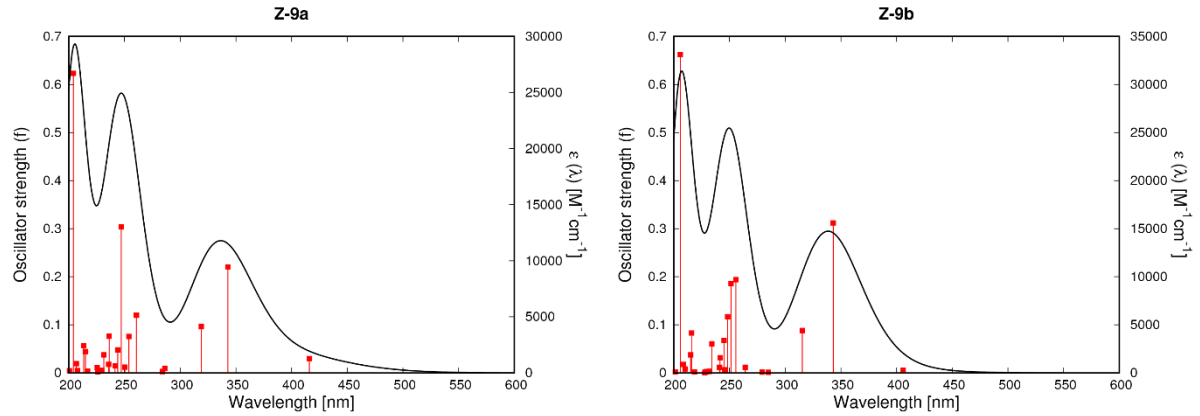
Z-9a
Oscillator strength (f)
ε (λ) [M-1cm-1]
Wavelength [nm]

Z-9b
Oscillator strength (f)
ε (λ) [M-1cm-1]
Wavelength [nm]

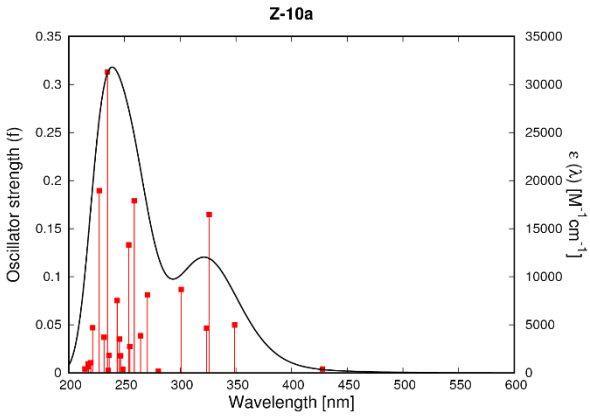
Z-10a
Oscillator strength (f)
ε (λ) [M-1cm-1]
Wavelength [nm]

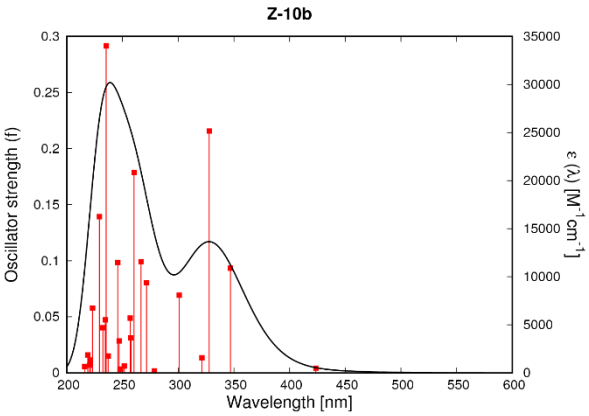
Z-10b
Oscillator strength (f)
ε (λ) [M-1cm-1]
Wavelength [nm]

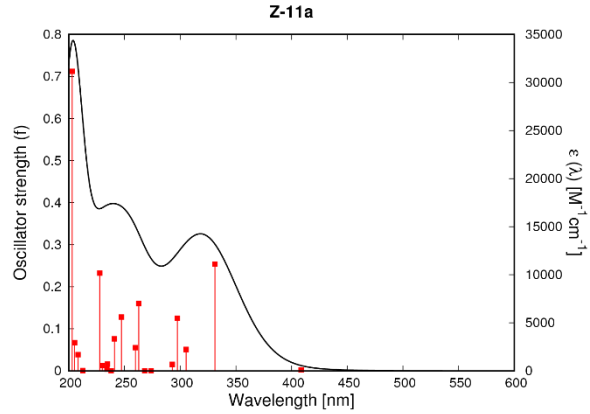
Z-11a
Oscillator strength (f)
ε (λ) [M-1cm-1]
Wavelength [nm]

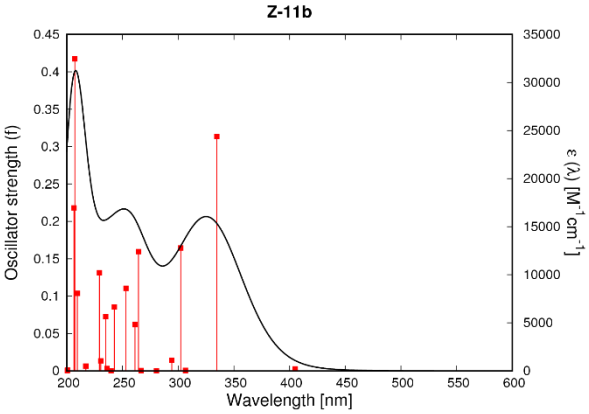
Z-11b
Oscillator strength (f)
ε (λ) [M-1cm-1]
Wavelength [nm]

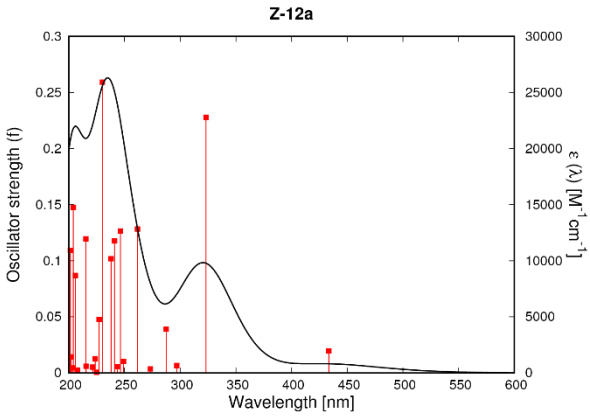
Z-12a
Oscillator strength (f)
ε (λ) [M-1cm-1]
Wavelength [nm]

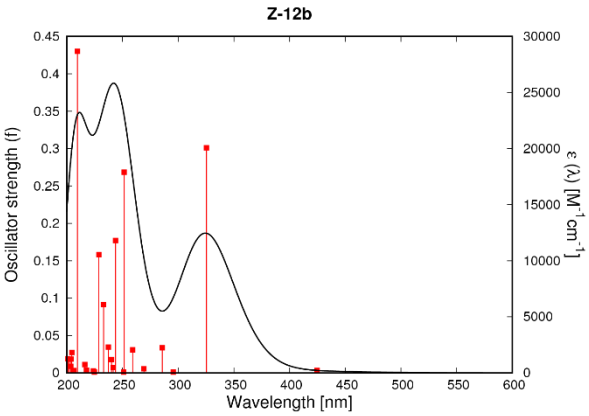
Z-12b
Oscillator strength (f)
ε (λ) [M-1cm-1]
Wavelength [nm]

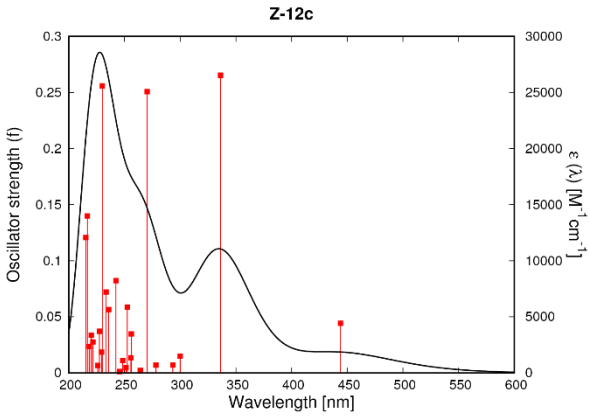
Z-12c
Oscillator strength (f)
ε (λ) [M-1cm-1]
Wavelength [nm]

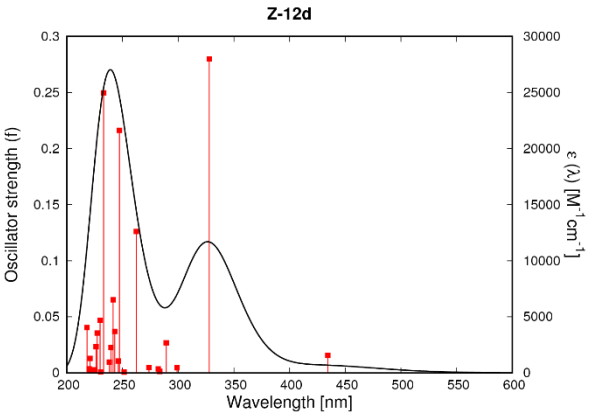
Z-12d
Oscillator strength (f)
ε (λ) [M-1cm-1]
Wavelength [nm]

7.2.4. MeOH

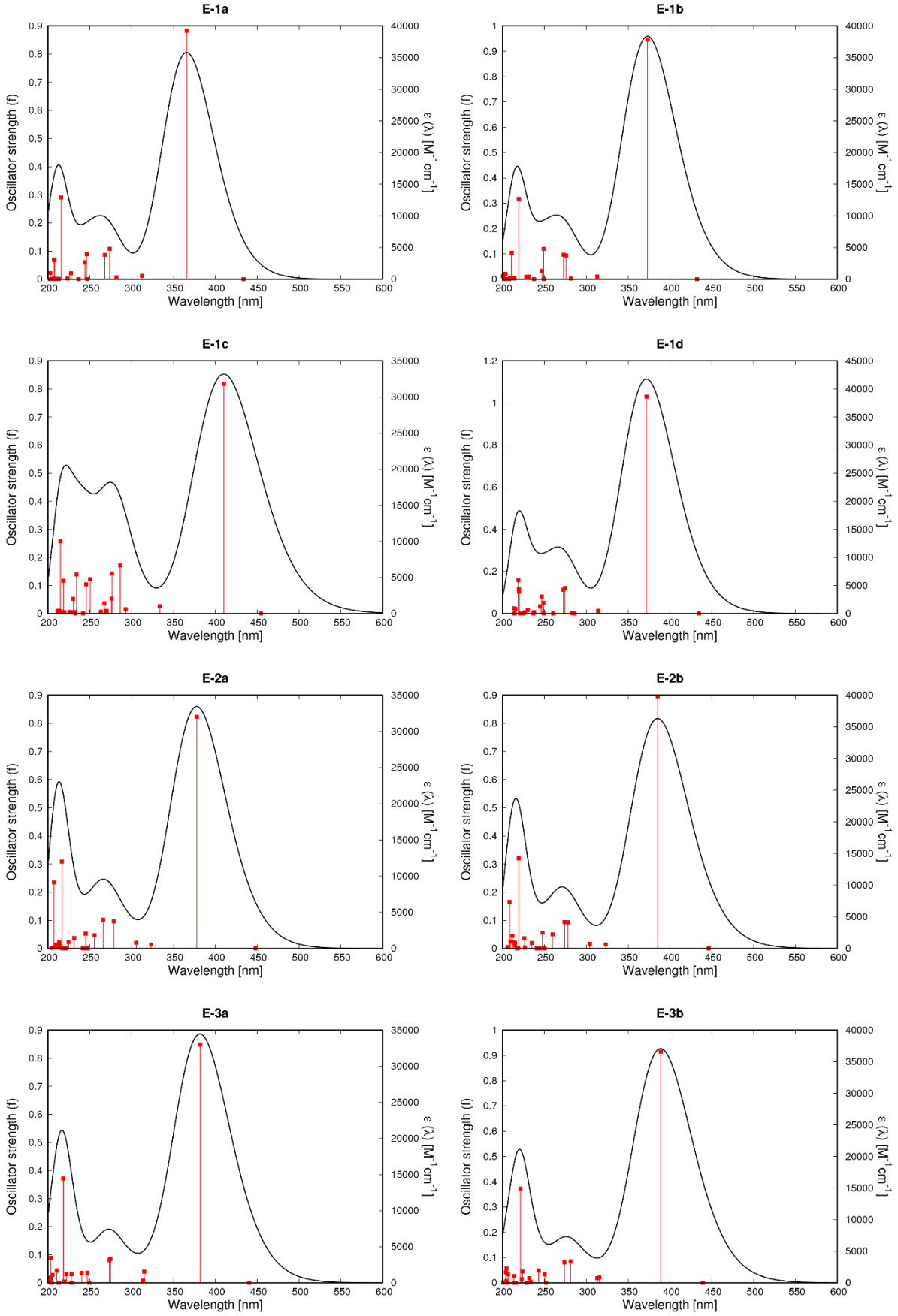
E-1a
E-1b
E-1c
E-1d
E-2a
E-2b
E-3a
E-3b
Oscillator strength (f)
ε (λ) [M-1cm-1]
Wavelength [nm]

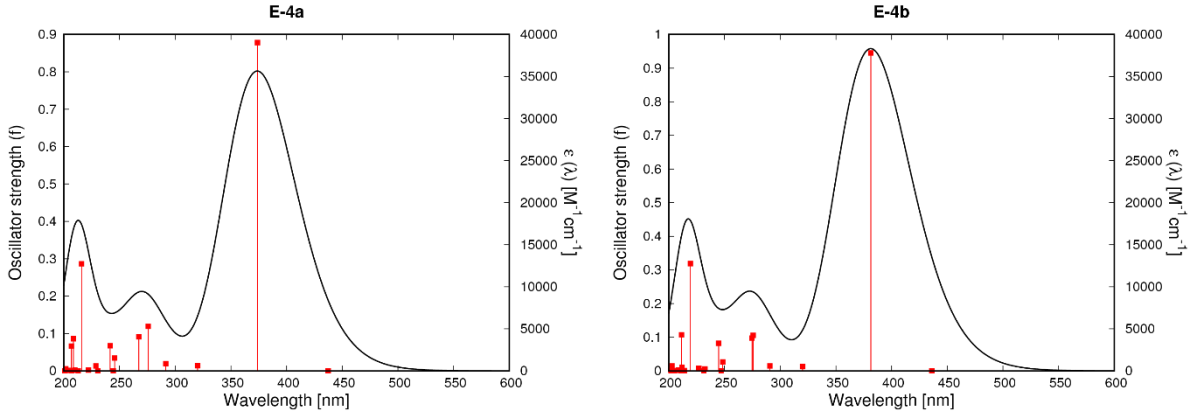
E-4a
Oscillator strength (f)
ε (λ) [M-1cm-1]
Wavelength [nm]

E-4b
Oscillator strength (f)
ε (λ) [M-1cm-1]
Wavelength [nm]

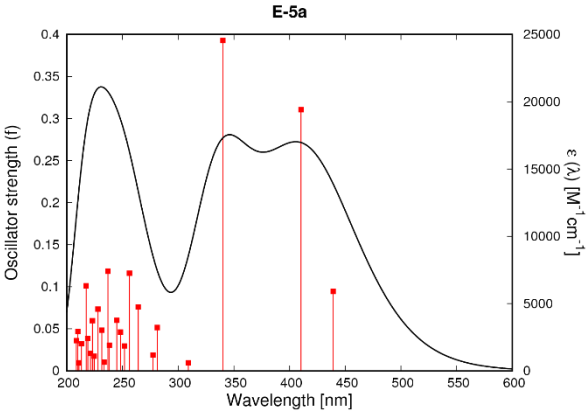
E-5a
Oscillator strength (f)
ε (λ) [M-1cm-1]
Wavelength [nm]

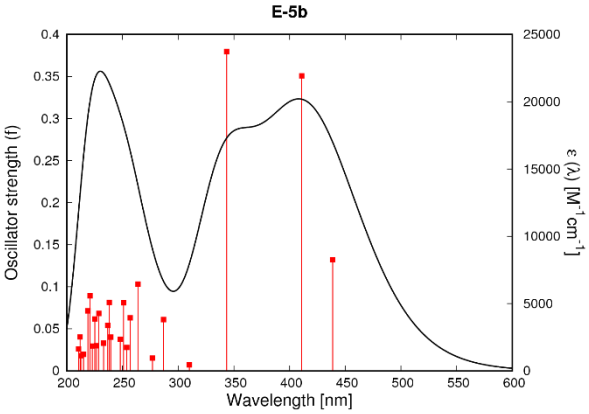
E-5b
Oscillator strength (f)
ε (λ) [M-1cm-1]
Wavelength [nm]

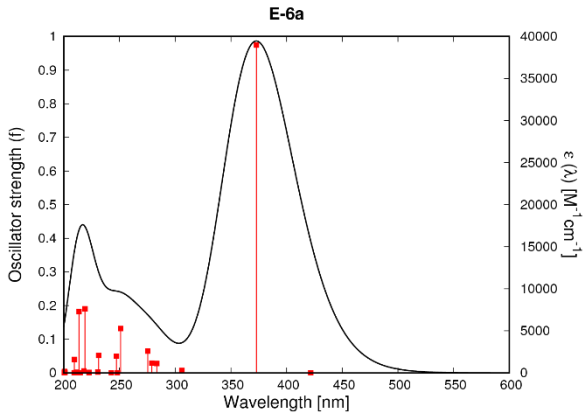
E-6a
Oscillator strength (f)
ε (λ) [M-1cm-1]
Wavelength [nm]

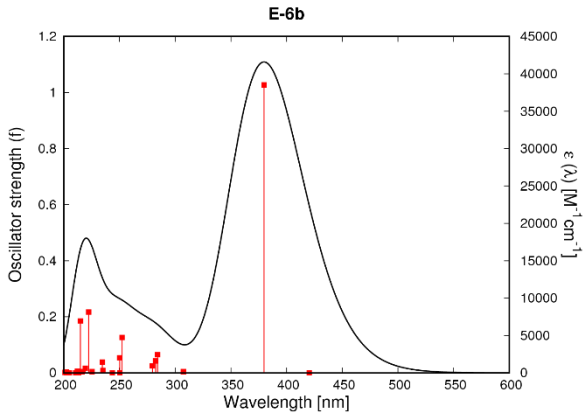
E-6b
Oscillator strength (f)
ε (λ) [M-1cm-1]
Wavelength [nm]

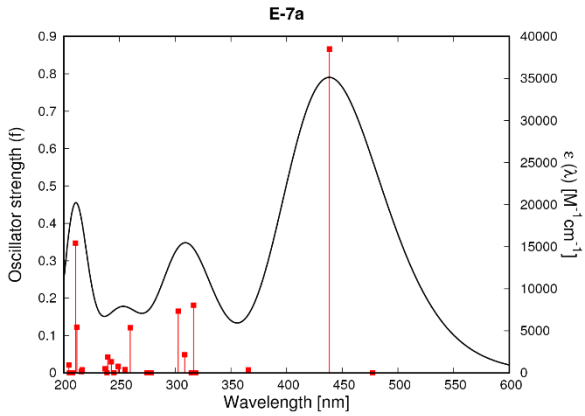
E-7a
Oscillator strength (f)
ε (λ) [M-1cm-1]
Wavelength [nm]

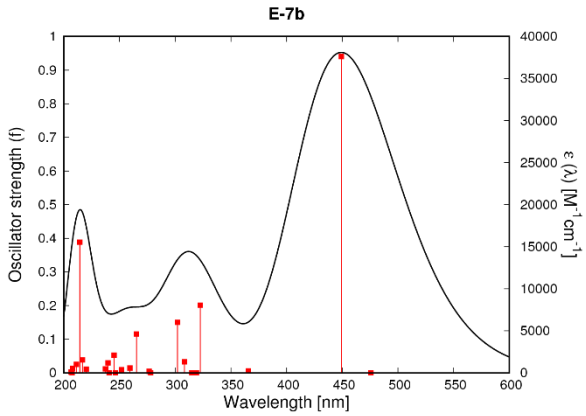
E-7b
Oscillator strength (f)
ε (λ) [M-1cm-1]
Wavelength [nm]

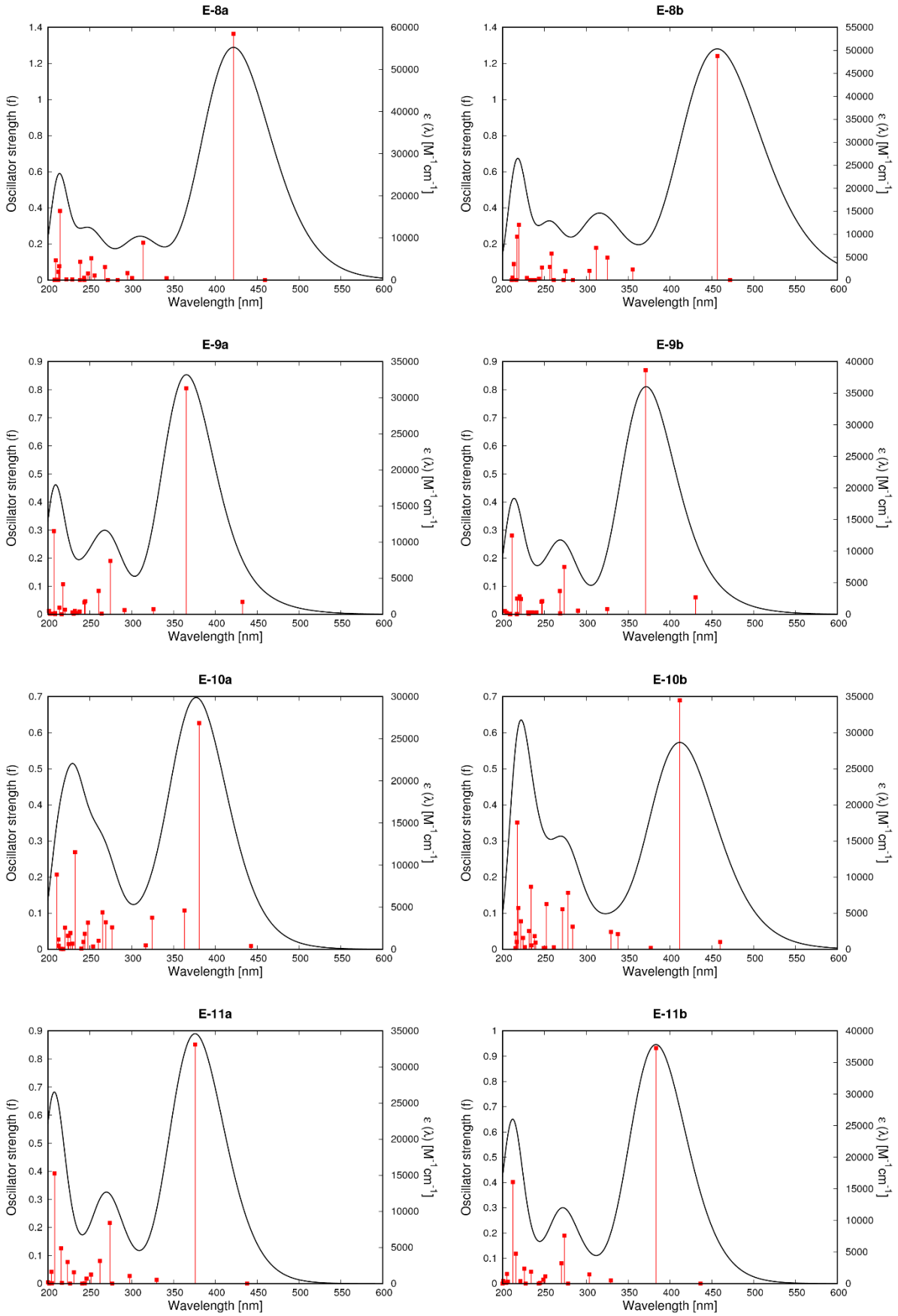
E-8a
E-8b
E-9a
E-9b
E-10a
E-10b
E-11a
E-11b
Oscillator strength (f)
ε (λ) [M-1cm-1]
Wavelength [nm]

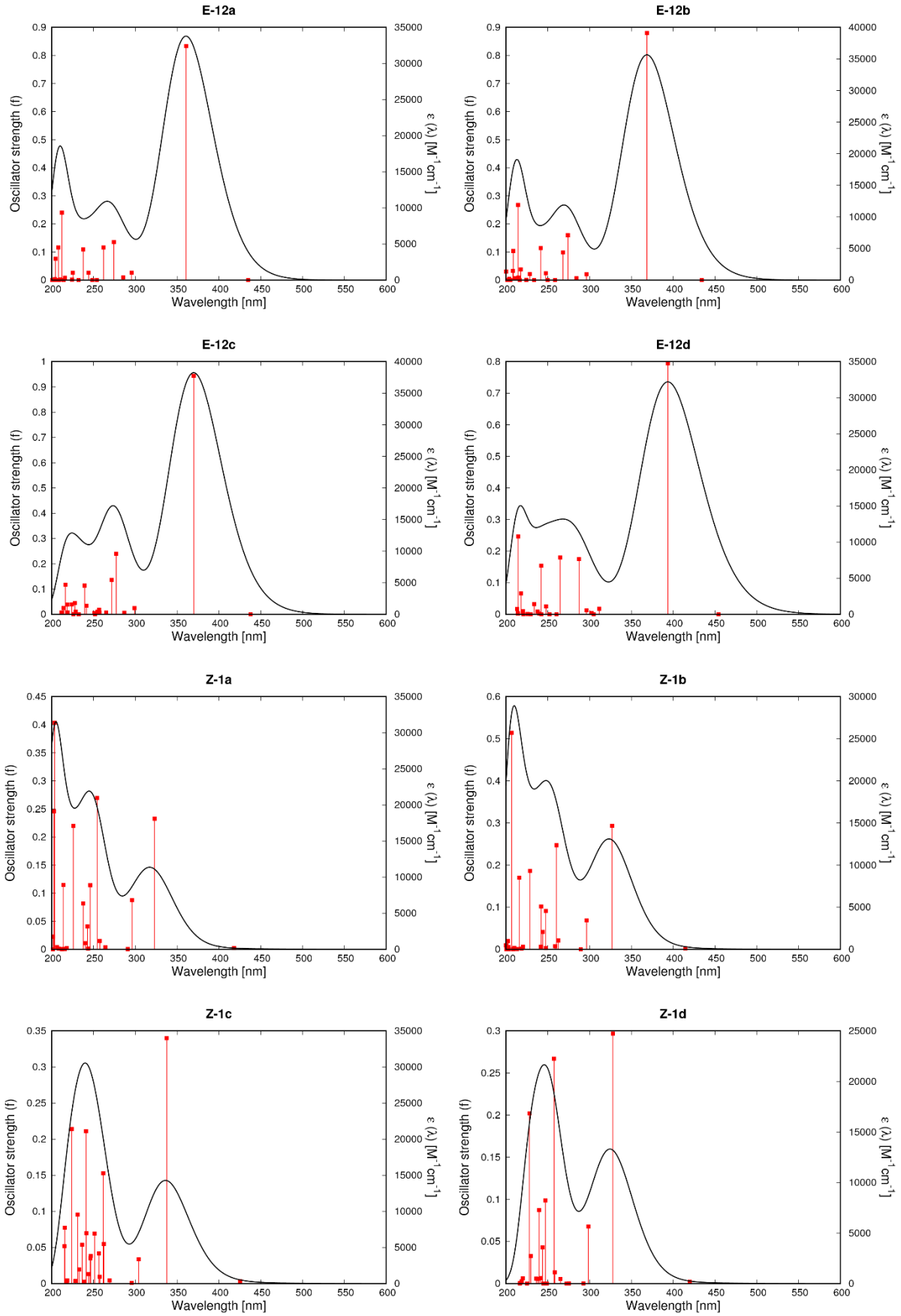
E-12a
E-12b
E-12c
E-12d
Z-1a
Z-1b
Z-1c
Z-1d
Oscillator strength (f)
ε (λ) [M-1cm-1]
Wavelength [nm]

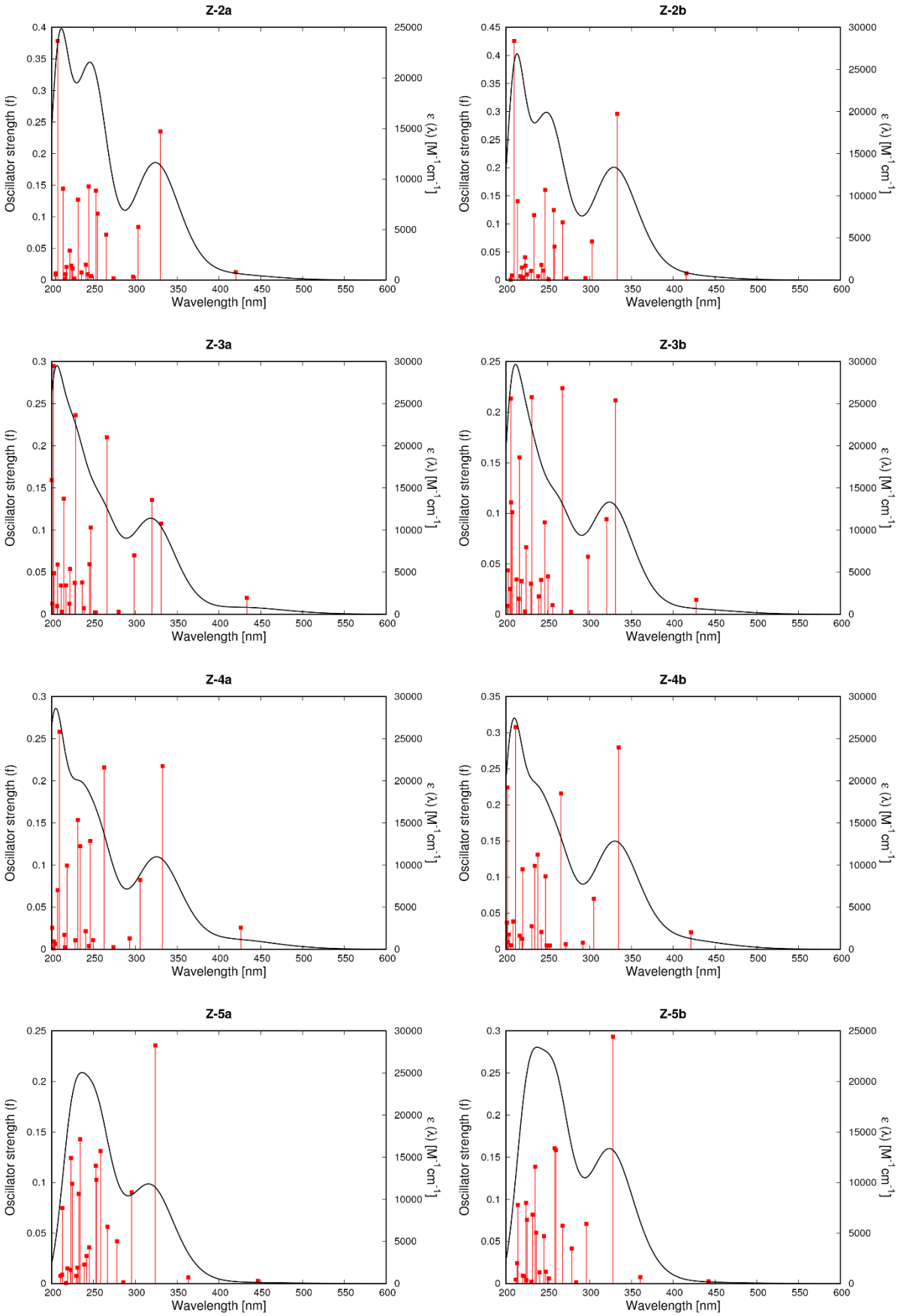
Z-2a
Z-2b
Z-3a
Z-3b
Z-4a
Z-4b
Z-5a
Z-5b
Oscillator strength (f)
ε (λ) [M-1cm-1]
Wavelength [nm]

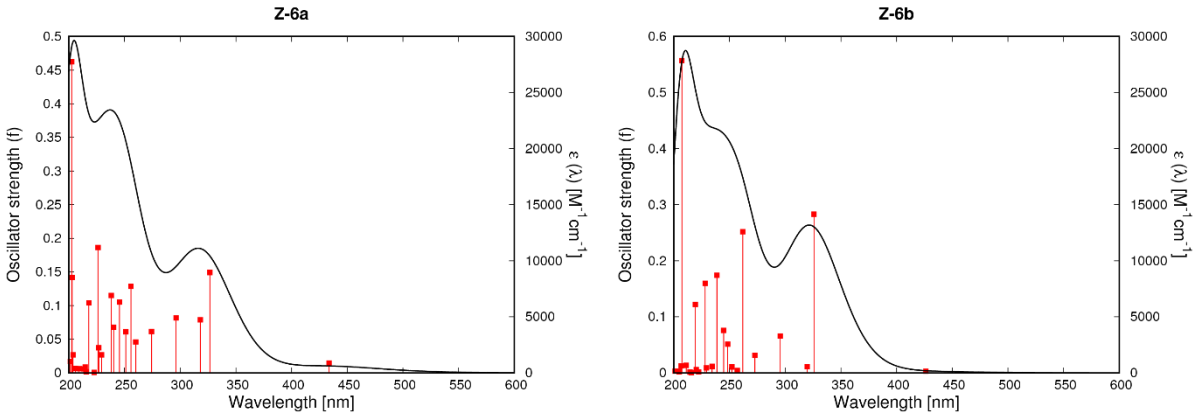
Z-6a
Oscillator strength (f)
ε (λ) [M-1cm-1]
Wavelength [nm]

Z-6b
Oscillator strength (f)
ε (λ) [M-1cm-1]
Wavelength [nm]

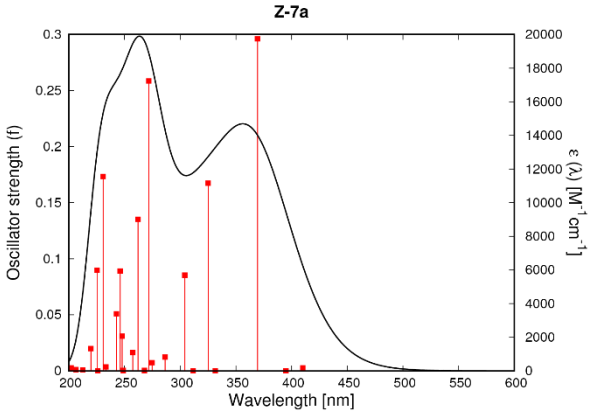
Z-7a
Oscillator strength (f)
ε (λ) [M-1cm-1]
Wavelength [nm]

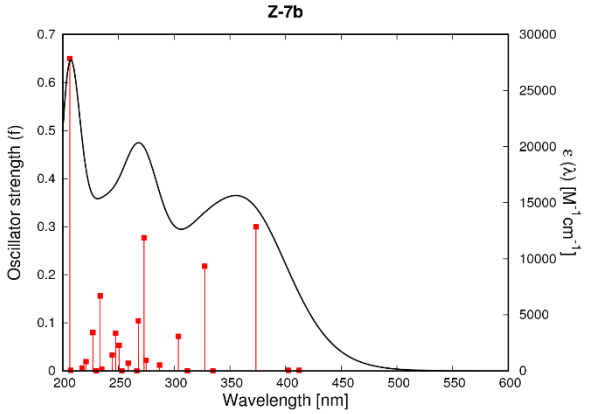
Z-7b
Oscillator strength (f)
ε (λ) [M-1cm-1]
Wavelength [nm]

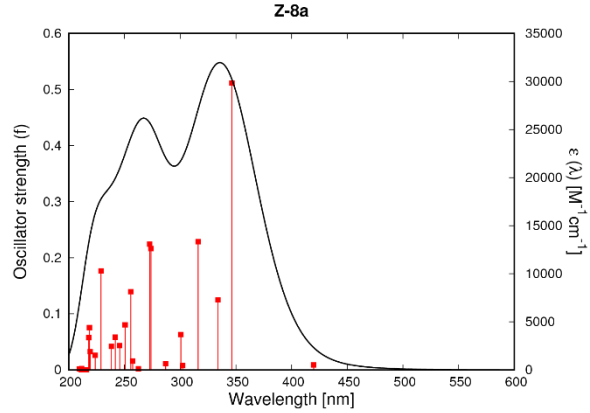
Z-8a
Oscillator strength (f)
ε (λ) [M-1cm-1]
Wavelength [nm]

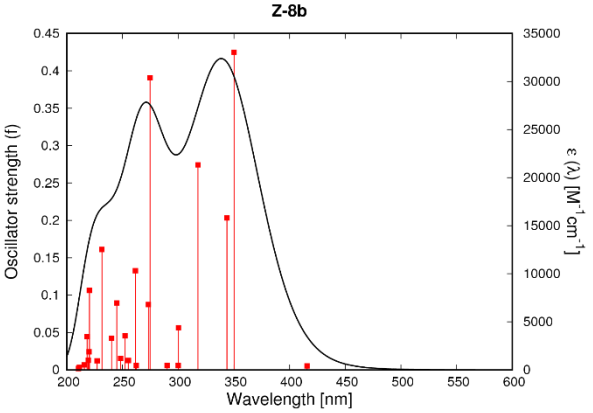
Z-8b
Oscillator strength (f)
ε (λ) [M-1cm-1]
Wavelength [nm]

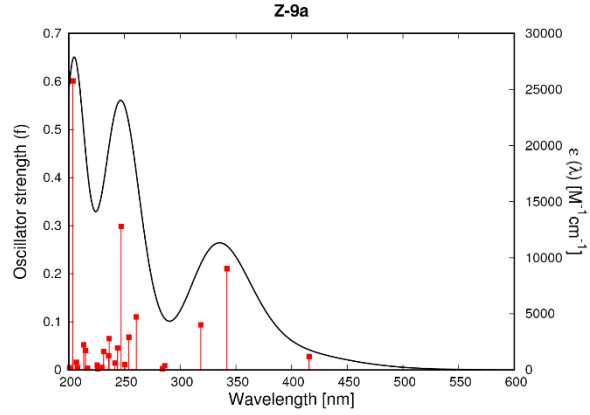
Z-9a
Oscillator strength (f)
ε (λ) [M-1cm-1]
Wavelength [nm]

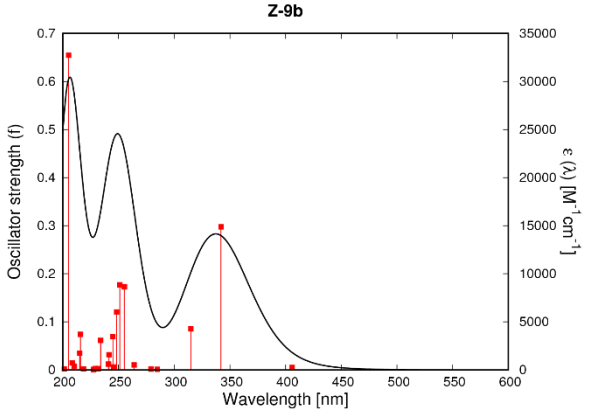
Z-9b
Oscillator strength (f)
ε (λ) [M-1cm-1]
Wavelength [nm]

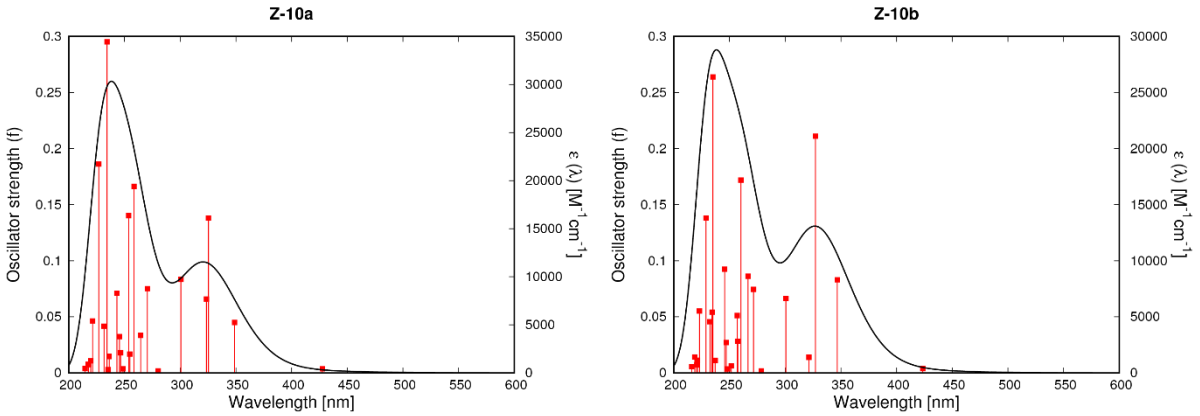
Z-10a
Oscillator strength (f)
ε (λ) [M-1cm-1]
Wavelength [nm]

Z-10b
Oscillator strength (f)
ε (λ) [M-1cm-1]
Wavelength [nm]

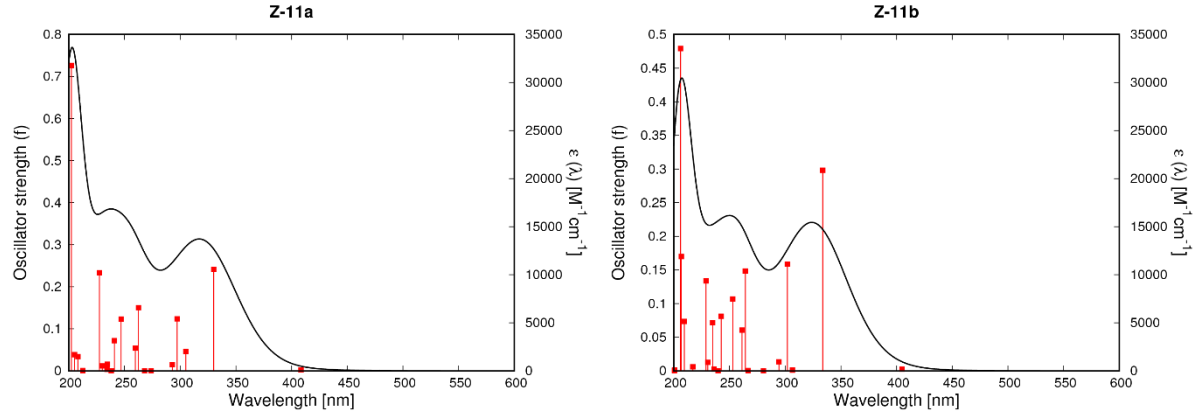
Z-11a
Oscillator strength (f)
ε (λ) [M-1cm-1]
Wavelength [nm]

Z-11b
Oscillator strength (f)
ε (λ) [M-1cm-1]
Wavelength [nm]

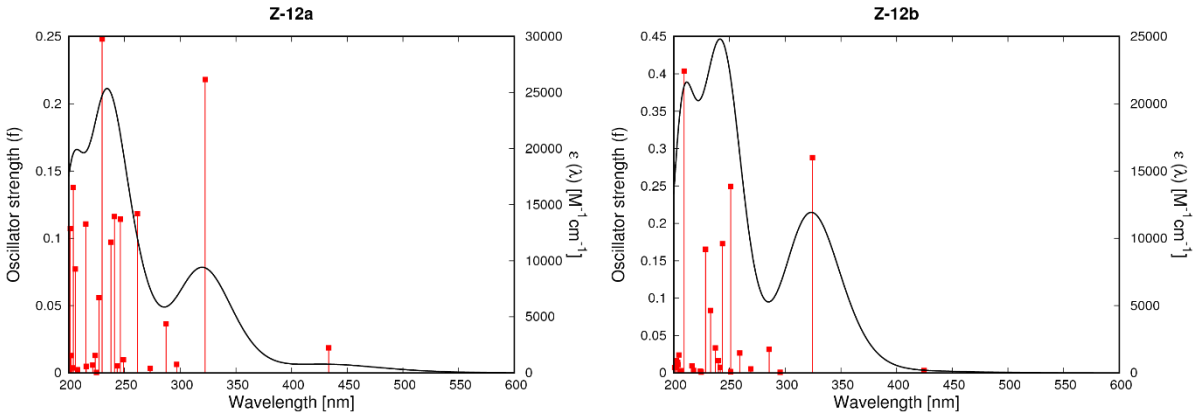
Z-12a
Oscillator strength (f)
ε (λ) [M-1cm-1]
Wavelength [nm]

Z-12b
Oscillator strength (f)
ε (λ) [M-1cm-1]
Wavelength [nm]

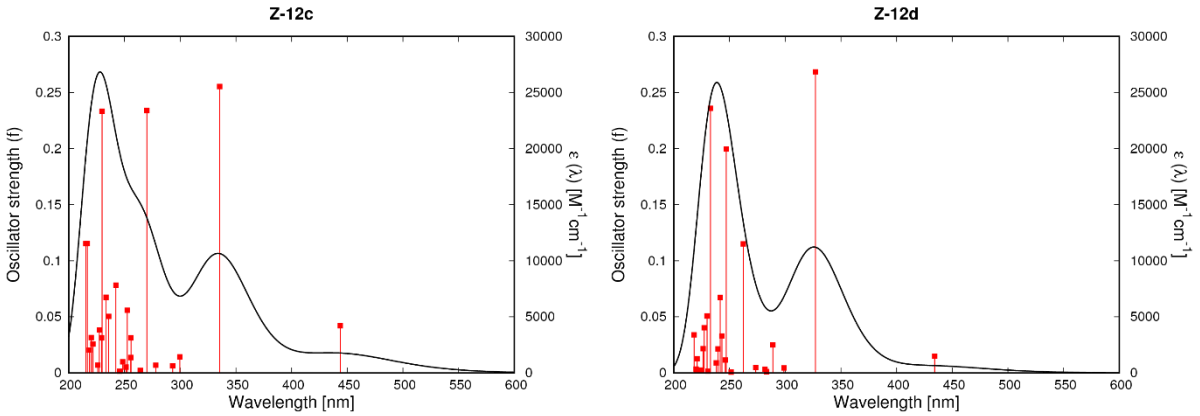
Z-12c
Oscillator strength (f)
ε (λ) [M-1cm-1]
Wavelength [nm]

Z-12d
Oscillator strength (f)
ε (λ) [M-1cm-1]
Wavelength [nm]

7.3. Electronic transitions

The five lowest transitions computed in the TD single-point calculations (25 states in total) are reported. For each excited state the energy (in eV), the associated wavelength (in nm) and the oscillator strength of the transition is given. The numbers of the orbitals involved in the transition (with general formula occupied → unoccupied) and the associated (largest) coefficient in the CI expansion is printed.

7.3.1. Transitions in Vacuum

***E*-1a**

Excited State 1: 2.7932 eV 443.88nm f=0.0000
57 → 59 0.70049
Excited State 2: 3.5782 eV 346.50nm f=0.7581
58 → 59 0.69987
Excited State 3: 4.0926 eV 302.95nm f=0.0062
56 → 59 0.67272
58 → 60 0.18604
Excited State 4: 4.3920 eV 282.29nm f=0.0050
54 → 59 0.55691
55 → 59 -0.34153
55 → 61 -0.11106
58 → 61 0.22951
Excited State 5: 4.5765 eV 270.92nm f=0.1071
54 → 59 0.32144
55 → 59 0.58703
56 → 60 -0.15070

***E*-1b**

Excited State 1: 2.7986 eV 443.02nm f=0.0000
61 → 63 0.69992
Excited State 2: 3.5160 eV 352.63nm f=0.8222
62 → 63 0.70084
Excited State 3: 4.0838 eV 303.60nm f=0.0029
60 → 63 0.65334
62 → 64 0.24433
Excited State 4: 4.3977 eV 281.93nm f=0.0022
58 → 63 0.53901
59 → 63 -0.34630
59 → 65 -0.11066
62 → 65 0.24949
Excited State 5: 4.5059 eV 275.16nm f=0.0728
60 → 63 -0.23711
62 → 64 0.63868

***E*-1c**

Excited State 1: 2.6668 eV 464.92nm f=0.0000
77 → 79 0.69869
Excited State 2: 3.1819 eV 389.66nm f=0.7119
78 → 79 0.70527
Excited State 3: 3.8292 eV 323.79nm f=0.0302
76 → 79 0.68743
78 → 82 0.10575
Excited State 4: 4.2475 eV 291.90nm f=0.0654
74 → 79 0.17082
75 → 79 0.18013
78 → 80 0.61448
78 → 81 -0.18645
Excited State 5: 4.2653 eV 290.68nm f=0.0009
74 → 79 0.57869
75 → 79 0.22874
75 → 83 0.10172
78 → 80 -0.24141
78 → 83 -0.18218

***E*-1d**

Excited State 1: 2.7922 eV 444.04nm f=0.0000
89 → 91 0.70010
Excited State 2: 3.4986 eV 354.38nm f=0.9154
90 → 91 0.70056
Excited State 3: 4.0495 eV 306.17nm f=0.0058
88 → 91 0.66737
90 → 93 0.20127
Excited State 4: 4.3984 eV 281.88nm f=0.0001
90 → 92 0.69676
Excited State 5: 4.4004 eV 281.75nm f=0.0028
86 → 91 0.56917
87 → 91 0.29147
87 → 95 0.11459
90 → 95 0.24648

***E*-2a**

Excited State 1: 2.6977 eV 459.60nm f=0.0000

74 → 76 0.69970
Excited State 2: 3.4355 eV 360.89nm f=0.6757
75 → 76 0.69749
Excited State 3: 3.9335 eV 315.20nm f=0.0085
73 → 76 0.68458
75 → 77 0.13026
Excited State 4: 4.0049 eV 309.58nm f=0.0200
72 → 76 0.67415
75 → 78 0.13835
Excited State 5: 4.4759 eV 277.00nm f=0.1004
71 → 76 0.66688
72 → 76 -0.10199
73 → 77 0.12397

***E*-2b**

Excited State 1: 2.7040 eV 458.52nm f=0.0000
78 → 80 0.69937
Excited State 2: 3.3809 eV 366.72nm f=0.7499
79 → 80 0.69901
Excited State 3: 3.9390 eV 314.76nm f=0.0067
77 → 80 0.67846
79 → 81 0.16249
Excited State 4: 4.0186 eV 308.52nm f=0.0171
76 → 80 0.67204
79 → 82 0.15268
Excited State 5: 4.4879 eV 276.26nm f=0.0913
75 → 80 0.64430
76 → 80 -0.10613
77 → 81 0.13632
79 → 81 -0.14102

***E*-3a**

Excited State 1: 2.7284 eV 454.43nm f=0.0000
61 → 63 0.70021
Excited State 2: 3.4210 eV 362.42nm f=0.7192
62 → 63 0.69576
Excited State 3: 4.0137 eV 308.90nm f=0.0242
60 → 63 0.67693
62 → 66 -0.11251
Excited State 4: 4.0332 eV 307.41nm f=0.0096
59 → 63 0.67280

62 → 64 0.17756
Excited State 5: 4.5521 eV 272.37nm f=0.0756
58 → 63 0.47450
59 → 63 0.17210
59 → 64 0.11075
62 → 64 -0.45691

***E*-3b**

Excited State 1: 2.7330 eV 453.66nm f=0.0000
65 → 67 0.69976
Excited State 2: 3.3673 eV 368.20nm f=0.7862
66 → 67 0.69777
Excited State 3: 4.0175 eV 308.61nm f=0.0235
64 → 67 0.67297
66 → 68 -0.10101
66 → 70 -0.10419
Excited State 4: 4.0265 eV 307.92nm f=0.0027
63 → 67 0.66271
66 → 68 -0.21123
Excited State 5: 4.4410 eV 279.18nm f=0.0648
63 → 67 0.20474
64 → 67 0.11387
66 → 68 0.64435

***E*-4a**

Excited State 1: 2.7548 eV 450.06nm f=0.0000
61 → 63 0.70066
Excited State 2: 3.4880 eV 355.46nm f=0.7412
62 → 63 0.69981
Excited State 3: 3.9729 eV 312.08nm f=0.0079
60 → 63 0.68301
62 → 64 0.14327
Excited State 4: 4.2550 eV 291.38nm f=0.0136
58 → 63 0.23575
59 → 63 0.62897
62 → 65 0.16879
Excited State 5: 4.5353 eV 273.38nm f=0.1362
58 → 63 0.63367
59 → 63 -0.24094
60 → 64 0.13939

***E*-4b**

Excited State 1: 2.7599 eV 449.23nm f=0.0000
65 → 67 0.70026
Excited State 2: 3.4301 eV 361.46nm f=0.8109
66 → 67 0.70089
Excited State 3: 3.9753 eV 311.89nm f=0.0053
64 → 67 0.67404
66 → 68 0.18022
Excited State 4: 4.2651 eV 290.70nm f=0.0103
62 → 67 0.22445
63 → 67 0.62811
66 → 69 0.18214
Excited State 5: 4.5190 eV 274.36nm f=0.0783
62 → 67 -0.22231
63 → 67 0.11954
64 → 67 -0.18418
66 → 68 0.61066

***E*-5a**

Excited State 1: 2.7656 eV 448.32nm f=0.0326
79 → 82 0.54880
80 → 82 0.36070
81 → 82 -0.22115
Excited State 2: 3.0772 eV 402.91nm f=0.2432
80 → 82 0.27999
81 → 82 0.63920
Excited State 3: 3.7503 eV 330.59nm f=0.3874
79 → 82 -0.41332
80 → 82 0.52655
81 → 82 -0.18204
Excited State 4: 4.1155 eV 301.27nm f=0.0024
78 → 82 0.62196
81 → 83 0.30021
Excited State 5: 4.3694 eV 283.76nm f=0.0307
78 → 82 -0.30371
81 → 83 0.61051

***E*-5b**

The TD-DFT of ***E*-5b** in vacuum is ridden by an internal error in the calculation of the transition vectors. Due to we are not directly interested in

the spectra in vacuum for this work, we decided to skip to report this data

***E*-6a**

Excited State 1: 2.8712 eV 431.81nm f=0.0000
61 → 63 0.70031
Excited State 2: 3.5144 eV 352.79nm f=0.8495
62 → 63 0.70050
Excited State 3: 4.1472 eV 298.96nm f=0.0022
60 → 63 0.64357
62 → 64 -0.27117
Excited State 4: 4.4327 eV 279.70nm f=0.0225
59 → 63 0.65067
60 → 64 -0.11294
62 → 65 -0.16964
Excited State 5: 4.4698 eV 277.38nm f=0.0294
58 → 63 0.42246
59 → 63 0.12417
59 → 65 0.10080
60 → 63 -0.13617
62 → 64 -0.30092
62 → 65 0.41460

***E*-6b**

Excited State 1: 2.8764 eV 431.04nm f=0.0000
65 → 67 0.69959
Excited State 2: 3.4567 eV 358.67nm f=0.9028
66 → 67 0.70138
Excited State 3: 4.1207 eV 300.88nm f=0.0005
64 → 67 0.58809
66 → 68 0.36913
Excited State 4: 4.4057 eV 281.42nm f=0.0609
62 → 67 -0.10665
63 → 67 -0.20499
64 → 67 -0.36653
66 → 68 0.53459
Excited State 5: 4.4332 eV 279.67nm f=0.0088
62 → 67 -0.27166
63 → 67 0.48417
66 → 69 -0.38594

***E*-7a**

Excited State 1: 2.6121 eV 474.66nm f=0.0000
68 → 70 0.66174
68 → 71 0.23613
Excited State 2: 3.1464 eV 394.05nm f=0.7834
69 → 70 0.70369
Excited State 3: 3.6541 eV 339.30nm f=0.0081
67 → 70 0.68877
67 → 71 0.10813
Excited State 4: 3.7714 eV 328.75nm f=0.0000
64 → 70 0.60442
64 → 71 -0.34794
Excited State 5: 4.1348 eV 299.85nm f=0.0187
65 → 70 0.59779
66 → 70 -0.13484
69 → 71 -0.27618
69 → 73 0.15523

***E*-7b**

Excited State 1: 2.6167 eV 473.82nm f=0.0000
72 → 74 0.66175
72 → 75 0.23383
Excited State 2: 3.0860 eV 401.77nm f=0.8602
73 → 74 0.70434
Excited State 3: 3.6643 eV 338.36nm f=0.0056
71 → 74 0.68619
71 → 75 0.10837
Excited State 4: 3.7741 eV 328.52nm f=0.0000
68 → 74 0.60475
68 → 75 -0.34594
Excited State 5: 4.1042 eV 302.09nm f=0.0947
69 → 74 -0.32925
73 → 75 0.59522
73 → 77 -0.10838

***E*-8a**

Excited State 1: 2.6525 eV 467.42nm f=0.0000
75 → 77 0.67040
75 → 78 0.20402
Excited State 2: 3.1300 eV 396.11nm f=1.2239

76 → 77 0.70347
Excited State 3: 3.7712 eV 328.76nm f=0.0077
74 → 77 0.68538
Excited State 4: 4.0033 eV 309.70nm f=0.1690
73 → 77 0.64594
76 → 78 0.24798
Excited State 5: 4.1563 eV 298.30nm f=0.0158
72 → 77 0.64015
73 → 80 0.11140
76 → 78 -0.10244
76 → 80 0.24218

***E*-8b**

Excited State 1: 2.5728 eV 481.90nm f=0.0000
79 → 81 0.67453
79 → 82 0.19067
Excited State 2: 2.9004 eV 427.47nm f=1.0972
80 → 81 0.70529
Excited State 3: 3.6287 eV 341.68nm f=0.0801
78 → 81 0.68908
Excited State 4: 3.8772 eV 319.77nm f=0.1117
77 → 81 0.59287
80 → 82 0.36562
Excited State 5: 4.0884 eV 303.26nm f=0.0304
76 → 81 0.52484
77 → 81 0.20413
80 → 82 -0.35697
80 → 84 0.18829

***E*-9a**

Excited State 1: 2.7856 eV 445.09nm f=0.0199
74 → 79 -0.10780
77 → 79 0.66084
78 → 79 -0.20320
Excited State 2: 3.5565 eV 348.61nm f=0.6926
77 → 79 0.20314
78 → 79 0.66829
Excited State 3: 3.9164 eV 316.57nm f=0.0108
76 → 79 0.68595
78 → 80 0.11673
Excited State 4: 4.1996 eV 295.23nm f=0.0123

75 → 79 0.67950
78 → 82 0.15469
Excited State 5: 4.5475 eV 272.64nm f=0.1898
74 → 79 0.66938
76 → 80 -0.14276

***E*-9b**

Excited State 1: 2.7960 eV 443.44nm f=0.0248
78 → 83 0.10263
81 → 83 0.66130
82 → 83 -0.20290
Excited State 2: 3.5117 eV 353.06nm f=0.7701
81 → 83 0.20228
82 → 83 0.66978
Excited State 3: 3.9332 eV 315.22nm f=0.0091
80 → 83 0.68184
82 → 84 -0.14126
Excited State 4: 4.2190 eV 293.87nm f=0.0112
79 → 83 0.67592
82 → 86 0.16733
Excited State 5: 4.5625 eV 271.74nm f=0.1632
78 → 83 0.66305
80 → 84 -0.15696

***E*-10a**

Excited State 1: 2.7193 eV 455.93nm f=0.0038
72 → 76 0.46148
73 → 76 0.35370
74 → 76 0.32730
75 → 76 0.20650
Excited State 2: 3.1926 eV 388.35nm f=0.0544
72 → 76 -0.25838
73 → 76 -0.21628
74 → 76 0.25651
75 → 76 0.56260
Excited State 3: 3.3844 eV 366.35nm f=0.4624
73 → 76 -0.26248
74 → 76 0.54191
75 → 76 -0.35555
Excited State 4: 3.7674 eV 329.10nm f=0.1484
72 → 76 -0.44866

73 → 76 0.49735
74 → 76 0.15889
Excited State 5: 3.9788 eV 311.61nm f=0.0079
71 → 76 0.68252
75 → 77 0.10843

***E*-10b**

Excited State 1: 2.6175 eV 473.68nm f=0.0062
76 → 80 0.51803
77 → 80 0.18514
78 → 80 0.42279
Excited State 2: 3.1274 eV 396.44nm f=0.3992
76 → 80 0.18215
78 → 80 -0.34149
79 → 80 0.58802
Excited State 3: 3.1682 eV 391.34nm f=0.1665
76 → 80 -0.32211
77 → 80 -0.23449
78 → 80 0.44673
79 → 80 0.37128
Excited State 4: 3.6292 eV 341.63nm f=0.0467
76 → 80 -0.27847
77 → 80 0.62989
Excited State 5: 3.8711 eV 320.28nm f=0.0508
75 → 80 0.68420
79 → 81 0.13640

***E*-11a**

Excited State 1: 2.7781 eV 446.28nm f=0.0000
89 → 91 0.69928
Excited State 2: 3.4656 eV 357.76nm f=0.7184
90 → 91 0.69969
Excited State 3: 3.8605 eV 321.16nm f=0.0085
88 → 91 0.68941
90 → 93 0.10751
Excited State 4: 4.2951 eV 288.67nm f=0.0120
86 → 91 0.25048
90 → 92 0.64173
Excited State 5: 4.5171 eV 274.48nm f=0.0000
89 → 92 0.70594

***E*-11b**

Excited State 1: 2.7848 eV 445.22nm f=0.0000
93 → 95 0.69906
Excited State 2: 3.4110 eV 363.48nm f=0.8029
94 → 95 0.70076
Excited State 3: 3.8722 eV 320.19nm f=0.0063
92 → 95 0.68537
94 → 97 0.12803
Excited State 4: 4.2269 eV 293.32nm f=0.0213
90 → 95 0.21862
94 → 96 0.65817
Excited State 5: 4.4922 eV 276.00nm f=0.0000
93 → 96 0.70586

***E*-12a**

Excited State 1: 2.7766 eV 446.53nm f=0.0000
73 → 75 0.70095
Excited State 2: 3.6109 eV 343.36nm f=0.7060
74 → 75 0.69872
Excited State 3: 4.3024 eV 288.17nm f=0.0146
71 → 75 0.55987
72 → 75 0.33462
74 → 76 0.20536
74 → 78 -0.13624
Excited State 4: 4.3107 eV 287.62nm f=0.0090
70 → 75 -0.23302
71 → 75 -0.34046
72 → 75 0.52271
74 → 76 0.18683
74 → 78 0.10711
Excited State 5: 4.5347 eV 273.41nm f=0.1359
70 → 75 0.60440
71 → 75 -0.13998
72 → 75 0.24363
74 → 76 -0.14322

***E*-12b**

Excited State 1: 2.7791 eV 446.14nm f=0.0000
77 → 79 0.70066

Excited State 2: 3.5450 eV 349.75nm f=0.7547
78 → 79 0.70040
Excited State 3: 4.2909 eV 288.95nm f=0.0074
74 → 79 -0.13086
75 → 79 0.21484
76 → 79 0.54281
78 → 80 0.36347
Excited State 4: 4.3286 eV 286.43nm f=0.0067
74 → 79 0.23490
75 → 79 0.60091
76 → 79 -0.18320
78 → 82 -0.18469
Excited State 5: 4.5375 eV 273.24nm f=0.1487
74 → 79 0.51937
75 → 79 -0.13682
76 → 79 0.33608
76 → 80 0.10808
78 → 80 -0.24140

***E*-12c**

Excited State 1: 2.7628 eV 448.77nm f=0.0000
93 → 95 0.69929
Excited State 2: 3.5091 eV 353.33nm f=0.8237
94 → 95 0.70044
Excited State 3: 4.2315 eV 293.01nm f=0.0158
90 → 95 0.11700
91 → 95 0.15158
92 → 95 0.53597
94 → 96 0.36683
94 → 98 0.16570
Excited State 4: 4.3112 eV 287.59nm f=0.0046
90 → 95 -0.32218
91 → 95 0.57279
92 → 95 -0.13417
94 →100 0.17439
Excited State 5: 4.3724 eV 283.56nm f=0.1150
92 → 95 -0.31986
94 → 96 0.56567
94 → 97 -0.11035
94 → 98 -0.18880

***E*-12d**

Excited State 1: 2.6671 eV 464.86nm f=0.0000
105 →107 0.69911
Excited State 2: 3.2814 eV 377.84nm f=0.6824
106 →107 0.70505
Excited State 3: 4.0644 eV 305.05nm f=0.0121
103 →107 -0.13478
104 →107 0.66872
106 →109 -0.15493
Excited State 4: 4.1941 eV 295.61nm f=0.0096
100 →107 0.55843
102 →107 0.16176
103 →107 0.35144
106 →112 -0.14995
Excited State 5: 4.3407 eV 285.63nm f=0.1709
100 →107 -0.35205
103 →107 0.56542
104 →107 0.15518

***Z*-1a**

Excited State 1: 2.8555 eV 434.20nm f=0.0016
55 → 59 -0.12976
57 → 59 -0.13223
58 → 59 0.67318
Excited State 2: 3.9787 eV 311.62nm f=0.1557
57 → 59 0.67656
58 → 59 0.13472
Excited State 3: 4.3240 eV 286.74nm f=0.0084
55 → 59 0.63434
56 → 59 0.24323
58 → 59 0.12245
Excited State 4: 4.3283 eV 286.45nm f=0.0568
55 → 59 -0.24204
56 → 59 0.63490
57 → 60 0.13653
Excited State 5: 4.5853 eV 270.40nm f=0.0049
54 → 61 -0.10375
57 → 60 -0.11453
58 → 60 0.65128
58 → 62 0.18777

***Z*-1b**

Excited State 1: 2.8763 eV 431.06nm f=0.0016
59 → 63 -0.12435
61 → 63 0.68422
Excited State 2: 3.9308 eV 315.42nm f=0.1976
61 → 65 0.11300
62 → 63 0.68976
Excited State 3: 4.3136 eV 287.43nm f=0.0468
60 → 63 0.66646
62 → 64 -0.19570
Excited State 4: 4.3519 eV 284.90nm f=0.0001
59 → 63 0.67581
61 → 63 0.13662
Excited State 5: 4.5495 eV 272.53nm f=0.0045
58 → 65 -0.10369
61 → 64 0.66499
61 → 66 0.16938

***Z*-1c**

Excited State 1: 2.8161 eV 440.27nm f=0.0021
75 → 79 -0.12339
77 → 79 0.55887
78 → 79 0.38565
Excited State 2: 3.7885 eV 327.26nm f=0.2443
77 → 79 -0.38371
78 → 79 0.57659
Excited State 3: 4.1920 eV 295.76nm f=0.0284
76 → 79 0.67480
78 → 82 0.11001
Excited State 4: 4.2695 eV 290.39nm f=0.0005
75 → 79 0.66554
77 → 79 0.13458
Excited State 5: 4.5151 eV 274.60nm f=0.0338
77 → 80 -0.23595
77 → 82 -0.10138
78 → 80 0.62355
78 → 81 -0.12408

***Z*-1d**

Excited State 1: 2.8599 eV 433.53nm f=0.0014
85 → 91 0.11502

89 → 91 0.63860
90 → 91 -0.24806
Excited State 2: 3.9036 eV 317.61nm f=0.2197
89 → 91 0.24951
89 → 95 0.10134
90 → 91 0.64383
Excited State 3: 4.2777 eV 289.84nm f=0.0438
88 → 91 0.67604
90 → 93 -0.15377
Excited State 4: 4.3273 eV 286.52nm f=0.0001
85 → 91 0.51292
87 → 91 -0.44459
89 → 91 -0.12427
Excited State 5: 4.5584 eV 271.99nm f=0.0039
84 → 95 -0.10451
89 → 93 0.58587
89 → 94 0.20020
89 → 96 -0.15603
90 → 93 -0.23297

***Z*-2a**

Excited State 1: 2.8430 eV 436.10nm f=0.0062
72 → 76 0.11188
74 → 76 -0.44103
75 → 76 0.52311
Excited State 2: 3.8909 eV 318.66nm f=0.1642
74 → 76 0.50576
75 v 76 0.45891
Excited State 3: 4.2036 eV 294.95nm f=0.0036
71 → 76 -0.28015
72 → 76 0.60317
73 → 76 -0.11552
74 → 76 0.16244
Excited State 4: 4.2419 eV 292.29nm f=0.0624
72 → 76 0.11140
73 → 76 0.66984
75 → 77 0.14001
Excited State 5: 4.4844 eV 276.48nm f=0.0263
71 → 76 0.13699
72 → 78 0.10052
74 → 77 -0.29757
75 → 77 0.58199

***Z*-2b**

Excited State 1: 2.8694 eV 432.09nm f=0.0057
76 → 80 0.10692
78 → 80 0.51249
79 → 80 -0.45256
Excited State 2: 3.8554 eV 321.59nm f=0.2067
78 → 80 0.43732
79 → 80 0.52669
Excited State 3: 4.2336 eV 292.86nm f=0.0300
75 → 80 0.20246
76 → 80 0.39766
77 → 80 0.50741
78 → 80 -0.10579
Excited State 4: 4.2439 eV 292.14nm f=0.0196
75 → 80 0.20117
76 → 80 0.46575
77 → 80 -0.43404
78 → 80 -0.11049
79 → 81 -0.15314
Excited State 5: 4.4525 eV 278.46nm f=0.0319
77 → 80 -0.11956
78 → 81 -0.36536
79 → 81 0.55136

***Z*-3a**

Excited State 1: 2.7824 eV 445.60nm f=0.0109
59 → 63 -0.13130
61 → 63 0.30148
62 → 63 0.60559
Excited State 2: 3.8853 eV 319.11nm f=0.0911
58 → 63 -0.14255
59 → 63 -0.35990
60 → 63 -0.26862
61 → 63 0.39067
62 → 63 -0.33285
Excited State 3: 4.0244 eV 308.08nm f=0.0814
58 → 63 0.16551
59 → 63 0.35870
60 → 63 0.28070
61 → 63 0.47901
Excited State 4: 4.3027 eV 288.15nm f=0.0447

59 → 63 -0.37015
60 → 63 0.54502
62 → 64 -0.19056
Excited State 5: 4.4666 eV 277.58nm f=0.0792
58 → 63 0.16532
59 → 63 -0.17316
61 → 64 0.15651
62 → 64 0.59432
62 → 65 -0.11361

***Z*-3b**

Excited State 1: 2.8140 eV 440.59nm f=0.0079
63 → 67 -0.13467
65 → 67 -0.35075
66 → 67 0.57734
Excited State 2: 3.8840 eV 319.21nm f=0.1598
63 → 67 0.27516
64 → 67 0.15918
65 → 67 0.46952
66 → 67 0.38667
Excited State 3: 4.0226 eV 308.22nm f=0.0537
62 → 67 0.19804
63 → 67 0.46996
64 → 67 0.29427
65 → 67 -0.36058
Excited State 4: 4.2986 eV 288.43nm f=0.0323
63 → 67 -0.30277
64 → 67 0.56356
65 → 68 -0.10015
66 → 68 -0.23269
Excited State 5: 4.4575 eV 278.15nm f=0.0891
63 → 67 -0.15836
64 → 67 0.13076
65 → 68 -0.20904
66 → 68 0.59459
66 → 69 0.10190

***Z*-4a**

Excited State 1: 2.8107 eV 441.11nm f=0.0138
61 → 63 0.43643
62 → 63 0.53189

Excited State 2: 3.8513 eV 321.93nm f=0.1558
59 → 63 -0.11491
61 → 63 0.51014
62 → 63 -0.45147
Excited State 3: 4.1975 eV 295.38nm f=0.0613
59 → 63 -0.12128
60 → 63 0.66923
Excited State 4: 4.3044 eV 288.04nm f=0.0074
58 → 63 0.33200
59 → 63 0.55643
60 → 63 0.13450
61 → 63 0.15331
62 → 64 0.13568
Excited State 5: 4.5379 eV 273.22nm f=0.0715
58 → 63 0.14187
59 → 63 -0.18358
61 → 64 0.21987
62 → 64 0.58129
62 → 66 0.10812

***Z*-4b**

Excited State 1: 2.8388 eV 436.74nm f=0.0122
65 → 67 0.49247
66 → 67 -0.47921
Excited State 2: 3.8286 eV 323.84nm f=0.1993
65 → 67 0.46053
66 → 67 0.50575
Excited State 3: 4.2058 eV 294.79nm f=0.0521
64 → 67 0.66617
66 → 68 -0.14057
Excited State 4: 4.3209 eV 286.94nm f=0.0025
62 → 67 -0.32207
63 → 67 0.56892
65 → 67 -0.14652
66 → 68 0.15048
Excited State 5: 4.5129 eV 274.73nm f=0.0911
63 → 67 -0.16410
64 → 67 0.12147
65 → 68 -0.26021
66 → 68 0.58419

***Z*-5a**

Excited State 1: 2.7417 eV 452.22nm f=0.0020
79 → 82 0.33878
81 → 82 0.60705
Excited State 2: 3.4542 eV 358.93nm f=0.0045
76 → 82 -0.11123
77 → 82 0.13342
79 → 82 0.57904
81 → 82 -0.35376
Excited State 3: 3.9433 eV 314.42nm f=0.1605
80 → 82 0.68434
81 → 84 0.10687
Excited State 4: 4.3089 eV 287.74nm f=0.0755
78 → 82 0.65927
80 → 83 0.14047
Excited State 5: 4.4010 eV 281.72nm f=0.0145
76 → 82 -0.21915
77 → 82 0.24238
78 → 82 -0.15932
81 → 83 0.41862
81 → 84 0.35598
81 → 85 -0.12603

***Z*-5b**

Excited State 1: 2.7677 eV 447.97nm f=0.0020
83 → 86 0.33216
85 → 86 0.60825
Excited State 2: 3.4869 eV 355.57nm f=0.0053
81 → 86 0.13999
83 → 86 0.58179
85 → 86 -0.34956
Excited State 3: 3.8951 eV 318.31nm f=0.2013
84 → 86 0.68484
85 → 88 -0.11971
Excited State 4: 4.2959 eV 288.61nm f=0.0561
82 → 86 0.65591
84 → 87 -0.18384
Excited State 5: 4.3931 eV 282.23nm f=0.0255
85 → 87 0.51131
85 → 88 0.39349

***Z*-6a**

Excited State 1: 2.7777 eV 446.36nm f=0.0079
59 → 63 -0.21946
61 → 63 0.20773
62 → 63 0.62971
Excited State 2: 3.8974 eV 318.12nm f=0.0692
59 → 63 0.54568
61 → 63 -0.30277
62 → 63 0.29829
Excited State 3: 4.0115 eV 309.07nm f=0.0854
59 → 63 0.35530
61 → 63 0.58691
Excited State 4: 4.3047 eV 288.02nm f=0.0281
60 → 63 0.56059
62 → 64 0.40189
Excited State 5: 4.3683 eV 283.83nm f=0.0607
60 → 63 -0.37737
61 → 64 0.16718
62 → 64 0.52661
62 → 65 -0.16420

***Z*-6b**

Excited State 1: 2.8198 eV 439.69nm f=0.0020
63 → 67 -0.21287
66 → 67 0.65608
Excited State 2: 3.9396 eV 314.71nm f=0.1406
63 → 67 -0.37060
65 → 67 0.54827
66 → 67 -0.20427
Excited State 3: 3.9687 eV 312.41nm f=0.0562
63 → 67 0.53995
65 → 67 0.41308
66 → 67 0.12527
Excited State 4: 4.3211 eV 286.92nm f=0.0355
64 → 67 0.62623
65 → 68 -0.16313
66 → 68 0.23712
Excited State 5: 4.3483 eV 285.13nm f=0.0202
64 → 67 -0.21254
65 → 68 0.12534
66 → 68 0.63076
66 → 69 -0.13309

***Z*-7a**

Excited State 1: 2.8958 eV 428.15nm f=0.0017
66 → 71 0.11003
68 → 71 0.69046
Excited State 2: 3.4191 eV 362.62nm f=0.0001
69 → 70 0.69906
Excited State 3: 3.4597 eV 358.36nm f=0.2150
68 → 70 0.66423
69 → 71 0.22299
Excited State 4: 3.8678 eV 320.55nm f=0.0000
63 → 70 0.66061
63 → 75 -0.11387
64 → 70 -0.19404
Excited State 5: 3.9240 eV 315.97nm f=0.1062
68 → 70 -0.21579
69 → 71 0.65807

***Z*-7b**

Excited State 1: 2.9188 eV 424.78nm f=0.0018
70 → 75 0.10574
72 → 75 0.68770
Excited State 2: 3.3029 eV 375.38nm f=0.0000
73 → 74 0.69841
Excited State 3: 3.4073 eV 363.87nm f=0.2135
72 → 74 0.66136
73 → 75 0.23244
Excited State 4: 3.8673 eV 320.60nm f=0.0000
67 → 74 0.67919
67 → 79 -0.10599
68 → 74 0.11322
Excited State 5: 3.8970 eV 318.15nm f=0.1451
72 → 74 -0.22558
73 → 75 0.65490

***Z*-8a**

Excited State 1: 2.8425 eV 436.18nm f=0.0050
73 → 78 0.22375
75 → 78 0.21359
76 → 77 0.19192

76 → 78 0.59308
Excited State 2: 3.5932 eV 345.05nm f=0.4247
75 → 78 -0.29037
76 → 77 0.62416
Excited State 3: 3.7563 eV 330.07nm f=0.0294
75 → 77 0.67498
75 → 78 -0.17499
Excited State 4: 3.9968 eV 310.21nm f=0.0994
73 → 77 0.12339
75 → 77 0.15698
75 → 78 0.54285
76 → 77 0.20605
76 → 78 -0.31369
Excited State 5: 4.1186 eV 301.03nm f=0.0123
69 → 78 0.14963
73 → 77 0.19778
73 → 78 0.60126
75 → 78 -0.16921
76 → 78 -0.16549

***Z*-8b**

Excited State 1: 2.8691 eV 432.13nm f=0.0031
77 → 82 0.21925
79 → 82 0.39049
80 → 81 0.10361
80 → 82 0.52286
Excited State 2: 3.5462 eV 349.63nm f=0.4111
79 → 81 0.16344
79 → 82 -0.28362
80 → 81 0.60879
Excited State 3: 3.6344 eV 341.14nm f=0.0291
79 → 81 0.64179
79 → 82 -0.11332
80 → 81 -0.24136
Excited State 4: 3.9682 eV 312.45nm f=0.1368
77 → 81 0.11735
79 → 81 0.20589
79 → 82 0.45982
80 → 81 0.19958
80 → 82 -0.41701
Excited State 5: 4.1554 eV 298.37nm f=0.0057
73 → 82 -0.15229
77 → 81 0.11774

77 → 82 0.63019
79 → 82 -0.16730
80 → 82 -0.15161

***Z*-9a**

Excited State 1: 2.8644 eV 432.85nm f=0.0132
74 → 79 -0.14006
77 →79 0.55456
78 → 79 0.40523
Excited State 2: 3.7453 eV 331.04nm f=0.1495
77 → 79 -0.39486
78 → 79 0.56665
Excited State 3: 4.0477 eV 306.31nm f=0.0780
76 → 79 0.69247
Excited State 4: 4.3290 eV 286.41nm f=0.0056
74 → 79 0.66839
77 → 79 0.14955
Excited State 5: 4.4102 eV 281.13nm f=0.0020
75 → 79 0.69790

***Z*-9b**

Excited State 1: 2.9225 eV 424.25nm f=0.0026
78 → 83 -0.13592
81 → 83 0.67077
82 → 83 0.14722
Excited State 2: 3.7589 eV 329.85nm f=0.2054
81 → 83 -0.14307
82 → 83 0.67786
Excited State 3: 4.0944 eV 302.81nm f=0.0742
80 → 83 0.68930
82 → 85 -0.11164
Excited State 4: 4.3516 eV 284.91nm f=0.0007
78 → 83 0.67754
81 → 83 0.14004
Excited State 5: 4.4969 eV 275.71nm f=0.0014
79 → 83 0.70345

***Z*-10a**

Excited State 1: 2.8093 eV 441.33nm f=0.0023

72 → 76 0.30259
74 → 76 0.59452
75 → 76 -0.16777
Excited State 2: 3.4267 eV 361.82nm f=0.0126
74 → 76 0.14949
75 → 76 0.68195
Excited State 3: 3.7885 eV 327.26nm f=0.0037
70 → 76 0.18424
72 → 76 0.57541
73 → 76 0.19393
74 → 76 -0.29158
Excited State 4: 3.9120 eV 316.93nm f=0.1547
72 → 76 -0.10702
73 → 76 0.65044
74 → 76 0.17886
74 → 78 0.11134
Excited State 5: 4.2458 eV 292.02nm f=0.0678
71 → 76 0.67567

***Z*-10b**

Excited State 1: 2.8347 eV 437.37nm f=0.0023
76 → 80 0.28594
77 → 80 -0.16479
78 → 80 0.59210
79 → 80 -0.13557
Excited State 2: 3.4711 eV 357.19nm f=0.0174
77 → 80 -0.14690
79 → 80 0.68230
Excited State 3: 3.8279 eV 323.90nm f=0.0032
74 → 80 0.18297
76 → 80 0.58402
77 → 80 0.21254
78 → 80 -0.25516
Excited State 4: 3.8751 eV 319.95nm f=0.1923
77 → 80 0.61843
78 → 80 0.25809
78 → 82 0.12205
79 → 80 0.10427
Excited State 5: 4.2393 eV 292.46nm f=0.0521
75 -> 80 0.66285

***Z*-11a**

Excited State 1: 2.9111 eV 425.91nm f=0.0017
89 → 91 0.69341
Excited State 2: 3.8465 eV 322.33nm f=0.1523
89 → 93 0.14017
90 → 91 0.68265
Excited State 3: 4.0315 eV 307.54nm f=0.0081
89 → 92 0.69841
Excited State 4: 4.1263 eV 300.48nm f=0.0000
88 → 91 -0.46538
90 → 92 0.51590
Excited State 5: 4.2090 eV 294.57nm f=0.1523
88 → 91 0.51402
90 → 92 0.46739

***Z*-11b**

Excited State 1: 2.9358 eV 422.32nm f=0.0017
93 → 95 0.69194
Excited State 2: 3.8083 eV 325.57nm f=0.1844
93 → 97 0.15423
94 → 95 0.67732
Excited State 3: 3.9944 eV 310.39nm f=0.0077
93 → 96 0.69886
Excited State 4: 4.0497 eV 306.16nm f=0.0376
92 → 95 -0.20542
94 → 96 0.66406
Excited State 5: 4.1909 eV 295.84nm f=0.1191
92 → 95 0.65740
94 → 96 0.20585
94 → 98 -0.12241

***Z*-12a**

Excited State 1: 2.7446 eV 451.74nm f=0.0103
71 → 75 -0.13125
73 → 75 -0.29697
74 → 75 0.61709
Excited State 2: 3.9337 eV 315.19nm f=0.1475
71 → 75 0.12576
73 → 75 0.60242
74 → 75 0.32018
Excited State 3: 4.2278 eV 293.26nm f=0.0039

71 → 75 0.63135
72 → 75 -0.20238
73 → 75 -0.17218
Excited State 4: 4.3975 eV 281.94nm f=0.0113
71 → 75 0.16430
72 → 75 0.59056
74 → 76 0.31341
Excited State 5: 4.5798 eV 270.72nm f=0.0498
71 → 75 -0.12669
72 → 75 -0.25650
73 → 76 -0.21133
74 → 76 0.55179
74 → 77 0.14024
74 → 78 -0.12106

***Z*-12b**

Excited State 1: 2.7920 eV 444.07nm f=0.0020
75 → 79 0.12780
77 → 79 0.21609
78 → 79 0.64951
Excited State 2: 3.9223 eV 316.10nm f=0.1909
77 → 79 0.65475
78 → 79 -0.22398
Excited State 3: 4.2543 eV 291.43nm f=0.0004
75 → 79 0.67539
78 → 79 -0.12295
Excited State 4: 4.4377 eV 279.39nm f=0.0143
76 → 79 0.64496
77 → 80 0.17685
77 → 84 0.10740
78 → 80 -0.15990
Excited State 5: 4.5548 eV 272.20nm f=0.0077
77 → 80 0.20537
78 → 80 0.63585
78 → 82 -0.11648

***Z*-12c**

Excited State 1: 2.7089 eV 457.69nm f=0.0239
91 → 95 0.12156
93 → 95 0.35374
94 → 95 0.58315

Excited State 2: 3.7706 eV 328.82nm f=0.1893
91 → 95 0.12177
93 → 95 0.56491
94 → 95 -0.38332
Excited State 3: 4.2200 eV 293.80nm f=0.0108
91 → 95 0.47294
92 → 95 -0.45891
93 → 95 -0.16434
Excited State 4: 4.2735 eV 290.12nm f=0.0105
91 → 95 -0.36984
92 → 95 -0.34287
94 → 96 0.38608
94 → 98 0.23709
Excited State 5: 4.4598 eV 278.01nm f=0.0850
91 → 95 0.21935
92 → 95 0.30857
94 → 96 0.55712
94 → 98 -0.14362

***Z*-12d**

Excited State 1: 2.7594 eV 449.32nm f=0.0087
101 →107 0.12739
105 →107 0.34526
106 →107 0.59155
Excited State 2: 3.8659 eV 320.71nm f=0.1960
105 →107 0.58424
106 →107 -0.36374
Excited State 3: 4.2373 eV 292.60nm f=0.0023
101 →107 0.57897
102 →107 0.28076
104 →107 -0.19528
105 →107 -0.13755
Excited State 4: 4.3732 eV 283.51nm f=0.0070
101 →107 0.14956
104 →107 0.59987
106 →108 -0.14266
106 →109 0.26094
Excited State 5: 4.5462 eV 272.72nm f=0.0380
102 →107 -0.13759
104 →107 -0.22673
105 →108 -0.11694
105 →109 0.22616
106 →108 -0.25465

106 →109 0.49427
106 →111 -0.12159

7.3.2. Transitions in Toluene

***E*-1a**

Excited State 1: 2.8208 eV 439.53nm f=0.0000
57 → 59 0.70052
Excited State 2: 3.3867 eV 366.09nm f=0.9261
58 → 59 0.70157
Excited State 3: 4.0264 eV 307.92nm f=0.0126
56 → 59 0.68370
58 → 60 0.15004
Excited State 4: 4.3863 eV 282.66nm f=0.0082
54 → 59 0.57915
55 → 59 0.30756
55 → 61 0.10827
58 → 61 0.22514
Excited State 5: 4.5319 eV 273.58nm f=0.1066
54 → 59 -0.28677
55 → 59 0.60935
56 → 60 0.14439

***E*-1b**

Excited State 1: 2.8286 eV 438.33nm f=0.0000
61 → 63 0.70012
Excited State 2: 3.3204 eV 373.40nm f=0.9915
62 → 63 0.70220
Excited State 3: 4.0193 eV 308.48nm f=0.0083
60 → 63 0.67296
62 → 64 0.19286
Excited State 4: 4.3935 eV 282.20nm f=0.0025
58 → 63 0.56330
59 → 63 0.30099
59 → 65 0.10885
62 → 64 -0.10205
62 → 65 0.24845
Excited State 5: 4.4723 eV 277.23nm f=0.1158
60 → 63 -0.18602
62 → 64 0.65902

***E*-1c**

Excited State 1: 2.6918 eV 460.60nm f=0.0001
77 → 79 0.69337
Excited State 2: 3.0230 eV 410.13nm f=0.8524
78 → 79 0.70519
Excited State 3: 3.7645 eV 329.35nm f=0.0334
76 → 79 0.68722
Excited State 4: 4.2405 eV 292.38nm f=0.0182
74 → 79 0.59641
75 → 79 0.30759
78 → 83 -0.17521
Excited State 5: 4.3310 eV 286.27nm f=0.1491
74 → 79 -0.28039
75 → 79 0.55394
78 → 80 0.27953

***E*-1d**

Excited State 1: 2.8179 eV 439.99nm f=0.0000
89 → 91 0.70023
Excited State 2: 3.3244 eV 372.95nm f=1.0719
90 → 91 0.70159
Excited State 3: 3.9922 eV 310.56nm f=0.0113
88 → 91 0.68059
90 → 92 -0.16350
Excited State 4: 4.3871 eV 282.61nm f=0.0048
84 → 91 0.58073
85 → 91 0.28829
85 → 95 0.10951
90 → 95 0.23706
Excited State 5: 4.5190 eV 274.36nm f=0.1482
84 → 91 0.17948
85 → 91 -0.28510
88 → 91 0.16206
90 → 92 0.57074

***E*-2a**

Excited State 1: 2.7282 eV 454.46nm f=0.0000
74 → 76 0.69975
Excited State 2: 3.2684 eV 379.35nm f=0.8587
75 → 76 0.70094
Excited State 3: 3.8795 eV 319.59nm f=0.0158

73 → 76 0.69105
75 → 77 0.10922
Excited State 4: 4.0220 eV 308.27nm f=0.0258
71 → 76 -0.10201
72 → 76 0.67505
75 → 78 0.13626
Excited State 5: 4.4445 eV 278.96nm f=0.0983
71 → 76 0.66960
72 → 76 0.11315
73 → 77 -0.12135

***E*-2b**

Excited State 1: 2.7370 eV 452.99nm f=0.0001
78 → 80 0.69950
Excited State 2: 3.2066 eV 386.65nm f=0.9338
79 → 80 0.70172
Excited State 3: 3.8819 eV 319.39nm f=0.0135
77 → 80 0.68726
79 → 81 0.13330
Excited State 4: 4.0385 eV 307.01nm f=0.0218
76 → 80 0.67144
79 → 82 0.15327
Excited State 5: 4.4592 eV 278.04nm f=0.0948
75 → 80 0.65240
76 → 80 -0.11950
77 → 81 0.13340
79 → 81 -0.12061

***E*-3a**

Excited State 1: 2.7669 eV 448.10nm f=0.0000
61 → 63 0.70027
Excited State 2: 3.2400 eV 382.67nm f=0.8886
62 → 63 0.69957
Excited State 3: 3.9573 eV 313.30nm f=0.0393
59 → 63 -0.15386
60 → 63 0.66728
62 → 65 -0.10192
Excited State 4: 3.9883 eV 310.87nm f=0.0097
59 → 63 0.66663
60 → 63 0.15082
62 → 64 -0.15220

Excited State 5: 4.5140 eV 274.66nm f=0.0893
58 → 63 0.51646
59 → 63 -0.10714
59 → 64 -0.11187
60 → 63 -0.10805
62 → 64 -0.42723

***E*-3b**

Excited State 1: 2.7736 eV 447.01nm f=0.0000
65 → 67 0.69993
Excited State 2: 3.1818 eV 389.67nm f=0.9562
66 → 67 0.70070
Excited State 3: 3.9598 eV 313.11nm f=0.0351
63 → 67 -0.31959
64 → 67 0.60037
Excited State 4: 3.9838 eV 311.22nm f=0.0039
63 → 67 0.60217
64 → 67 0.30658
66 → 68 0.17361
Excited State 5: 4.3989 eV 281.85nm f=0.1033
63 → 67 -0.10175
64 → 67 -0.17208
66 → 68 0.66281

***E*-4a**

Excited State 1: 2.7897 eV 444.43nm f=0.0000
61 → 63 0.70061
Excited State 2: 3.3050 eV 375.14nm f=0.9160
62 → 63 0.70177
Excited State 3: 3.9192 eV 316.35nm f=0.0145
60 → 63 0.68949
62 → 64 0.12062
Excited State 4: 4.2405 eV 292.38nm f=0.0226
58 → 63 -0.23323
59 → 63 0.63374
62 → 65 0.16066
Excited State 5: 4.4939 eV 275.89nm f=0.1216
58 → 63 0.63836
59 → 63 0.23926
60 → 64 -0.13542

***E*-4b**

Excited State 1: 2.7969 eV 443.29nm f=0.0000
65 → 67 0.70031
Excited State 2: 3.2415 eV 382.49nm f=0.9857
66 → 67 0.70242
Excited State 3: 3.9196 eV 316.32nm f=0.0115
64 → 67 0.68410
66 → 68 0.14908
Excited State 4: 4.2531 eV 291.51nm f=0.0175
62 → 67 -0.22414
63 → 67 0.63156
66 → 69 0.17545
Excited State 5: 4.4840 eV 276.50nm f=0.1176
62 → 67 0.16564
63 → 67 0.10438
64 → 67 -0.15471
66 → 68 0.64569

***E*-5a**

Excited State 1: 2.7844 eV 445.29nm f=0.0896
79 → 82 0.55218
80 → 82 0.29405
81 → 82 -0.29880
Excited State 2: 3.0103 eV 411.87nm f=0.3384
79 → 82 0.18850
80 → 82 0.26642
81 → 82 0.62154
Excited State 3: 3.6476 eV 339.91nm f=0.4200
79 → 82 -0.36859
80 → 82 0.57572
81 → 82 -0.13190
Excited State 4: 4.0635 eV 305.12nm f=0.0081
78 → 82 0.66093
81 → 83 0.21480
Excited State 5: 4.3726 eV 283.55nm f=0.0563
77 → 82 0.10738
78 → 82 -0.22171
81 → 83 0.64441

***E*-5b**

Excited State 1: 2.7868 eV 444.89nm f=0.1209
83 → 86 0.55608
84 → 86 -0.24612
85 → 86 0.33310
Excited State 2: 3.0058 eV 412.48nm f=0.3862
83 → 86 -0.23214
84 → 86 0.27449
85 → 86 0.60263
Excited State 3: 3.6119 eV 343.26nm f=0.4076
83 → 86 0.33686
84 → 86 0.59432
85 → 86 -0.13824
Excited State 4: 4.0455 eV 306.48nm f=0.0026
82 → 86 0.62533
85 → 87 -0.30104
Excited State 5: 4.2947 eV 288.69nm f=0.0701
82 → 86 0.30782
85 → 87 0.61790

***E*-6a**

Excited State 1: 2.9003 eV 427.48nm f=0.0000
61 → 63 0.70044
Excited State 2: 3.3211 eV 373.33nm f=1.0164
62 → 63 0.70213
Excited State 3: 4.0990 eV 302.47nm f=0.0062
60 → 63 0.66236
62 → 64 0.22408
Excited State 4: 4.3823 eV 282.92nm f=0.0267
59 → 63 0.67516
60 → 64 0.10423
Excited State 5: 4.4478 eV 278.76nm f=0.0497
58 → 63 0.39452
59 → 65 0.10403
60 → 63 0.12883
62 → 64 -0.37801
62 → 65 0.40089

***E*-6b**

Excited State 1: 2.9076 eV 426.42nm f=0.0000
65 → 67 0.69993

Excited State 2: 3.2620 eV 380.09nm f=1.0710
66 → 67 0.70268
Excited State 3: 4.0776 eV 304.06nm f=0.0014
64 → 67 0.62481
66 → 68 0.30731
Excited State 4: 4.3612 eV 284.29nm f=0.0962
63 → 67 -0.25342
64 → 67 -0.31230
66 → 68 0.56224
Excited State 5: 4.3922 eV 282.28nm f=0.0318
62 → 67 -0.14723
63 → 67 0.58509
66 → 68 0.22623
66 → 69 -0.23085

***E*-7a**

Excited State 1: 2.6037 eV 476.19nm f=0.0000
68 → 70 0.65118
68 → 71 -0.26566
Excited State 2: 2.9048 eV 426.82nm f=0.9430
69 → 70 0.70350
Excited State 3: 3.5200 eV 352.23nm f=0.0107
67 → 70 0.69011
67 → 71 -0.12004
Excited State 4: 3.8488 eV 322.14nm f=0.0000
64 → 70 0.61635
64 → 71 0.31729
Excited State 5: 4.0077 eV 309.36nm f=0.1153
65 → 70 0.22554
69 → 71 0.65324

***E*-7b**

Excited State 1: 2.6102 eV 475.00nm f=0.0000
72 → 74 0.65145
72 → 75 -0.26381
Excited State 2: 2.8371 eV 437.01nm f=1.0203
73 → 74 0.70390
Excited State 3: 3.5253 eV 351.70nm f=0.0082
71 → 74 0.68888
71 → 75 -0.11991
Excited State 4: 3.8509 eV 321.96nm f=0.0000

68 → 74 0.61542
68 → 75 0.31409
72 → 75 -0.10911
Excited State 5: 3.9359 eV 315.01nm f=0.1413
69 → 74 0.10592
73 → 75 0.68240

***E*-8a**

Excited State 1: 2.6713 eV 464.13nm f=0.0000
75 → 77 0.66724
75 → 78 0.21745
Excited State 2: 2.9401 eV 421.69nm f=1.4206
76 → 77 0.70308
Excited State 3: 3.6952 eV 335.53nm f=0.0114
74 → 77 0.68844
74 → 78 0.10394
Excited State 4: 3.9549 eV 313.49nm f=0.1895
73 → 77 0.66617
76 → 78 0.19915
Excited State 5: 4.1291 eV 300.27nm f=0.0207
72 → 77 0.63622
73 → 80 0.10246
76 → 78 -0.17071
76 → 80 0.21592

***E*-8b**

Excited State 1: 2.5953 eV 477.74nm f=0.0000
79 → 81 0.67167
79 → 82 0.20382
Excited State 2: 2.7175 eV 456.24nm f=1.2821
80 → 81 0.70436
Excited State 3: 3.5497 eV 349.28nm f=0.0732
78 → 81 0.69184
Excited State 4: 3.8301 eV 323.71nm f=0.1395
77 → 81 0.60482
80 → 82 0.34561
Excited State 5: 3.9865 eV 311.01nm f=0.1475
76 → 81 -0.12312
77 → 81 -0.33829
80 → 82 0.59390

***E*-9a**

Excited State 1: 2.8205 eV 439.58nm f=0.0429
74 → 79 0.10852
77 → 79 0.65436
78 → 79 -0.22268
Excited State 2: 3.3869 eV 366.07nm f=0.8431
77 → 79 0.21788
78 → 79 0.66518
Excited State 3: 3.8519 eV 321.88nm f=0.0186
76 → 79 0.69167
Excited State 4: 4.2207 eV 293.75nm f=0.0183
75 → 79 0.67884
78 → 82 -0.15737
Excited State 5: 4.5095 eV 274.94nm f=0.1891
74 → 79 0.67115
76 → 80 -0.14473
77 → 79 -0.10127

***E*-9b**

Excited State 1: 2.8316 eV 437.86nm f=0.0572
78 → 83 0.10237
81 → 83 0.65123
82 → 83 -0.23285
Excited State 2: 3.3365 eV 371.60nm f=0.9121
81 → 83 0.22930
82 → 83 0.66243
Excited State 3: 3.8660 eV 320.70nm f=0.0167
80 → 83 0.69008
82 → 84 -0.11453
Excited State 4: 4.2423 eV 292.26nm f=0.0162
79 → 83 0.67420
82 → 86 0.17355
Excited State 5: 4.5282 eV 273.81nm f=0.1682
78 → 83 0.66876
80 → 84 -0.15827

***E*-10a**

Excited State 1: 2.7565 eV 449.79nm f=0.0092
72 → 76 0.44760

73 → 76 0.37401
74 → 76 0.38219
Excited State 2: 3.2163 eV 385.49nm f=0.5218
72 → 76 -0.12610
74 → 76 0.14863
75 → 76 0.67332
Excited State 3: 3.3389 eV 371.33nm f=0.2323
72 → 76 -0.20853
73 → 76 -0.30717
74 → 76 0.56823
75 → 76 -0.18418
Excited State 4: 3.7727 eV 328.63nm f=0.1127
72 → 76 -0.47000
73 → 76 0.50176
Excited State 5: 3.9419 eV 314.53nm f=0.0132
71 → 76 0.68868
75 → 77 0.11831

***E*-10b**

Excited State 1: 2.6529 eV 467.36nm f=0.0186
76 → 80 0.51999
77 → 80 0.15096
78 → 80 0.41327
79 → 80 0.11812
Excited State 2: 3.0042 eV 412.70nm f=0.7153
78 → 80 -0.10871
79 → 80 0.69201
Excited State 3: 3.2327 eV 383.53nm f=0.0058
76 → 80 -0.37977
77 → 80 -0.18026
78 → 80 0.55969
Excited State 4: 3.6455 eV 340.10nm f=0.0510
76 → 80 -0.23516
77 → 80 0.65300
Excited State 5: 3.8061 eV 325.75nm f=0.0564
75 → 80 0.68218
76 → 80 -0.11185
79 → 81 0.10594

***E*-11a**

Excited State 1: 2.7993 eV 442.91nm f=0.0000

89 → 91 0.69879
Excited State 2: 3.2910 eV 376.74nm f=0.8850
90 → 91 0.70202
Excited State 3: 3.8032 eV 326.00nm f=0.0147
88 → 91 0.69363
Excited State 4: 4.2247 eV 293.47nm f=0.0245
86 → 91 0.20293
90 → 92 0.66410
Excited State 5: 4.4970 eV 275.70nm f=0.0000
89 → 92 0.70595

***E*-11b**

Excited State 1: 2.8080 eV 441.55nm f=0.0000
93 → 95 0.69865
Excited State 2: 3.2283 eV 384.06nm f=0.9695
94 → 95 0.70268
Excited State 3: 3.8112 eV 325.32nm f=0.0120
92 → 95 0.69142
94 → 97 0.10583
Excited State 4: 4.1469 eV 298.98nm f=0.0347
90 → 95 0.17581
94 → 96 0.67498
Excited State 5: 4.4723 eV 277.23nm f=0.0000
93 → 96 0.70592

***E*-12a**

Excited State 1: 2.8096 eV 441.29nm f=0.0000
73 → 75 0.70098
Excited State 2: 3.4387 eV 360.55nm f=0.8768
74 → 75 0.70213
Excited State 3: 4.2473 eV 291.91nm f=0.0235
72 → 75 0.65647
74 → 76 0.22320
Excited State 4: 4.3122 eV 287.52nm f=0.0121
70 → 75 -0.31458
71 → 75 0.59353
74 → 78 -0.16933
Excited State 5: 4.5039 eV 275.28nm f=0.1326
70 → 75 0.57895
71 → 75 0.30390
72 → 75 -0.15010

72 → 76 -0.10504
74 → 76 0.14055

***E*-12b**

Excited State 1: 2.8134 eV 440.69nm f=0.0000
77 → 79 0.70078
Excited State 2: 3.3670 eV 368.24nm f=0.9242
78 → 79 0.70289
Excited State 3: 4.2359 eV 292.70nm f=0.0138
75 → 79 0.10805
76 → 79 0.62694
78 → 80 0.29145
Excited State 4: 4.3334 eV 286.11nm f=0.0088
74 → 79 -0.37897
75 → 79 0.54515
78 → 82 -0.18532
Excited State 5: 4.5046 eV 275.24nm f=0.1635
74 → 79 0.48669
75 → 79 0.30720
76 → 79 -0.23377
76 → 80 -0.11556
78 → 80 0.28084

***E*-12c**

Excited State 1: 2.7935 eV 443.83nm f=0.0001
93 → 95 0.69993
Excited State 2: 3.3497 eV 370.14nm f=0.9927
94 → 95 0.70273
Excited State 3: 4.1879 eV 296.05nm f=0.0168
92 → 95 0.63458
94 → 96 -0.25035
Excited State 4: 4.3060 eV 287.93nm f=0.0070
90 → 95 -0.42489
91 → 95 0.51506
94 → 99 -0.16804
Excited State 5: 4.4354 eV 279.53nm f=0.2706
90 → 95 -0.31955
91 → 95 -0.19106
92 → 95 0.24319
92 → 96 -0.10005
94 → 96 0.50607

***E*-12d**

Excited State 1: 2.6945 eV 460.14nm f=0.0000
105 →107 0.69494
Excited State 2: 3.1417 eV 394.64nm f=0.8215
106 →107 0.70514
Excited State 3: 4.0146 eV 308.84nm f=0.0213
103 →107 0.11484
104 →107 0.67291
106 →108 0.13056
Excited State 4: 4.1798 eV 296.63nm f=0.0149
100 →107 0.56736
101 →107 0.37840
106 →111 -0.13896
Excited State 5: 4.2150 eV 294.15nm f=0.0001
102 →107 0.69527

***Z*-1a**

Excited State 1: 2.9067 eV 426.54nm f=0.0025
55 → 59 -0.14919
57 → 59 0.67308
58 → 59 -0.11836
Excited State 2: 3.8679 eV 320.55nm f=0.2410
57 → 59 0.11856
58 → 59 0.68512
Excited State 3: 4.2475 eV 291.90nm f=0.0973
56 → 59 0.69067
58 → 60 -0.11390
Excited State 4: 4.2926 eV 288.83nm f=0.0006
55 → 59 0.67716
57 → 59 0.15285
Excited State 5: 4.7029 eV 263.63nm f=0.0100
54 → 61 -0.12337
57 → 60 0.62993
57 → 62 0.22087
58 → 60 -0.14609

***Z*-1b**

Excited State 1: 2.9300 eV 423.15nm f=0.0026

59 → 63 -0.14408
61 → 63 0.68253
Excited State 2: 3.8174 eV 324.79nm f=0.3011
62 → 63 0.69552
Excited State 3: 4.2396 eV 292.44nm f=0.0757
60 → 63 0.68286
62 → 64 -0.15002
Excited State 4: 4.3193 eV 287.05nm f=0.0004
59 → 63 0.67660
61 → 63 0.15149
Excited State 5: 4.6733 eV 265.31nm f=0.0083
58 → 65 -0.11812
61 → 64 0.65234
61 → 66 0.20797

***Z*-1c**

Excited State 1: 2.8627 eV 433.10nm f=0.0034
75 → 79 -0.14217
77 → 79 0.64118
78 → 79 -0.22377
Excited State 2: 3.6926 eV 335.76nm f=0.3515
77 → 79 0.22066
78 → 79 0.66078
Excited State 3: 4.1299 eV 300.21nm f=0.0410
76 → 79 0.68580
Excited State 4: 4.2317 eV 292.99nm f=0.0011
75 → 79 0.66694
77 → 79 0.15411
Excited State 5: 4.6246 eV 268.10nm f=0.0923
78 → 80 0.64328
78 → 81 -0.20270

***Z*-1d**

Excited State 1: 2.9035 eV 427.01nm f=0.0023
85 → 91 0.14862
89 → 91 0.68206
Excited State 2: 3.8047 eV 325.87nm f=0.3133
90 → 91 0.69492
Excited State 3: 4.2064 eV 294.75nm f=0.0737
88 → 91 0.68860
90 → 92 0.12687

Excited State 4: 4.2824 eV 289.52nm f=0.0003
85 → 91 0.63811
86 → 91 -0.23186
89 → 91 -0.14563
Excited State 5: 4.6713 eV 265.42nm f=0.0038
86 → 91 -0.35268
89 → 92 0.56131
89 → 96 -0.15125

***Z*-2a**

Excited State 1: 2.8926 eV 428.63nm f=0.0112
71 → 76 -0.10961
72 → 76 0.11981
74 → 76 0.52012
75 → 76 0.44016
Excited State 2: 3.7847 eV 327.60nm f=0.2462
74 → 76 -0.42532
75 → 76 0.54179
Excited State 3: 4.1522 eV 298.60nm f=0.0892
73 → 76 0.68328
Excited State 4: 4.1912 eV 295.82nm f=0.0087
71 → 76 -0.30270
72 → 76 0.59185
73 → 76 0.11486
74 → 76 -0.17458
Excited State 5: 4.5572 eV 272.06nm f=0.0271
71 → 76 0.41492
72 → 76 0.20143
74 → 77 0.26009
75 → 77 0.41528

***Z*-2b**

Excited State 1: 2.9217 eV 424.36nm f=0.0107
75 → 80 -0.10489
76 → 80 0.11525
78 → 80 0.57283
79 → 80 0.36907
Excited State 2: 3.7463 eV 330.95nm f=0.3064
78 → 80 -0.35591
79 → 80 0.59151
Excited State 3: 4.1555 eV 298.36nm f=0.0754

77 → 80 0.68440
79 → 81 0.10800
Excited State 4: 4.2242 eV 293.51nm f=0.0042
75 → 80 -0.31288
76 → 80 0.59611
78 → 80 -0.16820
Excited State 5: 4.5393 eV 273.13nm f=0.0694
75 → 80 0.15744
78 → 81 0.33656
79 → 81 0.56205

***Z*-3a**

Excited State 1: 2.8170 eV 440.13nm f=0.0177
58 → 63 -0.10365
59 → 63 -0.15475
60 → 63 -0.10043
61 → 63 -0.34556
62 → 63 0.57088
Excited State 2: 3.7921 eV 326.96nm f=0.1556
58 → 63 0.14734
59 → 63 0.32680
60 → 63 0.23570
61 → 63 0.38430
62 → 63 0.39523
Excited State 3: 3.9311 eV 315.39nm f=0.0993
58 → 63 -0.17934
59 → 63 -0.36486
60 → 63 -0.31089
61 → 63 0.46300
Excited State 4: 4.2210 eV 293.73nm f=0.0775
59 → 63 -0.39763
60 → 63 0.55603
62 → 64 -0.11240
Excited State 5: 4.4997 eV 275.54nm f=0.0260
58 → 63 0.51875
59 → 63 -0.23214
62 → 64 0.35601
62 → 65 0.11607

***Z*-3b**

Excited State 1: 2.8538 eV 434.45nm f=0.0131

63 → 67 0.15987
65 → 67 -0.42321
66 → 67 0.51577
Excited State 2: 3.7803 eV 327.97nm f=0.2571
63 → 67 -0.23394
64 → 67 -0.12881
65 → 67 0.42899
66 → 67 0.47012
Excited State 3: 3.9368 eV 314.93nm f=0.0579
62 → 67 0.21427
63 → 67 0.46704
64 → 67 0.31958
65 → 67 0.34521
Excited State 4: 4.2243 eV 293.51nm f=0.0621
63 → 67 -0.34087
64 → 67 0.58222
66 → 68 0.14584
Excited State 5: 4.5209 eV 274.25nm f=0.1025
62 → 67 -0.35402
63 → 67 0.20454
65 → 68 -0.15348
66 → 68 0.50906
66 → 69 0.11224

***Z*-4a**

Excited State 1: 2.8541 eV 434.41nm f=0.0230
58 → 63 -0.10985
61 → 63 0.49049
62 → 63 -0.47961
Excited State 2: 3.7506 eV 330.57nm f=0.2306
59 → 63 -0.10385
61 → 63 0.45873
62 → 63 0.51016
Excited State 3: 4.1149 eV 301.31nm f=0.0875
60 → 63 0.68677
Excited State 4: 4.2658 eV 290.65nm f=0.0157
58 → 63 0.38029
59 → 63 0.53972
61 → 63 0.17791
Excited State 5: 4.5777 eV 270.84nm f=0.0478
58 → 63 0.38976
59 → 63 -0.32249
61 → 64 -0.15906

62 → 64 0.42324

***Z*-4b**

Excited State 1: 2.8862 eV 429.57nm f=0.0210
62 → 67 -0.10286
65 → 67 0.54230
66 → 67 -0.41936
Excited State 2: 3.7222 eV 333.10nm f=0.2923
65 → 67 0.40127
66 → 67 0.55992
Excited State 3: 4.1259 eV 300.50nm f=0.0759
64 → 67 0.68376
66 → 68 0.10675
Excited State 4: 4.2854 eV 289.32nm f=0.0097
62 → 67 -0.37403
63 → 67 0.54915
65 → 67 -0.16738
Excited State 5: 4.5684 eV 271.40nm f=0.1590
62 → 67 0.16778
63 → 67 0.18812
65 → 68 -0.19642
66 → 68 0.59633

***Z*-5a**

Excited State 1: 2.7597 eV 449.27nm f=0.0030
79 → 82 0.33879
81 → 82 0.60718
Excited State 2: 3.4276 eV 361.72nm f=0.0068
76 → 82 -0.11598
77 → 82 0.14871
79 → 82 0.57352
81 → 82 -0.35519
Excited State 3: 3.8475 eV 322.24nm f=0.2438
80 → 82 0.69089
Excited State 4: 4.2401 eV 292.41nm f=0.1042
78 → 82 0.67694
80 → 83 -0.11301
Excited State 5: 4.3777 eV 283.22nm f=0.0009
76 → 82 -0.41485
77 → 82 0.49276
78 → 82 -0.12323

79 → 82 -0.19123

***Z*-5b**

Excited State 1: 2.7873 eV 444.82nm f=0.0031
83 → 86 0.33474
85 → 86 0.60761
Excited State 2: 3.4578 eV 358.57nm f=0.0086
81 → 86 0.15542
83 → 86 0.57458
85 → 86 -0.35310
Excited State 3: 3.7971 eV 326.52nm f=0.3005
84 → 86 0.69113
85 → 88 -0.10096
Excited State 4: 4.2321 eV 292.96nm f=0.0817
82 → 86 0.67133
84 → 87 -0.14815
Excited State 5: 4.4042 eV 281.52nm f=0.0139
80 → 86 -0.30218
81 → 86 0.44134
82 → 86 -0.10919
83 → 86 -0.13688
85 → 87 -0.28217
85 → 88 -0.27009

***Z*-6a**

Excited State 1: 2.8157 eV 440.33nm f=0.0130
59 → 63 -0.24598
61 → 63 0.24204
62 → 63 0.60887
Excited State 2: 3.8232 eV 324.30nm f=0.1626
59 → 63 0.43517
61 → 63 -0.41799
62 → 63 0.34766
Excited State 3: 3.9339 eV 315.17nm f=0.0748
59 → 63 0.47610
61 → 63 0.50147
Excited State 4: 4.2424 eV 292.25nm f=0.0853
60 → 63 0.68076
62 → 64 0.12987
Excited State 5: 4.4376 eV 279.39nm f=0.0655
60 → 63 -0.10492

61 → 64 0.13093
62 → 64 0.63460
62 → 65 -0.19668

***Z*-6b**

Excited State 1: 2.8627 eV 433.10nm f=0.0031
63 → 67 -0.24298
65 → 67 0.16402
66 → 67 0.63354
Excited State 2: 3.8315 eV 323.59nm f=0.2932
63 → 67 -0.12066
65 → 67 0.65121
66 → 67 -0.21718
Excited State 3: 3.9169 eV 316.54nm f=0.0079
63 → 67 0.63578
65 → 67 0.18665
66 → 67 0.20337
Excited State 4: 4.2519 eV 291.60nm f=0.0707
64 → 67 0.67978
65 → 68 -0.13830
Excited State 5: 4.4476 eV 278.77nm f=0.0308
62 → 70 -0.10722
65 → 68 0.12497
66 → 68 0.64889
66 → 69 -0.18958

***Z*-7a**

Excited State 1: 2.9580 eV 419.14nm f=0.0027
66 → 71 -0.11834
68 → 71 0.68730
Excited State 2: 3.2613 eV 380.16nm f=0.0001
69 → 70 0.69795
Excited State 3: 3.3696 eV 367.95nm f=0.2987
68 → 70 0.66257
69 → 71 -0.23034
Excited State 4: 3.8264 eV 324.02nm f=0.1744
68 → 70 0.22745
69 → 71 0.65957
Excited State 5: 3.8766 eV 319.83nm f=0.0002
67 → 70 0.69755

***Z*-7b**

Excited State 1: 2.9802 eV 416.03nm f=0.0028
70 → 75 0.11295
72 → 75 0.67715
73 → 74 0.13496
Excited State 2: 3.1541 eV 393.08nm f=0.0000
72 → 75 -0.13371
73 → 74 0.68907
Excited State 3: 3.3254 eV 372.84nm f=0.3001
72 → 74 0.65787
73 → 75 0.24435
Excited State 4: 3.7941 eV 326.78nm f=0.2277
72 → 74 -0.24176
73 → 75 0.65434
Excited State 5: 3.8321 eV 323.54nm f=0.0002
71 → 74 0.70339

***Z*-8a**

Excited State 1: 2.8946 eV 428.33nm f=0.0084
73 → 78 -0.24513
75 → 77 0.11464
75 → 78 0.42519
76 → 77 0.16317
76 → 78 0.45389
Excited State 2: 3.5476 eV 349.49nm f=0.5865
75 → 77 0.17509
75 → 78 -0.32725
76 → 77 0.58747
Excited State 3: 3.7207 eV 333.22nm f=0.0573
75 → 77 0.60569
75 → 78 -0.16486
76 → 77 -0.28905
76 → 78 0.11030
Excited State 4: 3.9140 eV 316.77nm f=0.2015
75 → 77 -0.26956
75 → 78 -0.36136
76 → 77 -0.17662
76 → 78 0.49602
Excited State 5: 4.1114 eV 301.56nm f=0.0113
69 → 78 0.15131
73 → 77 0.22233

73 → 78 0.59176
75 → 78 0.21062
76 → 78 0.13550

***Z*-8b**

Excited State 1: 2.9232 eV 424.14nm f=0.0052
77 → 82 -0.24273
79 → 82 0.61650
80 → 82 0.18799
Excited State 2: 3.5078 eV 353.45nm f=0.5716
79 → 81 0.45409
79 → 82 -0.19087
80 → 81 0.40747
80 → 82 0.28474
Excited State 3: 3.6043 eV 343.99nm f=0.0556
79 → 81 -0.37857
80 → 81 0.56377
80 → 82 -0.16622
Excited State 4: 3.8839 eV 319.23nm f=0.2555
79 → 81 -0.35267
79 → 82 -0.10911
80 → 82 0.58535
Excited State 5: 4.1467 eV 299.00nm f=0.0078
73 → 82 -0.15279
77 → 81 0.13871
77 → 82 0.61926
79 → 82 0.24234

***Z*-9a**

Excited State 1: 2.9176 eV 424.95nm f=0.0238
74 → 79 -0.15130
77 → 79 0.57797
78 → 79 0.36659
Excited State 2: 3.6441 eV 340.24nm f=0.2224
77 → 79 -0.35530
78 → 79 0.59623
Excited State 3: 3.9538 eV 313.59nm f=0.1019
76 → 79 0.69802
Excited State 4: 4.3320 eV 286.21nm f=0.0094
74 → 79 0.66796
77 → 79 0.16569

Excited State 5: 4.3933 eV 282.21nm f=0.0029
75 → 79 0.69948

***Z*-9b**

Excited State 1: 2.9855 eV 415.28nm f=0.0047
78 → 83 -0.15063
81 → 83 0.67349
82 → 83 -0.12341
Excited State 2: 3.6441 eV 340.24nm f=0.3062
81 → 83 0.11921
82 → 83 0.68680
Excited State 3: 3.9998 eV 309.97nm f=0.0970
80 → 83 0.69687
Excited State 4: 4.3562 eV 284.62nm f=0.0013
78 → 83 0.67589
81 → 83 0.15402
Excited State 5: 4.4758 eV 277.01nm f=0.0016
79 → 83 0.70451

***Z*-10a**

Excited State 1: 2.8523 eV 434.69nm f=0.0038
70 → 76 0.10670
71 → 76 0.10385
72 → 76 0.28762
73 → 76 -0.15433
74 → 76 0.58124
75 → 76 -0.15691
Excited State 2: 3.4970 eV 354.54nm f=0.0310
73 → 76 -0.13178
74 → 76 0.11893
75 → 76 0.68086
Excited State 3: 3.8125 eV 325.21nm f=0.0179
70 → 76 0.17148
71 → 76 0.15641
72 → 76 0.48016
73 → 76 0.41632
74 → 76 -0.17231
Excited State 4: 3.8276 eV 323.92nm f=0.2083
70 → 76 -0.13134
72 → 76 -0.26930
73 → 76 0.51950

74 → 76 0.33331
Excited State 5: 4.1733 eV 297.09nm f=0.0948
71 → 76 0.64989
72 → 76 -0.23512

***Z*-10b**

Excited State 1: 2.8796 eV 430.57nm f=0.0040
74 → 80 0.10239
75 → 80 -0.13862
76 → 80 0.25935
77 → 80 -0.24287
78 → 80 0.57572
Excited State 2: 3.5307 eV 351.16nm f=0.0540
77 → 80 -0.19755
79 → 80 0.67267
Excited State 3: 3.7921 eV 326.95nm f=0.2518
77 → 80 0.58936
78 → 80 0.30155
79 → 80 0.19747
Excited State 4: 3.8501 eV 322.02nm f=0.0102
74 → 80 0.20773
75 → 80 -0.25254
76 → 80 0.52636
77 → 80 0.20370
78 → 80 -0.25650
Excited State 5: 4.1719 eV 297.19nm f=0.0764
75 → 80 0.60727
76 → 80 0.31719

***Z*-11a**

Excited State 1: 2.9687 eV 417.64nm f=0.0027
87 → 91 0.10552
89 → 91 0.69283
Excited State 2: 3.7599 eV 329.75nm f=0.2444
89 → 93 0.11406
90 → 91 0.69190
Excited State 3: 4.0939 eV 302.85nm f=0.0286
88 → 91 0.62318
90 → 92 0.31087
Excited State 4: 4.1283 eV 300.33nm f=0.0176
89 → 92 0.69189

Excited State 5: 4.1653 eV 297.66nm f=0.1634
88 → 91 -0.30411
90 → 92 0.62465

***Z*-11b**

Excited State 1: 2.9947 eV 414.01nm f=0.0028
91 → 95 0.10204
93 → 95 0.69183
Excited State 2: 3.7186 eV 333.42nm f=0.3004
93 → 97 0.12179
94 → 95 0.69066
Excited State 3: 4.0426 eV 306.69nm f=0.0286
92 → 95 -0.24428
94 → 96 0.65576
Excited State 4: 4.1007 eV 302.35nm f=0.0136
93 → 96 0.69845
Excited State 5: 4.1255 eV 300.53nm f=0.1593
92 → 95 0.64989
94 → 96 0.24907

***Z*-12a**

Excited State 1: 2.7986 eV 443.02nm f=0.0167
71 → 75 0.14443
73 → 75 0.35415
74 → 75 0.58271
Excited State 2: 3.8575 eV 321.41nm f=0.2202
71 → 75 0.10687
73 → 75 0.56880
74 → 75 -0.38242
Excited State 3: 4.2003 eV 295.18nm f=0.0062
70 → 75 -0.20605
71 → 75 0.59293
72 → 75 -0.21719
73 → 75 -0.18737
Excited State 4: 4.3584 eV 284.47nm f=0.0333
71 → 75 0.22070
72 → 75 0.62820
74 → 76 0.20254
Excited State 5: 4.6043 eV 269.28nm f=0.0030
70 → 75 0.64110
71 → 75 0.19111

74 → 77 0.10308

***Z*-12b**

Excited State 1: 2.8533 eV 434.52nm f=0.0031
75 → 79 0.14867
77 → 79 0.49468
78 → 79 0.46885
Excited State 2: 3.8335 eV 323.42nm f=0.2881
77 → 79 -0.47413
78 → 79 0.50979
Excited State 3: 4.2254 eV 293.43nm f=0.0007
75 → 79 0.67354
77 → 79 -0.13074
Excited State 4: 4.3878 eV 282.57nm f=0.0312
76 → 79 0.66640
78 → 80 -0.15983
Excited State 5: 4.6728 eV 265.33nm f=0.0156
74 → 79 -0.10245
74 → 81 0.10350
77 → 80 0.44274
78 → 80 0.48517
78 → 82 -0.11940

***Z*-12c**

Excited State 1: 2.7463 eV 451.46nm f=0.0385
90 → 95 -0.10657
93 → 95 0.37477
94 → 95 0.56729
Excited State 2: 3.7038 eV 334.75nm f=0.2644
90 → 95 -0.12720
93 → 95 0.54484
94 → 95 -0.40948
Excited State 3: 4.1747 eV 296.99nm f=0.0158
90 → 95 0.41430
91 → 95 -0.23604
92 → 95 0.45243
93 → 95 0.19699
Excited State 4: 4.2626 eV 290.86nm f=0.0040
90 → 95 -0.31261
91 → 95 0.28235
92 → 95 0.44572

94 → 96 -0.28050
94 → 97 -0.13443
Excited State 5: 4.5168 eV 274.49nm f=0.2224
91 → 95 0.30398
92 → 95 0.21248
94 → 96 0.58063

***Z*-12d**

Excited State 1: 2.8050 eV 442.01nm f=0.0140
101 →107 0.14563
105 →107 0.40196
106 →107 0.55043
Excited State 2: 3.7973 eV 326.51nm f=0.2787
105 →107 0.54323
106 →107 -0.42615
Excited State 3: 4.1918 eV 295.78nm f=0.0042
100 →107 0.16095
101 →107 0.58159
102 →107 0.23282
104 →107 -0.18439
105 →107 -0.15744
Excited State 4: 4.3343 eV 286.05nm f=0.0241
101 →107 0.17599
103 →107 -0.10221
104 →107 0.63311
106 →108 0.19361
Excited State 5: 4.5281 eV 273.81nm f=0.0016
101 →107 -0.21088
102 →107 0.63890
106 →108 -0.15091

7.3.3. Transitions in DMSO

***E*-1a**

Excited State 1: 2.8587 eV 433.70nm f=0.0000
57 → 59 0.70082
Excited State 2: 3.3669 eV 368.24nm f=0.9057
58 → 59 0.70159
Excited State 3: 3.9627 eV 312.88nm f=0.0133
56 → 59 0.68747
58 → 60 0.13311

Excited State 4: 4.3954 eV 282.08nm f=0.0073
54 → 59 0.59009
55 → 59 0.27378
55 → 61 0.11041
58 → 61 0.23934
Excited State 5: 4.5237 eV 274.08nm f=0.1079
54 → 59 -0.24792
55 → 59 0.62365
56 → 60 0.14891

***E*-1b**

Excited State 1: 2.8681 eV 432.28nm f=0.0000
61 → 63 0.70053
Excited State 2: 3.2992 eV 375.80nm f=0.9697
62 → 63 0.70222
Excited State 3: 3.9567 eV 313.35nm f=0.0116
60 → 63 0.68102
62 → 64 0.16346
Excited State 4: 4.4010 eV 281.72nm f=0.0026
58 → 63 0.57493
59 → 63 0.26062
59 → 65 0.11092
62 → 64 -0.10003
62 → 65 0.26835
Excited State 5: 4.4867 eV 276.34nm f=0.1000
60 → 63 -0.15732
62 → 64 0.66599

***E*-1c**

Excited State 1: 2.7267 eV 454.71nm f=0.0001
76 → 79 0.59876
77 → 79 0.36355
Excited State 2: 3.0037 eV 412.78nm f=0.8369
78 → 79 0.70546
Excited State 3: 3.7129 eV 333.93nm f=0.0272
76 → 79 -0.36220
77 → 79 0.59341
Excited State 4: 4.2297 eV 293.13nm f=0.0162
74 → 79 0.59653
75 → 79 0.31033
78 → 83 -0.17324

Excited State 5: 4.3231 eV 286.79nm f=0.1737
74 → 79 -0.29330
75 → 79 0.60459
78 → 83 0.10137

***E*-1d**

Excited State 1: 2.8522 eV 434.69nm f=0.0000
89 → 91 0.70058
Excited State 2: 3.3127 eV 374.27nm f=1.0515
90 → 91 0.70158
Excited State 3: 3.9423 eV 314.50nm f=0.0134
88 → 91 0.68459
90 → 92 -0.14492
Excited State 4: 4.3313 eV 286.25nm f=0.0002
86 → 91 0.67363
87 → 91 -0.19871
Excited State 5: 4.3796 eV 283.09nm f=0.0002
84 → 91 -0.13209
86 → 91 0.19322
87 → 91 0.65398

***E*-2a**

Excited State 1: 2.7671 eV 448.06nm f=0.0000
74 → 76 0.70010
Excited State 2: 3.2601 eV 380.30nm f=0.8472
75 → 76 0.70103
Excited State 3: 3.8315 eV 323.60nm f=0.0158
73 → 76 0.69222
75 → 77 0.10143
Excited State 4: 4.0569 eV 305.61nm f=0.0217
71 → 76 -0.11784
72 → 76 0.66867
75 → 78 0.14479
Excited State 5: 4.4449 eV 278.93nm f=0.0964
71 → 76 0.66508
72 → 76 0.13067
73 → 77 -0.12425

***E*-2b**

Excited State 1: 2.7780 eV 446.31nm f=0.0001
78 → 80 0.69992
Excited State 2: 3.1958 eV 387.96nm f=0.9196
79 → 80 0.70178
Excited State 3: 3.8315 eV 323.59nm f=0.0152
77 → 80 0.68959
79 → 81 0.12052
Excited State 4: 4.0730 eV 304.41nm f=0.0179
75 → 80 -0.11583
76 → 80 0.66337
79 → 82 0.16672
Excited State 5: 4.4581 eV 278.11nm f=0.0933
75 → 80 0.65197
76 → 80 0.13927
77 → 81 -0.13790

***E*-3a**

Excited State 1: 2.8142 eV 440.56nm f=0.0000
61 → 63 0.70063
Excited State 2: 3.2254 eV 384.41nm f=0.8716
62 → 63 0.69958
Excited State 3: 3.9315 eV 315.36nm f=0.0429
59 → 63 -0.48281
60 → 63 0.48613
Excited State 4: 3.9463 eV 314.18nm f=0.0072
59 → 63 0.48766
60 → 63 0.48373
62 → 64 0.11693
Excited State 5: 4.5063 eV 275.13nm f=0.0854
58 → 63 0.65069
60 → 64 -0.12961
62 → 64 0.17114

***E*-3b**

Excited State 1: 2.8227 eV 439.24nm f=0.0000
65 → 67 0.70036
Excited State 2: 3.1655 eV 391.68nm f=0.9376
66 → 67 0.70076
Excited State 3: 3.9224 eV 316.10nm f=0.0246
63 → 67 -0.16171
64 → 67 0.65957

66 → 68 0.14959
Excited State 4: 3.9532 eV 313.63nm f=0.0170
63 → 67 0.66574
64 → 67 0.15761
Excited State 5: 4.4016 eV 281.68nm f=0.0907
64 → 67 -0.17070
66 → 68 0.66856

***E*-4a**

Excited State 1: 2.8339 eV 437.50nm f=0.0000
61 → 63 0.70085
Excited State 2: 3.2934 eV 376.47nm f=0.9013
62 → 63 0.70175
Excited State 3: 3.8698 eV 320.39nm f=0.0146
60 → 63 0.69094
62 → 64 0.11309
Excited State 4: 4.2492 eV 291.78nm f=0.0208
58 → 63 -0.25352
59 → 63 0.62378
62 → 65 0.16727
Excited State 5: 4.4897 eV 276.15nm f=0.1179
58 → 63 0.62931
59 → 63 0.25901
60 → 64 -0.14102

***E*-4b**

Excited State 1: 2.8427 eV 436.15nm f=0.0000
65 → 67 0.70063
Excited State 2: 3.2279 eV 384.10nm f=0.9682
66 → 67 0.70240
Excited State 3: 3.8690 eV 320.46nm f=0.0137
64 → 67 0.68717
66 → 68 0.13511
Excited State 4: 4.2617 eV 290.93nm f=0.0159
62 → 67 -0.24412
63 → 67 0.62113
66 → 69 0.18389
Excited State 5: 4.4907 eV 276.09nm f=0.1109
62 → 67 0.25621
63 → 67 0.14747
64 → 67 -0.13880

66 → 68 0.60775

***E*-5a**

Excited State 1: 2.8203 eV 439.62nm f=0.1079
79 → 82 0.56290
80 → 82 -0.23995
81 → 82 0.32434
Excited State 2: 3.0133 eV 411.45nm f=0.3194
79 → 82 -0.22571
80 → 82 0.27308
81 → 82 0.60602
Excited State 3: 3.6339 eV 341.18nm f=0.3969
79 → 82 0.32843
80 → 82 0.59713
81 → 82 -0.14359
Excited State 4: 4.0076 eV 309.37nm f=0.0103
78 → 82 0.67552
81 → 83 0.17040
Excited State 5: 4.4052 eV 281.45nm f=0.0554
77 → 82 0.15375
78 → 82 -0.17442
81 → 83 0.64716

***E*-5b**

Excited State 1: 2.8224 eV 439.28nm f=0.1513
83 → 86 0.55554
84 → 86 -0.19093
85 → 86 0.36655
Excited State 2: 3.0084 eV 412.12nm f=0.3565
83 → 86 -0.27737
84 → 86 0.28021
85 → 86 0.58032
Excited State 3: 3.5982 eV 344.57nm f=0.3813
83 → 86 0.30002
84 → 86 0.61148
85 → 86 -0.14903
Excited State 4: 3.9963 eV 310.24nm f=0.0074
82 → 86 0.65772
85 → 87 0.22796
Excited State 5: 4.3178 eV 287.15nm f=0.0657
82 → 86 -0.23199

85 → 87 0.64804

***E*-6a**

Excited State 1: 2.9397 eV 421.76nm f=0.0000
61 → 63 0.70083
Excited State 2: 3.3022 eV 375.46nm f=0.9966
62 → 63 0.70228
Excited State 3: 4.0481 eV 306.28nm f=0.0080
60 → 63 0.67240
62 → 64 0.19317
Excited State 4: 4.3659 eV 283.98nm f=0.0278
59 → 63 0.67805
60 → 64 0.10733
Excited State 5: 4.4407 eV 279.20nm f=0.0322
58 → 63 0.42896
59 → 65 0.10970
62 → 64 -0.28792
62 → 65 0.45112

***E*-6b**

Excited State 1: 2.9484 eV 420.51nm f=0.0000
65 → 67 0.70045
Excited State 2: 3.2417 eV 382.46nm f=1.0497
66 → 67 0.70284
Excited State 3: 4.0306 eV 307.61nm f=0.0046
64 → 67 0.64949
66 → 68 0.25370
Excited State 4: 4.3560 eV 284.63nm f=0.0687
63 → 67 -0.42507
64 → 67 -0.24270
66 → 68 0.48608
Excited State 5: 4.3841 eV 282.81nm f=0.0474
62 → 67 -0.16568
63 → 67 0.48766
66 → 68 0.38208
66 → 69 -0.22779

***E*-7a**

Excited State 1: 2.5967 eV 477.46nm f=0.0000

68 → 70 0.64441
68 → 71 -0.28321
Excited State 2: 2.8069 eV 441.72nm f=0.8914
69 → 70 0.70420
Excited State 3: 3.3842 eV 366.36nm f=0.0083
67 → 70 0.69122
67 → 71 -0.12205
Excited State 4: 3.8923 eV 318.54nm f=0.0000
63 → 70 0.43648
63 → 71 0.19748
68 → 70 0.20608
68 → 71 0.46650
Excited State 5: 3.9054 eV 317.47nm f=0.1795
65 → 70 0.11630
69 → 71 0.68050

***E*-7b**

Excited State 1: 2.6046 eV 476.02nm f=0.0000
72 → 74 0.64523
72 → 75 -0.28063
Excited State 2: 2.7387 eV 452.71nm f=0.9661
73 → 74 0.70457
Excited State 3: 3.3859 eV 366.18nm f=0.0064
71 → 74 0.69063
71 → 75 -0.12132
Excited State 4: 3.8322 eV 323.53nm f=0.1983
73 → 75 0.68652
Excited State 5: 3.8828 eV 319.32nm f=0.0001
67 → 74 0.34492
67 → 75 0.15432
72 → 74 0.23652
72 → 75 0.53830

***E*-8a**

Excited State 1: 2.6989 eV 459.38nm f=0.0000
75 → 77 0.66524
75 → 78 0.22617
Excited State 2: 2.9182 eV 424.87nm f=1.3910
76 → 77 0.70327
Excited State 3: 3.6246 eV 342.06nm f=0.0108
74 → 77 0.68956

74 → 78 0.10631
Excited State 4: 3.9461 eV 314.19nm f=0.2079
73 → 77 0.65068
76 → 78 0.24701
Excited State 5: 4.1216 eV 300.82nm f=0.0116
72 → 77 0.59986
76 → 78 -0.26795
76 → 80 0.20409

***E*-8b**

Excited State 1: 2.6267 eV 472.01nm f=0.0000
79 → 81 0.66776
79 → 82 0.21089
Excited State 2: 2.6948 eV 460.08nm f=1.2658
80 → 81 0.70465
Excited State 3: 3.4845 eV 355.81nm f=0.0597
78 → 81 0.69049
Excited State 4: 3.8081 eV 325.58nm f=0.1273
77 → 81 0.55470
80 → 82 0.42233
Excited State 5: 3.9619 eV 312.94nm f=0.1804
76 → 81 -0.11698
77 → 81 -0.41342
80 → 82 0.54495

***E*-9a**

Excited State 1: 2.8658 eV 432.64nm f=0.0487
74 → 79 0.11415
77 → 79 0.65411
78 → 79 -0.22006
Excited State 2: 3.3741 eV 367.46nm f=0.8236
77 → 79 0.21272
78 → 79 0.66548
Excited State 3: 3.7979 eV 326.46nm f=0.0191
76 → 79 0.69091
Excited State 4: 4.2520 eV 291.59nm f=0.0162
75 → 79 0.67403
78 → 82 -0.17276
Excited State 5: 4.5096 eV 274.93nm f=0.1902
74 → 79 0.66824
76 → 80 -0.15106

77 → 79 -0.10450

***E*-9b**

Excited State 1: 2.8777 eV 430.84nm f=0.0674
78 → 83 0.10720
80 → 83 0.14735
81 → 83 0.63288
82 → 83 -0.23586
Excited State 2: 3.3226 eV 373.15nm f=0.8861
81 → 83 0.24096
82 → 83 0.66082
Excited State 3: 3.8104 eV 325.38nm f=0.0196
80 → 83 0.67978
81 → 83 -0.12579
82 → 84 0.10456
Excited State 4: 4.2725 eV 290.19nm f=0.0139
79 → 83 0.66761
82 → 86 0.19332
Excited State 5: 4.5248 eV 274.01nm f=0.1694
78 → 83 0.66574
80 → 84 0.16509
81 → 83 -0.10783

***E*-10a**

Excited State 1: 2.8003 eV 442.76nm f=0.0104
72 → 76 0.42064
73 → 76 0.40028
74 → 76 0.38507
Excited State 2: 3.2411 eV 382.53nm f=0.6687
74 → 76 0.12100
75 → 76 0.68837
Excited State 3: 3.4137 eV 363.20nm f=0.0917
72 → 76 -0.21819
73 → 76 -0.32486
74 → 76 0.57476
75 → 76 -0.11184
Excited State 4: 3.8182 eV 324.72nm f=0.0894
72 → 76 0.49983
73 → 76 -0.47065
Excited State 5: 3.9110 eV 317.02nm f=0.0119
71 → 76 0.68932

75 → 77 -0.11707

***E*-10b**

Excited State 1: 2.6948 eV 460.09nm f=0.0240
75 → 80 0.47538
76 → 80 0.25152
78 → 80 0.41146
79 → 80 0.13600
Excited State 2: 2.9944 eV 414.06nm f=0.7069
78 → 80 -0.10807
79 → 80 0.69002
Excited State 3: 3.2893 eV 376.93nm f=0.0044
75 → 80 -0.34717
76 → 80 -0.19912
77 → 80 -0.14164
78 → 80 0.56111
Excited State 4: 3.6686 eV 337.96nm f=0.0454
76 → 80 -0.16575
77 → 80 0.66699
Excited State 5: 3.7587 eV 329.86nm f=0.0491
75 → 80 -0.34414
76 → 80 0.59635

***E*-11a**

Excited State 1: 2.8292 eV 438.23nm f=0.0000
89 → 91 0.69865
Excited State 2: 3.2765 eV 378.40nm f=0.8728
90 → 91 0.70183
Excited State 3: 3.7551 eV 330.18nm f=0.0141
88 → 91 0.69398
Excited State 4: 4.1608 eV 297.98nm f=0.0285
86 → 91 0.17571
90 → 92 0.67435
Excited State 5: 4.4775 eV 276.91nm f=0.0000
89 → 92 0.70590

***E*-11b**

Excited State 1: 2.8393 eV 436.67nm f=0.0000
93 → 95 0.69857

Excited State 2: 3.2121 eV 385.99nm f=0.9543
94 → 95 0.70249
Excited State 3: 3.7606 eV 329.69nm f=0.0130
92 → 95 0.69237
Excited State 4: 4.0784 eV 304.00nm f=0.0379
90 → 95 -0.15349
94 → 96 0.68188
Excited State 5: 4.4544 eV 278.34nm f=0.0000
93 → 96 0.70590

***E*-12a**

Excited State 1: 2.8498 eV 435.06nm f=0.0000
73 → 75 0.70126
Excited State 2: 3.4173 eV 362.82nm f=0.8566
74 → 75 0.70220
Excited State 3: 4.1900 eV 295.91nm f=0.0272
72 → 75 0.67009
74 → 76 0.19490
Excited State 4: 4.3395 eV 285.71nm f=0.0103
70 → 75 0.49834
71 → 75 -0.44581
74 → 78 0.18243
Excited State 5: 4.5136 eV 274.69nm f=0.1350
70 → 75 0.43694
71 → 75 0.50282
72 → 75 -0.10930
72 → 76 -0.11118
74 → 76 0.10576

***E*-12b**

Excited State 1: 2.8545 eV 434.34nm f=0.0000
77 → 79 0.70111
Excited State 2: 3.3428 eV 370.90nm f=0.9032
78 → 79 0.70299
Excited State 3: 4.1791 eV 296.68nm f=0.0212
76 → 79 0.65402
78 → 80 0.24184
Excited State 4: 4.3573 eV 284.54nm f=0.0069
74 → 79 0.52571
75 → 79 -0.39754
78 → 81 0.20167

Excited State 5: 4.5153 eV 274.59nm f=0.1618
74 → 79 0.37384
75 → 79 0.47514
76 → 79 -0.17177
76 → 80 -0.12346
78 → 80 0.25523

***E*-12c**

Excited State 1: 2.8304 eV 438.05nm f=0.0001
93 → 95 0.70049
Excited State 2: 3.3329 eV 372.00nm f=0.9671
94 → 95 0.70280
Excited State 3: 4.1408 eV 299.42nm f=0.0247
92 → 95 0.65805
94 → 96 0.21815
Excited State 4: 4.3190 eV 287.07nm f=0.0067
90 → 95 0.50877
91 → 95 0.43138
94 → 99 0.17548
Excited State 5: 4.4678 eV 277.51nm f=0.2422
90 → 95 -0.39017
91 → 95 0.42564
92 → 95 0.16961
92 → 96 0.11655
94 → 96 -0.30705

***E*-12d**

Excited State 1: 2.7290 eV 454.32nm f=0.0000
102 →107 -0.17844
105 →107 0.67804
Excited State 2: 3.1327 eV 395.77nm f=0.8128
106 →107 0.70536
Excited State 3: 3.9758 eV 311.85nm f=0.0189
103 →107 0.50932
104 →107 -0.45545
106 →108 0.12010
Excited State 4: 4.0624 eV 305.20nm f=0.0001
102 →107 0.67037
103 →107 -0.10426
105 →107 0.18174
Excited State 5: 4.0948 eV 302.78nm f=0.0043

103 →107 0.44796
104 →107 0.53488

***Z*-1a**

Excited State 1: 2.9657 eV 418.06nm f=0.0025
55 → 59 -0.16858
57 → 59 0.67837
Excited State 2: 3.8265 eV 324.02nm f=0.2449
58 → 59 0.69470
Excited State 3: 4.1815 eV 296.51nm f=0.0916
56 → 59 0.69369
58 → 60 -0.10603
Excited State 4: 4.2588 eV 291.12nm f=0.0006
55 → 59 0.67472
57 → 59 0.17144
Excited State 5: 4.6888 eV 264.43nm f=0.0038
54 → 59 0.70272

***Z*-1b**

Excited State 1: 2.9900 eV 414.66nm f=0.0025
59 → 63 -0.16413
61 → 63 0.68004
Excited State 2: 3.7798 eV 328.02nm f=0.3076
62 → 63 0.69692
Excited State 3: 4.1761 eV 296.89nm f=0.0723
60 → 63 0.68810
62 → 64 -0.13411
Excited State 4: 4.2826 eV 289.51nm f=0.0005
59 → 63 0.67473
61 → 63 0.16861
Excited State 5: 4.7183 eV 262.78nm f=0.0255
58 → 63 0.67589
62 → 64 0.18577

***Z*-1c**

Excited State 1: 2.9141 eV 425.46nm f=0.0035
75 → 79 -0.14493
77 → 79 0.65788
78 → 79 -0.15953

Excited State 2: 3.6605 eV 338.71nm f=0.3544
77 → 79 0.15427
78 → 79 0.68040
Excited State 3: 4.0733 eV 304.38nm f=0.0353
76 → 79 0.68838
Excited State 4: 4.1910 eV 295.83nm f=0.0011
73 → 79 -0.17472
74 → 79 -0.19362
75 → 79 0.61049
77 → 79 0.16983
Excited State 5: 4.5984 eV 269.63nm f=0.0045
74 → 79 0.66826
75 → 79 0.21353

***Z*-1d**

Excited State 1: 2.9517 eV 420.05nm f=0.0022
84 → 91 0.16860
89 → 91 0.67872
Excited State 2: 3.7700 eV 328.87nm f=0.3102
90 → 91 0.69660
Excited State 3: 4.1473 eV 298.95nm f=0.0714
88 → 91 0.69197
90 → 92 0.11542
Excited State 4: 4.2329 eV 292.91nm f=0.0004
84 → 91 0.63950
86 → 91 -0.22766
89 → 91 -0.15373
Excited State 5: 4.4980 eV 275.64nm f=0.0003
84 → 91 0.20969
86 → 91 0.66147

***Z*-2a**

Excited State 1: 2.9505 eV 420.22nm f=0.0134
71 → 76 -0.12964
72 → 76 0.12662
74 → 76 0.56025
75 → 76 0.38137
Excited State 2: 3.7455 eV 331.02nm f=0.2471
74 → 76 -0.36473
75 → 76 0.58561
Excited State 3: 4.0805 eV 303.84nm f=0.0872

73 → 76 0.69407
Excited State 4: 4.1678 eV 297.48nm f=0.0055
71 → 76 -0.33318
72 → 76 0.58099
74 → 76 -0.19497
Excited State 5: 4.5200 eV 274.30nm f=0.0030
71 → 76 0.58123
72 → 76 0.36282

***Z*-2b**

Excited State 1: 2.9810 eV 415.92nm f=0.0130
75 → 80 -0.12538
76 → 80 -0.12244
78 → 80 0.59661
79 → 80 -0.32244
Excited State 2: 3.7106 eV 334.13nm f=0.3099
78 → 80 0.30762
79 → 80 0.61933
Excited State 3: 4.0853 eV 303.49nm f=0.0716
77 → 80 0.69070
Excited State 4: 4.1979 eV 295.35nm f=0.0039
75 → 80 0.34091
76 → 80 0.57961
78 → 80 0.18652
Excited State 5: 4.5520 eV 272.37nm f=0.0031
75 → 80 0.57481
76 → 80 -0.36246

***Z*-3a**

Excited State 1: 2.8594 eV 433.60nm f=0.0205
58 → 63 -0.12402
59 → 63 -0.18345
60 → 63 -0.11868
61 → 63 0.37368
62 → 63 0.53788
Excited State 2: 3.7390 eV 331.59nm f=0.1207
58 → 63 0.18747
59 → 63 0.37940
60 → 63 0.27256
61 → 63 -0.25555
62 → 63 0.41528

Excited State 3: 3.8664 eV 320.67nm f=0.1346
58 → 63 0.16048
59 → 63 0.30373
60 → 63 0.24008
61 → 63 0.53020
62 → 63 -0.17331
Excited State 4: 4.1458 eV 299.06nm f=0.0733
59 → 63 -0.38211
60 → 63 0.57350
Excited State 5: 4.4242 eV 280.24nm f=0.0034
58 → 63 0.62389
59 → 63 -0.26929
62 → 64 0.10242

***Z*-3b**

Excited State 1: 2.8987 eV 427.72nm f=0.0152
62 → 67 0.11969
63 → 67 0.18810
64 → 67 -0.10587
65 → 67 -0.46339
66 → 67 0.46356
Excited State 2: 3.7358 eV 331.88nm f=0.2311
62 → 67 -0.13018
63 → 67 -0.28605
64 → 67 0.17125
65 → 67 0.31599
66 → 67 0.51055
Excited State 3: 3.8641 eV 320.86nm f=0.0887
62 → 67 0.21261
63 → 67 0.42076
64 → 67 -0.28199
65 → 67 0.41522
66 → 67 0.12064
Excited State 4: 4.1529 eV 298.55nm f=0.0600
63 → 67 0.33757
64 → 67 0.59384
66 → 68 -0.12483
Excited State 5: 4.4578 eV 278.13nm f=0.0027
62 → 67 0.62282
63 → 67 -0.28312

***Z*-4a**

Excited State 1: 2.9078 eV 426.38nm f=0.0271
58 → 63 -0.13350
61 → 63 0.52221
62 → 63 -0.44024
Excited State 2: 3.7176 eV 333.51nm f=0.2283
59 → 63 -0.10585
61 → 63 0.41472
62 → 63 0.54458
Excited State 3: 4.0479 eV 306.29nm f=0.0852
60 → 63 0.69074
Excited State 4: 4.2245 eV 293.49nm f=0.0141
58 → 63 0.41427
59 → 63 0.51291
61 → 63 0.19940
Excited State 5: 4.5246 eV 274.02nm f=0.0028
58 → 63 0.51390
59 → 63 -0.44352
62 → 64 -0.12744

***Z*-4b**

Excited State 1: 2.9421 eV 421.42nm f=0.0252
62 → 67 -0.12768
65 → 67 0.56590
66 → 67 -0.38218
Excited State 2: 3.6913 eV 335.88nm f=0.2927
65 → 67 0.35985
66 → 67 0.58630
Excited State 3: 4.0588 eV 305.47nm f=0.0726
64 → 67 0.68796
Excited State 4: 4.2430 eV 292.21nm f=0.0101
62 → 67 -0.41557
63 → 67 0.51678
65 → 67 -0.18717
Excited State 5: 4.5622 eV 271.76nm f=0.0073
62 → 67 0.49468
63 → 67 0.43194
66 → 68 0.19875

***Z*-5a**

Excited State 1: 2.7755 eV 446.70nm f=0.0029

79 → 82 -0.32243
81 → 82 0.61628
Excited State 2: 3.4099 eV 363.60nm f=0.0066
76 → 82 -0.12144
77 → 82 0.16781
79 → 82 0.57422
81 → 82 0.34039
Excited State 3: 3.8161 eV 324.90nm f=0.2476
80 → 82 0.69277
Excited State 4: 4.1869 eV 296.13nm f=0.0942
78 → 82 0.67768
79 → 82 -0.11303
80 → 83 -0.10726
Excited State 5: 4.3373 eV 285.86nm f=0.0014
76 → 82 -0.39494
77 → 82 0.51546
78 → 82 -0.11993
79 → 82 -0.21199

***Z*-5b**

Excited State 1: 2.8027 eV 442.38nm f=0.0029
83 → 86 0.31883
85 → 86 0.61662
Excited State 2: 3.4365 eV 360.79nm f=0.0081
80 → 86 -0.10349
81 → 86 0.17460
83 → 86 0.57418
85 → 86 -0.33876
Excited State 3: 3.7685 eV 329.01nm f=0.3068
84 → 86 0.69313
Excited State 4: 4.1812 eV 296.52nm f=0.0744
82 → 86 0.67064
83 → 86 -0.12492
84 → 87 -0.13631
Excited State 5: 4.3630 eV 284.17nm f=0.0016
80 → 86 -0.34771
81 → 86 0.55095
82 → 86 -0.11770
83 → 86 -0.20497

***Z*-6a**

Excited State 1: 2.8582 eV 433.79nm f=0.0153
59 → 63 -0.26395
61 → 63 -0.27280
62 → 63 0.58973
Excited State 2: 3.7872 eV 327.37nm f=0.1651
59 → 63 0.43773
61 → 63 0.38787
62 → 63 0.37943
Excited State 3: 3.8919 eV 318.57nm f=0.0747
59 → 63 -0.46753
61 → 63 0.51139
Excited State 4: 4.1789 eV 296.69nm f=0.0857
60 → 63 0.68870
Excited State 5: 4.5177 eV 274.44nm f=0.0659
58 → 63 -0.11463
58 → 66 0.11622
61 → 64 -0.13149
62 → 64 0.61976
62 → 65 -0.21940

***Z*-6b**

Excited State 1: 2.9067 eV 426.54nm f=0.0031
63 → 67 -0.26332
65 → 67 -0.28449
66 → 67 0.58311
Excited State 2: 3.7928 eV 326.89nm f=0.2996
63 → 67 0.12788
65 → 67 0.59130
66 → 67 0.34801
Excited State 3: 3.8743 eV 320.02nm f=0.0092
63 → 67 0.62883
65 → 67 -0.23877
66 → 67 0.17319
Excited State 4: 4.1892 eV 295.96nm f=0.0689
64 → 67 0.68642
65 → 68 0.11315
Excited State 5: 4.5428 eV 272.93nm f=0.0342
62 → 70 -0.12828
65 → 68 -0.21665
65 → 69 0.10347
66 → 68 0.60602
66 → 69 -0.21417

***Z*-7a**

Excited State 1: 3.0229 eV 410.15nm f=0.0028
65 → 71 -0.12124
68 → 71 0.66141
69 → 70 -0.20077
Excited State 2: 3.1359 eV 395.37nm f=0.0000
68 → 71 0.19830
69 → 70 0.67297
Excited State 3: 3.3479 eV 370.33nm f=0.3076
68 → 70 0.66225
69 → 71 -0.23274
Excited State 4: 3.7353 eV 331.93nm f=0.0002
67 → 70 0.70497
Excited State 5: 3.8037 eV 325.96nm f=0.1772
68 → 70 0.22883
69 → 71 0.65824

***Z*-7b**

Excited State 1: 3.0057 eV 412.50nm f=0.0014
72 → 75 0.36770
73 → 74 0.59399
Excited State 2: 3.0779 eV 402.81nm f=0.0014
69 → 75 0.10569
72 → 75 0.58378
73 → 74 -0.37537
Excited State 3: 3.3125 eV 374.29nm f=0.3114
72 → 74 0.65596
73 → 75 0.25079
Excited State 4: 3.6995 eV 335.13nm f=0.0002
71 → 74 0.70501
Excited State 5: 3.7739 eV 328.53nm f=0.2294
72 → 74 -0.24733
73 → 75 0.65150

***Z*-8a**

Excited State 1: 2.9529 eV 419.87nm f=0.0093
73 → 78 -0.26321
75 → 77 0.17095
75 → 78 0.54179

76 → 77 0.12366
76 → 78 0.28157
Excited State 2: 3.5695 eV 347.35nm f=0.5416
75 → 77 0.25347
75 → 78 -0.28684
76 → 77 0.55068
76 → 78 0.19787
Excited State 3: 3.7101 eV 334.18nm f=0.1158
75 → 77 0.48137
75 → 78 -0.17835
76 → 77 -0.40649
76 → 78 0.24664
Excited State 4: 3.9099 eV 317.11nm f=0.2449
75 → 77 -0.38863
75 → 78 -0.12737
76 → 78 0.55013
Excited State 5: 4.1004 eV 302.37nm f=0.0072
69 → 78 0.15112
73 → 77 0.22333
73 → 78 0.58323
75 → 78 0.25777

***Z*-8b**

Excited State 1: 2.9816 eV 415.82nm f=0.0056
77 → 82 -0.26439
79 → 81 0.11165
79 → 82 0.62407
80 → 82 -0.11810
Excited State 2: 3.5323 eV 351.00nm f=0.4773
79 → 81 -0.36673
79 → 82 0.15758
80 → 81 0.48826
80 → 82 0.30520
Excited State 3: 3.6028 eV 344.13nm f=0.1711
79 → 81 0.38602
80 → 81 0.49978
80 → 82 -0.29493
Excited State 4: 3.8893 eV 318.78nm f=0.2941
79 → 81 0.42959
80 → 82 0.54208
Excited State 5: 4.1245 eV 300.61nm f=0.0619
77 → 82 0.11320
78 → 81 0.22373

78 → 82 0.63579
80 → 83 0.10794

***Z*-9a**

Excited State 1: 2.9807 eV 415.96nm f=0.0296
74 → 79 -0.16367
76 → 79 0.33699
77 → 79 0.48105
78 → 79 0.34876
Excited State 2: 3.6158 eV 342.90nm f=0.2207
76 → 79 -0.15607
77 → 79 -0.29897
78 → 79 0.60637
Excited State 3: 3.8869 eV 318.98nm f=0.0964
76 → 79 0.58470
77 → 79 -0.38303
Excited State 4: 4.3299 eV 286.35nm f=0.0092
74 → 79 0.66261
77 → 79 0.15336
Excited State 5: 4.3643 eV 284.09nm f=0.0028
75 → 79 0.69746

***Z*-9b**

Excited State 1: 3.0545 eV 405.91nm f=0.0056
78 → 83 -0.16599
81 → 83 0.67203
82 → 83 -0.11643
Excited State 2: 3.6130 eV 343.16nm f=0.3119
81 → 83 0.11215
82 → 83 0.68833
Excited State 3: 3.9310 eV 315.40nm f=0.0881
80 → 83 0.69800
Excited State 4: 4.3516 eV 284.92nm f=0.0013
78 → 83 0.67348
81 → 83 0.16857
Excited State 5: 4.4382 eV 279.36nm f=0.0015
79 → 83 0.70497

***Z*-10a**

Excited State 1: 2.8993 eV 427.64nm f=0.0040
70 → 76 0.12364
71 → 76 0.26686
72 → 76 -0.14920
73 → 76 -0.21261
74 → 76 0.57878
Excited State 2: 3.5528 eV 348.97nm f=0.0498
73 → 76 -0.21473
75 → 76 0.66780
Excited State 3: 3.8026 eV 326.05nm f=0.1647
73 → 76 0.62956
74 → 76 0.19827
75 → 76 0.20104
Excited State 4: 3.8295 eV 323.76nm f=0.0466
70 → 76 0.23870
71 → 76 0.47611
72 → 76 -0.29061
74 → 76 -0.34248
Excited State 5: 4.1188 eV 301.02nm f=0.0868
71 → 76 0.33761
72 → 76 0.60509

***Z*-10b**

Excited State 1: 2.9271 eV 423.57nm f=0.0042
74 → 80 0.11954
75 → 80 0.26759
76 → 80 0.12986
77 → 80 -0.25909
78 → 80 0.56282
Excited State 2: 3.5731 eV 347.00nm f=0.0934
77 → 80 -0.24789
78 → 80 -0.21398
79 → 80 0.62173
Excited State 3: 3.7812 eV 327.90nm f=0.2157
77 → 80 0.56356
78 → 80 0.26025
79 → 80 0.31007
Excited State 4: 3.8573 eV 321.43nm f=0.0134
74 → 80 0.22974
75 → 80 0.49880
76 → 80 0.28049
77 → 80 0.21274
78 → 80 -0.25291

Excited State 5: 4.1194 eV 300.98nm f=0.0693
75 → 80 -0.30785
76 → 80 0.61542

***Z*-11a**

Excited State 1: 3.0346 eV 408.56nm f=0.0027
87 → 91 0.11576
89 → 91 0.69213
Excited State 2: 3.7436 eV 331.19nm f=0.2539
89 → 93 -0.10041
90 → 91 0.69408
Excited State 3: 4.0600 eV 305.38nm f=0.0510
88 → 91 0.67042
90 → 92 0.19639
Excited State 4: 4.1683 eV 297.44nm f=0.1254
88 → 91 -0.19663
90 → 92 0.67172
Excited State 5: 4.2320 eV 292.97nm f=0.0155
89 → 92 0.69598

***Z*-11b**

Excited State 1: 3.0607 eV 405.08nm f=0.0027
91 → 95 0.11271
93 → 95 0.69148
Excited State 2: 3.7037 eV 334.76nm f=0.3135
93 → 97 -0.10647
94 → 95 0.69329
Excited State 3: 4.0430 eV 306.66nm f=0.0006
92 → 95 -0.46428
94 → 96 0.52240
Excited State 4: 4.1005 eV 302.36nm f=0.1644
92 → 95 0.51895
94 → 96 0.46845
Excited State 5: 4.2119 eV 294.36nm f=0.0144
93 → 96 0.69622

***Z*-12a**

Excited State 1: 2.8605 eV 433.44nm f=0.0195
70 → 75 0.16572

73 → 75 -0.40640
74 → 75 0.54342
Excited State 2: 3.8358 eV 323.23nm f=0.2279
70 → 75 -0.14117
73 → 75 0.52452
74 → 75 0.43874
Excited State 3: 4.1746 eV 297.00nm f=0.0065
70 → 75 0.61394
72 → 75 -0.23003
73 → 75 0.21245
Excited State 4: 4.3127 eV 287.48nm f=0.0389
70 → 75 0.20449
71 → 75 0.14299
72 → 75 0.63200
74 → 76 0.16368
Excited State 5: 4.5364 eV 273.31nm f=0.0036
70 → 75 -0.10566
71 → 75 0.67660

***Z*-12b**

Excited State 1: 2.9189 eV 424.77nm f=0.0033
74 → 79 0.16859
77 → 79 0.62948
78 → 79 0.25285
Excited State 2: 3.8091 eV 325.49nm f=0.3010
77 → 79 -0.25252
78 → 79 0.64950
Excited State 3: 4.1941 eV 295.62nm f=0.0009
74 → 79 0.66885
77 → 79 -0.17218
Excited State 4: 4.3373 eV 285.85nm f=0.0336
76 → 79 0.67268
78 → 80 0.16083
Excited State 5: 4.6039 eV 269.30nm f=0.0055
75 → 79 0.68900

***Z*-12c**

Excited State 1: 2.7926 eV 443.97nm f=0.0442
90 → 95 -0.13341
93 → 95 0.39163
94 → 95 0.55078

Excited State 2: 3.6871 eV 336.26nm f=0.2654
90 → 95 -0.13633
93 → 95 0.51942
94 → 95 -0.43309
Excited State 3: 4.1325 eV 300.02nm f=0.0150
88 → 95 0.15104
89 → 95 0.12345
90 → 95 -0.42527
92 → 95 0.45344
93 → 95 -0.23338
Excited State 4: 4.2252 eV 293.44nm f=0.0070
88 → 95 -0.15320
89 → 95 -0.10077
90 → 95 0.39199
91 → 95 -0.14491
92 → 95 0.47126
94 → 96 0.22148
Excited State 5: 4.4540 eV 278.37nm f=0.0070
91 → 95 0.67058
94 → 96 0.10112

***Z*-12d**

Excited State 1: 2.8548 eV 434.30nm f=0.0157
100 →107 0.16641
105 →107 -0.44287
106 →107 0.51248
Excited State 2: 3.7807 eV 327.94nm f=0.2798
100 →107 -0.11325
105 →107 0.50134
106 →107 0.47267
Excited State 3: 4.1457 eV 299.07nm f=0.0046
100 →107 0.59200
102 →107 -0.21599
103 →107 0.21170
105 →107 0.17400
Excited State 4: 4.2862 eV 289.26nm f=0.0268
100 →107 0.10832
101 →107 0.10750
102 →107 0.50683
103 →107 0.27397
104 →107 0.33331
106 →108 0.14925
Excited State 5: 4.3712 eV 283.64nm f=0.0013

100 →107 -0.24495
102 →107 -0.16939
103 →107 0.60744
104 →107 -0.11149

8.3.4. Transitions in MeOH

***E*-1a**

Excited State 1: 2.8592 eV 433.64nm f=0.0000
57 → 59 0.70085
Excited State 2: 3.3891 eV 365.83nm f=0.8831
58 → 59 0.70143
Excited State 3: 3.9658 eV 312.63nm f=0.0125
56 → 59 0.68675
58 → 60 0.13552
Excited State 4: 4.3968 eV 281.99nm f=0.0068
54 → 59 0.58959
55 → 59 0.27306
55 → 61 0.11117
58 → 61 0.24106
Excited State 5: 4.5288 eV 273.77nm f=0.1082
54 → 59 -0.24660
55 → 59 0.62347
56 → 60 0.15040

***E*-1b**

Excited State 1: 2.8686 eV 432.22nm f=0.0000
61 → 63 0.70056
Excited State 2: 3.3218 eV 373.24nm f=0.9467
62 → 63 0.70209
Excited State 3: 3.9599 eV 313.10nm f=0.0110
60 → 63 0.68006
62 → 64 0.16618
Excited State 4: 4.4023 eV 281.64nm f=0.0026
58 → 63 0.57454
59 → 63 0.26041
59 → 65 0.11157
62 → 65 0.27014
Excited State 5: 4.4919 eV 276.02nm f=0.0932
60 → 63 -0.16006

62 → 64 0.66470

***E*-1c**

Excited State 1: 2.7276 eV 454.56nm f=0.0001
76 → 79 0.58593
77 → 79 0.38395
Excited State 2: 3.0219 eV 410.28nm f=0.8182
78 → 79 0.70558
Excited State 3: 3.7164 eV 333.62nm f=0.0263
76 → 79 -0.38223
77 → 79 0.58029
Excited State 4: 4.2319 eV 292.97nm f=0.0153
74 → 79 0.59747
75 → 79 0.30690
78 → 83 -0.17548
Excited State 5: 4.3286 eV 286.43nm f=0.1720
74 → 79 -0.28919
75 → 79 0.60390
78 → 80 0.10582
78 → 83 0.10247

***E*-1d**

Excited State 1: 2.8528 eV 434.60nm f=0.0000
89 → 91 0.70061
Excited State 2: 3.3332 eV 371.97nm f=1.0304
90 → 91 0.70149
Excited State 3: 3.9448 eV 314.30nm f=0.0129
88 → 91 0.68387
90 → 92 -0.14722
Excited State 4: 4.3368 eV 285.89nm f=0.0002
86 → 91 0.67316
87 → 91 -0.20028
Excited State 5: 4.3846 eV 282.77nm f=0.0020
84 → 91 -0.39617
85 → 91 -0.20845
86 → 91 0.14539
87 → 91 0.48564
90 → 94 -0.16498

***E*-2a**

Excited State 1: 2.7674 eV 448.02nm f=0.0000
74 → 76 0.70013
Excited State 2: 3.2810 eV 377.89nm f=0.8234
75 → 76 0.70078
Excited State 3: 3.8342 eV 323.36nm f=0.0148
73 → 76 0.69164
75 → 77 0.10343
Excited State 4: 4.0581 eV 305.52nm f=0.0202
71 → 76 -0.11785
72 → 76 0.66810
75 → 78 0.14636
Excited State 5: 4.4490 eV 278.68nm f=0.0965
71 → 76 0.66449
72 → 76 0.13076
73 → 77 -0.12544

***E*-2b**

Excited State 1: 2.7782 eV 446.28nm f=0.0001
78 → 80 0.69996
Excited State 2: 3.2171 eV 385.39nm f=0.8954
79 → 80 0.70157
Excited State 3: 3.8345 eV 323.34nm f=0.0144
77 → 80 0.68889
79 → 81 0.12273
Excited State 4: 4.0740 eV 304.33nm f=0.0167
75 → 80 -0.11590
76 → 80 0.66275
79 → 82 0.16832
Excited State 5: 4.4618 eV 277.88nm f=0.0930
75 → 80 0.65132
76 → 80 0.13936
77 → 81 -0.13927

***E*-3a**

Excited State 1: 2.8144 eV 440.53nm f=0.0000
61 → 63 0.70066
Excited State 2: 3.2469 eV 381.85nm f=0.8490
62 → 63 0.69921
Excited State 3: 3.9357 eV 315.03nm f=0.0397
59 → 63 -0.44542

60 → 63 0.51982
Excited State 4: 3.9494 eV 313.93nm f=0.0084
59 → 63 0.52116
60 → 63 0.44634
62 → 64 0.11325
Excited State 5: 4.5107 eV 274.87nm f=0.0857
58 → 63 0.64863
60 → 64 -0.13064
62 → 64 0.17542

***E*-3b**

Excited State 1: 2.8228 eV 439.22nm f=0.0000
65 → 67 0.70039
Excited State 2: 3.1874 eV 388.98nm f=0.9148
66 → 67 0.70048
Excited State 3: 3.9257 eV 315.82nm f=0.0218
63 → 67 -0.13663
64 → 67 0.66424
66 → 68 0.15459
Excited State 4: 3.9571 eV 313.32nm f=0.0181
63 → 67 0.67060
64 → 67 0.13245
Excited State 5: 4.4067 eV 281.36nm f=0.0846
64 → 67 -0.17273
66 → 68 0.66711

***E*-4a**

Excited State 1: 2.8342 eV 437.45nm f=0.0000
61 → 63 0.70088
Excited State 2: 3.3155 eV 373.95nm f=0.8784
62 → 63 0.70158
Excited State 3: 3.8726 eV 320.16nm f=0.0137
60 → 63 0.69033
62 → 64 0.11514
Excited State 4: 4.2516 eV 291.62nm f=0.0193
58 → 63 -0.25534
59 → 63 0.62234
62 → 65 0.16901
Excited State 5: 4.4944 eV 275.86nm f=0.1193
58 → 63 0.62812
59 → 63 0.26059

60 → 64 -0.14239

***E*-4b**

Excited State 1: 2.8429 eV 436.12nm f=0.0000
65 → 67 0.70066
Excited State 2: 3.2505 eV 381.44nm f=0.9451
66 → 67 0.70226
Excited State 3: 3.8719 eV 320.22nm f=0.0131
64 → 67 0.68641
66 → 68 0.13739
Excited State 4: 4.2640 eV 290.77nm f=0.0147
62 → 67 -0.24581
63 → 67 0.61972
66 → 69 0.18571
Excited State 5: 4.4955 eV 275.79nm f=0.1059
62 → 67 0.27563
63 → 67 0.15504
64 → 67 -0.14017
64 → 68 -0.10310
66 → 68 0.59561

***E*-5a**

Excited State 1: 2.8231 eV 439.17nm f=0.0945
79 → 82 0.56918
80 → 82 -0.24372
81 → 82 0.30974
Excited State 2: 3.0215 eV 410.35nm f=0.3105
79 → 82 -0.20942
80 → 82 0.27408
81 → 82 0.61154
Excited State 3: 3.6447 eV 340.18nm f=0.3929
79 → 82 0.32863
80 → 82 0.59483
81 → 82 -0.15138
Excited State 4: 4.0103 eV 309.16nm f=0.0096
78 → 82 0.67440
81 → 83 0.17354
Excited State 5: 4.4077 eV 281.29nm f=0.0515
77 → 82 0.15604
78 → 82 -0.17702
81 → 83 0.64567

***E*-5b**

Excited State 1: 2.8260 eV 438.72nm f=0.1320
83 → 86 0.56443
84 → 86 -0.19560
85 → 86 0.34953
Excited State 2: 3.0167 eV 410.99nm f=0.3508
83 → 86 -0.25874
84 → 86 0.28174
85 → 86 0.58840
Excited State 3: 3.6083 eV 343.61nm f=0.3797
83 → 86 0.30036
84 → 86 0.60899
85 → 86 -0.15726
Excited State 4: 3.9989 eV 310.05nm f=0.0071
82 → 86 0.65610
85 → 87 0.23169
Excited State 5: 4.3211 eV 286.93nm f=0.0610
82 → 86 -0.23528
85 → 87 0.64662

***E*-6a**

Excited State 1: 2.9402 eV 421.69nm f=0.0000
61 → 63 0.70086
Excited State 2: 3.3246 eV 372.93nm f=0.9743
62 → 63 0.70216
Excited State 3: 4.0506 eV 306.09nm f=0.0073
60 → 63 0.67134
62 → 64 0.19611
Excited State 4: 4.3713 eV 283.63nm f=0.0280
59 → 63 0.67674
60 → 64 0.10957
Excited State 5: 4.4425 eV 279.08nm f=0.0288
58 → 63 0.43414
59 → 65 0.10958
62 → 64 -0.27400
62 → 65 0.45517

***E*-6b**

Excited State 1: 2.9489 eV 420.44nm f=0.0000
65 → 67 0.70048
Excited State 2: 3.2643 eV 379.82nm f=1.0271
66 → 67 0.70274
Excited State 3: 4.0330 eV 307.42nm f=0.0044
64 → 67 0.64792
66 → 68 0.25683
Excited State 4: 4.3607 eV 284.32nm f=0.0652
63 → 67 -0.42073
64 → 67 -0.24611
66 → 68 0.48704
Excited State 5: 4.3894 eV 282.46nm f=0.0427
62 → 67 -0.18115
63 → 67 0.48167
66 → 68 0.36924
66 → 69 -0.24859

***E*-7a**

Excited State 1: 2.5980 eV 477.23nm f=0.0000
68 → 70 0.64472
68 → 71 -0.28252
Excited State 2: 2.8275 eV 438.49nm f=0.8665
69 → 70 0.70448
Excited State 3: 3.3889 eV 365.85nm f=0.0078
67 → 70 0.69117
67 → 71 -0.12147
Excited State 4: 3.8935 eV 318.44nm f=0.0000
63 → 70 0.45910
63 → 71 0.20850
68 → 70 0.19542
68 → 71 0.44438
Excited State 5: 3.9164 eV 316.58nm f=0.1811
65 → 70 0.12540
69 → 71 0.67818

***E*-7b**

Excited State 1: 2.6058 eV 475.79nm f=0.0000
72 → 74 0.64552
72 → 75 -0.27997
Excited State 2: 2.7600 eV 449.22nm f=0.9405
73 → 74 0.70486

Excited State 3: 3.3908 eV 365.65nm f=0.0060
71 → 74 0.69053
71 → 75 -0.12074
Excited State 4: 3.8436 eV 322.57nm f=0.2012
73 → 75 0.68531
Excited State 5: 3.8848 eV 319.15nm f=0.0001
67 → 74 0.36753
67 → 75 0.16509
72 → 74 0.22907
72 → 75 0.52338

***E*-8a**

Excited State 1: 2.6994 eV 459.31nm f=0.0000
75 → 77 0.66540
75 → 78 0.22571
Excited State 2: 2.9395 eV 421.79nm f=1.3640
76 → 77 0.70345
Excited State 3: 3.6276 eV 341.78nm f=0.0100
74 → 77 0.68930
74 → 78 0.10568
Excited State 4: 3.9511 eV 313.80nm f=0.2070
73 → 77 0.64544
76 → 78 0.25971
Excited State 5: 4.1247 eV 300.59nm f=0.0116
72 → 77 0.60992
76 → 78 -0.24026
76 → 80 0.21023

***E*-8b**

Excited State 1: 2.6274 eV 471.88nm f=0.0000
79 → 81 0.66988
79 → 82 0.21103
Excited State 2: 2.7152 eV 456.63nm f=1.2416
80 → 81 0.70490
Excited State 3: 3.4880 eV 355.46nm f=0.0589
78 → 81 0.69244
Excited State 4: 3.8112 eV 325.31nm f=0.1247
77 → 81 0.54902
80 → 82 0.42973
Excited State 5: 3.9754 eV 311.88nm f=0.1784
76 → 81 -0.13634

77 → 81 -0.41734
80 → 82 0.53554

***E*-9a**

Excited State 1: 2.8669 eV 432.47nm f=0.0441
74 → 79 0.11494
77 → 79 0.65598
78 → 79 -0.21441
Excited State 2: 3.3939 eV 365.32nm f=0.8053
77 → 79 0.20828
78 → 79 0.66692
Excited State 3: 3.8010 eV 326.19nm f=0.0182
76 → 79 0.69060
Excited State 4: 4.2525 eV 291.56nm f=0.0152
75 → 79 0.67370
78 → 82 -0.17370
Excited State 5: 4.5145 eV 274.63nm f=0.1905
74 → 79 0.66778
76 → 80 -0.15205
77 → 79 -0.10400

***E*-9b**

Excited State 1: 2.8791 eV 430.63nm f=0.0604
78 → 83 0.10813
80 → 83 0.13088
81 → 83 0.63904
82 → 83 -0.22837
Excited State 2: 3.3427 eV 370.91nm f=0.8693
81 → 83 0.23408
82 → 83 0.66310
Excited State 3: 3.8137 eV 325.10nm f=0.0190
80 → 83 0.68222
81 → 83 -0.10702
82 → 84 0.10654
Excited State 4: 4.2730 eV 290.16nm f=0.0131
79 → 83 0.66728
82 → 86 0.19421
Excited State 5: 4.5291 eV 273.75nm f=0.1693
78 → 83 0.66513
80 → 84 0.16636
81 → 83 -0.10662

***E*-10a**

Excited State 1: 2.8005 eV 442.72nm f=0.0093
72 → 76 0.42192
73 → 76 0.39944
74 → 76 0.38496
Excited State 2: 3.2560 eV 380.79nm f=0.6269
74 → 76 0.14083
75 → 76 0.68317
Excited State 3: 3.4138 eV 363.18nm f=0.1077
72 → 76 -0.21346
73 → 76 -0.32628
74 → 76 0.57002
75 → 76 -0.13733
Excited State 4: 3.8205 eV 324.52nm f=0.0878
72 → 76 0.49870
73 → 76 -0.47032
Excited State 5: 3.9132 eV 316.84nm f=0.0114
71 → 76 0.68860
75 → 77 -0.11902

***E*-10b**

Excited State 1: 2.6957 eV 459.94nm f=0.0207
75 → 80 0.46859
76 → 80 0.26506
77 → 80 0.10153
78 → 80 0.41265
79 → 80 0.12868
Excited State 2: 3.0112 eV 411.74nm f=0.6899
78 → 80 -0.10520
79 → 80 0.69125
Excited State 3: 3.2884 eV 377.04nm f=0.0042
75 → 80 -0.34111
76 → 80 -0.20868
77 → 80 -0.14392
78 → 80 0.56071
Excited State 4: 3.6705 eV 337.79nm f=0.0425
76 → 80 -0.17161
77 → 80 0.66567
Excited State 5: 3.7624 eV 329.53nm f=0.0483
75 → 80 -0.36137

76 → 80 0.58521

***E*-11a**

Excited State 1: 2.8298 eV 438.14nm f=0.0000
89 → 91 0.69870
Excited State 2: 3.2971 eV 376.04nm f=0.8511
90 → 91 0.70160
Excited State 3: 3.7578 eV 329.94nm f=0.0133
88 → 91 0.69349
Excited State 4: 4.1640 eV 297.75nm f=0.0272
86 → 91 0.17784
90 → 92 0.67355
Excited State 5: 4.4782 eV 276.86nm f=0.0000
89 → 92 0.70590

***E*-11b**

Excited State 1: 2.8398 eV 436.59nm f=0.0000
93 → 95 0.69862
Excited State 2: 3.2334 eV 383.45nm f=0.9321
94 → 95 0.70228
Excited State 3: 3.7635 eV 329.44nm f=0.0124
92 → 95 0.69178
Excited State 4: 4.0819 eV 303.74nm f=0.0366
90 → 95 -0.15544
94 → 96 0.68124
Excited State 5: 4.4551 eV 278.30nm f=0.0000
93 → 96 0.70590

***E*-12a**

Excited State 1: 2.8502 eV 435.00nm f=0.0000
73 → 75 0.70129
Excited State 2: 3.4369 eV 360.74nm f=0.8337
74 → 75 0.70193
Excited State 3: 4.1930 eV 295.69nm f=0.0266
72 → 75 0.66842
74 → 76 0.19812
Excited State 4: 4.3408 eV 285.63nm f=0.0096
70 → 75 0.49405
71 → 75 -0.44973

74 → 78 0.18388
Excited State 5: 4.5186 eV 274.38nm f=0.1353
70 → 75 0.44034
71 → 75 0.49854
72 → 75 -0.11309
72 → 76 -0.11193
74 → 76 0.10392

***E*-12b**

Excited State 1: 2.8550 eV 434.28nm f=0.0000
77 → 79 0.70114
Excited State 2: 3.3628 eV 368.69nm f=0.8803
78 → 79 0.70281
Excited State 3: 4.1821 eV 296.47nm f=0.0208
76 → 79 0.65202
78 → 80 0.24533
Excited State 4: 4.3586 eV 284.46nm f=0.0065
74 → 79 0.52291
75 → 79 -0.40032
78 → 81 0.20318
Excited State 5: 4.5204 eV 274.28nm f=0.1600
74 → 79 0.37581
75 → 79 0.47320
76 → 79 -0.17545
76 → 80 -0.12441
78 → 80 0.25139

***E*-12c**

Excited State 1: 2.8309 eV 437.97nm f=0.0001
93 → 95 0.70052
Excited State 2: 3.3514 eV 369.95nm f=0.9441
94 → 95 0.70264
Excited State 3: 4.1439 eV 299.20nm f=0.0248
92 → 95 0.65626
94 → 96 0.22055
Excited State 4: 4.3207 eV 286.96nm f=0.0063
90 → 95 0.50676
91 → 95 0.43285
94 → 99 0.17711
Excited State 5: 4.4726 eV 277.21nm f=0.2399
90 → 95 -0.39002

91 → 95 0.42270
92 → 95 0.17394
92 → 96 0.11747
94 → 96 -0.30669

***E*-12d**

Excited State 1: 2.7299 eV 454.17nm f=0.0000
102 →107 -0.17647
105 →107 0.67902
Excited State 2: 3.1492 eV 393.70nm f=0.7949
106 →107 0.70545
Excited State 3: 3.9783 eV 311.65nm f=0.0177
103 →107 0.50554
104 →107 0.46357
106 →108 0.12226
Excited State 4: 4.0665 eV 304.90nm f=0.0001
102 →107 0.67778
105 →107 0.17815
Excited State 5: 4.0990 eV 302.48nm f=0.0041
103 →107 -0.46154
104 →107 0.52735

***Z*-1a**

Excited State 1: 2.9661 eV 418.01nm f=0.0024
55 → 59 -0.16773
57 → 59 0.67854
Excited State 2: 3.8378 eV 323.06nm f=0.2326
58 → 59 0.69423
Excited State 3: 4.1864 eV 296.16nm f=0.0876
56 → 59 0.69290
58 → 60 -0.10937
Excited State 4: 4.2602 eV 291.03nm f=0.0006
55 → 59 0.67495
57 → 59 0.17058
Excited State 5: 4.6915 eV 264.27nm f=0.0037
54 → 59 0.70260

***Z*-1b**

Excited State 1: 2.9904 eV 414.61nm f=0.0024

59 → 63 -0.16326
61 → 63 0.68024
Excited State 2: 3.7921 eV 326.96nm f=0.2931
62 → 63 0.69652
Excited State 3: 4.1807 eV 296.56nm f=0.0688
60 → 63 0.68709
62 → 64 -0.13789
Excited State 4: 4.2841 eV 289.41nm f=0.0005
59 → 63 0.67493
61 → 63 0.16775
Excited State 5: 4.7214 eV 262.60nm f=0.0212
58 → 63 0.68016
62 → 64 0.16996

***Z*-1c**

Excited State 1: 2.9147 eV 425.37nm f=0.0033
75 → 79 -0.14633
77 → 79 0.65791
78 → 79 -0.16031
Excited State 2: 3.6719 eV 337.66nm f=0.3399
77 → 79 0.15473
78 → 79 0.68002
Excited State 3: 4.0772 eV 304.09nm f=0.0337
76 → 79 0.68783
78 → 80 0.10000
Excited State 4: 4.1927 eV 295.72nm f=0.0011
73 → 79 -0.16961
74 → 79 -0.17320
75 → 79 0.61898
77 → 79 0.16913
Excited State 5: 4.6013 eV 269.45nm f=0.0044
74 → 79 0.67497
75 → 79 0.19060

***Z*-1d**

Excited State 1: 2.9523 eV 419.95nm f=0.0021
85 → 91 0.16743
89 → 91 0.67897
Excited State 2: 3.7803 eV 327.98nm f=0.2968
90 → 91 0.69630
Excited State 3: 4.1514 eV 298.65nm f=0.0677

88 → 91 0.69123
90 → 92 0.11873
Excited State 4: 4.2347 eV 292.78nm f=0.0003
85 → 91 0.63863
86 → 91 -0.22668
89 → 91 -0.15331
Excited State 5: 4.5037 eV 275.30nm f=0.0003
85 → 91 0.20856
86 → 91 0.66174

***Z*-2a**

Excited State 1: 2.9510 eV 420.14nm f=0.0126
71 → 76 -0.12896
72 → 76 0.12642
74 → 76 0.56046
75 → 76 0.38136
Excited State 2: 3.7559 eV 330.10nm f=0.2354
74 → 76 -0.36451
75 → 76 0.58530
Excited State 3: 4.0855 eV 303.47nm f=0.0839
73 → 76 0.69324
Excited State 4: 4.1690 eV 297.39nm f=0.0052
71 → 76 -0.33205
72 → 76 0.58166
74 → 76 -0.19415
Excited State 5: 4.5222 eV 274.17nm f=0.0027
71 → 76 0.58148
72 → 76 0.36127

***Z*-2b**

Excited State 1: 2.9815 eV 415.85nm f=0.0122
75 → 80 -0.12467
76 → 80 -0.12222
78 → 80 0.59712
79 → 80 -0.32186
Excited State 2: 3.7220 eV 333.11nm f=0.2961
78 → 80 0.30683
79 → 80 0.61932
Excited State 3: 4.0901 eV 303.14nm f=0.0687
77 → 80 0.68982
Excited State 4: 4.1992 eV 295.25nm f=0.0036

75 → 80 0.33985
76 → 80 0.58033
78 → 80 0.18577
Excited State 5: 4.5542 eV 272.24nm f=0.0029
75 → 80 0.57457
76 → 80 -0.36042

***Z*-3a**

Excited State 1: 2.8607 eV 433.40nm f=0.0194
58 → 63 -0.12341
59 → 63 -0.18268
60 → 63 -0.11801
61 → 63 0.37434
62 → 63 0.53796
Excited State 2: 3.7454 eV 331.03nm f=0.1078
58 → 63 0.19114
59 → 63 0.38787
60 → 63 0.28228
61 → 63 -0.23945
62 → 63 0.40904
Excited State 3: 3.8739 eV 320.05nm f=0.1358
58 → 63 0.15515
59 → 63 0.29355
60 → 63 0.22938
61 → 63 0.53707
62 → 63 -0.18675
Excited State 4: 4.1506 eV 298.72nm f=0.0700
59 → 63 -0.38219
60 → 63 0.57270
Excited State 5: 4.4272 eV 280.05nm f=0.0031
58 → 63 0.62361
59 → 63 -0.26847
62 → 64 0.10491

***Z*-3b**

Excited State 1: 2.8998 eV 427.56nm f=0.0144
62 → 67 0.11897
63 → 67 0.18725
64 → 67 -0.10513
65 → 67 -0.46371
66 → 67 0.46391

Excited State 2: 3.7452 eV 331.04nm f=0.2117
62 → 67 -0.13596
63 → 67 -0.29941
64 → 67 0.18289
65 → 67 0.30255
66 → 67 0.50554
Excited State 3: 3.8696 eV 320.40nm f=0.0941
62 → 67 0.20835
63 → 67 0.41231
64 → 67 -0.27465
65 → 67 0.42459
66 → 67 0.13808
Excited State 4: 4.1575 eV 298.22nm f=0.0570
63 → 67 0.33705
64 → 67 0.59311
66 → 68 -0.12826
Excited State 5: 4.4609 eV 277.93nm f=0.0025
62 → 67 0.62257
63 → 67 -0.28244

***Z*-4a**

Excited State 1: 2.9091 eV 426.20nm f=0.0257
58 → 63 -0.13298
61 → 63 0.52276
62 → 63 -0.43970
Excited State 2: 3.7277 eV 332.60nm f=0.2175
59 → 63 -0.10753
61 → 63 0.41376
62 → 63 0.54454
Excited State 3: 4.0528 eV 305.92nm f=0.0824
60 → 63 0.68982
Excited State 4: 4.2268 eV 293.33nm f=0.0130
58 → 63 0.41314
59 → 63 0.51335
61 → 63 0.19904
Excited State 5: 4.5273 eV 273.86nm f=0.0026
58 → 63 0.51390
59 → 63 -0.44217
62 → 64 -0.12979

***Z*-4b**

Excited State 1: 2.9431 eV 421.26nm f=0.0238
62 → 67 -0.12706
65 → 67 0.56660
66 → 67 -0.38130
Excited State 2: 3.7027 eV 334.84nm f=0.2797
65 → 67 0.35856
66 → 67 0.58646
Excited State 3: 4.0635 eV 305.12nm f=0.0700
64 → 67 0.68700
Excited State 4: 4.2452 eV 292.06nm f=0.0092
62 → 67 -0.41436
63 → 67 0.51737
65 → 67 -0.18680
Excited State 5: 4.5649 eV 271.60nm f=0.0070
62 → 67 0.49434
63 → 67 0.43044
66 → 68 0.20038

***Z*-5a**

Excited State 1: 2.7763 eV 446.58nm f=0.0027
79 → 82 -0.32249
81 → 82 0.61634
Excited State 2: 3.4111 eV 363.47nm f=0.0062
76 → 82 -0.12120
77 → 82 0.16711
79 → 82 0.57463
81 → 82 0.34023
Excited State 3: 3.8261 eV 324.05nm f=0.2357
80 → 82 0.69231
Excited State 4: 4.1913 eV 295.82nm f=0.0902
78 → 82 0.67703
79 → 82 -0.11217
80 → 83 -0.11023
Excited State 5: 4.3389 eV 285.75nm f=0.0014
76 → 82 -0.39539
77 → 82 0.51513
78 → 82 -0.12039
79 → 82 -0.21113

***Z*-5b**

Excited State 1: 2.8035 eV 442.25nm f=0.0028

83 → 86 0.31892
85 → 86 0.61665
Excited State 2: 3.4378 eV 360.65nm f=0.0077
80 → 86 -0.10326
81 → 86 0.17390
83 → 86 0.57465
85 → 86 -0.33861
Excited State 3: 3.7793 eV 328.06nm f=0.2930
84 → 86 0.69271
Excited State 4: 4.1854 eV 296.23nm f=0.0709
82 → 86 0.66990
83 → 86 -0.12363
84 → 87 -0.13965
Excited State 5: 4.3648 eV 284.05nm f=0.0016
80 → 86 -0.34807
81 → 86 0.55078
82 → 86 -0.11773
83 → 86 -0.20414

***Z*-6a**

Excited State 1: 2.8592 eV 433.63nm f=0.0146
59 → 63 -0.26337
61 → 63 -0.27306
62 → 63 0.58986
Excited State 2: 3.7945 eV 326.74nm f=0.1491
59 → 63 0.45648
61 → 63 0.36654
62 → 63 0.37768
Excited State 3: 3.8974 eV 318.12nm f=0.0789
59 → 63 -0.44956
61 → 63 0.52641
Excited State 4: 4.1836 eV 296.36nm f=0.0817
60 → 63 0.68772
62 → 64 0.10163
Excited State 5: 4.5191 eV 274.36nm f=0.0614
58 → 63 -0.11478
58 → 66 0.11749
61 → 64 -0.13460
62 → 64 0.61897
62 → 65 -0.21872

***Z*-6b**

Excited State 1: 2.9074 eV 426.44nm f=0.0029
63 → 67 -0.26239
65 → 67 -0.28112
66 → 67 0.58515
Excited State 2: 3.8048 eV 325.86nm f=0.2831
63 → 67 0.14385
65 → 67 0.58697
66 → 67 0.34842
Excited State 3: 3.8765 eV 319.84nm f=0.0112
63 → 67 0.62575
65 → 67 -0.25220
66 → 67 0.16508
Excited State 4: 4.1937 eV 295.65nm f=0.0655
64 → 67 0.68533
65 → 68 0.11686
Excited State 5: 4.5432 eV 272.90nm f=0.0315
62 → 70 -0.12942
65 → 68 -0.21632
66 → 68 0.60704
66 → 69 -0.21206

***Z*-7a**

Excited State 1: 3.0232 eV 410.12nm f=0.0026
65 → 71 -0.12108
68 → 71 0.66278
69 → 70 -0.19638
Excited State 2: 3.1391 eV 394.97nm f=0.0000
68 → 71 0.19402
69 → 70 0.67426
Excited State 3: 3.3559 eV 369.45nm f=0.2962
68 → 70 0.66276
69 → 71 -0.23133
Excited State 4: 3.7389 eV 331.61nm f=0.0002
67 → 70 0.70497
Excited State 5: 3.8140 eV 325.07nm f=0.1674
68 → 70 0.22668
69 → 71 0.65813

***Z*-7b**

Excited State 1: 3.0077 eV 412.22nm f=0.0013

72 → 75 0.37937
73 → 74 0.58634
Excited State 2: 3.0791 eV 402.67nm f=0.0013
69 → 75 0.10401
72 → 75 0.57638
73 → 74 -0.38721
Excited State 3: 3.3202 eV 373.42nm f=0.2997
72 → 74 0.65670
73 → 75 0.24891
Excited State 4: 3.7029 eV 334.83nm f=0.0002
71 → 74 0.70502
Excited State 5: 3.7853 eV 327.54nm f=0.2179
72 → 74 -0.24475
73 → 75 0.65168

***Z*-8a**

Excited State 1: 2.9533 eV 419.81nm f=0.0088
73 → 78 -0.26245
75 → 77 0.16921
75 → 78 0.54117
76 → 77 0.12399
76 → 78 0.28447
Excited State 2: 3.5782 eV 346.50nm f=0.5115
75 → 77 0.23738
75 → 78 -0.28231
76 → 77 0.56279
76 → 78 0.19004
Excited State 3: 3.7124 eV 333.97nm f=0.1246
75 → 77 0.48906
75 → 78 -0.18732
76 → 77 -0.38906
76 → 78 0.25253
Excited State 4: 3.9209 eV 316.22nm f=0.2287
75 → 77 -0.38744
75 → 78 -0.12876
76 → 78 0.54787
Excited State 5: 4.1015 eV 302.29nm f=0.0078
69 → 78 0.15114
73 → 77 0.22151
73 → 78 0.58465
75 → 78 0.25721

***Z*-8b**

Excited State 1: 2.9820 eV 415.78nm f=0.0053
77 → 82 -0.26348
79 → 81 0.11065
79 → 82 0.62454
80 → 82 -0.11865
Excited State 2: 3.5396 eV 350.27nm f=0.4249
79 → 81 -0.34038
79 → 82 0.15227
80 → 81 0.52056
80 → 82 0.28431
Excited State 3: 3.6059 eV 343.84nm f=0.2033
79 → 81 0.41020
80 → 81 0.46602
80 → 82 -0.31391
Excited State 4: 3.9013 eV 317.80nm f=0.2742
79 → 81 0.42713
80 → 82 0.54179
Excited State 5: 4.1282 eV 300.33nm f=0.0563
77 → 82 0.22690
78 → 81 0.21395
78 → 82 0.59725
79 → 82 0.10297
80 → 83 0.10494

***Z*-9a**

Excited State 1: 2.9816 eV 415.83nm f=0.0279
74 → 79 -0.16347
76 → 79 0.30085
77 → 79 0.50585
78 → 79 0.34675
Excited State 2: 3.6255 eV 341.97nm f=0.2105
76 → 79 -0.12722
77 → 79 -0.31106
78 → 79 0.60687
Excited State 3: 3.8920 eV 318.56nm f=0.0937
76 → 79 0.61246
77 → 79 -0.33553
Excited State 4: 4.3307 eV 286.29nm f=0.0086
74 → 79 0.66274
77 → 79 0.15953
Excited State 5: 4.3655 eV 284.01nm f=0.0026

75 → 79 0.69749

***Z*-9b**

Excited State 1: 3.0545 eV 405.90nm f=0.0052
78 → 83 -0.16534
81 → 83 0.67239
82 → 83 -0.11539
Excited State 2: 3.6250 eV 342.02nm f=0.2977
81 → 83 0.11120
82 → 83 0.68799
Excited State 3: 3.9361 eV 314.99nm f=0.0854
80 → 83 0.69739
Excited State 4: 4.3522 eV 284.88nm f=0.0012
78 → 83 0.67364
81 → 83 0.16786
Excited State 5: 4.4396 eV 279.27nm f=0.0015
79 → 83 0.70493

***Z*-10a**

Excited State 1: 2.8995 eV 427.61nm f=0.0037
70 → 76 0.12286
71 → 76 0.26455
72 → 76 -0.15289
73 → 76 -0.21235
74 → 76 0.57860
Excited State 2: 3.5533 eV 348.93nm f=0.0449
73 → 76 -0.22014
75 → 76 0.66613
Excited State 3: 3.8093 eV 325.48nm f=0.1380
71 → 76 0.13894
72 → 76 -0.10385
73 → 76 0.62752
74 → 76 0.15469
75 → 76 0.19554
Excited State 4: 3.8313 eV 323.61nm f=0.0659
70 → 76 0.23559
71 → 76 0.45947
72 → 76 -0.28478
74 → 76 -0.36471
Excited State 5: 4.1232 eV 300.70nm f=0.0834
71 → 76 0.34476

72 → 76 0.60034

***Z*-10b**

Excited State 1: 2.9273 eV 423.54nm f=0.0039
74 → 80 0.11876
75 → 80 0.26609
76 → 80 0.13227
77 → 80 -0.26004
78 → 80 0.56300
Excited State 2: 3.5751 eV 346.80nm f=0.0830
77 → 80 -0.25858
78 → 80 -0.21727
79 → 80 0.61617
Excited State 3: 3.7887 eV 327.25nm f=0.2111
77 → 80 0.56055
78 → 80 0.25462
79 → 80 0.32051
Excited State 4: 3.8579 eV 321.38nm f=0.0139
74 → 80 0.22973
75 → 80 0.49772
76 → 80 0.28434
77 → 80 0.20593
78 → 80 -0.25530
Excited State 5: 4.1236 eV 300.67nm f=0.0663
75 → 80 -0.31231
76 → 80 0.61230

***Z*-11a**

Excited State 1: 3.0349 eV 408.53nm f=0.0025
87 → 91 0.11527
89 → 91 0.69223
Excited State 2: 3.7541 eV 330.26nm f=0.2412
89 → 93 -0.10163
90 → 91 0.69352
Excited State 3: 4.0632 eV 305.14nm f=0.0460
88 → 91 0.66574
90 → 92 0.21082
Excited State 4: 4.1706 eV 297.28nm f=0.1239
88 → 91 -0.21046
90 → 92 0.66695
Excited State 5: 4.2304 eV 293.08nm f=0.0147

89 → 92 0.69569

***Z*-11b**

Excited State 1: 3.0609 eV 405.05nm f=0.0026
91 → 95 0.11222
93 → 95 0.69157
Excited State 2: 3.7152 eV 333.72nm f=0.2982
93 → 97 -0.10808
94 → 95 0.69260
Excited State 3: 4.0439 eV 306.59nm f=0.0010
92 → 95 -0.45164
94 → 96 0.53340
Excited State 4: 4.1049 eV 302.04nm f=0.1584
92 → 95 0.52928
94 → 96 0.45550
Excited State 5: 4.2101 eV 294.50nm f=0.0135
93 → 96 0.69615

***Z*-12a**

Excited State 1: 2.8612 eV 433.32nm f=0.0186
70 → 75 0.16504
73 → 75 -0.40616
74 → 75 0.54377
Excited State 2: 3.8448 eV 322.47nm f=0.2180
70 → 75 -0.14276
73 → 75 0.52424
74 → 75 0.43819
Excited State 3: 4.1763 eV 296.87nm f=0.0063
70 → 75 0.61393
72 → 75 -0.22803
73 → 75 0.21337
Excited State 4: 4.3155 eV 287.30nm f=0.0365
70 → 75 0.20185
71 → 75 0.14439
72 → 75 0.63155
74 → 76 0.16685
Excited State 5: 4.5391 eV 273.15nm f=0.0034
70 → 75 -0.10837
71 → 75 0.67567

***Z*-12b**

Excited State 1: 2.9190 eV 424.75nm f=0.0031
74 → 79 0.16759
77 → 79 0.62842
78 → 79 0.25605
Excited State 2: 3.8199 eV 324.57nm f=0.2879
77 → 79 -0.25558
78 → 79 0.64791
Excited State 3: 4.1954 eV 295.52nm f=0.0008
74 → 79 0.66862
77 → 79 -0.17132
Excited State 4: 4.3404 eV 285.65nm f=0.0316
76 → 79 0.67171
78 → 80 0.16351
Excited State 5: 4.6068 eV 269.13nm f=0.0054
75 → 79 0.68819

***Z*-12c**

Excited State 1: 2.7944 eV 443.69nm f=0.0421
90 → 95 -0.13471
93 → 95 0.39272
94 → 95 0.55011
Excited State 2: 3.6953 eV 335.51nm f=0.2554
90 → 95 -0.13799
93 → 95 0.51848
94 → 95 -0.43388
Excited State 3: 4.1351 eV 299.83nm f=0.0143
88 → 95 0.14674
89 → 95 0.11387
90 → 95 -0.42987
92 → 95 0.45271
93 → 95 -0.23341
Excited State 4: 4.2274 eV 293.29nm f=0.0064
88 → 95 -0.14883
90 → 95 0.39425
91 → 95 -0.14569
92 → 95 0.47075
94 → 96 0.22444
Excited State 5: 4.4569 eV 278.18nm f=0.0068
91 → 95 0.67025
94 → 96 0.10121

***Z*-12d**

Excited State 1: 2.8557 eV 434.16nm f=0.0150
100 →107 0.16564
105 →107 -0.44280
106 →107 0.51283
Excited State 2: 3.7890 eV 327.22nm f=0.2684
100 →107 -0.11428
105 →107 0.50125
106 →107 0.47222
Excited State 3: 4.1478 eV 298.92nm f=0.0044
100 →107 0.59202
102 →107 -0.21923
103 →107 0.20593
105 →107 0.17476
Excited State 4: 4.2890 eV 289.08nm f=0.0250
100 →107 0.10907
101 →107 0.10851
102 →107 0.49712
103 →107 0.28043
104 →107 0.34001
106 →108 0.15249
Excited State 5: 4.3756 eV 283.36nm f=0.0011
100 →107 -0.24341
102 →107 -0.18170
103 →107 0.60572
104 →107 -0.10464

8. Computational PSS Analysis

The code to generate a GUI based on Matlab code to automatise the PSS analysis is here reported. The code uses scripts downloaded from the Mathworks File Exchange (grep.m[2] and lorentzfit.m[3]) The computed spectra used for the PSS analysis were plotted using a Lorentzian function instead of a Gaussian, having found the former was giving better results than the latter. The general formula for the Lorentzian fit that was applied is the following one:

$$y(\lambda) = \sum_{i=1}^{n} y_i(\lambda) = \sum_{i=1}^{n} \left[\frac{f_i}{1 + \left(\frac{\lambda - \lambda_i}{h} \right)} \right]$$

Where f_i is the oscillator strength computed for each transition by the TD-DFT calculation and λ_i the wavelength associated to it. h represents the half of the full width at half maximum (FWHM) value (in nm) for the Lorentzian curve. This value was obtained fitting the experimental ππ* transition of the *E*-isomer with a Lorentzian function. The value for the amount of *Z*-form (Z_{PSS}) present in the PSS is obtained using the following equation:

$$Z_{PSS} = \frac{\frac{A_{PSS}}{A_{Eexp}} - 1}{\frac{f_{Zcalc}}{f_{Ecalc}} - 1}$$

Where A_{Eexp} is the value of the absorbance for the peak of the ππ* band found in the experimental spectrum of the *E*- isomer. A_{PSS} is the absorbance registered in the spectrum of the photostationary state at the same wavelength corresponding to A_{Eexp} in the experimental spectrum of the *E*- form. f_{Ecalc} is the oscillator strength corresponding to the maximum of the ππ* band after the Lorentzian fit, while f_{Zcalc} is the value corresponding to the oscillator strength of the calculated *Z*- spectrum at the same wavelength where f_{Ecalc} was found. (In the following figure the PSS calculation for **1b** is depicted. The experimental data are on the left side, while the computed ones on the right. The GUI furnishes the Z_{PSS} and not the percentage, that is $100 \cdot Z_{PSS}$, contrary to what is written on the GUI itself).

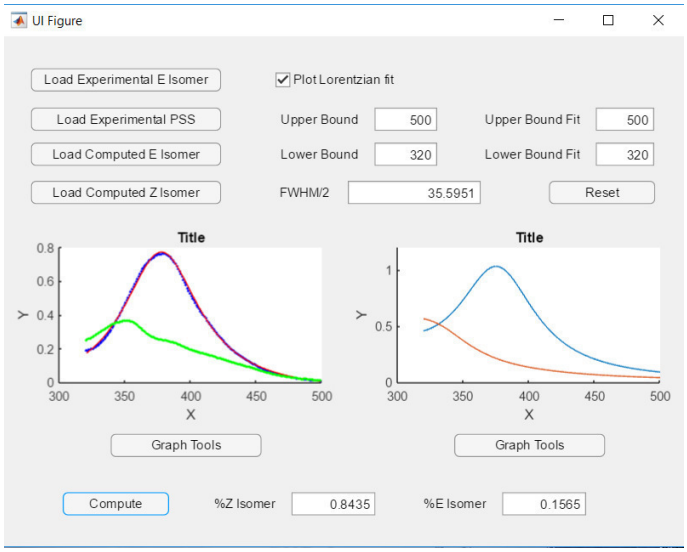

[2] https://www.mathworks.com/matlabcentral/fileexchange/9647-grep--a-pedestrian--very-fast-grep-utility
[3] https://www.mathworks.com/matlabcentral/fileexchange/33775-lorentzfit-x-y-varargin-

```
classdef app < matlab.apps.AppBase

    % Properties that correspond to app components
    properties (Access = public)
        UIFigure                    matlab.ui.Figure
        LoadExperimentalEIsomerButton  matlab.ui.control.Button
        LoadExperimentalPSSButton      matlab.ui.control.Button
        UIAxes                      matlab.ui.control.UIAxes
        UIAxes2                     matlab.ui.control.UIAxes
        LoadComputedEIsomerButton      matlab.ui.control.Button
        LoadComputedZIsomerButton      matlab.ui.control.Button
        UpperBoundEditFieldLabel       matlab.ui.control.Label
        UpperBoundEditField            matlab.ui.control.NumericEditField
        LowerBoundEditFieldLabel       matlab.ui.control.Label
        LowerBoundEditField            matlab.ui.control.NumericEditField
        PlotLorentzianfitCheckBox      matlab.ui.control.CheckBox
        ComputeButton                  matlab.ui.control.Button
        ZIsomerEditFieldLabel          matlab.ui.control.Label
        ZIsomerEditField               matlab.ui.control.NumericEditField
        EIsomerEditFieldLabel          matlab.ui.control.Label
        EIsomerEditField               matlab.ui.control.NumericEditField
        FWHM2EditFieldLabel            matlab.ui.control.Label
        FWHM2EditField                 matlab.ui.control.NumericEditField
        GraphToolsButton               matlab.ui.control.StateButton
        UpperBoundFitEditFieldLabel    matlab.ui.control.Label
        UpperBoundFitEditField         matlab.ui.control.NumericEditField
        LowerBoundFitEditFieldLabel    matlab.ui.control.Label
        LowerBoundFitEditField         matlab.ui.control.NumericEditField
        GraphToolsButton_2             matlab.ui.control.StateButton
        ResetButton                    matlab.ui.control.Button
    end


    properties (Access = public)
        Property
        %variables x&y from files
        x = [];
        y = [];

        %relevant data
        NormaExp = 0;
        TexpPeak = 0;
        indexPeak = 0;
        graphfit = [];
        valPhoto = 0;
        Norma = 0;
        tPeak = 0;
        cPeak = 0;
```

```
    indexComputedPeak = 0;

    %checks "Lorentzian fit" is selected
    Check = 0;

    %variables used to plot data using GraphTool buttons
    hlp1=[];
    hlp2=[];
    plt1=[];
    plt2=[];
    plt3=[];
    plt4=[];
    plt5=[];
    plt6=[];
    plt7=[];
    plt8=[];
    pltpss1=[];
    pltpss2=[];
    logic1=false;
    logic2=false;
    logicpss=false;
    logic3=false;
    logic4=false;

end


methods (Access = private)

    % Button pushed function: LoadExperimentalEIsomerButton
    function LoadExperimentalEIsomerButtonPushed(app, event)
        %clear variables
        app.hlp1=[];
        app.hlp2=[];
        app.plt1=[];
        app.plt2=[];
        app.plt3=[];
        app.plt4=[];
        app.x=[];
        app.y=[];
        %get file
        filter = {'*.txt';'*.*'}k;
        TextName = uigetfile(filter);
        [nmvalue_exp,f_exp] = textread(TextName, '%f %f');
        %nmvalue_exp: wavelenght - array
        %f_exp : osc. stregth - array
        Lbound = app.LowerBoundEditField.Value;
        Ubound = app.UpperBoundEditField.Value;
```

```
[rows,~] = size(f_exp);
index = 1;
app.hlp1=app.x;
app.hlp2=app.y;
%select bounds
   if Lbound < Ubound
      while index < rows +1
         if nmvalue_exp(index) < Ubound
            if nmvalue_exp(index) > Lbound
               app.x = [app.x,nmvalue_exp(index)];
               app.y = [app.y,f_exp(index)];
            end
         end
      index = index + 1;
      end
      %save relevant data and plot
      app.NormaExp = max(app.y);
      app.TexpPeak = max(app.y);
      app.indexPeak = find(app.y==app.TexpPeak);
      plot(app.UIAxes,app.x,app.y,'b.');
   end
   %save data for GraphTool
   app.plt1 = app.x;
   app.plt2 = app.y;
   app.logic1=true;

   %Lorentzian fit:
   if app.Check == 1
       %bounds for Lorentzian fit
       Lfitbound = app.LowerBoundFitEditField.Value;
       Ufitbound = app.UpperBoundFitEditField.Value;
       index = 1;
          if Lfitbound < Ufitbound
          while index < rows +1
             if nmvalue_exp(index) < Ufitbound
                if nmvalue_exp(index) > Lfitbound
                   app.hlp1 = [app.hlp1,nmvalue_exp(index)];
                   app.hlp2 = [app.hlp2,f_exp(index)];
                end
             end
          index = index + 1;
          end
      %using lorentzfit.m
      [app.graphfit param resnorm residual] = lorentzfit(app.hlp1,app.hlp2);
      app.FWHM2EditField.Value = sqrt(param(3));
      %plot fit
      hold(app.UIAxes);
      plot(app.UIAxes,app.hlp1,app.graphfit,'r-');
```

```
        hold(app.UIAxes,'off');
        end
    %save data for GraphTool
    app.plt3=app.hlp1;
    app.plt4=app.graphfit;
    app.logic2=true;
    end
end

% Button pushed function: LoadExperimentalPSSButton
function LoadExperimentalPSSButtonPushed(app, event)
  %clear variables
  app.Check = 0;
  app.pltpss1=[];
  app.pltpss2=[];
  app.hlp1=[];
  app.hlp2=[];
  app.x=[];
  app.y=[];
  %get file
  filter = {'*.txt';'*.*'};
  TextName = uigetfile(filter);
  [nmvalue_exp,f_exp] = textread(TextName, '%f %f');
  %nmvalue_exp: wavelenght - array
  %f_exp : osc. stregth - array
  Lbound = app.LowerBoundEditField.Value;
  Ubound = app.UpperBoundEditField.Value;
  [rows,~] = size(f_exp);
  index = 1;
  %bounds check
    if Lbound < Ubound
      while index < rows +1
        if nmvalue_exp(index) < Ubound
          if nmvalue_exp(index) > Lbound
            app.x = [app.x,nmvalue_exp(index)];
            app.y = [app.y,f_exp(index)];
          end
        end
      index = index + 1;
      end
      %save relevant data and plot
      app.valPhoto = app.y(app.indexPeak);
      hold(app.UIAxes);
      plot(app.UIAxes,app.x,app.y,'g.','LineWidth',2);
      hold(app.UIAxes,'off');
    end
        %save data for GraphTool
   app.pltpss1=app.x;
```

```
        app.pltpss2=app.y;
          app.logicpss=true;
    end

    % Button pushed function: LoadComputedEIsomerButton
    function LoadComputedEIsomerButtonPushed(app, event)
      %clear variables
      app.Check = 0;
      app.hlp1=[];
      app.hlp2=[];
      app.plt5=[];
      app.plt6=[];
      app.x=[];
      app.y=[];
      %get file
      filter = {'*.out';'*.log';'*.*'};
      FileName = uigetfile(filter);
      %diary: saves output lines
      diary on;
      diary(['GongBao_diary_',datestr(now,'dd-mm-yy','local'),'_',datestr(now,'hh-MM-
ss','local'),'.txt']);
      %using grep.m for parsing
      grep('Excited State',FileName);
      diary off;
      d=dir('*.txt');
      dates=[d.datenum];
      [~,newestIndex] = max(dates);
      %picks newest .txt file generated in the directory
      %it should be the one generated using GongBao.m
      New_File = d(newestIndex);
      Newest=New_File.name;
      %gets oscillator strength and wavelength:
      [~,~,~,~,~,~,~,~,nmvalue,~,f,~] = textread(Newest,'%s %s %s %s %s %s %s %s %f %s
f=%f %s');
      %nmvalue: wavelenght - array
      %f : osc. stregth - array
      [rows,~] = size(f)
      %bounds check
        Lbound = app.LowerBoundEditField.Value;
        Ubound = app.UpperBoundEditField.Value;
        if Lbound < Ubound
        app.x = Lbound:Ubound;
        index = 1;
        app.y = 0;
        %calculate spectrum
        while index < rows +1
          A = f(index)./(1+((app.x-nmvalue(index))./(app.FWHM2EditField.Value)).^2);
          app.y=app.y+A;
```

```
            index=index+1;
        end
        %save relevant data and plot
        app.Norma = max(app.y);
        app.tPeak = max(app.y);
        app.indexComputedPeak = find(app.y==app.tPeak);
        plot(app.UIAxes2,app.x,app.y);
        %save data for GraphTool
        app.plt5=app.x;
        app.plt6=app.y;
        app.logic3=true;
        end
    end

    % Button pushed function: LoadComputedZIsomerButton
    function LoadComputedZIsomerButtonPushed(app, event)
        %clear variables
        app.Check = 0;
        app.hlp1=[];
        app.hlp2=[];
        app.plt7=[];
        app.plt8=[];
        app.x=[];
        app.y=[];
        %get file
        filter = {'*.out';'*.log';'*.*'};
        FileName = uigetfile(filter);
        %diary: saves output lines
        diary on;
        diary(['GongBao_diary_',datestr(now,'dd-mm-yy','local'),'_',datestr(now,'hh-MM-
ss','local'),'.txt']);
        %using grep.m for parsing
        grep('Excited State',FileName);
        diary off;
        d=dir('*.txt');
        dates=[d.datenum];
        [~,newestIndex] = max(dates);
        %picks newest .txt file generated in the directory
        %it should be the one just generated using GongBao.m
        New_File = d(newestIndex);
        Newest=New_File.name;
        %gets oscillator strength and wavelength:
        [~,~,~,~,~,~,~,~,nmvalue,~,f,~] = textread(Newest,'%s %s %s %s %s %s %s %s %f %s
f=%f %s');
        %nmvalue: wavelenght - array
        %f : osc. stregth - array
        [rows,~] = size(f);
        %bounds check
```

```
            Lbound = app.LowerBoundEditField.Value;
            Ubound = app.UpperBoundEditField.Value;
            if Lbound < Ubound
            app.x = Lbound:Ubound;
            index = 1;
            app.y = 0;
            %calculate spectrum
            while index < rows +1
               A = f(index)./(1+((app.x-nmvalue(index))./(app.FWHM2EditField.Value)).^2);
               app.y=app.y+A;
               index=index+1;
            end
            %save relevant data and plot
            app.cPeak = app.y(app.indexComputedPeak);
            hold(app.UIAxes2);
            plot(app.UIAxes2,app.x,app.y);
            hold(app.UIAxes2,'off');
            end
            %save data for GraphTool
            app.plt7=app.x;
            app.plt8=app.y;
            app.logic4=true;
        end

        % Value changed function: PlotLorentzianfitCheckBox
        function PlotLorentzianfitCheckBoxValueChanged(app, event)
            %Allows Lorentzian Fit using Load Experimental E Isomer Button
            cla(app.UIAxes);
            app.Check = 1;
        end

        % Button pushed function: ComputeButton
        function ComputeButtonPushed(app, event)
            %calculate percentages of isomers
            app.ZIsomerEditField.Value = ((app.valPhoto/app.NormaExp)-
1)/((app.cPeak/app.Norma)-1);
            app.EIsomerEditField.Value = 1 - app.ZIsomerEditField.Value;
        end

        % Value changed function: GraphToolsButton
        function GraphToolsButtonValueChanged(app, event)
            %plots relevant data externally, allowing to modify the plot
            if (app.logic1==true) && (app.logic2==true) && (app.logicpss==true)
            plot(app.plt1,app.plt2,'b.');
            hold on
            plot(app.plt3,app.plt4,'-r');
            plot(app.pltpss1,app.pltpss2, 'g.');
            hold off
```

```
    elseif (app.logic1==true)
    plot(app.plt1,app.plt2,'b.');

    elseif (app.logicpss==true)
    plot(app.pltpss1,app.pltpss2,'g.');
    end

end

% Value changed function: GraphToolsButton_2
function GraphToolsButton_2ValueChanged(app, event)
    %plots relevant data externally, allowing to modify the plot
    if (app.logic3==true) && (app.logic4==true)
    plot(app.plt5,app.plt6,'-b');
    hold on
    plot(app.plt7,app.plt8,'-r');
    hold off
    elseif (app.logic3==true)
    plot(app.plt5,app.plt6,'-b');
    elseif (app.logic4==true)
    plot(app.plt7,app.plt8,'-r');
    end


end

% Button pushed function: ResetButton
function ResetButtonPushed(app, event)
%clear everything
cla(app.UIAxes);
cla(app.UIAxes2);
app.x = [];
app.y = [];
app.NormaExp = 0;
app.TexpPeak = 0;
app.indexPeak = 0;
app.graphfit = [];
app.valPhoto = 0;
app.Norma = 0;
app.tPeak = 0;
app.cPeak = 0;
app.indexComputedPeak = 0;
app.Check = 0;
app.hlp1=[];
app.hlp2=[];
app.plt1=[];
app.plt2=[];
```

```
        app.plt3=[];
        app.plt4=[];
        app.plt5=[];
        app.plt6=[];
        app.plt7=[];
        app.plt8=[];
        app.pltpss1=[];
        app.pltpss2=[];
        app.logic1=false;
        app.logic2=false;
        app.logicpss=false;
        app.logic3=false;
        app.logic4=false;
        end
    end

    % App initialization and construction
    methods (Access = private)

        % Create UIFigure and components
        function createComponents(app)

            % Create UIFigure
            app.UIFigure = uifigure;
            app.UIFigure.Position = [100 100 640 480];
            app.UIFigure.Name = 'UI Figure';

            % Create LoadExperimentalEIsomerButton
            app.LoadExperimentalEIsomerButton = uibutton(app.UIFigure, 'push');
            app.LoadExperimentalEIsomerButton.ButtonPushedFcn = createCallbackFcn(app,
@LoadExperimentalEIsomerButtonPushed, true);
            app.LoadExperimentalEIsomerButton.Position = [27 429 179 22];
            app.LoadExperimentalEIsomerButton.Text = 'Load Experimental E Isomer';

            % Create LoadExperimentalPSSButton
            app.LoadExperimentalPSSButton = uibutton(app.UIFigure, 'push');
            app.LoadExperimentalPSSButton.ButtonPushedFcn = createCallbackFcn(app,
@LoadExperimentalPSSButtonPushed, true);
            app.LoadExperimentalPSSButton.Position = [27 392 179 22];
            app.LoadExperimentalPSSButton.Text = 'Load Experimental PSS';

            % Create UIAxes
            app.UIAxes = uiaxes(app.UIFigure);
            title(app.UIAxes, 'Title')
            xlabel(app.UIAxes, 'X')
            ylabel(app.UIAxes, 'Y')
            app.UIAxes.Position = [11 118 300 185];
```

```
        % Create UIAxes2
        app.UIAxes2 = uiaxes(app.UIFigure);
        title(app.UIAxes2, 'Title')
        xlabel(app.UIAxes2, 'X')
        ylabel(app.UIAxes2, 'Y')
        app.UIAxes2.Position = [329 118 300 185];

        % Create LoadComputedEIsomerButton
        app.LoadComputedEIsomerButton = uibutton(app.UIFigure, 'push');
        app.LoadComputedEIsomerButton.ButtonPushedFcn = createCallbackFcn(app,
@LoadComputedEIsomerButtonPushed, true);
        app.LoadComputedEIsomerButton.Position = [27 359 179 22];
        app.LoadComputedEIsomerButton.Text = 'Load Computed E Isomer';

        % Create LoadComputedZIsomerButton
        app.LoadComputedZIsomerButton = uibutton(app.UIFigure, 'push');
        app.LoadComputedZIsomerButton.ButtonPushedFcn = createCallbackFcn(app,
@LoadComputedZIsomerButtonPushed, true);
        app.LoadComputedZIsomerButton.Position = [27 323 179 22];
        app.LoadComputedZIsomerButton.Text = 'Load Computed Z Isomer';

        % Create UpperBoundEditFieldLabel
        app.UpperBoundEditFieldLabel = uilabel(app.UIFigure);
        app.UpperBoundEditFieldLabel.HorizontalAlignment = 'right';
        app.UpperBoundEditFieldLabel.Position = [257 396 78 15];
        app.UpperBoundEditFieldLabel.Text = 'Upper Bound';

        % Create UpperBoundEditField
        app.UpperBoundEditField = uieditfield(app.UIFigure, 'numeric');
        app.UpperBoundEditField.Position = [350 392 59 22];
        app.UpperBoundEditField.Value = 500;

        % Create LowerBoundEditFieldLabel
        app.LowerBoundEditFieldLabel = uilabel(app.UIFigure);
        app.LowerBoundEditFieldLabel.HorizontalAlignment = 'right';
        app.LowerBoundEditFieldLabel.Position = [257 363 78 15];
        app.LowerBoundEditFieldLabel.Text = 'Lower Bound';

        % Create LowerBoundEditField
        app.LowerBoundEditField = uieditfield(app.UIFigure, 'numeric');
        app.LowerBoundEditField.Position = [350 359 59 22];
        app.LowerBoundEditField.Value = 320;

        % Create PlotLorentzianfitCheckBox
        app.PlotLorentzianfitCheckBox = uicheckbox(app.UIFigure);
        app.PlotLorentzianfitCheckBox.ValueChangedFcn = createCallbackFcn(app,
@PlotLorentzianfitCheckBoxValueChanged, true);
        app.PlotLorentzianfitCheckBox.Text = 'Plot Lorentzian fit';
```

```
        app.PlotLorentzianfitCheckBox.Position = [257 433 115 15];

        % Create ComputeButton
        app.ComputeButton = uibutton(app.UIFigure, 'push');
        app.ComputeButton.ButtonPushedFcn = createCallbackFcn(app,
@ComputeButtonPushed, true);
        app.ComputeButton.Position = [57 30 100 22];
        app.ComputeButton.Text = 'Compute';

        % Create ZIsomerEditFieldLabel
        app.ZIsomerEditFieldLabel = uilabel(app.UIFigure);
        app.ZIsomerEditFieldLabel.HorizontalAlignment = 'right';
        app.ZIsomerEditFieldLabel.Position = [192 34 65 15];
        app.ZIsomerEditFieldLabel.Text = '%Z Isomer';

        % Create ZIsomerEditField
        app.ZIsomerEditField = uieditfield(app.UIFigure, 'numeric');
        app.ZIsomerEditField.Position = [272 30 79 22];

        % Create EIsomerEditFieldLabel
        app.EIsomerEditFieldLabel = uilabel(app.UIFigure);
        app.EIsomerEditFieldLabel.HorizontalAlignment = 'right';
        app.EIsomerEditFieldLabel.Position = [389 34 66 15];
        app.EIsomerEditFieldLabel.Text = '%E Isomer';

        % Create EIsomerEditField
        app.EIsomerEditField = uieditfield(app.UIFigure, 'numeric');
        app.EIsomerEditField.Position = [470 30 79 22];

        % Create FWHM2EditFieldLabel
        app.FWHM2EditFieldLabel = uilabel(app.UIFigure);
        app.FWHM2EditFieldLabel.HorizontalAlignment = 'right';
        app.FWHM2EditFieldLabel.Position = [257 327 51 15];
        app.FWHM2EditFieldLabel.Text = 'FWHM/2';

        % Create FWHM2EditField
        app.FWHM2EditField = uieditfield(app.UIFigure, 'numeric');
        app.FWHM2EditField.ValueDisplayFormat = '%.4f';
        app.FWHM2EditField.Position = [325 323 125 22];

        % Create GraphToolsButton
        app.GraphToolsButton = uibutton(app.UIFigure, 'state');
        app.GraphToolsButton.ValueChangedFcn = createCallbackFcn(app,
@GraphToolsButtonValueChanged, true);
        app.GraphToolsButton.Text = 'Graph Tools';
        app.GraphToolsButton.Position = [102 85 142 22];

        % Create UpperBoundFitEditFieldLabel
```

```
            app.UpperBoundFitEditFieldLabel = uilabel(app.UIFigure);
            app.UpperBoundFitEditFieldLabel.HorizontalAlignment = 'right';
            app.UpperBoundFitEditFieldLabel.Position = [449 396 94 15];
            app.UpperBoundFitEditFieldLabel.Text = 'Upper Bound Fit';

            % Create UpperBoundFitEditField
            app.UpperBoundFitEditField = uieditfield(app.UIFigure, 'numeric');
            app.UpperBoundFitEditField.Position = [558 392 55 22];
            app.UpperBoundFitEditField.Value = 500;

            % Create LowerBoundFitEditFieldLabel
            app.LowerBoundFitEditFieldLabel = uilabel(app.UIFigure);
            app.LowerBoundFitEditFieldLabel.HorizontalAlignment = 'right';
            app.LowerBoundFitEditFieldLabel.Position = [449 363 94 15];
            app.LowerBoundFitEditFieldLabel.Text = 'Lower Bound Fit';

            % Create LowerBoundFitEditField
            app.LowerBoundFitEditField = uieditfield(app.UIFigure, 'numeric');
            app.LowerBoundFitEditField.Position = [558 359 55 22];
            app.LowerBoundFitEditField.Value = 320;

            % Create GraphToolsButton_2
            app.GraphToolsButton_2 = uibutton(app.UIFigure, 'state');
            app.GraphToolsButton_2.ValueChangedFcn = createCallbackFcn(app,
@GraphToolsButton_2ValueChanged, true);
            app.GraphToolsButton_2.Text = 'Graph Tools';
            app.GraphToolsButton_2.Position = [425 85 142 22];

            % Create ResetButton
            app.ResetButton = uibutton(app.UIFigure, 'push');
            app.ResetButton.ButtonPushedFcn = createCallbackFcn(app, @ResetButtonPushed,
true);
            app.ResetButton.Position = [514 323 100 22];
            app.ResetButton.Text = 'Reset';
        end
    end

    methods (Access = public)

        % Construct app
        function app = app

            % Create and configure components
            createComponents(app)

            % Register the app with App Designer
            registerApp(app, app.UIFigure)
```

```
        if nargout == 0
            clear app
        end
    end

    % Code that executes before app deletion
    function delete(app)

        % Delete UIFigure when app is deleted
        delete(app.UIFigure)
    end
  end
end
```

10. References

1. Albar, H. A.; Shawali, A. S.; Abdaliah, M. A., Substituent effects on azo coupling of indoles. *Canadian Journal of Chemistry* **1993**, *71*, 2144-2149.
2. Simeth, N. A.; Crespi, S.; Fagnoni, M.; König, B., Tuning the Thermal Isomerization of Phenylazoindole Photoswitches from Days to Nanoseconds. *Journal of the American Chemical Society* **2018**, *140*, 2940-2946.
3. Dolomanov, O. V.; Bourhis, L. J.; Gildea, R. J.; Howard, J. A. K.; Puschmann, H., OLEX2: a complete structure solution, refinement and analysis program. *Journal of Applied Crystallography* **2009**, *42*, 339-341.
4. Sheldrick, G. M., Crystal structure refinement with SHELXL. *Acta Crystallographica. Section C, Structural Chemistry* **2015**, *71*, 3-8.
5. Sheldrick, G., SHELXT - Integrated space-group and crystal-structure determination. *Acta Crystallographica Section A* **2015**, *71*, 3-8.
6. Frisch, M. J.; Trucks, G. W.; Schlegel, H. B.; Scuseria, G. E.; Robb, M. A.; Cheeseman, J. R.; Scalmani, G.; Barone, V.; Petersson, G. A.; Nakatsuji, H.; Li, X.; Caricato, M.; Marenich, A. V.; Bloino, J.; Janesko, B. G.; Gomperts, R.; Mennucci, B.; Hratchian, H. P.; Ortiz, J. V.; Izmaylov, A. F.; Sonnenberg, J. L.; Williams; Ding, F.; Lipparini, F.; Egidi, F.; Goings, J.; Peng, B.; Petrone, A.; Henderson, T.; Ranasinghe, D.; Zakrzewski, V. G.; Gao, J.; Rega, N.; Zheng, G.; Liang, W.; Hada, M.; Ehara, M.; Toyota, K.; Fukuda, R.; Hasegawa, J.; Ishida, M.; Nakajima, T.; Honda, Y.; Kitao, O.; Nakai, H.; Vreven, T.; Throssell, K.; Montgomery Jr., J. A.; Peralta, J. E.; Ogliaro, F.; Bearpark, M. J.; Heyd, J. J.; Brothers, E. N.; Kudin, K. N.; Staroverov, V. N.; Keith, T. A.; Kobayashi, R.; Normand, J.; Raghavachari, K.; Rendell, A. P.; Burant, J. C.; Iyengar, S. S.; Tomasi, J.; Cossi, M.; Millam, J. M.; Klene, M.; Adamo, C.; Cammi, R.; Ochterski, J. W.; Martin, R. L.; Morokuma, K.; Farkas, O.; Foresman, J. B.; Fox, D. J. *Gaussian 16 Rev. B.01*, Wallingford, CT, 2016.

A.II.1. Photochromic Coenzyme Q Derivatives: Switching Redox Potentials with Light

Contents

1. UV/Vis Spectroscopy: Further spectra

Compound **1a**^{o}

- Compound **1a**^{o} in toluene

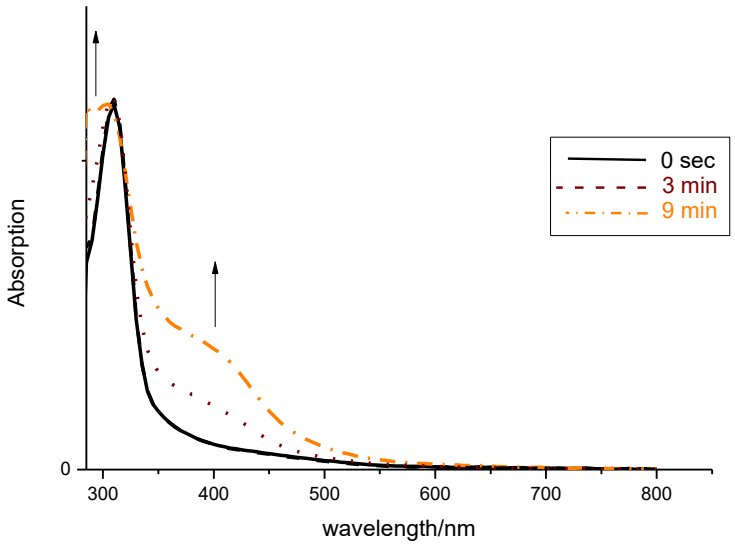

- Compound **1a**^{o} in DCM

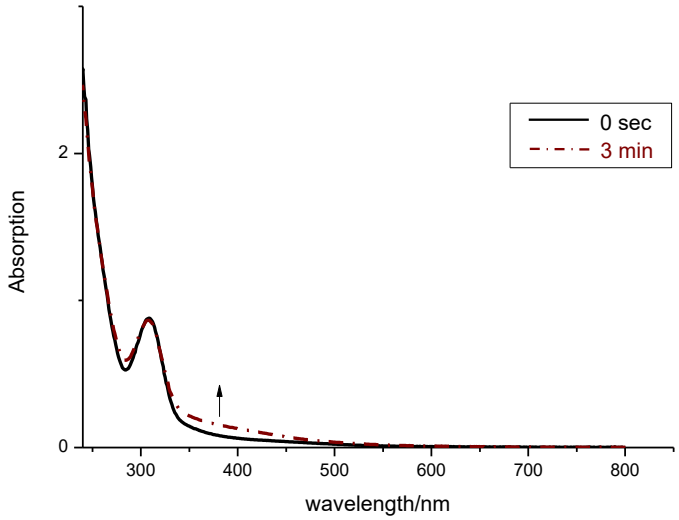

Compound **1b**^{o}

Table A1: Overview of spectroscopic properties of compound **1b**^{o} determined by UV/Vis spectroscopy and analytical HPLC.

Solvent	λ_{max} 1b^{o} [nm]	λ_{max} 1b^{c} [nm]	PSS [%]
MeCN	247, 297	307, 415, 582	20
DMSO	302	304, 410, 594	52
Toluene	298	296, 413, 580	47
Dioxane	301	294, 399, 595	42

- Compound **1b**^{o} in DMSO, fatigue resistance

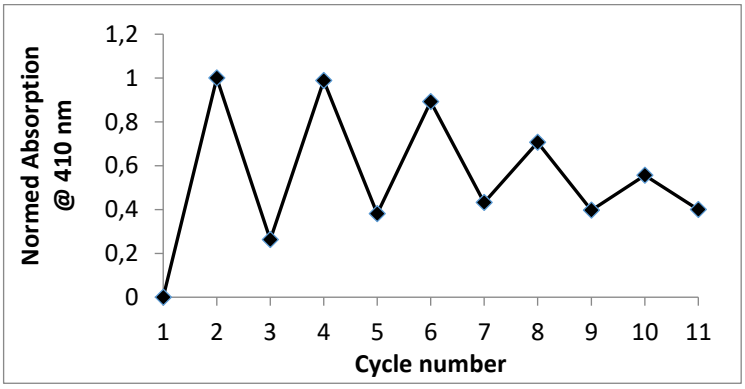

- Compound **1b**^{o} in toluene

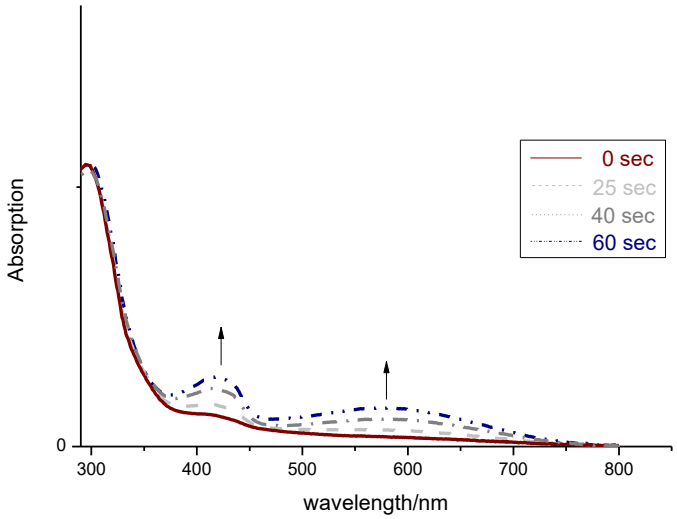

- Compound **1b**^{o} in MeCN

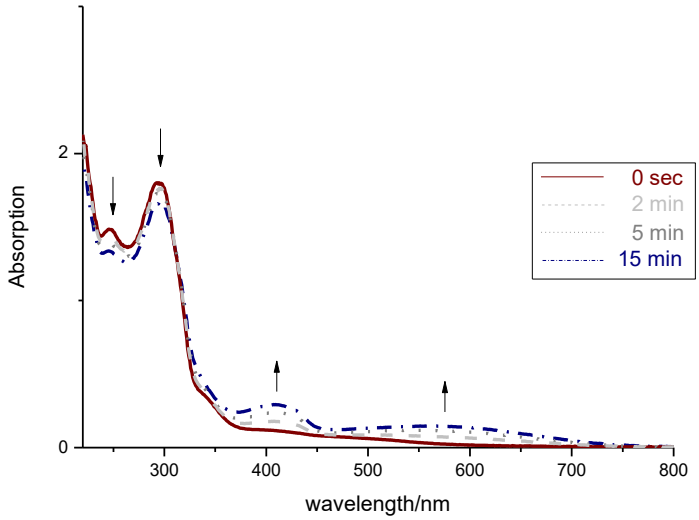

- Compound **1b**^{o} in toluene

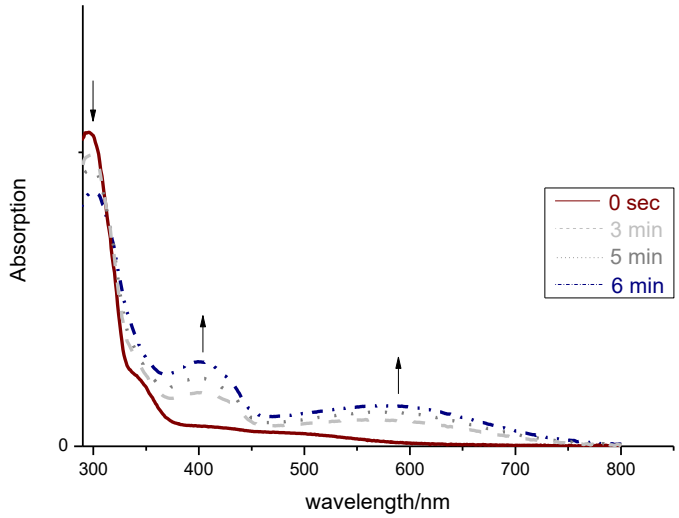

- Compound **1b**^{o} in toluene, fatigue resistance

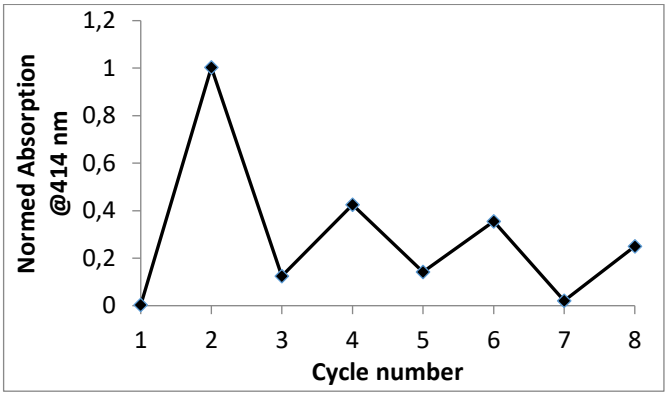

- Extinction coefficients

Compound	Solvent	Extinction coefficient [L/(mol*cm)]
1b^{a}	DMSO	ε_{300} = 582
1b^{a}	MeCN	ε_{296} =2539
1b^{c}	MeCN	ε_{579} =4928

2. Cyclic Voltammery and Spectroelectrochemical Studies (further material)

Molecules included in the study:

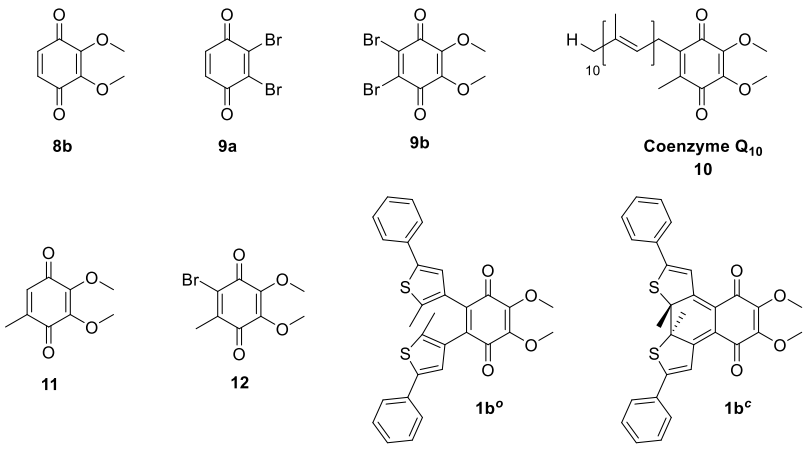

4.1. Compound **1b^o**

- Cyclic Voltammetry

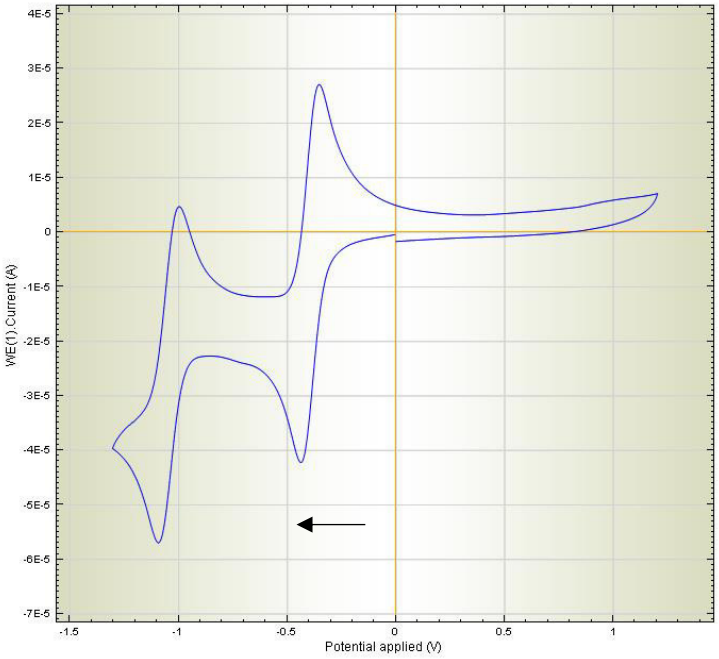

- Spectroelectrochemical studies

Peak 1

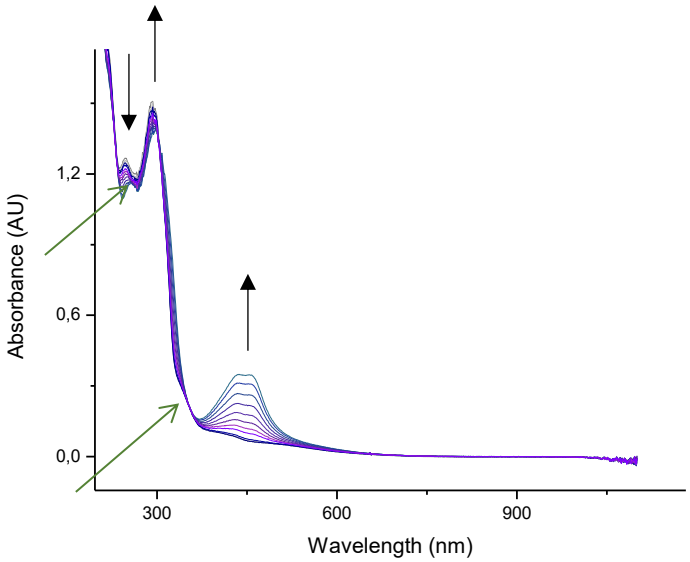

Peak 2

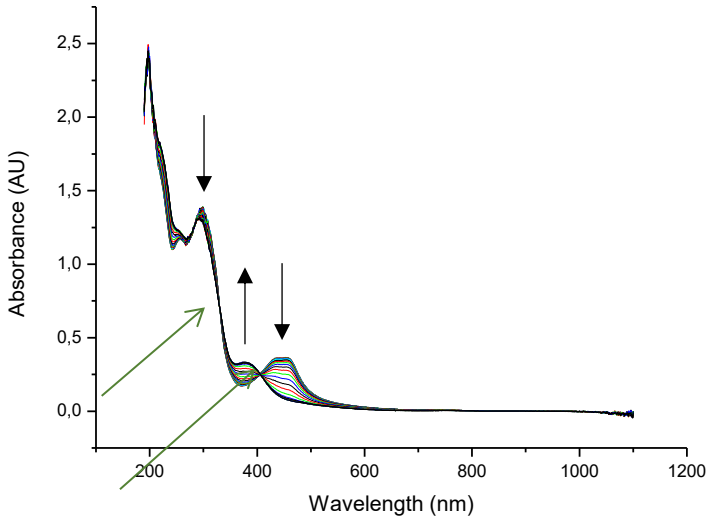

Peak 2 (invers)

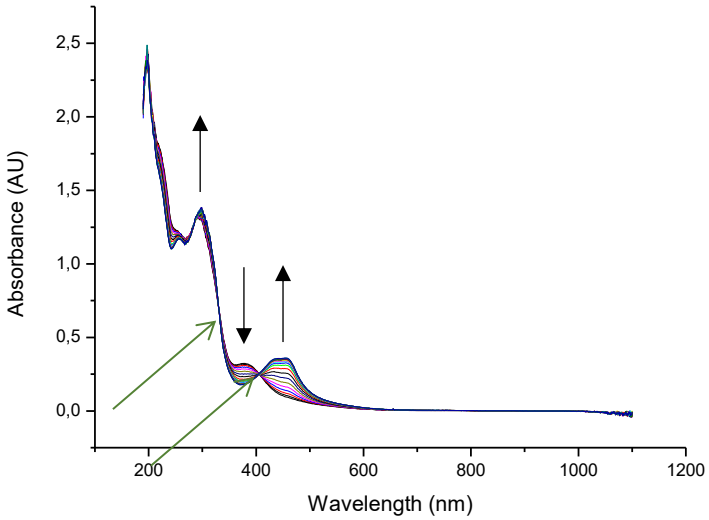

Peak 1 (invers)

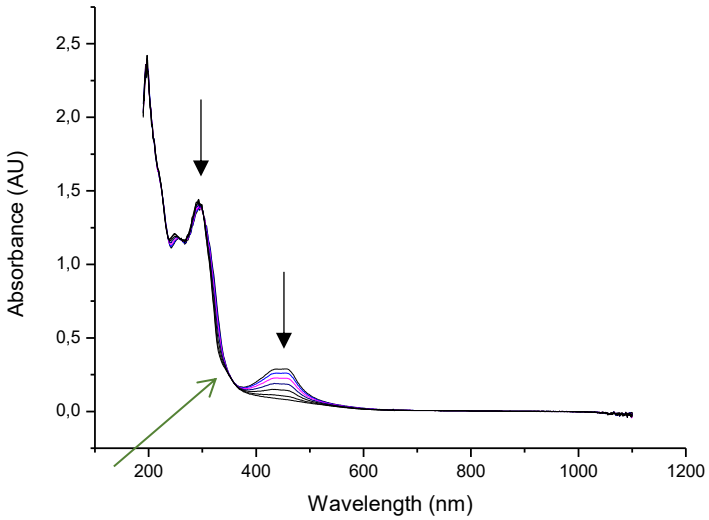

- Difference Spectra

Peak 1

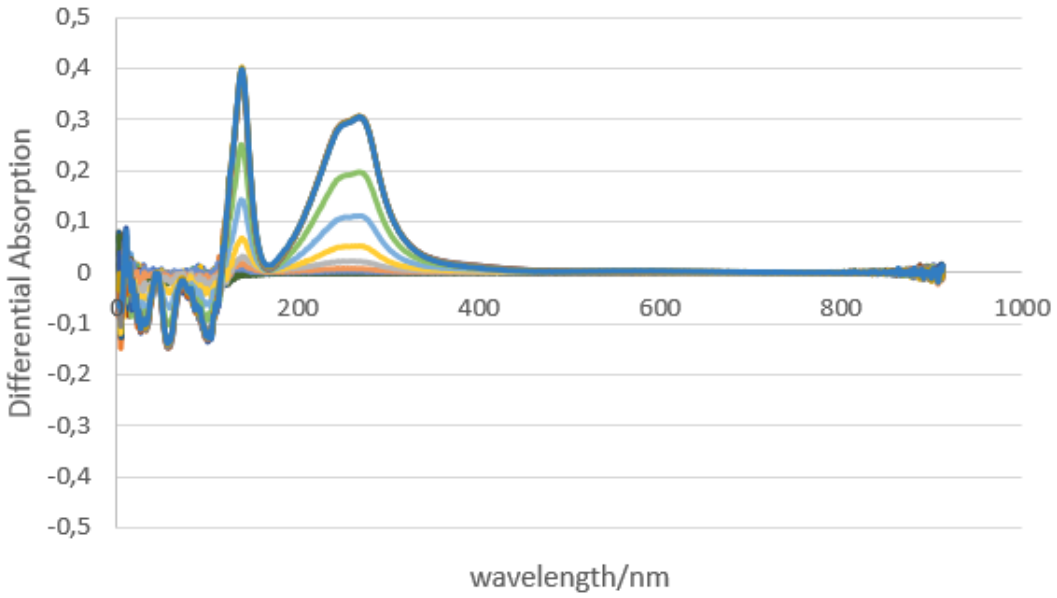

Peak 2

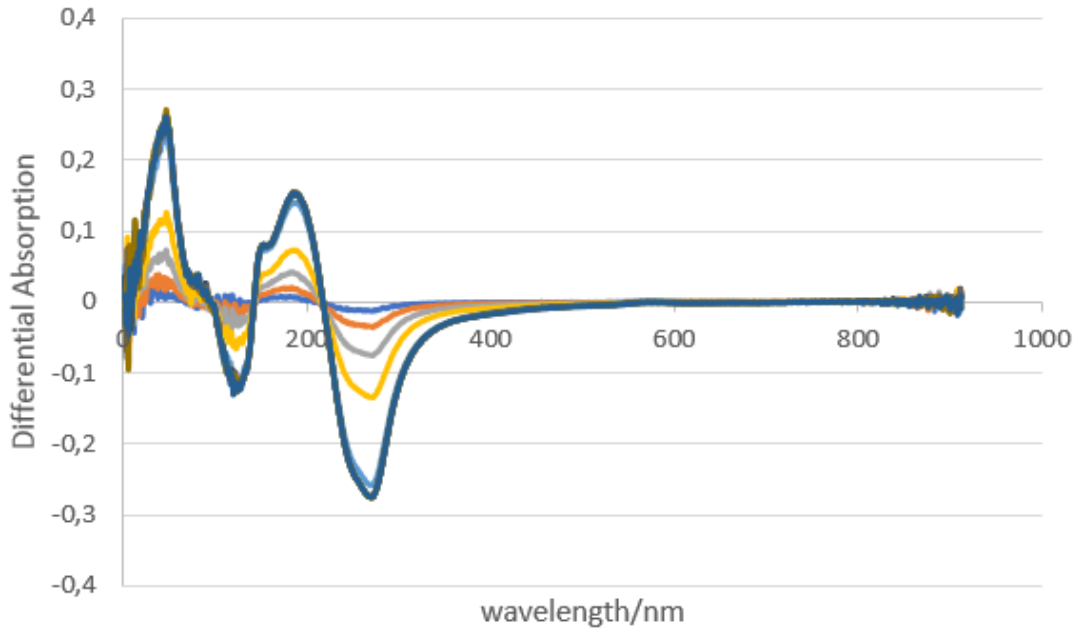

4.2. Compound **1b**^{c}

- Cyclic Voltammetry

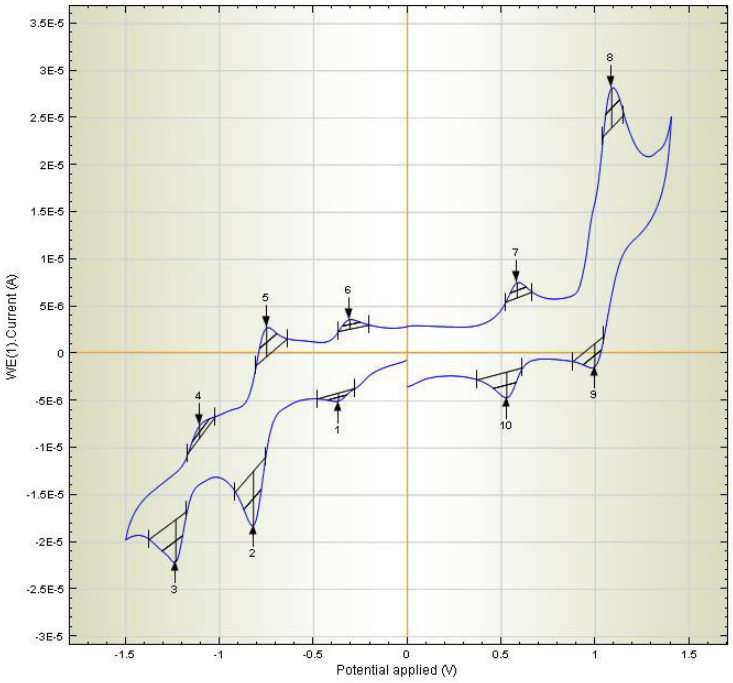

Compound **1b**^{c} with Ferrocene (peaks 7 and 10) as internal standard.

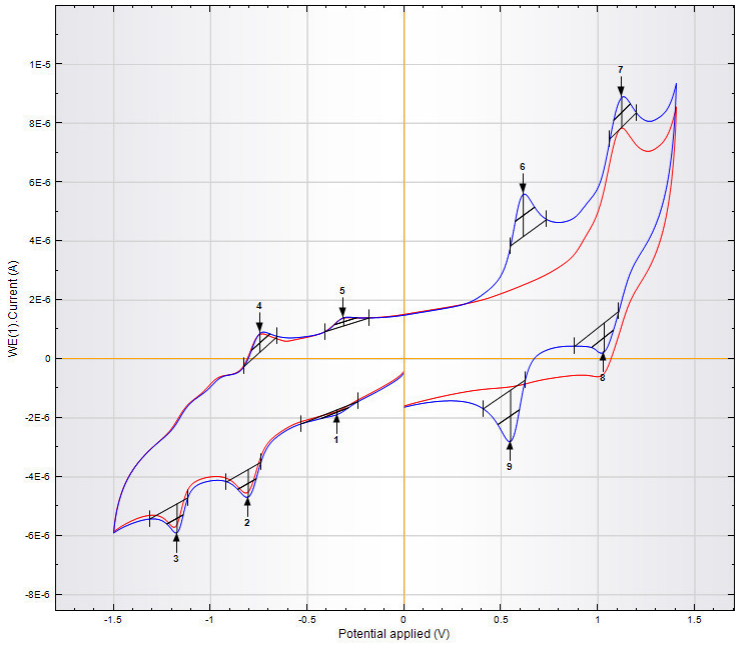

Two consecutive measurements of compound **1b**^{c}: Red: First round, without internal standard; Blue: Second round, after addition of ferrocene (peaks 6 and 9) as internal standard.

- Spectroelectrochemical studies

Peak 1 (0- -0.5 V)

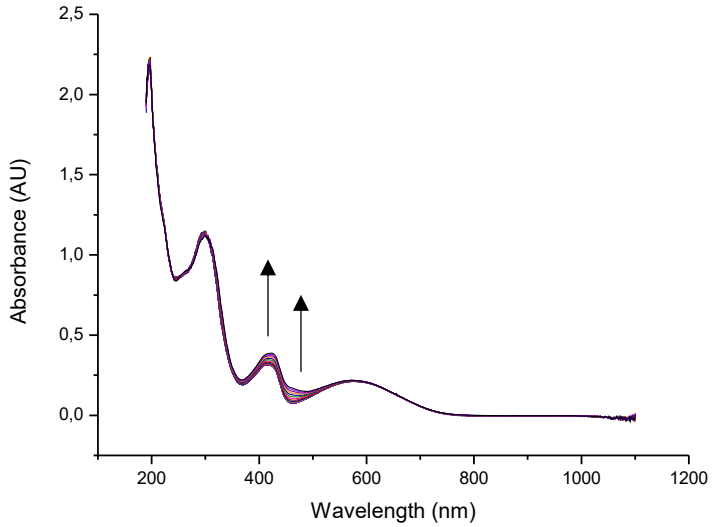

Peak 2 (-0.5 - -1.0V)

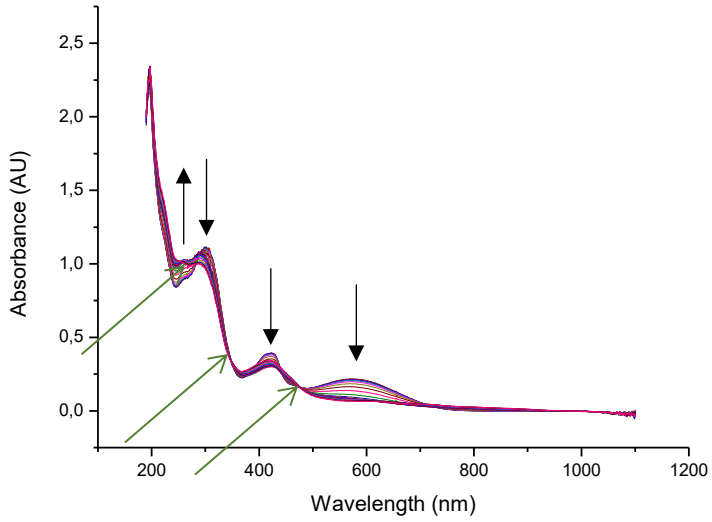

Peak 3 (-1.0 - -1.5V)

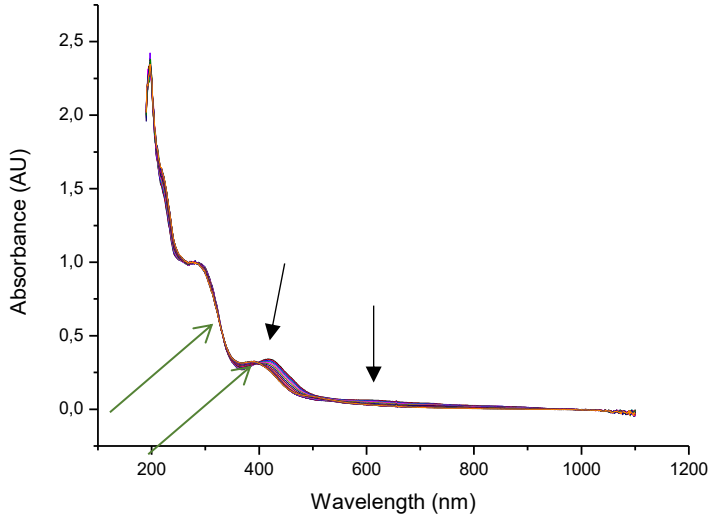

Peak 3 (invers, -1.5V - -1.0V)

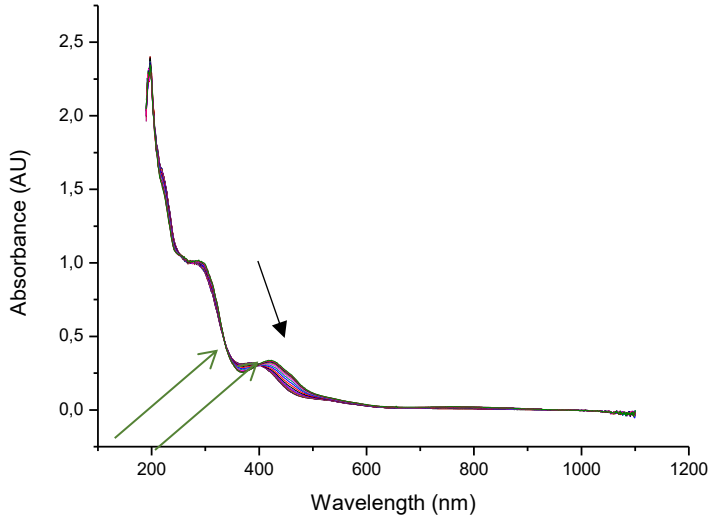

Peak 2 (invers, -1.0 - -0.5V)

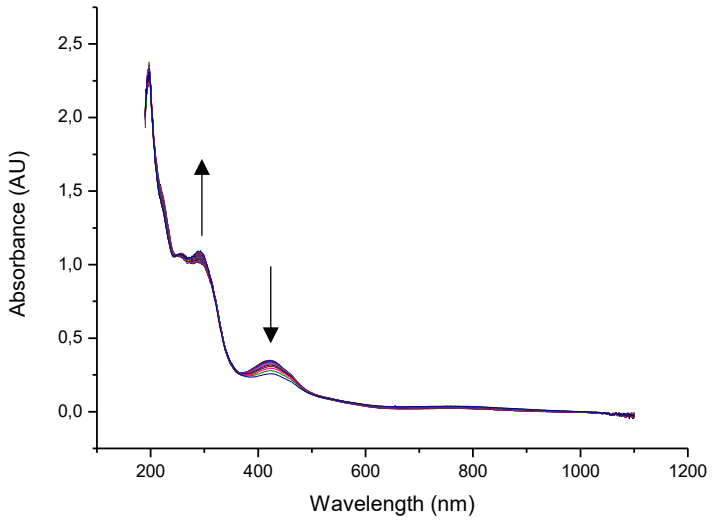

Peak 1 (invers, -0.5 – 0V)

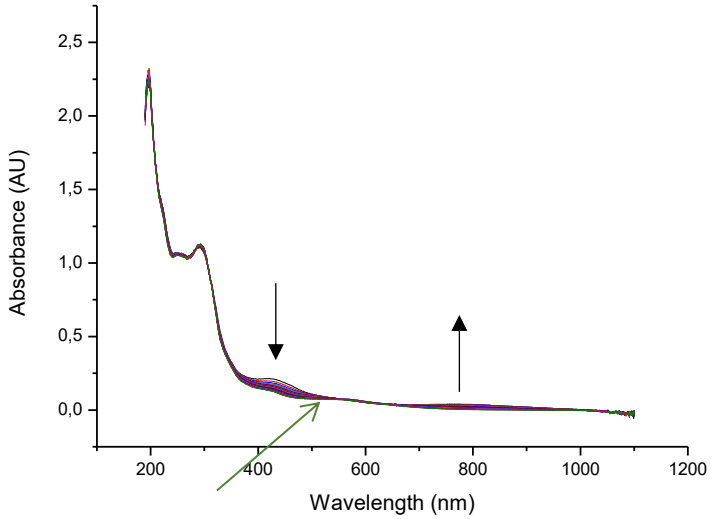

- Difference Spectra

Peak 1

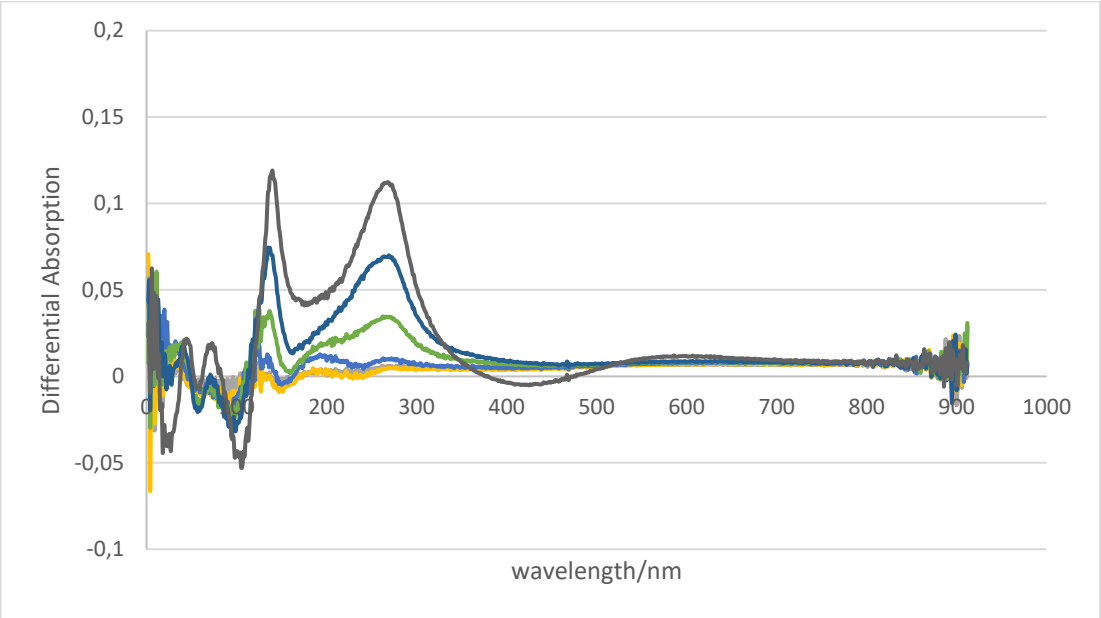

Peak 2

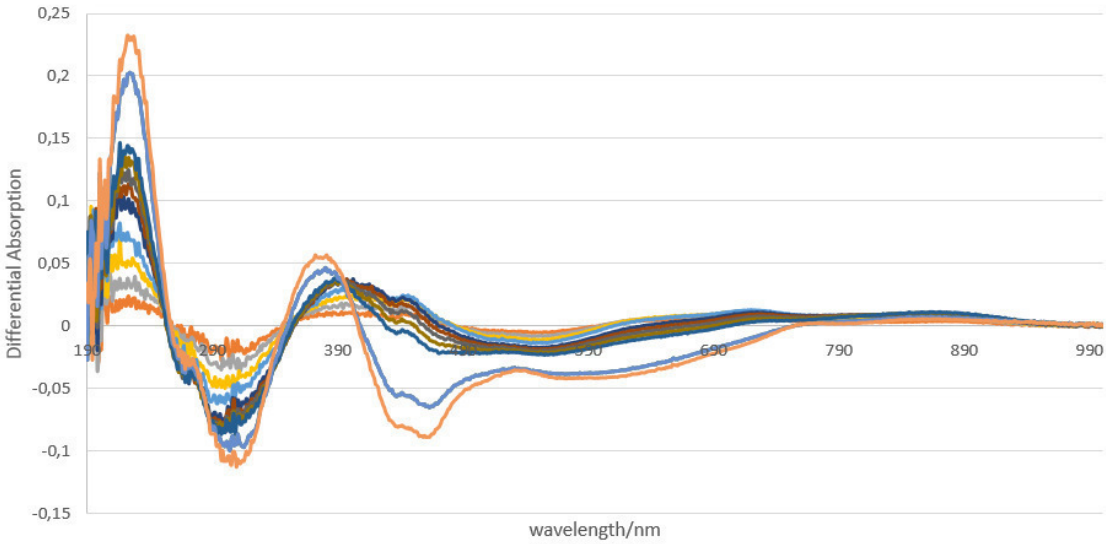

Peak 3

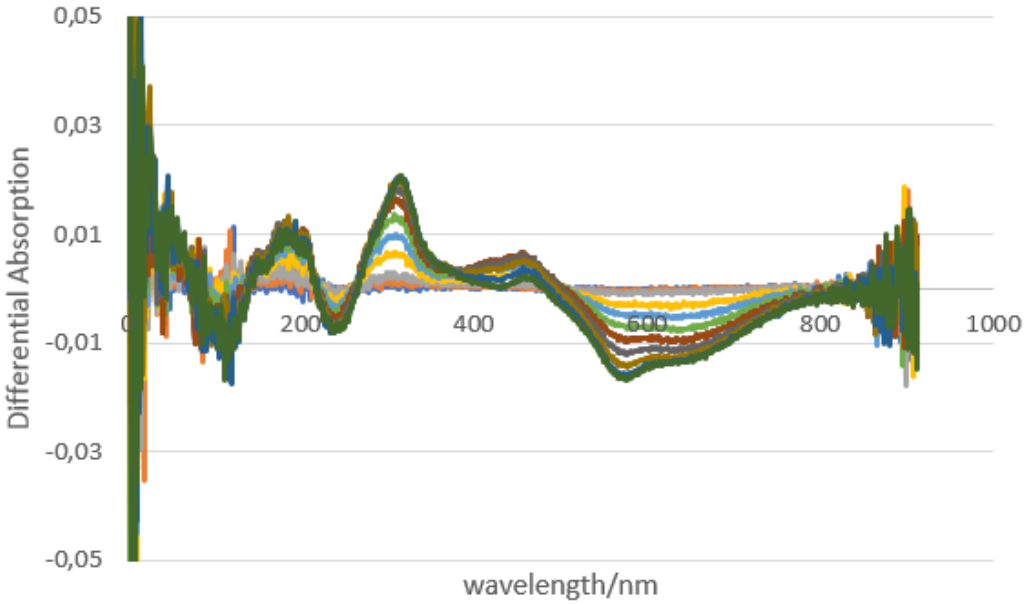

4.3. Compound **8b**

- Cyclic Voltammetry

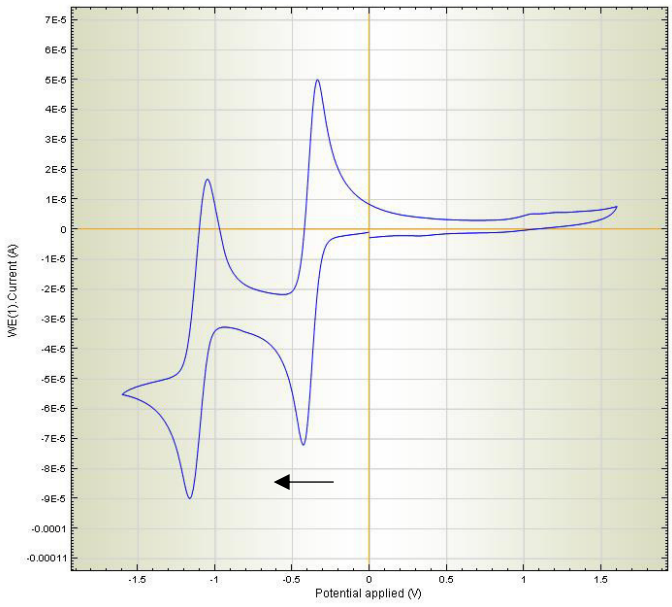

4.4. Compound **9b**

- Cyclic Voltammetry

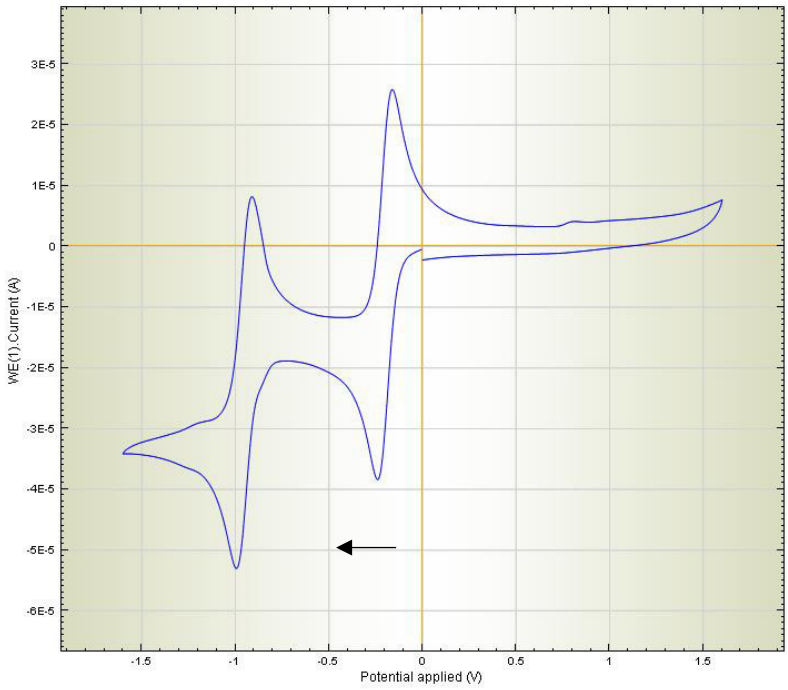

- Spectroelectrochemical studies

Peak 1 (0- -0.5V)

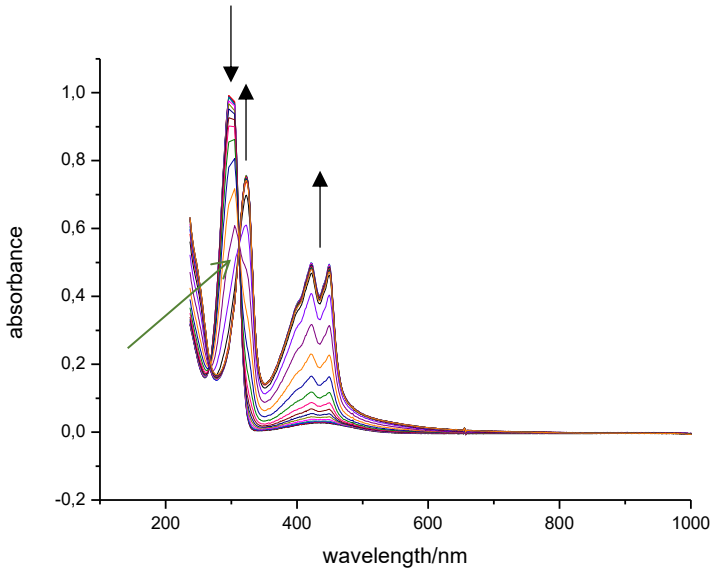

Peak 2 (-0.5 - -1.5V)

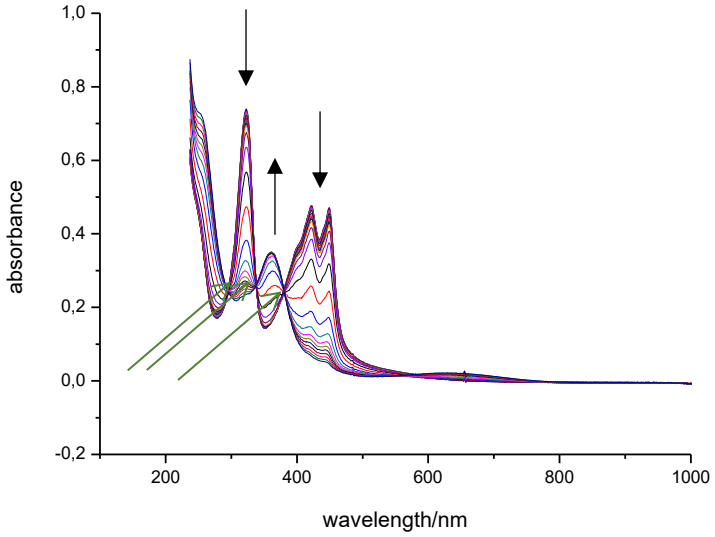

Peak 2 (invers, -1.5V - -0.5V)

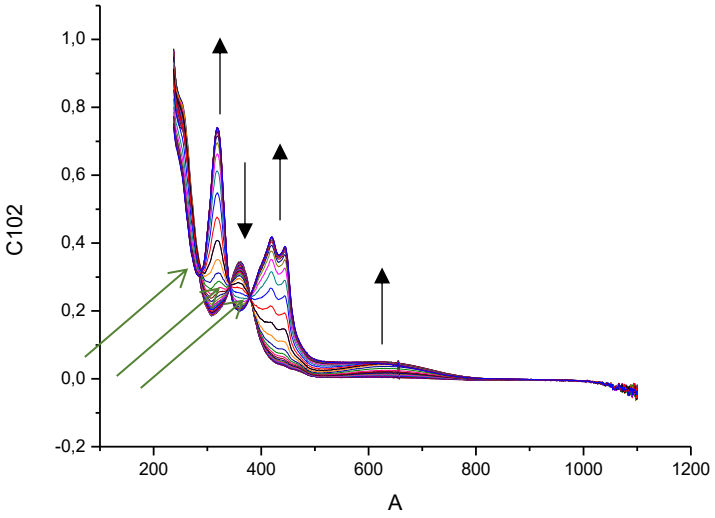

Peak 1 (invers, -0.5 – 0V, incomplete re-oxidation)

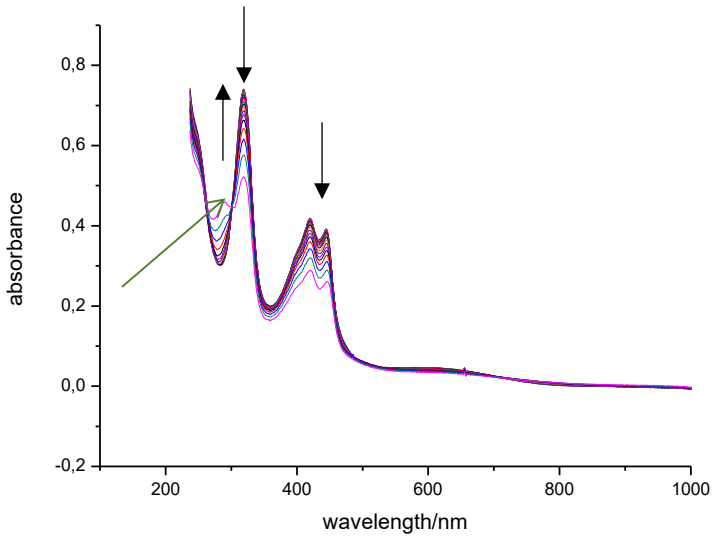

- Difference Spectra

Peak 1

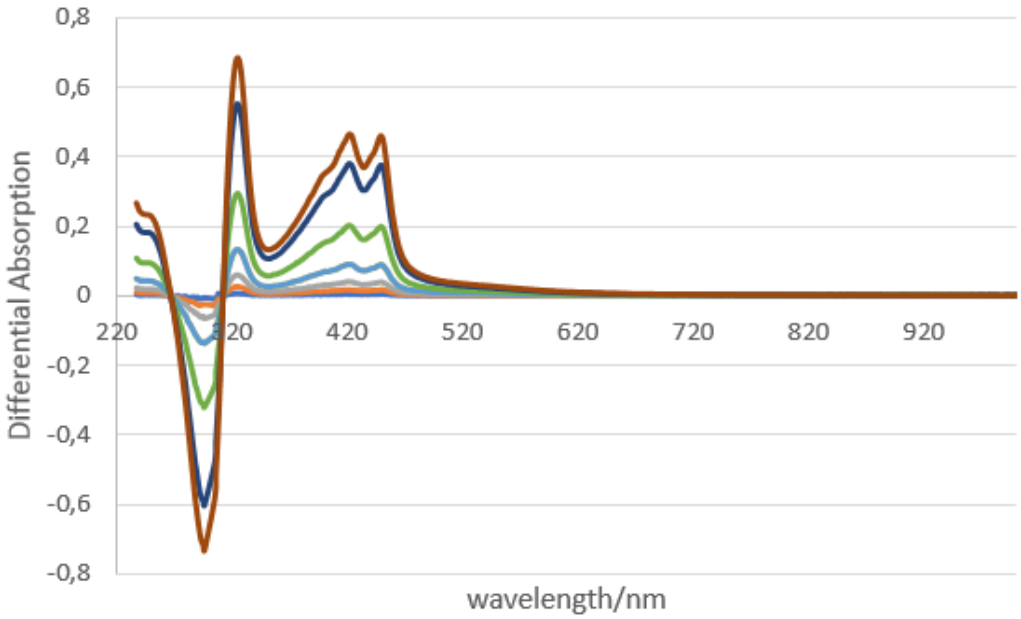

Peak 2

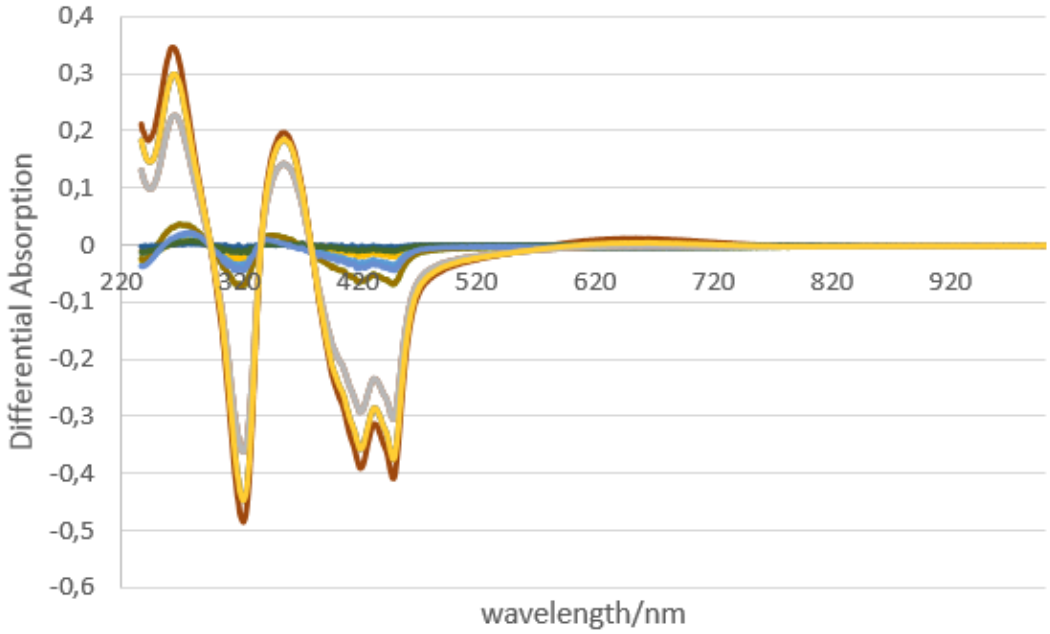

4.5. Compound **10** (CoQ_{10})

- Spectroelectric measurement

Peak 1

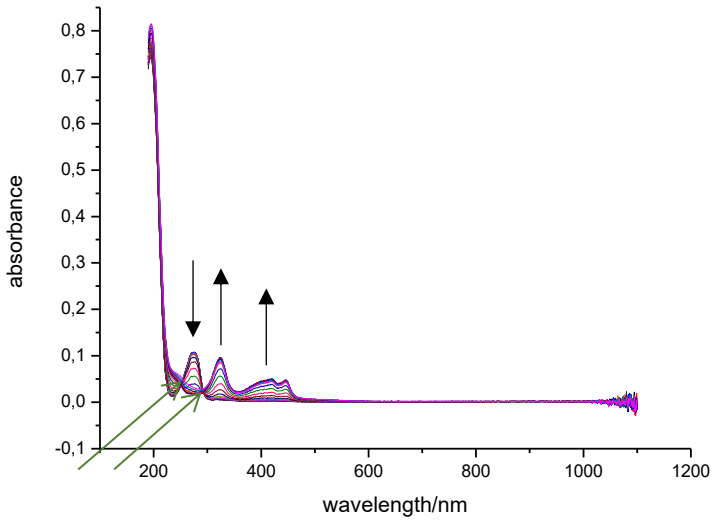

Peak 2

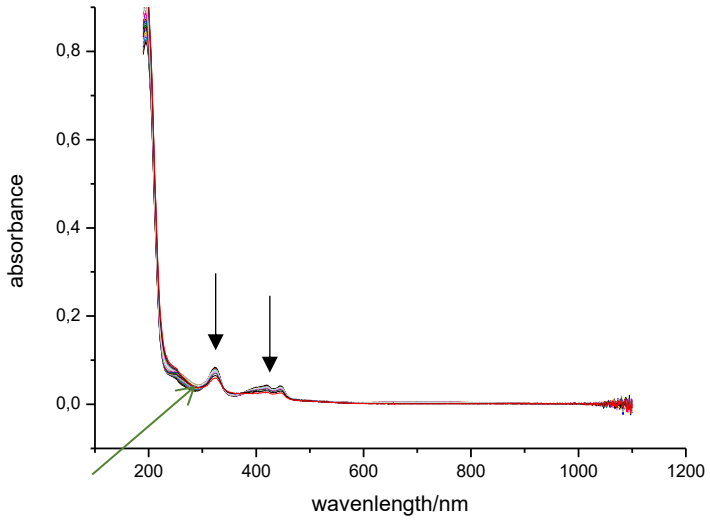

2nd peak (invers)

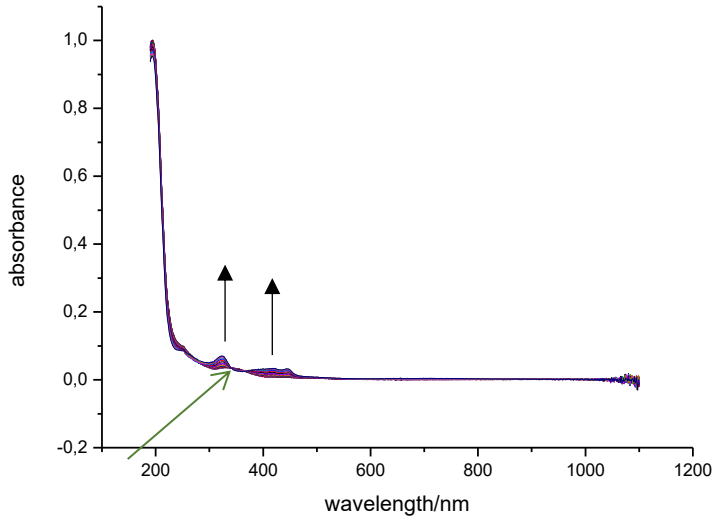

1st peak (invers)

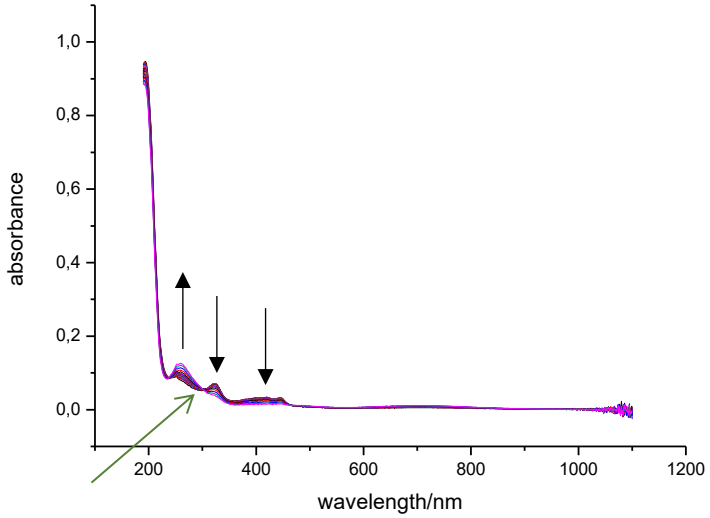

4.6. Compound **11**

- Cyclic Voltammetry

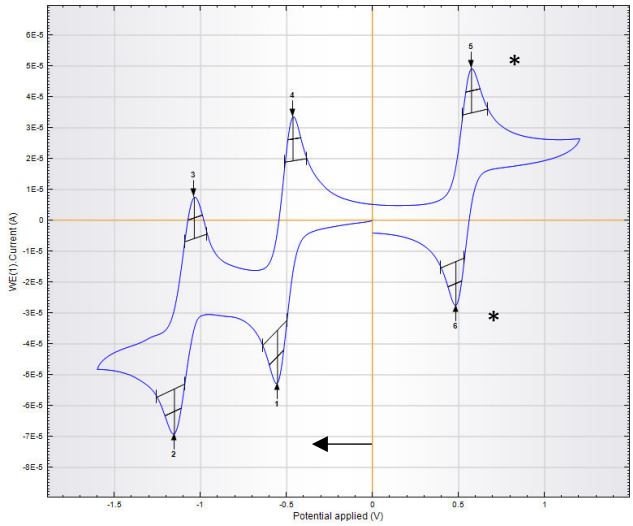

*Ferrocene as internal standard

- Spectroelectrochemical studies

Peak 1 (0- -0.7 V)

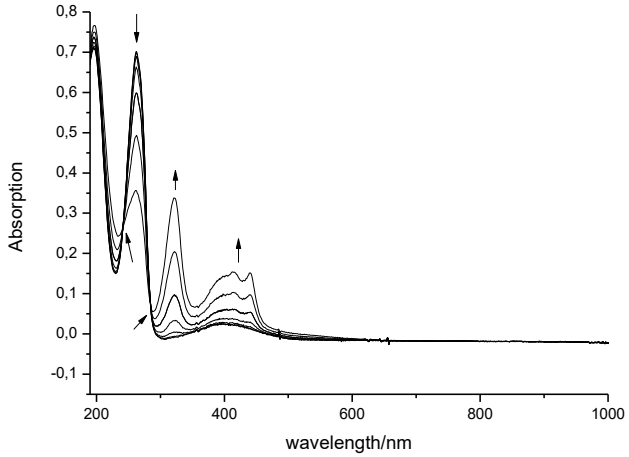

Peak 2 (-0.7- - 1.4V)

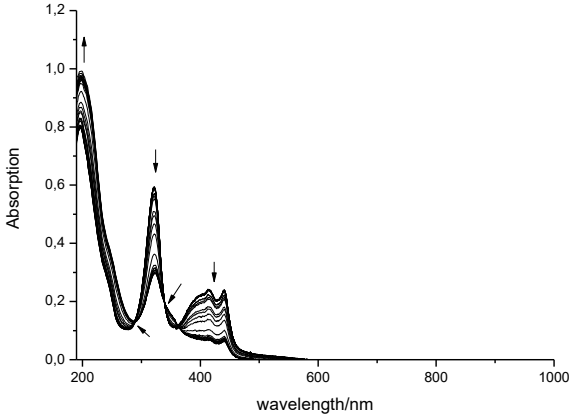

4.7. Compound **12**

- Cyclic Voltrammetry

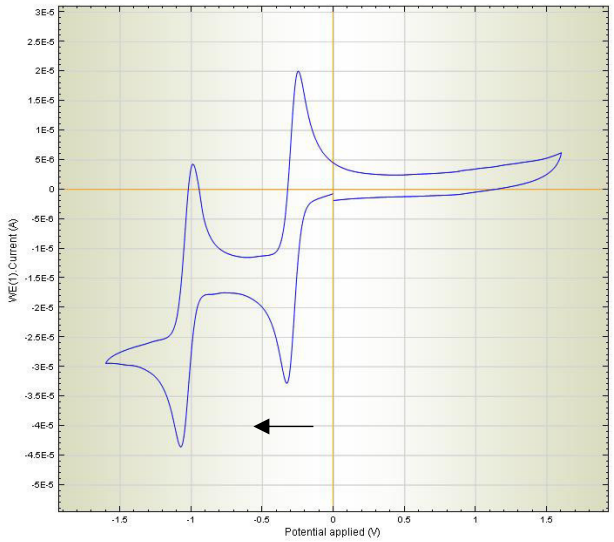

- Spectroelectrochemical studies

Peak 1 (0- -0.5V)

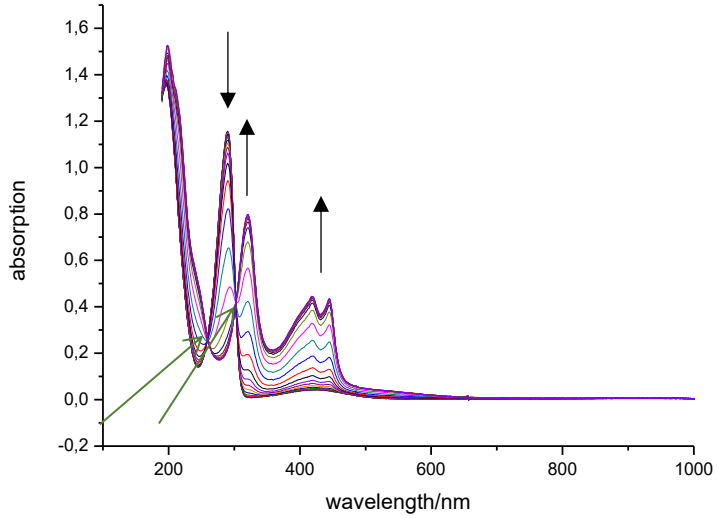

Peak 2 (-0.5 - -1.5V)

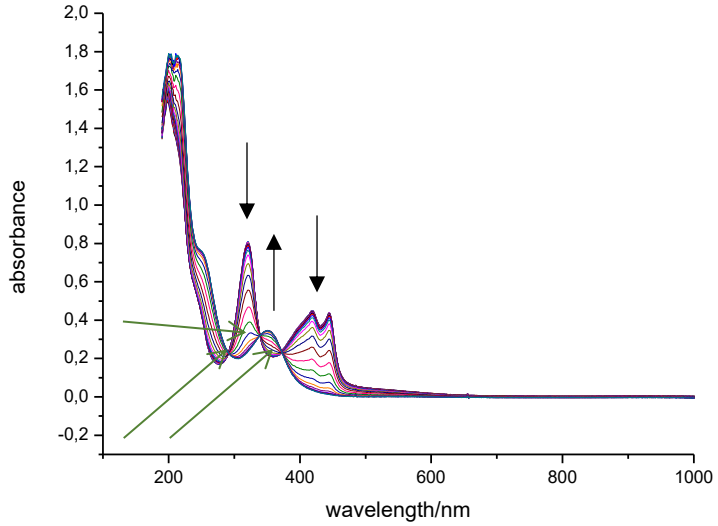

4.8. DCIP

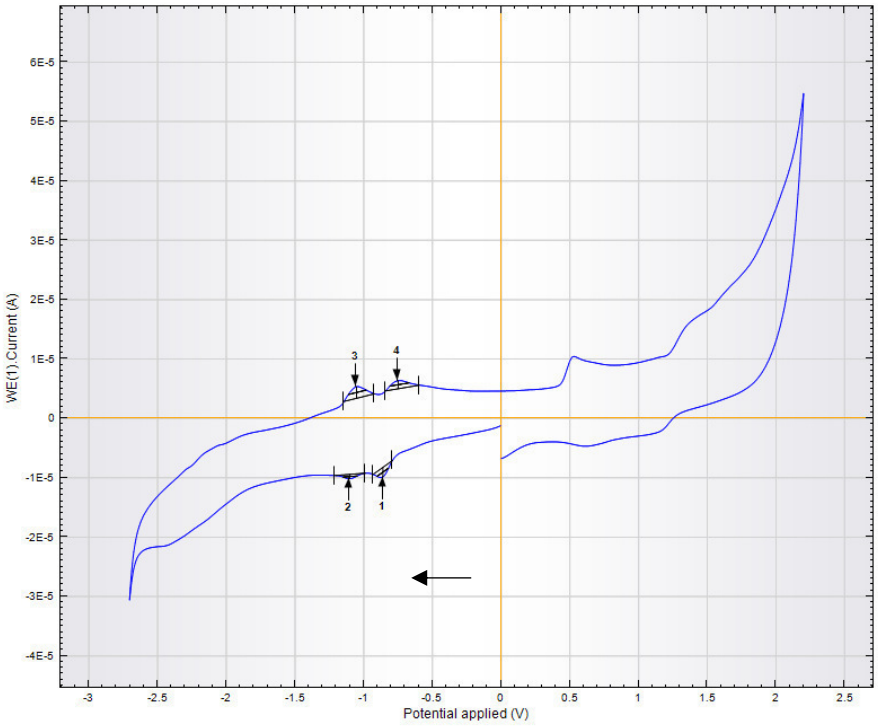

Potentials vs. SCN: -0.96 V, -1.23 V.

4.9. PMS

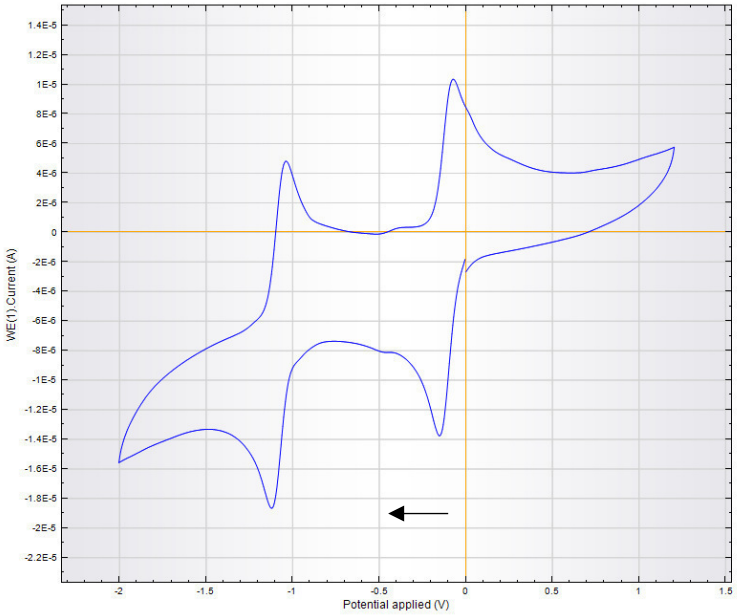

Potentials vs SCN: -0.11 V, -1.08 V.

5. Photoactivated Oxidation

5.1. Experimental Approach:

A Reduction of **1b**^{o}: A solution of **1b**^{o} (5 mM or 10 mM, DMSO, 600 µL) was dissolved in DMSO (1200 µL) and treated with a saturated solution of Hantzsch ester **13** (12 mM, DMSO, 600 µL) and stirred at ambient temperature in the dark.

To monitor the reaction, samples (100 µL) were taken and diluted with DMSO (100 µL), filtered and injected into analytical HPLC.

B Reduction of **1b**^{c}: A solution of **1b**^{c} (5 mM, DMSO, 50 µL) was dissolved in DMSO (100 µL) and treated with a saturated solution of Hantzsch ester **13** (12 mM, DMSO, 50 µL) and stirred at ambient temperature in the dark.

To monitor the reaction, samples (20 µL) were taken and diluted with DMSO (40 µL), filtered and injected into analytical HPLC.

C Reduction of **1b**^{c} and photoactivation: A solution of **1b**^{c} (10mM, DMSO, 50 µL) was dissolved in DMSO (100 µL) and treated with a saturated solution of Hantzsch ester **13** (12mM, DMSO, 50 µL) and stirred at ambient temperature in the dark. After three hours the sample was irradiated with a 590 nm single-spot LED for 10 min, then stirring was continued in the dark.

To monitor the reaction, samples (20 µL) were taken and diluted with DMSO (40 µL), filtered and injected into analytical HPLC.

5.2. Formation of **1b**^{o,red} using **1b**^{o} (10 mM, DMSO)

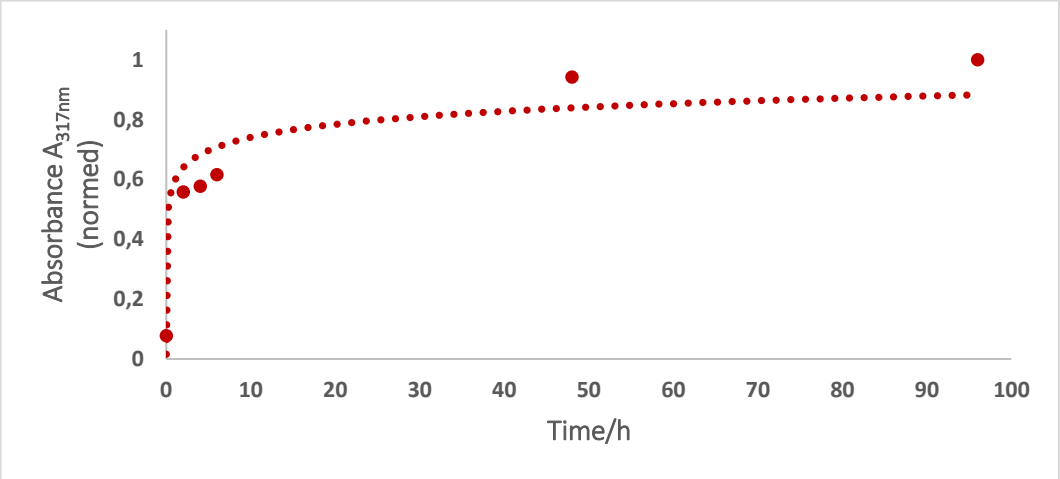

5.3. Representative HPLC traces (for Main Text, Figure 6 **A** and **B**)

Peaks: 7.2 min Hantzsch ester **13** (at the applied gradient oxidized and reduced form show the same retention time); 16.3 min: **1b**^{o,red}; 18.3 min: **1b**^{o}; 21.0 min: **1b**^{c}.

A_0h

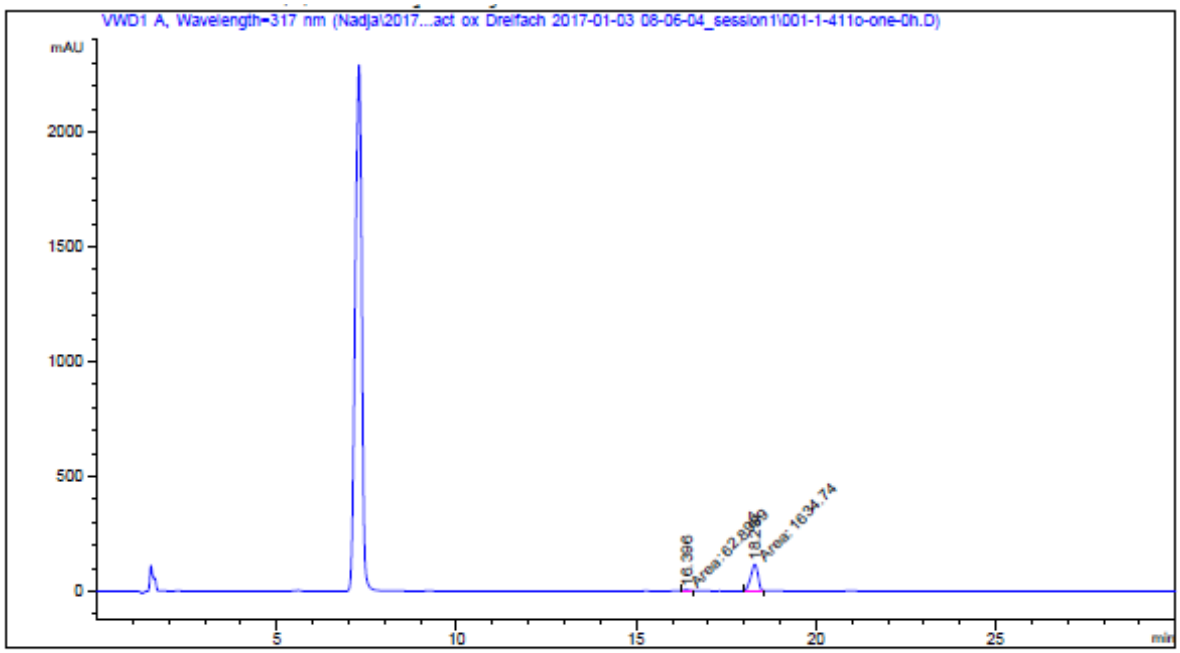


```
=====================================================================
                      Area Percent Report
=====================================================================

Sorted By             :      Signal
Multiplier            :      1.0000
Dilution              :      1.0000
Use Multiplier & Dilution Factor with ISTDs


Signal 1: VWD1 A, Wavelength=317 nm

Peak RetTime Type  Width     Area      Height     Area
  #   [min]        [min]   [mAU*s]     [mAU]       %
----|-------|----|-------|----------|----------|--------|
   1  16.396 MM    0.2133   62.89994    4.91378   3.7051
   2  18.297 MM    0.2337 1634.74426  116.57957  96.2949
```

A_11h

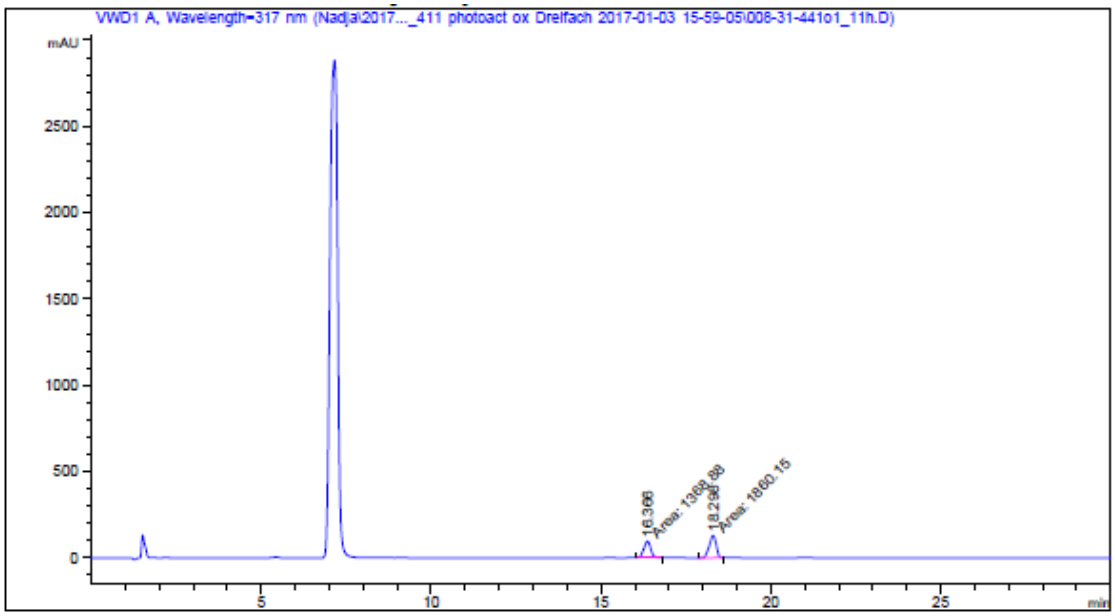


```
=====================================================================
                    Area Percent Report
=====================================================================

Sorted By             :      Signal
Multiplier            :      1.0000
Dilution              :      1.0000
Use Multiplier & Dilution Factor with ISTDs


Signal 1: VWD1 A, Wavelength=317 nm

Peak RetTime Type  Width     Area      Height     Area
  #   [min]        [min]   [mAU*s]     [mAU]       %
----|-------|----|-------|----------|----------|--------|
   1  16.366 MM    0.2389 1368.88477   95.50758  42.3930
   2  18.298 MM    0.2382 1860.14685  130.17055  57.6070
```

A_32h

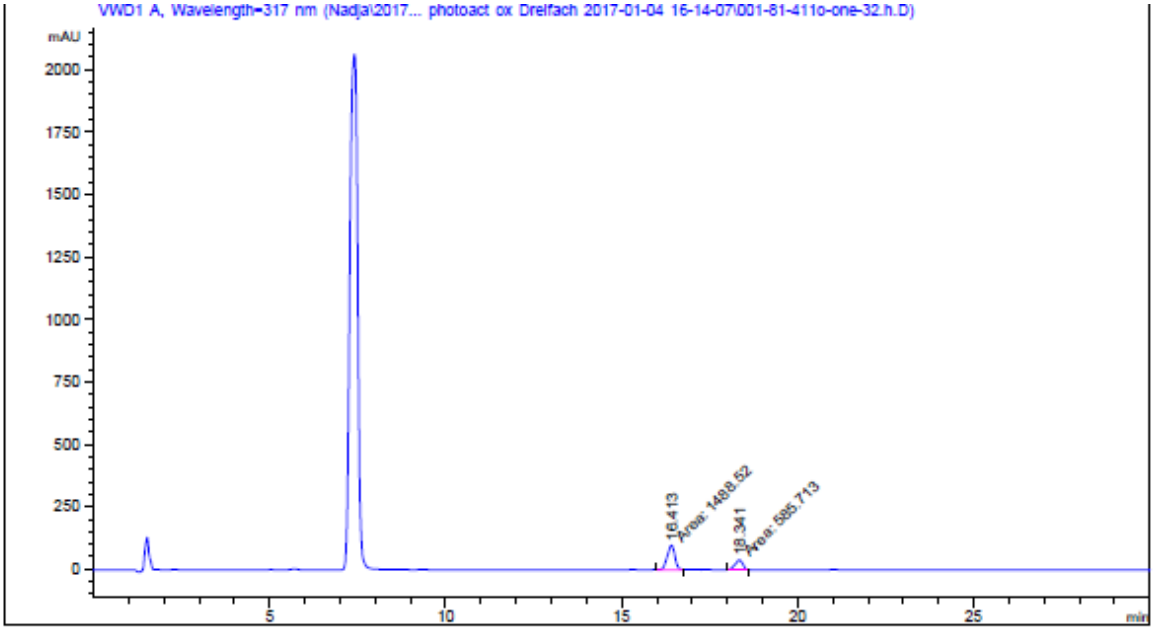


```
=====================================================================
                    Area Percent Report
=====================================================================

Sorted By             :      Signal
Multiplier            :      1.0000
Dilution              :      1.0000
Use Multiplier & Dilution Factor with ISTDs


Signal 1: VWD1 A, Wavelength=317 nm

Peak RetTime Type  Width     Area      Height     Area
  #   [min]        [min]   [mAU*s]     [mAU]       %
----|-------|----|-------|----------|----------|--------|
   1  16.413 MM    0.2525 1488.51843   98.24986  71.7624
   2  18.341 MM    0.2508  585.71344   38.92433  28.2376
```

A_47h

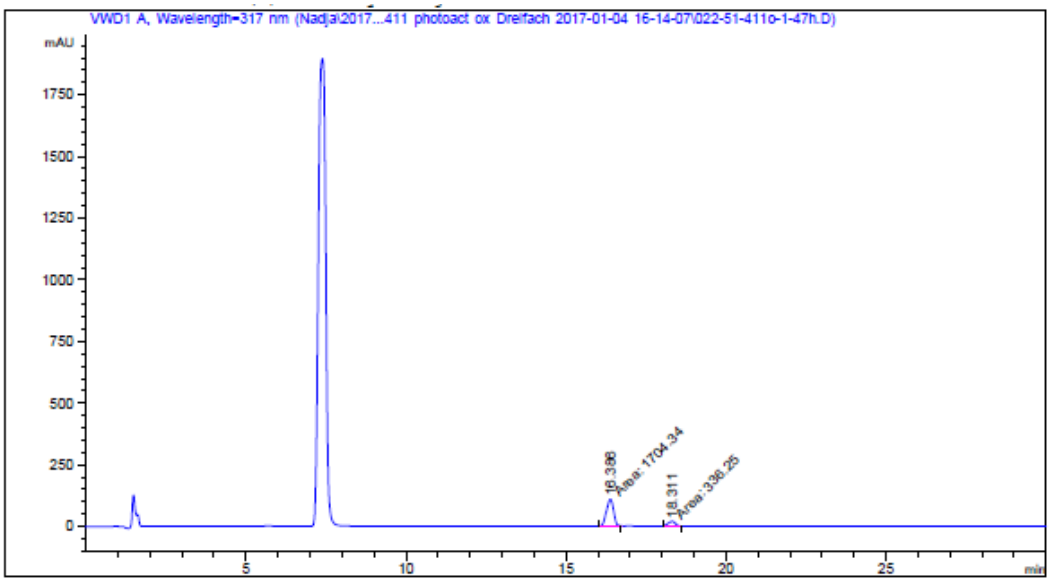


```
=====================================================================
                    Area Percent Report
=====================================================================

Sorted By             :      Signal
Multiplier            :      1.0000
Dilution              :      1.0000
Use Multiplier & Dilution Factor with ISTDs


Signal 1: VWD1 A, Wavelength=317 nm

Peak RetTime Type  Width     Area      Height     Area
  #   [min]        [min]   [mAU*s]     [mAU]       %
----|-------|----|-------|----------|----------|--------|
   1  16.386 MM    0.2598 1704.33765  109.34824  83.5219
   2  18.311 MM    0.2752  336.25031   20.36510  16.4781
```

B_0h/C_0h

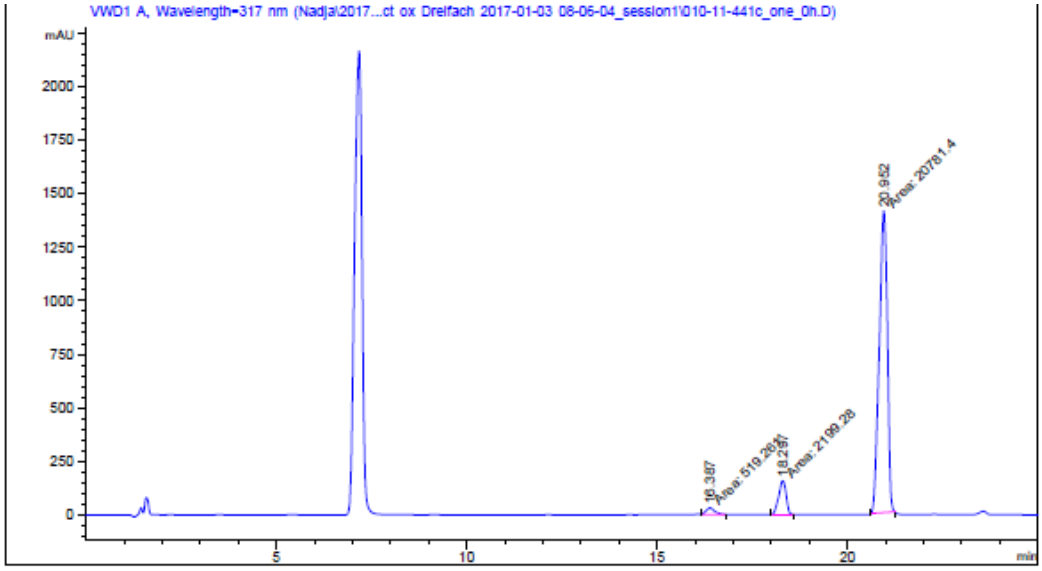


```
=====================================================================
                      Area Percent Report
=====================================================================

Sorted By             :      Signal
Multiplier            :      1.0000
Dilution              :      1.0000
Use Multiplier & Dilution Factor with ISTDs


Signal 1: VWD1 A, Wavelength=317 nm

Peak RetTime Type  Width     Area      Height     Area
  #   [min]        [min]   [mAU*s]     [mAU]       %
----|-------|----|-------|----------|----------|--------|
   1  16.387 MM    0.2781  519.26062   31.12502   2.2096
   2  18.297 MM    0.2289 2199.28003  160.10457   9.3587
   3  20.952 MM    0.2459 2.07814e4  1408.44507  88.4317
```

B_6h

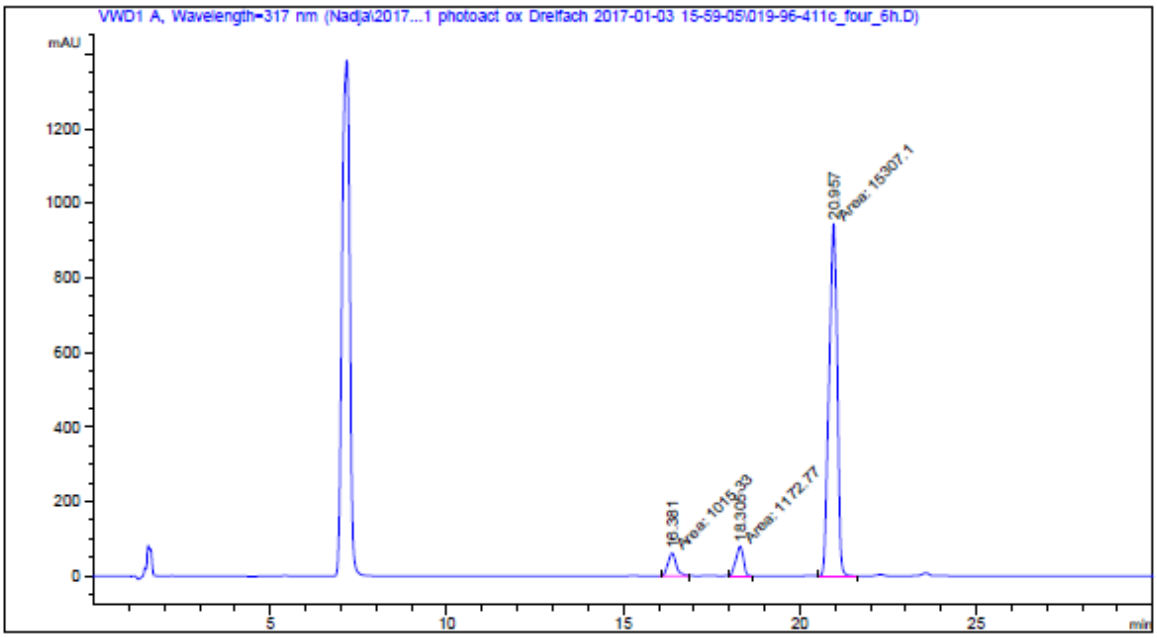


```
=====================================================================
                      Area Percent Report
=====================================================================

Sorted By             :      Signal
Multiplier            :      1.0000
Dilution              :      1.0000
Use Multiplier & Dilution Factor with ISTDs


Signal 1: VWD1 A, Wavelength=317 nm

Peak RetTime Type  Width     Area      Height     Area
  #   [min]        [min]   [mAU*s]     [mAU]       %
----|-------|----|-------|----------|----------|--------|
   1  16.381 MM    0.2752 1015.33301   61.48637   5.8035
   2  18.305 MM    0.2456 1172.76794   79.58045   6.7034
   3  20.957 MM    0.2697 1.53071e4   945.79211  87.4931
```

B_20h

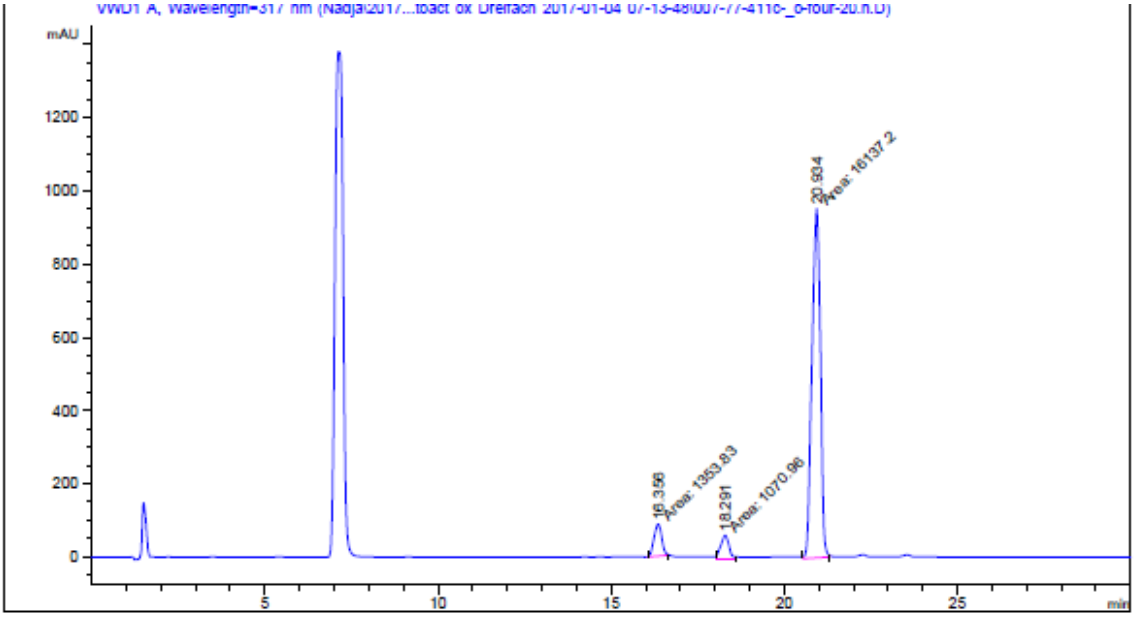


```
=====================================================================
                    Area Percent Report
=====================================================================

Sorted By             :      Signal
Multiplier            :      1.0000
Dilution              :      1.0000
Use Multiplier & Dilution Factor with ISTDs


Signal 1: VWD1 A, Wavelength=317 nm

Peak RetTime Type  Width     Area      Height     Area
  #   [min]        [min]   [mAU*s]     [mAU]       %
----|-------|----|-------|----------|----------|--------|
   1  16.356 MM    0.2586 1353.82556   87.26817   7.2935
   2  18.291 MM    0.2799 1070.96094   63.77544   5.7696
   3  20.934 MM    0.2822 1.61372e4   953.15631  86.9368
```

C_3h

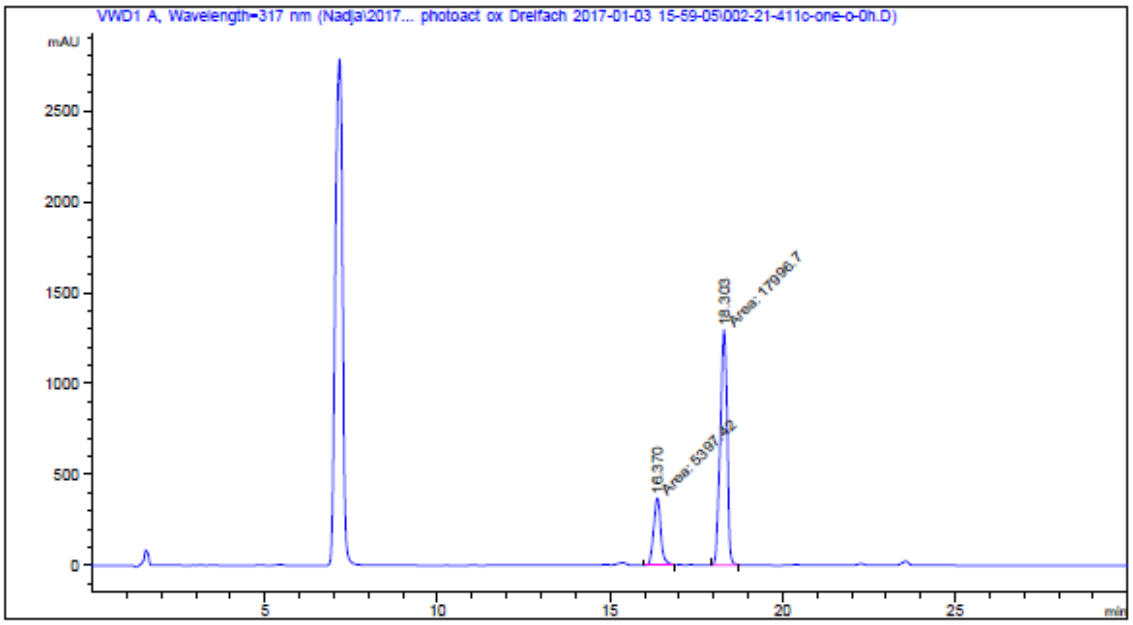


```
=====================================================================
                      Area Percent Report
=====================================================================

Sorted By             :      Signal
Multiplier            :      1.0000
Dilution              :      1.0000
Use Multiplier & Dilution Factor with ISTDs


Signal 1: VWD1 A, Wavelength=317 nm

Peak RetTime Type  Width     Area      Height     Area
  #   [min]        [min]   [mAU*s]     [mAU]       %
----|-------|----|-------|----------|----------|--------|
   1  16.370 MM    0.2431 5397.41650  370.02362  23.0717
   2  18.303 MM    0.2320 1.79967e4  1292.72192  76.9283
```

C_7.5h

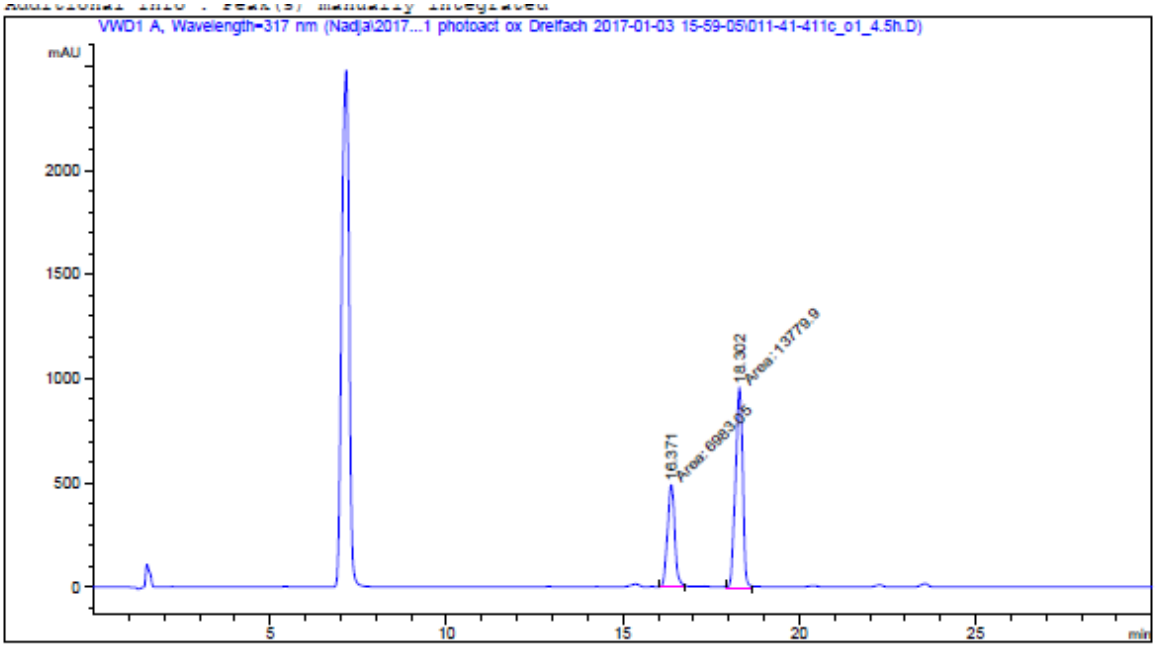


```
================================================================================
                          Area Percent Report
================================================================================

Sorted By             :      Signal
Multiplier            :      1.0000
Dilution              :      1.0000
Use Multiplier & Dilution Factor with ISTDs


Signal 1: VWD1 A, Wavelength=317 nm

Peak RetTime Type  Width     Area      Height     Area
  #   [min]        [min]   [mAU*s]     [mAU]       %
----|-------|----|-------|----------|----------|--------|
   1  16.371 MM    0.2390 6983.05029  486.93979  33.6323
   2  18.302 MM    0.2388 1.37799e4   961.71655  66.3677
```

C_39h

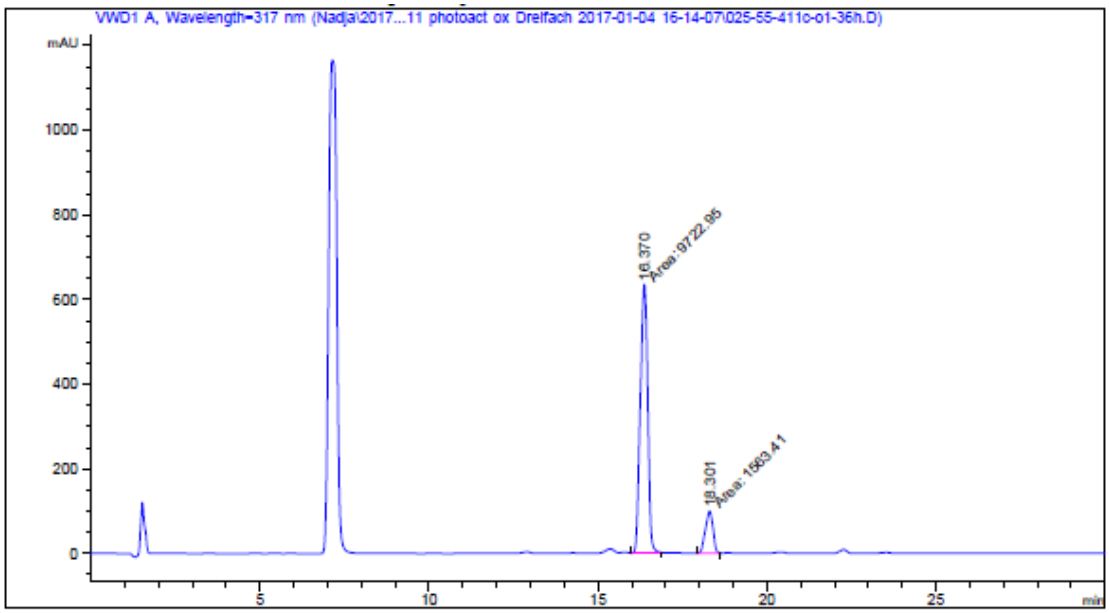


```
=====================================================================
                      Area Percent Report
=====================================================================

Sorted By             :      Signal
Multiplier            :      1.0000
Dilution              :      1.0000
Use Multiplier & Dilution Factor with ISTDs


Signal 1: VWD1 A, Wavelength=317 nm

Peak RetTime Type  Width     Area      Height     Area
  #   [min]        [min]   [mAU*s]     [mAU]       %
----|-------|----|-------|----------|----------|--------|
   1  16.370 MM    0.2555 9722.95117  634.16931  86.1478
   2  18.301 MM    0.2608 1563.40955   99.90733  13.8522
```

6. Activation of **1b**^{c} on isolated Mitochondria

- Stability of **1b**^{c} at elevated temperatures

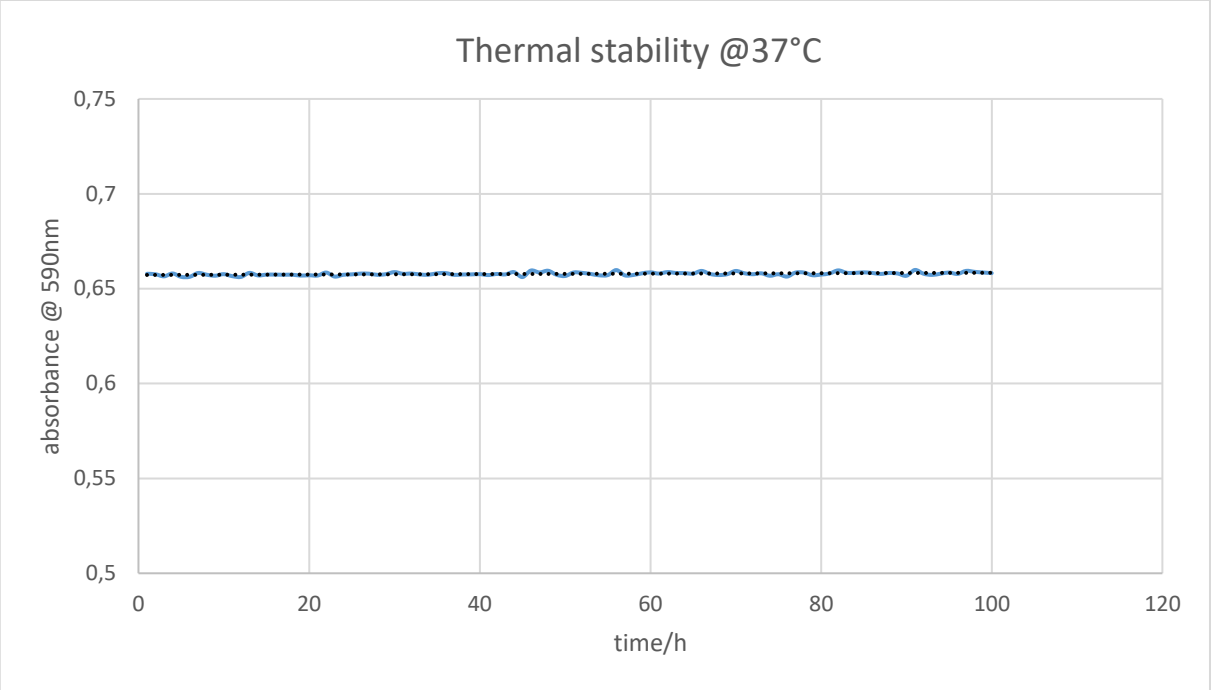

- Purity of compounds **1b**^{o} and **1b**^{c}

1b^{o}

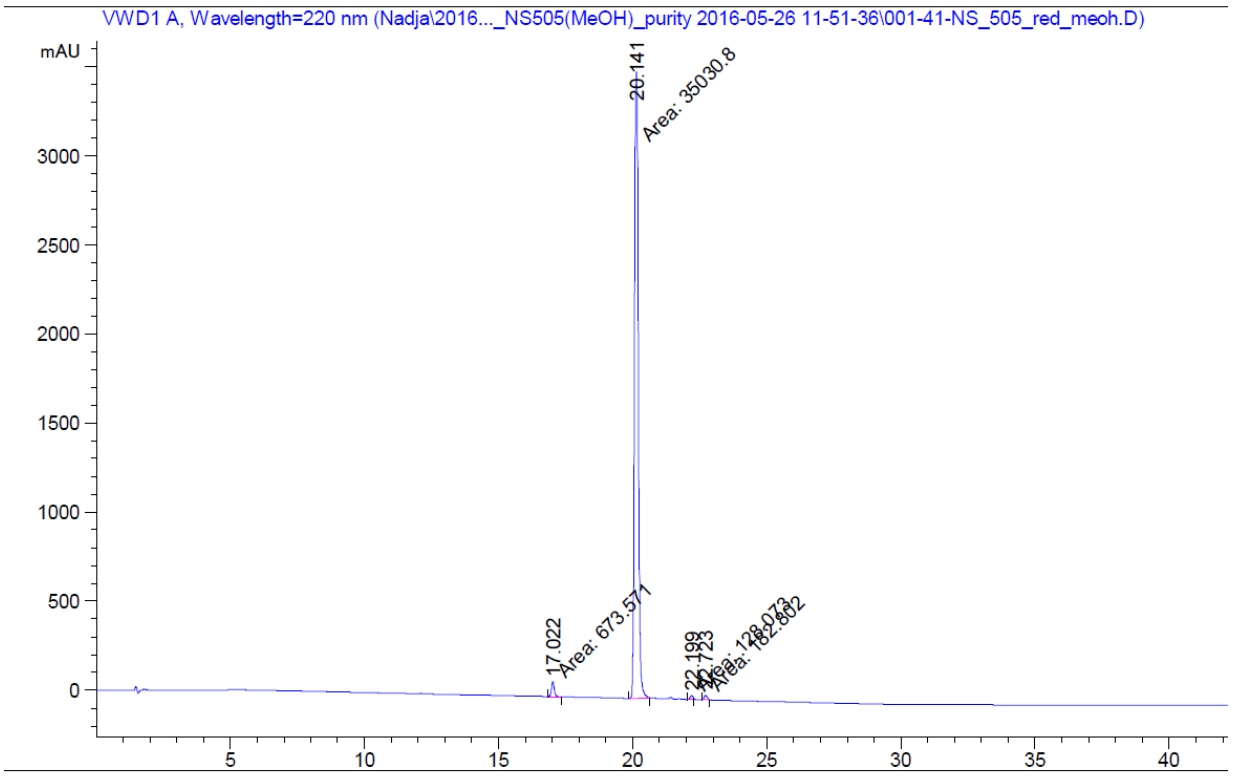

Peak #	RetTime [min]	Type	Width [min]	Area [mAU*s]	Height [mAU]	Area %
1	17.022	MM	0.1302	673.57086	86.23805	1.8702
2	20.141	MM	0.1661	3.50308e4	3515.66992	97.2666
3	22.199	MM	0.1065	128.07347	20.05158	0.3556
4	22.723	MM	0.1231	182.80190	24.75809	0.5076

1b^{c}

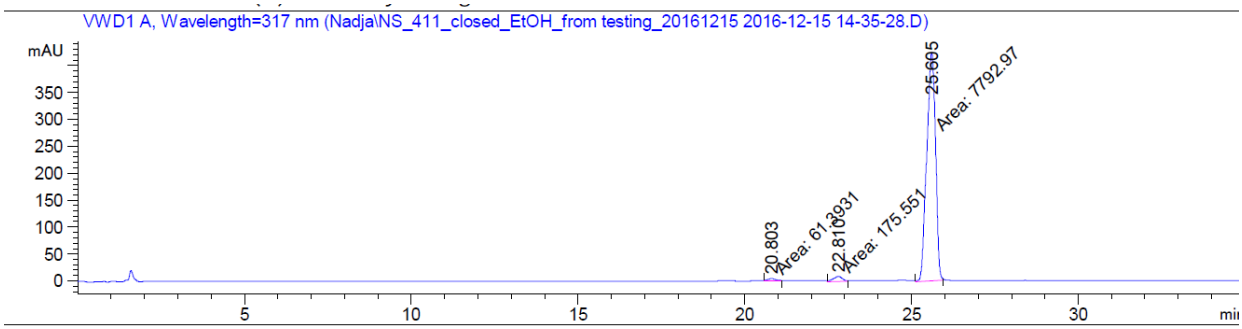

Peak #	RetTime [min]	Type	Width [min]	Area [mAU*s]	Height [mAU]	Area %
1	20.803	MM	0.2713	61.39307	3.77112	0.7646
2	22.810	MM	0.3193	175.55141	9.16268	2.1862
3	25.605	MM	0.3063	7792.96826	424.01196	97.0492
Totals :				8029.91273	436.94577	

- Isolation of mitochondria from yeast cells

A crude mitochondria extract was isolated from the wildtype yeast strain BY4742 (MATα his3Δ1 leu2Δ0 lys2Δ0 ura3Δ0), thankfully provided by the group of Herbert Tschochner, according to Gregg et al.[3] The protein concentration of the extract was determined with the Bradford assay[4] and the mitochondria were stored in 30 mM KP (pH 7.4), 2.2 mM EDTA and 0.1% (w/v) Thesit at -80 °C

- Mitochondrial reduction of 2,6-dichlorophenol indophenol

Reduction of 2,6-dichlorophenol indophenol (DCIP) was measured using the succinate dehydrogenase activity (SDH) of mitochondria as described previously.[5] Prior to the assays, SDH was activated with 8 mM succinate for 15 min at 37 °C. Triplet measurements were carried out in a 96-well plate of assays containing 40 µM **1b**^{c} and **1b**^{o} dissolved in ethanol, respectively, 10 mM succinate, 100 µM DCIP and 0.2 g/L mitochondria in 50 mM KP (pH 7.6), 0.006% (w/v) Thesit, 0.2 mM EDTA at 37 °C. Reduction of DCIP was followed at 520 nm ($\varepsilon_{DCIP,520}$ = 6.8 mM^{-1} cm^{-1}) continuously for 30 min or with 10 min interruption in which the samples were irradiated with 590 nm in the same plate reader used for activity measurements with an integrated 10 W xenon flash lamp (Tecan Trading AG). The resulting data were plotted and fitted with a linear function in the time frame of 0-10 min as well as 20-30 min to visualize the difference in reactivity.

7. Computational Studies

All DFT-calculations (B3LAP/6–31G(d) level) were performed with the Gaussian 09, Revision D01 software package.[6] Optimized structures (**1b**$^{o}_{min}$, **1b**$^{c}_{min}$, **13**$_{min}$, {**1b**$^{o}_{min}$–**13**$_{min}$}$_{ADJ}$, {**1b**$^{c}_{min}$–**13**$_{min}$}$_{ADJ}$) were confirmed to be minima through frequency calculations. Single-point energies were calculated for **1b**$^{o}_{ADJ}$, **1b**$^{c}_{ADJ}$, **13**$_{ADJ}$, {**1b**$^{o}_{min}$–**13**$_{min}$}$_{nonADJ}$ and {**1b**$^{c}_{min}$–**13**$_{min}$}$_{nonADJ}$. All cartesian coordinates are given in paragraph 10. later in the Supporting Information.

Adapting a published strategy, an energy cycle to gain insight into the presence of a non-covalent π stacking between both photoisomers and **13** was calculated according to the following scheme.[7]

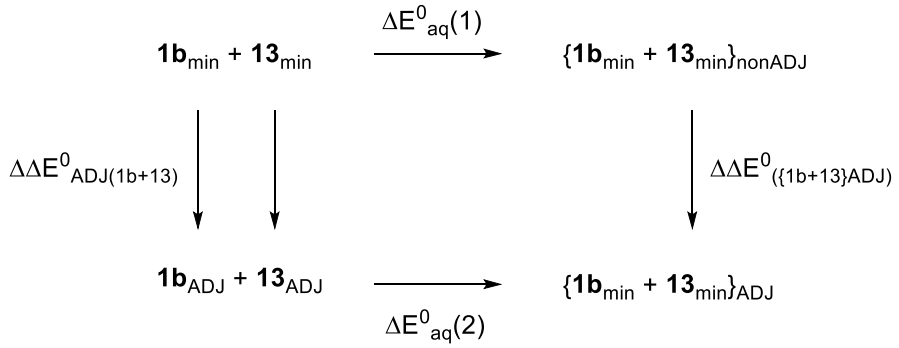

Then, the energies of the optimized structures (indicated with "min") of both photoisomers, the Hantzsch ester and the respective adduct complexes were compared with single point calculations of mixed structures, revealing the adjustment process (indicated with "ADJ") of the structures upon π stacking. The energy differences are given as follows:

	1b^{o}	**1b**^{c}	ΔΔE^{0}(**1b**^{c}-**1b**^{o})
ΔE$^{0}_{aq}$(1)*	-0,38	1,38	
ΔE$^{0}_{aq}$(2)*	-16,5	-22,9	
ΔΔEG$^{0}_{ADJ(1b+13)}$*	1,07	1,75	
ΔΔE$^{0}_{({1b+13}ADJ)}$*	-15,06	-22,53	-7,47

*Energy differences are expressed in Kcal/mol.

8. NMR spectra

- Compound **1a**^{o}

^{1}H NMR ($CDCl_3$, 400 MHz)

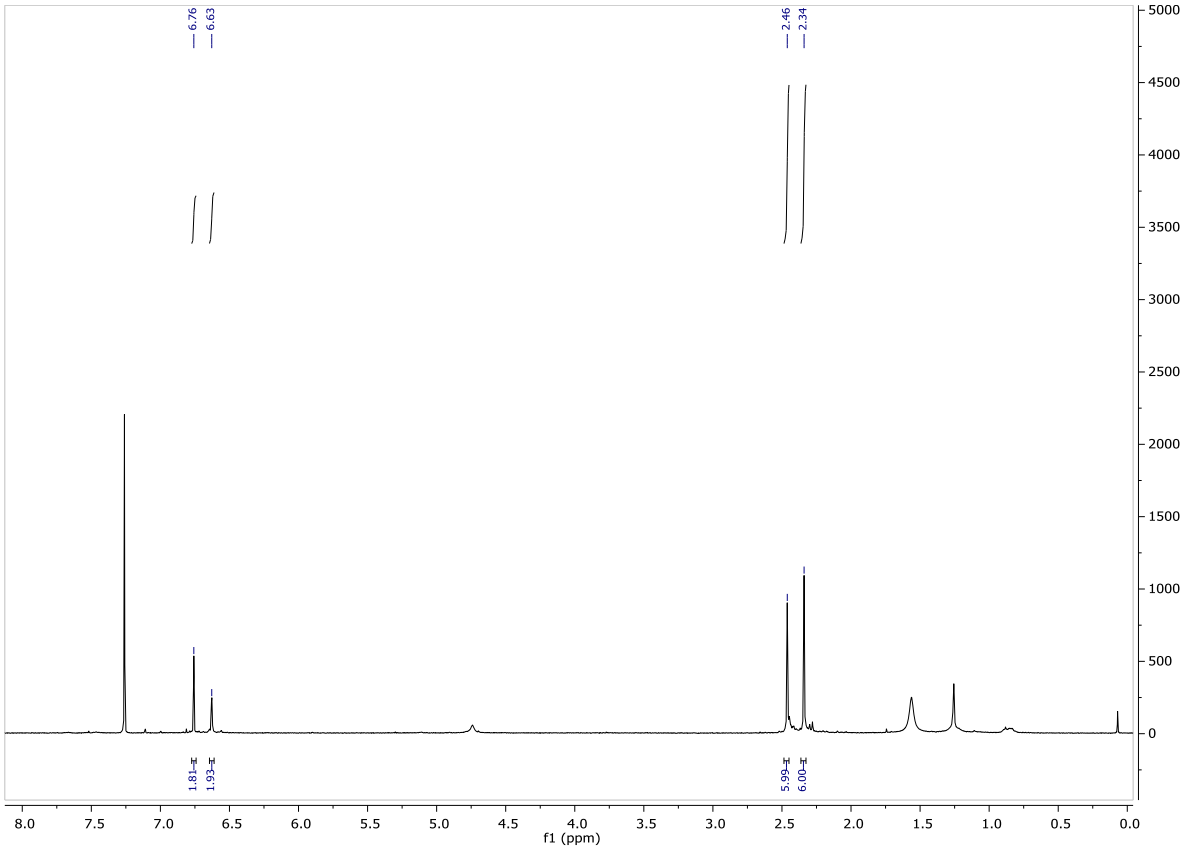

^{13}C NMR ($CDCl_3$, 101 MHz)

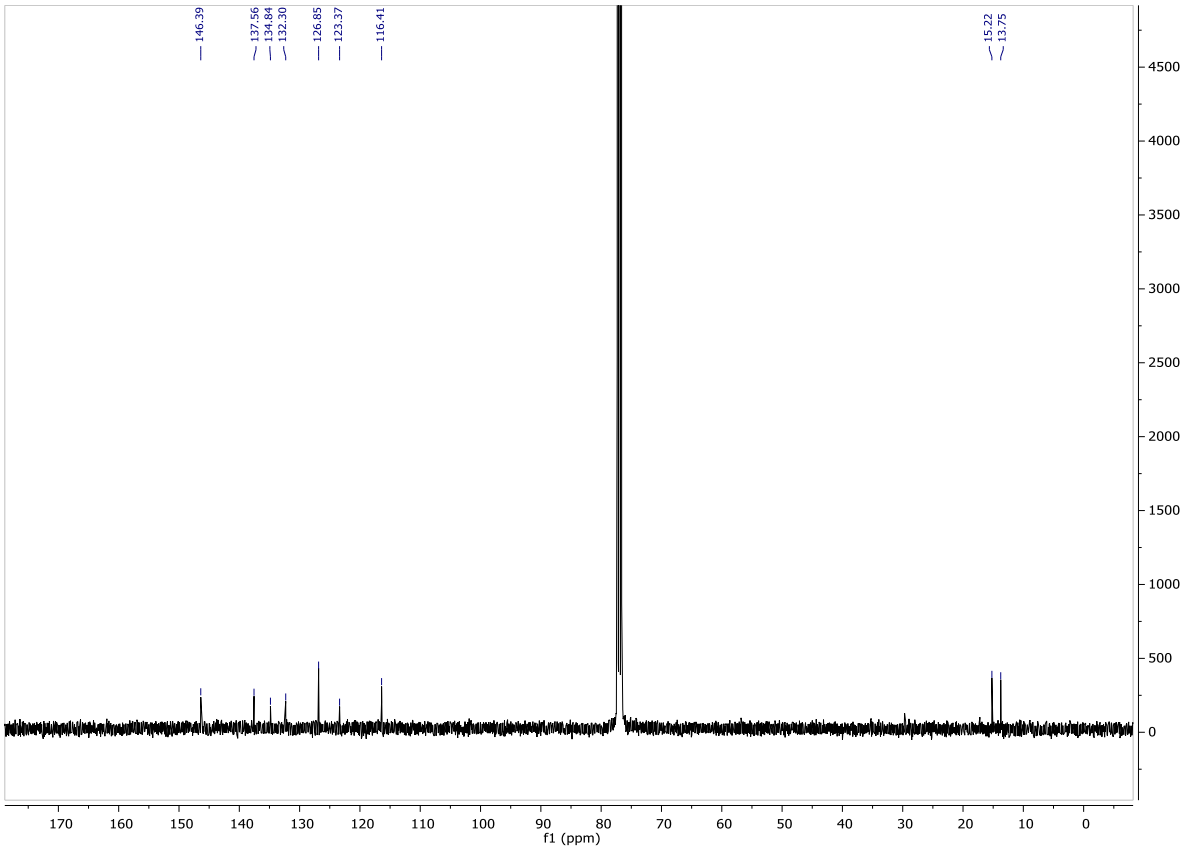

- Compound **1b**^{o}

^{1}H ($CDCl_3$, 600 MHz)

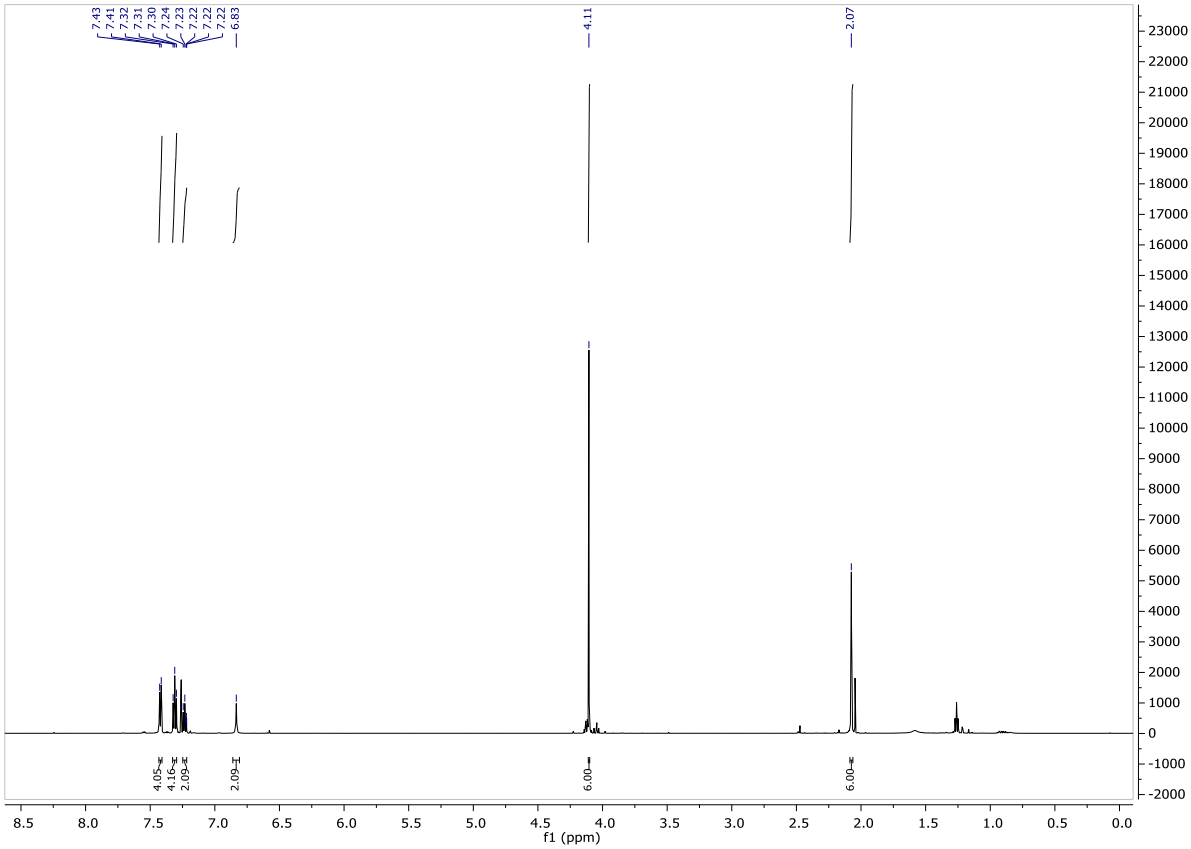

^{13}C ($CDCl_3$, 151 MHz)

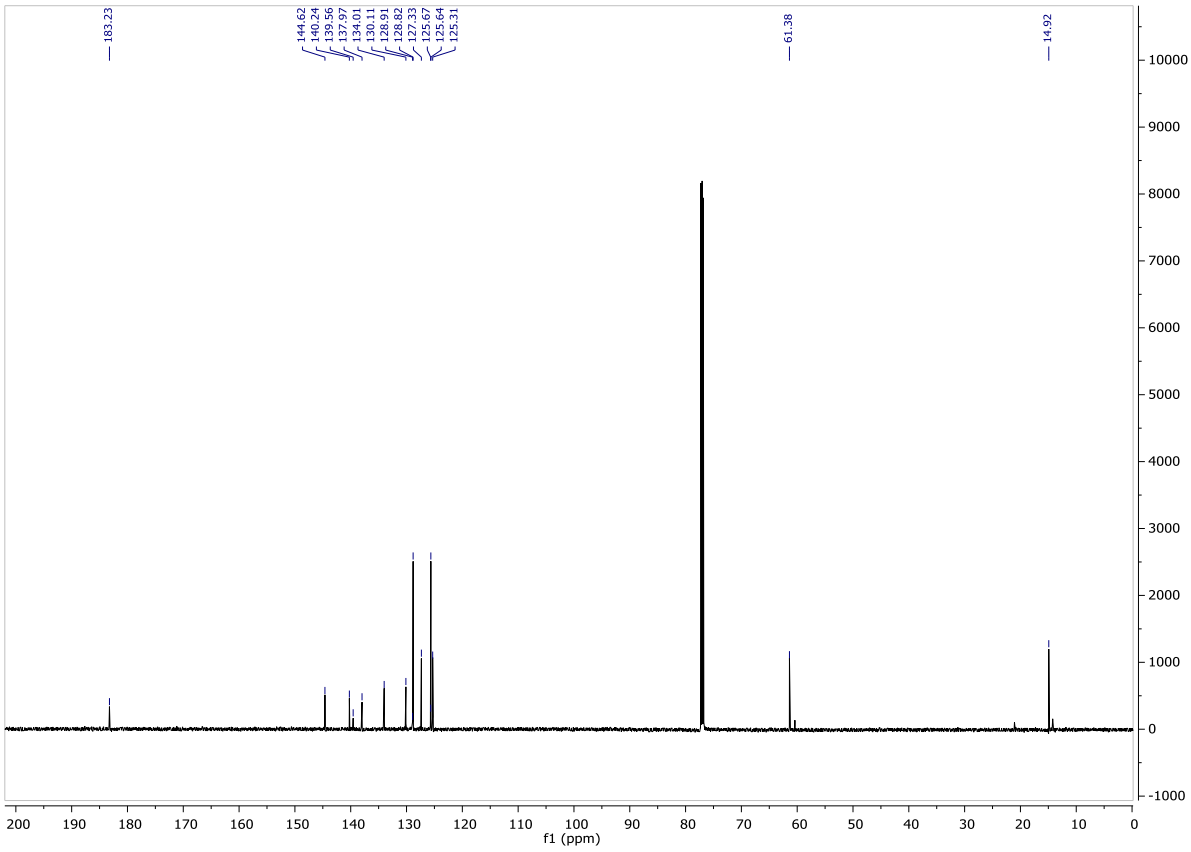

- Compound **1b**[c]

^{1}H NMR($CDCl_3$, 400MHz)

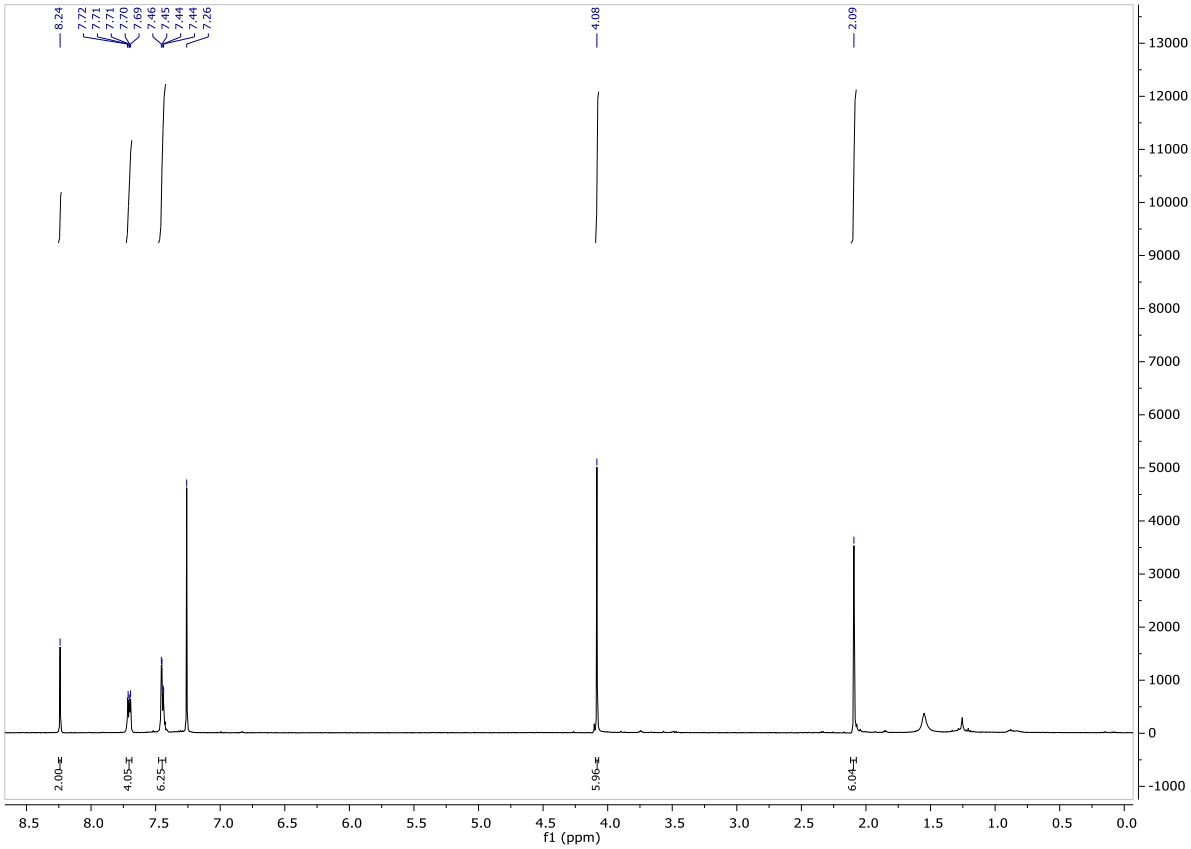

- Compound **9b**

^{1}H ($CDCl_3$, 300 MHz)

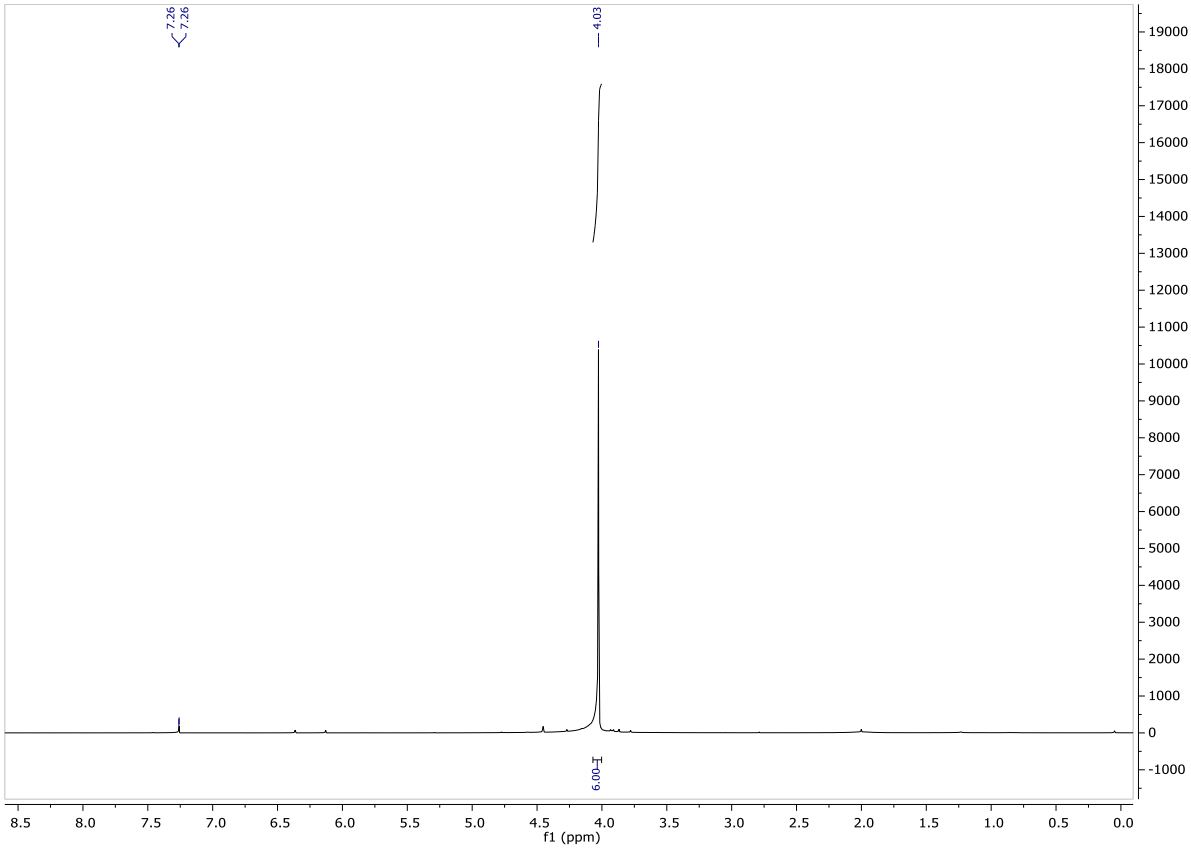

^{13}C NMR ($CDCl_3$, 75MHz)

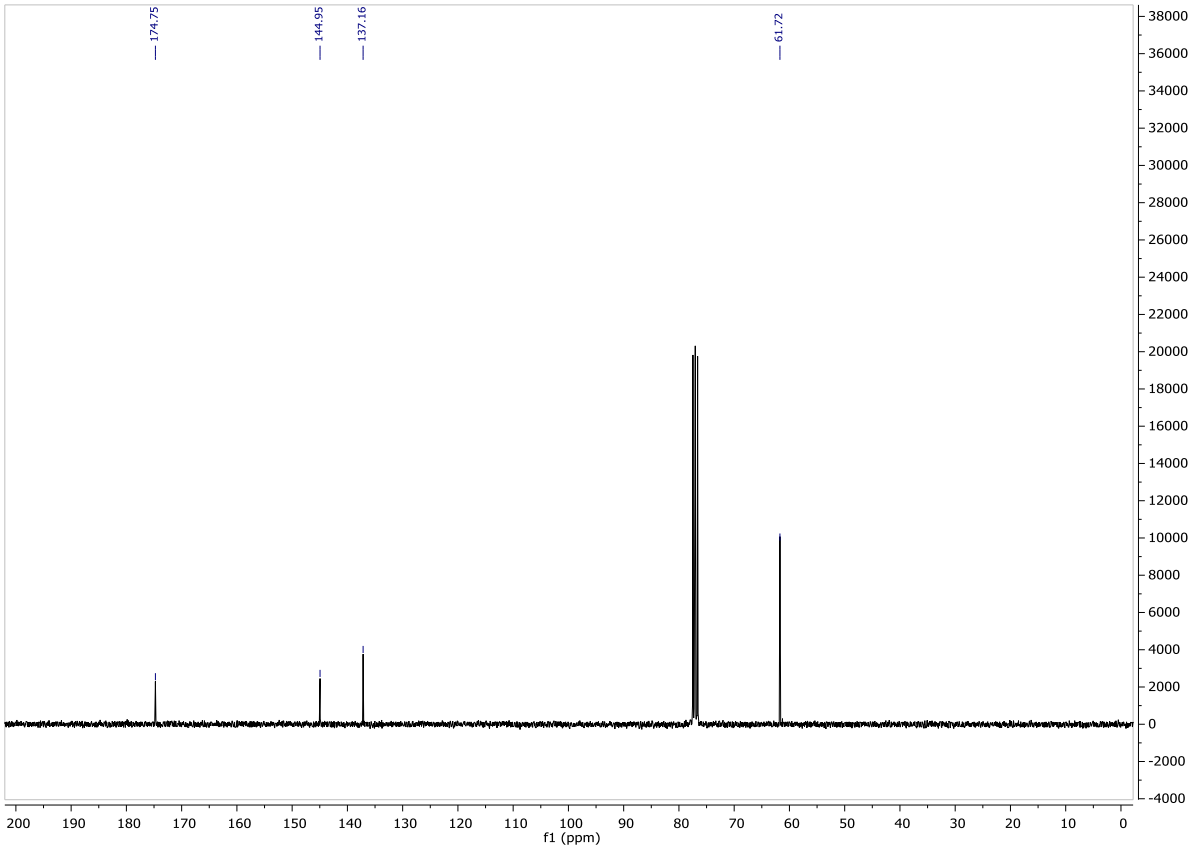

9. X-Ray Structure of 9b

Experimental. Single light red block-shaped crystals of (**9b**) were obtained by recrystallisation from .... A suitable crystal (0.25×0.18×0.10) mm^3 was selected and mounted on ... on a GV1000, TitanS2 diffractometer. The crystal was kept at T = 123.01(10) K during data collection. Using **Olex2**, the structure was solved with the **ShelXT** structure solution program, using the Direct Methods solution method. The model was refined with version 2016/6 of **ShelXL** using Least Squares minimisation.[8]

Crystal Data. $C_8H_6Br_2O_4$, M_r = 325.95, monoclinic, $P2_1/c$ (No. 14), a = 8.56023(6) Å, b = 16.31960(16) Å, c = 6.91885(5) Å, α = 94.8033(7)°, β = γ = 90°, V = 963.165(14) Å^3, T = 123.01(10) K, Z = 4, Z' = 1, μ(CuK) = 10.606, 13822 reflections measured, 1927 unique (R_{int} = 0.0288) which were used in all calculations. The final wR_2 was 0.0687 (all data) and R_1 was 0.0271 (I > 2(I)).

Compound	**9b**
Formula	$C_8H_6Br_2O_4$
$D_{calc.}$/ g cm^{-3}	2.248
□ /mm^{-1}	10.606
Formula Weight	325.95
Colour	light red
Shape	block
Size/mm^3	0.25×0.18×0.10
T/K	123.01(10)
Crystal System	monoclinic
Space Group	$P2_1/c$
a/Å	8.56023(6)
b/Å	16.31960(16)
c/Å	6.91885(5)
α/°	90
β/°	94.8033(7)
γ/°	90
V/Å^3	963.165(14)
Z	4
Z'	1
Wavelength/Å	1.54184
Radiation type	CuK□
μ_{min}/°	5.185
μ_{max}/°	73.474
Measured Refl.	13822
Independent Refl.	1927
Reflections Used	1907
R_{int}	0.0288
Parameters	129
Restraints	0
Largest Peak	0.519
Deepest Hole	-0.959
GooF	1.195
wR_2 (all data)	0.0687
wR_2	0.0685
R_1 (all data)	0.0276
R_1	0.0271

Images of the Crystal on the Diffractometer

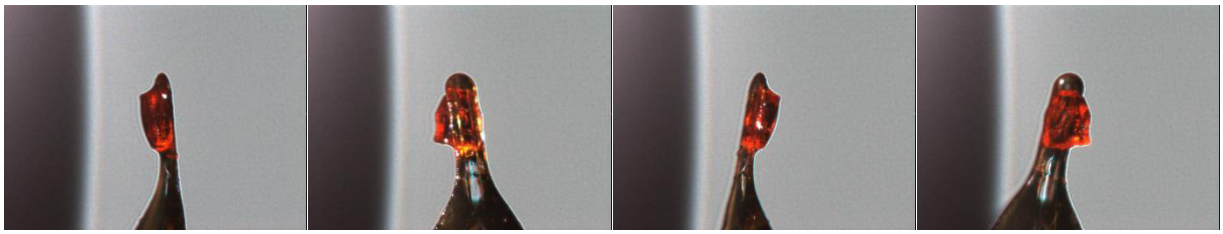

Table A2: Fractional Atomic Coordinates (×10⁴) and Equivalent Isotropic Displacement Parameters (Å²×10³) for **9b**. U_{eq} is defined as 1/3 of the trace of the orthogonalised U_{ij}.

Atom	x	y	z	U_{eq}
Br(01)	3602.1(3)	4478.8(2)	2540.8(4)	17.37(11)
Br(02)	6514.2(4)	3063.3(2)	2723.1(5)	24.33(11)
O(003)	5017(2)	6143.7(12)	2295(3)	20.8(4)
O(004)	7963(2)	6723.3(11)	2289(3)	16.2(4)
O(005)	10440(2)	5474.0(13)	2525(3)	25.2(5)
O(006)	9619(2)	3953.5(13)	2671(3)	25.2(4)
C(007)	5731(3)	4743.6(16)	2539(4)	14.6(5)
C(008)	7777(3)	7205.3(16)	4007(4)	18.4(5)
C(009)	6066(3)	5643.1(16)	2439(4)	13.9(5)
C(00A)	8896(3)	5350.6(17)	2538(4)	16.3(5)
C(00B)	7721(3)	5902.3(16)	2490(4)	14.2(5)
C(00C)	11073(3)	6289.2(18)	2343(5)	23.6(6)
C(00D)	8556(3)	4448.2(17)	2611(4)	17.0(6)
C(00E)	6881(3)	4187.5(16)	2614(4)	15.7(5)

Table A2: Anisotropic Displacement Parameters (×10⁴) **9b**. The anisotropic displacement factor exponent takes the form: $-2\pi^2[h^2a^{*2} \times U_{11} + ... + 2hka^* \times b^* \times U_{12}]$

Atom	U_{11}	U_{22}	U_{33}	U_{23}	U_{13}	U_{12}
Br(01)	14.53(16)	17.29(18)	20.33(16)	-0.73(10)	1.67(10)	-4.12(10)
Br(02)	27.31(18)	10.36(17)	34.83(19)	-0.58(11)	-0.37(13)	-0.24(11)
O(003)	15.3(9)	14.4(10)	32.8(11)	-0.2(8)	1.7(8)	2.5(8)
O(004)	19.0(9)	9.2(9)	20.7(9)	0.9(7)	2.9(7)	-1.3(7)
O(005)	10.9(9)	16.7(11)	47.9(13)	-0.4(9)	2.3(9)	0.8(7)
O(006)	21.3(10)	17(1)	37.0(11)	-1.0(9)	1.7(9)	7.9(9)
C(007)	16.4(12)	13.4(13)	14.1(11)	-0.5(9)	0.9(9)	-2.3(10)
C(008)	21.7(13)	9.6(13)	24.1(13)	-3.1(10)	1.9(10)	0.6(10)
C(009)	14.4(12)	11.5(13)	15.6(11)	-1.2(9)	0.0(9)	-0.9(10)
C(00A)	13.6(12)	14.2(14)	20.9(13)	-1.1(10)	0.3(10)	-0.7(10)
C(00B)	15.2(12)	10.8(13)	16.5(11)	-0.7(9)	0.6(9)	-0.8(10)
C(00C)	12.7(12)	18.5(16)	39.7(17)	0.0(12)	2.2(12)	-2.2(10)
C(00D)	15.5(14)	13.5(14)	22.0(13)	-1.5(10)	0.4(10)	3.1(10)
C(00E)	19.7(13)	8.8(13)	18.4(12)	-1.0(9)	-0.2(10)	-0.9(10)

Table A3: Bond Lengths in Å for **9b**.

Atom	Atom	Length/Å
Br(01)	C(007)	1.873(3)
Br(02)	C(00E)	1.864(3)
O(003)	C(009)	1.212(3)
O(004)	C(008)	1.445(3)
O(004)	C(00B)	1.365(3)
O(005)	C(00A)	1.338(3)
O(005)	C(00C)	1.446(3)
O(006)	C(00D)	1.214(3)
C(007)	C(009)	1.498(4)
C(007)	C(00E)	1.336(4)
C(009)	C(00B)	1.476(4)
C(00A)	C(00B)	1.348(4)
C(00A)	C(00D)	1.503(4)
C(00D)	C(00E)	1.496(4)

Table A4: Bond Angles in ° for **9b**.

Atom	Atom	Atom	Angle/°
C(00B)	O(004)	C(008)	115.00(19)
C(00A)	O(005)	C(00C)	121.1(2)
C(009)	C(007)	Br(01)	114.59(19)
C(00E)	C(007)	Br(01)	123.8(2)
C(00E)	C(007)	C(009)	121.6(2)
O(003)	C(009)	C(007)	121.4(2)
O(003)	C(009)	C(00B)	120.8(2)
C(00B)	C(009)	C(007)	117.8(2)
O(005)	C(00A)	C(00B)	129.4(3)
O(005)	C(00A)	C(00D)	110.0(2)
C(00B)	C(00A)	C(00D)	120.6(2)
O(004)	C(00B)	C(009)	115.6(2)
C(00A)	C(00B)	O(004)	122.6(2)
C(00A)	C(00B)	C(009)	121.4(3)
O(006)	C(00D)	C(00A)	120.4(2)
O(006)	C(00D)	C(00E)	121.7(3)
C(00E)	C(00D)	C(00A)	117.8(2)
C(007)	C(00E)	Br(02)	123.0(2)
C(007)	C(00E)	C(00D)	120.6(2)
C(00D)	C(00E)	Br(02)	116.39(19)

Table A5: Torsion Angles in ° for **9b**.

Atom	Atom	Atom	Atom	Angle/°
Br(01)	C(007)	C(009)	O(003)	-2.7(3)
Br(01)	C(007)	C(009)	C(00B)	178.23(17)
Br(01)	C(007)	C(00E)	Br(02)	0.2(3)
Br(01)	C(007)	C(00E)	C(00D)	-179.90(18)
O(003)	C(009)	C(00B)	O(004)	-2.5(4)
O(003)	C(009)	C(00B)	C(00A)	-176.2(3)
O(005)	C(00A)	C(00B)	O(004)	4.4(4)
O(005)	C(00A)	C(00B)	C(009)	177.6(3)
O(005)	C(00A)	C(00D)	O(006)	0.9(4)
O(005)	C(00A)	C(00D)	C(00E)	-179.4(2)
O(006)	C(00D)	C(00E)	Br(02)	0.2(3)
O(006)	C(00D)	C(00E)	C(007)	-179.7(3)
C(007)	C(009)	C(00B)	O(004)	176.6(2)
C(007)	C(009)	C(00B)	C(00A)	2.9(4)
C(008)	O(004)	C(00B)	C(009)	77.4(3)
C(008)	O(004)	C(00B)	C(00A)	-109.0(3)
C(009)	C(007)	C(00E)	Br(02)	-179.57(19)
C(009)	C(007)	C(00E)	C(00D)	0.3(4)
C(00A)	C(00D)	C(00E)	Br(02)	-179.59(19)
C(00A)	C(00D)	C(00E)	C(007)	0.5(4)
C(00B)	C(00A)	C(00D)	O(006)	-179.3(3)
C(00B)	C(00A)	C(00D)	C(00E)	0.4(4)
C(00C)	O(005)	C(00A)	C(00B)	-3.5(5)
C(00C)	O(005)	C(00A)	C(00D)	176.3(2)
C(00D)	C(00A)	C(00B)	O(004)	-175.4(2)
C(00D)	C(00A)	C(00B)	C(009)	-2.2(4)
C(00E)	C(007)	C(009)	O(003)	177.1(3)
C(00E)	C(007)	C(009)	C(00B)	-2.0(4)

Table A6: Hydrogen Fractional Atomic Coordinates (×10⁴) and Equivalent Isotropic Displacement Parameters (Å²×10³) for **9b**. U_{eq} is defined as 1/3 of the trace of the orthogonalised U_{ij}.

Atom	x	y	z	U_{eq}
H(00A)	8012.63	7768.54	3756.18	28
H(00B)	8477.96	7006.09	5057.56	28
H(00C)	6715.55	7161.56	4347.64	28
H(00D)	10594.01	6543.84	1190.43	35
H(00E)	12185.38	6255.54	2261.98	35
H(00F)	10860.34	6609.39	3454.57	35

10. Cartesian Coordinates

1b$^{o}_{min}$

Atom	x	y	z
C	-15.038.100.939	29.044.368.258	-189.601.034
C	-27.435.818.052	33.607.833.909	22.455.777.594
C	-39.483.644.619	25.473.892.067	19.515.662.397
C	-38.125.147.164	13.217.392.807	10.870.653.103
C	-2.576.252.481	0.8477607128	-0.7641834582
C	-13.509.790.066	15.744.334.641	-1.256.123.951
O	-0.2383080914	10.701.232.635	11.349.367.055
O	-50.459.938.542	28.802.618.984	23.898.102.771
O	-0.4325081838	36.197.832.826	22.979.630.224
C	0.7948298695	36.068.501.912	15.553.350.439
O	-2.818.761.995	44.928.455.524	29.748.998.423
C	-39.449.364.116	53.770.868.513	28.651.658.533
C	-50.842.932.396	0.7028804489	-0.6524457487
C	-23.479.058.148	-0.4412971071	-0.0741639194
C	-14.918.574.954	-0.6393755093	0.9922912281
S	-14.901.899.315	23.122.883.649	14.790.583.114
C	-26.387.026.896	27.639.229.878	0.2294284537
C	-29.935.817.273	16.545.008.209	-0.4902655318
C	-61.044.376.093	0.2791332862	15.684.984.657
C	-72.049.223.768	-0.277954771	-0.9709561582
S	-7.005.242.547	-0.2534301354	0.7742924737
C	-54.365.875.455	0.4948582063	0.6671830293
C	-30.987.181.919	41.484.777.864	0.0647001844
C	-0.6441714635	0.3443262569	17.451.250.838
C	-46.821.095.016	0.8236038157	19.198.924.874
C	-84.101.279.334	-0.8308376157	16.019.459.192
C	-22.860.412.204	52.412.126.554	0.4149864988

C	-27.364.384.881	65.489.214.316	0.2457982109
C	-40.040.023.534	67.944.416.967	-0.2849181614
C	-48.212.553.485	57.179.097.126	-0.6375918169
C	-43.789.617.457	44.094.763.898	-0.4585127408
C	-83.591.030.278	13.176.178.816	29.216.306.093
C	-9.497.525.022	18.294.484.571	35.387.835.005
C	107.110.847.683	-1.882.857.121	28.493.570.635
C	107.739.515.051	14.136.011.685	15.362.696.475
C	-96.390.531.138	-0.8895972542	-0.9207379426
H	13.074.429.393	45.262.454.292	18.479.294.282
H	0.6092753166	36.220.328.858	-0.4761841457
H	14.008.099.011	27.357.157.635	18.052.892.644
H	-35.747.774.314	63.438.235.029	32.145.844.027
H	-47.760.520.319	50.396.779.586	34.847.652.858
H	-42.810.350.822	54.681.818.263	18.273.184.849
H	-36.745.408.446	16.948.162.683	13.320.383.054
H	-60.198.696.384	0.4167866968	26.389.952.116
H	-10.561.703.299	13.545.542.054	16.613.424.732
H	-0.5935361254	0.0933615491	2.810.197.747
H	0.3773905385	0.3715086119	13.503.716.398
H	-395.448.197	16.176.406.824	17.278.834.578
H	-53.554.136.741	11.650.417.704	27.133.608.564
H	-41.290.904.004	-0.0453958374	2.297.640.016
H	-1.286.808.125	50.636.277.705	0.803819406
H	-2.090.187.574	73.781.833.972	0.5211265312
H	-4.353.597.776	78.144.288.417	-0.4189620466
H	-58.144.081.268	58.965.178.191	-1.041.203.447
H	-50.354.668.474	35.794.197.657	-0.7027585332
H	-74.148.691.772	-130.864.812	34.579.220.506

H	-9.433.260.732	-21.989.061.367	-45.588.770.773
H	-115.972.021.356	-22.882.190.083	-33.298.671.541
H	-117.126.422.404	-14.461.927.739	-0.9895893764
H	-97.106.405.417	-0.5039002113	0.0927701535

1b$^{c}_{min}$

Atom	x	y	z
C	-99.299.507.049	0.8515276913	0.3104560882
C	-9.799.601.403	-0.3774949452	0.9124215544
C	-85.209.763.459	-11.240.964.334	0.9064322419
C	-74.118.857.808	-0.5779458306	0.0957963348
C	-76.070.160.456	0.6628158584	-0.6655290947
C	-88.175.122.792	14.819.437.539	-0.4335020165
O	-89.522.350.412	26.308.484.045	-0.8741646675
O	-84.208.107.706	-21.557.114.744	-15.841.985.308
O	-110.936.788.922	150.449.798	0.5131187105
C	-116.498.259.109	23.821.995.491	-0.4760374544
O	-108.563.504.765	-0.8149636678	-16.286.791.853
C	-111.488.222.257	-22.129.752.161	1.763.784.573
C	-61.783.902.309	-12.046.479.283	0.0804706422
C	-66.629.593.781	10.560.956.137	-15.956.823.207
C	-55.232.731.308	0.0887480415	-19.359.982.381
S	-42.585.142.048	11.118.300.076	-28.540.863.606
C	-54.129.965.725	24.453.040.538	-30.443.010.807
C	-65.787.803.241	22.644.501.367	-23.489.638.241
C	-57.906.575.148	24.575.556.717	-0.6408409758
C	-45.539.989.842	29.120.006.676	-0.2658296033
S	-36.948.611.066	18.146.262.329	-0.8292329373
C	-50.051.265.181	-0.5011870533	-0.6109055868

C	-50.633.409.562	36.042.890.671	-38.702.366.783
C	-60.527.400.936	-0.9753659416	-29.306.112.916
C	-44.261.803.413	0.5585422611	0.3614765013
C	-39.348.118.641	41.774.116.552	-0.6700137811
C	-37.285.484.284	38.699.153.094	-42.291.944.909
C	-34.046.678.488	4.980.131.529	-50.052.137.651
C	-44.063.903.743	58.480.317.862	-54.425.828.793
C	-57.373.742.475	55.947.414.109	-50.989.277.141
C	-60.643.301.434	44.865.669.309	-4.324.762.396
C	-28.748.098.053	47.395.830.213	-0.0657504085
C	-23.023.168.947	59.496.611.372	-0.31826395
C	-27.727.373.786	-6.622.539.203	144.710.653
C	-38.204.467.474	-6.073.475.399	-21.917.603.375
C	-43.946.850.654	48.651.238.686	-1.811.176.367
H	-127.163.469.673	24.242.945.433	-0.2398004384
H	-112.059.646.404	33.761.983.243	-0.4214991621
H	-115.155.880.529	19.829.136.198	-14.861.451.645
H	-122.161.054.717	22.508.135.592	-1.997.579.188
H	-109.603.648.518	27.534.757.167	-0.8310202284
H	-105.649.357.469	26.660.430.441	-25.647.769.676
H	-73.588.158.484	3.009.088.532	-2.293.621.331
H	-64.712.608.811	30.250.282.302	-1.257.319.064
H	-64.606.368.872	-0.4738728787	-3.811.894.655
H	-52.528.952.309	16.476.443.136	-32.485.045.908
H	-6.847.086.337	15.686.491.901	-24.689.963.013
H	-35.442.681.451	10.413.373.784	-0.0650127334
H	-51.748.138.542	1.324.813.868	0.5811907574
H	-41.422.081.556	0.072605523	12.983.075.582
H	-29.361.711.056	32.120.130.099	-38.834.124.641

H	-23.668.667.817	51.683.555.181	-52.657.902.009
H	-41.538.675.912	67.131.852.382	-60.493.101.268
H	-65.249.446.414	62.601.097.232	-54.417.028.366
H	-71.037.113.941	42.901.508.559	-40.828.642.511
H	-25.090.918.657	42.347.535.409	-0.9555257965
H	-14.888.083.156	63.684.425.302	-0.267557469
H	-23.244.309.932	-7.565.426.226	17.477.322.014
H	-41.865.885.379	65.853.613.407	-30.773.895.157
H	-51.923.066.729	44.376.896.015	-24.099.693.386

13$_{min}$

Atom	x	y	z
C	-85.237.231.944	1.845.144.961	4.174.231.402
C	-77.780.346.415	21.896.299.724	30.908.716.649
N	-81.506.540.571	32.977.214.779	23.413.124.614
C	-92.539.323.754	41.020.512.402	25.944.422.176
C	-100.454.531.568	38.176.506.418	36.625.142.974
C	-9.747.192.847	26.479.033.066	45.879.731.578
C	-9.415.863.433	52.244.436.921	15.961.905.634
C	-65.410.991.917	1.501.336.992	25.620.059.942
C	-8.253.060.874	0.7006881917	50.554.962.711
O	-89.462.185.064	0.4373808372	60.250.694.453
O	-71.639.854.711	-0.0488835437	47.130.180.859
C	-6.876.094.058	11.777.251.462	-55.675.284.158
C	-76.910.744.956	24.020.238.852	-51.756.083.409
C	-112.434.406.052	45.749.946.065	-405.108.193
O	-119.165.696.212	42.868.234.045	-50.276.924.427
O	-115.502.309.254	56.304.935.087	-32.401.975.122
C	-127.236.746.206	63.906.951.862	-36.039.063.711
C	-139.950.325.138	57.583.863.983	-30.559.912.087

H	-7.581.787.103	35.280.268.013	15.418.089.482
H	-96.261.083.171	30.085.798.553	56.184.256.901
H	-106.227.808.678	19.880.074.937	46.474.682.686
H	-93.976.144.385	61.983.642.242	20.902.560.898
H	-86.127.758.779	51.992.431.914	0.8509081237
H	-103.731.392.482	5.154.501.943	10.747.795.022
H	-67.516.544.558	0.4651798938	22.875.529.625
H	-61.560.348.187	2.022.458.262	16.780.265.618
H	-57.517.854.132	14.720.828.541	-33.163.175.257
H	-58.050.166.589	13.528.033.513	-54.324.532.253
H	-70.691.217.244	-0.894450874	-66.049.045.887
H	-73.940.140.343	32.602.539.391	-57.898.445.528
H	-87.569.772.832	22.181.141.287	-53.341.221.523
H	-75.271.645.494	26.598.050.961	-41.236.787.681
H	-125.512.293.378	73.790.101.728	-31.684.226.409
H	-127.663.967.788	64.766.248.819	-469.220.384
H	-148.569.275.142	63.971.248.661	-32.823.519.076
H	-141.626.825.298	47.796.413.135	-35.133.195.294
H	-139.338.937.304	56.372.314.043	19.690.364.998

1b$^{o}_{ADJ}$

Atom	x	y	z
C	-0.80407314	349.775.721	-15.058.936
C	-207.115.394	392.368.047	-179.993.078
C	-322.183.471	299.959.576	-164.907.763
C	-297.730.862	160.333.084	-113.558.157
C	-17.214.937	118.960.893	-0.82168213
C	-0.56292178	214.493.641	-0.95931445
O	0.5663618	180.110.869	-0.61935797

O	-436.514.137	-335.173.676	-192.783.693
O	-0.20629407	-438.781.774	-158.489.269
C	-147.873.499	-397.970.545	-212.489.828
O	-223.091.921	-521.771.558	-213.226.349
C	-328.437.918	-566.789.326	-30.035.809
C	-418.515.763	-0.75676409	-0.98184586
C	-140.187.753	-0.20360185	-0.42931895
C	-0.70252086	-0.58842619	-0.69755785
S	-0.52539417	-232.353.261	-0.74765049
C	-137.936.463	-253.891.817	-0.77136128
C	-177.984.733	-131.898.097	-124.905.733
C	-502.004.666	-0.36654462	-20.800.463
C	-607.039.379	-0.44389611	-172.961.582
S	-606.654.767	-0.69825946	-0.0080325
C	-463.006.119	-0.26218373	-0.22656528
C	-159.246.256	-386.514.017	-136.250.269
C	-0.1377374	0.23915978	-181.482.925
C	-406.647.122	-0.45741426	-160.179.287
C	-709.883.527	-104.369.635	-258.867.137
C	-0.70309215	-492.966.732	-11.307.708
C	-0.91739511	-618.006.397	-170.760.516
C	-201.974.625	-639.542.017	-253.634.967
C	-291.298.897	-534.768.885	-27.740.735
C	-27.087.162	-409.958.779	-218.898.606
C	-738.860.876	-0.48460937	-384.860.303

C	-835.602.061	-105.280.301	-467.499.182
C	-906.622.802	-218.367.539	-426.392.498
C	-879.234.545	-274.425.729	-301.557.798
C	-781.825.994	-218.515.259	-219.041.541
H	-189.667.285	-488.326.595	-257.674.943
H	-213.515.316	-361.711.466	-133.176.829
H	-135.335.041	-320.456.288	-288.416.443
H	-294.462.863	-664.603.825	-335.324.252
H	-341.559.768	-499.315.309	-385.144.501
H	-422.533.101	-577.046.671	-245.971.095
H	-229.914.087	-119.545.317	-219.202.403
H	-481.479.699	-0.65910474	-310.343.234
H	-0.65281113	-12.013.264	-188.001.197
H	-0.24486959	-0.26788919	-278.022.455
H	0.92429182	-0.45131419	-165.284.401
H	-342.276.962	-134.128.186	-162.559.577
H	-486.032.038	-0.59726936	-23.436.296
H	-346.136.973	-0.40244361	-191.524.765
H	-0.1722729	-477.009.915	-0.50667087
H	-0.21505712	-698.653.238	-151.387.702
H	-218.573.254	-737.047.608	-298.603.605
H	-378.573.943	-550.778.751	-340.211.729
H	-343.233.254	-330.457.678	-234.440.606
H	-685.948.501	-0.40494442	-417.549.138
H	-856.675.645	-0.59878704	-56.401.158

H	-982.593.525	-261.927.032	-490.707.675
H	-933.387.407	-362.568.899	-268.231.005
H	-760.258.714	-264.831.274	-123.120.406

1b$^{c}_{ADJ}$

Atom	x	y	z
C	-907.836.258	112.179.091	0.17998013
C	-924.726.447	-0.12554757	0.73611198
C	-815.290.185	113.762.943	-0.69431059
C	-694.523.697	-0.80714238	-0.08928182
C	-681.491.236	0.51212176	-0.72062855
C	-779.981.716	156.271.355	-0.39190023
O	-760.456.436	277.328.926	-0.59725088
O	-828.416.733	220.368.065	-130.995.158
O	1.007.239.579	-203.590.213	0.34045185
C	1.058.567.529	-263.598.508	-0.85540958
O	1.041.569.911	-0.33691453	-13.524.679
C	1.081.948.342	-157.197.172	-196.805.019
C	-590.794.071	-172.138.538	-0.19599324
C	-579.357.693	0.75600729	-161.673.319
C	-493.130.236	-0.4216981	-20.809.625
S	-344.228.685	0.34925571	-290.484.382
C	-423.119.303	193.936.034	-293.689.147
C	-540.923.105	197.989.552	-224.007.228
C	-584.738.595	308.113.521	-0.22444285
C	-475.985.164	378.697.737	-0.22381751

S	-365.035.195	-283.206.065	-121.713.654
C	-459.226.653	126.455.115	-0.8373204
C	-360.215.613	305.280.399	-365.222.264
C	-570.017.456	-120.381.636	-317.548.716
C	-377.246.005	-0.49734521	0.23249255
C	-447.822.781	-52.011.553	0.03734703
C	-223.998.303	301.838.564	-400.493.006
C	-164.946.124	408.484.218	-467.827.892
C	-240.654.289	520.751.804	-501.701.297
C	-376.183.993	525.442.011	-467.827.806
C	-435.486.172	419.087.662	-400.629.632
C	-36.131.599	-593.889.001	-0.79250987
C	-336.095.349	-728.509.037	-0.54132164
C	-396.325.993	-79.214.929	-0.54553596
C	-481.979.987	720.023.733	-138.193.985
C	-507.446.994	585.533.758	-113.410.649
H	-1.136.975.463	-332.072.638	-0.52664653
H	-980.766.858	318.808.191	-138.854.447
H	-1.102.407.398	-18.720.126	-151.003.744
H	-1.186.766.634	-140.505.111	-222.473.308
H	-1.072.259.874	-242.219.114	-129.185.023
H	-1.022.808.837	-174.851.473	-286.923.586
H	-598.144.904	288.418.513	-209.069.091
H	-664.793.646	352.937.683	-0.79279585
H	-596.104.963	-0.52242689	-39.891.812
H	-509.090.056	-20.149.577	-358.014.319

H	-662.284.986	162.758.443	276.815.284
H	-279.703.169	0.20208691	0.16000492
H	-430.955.962	0.40000828	0.55251205
H	-362.234.795	114.084.185	110.288.635
H	-163.453.439	215.743.499	373.562.874
H	-0.59520121	403.886.562	493.651.851
H	-194.638.749	603.843.238	554.438.435
H	-436.093.433	612.042.707	494.586.719
H	-541.306.769	423.028.094	376.914.255
H	-31.507.692	545.957.671	-16.508.906
H	-269.511.505	783.846.986	119.756.157
H	-376.409.642	897.116.423	0.74266624
H	-528.469.006	768.558.584	223.549.721
H	-572.164.005	529.867.693	180.416.326

13_{ADJ} ($1b^{o}_{ADJ}$)

Atom	x	y	z
C	332.523.653	112.640.897	595.218.231
C	373.679.825	0.05903205	647.753.197
N	281.185.753	109.658.568	655.723.204
C	163.430.425	114.346.965	581.132.136
C	117.258.628	0.01880182	527.598.399
C	185.112.604	132.838.022	564.276.888
C	-10.575.818	-25.313.566	569.928.861
C	509.435.731	0.43450916	701.053.062

C	-416.649.765	-231.097.563	-572.761.441
O	-369.721.778	-341.967.111	-552.139.705
O	-551.085.145	-207.932.769	-572.213.859
C	-635.699.566	-322.903.665	-546.312.813
C	-657.820.609	-406.611.306	-671.398.715
C	-0.01163158	-0.15642699	-438.089.312
O	0.40416624	-12.458.593	-401.017.209
O	0.54063086	-101.253.475	-397.261.373
C	-164.752.222	-0.91976797	-30.400.643
C	-29.672.539	-0.68045628	-375.832.946
H	-31.534.672	-197.763.282	-691.418.331
H	-17.346.154	-204.255.236	-482.634.193
H	-134.154.586	-179.646.156	-650.158.122
H	-133.390.529	-312.336.261	-658.073.629
H	-0.02650442	-250.818.585	-561.705.431
H	-14.418.571	-304.882.361	-4.811.661
H	-56.832.203	-0.96469009	-625.179.527
H	-566.121.351	-0.44195252	-731.506.027
H	-498.097.224	-110.063.647	-78.751.919
H	-729.266.496	-279.159.863	-51.058.124
H	-590.865.325	-381.569.159	-465.878.746
H	-727.893.207	-488.016.367	-649.451.136
H	-563.755.246	-450.516.034	-705.620.158
H	-700.271.806	-345.970.049	-752.163.472
H	-16.386.812	-188.577.485	-25.295.147

H	143.568.847	-0.13009585	-231.640.933
H	378.975.454	-0.69125868	-303.358.868
H	296.323.201	0.29197779	-425.811.232
H	315.701.375	-146.136.803	-450.294.775

13_{ADJ} ($1b^{c}_{ADJ}$)

Atom	x	y	z
C	-858.894.485	177.736.855	414.837.596
C	-781.522.972	215.470.864	309.330.355
N	-823.806.398	319.812.407	228.353.399
C	-93.690.116	397.307.762	250.985.741
C	-1.016.354.515	368.846.977	35.762.785
C	-993.018.507	244.137.926	441.715.315
C	-951.506.933	507.879.554	149.463.994
C	-647.450.968	159.199.649	268.090.001
C	-827.513.523	0.68962655	508.256.571
O	-901.981.727	0.35654175	599.322.778
O	-70.948.059	0.04373206	-483.870.319
C	-680.436.919	109.732.804	-567.294.204
C	-753.608.305	233.409.362	-517.005.536
C	-1.133.692.055	446.333.645	-400.078.054
O	-1.211.088.197	407.149.093	-486.119.307
O	-1.148.566.381	568.040.598	-339.311.403
C	-1.263.070.463	645.674.499	38.033.826
C	-138.897.768	604.920.765	304.968.868
H	-778.842.975	330.174.612	138.307.863
H	-1.001.029.288	269.037.575	-548.164.277
H	-1.074.693.359	172.189.025	-425.109.012
H	-897.268.742	597.763.854	181.646.125
H	-909.516.158	475.374.795	0.53494787
H	-105.559.387	535.855.672	135.538.856
H	-651.160.781	0.50857605	255.757.661
H	-614.059.746	204.670.668	174.160.888

H	-571.780.764	179.506.668	34.454.252
H	-571.968.373	-121.904.003	55.992.159
H	-707.021.525	-0.8699352	670.874.972
H	-71.935.725	-322.436.714	571.111.588
H	-86.129.623	-223.066.138	533.041.365
H	-735.052.991	-248.177.418	410.031.823
H	1.235.048.877	749.065.827	35.801.003
H	-127.681.889	634.311.073	488.186.614
H	1.472.403.035	670.316.463	333.093.045
H	1.416.331.016	501.899.827	329.486.782
H	1.374.128.279	612.931.826	196.651.967

(1b$^{o}_{min}$-13$_{min}$)$_{ADJ}$

Atom	x	y	z
C	-0.8040730809	-34.977.569.396	-15.058.934.855
C	-20.711.537.808	-39.236.801.652	-17.999.306.454
C	-32.218.344.697	-29.995.955.349	-16.490.775.014
C	-29.773.083.957	-16.033.307.134	-11.355.814.853
C	-17.214.935.722	-11.896.088.458	-0.8216820681
C	-0.5629217323	21.449.362.409	-0.9593143737
O	0.5663617609	18.011.085.546	-0.6193579244
O	-43.651.410.342	-33.517.365.036	-19.278.367.776
O	0.2062940576	-43.878.173.992	-15.848.925.724
C	-1.478.734.882	-39.797.051.467	-21.248.981.172
O	-223.091.904	-52.177.151.798	-21.322.633.273
C	-32.843.789.287	-56.678.928.214	-30.035.806.748
C	-41.851.573.121	-0.7567640295	-0.9818457857

C	-14.018.774.251	-0.2036018311	-0.4293189171
C	-0.7025208105	-0.5884261487	0.6975577944
S	-0.5253941271	-23.235.324.344	0.7476504392
C	-13.793.645.274	-25.389.179.782	-0.7713612234
C	-17.798.471.965	-13.189.808.687	-12.490.572.345
C	-50.200.462.738	0.3665445912	-20.800.461.481
C	-60.703.933.248	-0.4438960709	-17.296.156.837
S	-60.665.472.163	-0.6982593997	0.0080324951
C	-46.300.608.387	0.2621837112	0.2265652618
C	-15.924.624.418	-38.651.398.723	-13.625.025.886
C	-0.1377373857	0.2391597656	-18.148.291.076
C	-4.066.470.907	0.4574142266	-16.017.927.455
C	-70.988.347.151	-10.436.962.684	-25.886.711.704
C	-0.70309209	-49.296.669.463	-11.307.707.087
C	-0.9173950396	-61.800.634.899	-17.076.050.223
C	-20.197.460.925	-63.954.196.599	-25.363.494.772
C	-29.129.887.545	-53.476.884.364	-27.740.732.856
C	-27.087.159.951	-40.995.874.779	-21.889.858.924
C	-7.388.608.182	-0.4846093346	-38.486.027.359
C	-83.560.199.847	-10.528.029.292	-46.749.914.647
C	-90.662.273.342	-21.836.752.202	-42.639.246.544
C	-87.923.447.993	-27.442.570.806	-30.155.777.422
C	-78.182.593.671	-21.851.524.226	-21.904.152.376
H	-18.966.727.034	-48.832.655.765	-25.767.492.377
H	-21.351.529.916	-36.171.143.877	-13.317.681.896
H	-13.533.503.084	-32.045.626.319	-28.841.642.061

H	-29.446.284.073	66.460.377.151	-33.532.422.633
H	-34.155.974.254	49.931.527.092	-3.851.444.711
H	-42.253.306.873	57.704.662.793	-24.597.107.658
H	-22.991.406.982	-11.954.530.753	-21.920.238.583
H	-48.147.966.225	0.6591046902	-31.034.320.972
H	-0.6528110757	12.013.263.058	1.880.011.825
H	-0.2448695742	-0.2678891665	27.802.243.357
H	0.9242917507	0.4513141603	16.528.438.905
H	-34.227.693.644	13.412.817.565	-16.255.956.418
H	-48.603.200.133	0.5972693176	-23.436.294.175
H	-34.613.694.635	-0.4024435798	-19.152.475.027
H	0.1722728827	-4.770.098.783	-0.5066708346
H	-0.2150571082	-69.865.318.642	-15.138.768.998
H	-21.857.323.743	-73.704.755.151	-29.860.358.181
H	-37.857.391.414	-550.778.711	-34.021.170.262
H	-34.323.322.744	-3.304.576.528	-23.444.058.834
H	-68.594.844.648	0.4049443936	-41.754.910.626
H	-85.667.557.943	-0.5987869915	-56.401.153.734
H	-98.259.344.754	-26.192.701.153	-49.070.763.801
H	-93.338.733.456	-36.256.887.201	-26.823.098.438
H	-76.025.865.778	-26.483.125.433	-12.312.039.622
C	-33.252.362.744	11.264.088.874	-59.521.818.802
C	-37.367.979.609	-0.0590320503	-64.775.314.575
N	-28.118.573.178	-10.965.855.975	-65.572.315.158
C	-16.343.041.307	-11.434.695.599	-58.113.209.227
C	-11.725.861.921	0.0188018177	-52.759.835.895
C	-18.511.258.988	-13.283.801.206	-56.427.684.228

C	-10.575.817.171	-25.313.564.093	-56.992.881.811
C	-50.943.569.166	-0.4345091282	-70.105.300.727
C	-41.664.973.301	2.310.975.455	-57.276.139.459
O	-36.972.175.025	34.196.708.509	-55.213.966.194
O	-55.108.510.385	20.793.275.293	-57.221.381.462
C	-63.569.951.875	32.290.363.991	-54.631.277.064
C	-65.782.055.933	40.661.127.557	-67.139.866.566
C	-0.0116315752	0.156426976	-43.808.927.846
O	0.4041662104	12.458.592.013	-40.101.717.818
O	0.5406308188	-10.125.346.773	-39.726.134.272
C	16.475.220.919	-0.9197679003	-30.400.640.635
C	29.672.536.738	-0.6804562234	-37.583.291.731
H	-31.534.669.658	-19.776.326.721	-69.141.827.849
H	-17.346.152.667	2.042.552.206	-48.263.415.644
H	-13.415.457.544	17.964.614.246	-6.501.580.742
H	-13.339.051.843	-31.233.623.744	-65.807.357.874
H	0.0265044204	-25.081.856.597	-56.170.538.846
H	-14.418.569.918	-30.488.233.777	-4.811.660.635
H	-56.832.198.695	-0.9646900149	-62.517.947.962
H	-56.612.130.977	0.4419524839	-73.150.596.965
H	-49.809.718.578	-11.006.363.899	-78.751.913.102
H	-7.292.664.396	27.915.984.229	-51.058.120.114
H	-59.086.528.017	38.156.913.048	-4.658.787.101
H	-72.789.315.292	48.801.632.997	-64.945.108.701
H	-56.375.520.202	45.051.599.964	-70.562.010.413

H	-70.027.175.365	34.597.002.253	-75.216.341.675
H	-16.386.810.753	-18.857.747.115	-25.295.145.088
H	-14.356.883.655	-0.1300958435	-23.164.091.522
H	-37.897.542.462	-0.6912586317	-30.335.884.474
H	-29.632.317.837	0.2919777636	-42.581.119.928
H	-31.570.135.069	-14.613.679.192	-45.029.474.075

(1b$^{c}_{min}$-13$_{min}$)$_{ADJ}$

Atom	x	y	z
C	-97.004.469.697	11.576.897.879	0.3124094828
C	-96.367.747.974	-0.0725992805	0.9032082039
C	-8.369.992.332	-0.853820236	0.9330678212
C	-72.665.719.045	-0.3882003749	0.0780252081
C	-7.409.501.795	0.8596594826	-0.6882739918
C	-8.564.090.081	17.411.407.164	-0.4306143476
O	-86.524.835.066	29.073.832.319	-0.8495768174
O	-82.940.963.455	-18.371.150.135	16.861.499.779
O	-108.219.976.372	19.147.453.412	0.4726162908
C	-115.891.298.624	21.544.497.797	-0.7216801132
O	-107.147.534.103	-0.4916692931	15.997.650.728
C	-110.869.669.311	-18.845.739.351	15.957.561.444
C	-60.748.234.533	10.960.795.727	-0.01895636
C	-64.789.340.304	11.826.314.148	-16.601.043.835
C	-5.421.130.263	0.1402566161	-20.359.669.844
S	-41.297.769.162	10.738.866.989	-30.110.471.758
C	-52.037.908.655	24.744.741.388	-31.745.977.417
C	-63.511.412.018	23.741.181.215	-24.309.623.681
C	-57.507.387.119	23.689.069.234	-0.5670555965

C	-45.620.392.621	29.091.894.153	-0.1421003401
S	-36.796.372.163	-1.874.271.102	-0.9886767604
C	-48.895.326.143	-0.476415182	-0.7274773279
C	-48.165.168.158	35.974.742.122	-4.032.173.842
C	-60.592.222.038	-0.8917054556	-30.008.531.479
C	-41.989.833.546	0.5473818614	0.2109441763
C	-40.129.699.057	42.115.712.698	-0.5265194477
C	-34.763.226.776	37.924.129.352	-4.418.592.111
C	-31.164.928.337	48.694.841.887	-52.256.577.912
C	-4.087.272.242	57.715.777.437	-56.670.343.625
C	-54.232.315.032	55.873.157.682	-52.966.083.396
C	-5.786.549.858	45.129.565.057	-44.903.012.248
C	-30.136.234.073	48.381.848.144	-0.2433855735
C	-25.050.565.471	60.814.738.589	-0.1252635883
C	-29.803.084.036	67.227.899.626	-12.716.118.372
C	-39.679.088.423	61.100.180.832	-20.494.878.015
C	-44.789.399.459	48.684.143.827	-16.843.956.226
H	-124.307.618.151	27.780.642.093	-0.4158762314
H	-109.932.916.666	26.775.153.939	-14.727.876.097
H	-119.636.878.949	1.208.001.244	-1.128.463.601
H	-121.623.736.903	18.907.047.669	-17.860.717.567
H	-108.873.510.952	23.413.740.794	-0.6223539253
H	-105.591.290.922	24.338.067.834	-23.742.915.974
H	-70.815.994.911	31.664.738.293	-23.635.040.018
H	-64.367.757.693	28.939.216.187	-12.136.070.044
H	-64.733.590.783	-0.3700796361	-3.867.261.622
H	-53.173.682.679	16.139.317.323	-33.483.440.438
H	-68.695.688.315	14.326.682.549	-25.039.706.133

H	-33.031.676.691	0.9629042898	-0.2551566537
H	-488.168.138	13.673.305.686	0.4502036474
H	-39.127.706.277	0.0518516357	11.420.295.489
H	-2.706.781.957	31.091.153.679	-40.704.632.918
H	-2.076.336.724	50.051.372.562	-55.071.376.252
H	-38.067.526.401	66.099.497.428	-62.980.338.718
H	-61.856.075.886	627.871.462	-56.436.601.848
H	-68.300.295.821	43.687.346.478	-42.302.489.529
H	-2.644.520.752	-43.599.827.098	-11.463.270.595
H	-17.390.068.173	-65.503.997.801	-0.4852364572
H	-25.819.808.907	-76.912.723.172	15.598.373.443
H	-4.335.436.419	-65.978.014.902	29.475.783.977
H	-52.275.727.006	-43.938.796.309	23.100.092.374
C	-85.025.823.675	0.9349295655	45.679.407.988
C	-720.514.493	0.9566062251	4.148.707.563
N	-67.477.167.587	20.567.597.688	3.443.278.669
C	-75.195.791.971	31.362.451.098	30.456.849.665
C	-88.270.631.765	31.869.035.338	34.282.083.811
C	-94.401.494.038	21.016.344.697	4.299.212.831
C	-67.667.221.216	41.270.199.193	21.916.569.567
C	-61.561.946.349	-0.1117538286	43.352.947.644
C	-91.329.402.013	-0.1626215751	5.306.346.888
O	-102.986.234.548	-0.1145608577	-56.894.242.183
O	-83.382.256.494	12.379.752.313	-55.439.371.736
C	-89.177.397.186	23.329.784.286	-6.292.522.427
C	-96.646.973.597	32.979.682.576	-5.384.494.069
C	-97.718.661.345	42.475.333.545	-30.663.028.629
O	-109.264.794.642	42.712.344.255	-34.830.126.347
O	-92.819.446.205	52.049.143.658	-22.384.149.345
C	-101.877.742.957	62.628.430.607	-18.448.628.039
C	-11.037.548.424	58.502.094.106	0.6524218138
H	-57.832.499.964	20.441.226.771	31.453.698.935
H	-97.865.377.763	25.331.047.675	52.507.439.849

H	-103.567.064.772	17.288.582.038	38.242.552.097
H	-56.987.949.616	38.882.822.947	21.752.394.156
H	-71.410.269.223	4.107.993.249	11.636.339.144
H	-68.900.947.925	51.452.379.185	25.624.565.058
H	-64.169.942.371	10.059.449.429	-37.613.235.534
H	-51.789.861.098	0.2446786852	39.955.487.063
H	-60.741.757.548	-0.4102206473	5.381.111.147
H	-80.608.510.431	28.181.845.165	-67.660.348.125
H	-95.730.497.734	19.265.791.347	-70.659.693.532
H	100.212.992.493	-41.547.700.352	-59.673.798.658
H	105.294.357.154	-28.084.179.423	-49.273.557.462
H	-9.009.190.832	36.712.830.961	-45.907.037.049
H	-95.305.394.883	70.986.113.547	15.932.510.072
H	108.073.035.747	-65.383.028.373	-27.012.559.398
H	116.309.603.177	-67.036.002.943	0.3053831617
H	117.205.633.769	-50.414.174.382	0.9266289814
H	104.036.021.902	-55.086.211.599	-0.1720667971

(1b$^{o}_{min}$-13$_{min}$)$_{nonADJ}$

Atom	x	y	z
C	-150.381.032	290.443.727	-189.601.063
C	-274.358.222	336.078.391	-22.455.781
C	-394.836.507	254.738.959	-195.156.654
C	-38.125.153	132.173.948	-108.706.548
C	-257.625.287	0.84776084	-0.76418358
C	-135.097.921	15.744.337	-125.612.414
O	-0.23830813	107.012.343	-113.493.688
O	-504.599.462	288.026.234	-238.981.064

O	-0.43250825	361.978.384	-229.796.337
C	0.79482999	360.685.073	-155.533.528
O	-281.876.242	449.284.623	-29.749.003
C	-394.493.701	537.708.766	-286.516.629
C	-508.429.402	0.70288055	-0.65244585
C	-234.790.618	-0.44129717	-0.07416394
C	-149.185.772	-0.63937561	0.99229139
S	-149.019.016	-231.228.872	147.905.853
C	-263.870.309	-276.392.341	0.22942849
C	-299.358.219	-165.450.108	-0.49026561
C	-610.443.856	0.27913333	-156.849.871
C	-720.492.346	-0.27795481	-0.9709563
S	-700.524.361	-0.25343017	0.77429259
C	-543.658.841	0.49485828	0.66718313
C	-309.871.867	-414.847.842	0.0647002
C	-0.64417156	0.34432631	174.512.535
C	-468.211.022	0.82360395	-191.989.278
C	-841.012.919	-0.83083775	-160.194.616
C	-228.604.157	-524.121.345	0.41498656
C	-273.643.891	-654.892.248	0.24579825
C	-400.400.296	-679.444.273	-0.2849182
C	-482.125.609	-571.791.057	-0.63759192
C	-437.896.242	-440.947.707	-0.45851282
C	-835.910.428	-131.761.808	-292.163.105
C	-949.752.647	-182.944.874	-353.878.404
C	-1.071.108.643	-188.285.742	-28.493.575
C	-1.077.395.317	-141.360.139	-153.626.988
C	-963.905.461	-0.88959739	-0.92073808
H	130.744.314	452.624.612	-184.792.971
H	0.60927541	362.203.344	-0.47618422
H	140.081.012	273.571.618	-180.528.954

H	-357.477.797	634.382.449	-32.145.849
H	-477.605.276	503.967.872	348.476.582
H	-428.103.574	546.818.267	182.731.876
H	-36.745.414	-169.481.653	133.203.851
H	-601.987.059	0.41678676	263.899.562
H	-105.617.049	135.455.441	166.134.273
H	-0.59353621	0.09336157	281.019.817
H	0.3773906	0.37150867	135.037.185
H	-395.448.257	161.764.093	172.788.372
H	-535.541.452	116.504.195	271.336.127
H	-412.909.103	-0.04539584	229.764.036
H	-128.680.832	-506.362.855	0.80381953
H	-209.018.789	-737.818.455	0.52112661
H	-435.359.844	-781.443.002	0.41896211
H	-5.814.409	-589.651.868	-10.412.036
H	-503.546.762	-357.942.031	0.70275864
H	-741.487.035	-130.864.832	345.792.257
H	-943.326.218	-219.890.647	455.887.778
H	-115.972.039	-228.821.935	332.986.766
H	1.171.264.402	-1.446.193	0.98958952
H	-971.064.202	-0.50390029	0.09277017
C	-561.317.887	1.086.924.755	405.491.909
C	-649.644.335	1.156.754.287	-32.929.363
N	-785.721.933	1.136.871.922	348.609.297
C	-841.606.419	1.048.735.118	440.213.197
C	-759.285.583	-975.567.009	519.908.751
C	-607.954.816	-988.537.863	511.651.385
C	-992.649.793	1.047.366.237	437.219.737
C	-618.963.258	1.257.796.692	-22.120.263
C	-415.035.688	1.097.333.695	396.012.963

O	-339.657.846	1.033.274.349	-467.520.235
O	-369.206.577	1.184.415.448	-301.309.165
C	-225.656.075	-119.658.286	-290.412.321
C	-166.576.065	1.087.907.934	-201.719.937
C	-803.846.223	-878.473.348	-620.826.853
O	-725.926.414	-81.590.553	-69.091.901
O	-939.222.437	-863.326.869	-630.886.068
C	-985.351.482	-768.452.879	-729.590.945
C	-985.838.341	-626.366.544	-675.047.317
H	-848.904.072	1.189.708.616	-290.515.712
H	-56.755.878	1.017.407.975	-609.633.506
H	-56.311.754	-889.992.679	-493.347.424
H	1.034.344.335	1.074.173.966	-534.546.323
H	1.030.586.417	1.118.127.695	-362.627.927
H	1.030.794.418	-94.791.679	-413.008.545
H	-560.360.417	1.212.988.643	-140.637.472
H	-711.499.747	1.298.079.125	-178.459.871
H	-560.005.026	1.340.960.733	-26.039.769
H	-210.136.873	1.295.903.513	-247.335.526
H	-182.170.495	1.193.317.242	-390.586.557
H	-0.58922283	1.104.441.396	-189.141.773
H	-181.199.148	-989.492.733	-247.014.512
H	-213.229.199	1.088.741.304	-102.616.311
H	1.086.515.322	-801.999.259	-754.127.073
H	-922.097.301	-776.136.992	-818.337.049

H	-1.028.436.872	-557.995.153	-749.422.116
H	-883.941.002	-593.689.516	-6.526.615
H	-1.046.149.766	-619.746.716	-583.846.524

$(1b^{c}_{min}\text{-}13_{min})_{nonADJ}$

Atom	x	y	z
C	-957.100.204	-174.607.876	-0.17104519
C	-944.065.278	-297.510.169	0.4309204
C	-81.620.274	-372.170.334	0.42493109
C	-705.293.655	-317.555.261	-0.385705
C	-724.806.685	-193.479.065	-114.703.061
C	-845.856.336	-111.566.256	-0.91500347
O	-859.328.612	0.03324235	-135.566.623
O	-806.186.182	-475.331.862	-110.269.755
O	-107.347.305	-109.310.834	0.03161747
C	-1.129.087.763	-0.21540657	-0.95753891
O	-1.049.740.201	-341.257.051	-114.717.821
C	-1.078.987.389	-481.058.238	-128.228.363
C	-581.944.068	-380.225.486	-0.40103069
C	-630.400.998	-15.415.108	-207.718.404
C	-516.432.348	-250.885.859	-241.750.003
S	-389.956.426	-148.577.639	-333.558.838
C	-505.404.691	-0.15230204	-352.580.314
C	-62.198.309	-0.33315601	-283.046.571
C	-543.170.791	-505.516.288	0.15933976
C	-41.950.491	-550.960.799	-0.2156717
S	-333.591.104	-441.223.331	-131.073.448
C	-464.617.673	-309.879.382	-109.240.709
C	-470.439.119	100.668.324	-435.173.892

C	-569.379.051	-357.297.281	-341.211.332
C	-406.723.043	-203.906.426	-0.12002477
C	-357.586.186	-677.501.928	0.18851257
C	-336.959.836	127.230.955	-471.069.682
C	-30.457.177	238.252.602	-548.671.626
C	-404.744.046	325.042.648	-592.408.549
C	-537.842.463	299.713.607	-558.043.021
C	-57.053.806	188.896.131	-480.626.475
C	-251.585.954	-733.719.078	-0.54725178
C	-19.433.665	-854.726.913	-0.16323733
C	-241.378.708	-922.014.737	0.96560551
C	-346.149.669	-867.108.343	171.025.948
C	-403.573.515	-746.273.163	132.967.542
H	-1.235.739.898	-0.17331155	-0.72130185
H	-108.470.163	0.77859244	-0.90300062
H	-1.115.663.976	-0.61469258	-196.764.686
H	-1.185.715.735	-484.842.073	-15.160.783
H	-1.060.141.641	-535.108.299	-0.34951907
H	-1.020.598.728	-52.636.503	-20.832.762
H	-699.986.658	0.41148257	-277.512.321
H	-611.231.145	-562.263.559	0.775818
H	-610.168.748	-307.147.964	-429.339.689
H	-489.394.551	-424.525.135	-373.000.668
H	-6.488.137	-416.625.621	-295.049.822
H	-318.531.804	-155.626.904	-0.5465141
H	-481.586.412	-127.279.249	0.09968954
H	-378.325.818	-252.500.112	0.81680649
H	-257.722.085	0.61440709	-43.649.147
H	-200.791.639	257.075.004	-574.729.276
H	-379.491.762	411.558.014	-653.081.281
H	-616.599.521	366.250.448	-592.320.546

H	-674.476.214	169.254.519	-456.436.654
H	-215.014.153	-683.236.119	-143.702.737
H	-112.985.774	-896.605.069	-0.74905889
H	-19.654.806	-101.630.346	126.623.124
H	-382.763.857	-918.296.949	259.588.887
H	-483.335.694	-703.529.728	192.846.854
C	-989.601.213	-600.006.919	-281.024.455
C	-871.306.731	-58.577.846	-346.506.305
N	-850.734.682	-472.855.385	-424.677.198
C	-942.933.701	-370.807.277	-44.385.983
C	-1.063.443.876	-378.291.396	-381.386.135
C	-1.099.199.386	-495.029.743	-290.660.542
C	-893.005.078	-261.755.667	-535.728.306
C	-753.403.595	-6.802.947	-346.195.893
C	-1.025.445.177	-71.389.156	-195.337.933
O	-1.132.697.484	-72.170.108	-13.759.137
O	-929.667.807	-810.656.722	-184.588.513
C	-96.255.297	-923.470.487	-100.534.027
C	-1.042.893.703	-1.028.368.744	-17.609.031
C	-1.170.641.863	-278.375.539	-39.246.359
O	-1.276.912.913	-288.994.582	-333.363.325
O	-1.142.726.747	-172.178.986	-473.706.218
C	-1.246.653.064	-0.72580841	-486.000.422
C	-1.349.025.509	-110.954.048	-591.883.159
H	-762.270.555	-465.070.944	-472.343.384
H	-1.124.360.004	-458.008.498	-190.350.061
H	-119.248.225	-541.645.216	-325.038.955

H	-892.536.074	-164.824.516	-485.392.551
H	-791.184.106	-2.834.904	-569.939.463
H	-957.389.057	-251.348.493	-623.351.263
H	-781.345.058	-778.534.605	-384.938.585
H	-671.856.172	-640.678.688	-407.784.937
H	-71.563.257	-696.065.635	-244.937.745
H	-865.530.532	-96.281.713	-0.68918552
H	-1.017.380.493	-88.764.042	-0.13088681
H	-1.059.487.238	-1.115.863.557	-1.121.355
H	-1.140.261.443	-988.167.576	-205.319.993
H	-989.525.479	-106.117.433	-265.947.784
H	-1.193.340.358	0.1886951	-513.497.589
H	-1.294.253.152	-0.58894763	-388.620.073
H	-1.422.041.581	-0.30100494	-604.222.143
H	-1.402.635.618	-201.476.413	-562.157.087
H	-1.300.556.404	-128.453.987	-68.854.429

11. References

1. Fröhlich, J.; Hametner, C.; Kalt, W., Synthesis of trisubstituted thiophenesvia a halogen dance reaction at 2-bromo-5-methylthiophene. *Monatshefte für Chemie / Chemical Monthly* **1996,** *127* (3), 325-330.
2. Wang, R.; Pu, S.; Liu, G.; Cui, S.; Liu, W., Synthesis and photochromism of isomeric unsymmetrical diarylethenes bearing both naphthalene and thiophene moieties. *Journal of Photochemistry and Photobiology A: Chemistry* **2012,** *243*, 47-55.
3. Gregg, C.; Kyryakov, P.; Titorenko, V. I., Purification of Mitochondria from Yeast Cells. **2009,** (30), e1417.
4. Bradford, M. M., A rapid and sensitive method for the quantitation of microgram quantities of protein utilizing the principle of protein-dye binding. *Anal Biochem* **1976,** *72* (1), 248-254.
5. Reddy, C. A.; Beveridge, T. J.; Breznak, J. A.; Marzluf, G. A.; Schmidt, T. M.; Snyder, L. R., *Methods for General and Molecular Microbiology, Third Edition*. American Society of Microbiology: 2007.
6. (a) Becke, A. D., Density-functional thermochemistry. III. The role of exact exchange. *The Journal of Chemical Physics* **1993,** *98* (7), 5648-5652; (b) Lee, C.; Yang, W.; Parr, R. G., Development of the Colle-Salvetti correlation-energy formula into a functional of the electron density. *Physical Review B* **1988,** *37* (2), 785-789; (c) Stephens, P. J.; Devlin, F. J.; Chabalowski, C. F.; Frisch, M. J., Ab Initio Calculation of Vibrational Absorption and Circular Dichroism Spectra Using Density Functional Force Fields. *The Journal of Physical Chemistry* **1994,** *98* (45), 11623-11627.
7. Kuhn, B.; Kollman, P. A., A Ligand That Is Predicted to Bind Better to Avidin than Biotin: Insights from Computational Fluorine Scanning. *Journal of the American Chemical Society* **2000,** *122* (16), 3909-3916.
8. (a) Dolomanov, O. V.; Bourhis, L. J.; Gildea, R. J.; Howard, J. A. K.; Puschmann, H., OLEX2: a complete structure solution, refinement and analysis program. *Journal of Applied Crystallography* **2009,** *42* (2), 339-341; (b) Sheldrick, G. M., Crystal structure refinement with SHELXL. *Acta Crystallographica. Section C, Structural Chemistry* **2015,** *71* (Pt 1), 3-8; (c) Linden, A., Chemistry and structure in Acta Crystallographica Section C. *Acta Crystallographica Section C* **2015,** *71* (1), 1-2.

A.II.2. Synthesis and Characterization of Generation II Coenzyme Q Switches

Compound ***7***

^{1}H-NMR (300 MHz, Chloroform-*d*)

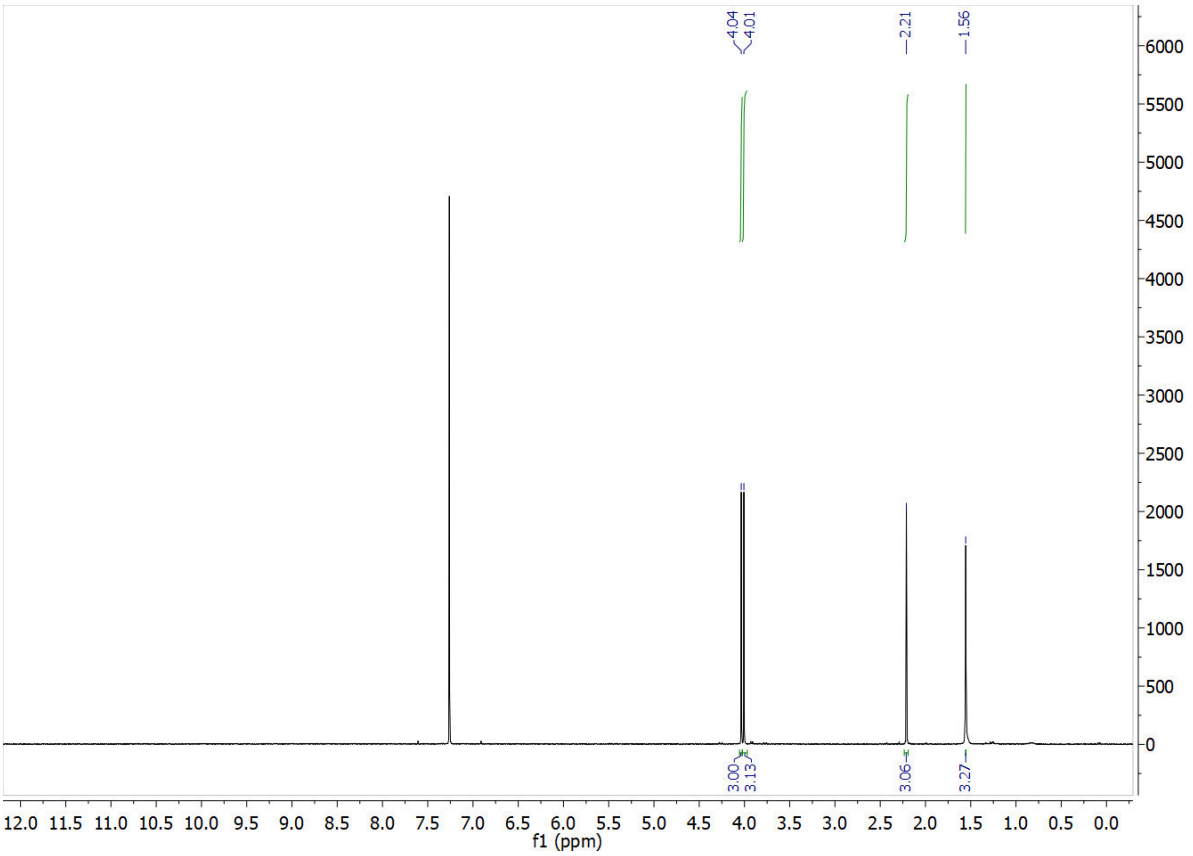

Compound **8a**

^{1}H NMR (600 MHz, Chloroform-*d*)

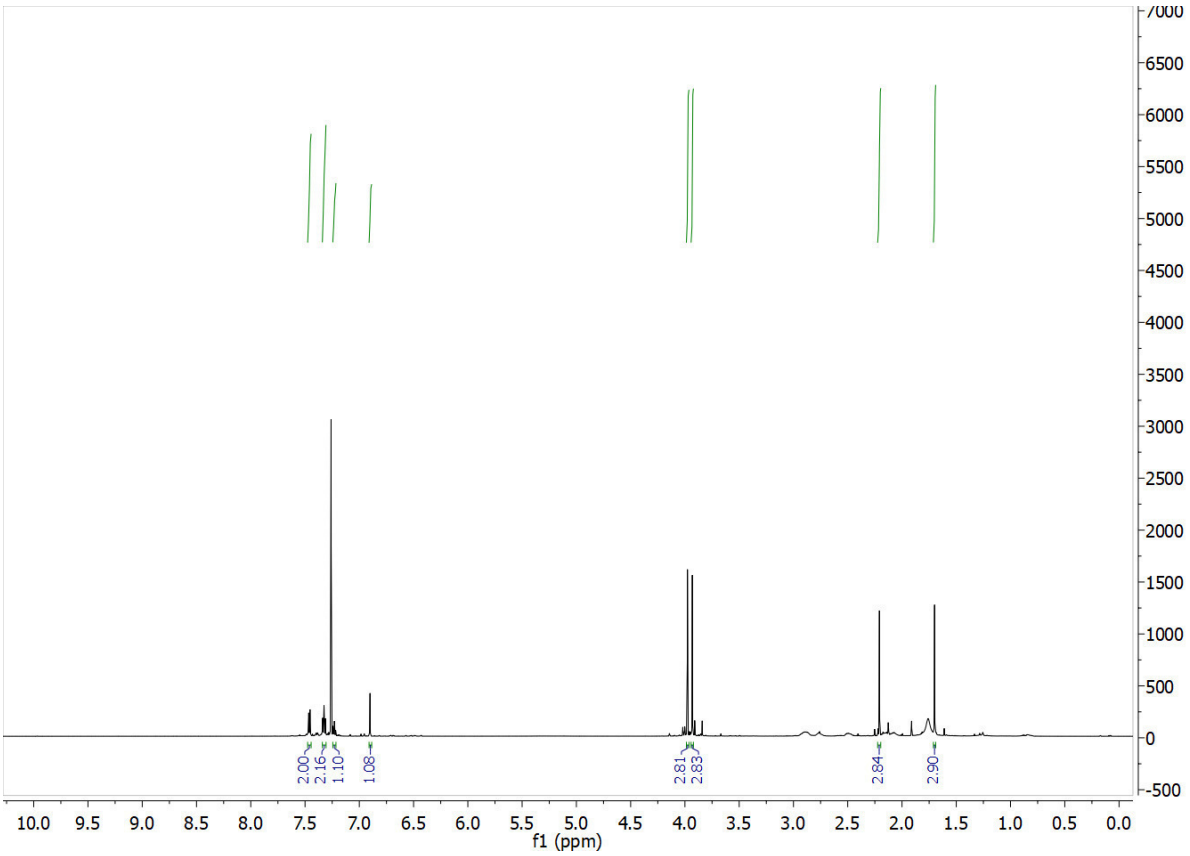

^{1}H NMR (151 MHz, Chloroform-*d*)

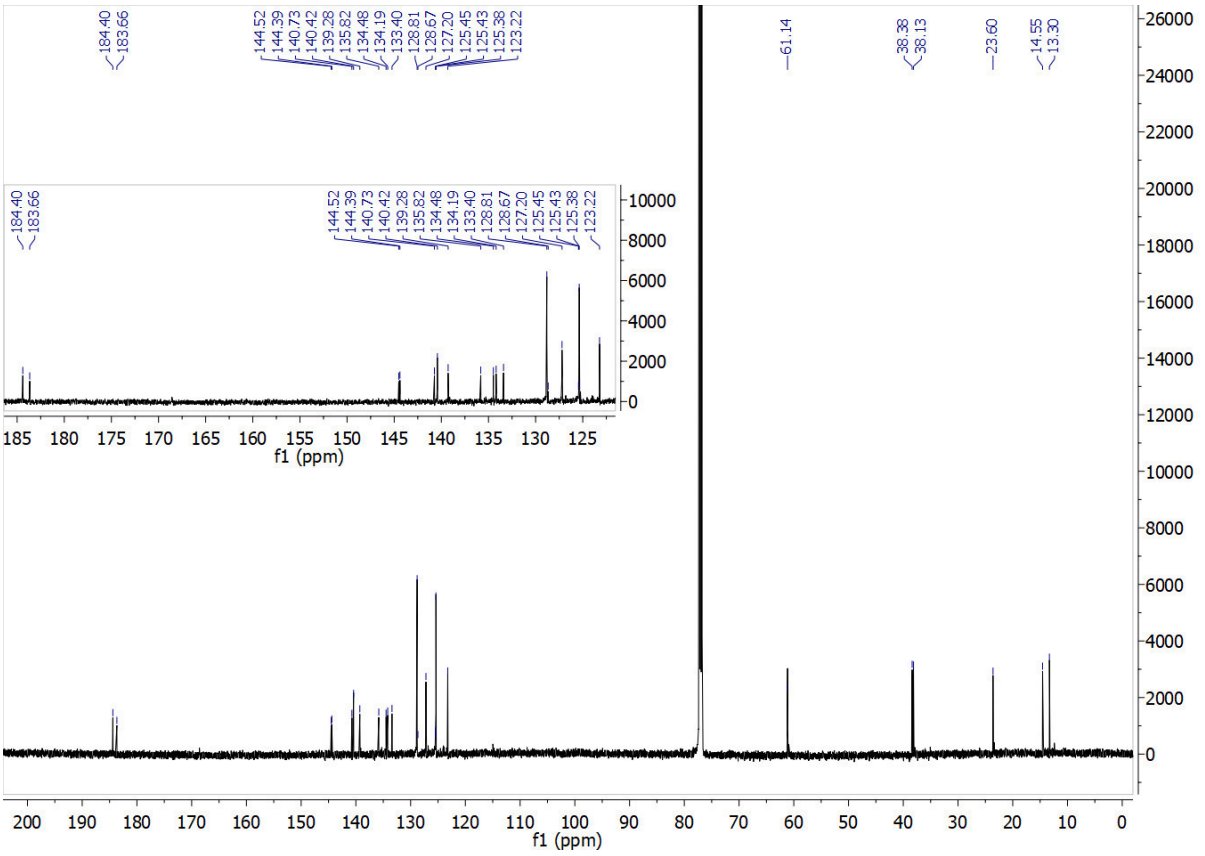

Compound **12**

^{1}H NMR (400 MHz, Chloroform-*d*)

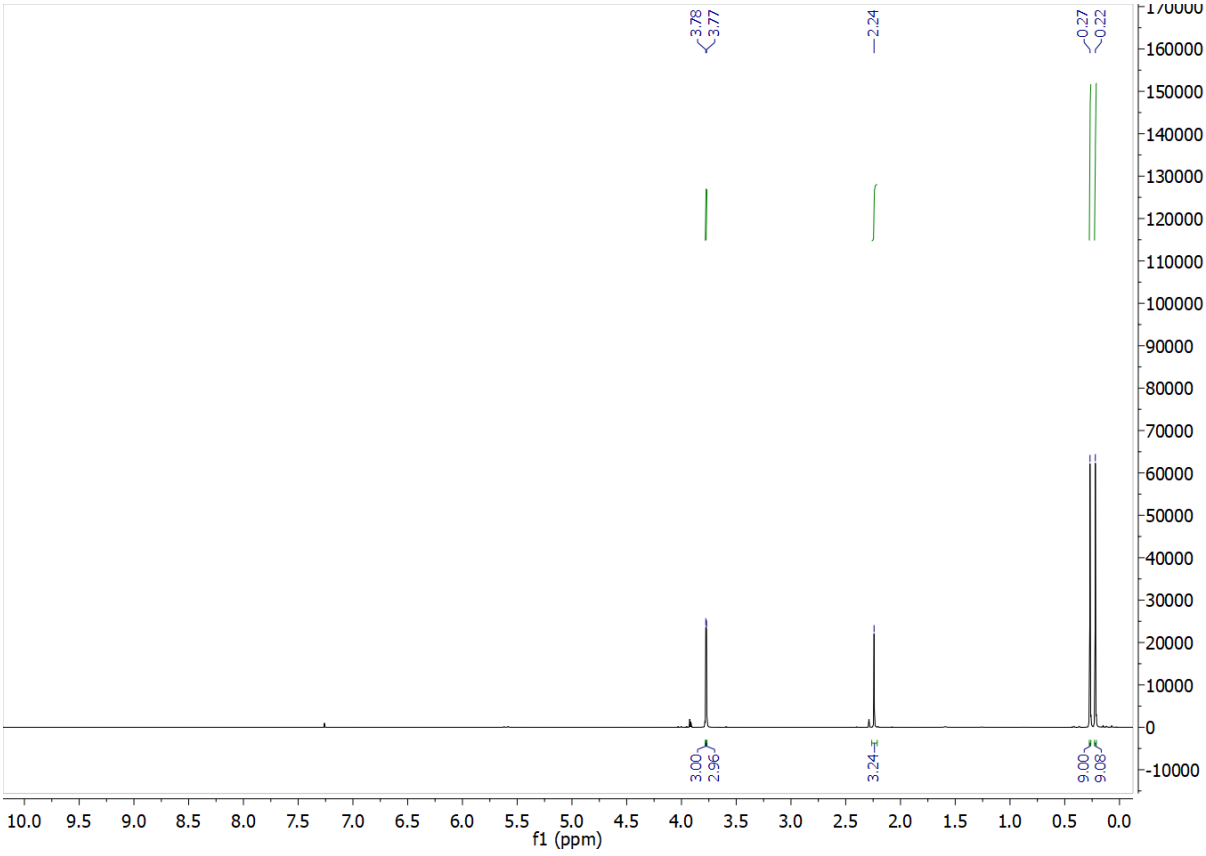

^{1}H NMR (101 MHz, Chloroform-*d*)

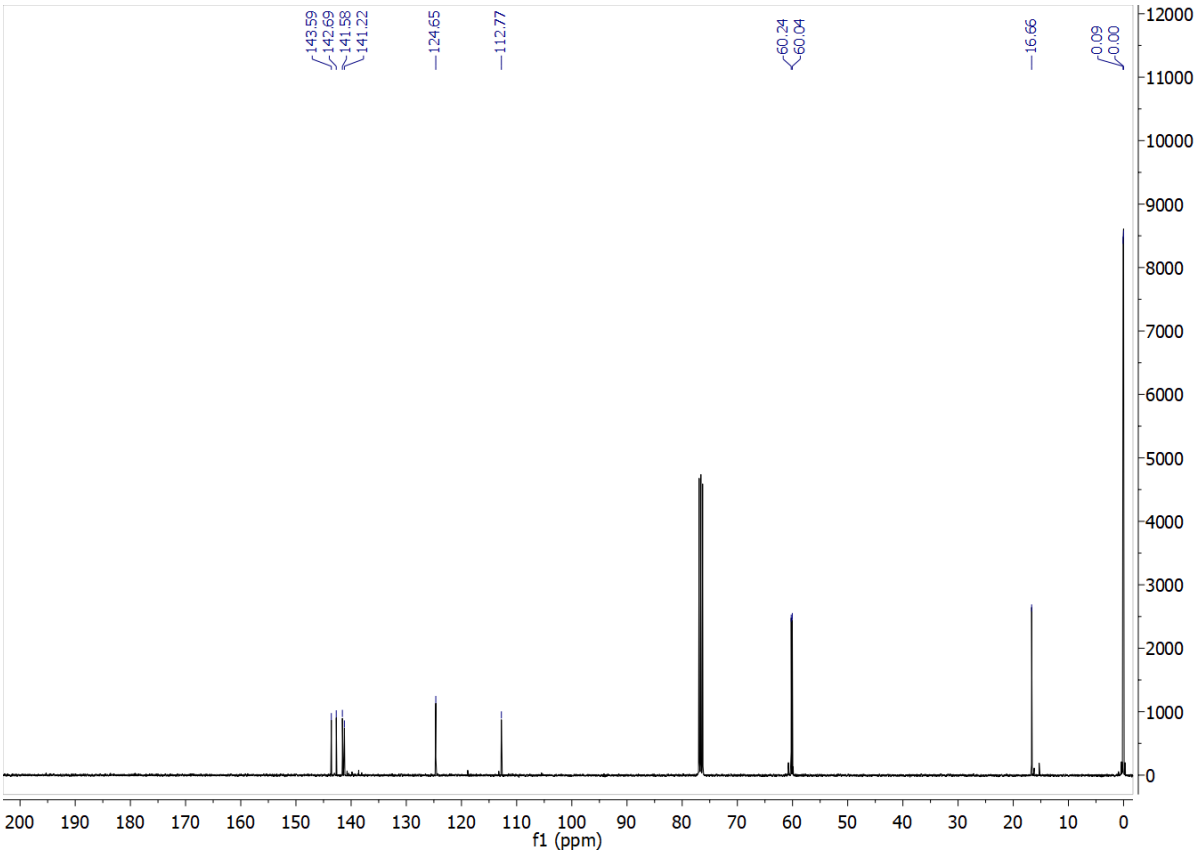

A.II.3. Towards Photocontrollable NAD^+ Analogues

Table of Contents

1. NMR

7a^{o} ^{1}H NMR (600 MHz, Methanol-d_4)

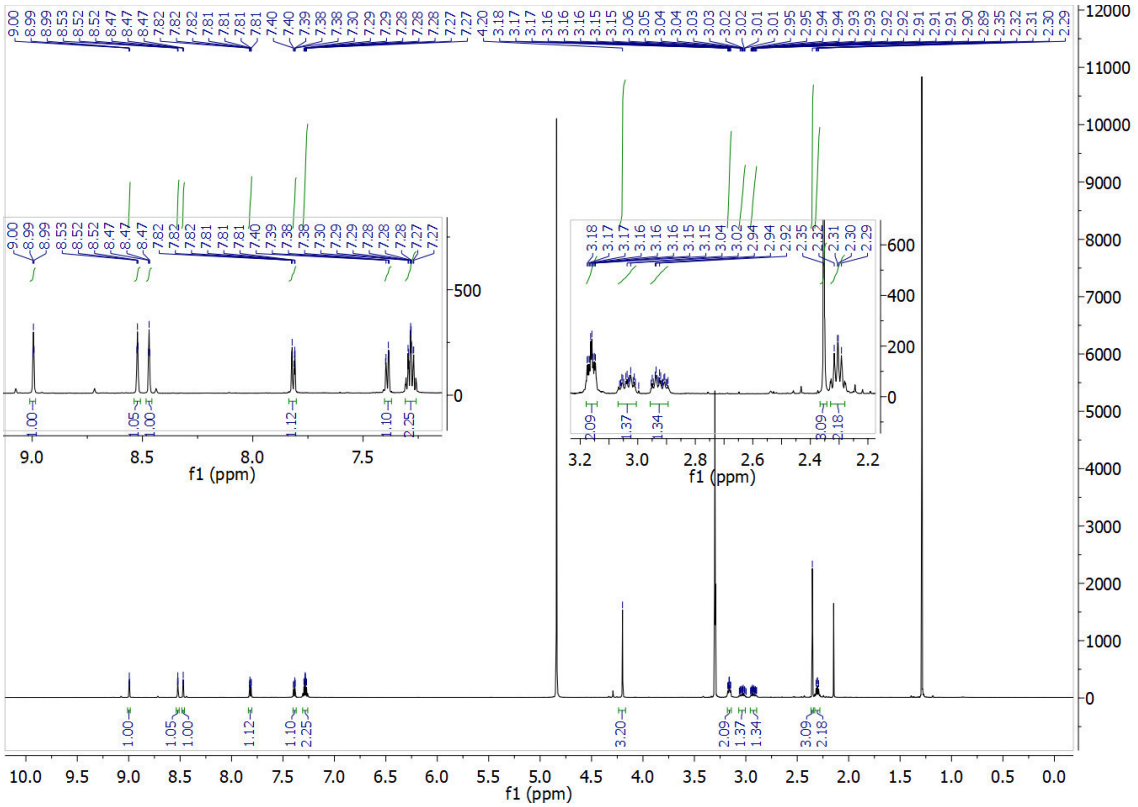

^{13}C NMR (151 MHz, Methanol-d_4)

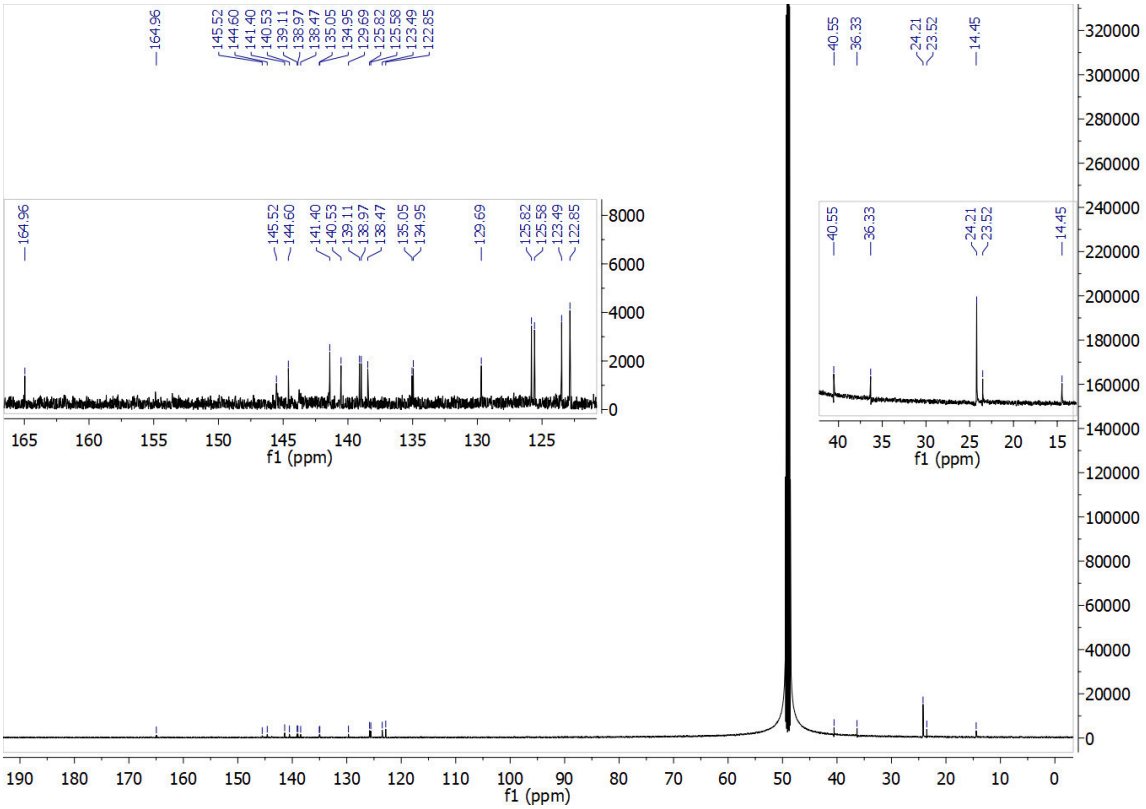

7b^{o} ^{1}H NMR (600 MHz, Methanol-d_4)

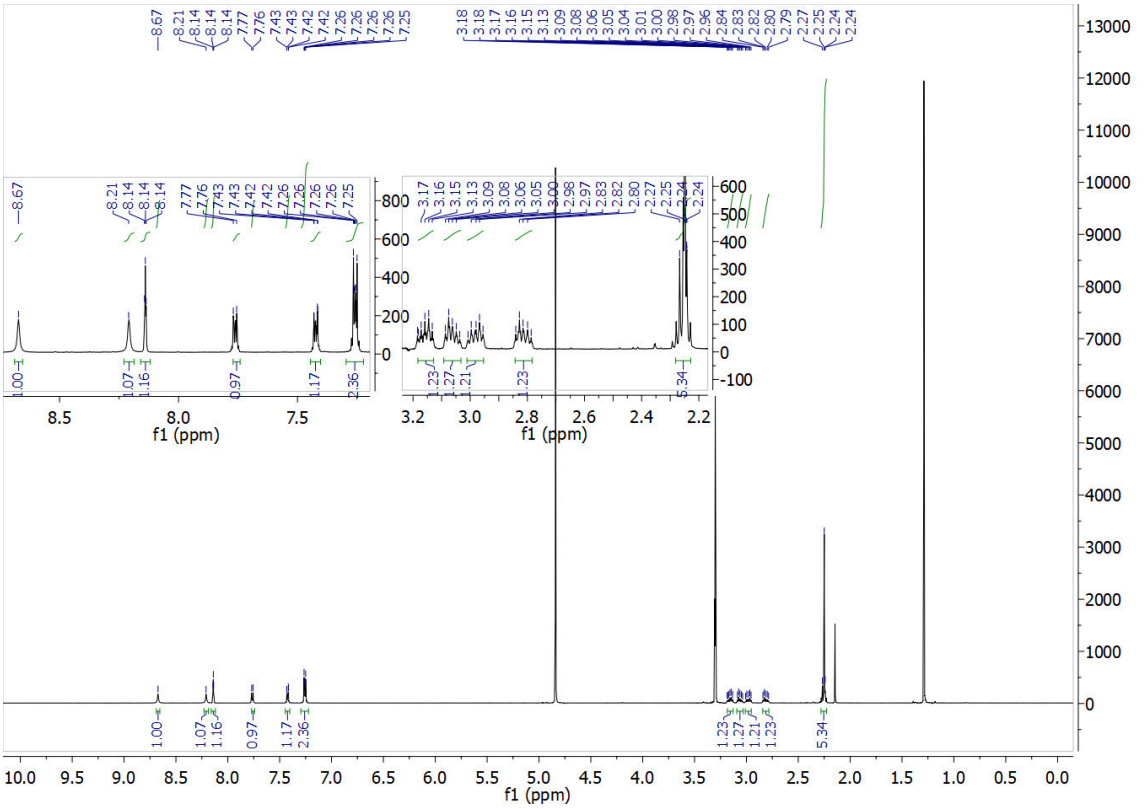

^{13}C NMR (151 MHz, Methanol-d_4)

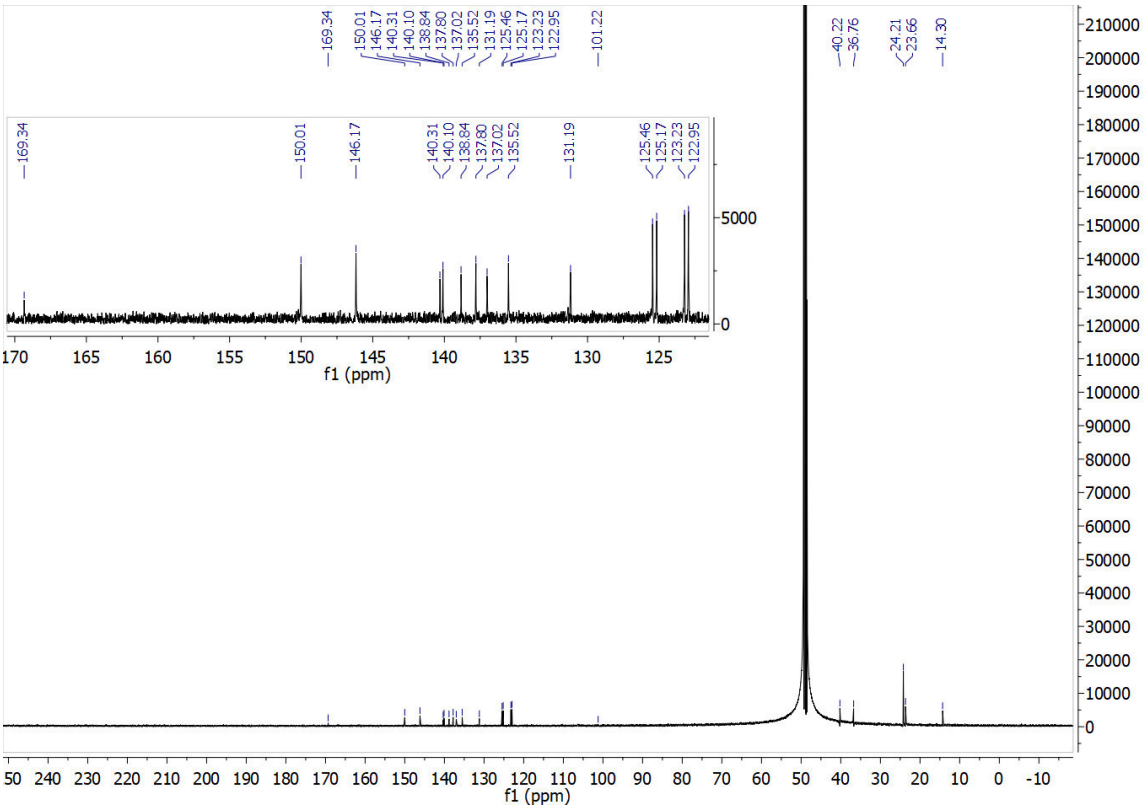

8c^{o} ^{1}H NMR (600 MHz, Methanol-d_4)

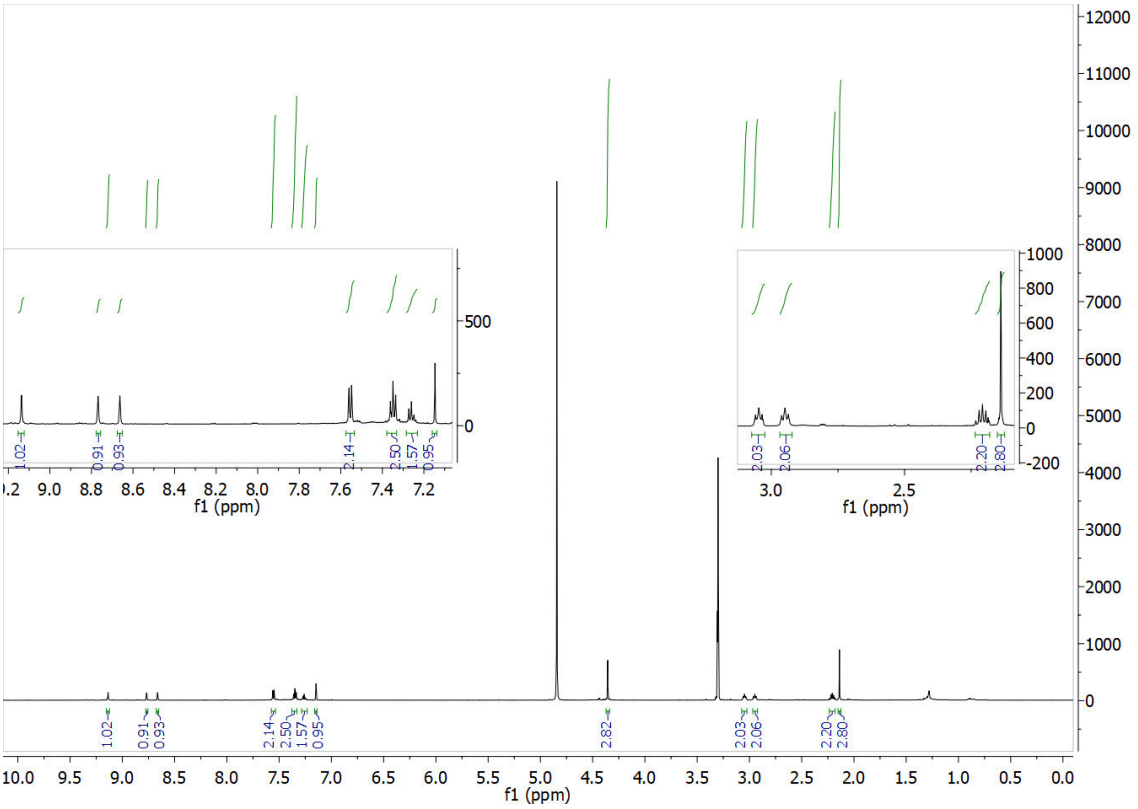

^{13}C NMR (151 MHz, Methanol-d_4)

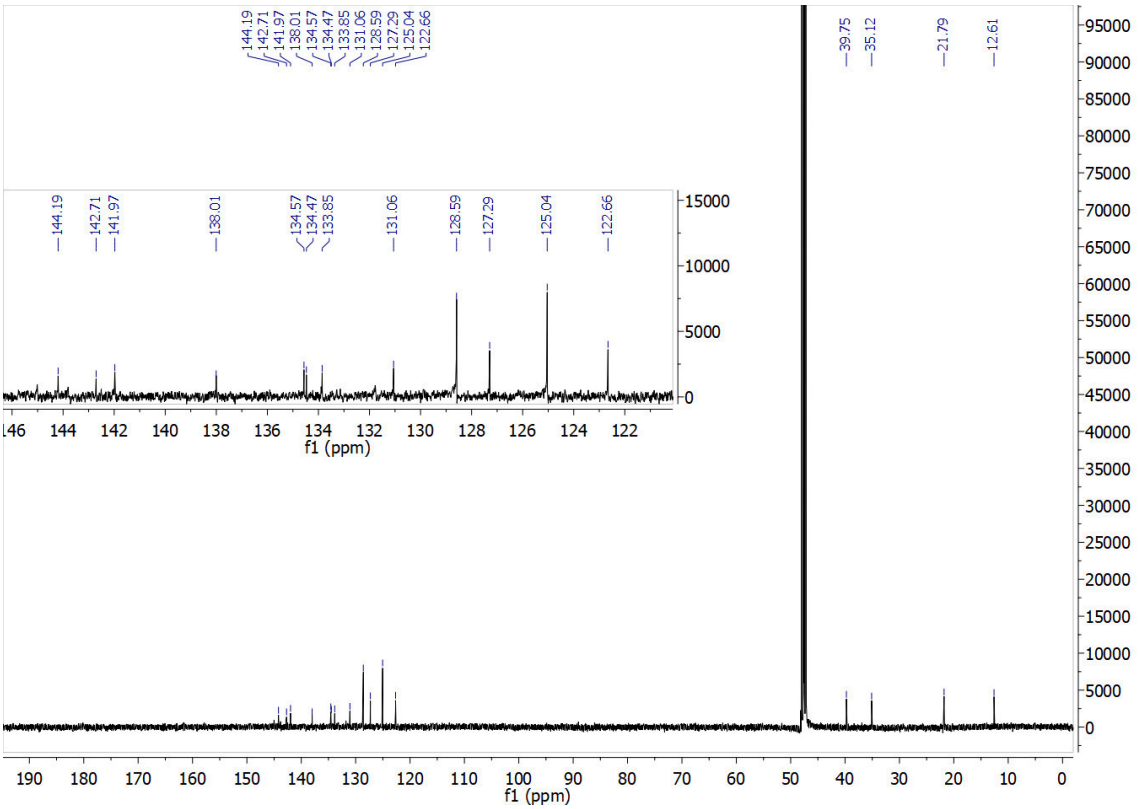

8a^{o} ^{1}H NMR (600 MHz, Methanol-d_4)

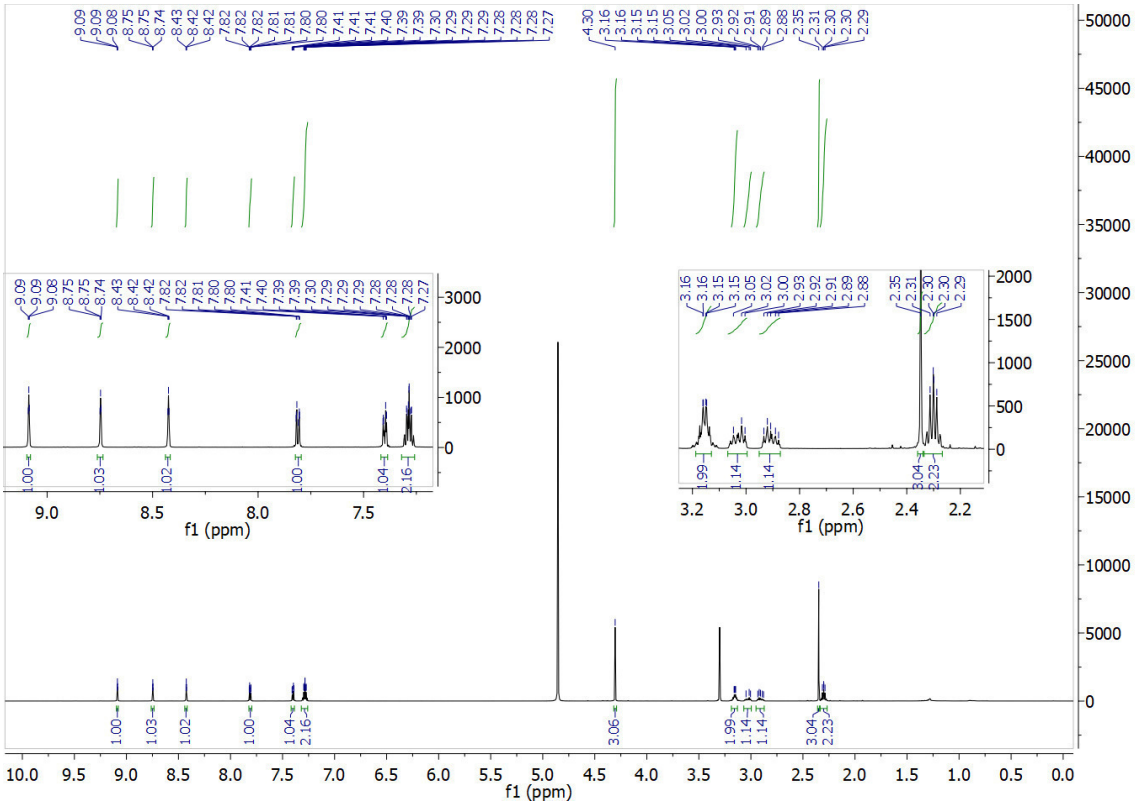

^{13}C NMR (151 MHz, Methanol-d_4)

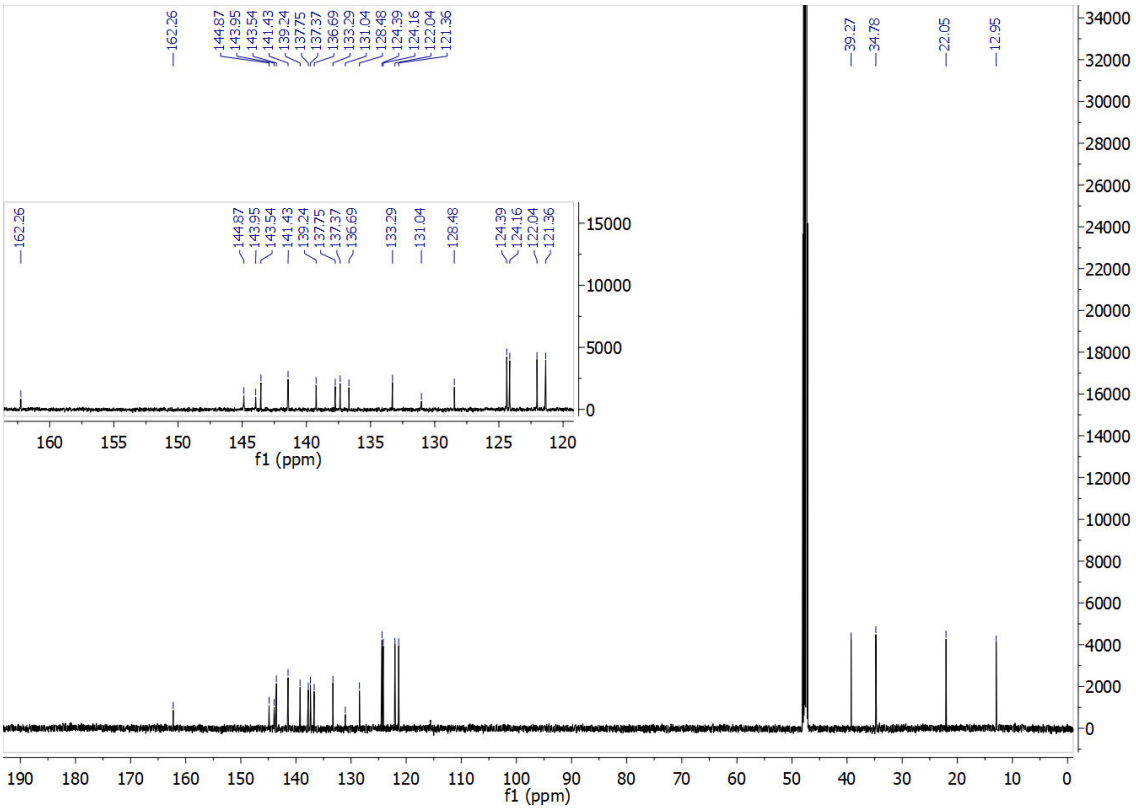

9^{o} ^{1}H NMR (300 MHz, Methanol-d_4

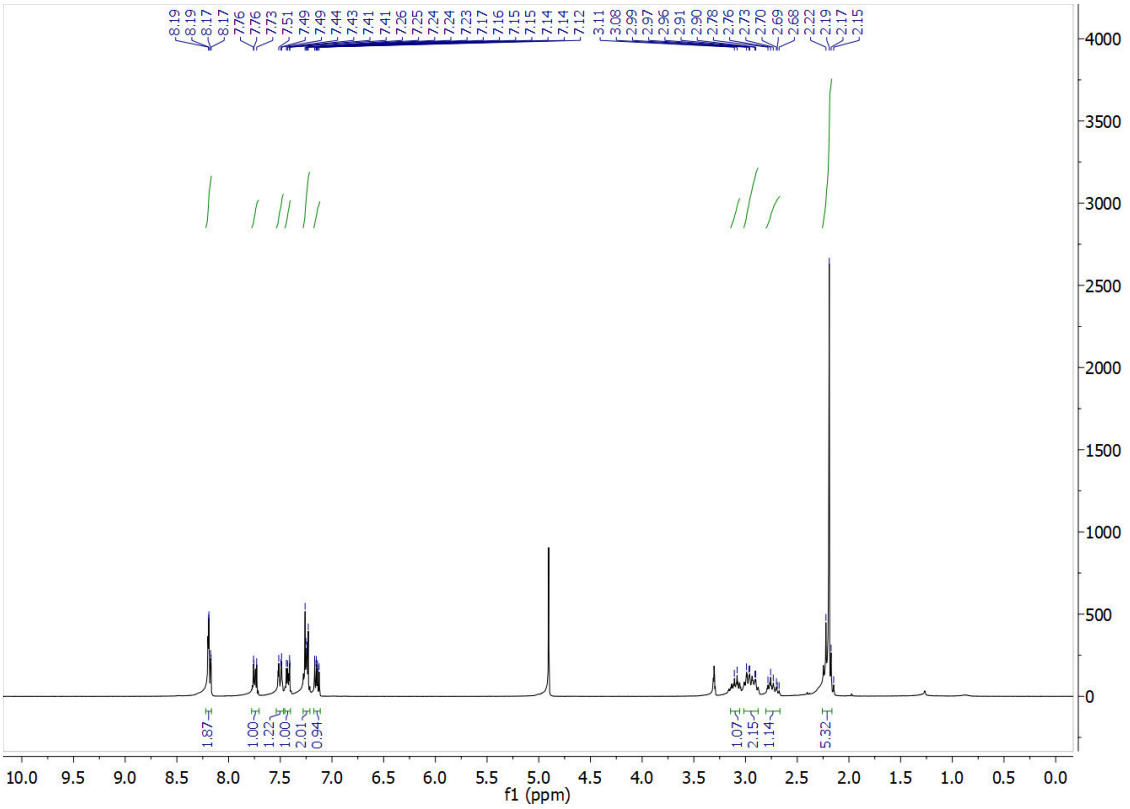

^{13}C NMR (75 MHz, Methanol-d_4)

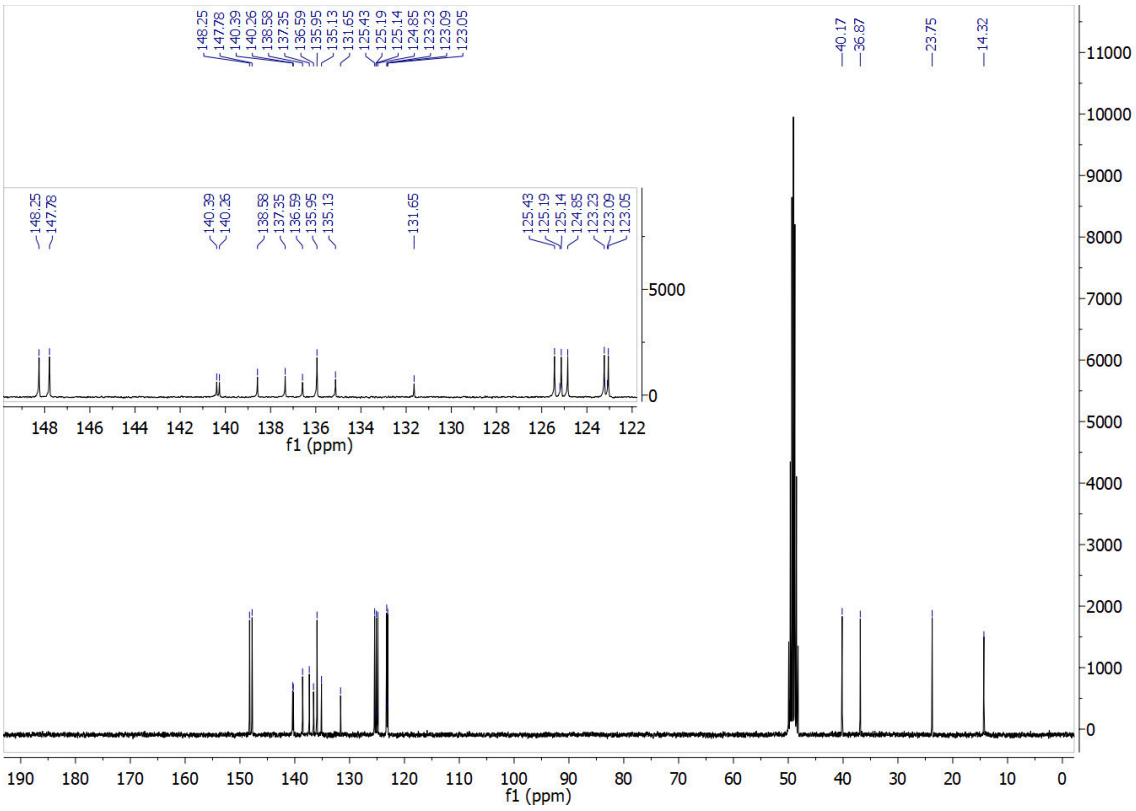

2. Mass and Purity

7a[o]

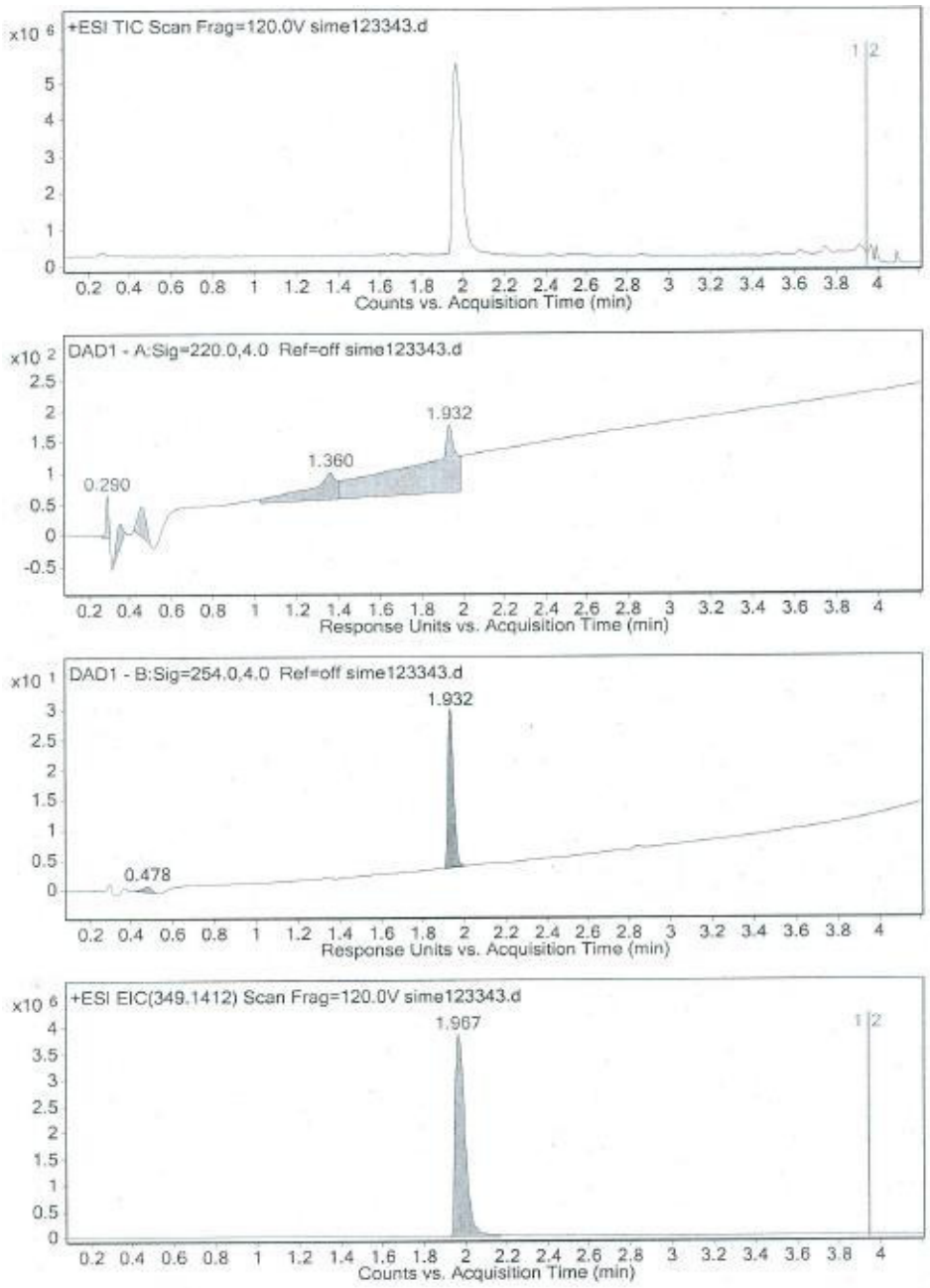

7b^{o}

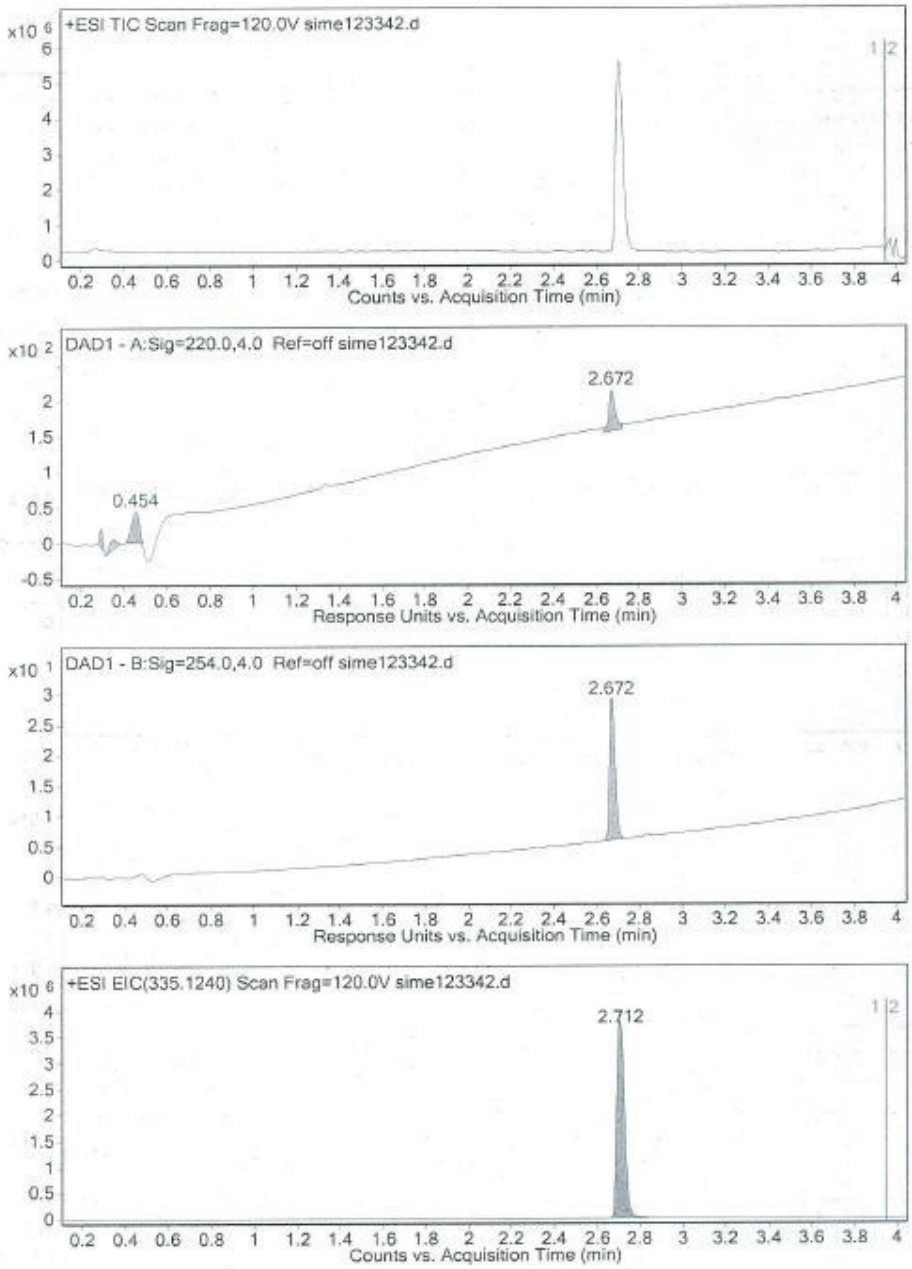
+ESI TIC Scan Frag=120.0V sime123342.d
Counts vs. Acquisition Time (min)
DAD1 - A:Sig=220.0,4.0 Ref=off sime123342.d
2.672
0.454
Response Units vs. Acquisition Time (min)
DAD1 - B:Sig=254.0,4.0 Ref=off sime123342.d
2.672
Response Units vs. Acquisition Time (min)
+ESI EIC(335.1240) Scan Frag=120.0V sime123342.d
2.712
Counts vs. Acquisition Time (min)

8a[o]

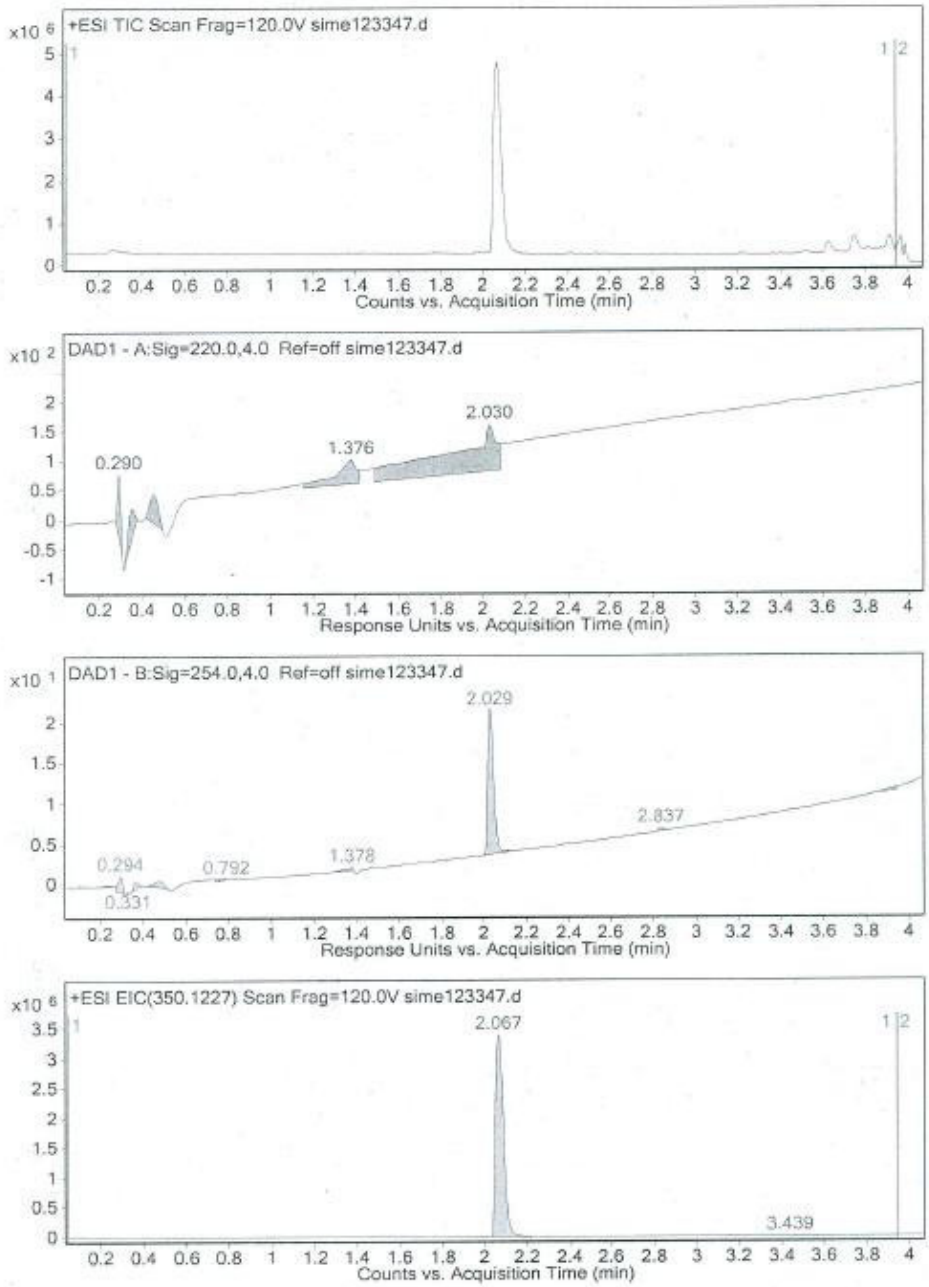
+ESI TIC Scan Frag=120.0V sime123347.d
Counts vs. Acquisition Time (min)
DAD1 - A:Sig=220.0,4.0 Ref=off sime123347.d
0.290
1.376
2.030
Response Units vs. Acquisition Time (min)
DAD1 - B:Sig=254.0,4.0 Ref=off sime123347.d
0.294
0.331
0.792
1.378
2.029
2.837
Response Units vs. Acquisition Time (min)
+ESI EIC(350.1227) Scan Frag=120.0V sime123347.d
2.067
3.439
Counts vs. Acquisition Time (min)

11

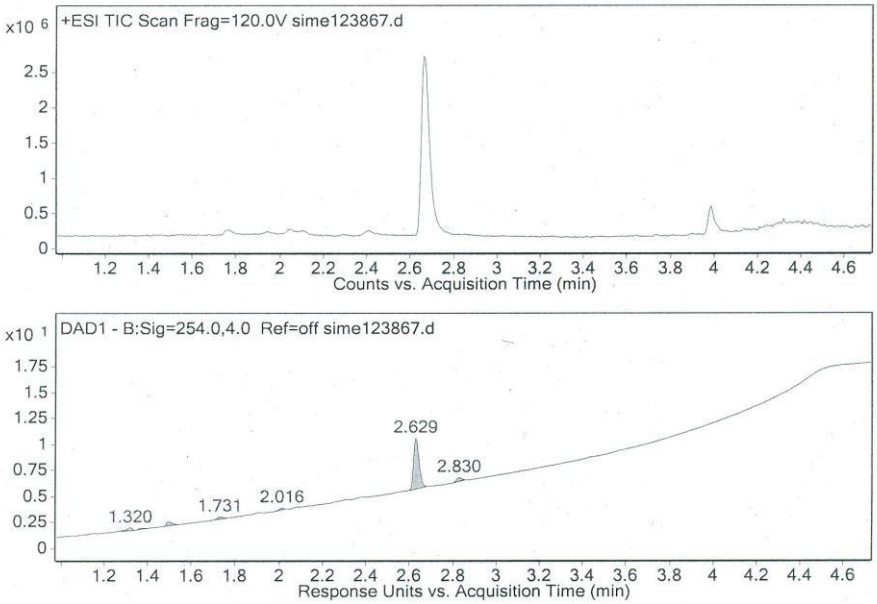
x10 6
+ESI TIC Scan Frag=120.0V sime123867.d
2.5
2
1.5
1
0.5
0
1.2 1.4 1.6 1.8 2 2.2 2.4 2.6 2.8 3 3.2 3.4 3.6 3.8 4 4.2 4.4 4.6
Counts vs. Acquisition Time (min)
x10 1
DAD1 - B:Sig=254.0,4.0 Ref=off sime123867.d
1.75
1.5
1.25
1
0.75
0.5
0.25
0
2.629
2.830
1.320
1.731
2.016
1.2 1.4 1.6 1.8 2 2.2 2.4 2.6 2.8 3 3.2 3.4 3.6 3.8 4 4.2 4.4 4.6
Response Units vs. Acquisition Time (min)

3. Cyclic Voltammetry

All measurements were performed in MeOH or MeOH/water with 0.1M Bu_4NBF_4 using ferrocene (0.005M) as internal standard (*Marked yellow*).

Table A1: Overview of measured potentials.

Compound	Potential VS Ferrocene		Potential VS SCN	
Vitamin C	-1.83293	0.19638	-1.45293	0.57638
NADH	0.845915	1.339415	1.225915	1.719415
Hantzsch ester	0.380175		0.760175	
NAD+	-134579	-1.57739	-134578.62	-1.19739
7ao	-0.4305275	-1.480415	-0.0505275	-1.100415
7bo	-1.71383		-1.33383	
8ao	-0.845955	-1.500555	-0.465955	-1.120555

Reducing Agents

Vitamin C (H_2O:MeOH, 1:1)

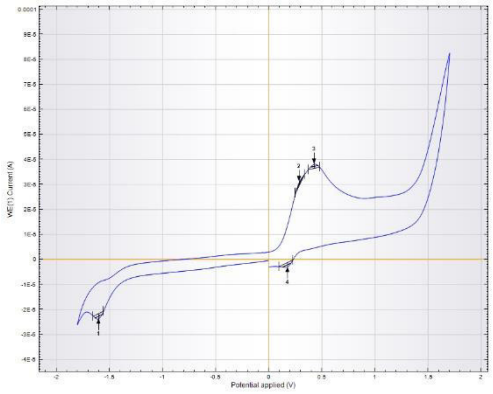

Index	Peak position
1	-1.6013
2	0.28702
3	0.42801
4	0.17624

NADH (H_2O:MeOH, 1:1)

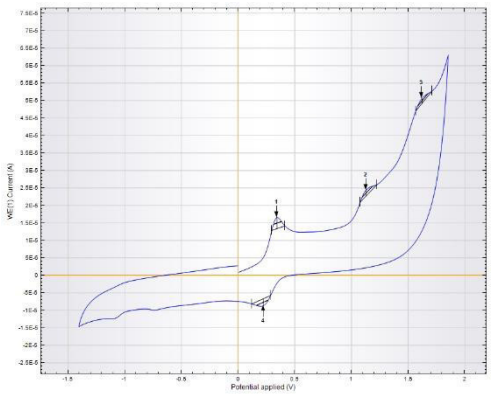

Index	Peak position
1	0.34241
2	1.1279
3	1.6214
4	0.22156

Hantzsch ester (**9**, in MeOH)

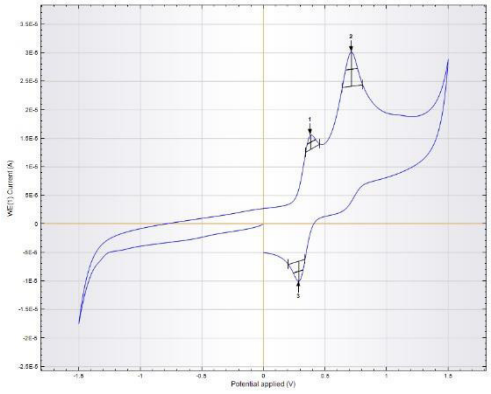

Index	Peak position
1	0.38269
2	0.71503
3	0.28702

Oxidizing Agents

NAD^+ (H_2O:MeOH, 1:1)

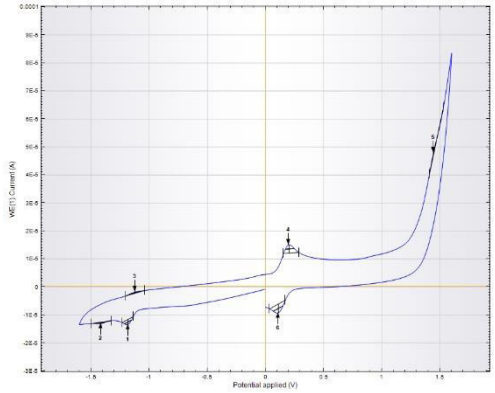

Index	Peak position
1	-1.1833
2	-1.4149
3	-1.1229
4	0.20142
5	1.4452
6	0.11078

7a^o

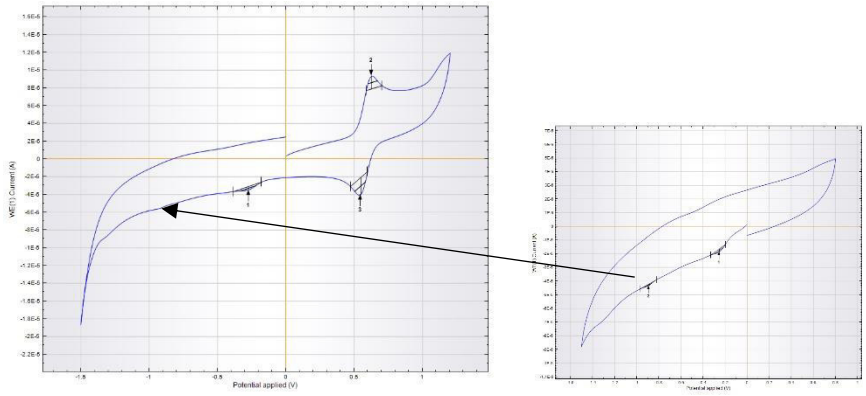

Index	Peak position
1	-0.27191
	-0.89127 (excerpt)
2	0.62943
3	0.54886

7b^{o}

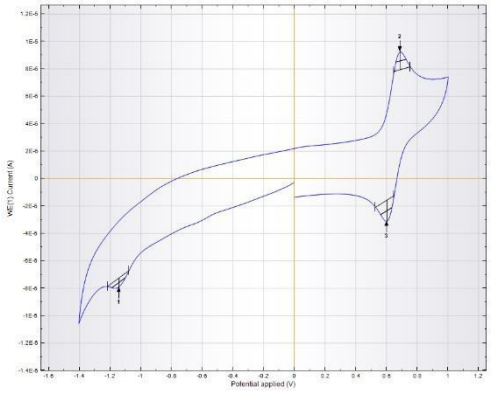

Index	Peak position
1	-1.143
2	0.68985
3	0.60425

8a^{o}

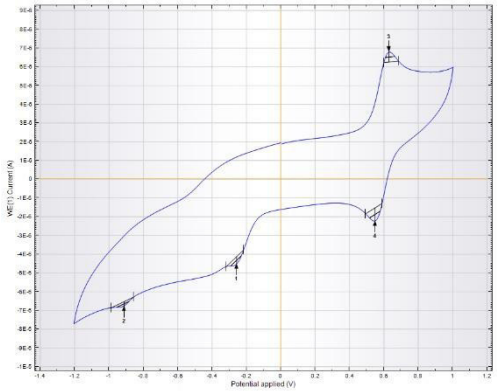

Index	Peak position
1	-0.25681
2	-0.91141
3	0.62943
4	0.54886

4. Redox Reactions with Hantzsch ester

MeOH

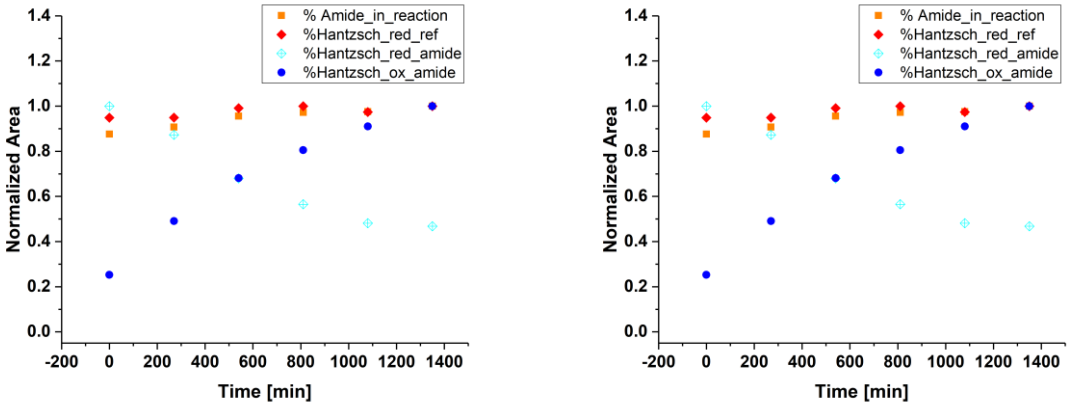

Figure A1: *left:* Kinetic profile of Hantzsch ester oxidation through compound **7a**^{o} (3.3 μM in MeOH); relative amount of **7a**^{o} (gray) **9** (blue) and **10** (brown) in the reaction mixture and **9** without addition of **7a**^{o} (green) under the same conditions; *left:* Kinetic profile of Hantzsch ester oxidation through compound **8a**^{o} (3.3 μM in MeOH); relative amount of **8a**^{o} (gray) **9** (blue) and **10** (brown) in the reaction mixture and **9** without addition of **8a**^{o} (green) under the same conditions.

MeCN

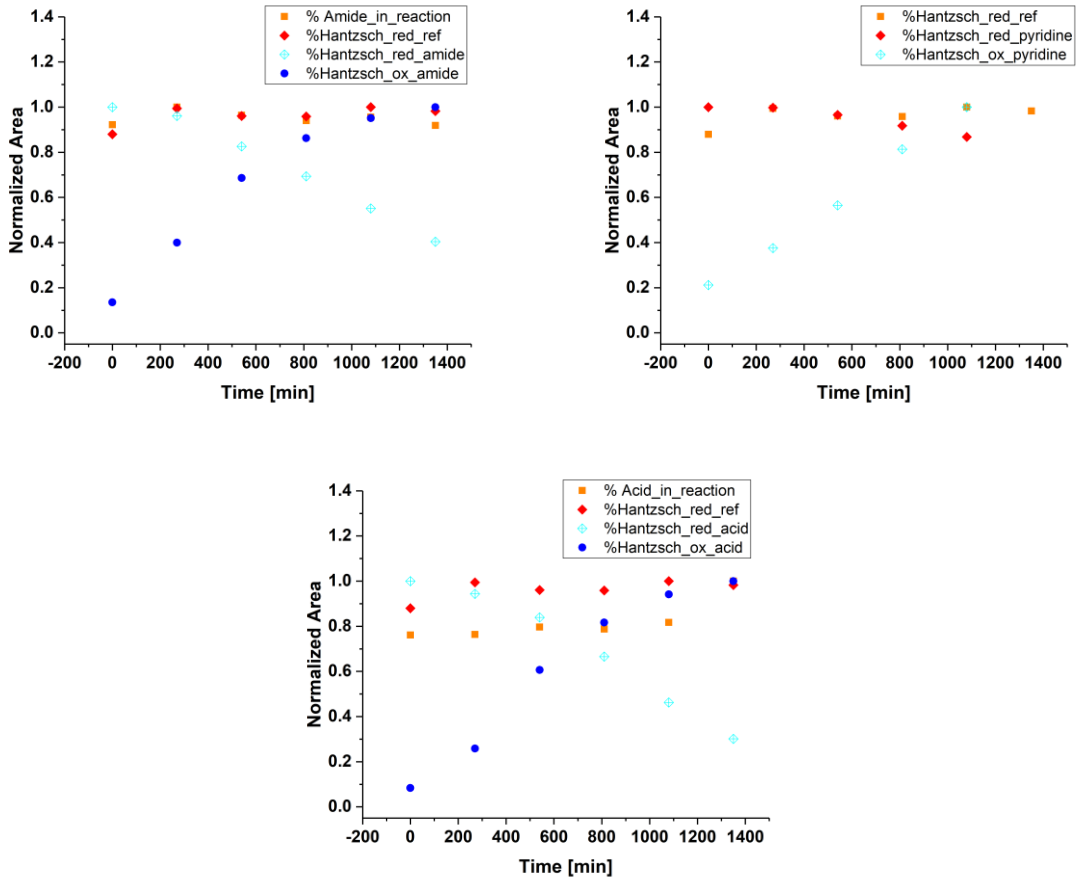

Figure A2: *left:* Kinetic profile of Hantzsch ester oxidation through compound **7a**^{o} (3.3 μM in MeCn); relative amount of **7a**^{o} (gray) **9** (blue) and **10** (brown) in the reaction mixture and **9** without addition of **7a**^{o} (green) under the same conditions; *right:* Kinetic profile of Hantzsch ester oxidation through compound **7b**^{o} (3.3 μM in MeCN); relative amount **9** (blue) and **10** (brown) in the reaction mixture and **9** without addition of **7b**^{o} (green) under the same conditions; *bottom:* Kinetic profile of Hantzsch ester oxidation through compound **8a**^{o} (3.3 μM in MeCN); relative amount of **8a**^{o} (gray) **9** (blue) and **10** (brown) in the reaction mixture and **9** without addition of **8a**^{o} (green) under the same conditions.

DMSO

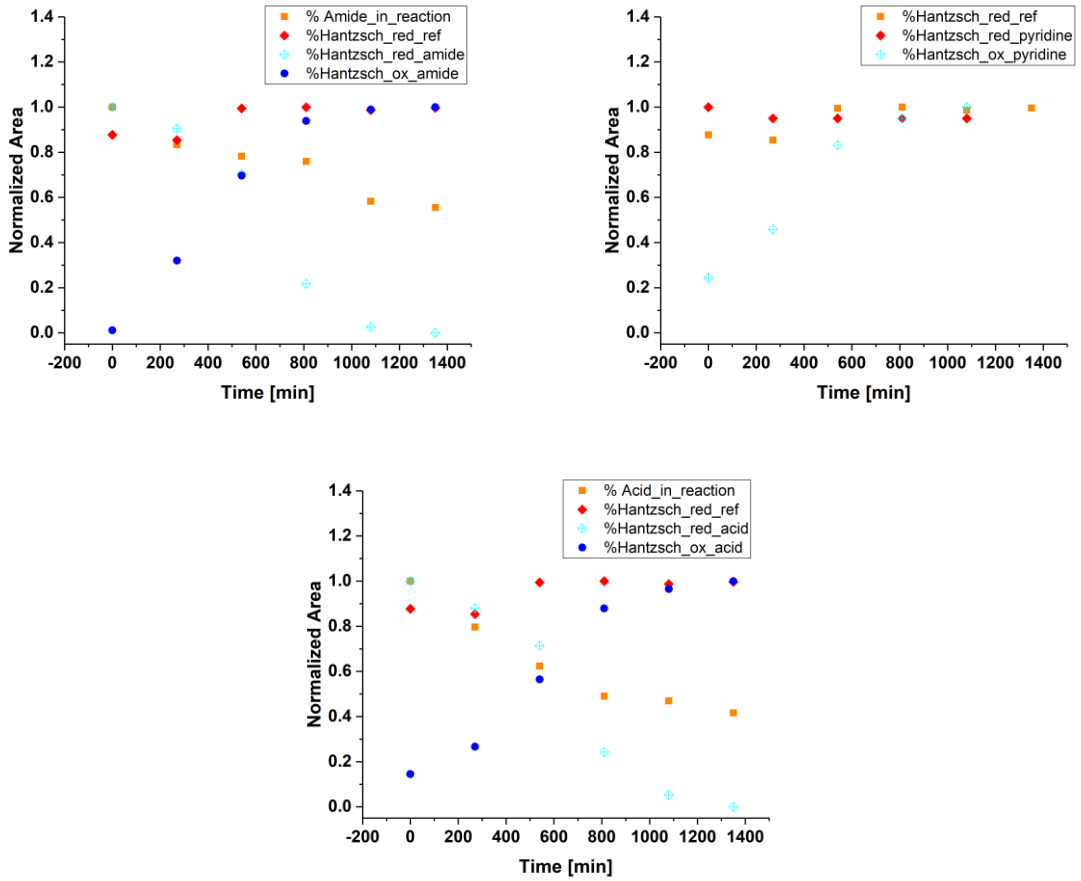

Figure A3: *left:* Kinetic profile of Hantzsch ester oxidation through compound **7a**^{o} (3.3 μM in DMSO); relative amount of **7a**^{o} (gray) **9** (blue) and **10** (brown) in the reaction mixture and **9** without addition of **7a**^{o} (green) under the same conditions; *right:* Kinetic profile of Hantzsch ester oxidation through compound **7b**^{o} (3.3 μM in DMSO); relative amount **9** (blue) and **10** (brown) in the reaction mixture and **9** without addition of **7b**^{o} (green) under the same conditions; *bottom:* Kinetic profile of Hantzsch ester oxidation through compound **8a**^{o} (3.3 μM in DMSO); relative amount of **8a**^{o} (gray) **9** (blue) and **10** (brown) in the reaction mixture and **9** without addition of **8a**^{o} (green) under the same conditions.

Redox Reaction with Hantzsch ester under irradiation

Table A2: Conversion of Hantzsch ester through **8a** or **7a**, respectively, under irradiation.

			9 control	9 irradiated	9+Switch control	9+Switch irradiated
Area from HPLC	**8a**	**9**	5044	24956	26893	16603
		9-ox	32391	11604	38568	11672
	7a	**9**	31101	17836	10948	0
		9-ox	5701	38215	36062	38676
Normalized Value	**8a**	**9**	0.13	0.68	0.41	0.59
		9-ox	0.87	0.32	0.59	0.41
	7a	**9**	0.85	0.32	0.23	0.00
		9-ox	0.15	0.68	0.77	1.00
Relative Value [%]	**8a**	**9**	13	68	41	59
		9-ox	87	32	59	41
	7a	**9**	85	32	23	0
		9-ox	15	68	77	100

A.III.1. Allosteric Regulation of the Imidazole Glycerol Phosphate Synthase Multienzyme Complexes with Light-Controllable Ligands

Table of Contents

1. UV/Vis Spectroscopy

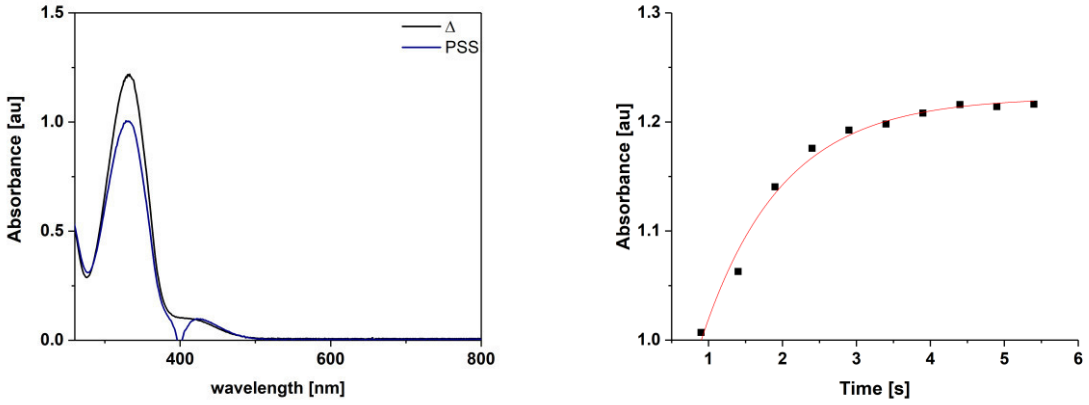

Equation	y = A1*exp(-x/t1) + y0
y0	1.22258 ± 0.00635
A1	-0.51383 ± 0.05063
t1	1.0777 ± 0.11851
R-Square(COD)	0.98737
Adj. R-Square	0.98376

Figure A1: UV-Vis absorption spectrum (left) of compound **29** in buffer (67 μM, 0.001% DMSO) and its lifetime (right).

2. NMR

*3-(5-Methyl-4-(4-(2-methyl-5-(3-(phosphonooxy)phenyl)thiophen-3-yl)-2,5-dioxo-2,5-dihydro-1H-pyrrol-3-yl)thiophen-2-yl)phenyl dihydrogen phosphate (**1a**)*

^{1}H NMR (400 MHz, Methanol-d_4)

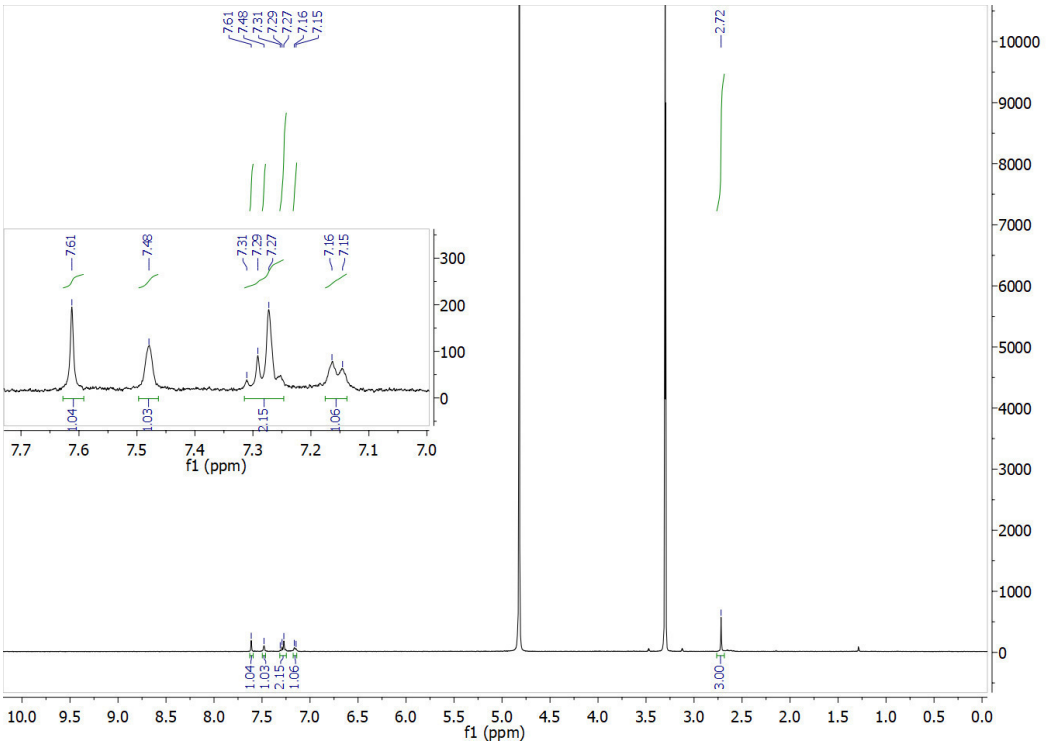

^{31}P NMR (162 MHz, Methanol-d_4)

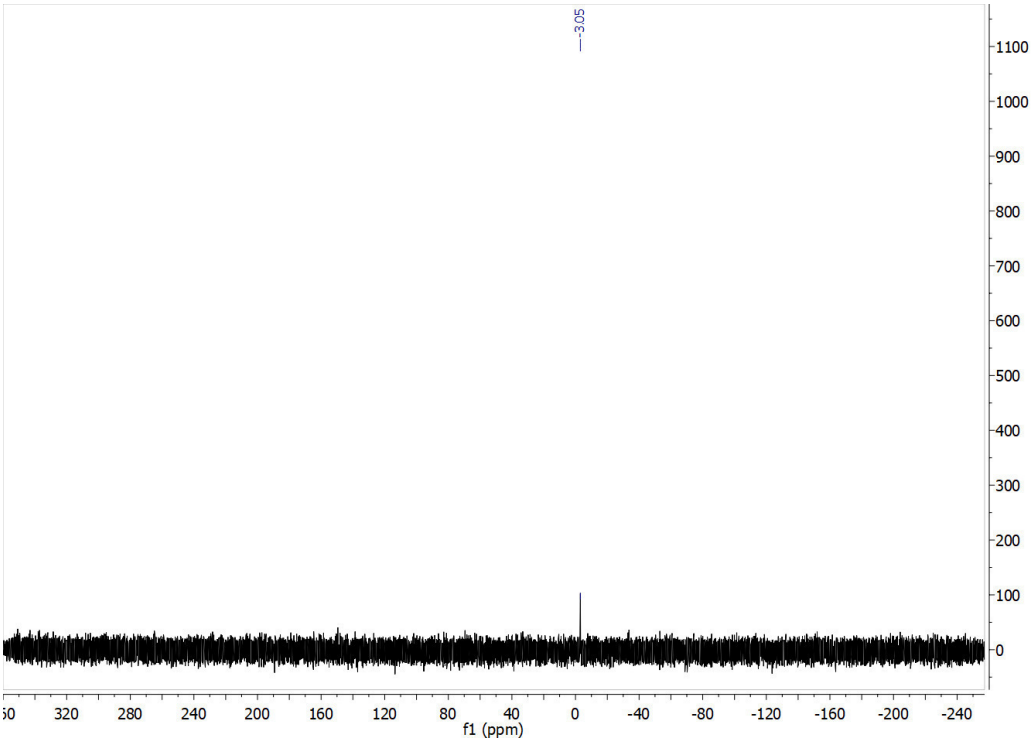

*Methyl 2-(5-(3-hydroxyphenyl)-2-methylthiophen-3-yl)-2-oxoacetate (**8**)*

^{1}H NMR (400 MHz, Chloroform-*d*)

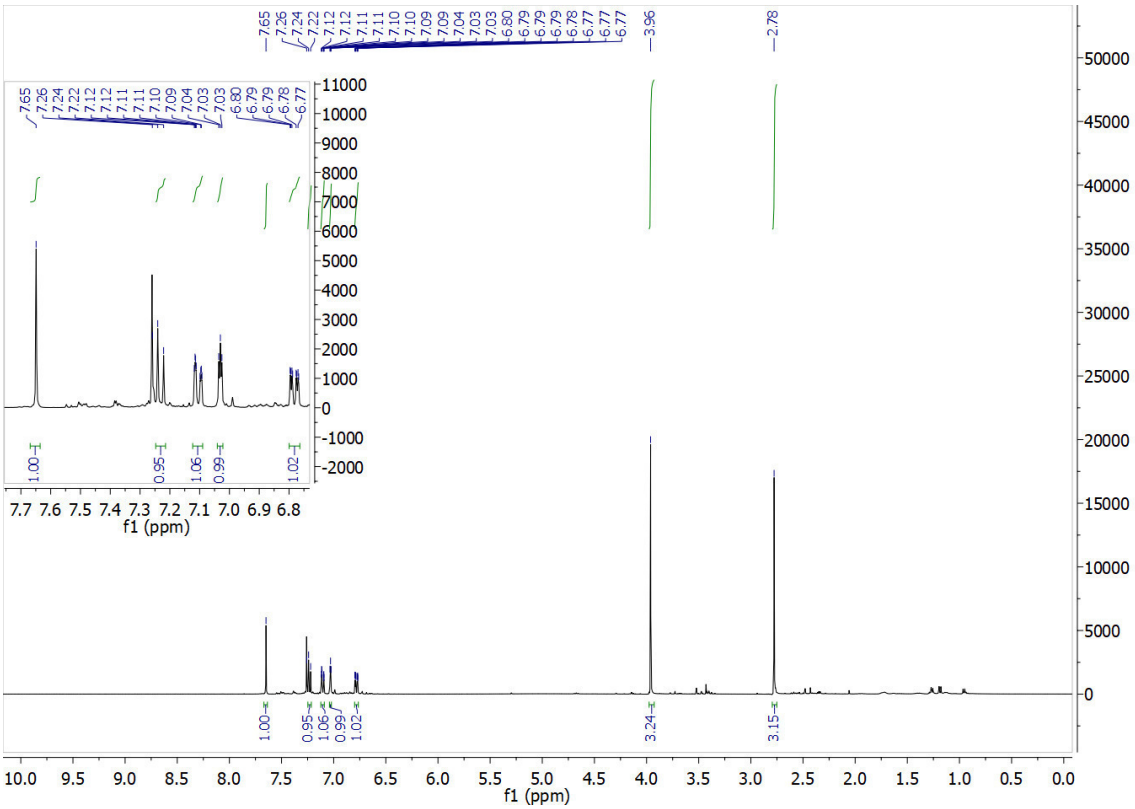

^{13}C NMR (101 MHz, Chloroform-*d*)

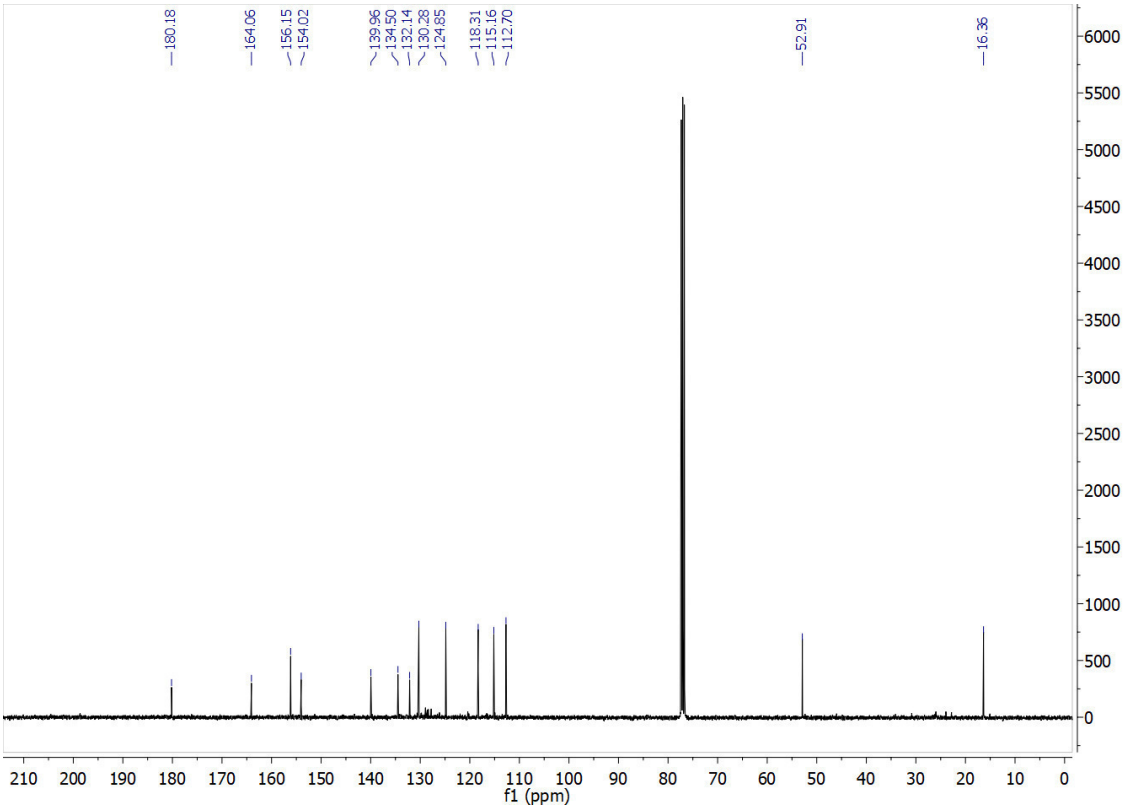

*2-(5-(3-Hydroxyphenyl)-2-methylthiophen-3-yl)-2-oxoacetamide (**9**)*

^{1}H NMR (400 MHz, Chloroform-*d*)

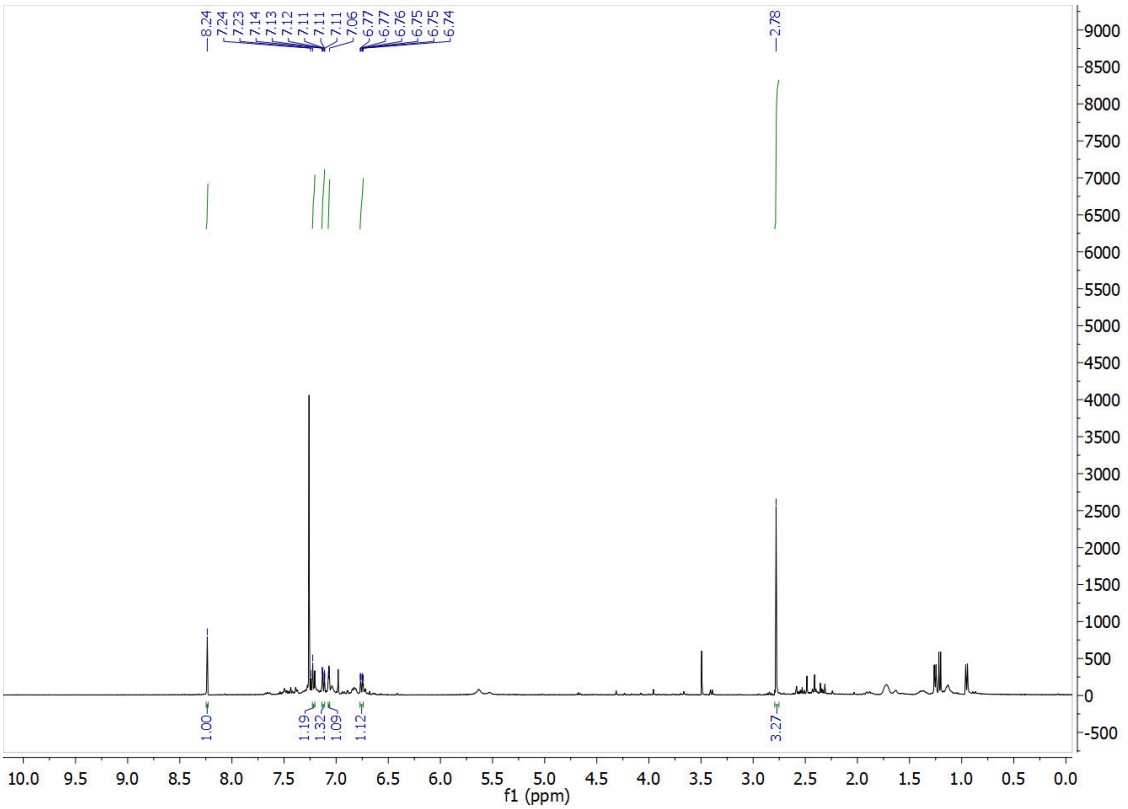

^{13}C NMR (101 MHz, Chloroform-*d*)

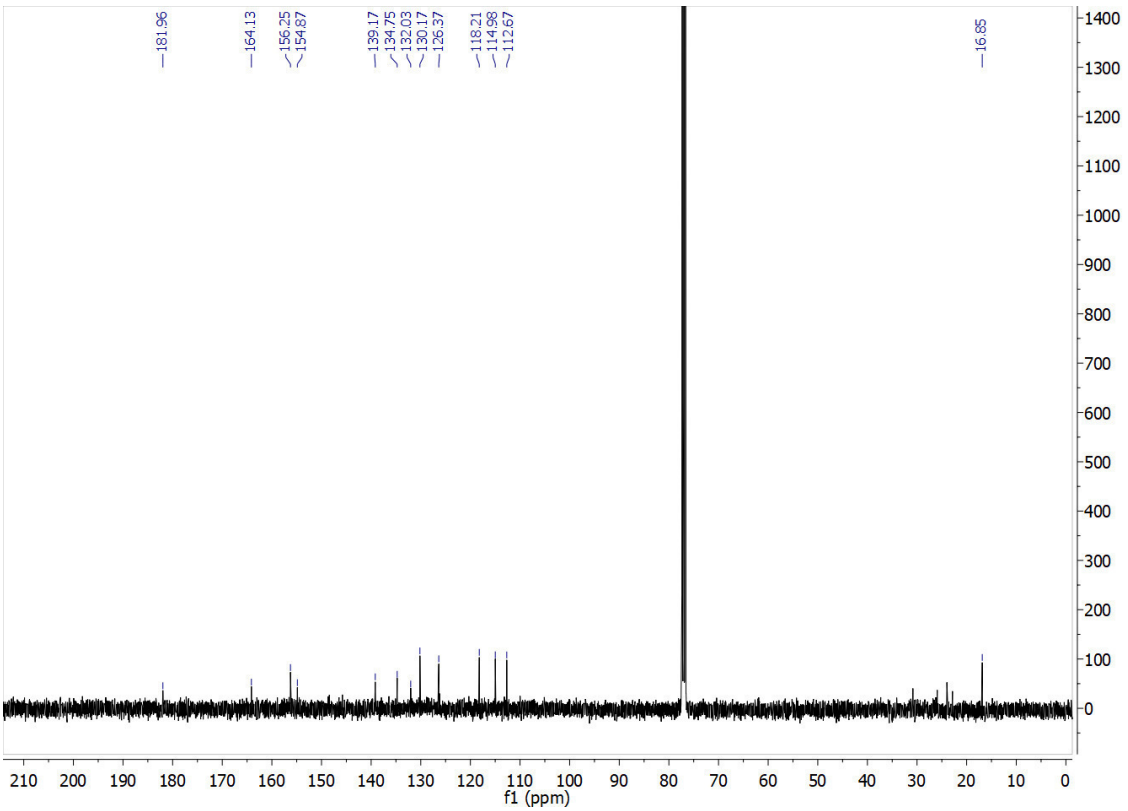

*Methyl 2-(5-(3-hydroxyphenyl)-2-methylthiophen-3-yl)acetate (**11**)*

^{1}H NMR (400 MHz, Chloroform-*d*)

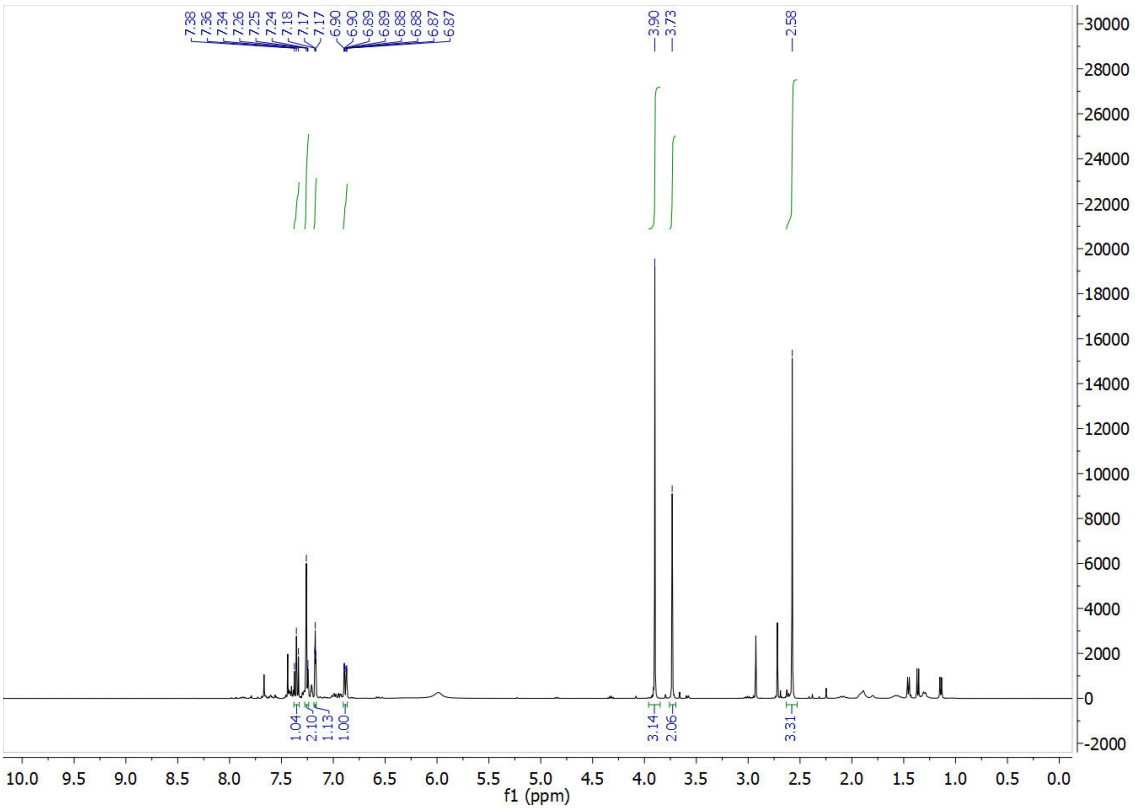

^{13}C NMR (101 MHz, Chloroform-*d*)

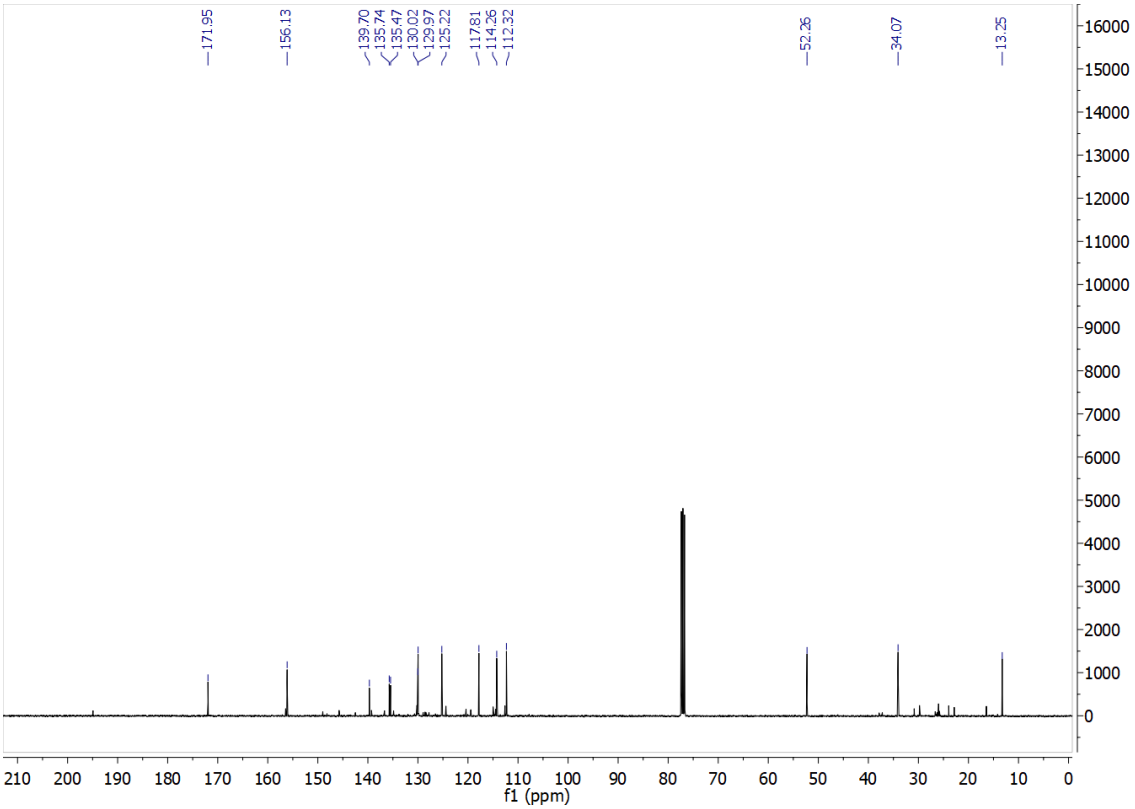

*3,4-Bis(5-(3-hydroxyphenyl)-2-methylthiophen-3-yl)-1H-pyrrole-2,5-dione (**12**)*

^{1}H NMR (400 MHz, Acetone-d_6)

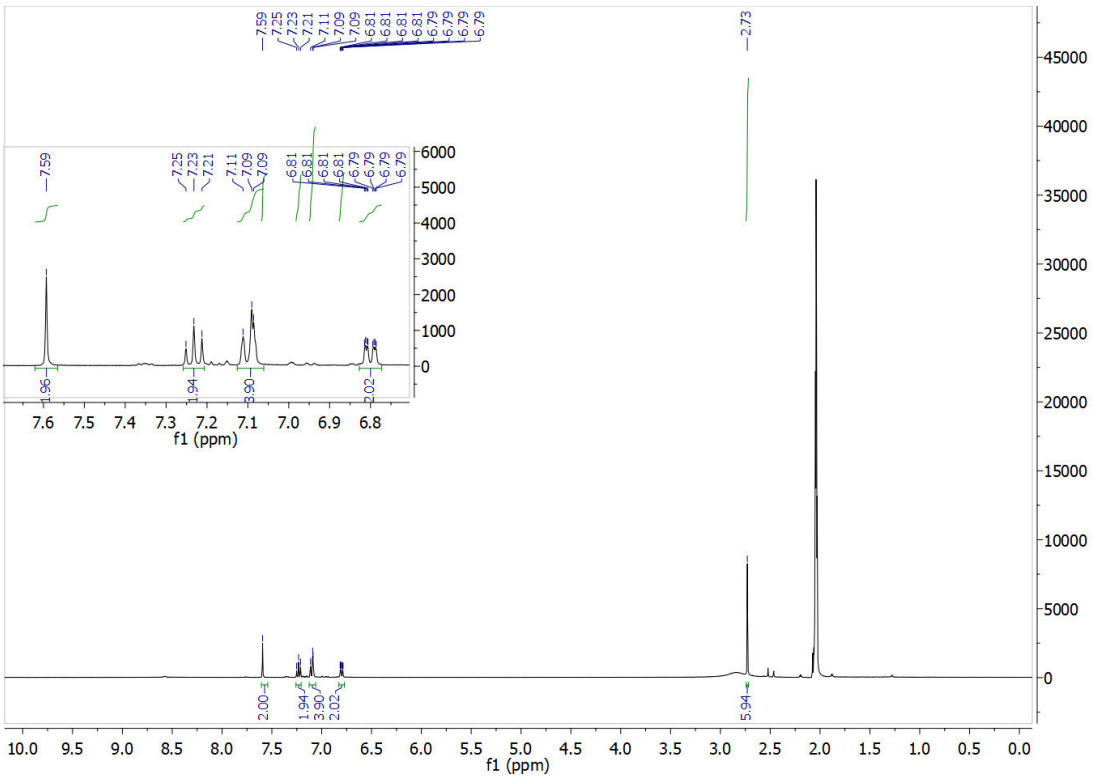

*Methyl 2-(5-(3-methoxyphenyl)-2-methylthiophen-3-yl)acetate (**14**)*

^{1}H NMR (400 MHz, Chloroform-d)

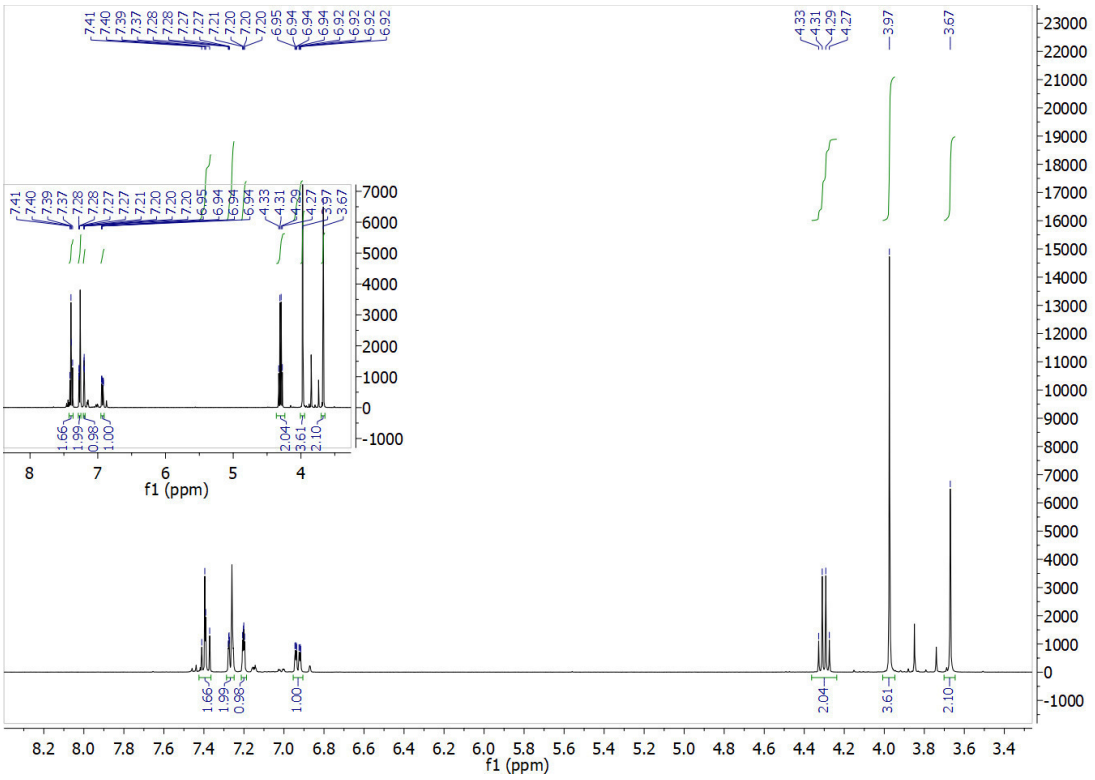

^{13}C NMR (101 MHz, Chloroform-*d*)

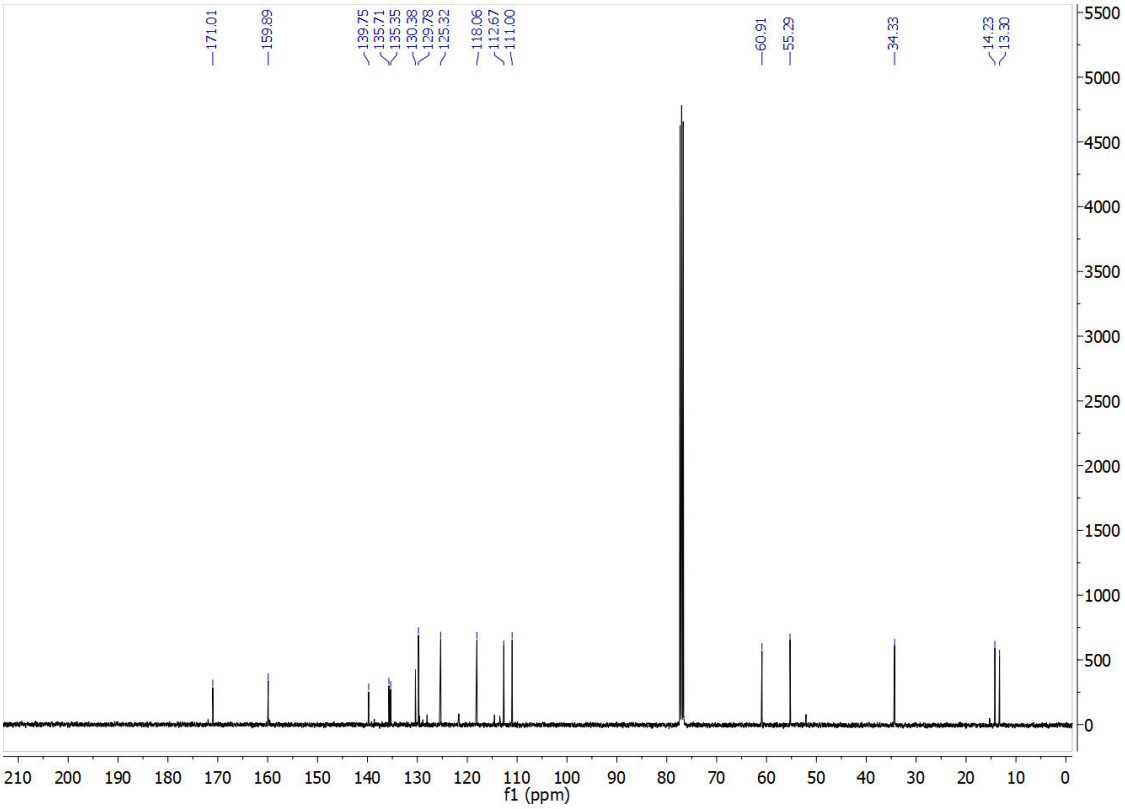

*2-(5-(3-Methoxyphenyl)-2-methylthiophen-3-yl)-2-oxoacetamide (**17**)*

^{1}H NMR (300 MHz, Chloroform-*d*)

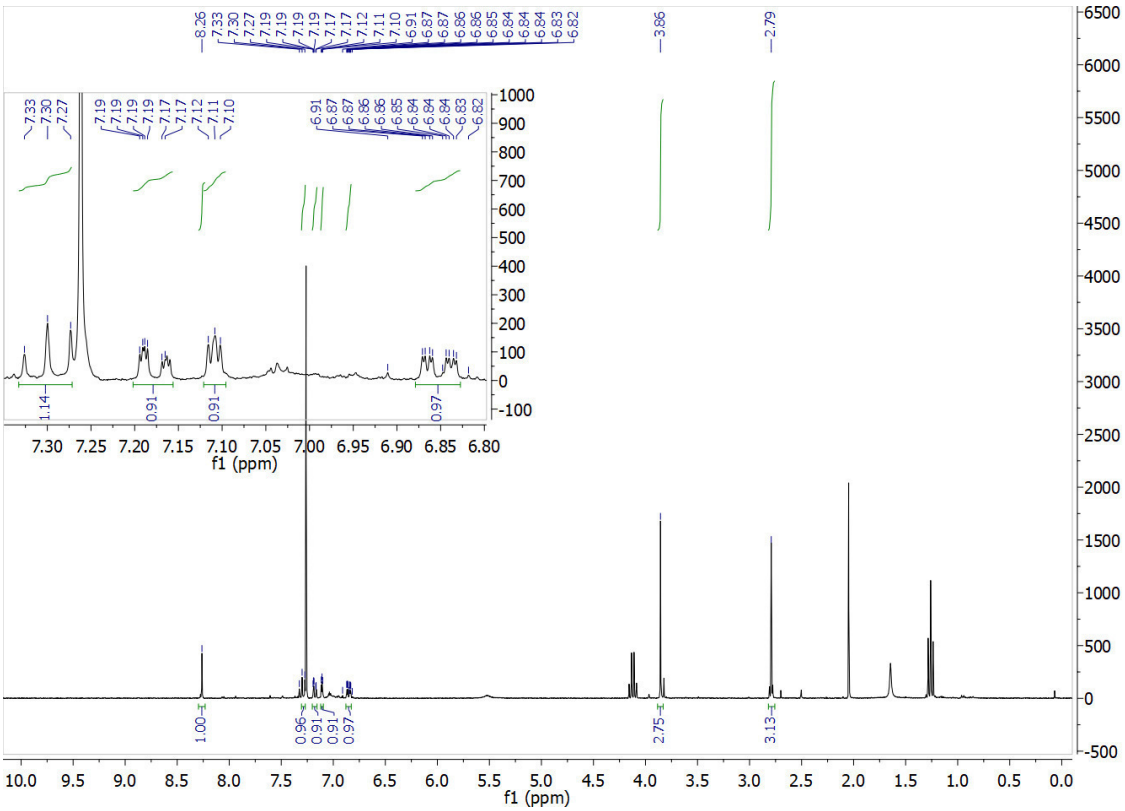

^{13}C NMR (101 MHz, Chloroform-*d*)

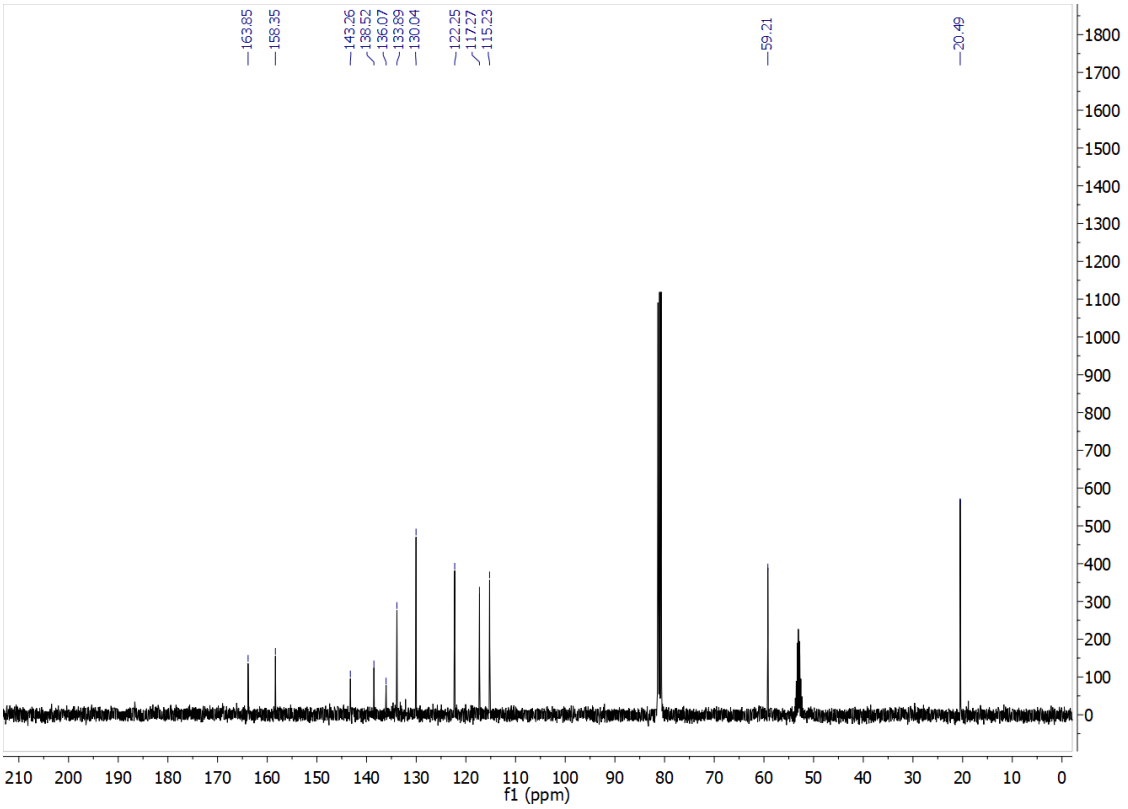

*3,4-bis(5-(3-methoxyphenyl)-2-methylthiophen-3-yl)-1H-pyrrole-2,5-dione (**19**)*

^{1}H NMR (400 MHz, Chloroform-*d*)

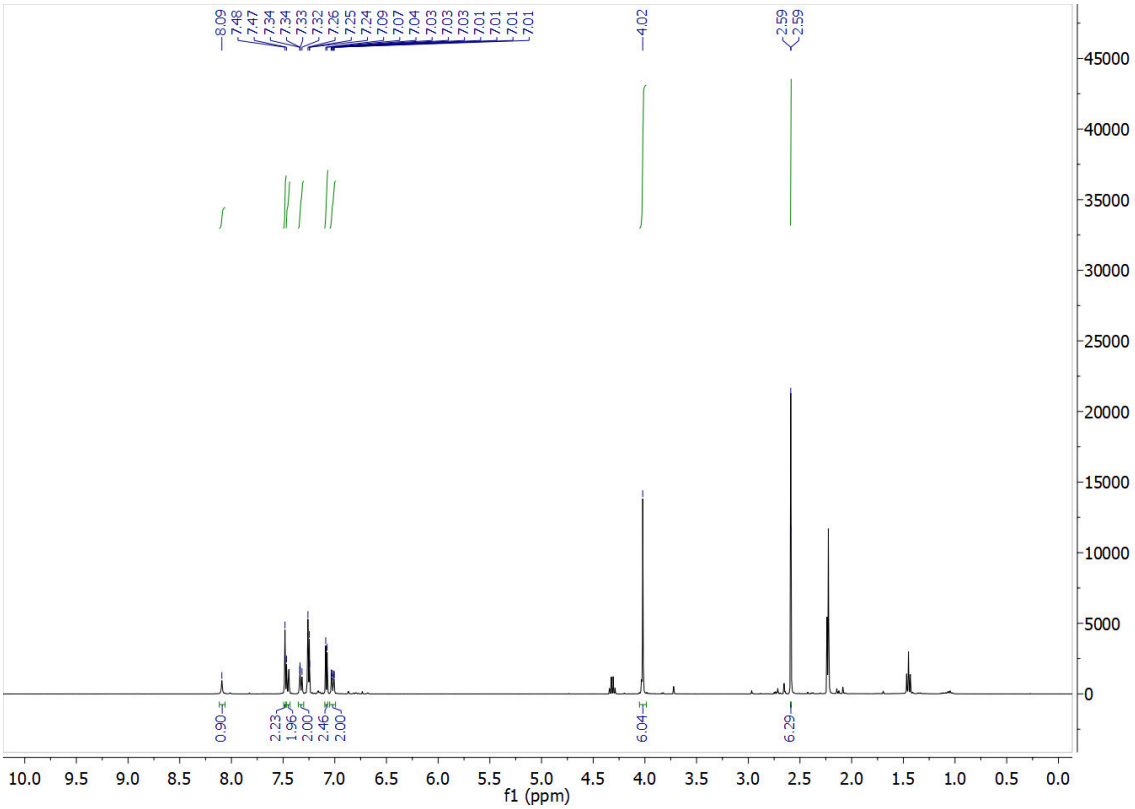

^{13}C NMR (101 MHz, Chloroform-*d*)

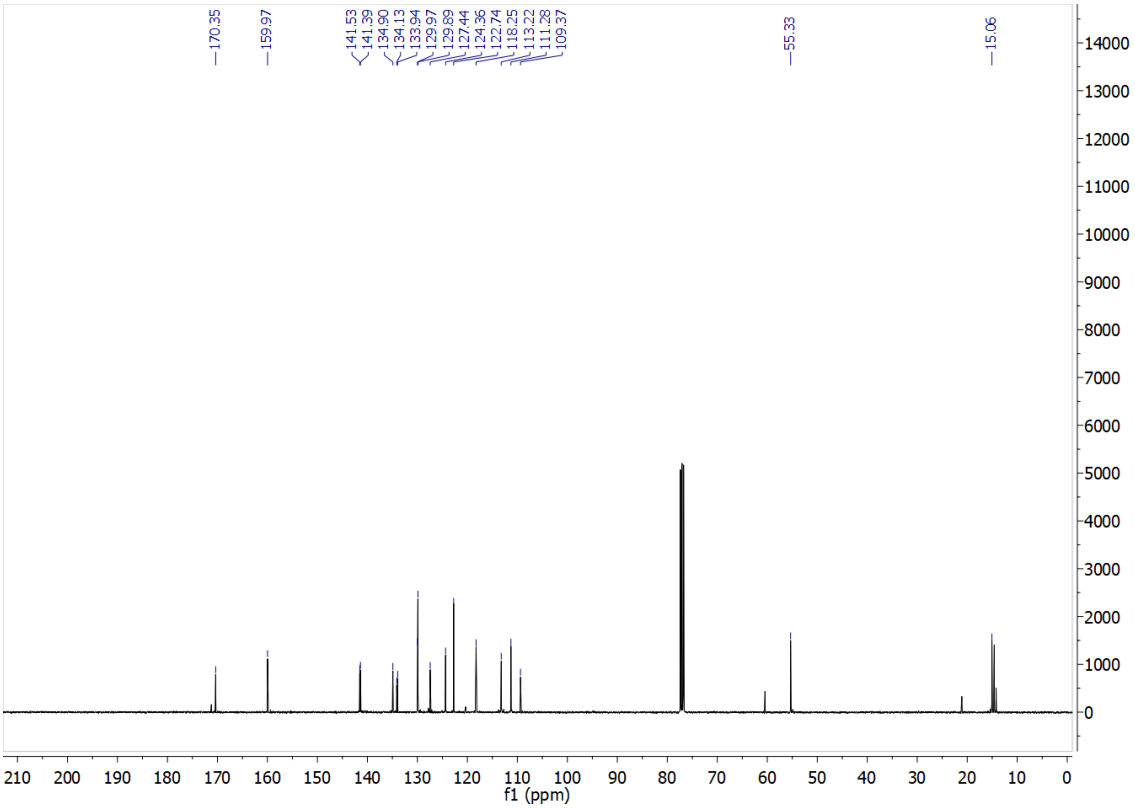

*3-(4-(2-Ethoxy-2-oxoethyl)-5-methylthiophen-2-yl)benzoic acid (**20**)*

^{1}H NMR (400 MHz, Chloroform-*d*)

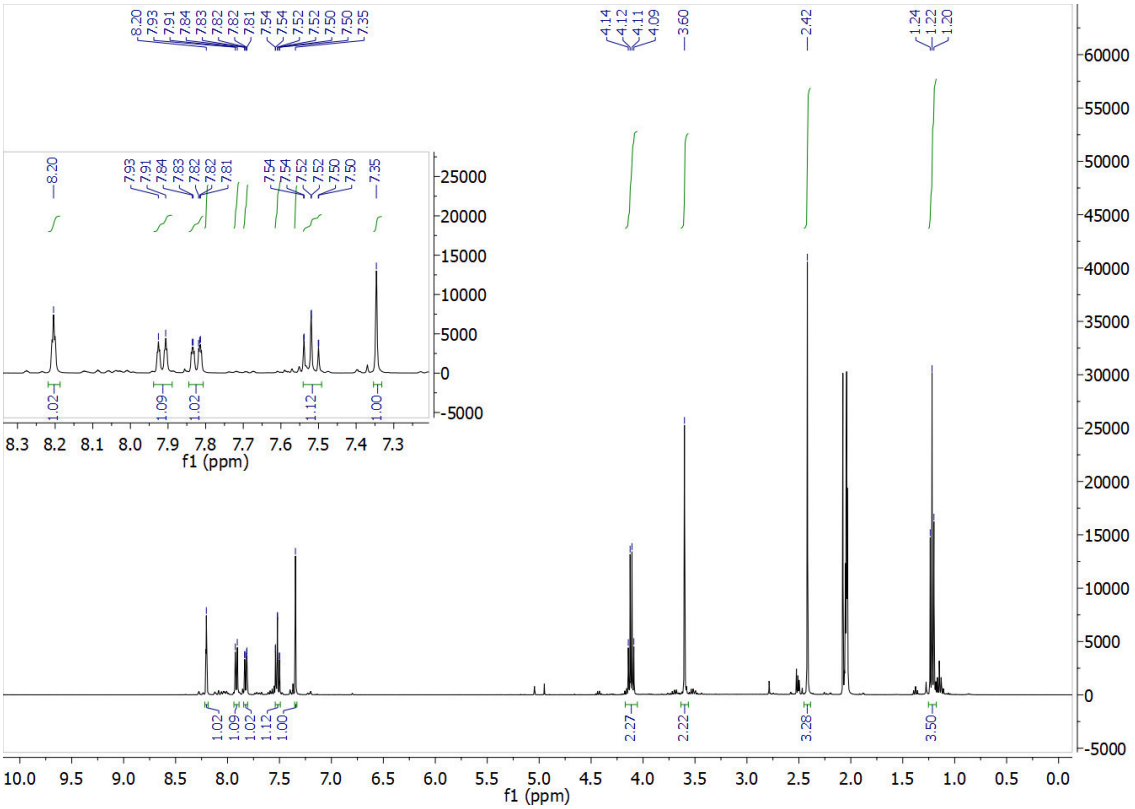

^{13}C NMR (101 MHz, Chloroform-*d*)

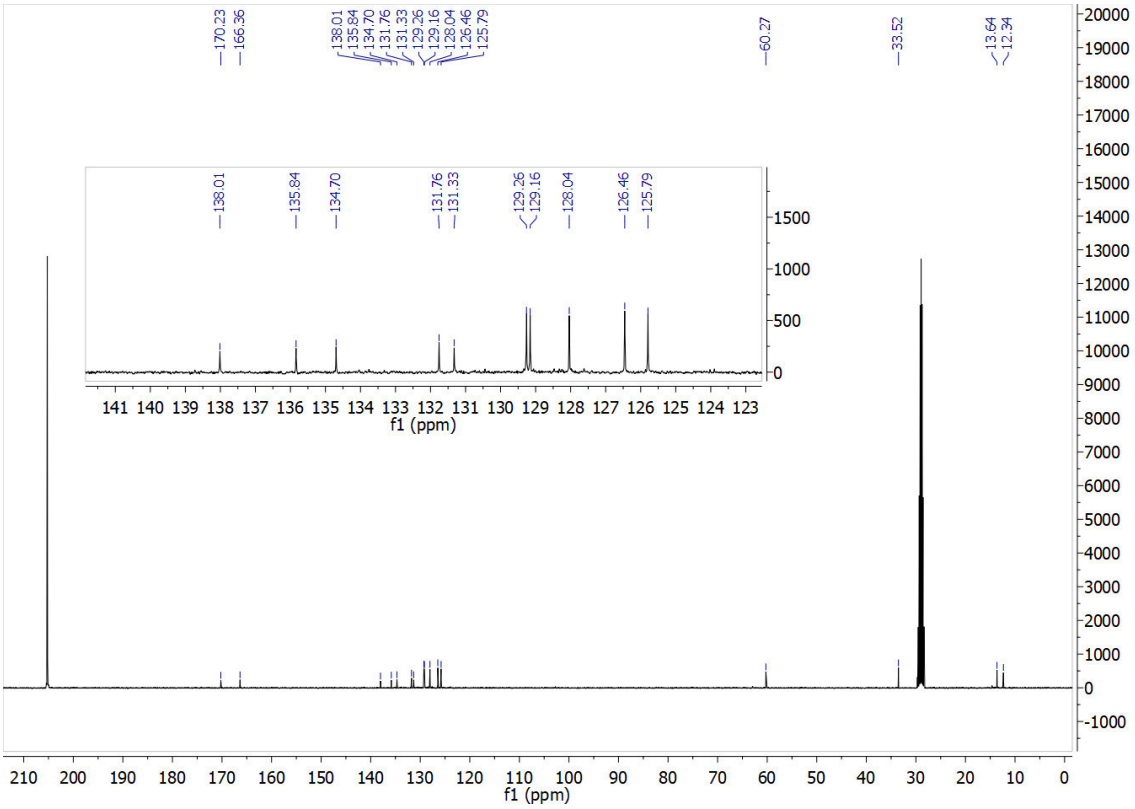

5-(2-(2,4-Dioxopentan-3-ylidene)hydrazineyl)isophthalic acid (***24***)

^{1}H NMR (300 MHz, DMSO-d_6)

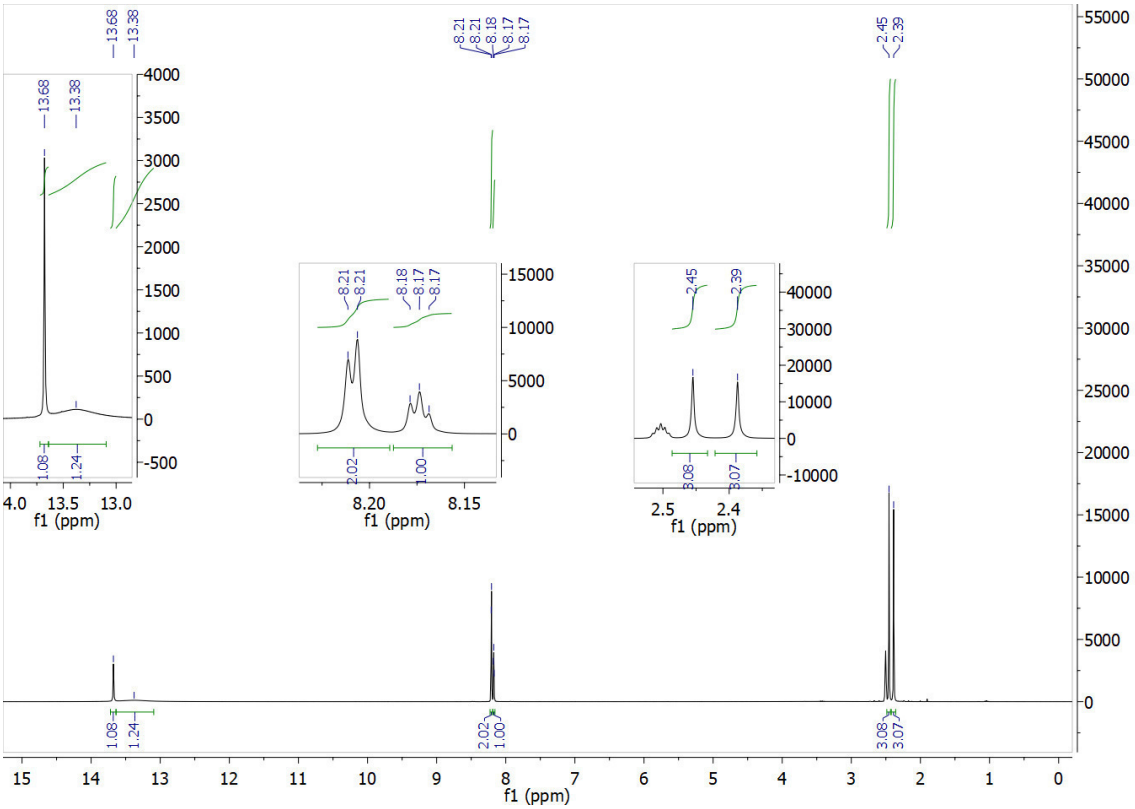

^{13}C NMR (75 MHz, DMSO-d_6)

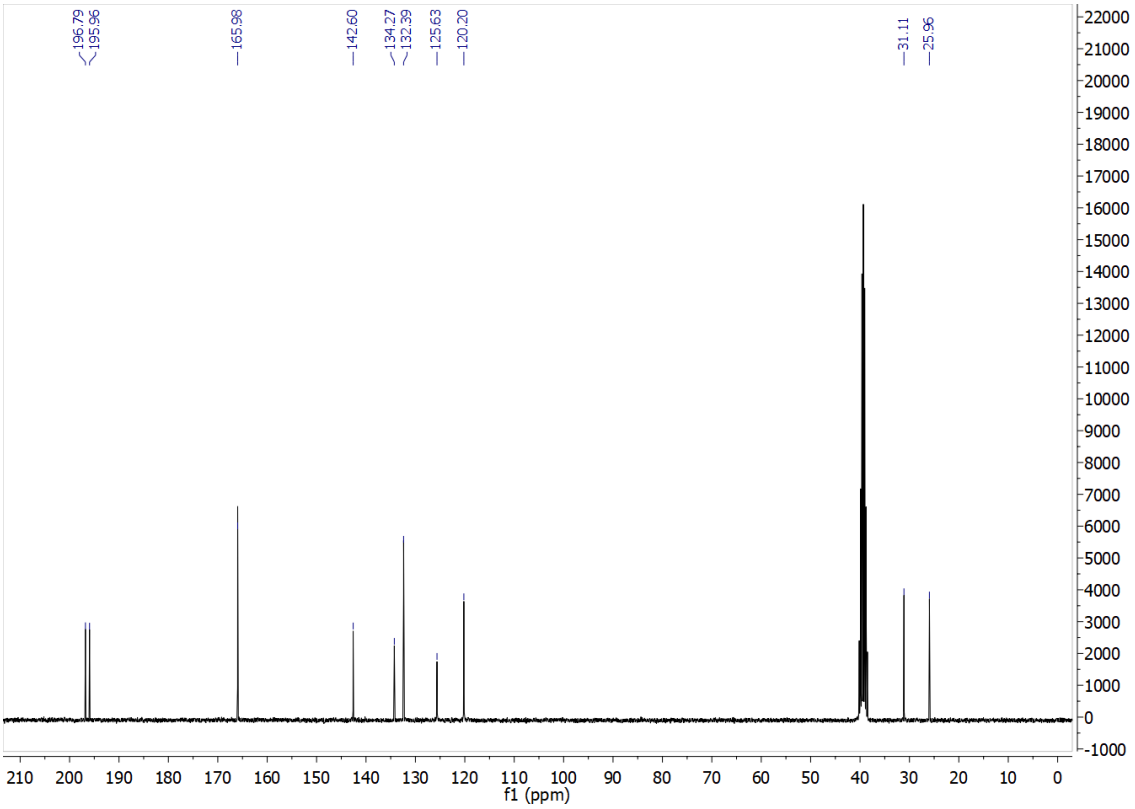

*(E)-5-((3,5-Dimethyl-1H-pyrazol-4-yl)diazenyl)isophthalic acid (**25**)*

^{1}H NMR (300 MHz, DMSO-d_6)

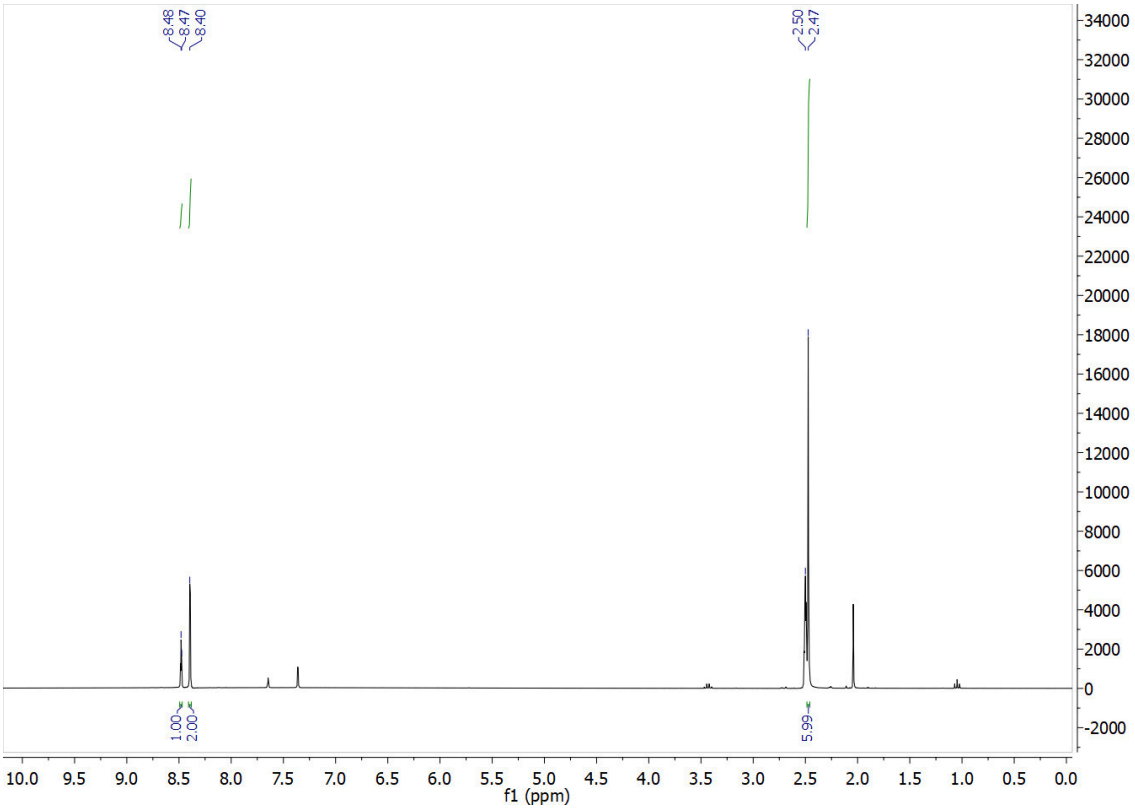

^{13}C NMR (75 MHz, DMSO-d_6)

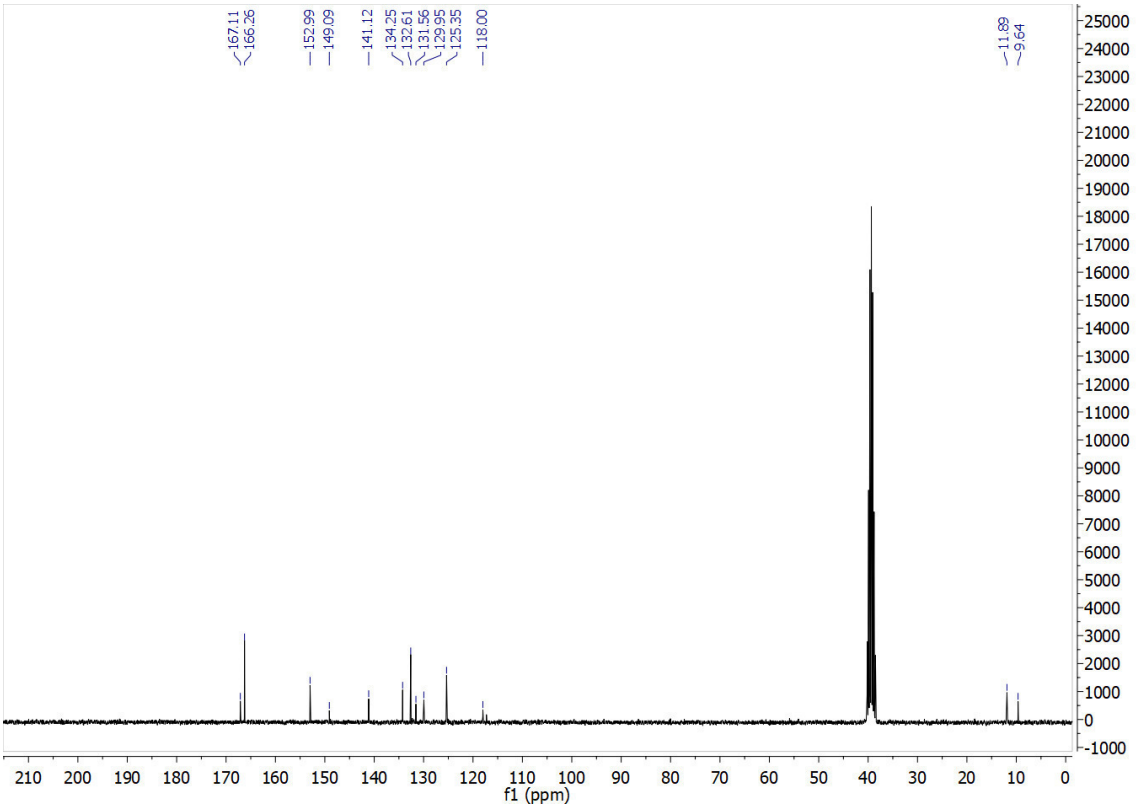

(E)-5-((3,5-Dimethyl-1H-pyrazol-4-yl)diazenyl)-N1,N3-bis(3-hydroxypropyl)isophthalamide (***27***)

^{1}H NMR (400 MHz, Methanol-d_4)

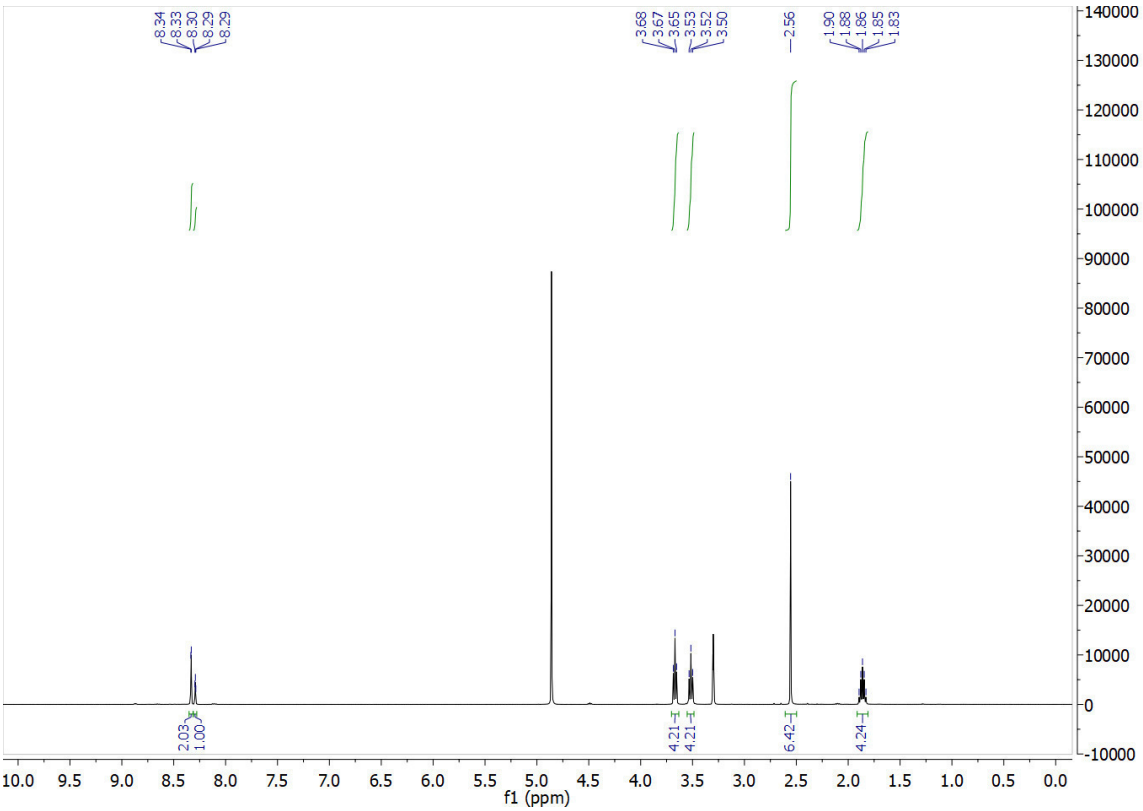

^{13}C NMR (101 MHz, Methanol-d_4)

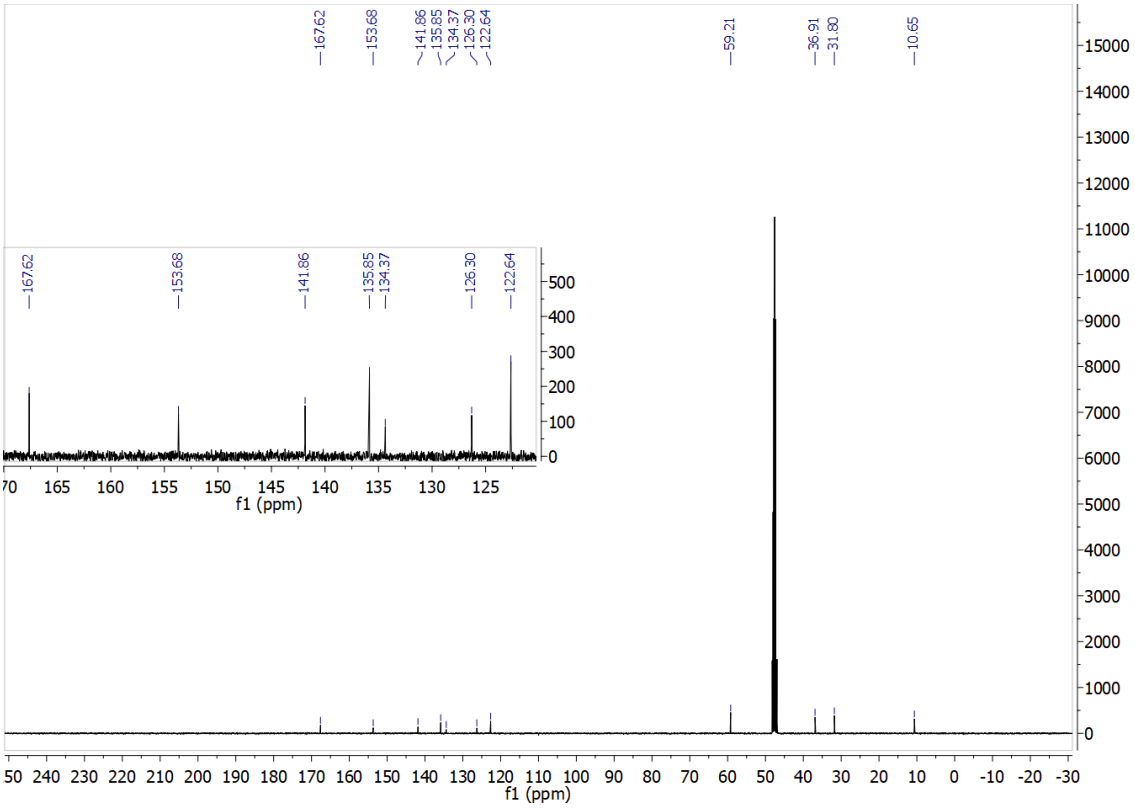

*(E)-5,5'-((5-((3,5-Dimethyl-1H-pyrazol-4-yl)diazenyl)isophthaloyl)bis(azanediyl))dipentanoic acid (**29**)*

^{1}H NMR (400 MHz, Methanol-d_4)

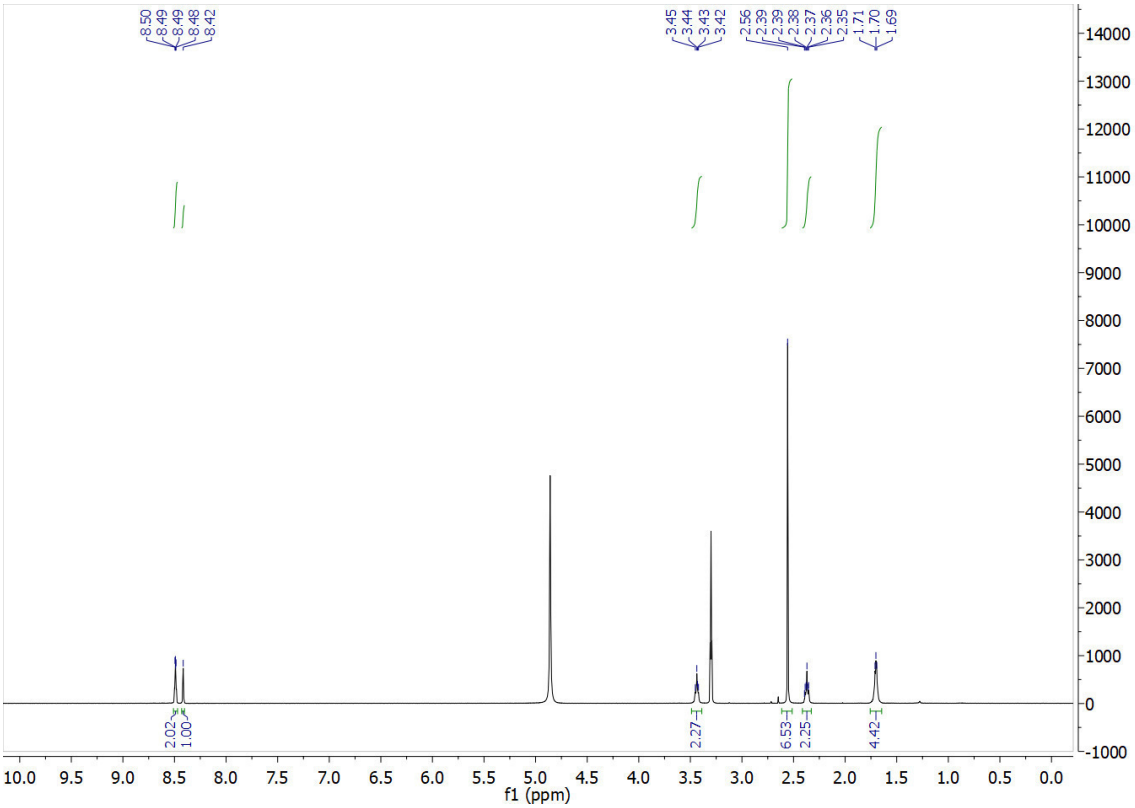

^{13}C NMR (101 MHz, Methanol-d_4)

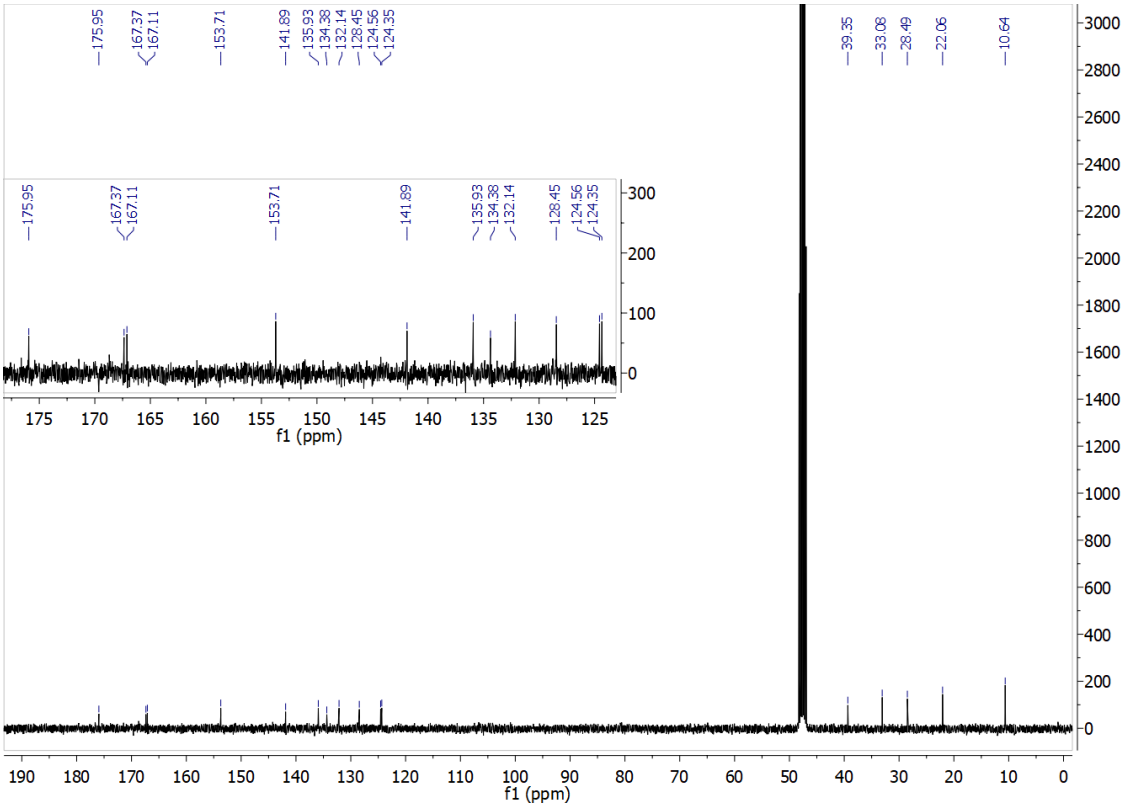

*3-(2-(4-Hydroxy-2-methylphenyl)hydrazineylidene)pentane-2,4-dione (**31**)*

^{1}H NMR (400 MHz, DMSO-d_6)

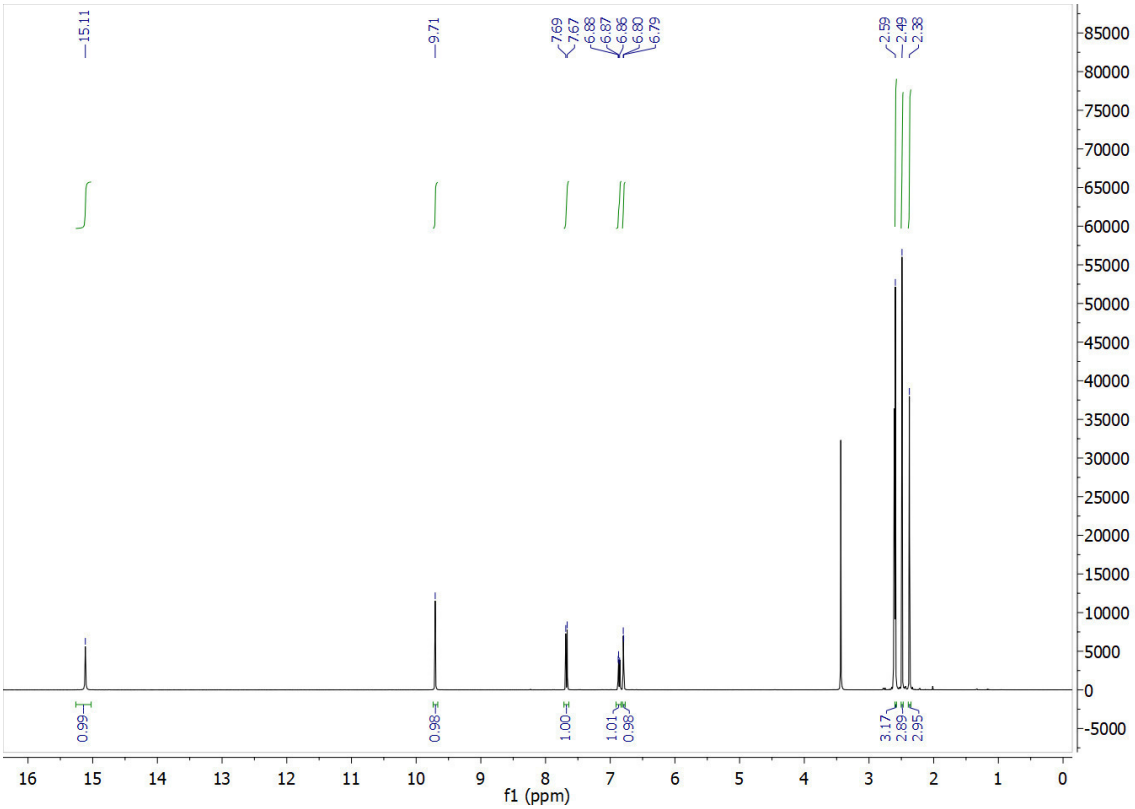

^{13}C NMR (101 MHz, DMSO-d_6)

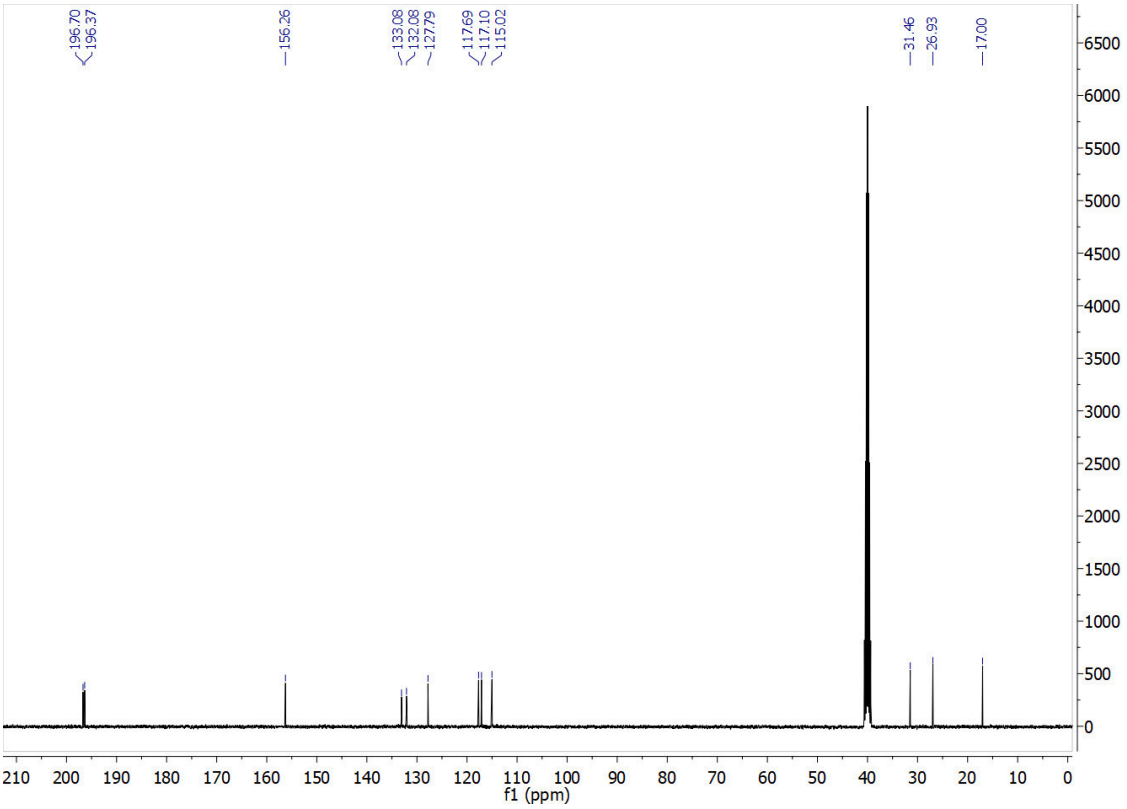

*3-(2-(4-(2-Hydroxyethoxy)-2-methylphenyl)hydrazineylidene)pentane-2,4-dione (**32**[2])*

^{1}H NMR (400 MHz, Methanol-d_4)

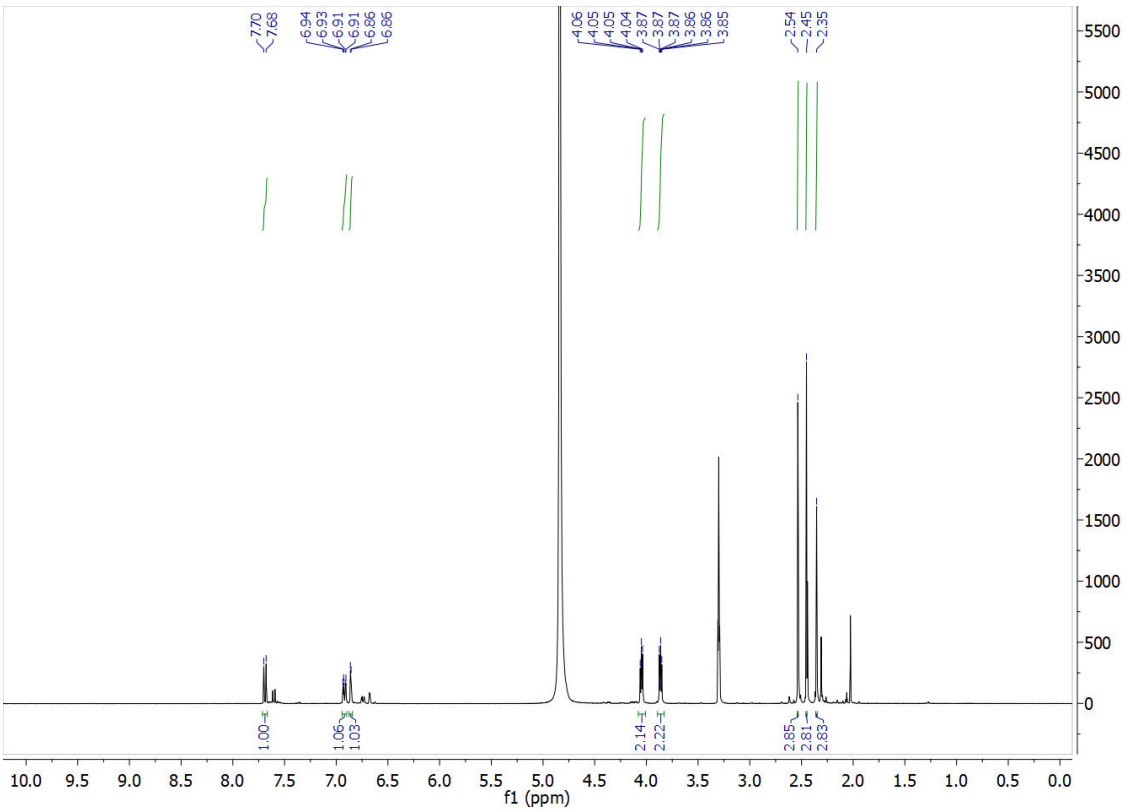

^{13}C NMR (101 MHz, Methanol-d_4)

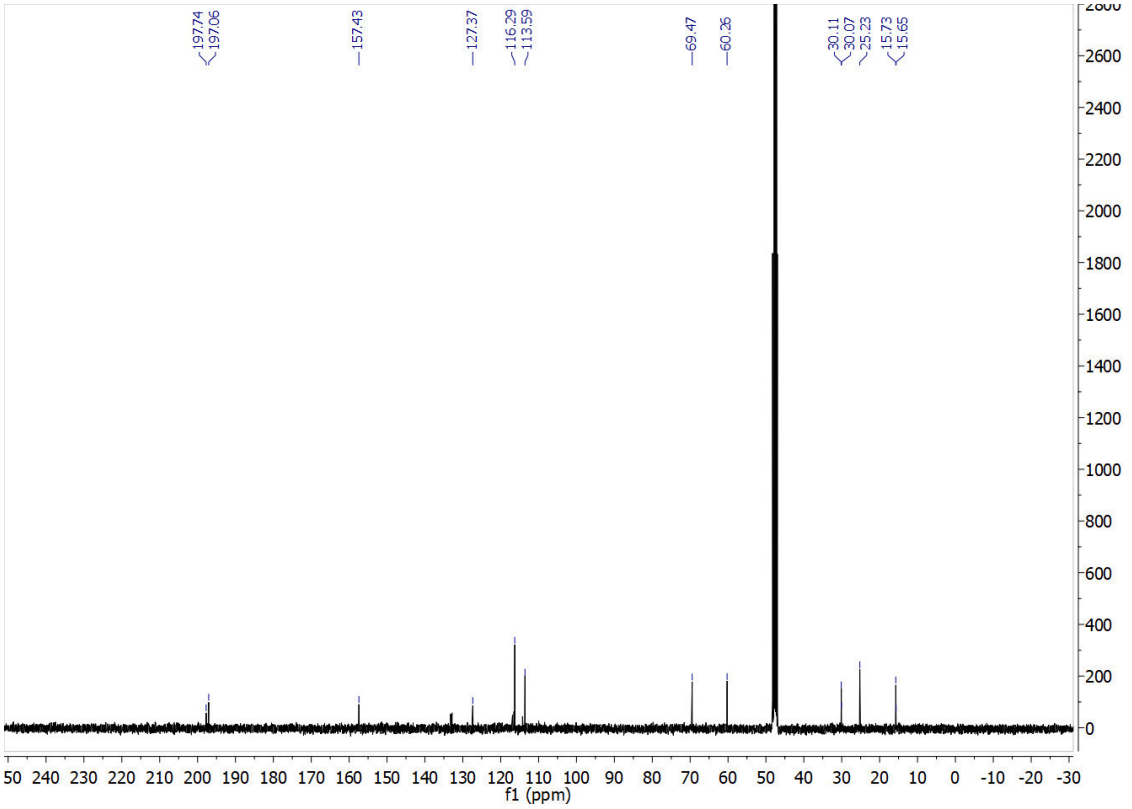

*3-(2-(4-(3-Hydroxypropoxy)-2-methylphenyl)hydrazineylidene)pentane-2,4-dione (**32**[3])*

^{1}H NMR (400 MHz, Methanol-d_4)

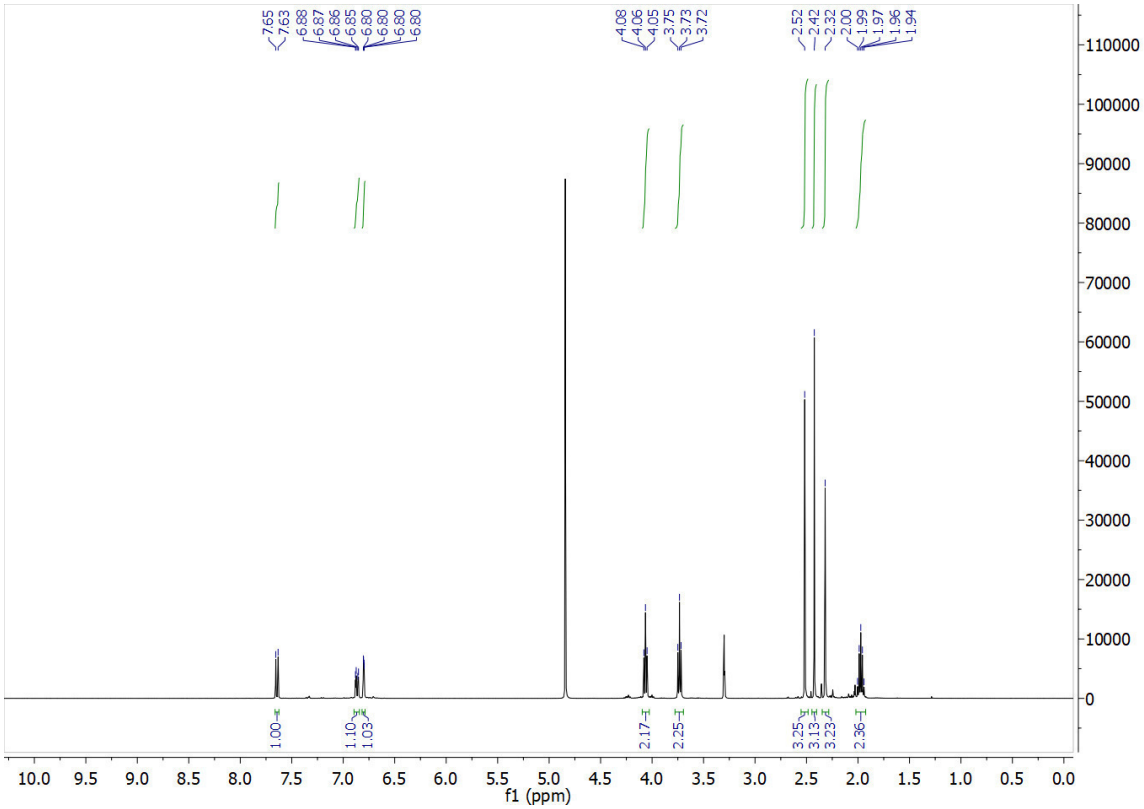

^{13}C NMR (101 MHz, Methanol-d_4)

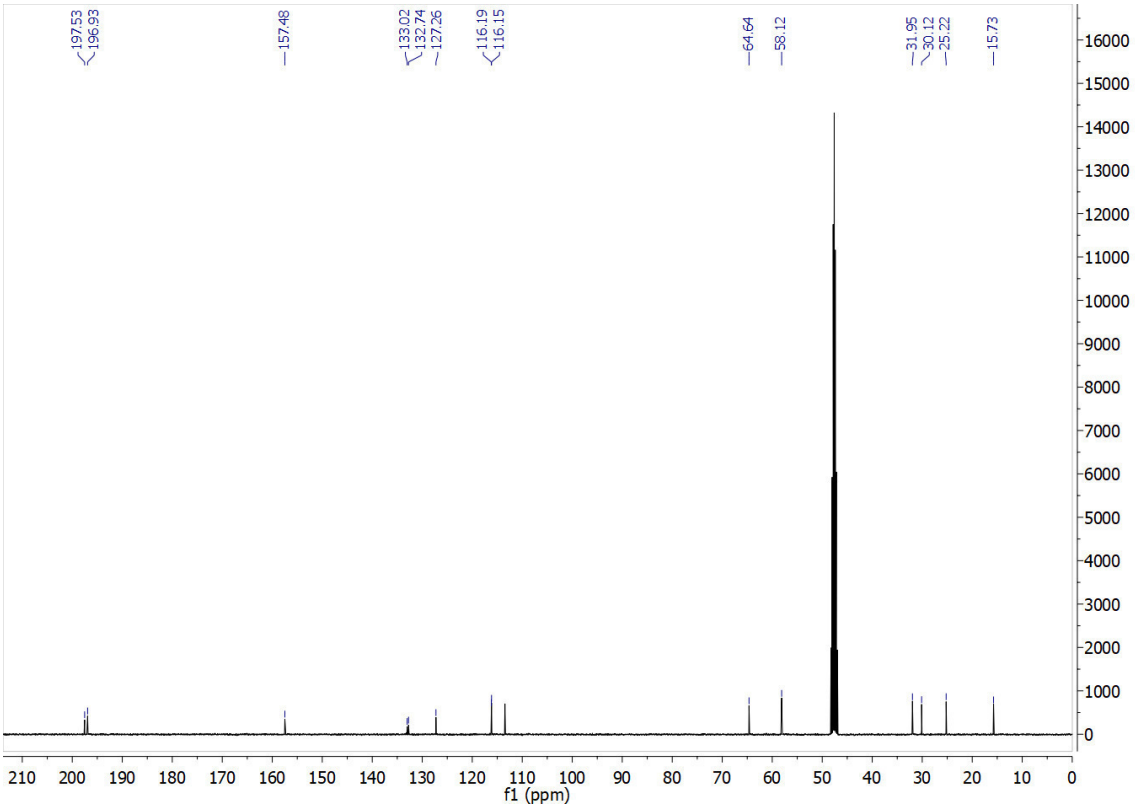

*3-(2-Bromophenoxy)propan-1-ol (**39**[3])*

^{1}H NMR (400 MHz, Chloroform-*d*)

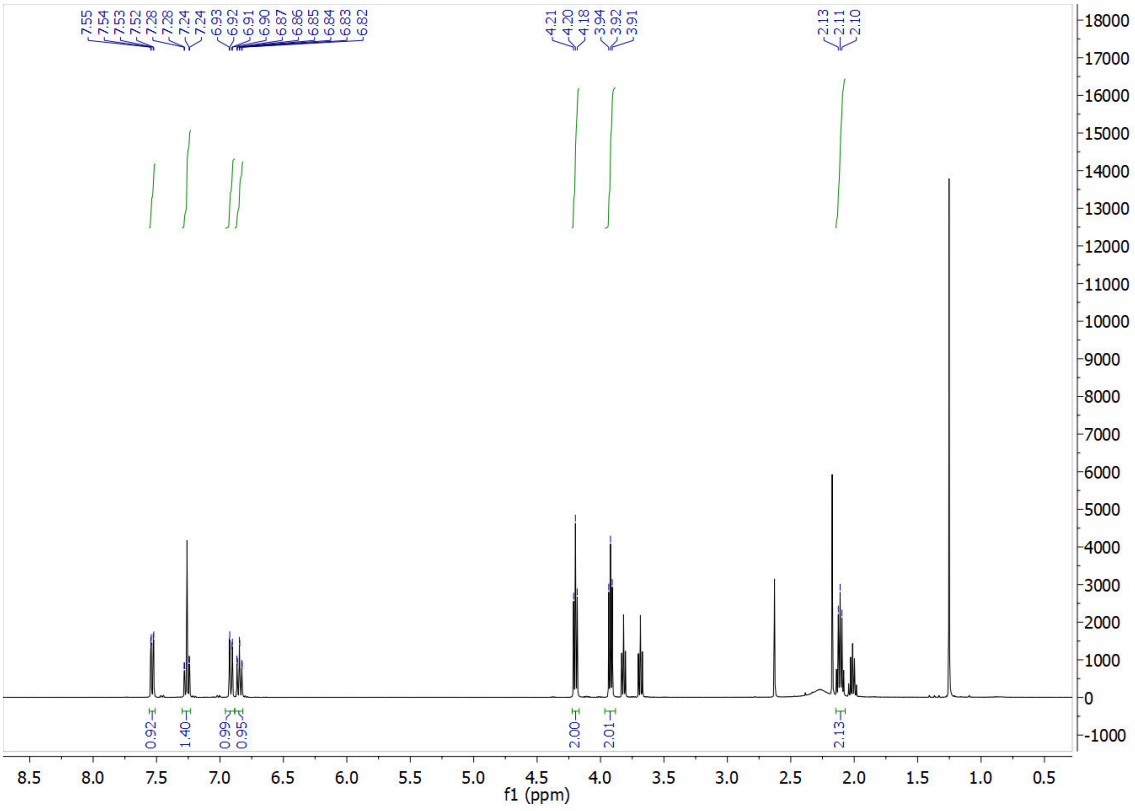

^{13}C NMR (101 MHz, Chloroform-*d*)

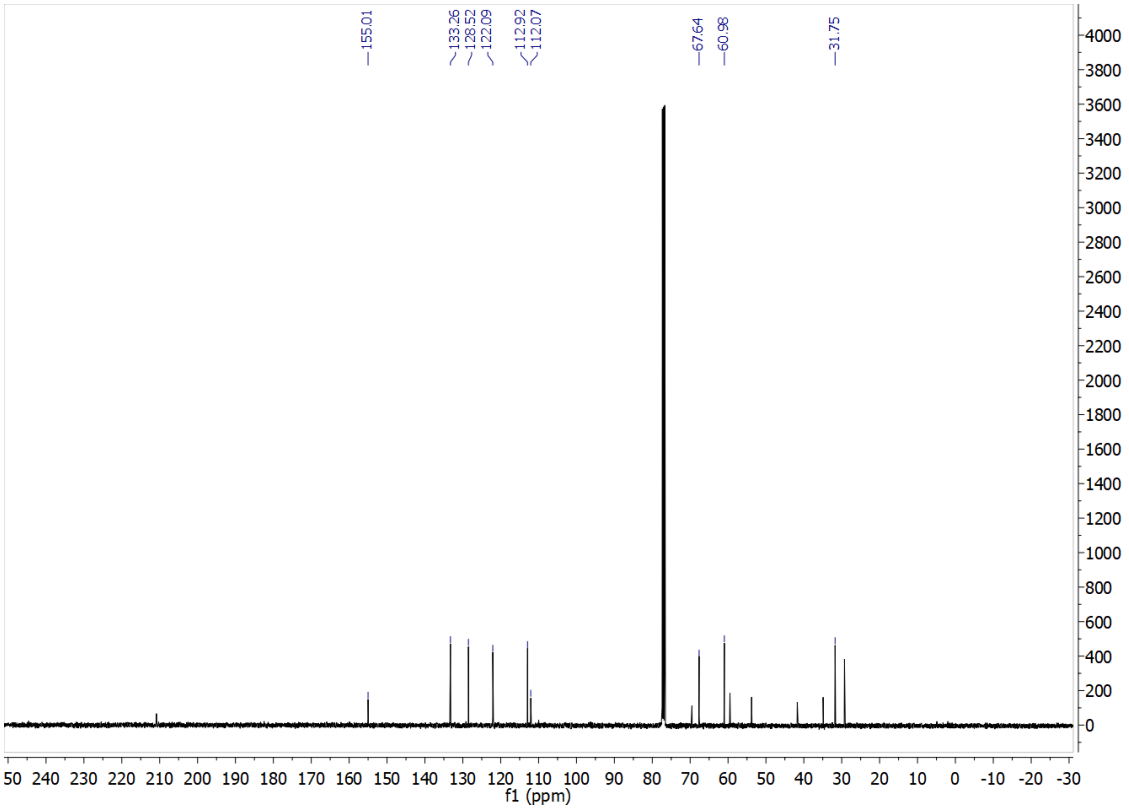

3. Biological Evaluation of DTE1–4

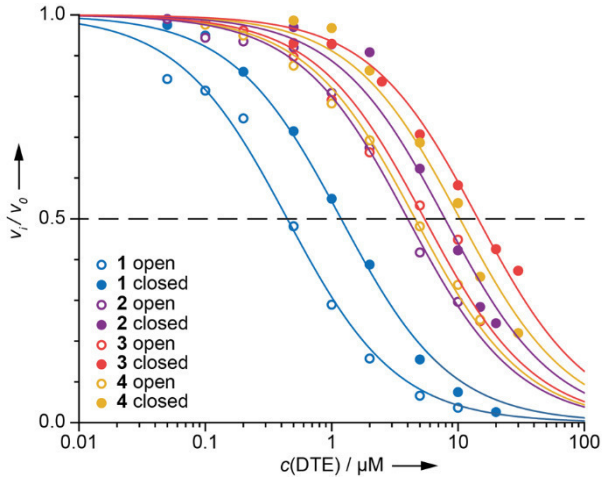

Figure A2. Related to Table 1. IC_{50} inhibition curves of HisF in the presence of compounds **1**-**4** in their ring-open (open circle) and ring-closed (filled circle) state. Reaction conditions: 50 mM Tris acetate pH 8.5, 100 mM ammonium acetate, 7 µM PRFAR and increasing concentrations (0–30 µM) of a DTE ligand. The reactions were started by the addition of 0.1 µM ImGP-S. Activities (v_i) were normalized by the measured reaction rates without DTE ligand (v_0). The IC_{50} value for each DTE ligand was determined at a v_i/v_0 value of 0.5 representing 50% inhibition.

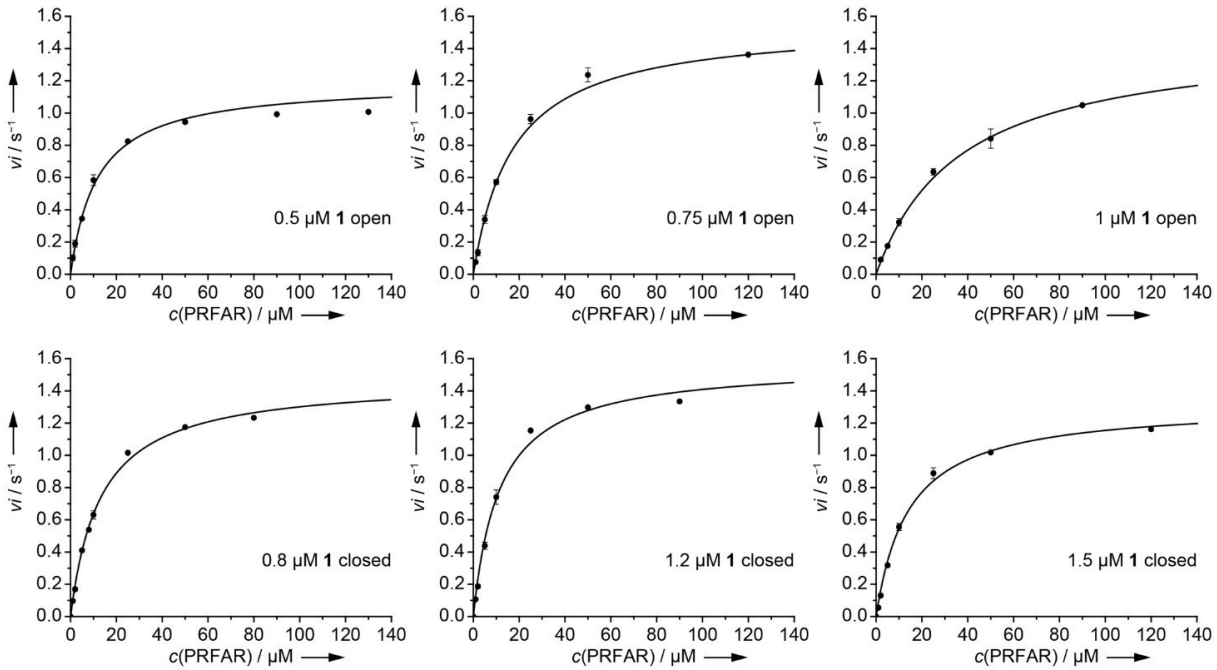

Figure A3. Related to Table 1. Representative substrate saturation curves of HisF in the presence of compound **1** in its open (top) and closed (bottom) form. Reaction conditions: 50 mM Tris acetate pH 8.5, 0.1 µM ImGP-S, 100 mM ammonium acetate, 1–200 µM PRFAR and three succinct concentrations of the DTE ligand **1** that resulted in 30–70 % inhibition in IC_{50} measurements (see Figure S1). See Table S2 for deduced steady-state kinetic parameters.

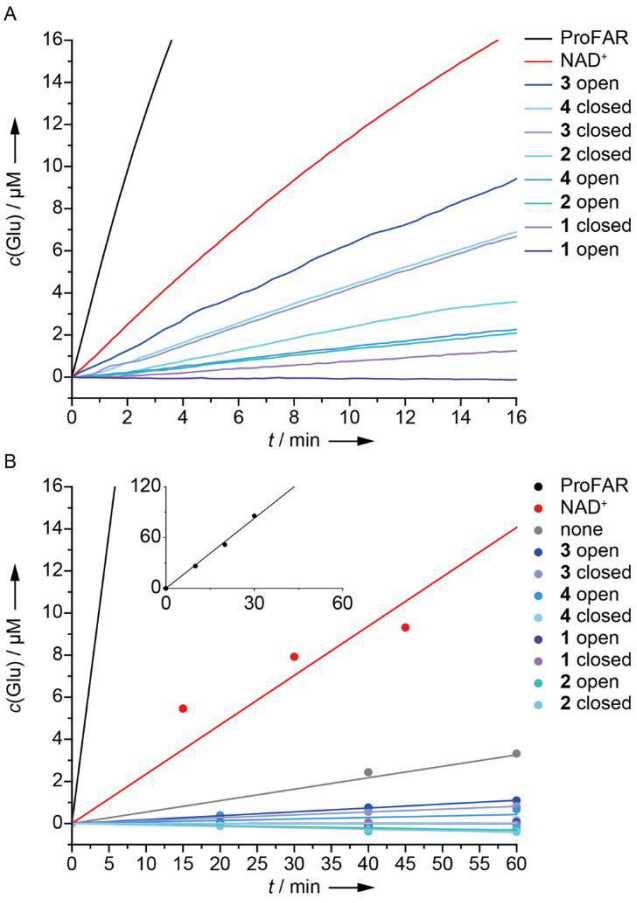

C

HisF ligand	conformation	$v_{A,cont}$ / min^{-1}	$v_{B,discont}$ / min^{-1}
1	open	0.0 ± 0.0	0.00
	closed	0.1 ± 0.0	0.00
2	open	0.1 ± 0.0	−0.01
	closed	0.2 ± 0.1	−0.01
3	open	0.5 ± 0.3	0.03
	closed	0.5 ± 0.1	0.02
4	open	0.1 ± 0.0	0.01
	closed	0.3 ± 0.2	0.00
none		---	0.05
NAD$^+$		1.3 ± 0.2	0.23
ProFAR		4.7 ± 0.3	2.76

Figure A4: Effect of compounds **1–4** on HisH activity compared to known HisF ligands ProFAR and NAD$^+$. A) HisH transition curves of the continuous assay. Either no ligand (besides NAD$^+$), ProFAR, or compounds **1–4** in their open or closed forms were added. Reaction conditions: 50 mM Tricine/KOH pH 8.0, 1 µM ImGP-S, 1g/L GDH, 10mM NAD$^+$, 8 mM glutamine, and 40 µM ligand (if applicable). B) HisH transition curves of the discontinuous assay. Either no ligand, ProFAR, NAD$^+$, or compounds **1–4** were added. The inset window shows the data points of the ProFAR reaction. Reaction conditions: 50 mM Tricine/KOH pH 8.0, 1 µM ImGP-S, 8 mM glutamine, 50 µM ProFAR or 10 mM NAD$^+$ or 100 µM DTE ligand. Conditions of the glutamate detection step: 50 mM Tricine/KOH, pH 8.0, 1 g/L GDH 10 mM NAD$^+$. C) Initial velocities of the HisH activities in the continuous ($v_{A,cont}$) and discontinuous ($v_{B,discont}$) assay. For further inhibition studies on HisH see also Figure A5.

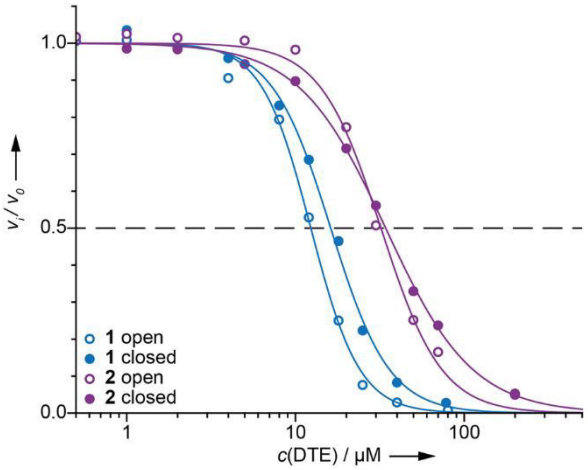

Figure A5: IC_{50} inhibition curves of HisH in the presence of compounds **1** and **2** in their open (open circle) and closed (filled circle) form. Conditions: 50 mM Tricine/KOH pH 8.0, 10 mM NAD^+, 8 mM glutamine, 40 µM ProFAR and increasing concentrations (0–200 µM) of a DTE ligand. The reactions were started by addition of 1 µM ImGP-S. Activities (v_i) were normalized by the reaction rate without DTE ligand (v_0). The IC_{50} value for each DTE ligand was determined at a v_i/v_0 value of 0.5 representing 50 % inhibition.

Table A1. Related to Table 1. Steady-state kinetic constants and deduced inhibitions constants for the activity of HisF in presence of compounds **1–4** in their ring-open and ring-closed forms.

compound	conformation	*c*(compound)/ μM	K_m^{app} / μM	k_{cat} / s^{-1}	*Ki* / μM
1	open	0.50	11.7	1.2	0.2
		0.75	17.4	1.6	0.2
		1.00	36.8	1.5	0.1
	closed	0.80	13.1	1.5	0.3
		1.20	11.4	1.6	0.6
		1.50	14.2	1.3	0.5
2	open	2.50	9.8	1.5	1.5
		4.50	11.3	1.4	2.1
		6.50	13.7	1.1	2.4
	closed	5.00	12.9	1.3	2.0
		6.00	15.6	1.4	1.8
		7.00	19.5	1.4	1.7
3	open	3.00	7.3	1.4	2.9
		4.50	8.5	1.3	3.3
	closed	5.00	9.1	1.3	3.3
		9.00	14.6	1.1	3.0
4	open	2.50	8.2	1.5	2.0
		4.00	11.1	1.5	1.9
		5.50	8.9	1.4	2.7
	closed	5.00	9.3	1.2	3.2
		9.00	7.4	1.3	8.5
		13.00	11.1	1.1	6.3

Three substrate saturation curves were recorded with measurement points at least as duplicates, and at succinct DTE ligand concentrations that resulted in 30-70 % inhibition in IC_{50} measurements (see Figure S1). By fitting the curves with the Michaelis-Menten equation, K_m^{app} and k_{cat} values were determined. Inhibition constants K_i were calculated as described in the experimental section from the increase of the K_m^{app} value with respect to the K_m value in absence of inhibitor. The mean values and standard deviations of K_i for each inhibitor are given in Table 1.

Table A2. Related to Figure 5. Activities prior and after UV-irradiation of HisF-, HisH-, and ImGP-S reactions with compounds **1** and **2** added in their ring-open form.

Figure 6	reaction	HisF ligand	v / min^{-1}		activation factor
			prior	after	
A	HisF	**1**	9.8	25.4	2.6
B	HisH	**1**	0.5	1.0	2.0
C	ImGP-S	**1**	6.0	13.5	2.8
D	ImGP-S	**2**	13.5	13.5	1.0

A.III.2. Photochromic Ligands for the Trp-Synthase Multienzyme Complex

Table of Contents

1. NMR Spectra

3a: ^{1}H NMR (300 MHz, 10% MeOD-*d4* in Chloroform-*d*)

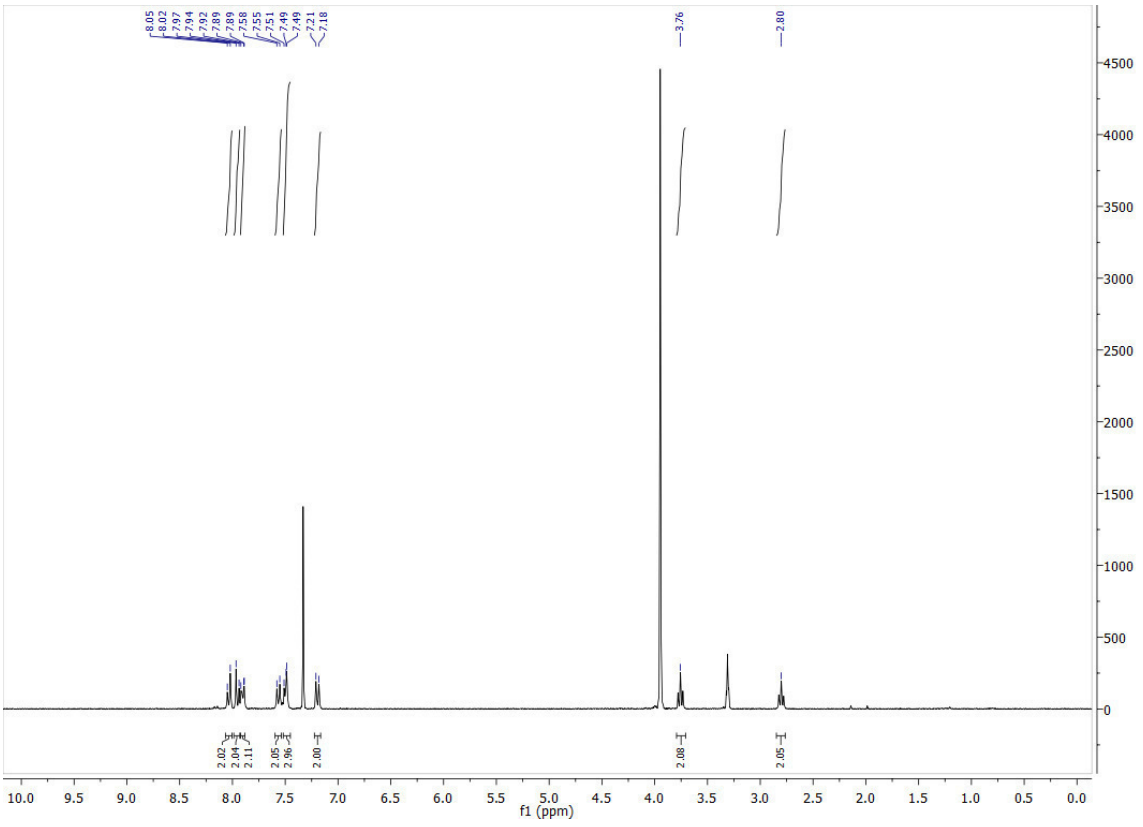

HSQC (151 MHz, Acetone-d_6):

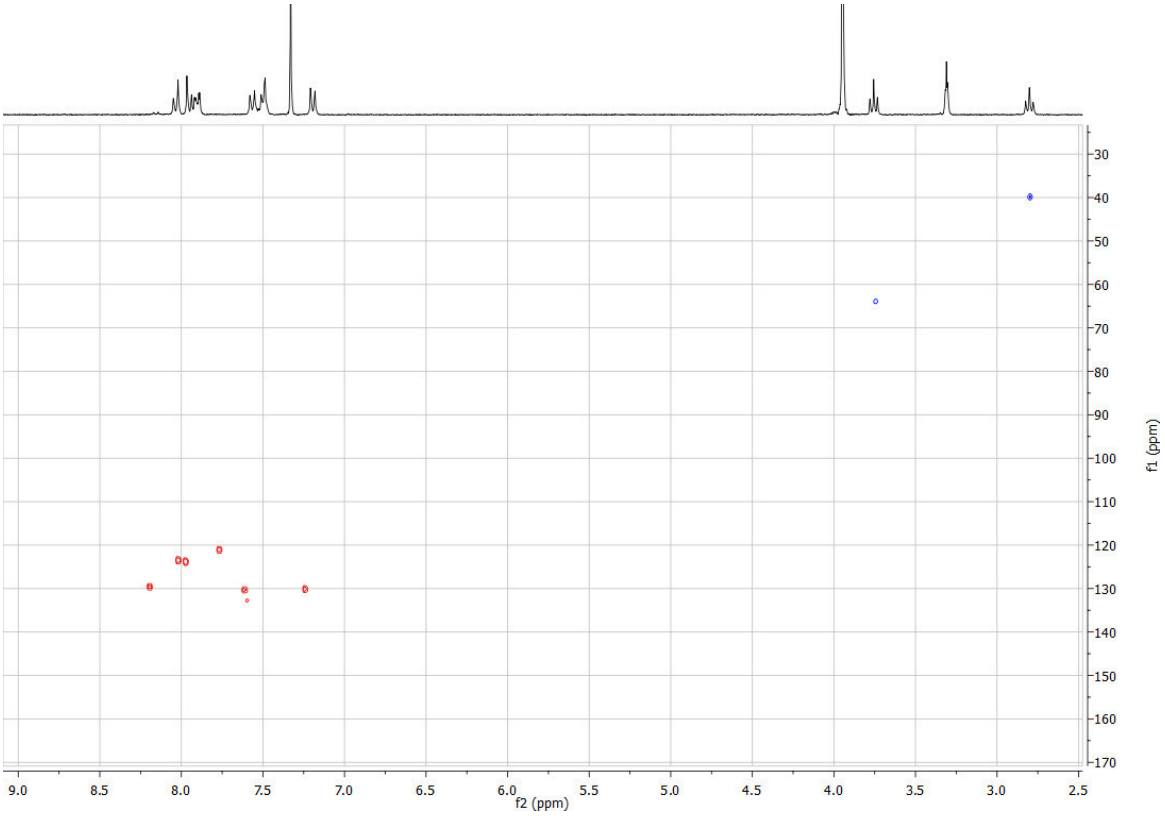

3b: ^{1}H NMR (400 MHz, Acetone-d_6)

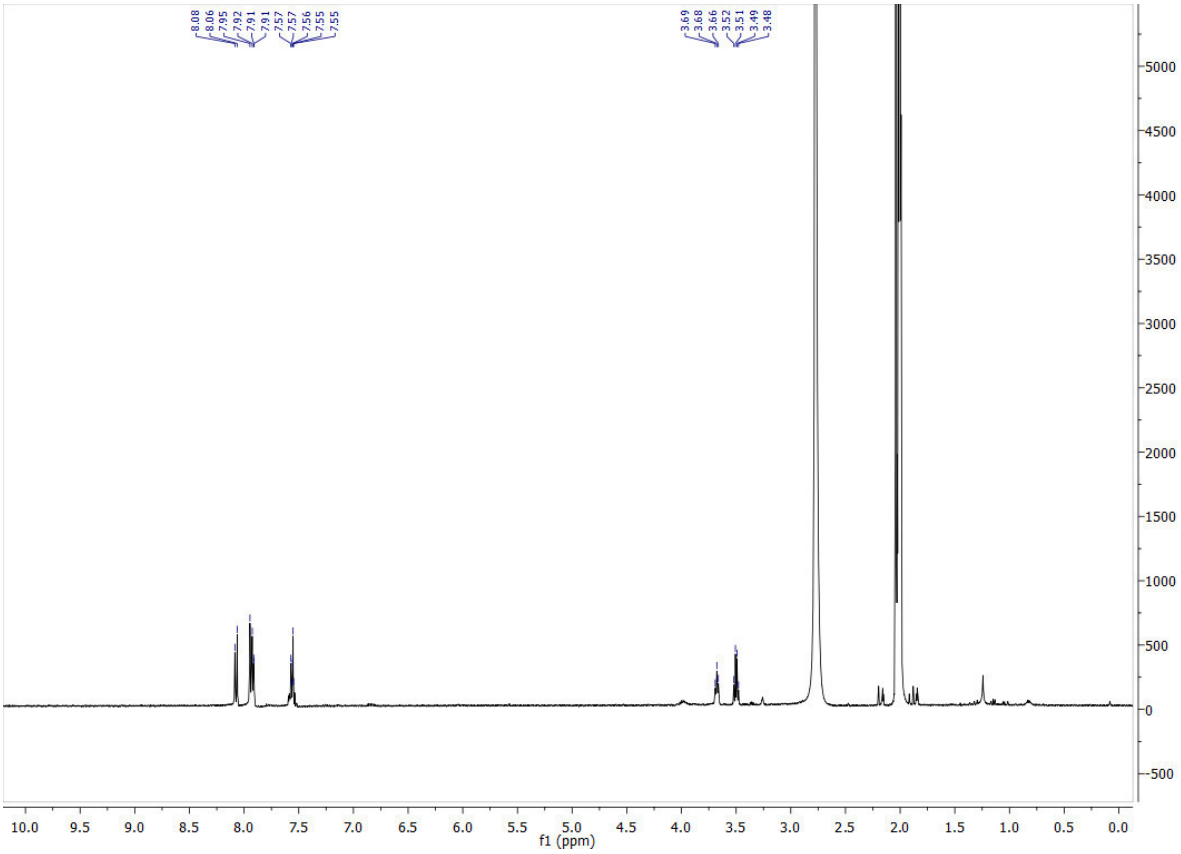

HSQC (151 MHz, Acetone-d_6)

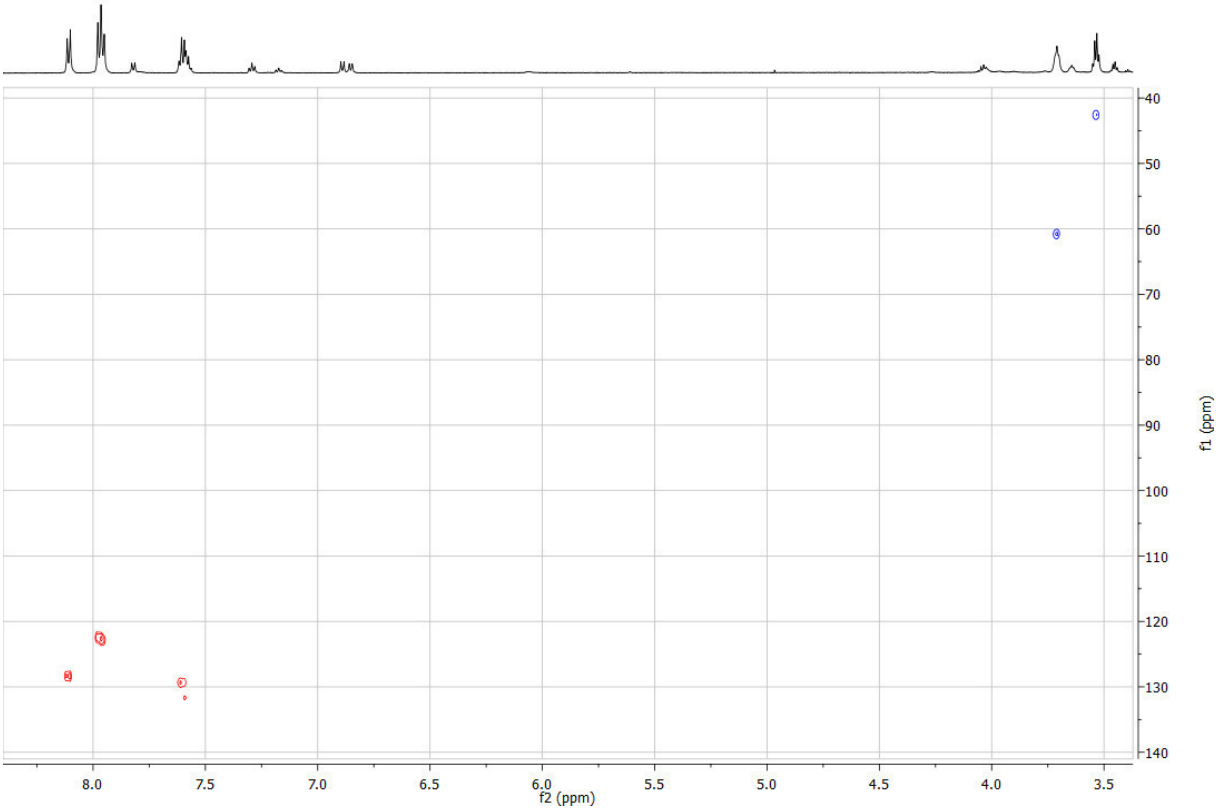

3c: ^{1}H NMR (400 MHz, Acetone-d_6)

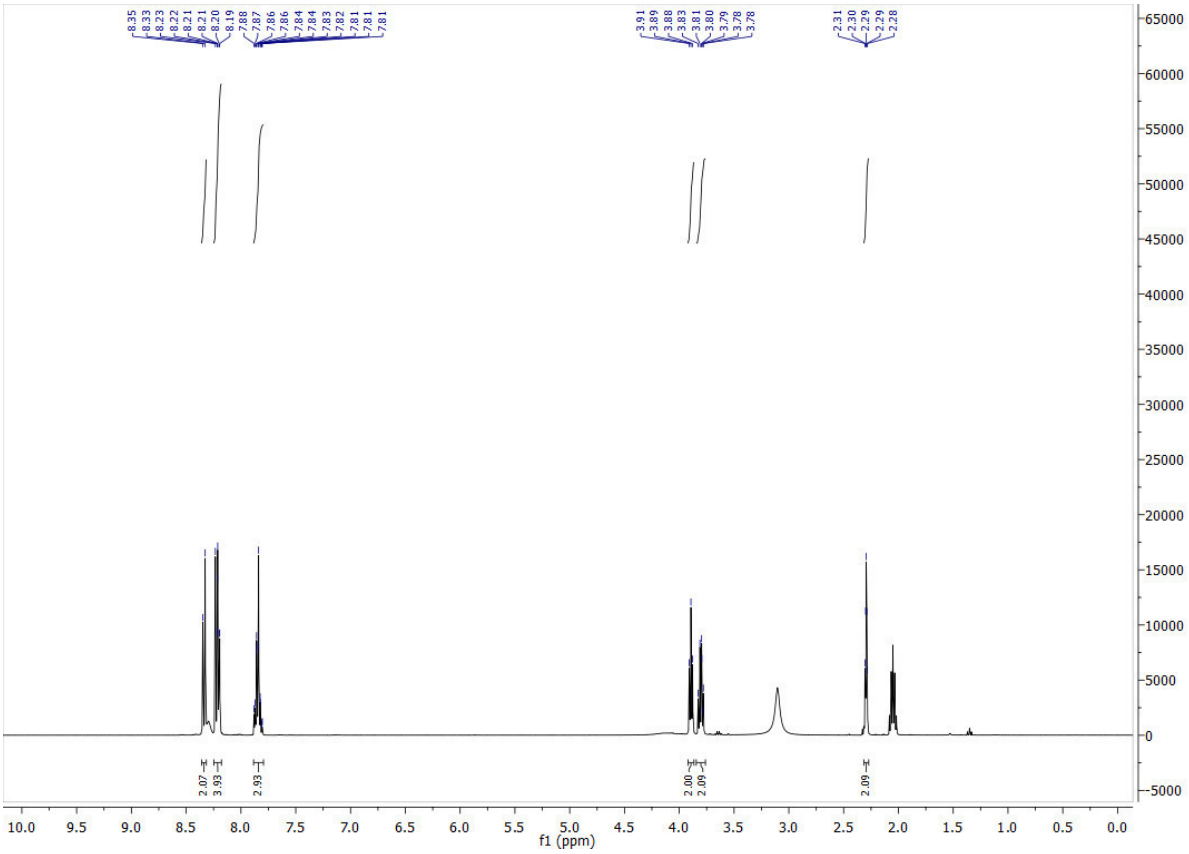

3c: ^{13}C NMR (101 MHz, Acetone-d_6)

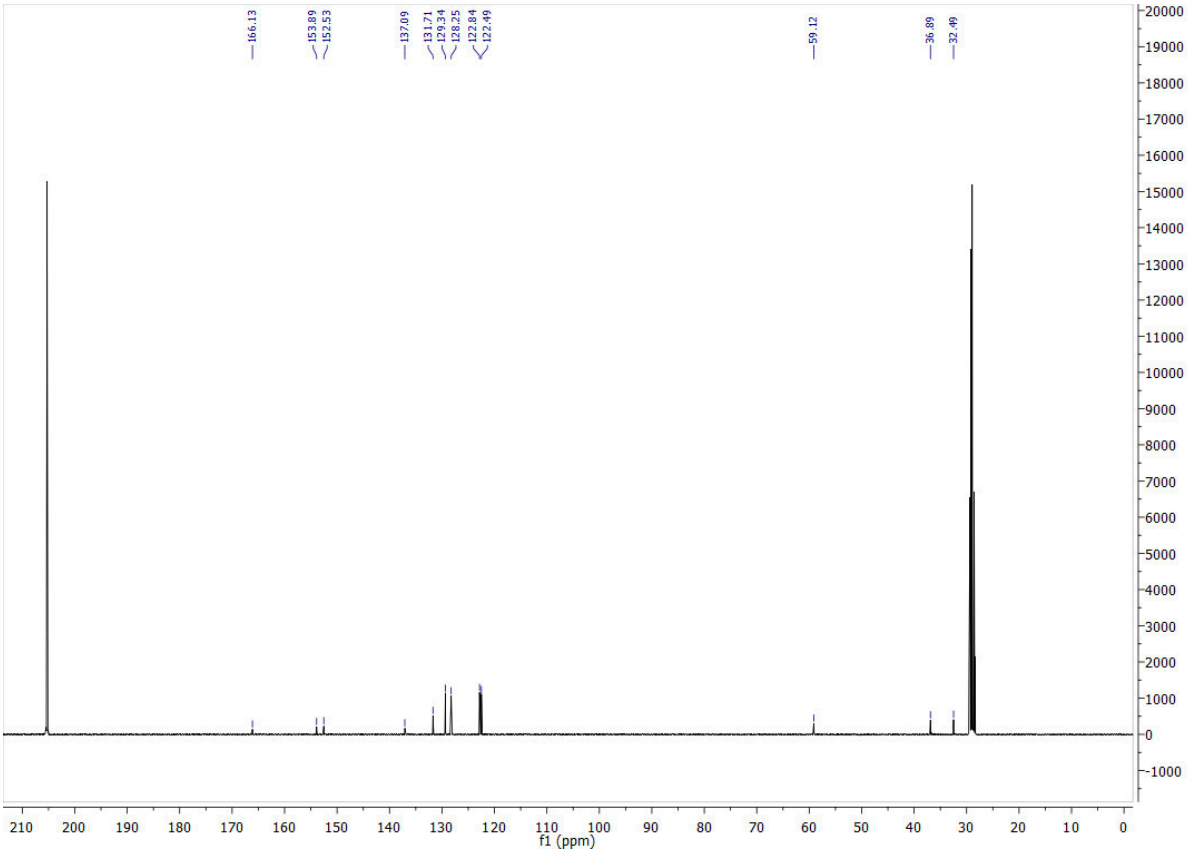

3d: ^{1}H NMR (400 MHz, Acetone-d_6)

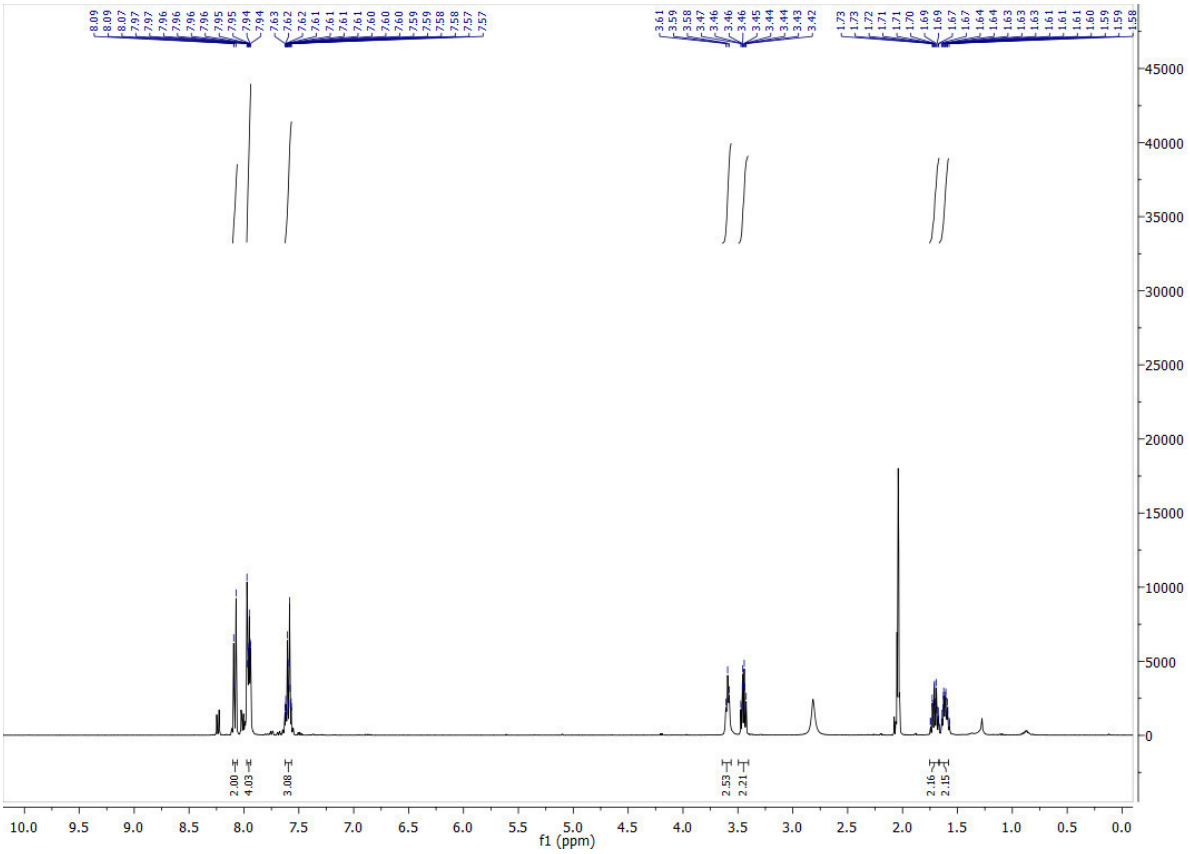

^{13}C NMR (101 MHz, Acetone-d_6)

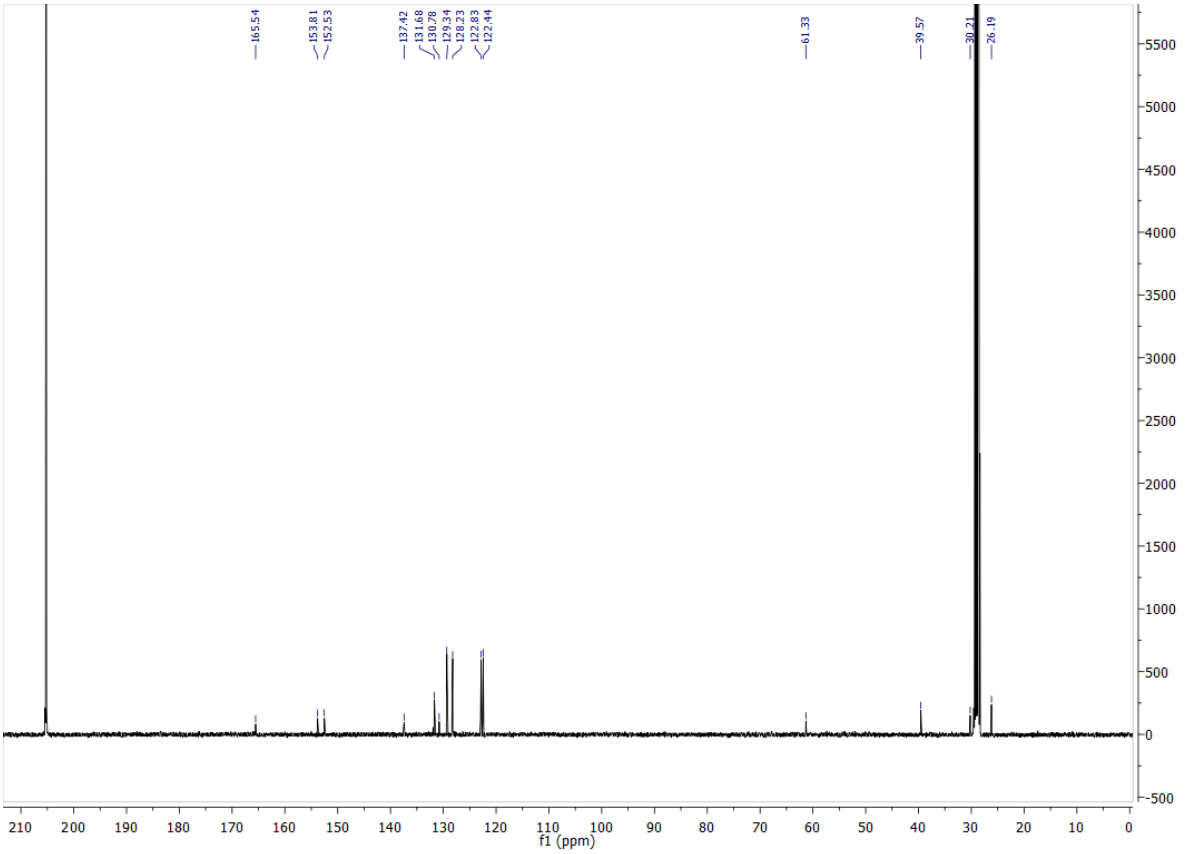

3e: ^{1}H NMR (400 MHz, Acetone-d_6)

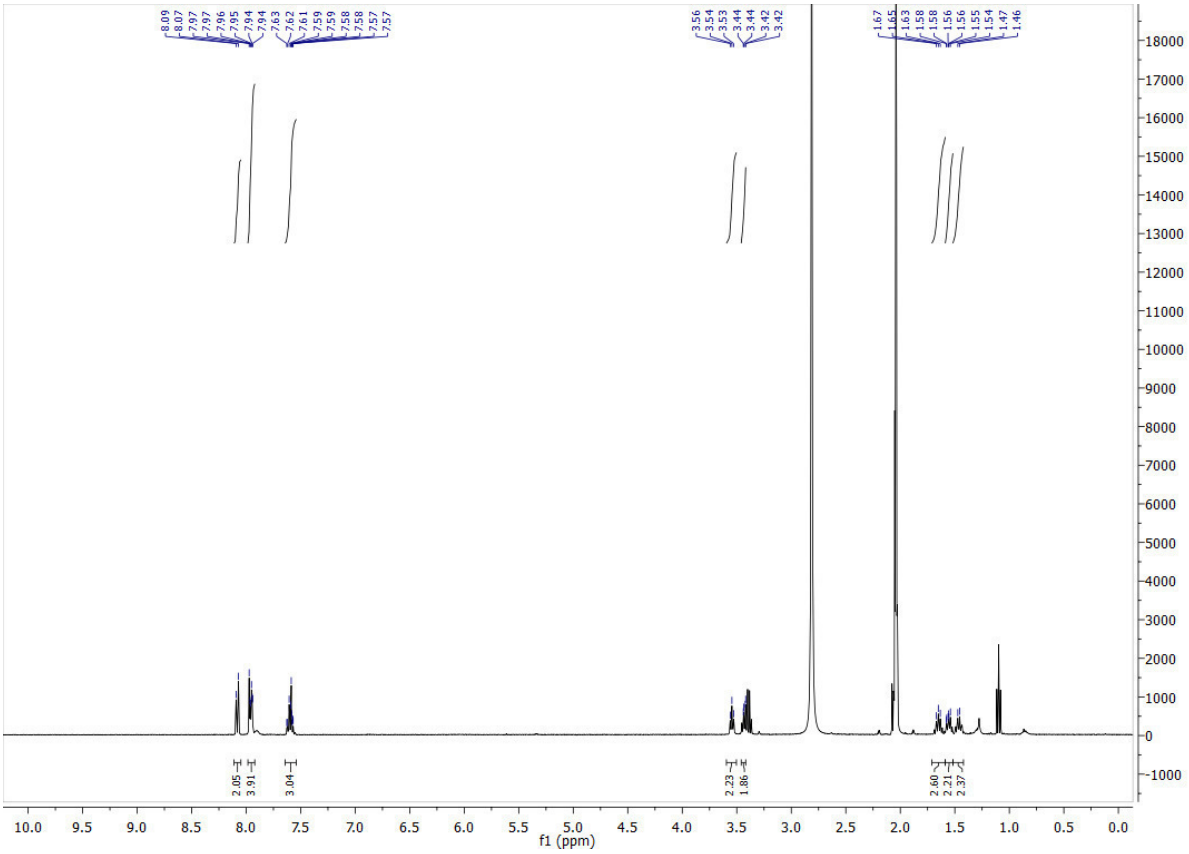

HSQC (151 MHz, Acetone-d_6):

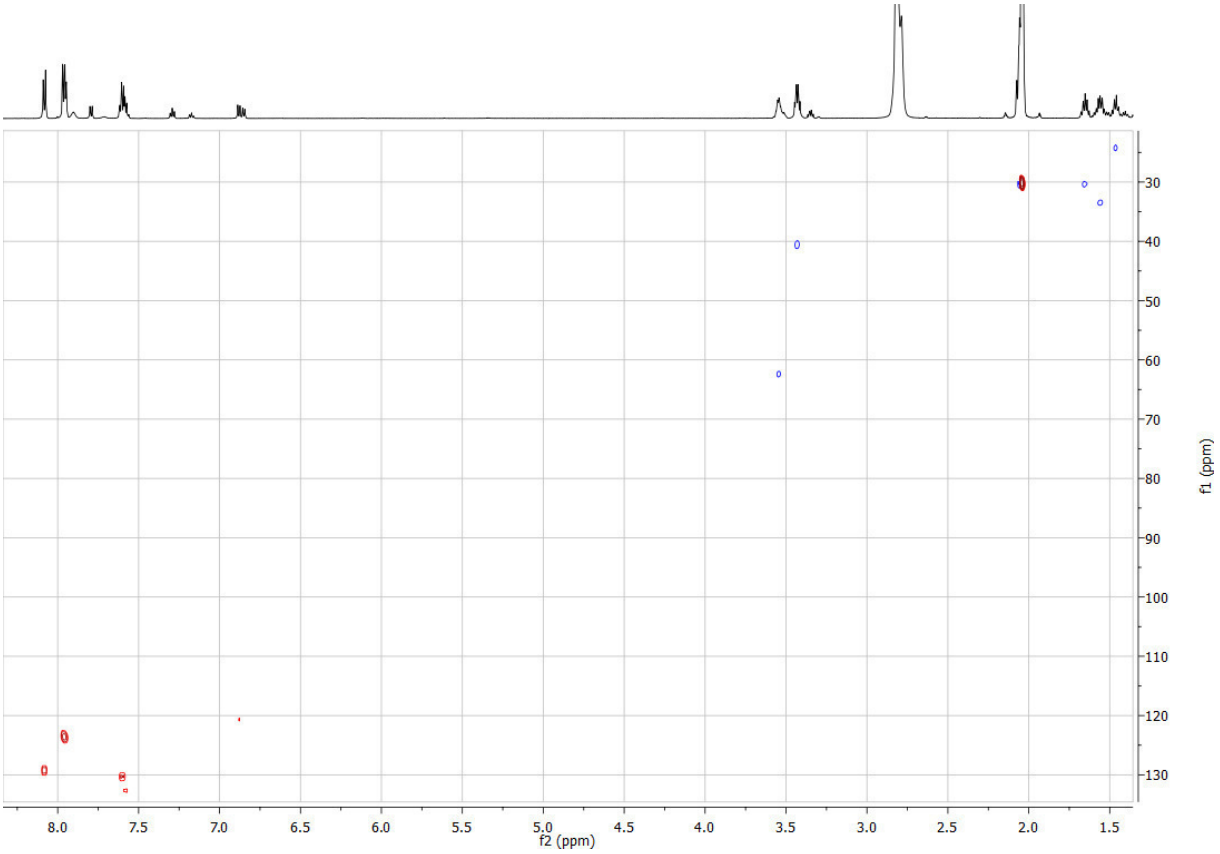

3f: ^{1}H NMR (400 MHz, Acetone-d_6)

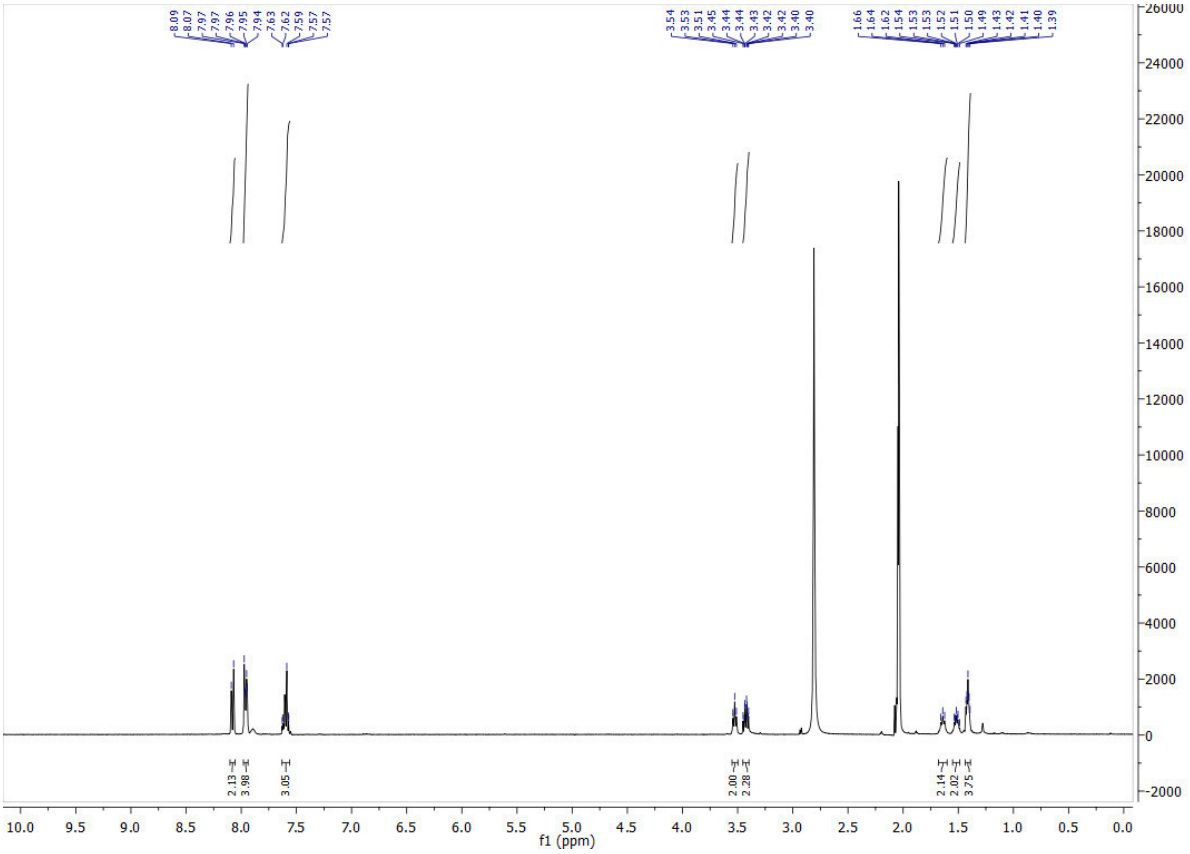

HSQC (151 MHz, Acetone-d_6)

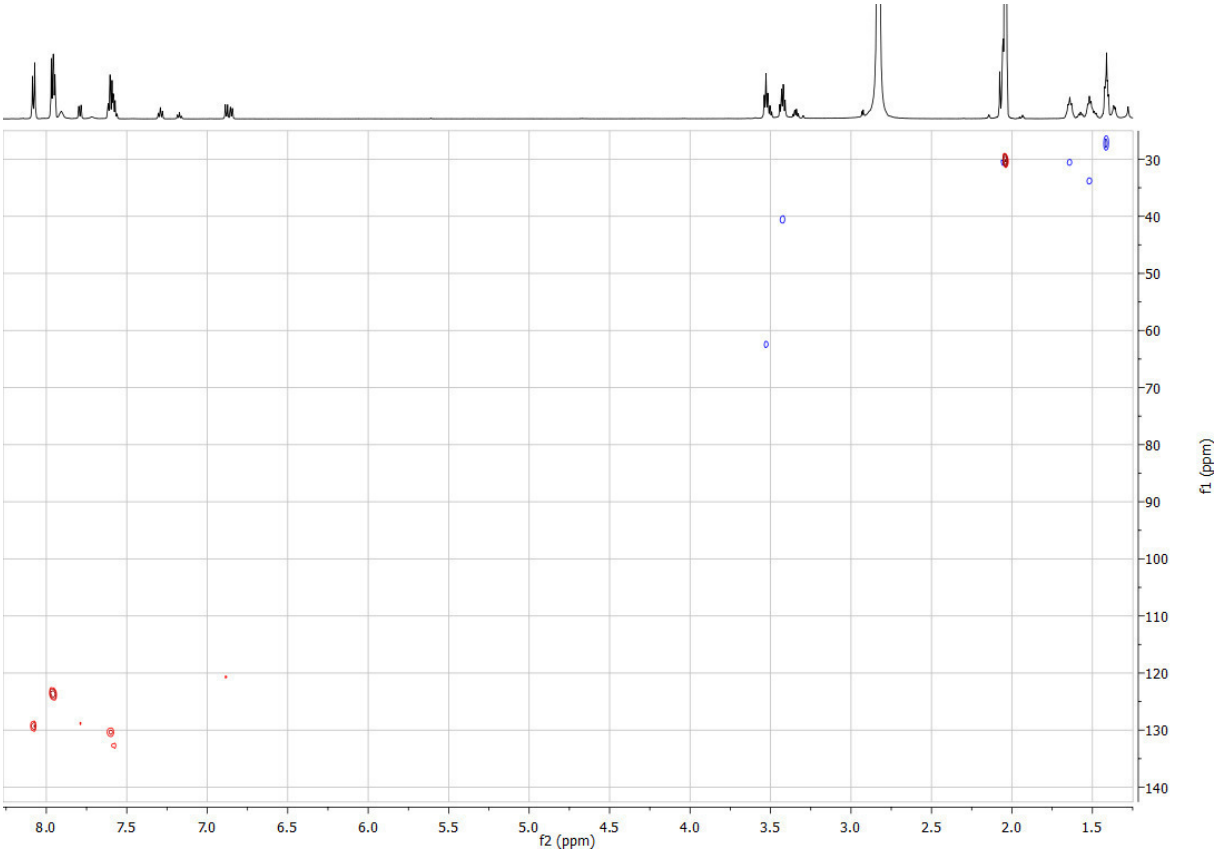

4a: ^{1}H NMR (400 MHz, Methanol-d_4)

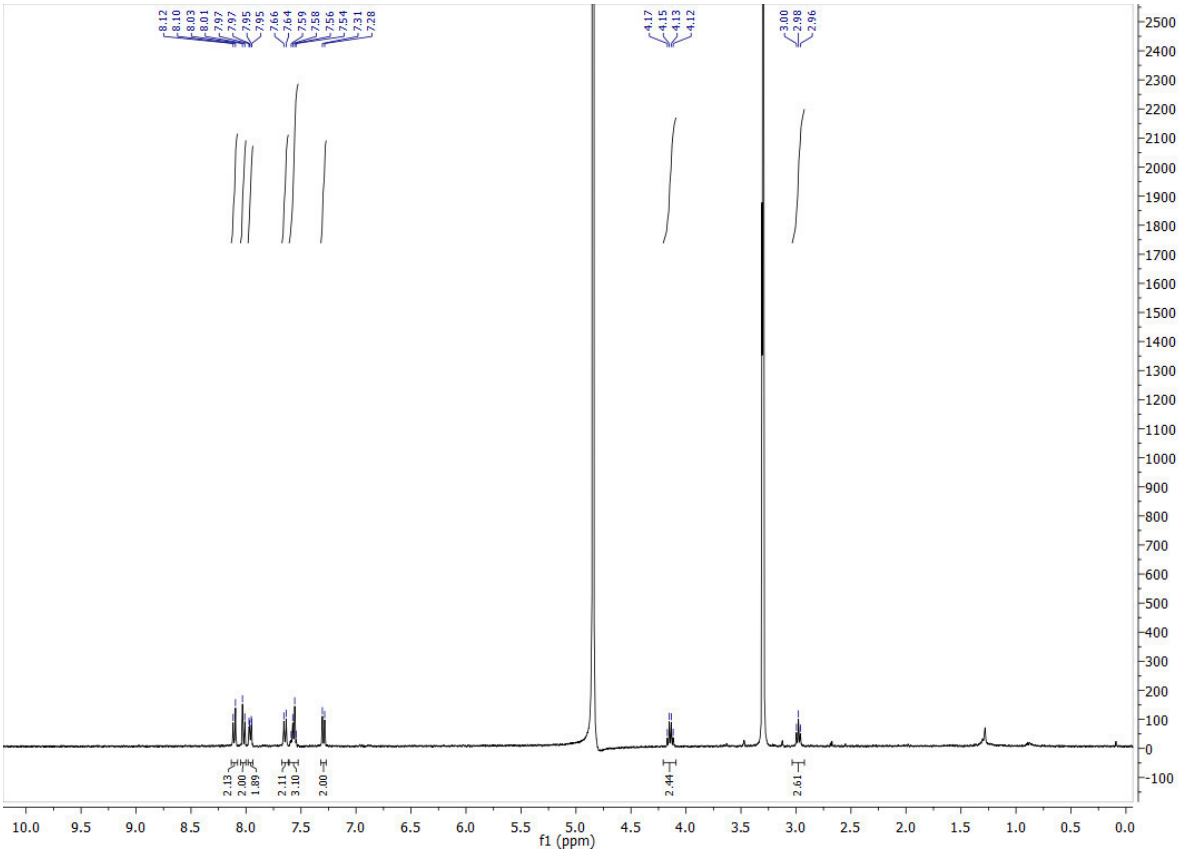

^{31}P NMR (162 MHz, Methanol-d_4)

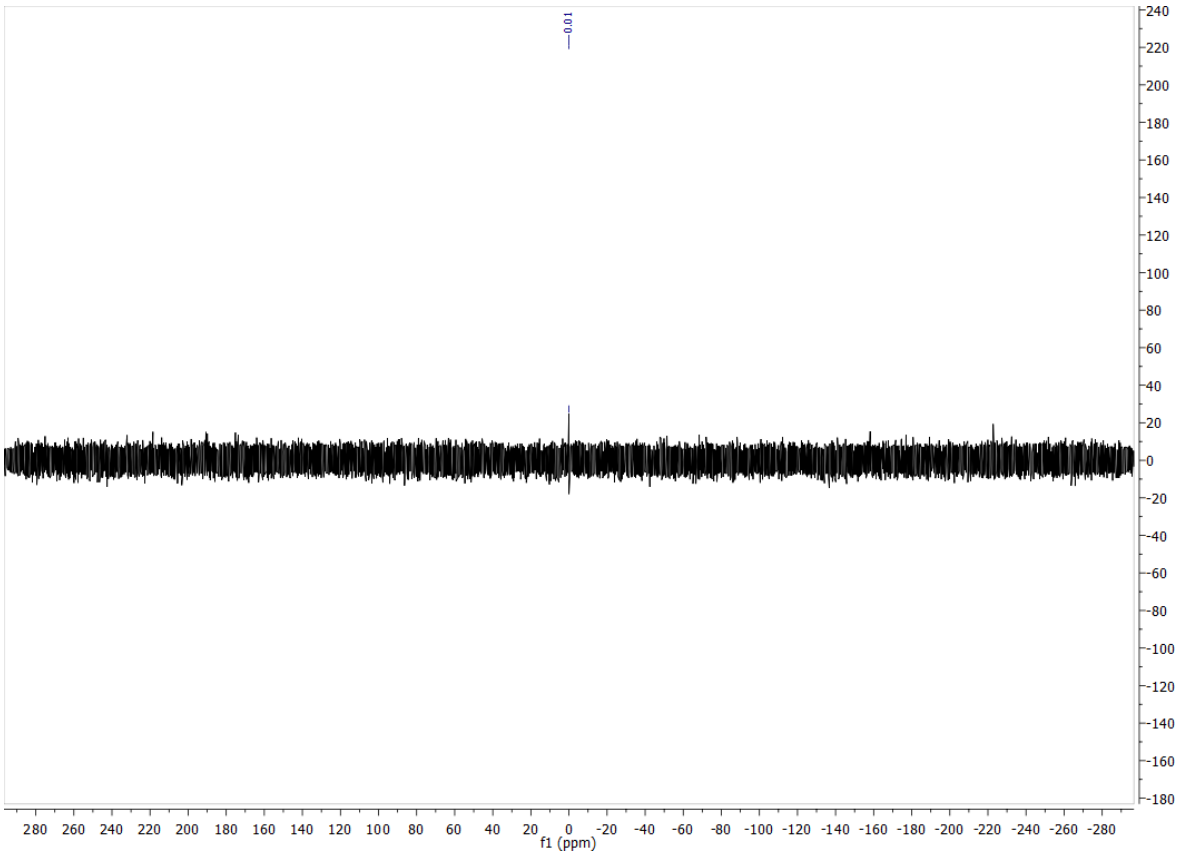

4b: ^{1}H NMR (400 MHz, Methanol-d_4)

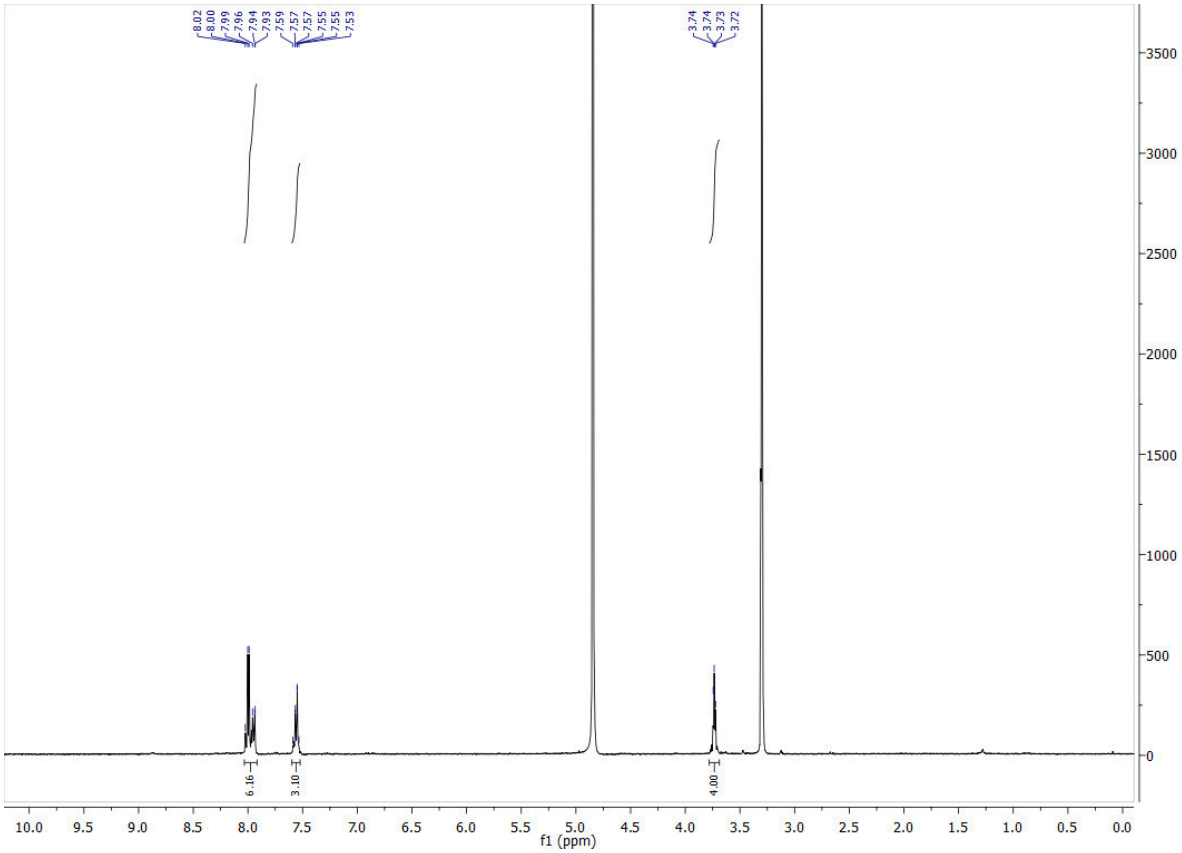

^{31}P NMR (162 MHz, Methanol-d_4)

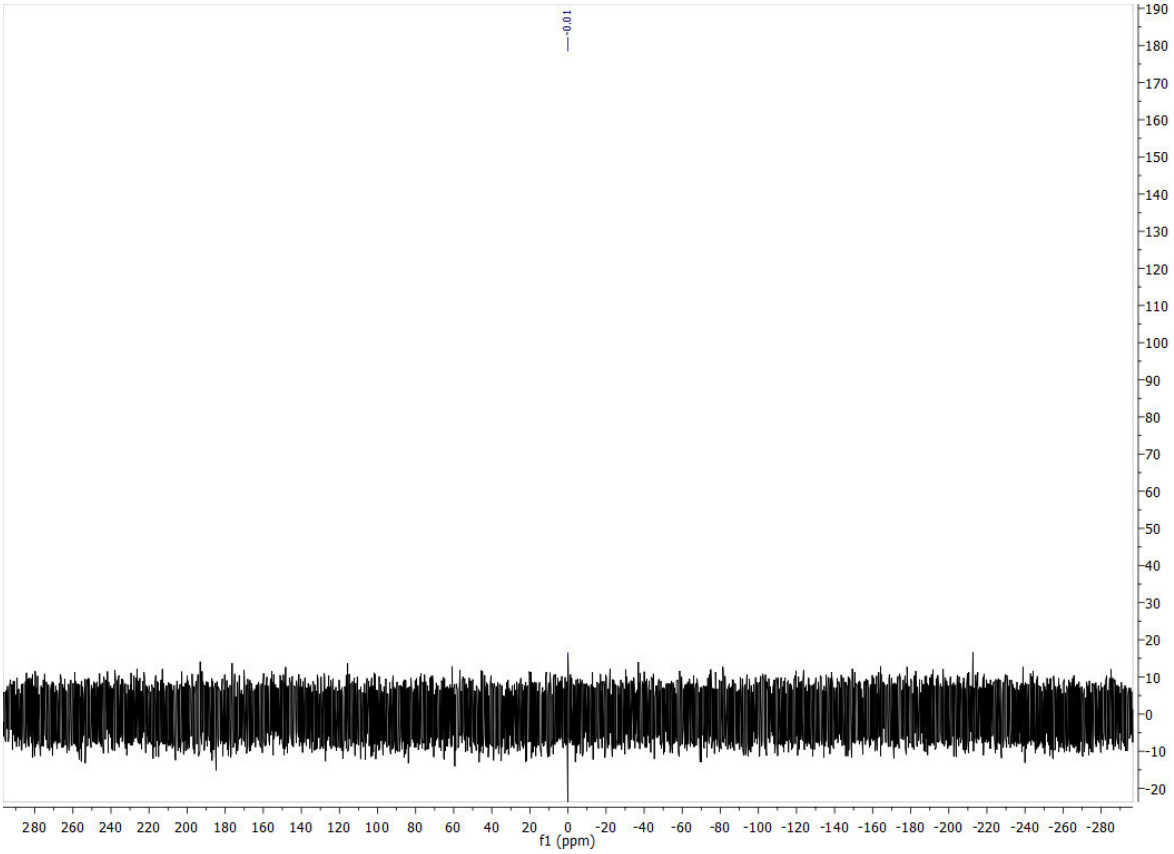

4c: ^{1}H NMR (400 MHz, Methanol-d_4)

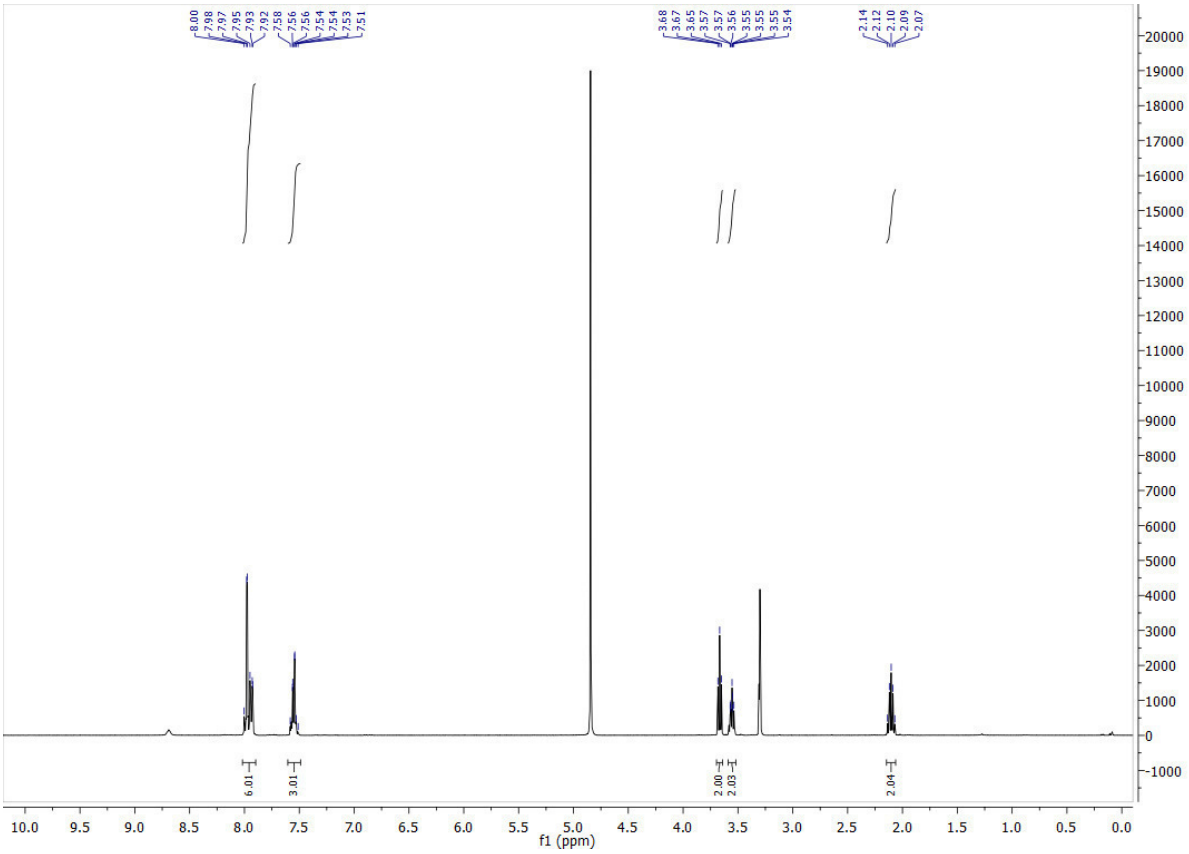

^{31}P NMR (162 MHz, Methanol-d_4)

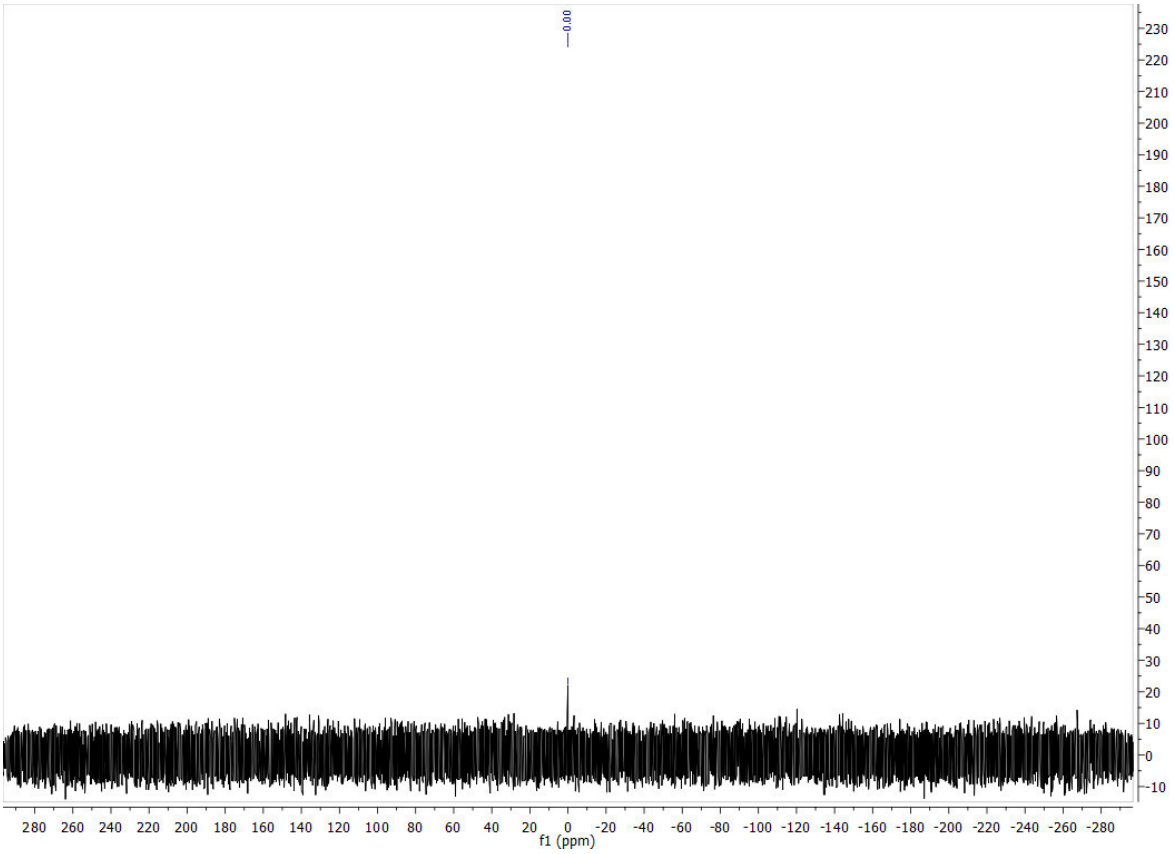

4d: ^{1}H NMR (400 MHz, Methanol-d_4)

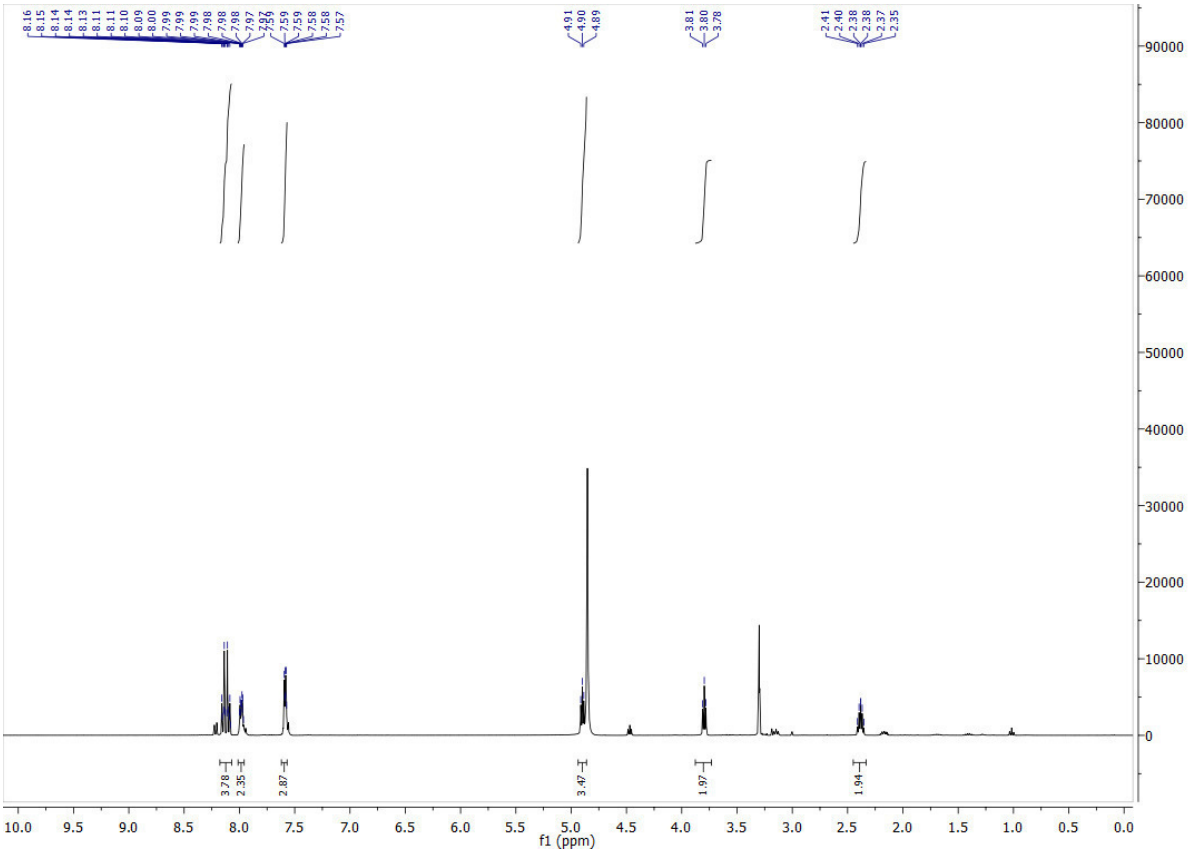

^{31}P NMR (162 MHz, Methanol-d_4)

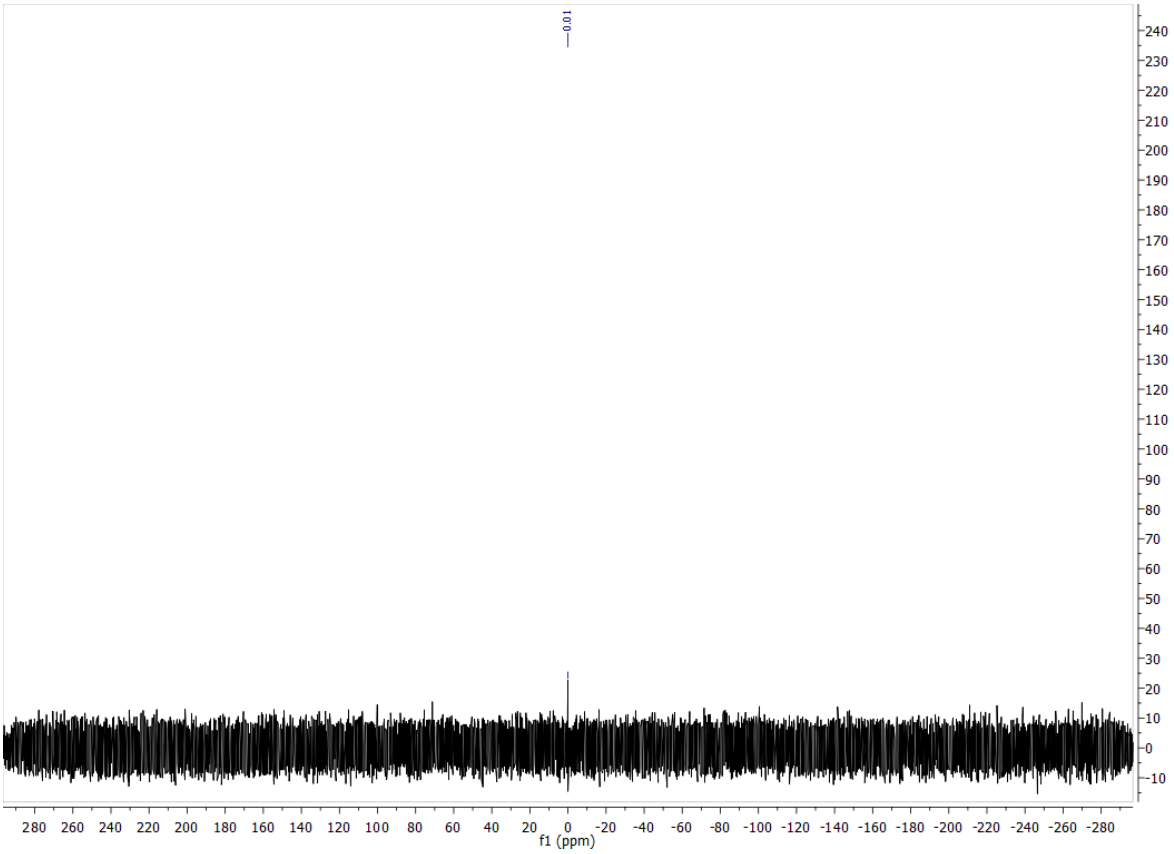

4e: ^{1}H NMR (400 MHz, Methanol-d_4)

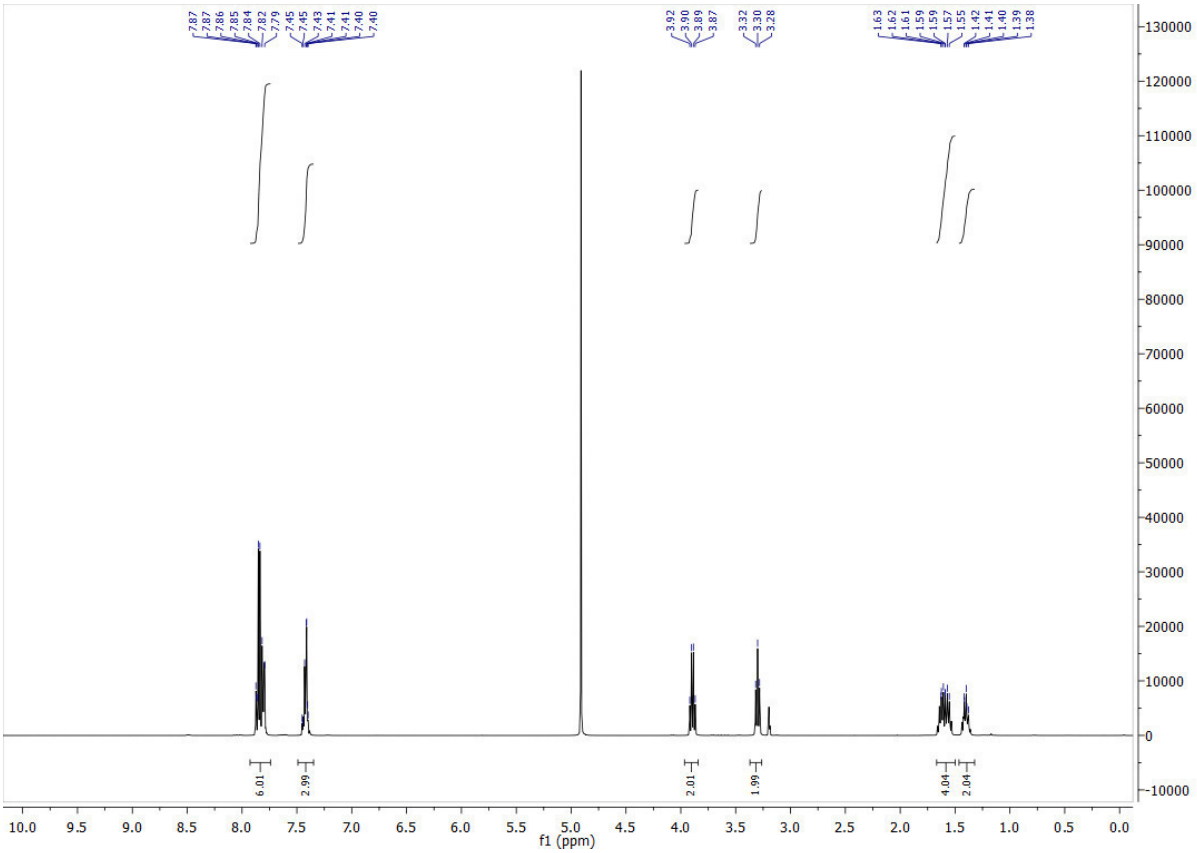

^{13}C NMR (101 MHz, Methanol-d_4)

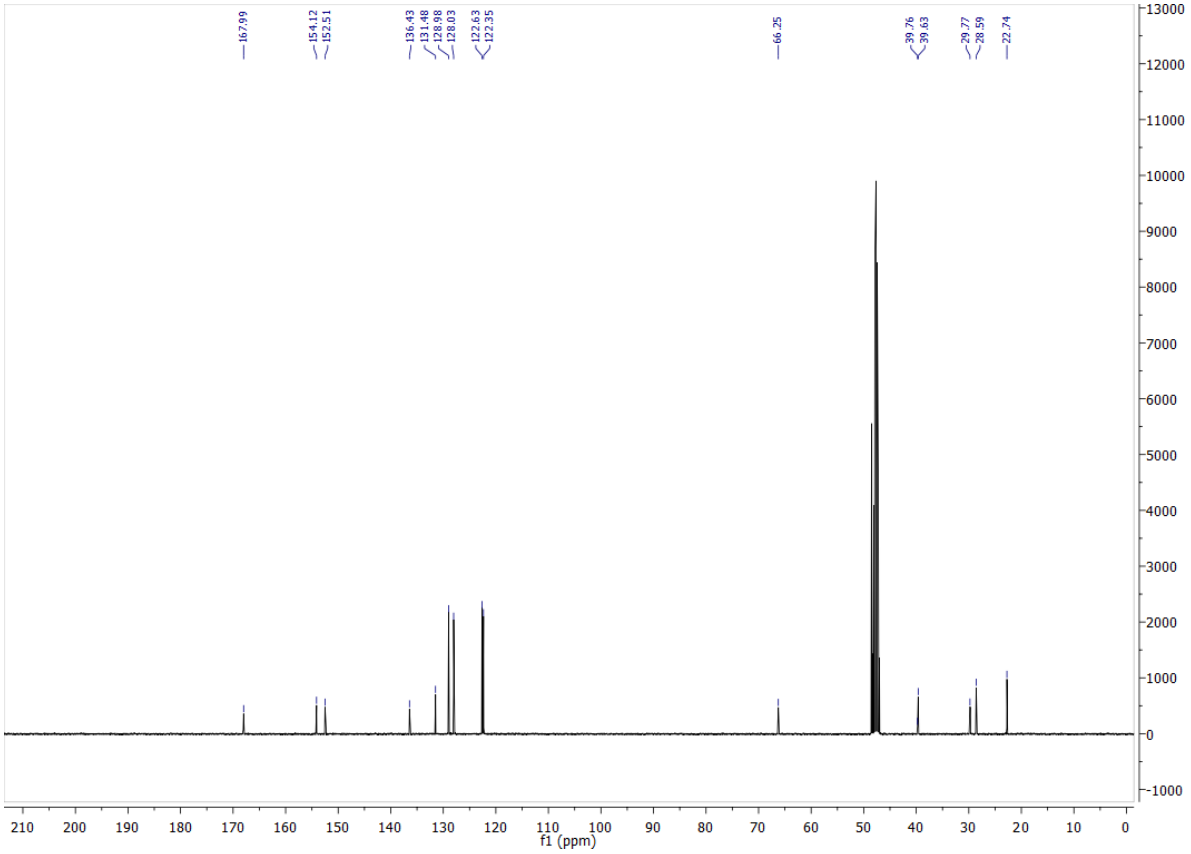

^{31}P NMR (162 MHz, Methanol-d_4)

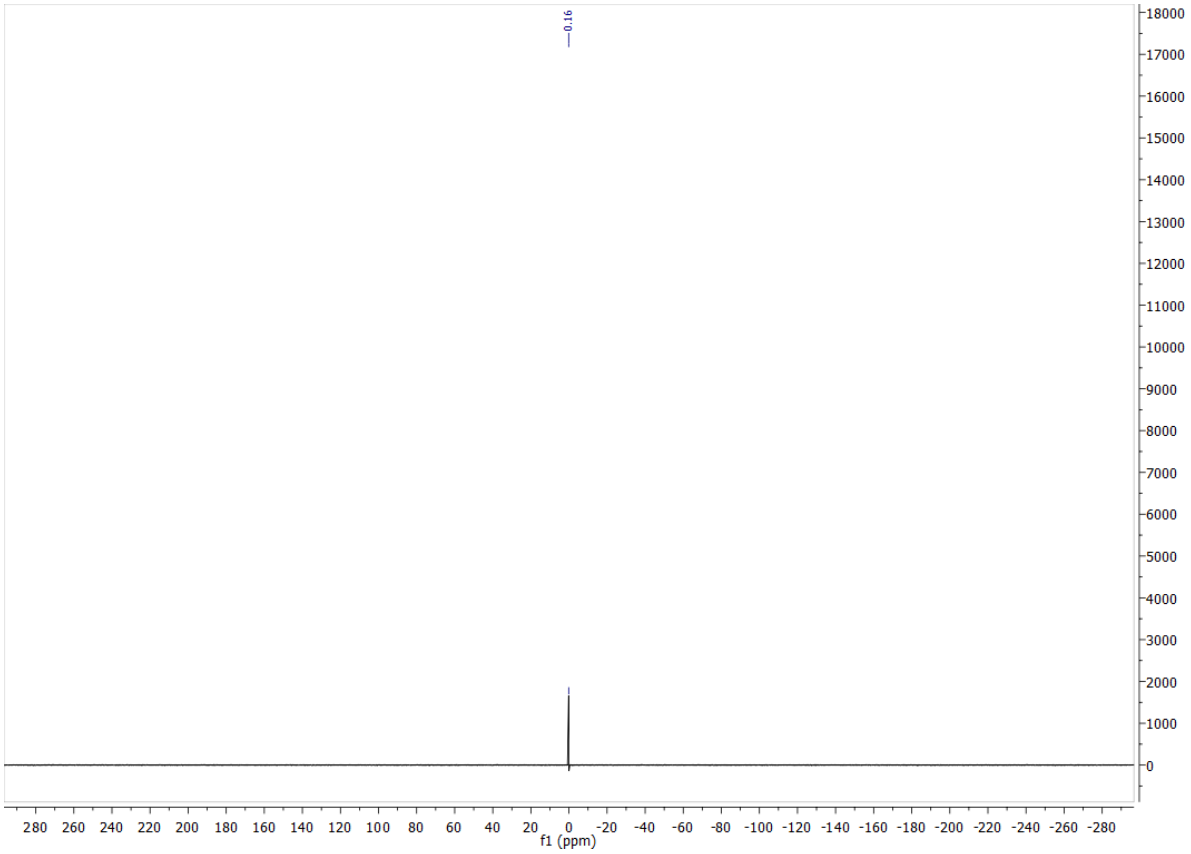

4f: ^{1}H NMR (400 MHz, Methanol-d_4)

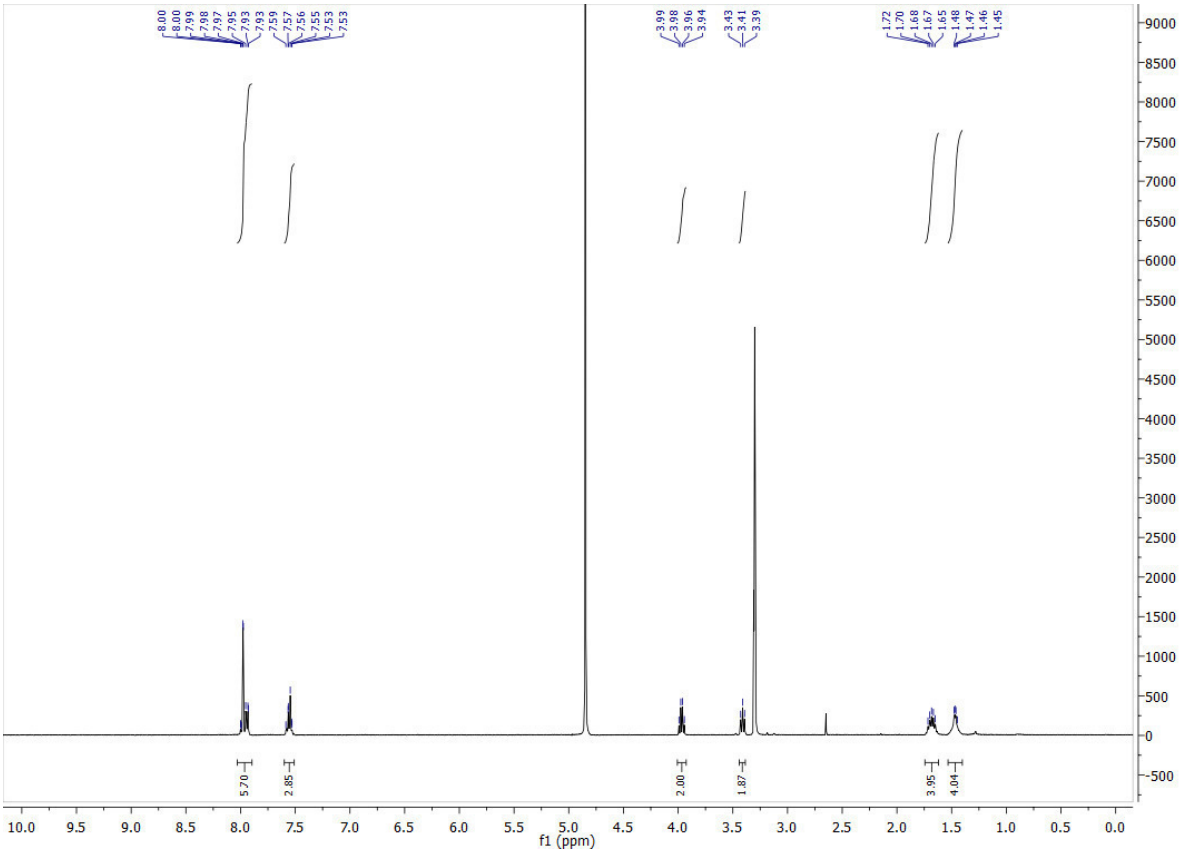

^{31}P NMR (162 MHz, Methanol-d_4)

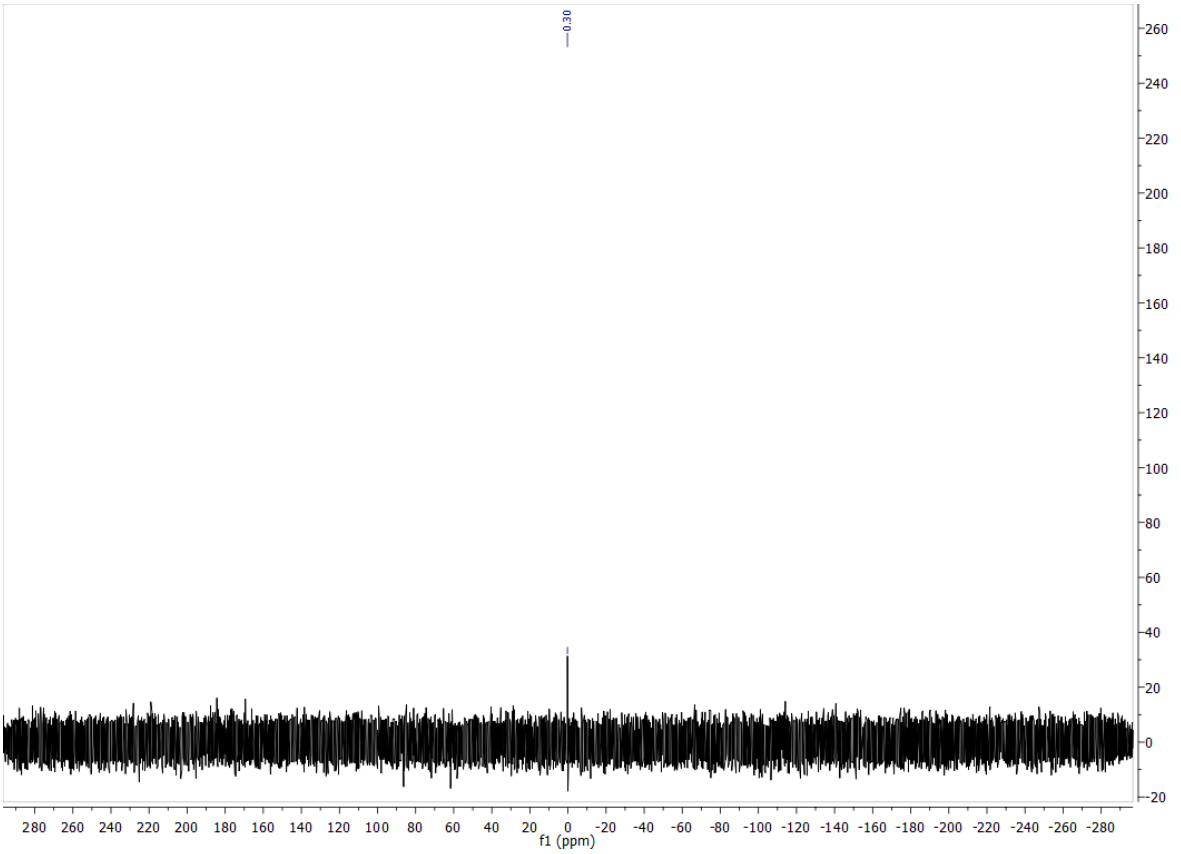

2. HPLC Trances

Method: 5-95% MeCN in H_2O/0.05% TFA in 20 min + 5min 98% MeCN in H_2O/0.05% TFA

4a

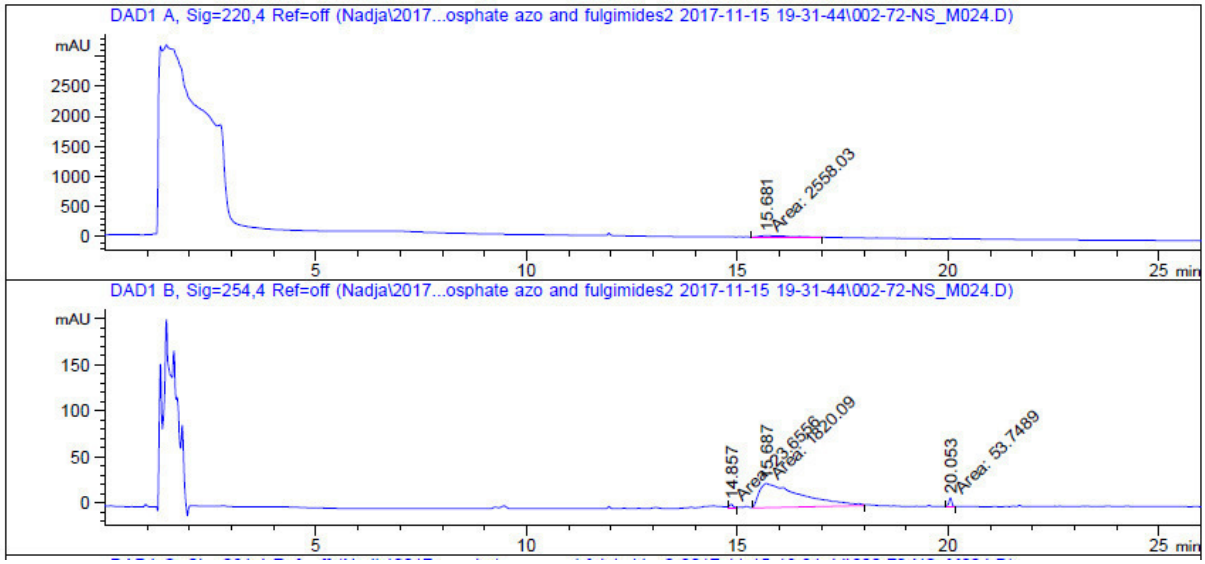

>99% purity (220nm), 96% purity (254 nm trace).

4c

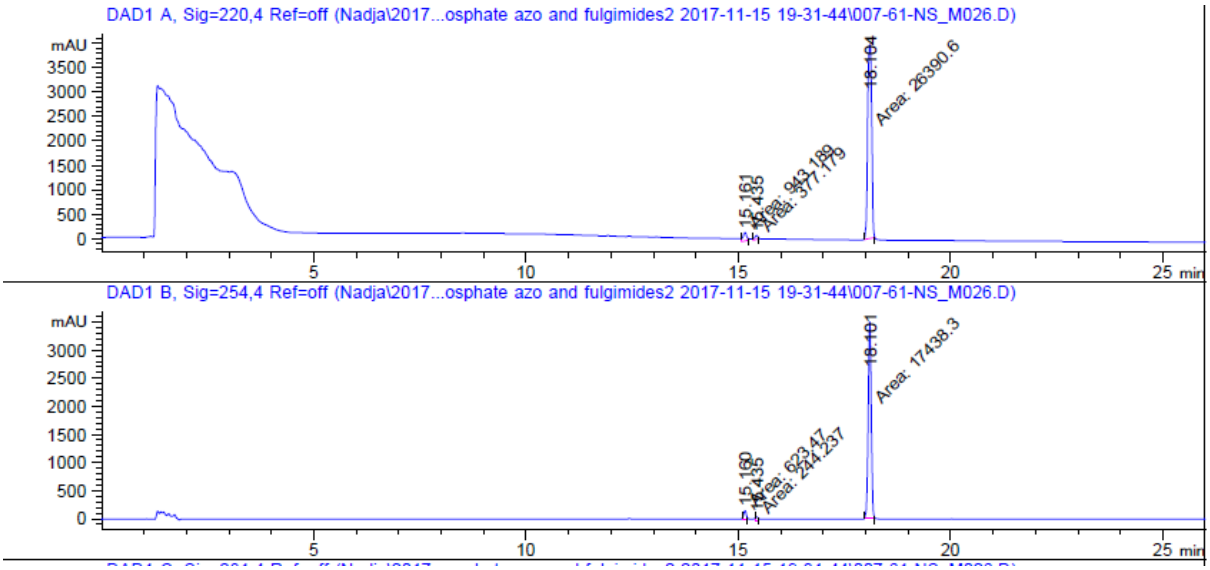

95% purity (220 nm and 254 nm).

4d

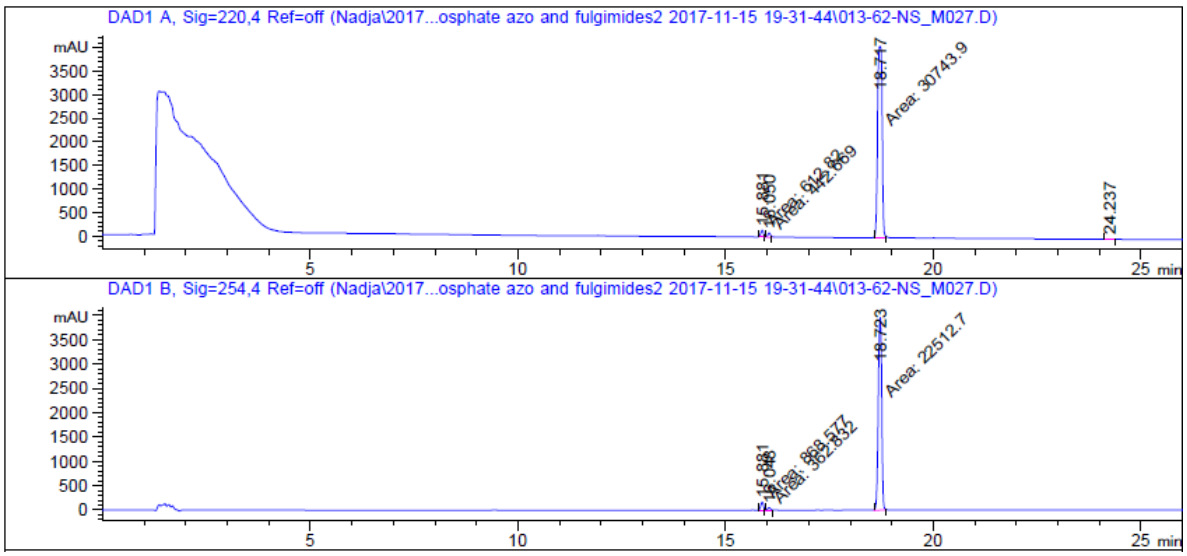

97% purity (220 nm), 95% purity (254 nm).

4e

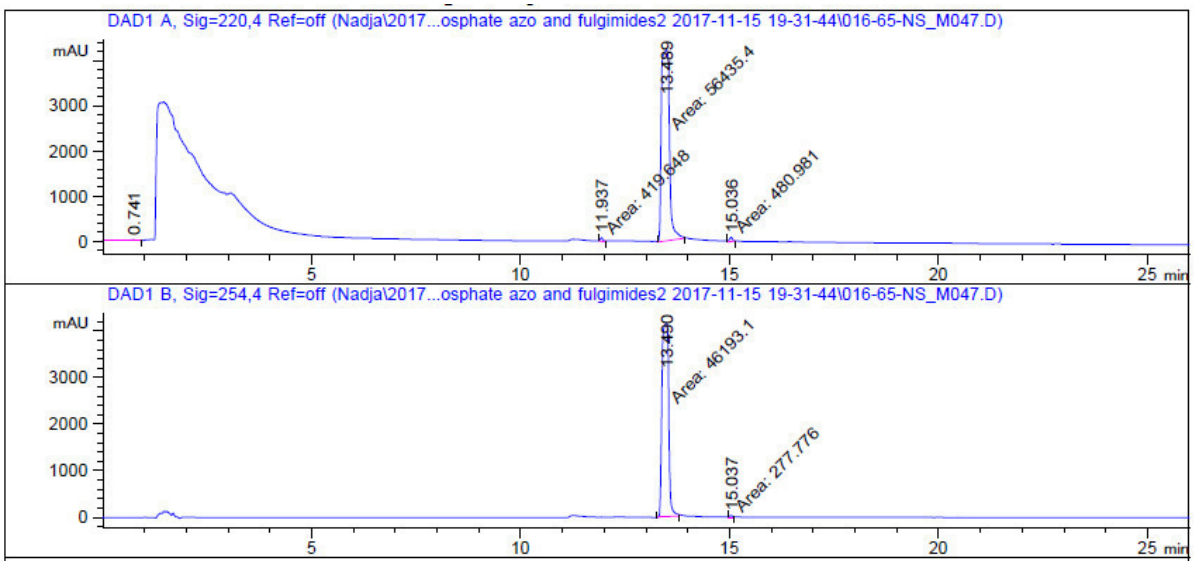

98% purity (220 nm), <99% purity (254 nm).

4f

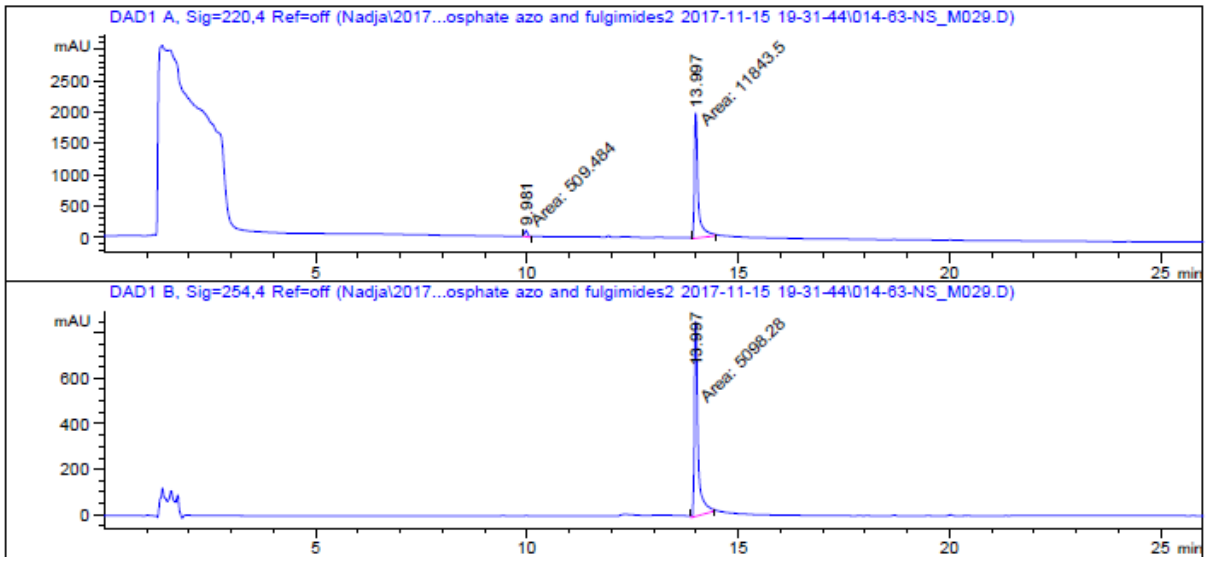

95% purity (220 nm), <99% purity (254 nm).

3. UV/Vis Spectra

Table A1: UV/Vis properties of compounds **4a-f**.

Compound	solvent mixture[a]	λ_{max} [nm]	$\varepsilon_{\lambda max}$[$M^{-1}cm^{-1}$][b]	concentration [µM]
4a	DMSO	335	15803	44
4b	10% DMSO in buffer[c]	326	15276	41
4c	15% DMSO in buffer[c]	326	15301	19
4d	5% DMSO in buffer[c]	326	15298	41
4e	buffer[c]	324	15336	68
4f	5% DMSO in buffer[c]	326	15324	22

[a]A DMSO stock solution (10 mM) was diluted into buffer to avoid precipitation. [b]molar decadic extinction coefficient at the individual absorption maximum of the compound in the used solvent. [c]used buffer: Dulbecco's Phosphate buffered Saline.

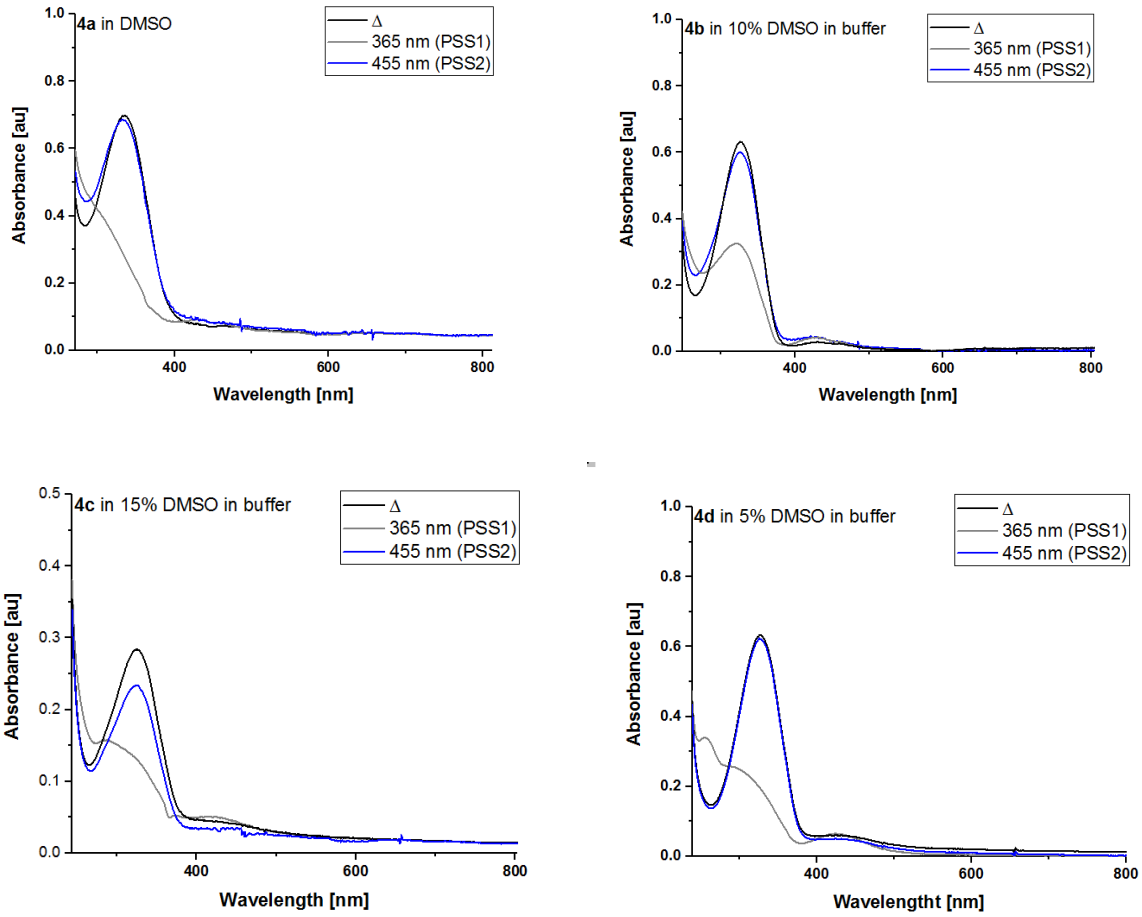

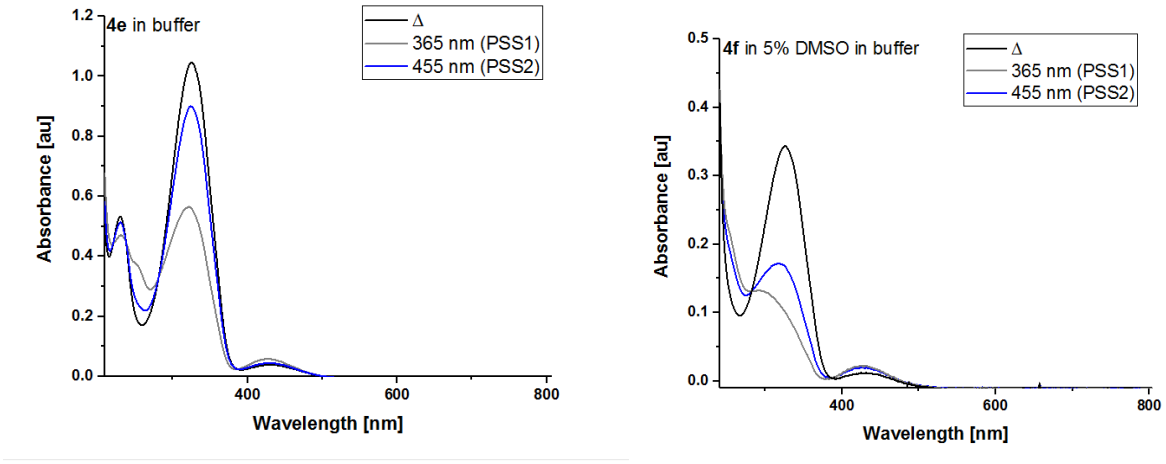

Figure A1: UV/Vis spectra of compounds **4a**-**f**. The individual solvents are specified in the spectrum. Black lines depict the absorption spectrum at the thermal equilibrium, grey lines at the PSS1 (irradiation with 365 nm LED), blue lines at the PSS2 (irradiation of PSS1 with a 455 nm LED).

Thermal *Z*-to-*E* Isomerization (exemplary of **4e** in buffer, 65µM)

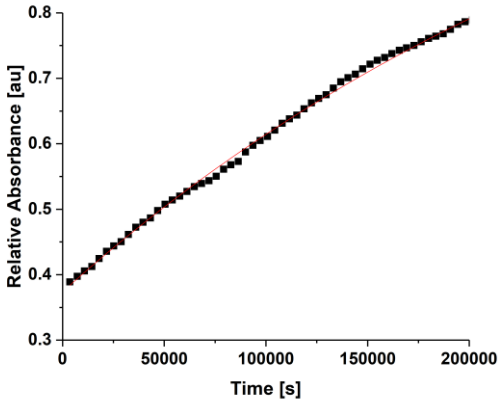

Equation	y = A1*exp(-x/t1) + y0
y0	1.28111 ± 0.04683
A1	-0.90721 ± 0.04506
t1	324851.55908 ± 23167.52726
R-Square(COD)	0.99791
Adj. R-Square	0.99784

A.IV.1. Photochromic Indolyl Fulgimides as Chromo-Pharmacophores Towards Sirtuins

Table of Contents

1. NMR Spectra

1a: ^{1}H-NMR (300 MHz, Methanol-d_4)

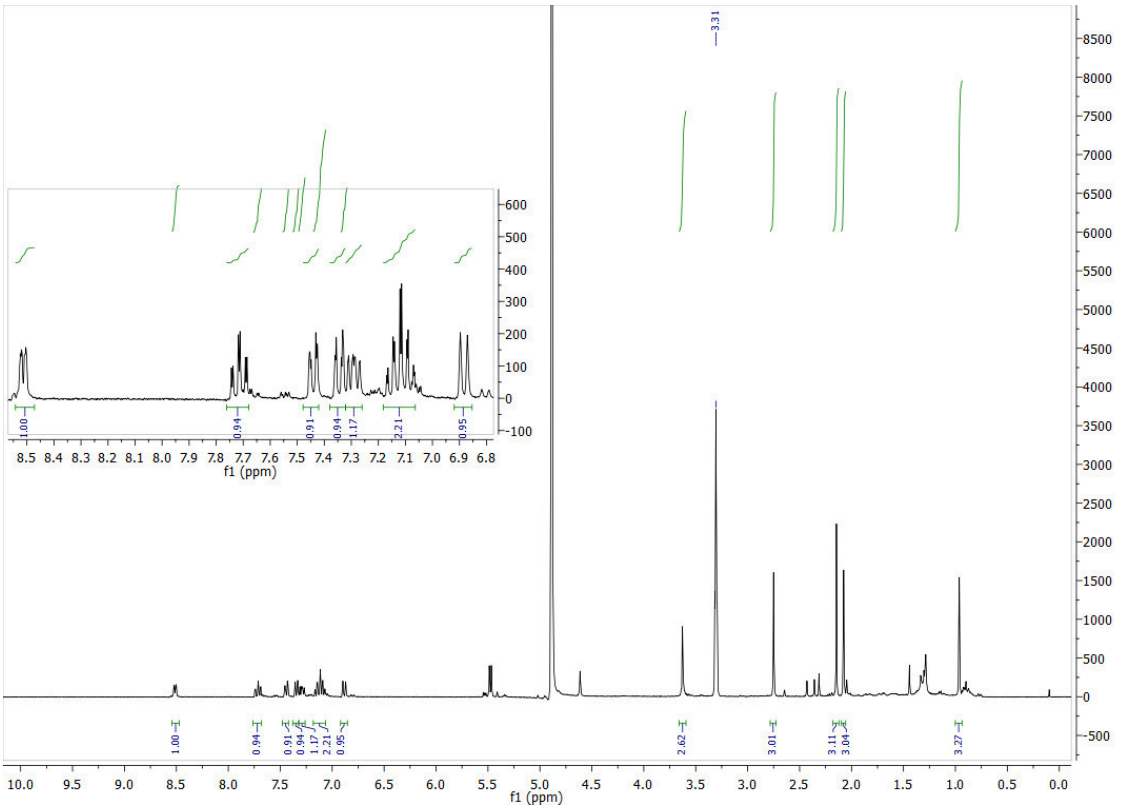

^{13}C-NMR (151 MHz, Methanol-d_4)

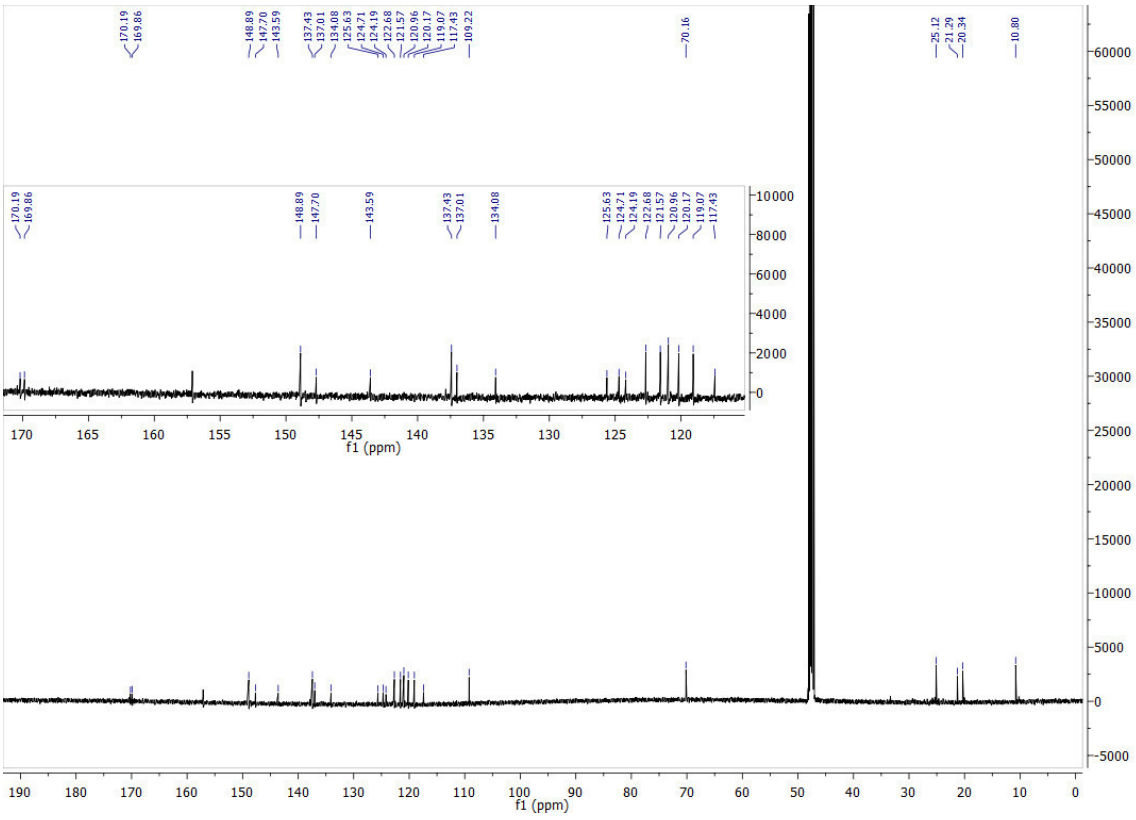

1b: ^{1}H-NMR (300 MHz, Methanol-d_4)

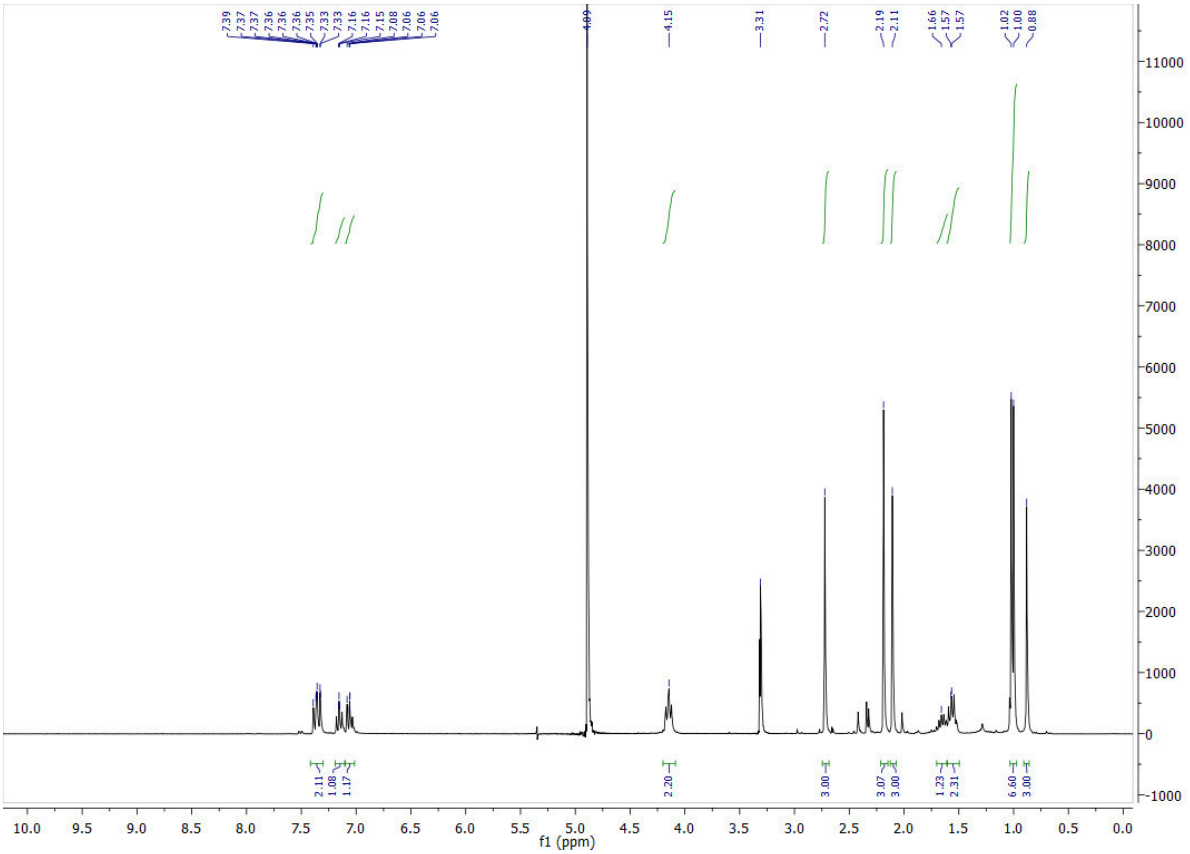

^{13}C-NMR (75 MHz, Methanol-d_4)

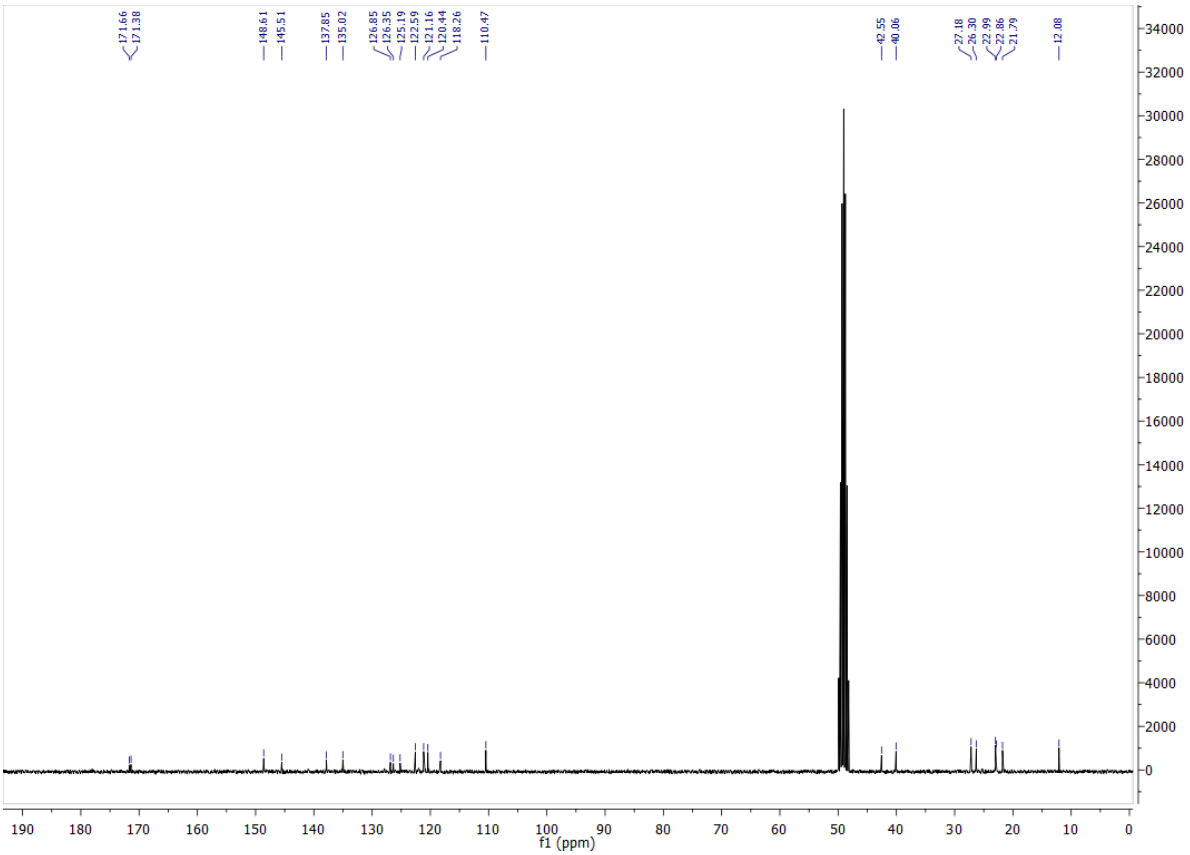

1c: ^{1}H-NMR (400 MHz, Acetonitrile-d_3)

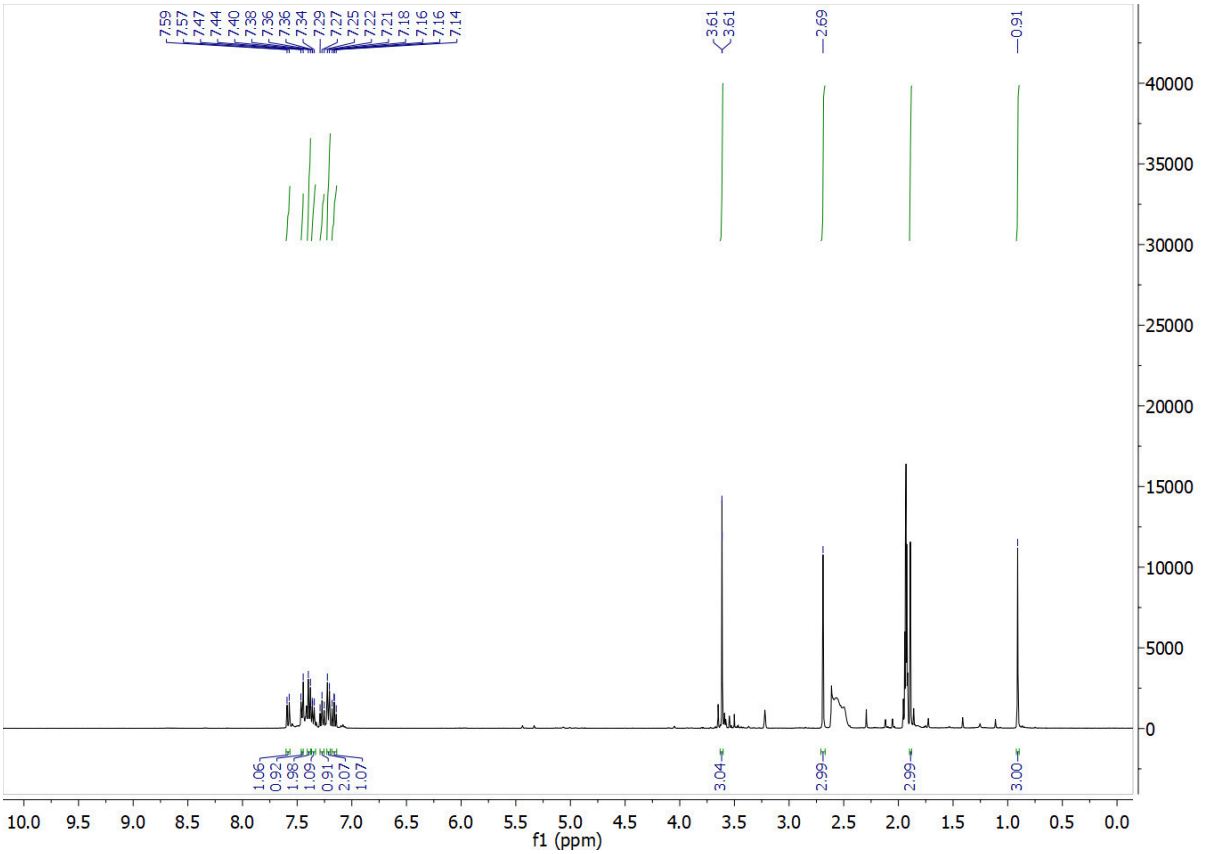

^{13}C-NMR (151 MHz, Acetonitrile-d_3)

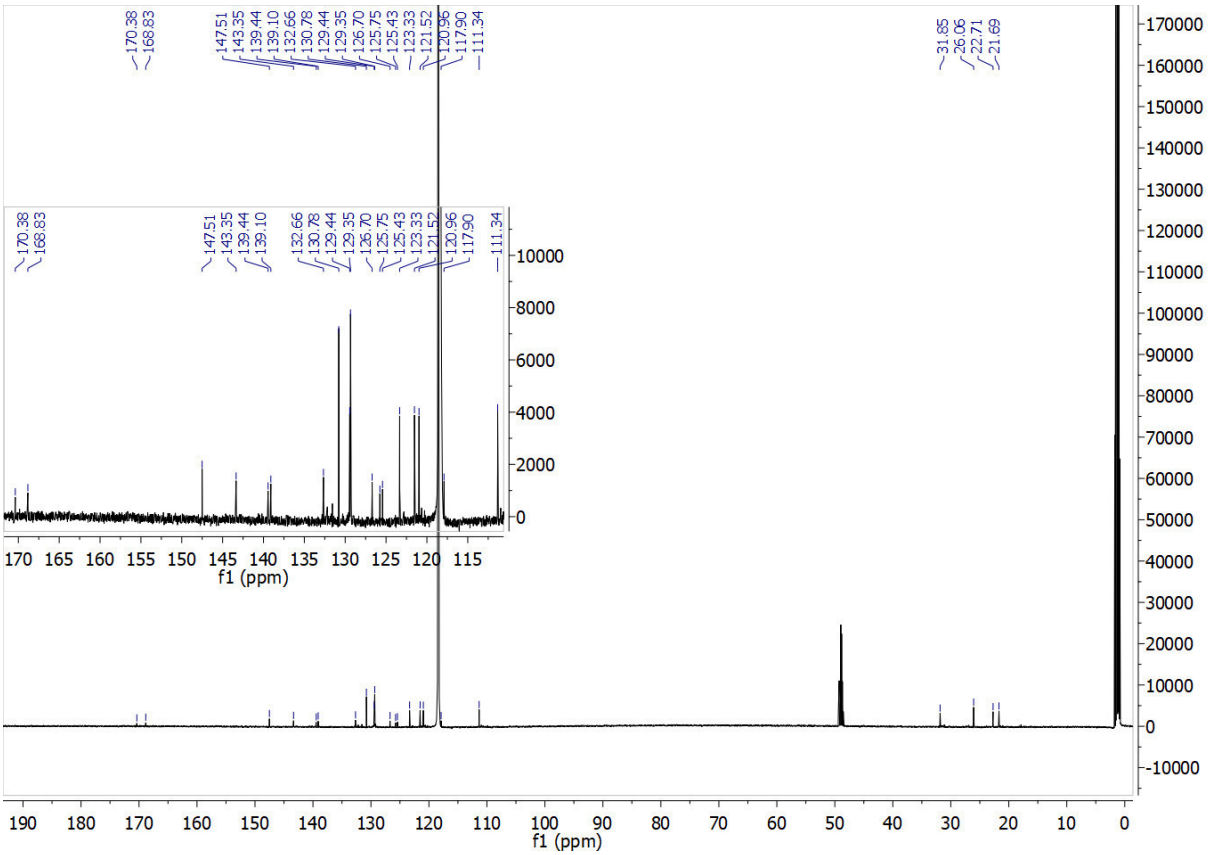

5: ^{1}H-NMR (400 MHz, Acetone-d_6)

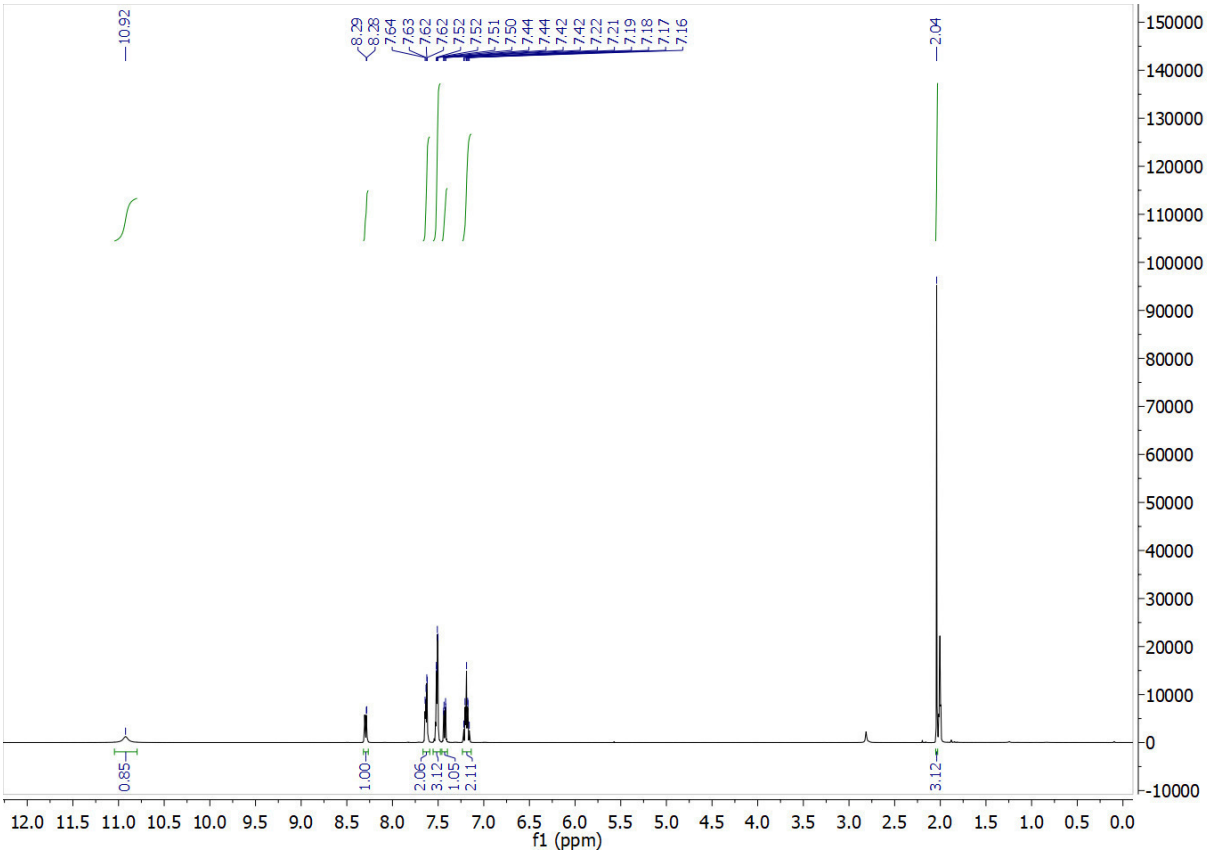

^{13}C-NMR (101 MHz, Acetone-d_6)

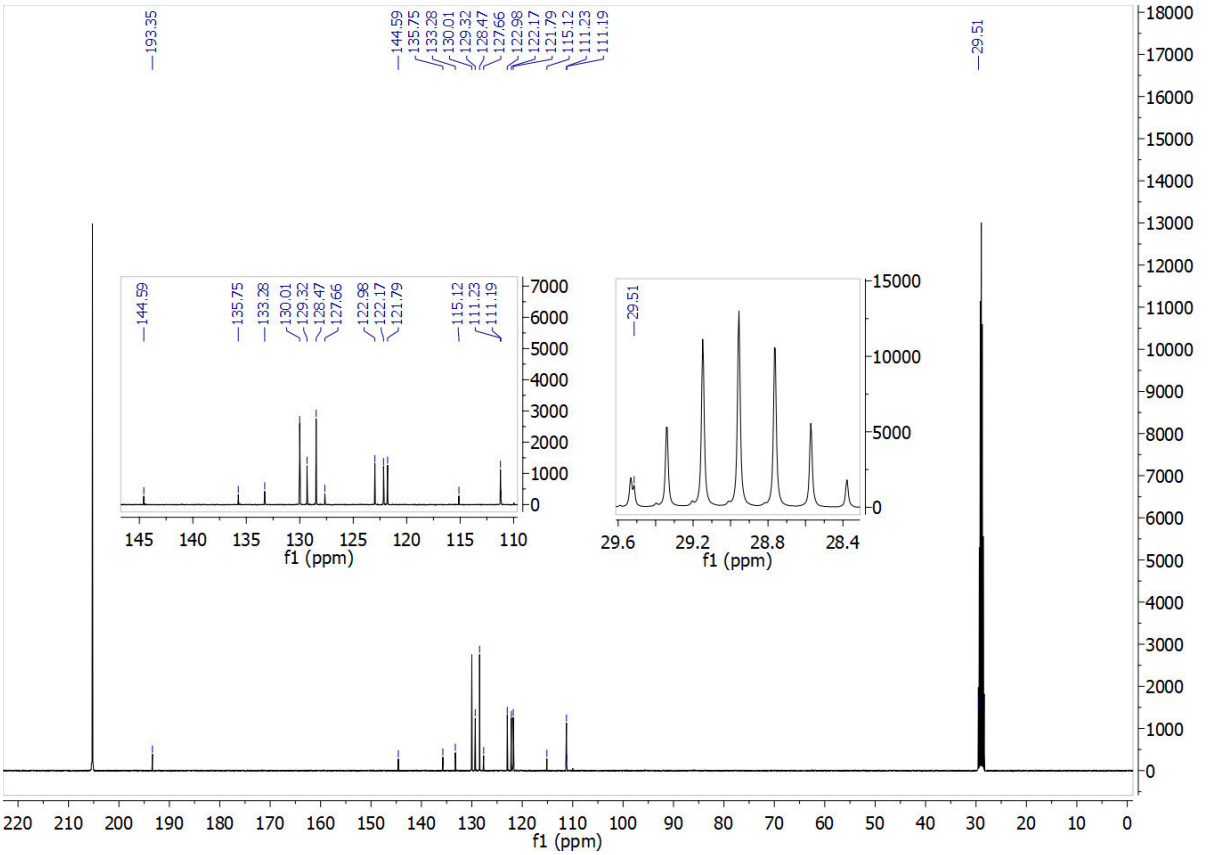

6a: ^{1}H-NMR (400 MHz, Chloroform-*d*)

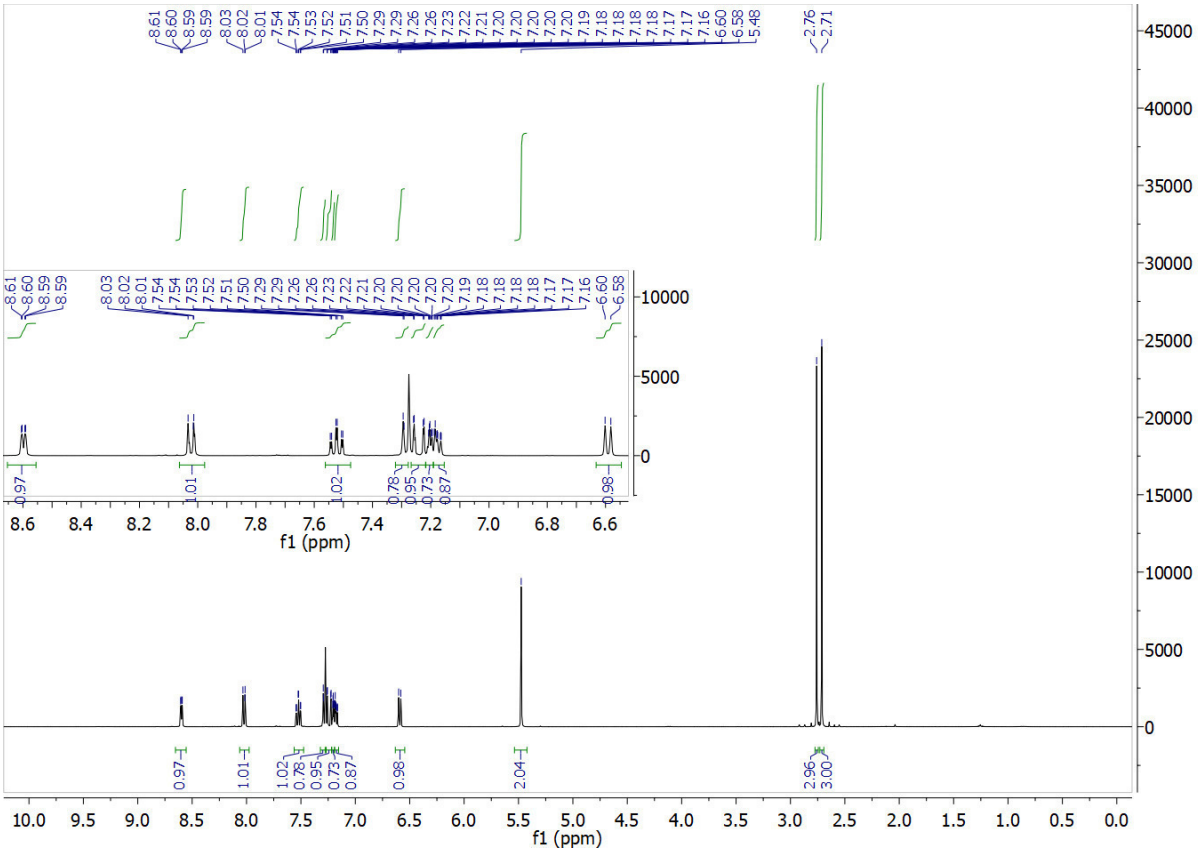

^{13}C-NMR (101 MHz, Chloroform-*d*)

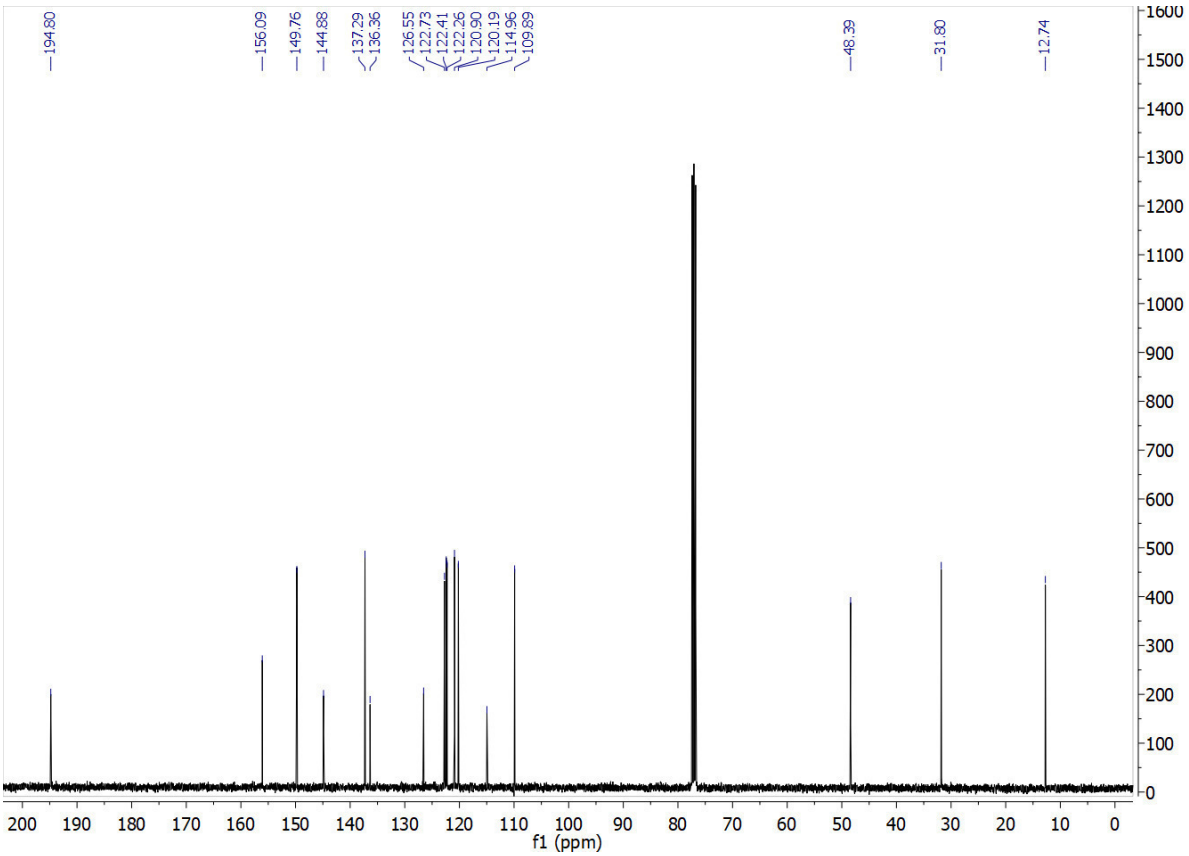

6b: ^{1}H-NMR (400 MHz, Chloroform-*d*)

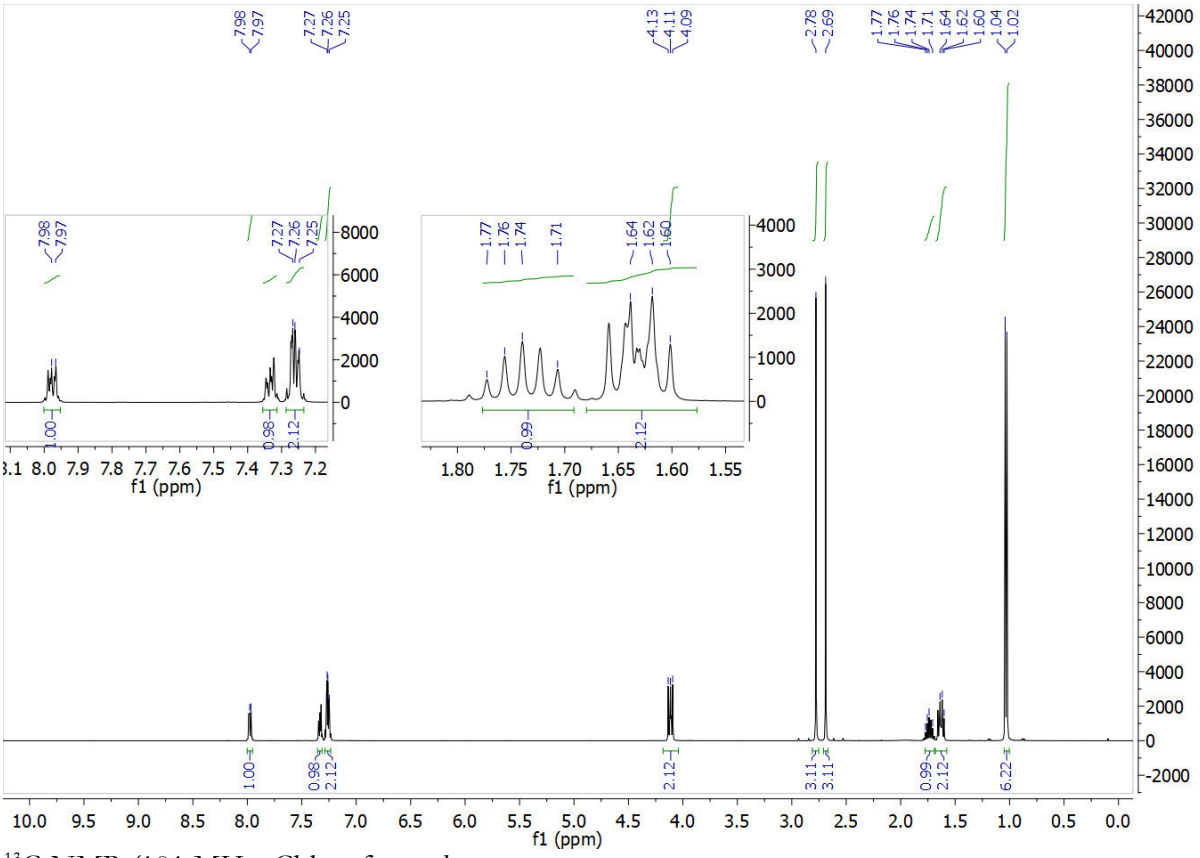

^{13}C-NMR (101 MHz, Chloroform-*d*)

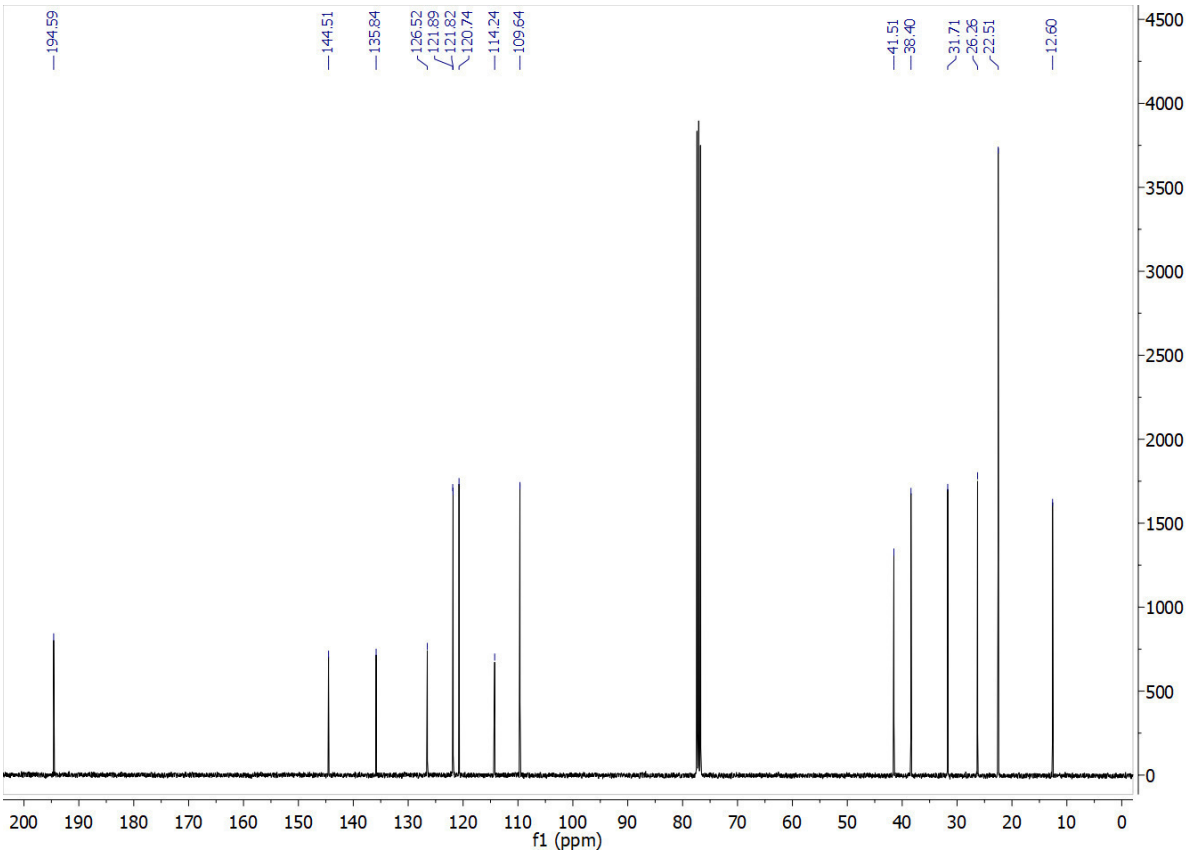

6c: ^{1}H-NMR (400 MHz, Acetone-d_6)

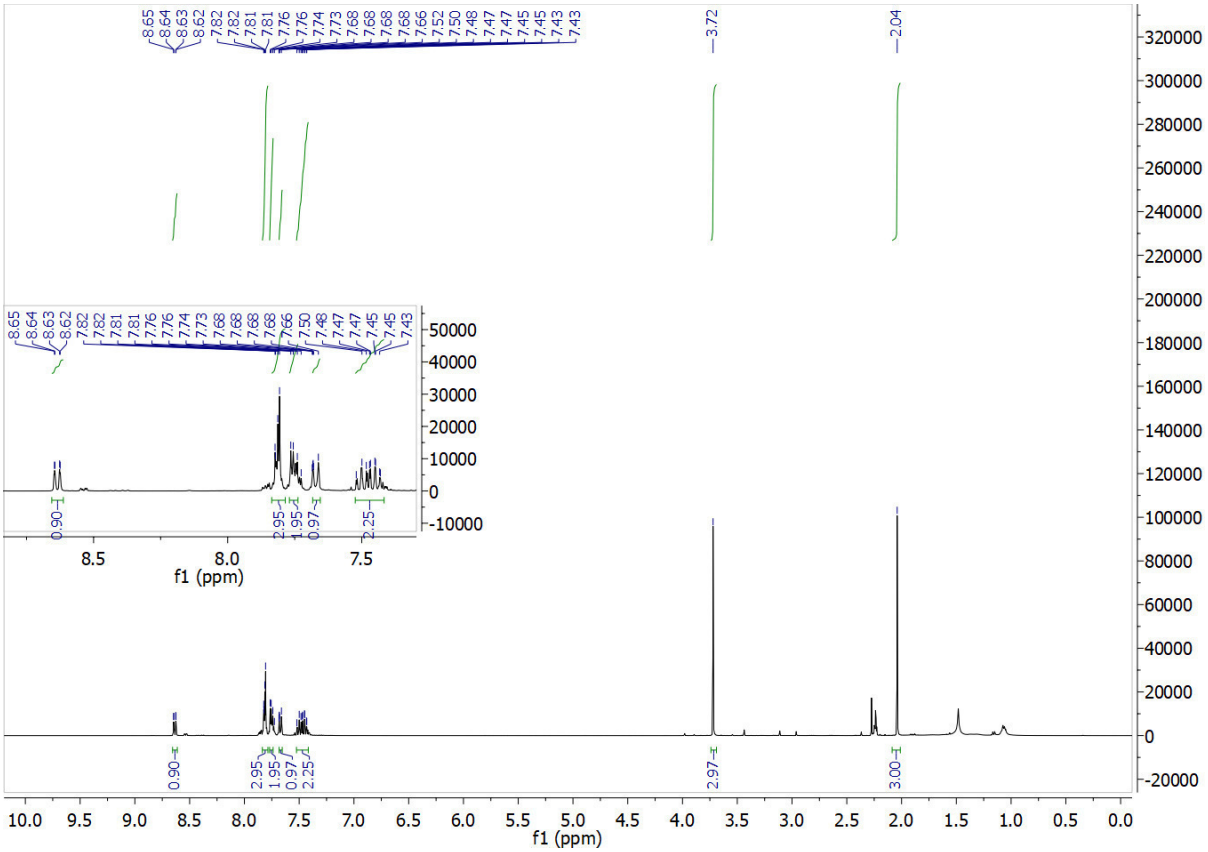

^{13}C-NMR (101 MHz, Acetone-d_6)

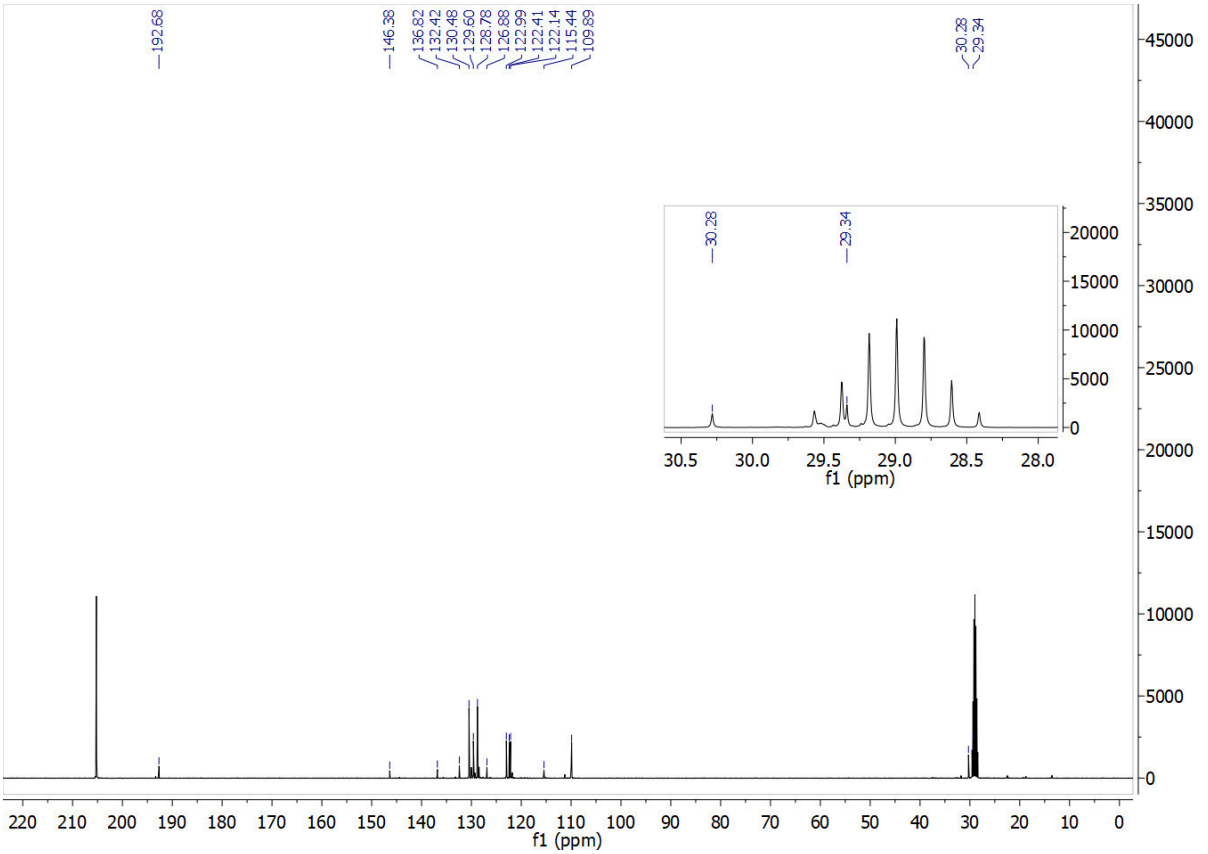

6d: ^{1}H-NMR (300 MHz, Chloroform-*d*)

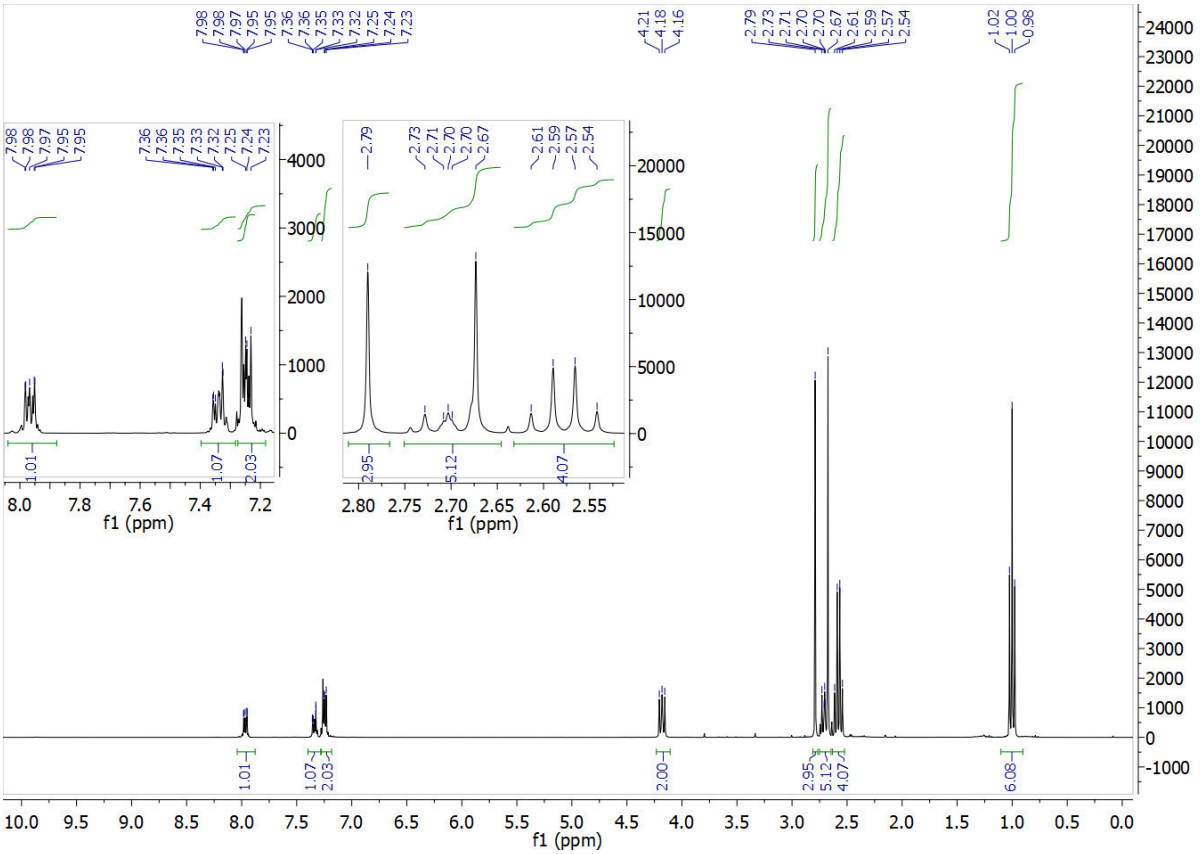

^{13}C-NMR (75 MHz, Chloroform-*d*)

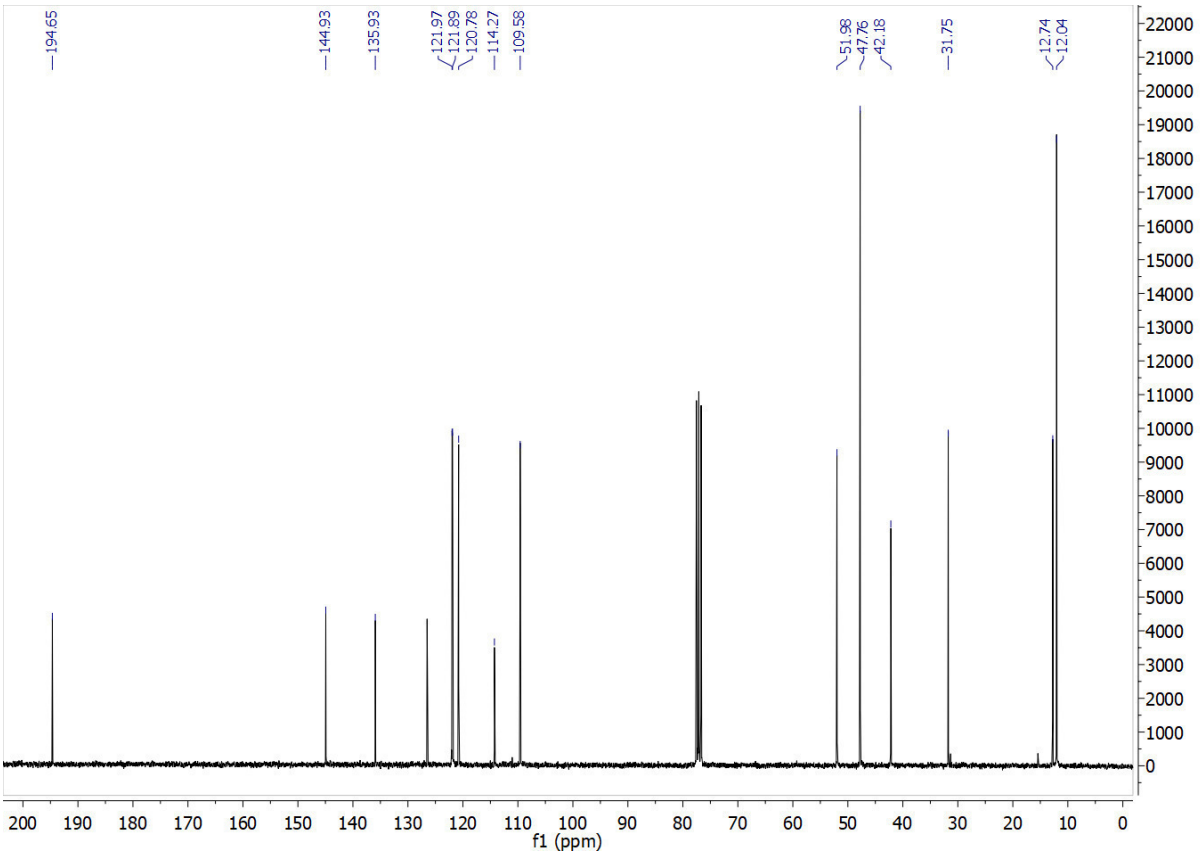

6e: ^{1}H-NMR (400 MHz, Chloroform-*d*)

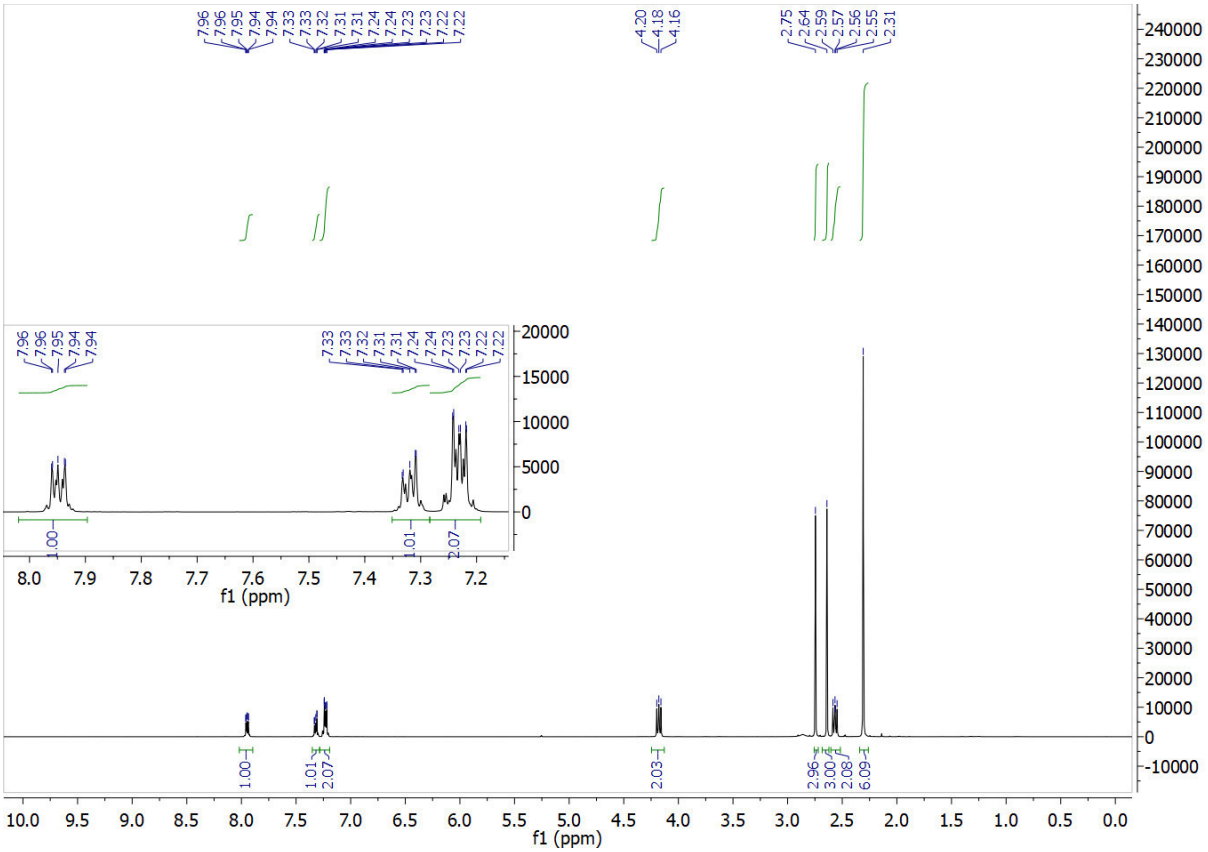

^{13}C-NMR (101 MHz, Chloroform-*d*)

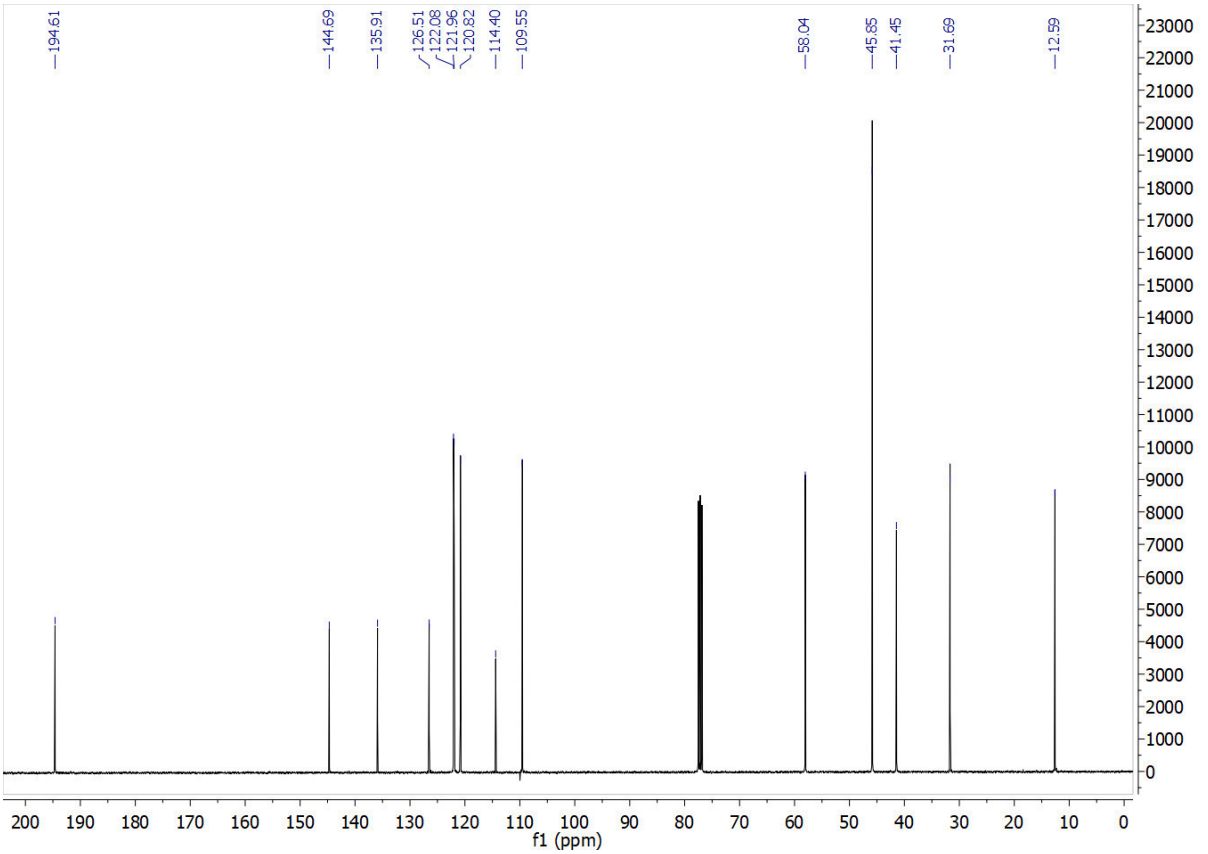

6f: ^{1}H-NMR (400 MHz, Chloroform-*d*)

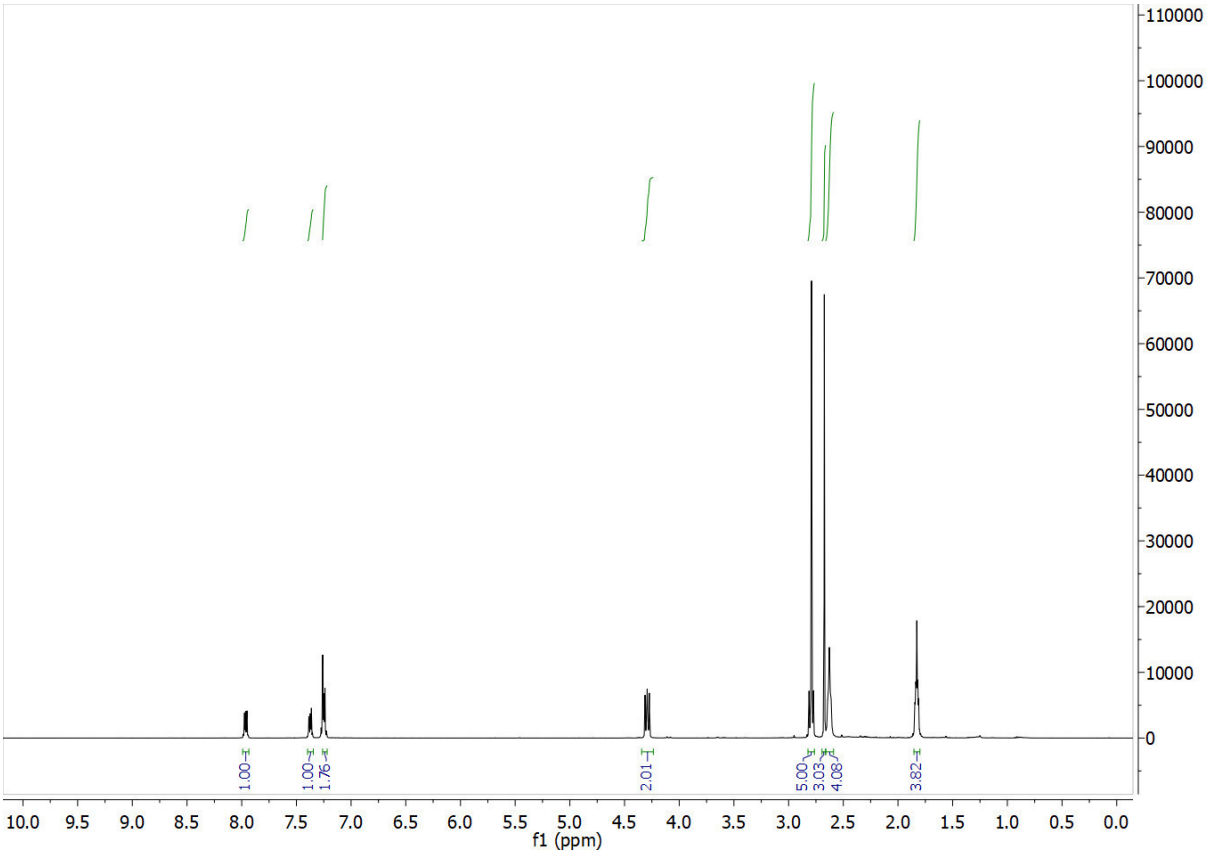

^{13}C-NMR (101 MHz, Chloroform-*d*)

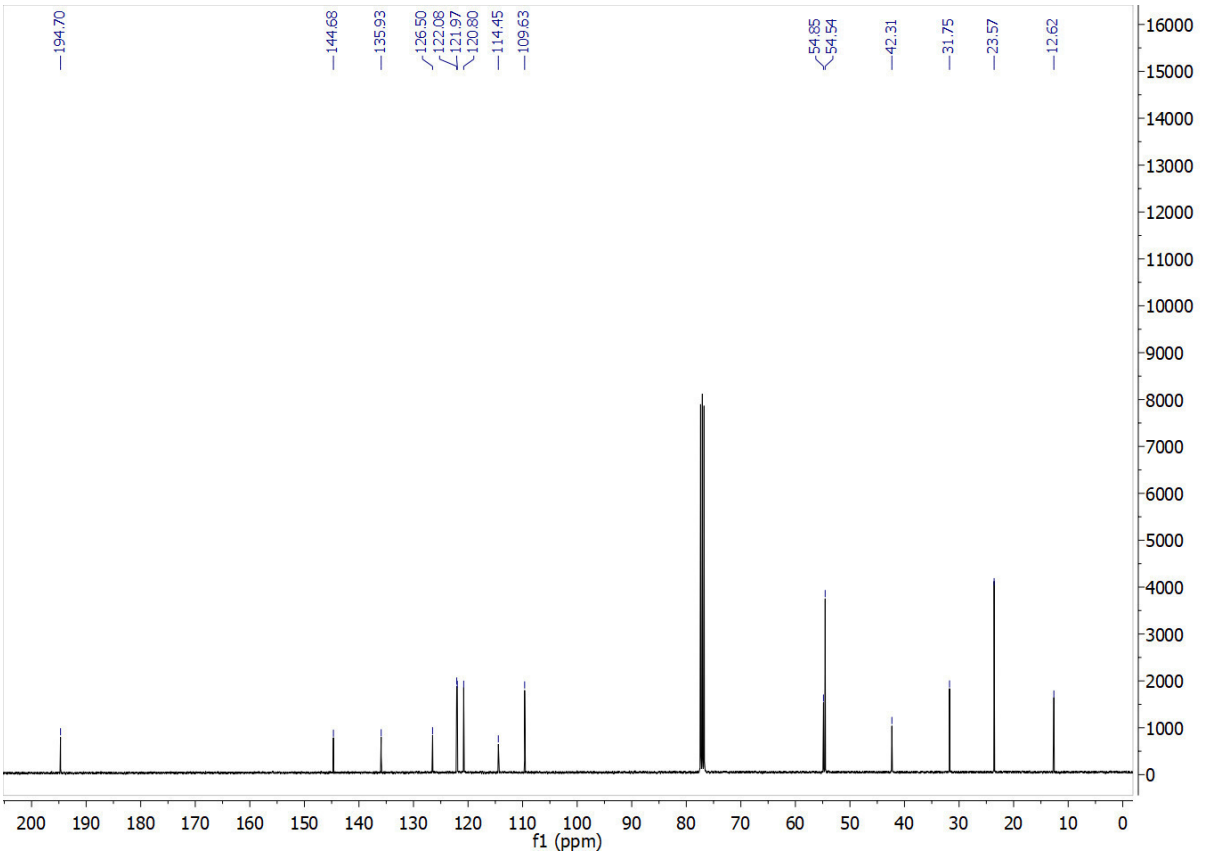

7a: ^{1}H-NMR (400 MHz, Chloroform-*d*)

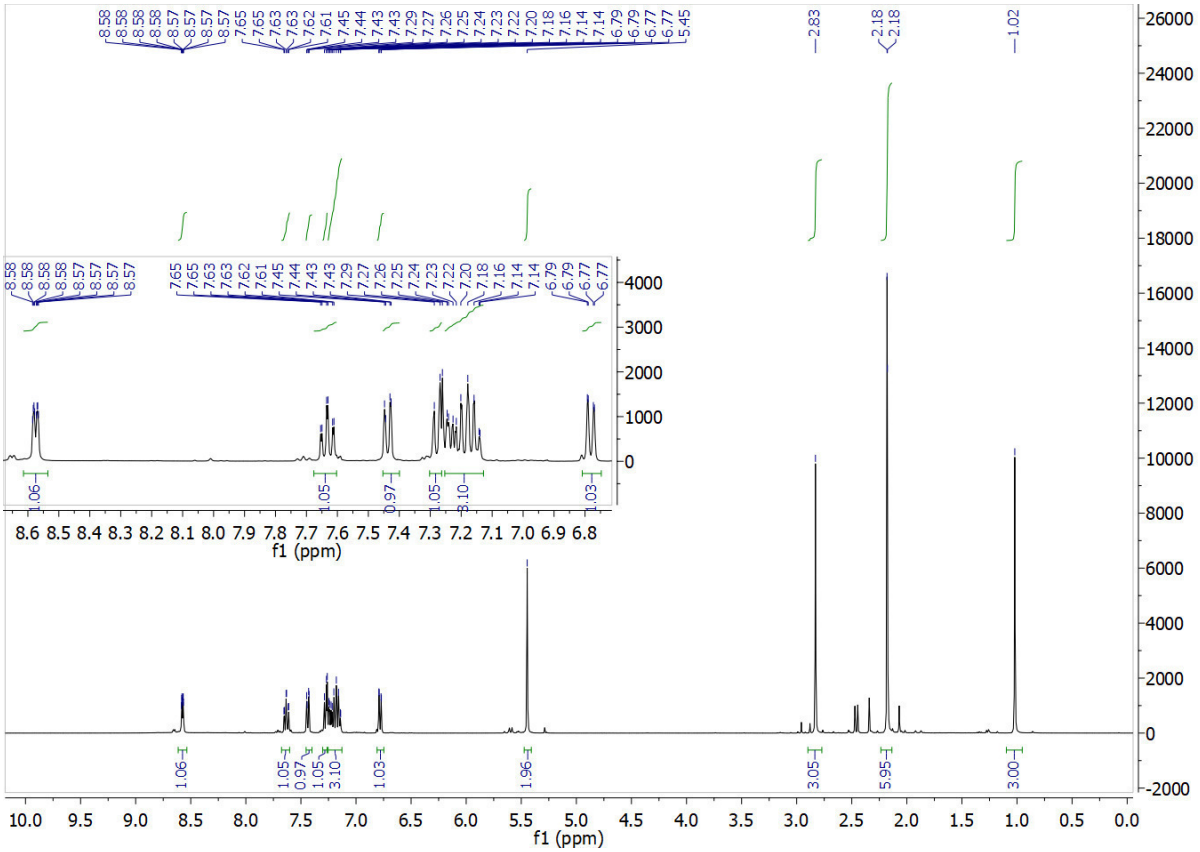

^{13}C-NMR (101 MHz, Chloroform-*d*)

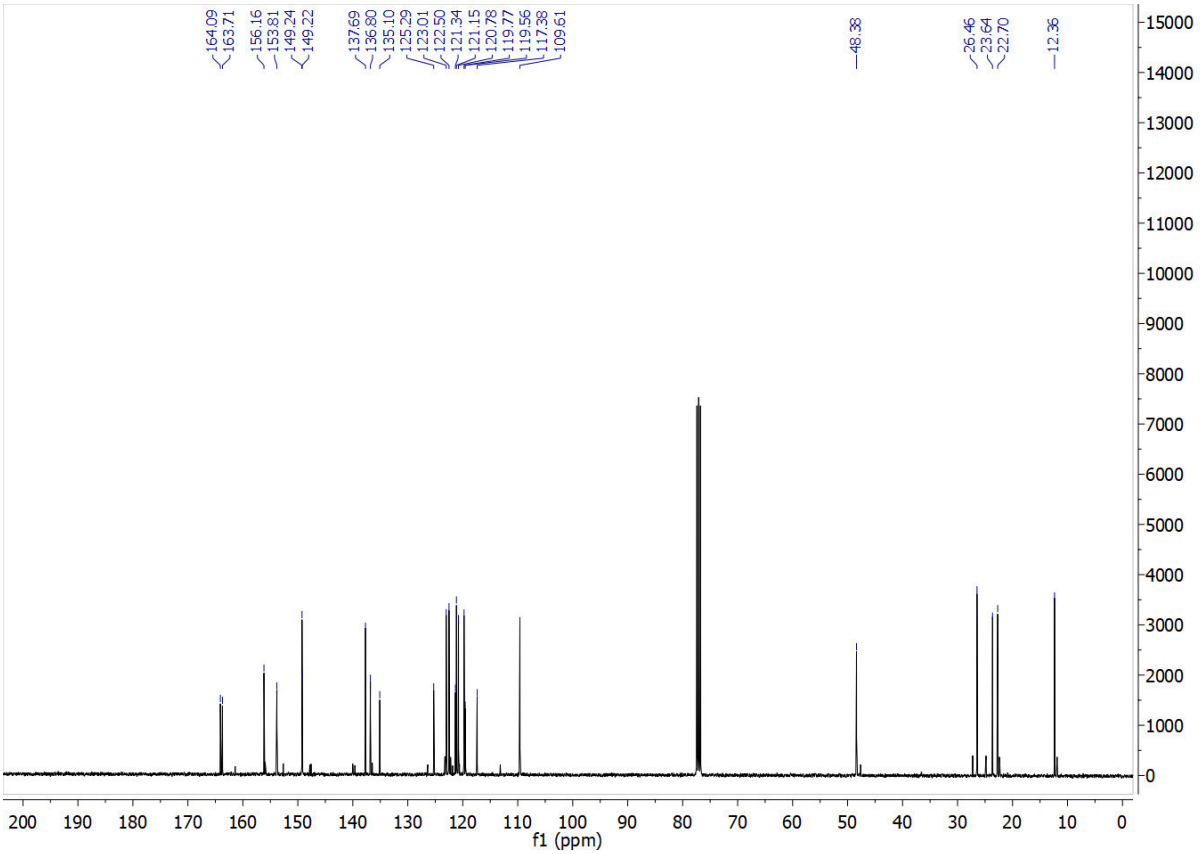

7b: ^{1}H-NMR (400 MHz, Chloroform-*d*)

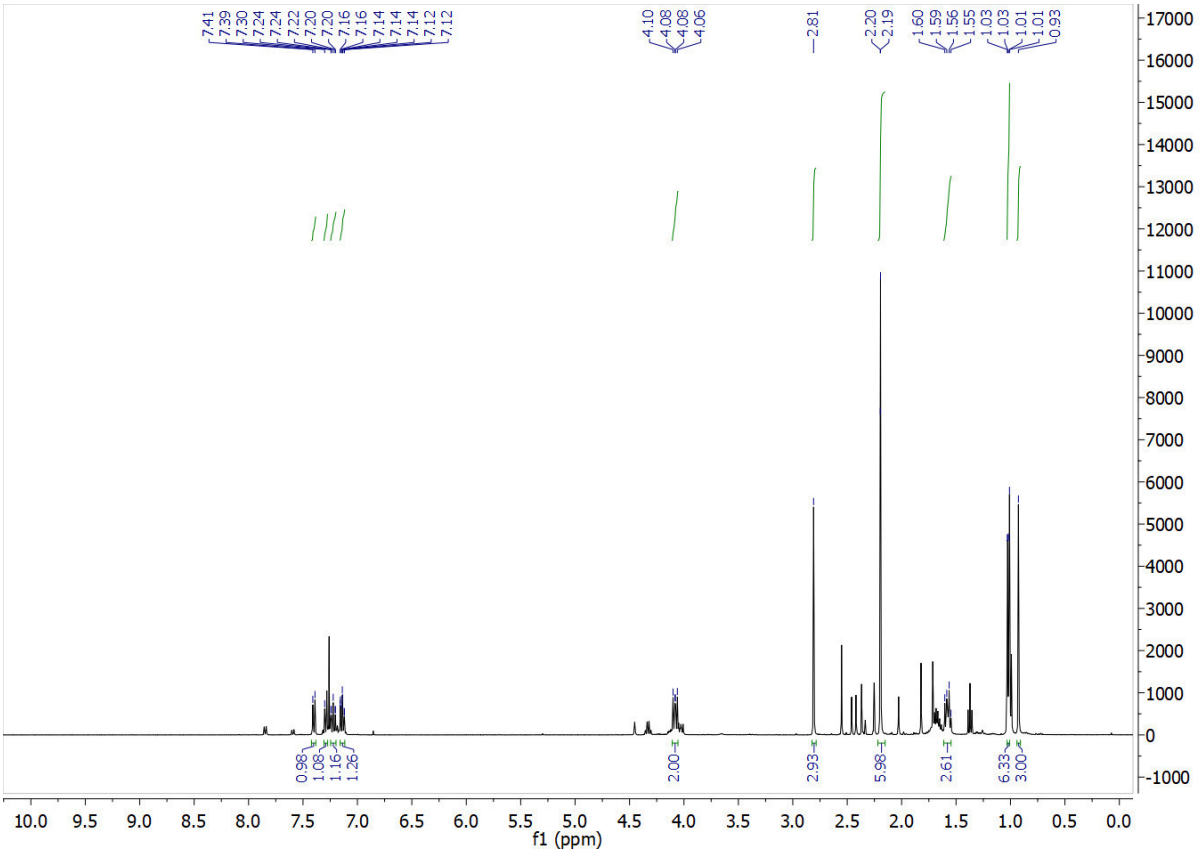

2. HPLC Traces for Purity, PSS Composition and Thermal Stability

HPLC traces at 220 nm and 254 nm allowed us to determine the purity and isomer composition at the thermal equilibrium.

To determine PSS composition *via* analytical HPLC, the compounds were eluted using an isocratic gradient over 15 min separating the peaks of the *E*-, *Z*- and closed isomer. Hence, 100 μM solutions of the photoswitch in the appropriate solvent (solvents are indicated for each measurement) were prepared. 20 μL samples were injected to the HPLC before and after irradiation, which was performed in a cuvette and followed *via* UV-Vis spectroscopy. Then, we integrated the peak area at the isosbestic points of the photoisomers in the respective solvent mixture (*vide infra*, Section 3), *i.e.* 40% MeCN in H_2O for compound **1a** and 70% MeCN in H_2O for compounds **1b** and **1c**.

Thermal stability of the compounds regarding the assay conditions was analyzed spectroscopically (vide infra) and via analytical HPLC comparing the composition and purity of the solutions at the thermal equilibrium and the PSS after incubation at 37 °C for 4 h

Table A1 gives an overview over the obtained data.

Table A1: Overview of PSS composition, purity and thermal stability of compounds **1a**, **1b**, **1c**.

		1a[a]			**1b**[b]			**1c**[c]		
		E	*Z*	C	*E*	*Z*	C	*E*	*Z*	C
ACN-water	Δ	73	27	0	94	6	0	98	2	0
	PSS	27	26	47	17	8	75	44	24	32
	PSS2	68	17	15	91	9	0	67	25	8
	Purity	*E*+*Z*-isomer > 99%			*E*+*Z*-isomer > 99%			*E*+*Z*-isomer > 99%		
DMSO	Δ	n.d.	n.d.	n.d.	96	4	0	100	0	0
	PSS	n.d.	n.d.	n.d.	23	10	66	45	24	31
DMSO-buffer (1:2)	Δ	n.d.	n.d.	n.d.	85	15	0	96	4	0
	PSS	n.d.	n.d.	n.d.	23	4	73	53	18	29
buffer	Δ	n.d.	n.d.	n.d.	92	8	0	100	0	0
	PSS	62	19	19	n.d.	n.d.	n.d.	65	3	32
	Δ 40 °C	76	24	0	decomposition			100	0	0
	PSS 40°C	57	8	36	decomposition			67	5	28

[a] λ^{obs}=400 nm. [b] λ^{obs}=270 nm. [c] λ^{obs}=271 nm.

Compound ***1a***

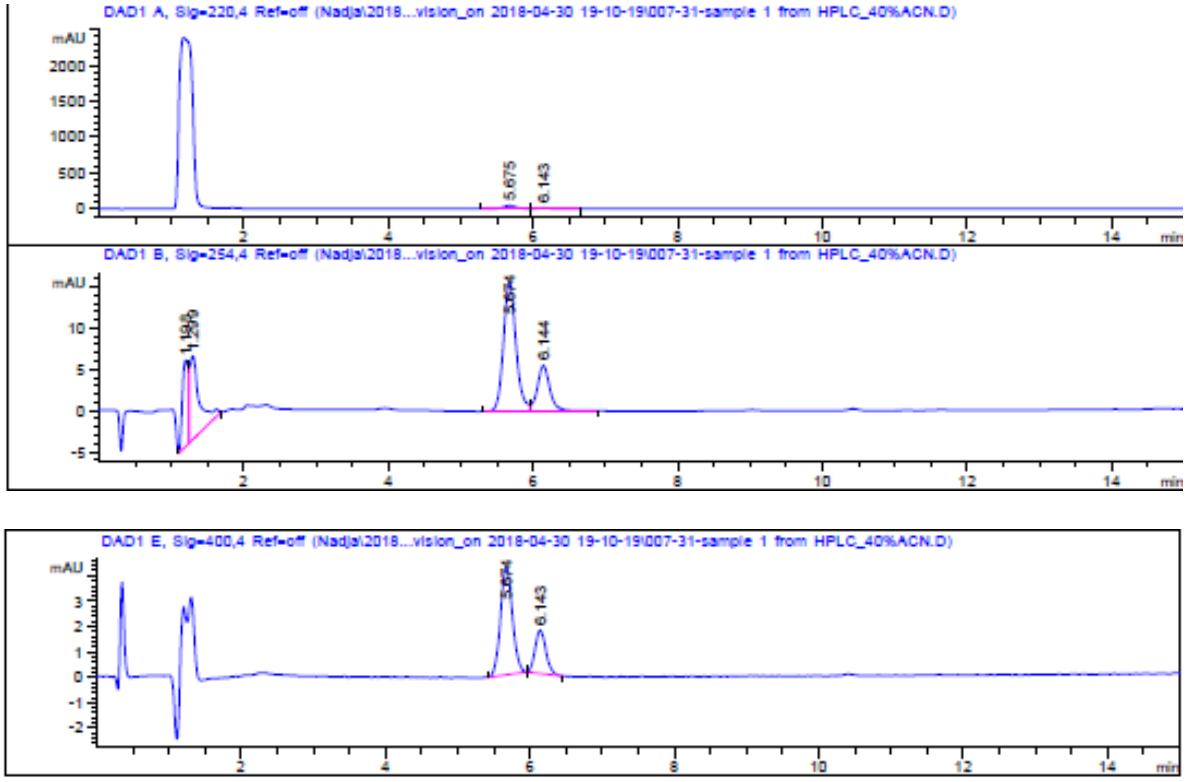

Figure A1: HPLC trace of **1a** (in 40% MeCN in H_2O from 10 mM DMSO stock) at 220 nm, 254 nm and at the isosbestic point at 400 nm. Through origin from the first fraction of the first peak in preparative HPLC, the sample exhibits both the *E*- and the *Z*-isomer of the open form of the switch at the thermal equilibrium.

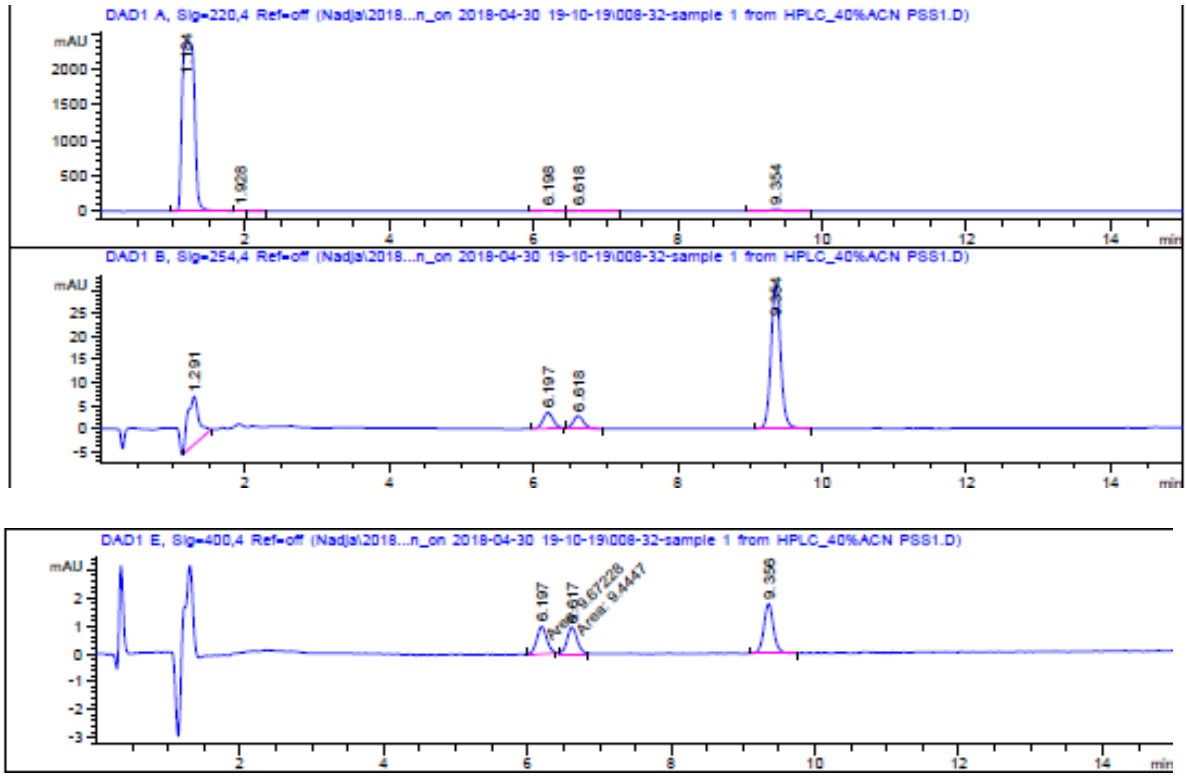

Figure A2: HPLC trace of **1a** (in 40% MeCN in H_2O from 10 mM DMSO stock) at 220 nm, 254 nm and at the isosbestic point at 400 nm at the PSS after irradiation with 400nm.

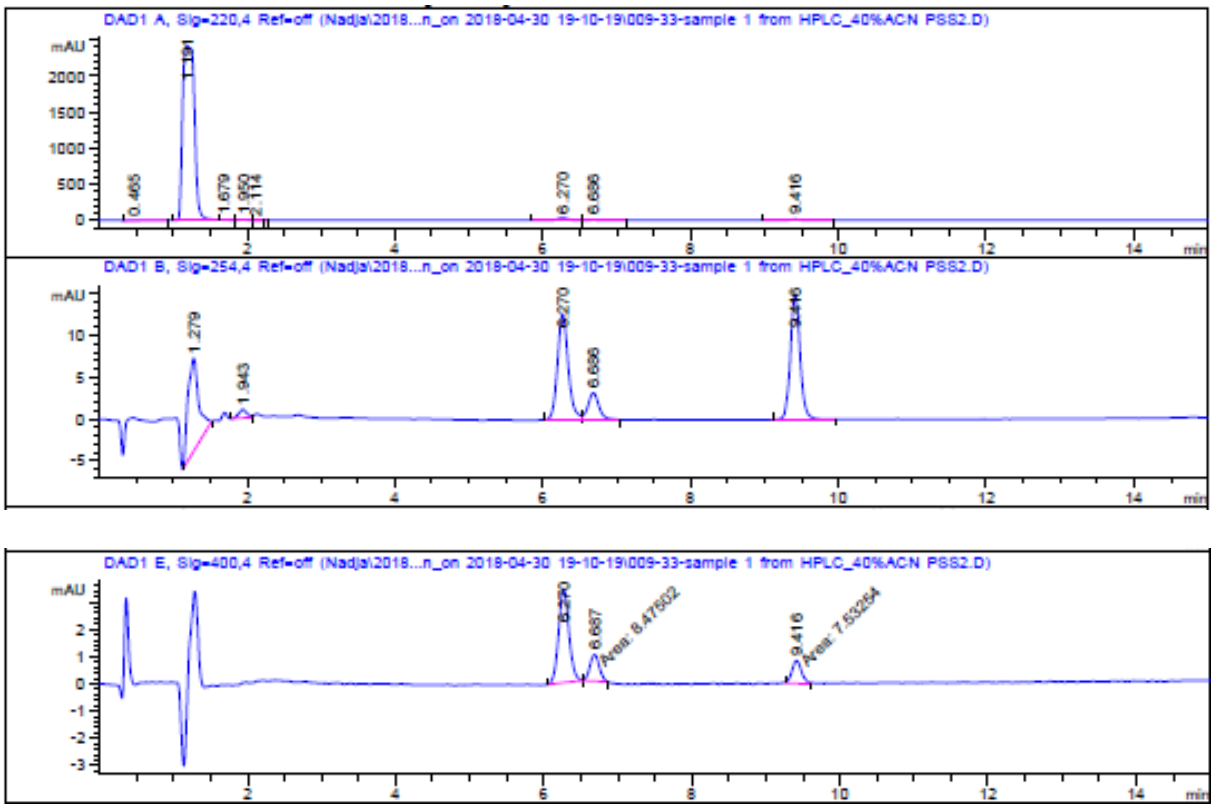

Figure A3: HPLC trace of **1a** (in 40% MeCN in H_2O from 10 mM DMSO stock) at 220 nm, 254 nm and at the isosbestic point at 400 nm at the PSS2 after irradiation with 590 nm.

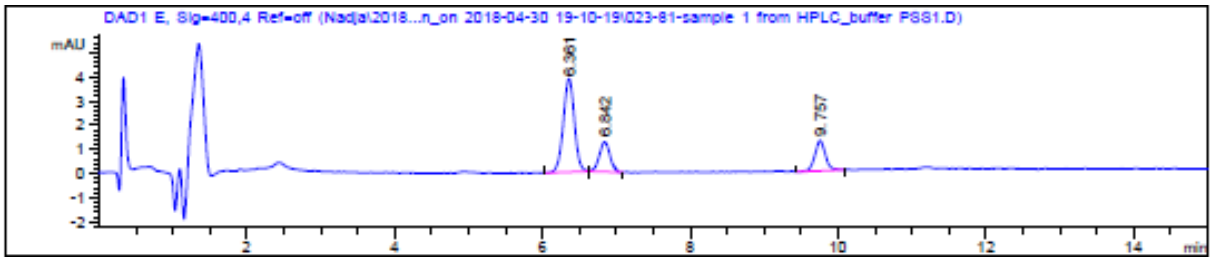

Figure A4: HPLC trace of **1a** (in buffer (5%DMSO)) at the isosbestic point at 400 nm at the PSS.

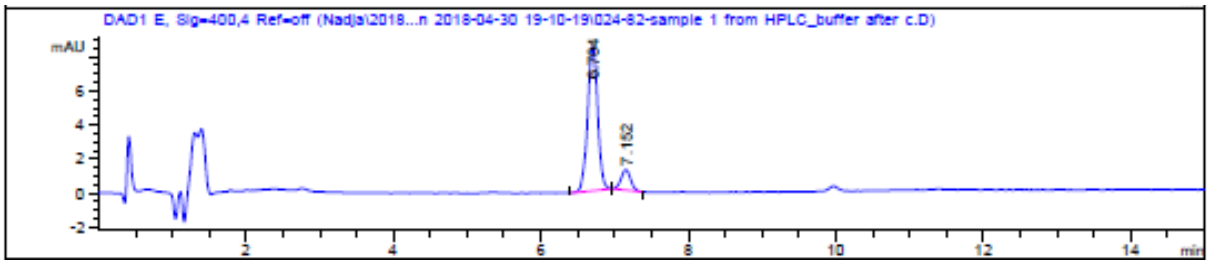

Figure A5: HPLC trace of **1a** (in buffer (5%DMSO)) at the isosbestic point at 400 nm at the PSS2 after six irradiation cycles.

Compound ***1b***

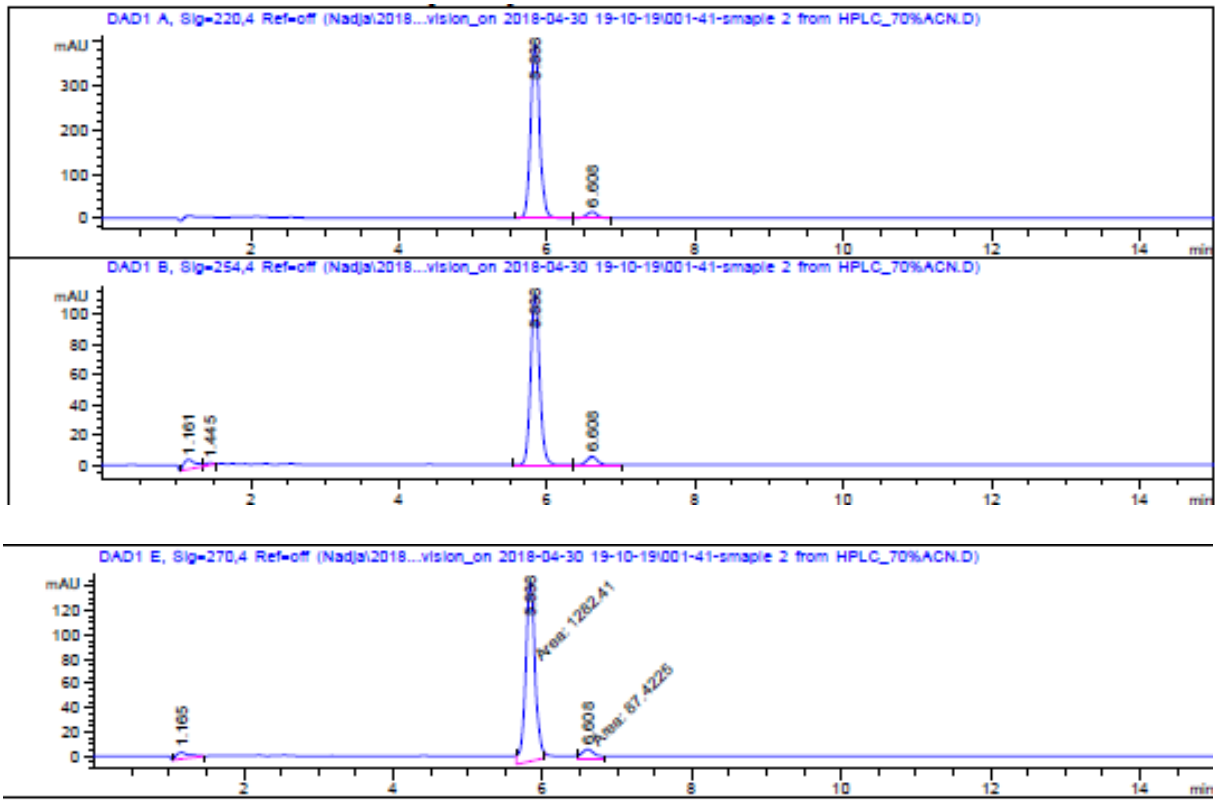

Figure A6: HPLC trace of **1b** (in 70% MeCN in H_2O) at 220 nm, 254 nm and at the isosbestic point at 270 nm. Through origin from the first fraction of the first peak in preparative HPLC, the sample exhibits both the *E*- and the *Z*-isomer of the open form of the switch at the thermal equilibrium.

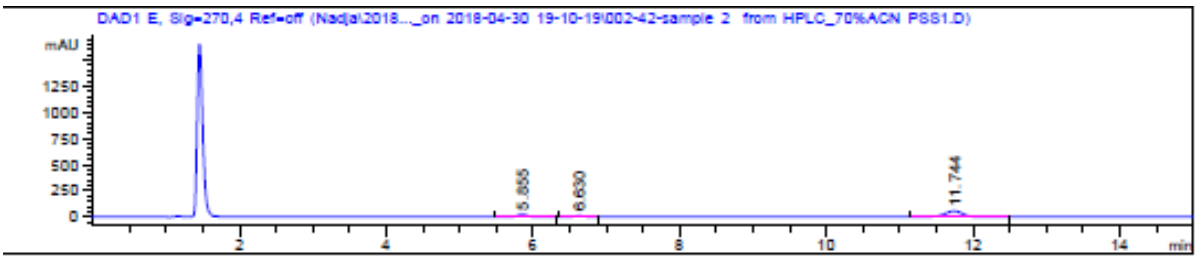

Figure A7: HPLC trace of **1b** (in 70% MeCN in H_2O) at the isosbestic point at 270 nm at the PSS after irradiation with 400 nm.

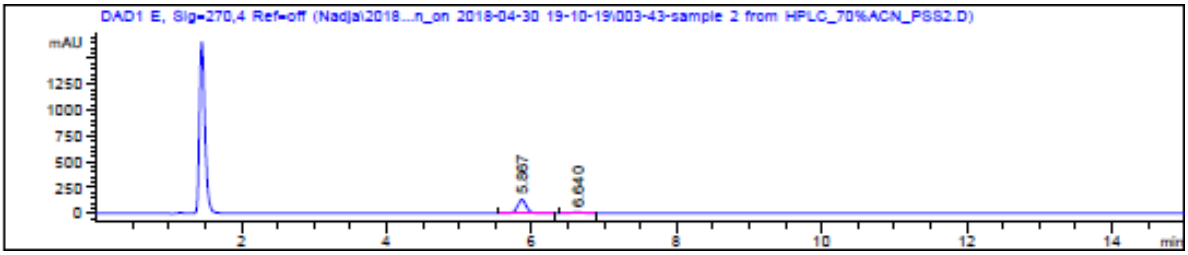

Figure A8: HPLC trace of **1b** (in 70% MeCN in H_2O) at the isosbestic point at 270 nm at the PSS after irradiation with 590 nm.

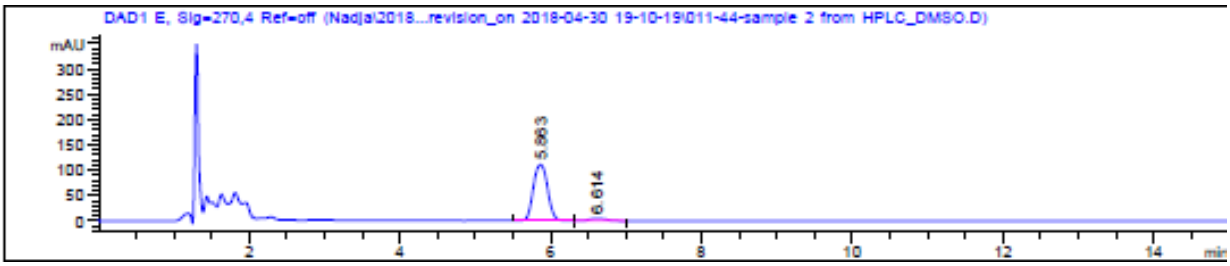

Figure A9: HPLC trace of **1b** (in DMSO) at the isosbestic point at 270 nm at the thermal equilibrium.

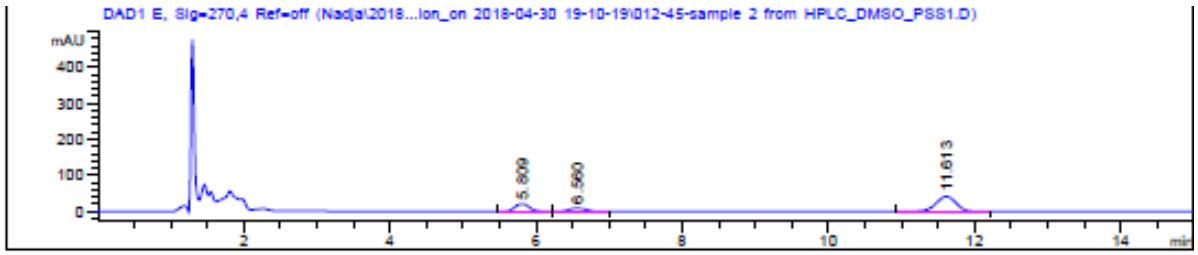

Figure A10: HPLC trace of **1b** (in DMSO) at the isosbestic point at 270 nm at the PSS.

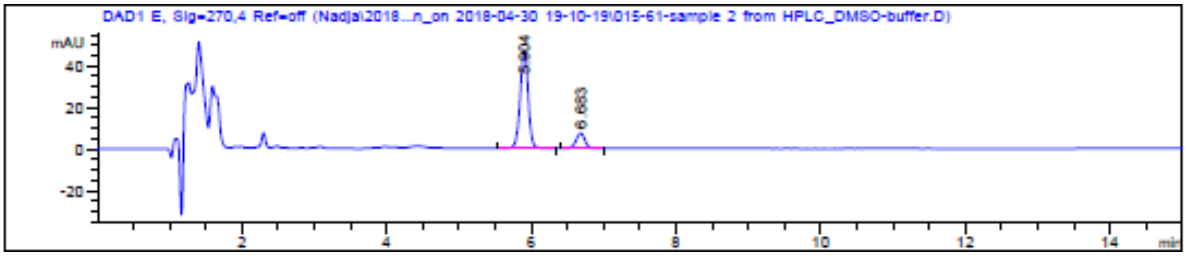

Figure A11: HPLC trace of **1b** (in DMSO-buffer 1:2) at the isosbestic point at 270 nm at the thermal equilibrium.

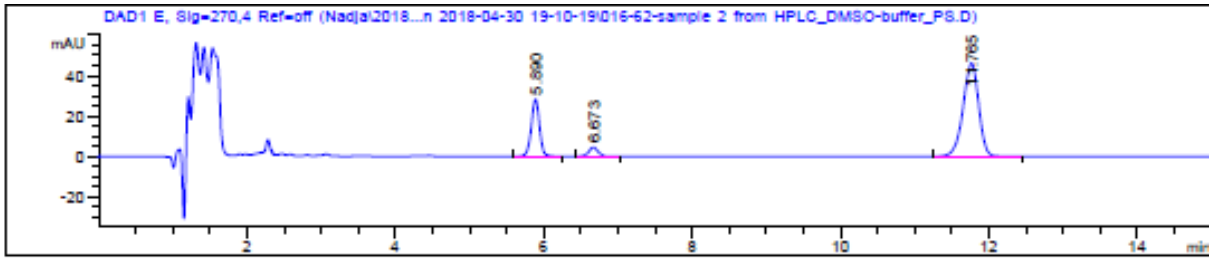

Figure A12: HPLC trace of **1b** (in DMSO-buffer 1:2) at the isosbestic point at 270 nm at the PSS.

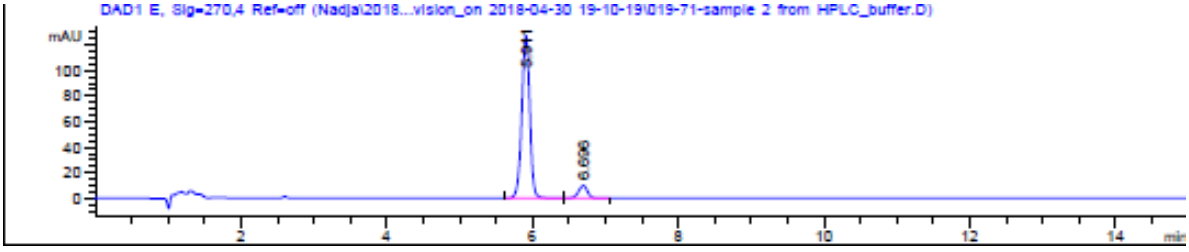

Figure A13: HPLC trace of **1b** (in buffer (5% DMSO)) at the isosbestic point at 270 nm at the thermal equilibrium.

Compound ***1c***

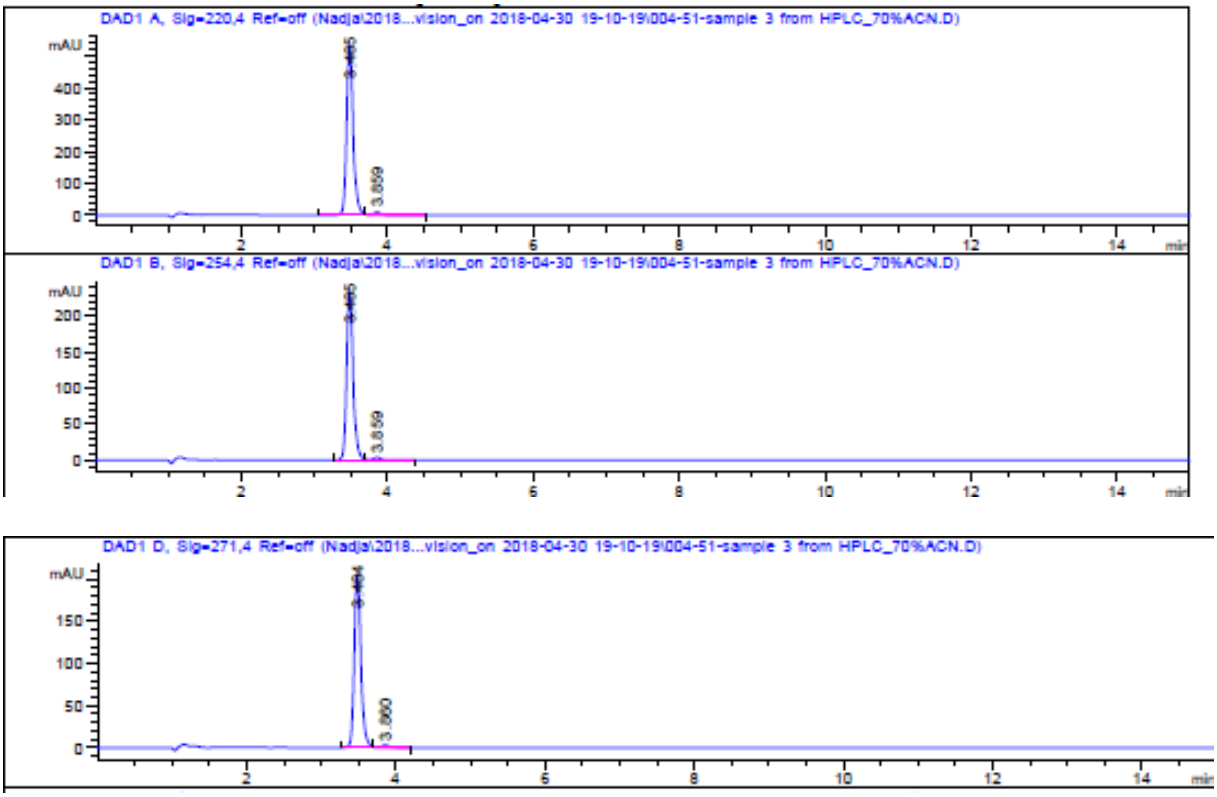

Figure A14: HPLC trace of **1c** (in 70% MeCN in H_2O) at 220 nm, 254 nm and at the isosbestic point at 271 nm. Through origin from the first fraction of the first peak in preparative HPLC, the sample exhibits both the *E*- and the *Z*-isomer of the open form of the switch at the thermal equilibrium.

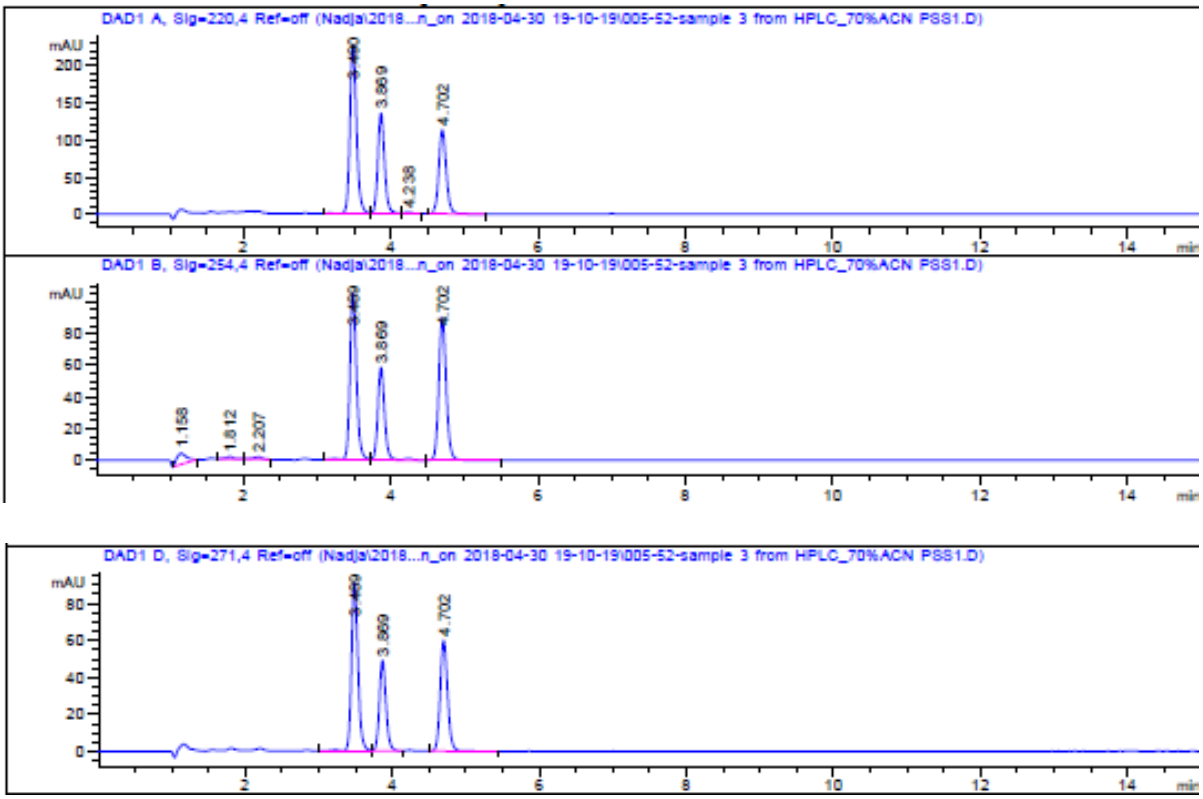

Figure A15: HPLC trace of **1c** (in 70% MeCN in H_2O) at 220 nm, 254 nm and 271 nm at the PSS after irradiation with 400 nm.

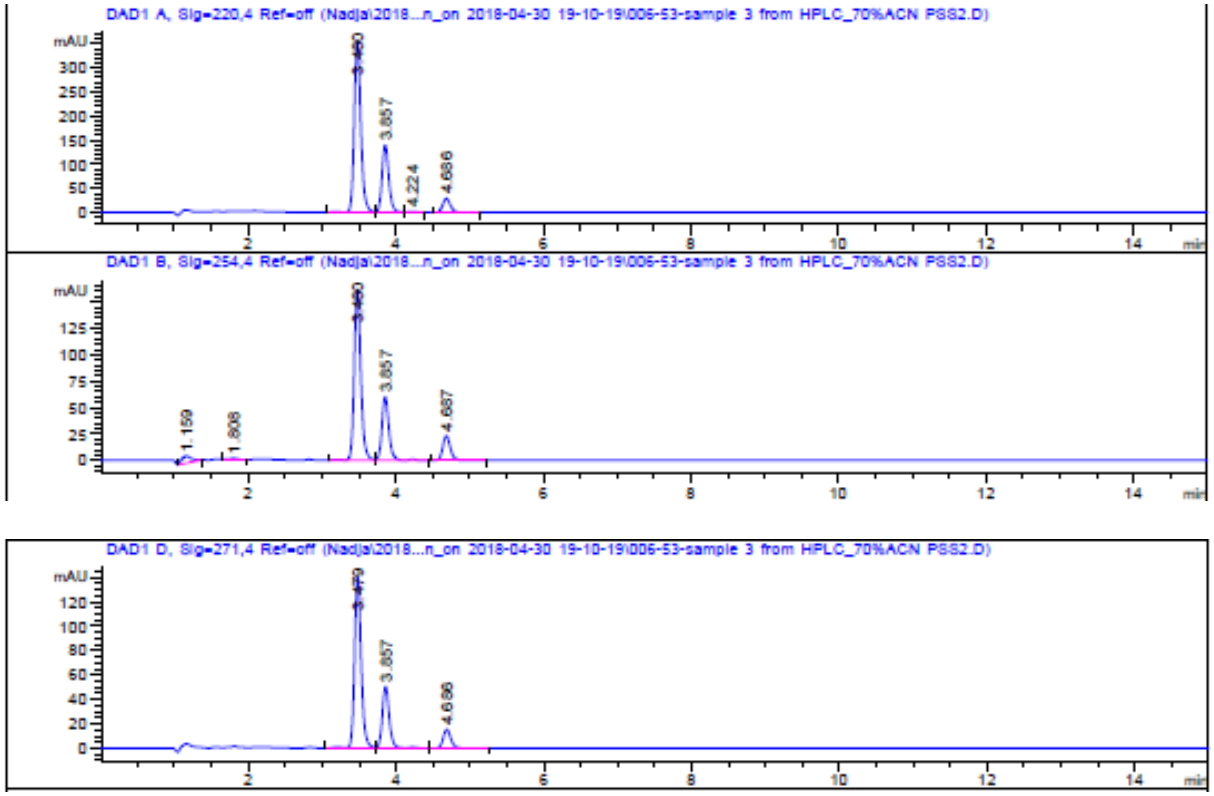

Figure A16: HPLC trace of **1c** (in 70%MeCN in H_2O) at 220 nm, 254 nm and 271 nm at the PSS2 after irradiation with 590 nm.

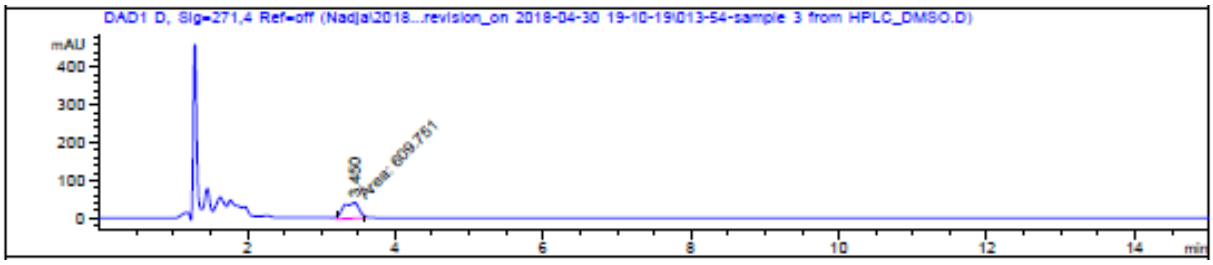

Figure A17: HPLC trace of **1c** (in DMSO) at the isosbestic point at 271 nm at the thermal equilibrium.

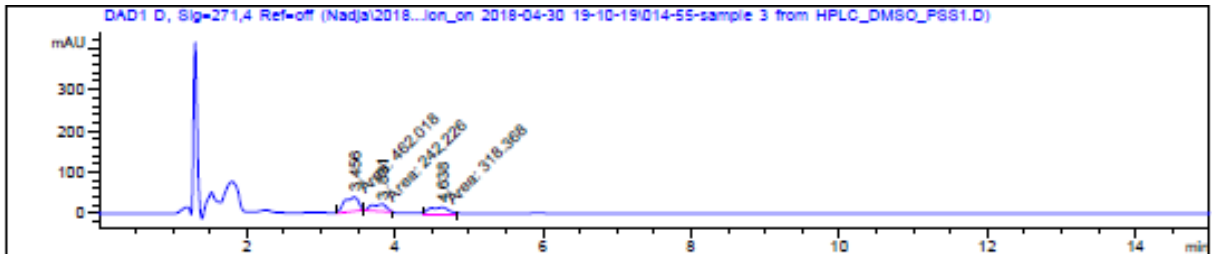

Figure A18: HPLC trace of **1c** (in DMSO) at the isosbestic point at 271 nm at the PSS after irradiation with 400 nm.

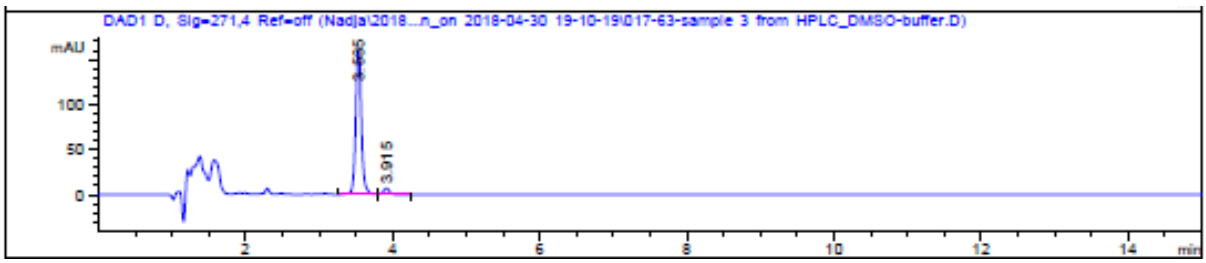

Figure A19: HPLC trace of **1c** (in DMSO-buffer 1:2) at the isosbestic point at 271 nm at the thermal equilibrium.

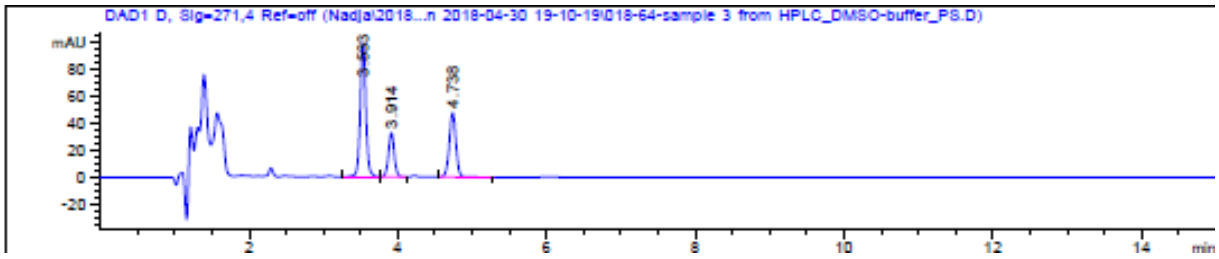

Figure A20: HPLC trace of **1c** (in DMSO-buffer 1:2) at the isosbestic point at 271 nm at the PSS state after irradiation with 400 nm.

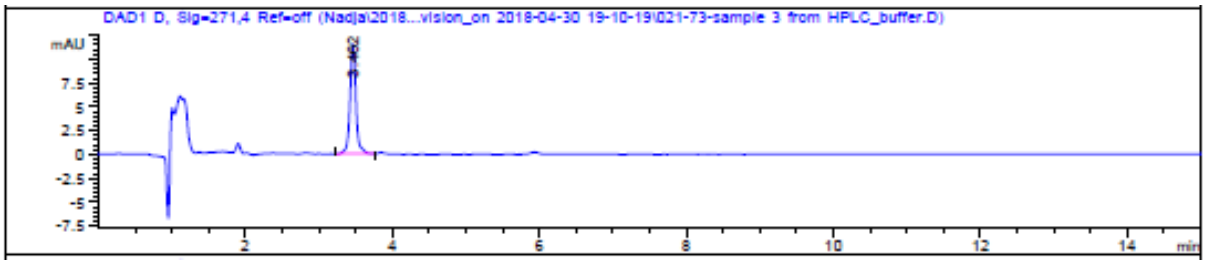

Figure A21: HPLC trace of **1c** (buffer (5% DMSO)) at the isosbestic point at 271 nm at the thermal equilibrium.

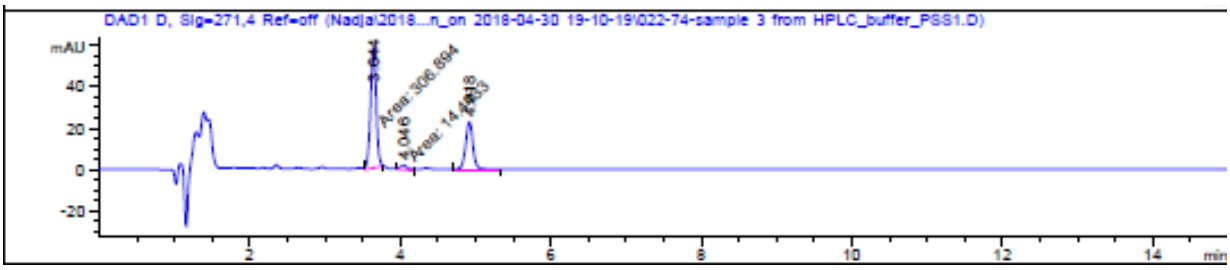

Figure A22: HPLC trace of **1c** (buffer (5% DMSO)) at the isosbestic point at 271 nm at the PSS after irradiation with 400 nm.

Thermal stability

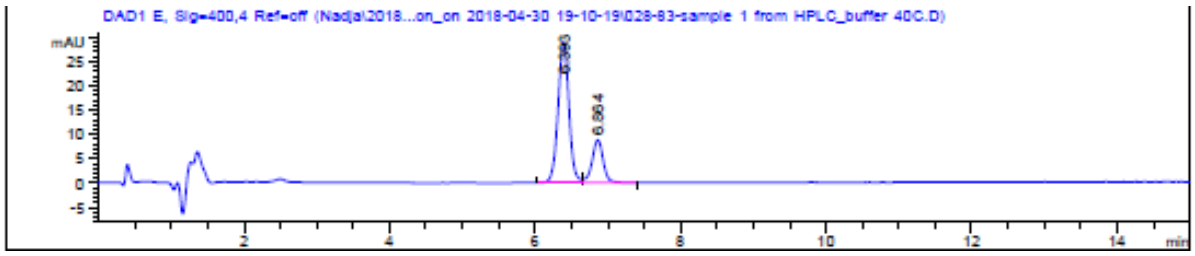

Figure A23: HPLC trace of **1a** (in buffer (5% DMSO)) at the isosbestic point at 400 nm at the thermal equilibrium after incubation at 40 C for 4h.

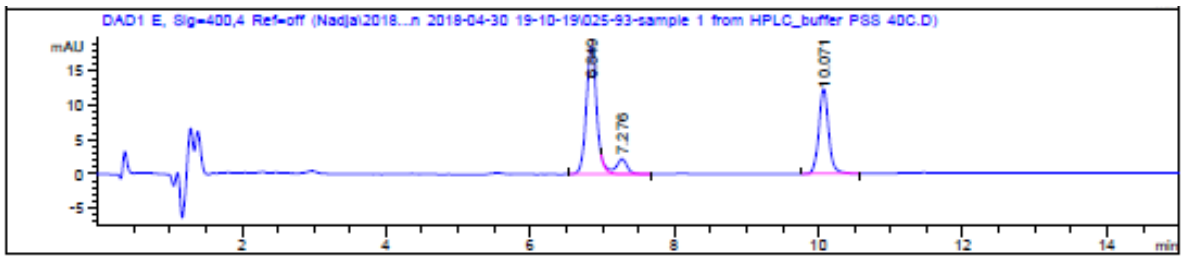

Figure A24: HPLC trace of **1a** (in buffer (5% DMSO)) at the isosbestic point 400 nm at the PSS after incubation at 40 C for 4h.

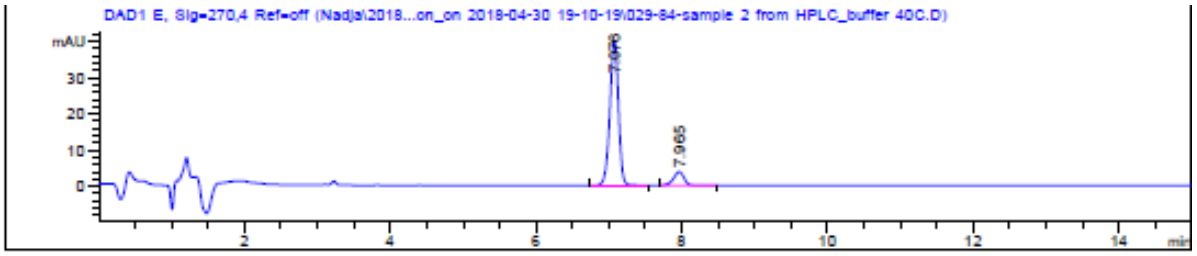

Figure A25: HPLC trace of **1b** (in buffer (5% DMSO)) at the isosbestic point at 270 nm at the thermal equilibrium after incubation at 40 C for 4h.

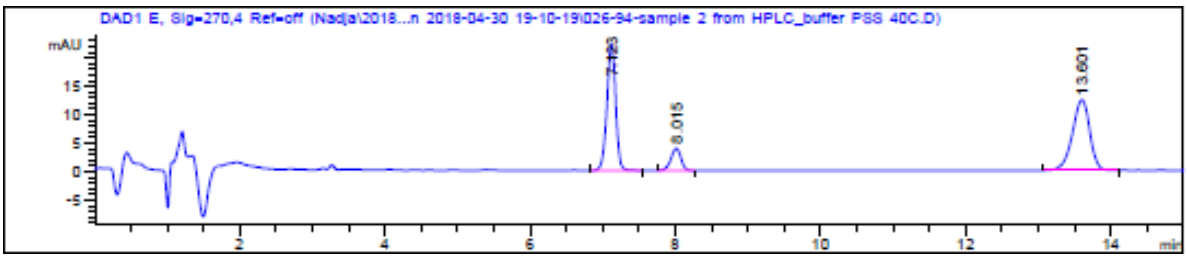

Figure A26: HPLC trace of **1b** (in buffer (5% DMSO)) at the isosbestic points at 270 nm at the PSS after incubation at 40 C for 4h.

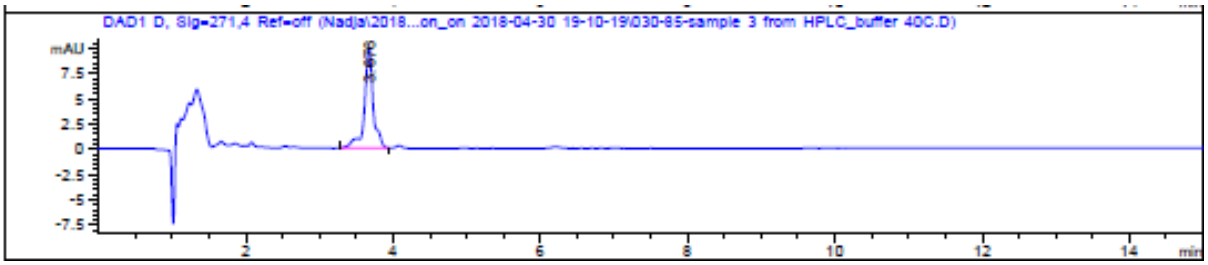

Figure A27: HPLC trace of **1c** (in buffer (5% DMSO)) at the isosbestic point at 271 nm at the thermal equilibrium after incubation at 40 C for 4h.

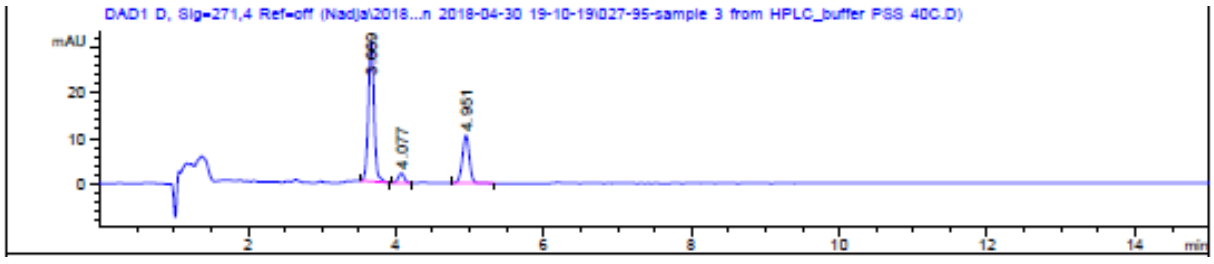

Figure A28: HPLC trace of **1c** (in buffer (5% DMSO)) at the isosbestic point at 271 nm at the PSS after incubation at 40 C for 4h.

3. Spectroscopy

UV-Vis absorption and fluorescence spectra were determined using an appropriate 1cmx1cm quartz cuvette. The concentration of the solutions as well as the solvent (mixtures) are stated for every measurement.

The molar attenuation coefficient ε at a certain wavelength λ was determined according to the Lambert-Beer law:

$$A = \varepsilon_\lambda c l$$

With A being the absorbance, c being the concentration and l being the pathlength (1 cm in our case). Hence, in a linear plot of A *versus* c, $\varepsilon_{\lambda max}$ can be determined directly from the slope of the line.

Determination of $\varepsilon_{\lambda max}$ of the closed forms is shown exemplarily for compound 1c in DMSO-buffer (1:2).

Table A2: Absorbance at λ_{max} =606 nm of the closed isomer of 1c at the PSS at different concentrations.

Absorbance [a.u.]	Concentration of **C-1c** [M]	Concentration of **1c** [M]
	at PSS (29% from HPLC)	
0.14182	2.90E-05	1.00E-04
0.05037	1.45E-05	5.00E-05
0.34923	5.80E-05	2.00E-04
0.764	1.45E-04	5.00E-04

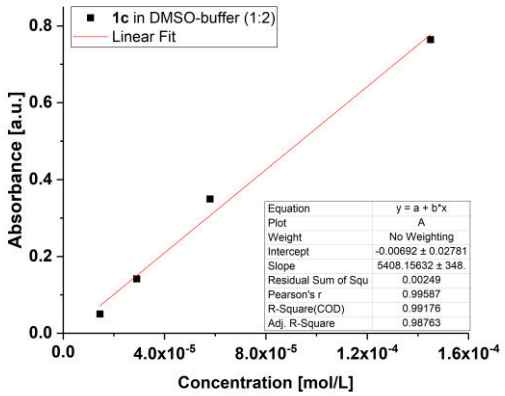

Figure A29: Plot of the absorbance of different concentrations of the amount of the closed form in 1c in DMSO-buffer (1:2).

From the sloe of the plot it can be concluded that $\varepsilon_{\lambda max}$=5408 L/(mol*cm) for ***C*-1c** at λ_{max} =606 nm.

Determination of Isosbestic Point for PSS Determination *via* HPLC

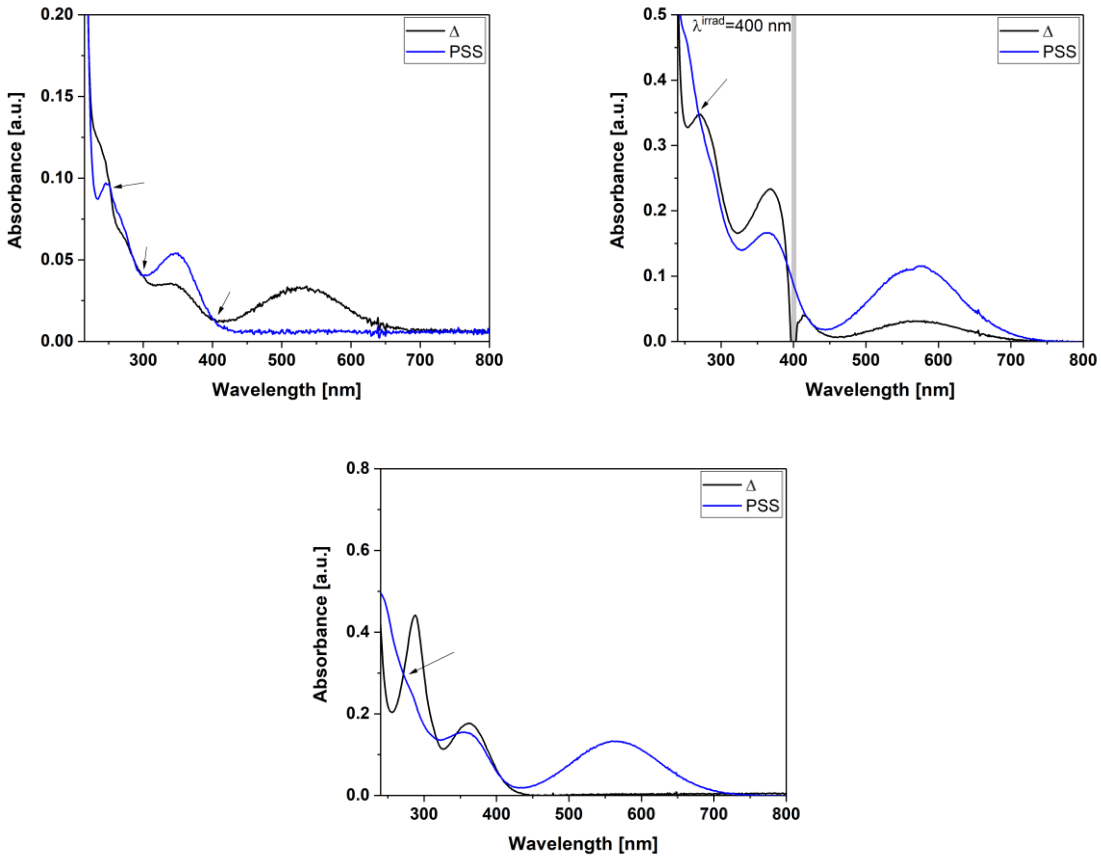

Figure A30: UV/Vis spectrum of **1a** (top left, 25 μM in 40% MeCN in water), **1a** (top right, 100 μM in 70% MeCN in water) and **1c** (bottom, 100 μM in 70% MeCN in water) at the thermal equilibrium (D, black line) and the PSS (blue line, upon irradiation with 400 nm). The isosbestic points at 400 nm, 270 nm and 271 nm, respectively, were chosen for PSS-analysis through analytical HPLC.

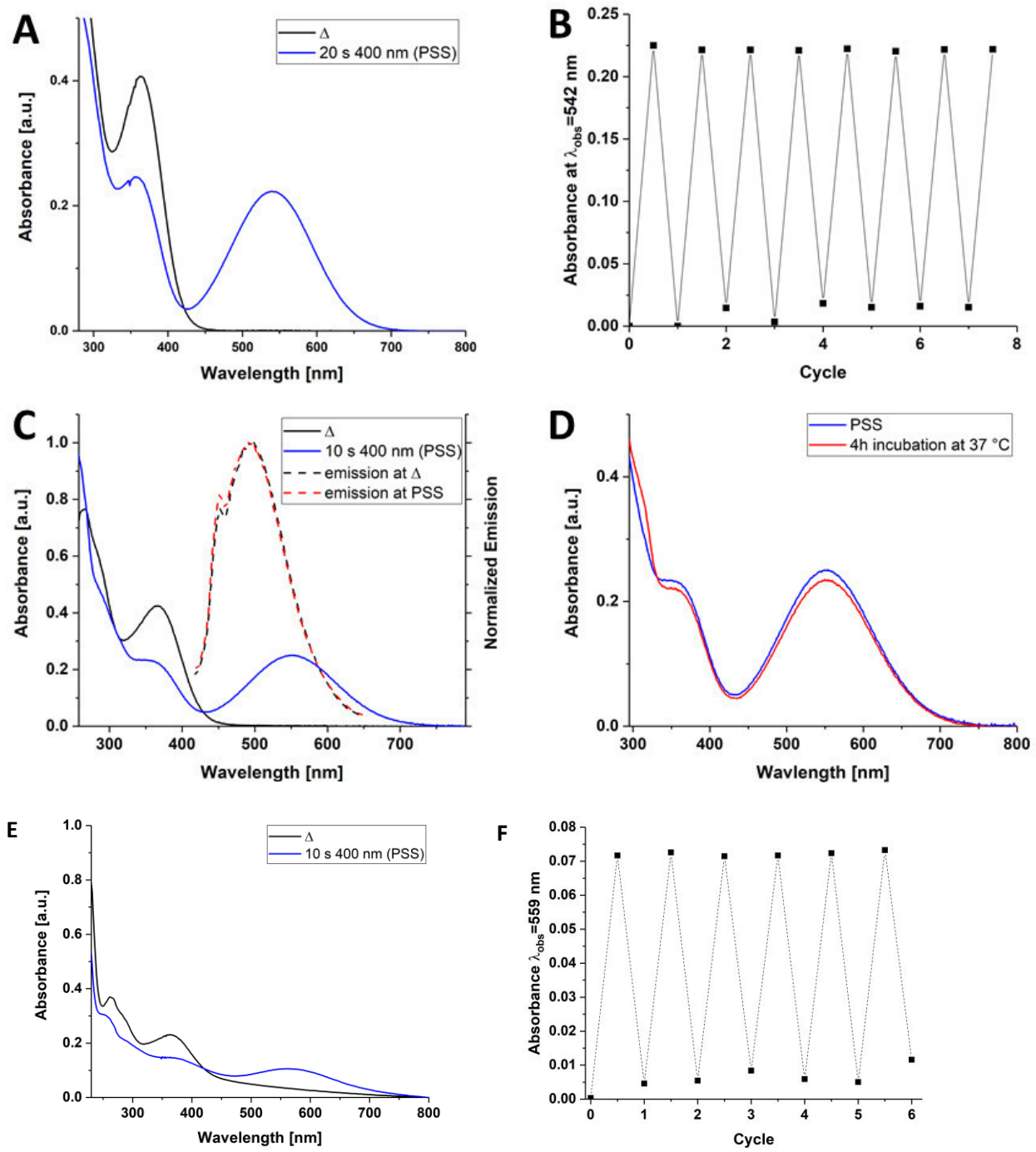

Figure A31: Spectroscopic properties of compound **1a** in various solvents. **A:** UV/Vis spectrum of **1a** 100µM in DMSO (black: open form, blue: PSS). **B:** Fatigue resistance of **1a** 100µM in DMSO over eight cycles (λ_{obs}= 542 nm). **C:** Spectra of 1a 100µM in assay buffer/DMSO 1:2 (solid black: UV/Vis spectrum of open form, solid blue: UV/Vis spectrum of PSS, dashed black: emission spectrum of open form, dashed blue: emission spectrum at PSS). **D:** Temperature stability of ***C*-1a** at 40 °C. **E:** UV/Vis spectrum of **1a** 100µM in assay buffer (black: open form, blue: PSS). **F:** Fatigue resistance of **1a** 10µM in assay buffer over six cycles (λ_{obs}= 559 nm).

1b

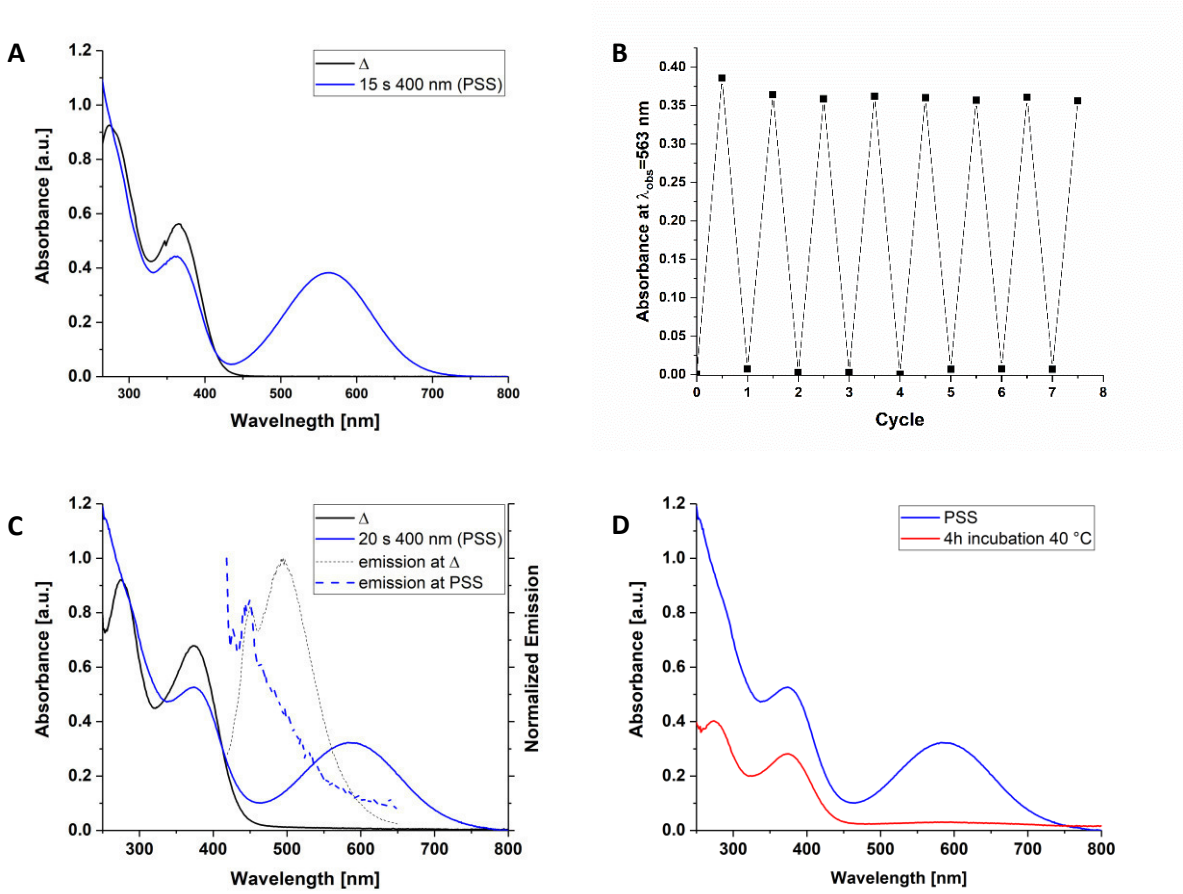

Figure A32: Spectroscopic properties of compound **1b** in various solvents. **A:** UV/Vis spectrum of **1b** 100µM in DMSO (black: open form, blue: PSS). **B:** Fatigue resistance of **1b** 100µM in DMSO over eight cycles (λ_{obs}= 563 nm). **C:** Spectra of **1b** 100µM in assay buffer/DMSO 1:2 (solid black: UV/Vis spectrum of open form, solid blue: UV/Vis spectrum of PSS, dashed black: emission spectrum of open form, dashed blue: emission spectrum at PSS). **D:** Temperature stability of ***C*-1b** at 40 °C.

1c

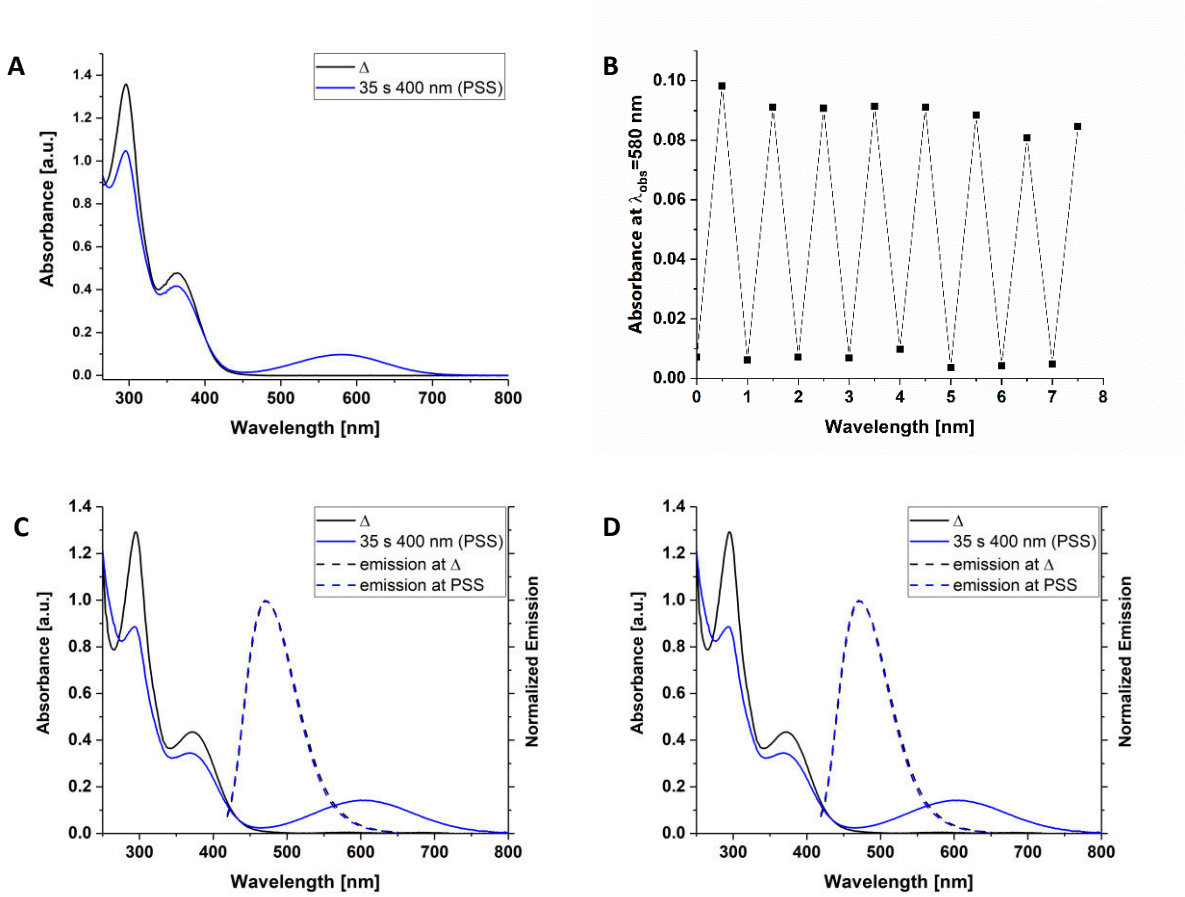

Figure A33: Spectroscopic properties of compound **1c** in various solvents. **A:** UV/Vis spectrum of **1c** 100µM in DMSO (black: open form, blue: PSS). **B:** Fatigue resistance of **1c** 100µM in DMSO over eight cycles (λ_{obs}= 580 nm). **C:** Spectra of **1c** 100µM in assay buffer/DMSO 1:2 (solid black: UV/Vis spectrum of open form, solid blue: UV/Vis spectrum of PSS, dashed black: emission spectrum of open form, dashed blue: emission spectrum at PSS). **D:** Temperature stability of ***C*-1c** at 40 °C.

4. Biological Evaluation

a) Cloning, expression and purification of recombinant proteins

The class I sirtuins ($Sirt1_{133-747}$, $Sirt2_{50-356}$, $Sirt3_{118-395}$) were expressed and purified as described previously.[1] SDS-PAGE was used for verification of identity and purity of the expressed enzymes.[2] Protein concentrations were determined by Bradford assay.[3] NAD^+ dependence of Deacetylase activity was confirmed and could be inhibited by nicotinamide.

b) Homogeneous ZMAL-based fluorescence assay

The ZMAL-assay was performed in black 96 well plates (OptiPlateTM -96F, black, 96 well, Pinch bar design, PerkinElmer, USA). ZMAL (Z-Lys(acetyl)-AMC was used as substrate.[4] The respective sirtuins were mixed with 5 µL substrate (10.5 µM final assay concentration) and 3 µL of DMSO as a control (5 % (v/v) final assay concentration) or various concentrations of inhibitor solved in DMSO. The mixture was filled up to 55 µL with assay buffer (50 mM Tris/HCl, 137 mM NaCl, 2.7 mM KCl, 1 mM $MgCl_2$, pH 8.0). The enzyme concentration was adjusted to 20-30 % conversion. The plates were irradiated from 1 cm distance with a custom made 96-well irradiation setup (each LED 400 nm, 5 mW, Figure A10) for 15 min for conversion to the closed isomer (or with a single LED for 1 min (590 nm, 5 mW) to retain the open isoform).

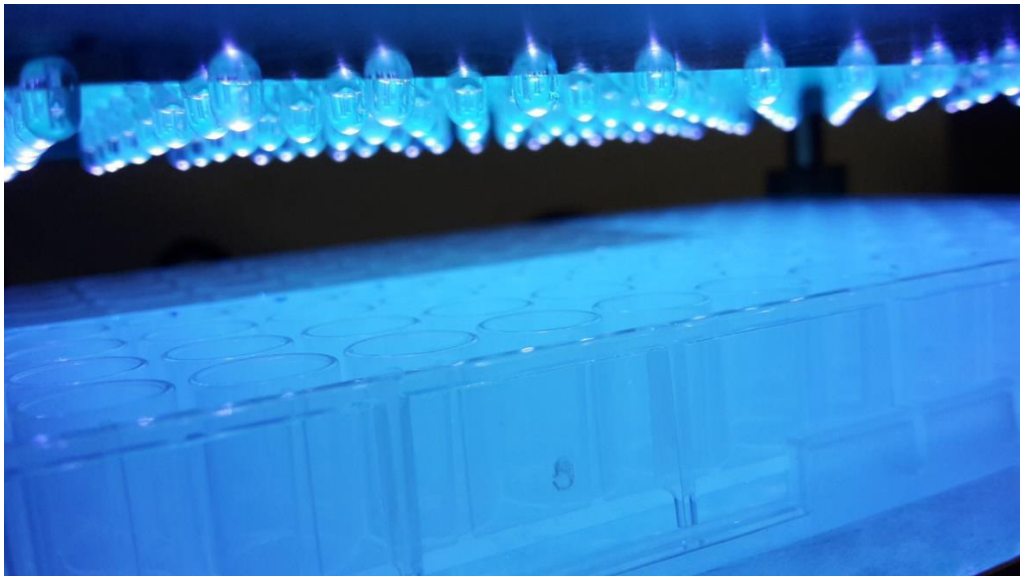

Figure A34: 96-well irradiation setup and an exemplary 96-well plate.

Addition of 5 µL NAD^+ (6 mM in assay buffer, final assay concentration 500 µM) initiated the enzymatic reaction. After incubation at 37 °C for 4 h with agitation at 140 rpm the catalytic reaction was stopped by addition of 60 µL stop solution (50 mM Tris, 100 mM NaCl, 6.7 % (v/v) DMSO, trypsin 5.5 U/µL, 8 mM nicotinamide, pH 8.0). The plate was incubated for another 20 min at 37 °C

and 140 rpm to cleave off the AMC fluorophore from the deacetylated substrate. The fluorescence intensity was measured in a microplate reader (λ_{Ex} = 390 nm, λ_{Em} = 460 nm, BMG POLARstar Optima, BMG Labtech, Germany). Additionally, a blanc control without substrate and a 100 % control with AMC instead of ZMAL were measured. To measure the intrinsic fluorescence of the compunds 1a-c a no-conversion control was employed using the same conditions as described above (similar concentration, irradiation and incubation times) without addition of the substrate. The substrate was added after the reaction was stopped to get a composition similar to the normal assay conditions without any substrate conversion. The Blanc corrected values for the no-conversion control was subtracted from the measured fluorescence intensities. EC_{50} values were calculated with GraphPad Prism software (La Jolla, CA) using a nonlinear regression to fit the dose response curve. IC_{50} values were calculated from EC_{50} and hill slope values by this formula $IC_{50} = \left(\frac{y_{max} - y_{min}}{50 - y_{min}} - 1\right)^{\frac{1}{H}} * EC_{50}$.

5. X-Ray

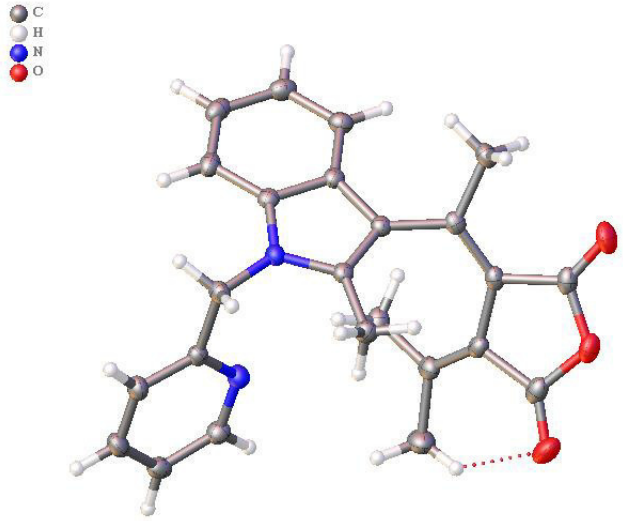

Experimental. Single clear orange plate-shaped crystals of **7a** were obtained from crystallization aqueous MeCN. A suitable crystal (0.13×0.11×0.07) mm^3 was selected and mounted on on a SuperNova, Single source at offset, Atlas diffractometer. The crystal was kept at T = 293.48(10) K during data collection. Using **Olex2**,[5] the structure was solved with the **ShelXT**[6] structure solution program, using the Intrinsic Phasing solution method. The model was refined with version 2016/6 of **ShelXL**[7] using Least Squares minimisation.

Crystal Data. $C_{24}H_{22}N_2O_3$, M_r = 386.43, triclinic, P-1 (No. 2), a = 9.6373(3) Å, b = 9.6529(3) Å, c = 11.2938(4) Å, a = 104.087(3)°, b = 108.553(3)°, g = 93.234(2)°, V = 955.79(6) Å^3, T = 293.48(10) K, Z = 2, Z' = 1, m(CuK$_a$) = 0.718, 21114 reflections measured, 3801 unique (R_{int} = 0.0360) which were used in all calculations. The final wR_2 was 0.0909 (all data) and R_1 was 0.0351 (I > 2(I)).

Compound	**7a**
Formula	$C_{24}H_{22}N_2O_3$
$D_{calc.}$/ g cm^{-3}	1.343
m/mm^{-1}	0.718
Formula Weight	386.43
Colour	clear orange
Shape	plate
Size/mm^3	0.13×0.11×0.07
T/K	293.48(10)
Crystal System	triclinic
Space Group	P-1
a/Å	9.6373(3)
b/Å	9.6529(3)
c/Å	11.2938(4)
a/°	104.087(3)
b/°	108.553(3)
g/°	93.234(2)
V/Å^3	955.79(6)
Z	2
Z'	1
Wavelength/Å	1.54184
Radiation type	CuK$_a$
Q_{min}/°	4.296
Q_{max}/°	73.596
Measured Refl.	21114
Independent Refl.	3801
Reflections Used	3345
R_{int}	0.0360
Parameters	306
Restraints	0
Largest Peak	0.241
Deepest Hole	-0.248
GooF	1.035
wR_2 (all data)	0.0909
wR_2	0.0866
R_1 (all data)	0.0407
R_1	0.0351

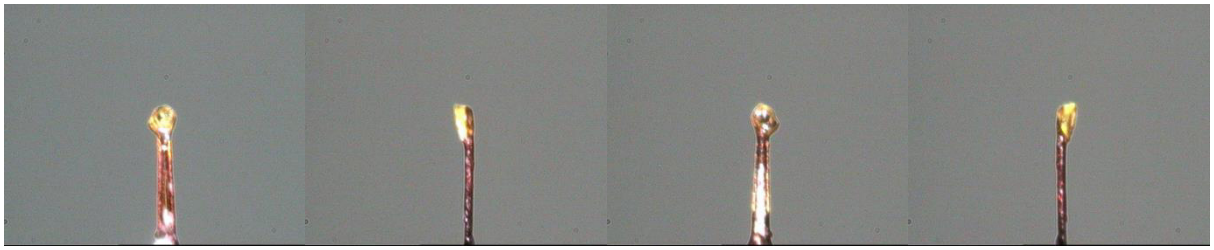

Figure A35: Images of the Crystal on the Diffractometer.

Table A3: Fractional Atomic Coordinates ($\times 10^4$) and Equivalent Isotropic Displacement Parameters ($Å^2 \times 10^3$) for **7a**. U_{eq} is defined as 1/3 of the trace of the orthogonalised U_{ij}.

Atom	x	y	z	U_{eq}
O1	1682.6(11)	3505.7(11)	10869.3(9)	28.8(2)
O2	1617.5(11)	5878.9(11)	11223.5(9)	32.8(2)
O3	1893.8(13)	1188.3(11)	10106.9(10)	37.7(3)
N1	1522.0(11)	4091.5(11)	5241.8(10)	18.7(2)
N2	2368.2(12)	1386.9(11)	4778.7(10)	22.5(2)
C1	2628.7(13)	5221.0(12)	5511.0(12)	18.7(2)
C2	3092.0(13)	5917.5(12)	6849.5(12)	18.5(2)
C3	2244.2(13)	5138.2(12)	7391.6(11)	17.7(2)
C20	1406.9(13)	1678.4(13)	3754.4(12)	18.8(2)
C4	1313.8(13)	4023.2(12)	6378.3(11)	18.0(2)
C6	2282.3(13)	5516.5(13)	8735.6(11)	18.9(2)
C8	2667.7(14)	3037.0(13)	9199.8(12)	20.7(3)
C19	778.1(14)	3090.0(13)	3972.9(12)	22.1(3)
C18	3267.1(15)	5654.3(14)	4683.4(13)	23.3(3)
C7	2361.3(13)	4538.7(13)	9436.6(11)	19.9(3)
C11	4434.2(14)	3109.7(14)	7997.9(12)	23.8(3)
C13	1882.0(14)	4810.2(15)	10582.2(12)	24.4(3)
C5	186.8(14)	2912.7(13)	6388.6(12)	22.1(3)
C23	2529.1(15)	-853.1(14)	3361.1(13)	24.7(3)
C15	4266.7(14)	7066.6(13)	7385.8(13)	22.4(3)
C21	950.5(15)	744.6(14)	2506.0(12)	23.3(3)
C10	3545.5(14)	2360.6(13)	8587.6(12)	22.7(3)
C16	4906.7(15)	7494.1(14)	6572.1(14)	26.2(3)
C9	2061.1(15)	2395.8(15)	10026.8(12)	26.3(3)
C22	1523.8(15)	-537.8(14)	2309.9(13)	26.8(3)
C17	4403.2(15)	6799.7(14)	5237.8(14)	26.4(3)
C24	2910.2(14)	133.0(14)	4564.2(13)	24.1(3)
C14	2094.7(15)	7063.4(14)	9268.8(12)	24.1(3)
C12	3716.2(18)	797.2(15)	8457.3(15)	34.3(3)

Table A4: Anisotropic Displacement Parameters ($\times 10^4$) **7a**. The anisotropic displacement factor exponent takes the form: $-2p^2[h^2a^{*2} \times U_{11} + ... + 2hka^* \times b^* \times U_{12}]$

Atom	U_{11}	U_{22}	U_{33}	U_{23}	U_{13}	U_{12}
O1	28.8(5)	38.7(5)	22.7(5)	11.2(4)	12.4(4)	2.2(4)
O2	35.1(5)	40.6(6)	23.7(5)	1.9(4)	16.1(4)	7.7(4)
O3	47.6(6)	34.1(6)	33.6(6)	16.6(4)	12.9(5)	-4.0(5)
N1	20.8(5)	18.3(5)	16.7(5)	3.9(4)	6.3(4)	4.9(4)
N2	22.9(5)	23.1(5)	20.3(5)	5.3(4)	6.2(4)	5.4(4)
C1	18.9(6)	17.9(5)	21.4(6)	7.6(5)	7.4(5)	7.4(4)
C2	19.5(6)	17.4(5)	20.7(6)	6.3(4)	8.2(5)	6.6(4)
C3	17.5(5)	17.6(5)	19.0(6)	5.1(4)	7.0(5)	5.0(4)
C20	17.9(6)	19.6(6)	19.5(6)	5.0(5)	7.7(5)	1.8(4)
C4	18.5(6)	18.1(5)	19.0(6)	6.1(4)	7.1(5)	6.5(4)
C6	14.3(5)	21.8(6)	18.5(6)	2.7(5)	5.0(5)	2.2(4)
C8	21.4(6)	22.5(6)	16.5(6)	6.4(5)	4.0(5)	0.0(5)
C19	23.8(6)	22.2(6)	16.6(6)	2.9(5)	3.4(5)	6.0(5)
C18	27.2(6)	26.1(6)	23.4(6)	11.4(5)	13.0(5)	11.7(5)
C7	17.2(6)	24.8(6)	16.3(6)	3.0(5)	5.8(5)	1.6(5)
C11	21.2(6)	30.9(7)	20.8(6)	7.8(5)	7.7(5)	9.7(5)
C13	20.3(6)	33.4(7)	18.4(6)	5.9(5)	6.4(5)	1.8(5)
C5	19.8(6)	21.5(6)	23.1(6)	4.7(5)	6.3(5)	0.6(5)
C23	25.5(6)	20.2(6)	31.5(7)	6.6(5)	14.4(6)	4.6(5)
C15	21.2(6)	19.5(6)	25.9(7)	5.7(5)	7.5(5)	3.7(5)
C21	24.6(6)	25.3(6)	18.4(6)	4.3(5)	6.3(5)	4.1(5)
C10	25.3(6)	23.2(6)	16.8(6)	5.2(5)	3.4(5)	4.2(5)
C16	23.4(6)	21.9(6)	37.0(7)	10.8(5)	13.0(6)	4.1(5)
C9	24.7(6)	32.4(7)	19.9(6)	9.4(5)	4.4(5)	-1.2(5)
C22	31.2(7)	23.7(6)	23.9(7)	0.3(5)	12.3(6)	2.5(5)
C17	27.7(7)	28.2(7)	35.0(7)	17.4(6)	18.5(6)	11.3(5)
C24	23.9(6)	24.8(6)	26.1(7)	9.9(5)	9.1(5)	6.9(5)
C14	26.3(6)	23.7(6)	19.8(6)	1.8(5)	7.3(5)	6.1(5)
C12	45.7(9)	25.4(7)	33.4(8)	9.4(6)	13.6(7)	11.1(6)

Table A5: Bond Lengths in Å for **7a**.

Atom	Atom	Length/Å
O1	C13	1.3925(17)
O1	C9	1.3981(17)
O2	C13	1.1988(16)
O3	C9	1.1968(17)
N1	C1	1.3855(15)
N1	C4	1.3769(15)
N1	C19	1.4477(15)
N2	C20	1.3347(17)
N2	C24	1.3438(17)
C1	C2	1.4066(17)
C1	C18	1.3980(17)
C2	C3	1.4427(16)
C2	C15	1.4049(17)
C3	C4	1.3822(17)
C3	C6	1.4601(16)
C20	C19	1.5197(17)

Atom	Atom	Length/Å
C20	C21	1.3913(17)
C4	C5	1.4871(16)
C6	C7	1.3627(18)
C6	C14	1.5122(16)
C8	C7	1.4731(17)
C8	C10	1.3546(18)
C8	C9	1.4782(17)
C18	C17	1.3796(19)
C7	C13	1.4781(16)
C11	C10	1.4925(18)
C23	C22	1.385(2)
C23	C24	1.3786(18)
C15	C16	1.3827(18)
C21	C22	1.3814(19)
C10	C12	1.5039(18)
C16	C17	1.401(2)

Table A6: Bond Angles in ° for **7a**.

Atom	Atom	Atom	Angle/°
C13	O1	C9	110.50(10)
C1	N1	C19	124.79(10)
C4	N1	C1	109.32(10)
C4	N1	C19	125.77(10)
C20	N2	C24	117.17(11)
N1	C1	C2	107.74(10)
N1	C1	C18	129.80(11)
C18	C1	C2	122.44(11)
C1	C2	C3	106.82(10)
C15	C2	C1	119.00(11)
C15	C2	C3	133.96(11)
C2	C3	C6	126.53(11)
C4	C3	C2	106.97(10)
C4	C3	C6	126.36(11)
N2	C20	C19	118.13(10)
N2	C20	C21	122.95(11)
C21	C20	C19	118.91(11)
N1	C4	C3	109.09(10)
N1	C4	C5	121.39(11)
C3	C4	C5	129.47(11)
C3	C6	C14	114.86(10)
C7	C6	C3	123.31(11)
C7	C6	C14	121.63(11)
C7	C8	C9	105.69(10)
C10	C8	C7	131.10(11)
C10	C8	C9	122.10(12)
N1	C19	C20	114.18(10)
C17	C18	C1	117.07(12)
C6	C7	C8	132.30(11)
C6	C7	C13	121.34(11)
C8	C7	C13	105.77(10)
O1	C13	C7	108.44(11)
O2	C13	O1	119.06(11)
O2	C13	C7	132.46(13)
C24	C23	C22	118.18(12)
C16	C15	C2	118.73(12)
C22	C21	C20	118.80(12)
C8	C10	C11	122.75(11)
C8	C10	C12	122.77(12)
C11	C10	C12	114.48(11)
C15	C16	C17	121.05(12)
O1	C9	C8	108.23(11)
O3	C9	O1	119.05(12)
O3	C9	C8	132.68(13)
C21	C22	C23	118.99(12)
C18	C17	C16	121.68(12)
N2	C24	C23	123.91(12)

Table A7: Hydrogen Fractional Atomic Coordinates ($\times 10^4$) and Equivalent Isotropic Displacement Parameters ($Å^2 \times 10^3$) for **7a**. U_{eq} is defined as 1/3 of the trace of the orthogonalized U_{ij}.

Atom	x	y	z	U_{eq}
H11A	3883.49	2967.61	7093.92	36
H11B	5344.67	2719.88	8084.6	36
H11C	4646.15	4123.54	8435.87	36
H5A	-694.23	2792.4	5649.74	33
H5B	-41.84	3216.69	7171.55	33
H5C	569.12	2011.95	6351.08	33
H14A	2268.86	7630.05	8725.91	36
H14B	2789.69	7444.99	10135.3	36
H14C	1106.57	7097.1	9283.54	36
H12A	3136.61	401.26	8880.7	51
H12B	4738.38	717.57	8854.27	51
H12C	3382.6	274.63	7553.64	51
H16	5704(19)	8274(18)	6929(16)	32(4)
H22	1237(19)	-1199(18)	1456(17)	36(4)
H17	4913(18)	7105(17)	4692(16)	29(4)
H18	2926(18)	5139(17)	3744(16)	28(4)
H21	283(19)	1019(17)	1811(17)	32(4)
H15	4630(17)	7550(16)	8315(15)	23(4)
H23	2937(19)	-1753(19)	3263(16)	33(4)
H24	3602(19)	-61(17)	5323(17)	31(4)
H19A	-279(17)	2881(16)	3843(14)	22(4)
H19B	828(17)	3563(17)	3297(16)	27(4)

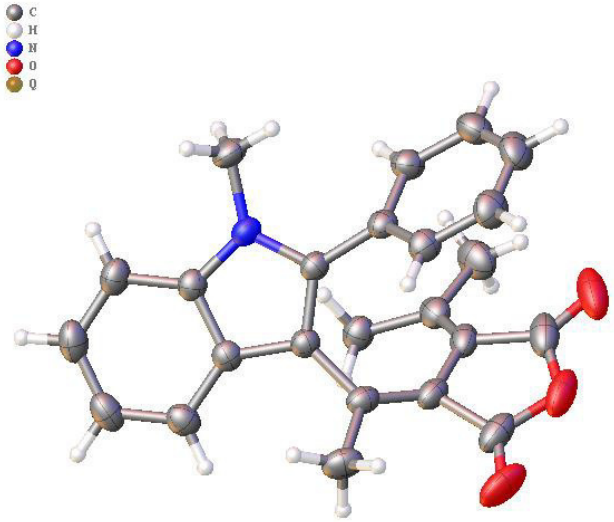

Experimental. Single clear yellow prism-shaped crystals of **7c** were obtained by recrystallisation from ethyl acetate. A suitable crystal (0.17×0.09×0.06) mm^3 was selected and mounted on a glass fibre with superglue on a XtaLAB Synergy R, DW system, HyPix diffractometer. The crystal was kept at T = 122.99(10) K during data collection. Using **Olex2**,[5] the structure was solved with the ShelXT[6] structure solution program, using the Intrinsic Phasing solution method. The model was refined with version 2016/6 of **ShelXL**[7] using Least Squares minimisation.

Crystal Data. $C_{24}H_{21}NO_3$, M_r = 371.42, monoclinic, $P2_1/c$ (No. 14), a = 10.6727(2) Å, b = 12.2092(2) Å, c = 15.0377(2) Å, β = 101.4650(10)°, α = γ = 90°, V = 1920.39(5) Å^3, T = 122.99(10) K, Z = 4, Z' = 1, μ(CuK$_\alpha$) = 0.678, 40249 reflections measured, 3936 unique (R_{int} = 0.0383) which were used in all calculations. The final wR_2 was 0.1129 (all data) and R_1 was 0.0400 (I > 2(I)).

Compound	**7c**
Formula	$C_{24}H_{21}NO_3$
$D_{calc.}$/ g cm^{-3}	1.285
μ/mm^{-1}	0.678
Formula Weight	371.42
Colour	clear yellow
Shape	prism
Size/mm^3	0.17×0.09×0.06
T/K	122.99(10)
Crystal System	monoclinic
Space Group	$P2_1/c$
a/Å	10.6727(2)
b/Å	12.2092(2)
c/Å	15.0377(2)
α/°	90
β/°	101.4650(10)
γ/°	90
V/Å^3	1920.39(5)
Z	4
Z'	1
Wavelength/Å	1.54184
Radiation type	CuK$_\alpha$
Θ_{min}/°	4.227
Θ_{max}/°	74.682
Measured Refl.	40249
Independent Refl.	3936
Reflections Used	3541
R_{int}	0.0383
Parameters	257
Restraints	0
Largest Peak	0.217
Deepest Hole	-0.263
GooF	1.058
wR_2 (all data)	0.1129
wR_2	0.1099
R_1 (all data)	0.0436
R_1	0.0400

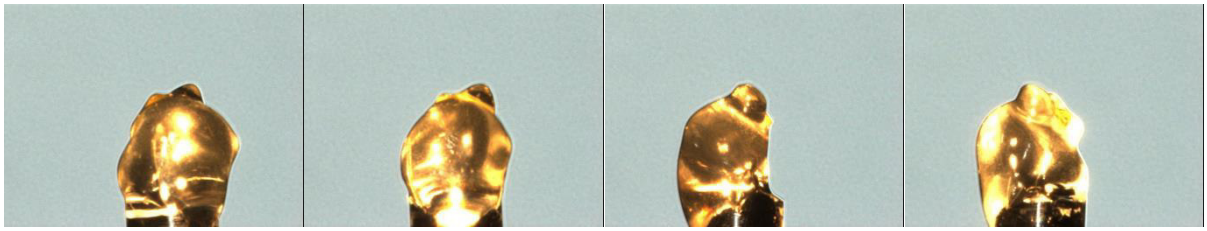

Figure A36: Images of the Crystal on the Diffractometer.

Table A8: Fractional Atomic Coordinates (×10⁴) and Equivalent Isotropic Displacement Parameters (Å²×10³) for **7c**. U_{eq} is defined as 1/3 of the trace of the orthogonalised U_{ij}.

Atom	x	y	z	U_{eq}
N9	1988.6(9)	5326.8(8)	5348.8(7)	31.4(2)
O23	4086.8(12)	9139.8(9)	3184.4(8)	60.4(3)
O25	5554.4(12)	7910.8(12)	2965.0(8)	67.9(4)
O24	2371.5(16)	10016.2(9)	3473.1(9)	72.7(4)
C10	2753.4(11)	7260.6(10)	5348.8(8)	31.4(3)
C8	2601.8(10)	6146.9(10)	4966.6(8)	29.3(2)
C7	3064.2(10)	5719.1(10)	4239.1(8)	29.6(2)
C6	2740.8(11)	4574(1)	4186.6(8)	31.3(3)
C1	2074.4(11)	4361.6(10)	4888.8(8)	32.1(3)
C16	3826.9(11)	6303.6(11)	3684.6(8)	33.1(3)
C20	3527.8(12)	7328.3(11)	3355.9(8)	35.9(3)
C21	2395.0(14)	8014.3(10)	3346.5(8)	37.6(3)
C26	1138.9(13)	7754.2(11)	3159.9(8)	38.0(3)
C11	3968.9(12)	7730.8(11)	5551.8(9)	37.8(3)
C15	1708.6(13)	7878.4(11)	5487.6(9)	38.0(3)
C28	689.2(12)	6611.7(11)	2932.2(9)	38.7(3)
C5	2939.0(12)	3711.9(11)	3613.8(9)	38.2(3)
C2	1660.9(12)	3312.2(11)	5060.9(10)	40.2(3)
C18	1519.8(13)	5387.8(12)	6190.5(9)	39.7(3)
C4	2525.5(13)	2673.3(11)	3781.6(11)	44.2(3)
C17	5034.1(12)	5732.8(14)	3559.8(10)	44.9(3)
C3	1904.6(13)	2473.9(11)	4501.5(11)	45.7(3)
C14	1878.4(15)	8945.8(12)	5803.8(10)	46.0(3)
C19	4514.3(15)	8064.1(14)	3128.7(10)	50.2(4)
C12	4128.7(15)	8796.1(13)	5867(1)	47.6(3)
C22	2864.1(18)	9156.9(12)	3368.2(10)	52.7(4)
C13	3087.4(17)	9406.1(12)	5991.3(10)	50.6(4)
C27	96.7(17)	8582.9(13)	3149.5(12)	54.9(4)

Table A9: Anisotropic Displacement Parameters (×10⁴) **7c**. The anisotropic displacement factor exponent takes the form: $-2\pi^2[h^2a^{*2} \times U_{11} + \ldots + 2hka^* \times b^* \times U_{12}]$

Atom	U_{11}	U_{22}	U_{33}	U_{23}	U_{13}	U_{12}
N9	30.8(5)	33.6(5)	31.3(5)	1.2(4)	9.6(4)	-4.6(4)
O23	78.6(8)	50.3(7)	49.6(6)	7.9(5)	6.4(5)	-33.1(6)
O25	53.7(7)	97.7(10)	56.0(7)	9.9(6)	19.7(5)	-34.8(6)
O24	123.8(12)	30.8(6)	56.9(7)	-0.6(5)	1.8(7)	-5.1(6)
C10	34.7(6)	33.8(6)	26.1(5)	-0.6(4)	6.8(4)	-4.1(5)
C8	26.5(5)	32.1(6)	29.4(5)	1.7(5)	5.6(4)	-2.5(4)
C7	26.7(5)	31.7(6)	30.7(6)	0.0(4)	6.3(4)	-1.4(4)
C6	26.0(5)	32.7(6)	34.5(6)	-0.7(5)	4.4(4)	-0.2(4)
C1	28.1(5)	31.9(6)	35.5(6)	1.1(5)	4.6(5)	-2.1(4)
C16	29.8(6)	41.6(7)	28.7(6)	-3.8(5)	7.9(4)	-7.1(5)
C20	38.8(6)	40.8(7)	29.1(6)	-0.3(5)	8.9(5)	-13.0(5)
C21	53.6(8)	30.3(6)	28.4(6)	2.0(5)	6.7(5)	-6.9(5)
C26	48.7(7)	34.4(6)	31.1(6)	4.4(5)	8.7(5)	4.1(5)
C11	36.6(6)	40.2(7)	35.7(6)	-2.4(5)	5.1(5)	-6.0(5)
C15	38.2(6)	39.6(7)	37.6(6)	-4.1(5)	10.7(5)	-1.9(5)
C28	34.5(6)	38.6(7)	42.6(7)	3.6(5)	7.0(5)	-2.1(5)
C5	32.2(6)	38.5(7)	43.9(7)	-5.9(5)	7.2(5)	1.8(5)
C2	34.7(6)	37.2(7)	48.2(7)	5.2(6)	7.3(5)	-6.5(5)
C18	43.3(7)	45.9(7)	33.1(6)	2.6(5)	15.3(5)	-5.8(6)
C4	36.6(7)	34.4(7)	59.1(9)	-10.1(6)	3.2(6)	1.9(5)
C17	31.7(6)	63.2(9)	42.2(7)	-1.2(6)	13.3(5)	-1.1(6)
C3	39.0(7)	31.3(6)	63.7(9)	1.6(6)	3.1(6)	-4.4(5)
C14	55.4(8)	41.3(7)	43.7(7)	-6.3(6)	15.7(6)	5.5(6)
C19	55.5(9)	59.4(9)	34.9(7)	5.4(6)	6.8(6)	-25.3(7)
C12	50.2(8)	44.7(8)	45.8(8)	-7.0(6)	4.3(6)	-14.6(6)

Atom	U_{11}	U_{22}	U_{33}	U_{23}	U_{13}	U_{12}
C22	82.7(11)	34.4(8)	35.6(7)	2.9(6)	-1.0(7)	-12.0(7)
C13	68.6(10)	37.2(7)	44.9(8)	-10.1(6)	8.3(7)	-8.5(7)
C27	63.5(10)	46.3(8)	53.1(9)	3.9(7)	6.9(7)	16.9(7)

Table A10: Bond Lengths in Å for **7c**.

Atom	Atom	Length/Å
N9	C8	1.3824(15)
N9	C1	1.3787(16)
N9	C18	1.4524(16)
O23	C19	1.398(2)
O23	C22	1.387(2)
O25	C19	1.199(2)
O24	C22	1.198(2)
C10	C8	1.4726(17)
C10	C11	1.3957(17)
C10	C15	1.3958(18)
C8	C7	1.3883(16)
C7	C6	1.4385(17)
C7	C16	1.4619(16)
C6	C1	1.4094(17)
C6	C5	1.4025(18)
C1	C2	1.3960(18)

Atom	Atom	Length/Å
C16	C20	1.3597(19)
C16	C17	1.5089(18)
C20	C21	1.468(2)
C20	C19	1.4749(18)
C21	C26	1.352(2)
C21	C22	1.4804(19)
C26	C28	1.4927(19)
C26	C27	1.501(2)
C11	C12	1.383(2)
C15	C14	1.387(2)
C5	C4	1.382(2)
C2	C3	1.382(2)
C4	C3	1.398(2)
C14	C13	1.384(2)
C12	C13	1.381(2)

Table A11: Bond Angles in ° for **7c**.

Atom	Atom	Atom	Angle/°
C8	N9	C18	126.78(11)
C1	N9	C8	109.04(10)
C1	N9	C18	123.36(10)
C22	O23	C19	110.93(11)
C11	C10	C8	119.37(11)
C11	C10	C15	118.72(12)
C15	C10	C8	121.88(11)
N9	C8	C10	122.07(10)
N9	C8	C7	109.09(10)
C7	C8	C10	128.77(11)
C8	C7	C6	106.85(10)
C8	C7	C16	126.25(11)
C6	C7	C16	126.72(11)
C1	C6	C7	106.80(10)
C5	C6	C7	134.37(12)
C5	C6	C1	118.83(12)
N9	C1	C6	108.20(10)
N9	C1	C2	129.53(12)
C2	C1	C6	122.21(12)
C7	C16	C17	115.56(11)
C20	C16	C7	122.64(11)
C20	C16	C17	121.63(12)
C16	C20	C21	131.43(11)
C16	C20	C19	121.18(13)
C21	C20	C19	105.94(12)
C20	C21	C22	105.25(12)
C26	C21	C20	130.44(12)
C26	C21	C22	122.89(13)
C21	C26	C28	121.84(12)
C21	C26	C27	123.09(13)
C28	C26	C27	115.06(13)
C12	C11	C10	120.50(13)

Atom	Atom	Atom	Angle/°
C14	C15	C10	120.35(12)
C4	C5	C6	118.93(13)
C3	C2	C1	117.53(13)
C5	C4	C3	121.24(13)
C2	C3	C4	121.19(13)
C13	C14	C15	120.29(14)
O23	C19	C20	107.57(13)
O25	C19	O23	119.04(14)
O25	C19	C20	133.27(17)
C13	C12	C11	120.38(13)
O23	C22	C21	108.00(14)
O24	C22	O23	119.63(15)
O24	C22	C21	132.29(18)
C12	C13	C14	119.75(13)

Table A12: Hydrogen Fractional Atomic Coordinates (×10⁴) and Equivalent Isotropic Displacement Parameters (Å²×10³) for **7c**. U_{eq} is defined as 1/3 of the trace of the orthogonalised U_{ij}.

Atom	x	y	z	U_{eq}
H11	4676.71	7324.66	5474.6	45
H15	894.37	7572.5	5367.37	46
H28A	1340.53	6210.79	2713.73	58
H28B	-75.12	6629.15	2471.2	58
H28C	512.88	6260.52	3465.16	58
H5	3342.21	3837.07	3128.91	46
H2	1237.13	3182.01	5534.42	48
H18A	1791.51	6064.68	6493.1	60
H18B	1855.15	4784.95	6574.74	60
H18C	602.81	5354.27	6059.92	60
H4	2662.73	2096.29	3408.64	53
H17A	5131.08	5061.13	3898.44	67
H17B	5756.09	6198.3	3773.64	67
H17C	4983.14	5575.96	2928.1	67
H3	1651.19	1764.44	4605.72	55
H14	1176.74	9354.21	5890.27	55
H12	4942.02	9103.33	5995.94	57
H13	3198.11	10123.39	6200.24	61
H27A	461.33	9255.32	3413.52	82
H27B	-504.19	8310	3493.42	82
H27C	-333.48	8713.3	2534.91	82

6. Computational Methods

All DFT-calculations (M06-2x/def2TZVP level of theory) were performed with the Gaussian 09, Revision D01 software package.[8, 9] Optimized structures were confirmed to be minima through frequency calculations. Visualization was done using CYLview Visualization Software.[10]

Cartesian Coordinates

***O*-1a**			
Atom	x	y	z
C	-7.98619	-0.25692	1.82818
C	-8.69018	0.4294	0.69527
C	-10.07692	0.67561	1.157
C	-10.05616	0.50615	2.65259
N	-8.83153	-0.09848	2.92987
O	-6.89708	-0.80018	1.9024
O	-10.89132	0.75356	3.50457
C	-11.22799	0.75585	0.43736
C	-8.01036	1.02345	-0.33779
C	-11.27463	0.52422	-1.0507
C	-12.57651	1.01414	1.06032
C	-8.62044	2.14761	-1.14635
C	-6.6407	0.65028	-0.69687
C	-5.50763	1.53934	-0.87801
C	-4.40655	0.726	-1.24643
N	-4.85119	-0.58819	-1.31822
C	-6.18921	-0.6341	-0.9728
C	-5.28895	2.91646	-0.69789
C	-4.01975	3.4397	-0.91858
C	-2.94775	2.61217	-1.30009
C	-3.12489	1.24155	-1.45846
C	-6.94379	-1.92256	-0.98482
C	-3.98257	-1.7259	-1.56076
C	-3.20497	-2.20453	-0.3393
C	-3.63411	-1.96189	0.96995
C	-2.87099	-2.47495	2.01871
C	-1.71997	-3.20528	1.72794
C	-1.3811	-3.39107	0.3873
N	-2.09848	-2.90461	-0.63151
H	-8.56964	-0.39488	3.86147
H	-10.37064	0.04306	-1.42922
H	-12.13443	-0.1142	-1.29016
H	-11.42069	1.46123	-1.60529

H	-12.52231	1.16136	2.13689
H	-13.02475	1.90622	0.59967
H	-13.25976	0.18174	0.84173
H	-9.45037	2.62885	-0.62334
H	-7.86176	2.89856	-1.37778
H	-8.98921	1.78455	-2.11423
H	-6.09119	3.57084	-0.36998
H	-3.84981	4.50431	-0.78292
H	-1.96419	3.04545	-1.45842
H	-2.29053	0.59788	-1.72033
H	-6.8238	-2.45537	-1.93646
H	-6.61487	-2.58625	-0.17679
H	-8.00773	-1.73063	-0.83541
H	-4.58871	-2.54982	-1.95021
H	-3.26793	-1.47247	-2.34899
H	-4.53619	-1.39156	1.1687
H	-3.17574	-2.30355	3.04758
H	-1.09698	-3.61925	2.51516
H	-0.48861	-3.95292	0.11545

***C*-1a**			
Atom	x	y	z
C	4.24269288	-0.15500655	-0.83120797
C	2.82035636	0.10680251	-0.3985376
C	2.34598625	-1.00507829	0.18943439
C	3.43762994	-2.01756894	0.25254319
N	4.52218837	-1.44334957	-0.40871417
O	5.00174096	0.56293708	-1.42300035
O	3.44678439	-3.10375912	0.76968194
C	0.97908818	-1.12516549	0.81399795
C	2.07956239	1.34728889	-0.48790342
C	1.13219066	-0.77001968	2.30307478
C	0.48020507	-2.57291928	0.66032946
C	2.76048534	2.64608521	-0.81916161
C	0.77568022	1.25365633	-0.15002322
C	-0.21870942	2.28662112	0.05752261
C	-1.33858297	1.67162396	0.65306139
N	-1.11383269	0.32776635	0.85119305
C	0.0735862	-0.09267928	0.07825992
C	-0.22434207	3.65840415	-0.18554819
C	-1.33735306	4.40712994	0.16364943

C	-2.44136981	3.78429831	0.74233775
C	-2.46537648	2.41993384	0.98413897
C	-0.34111795	-0.59739771	-1.31865769
C	-2.14690416	-0.55292962	1.32902251
C	-3.0609227	-1.14071209	0.27114088
C	-3.39295345	-2.49106502	0.28056469
C	-4.23551706	-2.98021533	-0.70578166
C	-4.71729474	-2.10478493	-1.66429242
C	-4.33687561	-0.7711487	-1.58425004
N	-3.53128078	-0.29506981	-0.64297319
H	5.41255353	-1.89708615	-0.53152098
H	1.89076135	-1.41232849	2.75189547
H	1.43475179	0.27160994	2.42242647
H	0.19792873	-0.91586087	2.84476029
H	1.04946566	-3.22568471	1.31846247
H	-0.57648453	-2.66776395	0.90060379
H	0.62157252	-2.93522385	-0.35780164
H	3.82748148	2.50575352	-0.96050401
H	2.35530499	3.07773325	-1.73662086
H	2.60423897	3.37052776	-0.01684939
H	0.61843457	4.13968119	-0.65836015
H	-1.35569844	5.47108216	-0.02757107
H	-3.31300793	4.37528319	0.99410202
H	-3.35478409	1.95367418	1.38271555
H	-0.93196372	0.17193251	-1.81521697
H	0.5457311	-0.80812759	-1.91798343
H	-0.94358665	-1.50287033	-1.2557076
H	-1.70660541	-1.35778121	1.91605049
H	-2.75911854	0.022037	2.02809127
H	-2.99059777	-3.14581359	1.0434522
H	-4.50510492	-4.02838617	-0.72799872
H	-5.37265312	-2.43967627	-2.45625768
H	-4.69721065	-0.05248387	-2.31244468

***O*-1c**			
Atom	x	y	z
C	2.13887701	-2.47755518	-0.4443289
C	1.02742806	-1.61385089	0.05419467
C	1.64045113	-0.64943137	0.98762786
C	3.11766323	-0.71430041	0.73520668
N	3.30863706	-1.84185845	-0.05161232
O	2.11006152	-3.48170903	-1.11079693
O	4.02180541	-0.02018968	1.12666149

C	1.09878314	-0.00744892	2.03679204
C	-0.18423946	-1.63269739	-0.54412318
C	-0.32500139	-0.20378019	2.45646991
C	1.86468347	0.94069625	2.91100675
C	-0.58891521	-2.75609222	-1.46958237
C	-1.14945396	-0.5354564	-0.43743283
C	-2.5487893	-0.66349283	-0.13672544
C	-3.08654367	0.63777274	-0.13446787
N	-2.07487524	1.52026153	-0.43068267
C	-0.90585721	0.81047333	-0.61453383
C	-3.37907519	-1.74236529	0.18624921
C	-4.70988114	-1.4996445	0.46065013
C	-5.23171324	-0.1970375	0.42997822
C	-4.430253	0.88883336	0.13686857
C	-2.296277	2.9259772	-0.68874306
C	0.37841503	1.46650082	-0.88566222
C	1.22213505	0.97958043	-1.88284118
C	2.49571914	1.5035653	-2.04019959
C	2.93868245	2.52594374	-1.21077514
C	2.09635265	3.03374667	-0.23203324
C	0.82391582	2.50736829	-0.07079345
H	4.22459153	-2.1705355	-0.31682009
H	-0.74529845	-1.13826086	2.09159686
H	-0.38351893	-0.18213703	3.54653019
H	-0.95550888	0.61139599	2.08414829
H	2.83239768	1.20938775	2.50505408
H	1.26414467	1.84384195	3.05481136
H	1.9997654	0.49870828	3.90258925
H	0.04712494	-2.75609785	-2.35782966
H	-0.45717889	-3.73237896	-1.00689044
H	-1.62193003	-2.62955359	-1.78498526
H	-2.98436183	-2.7503674	0.22042585
H	-5.3651115	-2.32496241	0.70564852
H	-6.27951792	-0.04022889	0.64938782
H	-4.82991708	1.89468146	0.13345228
H	-3.17578517	3.04511292	-1.32232711
H	-2.45452868	3.47729166	0.24048604
H	-1.43438559	3.34070324	-1.20366037
H	0.8773817	0.1756457	-2.52137498
H	3.146708	1.10991887	-2.80991665
H	3.93972567	2.92022509	-1.32271622
H	2.43850606	3.82529041	0.42176277
H	0.1827906	2.87485703	0.72296556

***C*-1c**			
Atom	x	y	z
C	-3.07296611	-1.57630769	-0.98727111
C	-1.73919346	-1.17077519	-0.42169365
C	-1.95066621	-0.41179699	0.66803682
C	-3.42042854	-0.31503153	0.90617013
N	-4.01644268	-1.01279719	-0.14037296
O	-3.31921116	-2.23329408	-1.96176401
O	-4.01666597	0.23657936	1.79401365
C	-0.82437951	0.10453697	1.53006491
C	-0.41749836	-1.56616104	-0.87196593
C	-0.46481709	-1.05372323	2.48810216
C	-1.185125	1.31110944	2.40548751
C	-0.22069626	-2.75714512	-1.76716941
C	0.59899056	-0.87209641	-0.32162522
C	2.02597135	-1.13591493	-0.30296035
C	2.5875841	-0.29786874	0.6825616
N	1.63793773	0.51556502	1.25601067
C	0.35446183	0.37702908	0.5520195
C	2.83843654	-2.01576866	-1.0066603
C	4.20005922	-2.05970213	-0.72490906
C	4.73848963	-1.23176509	0.25308126
C	3.94690352	-0.33895712	0.96822178
C	2.02329633	1.73460252	1.93434375
C	0.15482969	1.56443068	-0.41605005
C	1.2749732	2.03368218	-1.1088498
C	1.17516767	3.05474719	-2.03913114
C	-0.05495513	3.63900877	-2.30730354
C	-1.17516258	3.18850042	-1.6301782
C	-1.07256184	2.1647496	-0.69551909
H	-5.01124714	-1.12396158	-0.24969117
H	-1.32477299	-1.26519486	3.12460904
H	-0.20038262	-1.96011914	1.94363958
H	0.37603204	-0.769653	3.12013194
H	-2.0961215	1.10172798	2.96231602
H	-0.38164293	1.48119318	3.12218873
H	-1.33754292	2.2288241	1.84207121
H	-1.17109675	-3.21140713	-2.03050314
H	0.28135533	-2.47071509	-2.69336621
H	0.40258082	-3.50545932	-1.27110907
H	2.42969352	-2.64691781	-1.78194393
H	4.8411905	-2.7374015	-1.27130106
H	5.79917592	-1.27843381	0.46499156

H	4.37809205	0.29481062	1.73116727
H	2.93827157	2.14657471	1.49826666
H	1.23905449	2.48054159	1.82225341
H	2.19284574	1.5642084	3.00101084
H	2.24538202	1.58943392	-0.92642221
H	2.06330151	3.39226494	-2.55756137
H	-0.13693335	4.43753623	-3.03288826
H	-2.14259955	3.63514173	-1.82007887
H	-1.97236524	1.85505089	-0.18605739

7. References

1. Schiedel, M.; Herp, D.; Hammelmann, S.; Swyter, S.; Lehotzky, A.; Robaa, D.; Olah, J.; Ovadi, J.; Sippl, W.; Jung, M., Chemically Induced Degradation of Sirtuin 2 (Sirt2) by a Proteolysis Targeting Chimera (PROTAC) Based on Sirtuin Rearranging Ligands (SirReals). *J Med Chem* **2017,** *2*.
2. Laemmli, U. K., Cleavage of Structural Proteins during the Assembly of the Head of Bacteriophage T4. *Nature* **1970,** *227*, 680.
3. Bradford, M. M., A rapid and sensitive method for the quantitation of microgram quantities of protein utilizing the principle of protein-dye binding. *Analytical Biochemistry* **1976,** *72* (1), 248-254.
4. Heltweg, B.; Trapp, J.; Jung, M., In vitro assays for the determination of histone deacetylase activity. *Methods* **2005,** *36* (4), 332-337.
5. Dolomanov, O. V.; Bourhis, L. J.; Gildea, R. J.; Howard, J. A. K.; Puschmann, H., OLEX2: a complete structure solution, refinement and analysis program. *Journal of Applied Crystallography* **2009,** *42* (2), 339-341.
6. Sheldrick, G. M., Crystal structure refinement with SHELXL. *Acta Crystallographica. Section C, Structural Chemistry* **2015,** *71* (Pt 1), 3-8.
7. Sheldrick, G., SHELXT - Integrated space-group and crystal-structure determination. *Acta Crystallographica Section A* **2015,** *71* (1), 3-8.
8. Stephens, P. J.; Devlin, F. J.; Chabalowski, C. F.; Frisch, M. J., Ab Initio Calculation of Vibrational Absorption and Circular Dichroism Spectra Using Density Functional Force Fields. *The Journal of Physical Chemistry* **1994,** *98* (45), 11623-11627.

A.IV.2. Design and Synthesis of Photochromic Histamin H1 Antagonists Addressable with Visible Light

Table of Contents

1. NMR

1a: ^{1}H-NMR (300 MHz, MeOD-d4)

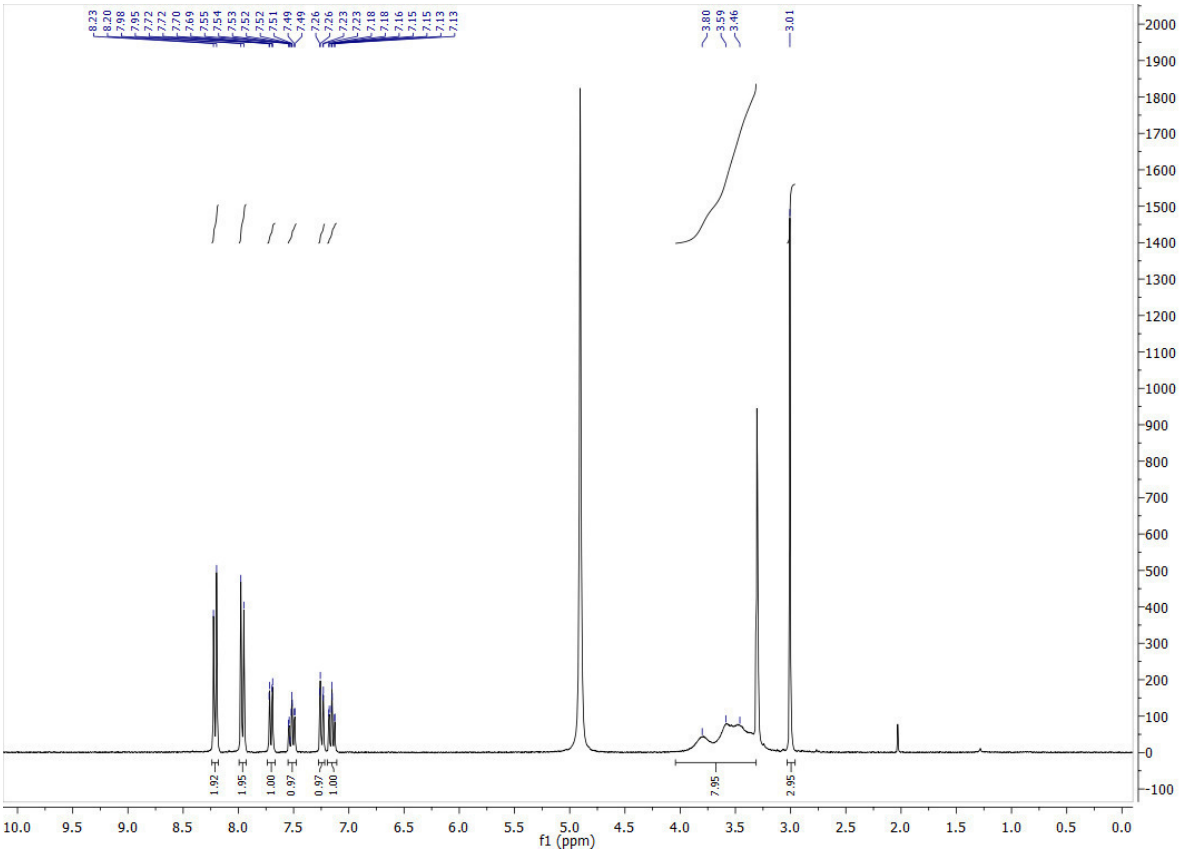

^{13}C-NMR (75 MHz, MeOD-d4)

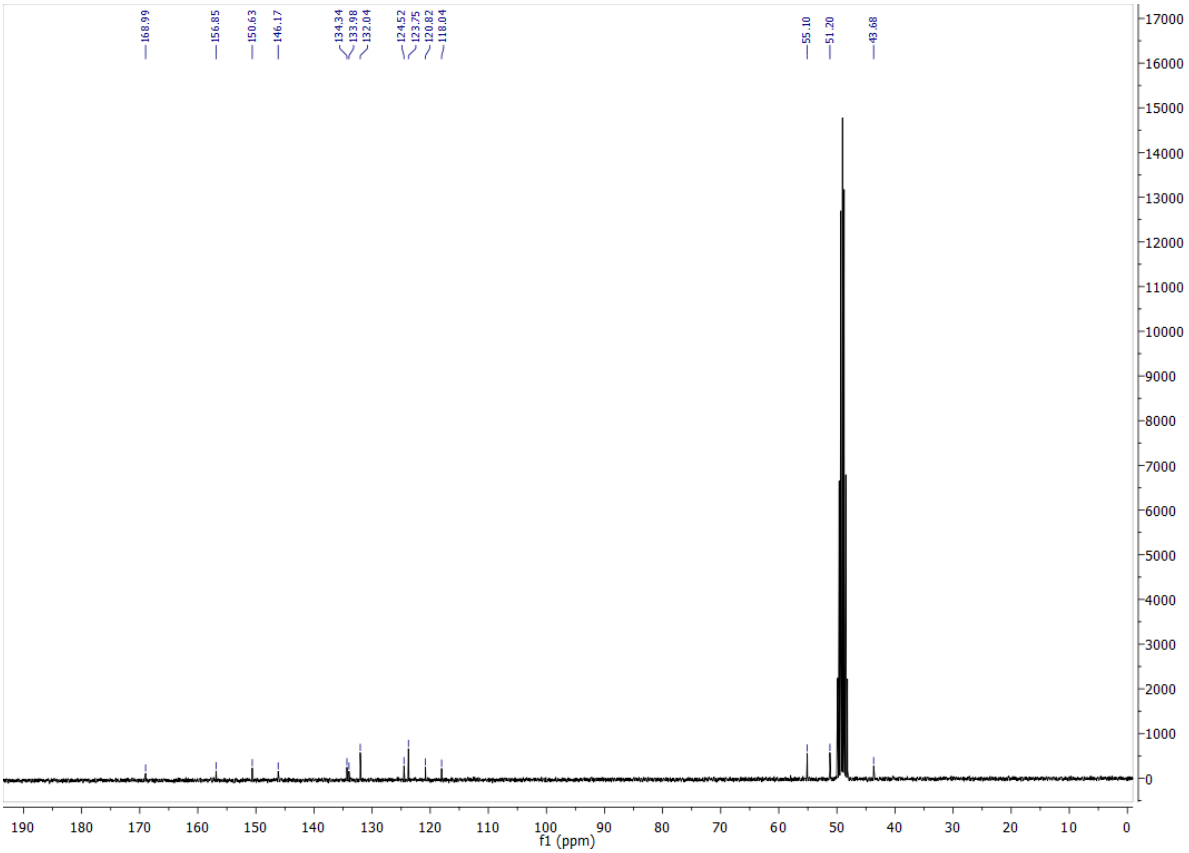

1b: ^{1}H-NMR (300 MHz, MeOD-d4)

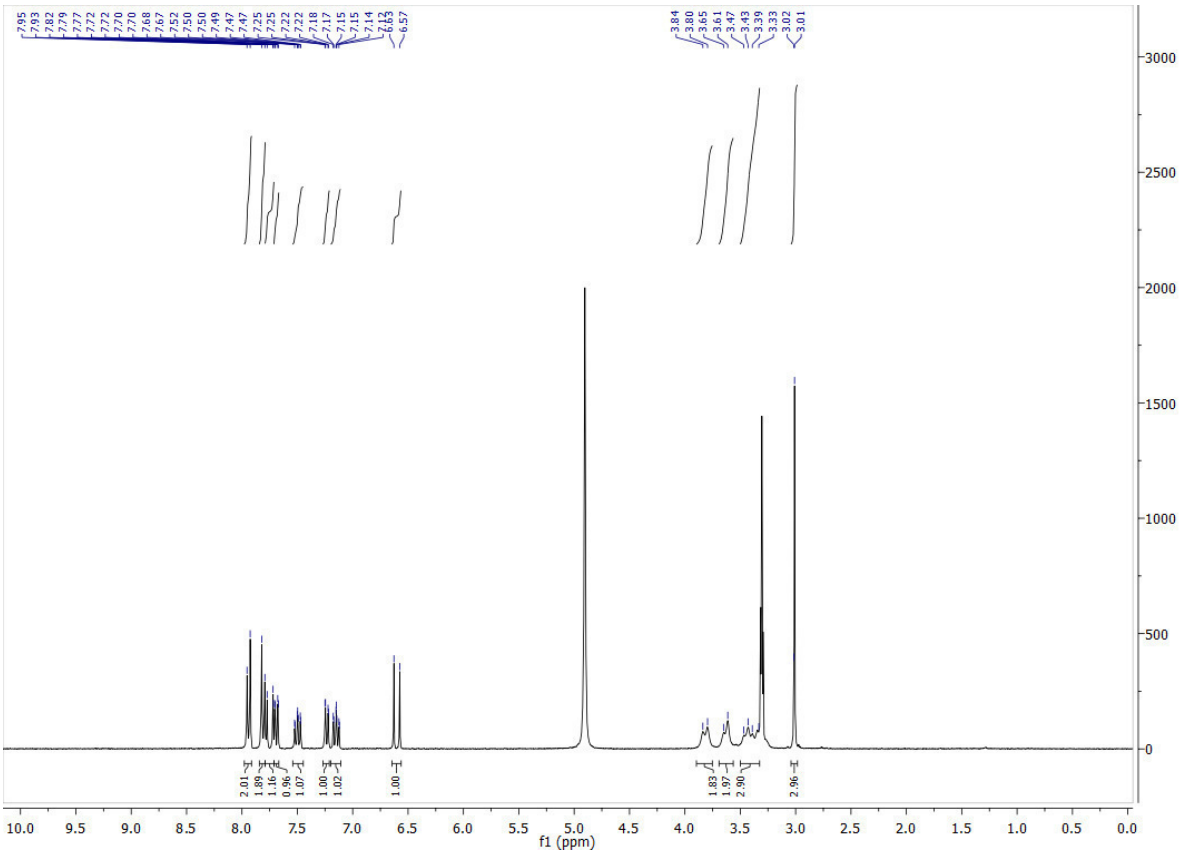

^{13}C-NMR (75 MHz, MeOD-d4)

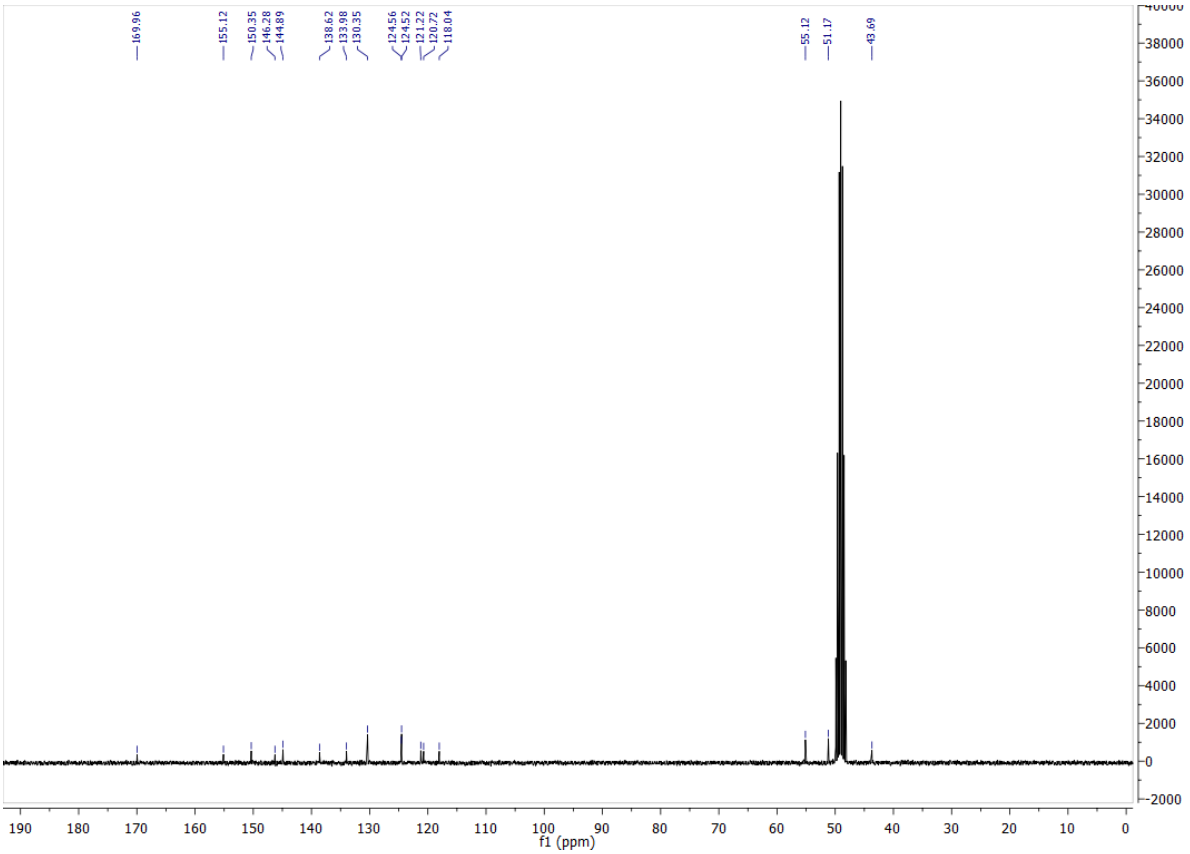

2. HPLC

1a

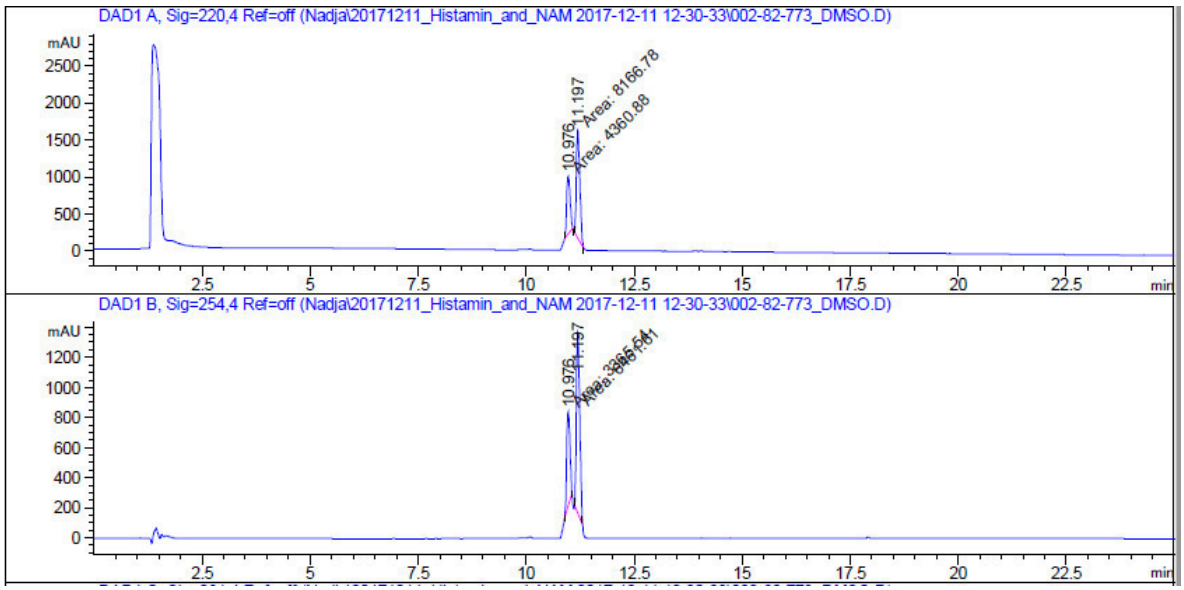
DAD1 A, Sig=220,4 Ref=off (Nadja\20171211_Histamin_and_NAM 2017-12-11 12-30-33\002-82-773_DMSO.D)
mAU
10.976
11.197
Area: 8166.78
Area: 4360.88
DAD1 B, Sig=254,4 Ref=off (Nadja\20171211_Histamin_and_NAM 2017-12-11 12-30-33\002-82-773_DMSO.D)
mAU
10.976
11.197
min

1b

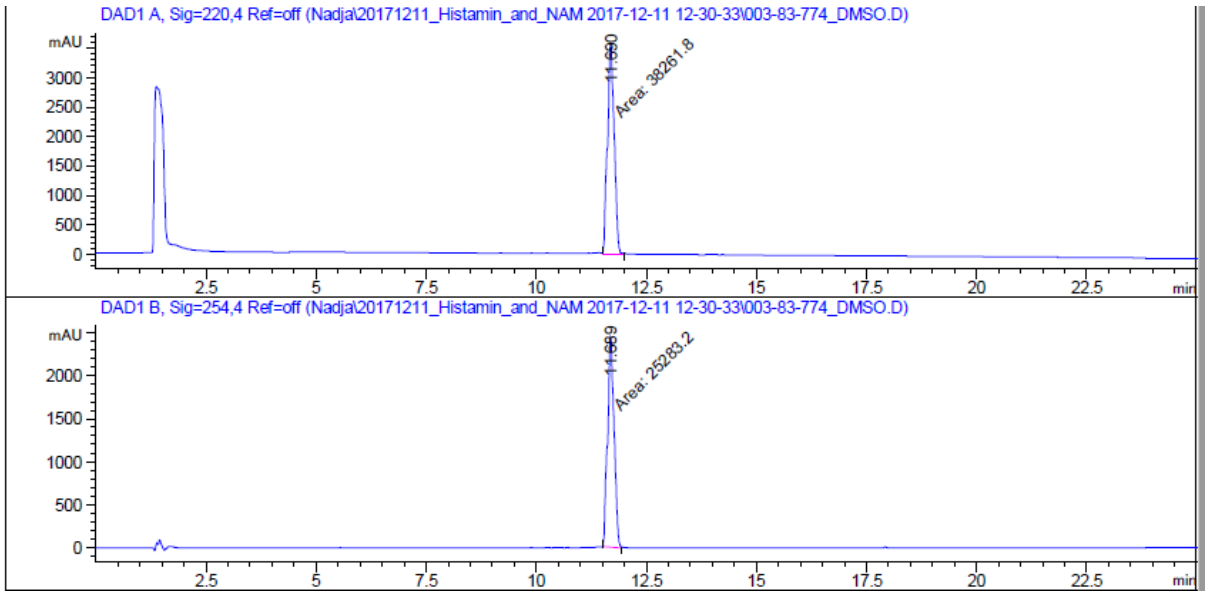
DAD1 A, Sig=220,4 Ref=off (Nadja\20171211_Histamin_and_NAM 2017-12-11 12-30-33\003-83-774_DMSO.D)
mAU
11.690
Area: 38261.8
DAD1 B, Sig=254,4 Ref=off (Nadja\20171211_Histamin_and_NAM 2017-12-11 12-30-33\003-83-774_DMSO.D)
mAU
11.689
Area: 25283.2
min

3. UV/Vis

1a in DMSO (left) and buffer (right)

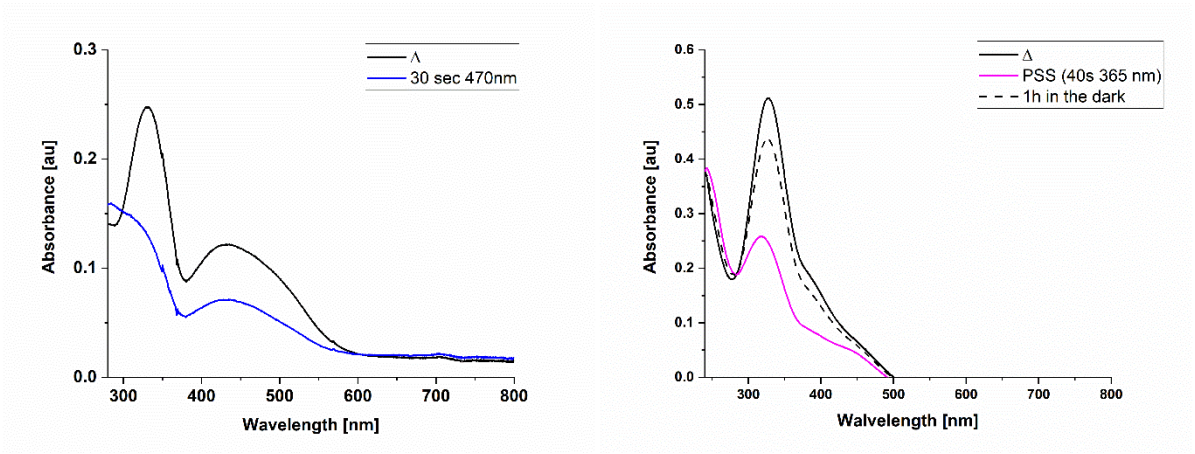

1b in DMSO (left) and buffer (right)

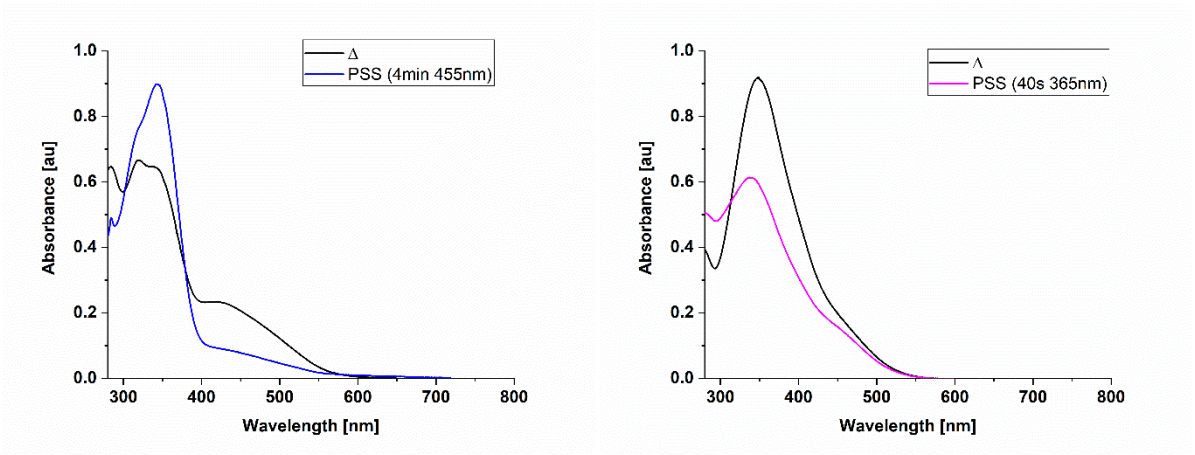

Lifetime in DMSO of **1a** (left) and **1b** (right).

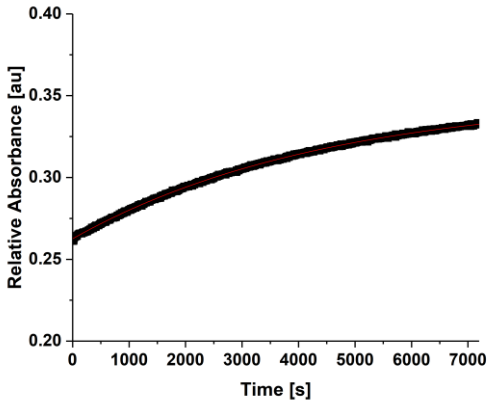

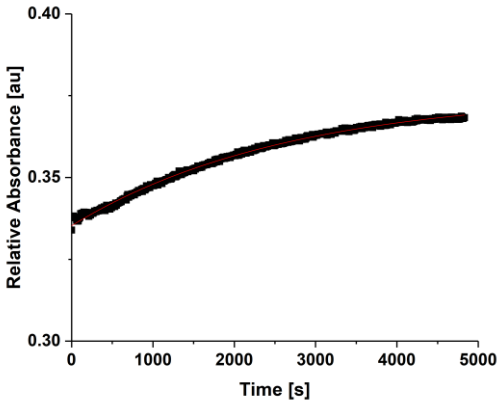

	1a	**1b**
Equation	y = A1*exp(-x/t1) + y0	y = A1*exp(-x/t1) + y0
y0	0.35019 ± 1.1675E-4	0.37556 ± 2.0687E-4
A1	-0.08765 ± 9.83248E-5	-0.04029 ± 1.69958E-4
t1	4490.7513 ± 12.20893	2645.25843 ± 30.21326
R-Square(COD)	0.9996	0.99702
Adj. R-Square	0.9996	0.997